*The Proceedings*

OF

# THE INSTITUTION OF ELECTRICAL ENGINEERS

FOUNDED 1871: INCORPORATED BY ROYAL CHARTER 1921

## PART C

MONOGRAPHS Nos. 246–282

# The Institution of Electrical Engineers

FOUNDED 1871

INCORPORATED BY ROYAL CHARTER 1921

---

PATRON: HER MAJESTY THE QUEEN

---

## COUNCIL 1957–1958

### President

T. E. GOLDUP, C.B.E.

### Past-Presidents

SIR JAMES SWINBURNE, Bart., F.R.S.
W. H. ECCLES, D.Sc., F.R.S.
THE RT. HON. THE EARL OF MOUNT EDGCUMBE, T.D.
J. M. DONALDSON, M.C.
PROFESSOR E. W. MARCHANT, D.Sc.
H. T. YOUNG.
SIR GEORGE LEE, O.B.E., M.C.
SIR ARTHUR P. M. FLEMING, C.B.E., D.Eng., LL.D.
J. R. BEARD, C.B.E., M.Sc.
SIR NOEL ASHBRIDGE, B.Sc.(Eng.).
COLONEL SIR A. STANLEY ANGWIN, K.C.M.G., K.B.E., D.S.O., M.C., T.D., D.Sc.(Eng.).

SIR HARRY RAILING, D.Eng.
P. DUNSHEATH, C.B.E., M.A., D.Sc.(Eng.).
SIR VINCENT Z. DE FERRANTI, M.C.
T. G. N. HALDANE, M.A.
PROFESSOR E. B. MOULLIN, M.A., Sc.D.
SIR ARCHIBALD J. GILL, B.Sc.(Eng.).
SIR JOHN HACKING.
COLONEL B. H. LEESON, C.B.E., T.D.
SIR HAROLD BISHOP, C.B.E., B.Sc.(Eng.).
SIR JOSIAH ECCLES, C.B.E., D.Sc.
SIR GEORGE H. NELSON, Bart.
SIR GORDON RADLEY, K.C.B., C.B.E., Ph.D.(Eng.).

### Vice-Presidents

S. E. GOODALL, M.Sc.(Eng.).
WILLIS JACKSON, D.Sc., D.Phil., Dr.Sc.Tech., F.R.S.
G. S. C. LUCAS, O.B.E.

SIR HAMISH D. MACLAREN, K.B.E., C.B., D.F.C., LL.D., B.Sc.
C. T. MELLING, C.B.E., M.Sc.Tech.

### Honorary Treasurer

THE RT. HON. THE VISCOUNT FALMOUTH.

### Ordinary Members of Council

PROFESSOR H. E. M. BARLOW, Ph.D., B.Sc.(Eng.).
J. A. BROUGHALL, B.Sc.(Eng.).
C. M. COCK.
SIR JOHN DEAN, B.Sc.
B. DONKIN, B.A.
J. S. FORREST, D.Sc., M.A.
PROFESSOR J. GREIG, M.Sc., Ph.D.
E. M. HICKIN.
J. B. HIGHAM, Ph.D., B.Sc.
D. McDONALD, B.Sc.
F. C. McLEAN, C.B.E., M.Sc.

B. L. METCALF, B.Sc.(Eng.).
J. R. MORTLOCK, B.Sc.(Eng.).
H. H. MULLENS, B.Sc.
A. H. MUMFORD, O.B.E., B.Sc.(Eng.).
R. H. PHILLIPS, T.D.
D. P. SAYERS, B.Sc.
C. E. STRONG, O.B.E., B.A., B.A.I.
H. WATSON-JONES, M.Eng.
D. B. WELBOURN, M.A.
H. WEST, M.Sc.

### Chairmen and Past-Chairmen of Sections

*Measurement and Control:*
H. S. PETCH, B.Sc.(Eng.).
*D. TAYLOR, M.Sc., Ph.D.

*Radio and Telecommunication:*
J. S. McPETRIE, Ph.D., D.Sc.
*R. C. G. WILLIAMS, Ph.D., B.Sc.(Eng.).

*Supply:*
PROFESSOR M. G. SAY, Ph.D., M.Sc., F.R.S.E.
*P. J. RYLE, B.Sc.(Eng.).

*Utilization:*
J. VAUGHAN HARRIES.
*H. J. GIBSON, B.Sc.

### Chairmen and Past-Chairmen of Local Centres

*East Midland Centre:*
J. D. PIERCE.
*H. L. HASLEGRAVE, M.A., Ph.D., M.Sc. (Eng.).

*Mersey and North Wales Centre:*
T. MAKIN.
*P. D'E. STOWELL, B.Sc.(Eng.).

*North Midland Centre:*
A. J. COVENEY.
*W. K. FLEMING.

*North-Eastern Centre:*
T. W. WILCOX.
*J. CHRISTIE.

*North-Western Centre*
F. R. PERRY, M.Sc.Tech.
*T. E. DANIEL, M.Eng.

*Northern Ireland Centre:*
C. M. STOUPE, B.Sc.
*DOUGLAS S. PARRY.

*Western Centre:*
J. F. WRIGHT.
*PROFESSOR G. H. RAWCLIFFE, M.A., D.Sc.

*Scottish Centre:*
E. O. TAYLOR, B.Sc.
*PROFESSOR F. M. BRUCE, M.Sc., Ph.D.

*South Midland Centre:*
L. L. TOLLEY, B.Sc.(Eng.).
*C. J. O. GARRARD, M.Sc.

*Southern Centre:*
L. G. A. SIMS, D.Sc., Ph.D.
*H. ROBSON, B.Sc.

* Past Chairman.

---

### Secretary

W. K. BRASHER, C.B.E., M.A., M.I.E.E.

**Deputy Secretary**
F. JERVIS SMITH, M.I.E.E.

**Assistant Secretary**
F. C. HARRIS.

**Editor-in-Chief**
G. E. WILLIAMS, B.Sc.(Eng.), M.I.E.E.

# THE PROCEEDINGS OF
# THE INSTITUTION OF ELECTRICAL ENGINEERS

## THE CONCEPT OF HETEROGENEOUS SURFACE IMPEDANCE AND ITS APPLICATION TO CYLINDRICAL CAVITY RESONATORS

### By A. E. KARBOWIAK, Ph.D.

### SUMMARY

The concept of heterogeneous surface impedance is introduced. This is defined as an impedance sheet whose surface impedance varies from point to point in an arbitrary manner. The approach is found to yield useful results in a variety of physical situations, and a few applications are illustrated by numerical examples.

Physical heterogeneous impedance sheets are extremely common. Typical examples are provided by resonators which are built up of several pieces of metals of various conductivities, resonators imperfectly assembled (e.g. by having small gaps between various parts), effects of imperfect machining or annealing, etc.

The formulae developed relate the Q-factor and the resonant frequency of a cavity to its dimensions and the Fourier components of the surface impedance function, which, in general, may be anisotropic. The analysis is kept as general as possible, and the formulae developed do not exclude any of the practical cases.

In the case of circumferential heterogeneity it is shown that all $E_{m,n,l}$- and $H_{m,n,l}$-modes (other than $E_0$- and $H_0$-modes) are unstable unless the $2m$th harmonic of the heterogeneous surface impedance is absent. It is further concluded that such cavities are characterized by a double-humped resonance curve, but so far as the $E_0$- and $H_0$-modes are concerned, the cavity may be regarded as homogeneous with surface impedance equal to the mean value of the surface-impedance function.

With the exception of a few isolated cases (discussed in detail) an axially heterogeneous cavity, when supporting any $E_{m,n,l}$ or $H_{m,n,l}$-mode, may be regarded as a homogeneous one whose axial anisotropic component is the sum of the mean value of the surface-impedance function and one-half of its $l$th harmonic, and whose circumferential component is given by the difference between the mean value of the surface-impedance function and one-half of its $l$th harmonic.

It is shown that, in general, a unique value of the surface impedance cannot be ascribed to an unbounded periodic sheet, but if its period is sufficiently small (in comparison with the wavelength), the heterogeneous sheet behaves as if it were homogeneous of surface impedance equal to the mean value of the surface-impedance function.

### LIST OF PRINCIPAL SYMBOLS

$\mu_0, \epsilon_0$ = Permeability and permittivity of free space, respectively.

$Z_0 = \sqrt{\dfrac{\mu_0}{\epsilon_0}}$ = Free-space impedance.

$Z_s = R_s + jX_s$ = Surface impedance normalized with respect to $Z_0$.

$Z_\eta, Z_\xi$ = Anisotropic components of surface impedance.

$Z_e$ = Equivalent uniform surface impedance.

$f(\phi, z)$ = Surface-impedance function of the heterogeneous surface.

$C_q^{(z)}, S_q^{(z)}, C_q^{(\phi)}, S_q^{(\phi)}$ = Fourier coefficients of the surface-impedance function.

$k_0 = 2\pi/\lambda_0$ = Wave number of a perfect cavity.

$f_0 = c/\lambda_0$ = Resonant frequency of a perfect cavity.

$\beta_l = \pi l/L$ = Axial propagation coefficient.

$h_{m,n}$ = Cut-off coefficient.

$k = k_0 + \delta k$ = Wave number of an imperfect cavity.

$h = h_0 + \delta h$ = Cut-off coefficient of an imperfect cavity.

$\nu$ = Perturbation parameter (essentially small).

$\delta h = \nu h^{(1)} + \nu^2 h^{(2)}, \dots$

$\delta k = \nu k^{(1)} + \nu^2 k^{(2)}, \dots$

$m$ = Radial-mode index.

$n$ = Circumferential-mode index.

$l$ = Axial-mode index.

$L$ = Length of the cavity.

$s$ = Radius of the cavity.

$t = \beta m/h_n^2 s$.

$w = k/h$.

$\Delta = \Delta_1 + j\Delta_2 = \Delta k/k_0 = \Delta f/f_0$ = Complex fractional change in the resonant frequency [eqn. (17)].

$c_n, s_n, c_n', s_n'$ = Coupling coefficients of various modes.

$\tau$ = Coupling coefficient between $_sH$ and $_cH$ modes or $_sE$ and $_cE$ modes.

The quantity $Z_0$ (= 377 ohms) is absorbed in the symbol $H$ (magnetic-field vector), and consequently all impedances and coupling coefficients are normalized with respect to that quantity. It is therefore immaterial which system of units is used, since all quantities, unless otherwise specified, are normalized; e.g. distance

is measured in the same units in which it is chosen to measure wavelength.

The time factor $\exp(j\omega t)$ is implied throughout.

## (1) INTRODUCTION

Acoustical resonant cavities were studied by Lord Rayleigh[1] as far back as the end of the last century, and his expressions for the resonant frequency of a rectangular box resonator (with perfectly conducting walls) apply with little modification to microwave cavities. Since then, more thorough analytical treatments of resonant electromagnetic cavities have appeared,[2, 3] and descriptions have been given on how to calculate the Q-factor of a cavity made of a good conductor.[4, 5, 6]

The effect of coupling devices on the performance of micro-wave cavities has been investigated theoretically by Bethe[7] and Condon.[8]

As far as the experimental work is concerned, most of our knowledge is derived from various designs of reference cavities, echo boxes and cavity wavemeters,[9, 10, 11, 12] but invariably the cavities investigated were (or were assumed to be) homogeneous and isotropic.

The study of anisotropic cavities presents no difficulty if the surface-impedance approach[13] is adopted, and furthermore, the performance of cavities whose walls are made of *any* homogeneous impedance surfaces (not necessarily homogeneous conductor) is easily predictable using this approach.

If, as with a circular cylindrical cavity, the cavity end-walls have an impedance which is different from that of the curved walls, then, in a strict sense, the cavity is (physically) no longer homogeneous. Formulae for such cavities have been obtained elsewhere,[13] and will not be discussed in the paper.

In contrast, the purpose of the paper is to analyse cavities whose walls are not representable by homogeneous impedance sheets but are themselves heterogeneous, and only such cavities will be termed heterogeneous.

## (2) STATEMENT AND APPROACH TO THE PROBLEMS

### (2.1) General

The type of problem it is proposed to tackle is to find, for example, the resonant frequency and the Q-factor of a cavity made up of two or more pieces of different materials that are assembled, possibly in an imperfect manner, e.g. by leaving small gaps between the various parts. Another example would be a cavity the inner surface of which (owing to a machining process) acquired a hardened skin which varied in its physical properties from one part of the cavity to another.

The analysis is based on the assumption that the surface impedance of all cavity walls is small. Consequently the Q-factor of such a cavity is high, and the resonant frequency is close to that of a perfect cavity.

### (2.2) Surface-Impedance Concept: its Interpretation and Uses

Fig. 1 illustrates a fragment of the cavity wall; $\bar{n}$ is the outward-drawn normal to the surface, $\phi$ is the circumferential co-ordinate, and $z$ is the axial co-ordinate. The surface impedance[13] $Z_s$, which is a characteristic property of the guide wall S, is measured in the direction of the normal $\bar{n}$ and is defined by the ratio of the tangential components (to the surface S) of the electric field vector $E_t$ and the magnetic field vector, $H_t$.

Thus
$$Z_s = \frac{E_t}{H_t}\bigg|_S \quad . \quad . \quad . \quad . \quad . \quad . \quad . \quad (1)$$

If this quantity is unaffected by the orientation of the $E_t$-vector, and if, in addition, it is independent of the value of the
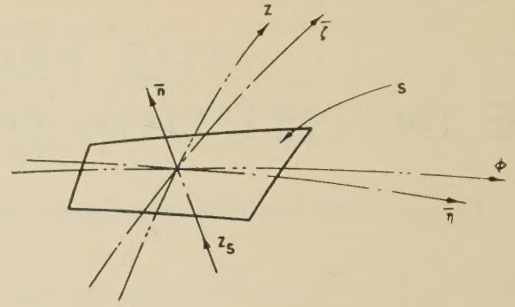


Fig. 1.—Fragment of the cavity wall.

co-ordinates, this single complex quantity is sufficient to describe the guide surface; such a surface is termed homogeneous and isotropic, a plain metal surface being an example.

A guide surface may be homogeneous, in that it is not a function of the guide co-ordinates, and yet the surface impedance as given by eqn. (1) may be dependent on the orientation of the $E_t$ vector; such a surface is called 'anisotropic'.[14] An anisotropic surface impedance, $Z_s$, is no longer scalar, but its component form, with respect to the $\phi$, $z$ co-ordinate system, a $2 \times 2$ matrix. This matrix can conveniently be reduced to a diagonal matrix in some other co-ordinate system $\eta$, $\xi$. The axes $\eta$ and $\xi$ are referred to as the principal axes of the anisotropic surface and the impedance components $Z_\eta$ and $Z_\xi$, defined by

$$Z_\eta = \frac{E_\eta}{H_\xi}\bigg|_S \\ -Z_\xi = \frac{E_\xi}{H_\eta}\bigg|_S \Bigg\} \quad . \quad . \quad . \quad . \quad . \quad (2)$$

are termed the principal impedance components of the surface impedance $Z_s$. The two complex numbers $Z_\eta$ and $Z_\xi$ are sufficient for adequate description of a homogeneous and anisotropic surface.

If the surface impedance $Z_s$, defined by eqn. (1), is not constant but is a function of the surface co-ordinates, evidently $Z_s$ can be regarded as heterogeneous in $\phi$ or $z$, or $\phi$ and $z$ co-ordinates. Evidently, an adequate description of the quantity $Z_s$ calls for the use of functions and we may put

$$Z_s = f(\phi, z) = \frac{E_t}{H_t}\bigg|_S \quad . \quad . \quad . \quad . \quad (3)$$

where $f(\phi, z)$ is a function of $\phi$ and $z$, characteristic of the surface. Eqn. (3) defines an isotropic heterogeneous surface.

For the general case the concept of the anisotropic heterogeneous surface has yet to be introduced. The surface impedance of such a surface has two principal components, defined by*

$$Z_\eta = f_\eta(\eta, \xi) = \frac{E_\eta}{H_\xi}\bigg|_S \\ Z_\xi = f_\xi(\eta, \xi) = \frac{E_\xi}{H_\eta}\bigg|_S \Bigg\} \quad . \quad . \quad . \quad (4)$$

The performance of cavities with homogeneous walls (either isotropic or anisotropic) is now readily predictable,[13] and here it is desired to study the properties of cavities whose walls are heterogeneous, i.e. whose surface impedance is not constant but can vary in an arbitrary manner over the surface of the

* The angle of anisotropy (the angle between the $z$ and $\xi$ co-ordinates) is assumed to be constant.

cavity. This variation can either be isotropic, as described by eqn. (3), or anisotropic, as described by eqn. (4).

### (2.3) Analytical Approach

Consider a cylindrical cavity as shown in Fig. 2, in which parts A and B are made of different metals, say copper and brass.
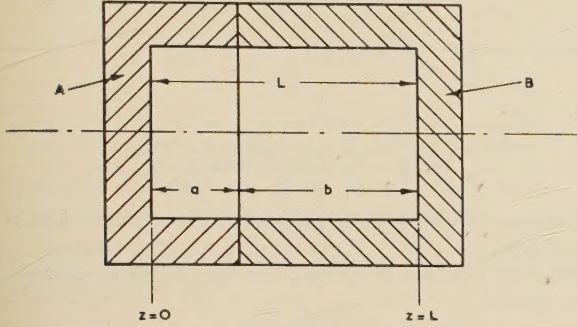


Fig. 2.—A heterogeneous cavity.

Evidently, one of the cavity end-plates has a surface impedance equal to the copper intrinsic impedance, $Z_A$, and the other equal to the brass intrinsic impedance $Z_B$: their effect on the resonant frequency and Q-factor may be calculated in the conventional manner.[13] The curved wall of the cavity is, however, heterogeneous, and its surface impedance is given by

$$Z_s = Z_A(0 < z < a) \left.\right\} \quad = Z_B(a < z < L) \left.\right\} \quad \cdots \quad (5)$$

The function $Z_s = f(z)$ can be expanded in an infinite series of orthogonal functions. For example, f(z) can be expanded in the interval $0 < z < L$ in a cosine series or in its Fourier series (the choice is a matter of convenience only). In the latter representation we evidently have

$$Z_s = f(z)$$
$$= Z_A \frac{a}{L} + Z_B \frac{L-a}{L} + \sum_{n=1}^{\infty} \left( \frac{Z_B - Z_A}{\pi n} \sin 2\pi n \frac{a}{L} \right) \cos \frac{2\pi n}{L} z$$
$$\cdots \quad (6)$$

For a second example, consider a cylindrical cavity as shown in Fig. 3. Here, owing to an imperfect construction, small gaps are present where the end-plates meet the body of the cavity.

The impedance of a narrow circumferential gap depends on the polarization of the wave. Thus, for a narrow groove, whose depth, $l$, is small in comparison with the wavelength, the input impedance is given by (see Appendix 8.1):

$$Z_E = j2\pi \frac{l}{\lambda_0} + \left( 2\frac{l}{t} + 1 \right) R_m \quad \cdots \quad (7)$$

for the E-vector normal to the edges of the groove, and

$$Z_H = j2 \frac{t}{\lambda_0} + \frac{2}{\pi} R_m \quad \cdots \quad (8)$$

for the E-vector parallel to the edges of the groove, where $l$ is the depth of the groove, $t$ is its width and $R_m$ is the intrinsic resistance of the metal in which the groove is cut.

Let us now return to the problem of the cavity depicted in Fig. 3. Here, evidently, $Z_s$ is not a function of $\phi$, but is aniso-tropic and heterogeneous in the co-ordinate z. Furthermore, the principal axes of the surface $\eta$, $\xi$ coincide with the $\phi$ and z co-ordinates respectively. Two simple examples of functions
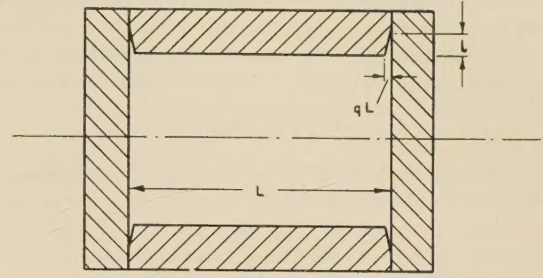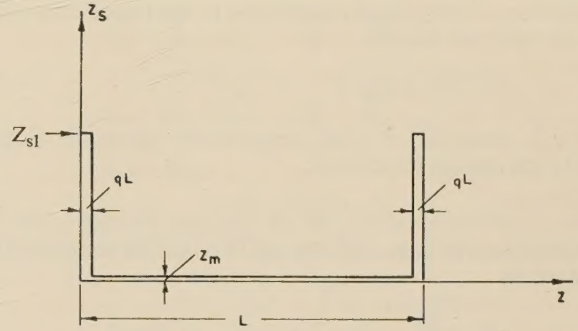


Fig. 3.—An imperfectly assembled cavity.



Fig. 4.—A possible surface impedance function of the cavity shown in Fig. 3.
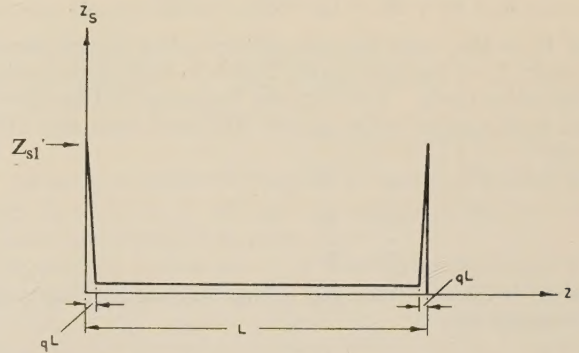


Fig. 5.—A possible surface impedance function of the cavity shown in Fig. 3.

appropriate to the case considered are shown in Figs. 4 and 5. Here again $Z_s$ can be expanded in its Fourier series. Thus, in the case of a rectangular gap (Fig. 4), we have

$$Z_\eta = Z_\phi = f_\phi(z)$$
$$= Z_m + Z_H \left( q + \frac{2}{\pi} \sum_{n=1}^{\infty} \frac{1}{n} \sin nq\pi \cos \frac{2\pi n}{L} \right) \quad \cdots \quad (9)$$

while $Z_z$ is given by eqn. (9) with $Z_E$ in place of $Z_H$.

In the case of a triangular gap (Fig. 5) we have the same expressions for $Z_\phi$ and $Z_z$, but with the expression in brackets in eqn. (9) replaced by

$$\frac{q}{2} + \sum_{n=1}^{\infty} \left[ \frac{2}{n\pi} \sin n\pi q - \frac{2}{n^2\pi^2 q} \left( n\pi q \sin n\pi q - 2 \sin^2 \frac{n\pi q}{2} \right) \right] \cos \frac{2\pi n}{L}$$
$$\cdots \quad (10)$$

Having learned how to translate various physical imperfections in a cavity into mathematical language we can now proceed with the analysis of a general case.

Accordingly it is assumed that the nature of the cavity imperfection is fully described by eqn. (4).

Let $M_{m,n,l}$ be the mode appropriate to a perfect cavity and let its resonant frequency be $f_0$. The following relation holds:

$$k_0^2 = h_{m,n}^2 + \beta_l^2 \quad \ldots \ldots \quad (11)$$

where, if the mode considered is an $E_{m,n,l}$- or an $H_{m,n,l}$-mode, $h_{m,n}$ is its cut-off coefficient and*

$$\beta_l = \pi l/L \quad \ldots \ldots \ldots \quad (12)$$

is the axial coefficient.

In the case of an axially heterogeneous cavity the originally pure mode, $M_{m,n,l} = \psi_0$ will become contaminated by a denumerable infinity of other modes appropriate to the region considered. Thus the field will become

$$\psi = \psi_0 + \nu \sum_q \psi^{(1)} + \nu^2 \sum_q \psi^{(2)} + \ldots \quad \ldots \quad (13)$$

where $\nu$ is essentially a small perturbation parameter proportional to the surface impedance;

i.e.

$$Z_s = \mathrm{f}(z) = \nu F(z) \quad \ldots \quad \ldots \quad (14)$$

The summation in eqn. (13) extends over all the discrete values of $\beta$ given by

$$\beta_q = \frac{\pi q}{L} \quad (q = 0, 1, 2, \ldots; q \neq l) \quad \ldots \quad (15)$$

The resonant frequency of the so perturbed mode is given by

$$k = k_0 + \delta k = k_0 + \nu k^{(1)} + \nu^2 k^{(2)} + \ldots \quad \ldots \quad (16)$$

where $k_0$ is the wave number corresponding to the resonant frequency, $f_0$, of the pure mode, and $k$ is a similar quantity of the perturbed mode. The resonant frequency and the Q-factor of the contaminated mode can be calculated from eqn. (16) as follows:

The fractional change in resonant frequency is given by

$$\frac{\delta \omega}{\omega_0} = \frac{\delta k}{k_0} = \Delta_1 + j\Delta_2. \quad \ldots \ldots \quad (17)$$

where $\Delta_1$ is the real fractional change in resonant frequency of the resonator and[13]

$$\Delta_2 = \frac{1}{2Q} \quad \ldots \ldots \ldots \quad (18)$$

In the case of a circumferentially heterogeneous cavity the summation in eqn. (13) extends over all the discrete values of $m$, the circumferential index of the mode. The calculation is otherwise the same as for an axially heterogeneous cavity.

## (3) FIRST-ORDER THEORY OF THE HETEROGENEOUS CAVITY

### (3.1) The Purpose of the First-Order Analysis

The first-order solution includes all terms up to and including the first power of the perturbation quantity $\nu$. This solution, which is relatively easy to obtain and is sufficient for quantitative computation in most practical cases, will be the first aim.

### (3.2) E-modes

Imagine a parallel-plate waveguide, of length $L$, short-circuited at both ends, as shown in Fig. 6. The plates are infinite in extent in the direction of the $y$ co-ordinate and they are separated

* It has been assumed that the end-plates are perfect; otherwise allowance must be made for the imperfection in the manner indicated in Reference 13 (see also numerical examples in Section 3.5).
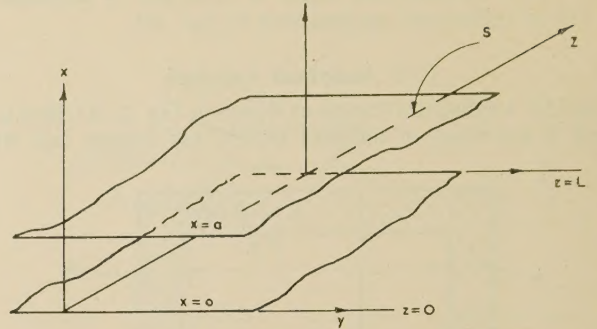


Fig. 6.—Parallel-plate resonator.

by a distance $a$; the field is assumed to be independent of the $y$ co-ordinate.

When the resonator is perfect, the field of an $E_0$-wave in it is derived from[13]

$$\left. \begin{aligned} E_z &= \sin h_0 x \cos \beta z \\ H_y &= -j\frac{k_0}{h_0} \cos h_0 x \cos \beta z \end{aligned} \right\} \quad \ldots \quad (19)$$

where the axial propagation coefficient, $\beta$, is given by

$$\beta = \frac{\pi}{L} \quad \ldots \ldots \ldots \quad (20)$$

the cut-off coefficient, $h$, is given by

$$h_0 = \frac{\pi}{a} \quad \ldots \ldots \quad (21)$$

and the wave number, $k_0$, from which the resonant frequency is derived, is given by

$$k_0^2 = h_0^2 + \beta^2 \quad \ldots \ldots \quad (22)$$

Let us replace the perfectly conducting surface S, at $x = a$, by a sheet of surface impedance, $Z_s$, which is isotropic and given by

$$Z_s = \nu \mathrm{f}(z) = \nu \sum_{r=0}^{\infty} (C_r \cos p_r z + S_r \sin p_r z) \quad . \quad (23)$$

In this expression $C_r$, $S_r$ are amplitude coefficients, $\nu$ is the perturbation parameter (essentially small) and

$$p_r = 2\pi \frac{r}{L} \quad \ldots \ldots \ldots \quad (24)$$

The boundary condition to be satisfied at $x = a$ is evidently[13]

$$Z_s = -\frac{E_z}{H_y}\bigg|_{x=a} \quad \ldots \ldots \quad (25)$$

Where $E_z$ and $H_y$ are now given by

$$E_z = \sin hx \cos \beta z + \nu \sum_u c_u^{(1)} \sin h_v x \cos \beta_u z$$
$$+ \nu^2 \sum_u c_u^{(2)} \sin h_v x \cos \beta_u z + \ldots \quad (26)$$

$$jH_y = \frac{k}{h} \cos hx \cos \beta z + \nu \sum_u c_u^{(1)} \frac{k}{h_v} \cos h_v x \cos \beta_u z$$
$$+ \nu^2 \sum_u c_u^{(2)} \frac{k}{h_v} \cos h_v x \cos \beta_u z + \ldots$$

In these equations the term $m = 1$ is excluded from the summations and the propagation coefficients are

$$h = h_0 + \delta h = h_0 + \nu h^{(1)} + \nu^2 h^{(2)} + \ldots \quad . \quad (27)$$

$$k = k_0 + \delta k = k_0 + \nu k^{(1)} + \nu^2 k^{(2)} + \ldots$$

and

$$k^2 = h^2 + \beta^2 = h_v^2 + \beta_u^2 \quad . \quad . \quad . \quad . \quad (28)$$

Eqns. (26) and (23) are now substituted in eqn. (25) and $\sin ha$ is expanded in the Taylor's series about the point $h_0 a$. Subsequently the terms in the first power of $\nu$ are extracted, resulting in an equation which, when multiplied through by $\cos \beta_1 z$ and integrated over the period $L$, leads to

$$\delta h = j \frac{1}{a} \frac{k_0}{h_0} \left( B_0 + \frac{B_1}{2} \right) \quad . \quad . \quad . \quad . \quad (29)$$

where

$$\left. \begin{aligned} B_0 &= \nu C_0 = \text{Average value of the surface impedance} \\ B_l &= \nu C_l = \text{Amplitude of the } l\text{th harmonic of the} \\ &\qquad \text{surface impedance function} \end{aligned} \right\} \quad (30)$$

For a cavity whose walls are homogeneous and isotropic the quantity $\delta h$ is given by[13]

$$\delta h = j \frac{1}{a} \frac{k_0}{h_0} Z_s \quad . \quad . \quad . \quad . \quad (29a)$$

Comparing this with eqn. (29) it is seen that, to the first order of quantities, a heterogeneous cavity behaves as if it had a uniform surface impedance, given by

$$Z_e = B_0 + \frac{B_1}{2} \quad . \quad . \quad . \quad . \quad (31)$$

Thus, so far as the performance of the cavity is concerned, the steady term and the first-harmonic components are the only two that matter. The only manifestation of the heterogeneous nature of the surface is the presence of the $B_1/2$ term in the expression for the equivalent homogeneous surface impedance $Z_e$.

Using a similar method it can be shown that the coefficients $c_l$ are given by

$$c_l = \frac{j}{2} \frac{1}{\sin h_v a} [C_{(l-1)/2} + C_{(l+1)/2}], \quad (l = 3, 5, 7, \ldots) \quad (32)$$

Thus to the first order of approximation, the $E_{0,n,1}$-mode becomes contaminated by a denumerable infinity of $E_{0,v,l}$-modes, where $l$ is odd.

### (3.3) Plane H-modes

Since the method of approach for cavities excited in $H_0$-modes is similar to that for E-modes, the details of analysis will be omitted.

It can be shown that the quantity $\delta h$ is given by

$$\delta h \simeq [\nu h^{(1)}] = j \frac{1}{a} \frac{h_0}{k_0} Z_e \quad . \quad . \quad . \quad . \quad (33)$$

where

$$Z_e = B_0 - \frac{B_1}{2} \quad . \quad . \quad . \quad . \quad (34)$$

Further, the $H_{0,n,1}$-mode becomes contaminated by a denumerable infinity of $H_{0,v,l}$-modes, where $l$ is an odd number. The coupling coefficients are

$$s_l^{(1)} = \frac{j}{2k_0} \frac{h_v}{\sin h_v a} [C_{(l-1)/2} - C_{(l+1)/2}] \quad \text{(where } l = 3, 5, 7 \ldots) \quad (35)$$

### (3.4) Application to Circular Cylindrical Resonators

If, in Sections 3.2 and 3.3, the surface impedance, $Z_s$, is anisotropic it is easy to see that, as far as the performance of E-waves is concerned, it is the $Z_z$ component that should be used

and the circumferential component, $Z_\phi$, neglected. The roles of $Z_z$ and $Z_\phi$ components are, however, interchanged so far as the propagation of $H_0$-waves is concerned (cf. reference 13).

Imagine a circular cylindrical resonator whose curved surface is anisotropic and axially heterogeneous. Here, to the first order of quantities, the effective anisotropic components are*

$$\left. \begin{aligned} Z_z &= B_0^{(z)} + \frac{B_1^{(z)}}{2} \\ Z_\phi &= B_0^{(\phi)} - \frac{B_1^{(\phi)}}{2} \end{aligned} \right\} \quad . \quad . \quad . \quad . \quad (36)$$

For $E_{m,n,l}$- and $H_{m,n,l}$-modes these quantities will become

$$\left. \begin{aligned} Z_z &= R_z + jX_z = B_0^{(z)} + \frac{B_l^{(z)}}{2} \\ Z_\phi &= R_\phi + jX_\phi = B_0^{(\phi)} - \frac{B_l^{(\phi)}}{2} \end{aligned} \right\} \quad (l \neq 0) \quad . \quad . \quad (37)$$

$$Z_z = B_0^{(z)} \qquad (l = 0) \quad . \quad . \quad (38)$$

These formulae can now be used in the expressions for the Q-factor of a cavity.[13] Thus, for $E_{m,n,l}$-modes,

$$\frac{1}{2Q} = \frac{1}{k_0} \left( \frac{R_z}{s} + \frac{2}{L} R_1 \right) \quad (l \neq 0) \quad . \quad . \quad (39)$$

and

$$\frac{1}{2Q} = \frac{1}{k_0} \left\{ \frac{\mathscr{R}[B_0^{(z)}]}{s} + \frac{R_1}{L} \right\} \quad (l = 0) \quad . \quad . \quad (40)$$

while, for $H_{m,n,l}$-modes,

$$\frac{1}{2Q} = \frac{1}{k} \left\{ \frac{1}{s} \left( \frac{h_0}{k} \right)^2 \left[ R_\phi + R_z \left( \frac{\beta_0}{h_0} \right)^2 \left( \frac{m}{h_0 s} \right)^2 \right] \right.$$

$$\left. \times \left[ 1 - \left( \frac{m}{h_0 s} \right)^2 \right]^{-1} + \left( \frac{\beta_0}{k_0} \right)^2 \frac{2}{L} R_1 \right\} \quad (41)$$

where $Z_1 = R_1 + jX_1$ denotes the surface impedance of the resonator end-plates.

The quantity $\Delta_1$ [see eqn. (17)] which gives the fractional real shift of the resonant frequency, is given for E- and H-waves by eqns. (39) or (40) and (41), respectively, but with the imaginary parts of the component impedances instead of the real parts.

### (3.5) Numerical Examples

Numerous examples of practical significance could be cited, but to illustrate the method, two distinct examples will be considered.

(3.5.1) An Isotropic Heterogeneous Cavity.

As a numerical example, consider a cylindrical cavity made up of two pieces as shown in Fig. 2.

Suppose that the length of the cavity is $0 \cdot 45$ cm and its diameter $0 \cdot 6$ cm. Let part A be made of copper ($\sigma_a = 5 \cdot 8 \times 10^7$ mhos/m) and part B be made of brass ($\sigma_b = \sigma_a/4 \cdot 4$); the length of the copper part is $0 \cdot 15$ cm ($= a$).

Had the cavity been perfect its resonant frequency, when excited in the $H_{11}$-mode, would have been $44 \cdot 4$ Gc/s.

The imperfect cavity has surface impedances $Z_A = (1 + j) 1 \cdot 44 \times 10^{-4}$ and $Z_B = (1 + j) 3 \cdot 10 \times 10^{-4}$.

Using eqns. (6) and (36) we find that $Z_z = 2 \cdot 71 \times 10^{-4}$, $Z_\phi = 2 \cdot 28 \times 10^{-4}$. Inserting these values in eqn. (41) we get

$$Q_{AB} = 3\,730$$

---

* The bracketed superscripts $(z)$ and $(\phi)$ have been used to differentiate between the anisotropic components.

Had the cavity been made of pure copper or brass throughout, the Q-factors would have been, respectively,

$$Q_A = 6\,050$$
$$Q_B = 2\,890$$

The resonant frequency of the cavity is, in all cases, lower than that for a perfect cavity by

$$\Delta_{AB} = 6\cdot0\,\text{Mc/s}$$
$$\Delta_A = 3\cdot7\,\text{Mc/s}$$
$$\Delta_B = 7\cdot7\,\text{Mc/s}$$

respectively.

### (3.5.2) An Anisotropic Heterogeneous Cavity.

Consider a cavity as illustrated in Fig. 3 with $L = 4\cdot2\,\text{cm}$ and $s = 3\cdot5\,\text{cm}$. Suppose that the cavity has been assembled in an imperfect manner by leaving small circumferential gaps between the end-plates and the body of the cavity, and that subsequent measurements have shown that the gaps are approximately rectangular with a width, $t$, of $0\cdot002\,5\,\text{cm}$ and a depth, $l$, of $0\cdot05\,\text{cm}$. It is required to investigate the performance of the cavity close to the resonant frequency of the $H_{011}$-mode.

A perfect cavity of the above measurements has a resonant frequency of $6\,340\,\text{Mc/s}$ in the $H_{01}$-mode, and this is degenerate with the $E_{11}$-mode. A cavity of the above measurements made of solid copper without the gaps would have two distinct resonant frequencies, one due to the $H_{01}$-mode and the other due to the $E_{11}$-mode. The respective resonant frequencies would be less than $6\,340\,\text{Mc/s}$ by

$$\Delta_H = 89\,\text{kc/s}$$
$$\Delta_E = 198\,\text{kc/s}$$

having Q-factors, respectively,

$$Q_H = 35\,500$$
$$Q_E = 15\,900$$

When the cavity is assembled in an imperfect manner as shown in Fig. 3, the impedance of the slots so formed is, for the two polarizations, given by eqns. (7) and (8), and with the numerical values given above we have $Z_E = (2\cdot4 + j67\cdot0) \times 10^{-3}$ and $Z_H = (0\cdot348 + j10\cdot6) \times 10^{-4}$. Consequently, using eqns. (9) and (36) we find that $Z_\phi = 0\cdot544 \times 10^{-4}(1 + j)$, $Z_z = (0\cdot596 + j2\cdot15) \times 10^{-4}$.

In other words, as a result of imperfect assembly, the effective value of $Z_\phi$ has remained unchanged but $Z_z$ has increased by $5\cdot22 \times 10^{-6} + j1\cdot61 \times 10^{-4}$. Thus $Q_H$ as well as the resonant frequency of the $H_{01}$-mode remains unchanged, but $Q_E$ and the resonant frequency of the $E_{11}$-wave suffer a noticeable change. The new values are as follows:

$$Q_E = 15\,100$$
$$\Delta_E = 439\,\text{kc/s}$$

so that now the cavity has two distinct resonant frequencies separated by $350\,\text{kc/s}$. The response of the cavity for the three cases, (a) a perfect cavity, (b) a copper cavity assembled without fault, and (c) a copper cavity assembled imperfectly, are illustrated in Fig. 7.

### (4) HIGHER-ORDER EFFECTS

If the analysis of Section 3 is continued with the retention of terms of the second order in $\nu$, the effective surface impedances for E- and H-modes are found to be

$$Z_e = B_0 + \frac{B_1}{2} + j\frac{ah_0}{4} \sum_u \frac{\cot h_v a}{h_v}[B_{(u-1)/2} + B_{(u+1)/2}]^2 \quad (42)$$
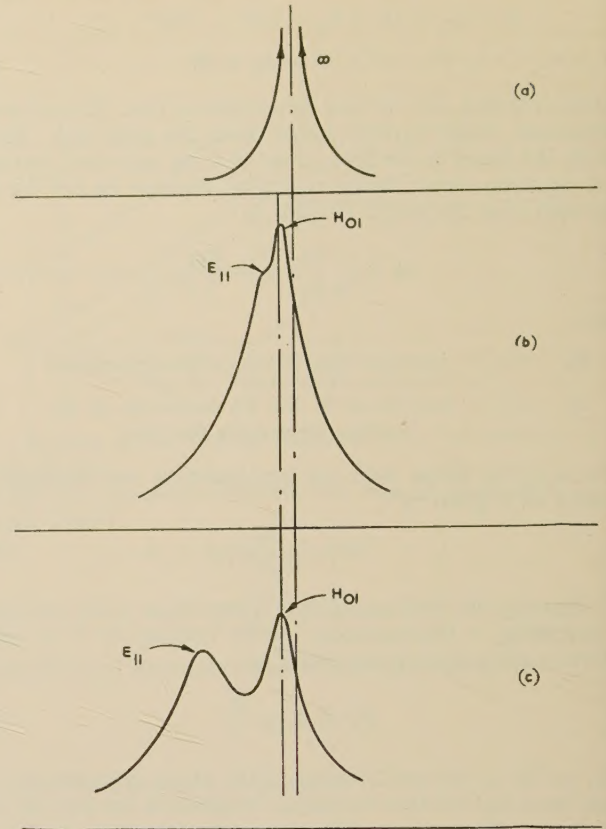$$(u = 3, 5, 7, \ldots)$$

for E-waves and



Fig. 7.—Response of a cavity with degenerate modes.

$$Z_e = \left(B_0 - \frac{B_1}{2}\right) + j\frac{1}{4k_0} \sum_u \frac{h_v}{\tan h_v a}[B_{(u-1)/2} - B_{(u+1)/2}]^2 \quad (43)$$

for H-waves.

If the coefficients, $B$, are sufficiently small, we observe from eqn. (42) or (43) that the expressions for $Z_e$ as given by eqn. (31) or (34) is sufficiently accurate, provided, of course, that $h_v a$ is not equal (or approximately equal) to a real multiple of $\pi$. Evidently, whenever $h_v a$ is equal (or approximately equal) to a multiple of $\pi$, eqn. (31) or (34) does not hold and eqn. (42) or (43) has to be used. However, these cases are rare, particularly since all higher values of $h_v$ are usually imaginary.

Referring to eqns. (32) and (35) we note that the case of $h_v a$ equal approximately to a real multiple of $\pi$ corresponds to one of the coupling coefficients being very large. The results can thus be summarized as follows:

For most practical cases, i.e. when none of the values of $h_v a$ are equal, or approximately equal, to a real multiple of $\pi$, the formulae derived in Section 3 are applicable, and here there is a small coupling between the wanted mode and a denumerable infinity of the $E_{0,v,r}$-modes or $H_{m,n,r}$-modes. In the few cases when one or more of the values of $h_v a$ are equal, or approximately equal, to a real multiple of $\pi$ there is, corresponding to each such value of $h_v a$, an $E_{0,v,r}$-mode that is coupled to an appreciable extent, and this brings about an appreciable change in the effective surface impedance, as given by eqn. (34). This surface impedance is calculable using eqn. (42) or (43).

### (5) ANALYSIS OF THE RIGHT CIRCULAR CYLINDRICAL CAVITY

#### (5.1) General

The results of the simple first-order analysis presented in Section 3 are, as shown, directly applicable to cavities of circular

cross-section. The surface-impedance approach therefore makes the complete solution of the field problem unnecessary, which has the great advantage that the relatively uninitiated can follow and apply the method with little effort. Unfortunately, in a few isolated cases the results obtained by the first-order theory are, as noted, inaccurate. Therefore, for successful application of the first-order analysis, it is necessary, at least, to be able to locate these cases. In general, these pitfalls can be noted easily, but to deal with them quantitatively we must resort to a more thorough analysis, and this is the purpose of the subsequent Sections.

A right circular cylindrical cavity, of length $L$, for which the $E_{m, n, l}$-mode has the following field components running parallel to the curved surface of the resonator[13] will be considered.

$$
\left.\begin{aligned}
E_z &= J_m(h_n r) \cos m\phi \cos \beta_l z \\
E_\phi &= \frac{\beta_l m}{h_n^2 r} J_m(h_n r) \sin m\phi \sin \beta_l z \\
H_\phi &= -j\frac{k_0}{h_n} J_m'(h_n r) \cos m\phi \cos \beta_l z
\end{aligned}\right\} \quad . \quad . \quad (44)
$$

The $H_{m,n,l}$-mode has the following components:

$$
\left.\begin{aligned}
H_z &= j J_m(h_n r) \sin m\phi \sin \beta_l z \\
E_\phi &= -\frac{k_0}{h_n} J_m'(h_n r) \sin m\phi \sin \beta_l z \\
H_\phi &= j\frac{\beta_l m}{h_n^2 r} J_m(h_n r) \cos m\phi \cos \beta_l z
\end{aligned}\right\} \quad . \quad . \quad (45)
$$

In every case the separation constants are, with a perfect waveguide, connected by

$$
k_0^2 = h_{n0}^2 + \beta_l^2 = h_v^2 + \beta_u^2 \quad . \quad . \quad . \quad (46)
$$

where $h_{n0}$ is the cut-off coefficient of a perfect waveguide and

$$
\beta_l = \frac{\pi l}{L} \quad . \quad . \quad . \quad . \quad (47)
$$

With an imperfect waveguide the boundary conditions to be satisfied on the curved surface are

$$
\left.\begin{aligned}
\frac{E_\phi}{H_z}\bigg|_S &= Z_\phi = \nu f_\phi(z) = \nu \sum_r \left[C_r^{(\phi)} \cos p_r z + S_r^{(\phi)} \sin p_r z\right] \\
\text{and} \\
-\frac{E_z}{H_\phi}\bigg|_S &= Z_z = \nu f_z(z) = \nu \sum_r \left[C_r^{(z)} \cos p_r z + S_r^{(z)} \sin p_r z\right]
\end{aligned}\right\} \quad . \quad (48)
$$

Here the separation constants are connected by

$$
k^2 = h_n^2 + \beta_l^2 = h_v^2 + \beta_u^2 \quad . \quad . \quad . \quad (49)
$$

where

$$
h_n = h_{n0} + \delta h = h_{n0} + \nu h^{(2)} + \nu^2 h^{(2)} + \ldots \quad . \quad (50)
$$

and $k$ is the wave number, from which the resonant frequency of the cavity may be calculated, as explained in Section 2.3.

### (5.2) Axially Heterogeneous Cavity

#### (5.2.1) E-modes.

In the case of an $E_{m,n,l}$-mode—originally a pure mode in a perfect cavity with field components given by eqn. (44)—the perturbed field will contain, as a rule, a denumerable infinity of H- as well as E-modes. Consequently the relevant field components inside a heterogeneous resonator excited in the $E_{m,n,l}$-mode will be

$$
\left.\begin{aligned}
E_z &= J_m(h_n r) \cos m\phi \cos \beta_l z \\
&\quad + \nu \sum_u c_u J_m(h_v r) \cos m\phi \cos \beta_u z + \ldots \\
E_\phi &= \frac{\beta_l m}{h_n^2 r} J_m(h_n r) \sin m\phi \sin \beta_l z \\
&\quad + \nu \sum_u c_u \frac{\beta_u m}{h_v^2 r} J_m(h_v r) \sin m\phi \sin \beta_u z + \ldots \\
&\quad - \nu \sum_u s_u \frac{k_0}{h_v} J_m'(h_v r) \sin m\phi \sin \beta_u z + \ldots
\end{aligned}\right\} \quad . \quad (51)
$$

$$
\left.\begin{aligned}
H_\phi &= -j\frac{k_0}{h_n} J_m'(h_n r) \cos m\phi \cos \beta_l z \\
&\quad - jv \sum_u c_u \frac{k_0}{h_v} J_m'(h_v r) \cos m\phi \cos \beta_u z + \ldots \\
&\quad + jv \sum_u s_u \frac{\beta_u m}{h_u^2 r} J_m(h_v r) \cos m\phi \cos \beta_u z \\
H_z &= jv \sum_u s_u J_m(h_v r) \sin m\phi \sin \beta_u z
\end{aligned}\right\} \quad . \quad (52)
$$

Substitution of eqns. (51) and (52) into the boundary condition [eqn. (48)] leads to a set of simultaneous equations which can be solved in the manner somewhat similar to that explained in Section 3. For the first-order solution we get

$$
Z_e = B_0^{(z)} + \frac{B_l^{(z)}}{2} = Z_z \quad . \quad . \quad . \quad (53)
$$

which, of course, is in confirmation of the first-order analysis [see eqn. (36)].

The $E_{m,n,l}$-mode is coupled to the $H_{m,v,l}$-mode and the $H_{m,n,l}$-mode coupling coefficient, $s_l$, is given by

$$
\nu s_l = j\frac{\beta_l m}{h_n^2 s} Z_e \quad . \quad . \quad . \quad . \quad (54)
$$

The $E_{m,n,l}$-mode is also coupled to a denumerable infinity of other E- and H-modes, and the coupling coefficients are given by

$$
c_u = \frac{j}{2} \frac{J_m'(h_n s)}{J_m(h_v s)}\left[C_{(u-l)/2}^{(z)} + C_{(u+l)/2}^{(z)}\right] \quad . \quad . \quad (55)
$$

$$
s_u = \frac{j}{2s} \frac{\beta_l m}{h_v k_0} \frac{J_m'(h_n s)}{J_m'(h_v s)}\left[C_{(u-l)/2}^{(z)} + C_{(u+l)/2}^{(z)}\right] \quad . \quad (56)
$$

where $u$ is odd if $l$ is odd and even if $l$ is even. All other coupling coefficients are zero.

If the terms in $\nu^2$ are retained and we proceed with the analysis to that order of quantities, we arrive at the following expression for $\delta h$:

$$
\delta h \simeq \nu h^{(1)} + \nu^2 h^{(2)} = j\frac{1}{s} \frac{k_0}{h_n}\left[\nu C_0^{(z)} + \nu \frac{C_l^{(z)}}{2}\right]
$$
$$
- \frac{1}{4s} \sum_n \left[\frac{k_0}{h_v} \frac{J_m'(h_v s)}{J_m(h_v s)} - \left(\frac{\beta_u m}{h_v s}\right)^2 \frac{1}{h_v s}\right] \times \left[\nu C_{(u-l)/2}^{(z)} + \nu C_{(u+l)/2}^{(z)}\right]^2
$$
$$
. \quad . \quad . \quad (57)
$$

It thus transpires that the simple first-order theory, as developed in Section 3, is adequate, unless one or more of the $h_v$ coefficients given by

$$
h_v = \sqrt{(k^2 - \beta_u^2)}, \quad (u \neq l) \quad . \quad . \quad . \quad (58)
$$

(where $u$ is odd if $l$ is odd and even if $l$ is even) is such that $h_v s$ is equal, or very nearly equal, to one of the roots of the $m$th-order Bessel function, including zero. One of the terms of the infinite summation of eqn. (57) then becomes signi-

ficant and must therefore be considered; further, the excited $E_{m,n,l}$-mode becomes tightly coupled [coupling coefficient is given by eqns. (55) or (56)] to one of the other modes unless the two Fourier coefficients, $C_{(u-l)/2}^{(z)}$ and $C_{(u+l)/2}^{(z)}$ are zero.

### (5.2.2) H-modes.

The case of H-modes is a little more complicated. Here, proceeding as with E-modes, we get, analogously to eqns. (51) and (52), infinite series expansions for each of the field components. These expansions, when subjected to the boundary conditions of eqn. (48), lead eventually to the following expression for the first-order value of $\delta h$:

$$vh^{(1)} = j\frac{1}{s}\frac{h_n}{k_0}\left[Z_\phi + Z_z\left(\frac{\beta_l}{h_n}\right)^2\left(\frac{m}{h_n s}\right)^2\right]\left[1 - \left(\frac{m}{h_n s}\right)^2\right]^{-1} . \quad (59)$$

where

$$\left.\begin{array}{l} Z_\phi = vC_0^{(\phi)} - \dfrac{vC_l^{(\phi)}}{2} \\[2mm] Z_z = vC_0^{(z)} + \dfrac{vC_l^{(z)}}{2} \end{array}\right\} \quad . \quad . \quad . \quad (60)$$

These equations are, of course, in confirmation of the first-order theory.

All coupling coefficients, $c_l$ and $s_l$, are determined as indicated in the last Section and are of the order of the surface impedance or higher, while the second-order perturbation term in $\delta h$ can be shown to be of the form

$$v^2h^{(2)} = -\frac{v^2}{4}\frac{h_n}{k_0}\left[\left(\frac{m}{h_n s}\right)^2 - 1\right]^{-1}\sum_u\left\{[C_{(u-l)/2}^{(\phi)} - C_{(u+l)/2}^{(\phi)}]\right.$$

$$\frac{J_m(h_v s)}{J'_m(h_v s)}N_u + \frac{\beta_l m}{h_n^2 s}[C_{(u-l)/2}^{(z)} + C_{(u+l)/2}^{(z)}]$$

$$\left.\left[\frac{\beta_u m}{h_n^2 s}\frac{J_m(h_v s)}{J'_m(h_v s)}N_u + \frac{k_0}{h_v}\frac{J'_m(h_v s)}{J_m(h_v s)}M_u\right]\right\} \quad . \quad . \quad . \quad (61)$$

Here again, $u$ is even when $l$ is even and odd when $l$ is odd, but $u \neq l$.

Thus, including second-order quantities, $\delta h$ is given by the sum of eqns. (59) and (61).

For a small value of surface impedance, we note that, with the exception of the singular points of eqn. (61), $\delta h$ is given to an adequate degree of accuracy by eqn. (59); in other words, the first-order solution is satisfactory provided that none of the $h_v s$ is a root of $J_m(h_v s) = 0$ or $J'_m(h_v s)$. In these exceptional cases there is a large coupling between the excited $H_{m,n,l}$-mode and some other mode (whose coupling coefficient becomes large), with a consequent appreciable change in the resonant conditions. In such cases $\delta h$ must be calculated from

$$\delta h = vh^{(1)} + v^2h^{(2)}$$

where $vh^{(1)}$ and $v^2h^{(2)}$ are, respectively, given by eqns. (59) and (61). But we observe further from eqn. (61) that, if to each such singular value $(h_v s)$ there is a zero value of coefficients $C_{(u-l)/2}$ and $C_{(u+l)/2}$, the first-order theory is still applicable.

### (5.3) Circumferentially Heterogeneous Cavity

When dealing with circumferentially heterogeneous cavities we must, in order not to lose generality, include in the expressions for the field components [eqns. (44) and (45)] the $\cos m\phi$ as well as the $\sin m\phi$ dependence. In other respects the analysis is analogous to that for axially heterogeneous cavity, and therefore details of the analysis will be omitted.

However, it must be stressed that the surface-impedance components $Z_\phi$ and $Z_z$ are now functions not of $z$ but of $\phi$,

and are periodic of period $2\pi$. In Section 5.3.1 and 5.3.2 we therefore take

$$\left.\begin{array}{l} Z_\phi = vf_\phi(\phi) = v\sum_q\left[C_q^{(\phi)}\cos q\phi + S_q^{(\phi)}\sin q\phi\right] \\[2mm] Z_z = vf_z(\phi) = v\sum_q\left[C_q^{(z)}\cos q\phi + S_q^{(z)}\sin q\phi\right] \end{array}\right\} \quad . \quad (62)$$

where $q$ takes all positive integral values.

### (5.3.1) E-modes.

It can be shown that, to the first order of quantities, the coupling coefficient, $\tau$, between* $_sE_{m,n,l}$ and $_cE_{m,n,l}$-modes is given by the solution of the quadratic

$$\tau^2 + \frac{2}{\tau^{(z)}}\tau - 1 = 0 \quad . \quad . \quad . \quad . \quad (63)$$

where

$$\tau^{(z)} = S_{2m}^{(z)}/C_{2m}^{(z)} \quad . \quad . \quad . \quad . \quad (64)$$

and

$$\tau = \frac{S_m}{C_m} \quad . \quad . \quad . \quad . \quad (65)$$

All the remaining coupling coefficients are of the order of the $Z_s$ quantity or smaller.

The two solutions for $\tau$,

$$\tau = -\frac{1}{\tau^{(z)}} + \begin{bmatrix} +1 \\ -1 \end{bmatrix}\sqrt{\left[\left(\frac{1}{\tau^{(z)}}\right)^2 + 1\right]} \quad . \quad . \quad (66)$$

can evidently be put into the form

$$\left.\begin{array}{l} \tau = \tan\left\{\frac{1}{2}\arctan\left[\tau^{(z)}\right]\right\} \\[2mm] = \tan\Phi = \tan\frac{1}{2}\Phi^{(z)} \end{array}\right\} \quad . \quad . \quad . \quad (67)$$

where

$$\Phi^{(z)} = \arctan\tau^{(z)} \quad . \quad . \quad . \quad . \quad (68)$$

Each value of $\tau$ is associated with a different value of $vh^{(1)}$ and therefore a different value of the propagation coefficient. Evidently the two values of $vh^{(1)}$ are given by

$$\delta h \simeq vh^{(1)} = -j\frac{v}{s}\left\{\left[C_0^{(z)} + \frac{C_{2m}^{(z)}}{2}\right] + \tau\frac{S_{2m}^{(z)}}{2}\right\} \quad . \quad (69)$$

We conclude, therefore, that all $E_{m,n,l}$-modes are unstable in waveguides whose surface impedance is circumferentially heterogeneous, unless $m = 0$. The above results have the obvious significance that a wave in a circular waveguide varies with the co-ordinate $\phi$ in the following manner:

$$c_m\cos m\phi + s_m\sin m\phi$$

If $s_m = 0$ we deal with an $_cE$-mode and if $c_m = 0$ we deal with an $_sE$-mode. In a perfect waveguide there is no connection between $c_m$ and $s_m$ coefficients, and $_cE$ and $_sE$ waves can be present in any proportion, as determined, for example, by the launching condition. In the present case, however, $c_m$ and $s_m$ must be combined in a definite proportion [given by eqn. (67)] which is determined solely by the magnitude of the $2m$th harmonic component of the surface impedance [eqn. (64)]. Clearly as a result of this phenomenon the cavity exhibits two resonance peaks, corresponding to the two values of $\delta h$ given by eqn. (69).

The expressions for the second-order approximations tend to be rather lengthy, and to save space it is not proposed to quote them; they contain singularities at points given by $J_q(h_n s) = 0$ and $J'_q(h_n s) = 0$.

### (5.3.2) H-modes.

To the first order of quantities the resonant conditions of H-modes are also given by the solution of a quadratic, as with

* $_sE$ denotes a mode whose $E_z$ component is proportional to $\sin m\phi$ and $_cE$ denotes one whose functional dependence is $\cos m\phi$.

E-modes, but the expressions are slightly more complicated. They are as follows:

$$\frac{k_0}{h_0}\left[\left(\frac{m}{h_0 s}\right)^2 - 1\right]s\begin{bmatrix}(\delta h)_1\\(\delta h)_2\end{bmatrix}$$

$$= -jC_0^{(e)} + \begin{bmatrix}+1\\-1\end{bmatrix}\left\{[C_{2m}^{(e)}]^2 - \left[\frac{S_{2m}^{(e)}}{2}\right]^2\right\}^{1/2} \quad . \quad (70)$$

$$\tau = \frac{s_m'}{c_m'} = \tan\left[\tfrac{1}{2}\arctan\tau^{(e)}\right] . \quad . \quad . \quad (71)$$

where

$$\tau^{(e)} = \frac{S_{2m}^{(e)}}{C_{2m}^{(e)}} \quad . \quad . \quad . \quad . \quad (72)$$

and

$$\left.\begin{aligned}C_{2m}^{(e)} &= t^2 C_{2m}^{(z)} - C_{2m}^{(\phi)}\\ S_{2m}^{(e)} &= t^2 S_{2m}^{(z)} - S_{2m}^{(\phi)}\\ C_0^{(e)} &= t^2 C_0^{(z)} + C_0^{(\phi)}\end{aligned}\right\} \quad . \quad . \quad . \quad (73)$$

where

$$t = \frac{\beta m}{h_n^2 s} . \quad . \quad . \quad . \quad . \quad (74)$$

The interpretation of these results is similar to those given in connection with E-waves in Section 5.3.1. In the first place, it will be observed, from eqn. (70), that there is always a unique solution for $H_0$-waves ($m = 0$). Secondly, if $m \neq 0$ the cavity has two distinct resonant frequencies calculable from eqn. (70), provided that the coefficients $C_{2m}$ and $S_{2m}$ are finite. In such cases $_cH$ and $_sH$-modes cannot exist separately in a pure form but must be combined in a definite proportion $\tau$, given by eqn. (71); this depends solely on the ratio $\tau^{(e)} = S_{2m}^{(e)}/C_{2m}^{(e)}$, which, of course, is independent of the absolute value of any coefficients of the series expansion even if they are extremely small. It must, however, be stressed that it is the presence of the $S_{2m}^{(e)}$ coefficient that is responsible for the tight coupling between the $_cH$- and $_sH$-modes, and if $S_{2m}^{(e)} = 0$, the cavity will support $_cH$- and $_sH$-modes, corresponding to two different resonant frequencies [eqn. (70)], which are not coupled together.

The second-order approximations possess singular points given by $J_q(h_n s) = 0$ and $J_q'(h_n s) = 0$, but the expressions are rather lengthy and will not be given.

## (6) DISCUSSION OF RESULTS

### (6.1) Collection of Formulae, their Discussion and Conclusions

As we have seen, the two anisotropic components ($Z_\phi$ and $Z_z$) of a heterogeneous cavity (length $L$) can be expressed in terms of their respective Fourier series by

$$\left.\begin{aligned}Z_z &= \nu f_z(z) = \nu\sum_r\left[C_r^{(z)}\cos p_r z + S_r^{(z)}\sin p_r z\right]\\ Z_\phi &= \nu f_\phi(z) = \nu\sum_r\left[C_r^{(\phi)}\cos p_r z + S_r^{(\phi)}\sin p_r z\right]\end{aligned}\right\} \quad . \quad (48)$$

where

$$p_r = \frac{2\pi r}{L}$$

for an axially heterogeneous cavity, and

$$\left.\begin{aligned}Z_z &= \nu f_z(\phi) = \nu\sum_q\left[C_q^{(z)}\cos q\phi + S_q^{(z)}\sin q\phi\right]\\ Z_\phi &= \nu f_\phi(\phi) = \nu\sum_q\left[C_q^{(\phi)}\cos q\phi + S_q^{(\phi)}\sin q\phi\right]\end{aligned}\right\} \quad . \quad (62)$$

$$(q = 0, 1, 2 \ldots)$$

for a circumferentially heterogeneous cavity.

An axially heterogeneous cavity, when excited in any of the $H_{m,n,l}$- or $E_{m,n,l}$-modes, behaves as if it were homogeneous and had a surface impedance given by

$$\left.\begin{aligned}Z_z &= \nu C_0^{(z)} + \tfrac{1}{2}\nu C_l^{(z)}\\ Z_\phi &= \nu C_0^{(\phi)} - \tfrac{1}{2}\nu C_l^{(\phi)}\end{aligned}\right\}(l \neq 0) \quad . \quad . \quad . \quad (60)$$

and

$$Z_z = \nu C_0^{(z)} \quad\quad (l = 0) \quad . \quad . \quad . \quad (60a)$$

There is always a small coupling to a denumerable infinity of other modes, but in practice this may be neglected, since the coupling coefficients are small (of the order of $Z_z$ or smaller).

There is, however, an exception to the above rule. If there are one or more values of $h_v$ such that $h_v s$ is (or is close to) a root of the $m$th-order Bessel function or its derivative, then at each such point there is a tight coupling between the excited mode and the mode to which $h_v$ belongs. Eqns. (60) are not then applicable, and to evaluate the resonant conditions eqns. (57) or (61) must be used.

For example, if a cavity whose length was $1 \cdot 26$ times its radius were excited in the $E_{020}$-mode, there would be a tight coupling between this mode and the $E_{012}$-mode, and, of course, the simple first-order theory could not account for the behaviour of the cavity; in order to evaluate the resonant frequency and the Q-factor, eqn. (57) would have to be used.

For a circumferentially heterogeneous cavity it has been established that, with the exception of $E_0$- and $H_0$-modes, all modes are unstable. With $E_0$- and $H_0$-modes the heterogeneity is of no consequence; it is the mean value of the surface impedance that determines the behaviour of the cavity [$C_0^{(z)}$ in the case of $E_0$-waves and $C_0^{(\phi)}$ in the case of $H_0$-waves]. However, as a result of their instability, all higher-order modes exhibit two distinct resonant frequencies corresponding to two different coupling coefficients between the $_cH_m$- and $_sH_m$- or $_cE_m$- and $_sE_m$-waves, as the case may be. This coupling coefficient depends solely on the relative magnitudes of the $S_{2m}$ and $C_{2m}$ coefficients of the surface-impedance function, and in the absence of these coefficients, the cavity behaves as if it were homogeneous of surface impedance equal to the mean value of the surface-impedance function ($C_0$-coefficient).

So far as the effect of circumferential heterogeneity is concerned the higher-order approximations, though calculable, need not be considered. This follows from examination of the results obtained in Section 5.3. Thus, with E-waves, we observe that the case $q = m$ is excluded from the infinite summations; but ($h_n s$) is a root of the $m$th-order Bessel function, and this cannot simultaneously be a root of the $q$th-order Bessel function or its derivative.

These properties can best be understood with the help of the mode chart[15] shown in Fig. 8. It will be seen that the mode lines are parallel whenever the modes concerned have the same axial index; otherwise they intersect, and the points of intersection are the singular points referred to above.

Thus, with axial heterogeneity, the summations occurring in eqns. (57) and (61) extend over the axial index, and consequently the singular points of these equations are given as the intersections of the mode line belonging to the investigated mode with the mode lines of modes whose axial index differs from the investigated mode by multiples of 2.

However, with circumferential heterogeneity the summations occurring in the second-order equations extend over the circumferential index while the axial index is held constant, and under such conditions all mode lines, as mentioned above, are parallel and consequently there are no singular points.

The question of degenerate modes must be investigated. Two mode lines then coincide, and there might appear to be a pitfall. But the degenerate modes are the $H_{0n}$- and $E_{1n}$-modes. The inspection of eqns. (57) and (61) reveals, however, that the
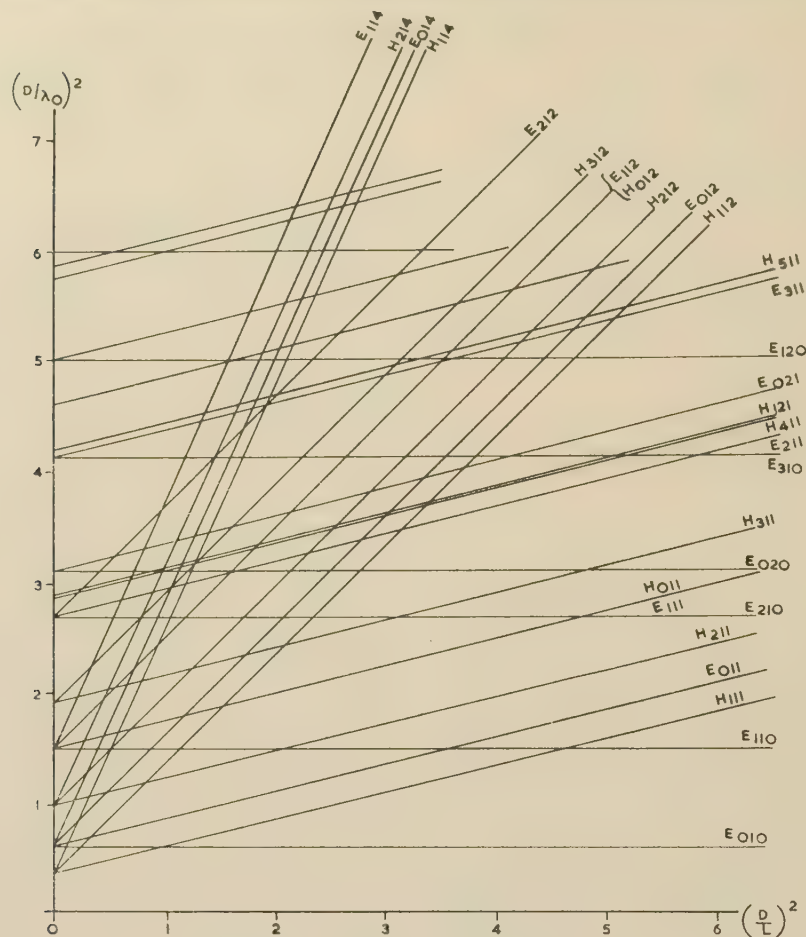
Fig. 8.—Mode chart for a right circular cavity.

axial heterogeneity does not bring a coupling between them. Similarly it can be shown that the circumferential heterogeneity can never be responsible for the coupling between these modes.

### (6.3) The Surface Impedance of a Periodic Surface

With homogeneous and isotropic surfaces a knowledge of the surface impedance is all that is required (apart from the dimensions of the cavities) for the determination of the resonant frequency of the cavity and its Q-factor.

With homogeneous and anisotropic surfaces it is not possible to predict the behaviour of a cavity unless the orientation of the surface with respect to the cavity co-ordinates is specified.

In an analogous manner, with heterogeneous surfaces it is, in general, not possible to predict the behaviour of a cavity unless it is specified which particular fragment of the surface is used as the wall of the cavity. This will be immediately obvious from the following consideration.

Imagine an impedance sheet whose surface-impedance function, $f(z)$, is expandable in a Fourier series. If this impedance sheet is employed as the curved surface of a resonator of length $l$, then, unless the length of the cavity is commensurable with the period of the surface impedance function, the mean value of $f(z)$ over the period $l$ ($C_0$-coefficient) will depend on the choice of the origin; similar remarks apply to the $C_l$-coefficient. It therefore transpires that the effect of the impedance sheet on the performance of a cavity depends (among other factors) on which particular fragment of the surface is chosen, and hence the name 'heterogeneous surface impedance' is used.
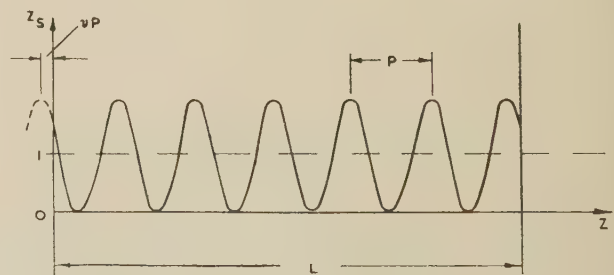


Fig. 9.—Fragment of a periodic surface in relation to the co-ordinate system.

Suppose that a certain impedance sheet with surface-impedance function $\cos(2\pi/p)z$ is used as the curved surface of a resonator, of length $l$. Evidently, we may expand this function in a Fourier series, which, with the co-ordinate system shown in Fig. 9, reads

$$Z_s = \nu f(z) = \nu\left[1 + \cos 2\pi\left(\frac{z}{P} + V\right)\right] = \sum_r (C_r \cos p_r z + S_r \sin p_r z)$$

where

$$p_r = \frac{2\pi r}{L} \quad . \quad . \quad . \quad . \quad . \quad (75)$$

Suppose the excited mode is an $E_{m,n,l}$-mode: the effective surface impedance is given by eqn. (60) as follows:

$$Z_z = \nu C_0 + \tfrac{1}{2}\nu C_l \quad . \quad . \quad . \quad . \quad (76)$$

where

$$C_0 = 1 + \frac{P}{\pi L} \sin \pi \frac{L}{P} \sin \pi \left( \frac{L}{P} + 2V \right)$$

$$C_l = \frac{1}{2\pi P} \cos \pi \left( \frac{L}{P} + 2V \right) \sin \pi \frac{L}{P} \frac{2}{\left[ \left( \frac{L}{P} \right)^2 - l^2 \right]}$$

$$\left. \right\} \quad . \quad (77)$$

hence the effective surface impedance is given by the substitution of eqn. (77) into (76).

It will be observed that if $L$ and $P$ are commensurable,

$$C_0 = 1$$
$$C_l = 0 \qquad \text{(if } L/P \neq l \text{)}$$
$$C_l = \cos 2\pi V \qquad \text{(if } L/P = l \text{)}$$

so that, even in this case, the effective surface impedance is a function of $V$ (provided that $L/P = l$). In other words, the surface impedance depends on the origin chosen, i.e. the particular fragment of the surface.

The effective surface impedance, given by eqn. (76), with the values of $C_0$ and $C_l$ given by eqn. (77), is plotted in Figs. 10(a)
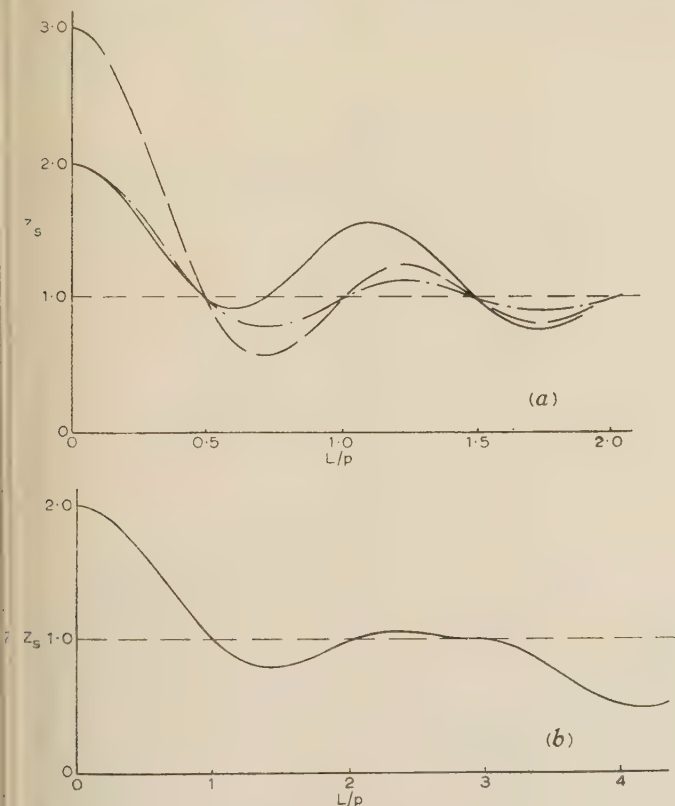


Fig. 10.—$Z_s$ as a function of $L/p$.

(a) ———————   $Z_s$ function ($L = 1$).
    — — — —   $2(\sin x)/x$.
    – – – – –   $(\sin x)/x$.
(b) For $l = 2$.

and 10(b) as a function of $L/P$ for $l = 1$ and $l = 2$, respectively. It will be observed that, if $L/P$ is commensurable and greater than $l$, the effective surface impedance acquires a unique value $v$. In all other cases there is no unique value that could be ascribed to a heterogeneous surface unless $L/Pl \to \infty$: evidently, for large values of $L/Pl$, the effective surface impedance tends to the mean value of the surface-impedance function, and then the surface loses its heterogeneous nature and may be regarded as homogeneous of surface impedance equal to the mean value of the surface-impedance function.

It transpires from eqns. (77) that, if $L/P = 10$, the fluctuation of the effective surface impedance about the mean of the surface-impedance function amounts to only about 3%.

It may therefore be concluded that, in general, if the period of a surface is small in comparison with the wavelength in the resonator (say, a factor of 10 or more), such a surface may be regarded as homogeneous of surface impedance equal to the mean surface-impedance function; otherwise it must be regarded as heterogeneous, and its effective surface impedance will be a function of the particular geometrical relation of the resonator to the surface. For example, if we attempted to calculate the surface impedance of a heterogeneous resonator from its conditions of resonance, for slightly different resonator lengths, then, as a result of the above phenomenon, the experimental points would appear to have a large scatter, which would increase with the decrease of the ratio $L/Pl$, while, for large values of $L/Pl$ there would be no noticeable scatter of experimental points (in qualitative agreement with Fig. 10). There is experimental evidence[16] in support of the theory, although at the time the authors explained this scatter of experimental points by a different argument.

### (7) ACKNOWLEDGMENTS

### (8) REFERENCES

(1) STRUTT, J. W.: 'The Theory of Sound' (Macmillan, 1888).
(2) BATEMAN, H.: 'Electrical and Optical Wave Motion' (Cambridge University Press, 1915).
(3) HANSON, W. W.: *Journal of Applied Physics*, 1938, **9**, p. 654.
(4) BORGNIS, F.: 'Electromagnetische Eigenschwingungen Dielectrischer Raume', *Annalen der Physik*, 1939, **35**, p. 359.
(5) MÜLLER, J.: 'Untersuchung über Electromagnetische Hohlraüme', *Hochfrequenztechnik und Electroakustik*, 1939, **54**, p. 157.
(6) WILSON, I. G., SCHRAMM, C. W., and KINZER, J. P.: 'High Q Resonant Cavities for Microwave Testing', *Bell System Technical Journal*, 1946, **25**, p. 408.
(7) BETHE, H. A.: 'Theory of Diffraction by Small Holes', *Physical Review*, 1944, **66**, p. 163.
(8) CONDON, E. U.: 'Forced Oscillations in Cavity Resonators', *Journal of Applied Physics*, 1941, **12**, p. 129.
(9) BLEANEY, B., LOUBSER, J. H. N., and PENROSE, R. P.: 'Cavity Resonators for Measurement with Centimetre Electromagnetic Waves', *Proceedings of the Physical Society*, 1947, **59**, p. 185.
(10) BRENIER, J.: 'Sur les cavities electromagnetiques', *L'Onde Electrique*, 1946, **26**, p. 305.
(11) ESSEN, L.: 'The Design, Calibration and Performance of Resonance Wavemeters for Frequencies between 1 000 and 25 000 Mc/s', *Journal I.E.E.*, 1946, **93**, Part IIIA, p. 1413.
(12) COMTE, G., and PARIS, J. M.: 'Experimental Study of Circular Waveguides using the TE$_{01}$ Mode in the Vicinity of 25 000 Mc/s', *Câbles et Transmission*, 1954, **8**, p. 311.
(13) KARBOWIAK, A. E.: 'Theory of Imperfect Waveguides; the Effect of Wall Impedance', *Proceedings I.E.E.*, Paper No. 1841 R, September, 1955 (**102** B, p. 698).
(14) KARBOWIAK, A. E.: 'Microwave Propagation in Anisotropic Waveguides', *Proceedings I.E.E.*, Monograph No. 147 R, August, 1955 (**103** C, p. 139).

(15) MONTGOMERY, C. G.: 'Technique of Microwave Measurements' (McGraw-Hill, Radiation Laboratory Series No. 11), p. 298.
(16) BARLOW, H. E. M., and KARBOWIAK, A. E.: 'An Experimental Investigation of the Properties of Corrugated Cylindrical Surface Waveguides', *Proceedings I.E.E.*, Paper No. 1625 R, May, 1954 (**101**, Part III, p. 182).

## (9) APPENDICES

### (9.1) Impedance of a Slot in a Metal Surface

#### (9.1.1) E-vector normal to the Edges of the Slot.

For a sufficiently narrow slot the wave inside it will be principally in the TEM-mode, and for a slot whose depth, $l$, is small in comparison with the wavelength the input impedance, $Z_{sl}$, in the absence of losses, is given by

$$Z_0 Z_{sl} \simeq j k_0 l Z_0 \quad . \quad . \quad . \quad . \quad (78)$$

while for an imperfect slot it is

$$Z_0 Z_{sl} = j h l Z_0' \quad . \quad . \quad . \quad . \quad . \quad (79)$$

where

$$h = k_0 + \delta h \quad . \quad . \quad . \quad . \quad . \quad (80)$$

$$Z_0' = Z_0 + \delta Z$$

But $Z_0'$, the characteristic impedance in the slot, is given by

$$Z_0' = \frac{k}{h} Z_0 \quad . \quad . \quad . \quad . \quad . \quad (81)$$

Using the surface impedance approach $\delta h$ can be shown to be given by

$$j \delta h = \frac{1}{t} Z_m = \frac{1}{t}(R_m + j X_m) \quad . \quad . \quad . \quad . \quad (82)$$

where $Z_m$ is the surface impedance of the metal of which the slot is made and $t$ is the width of the slot.

With these substitutions eqn. (79) yields

$$Z_{sl} = j k_0 l + 2 R_m \frac{l}{t} \quad . \quad . \quad . \quad . \quad (83)$$

However, to allow for the loss in the bottom of the slot, we must add $R_m$ to the above, so that we finally obtain

$$Z_{sl} = Z_E = R_m \left( 2\frac{l}{t} + 1 \right) + j 2\pi \frac{l}{\lambda_0} \quad . \quad . \quad (84)$$

#### (9.1.2) E-vector parallel to the Edges of the Slot.

For a sufficiently narrow slot the wave inside it will be principally in the $H_{01X}$ mode, the evanescent direction being the depth of the slot. Since we have assumed that the depth of the slot is much larger than its width, its input impedance will be equal to that of a waveguide below cut-off, which, in turn, is equal to the characteristic impedance of the waveguide. If $\gamma$ is the propagation coefficient in the evanescent direction then evidently

$$Z_{sl} = j \frac{k_0}{\gamma} \quad . \quad . \quad . \quad . \quad . \quad (85)$$

since $\gamma = \alpha + j\beta$ and here $\alpha \gg \beta$.

Therefore

$$Z_{sl} = j \frac{k_0}{\alpha} + \frac{k_0 \beta}{\alpha^2} \quad . \quad . \quad . \quad . \quad (86)$$

and substituting for $\alpha$ and $\beta$, we get

$$Z_{sl} = Z_H = j \frac{2t}{\lambda_0} + \frac{2}{\pi} R_m \quad . \quad . \quad . \quad (87)$$

# THE APPROXIMATE CALCULATION OF THE ELECTRIC FIELD BETWEEN A ROD AND A CONCENTRIC RING BY MEANS OF TOROIDAL FUNCTIONS

## By Professor G. W. CARTER, M.A., Member, and S. C. LOH, B.Sc., Student.

### SUMMARY

The electric field set up when a live conductor in the form of a rod passes through the centre of an earthed ring of circular section is approximately calculated by replacing the rod by an hour-glass-shaped conductor of the same minimum radius. The resulting field is found in terms of toroidal functions, numerical Tables of which are given. To find how closely the calculated results approach the true values for a rod and ring, a systematic electrolytic-tank study is undertaken, and charts of the differences between theory and experiment are given. It is found that the theoretical attack is successful in predicting the smallest figure to which the voltage gradient on the electrodes can be reduced, but that the conductor radii which will enable that figure to be realized are somewhat different in practice from those suggested by the theory.



Fig. 2.—Equivalent system with toroidal electrodes.

### (1) INTRODUCTION

The electric field between electrodes comprising a rod and a concentric ring of circular section (Fig. 1) is not exactly calculable by any known method, but it has an application in the design of
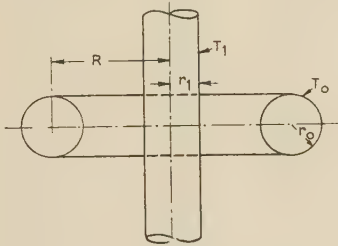


Fig. 1.—Rod-and-ring electrode system.

bushings, which may be regarded as practical embodiments of this ideal arrangement. The problem is discussed by Schwaiger[1] in terms of experimentally determined breakdown voltages, mostly obtained by measuring the sparkover voltage between a pair of crossed rods. On the theoretical side the allied problem of a wire passed through a circular hole in a plate was attacked by Bolliger[2] by a method which would furnish an approximate solution to the problem under discussion, namely by regarding the electrodes as two members of the system of hyperboloids formed by rotating a set of confocal hyperbolas about their conjugate axis.

The theoretical part of the paper also proceeds by attacking an allied problem—that of the field between electrodes which are tores of the system formed when a set of coaxial circles is rotated about its radical axis (Fig. 2). Thus the ring electrode $T_0$ is correctly represented, but the rod $T_1$ is replaced by an hour-glass-shaped solid, $T_1'$, having the same radius on the central plane. The toroidal functions necessary for the solution of this problem were first discussed by Neumann[3] and were fully investigated by Hicks;[4,5] but the authors have been able to trace only one
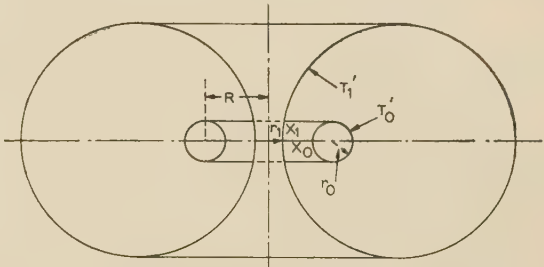
numerical Table of these functions, namely that published by Fouquet[6] in 1937. Since Fouquet's Table does not cover a sufficient range for the present purpose, an extended Table has been computed and included in the paper. The values have been used to calculate the potential gradients on the electrodes at the points of nearest approach. The question of the error introduced in replacing the rod by an hour-glass is investigated with the aid of an electrolytic tank, and conclusions are drawn about the most efficient radii for the conductors.

### (2) TOROIDAL FUNCTIONS

It is unnecessary to give more than a brief outline of the theory of toroidal functions, since the details are given in Hicks's papers.

If the cylindrical polar co-ordinates of a point are $\rho$ (radial), $z$ (axial), and $\chi$ (azimuth angle), and if these are related to another set of co-ordinates, $u$, $v$ and $w$, by the equations

$$\left.\begin{aligned} \rho &= \frac{a \sinh u}{\cosh u - \cos v} \\ z &= \frac{a \sin v}{\cosh u - \cos v} \\ \chi &= w \end{aligned}\right\} \quad . \quad . \quad . \quad (1)$$

then $u$, $v$ and $w$ are known as the *toroidal co-ordinates* of the point. In any radial plane the lines $u$ = constant are coaxial circles having limiting points at a distance $a$ from the axis, while $v$ = constant are the orthogonal system of coaxial circles intersecting at the limiting points of the former system (Fig. 3). Thus the surfaces $u$ = constant are anchor-rings or tores, while $v$ = constant are spheres having their centres on the axis of the tores. When a point is displaced so that its co-ordinates change by small amounts, $\delta u$, $\delta v$ and $\delta w$, its linear displacements in the three co-ordinate directions may be shown to be

$$\left.\begin{aligned} \delta s_u &= \frac{a\delta u}{\cosh u - \cos v} \\ \delta s_v &= \frac{a\delta v}{\cosh u - \cos v} \\ \delta s_w &= \frac{a \sinh u \delta w}{\cosh u - \cos v} \end{aligned}\right\} \quad . \quad . \quad . \quad (2)$$
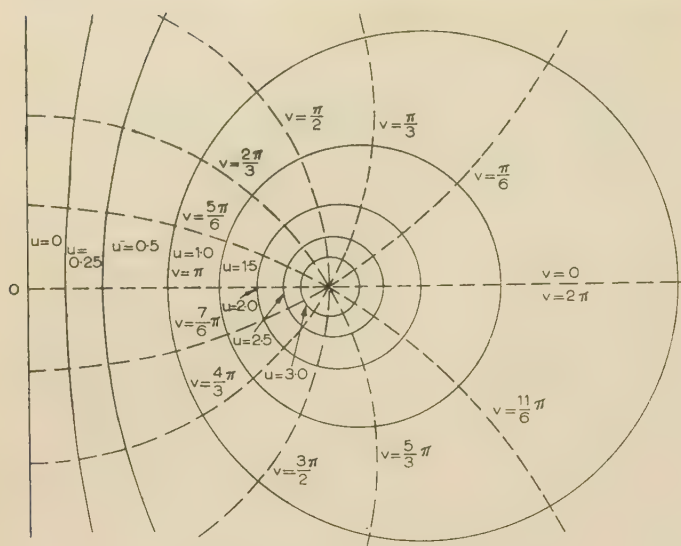
Fig. 3.—Toroidal co-ordinates.

The potential, $\phi$, of an electrostatic field always satisfies the differential equation known as Laplace's equation, which, for a 3-dimensional field, contains, in general, three independent variables. In the paper, however, we are concerned solely with problems having cylindrical symmetry, so that the variable $w$ becomes irrelevant. Expressed in terms of the two remaining toroidal co-ordinates $u$ and $v$, Laplace's equation becomes

$$\frac{\partial}{\partial u}\left(\frac{\sinh u}{\cosh u - \cos v}\frac{\partial \phi}{\partial u}\right) + \frac{\partial}{\partial v}\left(\frac{\sinh u}{\cosh u - \cos v}\frac{\partial \phi}{\partial v}\right) = 0 \quad (3)$$

The substitution

$$\phi = \psi\sqrt{(\cosh u - \cos v)} \quad . \quad . \quad . \quad . \quad (4)$$

reduces eqn. (3) to

$$\frac{\partial^2 \psi}{\partial u^2} + \frac{\partial^2 \psi}{\partial v^2} + \coth u \frac{\partial \psi}{\partial u} + \frac{1}{4}\psi = 0 \quad . \quad . \quad . \quad (5)$$

This equation is solved by assuming $\psi = UV$, where $U$ is a function of $u$ only and $V$ is a function of $v$ only. By this substitution, eqn. (5) is transformed into

$$\frac{1}{U}\left(\frac{d^2 U}{du^2} + \coth u \frac{dU}{du} + \frac{1}{4}U\right) + \frac{1}{V}\frac{d^2 V}{dv^2} = 0$$

and since the first term cannot contain $v$ and the second cannot contain $u$, both must be constants, which are written $+n^2$ and $-n^2$ respectively. Thus the separate differential equations for $U$ and $V$ are

$$\frac{d^2 U}{du^2} + \coth u \frac{dU}{du} - \left(n^2 - \frac{1}{4}\right)U = 0 \quad . \quad . \quad (6)$$

and

$$\frac{d^2 V}{dv^2} + n^2 V = 0 \quad . \quad . \quad . \quad . \quad . \quad (7)$$

The independent solutions of eqn. (7) are $\cos nv$ and $\sin nv$, and it is known from the theory of Fourier series that a sum of terms in which $n$ takes all integral values from zero to infinity will be capable of describing any distribution of charge on the surface of a tore. By direct substitution it may be proved that the following are solutions of eqn. (6):

$$p_n(u) = \frac{1}{\pi}\int_0^{\pi}\frac{d\theta}{(\cosh u - \sinh u \cos \theta)^{n+1/2}} \quad . \quad (8)$$

$$q_n(u) = \int_0^{\infty}\frac{d\theta}{(\cosh u + \sinh u \cosh \theta)^{n+1/2}} \quad . \quad (9)$$

$p_n(u)$ and $q_n(u)$ are known as *toroidal functions.*[*]

The toroidal functions can be expressed in terms of elliptic integrals, the necessary formulae being given by Hicks. Using these, the following Tables of values for the first four functions

### Table 1
#### TOROIDAL FUNCTIONS (FIRST KIND)

| $u$ | $p_0(u)$ | $p_1(u)$ | $p_2(u)$ | $p_3(u)$ |
|---|---|---|---|---|
| 0·0 | 1·000 | 1·000 | 1·000 | 1·000 |
| 0·1 | 0·999 4 | 1·002 | 1·009 | 1·022 |
| 0·2 | 0·997 5 | 1·008 | 1·038 | 1·089 |
| 0·3 | 0·994 4 | 1·017 | 1·086 | 1·206 |
| 0·4 | 0·990 1 | 1·030 | 1·155 | 1·379 |
| 0·5 | 0·984 6 | 1·047 | 1·246 | 1·620 |
| 0·6 | 0·978 0 | 1·068 | 1·362 | 1·942 |
| 0·7 | 0·970 2 | 1·092 | 1·504 | 2·366 |
| 0·8 | 0·961 4 | 1·120 | 1·678 | 2·918 |
| 0·9 | 0·951 6 | 1·153 | 1·885 | 3·631 |
| 1·0 | 0·940 9 | 1·189 | 2·132 | 4·551 |
| 1·1 | 0·929 2 | 1·229 | 2·424 | 5·733 |
| 1·2 | 0·916 8 | 1·273 | 2·767 | 7·252 |
| 1·3 | 0·903 5 | 1·321 | 3·169 | 9·202 |
| 1·4 | 0·889 7 | 1·373 | 3·640 | (1) 1·170 |
| 1·5 | 0·875 2 | 1·429 | 4·190 | 1·491 |
| 1·6 | 0·860 1 | 1·489 | 4·832 | 1·903 |
| 1·7 | 0·844 6 | 1·554 | 5·580 | 2·432 |
| 1·8 | 0·828 6 | 1·624 | 6·452 | 3·110 |
| 1·9 | 0·812 3 | 1·698 | 7·466 | 3·981 |
| 2·0 | 0·795 7 | 1·777 | 8·646 | 5·098 |
| 2·1 | 0·778 8 | 1·860 | (1) 1·002 | 6·532 |
| 2·2 | 0·761 7 | 1·949 | 1·162 | 8·373 |
| 2·3 | 0·744 4 | 2·043 | 1·347 | (2) 1·074 |
| 2·4 | 0·727 1 | 2·142 | 1·563 | 1·377 |
| 2·5 | 0·709 7 | 2·247 | 1·814 | 1·766 |
| 2·6 | 0·692 3 | 2·358 | 2·105 | 2·266 |
| 2·7 | 0·675 0 | 2·476 | 2·444 | 2·908 |
| 2·8 | 0·657 7 | 2·599 | 2·838 | 3·732 |
| 2·9 | 0·640 5 | 2·730 | 3·296 | 4·790 |
| 3·0 | 0·623 4 | 2·867 | 3·828 | 6·148 |
| 3·1 | 0·606 4 | 3·012 | 4·446 | 7·892 |
| 3·2 | 0·589 7 | 3·164 | 5·164 | (3) 1·013 |
| 3·3 | 0·573 1 | 3·324 | 5·998 | 1·300 |
| 3·4 | 0·556 8 | 3·493 | 6·967 | 1·670 |
| 3·5 | 0·540 7 | 3·671 | 8·093 | 2·144 |
| 3·6 | 0·524 8 | 3·858 | 9·402 | 2·753 |
| 3·7 | 0·509 2 | 4·054 | (2) 1·092 | 3·534 |
| 3·8 | 0·493 9 | 4·261 | 1·269 | 4·537 |
| 3·9 | 0·478 8 | 4·479 | 1·474 | 5·826 |
| 4·0 | 0·464 1 | 4·708 | 1·713 | 7·480 |

of each kind have been worked out. There are differences between these figures and those contained in Fouquet's table, in which there are undoubtedly a number of errors.

Hicks proves a number of theorems relating to toroidal functions, two of which will be mentioned here. The derivatives of $p_n(u)$ and $q_n(u)$ are shown to be given by

$$\left.\begin{array}{l}\dfrac{dp_n}{du} = \dfrac{(2n + 1)}{2 \sinh u}(p_{n+1} - \cosh u \cdot p_n) \\[2mm] \dfrac{dq_n}{du} = \dfrac{(2n + 1)}{2 \sinh u}(q_{n+1} - \cosh u \cdot q_n)\end{array}\right\} \quad . \quad . \quad (10)$$

* $p_n(u)$ and $q_n(u)$ are particular cases of the class of the functions known as *Legendre functions*: the relations between $p_n$ and $q_n$ and the corresponding Legendre functions are $p_n(u) = P_{n-1/2}(ju)$ and $q_n(u) = Q_{n-1/2}(ju)$. Hicks borrows the customary symbols for Legendre functions to designate the toroidal functions, writing $P_n(u)$ for $\pi p_n(u)$ and $Q_n(u)$ for $q_n(u)$; but this may lead to confusion, and we have preferred to employ a new notation.

## Table 2

### TOROIDAL FUNCTIONS (SECOND KIND)

| $u$ | $q_0(u)$ | $q_1(u)$ | $q_2(u)$ | $q_3(u)$ |
|---|---|---|---|---|
| 0·0 | ∞ | ∞ | ∞ | ∞ |
| 0·1 | 4·380 | 2·389 | 1·742 | 1·367 |
| 0·2 | 3·681 | 1·712 | 1·102 | (−1) 7·714 |
| 0·3 | 3·267 | 1·329 | (−1) 7·640 | 4·802 |
| 0·4 | 2·969 | 1·069 | 5·512 | 3·120 |
| 0·5 | 2·735 | (−1) 8·768 | 4·067 | 2·076 |
| 0·6 | 2·540 | 7·283 | 3·043 | 1·407 |
| 0·7 | 2·373 | 6·101 | 2·300 | (−2) 9·567 |
| 0·8 | 2·226 | 5·143 | 1·750 | 6·582 |
| 0·9 | 2·095 | 4·354 | 1·338 | 4·549 |
| 1·0 | 1·975 | 3·700 | 1·027 | 3·158 |
| 1·1 | 1·866 | 3·152 | (−2) 7·907 | 2·200 |
| 1·2 | 1·765 | 2·690 | 6·102 | 1·536 |
| 1·3 | 1·672 | 2·300 | 4·717 | 1·073 |
| 1·4 | 1·585 | 1·969 | 3·651 | (−3) 7·514 |
| 1·5 | 1·503 | 1·687 | 2·830 | 5·268 |
| 1·6 | 1·426 | 1·447 | 2·195 | 3·697 |
| 1·7 | 1·354 | 1·242 | 1·704 | 2·596 |
| 1·8 | 1·286 | 1·067 | 1·324 | 1·825 |
| 1·9 | 1·222 | (−2) 9·164 | 1·029 | 1·283 |
| 2·0 | 1·161 | 7·875 | (−3) 7·999 | (−4) 9·024 |
| 2·1 | 1·104 | 6·769 | 6·221 | 6·350 |
| 2·2 | 1·049 | 5·821 | 4·839 | 4·469 |
| 2·3 | (−1) 9·973 | 5·006 | 3·765 | 3·147 |
| 2·4 | 9·482 | 4·305 | 2·930 | 2·216 |
| 2·5 | 9·016 | 3·703 | 2·281 | 1·560 |
| 2·6 | 8·574 | 3·186 | 1·775 | 1·099 |
| 2·7 | 8·154 | 2·741 | 1·382 | (−5) 7·741 |
| 2·8 | 7·754 | 2·359 | 1·076 | 5·453 |
| 2·9 | 7·375 | 2·030 | (−4) 8·377 | 3·841 |
| 3·0 | 7·014 | 1·747 | 6·523 | 2·706 |
| 3·1 | 6·671 | 1·503 | 5·079 | 1·907 |
| 3·2 | 6·346 | 1·294 | 3·955 | 1·343 |
| 3·3 | 6·036 | 1·113 | 3·080 | (−6) 9·466 |
| 3·4 | 5·741 | (−3) 9·581 | 2·398 | 6·670 |
| 3·5 | 5·460 | 8·246 | 1·868 | 4·700 |
| 3·6 | 5·194 | 7·097 | 1·454 | 3·312 |
| 3·7 | 4·941 | 6·108 | 1·133 | 2·333 |
| 3·8 | 4·700 | 5·257 | (−5) 8·820 | 1·644 |
| 3·9 | 4·470 | 4·524 | 6·869 | 1·159 |
| 4·0 | 4·252 | 3·894 | 5·349 | (−7) 8·165 |

The numbers in parentheses indicate the power of 10 by which tabulated values are to be multiplied, e.g. $q_3(3\cdot0) = 0\cdot000\,027\,06$.

while another integral form for $q_n(u)$ is

$$q_n(u) = \frac{1}{\sqrt{2}}\int_0^\pi \frac{\cos n\theta\, d\theta}{\sqrt{(\cosh u - \cos\theta)}} \quad . \quad . \quad . \quad (11)$$

### (3) SOLUTION OF THE PROBLEM OF COAXIAL TORES

The general solution of eqn. (5), which is the product of the solutions of eqns. (6) and (7), may thus be written

$$\psi = \sum_{n=0}^{\infty} [a_n p_n(u) + b_n q_n(u)]\cos(nv + \alpha_n) \quad . \quad . \quad (12)$$

where $a_n$, $b_n$ and $\alpha_n$ are arbitrary constants. When the central plane is a plane of symmetry (as here), $\alpha_n = 0$; therefore, using eqn. (4), the potential of the field between charged coaxial tores $T_0'$, $T_1'$ is given by

$$\phi = \sqrt{(\cosh u - \cos v)} \sum_{n=0}^{\infty} [a_n p_n(u) + b_n q_n(u)]\cos nv \quad (13)$$

The constants $a_n$ and $b_n$ must be so chosen as to make $\phi = 0$ on $T_0'$ (where $u = u_0$) and $\phi = V$ on $T_1'$ (where $u = u_1$); thus

$$\sum_{n=0}^{\infty} [a_n p_n(u_0) + b_n q_n(u_0)]\cos nv = 0$$

or

$$a_n p_n(u_0) + b_n q_n(u_0) = 0 \quad . \quad . \quad . \quad . \quad (14)$$

and $\sum_{n=0}^{\infty} [a_n p_n(u_1) + b_1 q_n(u_1)]\cos nv = \dfrac{V}{\sqrt{(\cosh u_1 - \cos v)}}$

from which, by the usual method of evaluating Fourier coefficients,

$$a_n p_n(u_1) + b_n q_n(u_1) = \frac{2V}{\pi}\int_0^\pi \frac{\cos nv\, dv}{\sqrt{(\cosh u_1 - \cos v)}}$$

$$= \frac{2\sqrt{2}}{\pi} V q_n(u_1) \quad . \quad . \quad . \quad . \quad (15)$$

from eqn. (11). The factor $2/\pi$ becomes $1/\pi$ when $n = 0$. From eqns. (14) and (15) we obtain the values of the coefficients as

$$
\left.
\begin{aligned}
a_n &= \frac{2\sqrt{2}}{\pi} V \frac{\delta_n q_n(u_0) q_n(u_1)}{p_n(u_1)q_n(u_0) - p_n(u_0)q_n(u_1)} \\
b_n &= \frac{-2\sqrt{2}}{\pi} V \frac{\delta_n p_n(u_0) q_n(u_1)}{p_n(u_1)q_n(u_0) - p_n(u_0)q_n(u_1)}
\end{aligned}
\right\} \quad . \quad (16)
$$

where $\delta_n = 1$ when $n \geqslant 1$, but $\delta_0 = \frac{1}{2}$.

We are chiefly interested in the potential gradients on the surfaces of the two conductors; since $u$ is constant on each of these surfaces, the direction of the field is the direction of variation of $u$. The gradient is $-\partial\phi/\partial s_u$, where $\delta s_u$ is given by eqn (2); thus

$$E_u = -\frac{\partial\phi}{\partial s_u} = -\left(\frac{\cosh u - \cos v}{a}\right)\frac{\partial\phi}{\partial u} \quad . \quad . \quad (17)$$

The points of especial interest are $X_0$ and $X_1$ (see Fig. 2), where the two conductors are closest together, and where the co-ordinates $(u, v)$ are $(u_0, \pi)$ and $(u_1, \pi)$, $u_0$ being greater than $u_1$ if $u_1$ denotes the central conductor. At any point on the plane $v = \pi$,

$$E_u = -\left(\frac{1 + \cosh u}{a}\right)\frac{\partial\phi}{\partial u} \quad . \quad . \quad . \quad (18)$$

Evaluating this with the help of the identities (10) gives

$$E_u = \frac{\sqrt{2}}{a}\frac{\cosh^2\frac{u}{2}}{\sinh\frac{u}{2}}\sum_{n=0}^{\infty}(-1)^n\Big\{(n\cosh u + \tfrac{1}{2})[a_n p_n(u) + b_n q_n(u)]$$
$$- (n + \tfrac{1}{2})[a_n p_{n+1}(u) + b_n q_{n+1}(u)]\Big\}$$
$$. \quad . \quad . \quad . \quad (19)$$
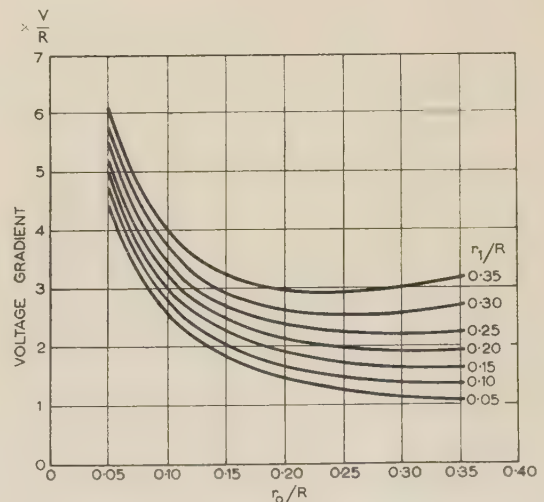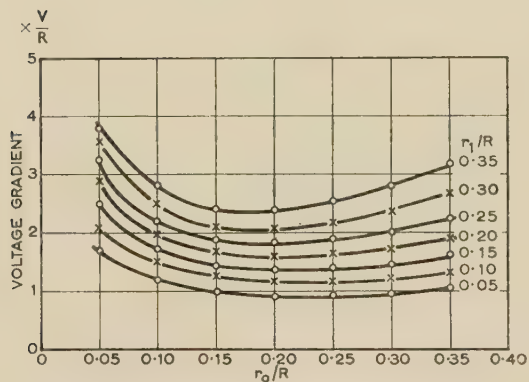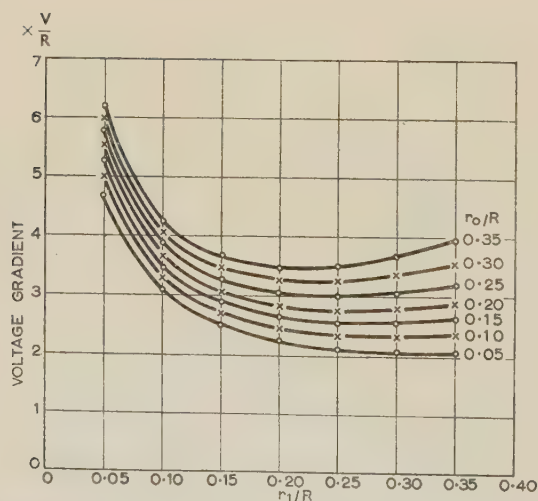
Fig. 4.—Voltage gradient on tore (calculated).
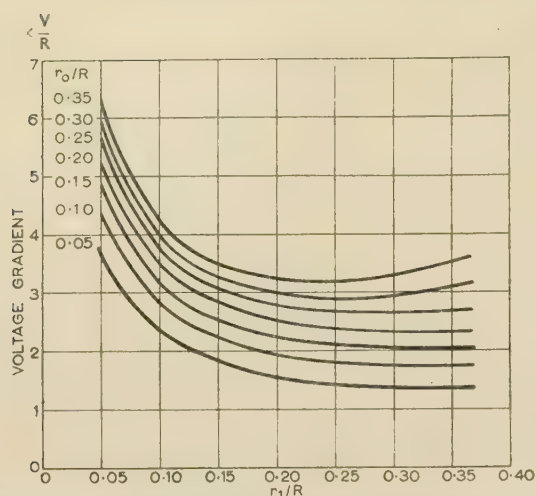
Fig. 5.—Voltage gradient on central conductor (calculated).



Fig. 8.—Approximate correction chart for voltage gradient on tore.



Fig. 6.—Voltage gradient on tore (measured).



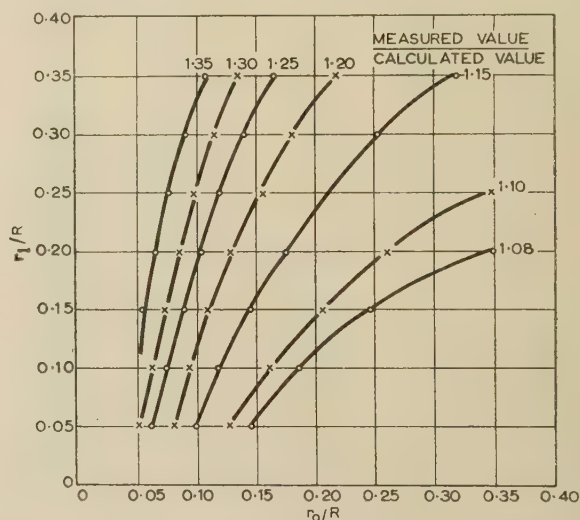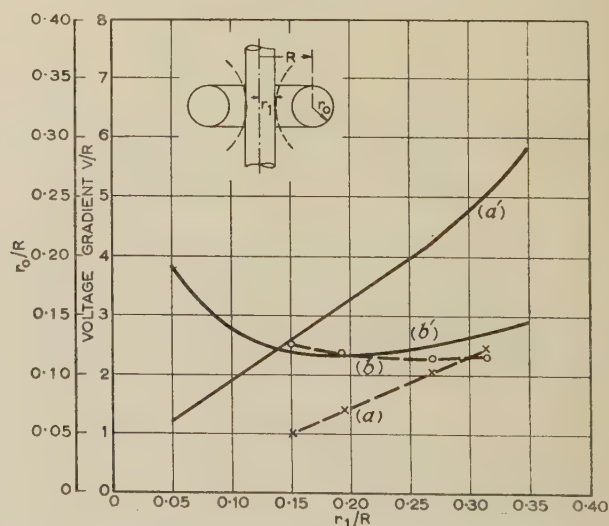Fig. 9.—Approximate correction chart for voltage gradient on central conductor.



Fig. 10.—Curves for equal gradient condition.

(a), (a') Relation between $r_0/R$ and $r_1/R$ for equal voltage gradients.
(b), (b') Value of the gradient on either electrode when relation (a) or (a') is satisfied.
(a), (b) by electrolytic tank.
(a'), (b') by toroidal functions.



Fig. 7.—Voltage gradient on central conductor (measured).

On the earthed conductor, $u = u_0$ and eqn. (19) reduces to

$$E_0 = -\frac{\sqrt{2}}{a} \frac{\cosh^2 \frac{u_0}{2}}{\sinh \frac{u_0}{2}} \sum_{n=0}^{\infty} (-1)^n (n + \tfrac{1}{2})[a_n \mathrm{p}_{n+1}(u_0) + b_n \mathrm{q}_{n+1}(u_0)] \qquad \cdots \qquad (20)$$

while on the live conductor, $u = u_1$ and eqn. (19) becomes

$$E_1 = \frac{\sqrt{2}}{a} \frac{\cosh^2 \frac{u_1}{2}}{\sinh \frac{u_1}{2}} \sum_{n=0}^{\infty} (-1)^n \left\{ \frac{2\sqrt{2}}{\pi} V(n \cosh u_1 + \tfrac{1}{2}) \delta_n \mathrm{q}_n(u_1) \right.$$
$$\left. - (n + \tfrac{1}{2})[a_n \mathrm{p}_{n+1}(u_1) + b_n \mathrm{q}_{n+1}(u_1)] \right\} \qquad \cdots \qquad (21)$$

The potential gradients given by eqns. (20) and (21) are plotted in Figs. 4 and 5. Instead of using $u_0$ and $u_1$ as independent variables, the dimension ratios $r_0/R$ and $r_1/R$ (see Fig. 1) have been employed. The relations between $r_0$, $r_1$, $R$ and $a$, $u_0$, $u_1$ are

$$a = \surd(R^2 - r_0^2)$$
$$u_0 = \text{arc sech} \ (r_0/R)$$
$$u_1 = 2 \ \text{arc tanh} \ \frac{r_1}{\surd(R^2 - r_0^2)} \qquad \cdots \qquad (22)$$

## (4) ELECTROLYTIC-TANK INVESTIGATION

To ascertain how closely the field between coaxial tores approximates to that between a coaxial rod and ring, the latter was investigated in a wedge-shaped electrolytic tank. Copper electrodes coated with Aquadag were used, with tap-water as the electrolyte; from a preliminary test with electrodes representing concentric cylinders it was concluded that the curve of potential variation could be drawn with an accuracy of 1%. The radial variation in potential in the mid-plane was plotted for different combinations of electrode radii, and the voltage gradients on the electrodes were deduced; the results are set forth in Figs. 6 and 7. Fig. 6, showing the voltage gradient on the ring, is to be compared with Fig. 4, and Fig. 7, showing that on the central conductor, with Fig. 5.

## (5) CONCLUSIONS

The relationship between the two sets of curves is summed up in Figs. 8 and 9, in which the ratio between measured and calculated voltage gradient is plotted. On the tore, the ratio approaches unity for large values of $r_0$ (i.e. for thick rings); but, in general, the measured value is less than the calculated one. On the central conductor the reverse is true, the measured value exceeding the calculated one, and again the ratio approaches unity for large values of $r_0$. These tendencies can be deduced

from a general consideration of the field, the hour-glass shape of the central conductor tending to produce a reduced gradient on itself and an increased gradient on the surrounding ring, as compared with a central conductor of cylindrical shape. It may therefore be said that the general correctness of the measurements is confirmed by the calculations, which are thus shown to have practical value as an independent check, quite apart from their theoretical interest as a new application of field theory.

For any given value of $r_1/R$ there must be a value of $r_0/R$ which will make the maximum voltage gradients on the two electrodes equal. This relation is given by curves (a) and (a') in Fig. 10, curve (a) referring to the measured values of voltage gradient and curve (a') to the calculated values. The considerable discrepancy between these two curves is due to the fact that the measured gradients on the two electrodes diverge from the calculated ones in opposite directions.

The relation given by these curves represents an optimum design condition. Assuming it to be satisfied, the voltage gradient on either electrode is given by curves (b) (measured) or (b') (calculated). Either curve shows a minimum attainable gradient of about $2 \cdot 3 V/R$; theory suggests that this will occur when $r_0 = 0 \cdot 165R$ and $r_1 = 0 \cdot 20R$, while measurement corrects these values to $r_0 = 0 \cdot 10R$ and $r_1 = 0 \cdot 27R$. So long as the relation between $r_0$ and $r_1$ is correctly maintained, their values can depart quite a long way from those cited without greatly increasing the voltage gradient.

## (7) REFERENCES

(1) SCHWAIGER, A.: 'Theory of Dielectrics', translated by R. W. SORENSEN (Wiley, New York, 1932).
(2) BOLLIGER, A.: 'Probleme der Potentialtheorie', *Archiv für Elektrotechnik*, 1918, **6**, p. 134.
(3) NEUMANN, C.: 'Allgemeine Lösung des Problems über den stationären Temperaturzustand eines homogenen Körpers welcher von irgend zwei nichtconzentrischen Kugelflächen begrenzt wird' (Schmidt, Halle, 1864).
(4) HICKS, W. M.: 'On Toroidal Functions', *Philosophical Transactions of the Royal Society*, 1881, **31**, p. 609.
(5) HICKS, W. M.: 'On the Steady Motion of a Hollow Vortex', *ibid.*, 1884, **35**, p. 161.
(6) FOUQUET, W.: 'Dipolare Koordinaten und Kugelfunktionen', *Zeitschrift für angewandte Mathematik und Mechanik*, 1937, **17**, p. 48.

# A SPECTROMETER METHOD FOR MEASURING THE ELECTRICAL CONSTANTS OF LOSSY MATERIALS

By J. S. SEELEY, Ph.D., B.Sc.(Eng.), Graduate.

## SUMMARY

The analysis of the propagation of a plane wave at oblique incidence through a strip of lossy material is stated, the behaviour of the lossy material being completely represented by the use of a complex refractive index and a complex reflection coefficient. A measurement technique is described whereby these constants can be measured from a strip of material used in a 1 cm parallel-plate spectrometer. The analysis and measurement technique are checked by the application of the spectrometer method and the established waveguide method to the measurement of two ordinary lossy dielectrics. The spectrometer method may be used for the measurement of any homogeneous material, and is especially suitable for the examination of anisotropic artificial dielectrics. The accuracy of the method is discussed for the measurement of the electrical constants of medium-loss materials with refractive indices between 0·5 and 2·0.

## LIST OF PRINCIPAL SYMBOLS

$A = \varepsilon^{-\alpha d}$ = Attenuation factor after transmission through strip of thickness $d$.

$k = \alpha/\beta$ = Index of absorption.

$\boldsymbol{n} = n(1 - jk)$ = Complex refractive index.

$\quad n$ = Real part of refractive index.

$\boldsymbol{r} = r\varepsilon^{-jx}$ = Complex reflection coefficient of intensity for a single interface.

$\quad r$ = Modulus of reflection coefficient.

$R, T$ = Power reflection and transmission coefficients of a strip of material.

$\boldsymbol{\gamma} = \alpha + j\beta$ = Complex propagation coefficient.

$\quad \delta$ = Loss angle.

$\boldsymbol{\epsilon} = \epsilon_r(1 - j\tan\delta)$ = Complex permittivity.

$\quad \epsilon_r$ = Relative permittivity.

$\quad \lambda_0$ = Free-space operating wavelength.

$\quad \lambda_g$ = Corresponding waveguide wavelength.

$\phi = \dfrac{2\pi d}{\lambda_0}\sqrt{(n^2 - \sin^2\psi)}$ = Effective electrical thickness of strip at oblique incidence.

$\quad \chi$ = Phase angle of reflection coefficient.

$\quad \psi$ = Angle of incidence.

## (1) INTRODUCTION

The power transmitted through a strip of lossless dielectric is a function of the angle of incidence when the strip is illuminated obliquely by a plane wave. Destructive interference between the reflections from the parallel interfaces allows all the incident power to be transmitted at a particular angle of incidence. The position of this angle of incidence can be accurately determined, because the associated zero of reflected power is sharply defined. The refractive index of the material can be calculated from the values of this angle of incidence, the free-space wavelength and

the thickness of the strip, when ambiguity has been resolved by making measurements on at least two strips of different thicknesses.

Measurements of this kind have been carried out by Culshaw[1] on polystyrene and Perspex using a free-space microwave spectrometer. The loss tangent of Perspex ($\simeq 0·010$) was calculated by Culshaw from the small decrease in amplitude of transmitted power at the position for minimum reflection. Sollom[2,3] has reported similar measurements on polystyrene, using a parallel-plate spectrometer. The accuracy of relative power measurements in a microwave spectrometer is increased by enclosing the transmitting region between parallel plates.

Experiments in the parallel-plate spectrometer with a strip of an artificial dielectric have yielded maximum transmission coefficients less than unity, and finite, though small, values of minimum reflection coefficient. The angles of incidence for maximum transmission were larger than those for minimum reflection, so that a simple calculation of the refractive index is not possible. The analysis given in Section 2 shows that these extra effects are produced by attenuation in the strip. A technique has been developed to determine all the electrical constants of a lossy material from measurements made on a strip.

## (2) PROPAGATION AT OBLIQUE INCIDENCE THROUGH A LOSSY MATERIAL

Consider the propagation of a plane wave through an infinitely wide strip of lossy material B, as shown in Fig. 1. If the medium
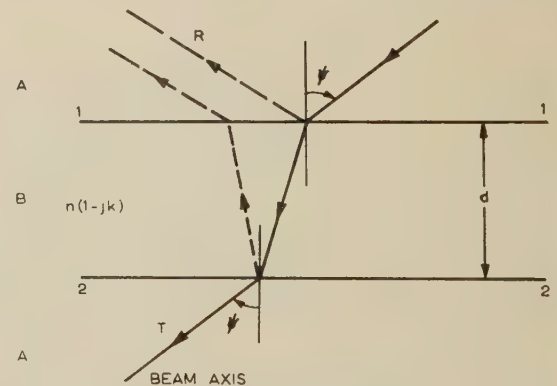


Fig. 1.—Refraction through a lossy strip.

A is free space, B may be specified in terms of a complex refractive index $\boldsymbol{n}$, and a complex reflection coefficient $\boldsymbol{r}$, where

$$\boldsymbol{n} = n(1 - jk) \quad \cdots \cdots \quad (1)$$

$$\boldsymbol{r} = r\varepsilon^{-\chi} \quad \cdots \cdots \quad (2)$$

The refractive index is used as a basic constant, as in optics, because optical-type measurements are to be made. This will be convenient in measurements on artificial dielectrics. A mag-

netic effect is associated with the conducting elements making up the artificial-dielectric array, implying that $n \neq \sqrt{\epsilon}$. This follows Brown and Willis Jackson,[4] who have discussed the use of a refractive index and an impedance to describe the behaviour of an artificial medium giving,

$$n = [\epsilon\mu]^{1/2} \quad . \quad . \quad . \quad . \quad . \quad (3)$$

To apply the analysis to conventional dielectrics, some equations will be expressed in terms of $n$ as $\sqrt{\epsilon_r}\sqrt{(1 - j \tan \delta)}$. The reflection coefficient, $r$, will be used as a basic constant instead of an impedance, $Z$, which can be obtained from the equation

$$r = \frac{Z - Z_0}{Z + Z_0} \quad . \quad . \quad . \quad . \quad . \quad (4)$$

### (2.1) Propagation through a Lossy Strip

The effective propagation coefficient through a strip of lossy material in the direction perpendicular to its parallel interfaces is given by

$$\gamma = \frac{2\pi}{\lambda_0}\sqrt{(n^2 - \sin^2 \psi)} \quad . \quad . \quad . \quad . \quad (5)$$

The expansion of eqn. (5) into the form $\gamma = \alpha + j\beta$ is a standard derivation. If $n^2 k \ll (n^2 - \sin^2 \psi)$,

$$\gamma = \alpha + j\beta \simeq \frac{2\pi}{\lambda_0}\sqrt{(n^2 - \sin^2 \psi)}\left(\frac{n^2 k}{n^2 - \sin^2 \psi} + j\right) \quad (6)$$

where $n$ and $k$ are assumed to be constant with variation in angle of incidence. The approximation represented by eqn. (6) is valid for medium-loss materials, where $k \not\gg 0\cdot 1$, provided that the angle of incidence does not exceed 60°. For an ordinary medium-loss dielectric, where $\mu_r = 1$,

$$\gamma = \frac{2\pi}{\lambda_0}\sqrt{(\epsilon_r - \sin^2 \psi)}\left[\frac{\epsilon_r \tan \delta}{2(\epsilon_r - \sin^2 \psi)} + j\right] \quad . \quad (7)$$

A refractive index $n_\psi$, occurring at the angle of incidence $\psi$, must be defined when the approximation (6) is not valid. Stratton[5] and Mahan[6] have given expressions for $n_\psi$. Two classes of material exhibit values of $n_\psi$ sensibly greater than $n$: the first comprises conducting or semi-conducting materials, where $k \gg 0\cdot 1$; the second comprises materials where $n < 1$ at angles of incidence in the immediate vicinity of the critical angle where $(n^2 - \sin^2 \psi)$ tends to zero. These cases will not be further considered in the paper.

The effective electrical thickness of a strip, whose actual thickness is $d$, is given by

$$\phi = \beta d = \frac{2\pi d}{\lambda_0}\sqrt{(n^2 - \sin^2 \psi)} \quad . \quad . \quad . \quad (8)$$

Birks[7] and others[8] have extended the basic treatment given by Stratton[5] to obtain equations for the power transmission and reflection coefficients of a strip in terms of $\phi$, $r\epsilon^{-jx}$, and $A$, namely

$$R = \frac{r^2[(1 - A^2)^2 + 4A^2 \sin^2 \phi]}{(1 - r^2A^2)^2 + 4A^2r^2 \sin^2 (\phi + X)} \quad . \quad . \quad (9)$$

$$T = \frac{A^2[(1 - r^2)^2 + 4r^2 \sin^2 X]}{(1 - r^2A^2)^2 + 4A^2r^2 \sin^2 (\phi + X)} \quad . \quad . \quad (10)$$

where $\quad A = \epsilon^{-\alpha d} = \exp\left[-\frac{2\pi d}{\lambda_0}\frac{n^2 k}{\sqrt{(n^2 - \sin^2 \psi)}}\right] \quad . \quad (11)$

Eqns. (9) and (10) show that $R$ and $T$ are cyclical functions of $\phi$. For a strip of fixed thickness, $\phi$ can be conveniently controlled by varying the angle of incidence.

For lossless materials, $A = 1$ and $X = 0$, and for this case $R = 0$ and $T = 1$ when $\phi = m\pi$ (corresponding to the half-wavelength thickness at normal incidence). $R$ and $T$ will have maximum and minimum values respectively when $\phi = m\pi \pm \pi/2$ (corresponding to the quarter-wavelength thickness at normal incidence), given by

$$R = \frac{4r^2}{(1 + r^2)^2} \text{ and } T = 1 - R \quad . \quad . \quad . \quad (12)$$

For lossy materials, $A < 1$ and $X \neq 0$. The minimum value of $R$, $\check{R}$, and the maximum value of $T$, $\hat{T}$, occur at $\phi_1$ and $\phi_3$ respectively, which are slightly removed from $m\pi$; the maximum value of $R$, $\hat{R}$, and the minimum value of $T$, $\check{T}$, occur at $\phi_2$ and $\phi_4$ respectively, which are slightly removed from $m\pi \pm \pi/2$. The displacements from the $\pi$ and $\pi/2$ positions of $\phi$ can be illustrated by a phase diagram, as shown in Fig. 2. The values
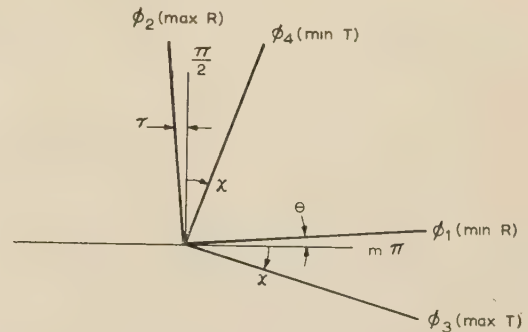


Fig. 2.—Phase-angle diagram.

of $\phi_1$–$\phi_4$ are derived in Section 9.1, expressions for $\theta$ and $\tau$ being given in eqns. (30) and (31).

An expression for $T/R$ is obtained by dividing eqn. (10) by eqn. (9), giving

$$\frac{T}{R} = \frac{A^2[(1 - r^2)^2 + 4r^2\sin^2 X]}{r^2[(1 - A^2)^2 + 4A^2 \sin^2 \phi]} \quad . \quad . \quad . \quad (13)$$

$T/R$ is a function of $\sin^2 \phi$ only ($\sin^2 X$ can be assumed to be constant for 5° changes in $\psi$), so that $T/R$ will have a maximum value when $\phi = m\pi$ and a minimum value when $\phi = m\pi \pm \pi/2$. The refractive index can therefore be calculated from eqn. (8), provided that ambiguity in the value of $m$ has been resolved, by determining the angle of incidence at which a minimum or maximum value of $T/R$ occurs.

Exact expressions for the minimum and maximum values of $R$ and $T$ are found by substituting the values $\phi_1$–$\phi_4$ in eqns. (9) and (10): these expressions are given in eqns. (36)–(39). A simultaneous solution to extract values of $A$, $r$ and $X$ from the minimum and maximum values of $R$ and $T$ and the values $\phi_1$–$\phi_4$ is not possible, because eqns. (36)–(39) and (34) and (35) are interlinked. An additional complication is that the values of $A$ and $r$ in the expression for $\check{R}$ are not exactly equal to those in the expression for $\hat{T}$, because of the different angles of incidence at which $\check{R}$ and $\hat{T}$ occur. Similarly, the values of $A$ and $r$ in the expression for $\hat{R}$ are not equal to those in the expression for $\check{T}$. The displacement of the minima and maxima from the exact $\pi$ or $\pi/2$ angular positions will not exceed 3° for medium-loss materials, provided that the angle of incidence does not exceed 60°. The changes in the values of $A$ and $r$ for increments of 3° in angle of incidence are less than the inherent errors discussed in Section 5. Therefore it can be assumed that, in determining $A$ and $r$ from eqns. (36)–(39), the values occur at the angles of incidence given by $\phi_1 \simeq \phi_3 \simeq m\pi$, $\phi_2 \simeq \phi_4 \simeq m\pi \pm \pi/2$.

An iterative process has to be used to extract the values of $A$, $r$ and $X$ from eqns. (34)–(39). It has been found in practice that sufficiently accurate results are obtained for medium-loss materials by assuming that $X$, $\theta$ and $\tau = 0$ in eqns. (36)–(39). $A$ and $r$ are therefore obtained from the solutions of the following equations provided that $A \ll 0 \cdot 6$, $X \gg 10°$ and $r \gg 0 \cdot 7$:

At $\qquad \phi = \phi_1 \simeq m\pi, \qquad \check{R} \simeq \dfrac{r^2(1 - A^2)^2}{(1 - r^2A^2)^2}$ . . (14)

At $\qquad \phi = \phi_2 \simeq m\pi \pm \dfrac{\pi}{2}, \hat{R} \simeq \dfrac{r^2(1 + A^2)^2}{(1 + r^2A^2)^2}$ . . (15)

At $\qquad \phi = \phi_3 \simeq m\pi, \qquad \hat{T} \simeq \dfrac{A^2(1 - r^2)^2}{(1 - r^2A^2)^2}$ . . (16)

At $\qquad \phi = \phi_4 \simeq m\pi \pm \dfrac{\pi}{2}, \check{T} \simeq \dfrac{A^2(1 - r^2)^2}{(1 + r^2A^2)^2}$ . . (17)

Figs. 3 and 4 provide a graphical solution for the simultaneous equations, (14) and (16), (15) and (17), and can be used to obtain
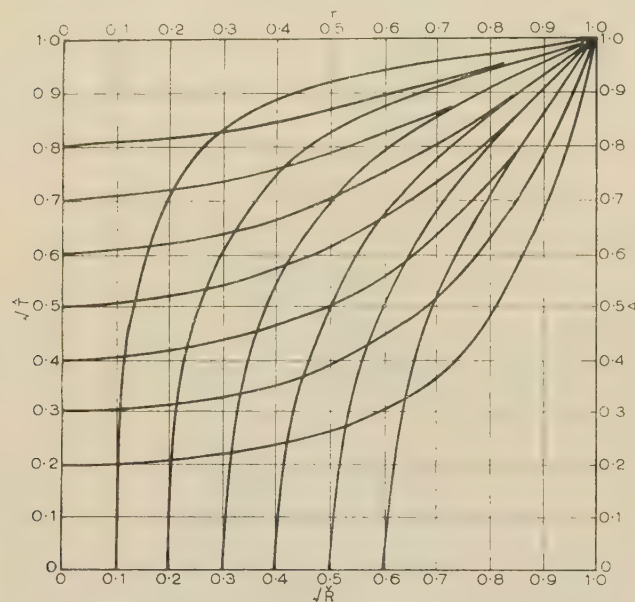


Fig. 3.—$\sqrt{\check{R}}$ and $\sqrt{\hat{T}}$ as functions of $A$ and $r$.

values of $A$ and $r$ from pairs of values of $\sqrt{\check{R}}$ and $\sqrt{\hat{T}}$, and of $\sqrt{\hat{R}}$ and $\sqrt{\check{T}}$. Fig. 4 is the most accurate chart to use for this purpose, because of the wide range of orthogonal intersection of the $\sqrt{\hat{R}}$ and $\sqrt{\check{T}}$ curves. The use of Fig. 3 will result in larger errors in $r$, because of the shape of the chart and also because $\sqrt{\check{R}}$ is small and will be liable to errors in measurement. The $\sqrt{\hat{T}}$ curves have a gradual slope, so that the values of $A$ can be obtained almost directly from the values of $\sqrt{\hat{T}}$. Then, since $A = \varepsilon^{-\alpha d}$

$$k = \frac{(\alpha d)(n^2 - \sin^2 \psi)}{n^2 \phi} \qquad . \quad . \quad . \quad (18)$$

The values of $A$ and $r$ can be substituted in eqns. (34) and (35) to determine the phase angle, $X$. If $\psi_1$, $\psi_2$, $\psi_3$ and $\psi_4$ are respectively the angles of incidence at which $\check{R}$, $\hat{R}$, $\hat{T}$ and $\check{T}$ occur (see Fig. 2),

$$\frac{2\pi d}{\lambda_0}[(n^2 - \sin^2 \psi_1)^{1/2} - (n^2 - \sin^2 \psi_3)^{1/2}]$$
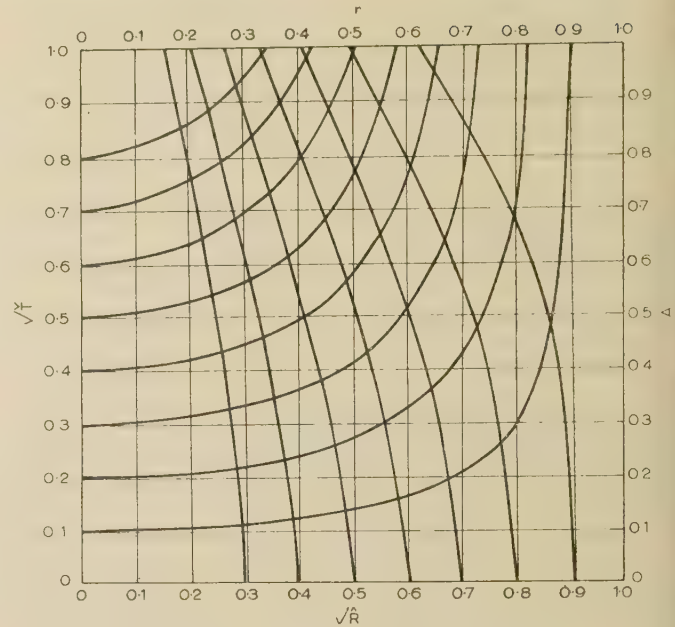$$= X\left[1 + \frac{r^2(1 - A^2)^2}{(1 - r^2)(1 - r^2A^4)}\right] \quad (19)$$



Fig. 4.—$\sqrt{\hat{R}}$ and $\sqrt{\check{T}}$ as functions of $A$ and $r$.

and

$$\frac{2\pi d}{\lambda_0}[(n^2 - \sin^2 \psi_2)^{1/2} - (n^2 - \sin^2 \psi_4)^{1/2}]$$
$$= X\left[1 + \frac{r^2(1 + A^4)}{(1 - r^2)(1 - r^2A^4)}\right] \quad (20)$$

Expressions for the reflection coefficient at the interface of a lossy material are given in the form $r\varepsilon^{-jX}$ in eqns. (42) and (43).

## (3) MEASUREMENT TECHNIQUES

To apply the analysis given in Section 2 to the determination of the electrical constants of a lossy material, it will be necessary to measure the relative powers reflected from and transmitted through a strip at various angles of incidence. The refractive index must be known before $k$ and $X$ can be calculated, and it can be determined from eqn. (8) once the ambiguity in the effective electrical thickness of the strip has been resolved. It will be difficult to resolve this ambiguity for dispersive materials, so the refractive index is best obtained from some alternative unambiguous method. Deviation measurements with a prism and an application of Snell's law, as described by Sollom,[2,3] can be used for this purpose.

### (3.1) Diffraction Effects in the Spectrometer

The 1 cm parallel-plate spectrometer used to make the measurements discussed in the paper has been fully described elsewhere.[2,3] The diameter of the spectrometer table is equal to the Rayleigh distance, so that specimens placed at the centre are in the Fresnel region of diffraction where the radiated field pattern has local disturbances in amplitude and phase.

Culshaw[1] deliberately operated a free-space spectrometer in both the Fresnel and Fraunhofer regions, and found that the diffraction and stray reflection effects occurring in the Fresnel region did not affect the accuracy of direction measurements. Amplitude measurements of the power transmitted through and reflected from a strip, as well as measurements of direction, are needed to apply the analysis given in Section 2. The work of Woonton[9–11] and of Bates and Elliott[12] shows that the central

portion of the radiation pattern is substantially unaltered for some distance inside the Fresnel region, indicating that a comparative method of power measurement would overcome any possible diffraction effects. If a calibrating strip of known reflecting properties is used, any diffraction effects will be eliminated, because they are common to both the unknown strip and the calibrating strip. This technique is described in Section 3.3. The analysis in Section 2 assumes that the incident waves are plane at all refracting boundaries, and also that no limitations are imposed by the finite widths of strips. Sollom's experimental work has justified the use of these assumptions for the 1 cm parallel-plate spectrometer, working at normal incidence, provided that specimens are placed at the centre of the table, and are at least twice the width of the aperture of the transmitting aerial (corners and edges which might produce diffraction effects can be 'masked' with tapered absorbing wedges). A rigorous examination of the application of the present method could be provided by an analysis using the concept of an angular spectrum of plane waves, developed by Booker and Clemmow.[13] ·

### (3.2) Prism Measurements

Consider the deviation, $D$, which is produced by a lossless prism, of refracting angle $\rho$, aligned for normal incidence as
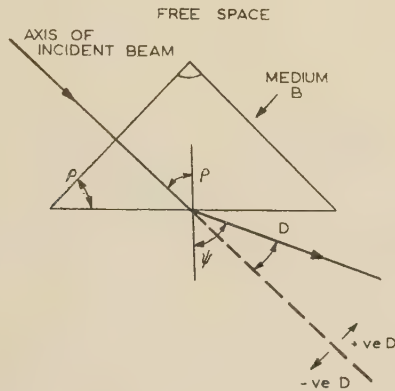


Fig. 5.—Refraction through a prism.

shown in Fig. 5. Snell's law applied to the refraction at the hypotenuse gives

$$n = \frac{\sin \psi}{\sin \rho} = \frac{\sin (\rho + D)}{\sin \rho} \quad . \quad . \quad . \quad (21)$$

$D$ is negative if $n < 1$ and positive if $n > 1$. If the prism material is lossy, Snell's law at the refracting boundary must be expressed in terms of a complex refractive index, i.e.

$$\frac{\sin \psi}{\sin \rho} = n(1 - jk) \quad . \quad . \quad . \quad . \quad (22)$$

The significance of this equation has been discussed by Stratton.[5] Planes of constant phase no longer coincide with planes of constant amplitude after refraction (waves of this type are called 'hybrid' or 'inhomogeneous' plane waves). The direction of the refracted beam (given by the normal to the planes of constant phase) is still determined by $n$ for medium-loss substances, but there is an amplitude taper across the width of the beam owing to the different path lengths travelled through the lossy medium. Eqn. (21) can be used to determine $n$. The direction of the refracted beam is obtained by plotting the receiver response over 10° of arc, and defining the direction as the centre of area of the response curve.

### (3.3) Strip Measurements

Measurements of transmitted and reflected power are made by moving the receiving aerial through the appropriate arcs (Fig. 6).
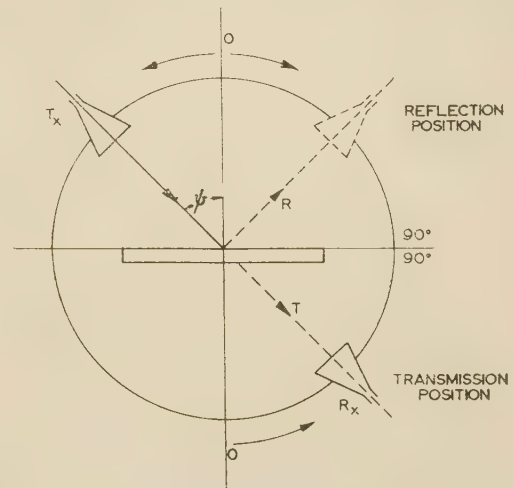


Fig. 6.—Positioning of the strip in the spectrometer.

The power coupled into or out of an aerial depends on its penetration into the parallel-plate gap. Sollom has shown that each aerial can be adjusted independently for maximum power transfer by varying this penetration. Thus, if the transmitting aerial is set for maximum power transfer into the empty spectrometer, the alterations in the path length through the strip produced by changes in the angle of incidence can be compensated by adjusting the receiving aerial for maximum signal. Relative power measurements at different angular positions are limited in accuracy by alterations in plate spacing and aerial penetrations around the circumference of the spectrometer. It has been found that these measurements can be made with sufficient accuracy to obtain results from the analysis given in Section 2 by taking great care in the angular alignment of the two aerials and continuously adjusting the penetration of the receiving aerial. When the receiving aerial has been adjusted for maximum signal, the peak value of the received response is used as a basis for comparison. Power-transmission coefficients are directly measured as the ratio of the power transmitted through the strip to that transmitted through the empty spectrometer. A polystyrene strip is used for calibration purposes in reflection measurements; this material satisfies the conditions for lossless transmission, and has a reflection coefficient comparable to those of most lossy materials. The power-reflection coefficient will have a maximum value for the $\pi/2$ position [see eqn. (12)] given by $4r^2/(1 + r^2)^2$, where $r$ is the reflection coefficient of a single interface at the appropriate angle of incidence. For the parallel-plate spectrometer, $r$ is the Fresnel perpendicular reflection coefficient, as expressed in eqn. (43). Curves for calibration with polystyrene ($\epsilon_r = 2 \cdot 56$) have been drawn of $r$ and $R_{lossless}$ (see Figs. 7 and 8). Values of maximum power reflected from the polystyrene strip can be standardized from $R_{lossless}$ computed from Figs. 7 and 8. This calibration can be applied to the maximum and minimum power reflected from the lossy strip, measured under the same transmitting conditions, to give values of $\hat{R}$ and $\check{R}$ for the strip.

### (4) EXPERIMENTAL RESULTS

The technique which has just been described provides the most convenient method of measuring the behaviour of dispersive artificial dielectrics, for which the reflection coefficient is not a
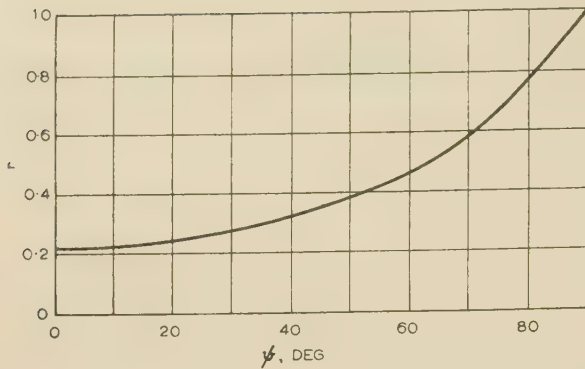
**Fig. 7.**—Intensity reflection coefficient of a free-space/polystyrene interface ($\epsilon_r = 2 \cdot 56$), at oblique incidence.

$$r = \frac{\sqrt{(2 \cdot 56 - \sin^2 \psi)} - \cos \psi}{\sqrt{(2 \cdot 56 - \sin^2 \psi)} + \cos \psi}$$
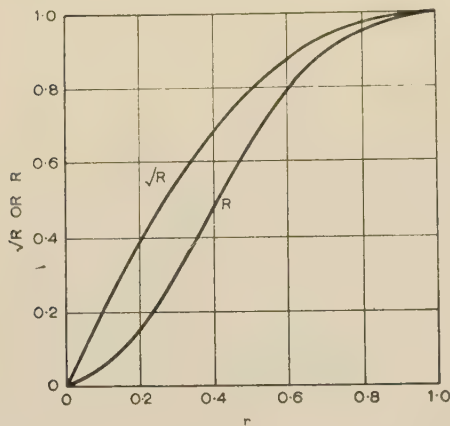


**Fig. 8.**—Graphs of the function $R_{lossless}$ (power reflection coefficient) of a lossless strip.

$R_{lossless} = 4r^2/(1 + r^2)^2$, where $r$ is the reflection coefficient of a single interface at any angle of incidence.

simple function of the refractive index, and where the refractive index, reflection coefficient and attenuation are frequency dependent. Resonant-cavity and waveguide techniques are well established for the unique determination of $\epsilon_r$ and $\tan \delta$ for ordinary dielectrics, so that a check can be made of the spectrometer method by determining the electrical constants of a lossy dielectric in the spectrometer and by one of the established methods.

The waveguide method was chosen as the alternative, because of its simplicity and the availability of waveguide components. This method, which is fully described elsewhere,[14,15] is based on a measurement of $\gamma$, the complex propagation coefficient. An approximate value of $\epsilon_r$ is needed before an accurate measurement can be made, and this was obtained in the present instance from input impedance measurements made on an arbitrary length of sample with short-circuit and open-circuit terminations. A quarter-wavelength sample was then prepared for an accurate short-circuit measurement to obtain the value of the function $(\tanh \gamma l)/\gamma l$, where $l$ is the length of the sample and is desirably a quarter-wavelength. Values of $\epsilon_r$ and $\tan \delta$ are extracted from this function by use of suitable hyperbolic charts.

The best check of the spectrometer method is provided by a material with a large ratio of $\tan \delta/\epsilon_r$, and with a value of $\epsilon_r$ not greater than $4 \cdot 0$ (if $\epsilon_r > 4$ the rate of change of $\phi$ with $\sin \psi$ will be too slow to permit the measurement of the maxima and

minima of reflection and transmission). Two materials were examined, namely fabric Bakelite laminate (Tufnol) and fibre board (a red-coloured plastic used in insulation boards). The internal dimensions of the 1 cm waveguide were $0 \cdot 420$ in $\times 0 \cdot 170$ in, and the quarter-wavelength samples of the materials examined were approximately $0 \cdot 060$ in long. The samples were hand-finished to the necessary tolerance, $\pm 0 \cdot 000\,5$ in. Strips were machined from the same sheets of material for use in the spectrometer, 10 in long and $0 \cdot 192$ in thick (spectrometer-plate spacing plus $0 \cdot 005$ in for uniform contact), and approximately two wavelengths in depth to ensure adequate attenuation. Each material was examined at three wavelengths, $\lambda_g$ in the waveguide corresponding to $\lambda_0$ in the spectrometer. The parallel surfaces of the strips were covered with tinfoil to ensure electrical contact with the spectrometer plates. It was found that additional weight had to be applied to press the top plate down on to the strip to obtain consistent reflection measurements.

The arrangement of the strip in the spectrometer is shown in Fig. 6. The angle of incidence used in calculations is that of the transmitter position. Typical maximum and minimum reflected responses for the fibre-board strip and the maximum response for the calibrating polystyrene strip are given in Fig. 9.
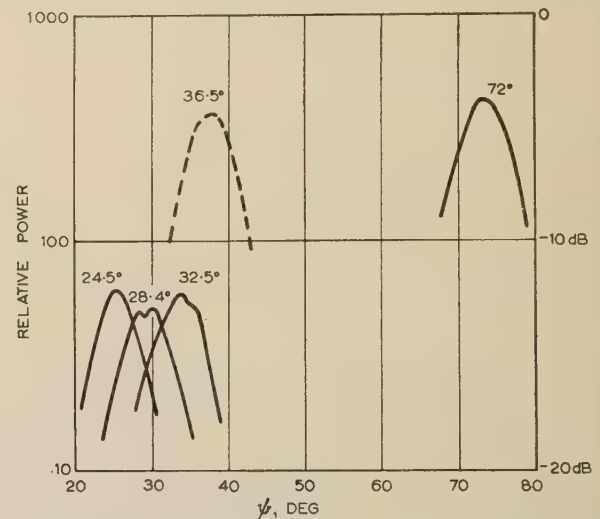


**Fig. 9.**—Maximum and minimum reflected responses from a lossy strip, and calibrating maximum reflected response from lossless strip.

———— Fibre-board response.
– – – – Calibrating polystyrene response.
$\lambda_0 = 1 \cdot 227$ cm.

Fibre-board: $1 \cdot 43$ cm thick, $\epsilon_r = 3 \cdot 04$, $\tan \delta = 0 \cdot 13$, electrical length is $2\lambda$ at $29°$, $1 \cdot 75\lambda$ at $73°$.
Polystyrene: $2 \cdot 67$ cm thick, $\epsilon_r = 2 \cdot 56$, $\tan \delta < 0 \cdot 001$, electrical length is $3 \cdot 25\lambda$ at $36 \cdot 5°$, $3\lambda$ at $53°$.

The minimum polystyrene response, at $\psi = 53°$, was more than 40 dB below the maximum response. The corresponding transmitted responses, with the calibrating responses through the empty spectrometer, are shown in Fig. 10. The minimum reflected response has a slight double-hump effect, which was even more noticeable in the polystyrene minimum response (more than 20 dB lower). This feature can be explained as a diffraction effect as follows: the reflection coefficient of the strip is changing rapidly with angle of incidence at the minimum reflection position (the lower the attenuation of the strip the more rapid this change will be), and the wide aperture of the receiving aerial gathers contributions over a 10° arc of incidence angles; the reduced sensitivity of the aerial at angles on the response 'skirt' may be offset by rapid changes in reflection coefficient to produce a flat,
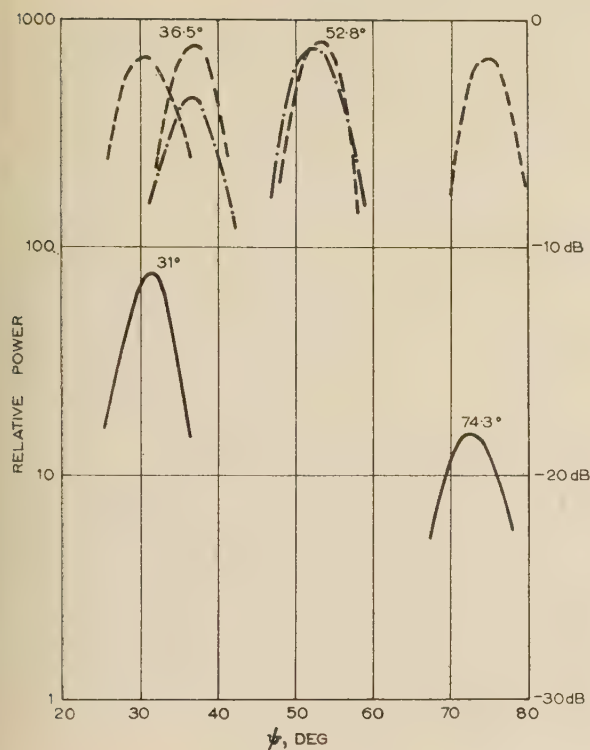
**Fig. 10.**—Maximum and minimum transmitted responses from lossy and lossless strips, and calibrating empty spectrometer responses.

——— Fibre-board response.
—·— Polystyrene response.
– – – Calibrating empty response.

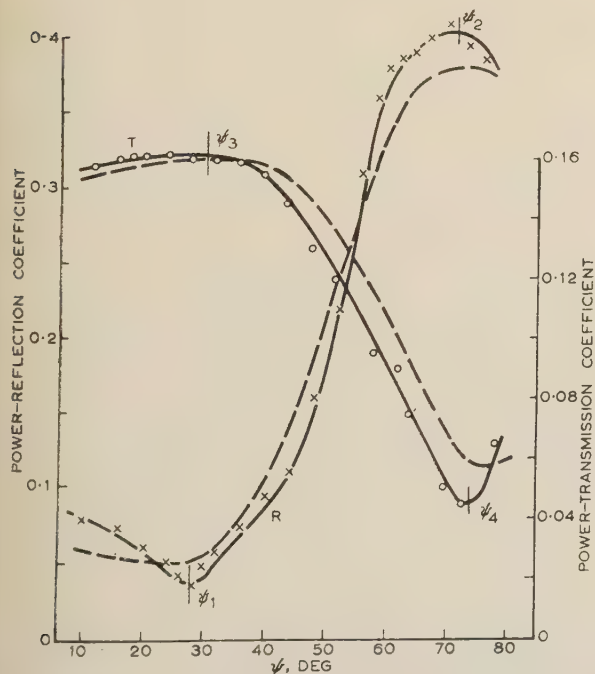The angle at each response is the position of the transmitter, used as a reference.



**Fig. 11.**—Calculated and measured values of power reflection and transmission coefficients of a lossy strip at oblique incidence.

– – – Calculated values.

$\lambda_0 = 1 \cdot 227$ cm; $d = 1 \cdot 43$ cm; $\epsilon_r = 3 \cdot 04$; $\tan \delta = 0 \cdot 13$.

or even double-humped, response curve when the aerial is in the minimum reflection position.

Complete curves of $R$ and $T$ for the fibre-board strip are shown in Fig. 11. Plots of $T/R$ near the $\pi$ and $\pi/2$ positions are given in Fig. 12, showing the location of the exact values of $\phi$, leading to calculation of $\epsilon_r$.
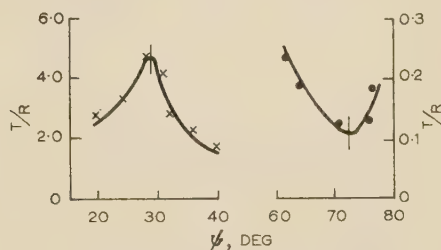


**Fig. 12.**—Plot of the function $T/R$ to find the positions for exact values of $\phi$ (values from Fig. 11).

The complete experimental results are shown in Table 1. The angles of incidence at which $\breve{R}$ and $\hat{R}$ occur, $\psi_1$ and $\psi_2$, are given in row (a), and those at which $\hat{T}$ and $\breve{T}$ occur, $\psi_3$ and $\psi_4$, in row (b). The thicknesses of the two strips have been chosen so that $\phi/2\pi = 2 \cdot 0$ at small, and $1 \cdot 75$ at large, angles of inci-

**Table 1A**

RESULTS FOR FABRIC BAKELITE

| $\lambda_0$ | | $1 \cdot 206$ cm | | $1 \cdot 227$ cm | | $1 \cdot 255$ cm |
|---|---|---|---|---|---|---|
| (a) $\psi_1, \psi_2$ .. | | $26°$ | $74°$ | $11°$ | $72°$ | $63 \cdot 5°$ |
| (b) $\psi_3, \psi_4$ .. | | $28 \cdot 5°$ | $78°$ | $17°$ | $75°$ | $66°$ |
| (c) $\epsilon_r$ .. .. | | $3 \cdot 75$ | $3 \cdot 73$ | $3 \cdot 75$ | $3 \cdot 73$ | $3 \cdot 71$ |
| (d) $\epsilon_r^*$ .. | | | $3 \cdot 72$ | | $3 \cdot 78$ | $3 \cdot 82$ |
| (e) $\tan \delta$ .. | | $0 \cdot 058$ | $0 \cdot 062$ | $0 \cdot 058$ | $0 \cdot 064$ | $0 \cdot 065$ |
| (f) $\tan \delta^*$ .. | | | $0 \cdot 047$ | | $0 \cdot 051$ | $0 \cdot 055$ |
| (g) $r$ .. .. | | $0 \cdot 32$ | $0 \cdot 76$ | $0 \cdot 34$ | $0 \cdot 78$ | $0 \cdot 68$ |
| (h) Calculated $r$ | | $0 \cdot 36$ | $0 \cdot 76$ | $0 \cdot 34$ | $0 \cdot 71$ | $0 \cdot 64$ |
| (i) $\chi$ .. .. | | $3 \cdot 0°$ | $3 \cdot 2°$ | $3 \cdot 0°$ | $3 \cdot 2°$ | $2 \cdot 8°$ |
| (j) Calculated $\chi$ | | $2 \cdot 5°$ | $2 \cdot 8°$ | $2 \cdot 4°$ | $2 \cdot 8°$ | $2 \cdot 7°$ |

* Results obtained from waveguide measurements with a sample $0 \cdot 165$ cm long, at the guide wavelengths corresponding to the values of $\lambda_0$ used in the spectrometer.

$d = 1 \cdot 28$ cm for the spectrometer method.

**Table 1B**

RESULTS FOR FIBRE-BOARD

| $\lambda_0$ | | $1 \cdot 206$ cm | $1 \cdot 227$ cm | | $1 \cdot 255$ | |
|---|---|---|---|---|---|---|
| (a) $\psi_1, \psi_2$ .. | | $32°$ | $28 \cdot 5°$ | $72°$ | $23 \cdot 5°$ | $69°$ |
| (b) $\psi_3, \psi_4$ .. | | $37 \cdot 5°$ | $31°$ | $75°$ | $27 \cdot 5°$ | $72°$ |
| (c) $\epsilon_r$ .. .. | | $3 \cdot 07$ | $3 \cdot 04$ | $3 \cdot 06$ | $3 \cdot 06$ | $3 \cdot 08$ |
| (d) $\epsilon_r^*$ .. | | $3 \cdot 06$ | | $3 \cdot 09$ | | $3 \cdot 11$ |
| (e) $\tan \delta$ .. | | $0 \cdot 12$ | $0 \cdot 13$ | $0 \cdot 13$ | $0 \cdot 132$ | $0 \cdot 138$ |
| (f) $\tan \delta^*$ .. | | $0 \cdot 105$ | | $0 \cdot 115$ | | $0 \cdot 118$ |
| (g) $r$ .. .. | | $0 \cdot 28$ | $0 \cdot 29$ | $0 \cdot 70$ | $0 \cdot 27$ | $0 \cdot 60$ |
| (h) Calculated $r$ | | $0 \cdot 34$ | $0 \cdot 33$ | $0 \cdot 70$ | $0 \cdot 31$ | $0 \cdot 62$ |
| (i) $\chi$ .. .. | | $6 \cdot 9°$ | $5 \cdot 3°$ | $6 \cdot 2°$ | $6 \cdot 3°$ | $7 \cdot 1°$ |
| (j) Calculated $\chi$ | | $6 \cdot 65°$ | $6 \cdot 55°$ | $7 \cdot 15°$ | $6 \cdot 45°$ | $7 \cdot 4°$ |

* Results obtained from waveguide measurements with a sample $0 \cdot 179$ cm long, at the guide wavelengths corresponding to the values of $\lambda_0$ used in the spectrometer.

$d = 1 \cdot 43$ cm for the spectrometer method.

dence. The values of $\epsilon_r$, tan $\delta$, $r$ and $X$ measured in the spectro-meter are given in rows (c), (e), (g) and (i), respectively, and the values of $\epsilon_r$ and tan $\delta$ obtained from the waveguide measurements are given in rows (d) and (f). Values of $r$ and $X$ calculated from eqns. (43) with the waveguide values of $\epsilon_r$ and tan $\delta$ are given in rows (h) and (j), and are to be compared with the values measured in the spectrometer [rows (g) and (i)]. Graphs showing the values of $\phi$, $r$ and $X$ for the fibre-board strip are given in Fig. 13.
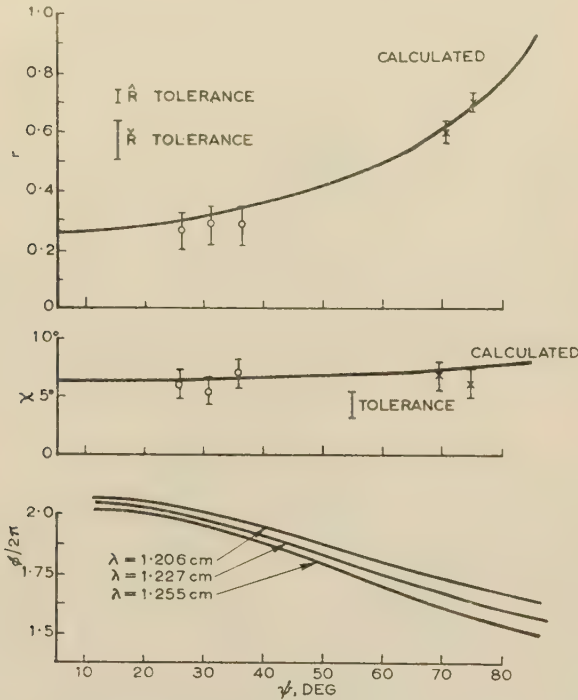


Fig. 13.—Theoretical characteristics of lossy strip.
$d = 1\cdot43$ cm; tan $\delta = 0\cdot13$; $\epsilon_r = 3\cdot04$.
x. $\hat{R}$ measurements.
o. $\check{R}$ measurements.

The differences between the spectrometer and waveguide measurements of $\epsilon_r$ are not greater than 2%. The measurements of tan $\delta$ in the spectrometer tend to be lower than those in waveguide, the greatest difference being 15% when tan $\delta \simeq 0\cdot04$. The values of $r$ obtained in the spectrometer are in good agree-ment with the calculated values, with the exception of those resulting from $\check{R}$ measurements, which seem to be low (a large error is expected from $\check{R}$ measurements). All the measured values of $X$ are in good agreement with the calculated values.

## (5) EXPERIMENTAL ACCURACIES
### (5.1) Waveguide Measurements

The waveguide impedance measurements were made in terms of the standing-wave ratio (s.w.r.) and minimum position. The small values of s.w.r. obtained with the short-circuit termination were measured by the Roberts–Von Hippel method. On the assumption that the error in the measurement of position is $\pm0\cdot002$ cm, then, from the analysis of Roberts,[15] the error in $\epsilon_r$ will not exceed $\pm1\cdot5$% at $\lambda_g = 1\cdot5$ cm, for values of $\epsilon_r$ between $2\cdot0$ and $4\cdot0$. For low-loss materials (tan $\delta \simeq 0\cdot01$), the error in tan $\delta$ will be $\pm25$%, while for medium-loss materials (tan $\delta \simeq 0\cdot10$), it will be $\pm10$%, and will vary proportionally between these values.

### (5.2) Spectrometer Method

Errors in the measurement of comparative power level are inherent in the spectrometer, and the accuracy of the method will depend on the order of accuracy of the measurement of the power coefficients. Theoretical curves of $R$ and $T$ for the fibre-board strip have been prepared from the values of $\epsilon_r$ and tan $\delta$ measured at $\lambda_0 = 1\cdot227$ cm; these are shown in Fig. 11, together with the measured values of $R$ and $T$. Examination of the curves justifies the adopted calibration procedure, and shows that $R$ and $T$ can be measured to within $\pm0\cdot02$. These errors can be applied to the worst cases of interpretation of $A$ and $r$ from Figs. 3 and 4 for both medium- and low-loss materials. If the reflection coefficient is about $0\cdot5$, for medium-loss material, $\check{T} \ll 0\cdot09$ at large angles of incidence and $\hat{R} \ll 0\cdot30$. Thus with $\check{T} = 0\cdot09 \pm 0\cdot02$ and $\hat{R} = 0\cdot30 \pm 0\cdot02$, tan $\delta \simeq 0\cdot10$ $\pm 7$% and $r = 0\cdot48 \pm 0\cdot015$. Similarly, $\hat{T} \ll 0\cdot20$ and $\check{R} \ll 0\cdot10$. Applying limits of $\pm0\cdot02$ to these values gives tan $\delta \simeq 0\cdot10 \pm 5$% and $r = 0\cdot42 \pm 0\cdot05$. For low-loss materials at large angles of incidence, $\check{T} \gg 0\cdot45$ and $\hat{T} \gg 0\cdot65$, $\hat{R} \simeq 0\cdot50$ and $\check{R} \simeq 0\cdot03$. Applying the limits of $\pm0\cdot02$ to these pairs of values gives, for $\hat{T}/\hat{R}$ measurements, tan $\delta \simeq 0\cdot01 \pm 20$% and $r = 0\cdot45 \pm 0\cdot02$; for $\hat{T}/\check{R}$ measurements, tan $\delta \simeq 0\cdot01 \pm 20$% and $r = 0\cdot40 \pm 0\cdot07$.

Finally, considering eqns. (19) and (20), the differences between $\psi_1$ and $\psi_3$, and between $\psi_2$ and $\psi_4$, can be read to within $\pm1°$ or better if the angles are close together; thus, for small differences (i.e. $X \gg 5°$) the tolerance on calculations of $X$ is $\pm 0\cdot5°$, and for larger differences ($X \gg 10°$) the tolerance is $\pm1\cdot0°$.

### Table 2
#### ACCURACIES OF THE SPECTROMETER METHOD

| Electrical constant | Range | Tolerance |
|---|---|---|
| $k$ or $\frac{1}{2}$ tan $\delta$ | $<0\cdot001$<br>$0\cdot01$<br>$0\cdot1$ | Limit of measurement<br>$\pm20$%<br>$\pm7$% |
| $X$ | $<5°$<br>$5°–10°$ | $\pm0\cdot5°$<br>$\pm1\cdot0°$ |
| $r$ | $0\cdot3–0\cdot6$<br><br>$>0\cdot6$ | $\pm0\cdot02$ (from $\hat{R}$)<br>$\pm0\cdot06$ (from $\check{R}$)<br>Greater than values given above |
| $n^2$ or $\epsilon_r$ | $4\cdot0–0\cdot25$ | $\pm2$% (strip)<br>$\pm1$% (prism) |

For values of $k$ between $0\cdot1$ and $0\cdot01$ the accuracy will vary between $\pm7$% and $\pm20$%. The difficulties of locating and giving values to maxima and minima on graphs of $T$ and $R$ are reduced with materials whose refractive index is near unity (such as artificial dielectrics), or materials which have low losses. In these cases the maxima and minima are more sharply defined. The accuracies claimed for the spectrometer method in Table 2 are seen to be justified by the results shown in Table 1 and Fig. 13, in view of the agreement of $\epsilon_r$ and tan $\delta$ with the waveguide values and the agreement of $r$ and $X$ with the calculated values.

## (6) CONCLUSIONS

The properties of all materials, including artificial dielectrics, can be specified by a complex refractive index and a complex reflection coefficient, which can be measured by inserting a strip of the material in a microwave spectrometer; possible ambiguities in the real refractive index can be resolved by using two strips of different thicknesses or by a separate measurement using a

prism. It is not suggested that the spectrometer method is a substitute for the established waveguide methods at wavelengths above 1 cm. The disadvantages of the method are that large homogeneous samples are required, and a parallel-plate spectrometer must be used to ensure the required accuracy of relative power measurements. The accuracies obtainable with the spectrometer method at 1 cm wavelengths are indicated in Table 2. It is reasonable to suggest that these should be maintained at wavelengths below 1 cm, where the accuracies obtainable with waveguide methods fall away. The spectrometer method will therefore be of value at these wavelengths.

A most valuable feature of the method described is that it can be used for anisotropic materials in which the properties depend on the direction of propagation.

### (7) ACKNOWLEDGMENTS

### (8) REFERENCES

(1) CULSHAW, W.: 'A Spectrometer for Millimetre Wavelengths', *Proceedings I.E.E.*, Paper No. 1445 M, February, 1953 (**100**, Part IIA, p. 5).

(2) SOLLOM, P. H.: 'An Accurate Parallel-Plate Microwave Spectrometer', University of London, Ph.D. Thesis, 1954.

(3) SOLLOM, P. H., and BROWN, J.: 'A Centimetre-wave Parallel-Plate Spectrometer', *Proceedings I.E.E.*, Paper No. 2008 R, May, 1956 (**103 B**, p. 419).

(4) BROWN, J., and WILLIS JACKSON: 'The Properties of Artificial Dielectrics at Centimetre Wavelengths', *ibid.*, Paper No. 1699 R, January, 1955 (**102 B**, p. 11).

(5) STRATTON, J. A.: 'Electromagnetic Theory' (McGraw-Hill, New York, 1941).

(6) MAHAN, A. L.: 'Reflection and Refraction at Oblique Incidence on a Dielectric/Metallic Interface as a Boundary Problem in Electromagnetic Theory', *Journal of the Optical Society of America*, 1956, **46**, p. 913.

(7) BIRKS, J. B.: 'Dielectric Housings for Centimetre-Wave Antennae', *Journal I.E.E.*, 1946, **93**, Part IIIA, p. 647.

(8) CADY, W. M., KARELITZ, M. B., and TURNER, L. A.: 'Radar Scanners and Radomes' (McGraw-Hill, New York, 1948).

(9) WOONTON, G. A., and CARRUTHERS, J. A.: 'Indoor Measurements of Microwave Antenna Radiation Patterns by means of a Metal Lens', *Journal of Applied Physics*, 1950, **21**, p. 428.

(10) WOONTON, G. A.: 'The Effect of an Obstacle in the Fresnel Field on the Distant Field of a Linear Radiator', *ibid.*, p. 577.

(11) WOONTON, G. A., CARRUTHERS, J. A., ELLIOTT, H. A., and RIGBY, E. C.: 'Diffraction Errors in an Optical Measurement at Radio Wavelengths', *ibid.*, 1951, **22**, p. 390.

(12) BATES, R. H. T., and ELLIOTT, J.: 'The Determination of the True Side-Lobe Level of Long Broadside Arrays from Radiation-Pattern Measurements made in the Fresnel Region', *Proceedings I.E.E.*, Monograph No. 169 R, March, 1956 (**103 C**, p. 307).

(13) BOOKER, H. G., and CLEMMOW, P. C.: 'The Concept of an Angular Spectrum of Plane Waves', *ibid.*, Paper No. 992 R (**97**, Part III, p. 11).

(14) BARLOW, H. M., and CULLEN, A. L.: 'Microwave Measurements' (Constable and Co., London, 1950).

(15) VON HIPPEL, A.: 'Dielectric Materials and Applications' (John Wiley and Sons, New York, 1955).

### (9) APPENDICES

#### (9.1) The Exact Values of $\varphi_1$–$\varphi_4$, $\breve{R}$, $\hat{R}$, $\breve{T}$ and $\hat{T}$

The expression for $R$ has been given in eqn. (9). Maximum and minimum reflections will occur when $d(R)/d\phi = 0$. $R$ is of the form $(M + \sin^2 \phi)/[N + \sin^2 (\phi + X)]$, where

$$M = \frac{(1 - A^2)^2}{4A^2} \text{ and } N = \frac{(1 - r^2A^2)^2}{4A^2r^2} \qquad . \quad . \quad (23)$$

$d(R)/d\phi = 0$ when $(2N + 1) \sin 2\phi - (2M + 1) \sin 2(\phi + X) + 2 \sin 2X = 0$. This expression can be arranged as a quadratic equation in $\tan \phi$. $X$ will not be greater than $10°$ for medium-loss materials, so that $\sin X \simeq X$ and $\cos X \simeq 1$. The roots of the equation are therefore obtained as

$$\tan \phi_1 \simeq X\frac{M}{(N - M)} \cdot \qquad . \quad . \quad . \quad (24)$$

and

$$\tan \phi_2 \simeq -\frac{1}{X}\frac{(N - M)}{(M + 1)} \qquad . \quad . \quad . \quad (25)$$

Suppose that $R$ has a minimum value at

$$\phi = \phi_1 = m\pi + \theta \qquad . \quad . \quad . \quad . \quad (26)$$

and a maximum value at

$$\phi = \phi_2 = m\pi \pm \frac{\pi}{2} + \tau \qquad . \quad . \quad . \quad (27)$$

$\theta$ and $\tau$ will be small, so therefore

$$\theta \simeq \tan \theta = X\frac{M}{(N - M)} \qquad . \quad . \quad . \quad (28)$$

and since $\tan \phi_2 \simeq -1/\tan \tau$,

$$\tau \simeq \tan \tau = X\frac{(M + 1)}{(N - M)} \qquad . \quad . \quad . \quad (29)$$

Substituting the values of $M$ and $N$ from eqns. (23) in eqns. (28) and (29) gives

$$\theta = X\frac{r^2(1 - A^2)^2}{(1 - r^2)(1 - r^2A^4)} \qquad . \quad . \quad . \quad (30)$$

$$\tau = X\frac{r^2(1 + A^4)}{(1 - r^2)(1 - r^2A^4)} \qquad . \quad . \quad . \quad (31)$$

Similarly, maximum and minimum transmissions will occur when $d(T)/d\phi = 0$. $T$ is of the form $(K + \sin^2 X)/[L + \sin^2 (\phi + X)]$, and $d(T)/d\phi = 0$ when $-(K + \sin^2 X)2 \sin (\phi + X) \cos (\phi + X) = 0$, i.e. either $\sin (\phi + X)$ or $\cos (\phi + X) = 0$.

So $T$ has a maximum value at

$$\phi_3 + X = m\pi \qquad . \quad . \quad . \quad . \quad (32)$$

and a minimum value at

$$\phi_4 + X = m\pi \pm \frac{\pi}{2} \qquad . \quad . \quad . \quad (33)$$

Eqns. (26)–(33) can be combined to give

$$\phi_1 - \phi_3 = \theta + X = X\left[ 1 + \frac{r^2(1 - A^2)^2}{(1 - r^2)(1 - r^2A^4)} \right] \qquad (34)$$

$$\phi_2 - \phi_4 = \tau + \chi = \chi \left[ 1 + \frac{r^2(1 + A^4)}{(1 - r^2)(1 - r^2 A^4)} \right] \quad (35)$$

The relative positions of $\phi_1$–$\phi_4$ are indicated in the phase diagram, Fig. 2.

The exact minimum and maximum values of $R$ and $T$ are determined by substituting the values of $\phi_1$–$\phi_4$ in eqns. (9) and (10), giving

At $\phi = \phi_1$:
$$\breve{R} = \frac{r^2[(1 - A^2)^2 + 4A^2 \sin^2 \theta]}{(1 - r^2 A^2)^2 + 4 A^2 r^2 \sin^2 (\theta + \chi)} \quad . \quad . \quad (36)$$

At $\phi = \phi_2$:
$$\hat{R} = \frac{r^2[(1 - A^2)^2 + 4A^2(1 - \sin^2 \psi)]}{(1 - r^2 A^2)^2 + 4A^2 r^2[1 - \sin^2 (\psi + \chi)]} \quad . \quad (37)$$

At $\phi = \phi_3$:
$$\hat{T} = \frac{A^2[(1 - r^2)^2 + 4r^2 \sin^2 \chi]}{(1 - r^2 A^2)^2} \quad . \quad . \quad (38)$$

At $\phi = \phi_4$:
$$\breve{T} = \frac{A^2[(1 - r^2)^2 + 4r^2 \sin^2 \chi]}{(1 - r^2 A^2)^2 + 4A^2 r^2} \quad . \quad . \quad (39)$$

### (9.2) The Reflection Coefficient at the Interface of a Lossy Material

The reflection coefficient will be considered for the case of perpendicular polarization only (where the direction of the electric vector is perpendicular to the plane of incidence), because the parallel-plate spectrometer is designed to work with this polarization.

Stratton[5] gives the following expression for the reflection coefficient at the interface of a dielectric material:

$$r_{\perp} = \frac{\sqrt{(n^2 - \sin^2 \psi)} - \cos \psi}{\sqrt{(n^2 - \sin^2 \psi)} + \cos \psi} \quad . \quad . \quad (40)$$

For a lossless dielectric, $\mathbf{n} = n$, giving

$$r = \frac{\sqrt{(n^2 - \sin^2 \psi)} - \cos \psi}{\sqrt{(n^2 - \sin^2 \psi)} + \cos \psi} \quad . \quad . \quad (41)$$

For a medium-loss material, $\mathbf{n} = n(1 - jk)$, where $k \not> 0 \cdot 1$ giving

$$r = \frac{\sqrt{(n^2 - \sin^2 \psi)} - \cos \psi}{\sqrt{(n^2 - \sin^2 \psi)} + \cos \psi} \varepsilon^{-j\chi}$$

where
$$\chi = \arctan \left[ \frac{2n^2 k}{(n^2 - 1)\sqrt{(n^2 - \sin^2 \psi)}} \right] \quad . \quad . \quad (42)$$

i.e. $\mathbf{r} = r\varepsilon^{-j\chi}$, where $r$ is evaluated as though the material were lossless. This form of expression has been used for the reflection coefficient in the analysis given in Sections 2 and 9.1. For ordinary dielectric material,

$$r = \frac{\sqrt{(\epsilon_r - \sin^2 \psi)} - \cos \psi}{\sqrt{(\epsilon_r - \sin^2 \psi)} + \cos \psi} \varepsilon^{-j\chi}$$

where
$$\chi = \arctan \left[ \frac{\epsilon_r \tan \delta}{(\epsilon_r - 1)\sqrt{(\epsilon_r - \sin^2 \psi)}} \right] \quad . \quad . \quad (43)$$

# THE STATISTICAL BASIS OF IMPULSE TESTING

## By T. J. LEWIS, M.Sc., Ph.D., Associate Member.

### SUMMARY

The normal procedure of impulse-testing insulation involves the average of a series of similar tests and the determination of the percentage breakdown at a given impulse ratio. The basis of this procedure involves the properties of a series of Bernoulli trials, the outcome of each trial being either breakdown or non-breakdown of the insulation tested. These properties, which are of a statistical nature, are analysed, and the results expected for various types of insulation and impulse waveshape are given and compared with existing experimental data where possible. The probable outcome of a series of $N$ impulse trials is shown to have a binomial distribution, and estimates of the errors involved are given. The effect of sample variation which applies particularly to tests on solid insulation is also treated briefly.

The paper provides a statistical background against which the results of impulse voltage experiments may be judged.

### LIST OF PRINCIPAL SYMBOLS

$I$ = Rate of appearance of electrons, etc., in the insulation.
$N$ = Number of impulse trials in a given test.
$n$ = Number of trials resulting in breakdown in time $t - t + \delta t$.
$P(t)$ = Probability that breakdown occurs within time $t$.
$p$ = Probability of breakdown for a trial at impulse voltage $V$.
$\bar{p}$ = Mean or expectation of $p$.
$S_N$ = Number of breakdowns in $N$ trials.
$t_1, t_2$ = Times corresponding to $V = V_0$.
$V$ = Impulse voltage.
$V_0$ = Threshold voltage, below which $\lambda = 0$.
$W$ = Probability that an electron, etc., causes a breakdown.
$\lambda = IW$ = Mean rate of occurrence of breakdown initiating events.
$\sigma$ = Standard deviation of $p$ = (Variance $p$)$^{1/2}$.

### (1) INTRODUCTION

The procedures adopted to determine the electric strength of insulating material, either alone or in assembled equipment, when subjected to impulse voltages are unlike those of most electrical measurements. The techniques have to allow for the fact that the impulse voltage is of a transient nature and that frequently a measurement cannot be repeated under identical conditions because of a change or even a failure of the test object. The impulse strength has to be decided on a statistical basis from the breakdown results of a given series of impulse applications either on a single test object or on a series of objects which are as uniform as possible, the reliability of the final estimate of the strength depending on the number of tests performed. The mathematical basis and the significance of the properties of this method of testing are not widely appreciated. The object of the paper is to outline the statistical nature of impulse testing so that practical results may be judged against a

statistical background. The separation of the statistical effects from the more physical processes of the actual breakdown discharge is important in the interpretation of such experiments. The analysis given uses a model which involves certain assumptions regarding the breakdown process. At present, this model appears to be definitely applicable to gas breakdown, and is also the likely model for impulse breakdown of pure liquids. Whether such a model is also applicable to certain forms of solid breakdown is not certain and must await further experimental evidence.

### (2) THE NATURE OF IMPULSE TESTS

The aspects of impulse breakdown measurements which are important for the present discussion are as follows:

(*a*) The outcome of a particular impulse voltage application to a test object has two possibilities, namely breakdown or non-breakdown, which might be termed success and failure, respectively. The probability of success, i.e. breakdown, is dependent on the duration and magnitude of the impulse voltage and also on the nature of the test object. Tests or trials of this sort which have two mutually exclusive outcomes of success and failure are termed Bernoulli trials, provided that they are independent.[1] A considerable portion of the theory of probability is concerned with trials of this sort and with the formulation of the statistical laws which are obeyed. We expect, therefore, that a series of impulse measurements will conform with the statistics of Bernoulli trials.

(*b*) A reliable impulse measurement can be obtained only from a series of similar impulse voltage applications, i.e. a series of trials or sampling operations. Such a measurement is different from those with direct or alternating voltages because the impulse voltage, of short duration, acts as a sampling probe, whereas continuous voltages provide monitoring of the test object over long periods. Theoretically, however, this difference disappears since direct voltage can be considered as an impulse of infinitely long duration. If a given impulse trial is to result in success, the breakdown must occur within the duration of the impulse, which may commonly be less than 100 microsec. Success will depend on the breakdown time-lag, therefore, and it is possible to apply an impulse at a voltage considerably above the direct or alternating voltage level without breakdown.

(*c*) Since an impulse measurement requires a series of similar trials for reliable interpretation, the effect of previous trials on a particular trial is important. Although this cannot be discussed generally, two main categories of breakdown may be distinguished, namely breakdown in insulants which are self-healing (gases and liquids) and in insulants which are damaged irrevocably (solid insulation). Insulants in the first category are frequently easy to test, and a series of Bernoulli trials can often be obtained, as, for instance, for a spark-gap in air. On the other hand, a test of a porcelain insulator in which puncture occurs is in the second category, since further tests must be made on a fresh insulator. This introduces the variation between insulation samples and reduces the overall accuracy of any estimate of impulse breakdown strength.

Correspondence on Monographs is invited for consideration with a view to publication.

Dr. Lewis is in the Electrical Engineering Department, Queen Mary College, University of London.

### (3) THE BREAKDOWN MECHANISM

The breakdown time-lag, which is the time between application of an impulse voltage and the collapse of voltage across the test object, can be divided into two intervals—a period up to the appearance of an initiating event which begins the breakdown process and then a further formative period during which the breakdown develops. The initiating event, which may be the appearance of an electron in a favourable position in the insulation, may be assumed to occur randomly in time and to be subject to statistical fluctuations, so that this period is referred to as the statistical lag. It is the randomness of this time-lag that causes impulse testing to depend on probability theory. Although the initiating events occur randomly, they will have a mean rate of occurrence $\lambda$ which might be assessed in a hypothetical experiment by counting over long periods of time.

The formative time-lag depends on the nature of the breakdown process, and its duration may change considerably with test conditions. In general, it will decrease with over-voltage and may be subject to fluctuations also.[2] It is clear that a breakdown cannot occur earlier than the formative time, but in certain cases, and especially for gases at large over-voltages, it is possible to ignore the formative lag in comparison with the statistical lag, as in the analysis of the next section. A further discussion on the formative lag is given in Section 7.

### (4) THEORETICAL BASIS

#### (4.1) Step-Function Voltages

Suppose that a test object is subjected to a step-function voltage, namely a voltage which, applied instantaneously at time $t = 0$, remains constant for $t > 0$, having a magnitude $V$. Provided that $V$ is greater than a certain threshold value $V_0$ (Fig. 1) breakdown will occur. Assuming that $\lambda$ is of the same
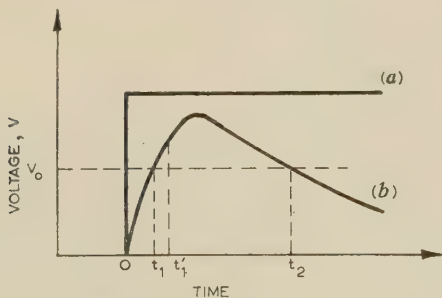


Fig. 1.—Test impulse voltages.

(a) Step-function voltage.
(b) Impulse $V = E(\varepsilon^{-\alpha t} - \varepsilon^{-\beta t})$.

form for each of a series of $N$ trials, $N$ being large, the probability $P(t)$ that a breakdown should occur within a time $t$ can be determined as follows. The number of trials, $n$, that result in breakdown in the interval $t - t + \delta t$ is, by definition,

$$n = N[P(t + \delta t) - P(t)]$$

which, in the limit, becomes

$$n = N P'(t)dt \quad . \quad . \quad . \quad . \quad . \quad (1)$$

Also we have

$$n = N[1 - P(t)]\lambda(t)dt \quad . \quad . \quad . \quad . \quad (2)$$

whence, from eqns. (1) and (2), we find after integration that

$$P(t) = 1 - \exp\left[-\int_0^t \lambda(t)dt\right] \text{ since } P(0) = 0 \quad . \quad (3)$$

Combining eqns. (2) and (3), $n$ may be expressed in the form

$$n = N\lambda \exp\left[-\int_0^t \lambda(t)dt\right]dt \quad . \quad . \quad . \quad (4)$$

Provided that $\lambda \neq 0$ a trial must always result in breakdown since $P(t) \to 1$ as $t \to \infty$. The above equations have frequently been applied to measurements with approximate step-function voltages for which $\lambda$ may be considered to be independent of time (see references cited by Saxe and Lewis[4]). Important deductions concerning the nature of $\lambda$ can be made in such cases since it is not difficult to show from eqn. (4) that the mean time lag for a large number of measurements is equal to $\lambda^{-1}$ and that the standard deviation (Appendix 14.2) is also equal to $\lambda^{-1}$. Such estimates can then be related to mechanisms of electron emission in the spark-gap under test.[4,5,6] However, the present paper is not primarily concerned with this aspect of impulse breakdown, and full accounts can be found in the literature cited.

#### (4.2) Finite Impulse Voltages

The usual test impulse voltage can be written as

$$V = E[\exp(-\alpha t) - \exp(-\beta t)] \text{ with } \beta \gg \alpha$$

$V$ now varies with $t$, and it is not possible to assume that $\lambda$ is constant as above, since generally $\lambda$ will be a function of $V$. As discussed in Section 5, $\lambda$ will be zero up to a threshold voltage $V_0$ and will then increase as $V$ increases above this value. Thus referring to Fig. 1, we may deduce from eqn. (3) that the probability of a breakdown for a particular impulse test, i.e. the probability $p$ of success in a trial with impulse voltage $V$ is given by

$$p = 1 - \exp\left[-\int_{t_1}^{t_2} \lambda(t)dt\right] \quad . \quad . \quad . \quad . \quad (5)$$

in which $t_1$ and $t_2$ correspond to the condition $V = V_0$. This result already has practical significance since it states the expected number of breakdowns in a large number of tests. It is, for instance, the spark-over ratio for a sphere spark-gap in air tested with the given impulse. Eqn. (5) will be discussed more fully in Section 6.

### (5) THE INITIATING EVENT

The parameter $\lambda$ has been defined as the mean rate of occurrence of breakdown initiating events. This definition visualizes an ideal experiment in which breakdown initiation can be recorded without the necessity for any further stages in the breakdown process; the test object recovering instantaneously after such an event. In practice, a continuous recording of these events is impossible because of the attendant breakdown, and a series of impulse trials as in Section 4 must be employed. The nature of this parameter, which is voltage dependent, will obviously depend greatly on the insulation under test, and can only be determined when the mechanism of breakdown is fully understood.

Only gases have been studied extensively, several investigators having discussed[3] the nature of $\lambda$. In an early treatment von Laue[7] considered that $\lambda$ consisted of the product of three factors: $I$, the number of primary electrons per unit time produced in the gas volume under stress between the electrodes, $w_1$ the probability that an electron appeared in a region suitable for spark initiation and $w_2$, the probability that the initiation did in fact, occur. The factors, $w_1$ and $w_2$, are really an artificial division, and we may consider that $\lambda$ equals $IW$, in which $W$ is the probability that an electron causes breakdown. Both $I$ and $W$ may vary with voltage $V$ and possibly with time also. The

magnitude of $I$ will be related to the degree of irradiation, whether natural or artificial, and when the field is sufficient, it will be augmented by electron emission from the cathode, thereby becoming dependent on $V$. On the other hand, $W$ will be zero below the threshold $V_0$ and will then increase with increasing $V$, finally becoming unity. It has been possible[8,9] to calculate $W$ and to give the voltage characteristic for some ideal cases. Such a characteristic is shown qualitatively in Fig. 2. If $I$ remains
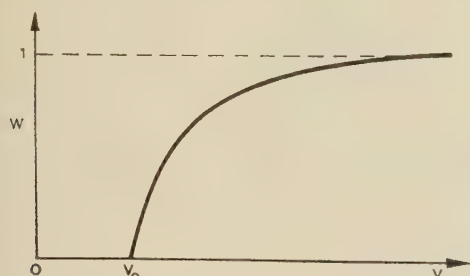


**Fig. 2.**—Typical variation of $W$ with voltage $V$.
This is also the shape of the $\lambda$ curve when $I$ remains constant.

constant, this Figure, to a different scale, also gives the form of $\lambda$ and would be applicable, for instance, to a sphere spark-gap in air at atmospheric pressure (Section 6). For highly compressed gases[10] and for small electrode spacings[4,5,6] the cathode field is great enough (greater than $5 \times 10^4$ volts/cm) to cause electron emission. This component of $I$, which will supplement that due to natural causes, may be expected to increase exponentially with the voltage $V$, producing the characteristic shown in Fig. 3. Both types of characteristic will be discussed in Section 6.
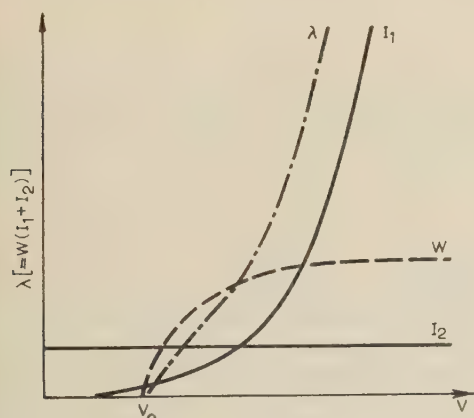


**Fig. 3.**—Variation of $\lambda$ with $V$ when $I$ is field-dependent.
$I = I_1 + I_2$, where $I_1$ is field-dependent and $I_2$ is due to external irradiation.

When the field becomes very non-uniform as in a point-plane or rod-gap arrangement, the limits of $W$ are likely to be extended over a very much greater voltage range, and probably $W$ will approach unity only asymptotically. There would be a corresponding effect on $\lambda$, but the general shape of the characteristics (Figs. 2 and 3) would not be seriously altered.

For liquid and solid insulation no clear picture of the nature of $\lambda$ has yet emerged. From work on the statistical time lag of pure liquids in the author's laboratory it would seem that the breakdown process is similar to that for gases and that we may postulate $\lambda = IW$ with a significance as for gases. It also seems likely that insulating oils come into the same category if the definition of $I$ is broadened to include initiations by ionic

impurity, by dust particles and by ionization in gas bubbles in the oil. Figs. 2 and 3 are then still applicable to illustrate the conditions in which $\lambda$ is dependent or otherwise on the applied voltage. Since the breakdown fields may often be as great as $10^6$ volts/cm, dependence on voltage is much more probable than in gases.

A complicating factor which would involve a different statistical behaviour and prevent the application of the present analysis is the possibility of a significant formative time lag. If this lag is constant it may easily be accounted for as in Section 7, but if it fluctuates and is voltage dependent in a complicated way, the results in the paper may not apply. These reservations, which may hold for some tests on liquids, are even more applicable to solids. Breakdown phenomena in solids appear to involve several distinct mechanisms[11] and are complicated by formative time lags which can be much larger than the statistical one. In some cases, as reported by Whitehead,[12] tests on homogeneous insulation under intrinsic breakdown conditions have yielded very short time lags ($10^{-7}$ sec) which could be related to large values of $\lambda$. If, under the high breakdown stress ($10^6$–$10^7$ volts/cm), a considerable number of free electrons arise in these materials, then with $I$ large, $W$ need not greatly exceed zero. The result would be an impulse ratio $V/V_0$ close to unity, as has indeed been observed. However, these are special cases, and for the majority of solid insulating materials including the insulants of engineering importance in which voids and other non-homogeneous regions may exist, the present statistical model for the time-lag distribution may not apply.

Lastly it should be noted that, for both liquids and solids, the discharge following a breakdown impairs the insulating property, destroying it altogether in the case of solid insulation. This prevents further tests on the same sample. Thus, a series of tests is complicated by the variations in samples and a further variable is thereby introduced. The effect of this extra variable will be discussed briefly in Section 10.

## (6) THE PROBABILITY OF BREAKDOWN

We now return to consider equation (5) for a typical case of gas breakdown in which $I$ is determined by natural causes. Suppose that the peak value of the impulse is greater than that required to attain the condition $W = 1$, then to a good approximation we may write $\lambda = I$ over the range $t_1$–$t_2$ in eqn. (5), or alternatively we may assume that $\lambda$ is independent of voltage over this range. Eqn. (5) then becomes

$$p = 1 - \varepsilon^{-I(t_2 - t_1)} \quad . \quad . \quad . \quad . \quad (6)$$

Fig. 4 shows values of $p$ computed from eqn. (6) for $0 \cdot 5/5$ and $1/50$ microsec impulses at various impulse ratios $V/V_0$ corresponding to over-voltages $V - V_0$. These results indicate the sensitiveness of $p$ to both $I$ and the waveshape. Since the approximate form eqn. (6) has been used, the results will tend to become inaccurate at small values of $p$ corresponding to small over-voltages. In this region, shown by dotted lines beginning at $V_0$ in Fig. 4, $W$ increases from zero up to unity. The foot of the probability curve will be determined by the variation of $W$ and will be prominent when $W$ extends over a wide range as might particularly occur for non-uniform field distributions. The theoretical results (Fig. 4) are strikingly supported by experimental evidence given in the papers by Garfitt,[13] Meek[14] and Ganger.[15] These authors investigated the impulse breakdown of sphere-gaps in air and the physical factors which influenced the scatter of measurements without always paying due regard to the statistics involved. For instance, Meek indicates a linear relationship between percentage breakdown $p$ and voltage $V$, although his experimental observations fit curves similar to
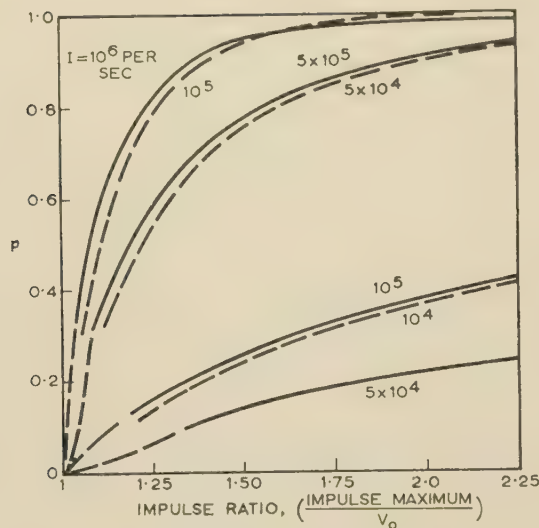
Fig. 4.—Dependence of the probability of breakdown on over-voltage.

——————— 0·5/5 microsec wave.
— — — — 1/50 microsec wave.

Fig. 4. The results given by Garfitt and Ganger and the additional results by Miranda[16] are also in close agreement with Fig. 4. All these authors find that increased irradiation $I$ causes the experimental probability curves to move to lower voltages and to become steeper, which is again in agreement with the theoretical deductions here. Fig. 5 shows a typical set
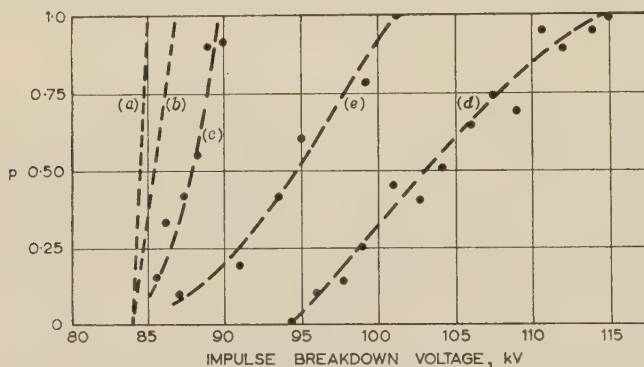


Fig. 5.—Dependence of breakdown probability $p$ on over-voltage.

Results obtained by Meek for a 3·0 cm gap between 12·5 cm diameter spheres.
(a), (b) and (c) Positive 1/5 microsec impulse wave. Effect of decreasing amounts of irradiation, i.e. reduction in $I$.
(d) Positive 1/5 microsec wave. Gap unirradiated.
(e) Positive 1/500 microsec wave. Gap unirradiated.

of results as obtained by Meek.[14] The effect of waveshape is shown most clearly by the results given by Garfitt.[13] As expected from eqn. (6), the condition $p = 0·5$ is found to move to higher voltages as the wavetail falls to half value in a shorter time, but more significant is the fact that a similar effect is found as the slope of the wavefront decreases. Since an increase of wavefront duration increases $t_1$ (Fig. 1) there will be a corresponding decrease in $p$ for a given voltage level. Thus the explanation given by Meek,[14] that the slower wavefront sweeps ions from the gap and so gives higher impulse breakdown voltages, may not be entirely correct.

There seems to be little relevant information concerning gas

breakdown between electrodes other than spheres. Miranda[16] gives a characteristic for six condenser bushings in parallel and states that additional irradiation does not affect the results, showing that $I$ was naturally large, probably as a result of corona and surface discharges. The shape of the characteristic was similar to those in Fig. 4. Most of the reports for rod-gaps and various forms of line insulators[17, 18] give information for the condition $p = 0·5$ only, and not the full breakdown characteristic. However, judging by the large discrepancies frequently occurring in measurements from different sources, a statistical influence was almost certainly present.

For very small gaps[4, 5, 6] highly compressed gases[10] and many pure liquids,[19] $I$ will be dependent on $V$, as in Fig. 3. The breakdown characteristic will now be similar to that for large values of $I$; in fact there may be an abrupt increase in $\lambda$ from small values corresponding to the foot of the $W$ curve up to nearly unity at slightly higher voltages. The test object would show a distinct impulse breakdown value with just a small probability of breakdowns below this value. These low values might be attributed, in practice, to inconsistencies, but would really be the expected result of a consistent series of trials. Experimental evidence concerning this exists for pure hydrocarbon liquids,[19] in which there is a clear distinction between breakdown and non-breakdown.

For certain forms of solid insulation, abrupt changes between the conditions $p = 0$ and $p = 1$ have been reported which would be in agreement with eqn. (5) when the exponent is large. In extreme cases even when $W$ is small, $\lambda$ is still large and $p$ is close to unity, giving an impulse ratio which is also near unity.[1]

It is relevant at this stage to comment on the effect of chopped waves as frequently used in tests on transformer windings. Suppose that the duration of the chopped wave is $T$, eqn. (5) can be written as

$$p = 1 - \exp\left[ -\int_{t_1}^{T} \lambda(t)\,dt \right] \quad . \quad . \quad . \quad . \quad (7)$$

Unless the chopped wave is accurately controlled and consistent, erratic results may be obtained. If a rod gap is used for chopping, $T$ is ill defined, and this will cause $p$ to vary considerably from test to test and no consistent result may appear. Circuits which control the chopping time $T$ have been introduced.[20]

### (7) EFFECT OF THE FORMATIVE TIME-LAG

The formulae developed so far have neglected the possible effect of a significant formative lag. This represents a dead time following the attainment of the condition $V = V_0$. If the formative lag is constant, eqn. (5) may be employed by substituting a time $t_1'$, instead of $t_1$, where the interval $t_1' - t_1$ represents the formative lag (Fig. 1). This is equivalent to stating that $W$ departs from zero, not at time $t_1$ but at $t_1'$. In gases, formative time lags greater than about 1 microsec are observed only when the over-voltage is less than a few per cent, so that it is safe to assume that the formative lag in gases will be appreciably less than 1 microsec for all impulse measurements having engineering usefulness. A similar condition appears to apply also to impulse breakdown of liquids unless the over-voltage is very small. In these cases, the reduction of the interval of integration required in eqn. (5) can be neglected whenever the over-voltage is greater than a few per cent.

In the case of solid breakdown, the formative time lag cannot be included in the analysis in such a straightforward manner. Experimental evidence[11, 12] indicates that the time lag might be very short ($< 10^{-7}$ sec) or very long (several microseconds) even under conditions of intrinsic breakdown. If the formative lag

varies in a complicated way with over-voltage or is subject to
the random fluctuations between large and small values or is
in any way dependent on the previous history of the sample,
the time lag distribution specified by eqns. (3), (4), and (5) will
not be realized.

## (8) ACCURACY OF MEASUREMENT

Assessment of experimental breakdown probabilities should
include the fact that frequently they have been obtained from
comparatively few trials. For instance, Meek[14] uses only ten
trials to obtain a particular value of $p$, while Ganger[15] uses 50.
In some cases there is no indication of the number of trials
involved.[17, 18] The theory developed so far has been based on a
large number of trials, but whenever the number is small there
is a definite and computable expected error which is quite
distinct from error arising from any lack of precise experimental
control.

The definition of the probability of breakdown $p$ [eqn. (5)]
is based on the intuitive argument that in a large number, $N$, of
independent but identical trials, the number of breakdowns will
be $pN$. In practice $N$ must remain finite and frequently is a
small number less than 100. With such a condition, an estimate
of the accuracy with which $p$ might be determined is required.
This is important in determining the significance of impulse
measurements in general, and particularly so when only a few
breakdown trials are possible, as often happens when testing
equipment involving solid insulation.

Let $S_N$ be the number of breakdowns in $N$ trials, each trial
having a probability $p$ for breakdown. The probability that
$S_N = k$ is given by the well-known binomial distribution,[1]
namely

$$P_r(S_N = k) = \binom{N}{k} p^k (1 - p)^{N-k} \quad . \quad . \quad . \quad (8)$$

This distribution has the expected mean value $pN$ and a standard
deviation $[p(1 - p)N]^{1/2}$. It is possible to replace the binomial
distribution by an asymptotic form involving the normal distri-
bution[1] which is more convenient for computation.

Thus $\quad \mathbf{P}_r(S_N = k) \sim [p(1 - p)N]^{-1/2} \phi\left\{\dfrac{k - pN}{[p(1 - p)N]^{1/2}}\right\} \quad . \quad (9)$

in which $\phi(x) = (2\pi)^{-1/2} \exp(-x^2/2)$ is the normal density
function. Although this is an asymptotic formula, the accuracy
is surprisingly good even for small values of $N$. The estimated
value of $p$ from a test will be $S_N/N$, resulting in percentage
distribution curves as shown in Fig. 6.

If $N$ is kept fixed, the standard deviation becomes a maximum,
having the value $\frac{1}{2}N^{-1/2}$ when $p = 0.5$, i.e. the maximum dis-
persion occurs at the 50% breakdown point. This is important
since the usual specifications for impulse testing adopt this 50%
criterion, and it would seem that it is not ideal since a 90%
criterion, say, could be obtained to the same accuracy with
fewer observations. If due regard is paid to the slope of the
$p/V$ curve (Fig. 4) it will be seen that this is not necessarily true
since $p$ is less sensitive to voltage change in the neighbourhood
of the 0·9 point. It is, however, true that optimum conditions
may not be obtained with a 50% criterion if the slope of the $p/V$
curve does not change greatly between, say, the 0·5 and 0·8
points.

Conclusions concerning the accuracy of results can be obtained
in an alternative and more useful way as follows: We wish to
establish the probability with which the estimated value of $p$,
i.e. $S_N/N$, may differ from the true value by less than an amount
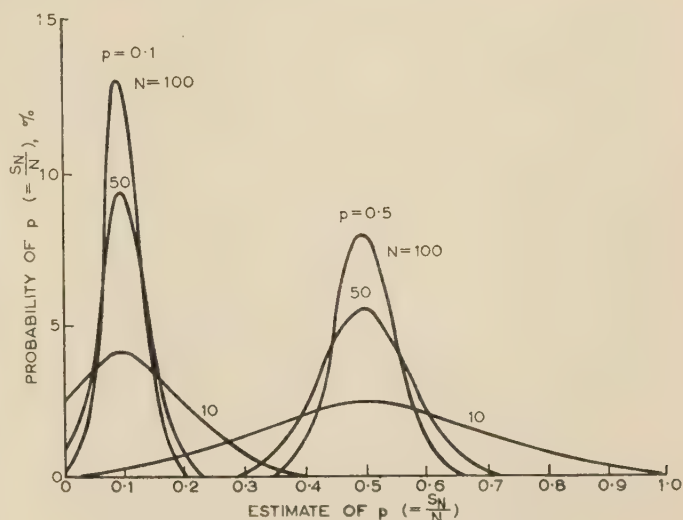$\eta$ say. Alternatively, we wish to know the requisite value of $N$



Fig. 6.—Distribution of the estimated value of $p$.
The possible error in the estimate decreases as $|p - 0.5|$ increases and as $N$ increases.

such that the difference $\eta$ has a probability greater than $\alpha$, say.
The formal statement is

$$P_r\left(\left|\frac{S_N}{N} - p\right| < \eta\right) > \alpha \quad . \quad . \quad . \quad (10)$$

Using eqn. (9) it may be shown (Appendix 14.1) that eqn. (10)
is approximately equivalent to

$$\Phi\left\{\eta\left[\frac{N}{p(1 - p)}\right]^{1/2}\right\} > (\alpha + 1)/2 \quad . \quad . \quad (11)$$

in which $\Phi(x)$ is the normal distribution function

$$(2\pi)^{-1/2} \int_{-\infty}^{x} \exp(-\tfrac{1}{2}y^2) dy$$

As an example, suppose a value $p = 0.9$ or a 90% breakdown
ratio is to be attained with an error of less than 5% at a con-
fidence level of 95%. Thus $\eta = 0.05$ and $\alpha = 0.95$, and from
Tables[21] of the function $\Phi(x)$ we find that $N \simeq 140$. However,
if a ratio of 50% is required with the same tolerances, $N \simeq 400$.
Again, for a ratio of 50% the likely error [with a 95% confidence
level and using the exact eqn. (21)] is 9·3% for $N = 100$ and as
great as 26% for $N = 10$. Since practically all the results
reported by Meek[14] have been obtained with $N = 10$, it is not
surprising that a large degree of scatter was found. Less
statistical error will occur in the results of Ganger[15] since he
used $N = 50$. A similar comment may be made concerning
many other impulse breakdown results. It is suggested that
reported differences in impulse measurements by various workers
may be due, not to lack of control in the measurements as so
often supposed, but merely to a property of the statistical pro-
cesses involved. A realization of this might allow more correct
interpretations, especially in those cases where very few trials
are possible.

## (9) NUMBER OF TRIALS BEFORE BREAKDOWN

It may occur that a sequence of trials will not cause break-
down. If, for a particular measurement, the total number of
trials is small, it is possible that a breakdown will not occur,
thus giving a false impression of the impulse strength of the test
object. It is therefore useful to know the probability for a given
number of successive trials not resulting in breakdown.

The probability that the first breakdown in a sequence occurs on the $m$th trial is $p(1-p)^{m-1}$, and the probability of a breakdown not occurring in the whole sequence is $(1-p)^N$. This latter probability is shown as a function of $N$ for various values of $p$ in Fig. 7. If $N = 10$, there is a significant probability of
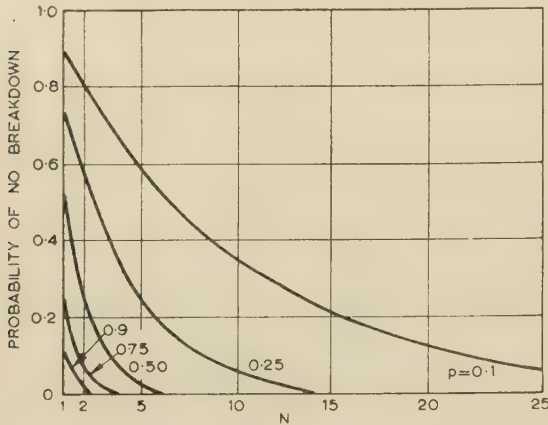


Fig. 7.—Probability of breakdown not occurring in a sequence of trials.

not recording a breakdown when $p < 0.25$ and this probably accounts for the frequent omission of results at the lower end of percentage breakdown curves.[14] There are also more far-reaching effects which will occur when $N \leqslant 10$, in measurements where the impulse breakdown strength is determined by a set of $N$ trials at a particular voltage level followed by similar sets at increasing voltage levels until breakdown occurs. Standard specifications invariably involve such a procedure. Measurements made in this way can give a false idea of the statistics involved, since the procedure tends to reduce the natural scatter in results and to raise the breakdown level. A full discussion of this, which concerns the statistics of test sequences, cannot be attempted here.

### (10) TEST SAMPLE DISTRIBUTIONS

It is frequently impossible to test identical samples in a series of trials because either breakdown ruins each sample or, if breakdown does not occur, each trial by a process of fatigue alters the insulation properties.[12] Thus, instead of postulating a constant value of $p$ in a series of trials, we have to consider that $p$ itself has a probability distribution for the samples tested. The distribution may assume a variety of forms, and if fatiguing occurs, the theory of test sequences will be involved. In the present treatment fatigue is not considered and only sample variation is included, i.e. it is assumed that the $p/V$ curve for each sample varies in position along the voltage axis. The $N$ trials at voltage $V$ then have breakdown probabilities $p_1, p_2 \ldots p_N$, and we need to consider the sum $S_N$ (the number of breakdowns in $N$ trials) as in Section 8. As shown in Appendix 14.2 the useful parameters of the distribution of $S_N$, namely the expectation and the variance, are

$$E(S_N) = \sum_{j=1}^{N} p_j \quad . \quad . \quad . \quad . \quad . \quad (12)$$

$$\text{Var}(S_N) = \sum_{1}^{N} p_j - \sum_{1}^{N} p_j^2 \quad . \quad . \quad . \quad (13)$$

The $p_j$ terms will themselves have a distribution with a discrete frequency distribution function $f_s(p_s)$ such that, in the $N$ trials,

$Nf_s(p_s)$ will have the breakdown probability $p_s$. Thus, from eqns. (12) and (13),

$$E(S_N) = N \sum f_s(p_s) \times p_s = N E(p) \quad . \quad . \quad . \quad (14)$$

and

$$\text{Var}(S_N) = N[\sum f_s p - \sum f_s p_s^2] = N[E(p) - E(p^2)] \quad . \quad . \quad . \quad . \quad (15)$$

If the distribution of $p$ has a mean value $\bar{p}$ and a standard deviation $\sigma$, then, from eqns. (14) and (15) and Appendix 14.2,

$$E(S_N) = N\bar{p} \quad . \quad . \quad . \quad . \quad . \quad (16)$$

$$\text{Var}(S_N) = N[\bar{p}(1-\bar{p}) - \sigma^2] \quad . \quad . \quad . \quad (17)$$

which revert to the results given in Section 8 when $\sigma = 0$. It should be noted that the above results have been obtained without knowledge of the distribution function of $S_N$ which
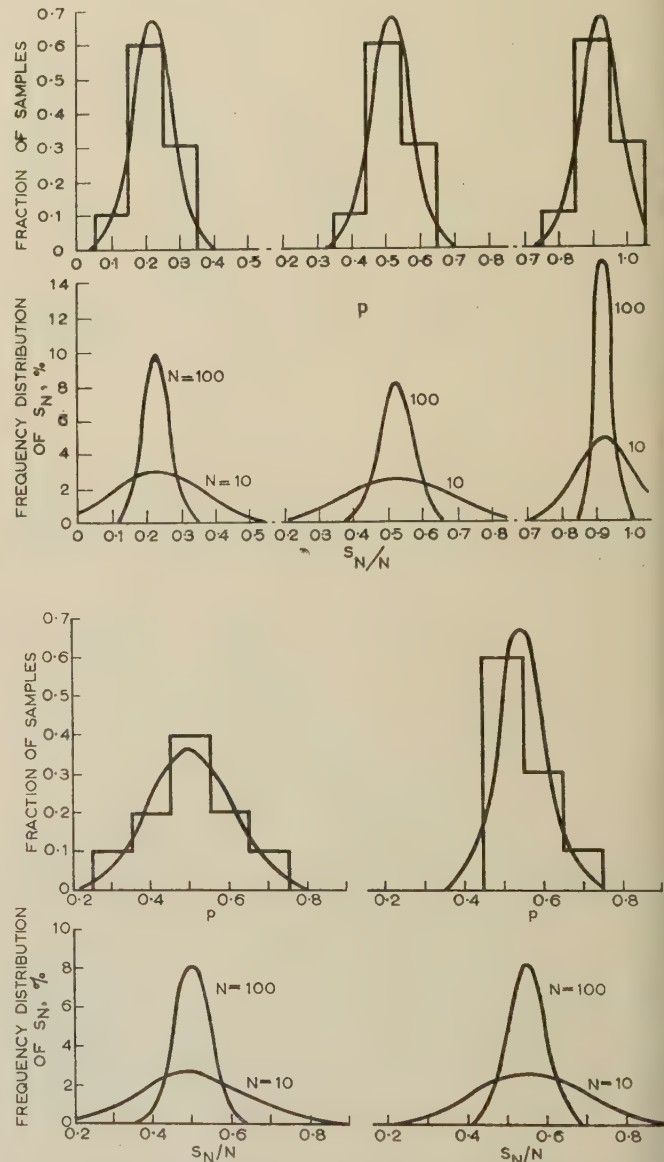




Fig. 8.—Comparison of actual and calculated distributions of $p$ from $S_N$.

Actual distributions of $p$ shown as histograms.
Distributions of $S_N$ are shown for $N = 10$ and 100 in each case. Distributions of $S_N$ and $p$ (calculated) are assumed to be normal.

will now no longer be of strict binomial form, although the deviation will be small if $\sigma$ is small and the estimates of probable error [eqns. (10) and (11)] could then be used. If values of $E(S_N)$ and Var $(S_N)$ can be found from tests, both $\bar{p}$ and $\sigma$ for the samples tested may be estimated using eqns. (16) and (17). In general, for this type of testing, $N$ will not be large since the number of samples will be limited and the accuracy will then be small. As examples of the results to be expected and of the accuracy with which the sample distribution of $p$ may be obtained, certain discrete distributions of $p$ have been assumed, and the corresponding estimates of the distribution have found from eqns. (12), (13), (16) and (17). The results are shown in Fig. 8. In this Figure histograms representing the actual distribution of among the individual samples of a given test series have been assumed. With these histograms, the expectation and variance of $S_N$ can be found from eqns. (12) and (13). If the distribution of $S_N$ is now assumed to be normal, $S_N/N$ can be drawn as in Fig. 8. At the same time, using eqns. (16) and (17) the estimated mean and standard deviation of $p$ can also be found. Assuming normality once more, the distribution of $p$ has been superimposed on the original histograms in Fig. 8. The asymmetric distributions of $p$ probably occur frequently in practice where attempts are made to produce consistent test samples by controlled preparation. Lapses in control will tend to produce a proportion of samples having lower strengths and therefore larger values of $p$ at a given voltage. Estimates of $\sigma$ from results of $S_N$ as in Fig. 8 will be inaccurate unless the sample variation is actually large, but a useful guide to this variation can usually be obtained. On the other hand an estimate of the mean, $\bar{p}$, can be obtained with reasonable accuracy especially if approaches unity (see Section 8).

## (11) CONCLUSIONS

The treatment given has been designed to show, first, that all impulse tests are dependent on the basic points given in Section 2 and embodied in eqn. (5), and secondly, that there are definite results to be expected from this type of testing which are of a statistical nature and distinct from any physical properties. The estimates of scatter to be expected when the number of trials is small [eqn. (10)] and the probable number of trials before a breakdown occurs (Section 9) provide a useful background in assessing the significance of experimental results. Probability theory is particularly applicable in the standardization of impulse voltage measurement with sphere-gaps[13, 14, 15] and confirms the importance of irradiation and the effect of waveshape.

There are further applications of the theory which have not been investigated. For instance, the effects of particular test procedures should be assessed. The statistical results will be modified if tests are made in which a chosen number of trials are made at each of several increasing voltage levels until breakdown occurs or in sequential tests in which the voltage level for a particular trial is determined by the outcome of the previous trial. The statistics will also be modified in tests in which fatigue occurs. The outcome of a trial then depends on the history of trials. Impulse tests on solid insulation are very likely to come into this category. The investigation of such statistics would be complicated but worth while in providing a basis on which experimental results might be judged.

## (12) ACKNOWLEDGMENTS

## (13) REFERENCES

(1) FELLER, W.: 'Probability Theory and its Applications' (John Wiley, 1950).

(2) MEEK, J. M., and CRAGGS, J. D.: 'Electrical Breakdown of Gases' (Oxford Clarendon Press, 1953) Chapters 4 and 6.

(3) MEEK, J. M., and CRAGGS, J. D.: *ibid.*, p. 111 and Chapter 8.

(4) SAXE, R. F., and LEWIS, T. J.: 'Measurement of the Statistical Time Lag of Breakdown in Gases and Liquids', *British Journal of Applied Physics*, 1955, **6**, p. 211.

(5) LLEWELLYN JONES, F., and DE LA PERRELLE, E. T.: 'Field Emission of Electrons in Discharges', *Proceedings of the Royal Society*, A, 1953, **216**, p. 267.

(6) LLEWELLYN JONES, F., and MORGAN, C. G.: 'Surface Films and Field Emission of Electrons', *ibid.*, 1953, **218**, p. 88.

(7) VON LAUE, M.: 'Remarks on K. Zuber's Measurement of Time of Lag with Spark Discharge', *Annalen der Physik*, 1925, **76**, p. 261.

(8) WIJSMAN, R. A.: 'Breakdown Probability of a Low Pressure Gas Discharge', *Physical Review*, 1949, **75**, p. 833.

(9) GREY MORGAN, C., and HARCOMBE, D.: 'Fundamental Processes of the Initiation of Electrical Discharges', *Proceedings of the Physical Society*, B, 1953, **66**, p. 665.

(10) HOWELL, A. H.: 'Breakdown Studies in Compressed Gases', *Transactions of the American I.E.E.*, 1939, **58**, p. 193.

(11) MASON, J. H.: 'Breakdown of Solid Dielectrics in Divergent Fields', *Proceedings I.E.E.*, Monograph No. 127, April, 1955 (**102 C**, p. 254).

(12) WHITEHEAD, S.: 'Dielectric Breakdown of Solids' (Oxford Clarendon Press, 1951), p. 89.

(13) GARFITT, D. E. M.: 'The Measurement of Impulse Voltages by Means of Small Sphere-Gaps', *Proceedings of the Physical Society*, 1942, **54**, p. 109.

(14) MEEK, J. M.: 'The Influence of Irradiation on the Measurement of Impulse Voltages with Sphere-Gaps', *Journal I.E.E.*, 1946, **93**, Part II, p. 97.

(15) GANGER, B. P.: 'The Influence of Irradiation on the Impulse Breakdown of Sphere-Gaps', *Brown Boveri Review*, 1953, **40**, p. 215.

(16) MIRANDA, F. J.: Discussion on Reference 14, *Journal I.E.E.*, 1946, **93**, Part II, p. 112.

(17) ALLIBONE, T. E.: 'International Comparison of Impulse Voltage Tests', *Journal I.E.E.*, 1937, **81**, p. 741.

(18) WEDMORE, E. B.: 'Surge Phenomena' (British Electrical and Allied Industries Research Association, 1941), Part IV.

(19) MACFADYEN, K. A.: 'Some Researches into the Electrical Conduction and Breakdown of Liquid Dielectrics', *British Journal of Applied Physics*, 1955, **6**, p. 1.

(20) JOHNSON, G. H.: 'An Impulse Generator Circuit for Chopped Waves on Transformers', *Transactions of the American I.E.E.*, 1953, **72**, Part III, p. 839.

(21) LINDLEY, D. V., and MILLER, J. C. P.: 'Cambridge Elementary Statistical Tables' (Cambridge University Press, 1953).

## (14) APPENDICES

### (14.1) Probable Error in Estimates of $p$

Let us consider the probability that $S_N$ should lie between the limits $\alpha$ and $\beta$.

This is equal to the sum of the probabilities that $S_N = k$, where $\alpha \leqslant k \leqslant \beta$. Using eqn. (9) this may be stated as

$$P_r\,(\alpha \leqslant S_N \leqslant \beta) \sim [Np(1-p)]^{-1/2} \sum_{k=\alpha}^{k=\beta} \phi(x_k)$$

in which $\phi(x)$ is the normal density function $(2\pi)^{-1/2} \exp(-x^2/2)$ and

$$x_k = (k - Np)[Np(1-p)]^{-1/2} \quad . \quad . \quad . \quad (18)$$

2

Replacing the summation by the integral which it approaches asymptotically,

$$P_r\,(\alpha \leqslant S_N \leqslant \beta) \sim \int_{x_{\alpha-\frac{1}{2}}}^{x_{\beta+\frac{1}{2}}} \phi(x)dx \equiv \Phi(x_{\beta+\frac{1}{2}}) - \Phi(x_{\alpha-\frac{1}{2}})\,. \quad (19)$$

where $\Phi(x)$ is the normal distribution function $\int_{-\infty}^{x} \phi(x)dx = (2\pi)^{-1/2} \int_{-\infty}^{x} \exp(-\frac{1}{2}y^2)dy$. Eqn. (19) is a statement of the De Moivre–Laplace limit theorem.

Comparing the limits $\alpha$, $\beta$ with the corresponding limits in eqn. (10) we have $\alpha = N(p - \eta)$, $\beta = N(p + \eta)$ so that, using eqn. (18), eqn. (19) can be written

$$P_r\left(\left|\frac{S_N}{N} - p\right| < \eta\right) \sim \Phi\left\{\frac{N\eta + \frac{1}{2}}{[Np(1-p)]^{1/2}}\right\}$$

$$- \Phi\left\{\frac{-N\eta + \frac{1}{2}}{[Np\,(1-p)]^{1/2}}\right\} = 2\Phi\left\{\frac{N\eta + \frac{1}{2}}{[Np\,(1-p)]^{1/2}}\right\} - 1 \quad . \quad (20)$$

since $\Phi(-x) = 1 - \Phi(x)$.

Thus, combining eqns. (20) and (10),

$$\Phi\left\{\frac{N\eta + \frac{1}{2}}{[Np(1-p)]^{1/2}}\right\} > \frac{1}{2}(\alpha + 1) \quad . \quad . \quad (21)$$

From this equation, if $N$, $p$ and $\alpha$ are known, $\eta$, the probable error in the estimate of $p$, may be computed from Tables[21] of $\Phi(x)$.

A less exact form of eqn. (21), which becomes more accurate as $N$ increases and is much easier to use in cases where $N$ has to be computed for given values of $p$, $\eta$ and $\alpha$, is

$$\Phi\left\{\frac{N\eta}{[Np(1-p)]^{1/2}}\right\} > \frac{1}{2}(\alpha + 1)$$

which corresponds to the Laplace limit theorem.[1]

### (14.2) Expectation and Variance

Probability distributions are conveniently described by certain parameters of the distribution, of which the expectation or mean and the variance are most important. Let us suppose that a random variable $X$ assumes the discrete values $x_1, x_2, \ldots$ with probabilities $f(x_1), f(x_2), \ldots$, the expected value of $X$ is defined by

$$E(X) = \Sigma f(x_j)x_j = \bar{x} \quad . \quad . \quad . \quad (22)$$

the summation being made over all possible values of the variable. Obviously by definition we also have the second moment

$$E(X^2) = \Sigma f(x_j)x_j^2 \quad . \quad . \quad . \quad (23)$$

It is convenient to introduce a new variable $X - \bar{x}$, which is the deviation from the mean and which has the property $E(X - \bar{x}) = 0$. The second moment is not zero, however, since

$$E[(X - \bar{x})^2] = \Sigma f(x_j)(x_j^2 - 2x_j\bar{x} + \bar{x}^2)$$

$$= E(X^2) - \bar{x}^2$$

This second moment is termed the variance of $X$ and therefore

$$\mathrm{Var}\,(X) = E(X^2) - \bar{x}^2 = \sigma^2 \quad . \quad . \quad (24)$$

The positive square root of Var $(X)$ is $\sigma$, the standard deviation of $X$, and is a measure of the dispersion of the distribution about the mean.

In Sections 8 and 10 we are interested in the sum, $S_N$, of random variables, $X_1, X_2, \ldots, X_N$, and it is not difficult to show provided that $X_1, X_2$, etc., are mutually independent, that

$$E(S_N) = \sum^{N} E(X_j) \quad . \quad . \quad . \quad (25)$$

and

$$\mathrm{Var}\,(S_N) = \sum^{N} \mathrm{Var}\,(X_j) \quad . \quad . \quad . \quad (26)$$

$X_j$ is a random variable corresponding to a Bernoulli trial and assumes the values zero and unity with probabilities $1 - p_j$ and $p_j$. Therefore, from eqns. (22) and (23), $E(X_j) = E(X_j^2) = p_j$ and from eqn. (24), Var $(X) = p_j(1 - p_j)$. Substitution in eqns. (25) and (26) gives

$$E(S_N) = \sum^{N} p_j$$

$$\mathrm{Var}\,(S_N) = \sum^{N} p_j(1 - p_j)$$

If $p_1, p_2$, etc., are all equal to $p$, then $E(S_N) = Np$ and Var $(S_N) = Np(1 - p)$ as in Section 8.

# THE THERMAL PROPERTIES OF HIGH-VOLTAGE INSULANTS

## By P. H. G. ALLEN, B.Sc.(Eng.), A.M.I.Mech.E., Associate Member.

### SUMMARY

Lack of agreement between published values of the thermal properties of high-voltage insulants necessitates the development of relatively simple methods for their measurement. Transient methods for the determination of the thermal diffusivity of solids and thermal conductivity of fluids are described, with examples of their use and an estimate of their accuracy. Allowance is made for anisotropy in the case of solids. Suitable methods for determination of specific heat are discussed, and the importance of the rate of change of density of liquids with temperature is stressed.

### LIST OF SYMBOLS

$k$ = Thermal conductivity of solid or fluid, watt per deg C-in.

$\alpha$ = Thermal diffusivity of solid or fluid, rad²/min or in²/sec. Suffixes $z$, $r$ and $c$ indicate value in axial, radial and circumferential directions, respectively, for solid cylindrical specimens.

$\rho$ = Density of solid or fluid, lb/in³.

$c_p$ = Specific heat per unit mass of solid or fluid, joules per deg C-lb.

$\theta_1$ = Specimen surface temperature for time $t < 0$, deg C.

$\theta_2$ = Specimen surface temperature for time $t > 0$, deg C.

$\theta$ = Temperature at point considered in solid or fluid, or along fine wire, deg C.

$t$ = Time, min or sec.

$A$ = Function (numeric) of position of point in solid = F($r$, $z$), say, for cylindrical specimen.

$B_c$ = Function of overall dimensions and material diffusivities for solid specimen.

$$= -\left[\alpha_z\left(\frac{\pi}{2c}\right)^2 + \alpha_r(x_1)^2\right]$$ for a hollow cylindrical

specimen, axial length $2c$.

$x_1$ = First root of the equation

$$J_0(x)Y_0\left(\frac{r_o}{r_i}x\right) - J_0\left(\frac{r_o}{r_i}x\right)Y_0(x) = 0$$

$J_0$, $Y_0$ = Bessel functions of the first and second kind, respectively, zero order.

$B_a$, $B_b$ = Functions (per minute) as $B_c$, but for axial lengths $2a$ and $2b$, respectively.

$a, b, c$ = Half-axial lengths ⎫ of hollow cylindrical specimens
$r_o$ = Outer radius ⎬ measured in multiples of $r_i$,
$r_i$ = Inner radius ⎭ rad.

$\epsilon$ = Percentage error in determination of $B_c$.

$\theta_s$ = Actual surface temperature of specimen, deg C.

$C'$, $\tau$ = Coefficient (numeric) and thermal time-constant (min) derived empirically to define the variation of $\theta_s$ with time, according to the equation

$$\theta_s = (\theta_2 - \theta_1)(1 - C'\varepsilon^{-t/\tau})$$

$\epsilon_d$ = Percentage error due to deviation of $\theta_s$ from step-function form.

$\theta_p$ = Temperature rise after time $t_p$ of a line source emitting thermal energy at a constant rate, deg C. (Similarly for suffix $q$.)

$q$ = Constant thermal-energy release rate in fine wire representing line source, watts/in.

$I$ = Current through the fine wire, amp.

$R$ = Resistance of the fine wire, ohms.

$V$ = Potential drop across the fine wire, volts.

$2l$ = Length of the fine wire, in.

$C, S, G$ = Thermal capacity (joules per deg C-in), thermal resistance (deg C/watt-in), and thermal conductance to ambient (watt per deg C-in), respectively, per unit length of the fine wire.

$g_m$ = Mutual conductance of valve employed in constant-power circuit, amp/volt or mA/volt.

$v_g$ = Control-grid potential of valve employed in constant-power circuit, volts.

$\Delta V$, $\Delta v_g$ = Change in $V$ and $v_g$, respectively, under constant-power conditions.

$\Delta R$ = Change in $R$ under constant-power conditions, ohms.

$\Delta I$ = Change in $I$ under constant-power conditions, amp.

$M_m$, $c_m$ = Mass (lb) and specific heat per unit mass (joules per deg C-lb) of substance M. (Similarly for suffix $n$.)

$W$ = Thermal capacity (water equivalent) of calorimeter, cal/deg C.

$R_\theta$ = Cooling rate of calorimeter, deg C/h.

$K_\theta$ = Cooling constant of calorimeter, cal/h.

$W_T$ = Total thermal capacity of calorimeter, with contents, cal per deg C.

$R_{\theta m}$ = Cooling rate of calorimeter containing substance M, deg C/h. (Similarly for suffix $n$.)

$\nu$ = Kinematic viscosity of fluid, stokes.

$\mu$ = Dynamic viscosity of fluid, poise.

$\beta$ = Coefficient of change of density with temperature, per deg C

$$= \frac{\rho_d - \rho_e}{\rho_d(\theta_e - \theta_d)},$$ suffixes indicating corresponding densities and temperatures.

$\gamma$ = Euler's constant.

$\Delta l$ = Elemental length of fine wire, in.

### (1) INTRODUCTION

Although much literature is available on the overall thermal behaviour of high-voltage equipment such as cables and transformer windings, very little published data have appeared on the thermal properties of the individual insulating materials which comprise the structure surrounding the copper conductors. Since it is through and by means of these that copper losses are transferred to the ambient medium, knowledge of such properties is an essential preliminary for any detailed investigation of the subject.

The thermal properties of present interest are the thermal conductivity $k$, thermal diffusivity (also called the thermometric conductivity) $\alpha$, and specific heat per unit volume, $\rho c_p$, where $\rho$

is the density, and $c_p$ is the specific heat per unit mass. These quantities are connected by the relationship

$$\alpha = \frac{k}{\rho c_p} \quad . \quad . \quad . \quad . \quad . \quad . \quad (1)$$

Thus, knowledge of any two quantities suffices to define all three. However, laminar grained solids of the type used for high-voltage insulation can exhibit anisotropy, so that diffusivity (and, with it, conductivity) may vary with direction. For example, without giving references or values, Jerrard[1] states that the thermal conductivity along the laminations of insulation used in rotating machines may be as much as six times that across them, while Taylor[2] found a ratio of about 5 : 1 in the corresponding values for kraft paper and mica. Experimental techniques must allow for this possibility.

## (2) AVAILABLE INFORMATION

In addition to the work of Taylor,[2] a comprehensive investigation into the thermal conductivity of solid electrical insulating materials has been made,[3] but the only material of present interest was kraft paper; this, however, was in much thinner form than is used in high-voltage apparatus, and measurements were made on the material in the dry state. So far as oil-impregnated materials are concerned, Table 1 gives published values[4-8] for thermal conductivity of paper and pressboard.

### Table 1

PUBLISHED VALUES OF THERMAL CONDUCTIVITY FOR
PRESSBOARD AND PAPER

Thermal conductivity, $k$
watt/deg C-in
$\times 10^{-3}$

| Pressboard: | 4·6 | King (1932) |
|---|---|---|
| | 6·5 | Gotter (1954) |
| | 2·9–3·6 | Montsinger (1951) |
| Paper: | 2·9 | Symons and Walker (1912) |
| | 3·8 | Gotter (1954) |
| | 4·7 | Marshall (1953) |

Evidently, no mean values can be derived with confidence, and scope exists for simple methods of convenient determination on any given material actually used.

A similar position with regard to transformer oil is revealed by Fig. 1. In this, since they are usually specified as being at a particular temperature, thermal conductivity values[6, 9-14] are shown plotted against temperature.
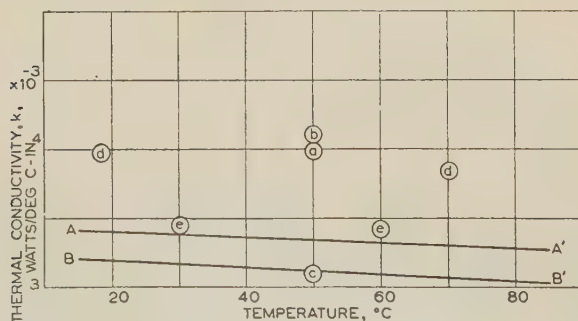


Fig. 1.—Thermal conductivity of transformer oil: comparison of published values.

(a) Montsinger (1917) ⎱ no specified temperature.
(b) Montsinger (1951) ⎰
(c) Davis (1924).
(d) Lorenz (1934).
(e) Smith (1934).
A–A′ Kaye and Higgins (1928).
B–B′ Schmidt and Leidenfrost (1953).

So far as specific heat is concerned, the only reliable figure available are for transformer oil.[15] Vague ranges of values are quoted in respect of 'insulation', but these are unsuitable for derivation of conductivity from diffusivity, or vice versa.

Two further factors affecting the thermal performance of liquids are viscosity and change of density with temperature. Values of these quantities are suggested in the appropriate British Standard,[16] and their determination is a routine matter.

## (3) EXPERIMENTAL METHODS
### (3.1) Thermal Conductivity of Solids
#### (3.1.1) Available Methods.

Classical methods for the determination of the thermal conductivity of solids are based on the uniform flow of thermal energy at a steady measured rate over a known area between defined isothermal surfaces. Most involve some type of guard ring arrangement to achieve uniformity, and, under these circumstances, determination of thermal conductivity in one reference direction only can be made. With oil-impregnated solids, particular difficulties arise from the use of standard laboratory forms of such steady-state apparatus, since measurements must be made with the material in an oil-immersed state. There is no reason why a special apparatus should not be constructed in which laminations of the insulating material under test are wound on to (if paper) or sprung into (if pressboard) a cylindrical former divided axially into guard ring and measuring surfaces, while the free surface of the material is kept substantially at constant temperature by oil circulation and cooling arrangements. Such apparatus has, however, little further use for routine laboratory thermal-conductivity investigations and can only furnish values of thermal conductivity in the radial direction, i.e. through the laminations of the material.

Transient thermal experimental techniques, on the other hand, give values of thermal diffusivity, $\alpha$. They are characterized by the use of temperature-measuring apparatus embedded within the specimens themselves, and are simplified by the absence of any need for calorimetric measurements. An outstanding advantage in their present application is the ease with which they can be adapted to take account of anisotropy.

#### (3.1.2) Theory of Transient Method Employed.

Transient methods depend on the fact that, at some time, after the surface of a solid specimen of prescribed shape is subjected to a sudden change of temperature from, say, $\theta_1$ to $\theta_2$, the temperature $\theta$ at any point within the specimen tends to an exponential dependence on time, i.e.

$$\frac{\theta_2 - \theta}{\theta_2 - \theta_1} = A \varepsilon^{B_c t} \quad . \quad . \quad . \quad . \quad . \quad ($$

where $A$ is a function of the position of the point considered and $B_c$ is a function of the overall dimensions of the solid and of its thermal diffusivities.

In the case of a hollow cylinder, inner radius $r_i$, outer radius $r_o$ and axial length $2c$, made of material having thermal diffusivity $\alpha_r$ in the radial direction, $\alpha_z$ in the axial direction, it is shown in Section 7.1 that

$$B_c = - \left[ \alpha_z \left(\frac{\pi}{2c}\right)^2 + \alpha_r (x_1)^2 \right] \quad . \quad . \quad . \quad ($$

$x_1$ being defined in that Section. From symmetry, it is evident that the thermal diffusivity, $\alpha_c$, in the circumferential direction does not enter the expression. Also, $B_c$ is the index of a term formed as the product of the two first terms of individual series giving solutions for a hollow cylinder of infinite axial length

and a slab of finite thickness but infinite area, respectively. At sufficiently large values of $t$ the products of other pairs of terms can be neglected, and the simple relationship given by eqn. (2) is obeyed.

Common values of the coefficient $A$ are given at points in the same relative positions in any given set of specimens, e.g. points on the mid-axial planes lying at the mean radii, $\frac{1}{2}(r_i + r_o)$, of hollow cylinders, and thus this coefficient can be made quite independent of the cylinder axial length. On the other hand, $B_c$ is inseparable from cylinder axial length, and for a pair of specimens having common radial dimensions, but different axial lengths, $2a$ and $2b$, say,

$$B_a = -\left[\alpha_z\left(\frac{\pi}{2a}\right)^2 + \alpha_r(x_1)^2\right] \quad . \quad . \quad . \quad (4)$$

$$B_b = -\left[\alpha_z\left(\frac{\pi}{2b}\right)^2 + \alpha_r(x_1)^2\right] \quad . \quad . \quad . \quad (5)$$

Subjecting the surfaces of these specimens to a step function of temperature at time zero, and noting the subsequent temperature history of points having a common value of $A$, a pair of linear graphs of the logarithms of $\theta_2 - \theta$ against time, having slopes $B_a$ and $B_b$, can be obtained. From these, and from the known specimen dimensions, $\alpha_z$ and $\alpha_r$ can be calculated by simultaneous solution of eqns. (4) and (5).

**(3.1.3) Experimental Procedure for Solids.**

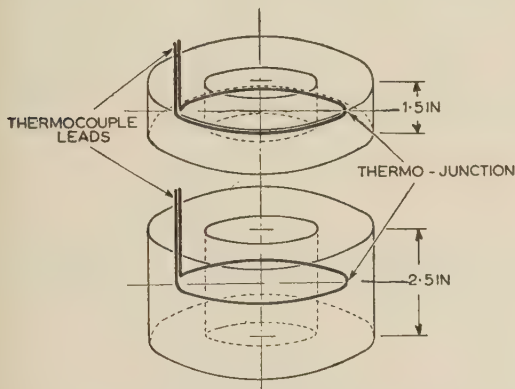Pairs of paper and pressboard specimens were made up in the form shown in Fig. 2, each having axial lengths of $1 \cdot 5$ in

THERMOCOUPLE LEADS

THERMO - JUNCTION

1·5 IN

2·5 IN

Fig. 2.—Layout of specimens for determination of thermal diffusivity.

and $2 \cdot 5$ in. The common radial dimensions were fixed, first, by the values of the ratio $r_o/r_i$ for which values of $x_1$ are available,[17,18] and secondly, by their practicability. This is governed in the case of paper by available mandrel sizes which determine the inner radius, and in the case of pressboard by the flexibility of the material, since this is built up of strips bent to form concentric laminae within a former which fixes the outer radius.

In each case, fine butt-jointed iron-constantan thermocouples, of section $0 \cdot 016$ in $\times 0 \cdot 009$ in throughout, were embedded when the mean radial dimension was reached, the leads, as well as the thermo-junction, lying circumferentially in the mid-axial plane. At a point in this plane diametrically opposite the junction, the leads were turned through a right angle and taken out axially. As they lie along an isothermal, the curved portions of the thermocouple leads require no thermal insulation. The axial portions were insulated within the specimens by means of asbestos tape, folded and sewn to form a sleeve, and outside the

specimen by varnished silk tubing, the two coverings being sealed together at the specimen surface with cellulose cement. The specimens were mounted in pairs of frames made from heavy-gauge copper wire and were subjected to the routine processes of dry-out and oil-impregnation, after which they remained oil-immersed.

For each experiment the pair of specimens was transferred as rapidly as possible to a thermostatically-controlled oil-filled bath set to a temperature a few degrees higher and kept moving to stir the oil. The subsequent temperature history of each embedded junction with respect to the reference, immersed in the same oil, was recorded using a precision potentiometer. Tests were repeated for each pair of specimens at different surface-temperature 'steps', and Fig. 3 shows the results obtained for
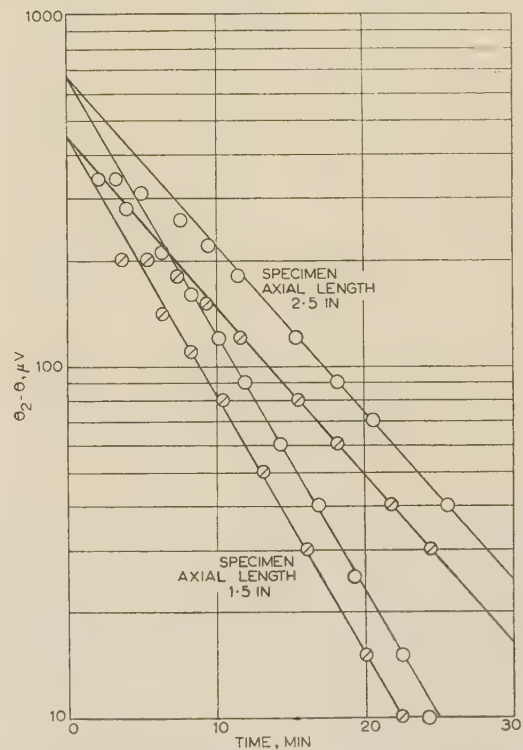
Fig. 3.—Results of tests on $7 \cdot 5$-mil paper specimen.

Temperature step: $4 \cdot 7°$C ⊘
$6 \cdot 7°$C ○
Mean temperature, $26°$ C

$7 \cdot 5$-mil kraft-paper specimens wound with the paper grain circumferential. The linearity of the thermal-e.m.f./temperature characteristic of iron against constantan over the small temperature ranges involved permits the measurements remaining in terms of microvolts.

It will be seen that owing to the equality, for each specimen, of the coefficient $A$ in eqn. (2) and the fact that they are both subjected to the same temperature boundary conditions, the curves for each specimen intersect at time zero, and this provides a useful aid in their correct alignment. Also, by dividing values by the corresponding common value at time zero, results of several tests can be correlated on a dimensionless basis in accordance with eqn. (2). The application of this procedure to the data of Fig. 3 is shown in Fig. 4, from which it will be seen that slopes can be estimated with confidence.

In order to investigate the thermal diffusivity at higher temperatures, pairs of specimens left overnight in an oil-filled
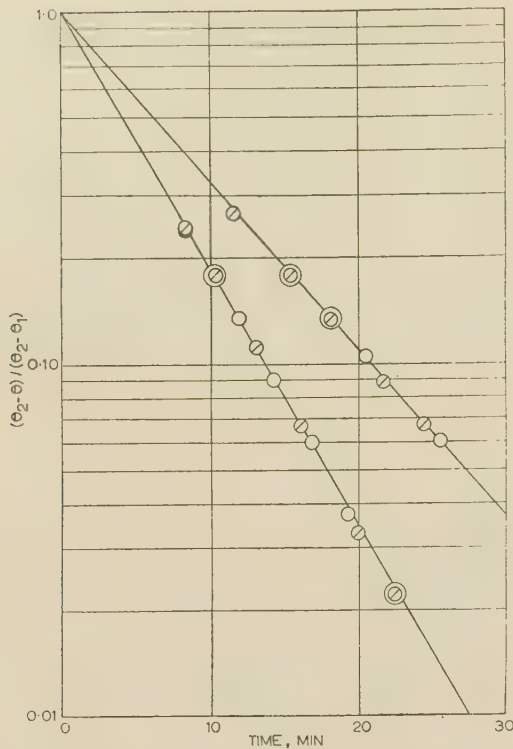
Fig. 4.—Correlated results for 7·5-mil paper specimen.

Temperature step:  4·7°C ⊘
                   6·7°C ○
Mean temperature, 26°C
Slopes: $B_a$, −0·167 per minute.
        $B_b$, −0·110 per minute.



Fig. 5.—Surface temperature rise during test.

$$\tau = 2\,\text{min}$$
$$C' = \frac{428 - 211}{428} = 0·51$$

container placed in a thermostatically controlled oven were transferred to the bath, which was maintained at a somewhat higher temperature. For measurement of thermal diffusivity along the grain of the material, specimens were made up having this aligned in the axial direction. These experiments gave a second determination of the radial diffusivity, which, when compared with that already obtained, provides an indication of the repeatability of results.

### (3.1.4) Accuracy of Method.

The main source of error lies in the probable deviation of surface temperature conditions from the theoretical postulation of a step function applied at time zero. In order to investigate this, a thermo-junction was attached to the surface of a pressboard specimen and its temperature history recorded during a typical test. Owing to their larger sizes compared with those of paper, and the greater specific heat of pressboard, specimens of this material represent the worst experimental condition in this respect. Fig. 5 shows the results of one such test plotted on cooling-curve graph paper by the usual technique.[19] From these it will be seen that the variation of the actual temperature of the surface, $\theta_s$, with time approximates very closely to the function

$$\theta_s = (\theta_2 - \theta_1)(1 - C'\varepsilon^{-t/\tau}) \quad . \quad . \quad . \quad . \quad (6)$$

The values of $\tau$ and $C'$ are readily estimated from this form of graphical presentation.

In this form, the response due to the actual surface temperature can be evaluated by application of Duhamel's theorem, and the error due to the deviation from a step function is found to be

$$\epsilon_d = \frac{100C'B_c\tau}{1 + B_c\tau}\left[1 - \frac{C'}{B_c\tau}\varepsilon^{-(1+B_c\tau)t/\tau}\right]\% \quad . \quad . \quad (7)$$
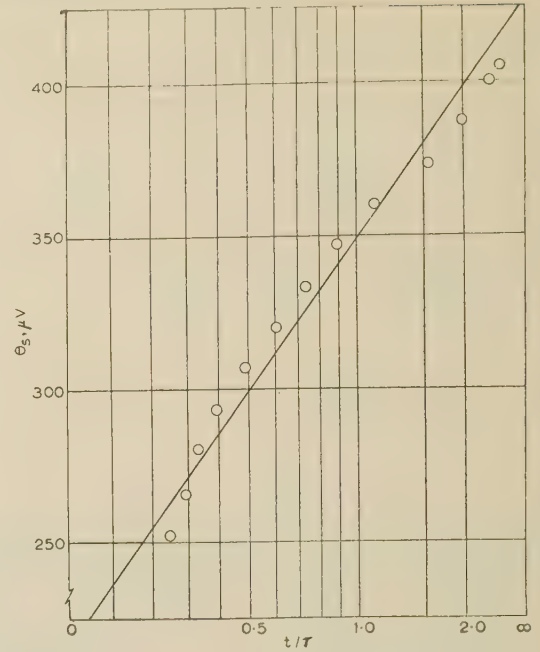
From this equation it is evident that the variable part of the error decays rapidly for small values of $\tau$, provided that $|B_c\tau|$ does not approach too closely to unity, while a constant error has no effect on the slope, $B_c$, of the log-linear graphs obtained.

Unfortunately, the expressions involved tend to magnify errors inherent in the experimental data. From eqns. (4) and (5) considering $|B_a| > |B_b|$,

$$\alpha_z = \frac{B_a - B_b}{\pi^2\left[\dfrac{1}{(2b)^2} - \dfrac{1}{(2a)^2}\right]} \quad . \quad . \quad . \quad (8)$$

and, since differences are involved, a percentage error of $\epsilon$ in each slope will lead to a percentage error in $\alpha_z$ of the order of

$$\epsilon\left(\frac{B_a + B_b}{B_a - B_b}\right)$$

Similarly,

$$\alpha_r = \frac{(2a)^2B_b - (2b)^2B_a}{[(2a)^2 - (2b)^2](x_1)^2} \quad . \quad . \quad . \quad (9)$$

and the experimental error is multiplied by a factor

$$\frac{B_b + (b/a)^2B_a}{B_b - (b/a)^2B_a}$$

Evidently, least error magnification occurs for $|B_a| \gg |B_b|$. This condition is furthered by making $b \gg a$, but the extent depends on the relative values of $\alpha_z$ and $\alpha_r$ and practical considerations set limits to this possibility. The maximum axial length of the larger specimen is limited by the following factors:

(a) Thermal capacity of specimens relative to bath oil. This does not exceed 10% in the present work.

(b) Time at which eqn. (2) begins to apply. This increases with specimen axial length.

The minimum axial length of the smaller specimen, on the other hand, is limited by:

(a) The proportionate error in dimensions and thermocouple location.

(b) The rate of change of temperature at which measurements can be made accurately and conveniently.

(c) The increase in the product $|B_c\tau|$ towards unity.

In the present work, the error-magnification factor did not exceed 5.

An estimate of accuracy is best obtained from the correlation shown between the results of different tests on the same pair of specimens and between values obtained for diffusivity in the radial direction derived from experiments on specimens of the same material differing only in circumferential alignment of grain direction. The order of correlation between tests on the same pair of paper specimens at the same temperature is shown in Fig. 4, which is an average result; better results were obtained. For pressboard, results were in general somewhat less satisfactory, and Fig. 6 shows a correlation of three sets of results, indicating the limits within which the steeper line may be taken to lie.
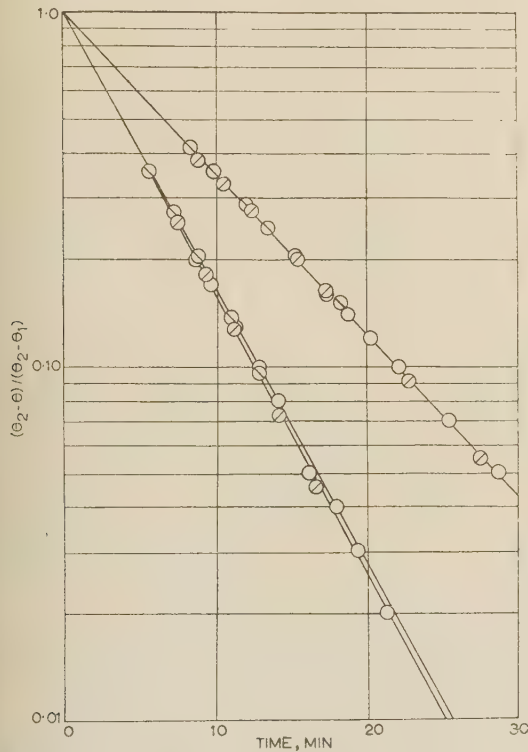


Fig. 6.—Correlated results for 100-mil pressboard specimen.

Temperature step:
Temperature step:  5·9°C ⊘
                   8·0°C ⊗
                   9·2°C ◯
Mean temperature, 28°C

Slopes: $B_a$, −0·181 ± 0·002 per minute.
        $B_b$, −0·105 per minute.

Table 2 shows some thermal diffusivity values obtained from similar tests on pairs of specimens differing only in grain direction. It is considered that, with care, an accuracy within ±5% is obtainable. This is of the order given by other methods and quite satisfactory for design purposes. The possibility of enhancing the accuracy for precision determinations is discussed in Section 4.

## (3.2) Thermal Conductivity of Transformer Oil

### (3.2 1) Available Methods.

Steady-state methods for the determination of liquid thermal conductivity are exactly analogous to those used for solids, except that special precautions are taken to avoid any motion of the liquid leading to the incidence of convective heat transfer.

## Table 2

### RADIAL THERMAL DIFFUSIVITY

| Material | Temperature | Radial thermal diffusivity $\alpha_r$ in$^2$/sec | |
| --- | --- | --- | --- |
| | | Grain circumferential | Grain axial |
| | deg C | × 10$^{-4}$ | × 10$^{-4}$ |
| Paper, 5 mil .. | 48 | 1·40 | 1·33 |
| Pressboard, 25 mil | 26 | 2·09 | 2·23 |

One simple precaution, when the liquid is contained between parallel horizontal plates, is to ensure that the direction of heat flow is from upper to lower plates. Other precautions include limiting thermal flux density and, consequently, temperature differences, as well as clearances between isothermal surfaces, to small values. Either step tends to limit the accuracy attainable, although some investigators, notably Bates[20] and Sakiadis and Coates,[21] consider the latter to be unnecessary.

In all the measurements on transformer oil quoted in Fig. 1 for which experimental details are available, very limited clearances were employed, except in the case of Davis,[10] who used a simple axially-suspended heated wire in a cylinder. Here again, the use of a fine wire limits accuracy.

The application of transient techniques to the determination of fluid thermal conductivity is very limited. A transient method for solids has been adapted by Sakiadis and Coates[21] for water, but the results are most unsatisfactory. The same authors report a method employing the periodic heating of a surface in contact with water but do not consider the results as better than average, which implies an experimental error of greater than ±12%.

A transient method for fluids, due to van der Held and van Drunen,[22] is of general application and has been applied to solids by Vos[23] and, in measurements on soil, by Mason and Kurtz.[24] The method has the advantage that no precision metrology or fabrication is required, and, as modified and improved* for the present work, employs standard laboratory apparatus.

### (3.2.2) Theory of Transient Method Employed.

It is shown in Section 7.2 that temperature rises $\theta_p$ and $\theta_q$ above ambient after times $t_p$ and $t_q$, respectively, at any point in the thermal field, due to a continuous line source in a medium of conductivity $k$, emitting thermal energy at a constant rate $q$ per unit length, commencing at time zero, is, after a certain time, given by

$$\theta_p - \theta_q = \frac{q}{4\pi k} \log_\varepsilon \frac{t_p}{t_q} \quad . \quad . \quad . \quad . \quad (10)$$

Since this holds at the source, the graph of temperature rise of a fine wire with constant power dissipation against the logarithm of time is linear. From its slope the thermal conductivity of the ambient medium can be derived. Further, over small time intervals, convective effects in a fluid medium, requiring time to develop, can be eliminated.

The experimental problem is, therefore, to maintain constant the dissipation, $I^2R$, in a wire of resistance $R$ carrying current $I$, while $R$, variation of which measures the wire temperature, is changing. A simple circuit to achieve this consists of a high-impedance thermionic valve supplied from a stable source of direct current with the wire connected in its cathode circuit, the control grid being kept at negative supply potential. Section 7.3

* British Patent Application No. 17427: 1955.

indicates that for small changes in $R$ the value of $I^2R$ remains constant, provided that the mutual conductance, $g_m$, of the valve obeys the relationship

$$g_m = \frac{1}{R} \quad \cdots \cdots \cdots \quad (11)$$

It is also shown that for small changes a proportionality exists under these conditions between changes in voltage across the wire and the resistance of the wire as follows:

$$\frac{\Delta R}{R} = 2\frac{\Delta V}{V} \quad \cdots \cdots \cdots \quad (12)$$

The voltage changes can be recorded continuously with respect to constant datum by oscillograph.

### (3.2.3) Experimental Procedure for Transformer Oil.

The data initially required are the resistance/temperature characteristic of the fine wire and the variation of mutual conductance with anode current under working conditions for the valve employed, in this case a 12E1 beam tetrode. The second of these characteristics is derived from the anode-current/control-grid-voltage characteristic at constant anode and screen-grid potentials, and is given in Fig. 7. The mutual conductance
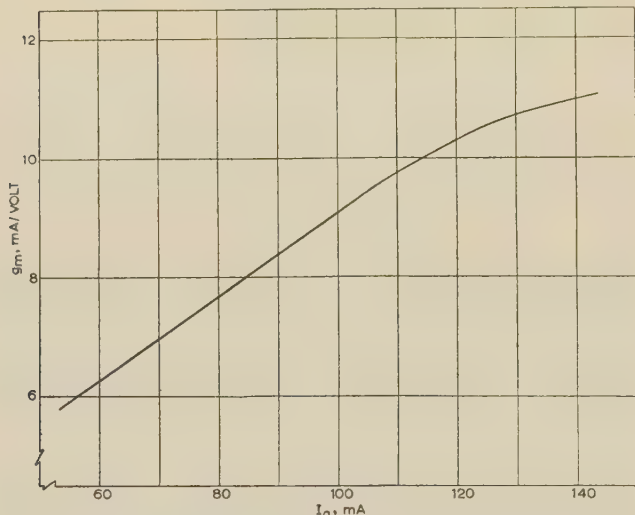


Fig. 7.—Mutual-conductance/anode-current characteristic of 12E1 valve.

$V_a = 204$ volts.
$V_{g2} = 144$ volts.

varies between 6 and 11 mA/volt, according to anode current, and so can be adjusted by grid bias. These values of mutual conductance correspond to a cathode load resistance range of 91–167 ohms, which amply covers the variation due to changes of temperature between 20 and 80° C.

Fig. 8 shows the essential details of the circuit employed. The oscillograph was a double-beam cathode-ray instrument with motor-driven camera, one beam being fed at 50 c/s from a peaking transformer to provide a datum for trace-deflection measurements and also time markings. To eliminate transient effects when switching anode and screen voltages on to the valve, a dummy load, consisting of a stable resistor R′, set equal to the initial value of the wire resistance, was used to obtain steady anode current before switching over at time zero to the 0·001 in diameter thermo-pure platinum wire. This was immersed in a thermostatically controlled bath containing the oil under investigation
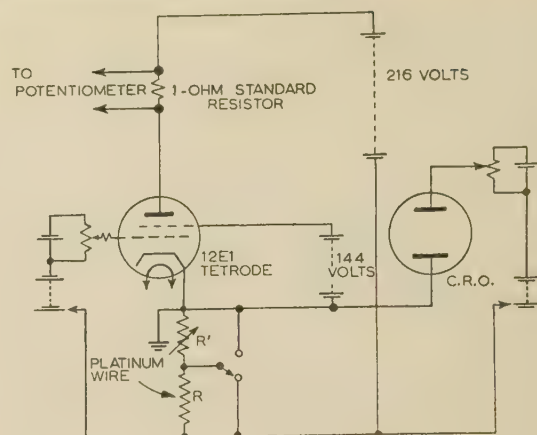


Fig. 8.—Constant-power circuit for thermal-conductivity determination.

and fitted with a mercury-in-glass thermometer graduated i 0·1° C. Spurious effects still obtained at the time of switchin had the effect of masking the exact switching point. Th difficulty was overcome by a method described later.

The anode current was measured in terms of the voltage dro measured by potentiometer, produced across a standard 1-ohi resistor. With modified connections, the potentiometer was als used, together with resistor R′, to measure wire resistance by substitution method.

To minimize 50 c/s pick-up, the valve heater was supplie from an accumulator, while anode, screen-grid, grid bias ar reference voltages were obtained from dry batteries. To avoi microphony due to operation of the change-over switch ar camera motor, the valve was mounted separately.

Preliminary tests were made to determine the order of overa current and resistance change between initial and final stead state values. These confirmed the constant-power performan of the circuit and indicated the order of resistance change, that a mean resistance could be estimated and the correspondir mean current obtained by grid-bias adjustment.

To make a measurement when the oil had attained the desir temperature, R′ was set to the same resistance as that of tl wire, and the grid bias potential adjusted to give the desir initial anode current passing through it. The reference volta was then adjusted for suitable location of the spot on the oscill graph screen, and, after switching off the bath-stirring mechanisr the camera clutch was engaged, the shutter opened and tl change-over switch operated. After about 3 sec, the came motor was switched off. The oscilloscope was calibrated I recording trace deflections for input voltages derived from tl potentiometer.

As an example, results are given for a test made on transform oil at 80° C. Using a travelling microscope, measurements we made of trace deflections at fixed time intervals, and, whe converted to voltage changes $\Delta V$, gave a graph against time as shown in Fig. 9. As shown in Section 7.2, correction for ze errors can be made by plotting the inverse, $dt/d\Delta V$, of the slo of this graph against time, the intercept of such a graph (Fig. 1 on the $t$-axis giving the corrected zero. Also, the slope theoretically equal to that finally obtained when the logarithm corrected time $t'$ is plotted against $\Delta V$, as shown in Fig. 11.

These graphs have slopes of 111 and 112 per volt, respectivel showing a good agreement. The latter figure, however, is bas on more data over a more reliable time interval. Using eqn. (1 together with the relationship $V = IR$, to interpret $\Delta V$ terms of $\Delta R$, and the wire resistance/temperature relationsh
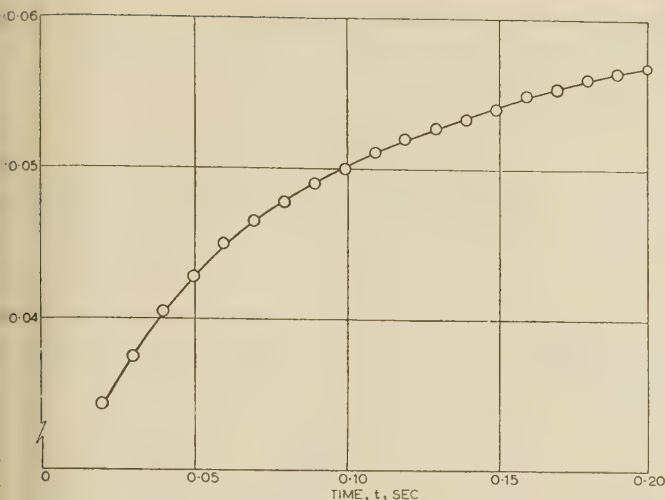
**Fig. 9.**—Temperature rise (proportional to $\Delta V$) of fine wire.
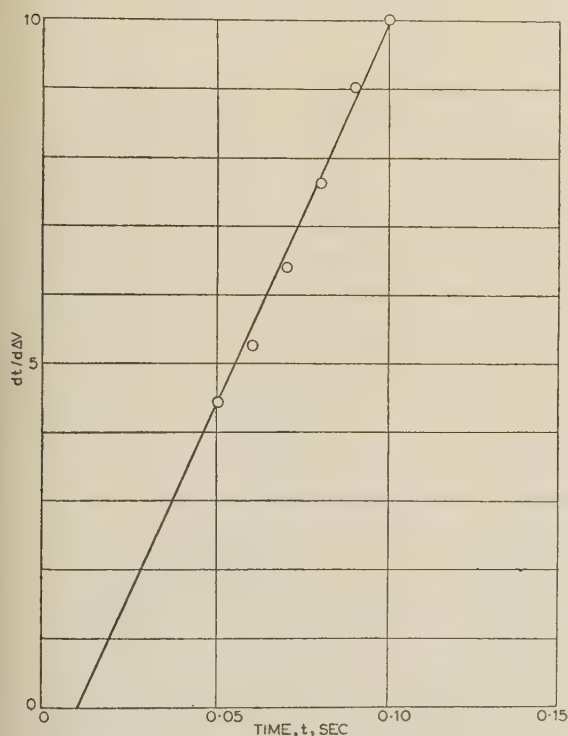


**Fig. 10.**—Inverse slope of Fig. 9 plotted against time.
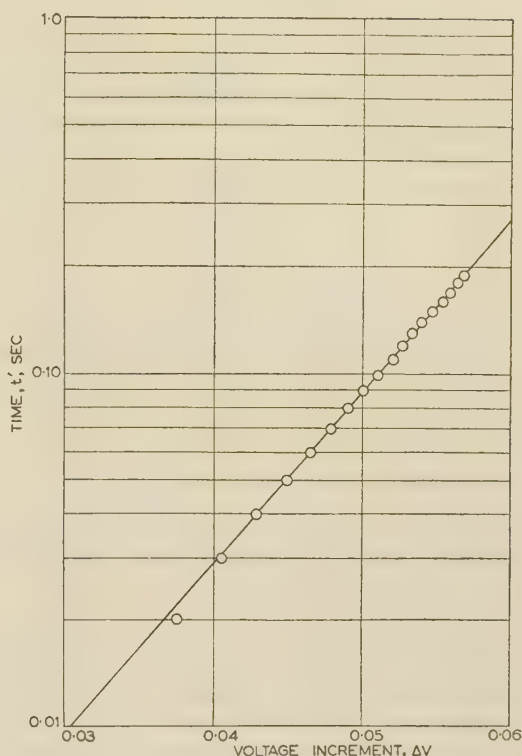
Slope: 111 per volt.



**Fig. 11.**—Graph of voltage increment against logarithm of corrected time.

Slope: 112 per volt.

**(3.2.4) Accuracy of Method.**

Since the current is cubed in eqn. (14), accuracy in its measurement is essential. By the use of a potentiometric method the accuracy of the $I^3$ term is kept within $\pm 0 \cdot 5 \%$. The accuracy of measurement of $R$ is limited to that of the standards used for comparison, namely $0 \cdot 1 \%$, the sensitivity of the measurement being of an order better than this. Subsequent calibration of the thermometer indicates a possible error of the order of $0 \cdot 3 \%$, and the resistance/temperature relationship can be taken as correct to within $\pm 0 \cdot 5 \%$. The measurement of 20 in of wire can easily be made to the same degree of accuracy, and change in its length due to thermal expansion does not exceed $0 \cdot 15 \%$. Such changes are taken up by mounting the wire under light tension. Apart from determination of the slope of the final graph, the following are considered to be possible sources of error inherent in the method:

*(a) Operation of the constant-power circuit.*

Measurements made at initial and final steady states indicate that power constancy is maintained to within $1 \%$ of the power change, i.e. $0 \cdot 01 \%$ of the total power involved.

*(b) Heat-storage effects in source.*

Eqn. (10) assumes constancy of power liberated into the ambient medium by the source, while the circuit design merely ensures a constant external supply of electrical energy to the source. Estimating the thermal capacity, $C$, of 1 in of $0 \cdot 001$ in diameter platinum wire as $3 \cdot 8 \times 10^{-5}$ joule per deg C, and differentiating eqn. (10) with respect to $t_p$,

$$\frac{d(\theta_p - \theta_q)}{dt_p} = \frac{q}{4\pi k t_p} \qquad . \qquad . \qquad . \qquad . \qquad (15)$$

$\cdot 447$ ohm per deg C) to convert this to temperature rise, from qn. (10) we have

$$\frac{q}{4\pi k} = \frac{2}{112 \times 0 \cdot 447 I} \quad . \quad . \quad . \quad . \quad (13)$$

fter obtaining $q$ from the initial current and resistance values ad length, $2l$, of the wire, we have, finally,

$$\frac{0 \cdot 447 I^3 R \times 112}{16\pi l} = \frac{0 \cdot 447 \times (0 \cdot 064)^3 \times 151 \cdot 8 \times 112}{8\pi \times 21 \cdot 5}$$
$$= 3 \cdot 69 \times 10^{-3} \text{ watt per deg C-in} \quad (14)$$

the rate of heat storage per inch of wire is

$$C\frac{d(\theta_p - \theta_q)}{dt_p} = \frac{qC}{4\pi k t_p} \quad . \quad . \quad . \quad . \quad (16)$$

which must be deducted from the total energy liberation rate, $q$, to give the net rate, $q'$, into the medium from the source:

$$q' = q\left(1 - \frac{C}{4\pi k t_p}\right)$$

$$= q\left(1 - \frac{8\cdot6}{10^4 t_p}\right) \quad . \quad . \quad . \quad (17)$$

The error is less than 1% for $t_p > 86$ millisec. It will be seen from Fig. 11, however, that no deviation from linearity is perceptible at times considerably below this, doubtless owing to the fact that this error is of the same order as, but opposite sign to, that discussed under (c) following.

(c) *Employment of approximate expression.*

Eqn. (10) is an approximation and is valid only for sufficiently large $t$. Investigation shows that the value of $t$ for negligible error due to this cause is about 50 millisec.

(d) *Thermal leakage at ends of wire.*

This error is minimized by the use of as long a wire as possible. Bath-size limitations necessitated the suspension of the wire in two series-connected lengths of about 10 in each. Even under these conditions, and assuming, pessimistically, no temperature rise of the wire extremities, the analysis given in Section 7.4 indicates a heat leakage amounting to about 0·25% of the total thermal energy involved.

Considering these sources of error and the way in which points plotted in Fig. 11 lie on a straight line, ±5% is indicated as a conservative claim for the accuracy of results obtained. While the method is capable of considerable refinement from this point of view, it is not worth while in the present application to attempt precision of an order higher than that attained in the measurements on solids.

### (3.3) Specific Heat of Solids and Transformer Oil

(3.3.1) **Method of Mixtures.**

The determination of specific heats by the method of mixtures is well-established laboratory practice. The temperature change is noted when known masses of substances, having known and unknown specific heats, respectively, are put into thermal contact in a well-lagged enclosure so as to assume a common temperature without loss of thermal energy. In the case of a liquid, this is easily achieved, using as the reference mass another liquid with which it is miscible, or solid of high thermal conductivity, either having known specific heat. Conversely, solids require a liquid of known specific heat. Those at present under investigation, however, can be immersed only in their own impregnant, so that transformer oil must be used as the reference liquid. The specific heat of transformer oil was determined by the method of mixtures and agreed with available values[15] to within 2%. When the method was applied to the solids, it was found that, owing to their low thermal diffusivity, times required to attain thermal equilibrium proved excessive. Normally, this period can be covered by observing the calorimeter temperature for a period before and after mixing and extrapolating the cooling curves obtained to the mixing time. Excessive extrapolation periods lead to loss of accuracy, and an alternative method was adopted for the solids.

(3.3.2) **Alternative Method for Poorly Conducting Solids.**

Provided that the impedance to heat flow within the calorimeter can be neglected in comparison with that between its inner walls

and the ambient medium, the cooling rate, $R_\theta$, at a given temperature for a calorimeter which, with its contents, has a total thermal capacity $W_T$, is given by

$$R_\theta = \frac{K_\theta}{W_T} \quad . \quad . \quad . \quad . \quad . \quad (18)$$

$K_\theta$ being a constant defined by this equation. For a calorimeter of thermal capacity $W$ containing mass $M_m$ of substance M having specific heat $c_m$ per unit mass,

$$R_{\theta m} = \frac{K_\theta}{W + M_m c_m} \quad . \quad . \quad . \quad . \quad (19)$$

If, in addition, the calorimeter contains mass $M_n$ of substance N with specific heat $c_n$,

$$R_{\theta m n} = \frac{K_\theta}{W + M_m c_m + M_n c_n} \quad . \quad . \quad . \quad (20)$$

so that

$$\frac{W + M_m c_m + M_n c_n}{W + M_m c_m} = \frac{R_{\theta m}}{R_{\theta m n}} \quad . \quad . \quad (21)$$

Specimens were prepared in paper and pressboard to size suitable for immersion in the one-gallon Thermos flask used as calorimeter. For each experiment, the specimen was heated in the oil bath to about 80°C and 2 kg of hot oil transferred to the flask. The specimen was also transferred, the cover secured, and the temperature of the flask contents noted by means of an immersed thermocouple at intervals of about 15 min over a period of about seven hours. The experiment was also performed with 2 kg of oil only, and again with 2 kg of oil and a suitable copper mass. During the tests, the ambient temperature was maintained as nearly as possible constant.

Cooling rates were estimated from graphs of logarithms of temperature rise above ambient plotted against time for the contents of the Thermos flask. The fact that the cooling proved to be Newtonian greatly facilitated cooling-rate evaluation. In the case of 7½-mil paper, substitution in eqn. (21) and use of the value of $W$ obtained by this method for the cooling of oil with and without the copper block, gives 410 cal as the thermal capacity of the specimen, volume 75·5 in³, at 70°C. Converting calories to joules gives 22·7 joules/in³-deg C as the specific heat per unit volume.

As the diffusivity of the materials is known, the thermal time constants of the specimens can be calculated. These are of the order of less than 2% of the values observed for the calorimeter and its contents, and neglect of thermal impedance within the calorimeter is justified. Little variation is possible in the location of the cooling curve over a period of about six hours, and the main source of error lies in the value taken for the thermal capacity, $W$, of the calorimeter. This, however, is minimized by the use of the same method for its determination, and values are quoted as correct to within ±3%.

### (3.4) Other Properties

The relevant remaining thermal properties of high-voltage insulants are those of liquids, namely viscosity and change of density with temperature. Measurements of these properties are routine laboratory practice and the methods call for no comment. Values for transformer oil are suggested in the British Standard[16] and in the case of viscosity are for kinematic viscosity, $v$. It is, however, the dynamic viscosity, $\mu$, the product of kinematic viscosity and density, which affects steady-state thermal performance. The coefficient, $\beta$, of change of density with temperature is defined as

$$\beta = \frac{\rho_d - \rho_e}{\rho_d(\theta_e - \theta_d)} \quad . \quad . \quad . \quad . \quad (22)$$

The suffixes of $\rho$ and $\theta$ indicate corresponding values. Evidently, $\beta$ is a function of $\rho_d$, i.e. of the lower reference temperature. A value for $\beta$ of 0·0008 per degC is suggested by the British Standard as typical for transformer oil, no reference temperature, $\theta_d$, being specified. Employment of this value in the case of the oil investigated would have given an error of the order of 20% in the evaluation of pressure head causing oil circulation or of the Grashof number, the dimensionless group characterizing natural convective cooling. The necessity for making measurements, rather than reference to the British Standard, needs no emphasis.

It has been suggested[25] that the rate of change of density with temperature is, for insulating oils, a function of density, being greater for oils having lower densities. Such oils would also require to have a lower dynamic viscosity, $\mu$, to give values of kinematic viscosity, $\nu$, to comply with the characteristics suggested for typical oils in the British Standard. Further, it is thought[26] that convective cooling is assisted in the parts of the apparatus where the oil is subjected to electric stress to a degree which is a function of change of permittivity with temperature. Since this is proportional to density change, the effect of this fluid property upon convective cooling of transformer windings may well be two-fold and a maximum value is desirable.

## (4) DISCUSSION AND CONCLUSIONS

It is not the object of the present paper to provide a source of design data for a complete class of materials. Rather, relatively simple methods have been described by means of which design engineers can investigate the thermal properties, as these are required, of existing and newly developed materials. Unless the properties of both are fully known, no reliable application of existing thermal test data obtained using one can be applied with confidence to the other. This applies especially in the case of liquids when estimation or comparison of thermal performance without actual experiment can be made only in terms of dimensionless groups. Evaluation of these requires a full knowledge of all relevant properties which must also be known if experimental results derived using other fluids are to be utilized.

So far as the methods themselves are concerned, discussion will be limited to those which are novel. That for the diffusivity determination is probably capable of little further refinement for fundamental reasons already discussed. Improvement of accuracy may be possible by careful control of thermostatic bath heat input to correspond to the calculated thermal absorption of the specimens during the experiment. In the work described, this complication is not considered necessary. It may be useful to point out that exactly the same analysis applies to the process of diffusion of moisture, and the constant for any such process, e.g. of water into dry paper, together with its variation with direction, etc., can be determined. The practicability of generating a 'step function' of humidity for such an experiment has been indicated.[27]

The method for the determination of liquid thermal conductivity, on the other hand, is considered capable of further development in two different directions. First, it should be possible to manufacture an electronic instrument, self-contained and incorporating a dip-stick, for thermal conductivity measurements of liquids in bulk, or a test cell for use with smaller quantities. Secondly, a much higher degree of accuracy may be achieved using a high-gain linear amplifier and more accurate means for trace-deflection measurement. As the only element exposed to the fluid under investigation is a platinum wire, investigations over wide pressure and temperature ranges would involve a minimum of complication.

## (6) REFERENCES

(1) JERRARD, R. P.: 'Temperature Drop to Resistance Temperature Detector in Stator Windings of Turbine Generators', *Transactions of the American I.E.E.*, 1954, **73**, p. 665.
(2) TAYLOR, T. S.: 'The Thermal Conductivity of Insulating and Other Materials', *Electrical Journal*, 1919, **16**, p. 526.
(3) 'The Thermal Resistivity of Solid Dielectrics', *Journal I.E.E.*, 1930, **68**, p. 1313.
(4) SYMONS, H. D., and WALKER, MILES: 'The Heat Paths in Electrical Machinery', *ibid.*, 1912, **48**, p. 674.
(5) KING, W. J.: 'The Basic Laws and Data of Heat Transmission', *Mechanical Engineering*, 1932, **54**, p. 275.
(6) BLUME, L. F. (Editor): 'Transformer Engineering' (Wiley, 1951).
(7) MARSHALL, T. A.: 'An Apparatus for Measuring the Coefficient of Thermal Conductivity of Solids and Liquids', *British Journal of Applied Physics*, 1953, **4**, p. 112.
(8) GOTTER, G.: 'Erwärmung und Kühlung elektrischer Maschinen' (Springer-Verlag, Berlin, 1954).
(9) MONTSINGER, V. M.: 'Cooling of Oil-Immersed Transformer Windings after Shut-Down', *Transactions of the American I.E.E.*, 1917, **36**, p. 711.
(10) DAVIS, A. H.: 'Convective Cooling of Wires in Streams of Viscous Liquids', *Philosophical Magazine*, 1924, **47**, p. 1057.
(11) LORENZ, H. H.: 'Die Warmeübertragung von einer ebenen senkrechten Platte an Öl bei natürlicher Konvektion', *Zeitschrift für Technische Physik*, 1934, **15**, p. 362.
(12) SMITH, J. F. D.: 'Heat Transfer and Pressure Drop for an Oil in a Copper Tube', *Transactions of the American Institute of Chemical Engineers*, 1934, **31**, p. 83.
(13) KAYE, G. W. C., and HIGGINS, W. F.: 'The Thermal Conductivity of Certain Liquids', *Proceedings of the Royal Society*, A, 1928, **117**, p. 459.
(14) SCHMIDT, E., and LEIDENFROST, W.: 'Der Einfluss elektrischer Felder auf den Wärmetransport in flüssigen elektrischen Nichtleitern', *Forschung auf dem Gebiete des Ingenieurwesens*, 1953, **19**, No. 3, p. 65.
(15) 'Report on Researches on the Chemical and Physical Properties of Insulating Oils', *Journal I.E.E.*, 1923, **67**, p. 661.
(16) B.S. 148: 1951: 'Insulating Oil for Transformers and Switchgear'.
(17) JAHNKE, E., and EMDE, F.: 'Tables of Functions' (Dover Publications, New York, 1945).
(18) LOWAN, A. N., and HILLMAN, A.: 'A Short Table of the First Five Zeros of the Transcendental Equation $J_0(x)Y_0(kx) - J_0(kx)Y_0(x) = 0$', *Journal of Mathematics and Physics*, 1943, **22**, p. 208.
(19) NARBUTOVSKIH, P.: 'Simplified Graphical Method of Computing Thermal Transients', *Transactions of the American I.E.E.*, 1947, **66**, p. 78.
(20) BATES, O. K.: 'Thermal Conductivity of Liquids', *Industrial and Engineering Chemistry*, 1933, **25**, p. 431.

(21) SAKIADIS, B. C., and COATES, J.: 'Studies of Thermal Conductivity of Liquids', Parts I, II and III, Engineering Experiment Station Bulletins Nos. 34 (1952), 35 (1953) and 45 (1954), Louisiana State University.

(22) VAN DER HELD, E. F. M., and VAN DRUNEN, F. G.: 'A Method of Measuring the Thermal Conductivity of Liquids', *Physica*, 1949, **15**, p. 865.

(23) VOS, B. H.: 'Measurements of Thermal Conductivity by a Non-Steady-State Method', *Applied Scientific Research A*, 1956, **5**, p. 425.

(24) MASON, V. V., and KURTZ, M.: 'Rapid Measurements of the Thermal Resistivity of Soil', *Transactions of the American I.E.E.*, 1952, **71**, Part III, p. 570.

(25) RILEY, T. N., and SCOTT, T. R.: 'Insulating Oils for High-Voltage Cables', *Journal I.E.E.*, 1928, **66**, p. 805.

(26) ALLEN, P. H. G.: 'The Distribution of Temperature in a Layer-Type Transformer Winding', *Proceedings of the BTH Third Summer School in Electrical Engineering*, 1956, p. 47.

(27) HASEGAWA, S., GARFINKEL, S. B., and WEXLER, A.: 'Simple Humidity Lag Apparatus', *Review of Scientific Instruments*, 1955, **26**, p. 1196.

(28) NEWMANN, A. B.: 'Heating and Cooling Rectangular and Cylindrical Solids', *Industrial and Engineering Chemistry*, 1936, **28**, p. 545.

(29) CARSLAW, H. S., and JAEGER, J. C.: 'Conduction of Heat in Solids' (Oxford University Press, 1947).

## (7) APPENDICES

### (7.1) Temperature Distribution within a Hollow Cylinder

Newmann[28] has pointed out the possibility of employing product solutions when the temperature, $\theta$, within a solid, the surfaces of which are subjected to a temperature step $\theta_2 - \theta_1$ at time zero, is expressed in the 'deficiency' form, namely $(\theta_2 - \theta)/(\theta_2 - \theta_1)$.

It can easily be shown that the product of solutions $[(\theta_2 - \theta)/(\theta_2 - \theta_1)]_x$, $[(\theta_2 - \theta)/(\theta_2 - \theta_1)]_y$ and $[(\theta_2 - \theta)/(\theta_2 - \theta_1)]_z$, say, for semi-infinite solids, X, Y and Z, gives the solution $[(\theta_2 - \theta)/(\theta_2 - \theta_1)]_{xyz}$ for the finite solid formed by their intersection.

In the case of a hollow cylinder, circular symmetry reduces the number of semi-infinite solids to two, namely a slab having finite thickness $2c$, i.e. bounded by infinite planes at $z = \pm c$, and a cylinder, inner radius $r_i$, outer radius $r_o$, of infinite axial ($z$-direction) length.

Solutions given by Carslaw and Jaeger[29] for these solids can be expressed as follows:

*Slab.*

$$\left(\frac{\theta_2 - \theta}{\theta_2 - \theta_1}\right)_z$$
$$= \frac{4}{\pi} \sum_{n=0}^{\infty} \left\{ \frac{(-1)^n}{2n+1} \cos \frac{(2n+1)\pi z}{2c} \exp\left[ -(2n+1)^2 \left(\frac{\pi}{2c}\right)^2 \alpha_z t \right] \right\}$$

$$\cdots \cdot (23)$$

*Hollow cylinder.*

$$\left(\frac{\theta_2 - \theta}{\theta_2 - \theta_1}\right)_r = \pi \sum_{n=1}^{\infty} \left[ \frac{J_0(x_n) U_0\left(\frac{r}{r_i}x_n\right)}{J_0(x_n) + J_0\left(\frac{r_o}{r_i}x_n\right)} \exp\left(-x_n^2 \alpha_r t\right) \right] \cdots \cdot (24)$$

$x_n$ being the $n$th root of the equation

$$J_0(x) Y_0\left(\frac{r_o}{r_i}x\right) - J_0\left(\frac{r_o}{r_i}x\right) Y_0(x) = 0 . \quad \cdots \quad (25)$$

and $U_0\left(\frac{r}{r_i}x_n\right) = J_0\left(\frac{r}{r_i}x_n\right) Y_0\left(\frac{r_o}{r_i}x_n\right) x_n - J_0\left(\frac{r_o}{r_i}x_n\right) Y_0\left(\frac{r}{r_i}x_n\right) . \quad (26)$

where $J_0$ and $Y_0$ are Bessel functions of the first and second kind, respectively, and zero order.

Neglecting terms other than the first in each series,

$$\left(\frac{\theta_2 - \theta}{\theta_2 - \theta_1}\right)_{zr} = \left(\frac{\theta_2 - \theta}{\theta_2 - \theta_1}\right)_z \left(\frac{\theta_2 - \theta}{\theta_2 - \theta_1}\right)_r$$

$$= \frac{J_0(x_1) U_0\left(\frac{r}{r_i}x_1\right)}{J_0(x_1) + J_0\left(\frac{r_o}{r_i}x_1\right)} \cos \frac{\pi z}{2c} \exp\left\{ -\left[ \alpha_z\left(\frac{\pi}{2c}\right)^2 + \alpha_r x_1^2 \right]t \right\}$$

$$\cdots \cdot (27)$$

and

$$\frac{J_0(x_1) U_0\left(\frac{r}{r_i}x_1\right)}{J_0(x_1) + J_0\left(\frac{r_o}{r_i}x_1\right)} \cos \frac{\pi z}{2c} = F(r, z) . \quad \cdots \quad (28)$$

$$-\left[ \alpha_z\left(\frac{\pi}{2c}\right)^2 + \alpha_r x_1^2 \right] = B_c . \quad \cdots \quad (29)$$

It should be noted that, as in eqn. (24) all radial dimensions are non-dimensionalized by division by $r_i$, this process must be applied to $c$ in eqn. (23). Hence, for convenience, calling the length $r_i$ 'one radius', values of diffusivity are obtained, initially, as '(radii)$^2$ per unit time'.

### (7.2) Temperature Rise due to a Continuous Line Source

For a continuous line source emitting thermal energy at constant rate $q$, the temperature rise $\theta$ at distance $r$ from the source is given[29] as

$$\theta = \frac{q}{4\pi k} \int_{\frac{r^2}{4\alpha t}}^{\infty} \frac{\varepsilon^{-u} du}{u} \quad \cdots \quad (30)$$

For small values of $\frac{r^2}{4\alpha t}$, eqn. (30) can be approximated as

$$\theta = \frac{q}{4\pi k} \left( \log_\varepsilon \frac{4\alpha t}{r^2} - \gamma \right) \quad \cdots \quad (31)$$

where $\gamma$ is Euler's constant.

By taking differences between the temperature, $\theta_p$, at time $t_p$ and some datum temperature, $\theta_q$, at time $t_q$, $r$ and $\gamma$ can be eliminated, giving

$$\theta_p - \theta_q = \frac{q}{4\pi k} \log_\varepsilon \frac{t_p}{t_q} \quad \cdots \quad (10)$$

From this, it follows that

$$\frac{dt_p}{d(\theta_p - \theta_q)} = \frac{4\pi k}{q} t_p \quad \cdots \quad (32)$$

and hence the graph of $dt_p/d(\theta_p - \theta_q)$ against time, $t_p$, has slope $4\pi k/q$ and passes through zero. A fuller analysis from the point of view of error compensation is given by van der Held[22] and Mason and Kurtz,[24] who used somewhat cruder experimental approximations to the ideal linear source postulated.

### (7.3) Constant-Power Circuit Operation

Since

$$\Delta(I^2R) = I^2\Delta R + 2IR\Delta I \quad . \quad . \quad . \quad (33)$$

for constancy of $I^2R$ during small changes $\Delta R$ in $R$,

$$\frac{\Delta R}{R} = -\frac{2\Delta I}{I} \quad . \quad . \quad . \quad . \quad (34)$$

Considering the circuit described in Section 3.2.2, the voltage, $v_g$, of the control grid relative to the cathode is given by

$$v_g = -V = -IR \quad . \quad . \quad . \quad . \quad (35)$$

whence $\dfrac{\Delta v_g}{\Delta R} = \dfrac{dv_g}{dR} = -\left(R\dfrac{\partial I}{\partial R} + I\right) = -\left(R\dfrac{\Delta I}{\Delta R} + I\right)$ . (36)

For constant $I^2R$, from eqn. (34),

$$\frac{\Delta I}{\Delta R} = -\frac{I}{2R} \quad . \quad . \quad . \quad . \quad (37)$$

and, substituting eqn (37) in eqn. (36),

$$\frac{\Delta v_g}{\Delta R} = -\frac{I}{2} \quad . \quad . \quad . \quad . \quad (38)$$

The mutual conductance, $g_m$, of the valve is defined as

$$g_m = \frac{\Delta I}{\Delta v_g} \quad . \quad . \quad . \quad . \quad (39)$$

which may be expressed as

$$g_m = \frac{\Delta I}{\Delta R}\frac{\Delta R}{\Delta v_g} \quad . \quad . \quad . \quad . \quad (40)$$

Substituting eqns. (37) and (38) in eqn. (40),

$$g_m = \frac{1}{R}. \quad . \quad . \quad . \quad . \quad (11)$$

for constant $I^2R$.

Also, from eqn. (35),

$$\frac{\Delta V}{V} = \frac{\Delta I}{I} + \frac{\Delta R}{R} \quad . \quad . \quad . \quad . \quad (41)$$

and substituting for $\Delta I/I$ from eqn. (34), under constant-power conditions,

$$\frac{\Delta V}{V} = \frac{\Delta R}{2R} \quad . \quad . \quad . \quad . \quad (42)$$

whence

$$\frac{\Delta R}{R} = \frac{2\Delta V}{V} \quad . \quad . \quad . \quad . \quad (12)$$

### (7.4) Temperature Distribution along a Fine Electrically Heated Wire

Neglecting internal radial temperature differences, the heat balance for an element $\Delta l$ of wire of length $2l$, dissipating $q$ watts per unit length, leads to the following differential equation for the temperature, $\theta$, of the wire:

$$\frac{\partial^2\theta}{\partial x^2} + Sq - SC\frac{\partial\theta}{\partial t} - SG\theta = 0 \quad . \quad . \quad . \quad (43)$$

Locating the origin at the centre of the wire and applying boundary conditions $\theta = 0$ at $x = \pm l$ with current switched on at time zero, eqn. (43) has the solution

$$\theta = \frac{q}{G}\left[\frac{\cosh\sqrt{(SG)}x}{\cosh\sqrt{(SG)}l} + 1 - 2\exp\left(-\frac{G}{C}t\right)\right.$$

$$\left. + \frac{2}{\pi}\sum_{n=-\infty}^{\infty}(-1)^n\frac{\cos\frac{1}{2}(2n+1)\pi x/l\exp\left\{-\dfrac{SG+[\frac{1}{2}(2n+1)\pi/l]^2}{SC}t\right\}}{\frac{1}{2}(2n+1)\left\{1+\dfrac{1}{SG}[\frac{1}{2}(2n+1)\pi/l]^2\right\}}\right]$$

$$. \quad . \quad . \quad (44)$$

At the wire extremities, thermal leakage is given by

$$\frac{\left(\dfrac{\partial\theta}{\partial x}\right)_l}{S} = \frac{q}{S}\left[\sqrt{\frac{S}{G}}\tanh\sqrt{(SG)}l\right.$$

$$\left. - \frac{2}{GL}\sum_{n=-\infty}^{\infty}\frac{\exp\left\{-\dfrac{SG+[\frac{1}{2}(2n+1)\pi/l]^2}{SC}t\right\}}{1+\dfrac{1}{SG}[\frac{1}{2}(2n+1)\pi/l]^2}\right]. \quad (45)$$

# THE CALCULATION OF CYCLIC RATING FACTORS AND EMERGENCY LOADING FOR ONE OR MORE CABLES LAID DIRECT OR IN DUCTS

## By H. GOLDENBERG, M.Sc.

### SUMMARY

The knowledge of the loss load factor of a load cyclically applied to a cable laid direct in the ground or in a duct, together with the detail of the load current for the six hours prior to maximum core temperature, is shown to be adequate for cyclic-rating-factor calculations. If the loss load factor is known without further calculation, the method is shorter than an earlier one described by the author. The method is extended to deal with short-term emergency loads within accepted temperature limits and with groups of cables carrying diverse cyclic loads.

## (1) INTRODUCTION

In a recent paper[1] a method was described for the calculation of cyclic rating factors for isolated cables laid direct or in ducts, taking into account the form of the whole cycle. In the present paper it is shown that it is adequate to consider only the loss load factor of the cycle and the detail of the load current for the six hours prior to maximum core temperature. This has led to a method of cyclic-rating-factor calculation, which, if the loss load factor of the cycle is known without further calculation, requires fewer arithmetical operations than the earlier method, and is extensible to deal with both short-term emergency loads within accepted temperature limits and groups of cables carrying diverse cyclic loads.

## (2) NEW BASIS OF CYCLIC-RATING-FACTOR CALCULATION

The maximum core-temperature response to a complicated cyclic load current may be approximated by the maximum core-temperature response to the actual applied current, for a time $T$ hours prior to the expected time of maximum core temperature, and a constant applied current for all earlier times, its amplitude being the root mean square of the cyclic current, i.e. $\sqrt{(\mu)}I$, where $\mu$ is the loss load factor of the cycle and $I$ is the peak cyclic current. (The loss load factor is the ratio of the mean square to the maximum square current of an applied cyclic load.) The heat dissipated in a cable may, with sufficient accuracy, be taken as directly proportional to the square of the applied current.

With $\theta_c(T)$ as the core-temperature rise above ambient at $T$ hours after the application to a cable of a step-function rated current $I_0$, the core-temperature rise at $T_2$ hours after the application to the cable of a rectangular current pulse of one-hour duration is given as a fraction of the steady-state core-temperature rise for the same current by

$$\frac{\theta_c(T_2 + 1) - \theta_c(T_2)}{\theta_c(\infty)}$$

Following the notation adopted in the earlier paper[1] and denoting the magnitudes of the hourly rectangular pulses into which the square of the daily cyclic current may be decomposed by $Y_0$,

$Y_1, \ldots, Y_{23}$, where each of the $Y$'s is expressed as fraction of their maximum value and $Y_r$ is a measure of the equivalent square current between $r$ and $(r + 1)$ hours prior to the expected time of maximum core temperature, the maximum core-temperature rise is given by

$$(I^2/I_0^2)\left\{\mu[\theta_c(\infty) - \theta_c(T)] + \sum_{r=0}^{T-1} Y_r[\theta_c(r + 1) - \theta_c(r)]\right\}$$

$$= (I^2\theta_c(\infty)/I_0^2)\left\{\mu + \sum_{r=0}^{T-1}(Y_r - \mu)\frac{[\theta_c(r + 1) - \theta_c(r)]}{\theta_c(\infty)}\right\}$$

In this equation $\mu(I^2/I_0^2)\theta_c(\infty)$ represents the temperature at $T = 0$ (the time of maximum core temperature) due to the r.m.s. current $\sqrt{(\mu)}I$ assumed applied as a uniform load, and the remaining term represents the correction to be made at $T = 0$ owing to the departure of the true current from the r.m.s. current for all times back to $T$ hours. If the thermal capacity of the cable itself be neglected, then, from Reference 1,

$$\frac{\theta_c(1) - \theta_c(0)}{\theta_c(\infty)} = 1 - k + k\alpha(1)$$

$$\frac{\theta_c(r + 1) - \theta_c(r)}{\theta_c(\infty)} = k[\alpha(r + 1) - \alpha(r)] \text{ for } r \geqslant 1$$

where $k$ = Ratio of cable surface temperature rise to core-temperature rise, under steady conditions.

$\alpha(T)$ = Ratio of transient cable surface temperature rise at $T$ hours after the application of a step-function current to the steady-state cable surface temperature rise.

Therefore the maximum core-temperature rise is given approximately by

$$(I^2\theta_c(\infty)/I_0^2)\left\{\mu + (Y_0 - \mu)[1 - k + k\alpha(1)]\right.$$
$$+ (Y_1 - \mu)k[\alpha(2) - \alpha(1)] + (Y_2 - \mu)k[\alpha(3) - \alpha(2)] \ldots$$
$$\left. + (Y_{T-1} - \mu)k[\alpha(T) - \alpha(T - 1)]\right\}$$
$$= (I^2\theta_c(\infty)/I_0^2)\left[(1 - k)Y_0 + k\{B + \mu[1 - \alpha(T)]\}\right]$$

where

$$B = Y_0\Phi_0 + Y_1\Phi_1 + Y_2\Phi_2 + \ldots + Y_{T-1}\Phi_{T-1}$$

$$\Phi_s = \alpha(s + 1) - \alpha(s)$$

For standard cyclic-rating-factor calculations the peak cyclic current $I$ is assumed to be initially equal to the steady rated current $I_0$. The cyclic current, as a whole, may then be multiplied by the following cyclic rating factor for the same core-temperature rise:

$$\frac{1}{\sqrt{\left[(1 - k)Y_0 + k\{B + \mu[1 - \alpha(T)]\}\right]}}$$

This differs from eqn. (6) of the earlier paper[1] in that the

Table 1

VALUES OF Φ FOR SOIL THERMAL DIFFUSIVITY OF 0·02 CM²/SEC.    (HOURLY INTERVALS FOR SIX HOURS.)

Cable diameter or inner duct diameter (in inches)

| $T_2$ | 0·50 | 0·75 | 1·00 | 1·25 | 1·50 | 1·75 | 2·00 | 2·25 | 2·50 | 2·75 | 3·00 | 3·25 | 3·50 | 3·75 | 4·00 | 4·25 | 4·50 | 5·00 | 6·00 |
|---|---|---|---|---|---|---|---|---|---|---|---|---|---|---|---|---|---|---|---|
| 0 | 0·529 | 0·494 | 0·464 | 0·439 | 0·417 | 0·397 | 0·378 | 0·361 | 0·345 | 0·330 | 0·315 | 0·302 | 0·289 | 0·276 | 0·264 | 0·253 | 0·241 | 0·220 | 0·183 |
| 1 | 0·061 | 0·066 | 0·070 | 0·073 | 0·075 | 0·078 | 0·080 | 0·082 | 0·084 | 0·086 | 0·087 | 0·089 | 0·090 | 0·091 | 0·093 | 0·094 | 0·095 | 0·096 | 0·098 |
| 2 | 0·036 | 0·038 | 0·041 | 0·043 | 0·044 | 0·046 | 0·047 | 0·048 | 0·050 | 0·051 | 0·052 | 0·053 | 0·054 | 0·054 | 0·055 | 0·056 | 0·057 | 0·058 | 0·060 |
| 3 | 0·025 | 0·027 | 0·029 | 0·030 | 0·031 | 0·033 | 0·034 | 0·034 | 0·035 | 0·036 | 0·037 | 0·038 | 0·038 | 0·039 | 0·039 | 0·040 | 0·041 | 0·042 | 0·043 |
| 4 | 0·020 | 0·021 | 0·023 | 0·024 | 0·024 | 0·025 | 0·026 | 0·027 | 0·027 | 0·028 | 0·029 | 0·029 | 0·030 | 0·030 | 0·031 | 0·031 | 0·032 | 0·032 | 0·034 |
| 5 | 0·016 | 0·017 | 0·018 | 0·019 | 0·020 | 0·021 | 0·021 | 0·022 | 0·022 | 0·023 | 0·023 | 0·024 | 0·024 | 0·025 | 0·025 | 0·026 | 0·026 | 0·027 | 0·028 |

Values of $1 - \alpha(6)$ for soil thermal diffusivity of 0·02 cm²/sec

| | 0·50 | 0·75 | 1·00 | 1·25 | 1·50 | 1·75 | 2·00 | 2·25 | 2·50 | 2·75 | 3·00 | 3·25 | 3·50 | 3·75 | 4·00 | 4·25 | 4·50 | 5·00 | 6·00 |
|---|---|---|---|---|---|---|---|---|---|---|---|---|---|---|---|---|---|---|---|
| | 0·313 | 0·336 | 0·356 | 0·373 | 0·388 | 0·401 | 0·414 | 0·425 | 0·436 | 0·447 | 0·457 | 0·466 | 0·475 | 0·484 | 0·493 | 0·501 | 0·509 | 0·525 | 0·554 |

VALUES OF Φ FOR SOIL THERMAL DIFFUSIVITY OF 0·01 CM²/SEC.    (HOURLY INTERVALS FOR SIX HOURS.)

Cable diameter or inner duct diameter (in inches)

| $T_2$ | 0·50 | 0·75 | 1·00 | 1·25 | 1·50 | 1·75 | 2·00 | 2·25 | 2·50 | 2·75 | 3·00 | 3·25 | 3·50 | 3·75 | 4·00 | 4·25 | 4·50 | 5·00 | 6·00 |
|---|---|---|---|---|---|---|---|---|---|---|---|---|---|---|---|---|---|---|---|
| 0 | 0·468 | 0·430 | 0·394 | 0·367 | 0·342 | 0·319 | 0·299 | 0·280 | 0·262 | 0·246 | 0·230 | 0·216 | 0·202 | 0·189 | 0·176 | 0·164 | 0·153 | 0·132 | 0·097 |
| 1 | 0·061 | 0·066 | 0·069 | 0·072 | 0·075 | 0·077 | 0·079 | 0·081 | 0·083 | 0·084 | 0·085 | 0·086 | 0·087 | 0·088 | 0·088 | 0·088 | 0·088 | 0·088 | 0·088 |
| 2 | 0·036 | 0·038 | 0·041 | 0·043 | 0·044 | 0·046 | 0·047 | 0·048 | 0·049 | 0·050 | 0·051 | 0·052 | 0·053 | 0·053 | 0·054 | 0·054 | 0·055 | 0·056 | 0·056 |
| 3 | 0·025 | 0·027 | 0·029 | 0·030 | 0·031 | 0·032 | 0·033 | 0·034 | 0·035 | 0·036 | 0·037 | 0·037 | 0·038 | 0·038 | 0·039 | 0·040 | 0·040 | 0·040 | 0·042 |
| 4 | 0·020 | 0·021 | 0·022 | 0·023 | 0·024 | 0·025 | 0·026 | 0·027 | 0·027 | 0·028 | 0·028 | 0·029 | 0·029 | 0·030 | 0·030 | 0·031 | 0·031 | 0·032 | 0·033 |
| 5 | 0·016 | 0·017 | 0·018 | 0·019 | 0·020 | 0·021 | 0·021 | 0·022 | 0·022 | 0·023 | 0·023 | 0·024 | 0·024 | 0·025 | 0·025 | 0·025 | 0·026 | 0·026 | 0·027 |

Values of $1 - \alpha(6)$ for soil thermal diffusivity of 0·01 cm²/sec

| | 0·50 | 0·75 | 1·00 | 1·25 | 1·50 | 1·75 | 2·00 | 2·25 | 2·50 | 2·75 | 3·00 | 3·25 | 3·50 | 3·75 | 4·00 | 4·25 | 4·50 | 5·00 | 6·00 |
|---|---|---|---|---|---|---|---|---|---|---|---|---|---|---|---|---|---|---|---|
| | 0·374 | 0·402 | 0·426 | 0·446 | 0·463 | 0·479 | 0·494 | 0·508 | 0·521 | 0·534 | 0·545 | 0·557 | 0·567 | 0·578 | 0·588 | 0·598 | 0·607 | 0·626 | 0·659 |

symbol $A$ of that equation is replaced by $B + \mu[1 - \alpha(T)]$. The calculation of the term $A$ involved the summation of a number of products which could be as large as 24, whereas the calculation of $B$ involves the summation of $T$ products, $T$ being the number of hours prior to the expected time of maximum core temperature for which an accurate representation of the applied current curve is considered. Hence the choice of $T$ is a compromise between the necessity of obtaining a reasonably accurate cyclic rating factor and the desire to limit the number of multiplications involved. A suitable value for $T$ appears to be 6 hours, and the cyclic-rating-factor error with this choice will be considered for the eight typical applied-current curves of Fig. 1.
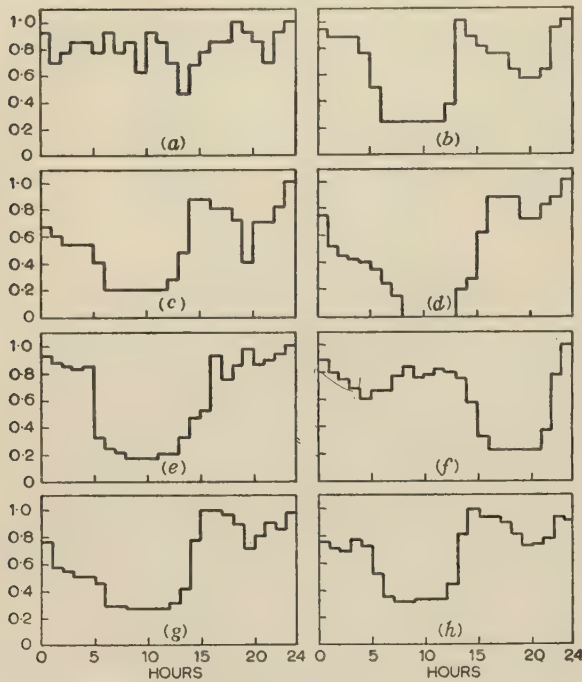


Fig. 1.—Eight typical load current curves.

To facilitate the application of the proposed method, Table 1 presents values of $\Phi$ and $1 - \alpha(6)$ for soil thermal diffusivities $0 \cdot 02$ and $0 \cdot 01 \, \text{cm}^2/\text{sec}$ for a range of cable diameters or inner duct diameters of $0 \cdot 5(0 \cdot 25) \, 4 \cdot 5$, $5 \cdot 0$ and $6 \cdot 0$ in, respectively.

Tabulated values of $k$ for representative cables conforming to B.S. 480: 1954, laid direct or in ducts, and for a soil thermal resistivity of $120° \, \text{C cm/watt}$, have been included in the earlier paper,[1] together with formulae for the calculation of $k$ for any other type of cable and for any other soil thermal resistivity.

In order to illustrate the present method, and to provide a comparison with the earlier method, let us consider example 1 of Reference 1. In this case the cyclic rating factor was calculated for a certain cyclic current applied to an isolated circuit comprising three single-core $1 \cdot 00 \, \text{in}^2$ 33 kV p.i.l.s. cables laid direct in the ground in trefoil touching formation. The cables were served, with added sheath protection, and they conformed to B.S. 480: 1954. The outer diameter of each cable was $2 \cdot 41$ in, and the upper cable axis was at a depth of 36 in below ground surface. The soil thermal resistivity and diffusivity were $120° \, \text{C cm/watt}$ and $0 \cdot 02 \, \text{cm}^2/\text{sec}$, respectively, while the appropriate value of the parameter $k$ was $0 \cdot 87$.

The present method of calculation is given in Table 2, and proceeds as follows:

(a) Enter in column 1 the six consecutive hourly intervals of

**Table 2**

CALCULATION OF CYCLIC RATING FACTOR. NATIONAL LOAD CURVE OF FIG. 2 OF EARLIER PAPER APPLIED TO ONE ISOLATED CIRCUIT COMPRISING THREE SINGLE-CORE $1 \cdot 00 \, \text{IN}^2$ 33 kV CABLES LAID DIRECT IN THE GROUND IN TREFOIL TOUCHING FORMATION

| 1<br>Time* | $Y$ step function equivalent to (cyclic current per peak current)$^2$ | 3<br>$\Phi$ factors for $D = 0 \cdot 02$ $d = 2 \cdot 50$ from Table 1 | 4<br>$Y \times \Phi$ i.e. col. 2 × col. 3 |
|---|---|---|---|
| h<br>0–1<br>1–2<br>2–3<br>3–4<br>4–5<br>5–6 | 0·99<br>0·75<br>0·625<br>0·625<br>0·625<br>0·80 | 0·345<br>0·084<br>0·050<br>0·035<br>0·027<br>0·022 | 0·342<br>0·063<br>0·031<br>0·022<br>0·017<br>0·018 |

Total $= B = \Sigma Y \Phi = 0 \cdot 493$.

Depth of upper cable axis below ground surface $= 36$ in.
Outer diameter $d$ of each cable of trefoil formation $= 2 \cdot 41$ in.
Soil thermal diffusivity, $D = 0 \cdot 02 \, \text{cm}^2/\text{sec}$.
Soil thermal resistivity, $g = 120° \, \text{C cm/watt}$.
Value of $k$ from previous paper $= 0 \cdot 87$.
Value of column 2 for time 0–1 hour $= Y_0 = 0 \cdot 99$.
Value of loss load factor, $\mu = 0 \cdot 506$.
Value of $1 - \alpha(6)$ for $D = 0 \cdot 02$, $d = 2 \cdot 50$ from Table 1.  $1 - \alpha(6) = 0 \cdot 436$.
Cyclic rating factor

$$= 1 \Big/ \big[ (1 - k) Y_0 + k \{ B + \mu[1 - \alpha(6)] \} \big]^{1/2} = 1 \cdot 15.$$

\* Time measured prior to expected time of maximum core temperature.

time directly prior to the expected time of maximum core temperature. (In the present example 17·5 hours.)

(b) Enter in column 2 the values of $Y$, namely the step function equivalent to (cyclic current per peak current)$^2$, for the appropriate hours, from Table 7 of Reference 1, measuring time prior to the expected time of maximum core temperature.

(c) Enter in column 3 the $\Phi$ factors for $D = 0 \cdot 02 \, \text{cm}^2/\text{sec}$ and cable diameter $2 \cdot 41$ in from Table 1. As no values are tabulated for exactly $d = 2 \cdot 41$ in, enter those for the nearest tabulated diameter ($2 \cdot 50$ in). The error in this procedure is negligible.

(d) Enter in column 4 the product of the corresponding entries of columns 2 and 3.

(e) Enter at the foot of column 4 the value of $B$, the sum of the individual entries in column 4. Here $B = 0 \cdot 493$.

(f) Note the value of $Y_0$, the entry in column 2 for the time 0–1 hour. Here $Y_0 = 0 \cdot 99$.

(g) Calculate the value of $\mu$ the loss load factor or ratio of mean square current to maximum square current for the applied cyclic current. From Table 6(a) of Reference 1, $\mu$ is given by the average value of (cyclic load current/peak load current)$^2$ at time $T$, and is $0 \cdot 504$. From Table 6(b) of the earlier paper $\mu$ is given by the corresponding weighted average, and is $0 \cdot 506$. In the present example $\mu$ is taken as $0 \cdot 506$.

(h) Note the value of $1 - \alpha(6)$ for $D = 0 \cdot 02$ and $d = 2 \cdot 50$ from Table 1. Here $1 - \alpha(6) = 0 \cdot 436$.

(i) Calculate the value of the cyclic rating factor

$$1 \Big/ \big[ (1 - k) Y_0 + k \{ B + \mu[1 - \alpha(6)] \} \big]^{1/2} = 1 \cdot 15$$

This is identical with the value obtained for the same problem by the method of the previous paper.

**(3) ACCURACY OF THE PRESENT METHOD AS ILLUSTRATED BY EIGHT TYPICAL CURRENT CURVES APPLIED TO CABLES OF VARIOUS DIAMETERS**

The formula for the cyclic rating factor given in the earlier paper differs from that of the present paper in that the symbol $A$ of the previous formula is now replaced by $B + \mu[1 - \alpha(6)]$. If these factors were equal numerically, the methods of the two papers would yield the same result.

The eight typical current curves of Fig. 1 are considered cyclically applied to cables of various outer diameters (or inner duct diameters in the case of ducted cables). The curves have been drawn so that the expected time of maximum core temperature is 24 hours in each case, allowing a direct comparison between the applied cyclic currents. It will be observed that, in some cases, the expected time of maximum core temperature does not coincide with the time of peak current.

The values of $A$ and $B + \mu[1 - \alpha(6)]$ have been calculated for the eight typical curves of Fig. 1 for various cable diameters and for a soil thermal diffusivity of $0 \cdot 01 \text{ cm}^2/\text{sec}$ and are presented in Table 3. It will be noticed that, in some cases, $A$ is numerically

the seventh day in question and the identical current of the six previous days for all remaining days prior to the individual seventh day in question.

If the maximum core-temperature rise occurs at $T$ hours on the seventh day and the loss load factor of the identical applied current for the six days in question is $\mu$, the required formula for the cyclic rating factor is given directly from Section 2 by

$$\frac{1}{\sqrt{\left[(1 - k)Y_0 + k\left\{B + (\mu I_1^2/I^2)[1 - \alpha(T)]\right\}\right]}}$$

where $B = Y_0\Phi_0 + Y_1\Phi_1 + \ldots + Y_{T-1}\Phi_{T-1}$

$I$ = Peak cyclic current of seventh day.

$I_1$ = Peak cyclic current of remaining six days.

All the other symbols have the same meaning as in Section 2. The minimum value of $T$ to be used in this formula is six, so that if the maximum core temperature occurs at a time earlier than 6 hours, the value of six must be taken for $T$ while the

**Table 3**

CALCULATED VALUES OF $A$ AND $B + \mu[1 - \alpha(6)]$ FOR THE EIGHT TYPICAL CURVES OF FIG. 1 APPLIED TO CABLES OF VARIOUS DIAMETERS

| Applied current as illustrated in | Calculated value of | Cable diameter or inner duct diameter (in inches) | | | | |
|---|---|---|---|---|---|---|
| | | 0·5 | 1·5 | 3·0 | 4·5 | 6·0 |
| Fig. 1(a) | $A$ | 0·833 | 0·794 | 0·759 | 0·735 | 0·717 |
| | $B + \mu[1 - \alpha(6)]$ | 0·840 | 0·801 | 0·767 | 0·744 | 0·728 |
| Fig. 1(b) | $A$ | 0·733 | 0·670 | 0·613 | 0·573 | 0·541 |
| | $B + \mu[1 - \alpha(6)]$ | 0·734 | 0·671 | 0·614 | 0·574 | 0·544 |
| Fig. 1(c) | $A$ | 0·683 | 0·608 | 0·541 | 0·494 | 0·457 |
| | $B + \mu[1 - \alpha(6)]$ | 0·680 | 0·604 | 0·536 | 0·488 | 0·453 |
| Fig. 1(d) | $A$ | 0·691 | 0·617 | 0·551 | 0·504 | 0·467 |
| | $B + \mu[1 - \alpha(6)]$ | 0·695 | 0·622 | 0·557 | 0·510 | 0·475 |
| Fig. 1(e) | $A$ | 0·762 | 0·704 | 0·654 | 0·617 | 0·588 |
| | $B + \mu[1 - \alpha(6)]$ | 0·775 | 0·721 | 0·672 | 0·638 | 0·611 |
| Fig. 1(f) | $A$ | 0·670 | 0·593 | 0·523 | 0·476 | 0·440 |
| | $B + \mu[1 - \alpha(6)]$ | 0·676 | 0·599 | 0·531 | 0·484 | 0·451 |
| Fig. 1(g) | $A$ | 0·732 | 0·677 | 0·627 | 0·592 | 0·564 |
| | $B + \mu[1 - \alpha(6)]$ | 0·728 | 0·672 | 0·620 | 0·585 | 0·558 |
| Fig. 1(h) | $A$ | 0·689 | 0·657 | 0·628 | 0·607 | 0·589 |
| | $B + \mu[1 - \alpha(6)]$ | 0·685 | 0·651 | 0·620 | 0·598 | 0·582 |

greater than $B + \mu[1 - \alpha(6)]$ or that the cyclic rating factor obtained by the present method is too large. However, this is seen to be the case by less than 1% while the maximum underestimate of cyclic rating factor by the method of the present paper is less than 2%.

### (4) WEEKLY CYCLIC LOAD

A weekly cyclic load of some importance consists of six days of an identical applied current and a seventh day with a substantially increased current, so that the maximum core temperature will be reached on each seventh day alone. For the determination of the maximum core temperature on any individual seventh day there is only a negligible error involved in considering the temperature response as being due to the correct current for

remaining values of $Y$ must correspond to the last hours of one of the six identical daily cycles.

Hourly values of $\Phi$ for a wide range of cable and inner-duct diameters, for the standard depth of laying of 36 in and for soil thermal diffusivities of $0 \cdot 02$ and $0 \cdot 01 \text{ cm}^2/\text{sec}$, together with corresponding values of $\alpha(T)$, have been given in Reference 2.

### (5) EMERGENCY LOAD

It is often important to calculate the maximum permissible constant current for a specified period of $T$ hours following either a constant current less than the rated current, or a cyclic current.

If the constant current continuously applied to a cable prior to emergency loading is $\sqrt{\mu}$ times the rated current, the subsequent emergency current for a period of $T$ hours has been shown

by Whitehead and Hutchings[3] to be given by $p$ times the rated load current, where

$$p = \left[ \mu + \frac{1 - \mu}{1 - k + k\alpha(T)} \right]^{1/2}$$

To facilitate calculation of the maximum load factor, Table 4 gives values of $\alpha(T)$ for 24 hourly values of $T$ for a soil thermal diffusivity of $0\cdot01\,\text{cm}^2/\text{sec}$ for a range of outer cable or inner duct diameters, and for the standard depth of laying of 36 in, while $k$

On equating the above expressions for the core-temperature rise above ambient at the end of the period of emergency load with the maximum permissible core-temperature rise above ambient and solving for $q$, we find, after some manipulation involving the relations given in Section 2,

$$q = \left[ \frac{1 - (kI^2/I_0^2)\{\mu[1 - \alpha(6)] + Y_T\Phi_T + Y_{T+1}\Phi_{T+1} \cdots + Y_5\Phi_5\}}{1 - k + k\alpha(T)} \right]^{1/2}$$

### Table 4

VALUES OF $\alpha(T)$ FOR SOIL THERMAL DIFFUSIVITIES OF $0\cdot01$ AND $0\cdot02\,\text{CM}^2/\text{SEC}$

| $D = 0\cdot01\,\text{cm}^2/\text{s}$ | Cable diameter or inner duct diameter (in inches) | | | | | | | | | | | $D = 0\cdot02\,\text{cm}^2/\text{s}$ |
|---|---|---|---|---|---|---|---|---|---|---|---|---|
| $T$ | $0\cdot50$ | $1\cdot00$ | $1\cdot50$ | $2\cdot00$ | $2\cdot50$ | $3\cdot00$ | $3\cdot50$ | $4\cdot00$ | $4\cdot50$ | $5\cdot00$ | $6\cdot00$ | $T$ |
| h | | | | | | | | | | | | h |
| 0 | 0·0000 | 0·0000 | 0·0000 | 0·0000 | 0·0000 | 0·0000 | 0·0000 | 0·0000 | 0·0000 | 0·0000 | 0·0000 | 0·0 |
| 1 | 0·4682 | 0·3945 | 0·3417 | 0·2989 | 0·2623 | 0·2302 | 0·2017 | 0·1761 | 0·1530 | 0·1323 | 0·0970 | 0·5 |
| 2 | 0·5293 | 0·4639 | 0·4168 | 0·3783 | 0·3450 | 0·3155 | 0·2887 | 0·2641 | 0·2414 | 0·2204 | 0·1825 | 1·0 |
| 3 | 0·5651 | 0·5046 | 0·4609 | 0·4251 | 0·3941 | 0·3664 | 0·3412 | 0·3179 | 0·2962 | 0·2760 | 0·2388 | 1·5 |
| 4 | 0·5905 | 0·5335 | 0·4923 | 0·4585 | 0·4292 | 0·4029 | 0·3789 | 0·3567 | 0·3360 | 0·3164 | 0·2805 | 2·0 |
| 5 | 0·6101 | 0·5559 | 0·5166 | 0·4844 | 0·4564 | 0·4313 | 0·4083 | 0·3870 | 0·3671 | 0·3483 | 0·3134 | 2·5 |
| 6 | 0·6263 | 0·5742 | 0·5366 | 0·5056 | 0·4787 | 9·4546 | 0·4325 | 0·4119 | 0·3927 | 0·3745 | 0·3407 | 3·0 |
| 7 | 0·6399 | 0·5897 | 0·5534 | 0·5236 | 0·4976 | 0·4743 | 0·4529 | 0·4331 | 0·4144 | 0·3968 | 0·3640 | 3·5 |
| 8 | 0·6516 | 0·6031 | 0·5680 | 0·5391 | 0·5140 | 0·4914 | 0·4707 | 0·4514 | 0·4333 | 0·4162 | 0·3842 | 4·0 |
| 10 | 0·6713 | 0·6256 | 0·5924 | 0·5651 | 0·5414 | 0·5204 | 0·5004 | 0·4822 | 0·4650 | 0·4487 | 0·4183 | 5 |
| 12 | 0·6874 | 0·6439 | 0·6123 | 0·5864 | 0·5638 | 0·5434 | 0·5247 | 0·5073 | 0·4910 | 0·4754 | 0·4463 | 6 |
| 14 | 0·7010 | 0·6594 | 0·6292 | 0·6044 | 0·5827 | 0·5632 | 0·5453 | 0·5287 | 0·5129 | 0·4980 | 0·4701 | 7 |
| 16 | 0·7128 | 0·6728 | 0·6438 | 0·6199 | 0·5991 | 0·5804 | 0·5632 | 0·5472 | 0·5320 | 0·5177 | 0·4908 | 8 |
| 18 | 0·7233 | 0·6847 | 0·6567 | 0·6337 | 0·6136 | 0·5956 | 0·5790 | 0·5635 | 0·5489 | 0·5350 | 0·5090 | 9 |
| 20 | 0·7325 | 0·6953 | 0·6682 | 0·6460 | 0·6266 | 0·6091 | 0·5931 | 0·5782 | 0·5640 | 0·5505 | 0·5254 | 10 |
| 22 | 0·7409 | 0·7049 | 0·6787 | 0·6571 | 0·6383 | 0·6214 | 0·6058 | 0·5913 | 0·5776 | 0·5646 | 0·5402 | 11 |
| 24 | 0·7486 | 0·7136 | 0·6882 | 0·6673 | 0·6490 | 0·6326 | 0·6175 | 0·6034 | 0·5901 | 0·5775 | 0·5537 | 12 |

may be calculated (or is given directly for cables to B.S. 480: 1954) using the earlier paper.[1] Further, as $\alpha(T)$ for a soil thermal diffusivity of $0\cdot02\,\text{cm}^2/\text{sec}$ is equal to $\alpha(2T)$ for a soil thermal diffusivity of $0\cdot01\,\text{cm}^2/\text{sec}$, Table 4 also gives $\alpha(T)$ for a soil thermal diffusivity of $0\cdot02\,\text{cm}^2/\text{sec}$ for a maximum period of $T = 12$ hours.

If the cyclic current is applied to a cable prior to emergency loading, we denote the amplitudes of the step-function current equivalent to the squared applied cyclic current for the one hour, two hours, three hours, etc., prior to the commencement of the emergency current by $I\sqrt{Y_T}$, $I\sqrt{Y_{T+1}}$, $I\sqrt{Y_{T+2}}$, etc., where $I$ is the peak cyclic current. The maximum emergency current for the period of $T$ hours is denoted by $q$ times the rated current. If $\theta_c$ is the maximum permissible core-temperature rise above ambient, and $I_0$ is the corresponding rated current, the core-temperature rise above ambient at the end of the period of emergency current is given by

$$(I^2/I_0^2)\{\mu\theta_c + (q_1^2 - \mu)\theta_c(T) + (Y_T - \mu)[\theta_c(T + 1) - \theta_c(T)]$$
$$+ (Y_{T+1} - \mu)[\theta_c(T + 2) - \theta_c(T + 1)] + \ldots$$
$$+ (Y_5 - \mu)[\theta_c(6) - \theta_c(5)]\} \quad \text{for } T < 6 \text{ hours}$$

$$(I^2/I_0^2)\{\mu\theta_c + (q_1^2 - \mu)\theta_c(T)\} \quad \text{for } T \geqslant 6 \text{ hours}$$

where $q_1 = qI_0/I$, and $\theta_c(T)$ is the core-temperature rise above ambient at $T$ hours after the application to the cable of a step-function rated current $I_0$.

for $T < 6$ hours, and

$$q = \left\{ \frac{1 - (k\mu I^2/I_0^2)[1 - \alpha(T)]}{1 - k + k\alpha(T)} \right\}^{1/2}$$

for $T \geqslant 6$ hours.

To illustrate the application of the present method, we consider the cable, the method of laying, the soil constants, the cyclic current and additional data required to be the same as in example 1 of Reference 1. With the peak cyclic current equal to the steady rated current, it is required to find the maximum permissible constant current for the period of $10\cdot5$–$12\cdot5$ hours, subsequent to the cyclic current at all earlier times.

The emergency is for a two-hour period, so that $T = 2$. The values of $Y$ for the 4-hour period prior to the emergency current are taken from the earlier paper,[1] and are as follows: $Y_2 = Y_3 = 0\cdot885$, $Y_4 = 1\cdot00$, $Y_5 = 0\cdot375$. The corresponding values of $\Phi$ for a soil thermal diffusivity of $0\cdot02\,\text{cm}^2/\text{sec}$ and a cable external diameter of $2\cdot50$ in are obtained from Table 1 and are as follows: $\Phi_2 = 0\cdot050$, $\Phi_3 = 0\cdot035$, $\Phi_4 = 0\cdot027$ and $\Phi_5 = 0\cdot022$. Further $1 - \alpha(6) = 0\cdot436$ from Table 1, while $\mu = 0\cdot506$, $k = 0\cdot87$, and $\alpha(2)$, for a soil thermal diffusivity of $0\cdot02\,\text{cm}^2/\text{sec}$ and a cable external diameter of $2\cdot50$ in, is obtained from Table 4 and equals $0\cdot429$. The insertion of these values in the previous formula gives an emergency current $19\%$ in excess of the rated value.

## (7) CABLE GROUPS

The temperature distribution due to an isolated cable laid direct in the ground, with a constant applied current, may be approximated by that due to a continuous line source of heat at the cable centre together with its image in the earth's surface, provided that there is a constant rate of heat liberation per unit time per unit length of the source, that the cable is assumed to possess the same thermal properties as the soil in which it is buried, and that the surface of the ground may be treated as an isothermal. The transient temperature rise, at a point distant $r_1$ from the line source and $r_2$ from the image of the line source in the earth's surface, is given as a proportion of the steady-state temperature rise at the same point by $\psi(t)$, where

$$\psi(t) = \frac{-\operatorname{Ei}\left(-\dfrac{r_1^2}{4Dt}\right) + \operatorname{Ei}\left(-\dfrac{r_2^2}{4Dt}\right)}{2\log_\varepsilon(r_2/r_1)}$$

$t$ = Time measured from the instant of application of heating, sec.

$D$ = Thermal diffusivity of the soil, cm²/sec.

$-\operatorname{Ei}(-x)$ is the exponential integral function defined by

$$-\operatorname{Ei}(-x) = \int_x^\infty \frac{\varepsilon^{-u}}{u}\,du$$

while the steady-state temperature rise itself is given by

$$\theta = (gP/2\pi)\log_\varepsilon(r_2/r_1)$$

where  $g$ = Soil thermal resistivity, deg C cm/watt.

$P$ = Rate of heating per unit length of line source, watts/cm.

The assumption that the cable material possesses the same properties as the soil is not so unjustified in practice for the times under consideration as would appear at first sight.[4,5] Excellent Tables of the exponential integral function have been published by the National Bureau of Standards.[6]

Let us consider a group of differently intermittently loaded cables laid direct in the ground, and suppose that it is required to calculate the peak intermittent current in a single cable in order that its maximum permissible temperature rise above ambient and the temperature rise above ambient of the other cables are not exceeded, the intermittent current in all other cables remaining the same. The maximum core-temperature rise due to the single cable, isolated from the remaining cables, is given by

$$I^2\theta_c(\infty)/R^2 I_0^2$$

where, for the isolated single cable,

$\theta_c(\infty)$ = Maximum permissible core-temperature rise above ambient.

$I$ = Peak intermittent current prior to the application of the intermittent rating factor.

$I_0$ = Continuous rated current.

$R$ = Cyclic rating factor.

It will be assumed that the time of maximum core temperature of the cable whose peak intermittent current is required is the same whether that cable is in the presence of other loaded conductors or not. This assumption is made for simplicity only, and is not essential for the present method.

On the temperature rise above ambient due to the single isolated cable must be superimposed the temperature contributions due to the remaining cables. The contribution from the $s$th additional cable is given by

$$\frac{gP_s}{2\pi}\left(\log_\varepsilon\frac{r_{2s}}{r_{1s}}\right)\left\{Y_{0s}[\psi_s(1) - \psi_s(0)] + Y_{1s}[\psi_s(2) - \psi_s(1)]\ldots\right.$$
$$\left.\ldots + Y_{(T-1),s}[\psi_s(T) - \psi_s(T-1)] + \mu_s[1 - \psi_s(T)]\right\}$$

where the $s$th additional cable is denoted by the symbol $s$, and

$I_s$ = Peak intermittent current on $s$th cable.

$I_{0s}$ = Rated current on $s$th cable.

$P_s$ = Rate of heating per unit length of $s$th cable with steady applied peak current $I_s$.

$r_{2s}$ = Distance from image of centre of cable $s$ in earth's surface to centre of single cable whose intermittent rating factor is required.

$r_{1s}$ = Distance from centre of cable $s$ to centre of single cable whose intermittent rating factor is required.

$Y_{0s}$, $Y_{1s}$, etc. = Values of $Y_0$, $Y_1$, etc., for the $s$th cable. Appropriate hourly rectangular pulses into which the square of each cyclic current is decomposed, with peak intermittent current assumed to be unity. Time measured prior to expected time of maximum core temperature of cable whose intermittent rating factor is required.

$\psi_s(T)$ = Value of $\psi(t)$, with $t$ replaced by $3\,600T$, for the $s$th cable.

$\mu_s$ = Loss load factor of the applied current of the $s$th cable.

Denoting

$$C_s = Y_{0s}[\psi_s(1) - \psi_s(0)] + Y_{1s}[\psi_s(2) - \psi_s(1)] + \ldots$$
$$\ldots + Y_{(T-1),s}[\psi_s(T) - \psi_s(T-1)] + \mu_s[1 - \psi_s(T)]$$

the total temperature rise at the centre of the cable whose intermittent rating factor is required is

$$[I^2\theta_c(\infty)/R^2 I_0^2] + \frac{g}{2\pi}\sum_s C_s P_s\log_\varepsilon(r_{2s}/r_{1s})$$

The peak intermittent current of an individual cable, with the current of all the remaining cables kept constant, is then given by the rated current of that cable when isolated, multiplied by the intermittent rating factor

$$R\left\{1 - [g/2\pi\theta_c(\infty)]\sum_s C_s P_s\log_\varepsilon(r_{2s}/r_{1s})\right\}^{1/2}$$

while a corresponding expression can also be obtained when all the cables are to be multiplied by the same cyclic rating factor.

When the remaining cables are 'sufficiently far' separated from the single cable whose intermittent rating factor is required, $C_s$ may be assumed to be equal to $\mu_s$, as the terms $\psi_s(T)$ in the equation for $C_s$ become negligible. In practice 'sufficiently far' may be interpreted as 12 in or more for cables conforming to B.S. 480: 1954, but for a large proportion of applied load curves this distance may be much reduced.

For calculation purposes calculated values of the power loss per centimetre for representative areas of cables conforming to B.S. 480: 1954, for a soil thermal resistivity of 120° C cm/watt for cables laid direct in the ground and in ducts, have been included in Reference 7.

If the single cable whose intermittent rating factor is required is too close to the remaining cables of the group for $C_s$ to be assumed equal to $\mu_s$, a simplification of the previous formula is nevertheless possible, as the intermittent rating factor may be expressed as

$$R\left\{1 - [g/4\pi\theta_c(\infty)]\sum P_s H_s\right\}^{1/2}$$

where

$$H_s = Y_{0s}[\Psi'_s(1) - \Psi'_s(0)] + Y_{1s}[\Psi'_s(2) - \Psi'_s(1)] \ldots$$
$$\ldots + Y_{(T-1),s}[\Psi'_s(T) - \Psi'_s(T-1)]$$
$$+ \mu_s[2 \log_\varepsilon (r_{2s}/r_{1s}) - \Psi'_s(T)]$$

$$\Psi'_s(T) = - \mathrm{Ei}\left(\frac{-r_{1s}^2}{4D \times 3\,600T}\right) + \mathrm{Ei}\left(\frac{-r_{2s}^2}{4D \times 3\,600T}\right)$$

A suitable value of $T$ for summation purposes is 24 hours for cables conforming to B.S. 480: 1954. The image term of $\Psi'_s(T)$ is then negligible, so that we take

$$\Psi'_s(T) = - \mathrm{Ei}\left(\frac{-r_{1s}^2}{4D \times 3\,600T}\right)$$

where $T$ = time, hours.

$\Psi'_s(T)$ may readily be calculated using Tables for the exponential integral given in Reference 5, but critical Tables for this purpose when $-\mathrm{Ei}(-x) = 0\cdot00\,(0\cdot01)\,2\cdot00$, together with Tables of $-\mathrm{Ei}(-x)$ for $x = 0\cdot00\,(0\cdot01)\,1\,(0\cdot1)\,10$ have been given in Reference 7.

It is necessary to check that the application of the calculated intermittent rating factor to the particular cable in question does not make the conductor temperatures of surrounding cables exceed their permissible values. If $R_1$ denotes the intermittent rating factor of the particular cable in question in the presence of remaining loaded cables, the maximum conductor temperature rise above ambient of an individual surrounding cable may be obtained in the form

$$(I^2\theta_c(\infty)/I_0^2)\left[(1-k)Y_0 + k\{B + \mu[1 - \alpha(6)]\}\right]$$
$$+ \frac{g}{2\pi}\sum_s' \mu_s P_s \log_\varepsilon \frac{r_{2s}}{r_{1s}} + \frac{R_1^2 g\mu}{2\pi} P \log_\varepsilon \frac{r_2}{r_1}$$

where the first term represents the conductor temperature rise above ambient of the isolated individual surrounding cable under consideration, the second term represents the conductor temperature rise above ambient of the same cable due to all remaining cables except the cable whose intermittent rating factor is required, and the final term represents the conductor temperature rise above ambient of the same cable due to the cable whose intermittent rating factor is required ($P$ is the rate of heating per unit length of the cable whose intermittent rating factor is required, subject to steady rated current).

If the temperature rise given by this expression is less than its maximum permissible value for all surrounding cables, the required intermittent rating factor is simply $R_1$.

If the conductor temperature rise of only one surrounding cable is exceeded, the cyclic rating factor is obtained by equating the above expression for that cable to the maximum permissible conductor temperature rise above ambient of the cable, $\theta_c(\infty)$, and solving the resultant equation for $R_1$, giving

$$R_1 = \left\{\frac{\theta_c(\infty) - (I^2\theta_c(\infty)/I_0^2)\left[(1-k)Y_0 + k\{B + \mu[1 - \alpha(6)]\}\right] - \frac{g}{2\pi}\sum_s' \mu_s P_s \log_\varepsilon \frac{r_{2s}}{r_{1s}}}{(g\mu P/2\pi)\log_\varepsilon (r_2/r_1)}\right\}^{1/2}$$

If the conductor temperature rise of more than one surrounding cable is exceeded, the appropriate intermittent rating factor may be calculated on a similar basis, but the details become correspondingly more complicated.

As an example, let us consider a trefoil touching group of cables, laid direct in the ground at a depth 36 in of upper-cable axis below ground surface, symmetrically disposed at a horizontal axial spacing of 18 in with respect to two identical 3-core cables,

each at a depth of 42 in of upper cable surface below ground surface. This geometrical configuration is given in Fig. 2. The trefoil touching group of cables, their current and the soil properties are taken to be the same as in the earlier example of Section 2. The 3-core cables are taken as screened $0\cdot25\,\mathrm{in}^2$, 33 kV p.i.l.s., single-wire armoured and served, with an outer-cable diameter of $3\cdot47$ in, a cable loss of $39\cdot0\,\mathrm{kW}/1\,000$ yd for a core-temperature rise above ground of $50°$ C due to a steady applied rated current. The intermittent current applied to each 3-core cable is assumed to have a loss load factor of $0\cdot472$ (corresponding to an intermittent current different from that applied to the trefoil touching group of cables). If the peak intermittent current of each 3-core cable is equal to its (isolated) rated current, the question arises as to the magnitude of the peak intermittent current of the trefoil cable group so that the maximum permissible core temperature of each cable is not exceeded. In particular, it is interesting to compare this figure with the corresponding peak value for the isolated trefoil group.

From Section 2 the cyclic rating factor $R$ for the isolated trefoil group is given as $1\cdot15$. The maximum permissible core temperature of the trefoil group is obtained from E.R.A. Report Ref. F/T183, and is $70°$ C, giving the value for $\theta_c(\infty)$, the maximum permissible core temperature rise above ambient, of $70 - 15 = 55°$ C, and a corresponding value for $g/2\pi\theta_c(\infty)$ of $120/2\pi \times 55 = 0\cdot347\,\mathrm{cm/watt}$. Further, the rate of heating per unit length of 3-core cable, with steady applied rated current, is $P = 39\cdot0\,\mathrm{kW}/1\,000$ yards $= 0\cdot427$ watts/cm.

The loss load factor $\mu$ of the load applied to the 3-core cables is $0\cdot472$, while from the geometrical configuration of Fig. 2,
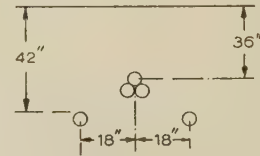


Fig. 2.—Cable configuration.

$\log_\varepsilon (r_2/r_1) = 1\cdot47$. Hence for the two 3-core cables the term $[g/2\pi\theta_c(\infty)] \sum_s P_s\mu_s \log_\varepsilon (r_{2s}/r_{1s})$ assumes the numerical value of $2 \times 0\cdot347 \times 0\cdot427 \times 0\cdot472 \times 1\cdot47 = 0\cdot206$, so that the intermittent rating factor for the trefoil cable group is given by $1\cdot15\sqrt{(1 - 0\cdot206)} = 1\cdot02$, provided that the 3-core cables do not exceed their permissible temperature.

It is now necessary to check that the 3-core cables do not exceed their permissible temperature when the amplitude of the current waveform applied to the trefoil group is multiplied by the 'tentative' intermittent rating factor of $1\cdot02$. The maximum permissible conductor temperature rise above ambient for the 3-core cable is $50°$ C, while the cyclic rating factor for an isolated 3-core cable (corresponding to a particular intermittent current detailed in Table 5, col. 5, and of loss load factor $0\cdot472$) is $1\cdot14$. The intermittent currents applied to the trefoil group of cables and to the 3-core cables have peak values occurring at approximately the same time.

The maximum core-temperature rise in either 3-core cable, due to its own current, is $50/1\cdot14^2 = 38\cdot4°$ C, the peak cyclic current of each 3-core cable being equal to its rated current. The temperature rise in either 3-core cable due to the remaining 3-core

**Table 5**

CALCULATION OF THE CYCLIC RATING FACTOR OF A TREFOIL GROUP IN THE PRESENCE OF TWO 3-CORE CABLES. INTERMITTENT CURRENT IN ALL CABLES

| 1<br>Time*<br>$T$ | 2<br>$\dfrac{1 \cdot 76}{T} = \dfrac{r_1^2}{4D \times 3\,600T}$ | 3<br>$-\mathrm{Ei}\left(-\dfrac{1 \cdot 76}{T}\right) = \Psi(T)$ | 4<br>Differences of col. 3<br>$\Psi(T) - \Psi(T-1)$ | 5<br>$Y$ step function equivalent to (cyclic load current per peak load current)² | 6<br>Col. 4 × col. 5 |
|---|---|---|---|---|---|
| h | | | | | |
| 0 | ∞ | 0·00 | | | |
| 1 | 1·76 | 0·07 | 0·07 | 0·94 | 0·066 |
| 2 | 0·880 | 0·27 | 0·20 | 0·63 | 0·126 |
| 3 | 0·587 | 0·47 | 0·20 | 0·36 | 0·072 |
| 4 | 0·440 | 0·64 | 0·17 | 0·31 | 0·053 |
| 5 | 0·352 | 0·79 | 0·15 | 0·35 | 0·053 |
| 6 | 0·293 | 0·92 | 0·13 | 0·48 | 0·062 |
| 7 | 0·251 | 1·04 | 0·12 | 0·56 | 0·067 |
| 8 | 0·220 | 1·15 | 0·11 | 0·61 | 0·067 |
| 9 | 0·196 | 1·24 | 0·09 | 0·71 | 0·064 |
| 10 | 0·176 | 1·33 | 0·09 | 0·88 | 0·079 |
| 11 | 0·160 | 1·41 | 0·08 | 0·56 | 0·045 |
| 12 | 0·147 | 1·48 | 0·07 | 0·12 | 0·008 |
| 13 | 0·135 | 1·56 | 0·08 | 0·06 | 0·005 |
| 14 | 0·126 | 1·62 | 0·06 | 0·06 | 0·004 |
| 15 | 0·117 | 1·68 | 0·06 | 0·06 | 0·004 |
| 16 | 0·110 | 1·74 | 0·06 | 0·06 | 0·004 |
| 17 | 0·104 | 1·79 | 0·05 | 0·06 | 0·003 |
| 18 | 0·0978 | 1·84 | 0·05 | 0·15 | 0·008 |
| 19 | 0·0926 | 1·89 | 0·05 | 0·39 | 0·020 |
| 20 | 0·0880 | 1·94 | 0·05 | 0·67 | 0·033 |
| 21 | 0·0838 | 1·98 | 0·04 | 0·77 | 0·031 |
| 22 | 0·0800 | 2·03 | 0·05 | 0·77 | 0·038 |
| 23 | 0·0765 | 2·07 | 0·04 | 0·83 | 0·033 |
| 24 | 0·0733 | 2·11 | 0·04 | 0·94 | 0·038 |
| | | | | Total .. .. | 0·983 |

From example, $\log_\varepsilon r_2/r_1 = 2 \cdot 21$, $\mu = 0 \cdot 472$, $g/2\pi\theta_c(\infty) = 0 \cdot 347$ and $P = 0 \cdot 427$

$$\mu[2 \log (r_2/r_1) - \Psi(24)] = 0 \cdot 472 \times 2 \cdot 31 = 1 \cdot 090$$
$$H = 0 \cdot 983 + 1 \cdot 090 = 2 \cdot 073$$

$$\frac{g}{4\pi\theta_c(\infty)} \sum_s P_s H_s = 2 \times 0 \cdot 173\,5 \times 0 \cdot 427 \times 2 \cdot 073 = 0 \cdot 307$$
(Two equally loaded cables)

Intermittent rating factor, $R$, of isolated trefoil group $= 1 \cdot 15$.
Intermittent rating factor of trefoil group in the presence of the two loaded 3-core cables $= 1 \cdot 15\sqrt{(1 - 0 \cdot 307)} = 0 \cdot 95$.

*Time measured prior to expected time of maximum core temperature of trefoil group.

cable is $(g/2\pi)\mu_s P_s \log_\varepsilon (r_{2s}/r_{1s})$, and with $g = 120° \mathrm{C\,cm/watt}$, $\mu_s = 0 \cdot 472$, $P_s = 0 \cdot 427$ watts/cm and $\log_\varepsilon (r_{2s}/r_{1s}) = 0 \cdot 96$ from the cable configuration of Fig. 2, the temperature rise due to the remaining 3-core cable is $3 \cdot 7° \mathrm{C}$. The temperature rise in either 3-core cable due to the trefoil group is given by $(R_1^2 g\mu P/2\pi) \log_\varepsilon (r_2/r_1)$, and with $R_1 = 1 \cdot 02$, $g = 120° \mathrm{C\,cm/watt}$, $\mu = 0 \cdot 506$, $P =$ trefoil cable group loss $= 0 \cdot 54$ watt/cm and $\log_\varepsilon (r_2/r_1) = 1 \cdot 47$ from the cable configuration of Fig. 2, the temperature rise due to the trefoil group is $8 \cdot 0° \mathrm{C}$. The maximum temperature increase of the conductor of the 3-core cable is therefore $38 \cdot 4 + 3 \cdot 7 + 8 \cdot 0 = 50 \cdot 1° \mathrm{C}$, which is practically the same as the permissible value of $50° \mathrm{C}$.

Thus the amplitude of the intermittent current of the trefoil group may be increased by only 2% with the two 3-core cables of the group loaded as specified, while a 15% increase is permissible for the isolated trefoil group. With large or close cable groups a reduction of peak intermittent current below its isolated rated value may often prove to be necessary. This is illustrated by the above example with a horizontal spacing of 6 in in place of 18 in, all other factors remaining the same. The amplitude of the intermittent current of the trefoil group must then be decreased by 5%.

It is instructive to give some details of the cyclic-rating-factor calculation for the case of 6 in horizontal spacing, based both on the averaging of the current in the 3-core cables, and on the more accurate intermittent current representation.

The intermittent rating factor based on the averaging of the current in the 3-core cables, and for 6 in horizontal spacing, is obtained in the same manner as for 18 in horizontal spacing, except that, from the geometrical configuration of Fig. 2, the term $\log_\varepsilon (r_2/r_1)$ now assumes the value of $2 \cdot 21$ in place of the previous value of $1 \cdot 47$. The intermittent rating factor based on the averaging of the current in the 3-core cables is then found to be $0 \cdot 95$.

When account is to be taken of the intermittent character of the current in the 3-core cables, the calculation may be presented

in a tabular manner. Table 5 gives the calculation for the present example. In column 1 is entered the time $T$ in hours, measured prior to the expected time of maximum core temperature of the trefoil group (in the present case $17 \cdot 5$ hours). In column 2 is entered the values of $r_1^2/4D \times 3\,600T$ for $T = 0(1)24$. The exponential integral of the latter values are entered in column 3. The differences of the entries in column 3 are inserted in column 4. Column 5 gives the step function equivalent to (cyclic current per peak current)$^2$ for each 3-core cable. The product of each corresponding pair of entries of columns 4 and 5 is inserted in column 6, and the latter column is totalled. On addition to this total of $\mu[2 \log_\varepsilon (r_2/r_1) - \Psi'(24)]$, the factor $H$ is obtained, and is equal to $2 \cdot 073$, giving an intermittent rating factor of $0 \cdot 95$, namely the same as that based on the averaging of the current in the 3-core cables. The direct cable centre separation in this example is $8 \cdot 9$ in—certainly less than the 12 in demarcation limit specified earlier. Nevertheless the method of averaging the current of surrounding cables is not sufficiently accurate for all cases of separation less than 12 in for all cables and for all current forms, so that a reduction of this figure does not appear desirable.

## (7) ACKNOWLEDGMENTS

## (8) REFERENCES

(1) GOLDENBERG, H.: 'The Calculation of Cyclic Rating Factors for Cables Laid Direct or in Ducts', *Proceedings I.E.E.*, Monograph No. 203 S, October, 1956 (**104** C, p. 154).
(2) GOLDENBERG, H.: 'A Further Simple Method for the Calculation of Cyclic Rating Factors and Emergency Loading for Cables Laid Direct or in Ducts' (E.R.A. Report Ref. F/T190; 1957).
(3) WHITEHEAD, S., and HUTCHINGS, E. E.: 'Current Rating of Cables for Transmission and Distribution', *Journal, I.E.E.*, 1938, **83**, p. 517.
(4) BULLER, F. H.: 'Thermal Transients on Buried Cables', *Transactions of the American I.E.E.*, 1951, **70**, Part I, p. 45.
(5) Supplement to Report Ref. F/T12, on the Heating of Buried Cables (E.R.A. Report Ref. F/T15; 1925).
(6) 'Tables of Sine, Cosine and Exponential Integrals', Vol. 1 (National Bureau of Standards, 1940).
(7) GOLDENBERG, H.: 'The Calculation of External Thermal Resistance and Cyclic Rating Factors for Groups of Cables Laid Direct in the Ground or in Ducts' (E.R.A. Report Ref. F/T192; 1957).

# COEFFICIENTS FOR 'DECOMPOSITION' OF FUNCTIONS INTO LAGUERRE-FUNCTION SERIES

## By J. W. HEAD, M.A., and GWYNNETH M. OULTON, B.Sc.

### SUMMARY

Given a function of time which behaves arbitrarily up to a certain time and is thereafter negligible, a satisfactory 10-term Laguerre-series approximation to the function can in general be written down in terms of the values of the function (obtained by graphical interpolation if necessary) at times proportional to the 10 zeros of the Laguerre function of order 10. The way in which the approximation fails when the procedure is deliberately applied to an unsuitable function is considered.

## (1) INTRODUCTION

If we wish to consider a function of time which is periodic but otherwise arbitrary, it is often helpful to find a Fourier series, by means of which the periodic function is broken up into a finite or infinite number of sinusoidal components, and a useful approximation to the original function is obtained by taking, say, the first $n$ of these components.

Frequently, however, we are concerned with a function of time which has no obvious periodicity, behaves in an arbitrary manner for small and moderate values of the time, and is negligible from a certain time $t_0$ onwards. A reasonable approximation to such a function will often be a series of Laguerre functions. The coefficients in the series can, like those in a Fourier series, be determined by integration, since Laguerre functions of the same argument $kt$ and different orders are orthogonal for the range $0 < t < \infty$. If, however, we know the greatest number of terms in the Laguerre series likely to be justified in practice by the accuracy with which the values of the given time function can be determined, the coefficients can be derived directly, without any integration, from certain constants which can be calculated in advance. These constants are discussed, and tabulated below on the assumption that a series of 10 terms is justified by the data.

$f(t)$ is negligible for $t \geqslant t_0$. We seek to determine the coefficients $b_s$ so that

$$\text{f}(t) \text{ and } \sum_{s=0}^{N-1} b_s \lambda_s(kt) \quad \ldots \quad \ldots \quad (1)$$

shall be approximately equal for $0 < t < t_0$ and negligible for $t \geqslant t_0$, $\lambda_s(kt)$ being the Laguerre function of argument $kt$ and order $s$, tabulated in a paper by Head and Wilson.* We are at liberty to choose $k$ as we please; for the time being we shall regard it as a known parameter until the considerations governing its choice can be explained.

Now suppose we choose $N$ times $t_1, t_2 \ldots t_N$ and make the two quantities (1) equal at these times. Then the $b_s$ will be determined by the linear simultaneous equations

$$\text{f}(t_r) = \sum_{s=0}^{N-1} b_s \lambda_s(kt_r) \, (r = 1, 2 \ldots N) \quad . \quad . \quad . \quad (2)$$

Now it happens that if

$$t_r = \alpha_{Nr}/k \quad . \quad . \quad . \quad . \quad . \quad (3)$$

where $\alpha_{Nr}$ is the $r$th zero (in ascending order) of the Laguerre function $\lambda_N(x)$, eqns. (2) have an explicit solution

$$b_s = \sum_{r=1}^{N} \frac{\alpha_{Nr}\lambda_s(\alpha_{Nr})}{N^2\lambda_{N-1}^2(\alpha_{Nr})} \text{f}(\alpha_{Nr}/k) \, (s = 0, 1 \ldots N-1) \quad (4)$$

so that if the matrix of coefficients

$$\beta_{rs} = \frac{\alpha_{Nr}\lambda_s(\alpha_{Nr})}{N^2\lambda_{N-1}^2(\alpha_{Nr})} \, (r = 1, 2 \ldots N; s = 0, 1 \ldots N-1) \quad (5)$$

is worked out, $b_s$ can be written down immediately once the $\text{f}(\alpha_{Nr}/k)$ are known. If $\text{f}(t)$ is only given graphically, $\text{f}(\alpha_{Nr}/k)$

### Table 1
#### VALUES OF $\beta_r$

| $r$ \ $s$ | 0 | 1 | 2 | 3 | 4 | 5 | 6 | 7 | 8 | 9 |
|---|---|---|---|---|---|---|---|---|---|---|
| 1 | 0·3304 | 0·2849 | 0·2425 | 0·2031 | 0·1666 | 0·1328 | 0·1015 | 0·07271 | 0·04630 | 0·02209 |
| 2 | 0·5777 | 0·1563 | −0·1114 | −0·2628 | −0·3284 | −0·3329 | −0·2963 | −0·2340 | −0·1581 | −0·07790 |
| 3 | 0·5386 | −0·4353 | −0·5286 | −0·2723 | 0·04319 | 0·2799 | 0·3928 | 0·3881 | 0·2962 | 0·1551 |
| 4 | 0·3403 | −0·8168 | −0·006122 | 0·5414 | 0·4916 | 0·1174 | −0·2611 | −0·4586 | −0·4365 | −0·2518 |
| 5 | 0·1526 | −0·6950 | 0·8106 | 0·3140 | −0·4944 | −0·5920 | −0·1256 | 0·3738 | 0·5513 | 0·3689 |
| 6 | 0·04851 | −0·3555 | 0·9233 | −0·7877 | −0·4304 | 0·5725 | 0·6135 | −0·08152 | −0·6047 | −0·5101 |
| 7 | 0·01054 | −0·1144 | 0·5005 | −1·065 | 0·9148 | 0·3320 | −0·8089 | −0·4182 | 0·5430 | 0·6826 |
| 8 | 0·001456 | −0·02225 | 0·1470 | −0·5380 | 1·1375 | −1·226 | 0·1307 | 0·9892 | −0·2726 | −0·9014 |
| 9 | 0·1100 × 10⁻³ | −2·310 × 10⁻³ | 0·02188 | −0·1224 | 0·4427 | −1·053 | 1·560 | −1·103 | −0·4005 | 1·203 |
| 10 | 3·113 × 10⁻⁶ | −0·09004 × 10⁻³ | 1·210 × 10⁻³ | −0·00996 | 0·05636 | −0·2278 | 0·6715 | −1·428 | 2·076 | −1·711 |

## (2) DERIVATION OF APPROXIMATING LAGUERRE SERIES

Suppose now that we wish to approximate to a function $\text{f}(t)$ of time, given either graphically or by explicit formula, and that

must be estimated by interpolation. The matrix of coefficients is given in Table 1 for $N = 10$.

Eqn. (4) is derived by multiplying eqn. (2) by

$$\lambda_s(\alpha_{Nr})/D_r^2 \quad . \quad . \quad . \quad . \quad . \quad . \quad (6)$$

and summing with respect to $r$, where

$$D_r^2 = \lambda_0^2(\alpha_{Nr}) + \lambda_1^2(\alpha_{Nr}) + \ldots + \lambda_{N-1}^2(\alpha_{Nr}) \qquad . \quad (7)$$

$$= N^2\lambda_{N-1}^2(\alpha_{Nr})/\alpha_{Nr} \qquad . \quad . \quad . \quad . \quad . \quad (8)$$

The fact that the quantities $\lambda_s(\alpha_{Nr})$ have orthogonal properties, and that $D_r^2$ defined by eqn. (7) has the simplified value given in eqn. (8), is explained in Section 13.2 of the paper by Head and Wilson. After the multiplication and summation, the right-hand side of eqn. (2) reduces to the single term $b_s$ if $t_r$ satisfies eqn. (3).

In determining $k$, there are three conflicting considerations: (a) $k$ must not be so small that $\alpha_{NN}/k$ exceeds $t_0$, or no useful information will be obtained from the last point where the two members of (1) are made equal; (b) $k$ must be sufficiently large to ensure that $|\lambda_s(kt)|$ is less than a predetermined amount $\epsilon$ for all $s$ up to and including $N-1$ and all $t \geqslant t_0$; (c) $k$ must be sufficiently small to ensure that the values of $t$ at which the members of (1) are made to agree are not too small and too close together. If no value of $k$ is suggested by the nature of the problem, $3\alpha_{NN}/(4t_0)$ would appear to be suitable.

### (3) APPLICATION

If $f(t)$ is replaced by $\lambda_u(kt)$ for $u = 0, 1 \ldots 9$ and the constants in Table 1 are used to determine the 10-term Laguerre series for $f(t)$, then we obtain, as expected from eqn. (4),

$$b_s = 0 \, (s \neq u); \, b_u = 1 \quad . \quad . \quad . \quad . \quad . \quad (9)$$

If $f(t)$ is in fact any expression of the form

$$\varepsilon^{-\frac{1}{2}kt} \times \text{(polynomial in } t) \quad . \quad . \quad . \quad (10)$$

and the polynomial is of degree not exceeding 9, the agreement between the two members of (1) will be exact when the $b_s$ are given by eqn. (4).

Only minor discrepancies are to be expected if $f(t)$ has no violent oscillations in the range $0 \leqslant t \leqslant t_0$, and therefore it would appear to be most useful deliberately to choose an unsuitable function for $f(t)$ and to see how the 10-term Laguerre-series approximation fails. This has been done for the case

$$f(t) = \begin{cases} \dfrac{\sin(t - 3\pi)}{t - 3\pi} & (0 < t \leqslant 6\pi) \\[2ex] 0 & t \geqslant 6\pi \end{cases} \qquad . \quad . \quad (11)$$

taking $k = \frac{5}{3}$ (Fig. 1).

The Laguerre-function approximation appears to be in sur-
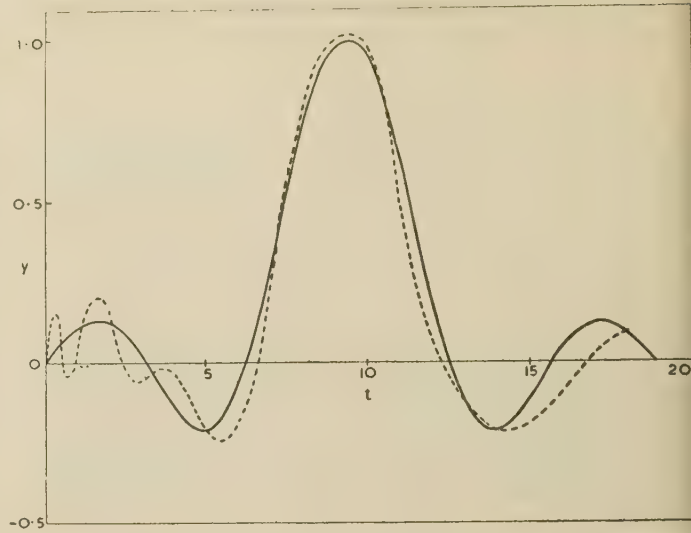


Fig. 1.—Ten-term Laguerre-function approximation (dotted) to $\sin(t - 3\pi)/(t - 3\pi)$.

prisingly good general agreement with the true $f(t)$ given by eqn. (11) in this case, except for the violent behaviour for small values of $t$.

It thus appears that a 10-term Laguerre-series approximation to a function of time which is negligible for $t \geqslant t_0$ and does not oscillate violently in the range $0 < t < t_0$ can be readily obtained by means of the data in Table 1 and the values of the function at 10 times which are spaced not equally but in the ratios of the zeros of the Laguerre function of order 10, and that such an approximation to the function of time is generally satisfactory.

For convenience the values of the zeros $\alpha_{10,r}$ of the Laguerre function of order 10 given in the paper by Head and Wilson are repeated here:

$$\alpha_{10,1} = 0 \cdot 137\,789; \quad \alpha_{10,2} = 0 \cdot 729\,46; \quad \alpha_{10,3} = 1 \cdot 808\,35;$$
$$\alpha_{10,4} = 3 \cdot 401\,43; \quad \alpha_{10,5} = 5 \cdot 552\,50; \quad \alpha_{10,6} = 8 \cdot 330\,15;$$
$$\alpha_{10,7} = 11 \cdot 843\,78; \quad \alpha_{10,8} = 16 \cdot 279\,25; \quad \alpha_{10,9} = 21 \cdot 996\,58;$$
$$\alpha_{10,10} = 29 \cdot 920\,70$$

### (4) ACKNOWLEDGMENT

# TRANSIENT HEATING OF BURIED CABLES

By Prof. J. C. JAEGER, M.A., D.Sc., and GORDON H. NEWSTEAD, M.E.E., Associate Member.

## SUMMARY

The paper develops exact methods of computing the thermal performance of buried cables, based on a solution of the relevant differential equations given by Jaeger in 1956.

The approach differs from that of other workers, who have used approximate methods of calculation. It is shown that the integrals occurring in the exact solution only require a small amount of computation, and if there is very great demand for this information, it could easily be codified by one of the national computing organizations.

The results obtained by the exact method are compared with those of other workers, particularly Whitehead and Hutchings (1938), and it is shown that, although their methods are generally satisfactory, they can lead to large discrepancies in particular cases, especially for small heating times. Calculations are made for a particular cable to show the application of the method.

## LIST OF SYMBOLS

The notation of Whitehead and Hutchings[6] has been followed as far as possible, to make comparison with their results easier. As in their notation, watt-C.G.S.-deg C units will be used and the mechanical equivalent of heat $J$ eliminated from the following equations. The results of the paper can be compared with those of authors who use calorie-C.G.S.-deg C units by transforming the symbols which occur in this paper as follows: replace $g$ by $1/JK$, $S$ by $SJ$, $G'$ by $G'/J$, $S_e$ by $S_eJ$ and $c$ by $cJ$. $D$, $\rho$, $h$, $\alpha_1$, $\alpha_2$ and $\tau$ remain unchanged.

$t$ = Time after switching on current in cable.
$I$ = Current in cable.
$I_{max}$ = Rated value of cable current.
$\theta$ = Core temperature of cable.
$\theta'$ = Sheath temperature of cable.
$\theta''$ = Temperature at radius $r$ in the surrounding medium.
$\theta_\infty$ = Asymptotic value of $\theta$ for large values of $t$.
$a$ = External radius of cable sheath.
$l$ = Depth of burial.
$S$ = Thermal capacity per unit length of cable.
$S_e$ = Thermal capacity per unity length of cable sheath.
$G'$ = Thermal resistance per unit length of cable insulation.
$R$ = Electrical resistance per unit length of cable conductor.
$g$ = Thermal resistivity of ground.
$\rho$ = Density of ground.
$c$ = Specific heat of ground.
$D$ = Thermal diffusivity of ground = $1/(g\rho c)$.

*Dimensionless Constants.*

$h = 2\pi G'/g$.
$\alpha_1 = 2\pi a^2 \rho c/S$.
$\alpha_2 = 2\pi a^2 \rho c/S_e$.
$\tau = Dt/a^2$.
$\mu = [h + \log_\varepsilon (2l/a)]/2\pi$.

## (1) INTRODUCTION

Calculations relating to the transient heating of buried cables have been made by many authors. Two problems, in particular,

have been considered: heating by constant current, which may be regarded as an approximation to the case of the superposition of a peak load on a base load, and instantaneous heating, e.g. by a short-circuit, in which case it is desired to know the way in which the excess heat is dissipated.

The fundamental work on the first problem from the engineer's point of view is that of Whitehead and Hutchings (1938),[6] who use a number of different approximations so that it is hard to see the order of accuracy of their final results. On the second problem the simplest idealization, that of a cylinder buried in an infinite material, has been discussed by Whitehead (1944),[5] who develops approximate formulae, and Tranter (1947),[4] who points out that it is more satisfactory to use the accurate results. Approximate formulae for a more complicated idealization of a cable have been given by Grünberg (1941)[8] and Grünberg and Sontz (1941).[7] The object of the present paper is to give accurate formulae for the simplest useful idealization of a practical cable and to point out that numerical values are, in fact, quite easily calculated from them for any given cable. Numerical results will be given for an actual cable and the status of the various approximations will be discussed.

The model used here will be that of Whitehead and Hutchings, namely a core consisting of the current-carrying elements, which is supposed to be a perfect thermal conductor and to have thermal capacity $S$ and electric resistance $R$ per unit length of cable. The core is separated from the surrounding sheath by insulation whose thermal resistance per unit length of cable is $G'$ and whose thermal capacity is neglected.* The sheath consists of perfect conductor of thermal capacity $S_e$ per unit length. The external radius of the sheath is $a$, and it is supposed to be surrounded by soil of density $\rho$, specific heat $c$, thermal resistivity $g$ and thermal diffusivity $D = 1/g\rho c$. For the preliminary calculation this material is supposed to be infinite in extent: the effect of burial at depth $l$ is considered subsequently.

Finally, it should be stated explicitly that the only problems of this type for which exact solutions can be obtained are those of approximately circular symmetry. There is no possibility of giving an exact treatment of a multi-core cable.

## (2) THE EXACT THEORY: CONSTANT CURRENT

Suppose that the cable described above is in a medium of infinite extent, both the cable and the surrounding material being initially at a constant temperature which may be taken to be zero, and that at time $t = 0$ constant current $I$ is switched into the cable. Then, if $\theta$ is the temperature in the core, $\theta'$ that in the sheath and $\theta''$ that at radius $r$ in the surrounding material, the differential equations satisfied by $\theta$, $\theta'$, $\theta''$ are

$$S\frac{d\theta}{dt} + \frac{\theta - \theta'}{G'} = RI^2 \quad . \quad . \quad . \quad . \quad (1)$$

$$S_e\frac{d\theta'}{dt} - \frac{\theta - \theta'}{G'} - \frac{2\pi a}{g}\left[\frac{\partial\theta''}{\partial r}\right]_{r=a} = 0 \quad . \quad . \quad (2)$$

* If this is not done the problem is still soluble but the solution is much more complicated. An empirical allowance can be made by adding half its value to $S$ and half to $S_e$.

$$\theta' = (\theta'')_{r=a} \quad . \quad . \quad . \quad . \quad . \quad . \quad (3)$$

$$\frac{\partial^2 \theta''}{\partial r^2} + \frac{1}{r} \frac{\partial \theta''}{\partial r} - \frac{1}{D} \frac{\partial \theta''}{\partial t} = 0 \quad r > a \quad . \quad . \quad (4)$$

The solution of these with $\theta = \theta' = \theta'' = 0$ when $t = 0$ has been given by Jaeger (1956).[1]  The interesting quantity is $\theta$ and its value is

$$\theta = gRI^2 G(h, \alpha_1, \alpha_2, \tau) \quad . \quad . \quad . \quad . \quad (5)$$

where

$$G(h, \alpha_1, \alpha_2, \tau) = \frac{2\alpha_1^2 \alpha_2^2}{\pi^3} \int_0^\infty \frac{(1 - \varepsilon^{-u^2\tau}) du}{u^3 \Delta(u)} \quad . \quad . \quad (6)$$

$$\Delta(u) = [u(\alpha_1 + \alpha_2 - hu^2)J_0(u) - \alpha_2(\alpha_1 - hu^2)J_1(u)]^2$$
$$+ [u(\alpha_1 + \alpha_2 - hu^2)Y_0(u) - \alpha_2(\alpha_1 - hu^2)Y_1(u)]^2 \quad . \quad (7)$$

$h$, $\alpha_1$, $\alpha_2$ and $\tau$ are the dimensionless parameters

$$h = \frac{2\pi G'}{g}, \quad \alpha_1 = \frac{2\pi a^2 \rho c}{S}, \quad \alpha_2 = \frac{2\pi a^2 \rho c}{S_e}, \quad \tau = \frac{Dt}{a^2} . \quad (8)$$

and $J_0$, $Y_0$, $J_1$, $Y_1$ are the Bessel functions of the first and second kinds of orders zero and unity, respectively.

The parameters $\alpha_1$ and $\alpha_2$ are the ratios of the thermal capacity of a cylinder of the surrounding material of radius $a$ and unit length to the thermal capacities of unit lengths of the core and sheath, respectively.  The order of magnitude of the parameter $\tau$ which involves the time is of importance: taking typical values of $D = 0.005$, $a = 2$ cm and $t = 1$ hour gives $\tau = 4.5$.  It follows that the values of $\tau$ involved in practical problems will very probably lie in the range $0.2 < \tau < 10$.  It is well known that it is easy to develop approximate solutions for integrals such as that of eqn. (6) for values of $\tau$ which are small, say $\tau < 0.2$, or large, say $\tau > 20$, but that in the intermediate range it is necessary to evaluate the integrals by numerical integration.  For any particular cable this is only a matter of a day's work for a skilled computer, and it may be remarked that some values of a related integral [eqn. (23) below] were tabulated by the National Physical Laboratory, so that if there is any great demand for information of this sort for a wide variety of cables it could easily be codified by one of the national computing organizations.

For large values of $\tau$,

$$G(h, \alpha_1, \alpha_2, \tau) \simeq \frac{1}{4\pi}\left(2h + \log_\varepsilon \frac{4\tau}{C}\right) . \quad . \quad . \quad (9)$$

where $\log_\varepsilon C$ is Euler's constant $\gamma$, so that

$$C = 1.7811 \quad . \quad . \quad . \quad . \quad . \quad (10)$$

The error of approximation (9) is of the order of $1/\tau$.

The theory above is the exact theory for an infinitely long cable surrounded by an indefinite amount of soil.  In the practical case the cable is regarded as being buried at depth $l$ in soil whose surface is kept at zero temperature.  This may be taken into account by adding to eqn. (5) the effect of a line sink of heat of equal amount at the 'image' point distant $2l$ from the cable.  The temperature at the cable due to this is (Reference 3, Section 104)

$$\frac{gRI^2}{4\pi} \text{Ei}\left(-\frac{l^2}{a^2\tau}\right) \quad . \quad . \quad . \quad . \quad (11)$$

where $-\text{Ei}(-x)$ is the exponential integral, which is tabulated, for example, in Reference 9.  Combining expressions (5) and (11) gives, for a cable buried at depth $l$ in soil whose surface is kept at zero,

$$\theta = gRI^2\left[G(h, \alpha_1, \alpha_2, \tau) + \frac{1}{4\pi} \text{Ei}\left(-\frac{l^2}{a^2\tau}\right)\right] \quad . \quad (12)$$

Since $\text{Ei}(-l^2/a^2\tau)$ is negligible if $(l^2/a^2\tau) > 10$, it follows that, for values of $\tau$ of the order of those mentioned earlier, the second term on the right-hand side of eqn. (12) may be omitted.  For large values of $\tau$, however, the approximation

$$\text{Ei}\left(-\frac{l^2}{a^2\tau}\right) \simeq \log_\varepsilon \frac{Cl^2}{a^2\tau} \quad . \quad . \quad . \quad (13)$$

holds, and using this and (9) in eqn (12) gives for the asymptotic value $\theta_\infty$ of $\theta$ for large values of the time

$$\theta_\infty = \frac{gRI^2}{4\pi}\left(2h + \log_\varepsilon \frac{4l^2}{a^2}\right) \quad . \quad . \quad . \quad (14)$$

Dividing eqn. (12) by eqn. (14) gives the temperature rise in terms of its asymptotic value, namely

$$\frac{\theta}{\theta_\infty} = \frac{4\pi G(h, \alpha_1, \alpha_2, \tau) + \text{Ei}(-l^2/a^2\tau)}{2h + \log_\varepsilon(4l^2/a^2)} \quad . \quad . \quad (15)$$

which involves the thermal properties of the soil in the time scale $\tau$.

## (3) CALCULATIONS FOR A PARTICULAR CABLE

As an illustration, calculations have been made for a $3\frac{1}{2}$-core cable.  This is a standard low-voltage lead-sheathed cable as used by the Hydro-Electric Commission in Tasmania.  It consists of three conductors, each $0.4$ in$^2$, and a half-conductor of $0.2$ in$^2$, and is as specified in B.S. 480: 1954, Part 1, Table 9.

For symmetry it is assumed that all the conductors are energized.  The measured external radius of the sheath, $a$, is $2.79$ cm and its internal radius $2.5$ cm.  Calculations are made for soils of three different conductivities referred to as very dry, sandy ($8\%$ moisture) and standard.  The conductivities and diffusivities of these soils are given in Table 1.  For all the soils we take $\rho = 1.75$, $c = 1.02$.*  The thermal resistance $G'$ per unit length

### Table 1

#### PROPERTIES OF THREE TYPES OF SOIL

| Soil type | $g$ | $D$ | $h$ | $\tau$ after 1 hour | $\alpha_1$ | $\alpha_2$ |
|---|---|---|---|---|---|---|
| Very dry .. | 360 | 0.0015 | 0.13 | 0.72 | 2 | 12.4 |
| Sandy ($8\%$ moisture) | 170 | 0.0033 | 0.28 | 1.53 | 2 | 12.4 |
| Standard | 120 | 0.0048 | 0.40 | 2.23 | 2 | 12.4 |

of cable is found by laboratory measurement to be $7.55$.  The values of the various parameters (8) are also given in Table 1, the value of $\tau$ given being at the end of one hour.

The quantity $G(h, 2, 12.4, \tau)$ as a function of $\tau$ for values of the parameters which include those given in Table 1 is shown in Fig. 1.  As mentioned above, for heating times of a few hours and reasonable depths of burial the second term in eqn. (12) is negligible, so that Fig. 1 gives $\theta/gRI^2$, where $\theta$ is the temperature rise in the cable.  The asymptotic value $\theta_\infty$, given by eqn. (14) for a depth of burial $l$, is

$$\theta_\infty = gRI^2[h + \log_\varepsilon(2l/a)]/2\pi = \mu gRI^2 \quad . \quad . \quad (16)$$

The quantity $\mu g$ will be recognized as the thermal resistance of the cable, for the given situation and soil, in thermal ohms.  Using these results, the behaviour of the cable under peak-load conditions may be calculated.  Suppose, for example, that the cable is buried at a depth of 18 in in sandy soil with a base load that gives a steady temperature which is $90\%$ of the maximum
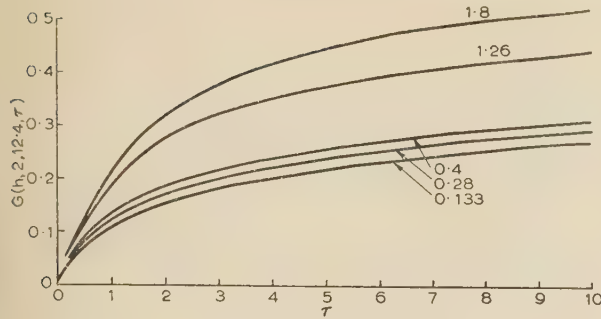
**Fig. 1.**—Values of $G(h, 2, 12\cdot4, \tau)$ for various values as a function of $\tau$.
Numbers on the curves are the values of $h$.

permissible temperature, and that a peak load corresponding to half the rated maximum current is superposed. The temperature rise is shown in Fig. 2, and it appears that it reaches the maximum permissible value after about 40 minutes. The effect of switching off the peak load after some time is equivalent to switching in an equal and opposite heat supply after that time, and so may
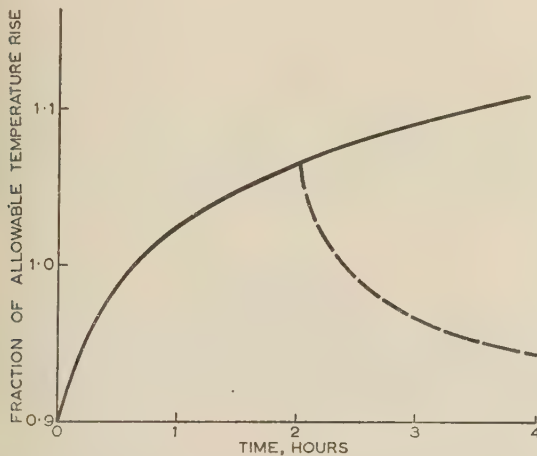


**Fig. 2.**—Temperature rise in a cable carrying a base load of 90% of its rated capacity when a peak load of 50% of its rated capacity is switched in.

Dotted curve is effect of switching off peak load after 2 hours.

also be determined. The dotted curves show the effect of switching off the peak load after 2 hours.

The above results can be put in a form more suitable for comparison with the overload-rating tables currently used. These tables give multiplying factors for determining the one-hour overload rating of the cable if it has previously been running at 50% and 75% of its rated load. Suppose that the cable has reached steady conditions when carrying a continuous load current $\alpha_0 I_{max}$ and that the current is suddenly increased to $\alpha I_{max}$, then

$$\alpha = \left[ \alpha_0^2 + \frac{(1 - \alpha_0^2)\mu}{G(h, \alpha_1, \alpha_2, \tau)} \right]^{1/2} . \quad . \quad . \quad (17)$$

This equation should be compared with eqn (9.3) of Reference 6. For the cable considered above for an emergency loading condition of one hour's duration in standard soil, we obtain $G(h, \alpha_1, \alpha_2, \tau) = 0\cdot19$ from Fig. 1. This gives $1\cdot66$ and $1\cdot45$ for the rating factors for 50% and 75% continuous loading, which should be compared with values of $1\cdot27$ and $1\cdot17$ taken from Fig. 17 of Reference 6. This shows that the divergence between these values and those given in normal rating tables,

e.g. E.R.A. Report FT/128, as adopted by manufacturers can considerably underrate the cable for transient loadings. It should be noted, however, that the Reference 6 rating factors include a factor of safety, so that their results would give safe values that could be used in general. This factor was arrived at by the process of taking $D = 0\cdot02$, but now that an exact solution of the problem has been found we suggest a better approach would be to calculate a rating factor using realistic values of the parameters concerned and then to allow the factor of safety. This procedure has the advantage that one knows what the factor of safety actually is, and, when conditions are known precisely, smaller factors can be used. This procedure is in keeping with the use of a factor of safety in other branches of engineering. In order to demonstrate the relations between the approximations of Reference 6 and the results of the present authors, Fig. 3
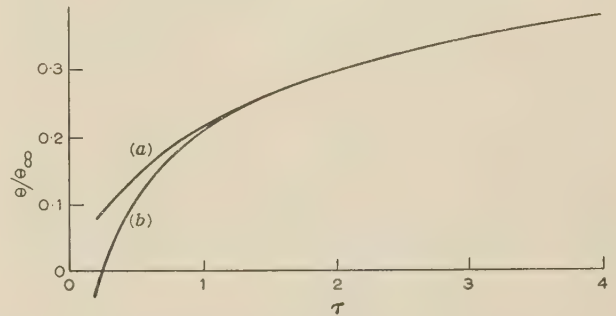


**Fig. 3.**—Comparison of exact calculation and approximation of Whitehead and Hutchings for $3\frac{1}{2}$-core cable.

(a) Accurate: hydro-electric cable, $g = 120$.
(b) Approximation of Whitehead and Hutchings.

shows a graph of $\theta/\theta_\infty$ against $\tau$ using the exact [curve (a)] and the approximate method [curve (b)] for the cable under consideration. It will be seen that for one hour ($\tau = 2\cdot2$) the curves agree quite accurately. It is also seen that as curve (b) lies under curve (a) for small values of $\tau$, the approximations of Reference 6 would tend to overrate the transient overload capacity of large cables or other cables for small times (the more so as Whitehead and Hutchings claim that their rating factors include a factor of safety).

## (4) APPROXIMATIONS FOR VARIOUS PRACTICAL TYPES OF CABLE

The cable for which calculations were made in Section 3 was of a type in which most of the thermal mass was in the core and the thermal resistance of the paper insulation was not high. In this case the effect of the sheath on the temperature rise in the core is in fact very small and to a first approximation may be neglected. This is the first of the special cases considered below.

(a) *The Thermal Capacity of the Sheath negligible.*

In this case $\alpha_2 = \infty$ and $\alpha_1$ is, in fact, of the order of 2 for most soils and for cables with thin insulation. The temperature rise is then given by $G(h, \alpha_1, \infty, \tau)$, which is the function written $G(h, \alpha_1, \tau)$ in Reference 1. Tables of $G(0, \alpha, \tau)$ and graphs of $G(h, 1, \tau)$ and $G(h, 2, \tau)$ are given in that paper, so that considerable numerical information is available.

(b) *The Thermal Capacity of the Sheath much Greater than that of the Core.*

This is the case discussed by Whitehead and Hutchings.[6] The case of negligible thermal mass in the core may be described as follows: power $RI^2$ per unit length is supplied to the sheath

through a thermal resistance of $G'$ per unit length. For this case the temperature $\theta'$ of the sheath is, by eqn. (12),

$$\theta' = gRI^2\left[ G(0, \infty, \alpha_2, \tau) + \frac{1}{4\pi}\,\text{Ei}\left(-\frac{l^2}{a^2\tau}\right)\right] \quad . \quad (18)$$

where $G(0, \infty, \alpha_2, \tau)$ is the function $G(0, \alpha_2, \tau)$ mentioned above, which is tabulated in Reference 1. The temperature $\theta$ of the core is that corresponding to the transfer of power $RI^2$ through thermal resistance $G'$ to the sheath at temperature $\theta'$, or

$$\theta = G'RI^2 + \theta' \quad . \quad . \quad . \quad . \quad . \quad . \quad . \quad . \quad (19)$$

$$= gRI^2\left[\frac{h}{2\pi} + G(0, \alpha_2, \tau) + \frac{1}{4\pi}\,\text{Ei}\left(-\frac{l^2}{a^2\tau}\right)\right] \quad . \quad (20)$$

The treatment of this problem by Whitehead and Hutchings must now be discussed. They separate it into two parts: an approximate calculation of $\theta'$, and the derivation of $\theta$ from $\theta'$. Their method of calculating $\theta'$ (Reference 6, Appendix 3) leads to the result

$$\theta' = \frac{gRI^2}{4\pi}\left[\log_\varepsilon\frac{4\tau}{C} + \text{Ei}\left(-\frac{l^2}{a^2\tau}\right)\right] \quad . \quad . \quad (21)$$

It appears from eqn. (9) that this is in fact the approximation to eqn. (18) valid for large values of the time, so that it will be unreliable for times of the order of an hour or less which are in question here. For example, for $\tau = 1$, $G(0, 2, \tau) = 0.098$, while the approximation gives $0.064$; for smaller values of $\tau$ the discrepancy rapidly becomes greater.

Having found $\theta'$ from eqn. (21), Whitehead and Hutchings determine $\theta$ from $\theta'$ by a method which attempts to take into account the finite thermal capacity of the core, instead of neglecting it completely as in eqn. (19). They, however, introduce additional approximations, so that it is difficult to see the error in their final result. The position is that for large values of $\tau$ their results can be no better than the use of eqn. (15) with the approximation (9); for values of $\tau < 1$ they are quite incorrect, and eqn. (15) must be used.

## (5) SUDDEN HEATING OF THE CORE

If the core, sheath and surrounding material are all at a constant temperature, which may be taken to be zero, and the temperature of the core is suddenly raised to $\theta_0$ at time $t = 0$, its temperature $\theta$ at time $t$ subsequently is found[1] to be given by

$$\frac{\theta}{\theta_0} = F(h, \alpha_1, \alpha_2, \tau) \quad . \quad . \quad . \quad . \quad (22)$$

where

$$F(h, \alpha_1, \alpha_2, \tau) = \frac{4\alpha_1\alpha_2^2}{\pi^2}\int_0^\infty \frac{\varepsilon^{-u^2\tau}du}{u\Delta(u)} \quad . \quad . \quad (23)$$

where $\alpha_1$, $\alpha_2$ and $\Delta(u)$ are defined in eqns. (8) and (7). The value of $F(h, \alpha_1, \alpha_2, \tau)$ for the cable studied in Section 3 is shown in Fig. 4.

If the thermal capacity of the sheath is small compared with that of the core, the value of $\theta/\theta_0$ is very nearly $F(h, \alpha_1, \infty, \tau)$, which is the function $F(h, \alpha_1, \tau)$ for which numerical values are given in Reference 1. Finally, it should be said that the present
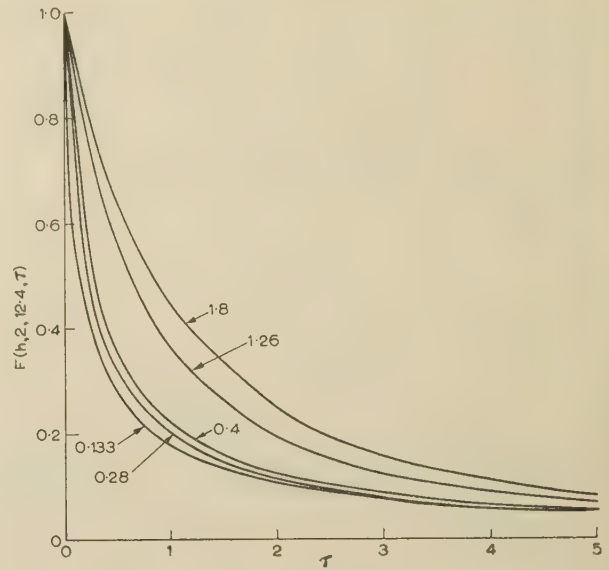


Fig. 4.—Temperature decay in a cable whose core is suddenly heated.
Numbers on the curves are the values of $h$.

theory does not apply to the still more complicated case considered by Grünberg and Sontz[7] and Grünberg[8] who introduce the additional complication of a cable of which the core is hollow and filled with oil. It is easy to write down accurate formulae of the present type instead of the approximate formulae used by the above authors.

## (6) REFERENCES

(1) JAEGER, J. C.: 'Conduction of Heat in an Infinite Region Bounded Internally by a Circular Cylinder of a Perfect Conductor', *Australian Journal of Physics*, 1956, **9**, p. 167.

(2) BULLARD, E.: 'The Flow of Heat through the Floor of the Atlantic Ocean', *Proceedings of the Royal Society A*, 1954, **222**, p. 408.

(3) CARSLAW, H. S., and JAEGER, J. C.: 'Conduction of Heat in Solids' (Oxford University Press, 1947).

(4) TRANTER, C. J.: 'Heat Flow in an Infinite Medium Heated by a Cylinder', *Philosophical Magazine*, 1947, **38**, p. 131.

(5) WHITEHEAD, S.: 'An Approximate Method for Calculating Heat Flow in an Infinite Medium Heated by a Cylinder', *Proceedings of the Physical Society, London*, 1944, **56**, p. 357.

(6) WHITEHEAD, S., and HUTCHINGS, E. E.: 'Current Rating of Cables for Transmission and Distribution', *Journal I.E.E.*, 1938, **83**, p. 517.

(7) GRÜNBERG, G., and SONTZ, M.: 'The Calculation of Short-Circuit Heating of H.V. Cables', *Journal of Physics of the the U.S.S.R.*, 1941, **4**, p. 97.

(8) GRÜNBERG, G.: 'Short-Circuit Heating of H.V. Cables', *ibid.*, 1941, **4**, p. 463.

(9) JAHNKE, E., and EMDE, F.: 'Tables of Functions' (Teubner, 1933).

# AN APPROXIMATE TRANSIENT ANALYSIS OF A SECOND-ORDER POSITION-CONTROL SYSTEM WHEN BACKLASH IS PRESENT

By E. A. FREEMAN, B.Sc., Graduate.

## SUMMARY

An approximate transient analysis is derived for a second-order position-control system with backlash. The general characteristics of the transient oscillations are discussed, and the relationship between the amplitude of overshoot and time is given explicitly. It is shown that there is a best choice for the ratio of the moments of inertia on opposite sides of the backlash if a maximum decrement of the transient oscillations is required. Furthermore, the conditions for which the settling time for the system is a minimum are also derived. The effect of derivative of input on the transient response is considered. Results from an electronic analogue of the system confirm the theoretical work.

## INTRODUCTION

Experience shows that control systems which have been designed from linear theory do not always meet their specifications. Discrepancies may occur between the predicted and measured transient response;[1,2] furthermore, after the initial transient has died away the system may exhibit an unexpected self-sustaining oscillation.[3,4] These discrepancies are invariably due to the non-linearities present in any practical system. The introduction of the describing function technique[5,6] has made it possible for the designer to predict and obviate the presence of sustained oscillations which arise due to non-linearities. However, the designer has no such generalized technique for determining the transient response when the system has some type of non-linearity. It follows, therefore, that each problem must be treated individually. In the present paper the effect of backlash on the transient performance of a second-order position-control system is investigated.

Recent work on the stability of control systems with backlash[7,8] has shown that a second-order system with backlash will exhibit sustained oscillations unless some form of divided reset is used. We assume, therefore, that the practical system under investigation employs divided reset for stabilization, output-velocity feedback being taken from the motor and positional reset from the load.

In order to determine the characteristics of the transient response in general terms it has been found necessary to make certain simplifying assumptions. However, these assumptions do not limit the application of the results of the analysis too severely. In particular, the results apply to the transient in response to a small step-function input, and to that part of the transient in response to a large step-function input for which the amplitude of the overshoot is small. It will be seen that in such cases the analysis gives the designer a quantitative measure of the effect of backlash on the transient performance of the system.

## (1) MOTION OF THE MOTOR AND LOAD DURING THE TRANSIENT RESPONSE

Consider the transient response of a second-order position-control system which has a motor connected to a load through gearing, the gearing being assumed to have backlash. If the system damping is less than the critical value, the transient in response to a step-function input is oscillatory, and because of the presence of backlash the motor and load become separated for a certain period during each cycle of this oscillatory transient. A separation occurs when the deceleration of the motor becomes greater than that of the load. However, if the frictional forces on the load produce a deceleration greater than the maximum deceleration of the motor, the motor and load will maintain contact during the period of deceleration and become separated only when the motor velocity reverses. The precise instant at which the motor and load become separated depends also on the nature of the frictional forces acting.

Consider one half-period of the transient oscillation, as shown in Fig. 1. If linear speed-dependent friction is the only frictional force, it may be shown (Section 7.2) that a separation occurs when

$$\dot{\theta}_l = \frac{\omega_0^2(\theta_i - \theta_l)}{\dfrac{\mu_v}{I} - \dfrac{\mu_{vl}}{I_l}} \qquad . \quad . \quad . \quad . \quad (1)$$

where $\theta_i$ = Amplitude of the input step-function.
  $\theta_l$ = Load position.
  $I_l$ = Moment of inertia of the load.
  $I = I_l + I_m$ = Total moment of inertia of motor and load.
  $\mu_{vl}$ = Coefficient of friction for the load.
  $\mu_v = \mu_{vl} + \mu_{vm}$ = Total coefficient of friction for motor and load.

It may be deduced from eqn. (1) that if $\mu_{vl}/\omega I_l$ is made large, a separation occurs near the instant of zero velocity. When coulomb friction is also applied to the load the condition for a separation is modified to (Section 7.2)

$$\dot{\theta}_l = \frac{F_c + \omega_0^2(\theta_i - \theta_l)}{\dfrac{\mu_v}{I} - \dfrac{\mu_{vl}}{I_l}} \qquad . \quad . \quad . \quad . \quad (2)$$

so that in the presence of coulomb friction a separation occurs at a lower velocity, and, what is more important to the analysis which follows, the waveform of the load velocity during a separation period is more nearly equal to the waveform of the motor velocity [see Fig. 1(b)]. The stiction present in any practical system also modifies the velocity of the load during a separation. Referring to Fig. 1(c), it may be seen that as the velocity of the load falls the friction force rises rapidly, causing an increase in the deceleration of the load.

In attempting to determine the characteristics of the transient response in the presence of backlash and non-linear friction two principal difficulties arise. First, because of the variable nature of the frictional forces occurring in practical systems, it is difficult to ascribe a particular form to the friction characteristic which will be applicable to a majority of such systems. Secondly, having assumed a particular friction characteristic, the equations
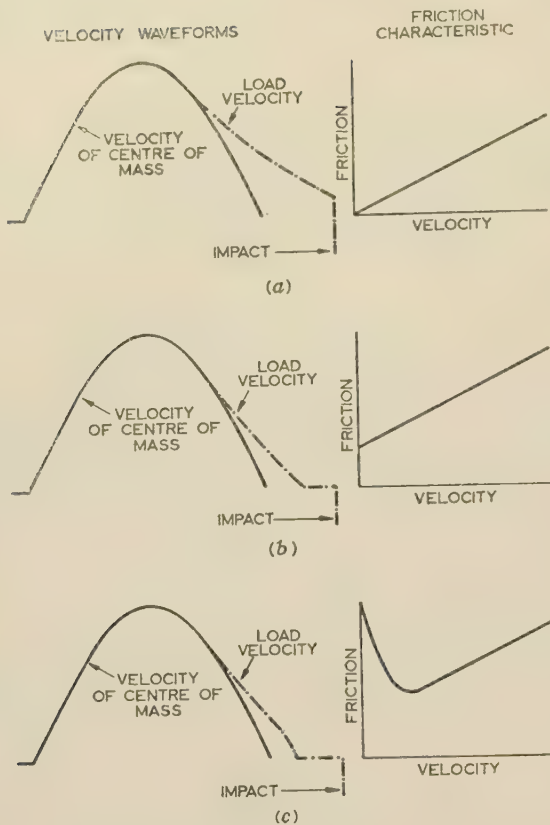
Fig. 1.—Waveforms showing effect of friction on load velocity when motor and load become separated.

    (a) Linear speed-dependent friction, or viscous friction.
    (b) Combined coulomb and viscous friction.
    (c) Combined stiction, coulomb and viscous friction.

defining the system become mathematically intractible. Therefore it becomes apparent at the outset that, if some estimate of the transient response is to be made, simplifying assumptions are necessary. In the analysis which follows it is assumed that the motor and load become separated at the instant of zero velocity. This assumption is made in order to anticipate the effects of the non-linear frictional forces, as illustrated in Fig. 1, and gives an exact representation of the motion when the frictional forces on the load are large compared with the load inertia. In general, a separation occurs before the instant of zero velocity, so that the analysis gives the designer a pessimistic estimate of the transient response (Section 7.2). It should be pointed out, however, that since the transient oscillations in the presence of backlash occur at a low frequency (Fig. 2) the assumption gives a good approximation to the transient in many cases. With regard to the instant of impact, it is assumed that the motor and load share their momentum according to the principle of the conservation of momentum,[10] and that they move on together after impact. Resilience in the coupling connecting motor and load is also neglected. The implication of these assumptions is illustrated by the transient shown in Fig. 2.

## (2) CHARACTERISTICS OF THE TRANSIENT RESPONSE

In the following analysis the transient response characteristics are derived, particular attention being focused on the relationship between the amplitude of overshoot and time. Derivation of the transient response involves the solution of the equations defining the system during the periods of contact and separation. How-
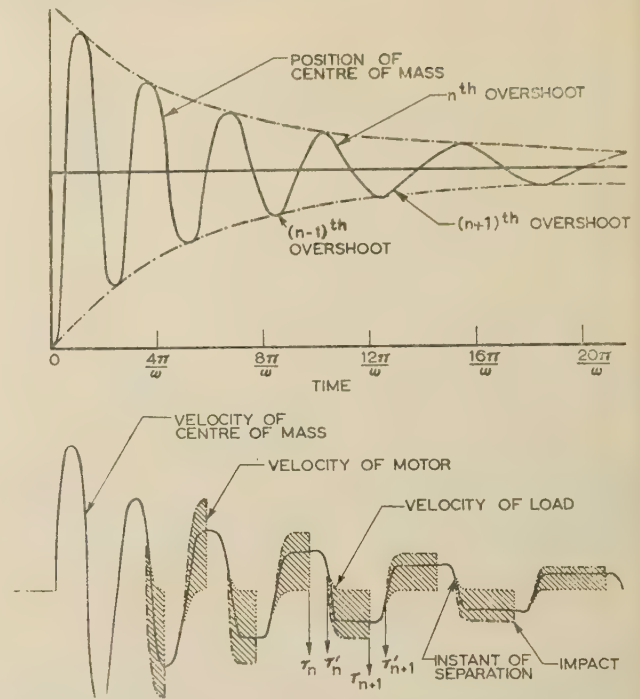


Fig. 2.—Waveforms illustrating the nature of transient oscillations in response to a step-function input when backlash is present.

ever, the solution of the equations defining the system for a separation period is found to depend on conditions existing at the end of the previous contact period, and, similarly, the response during a contact period depends on the conditions existing at the end of the previous separation period (see Fig. 2). By assuming the amplitude of the oscillation to be small,* it is possible to overcome this difficulty and to obtain a general expression for the transient response.

### (2.1) Half-Periodic Time

(2.1.1) Period of Separation.

Referring to the $n$th overshoot shown in Fig. 2 and assuming a separation to occur at the instant of zero velocity, the equation of motion for the separation period $\tau'_n \rightarrow \tau_{n+1}$ is

$$T_q = I_m \ddot{\theta}_m + \mu_{vm} \dot{\theta}_m$$

where $T_q$ is the motor torque, defined by $T_q = \mu(\theta_i - \theta_l)$. During a separation period, $\theta_i - \theta_l$ is a constant and equal to $a'_n$, the amplitude of the $n$th overshoot.

Hence
$$\mu a'_n = I_m \ddot{\theta}_m + \mu_{vm} \dot{\theta}_m \quad . \quad . \quad . \quad . \quad (3)$$

Using eqn. (3) it may be shown (Section 7.1) that the separation period is given approximately by

$$\tau_{n+1} - \tau'_n = \frac{I_m}{\mu_{vm}}\left(1 + \frac{f\theta_{BL}}{a'_n}\right) \quad . \quad . \quad . \quad . \quad (4)$$

The approximation involved is given quantitatively in Section 7.1, from which it follows that if $f\theta_{BL}/a'_n > 1 \cdot 2$ an error of less than 5% is introduced.

In order to illustrate the approximation involved in a particular case, consider $a'_n$ to be the first overshoot of the transient.

* The quantitative restrictions on the amplitude to be considered are given in Section 7.1.

This means that $a'_n$ is the amplitude of the step-function input $A$. Substituting for $f$, we have

$$f\frac{\theta_{BL}}{a'_n} = \frac{\theta_{BL}}{A}\frac{4I}{I_m}\left(\frac{\mu_{vm}}{2\omega_0 I}\right)^2$$

Clearly, the minimum value of $f\theta_{BL}/a'_n$ occurs when $I_m \to I$ and the damping factor $\mu_{vm}/(2\omega_0 I) \to 0$, and in this case the approximation to the separation period is inadmissible. However, for all practical purposes the damping must always be greater than zero, so that we will consider the approximation when the damping factor has a practical value, namely $0\cdot7$. We will also assume that $I_m = 2I_l$. Hence

$$f\frac{\theta_{BL}}{a'_n} = 3\cdot06\frac{\theta_{BL}}{A}$$

If a $5\%$ approximation is sufficient, $\theta_{BL}/A$ may be equal to $1\cdot2/3\cdot06$. In other words, provided that the amplitude of the initial step is less than $2\cdot6\theta_{BL}$, the approximation introduces an error of less than $5\%$.

As a second example, let us consider the case in which $I_m = \frac{1}{2}I_l$ and the damping factor is $0\cdot8$. In this case the initial step may be made equal to $6\cdot4\theta_{BL}$ without involving an error greater than $5\%$. It should be pointed out that if only a crude estimation of the initial part of the transient is required much larger amplitudes of oscillation may be considered (Section 7.1).

**(2.1.2) Period of Contact.**

At the end of a separation period an impact takes place and the motor and load move on together, assuming that there is no resilience in the coupling. It is shown in Section 7.2 that the velocity after impact is $a'_n\mu/\mu_{vm}$; therefore the equation defining the motion during contact becomes

$$I\ddot{\theta}_m + \mu_{vm}\dot{\theta}_m = \mu(\theta_i - \theta_l) \quad . \quad . \quad . \quad . \quad (5)$$

with the initial conditions:

$$\left.\begin{array}{l}\dot{\theta}_m = a'_n\mu/\mu_{vm} \\ \theta_l = a'_n\end{array}\right\} t = \tau_{n+1}$$

By solving eqn. (5) and determining the time taken for the velocity again to become zero, we obtain for the contact period (Section 7.2)

$$\tau'_{n+1} - \tau_{n+1} = \frac{1}{\omega_0\sqrt{(1-\zeta^2)}}\left[\pi - \arctan\frac{I_m}{2I_l+I_m}\frac{\sqrt{(1-\zeta^2)}}{\zeta}\right]$$
$$. \quad . \quad . \quad . \quad (6)$$

The time taken by the system to perform one half-cycle of the transient oscillation is made up of the contact period and the separation period. The half-periodic time thus becomes

$$\tau'_{n+1} - \tau'_n = \tau = \mu_1 + \mu_2/a'_n \quad . \quad . \quad . \quad . \quad (7)$$

where

$$\mu_1 = \frac{1}{\omega_0}\left\{\frac{1}{2\zeta} + \frac{1}{\sqrt{(1-\zeta^2)}}\left[\pi - \arctan\frac{I_m}{2I_l+I_m}\frac{\sqrt{(1-\zeta^2)}}{\zeta}\right]\right\}$$

and

$$\mu_2 = f\frac{\theta_{BL}}{2\zeta\omega_0}$$

**(2.2) Relationship between the Amplitudes of Successive Overshoots**

During the period of contact $\tau_{n+1} \to \tau'_{n+1}$ the load position is given by (Section 7.2)

$$\theta_l = \theta_i + B\varepsilon^{-\sigma t}\sin(\omega t + \beta) \quad . \quad . \quad . \quad (8)$$

In this equation the time $t$ is measured from the instant of making contact; thus by putting $t = 0$ in eqn. (8) we obtain the amplitude of $\theta_l$ at the time $\tau_{n+1}$. Therefore, we have

$$\theta_l(\tau_{n+1}) - \theta_i = B\sin\beta \quad . \quad . \quad . \quad . \quad (9)$$

Referring to Fig. 2, we see that $\theta_l(\tau_n - \theta_i = a'_{n+1})$, the amplitude of the $n$th overshoot.

Hence $$a'_n = B\sin\beta$$

At the end of the contact time $\theta_l - \theta_i = a'_{n+1}$, so that $a'_{n+1}$ may be obtained by putting $t = \tau'_{n+1} - \tau_{n+1}$ in eqn. (8). Thus

$$a'_{n+1} = \theta_l(\tau'_{n+1}) - \theta_i = B\varepsilon^{-\sigma(\tau'_{n+1}-\tau_{n+1})}\sin\left[\omega(\tau'_{n+1} - \tau_{n+1}) + \beta\right]$$
$$. \quad . \quad . \quad (10)$$

Dividing eqn. (9) by eqn. (10) the relationship between $a'_{n+1}$ and $a'_n$ is obtained:

$$\left|\frac{a'_{n+1}}{a'_n}\right| = \frac{\varepsilon^{-\sigma(\tau'_{n+1}-\tau_{n+1})}\sin\left[\omega(\tau'_{n+1} - \tau_{n+1}) + \beta\right]}{\sin\beta} \quad (11)$$

Substituting for the contact period as derived in Section 7.2, eqn. (11) becomes

$$\left|\frac{a'_{n+1}}{a'_n}\right| = \frac{\sqrt{(1-\zeta^2)}\varepsilon^{-\sigma(\tau'_{n+1}-\tau_{n+1})}}{\sin\beta} \quad . \quad . \quad . \quad (12)$$

where $$\tan\beta = \frac{\zeta^2}{\zeta^2 - \frac{1}{2}I_m/I}\sqrt{(1-\zeta^2)}$$

and $\tau'_{n+1} - \tau_{n+1}$ is given by eqn. (6).

Since $\tau'_{n+1} - \tau_{n+1}$ and $\tan\beta$ are constants for any given set of parameters, it follows from eqn. (12) that the ratio of the amplitudes of successive overshoots is a constant. Accordingly we can write

$$a'_{n+1} = ka'_n$$

where $k < 1$ for a damped oscillation.

**(2.3) Amplitude of Overshoot as a Function of Time**

The analysis presented above has been shown to be applicable when the amplitude of the overshoot is small. In this Section $a'_0$ is considered to be the amplitude of the first overshoot for which the analysis is accurately applicable, and may be regarded as the amplitude of a small step-function input or, alternatively, that of a small overshoot resulting from the application of a large step-function input. The problem is to determine the transient subsequent to $a'_0$.

Considering eqn. (7), the time taken to perform the $i$th overshoot after $a'_0$ is

$$\tau_i = \mu_1 + \mu_2/a'_i$$

Now the ratio of the amplitudes of successive overshoots has been shown to be constant and equal to $k$ so that $a'_1 = ka'_0$; thus $a'_i = k^i a'_0$, from which it follows that

$$\tau_i = \mu_1 + \mu_2/k^i a'_0$$

The total time taken to perform $r$ overshoots is therefore given by

$$\sum_{i=1}^r \tau_i = \mu_1 r + \frac{\mu_2}{a'_0}\left(\frac{1}{k} + \frac{1}{k^2} + \frac{1}{k^3} + \cdots \frac{1}{k^r}\right)$$

which leads to $$\sum_{i=1}^r \tau_i = \mu_1 r + \frac{\mu_2}{a'_0}\left(\frac{1 - 1/k^r}{1 - 1/k}\right) \quad . \quad . \quad (13)$$

The amplitude of the oscillation after this time is $a'_r = k^r a'_0$.

Substituting for $r$ and $k^r$ in eqn. (13) and writing $t_{NL}$ as the total time $\sum_{i=1}^{r} \tau_i$, we obtain

$$t_{NL} = \frac{\mu_1 \log (a'_r/a'_0)}{\log k} + \frac{\mu_2}{a'_0}\left(\frac{1 - a'_0/a'_r}{1 - 1/k}\right) \quad . \quad . \quad (14)$$

For a linear system the corresponding result is

$$t_L = \frac{\omega_0}{\zeta} \log (a'_r/a'_0) \quad . \quad . \quad . \quad . \quad . \quad (15)$$

Eqn. (14) gives the time taken by the control system to reduce the error from $a'_0$ to $a'_r$. Comparing this with the time taken in the absence of backlash, eqn. (15), it will be seen that the essential difference is due to the second term on the right-hand side of eqn. (14). Referring to eqn. (4), we see that this term arises because of the increase in the time taken by the motor to cross the backlash when the amplitude of the overshoot decreases. As the number of overshoots increases, $\dfrac{1 - a'_0/a'_r}{1 - 1/k}$ increases, thus causing a bigger difference between $t_{NL}$ and $t_L$. This effect is illustrated in the waveforms shown in Fig. 2 and in a more quantitative manner in Fig. 5. The curves of Fig. 5 are drawn for an inertia ratio $I_m/I = 0.225$, which, it will be shown later, corresponds to approximately the best choice of the ratio.

Although the curves are drawn for the special case in which the decrement per half-period is a maximum, the response with backlash is much more oscillatory than that of the linear system. In order to improve the response of the system with backlash it is necessary to minimize $\dfrac{1 - a'_0/a'_r}{1 - 1/k}$. This implies* that the desired output should be reached in a minimum number of overshoots, i.e. the damping on the system should be arranged to prevent any overshoot. If the damping on the system is made equal to the critical value the response consists of a finite delay, $\mu_2/a'_0$, followed by an exponential rise to the desired output. The finite delay arises because of the time taken by the motor to take up the backlash and can be reduced by advancing the phase of the input. However, as will be seen later, no appreciable improvement is possible.

### (2.4) Response with one Overshoot

Generally the designer of a practical control system is concerned not with the time taken by the system to reduce the error to zero but with that taken for the error to fall within specified limits.[11] In such cases the settling time may be regarded as the time taken for one overshoot, provided that the error existing after the first overshoot is within the specified accuracy limit. Since the amplitude of the first overshoot after $a'_0$ is $ka'_0$, it follows that by making $k$ a minimum the accuracy of the system is optimized. From eqn. (12) it can easily be shown that a minimum value of $k$ is obtained if the ratio of the moments of inertia $I_m/I$ and damping factor $\zeta$ are related by the following equation:

$$I_m/I = \zeta[(\zeta + 1) - \surd(\zeta^2 + 2\zeta)] \quad . \quad . \quad . \quad (16)$$

Fig. 3 shows this relationship graphically. It should be pointed out, however, that the ratio $I_m/I$ is not extremely critical, since the minimum of $k$ is not very pronounced. This may be taken to imply that if $I_m/I \simeq 0.225$ the decrement $k$ is very nearly the optimum value for all values of damping factor in the range $0.5 \leqslant \zeta \leqslant 1$. Having chosen $I_m/I$, the optimum decrement $k$ can be determined. Fig. 4 shows the optimum value of the decrement together with that for the linear system. For

*It may be proved that $t_{NL} - t_L$ is a minimum if the damping applied to the system prevents overshoot.
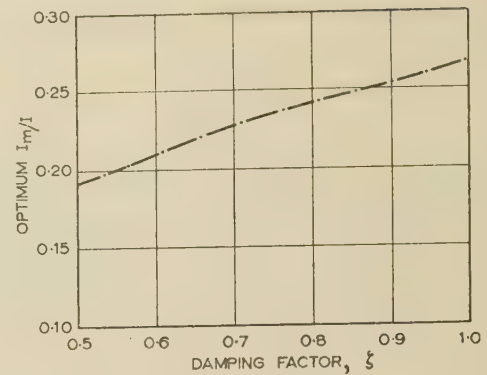


Fig. 3.—Optimum inertia ratio for maximum decrement per half-period of the transient oscillations.
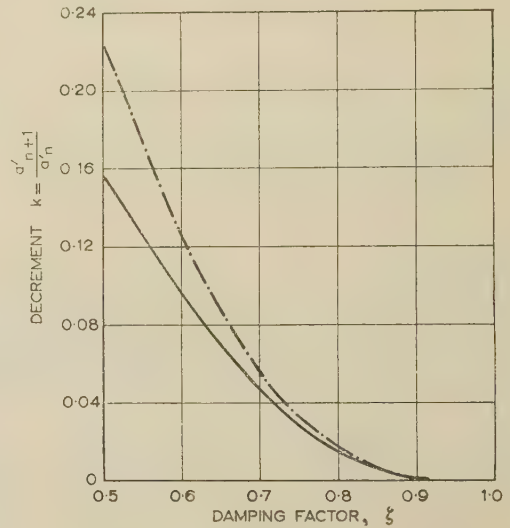


Fig. 4.—Optimum value of decrement $k$ per half-period ($k = a'_{n+1}/a'_n$) for a second-order control system with backlash.

      — · —   With backlash present.
      ———   Linear system.

all values of damping factor less than critical, the decrement with backlash is less than that of the linear system; however, for systems with $\zeta \geqslant 0.65$ no appreciable change in $k$ takes place due to the presence of backlash (Fig. 4). Nevertheless, it should be pointed out that, although the decrement per half-period may not be modified appreciably, the transient response appears to be much less damped because of the increase in the time taken to perform a given overshoot (Fig. 5).

### (2.5) Effect of Phase-Advancing the Input

When the damping applied to the system is critical, the response to a step-function input is made up of a finite delay, while the motor takes up the backlash, followed by an exponential rise to the desired output. By applying derivative of input the initial part of the transient is modified. The equation of motion during the initial separation period becomes

$$\theta_m = \frac{\mu}{\mu_{vm}} a'_0 t$$

Thus the initial delay $\tau_0$ is $\theta_{BL}/\omega_0 a'_0$ and the response time is reduced by $\frac{1}{2}\zeta$.

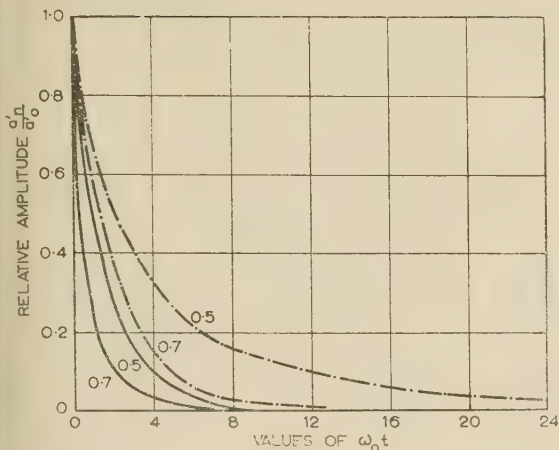If the initial delay is large, only a small reduction in response

Fig. 5.—Envelope of the transient oscillations for the linear system and in the presence of backlash.

——— Linear system.
— - — System with backlash.

The values marked on each curve refer to the damping factor ζ.

...ue is effected by derivative of input: alternatively, if the initial ...ay is short, derivative of input reduces this delay appreciably; ...wever, in this case the total response time is improved only ...h'ly. Consequently it may be concluded that derivative of ...ut is not a particularly effective method of reducing the ...ponse time for small step-function inputs.

## (3) TRANSIENT RESPONSE FROM THE ANALOGUE*

Observations of the transient in response to a small step-function input confirm the main points predicted by the theory.
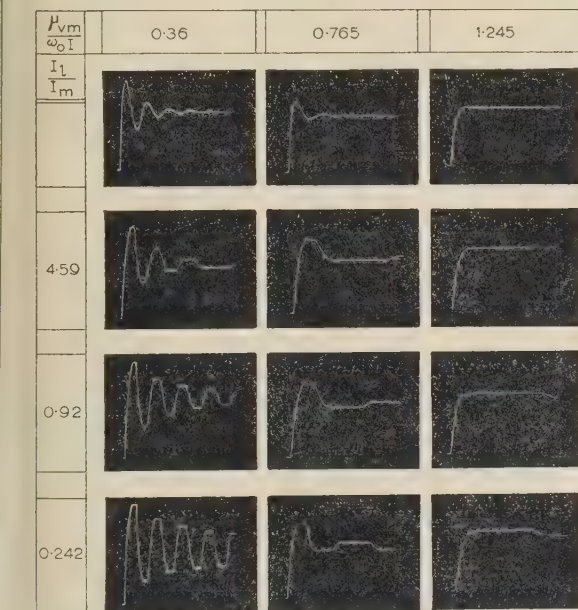


Fig. 6.—Step-function response of a second-order system with backlash when positional reset is taken from the load and output-velocity feedback from the motor.

$\theta_{BL}/\theta_i = 0.4$ for all transients.

...ferring to Fig. 6, it may be seen that as the amplitude of the ...ershoot decreases the half-periodic time of the oscillation ...creases. It is also apparent that, if the system damping is

...he arrangement and functioning of the analogue is discussed in Reference 8.

increased so that only a small overshoot occurs, the settling time becomes prohibitively large. For all values of damping shown, the waveforms illustrate that considerable improvement in the transient response can be obtained by increasing the ratio $I_l/I_m$. However, it will be seen from Fig. 7 that, although the response
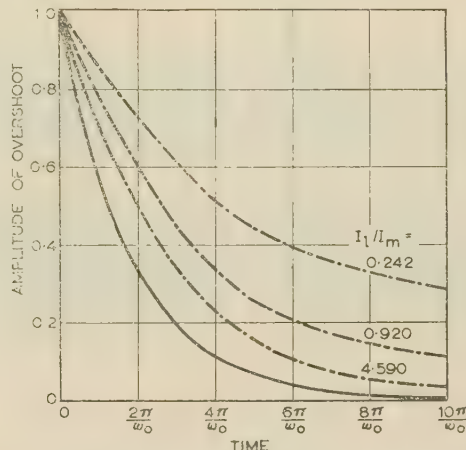


Fig. 7.—Effect of inertia ratio on the transient response.

Curves show the envelope of the transient oscillations in response to a step-function input when

$$\mu_{vm}/\omega_0 I = 0.36$$

——— Linear system response.
— - — System response in the presence of backlash.

can be improved by a correct choice of $I_l/I_m$, the transient in the presence of backlash is always more oscillatory than that of the linear system. Fig. 8 illustrates, in a more quantitative manner,
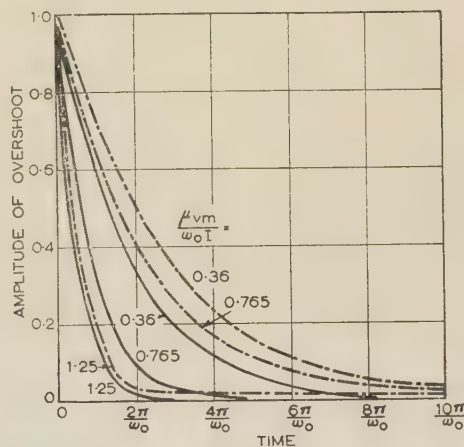


Fig. 8.—Effect of damping factor on transient response.

Curves show the envelope of the transient oscillations in response to a step-function input when $I_l/I_m = 4.59$.

——— Linear system response.
— - — System response in the presence of backlash.

the effect of varying the system damping, all curves being drawn for a ratio $I_l/I_m$ approximately equal to the optimum value. Clearly, the transient response with backlash and small damping is much more oscillatory than that of the linear system; however, when the damping is increased so as to permit only a small overshoot, the transient with backlash approaches that of the linear system. The small overshoot which occurs when the damping is less than critical persists for an extremely long time and is only permissible if the amplitude of this overshoot is within the desired accuracy limit of the system. It will be

3

remembered that the above findings are in agreement with the theoretical work, which showed that the response of the system with backlash was optimum when the inertia ratio, $I_m/I$, was approximately $0 \cdot 225$ and the damping on the system was critical.

The modification to the transient response, which takes place when derivative of input is applied, is shown in Fig. 9. Wave-
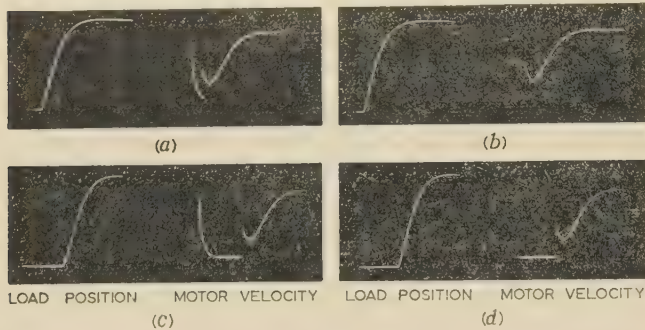


(a)    (b)

LOAD POSITION    MOTOR VELOCITY        LOAD POSITION    MOTOR VELOCITY
(c)    (d)

**Fig. 9.**—Effect of derivative of input on transient response of a second-order control system when backlash is present.

For all transients $\mu_{vm}/2\omega_0 I = 2$ and $I_l/I_m = 0 \cdot 92$.

(a), (c) Response without derivative of input.
(b), (d) Response with derivative of input.
(a), (b) Transients for $\theta_{BL}/\theta_i = 0 \cdot 528$.
(c), (d) Transients for $\theta_{BL}/\theta_i = 2 \cdot 64$. ·

forms are shown for a given inertia ratio and damping factor and two different amplitudes of input step-function. When the input step is large compared with the backlash angle the delay in the response can be reduced considerably by derivative of input. Unfortunately, for small input steps little improvement is obtained. In other words, derivative of input is effective in improving the response time only when the modification due to backlash is small.

### (4) DISCUSSION AND CONCLUSIONS

The approximate transient analysis, which has been derived for a second-order control system with backlash, has shown that the transient response in the presence of backlash always appears to be more oscillatory than that of the linear system. Conditions have been derived for obtaining a maximum decrement of the oscillation per half-period, and these give the best non-linear response provided that the first overshoot falls within the desired accuracy limit of the system. The optimum decrement thus obtained is not appreciably different from that of the linear response; however, it should be pointed out that the time taken by the system to perform a half-cycle of the oscillation is much greater when backlash is present and the amplitude of the oscillation is small. This means that, when the first overshoot after the initial step is greater than the desired accuracy of the control system, the persistence of this error for a prohibitively large time is equivalent to a very underdamped transient. In cases where it is desirable to have zero error after a sensibly short time, it has been shown to be better to have a critically damped system than to permit a small overshoot. When the system is critically damped and the ratio of inertias is optimum, the transient response of the system with backlash is made up of a finite delay followed by an exponential rise to the desired output. The initial delay may be reduced by applying derivative of input. However, as the oscillograms have illustrated, no appreciable reduction in the response time can be effected in this manner.

### (5) ACKNOWLEDGMENTS

The author is indebted to Prof. J. C. Prescott of King's College, Newcastle upon Tyne, for the facilities placed at his disposal during the course of the work described, and to D C. A. Walley and Mr. F. J. U. Ritson of the Electrical Engineering Department for their valuable advice and encouragement.

### (6) REFERENCES

(1) WEST, J. C., and DALTON, J. R.: 'The Step-Function Response of an R.P.C. Servo Mechanism possessing Torque Limitation', *Proceedings I.E.E.*, Paper N 1576 M, November, 1953 (**101**, Part II, p. 166).

(2) WEST, J. C., and NIKIFORUK, P. N.: 'The Response R.P.C. Systems with Hard-Spring Non-Linear Characteristics to Step-Function and Random Inputs', *ibid* Paper No. 1728 M, October, 1954 (**102** B, p. 575).

(3) WEST, J. C., and SOMERVILLE, M. J.: 'Integral Control with Torque Limitation', *ibid.*, Monograph No. 181 M June, 1956 (**103** C, p. 407).

(4) GOLDFARB, L. C.: 'On Some Non-Linear Phenomena Regulatory Systems', from OLDENBURGER, R. (Ed. 'Frequency Response' (Macmillan, New York, 1956).

(5) KOCHENBURGER, R. J.: 'A Frequency Response Method f Analysing and Synthesising Contactor Servomechanism *Transactions of the American I.E.E.*, 1950, **69**, p. 270.

(6) JOHNSON, E. C.: 'Sinusoidal Analysis of Feedback Contr Systems containing Non-Linear Elements', America I.E.E. Technical Paper No. 52–154, 1952.

(7) LIVERSIDGE, J. H.: 'Backlash and Resilience within th Closed Loop of Automatic Control Systems', Automat and Manual Control Conference, Cranfield, 1951.

(8) FREEMAN, E. A.: 'The Effect of Speed-Dependent Frictic and Backlash on the Stability of Control System Technical Report, Electrical Engineering Departmer King's College, Newcastle upon Tyne.

(9) BOWDEN, F. P., and TABOR, D.: 'The Friction and Lubric tion of Solids' (Clarendon Press, Oxford, 1950).

(10) RUTHERFORD, D. E.: 'Classical Mechanics' (Oliver ai Boyd, Ltd., London, 1951).

(11) TRUXAL, J. G.: 'Automatic Feedback Control Syste Synthesis' (McGraw-Hill, London, 1955).

### (7) APPENDICES

#### (7.1) The Separation Period

When the motor and load become separated the torq developed by the motor accelerates only the motor inertia, a the equation of motion may be written

$$T_q = I_m \ddot{\theta}_m + \mu_{vm} \dot{\theta}_m \quad \ldots \ldots (1$$

$T_q = \mu(\theta_i - \theta_l)$ and, since we assume that a separation occu at zero velocity, $\theta_i - \theta_l$ is constant during the separation peric Writing $a'_n$, the amplitude of the $n$th overshoot (Fig. 2), f $\theta_i - \theta_l$, eqn. (17) becomes

$$\mu a'_n = I_m \ddot{\theta}_m + \mu_{vm} \dot{\theta}_m \quad \ldots \quad \vdots \quad \ldots (1$$

Solution to eqn. (18) gives

$$\theta_m = \frac{\mu}{\mu_{vm}} a'_n \left[ t - \frac{I_m}{\mu_{vm}} (1 - \varepsilon^{-\mu_{vm}t/I_m}) \right] + \theta_m(\tau'_n) \quad . \quad (1$$

and

$$\dot{\theta}_m = \frac{\mu}{\mu_{vm}} a'_n (1 - \varepsilon^{-\mu_{vm}t/I_m}) \quad \ldots \quad . \quad (2$$

where $t$ is the time measured after the instant of separation.

Now        $$\theta_m(\tau'_n) = \theta_l(\tau'_n) \pm \tfrac{1}{2}\theta_{BL}$$

$$+ \text{ for } n \text{ odd.}$$

$$- \text{ for } n \text{ even.}$$

Thus eqn. (17) becomes

$$\theta_m = \frac{\mu}{\mu_{vm}} a_n' \left[ t - \frac{I_m}{\mu_{vm}} (1 - \varepsilon^{-\mu_{vm}t/I_m}) \right] + \theta_l(\tau_n') \pm \tfrac{1}{2}\theta_{BL} \quad (21)$$

The time to cross the backlash, $\theta_{BL}$, is obtained by putting $\theta_m - [\theta_l(\tau_n') \pm \tfrac{1}{2}\theta_{BL}] = \pm \theta_{BL}$ in eqn. (21):

$$\theta_{BL} = \frac{\mu}{\mu_{vm}} a_n' \left[ t - \frac{I_m}{\mu_{vm}} (1 - \varepsilon^{-\mu_{vm}t/I_m}) \right]$$

An approximation to the period of separation may be obtained by putting $\varepsilon^{-\mu_{vm}t/I_m} = 0$, in which case the separation time $\tau_{n+1} - \tau_n'$ is given by

$$\tau_{n+1} - \tau_n' = \frac{I_m}{\mu_{vm}} + \frac{\mu_{vm}}{\mu} \frac{\theta_{BL}}{a_n'} \quad . \quad . \quad (22)$$

Hence

$$\omega_0(\tau_{n+1} - \tau_n') = \frac{\omega_0 I_m}{\mu_{vm}} \left( 1 + \frac{f\theta_{BL}}{a_n'} \right) \quad . \quad . \quad (23)$$

where

$$f = \frac{4I}{I_m} \left( \frac{\mu_{vm}}{2\omega_0 I} \right)^2$$

When eqn. (22) is approximately correct, the percentage error in using it instead of the exact equation is given by

Percentage error in $\omega_0(\tau_{n+1} - \tau_n') =$

$$-\frac{100 \exp\left[ -\frac{\mu_{vm}}{I_m}(\tau_{n+1} - \tau_n') \right]}{1 + f\theta_{BL}/a_n'}$$

Substituting for $\tau_{n+1} - \tau_n'$ from eqn. (23), we obtain

Percentage error $= -\frac{100 \exp\left[ -(1 + f\theta_{BL}/a_n') \right]}{1 + f\theta_{BL}/a_n'}$ . (24)

From eqn. (24) it follows that if $f\theta_{BL}/a_n' < 1 \cdot 2$ the maximum error involved in using eqn. (22) to determine the separation time is 5%.

The error involved for any particular value of $f\theta_{BL}/a_n'$ may easily be obtained from Fig. 10.
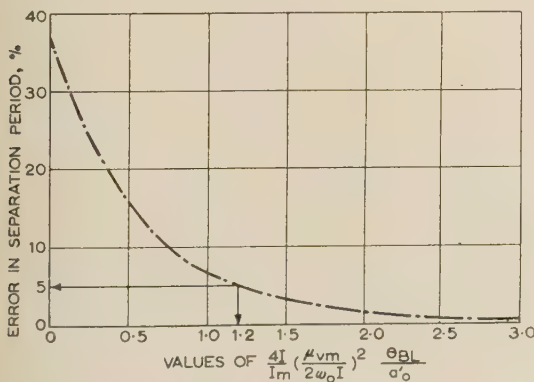


Fig. 10.—Curve showing percentage error introduced by using approximate formula for calculating the separation period.

## (7.2) The Contact Period

When the motor and load are in contact through the gearing, the torque developed by the motor, $\mu(\theta_i - \theta_l)$, accelerates the inertia of both the motor and the load. Thus the equation of motion becomes

$$I_m\ddot{\theta}_m + I_l\ddot{\theta}_l + \mu_{vm}\dot{\theta}_m + \mu_{vl}\dot{\theta}_l = \mu(\theta_i - \theta_l) \quad . \quad (25)$$

We require to solve eqn. (25) for the time interval $\tau_n \leqslant t \leqslant \tau_n$, i.e. the period of contact corresponding to the $n$th overshoot. Since $\theta_i$ is a constant, solution of eqn. (25) gives

$$\theta_l = \theta_i + B\varepsilon^{-\sigma t'} \sin(\omega t' + \beta) \quad . \quad . \quad (26)$$

where

$$\sigma = \frac{\mu_v}{2I}$$

and

$$\omega = \omega_0 \left[ 1 - \left( \frac{\mu_v}{2\omega_0 I} \right)^2 \right]^{1/2}$$

Eqn. (26) is based on the assumptions that there is no resilience in the coupling between the motor and load and that they move on together after impact. From eqn. (26), the load velocity, $\dot{\theta}_l$, is given by

$$\dot{\theta}_l = B\varepsilon^{-\sigma t'}[\omega \cos(\omega t' + \beta) - \sigma \sin(\omega t' + \beta)] \quad . \quad (27)$$

At the beginning of contact $\theta_l = \theta_l(\tau_n)$ and $\dot{\theta}_l = \dot{\theta}_l(\tau_n)$; hence, putting $t' = 0$ in eqns. (26) and (27), we obtain

$$\theta_l(\tau_n) = \theta_i + B \sin \beta \quad . \quad . \quad . \quad (28)$$

and

$$\dot{\theta}_l(\tau_n) = \omega_0 \left\{ \left[ 1 - \left( \frac{\mu_v}{2\omega_0 I} \right)^2 \right]^{1/2} B \cos \beta - \frac{\mu_v}{2\omega_0 I} B \sin B \right\} \quad . \quad (29)$$

Substituting from eqn. (28) into eqn. (29),

$$\tan \beta = \frac{\omega_0 \left[ 1 - \left( \frac{\mu_v}{2\omega_0 I} \right)^2 \right]^{1/2} [\theta_l(\tau_n) - \theta_i]}{\dot{\theta}_l(\tau_n) + \frac{\mu_v}{2I}[\theta_l(\tau_n) - \theta_i]} \quad . \quad . \quad (30)$$

### (7.2.1) The End of the Contact Period.

It has already been seen that the motor and load become separated when the deceleration of the motor becomes greater than that of the load. During the contact period eqn. (25) gives the deceleration of the motor as

$$I\ddot{\theta}_m = \mu(\theta_i - \theta_l) - \mu_v\dot{\theta}_m \quad . \quad . \quad . \quad (31)$$

At the instant of separation the deceleration of the load is due entirely to the frictional forces acting on the load. Therefore we obtain

$$\mu_{vl}\dot{\theta} + I_l\ddot{\theta}_l = 0$$

and

$$\ddot{\theta}_l = -\frac{\mu_{vl}\dot{\theta}_l}{I_l} \quad . \quad . \quad . \quad . \quad (32)$$

For separation, $-\frac{\mu_{vl}}{I_l}\dot{\theta}_l = \frac{\mu}{I}(\theta_i - \theta_l) - \frac{\mu_v}{I}\dot{\theta}_m$

and, since at the commencement of separation $\dot{\theta}_m = \dot{\theta}_l$, the condition for separation may be written

$$\dot{\theta}_m = \frac{\omega_0^2(\theta_i - \theta_l)}{\frac{\mu_v}{I} - \frac{\mu_{vl}}{I_l}} \quad . \quad . \quad . \quad . \quad (33)$$

It follows from eqn. (33) that if $\mu_{vl}/I_l$ is large a separation occurs for $\dot{\theta}_m = 0$.

### (7.2.2) Effect of Coulomb Friction on the Instant of Separation.

Let $F_c$ be the coulomb friction force applied to the load. The deceleration of the load just after separation is

$$-\left( F_c + \frac{\mu_{vl}}{I_l}\dot{\theta}_l \right)$$

hence a separation occurs for

$$-\left(F_c + \frac{\mu_{vl}}{I}\dot{\theta}_i\right) = \frac{\mu}{I}(\theta_i - \theta_l) - \frac{\mu_v}{I}\dot{\theta}_l$$

Therefore

$$\dot{\theta}_m = \frac{F_c + \frac{\mu}{I}(\theta_i - \theta_l)}{\frac{\mu_v}{I} - \frac{\mu_{vl}}{I_l}} \qquad \ldots \ldots (34)$$

It may be deduced from eqn. (34) that the presence of coulomb friction causes a separation to occur at a lower velocity.

In general, the frictional forces on the load will not be sufficiently large compared with the load inertia to cause a separation to occur at zero velocity. However, in cases of small load inertia it is reasonable to assume a separation for zero velocity. It should also be pointed out that, since the transient oscillations considered are of a low-frequency nature, errors in the comparatively short contact time will cause much smaller errors in the half-periodic time. The effect of the assumption on the subsequent separation period is to give a pessimistic estimate of this period. By assuming that a separation occurs for zero velocity, the results obtained from the analysis thus give the designer a pessimistic estimate of the transient response.

Assuming that the contact period ends when $\dot{\theta}_m = \dot{\theta}_l =$ the contact time is given by

$$\tau_n' - \tau_n = \frac{1}{\omega_0\sqrt{(1 - \zeta^2)}}\left[\arctan\frac{\sqrt{(1 - \zeta^2)}}{\zeta} - \beta\right]. \quad (3$$

**(7.2.3) Velocity after Impact.**

Using eqns. (20) and (23) from Section 7.1, the velocity aft impact is found to be

$$\dot{\theta}_l(\tau_{n+1}) = \frac{\mu}{\mu_{vm}}a_n' \qquad \ldots \ldots (3$$

Substituting in eqn. (30), we have

$$\tan\beta = \frac{\sqrt{(1 - \zeta^2)}}{\zeta}\left[1\Big/\left(1 - \frac{I_m}{2I}\frac{1}{\zeta^2}\right)\right] \qquad \ldots (3$$

Substituting for $\beta$ in eqn. (35), we obtain the contact time:

$$\omega_0(\tau_n' - \tau_n) = \frac{1}{\sqrt{(1 - \zeta^2)}}\left[\pi - \arctan\frac{I_m}{2I - I_m}\frac{\sqrt{(1 - \zeta^2)}}{\zeta}\right]$$

$$\ldots \ldots (3$$

# THE MEASUREMENT OF INDUCTION-MOTOR STRAY LOSS AND ITS EFFECT ON PERFORMANCE

By T. H. BARTON, Ph.D., Associate Member, and V. AHMAD, M.Sc., Graduate.

## SUMMARY

Stray losses are shown to affect the performance of induction motors to a very considerable extent—far greater than is indicated in B.S. 269. The sources of loss and methods for isolating the contribution of each to the whole are discussed. It is suggested that the total loss should be taken as the sum of the components, and this proposal is shown to be accurate except at small negative slips when the loss is much greater than such a calculation indicates. A single easy test, the reverse-rotation test, extrapolated according to simple rules, is shown to be sufficient to predict the stray loss under all conditions (including d.c. excitation) with sufficient accuracy for the majority of purposes, and it is proposed that such a test should replace the existing recommendations of B.S. 269.

## LIST OF SYMBOLS

$B$ = Air-gap flux density.
$I_1$ = Primary phase current.
$I_2$ = Secondary phase current.
$I_R$ = Full-load primary current.
$P_{st}$ = Stray-loss power, watts.
$V$ = Phase voltage.
$T$ = Torque in synchronous watts.
$f$ = Frequency, c/s.
$n$ = Speed of rotation, r.p.m.
$p$ = Number of poles.
$s$ = Fractional slip.
$S$ = Number of slots.
$R_1$ = Primary phase resistance, ohms.
$X_1$ = Primary phase leakage reactance, ohms.
$Z_1 = R_1 + jX_1$.
$R_2$ = Component of secondary resistance referred to the primary which is independent of frequency.
$\Delta R_2$ = Component of secondary resistance referred to the primary which is proportional to frequency.
$X_2$ = Secondary leakage reactance at standstill referred to the primary.
$R_m$ = Series resistive component of magnetizing impedance.
$X_m$ = Series reactive component of magnetizing impedance.
$Z_m = R_m + jX_m$
$\theta = \arg [Z_m/(Z_m + Z_1)]$
$w = |(Z_1 + Z_m)/Z_m|$
$R_2' = w^2 R_2$
$\Delta R_2' = w^2 \Delta R_2'$
$X_2' = w^2 X_2$
$R_s = \mathscr{R}[Z_1 Z_m/(Z_1 + Z_m)] + \Delta R_2'$
$X_s = \mathscr{I}[Z_1 Z_m/(Z_1 + Z_m)] + X_2'$

## (1) INTRODUCTION

B.S. 269 defines stray load losses as 'the additional losses, wherever occurring, caused by the load current due to changes in the flux distribution and to eddy currents'. This definition excludes losses due to tooth ripples in the main flux, probably because, in normal testing procedure, these are included in the no-load losses. However, in order to make the analysis complete, these losses have been separated from the no-load losses and are included in the term 'stray loss' used in the paper.

With the above proviso, the stray losses in an induction motor may be divided into losses at the fundamental frequency and losses at relatively high frequencies due to tooth ripples in the main and leakage fluxes. Methods have been developed by which these various components can be measured,[1,2,3] and the paper describes the results of such measurements on a 7·5 h.p. squirrel-cage motor. The sum of the components is then compared with the total stray loss obtained in practice, and the effect of stray loss on the starting, stopping and normal running performance is discussed.

## (2) THE EXPERIMENTAL MACHINE

The machine is the one designated No. 1 in Reference 4, in which full details are given. It is continuously rated at 7·5 h.p. 400 volts, 6·3 amp per phase, and has a synchronous speed of 1 500 r.p.m. at 50 c/s.

## (3) THE FUNDAMENTAL-FREQUENCY STRAY LOSS

The principal source of fundamental-frequency stray loss is iron loss produced by the leakage fluxes, although, in machines with conductors of large cross-section, the effects of eddy currents due to skin and proximity effects may be appreciable. In the iron losses associated with the leakage fluxes are included the losses in end-shields and core end-plates due to the end-winding leakage. All the leakage fluxes are produced by the primary and secondary currents, and, since the associated losses occur at the fundamental frequency, they appear in the equivalent circuit as resistances in addition to the d.c. resistances of the windings. They correspond, in fact, to the 15–30% which designers add to the calculated d.c. resistances.[5] It is to be noted that, since these losses are frequency dependent, the addition to the rotor resistance will be a function of frequency, usually of frequency raised to some power, of numerical value between one and two.

The effective a.c. resistance of the windings has been obtained from a study of the electrical and mechanical characteristics of the machine. Where, as in the majority of cases, only the a.c. resistance of the primary winding is required, two other tests, a standstill test and the one proposed by Ware,[2] may be used with a great reduction in the required number of experimental observations and computations. The results of these three tests on the experimental machine are in reasonable agreement, and, whilst

the standstill test may be preferable on theoretical grounds, Ware's test may be preferred because of its greater simplicity.

### (3.1) Determination from the Machine Characteristics

The effective impedance per phase of the machine, with the secondary winding short-circuited and the rotor driven by an external drive, is determined over the widest possible slip range (in this case $-0.2$ to $+2.2$), including an accurate measurement at zero slip. It is then most convenient to derive the equivalent circuit, as described by Morris,[6] from these results as an intermediate step in the derivation of the conventional circuit. It is essential when doing this to correct the results to a constant reference temperature, and, if saturation of the leakage flux paths occurs, to correct to a constant reference reactance, usually the unsaturated value. The conditions of the experiment and the value of the reference reactance should be so chosen that deviations from the basic conditions are minimized.

Harmonics of the main field produce small variations in both the magnitude and phase angle of the machine admittance, the maximum effect of the fifth harmonic in the experimental machine being approximately a 2% reduction in both these quantities; the effects of higher harmonics are not detectable electrically. These small variations are ignored by the method of analysis described, so that the resultant equivalent circuit is that for the fundamental only.

The equivalent circuit thus obtained and the conventional circuit derived from it are shown in Fig. 1.
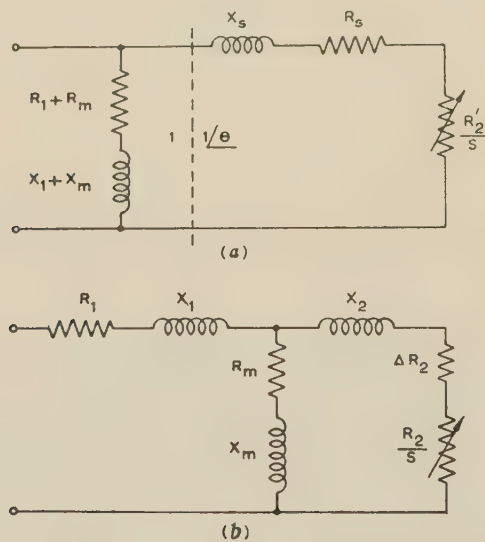


**Fig. 1.**—Equivalent circuits of the experimental machine.

(a) Morris circuit.
$R_s = 2.70 + 0.44$ ohms.
$X_s = 11.95$ ohms.
$R_1 + R_m = 26.4$ ohms.
$X_1 + X_m = 214.0$ ohms.
$R_2'/s = 2.70/s$ ohms.

(b) Conventional circuit.
$R_1 = 2.66$ ohms.
$X_1$ and $X_2 = 5.70$ ohms.
$R_m = 23.7$ ohms.
$X_m = 208.0$ ohms.
$\Delta R_2' = 0.42$ ohm.
$R_2/s = 2.55/s$ ohms.

The Morris circuit is obtained by the transformation of the normal T-circuit into an L-circuit and is convenient for experimental work because its parameters may be directly measured. For a transformer it uses the actual open-circuit transformation ratio at the point indicated by the dotted line of Fig. 1(a), and, since under these conditions it is usual for the secondary voltage

to lead the primary voltage by a small angle $\theta$, this ratio complex. The angle $\theta$ is $\arg[Z_m/(Z_1 + Z_m)]$. In an induction motor with equal numbers of primary and secondary phases the transformation ratio required is that obtained when the axes of the two phases concerned are coincident. In squirrel-cage machines the secondary terminals are not available and the ratio cannot be measured directly. Its argument $\theta$, but not its modulus, can, in theory, be obtained from measurements at the primary terminals and, since actual secondary quantities are not required, ignorance of the modulus is not a disadvantage. The modulus may be arbitrarily chosen in these circumstances, and it is the authors' practice to take it as unity, implying a turns ratio for the machine of $|(Z_1 + Z_m)/Z_m|$. In a practical machine $\theta$ is of the order of $0.5°$ and it cannot be measured, by primary measurements only, to better than about $\pm 0.5°$. Its precise value is only of importance when determining the stator leakage reactance $X_1$ from the reactance $X_s$, and it is the authors' practice, if there are no good reasons to the contrary, to choose a value of $\theta$ which makes $X_1$ and $X_2$ equal. For this reason $\theta$ is not quoted in Fig. 1; it has been taken as $0.51°$.

With the modulus of the transformation ratio taken as unity the reactance $X_s$ is the reactive component of $(Z_1 Z_m)/(Z_1 + Z_m)$ plus $X_2'$, and the resistance $R_s$ is the resistive component of $Z_1 Z_m/(Z_1 + Z_m)$ plus any component, $\Delta R_2'$, of the secondary resistance which is proportional to slip. Such a component is present owing to hysteresis loss associated with the secondary leakage flux. There are additional components proportional to $s^2$ due to skin effect and eddy-current loss associated with the leakage flux, but the experimental accuracy is insufficient to separate these, and they are satisfactorily dealt with by an appropriate resistance proportional to slip. $R_s$ cannot be divided into its two components by electrical measurements confined to the primary terminals, but this can be done by consideration of the torque produced by the normal induction motor action of the fundamental field.

This torque cannot be measured directly, because of the additional torques produced by the high-frequency stray losses and harmonic fields. The stray losses are zero when the rotor is stationary, and hence the standstill torque should be used. This, however, introduces the possibility of locking torques due to reluctance effects, and the standstill torque is best obtained as the mean of the output torques obtained with the machine rotating slowly, first forwards and then backwards. Harmonic torques can be minimized by keeping the speed of rotation well below the lowest harmonic synchronous speed which, in practice, is that of the $(2S/p + 1)$th harmonic. Unfortunately this does not entirely eliminate harmonic torque, so that some correction must be made. In the experimental machine this was limited to the fifth harmonic, higher ones being small as shown in Fig. 7. The fundamental torque is taken as the sum of the output and fifth-harmonic torques, the latter being obtained by calculation from an experimentally derived equivalent circuit. In practice it would probably be more convenient for the designer to calculate the harmonic circuit parameters.

The slope of the graph showing the fundamental torque as a function of the square of the voltage can be used to derive the resistance $\Delta R_2'$ from the equation

$$\frac{T}{V^2} = \frac{3(R_2' + \Delta R_2')}{(R_s + R_2')^2 + X_s^2} \text{ synchronous watts} \quad . \quad (1)$$

The result for the experimental machine is shown in Fig. 1(a), where the resistance $R_s$ is given as the sum of two resistances, the smaller of which is the quantity $\Delta R_2'$.

The a.c. resistance of the stator thus calculated is about 16% higher than the d.c. value, and the increase is entirely due to iron

loss, since the stator conductors are far too small to produce skin or proximity effects.

The constant component of the rotor resistance in Fig. 1(b) is due in part to iron loss and in part to skin effect in the rotor bars. Theoretically, only the hysteresis loss should give rise to a constant resistance, since eddy currents and skin effect lead to a quantity which is the product of a resistance and the slip. However, the experimental technique is insufficiently accurate to show up these finer details, and errors due to their neglect are extremely small. By analogy with the increase in stator resistance, the 0·42-ohm extra rotor resistance comprises approximately 0·36 ohm due to iron loss and 0·06 ohm due to skin effect in the bars. The latter figure is a reasonable average for the calculated skin effect over the experimental speed range.

### (3.2) Standstill Test

Although the multiplicity of results used in the previous test lend confidence to the final result, it is much too complicated for routine purposes. However, since, in general, only the stator resistance is required, it can be replaced by a much simpler test in which the input power, current and output torque at standstill are measured. The stator loss, and hence resistance, is obtained as the difference between the input power and air-gap power plus iron loss. The iron loss is usually negligible, but the air-gap power cannot be directly derived from the output torque because of frictional, reluctance and harmonic effects already discussed. These may be allowed for by the methods of the previous Section, but, from experience with the experimental machine, the authors consider that the corrections may be greatly simplified in many cases. In wound-rotor machines harmonic torques are negligible, and in squirrel-cage machines only the one of lowest order need be considered. The effect of this can be estimated with sufficient accuracy from a calculated equivalent circuit. Static friction is only likely to be of importance in machines with sleeve bearings; for example, the experimental machine with ball and roller bearings had a friction torque of 0·03 lb-ft. Reluctance effects in skewed machines are small—they were negligible in the experimental machine—and can be allowed for by taking sets of results with the rotor moved successively through appropriate fractions of a stator slot pitch.

This test gave the stator resistance of the experimental machine as 2·72 ohms, i.e. 2% higher than that given in the previous Section. This is within the accuracy of the experiment.

### (3.3) Determination by Ware's Test

A second alternative is the test proposed by Ware,[2] in which the power input to the stator, with polyphase excitation at the normal frequency, is measured with the rotor removed. The stator a.c. resistance is then taken as the ratio of the power per phase to the square of the phase current.

This test does not reproduce the normal flux conditions, the zigzag leakage flux being much reduced, and there is a small component of main flux present. Hence the resistance so measured will not include the loss associated with the zigzag leakage, but, as some compensation, will include a small loss associated with the main flux. It is evident that in most cases these two effects, though opposed in sign, will not exactly neutralize one another. This was observed to be so for the experimental machine, where the test gave a resistance of 2·5 ohms, which was appreciably lower than that given in the previous test. Hence it appears that, although better than a d.c. measurement, Ware's test cannot be expected to give a completely accurate result except in exceptional cases.

## (4) STRAY LOSSES AT TOOTH-RIPPLE FREQUENCIES

Stray losses are due to tooth ripples in the main and zigzag leakage fluxes, the mechanism of loss being illustrated in Fig. 2,
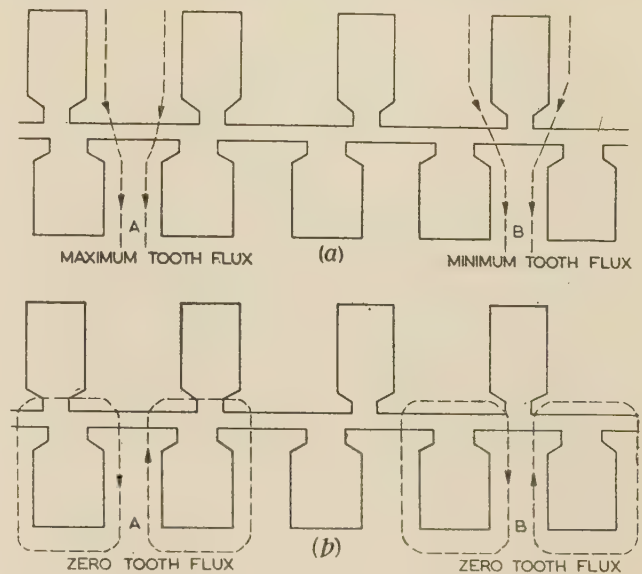


Fig. 2.—Modifications in the rotor tooth flux due to the stator slots.
(a) Effect on the main flux.
(b) Effect on the zigzag leakage flux.

which shows the stator and rotor teeth in various relative positions. Fig. 2(a) shows the disposition of the main flux, and it is evident that the flux passing down tooth A is a maximum whilst that down tooth B is a minimum. It is this variation of tooth flux at the slot-ripple frequency which is responsible for the voltage-dependent component of the stray loss.

Fig. 2(b) shows the zigzag leakage flux. Here, because of their symmetrical disposition relative to the stator teeth, the fluxes down teeth A and B are zero, whilst for all other positions, the zigzag leakage tooth flux is not zero. This variation of tooth flux is responsible for the current-dependent component of the stray loss. From Fig. 2 it is seen that the two kinds of high-frequency tooth ripple due respectively to voltage and current are in time quadrature; and hence, since the loss is approximately proportional to the square of the ripple amplitude, the two losses may be considered separately and numerically added to give the total loss. In both cases the frequency of tooth ripple is proportional to the speed of rotation; whilst, in the first case, the amplitude is proportional to the main flux density (i.e. to the ratio $V/f$), and, in the second case, to the current. It is known that iron loss in machine laminations can be represented by an equation of the form $kf^{\alpha}B^{\beta}$, where $\alpha$ and $\beta$, although approximately constant over limited ranges of frequency and flux density, tend to decrease somewhat with increase in both quantities. Hence it is to be expected that the high-frequency loss can be expressed by equations of similar form—an expectation borne out in practice.

The two losses can be separated by the tests described by Rawcliffe and Menon,[3] and by Morgan, Brown and Schumer.[1]

### (4.1) The Rawcliffe and Menon Test

The Rawcliffe and Menon test[3] consists in running the machine on no load and measuring the total input power, slip and voltage over the widest possible voltage range consistent with the slip being extremely small. Under these conditions the air-gap power is, to a high degree of approximation, equal to $3V^2{}_s/R_2$. This

supplies the friction and windage losses, which can be assumed constant, and the no-load stray loss, which can be taken as comprising the loss due to high-frequency tooth ripple in the main flux, and in the leakage flux produced by the magnetizing current. Although $R_2$ is not known accurately, especially in squirrel-cage machines, a scale is fixed for the quantity $3V^2s$ in terms of power by plotting both the product $V^2s$ and the input power against voltage, and extrapolating to zero voltage when the two quantities must be equal. $V^2s$ can be measured accurately and easily, but the authors find that the extrapolation is easier if the graphs are plotted to a base of $V^2$. When calculating the results allowance must be made for the synchronous-hysteresis torque, which is readily calculated to the required degree of accuracy.

The stray loss due to the leakage flux of the magnetizing current is small and can be obtained from the reverse-rotation test. This gives the total loss due to corresponding currents in both primary and secondary windings, whereas the secondary current on light load is very small indeed, compared with the primary current. The ratio of the two components of these losses can be calculated,[4] but it will be sufficient in the majority of cases to take one-half of the total loss given by the reverse-rotation test, at a primary current equal to the magnetizing current.

The stray loss associated with the main flux, as determined by this test, is shown plotted in Fig. 3(a) for a series of fixed flux
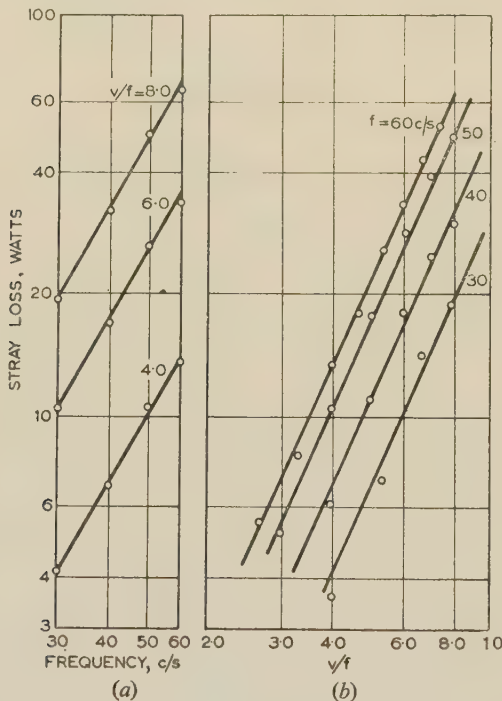


Fig. 3.—Stray loss associated with the main flux in the experimental machine.

(a) Constant flux densities.
(b) Constant speeds.

densities (i.e. fixed ratios of $V/f$) over a range of speeds. It is also shown in Fig. 3(b) for a series of fixed speeds over a range of flux densities. The loss in the experimental machine was found to be expressible as

$$P_{st} = 0 \cdot 51(n/1\,500)^{1 \cdot 7}(V/f)^{2 \cdot 2} \text{ watts} \quad . \quad . \quad . \quad (2)$$

This should be compared with the expression predicted in a previous paper,[4] which was

$$P_{st} = 0 \cdot 85(n/1\,500)^{1 \cdot 5}(V/f)^{2 \cdot 0} \text{ watts}$$

It is noteworthy that the latter expression gives a loss of 54 watt at 400 volts, 50 c/s, 1 500 r.p.m. compared with the measured los of 50 watts.

### (4.2) Reverse-Rotation Test

The reverse-rotation test was proposed by Morgan, Brown and Schumer,[1] and has been adopted by the American Standard Association.[7] It consists in measuring the primary electrical input power and the shaft power of the machine when driven backwards at synchronous speed, the primary being excited by the low voltage necessary to circulate full-load current and the secondary being short-circuited. The stray loss, except for the small effects of harmonic fields, is then obtained as the difference between the shaft and air-gap powers, and is extrapolated by assuming it to vary with the square of both speed and current. The test is easy to perform, but, since much of the input power is lost in the stator windings, it is essential to have an accurate value of the effective stator resistance when calculating the air-gap power, and, in view of Section 3, this may prove much more difficult to obtain. The results of the authors' investigations indicate that it is more accurate to take the index of extrapolation with speed as being $1 \cdot 5$ rather than $2 \cdot 0$. The method measures stray loss due to both leakage and main fluxes, but the latter is usually small enough to be neglected.

The results for the experimental machine are shown in Fig. 4 and can be expressed as

$$P_{st} = 210(n/1\,500)^{1 \cdot 5}(I/I_R)^{1 \cdot 9} \text{ watts} \quad . \quad . \quad (3$$
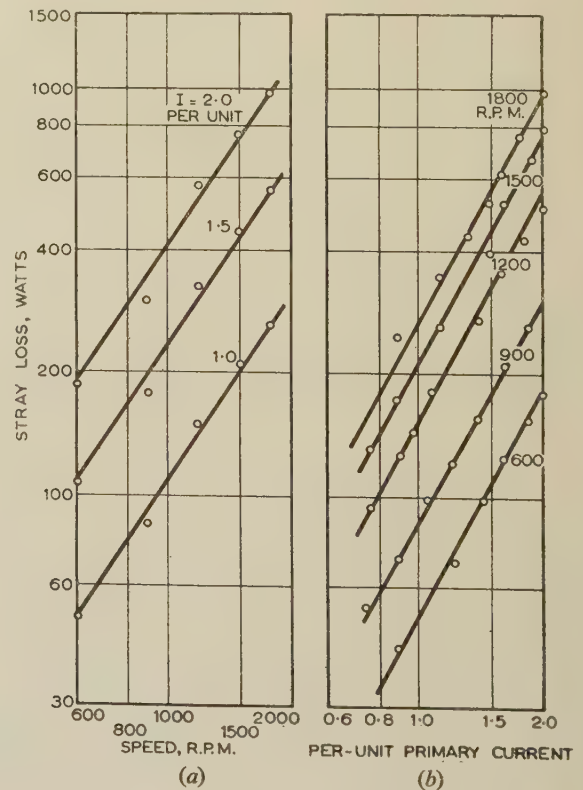


Fig. 4.—Stray loss associated with the leakage flux in the experimental machine.

(a) Constant primary currents.
(b) Constant speeds.

This result is not significantly different from that obtained by the much more complicated method described in an earlier paper,[4] and it is concluded that, provided that the speed is well removed

from the harmonic synchronous speeds, Morgan's method is satisfactory.

For the highest accuracy this result should be divided into rotor and stator components. This cannot be done experimentally, but the ratio of the two components can be calculated from the design data by the method described earlier,[4] and the division can then be performed, the result for the experimental machine being given as

$$P_{st} = \left(\frac{n}{1\,500}\right)^{1\cdot5}\left[144\left(\frac{I_1}{I_R}\right)^{1\cdot9} + 70\left(\frac{I_2}{I_R}\right)^{1\cdot9}\right] \text{watts} \quad . \quad (4)$$

However, for the majority of purposes it is sufficiently accurate to apply the result given in eqn. (3), using the stator current as the parameter. This approximation is only liable to appreciable error at very small loads, under which circumstances the stray loss is small.

## (5) STRAY LOSS AT SMALL SLIPS

The stray loss at small slips has been measured in the experimental machine by comparing the air-gap and output powers, and has been calculated from a combination of eqns. (2) and (4). The results are shown in Fig. 5, where the lines are calculated and
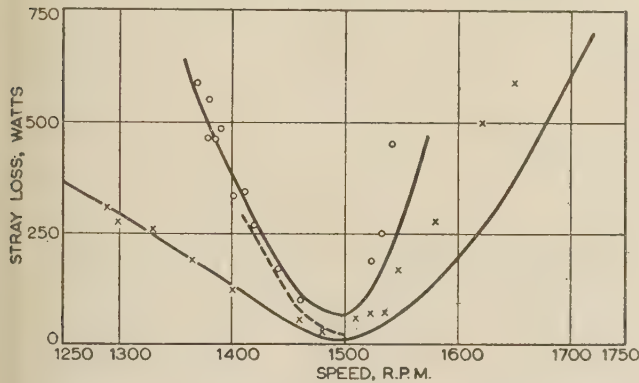


Fig. 5.—Stray loss in the experimental machine at small and moderate slips.

○    Measured at 400 volts per phase.
×    Measured at 200 volts per phase.
——   Predicted, at 200 and 400 volts per phase.
- - - -   Predicted, at 400 volts per phase, using only the results of the reverse rotation test.

the points are experimental. The agreement between calculated and measured results is good below synchronous speed but poor above this speed. This difference has been found in another machine, and it is noteworthy that in both cases the difference disappeared at the large negative slips obtained by running the machines at maximum speed whilst operating at half the normal frequency. The authors at present have no quantitative explanation of the effect, but consider that it may be due to the additive action of the zigzag leakage flux and main-flux slot ripples when the machine is generating at a high power factor. Under these circumstances the square of the sum of the ripple amplitudes should be considered, rather than the sum of the squares, and would result in a much higher calculated loss.

## (6) D.C. DYNAMIC BRAKING

There is little difference between operation with d.c. excitation and normal operation, except that a stationary primary m.m.f. wave of constant amplitude, rather than a rotating flux-wave of constant amplitude, is used. It is to be expected that the stray loss will be of similar form to that obtained in the reverse-

rotation test, except at low speeds when the machine saturates. This has, in fact, proved to be the case, the results being shown in Fig. 6. The currents are the equivalent a.c. values, and the
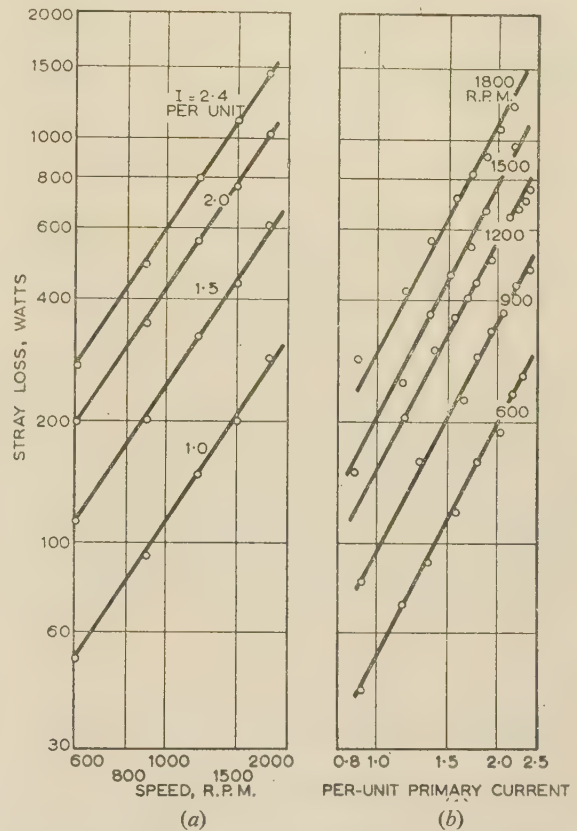


Fig. 6.—Stray loss in the experimental machine when it is excited by direct current. The currents shown are equivalent a.c. values.

   (a) Constant primary currents.
   (b) Constant speeds.

results are, within the limits of experimental error, identical to those obtained from the reverse-rotation test. It follows, therefore, that the latter can be used as the basis for calculating the loss with d.c. excitation.

The braking torque produced by the induction motor was subtracted from the torque required to drive it, to obtain the retarding torque due to high-frequency stray losses. The braking torque was calculated from the equivalent circuit of Fig. 1(a) but with slip replaced by fractional speed. Allowance was made for the variation of rotor resistance with temperature, frequent measurements of the resistance being made during the experiment.

## (7) THE EFFECT OF STRAY LOSSES ON THE PERFORMANCE

Stray losses adversely affect the performance of a machine by reducing its efficiency, pull-out torque and acceleration time. The stopping performance is improved when either plugging or d.c. injection is used, and the starting torque is not appreciably affected. The effect on the torque/speed curve of the experimental machine is shown in Fig. 7.

### (7.1) Effect on Efficiency

The efficiency is reduced by both supply-frequency losses and tooth-ripple-frequency losses. In the experimental machine the latter component is $0\cdot7\%$ of the rated output at no load, and $4\cdot5\%$ at full load. This loss must be supplied from the mech-
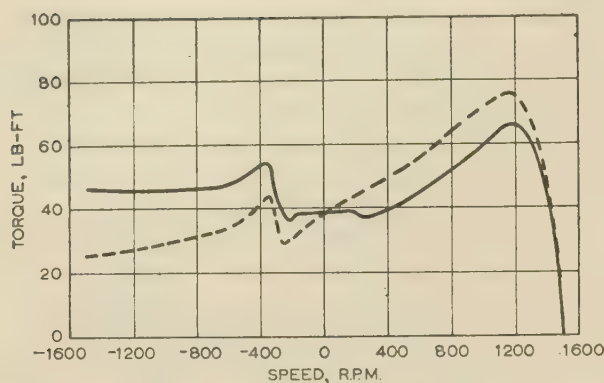
**Fig. 7.**—Torque/speed characteristics of the experimental machine showing the effect of stray loss.

---- Torque which would be obtained if the stray loss was zero.
—— Torque actually obtained.

gross error. Only the measurement and analysis of the loss for example by the reverse-rotation and the Rawcliffe and Menon tests, is sufficient for a true estimate of its effect.

Such a procedure is, however, too complicated for routine purposes, and the question therefore arises as to the possibility of a simpler test. This is, in fact, available in the reverse-rotation test. If the results of this test are applied directly to normal operation, without any attempt to divide them into rotor and stator components and with no allowance for the loss associated with the main flux, a close approximation to the actual loss is commonly obtained. This has been done for the experimental machine, with the result shown by the dotted line in Fig. 5, which refers to 400-volt operation. The fact that such a procedure overestimates the loss due to the rotor currents compensates to some extent for the neglect of the main flux loss. The value of the reverse-rotation test is shown by its inclusion in the American Standard Test Code.[7]

A similar detailed series of experiments has been performed on another squirrel-cage motor rated at 10 h.p., 1 420 r.p.m., 50 c/s (machine No. 2 of Reference 4) with similar results, but it would be of interest if the reverse-rotation test were performed for a number of substantially differing machines, under widely varying conditions of flux, speed and load current, in order to check its probable accuracy as a test for stray loss. As the authors of the present paper have no opportunity for performing a considerable number of tests, it is hoped that someone else will find the opportunity to do so.

anical output of the machine, and therefore compels additional supply-frequency input, so that the total stray loss at full load is about 5% and the full-load efficiency is about 85%. The stray loss at full load in this machine is therefore about equal to one-half of the total of the other losses—a figure which is typical of small and medium-size induction motors. The importance of stray losses is self evident, and it is seen that the process recommended in B.S. 269, whereby the stray losses at full load are arbitrarily taken as 0·625% of the rated output, is liable to

### Table 1

ACCELERATION AND RETARDATION CHARACTERISTICS OF THE EXPERIMENTAL MACHINE WHEN COUPLED TO A LOAD OF INERTIA $J$ LB-FT$^2$

The friction torque is assumed constant at 2 lb-ft. Relative values, taking the value including the effect of stray loss as unity, are given under the actual values to facilitate comparisons.

| | Time to complete operation | | Energy liberated in motor | | Revolutions during operation | |
|---|---|---|---|---|---|---|
| | Excluding stray loss | Including stray loss | Excluding stray loss | Including stray loss | Excluding stray loss | Including stray loss |
| | sec | sec | joules | joules | | |
| Acceleration, 0–1 450 r.p.m. .. .. | 0·090$J$ (0·81) | 0·111$J$ (1) | 1 054$J$ (0·75) | 1 400$J$ (1) | 0·93$J$ (0·76) | 1·22$J$ (1) |
| Retardation, using plugging, 1 450–0 r.p.m. | 0·155$J$ (1·47) | 0·105$J$ (1) | 2 630$J$ (1·35) | 1 950$J$ (1) | 1·98$J$ (1·62) | 1·22$J$ (1) |
| Total cycle .. .. .. .. .. | 0·245$J$ (1·13) | 0·216$J$ (1) | 3 680$J$ (1·10) | 3 350$J$ (1) | 2·91$J$ (1·19) | 2·44$J$ (1) |

### Table 2

RETARDATION CHARACTERISTICS OF EXPERIMENTAL MACHINE, WHEN EXCITED BY A DIRECT CURRENT EQUAL TO 1·6 TIMES THE FULL-LOAD CURRENT, SHOWING THE EFFECT OF STRAY LOSS

The load is of inertia $J$ lb-ft$^2$, and the friction torque is assumed constant at 2 lb-ft.

| | Time to complete operation | | Energy liberated in motor | | Revolutions during operation | |
|---|---|---|---|---|---|---|
| | Excluding stray loss | Including stray loss | Excluding stray loss | Including stray loss | Excluding stray loss | Including stray loss |
| | sec | sec | joules | joules | | |
| Retardation, 1 450–0 r.p.m. .. .. | 0·46$J$ (1·2) | 0·38$J$ (1) | 1 070$J$ (1·08) | 980$J$ (1) | 7·1$J$ (1·2) | 5·9$J$ (1) |

## (7.2) Effect on Pull-out and Starting Torques

The pull-out torque is appreciably reduced, that of the experimental machine being 88% of the value which would be obtained in the absence of stray loss. This is typical of small and medium-size machines, and the fact that it has not caused trouble in the past is probably due to the generosity of the various national standards when specifying pull-out torque.

The tooth-ripple losses are zero at standstill, so that the effect on the starting torque is limited to that due to the supply-frequency stray loss; the effect is therefore small.

## (7.3) Effect on Acceleration and Retardation

Although induction motors generally operate at constant speed there are many applications, such as centrifuge drives, where the principal duty is to start and stop a load. In these applications, stray loss will increase the duration of the accelerating period and the heating which then occurs; but, on the other hand, they will decrease the time of retardation and also the corresponding heating. The magnitude of the effect in the experimental machine when coupled to a pure inertia load is shown in Tables 1 and 2, which were calculated from test values of losses.

The results for d.c. braking are shown separately since they depend on the exciting current; in the Table this has been taken as equivalent to 10 amp, which was 1·6 times the full load current. The relationship between those values including the effects of stray losses and those excluding these effects will not be significantly affected by the current, since the induction torque is proportional to $I^2$ and the stray-loss torque to $I^{1·9}$.

Referring to Table 1, it will be seen that the effect of stray loss on the performance over one complete cycle of starting and stopping is not great, being of the order of a 12% improvement. This is, however, made up of two much greater effects, comprising a deterioration of about 20% in the starting performance and an improvement of about 40% in the stopping performance. In the case of d.c. braking the improvement is less, being about 20%. It is therefore evident that a knowledge of the stray loss could be of great help to the designer of such a drive when faced with difficult duty schedules.

## (8) CONCLUSIONS

There are three sources of stray loss in induction motors—eddy-current and iron losses at the supply frequency, tooth ripple in the main flux and tooth ripple in the zigzag leakage flux. In the small and medium-size motors the latter component predominates, but in large machines all three sources will be of comparable importance because of the reduced relative importance of zigzag leakage in such machines. The losses can be separated by three simple tests, the standstill test, the Rawcliffe and Menon test and the Morgan Brown and Schumer reverse-rotation test. Ware's test for the determination of the a.c. resistance of the primary windings is subject to certain inaccuracies, since it does not reproduce the flux conditions existing in the loaded machine, but, because of its simplicity, it is possible that it would be acceptable for routine purposes, especially if limits as to its accuracy in particular cases could be established.

The Rawcliffe and Menon test is suitable for the determination of stray loss associated with tooth ripple in the main flux, although an allowance must be made for loss associated with the leakage flux of the magnetizing current. The loss can be taken as constant over the working range, but, if necessary, can be extrapolated according to the law $(V/f)^2 n^{1·5}$. It is advantageous to plot the results to a base of $V^2$ rather than $V$ as suggested by Rawcliffe and Menon, since extrapolation of the graphs is then easier.

The Morgan, Brown and Schumer reverse-rotation test is easy to perform, but since a large proportion of the input power is lost in the stator, it is essential to use the best possible value for the stator resistance at the supply frequency. This is usually that obtained by Ware's test and its possible inaccuracy reflects on the reverse-rotation test. The indices of extrapolation of the result with current and speed should be modified from 2 as suggested by the originators of the test, to 2 and 1·5, respectively. No allowance is normally required for the loss associated with the main flux in this test, but it may be necessary to divide the loss into stator and rotor components. This can be done by the method given in Reference 4.

When calculating the stray loss from the results of the above tests, little error is caused in most cases if the loss associated with the main flux is neglected, thus eliminating the need for the Rawcliffe and Menon test. Machines where this procedure is inadvisable are those having an abnormally low zigzag leakage reactance, such as large machines with relatively long air-gaps and open slots.

Although the recommendations of B.S. 269 may be reasonable for large machines, they are totally unrealistic for the majority of induction motors, and it appears that the specification should be amended to include a more precise and scientific determination of the stray losses based, say, on the reverse-rotation test.

Stray losses do not significantly affect the starting torque but do appreciably reduce the pull-out torque. Since the authors have found no record of complaints on this account, it appears that the standard specification on the subject is sufficiently generous to mask the effect. Nevertheless, with the present tendency towards better utilization of material and smaller factors of safety, it is an effect that should be borne in mind.

The effect on start-stop performance may or may not be favourable, but it is small. However, the effect on the start or stop taken separately is appreciable, the starting performance being worsened and the stopping performance improved.

## (10) REFERENCES

(1) MORGAN, T., BROWN, W. E., and SCHUMER, A. J.: 'Reverse Rotation Tests for the Determination of Stray-Load Loss in Induction Motors', *Transactions of the American I.E.E.*, 1939, **58**, p. 319.

MORGAN, T., BROWN, W. E., and SCHUMER, A. J.: 'Induction Motor Characteristics at High Slips', *ibid.*, 1940, **59**, p. 464.

(2) WARE, D. H.: 'Measurement of Stray-Load Loss in Induction Motors', *ibid.*, 1945, **64**, p. 194.

(3) RAWCLIFFE, G. H., and MENON, A. M.: 'A Simple New Test for Harmonic-Frequency Losses in A.C. Machines', *Proceedings I.E.E.*, Paper No. 1222 U, April, 1952 (**99**, Part II, p. 145).

(4) BARTON, T. H., and AHMAD, V.: 'The Measurement and Prediction of Induction Motor Stray Loss at Large Slips', *ibid.*, Monograph No. 219 U, January, 1957 (**104** C, p. 299).

(5) KUHLMANN, J. H.: 'Design of Electrical Apparatus' (Chapman and Hall Ltd., 1950, 3rd edition), p. 332.

(6) MORRIS, D.: 'Some Tests of an Exact Practical Theory of the Transformer', *Proceedings I.E.E.*, Paper No. 902 S, February, 1950 (**97**, Part II, p. 17).

MORRIS, D.: 'Some Tests of an Exact Practical Theory of the Induction Motor', *ibid.*, Paper No. 1041 U, December, 1950 (**97**, Part II, p. 767).

(7) 'American Standard Test Code for Polyphase Induction Motors and Generators' (American Standards Association, New York, 1954).

# GENERALIZED OPERATORS FOR THE APPROXIMATE STEADY-STATE ANALYSIS OF LINEAR AND NON-LINEAR CIRCUITS

By A. J. O. CRUICKSHANK, B.Sc., Ph.D., Associate Member.

## SUMMARY

A method of approximate analysis is given for linear and non-linear circuits subjected to sinusoidal or non-sinusoidal applied voltages. In brief, the method may be said to be a periodic analogue of the technique of time series. Waveforms are represented by an $n$-component operator giving the values of the wave at each of $n$ ordinates. For waves containing only odd harmonics, the half-cycle is divided into $n$ parts, while for those containing even harmonics the complete cycle is divided into $n$ parts. The central feature of the method is the use of a shift operator, $u$, which translates any waveform to the right by $1/n$th of a half-cycle or of a complete cycle as the case may be. The fundamental relations $u^n = -1$ and $u^n = 1$ are obtained in the two cases respectively.

For linear circuit work the method is advantageous where the periodic input is numerically or graphically specified and where a similar description of the output is required. The procedure is then to form, according to certain rules, an impedance operator for the circuit and to operate on the inverse of the impedance operator, i.e. the admittance operator, by the input wave of applied voltage. The waveform of the current, or the output in the case of a transfer-function operator, is then obtained. From this, r.m.s. values and powers are easily computed. Since the method relates basically to operations on non-sinusoidal waveforms displaced with respect to each other, it is also suitable for e.m.f. calculations in distributed coil groups moving in non-sinusoidal fields.

In the solution of non-linear circuits, e.g. those containing iron-cored coils or non-linear resistors, the current is obtained by a process of continued approximation. This can be done very simply. An initial solution is assumed or a very rough calculation made in order to start the procedure. One particular method of doing this is to assume that all of the applied voltage acts across the non-linearity. From the static characteristic of the non-linearity a second estimation can then be made of the voltage acting across the non-linearity using the imposed circuit equation. The two estimations are averaged and the procedure is repeated until there is only a small change in any of the waveforms. The method appears to be of fairly general application. Both sinusoidal and non-sinusoidal applied voltages may be handled with the same amount of work. It is suitable for instantaneous and non-instantaneous non-linearities, and since it provides a response waveform, r.m.s. currents and powers may be obtained. It is also suitable for circuits containing more than one non-linearity.

The method, however, is approximate, numerical and relates to a fixed frequency. The accuracy is generally within 5% of the maximum ordinate in the waveform with the normal ordinate spacings employed. R.M.S. values and powers, however, may be obtained more accurately, the error in these seldom exceeding 2%.

## LIST OF PRINCIPAL SYMBOLS

$f(t)$ = Function periodic in time $2\pi/\omega$.

$n$ = Positive integer; number of ordinates of $f(t)$ in $\pi/\omega$ or $2\pi/\omega$.

$\tau$ = Interval between ordinates = $\pi/n\omega$ or $2\pi/n\omega$.

$f_k$ = Ordinate height of $f(t)$ at $t = k\tau$.

$\Delta_0(t)$ = Waveform of isosceles-triangular pulses of unit height and base $2\tau$, repeated with alternate sign in half period $\pi/\omega$; $\Delta_0(0) = 1$.

$\Delta_e(t)$ = As above, but repeated with same sign in period $2\pi/\omega$. $\Delta_e(0) = 1$.

$u$ = Shift operator for periodic functions; $uf(t) = f(t - \tau)$ i.e. $u$ translates to the right by $\tau$ sec.

$f$ = Operator form of waveform $f(t)$;

$$f = \sum_{n-1} f_k u^k = f_0 + f_1 u + f_2 u^2 + \ldots + f_{n-1} u^{n-1}.$$

$A = \sum_{n-1} A_k u^k$; general form of $n$-component or $u$-operator.

$p$ = Differential $u$-operator.

$p^{-1}$ = Integral $u$-operator.

$AB$ = Product of two operators; $AB = BA$.

$I = \sqrt{\left(\dfrac{1}{n} \sum_{n-1} I_k^2\right)}$; r.m.s. value of current waveform.

## (1) INTRODUCTION

In the last ten years or so there has been an increasing interest in the calculation of network and system responses by numerical methods based on the expression of time functions as a number series giving the ordinates of the function at regular intervals. These methods have been developed especially for dealing with transient inputs of arbitrary form, and the work has been directed to the study of both linear and non-linear circuits. In the latter the expression of time functions as a number series having a definite starting-point allows the response to be obtained in a step-by-step fashion, by which manner the non-linear relation may be set into the problem point by point.

In using the method of time series, Tustin[1] represented time functions by a series of delta units or isosceles triangles of varying heights and showed also how other shapes of pulse or other units might be used. His approach was from a geometric viewpoint. Since then, various authors[2-7] have attempted to organize the method on a theoretical basis and to relate it to existing Laplace or Fourier transform theory.

The question which the present paper takes up is whether a steady-state analysis exists for general periodic inputs based on the representation of such waveforms by a series of displaced unit waveforms of varying magnitude—in short, whether there is a periodic counterpart of time series. Such an analysis would, in fact, be suited to the non-linear problems which Moullin[8,9] and Slemon[10] have tackled using Fourier components and successive approximations, and to more general circuits containing non-linear resistors and iron-cored inductors. It would also be applicable to linear circuit analysis with arbitrary and numerically specified periodic inputs. An analysis can, in fact, be performed and is the subject of the paper. As it happens, the theory bears many resemblances to normal vector algebra concerning the $j$ operator and, in fact, a simple form of the analysis very like vector algebra results when the periodic inputs are of sine waveform. One particular point which emerges is that the method of polynomial division which can be used in

evaluating time series having a definite starting-point is now not generally applicable, and an inversion process takes its place. This is also the case with Thomson's[2] theory, which employs double-sided series. The method, however, is essentially different from that used by Thomson, in that the basic building-block of the waveform is itself periodic and not an isolated pulse. Furthermore, it is concerned distinctly with steady-state responses as against pulse responses.

The application of this method in calculating the forced oscillations of certain non-linear circuits is by a method of successive approximation and convergence. The non-linear element may be given analytically, or its characteristics may be displayed graphically as, for instance, by giving a set of magnetization loops for an iron-cored coil. An example is given of the calculation of magnetizing current waveform in such a coil. In linear circuits the steady-state response to non-sinusoidal inputs may be obtained; the use of the method in this case would be justified when the periodic input was known numerically or graphically and a similar description of the output was required. In these circumstances the method dispenses with the need for Fourier analysis of the input and subsequent point-by-point calculation of the output, both of which are extremely tedious processes. However, if the Fourier components of the input are known there would be no particular value in employing the method. With non-linear systems, whether the periodic input is given numerically or by its Fourier components, the method has very definite advantages.

The theory is for simplicity restricted first to periodic waveforms containing only odd Fourier components, and in these the negative half-cycle is a replica in time of the positive half-cycle, apart from sign. Later the analysis is extended to cover the case of both odd and even harmonics. This requires extra computational labour. The cardinal feature of the theory is the use of a shift operator $u$, which translates any function in real time to the right by an amount $\tau$. The operator $u$ is analogous to $z^{-1}$ of $z$-transform theory and is in some respects similar to the normal operator $j$ of vector algebra. Finally, it should be stated that calculations carried out by the theory are not exact, owing to the polygonal approximation of the waveform which is made. It is obvious that the order of accuracy will improve as more ordinates are chosen to represent the waveform.

## (2) *U*-OPERATORS

### (2.1) Basis

Consider Fig. 1(a), which shows a periodic input $f(t)$, of arbitrary waveform but containing only odd harmonics. This may be divided into a number of superposed and displaced triangular pulse waveforms of heights corresponding to the ordinates $f(0)$, $f(\tau)$, $f(2\tau)$, ... $f(n\tau)$, where $n$ is an even integer and $n\tau$ is equal to the half-period (the reason for restricting $n$ to even values will be apparent later). The triangular pulse waveforms corresponding to the ordinates at $t = 0$ and $t = \tau$ are shown in Fig. 1(b). Consideration of any polygonal element such as ABCD in Fig. 1(a) will show that it can be reduced to the isosceles-triangle element OPQ in Fig. 1(b). The representation is, in fact, the periodic analogue of that introduced by Tustin.[1] For waveforms having only odd harmonics the negative half-wave is a replica in time, apart from sign, of the positive half-wave and the ordinate at $(n + 1)\tau$ is the negative of the ordinate at $\tau$. For the particular waveform shown in Fig. 1(a), $n = 6$, which is a fairly coarse spacing in view of the waveshape. Let the triangular pulse waveform corresponding to an ordinate of unit height at $t = 0$ be denoted by $\Delta_0(t)$, as shown in Fig. 2(a). Let there now be a shift operator, $u$, which translates any wave-
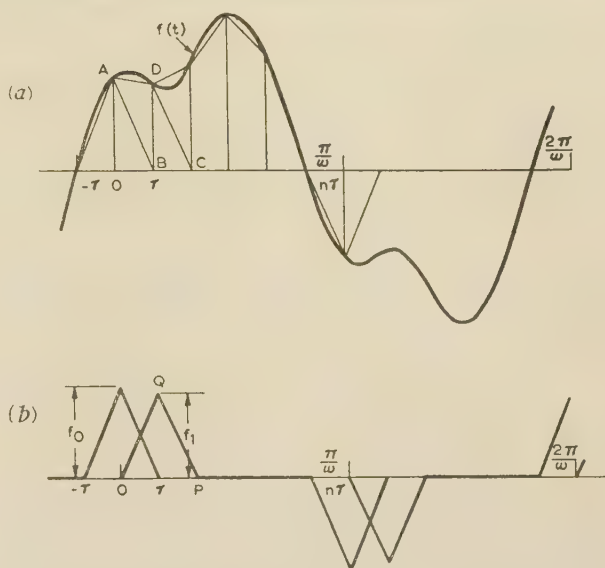


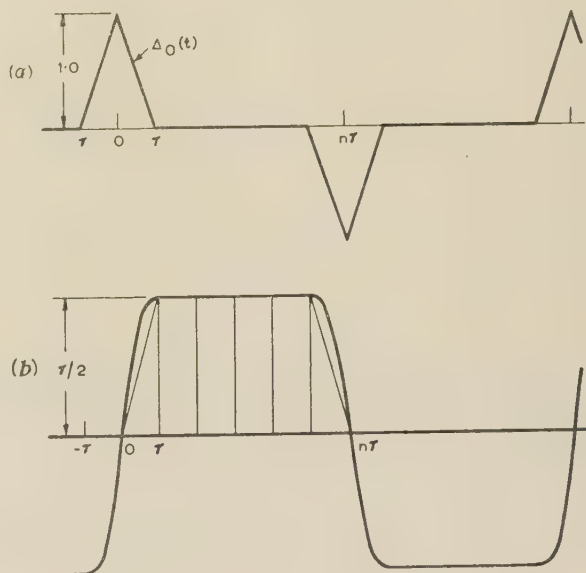Fig. 1.—Polygonal approximation of periodic input with only **odd** harmonics.



Fig. 2.—Integration of unit triangular-pulse waveform.

form one interval $\tau$ to the right, i.e. $u$ operates in the domain of real time and corresponds to a lag of $\tau$ sec. Then, if we write $f(n\tau) = f_n$, $f(t)$ may be given the polygonal representation

$$f(t) \simeq (u^0 f_0 + u f_1 + u^2 f_2 + \ldots + u^{n-1} f_{n-1})\Delta_0(t) \quad . \quad (1)$$

The series $uf$ consists of a finite number of terms equal to the number of ordinates chosen to represent the half-wave. The series of $n$ terms can, of course, commence with any particular ordinate desired, but after $n$ terms the ordinate values $f_0$, $f_1$, etc., repeat, apart from a negative sign. Hence $f(t)$ may be written

$$(u^{-r} f_{-r} + u^{-(r-1)} f_{-(r-1)} + \ldots + u^{-r+n-1} f_{-r+n-1})\Delta_0(t)$$

$r$ being any integer or zero. In the above expression $u^{-r}$ is defined by $u^{-r} u^r f(t) = f(t)$, i.e. for $r$ a positive integer the operator $u^{-r}$ shifts any time function $r$ intervals to the left.

The representation of f($t$) given in eqn. (1) may be written f($t$) $\simeq f\Delta_0(t)$, where

$$f = f_0 + f_1 u + f_2 u^2 + \ldots + f_{n-1} u^{n-1} = \sum_{n-1} f_k u^{k*}$$

In this expression $u$, $u^2$, ... $u^k$ are simple shift operators. More generally, a $u$-operator will be defined by an expression such as

$$a + u^q b + u^r c + u^s d \quad . \quad . \quad . \quad . \quad . \quad (2)$$

containing a finite number of terms, and where some of the coefficients may be zero and $q$, $r$, $s$, ... are positive or negative integers. Since, however, $\tau$ is 1/$n$th of the half-period, we have the fundamental relation

$$u^n = -1 \quad . \quad . \quad . \quad . \quad . \quad (3)$$

It follows that any expression of the form in eqn. (2) may be reduced to the form

$$a + ub' + u^2 c' + u^3 d' + \ldots + u^{n-1} g' \quad . \quad . \quad (4)$$

containing $n$ terms only if none of the coefficients are zero; e.g. if $n = 6$, $5u^{-3} + 3u^{-2} + 1 + u + 4u^7 = 1 - 3u - 5u^3 - 3u^4$. This is analogous to reducing a normal vector operator such as $a + jb + j^2 c + j^3 d$ to the form $a - c + j(b - d)$ by substituting $j^2 = -1$. In fact, all of the rules to be given for $u$-operators have their counterparts in $j$-operator theory, as might be expected. One can think of the $u$-operator as a generalized form of the $j$-operator, with the exception that $u$-operator theory is confined to the domain of real time so long as the waveform is non-sinusoidal. If, as a special case, the waveform is sinusoidal, a simplified version of $u$-operator theory is still applicable, but this will not generally hold any advantages over normal vector techniques.

The expression (4) may refer to the impedance, admittance or transfer-function operator for a circuit. An impedance operator will be denoted by $Z$, and admittance and transfer-function operators will be denoted by $Y$.

### (2.2) Operation on a Waveform

The operation by an operator $Z$ on a wave $f$ is written $Zf$. It is simply defined by the rule of polynomial multiplication, followed by reduction using $u^n = -1$. An example will make this clear.

If $n = 6$, let us suppose that $f$ is given by

$$f_0 + f_1 u + f_2 u^2 + f_3 u^3 + f_4 u^4 + f_5 u^5$$

Let $Z$ be $a + bu + cu^2$. Then the multiplication is

$$f_0 + f_1 u + f_2 u^2 + f_3 u^3 + f_4 u^4 + f_5 u^5$$
$$a + bu + cu^2$$

| $af_0$ | $af_1$ | $af_2$ | $af_3$ | $af_4$ | $af_5$ |
|---|---|---|---|---|---|
| $-bf_5$ | $bf_0$ | $bf_1$ | $bf_2$ | $bf_3$ | $bf_4$ |
| $-cf_4 -cf_5$ | | $cf_0$ | $cf_1$ | $cf_2$ | $cf_3$ |
| etc. | etc. | etc. | $(af_3 + bf_2$ etc. | etc. | |
| | | | $+ cf_1)u^3$ | | |

The ordinate series of the product will, of course, be periodic, and the waveform of the product is defined completely by any set of $n$ terms.

* In further work f($t$) is represented simply by $f$, where it is understood that $f$ has still to operate on $\Delta_0(t)$ in order that the equation f($t$) $\simeq f\Delta_0(t)$ may hold. This is similar to writing a voltage $V = a + jb$, where to be complete, the sine wave of voltage v($t$) should be written v($t$) $= VS = (a + jb)S$, $S$ being a reference sine wave. Also, in further work the operators $u^k$ may appear before or after the numbers upon which they operate. Logically they should always precede the operand, but since the handling of $u$-operators resembles to some extent the manipulation of polynomials, it is convenient sometimes to put the $u^k$ after the operand, which is then regarded as a coefficient.

Consideration of the above procedure leads one to the conclusion that the process of polynomial division will not be available when an interpretation is sought of the form $f/Z$, and this is so. This is in contrast to numerical analysis with transient inputs, where any series has a definite starting-point, say at $t = 0$, from which the division may be commenced. In the present case an inversion process has to be found in order to convert the problem to the usual operating procedure given above, i.e. $f/Z$ is interpreted as $Z^{-1}f$. This is similar to the evaluation of $(a + jb)/(c + jd)$ in vector algebra by a process of rationalization.

### (2.3) Differential and Integral Operators

Previous work[1,5] in the field of time series and $z$-transform theory has shown that the form $[2(1 - z^{-1})]/[\tau(1 + z^{-1})]$, when operating on a series $g_0 + g_1 z^{-1} + g_2 z^{-2}$, etc., representing a non-periodic time function g($t$) starting at $t = 0$, produces the derivative g'($t$). This operator is also applicable to periodic functions, and in terms of $u$ it is

$$p = \frac{2}{\tau} \frac{1 - u}{1 + u} \quad . \quad . \quad . \quad . \quad . \quad (5)$$

What is different in this case, however, is that the $u$-operator in the denominator is to be evaluated by a process of inversion instead of division.

The integral operator is the inverse of the differential operator, the integration of a periodic waveform being defined in a steady-state sense, i.e. having zero average value. Hence

$$p^{-1} = \frac{\tau}{2} \frac{(1 + u)}{(1 - u)} \quad . \quad . \quad . \quad . \quad (6)$$

An alternative form of this can be deduced geometrically. Fig. 2($a$) shows the unit triangular-pulse waveform $\Delta_0(t)$, and the full line in Fig. 2($b$) shows its steady-state integral having zero average value. The ordinates of $\Delta_0(t)$, taking $n = 6$, are 1, 0, 0, 0, 0, 0, while those of the integral are 0, $\tau/2$, $\tau/2$, $\tau/2$, $\tau/2$, $\tau/2$. One or two trials will show that the operator producing this result is

$$p^{-1} = \frac{\tau}{2}(u + u^2 + u^3 + u^4 + u^5) \quad . \quad . \quad (7)$$

Since this holds for the unit waveform $\Delta_0(t)$, it will also hold for any waveform built up from displaced triangular-pulse waveforms of varying magnitudes, and in general, therefore, the integral operator can be written

$$p^{-1} = \frac{\tau}{2}(u + u^2 + \ldots + u^{n-1}) \quad . \quad . \quad (8)$$

Eqn. (8) represents, in fact, the evaluation of eqn. (6). This will be shown later when the inverses of $u$-operators have been discussed. It will also transpire that

$$p = \frac{2}{\tau}(- u + u^2 - u^3 + \ldots - u^{n-1}) . \quad . \quad . \quad (9)$$

is the general operator form of eqn. (5).

### (3) ALGEBRA OF $U$-OPERATORS

#### (3.1) Unit Operator: Addition and Subtraction

The unit operator is one in which all the coefficients of powers of $u$ vanish, except that of $u^0$, which is unity.

The sum or difference of two operators $R$ and $S$ is found by taking the sum or difference of corresponding components, i.e.

f $$R = R_0 + R_1 u + R_2 u^2 \ldots + R_{n-1} u^{n-1} = \sum_{n-1} R_k u^k$$

and $$S = \sum_{n-1} S_k u^k, \text{ then } R \pm S = \sum_{n-1} (R_k \pm S_k) u^k$$

### (3.2) Multiplication

The reduction of an operator whose terms contain any powers of $u$ to the normal form $\sum_{n-1} R_k u^k$ by substituting $u^n = -1$ has been dealt with in Section 2.1. The product of two operators is formed according to the normal rule of polynomial multiplication, followed, if necessary, by reduction using $u^n = -1$. This is the same process as the operation of a $u$-operator on a waveform. Multiplication of $u$-operators is commutative, i.e. $RS = SR$. For practical computational purposes, multiplication or operation on a waveform is carried out with a desk calculating machine. If desired, the calculating-machine-and-strip method for forming successive sums of products may be advantageously applied here.

### (3.3) Division and Inversion

The ratio of two operators may be evaluated by polynomial division, provided that an exact quotient is obtained, i.e. a finite number of terms in powers of $u$. This is not usually the case. In general, therefore, the ratio of two $u$-operators is evaluated by inverting the operator in the denominator and multiplying it by the numerator; in symbols, $R/A = RA^{-1}$.

The inverse of the general operator $A = \sum_{n-1} A_k u^k$ is defined by the relation $AA^{-1} = A^{-1}A = 1$. As shown in Section 9.1 the inverse $A^{-1}$ is another operator $B = \sum_{n-1} B_k u^k$, where $B_k = A_{1,k+1}/A$, and $A_{1,k+1}$ is the cofactor of the element in the first row and $(k+1)$th column of the determinant $A$. It therefore follows that a condition for the existence of an inverse operator is that $A \neq 0$, and for practical circuits this condition is nearly always fulfilled. Although the inverse of $A$ has been formally stated in terms of the determinant $A$ and the cofactors of the elements of its first row, in practice it is better simply to solve the set of $n$ simultaneous equations given in Section 9.1; it is suggested that Crout's[11] method is superior to most others in accomplishing this. Nevertheless, the calculation of the inverse of a general $n$-term operator requires a fair amount of arithmetical labour. This may be reduced by the use in appropriate circumstances of the forms for $p$ and $p^{-1}$ given in eqns. (5) and (6), rather than those in eqns. (9) and (8). Also, a branch-by-branch analysis of a particular circuit, or similar approach, will restrict the order of the operators which have to be inverted. Circuits having characteristic equations of the first, second . . . $m$th order will give $u$-operators in the denominator having two, three . . . $(m + 1)$ terms respectively (where $m < n$, the number of ordinates chosen). In the formation of the inverses of these simple operators the matrix $A$ in Section 9.1 will then contain a large number of zeros. The use of a desk calculating machine is essential in performing the arithmetical work.

For non-linear circuits, where the solution is obtained by successive approximations, inverses are not required. This method can equally well be applied to linear circuits, although it is not done in the linear-circuit examples in the paper, for which exact inverses are given.

The inverse of a 2-term operator may be worked out in general symbols using the rule given. If $A = x + yu$, we have

$$^{-1} = (x + yu)^{-1} = (x^n + y^n)^{-1}(x^{n-1} - x^{n-2} yu$$
$$+ x^{n-3}y^2u^2 - \ldots + xy^{n-2}u^{n-2} - y^{n-1}u^{n-1}) \quad (10)$$

In particular, for $x = y = 1$,

$$(1 + u)^{-1} = \tfrac{1}{2}(1 - u + u^2 - \ldots - u^{n-1})$$

and for $x = 1, y = -1$,

$$(1 - u)^{-1} = \tfrac{1}{2}(1 + u + u^2 + \ldots + u^{n-1})$$

Evaluating $p = \dfrac{2}{\tau} \dfrac{(1 - u)}{(1 + u)}$ gives, for example,

$$\frac{1}{\tau}(1 - u)(1 - u + u^2 \ldots - u^{n-1})$$

$$= \frac{2}{\tau}(- u + u^2 - u^3 \ldots - u^{n-1})$$

Another convenient form of $(x + yu)^{-1}$ is

$$x^{-1}(1 + a^n)^{-1}(1 - au + a^2 u^2 - a^3 u^3 \ldots - a^{n-1}u^{n-1})$$

where $a = y/x$.

It is appropriate to explain at this stage the choice of an even number of ordinates to describe the half-cycle of a waveform containing only odd harmonics. Since $u^n = -1$, one solution of this when $n$ is odd is $u = -1$. Hence, if $n$ is odd the inverse of $1 + u$ will give a zero denominator. This means that, when $n$ is odd, an exact inverse will not exist for the operator $1 + u$, and this occurs in the denominator of the differentiating operator $p$. The integrating operator $p^{-1} = \dfrac{\tau}{2} \dfrac{(1 + u)}{(1 - u)}$, on the other hand, can be evaluated when $n$ is odd. Both $p$ and $p^{-1}$, however, may be evaluated exactly if $n$ is restricted to even values. This is the sole reason for the restriction.

This particular difficulty and any similar one may always, of course, be avoided by taking an approximation to the operator, e.g. in the above case with $n$ odd by inverting $(1 + 0 \cdot 99u)$ instead of $1 + u$. Such a process is quite logical in an approximate method of calculation, where the error introduced by so doing is less than that originating from the segmental representation of a curve. The approximation to a particular operator may, moreover, be improved indefinitely if one is prepared to accept the larger number of significant figures necessary in performing a calculation; this usually can be done without effort if the number is still within the capacity of the calculating machine available. The procedure of approximation to an operator is necessary when more general waveforms are considered, as in the next Section. A further point to bear in mind is that pure differential or integral operators are seldom required. In the course of normal circuit analysis an operator which does not have an exact inverse is not likely to arise.

### (3.4) Extension to Waveforms containing Even Harmonics

The theory so far given has been restricted to waveforms having only odd harmonics, and in consequence, a negative half-wave which is a replica in time of the positive half-wave, apart from sign. This has been done, first, because a large number of engineering waveforms are of this type and many non-linear elements have input/output relationships which are symmetrical about the origin; secondly, the theory for only odd-harmonic-type waveforms can be made more complete than that for even and odd harmonic waveforms in the sense that, by restricting $n$ to even values, there is no need to have approximate operators—which is not so in the case about to be considered, where an approximate integral operator must be introduced when it is required; finally, it is possible to consider general waveforms by adding only a few remarks to the foregoing theory.

There remains, however, one case not generally covered but which can be dealt with if the operator contains only differential
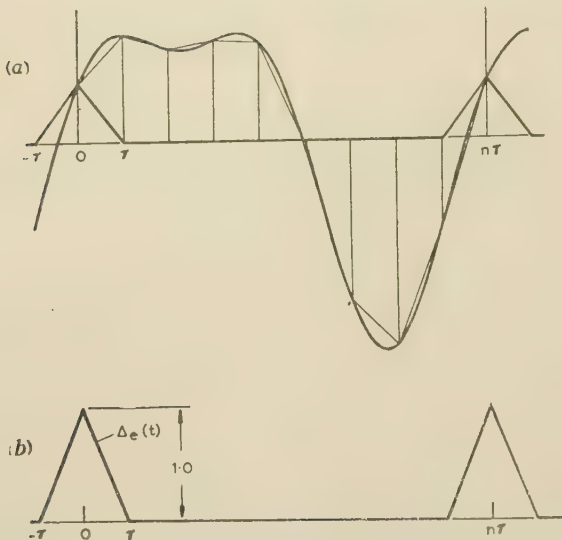
Fig. 3.—Polygonal approximation of general periodic input.

components, namely that of a periodic function having a d.c. component, or non-zero average value. The procedure here is to consider the d.c. component separately. This will be valid for both linear and non-linear systems, provided that the information about the non-linear element is in terms of an input/output relationship about the working point determined by the d.c. component.

The building-block of a general waveform is the triangular-pulse waveform, $\Delta_e(t)$, in Fig. 3(b), of unit height and of period equal to that of the waveform being represented. If this period is divided into $n$ intervals of length $\tau$, $n$ being odd, a segmental approximation of the periodic function $f(t)$ is

$$f(t) \simeq \left( \sum_{n-1} f_k u^k \right) \Delta_e(t)$$

In other words, the representation is of the same nature as previously used but summation takes place over a whole cycle.

The waveform may be written as $f\Delta_e(t) = \left( \sum_{n-1} f_k u^k \right) \Delta_e(t)$, or simply $f$.

The results regarding the formation and the algebra of $u$-operators remain the same as before, with the exception that the fundamental relationship $u^n = 1$ now holds. In consequence, the inversion matrix is slightly different, the signs of the elements being all positive. Formally, however, we have the same rule. The inverse of $A = \sum_{n-1} A_k u^k$ is $B = \sum_{n-1} B_k u^k$, where $B_k = A_{1,k+1}/A$ and $A_{1,k+1}$ is the cofactor of the element in the first row and $(k + 1)$th column of the determinant $A$ of the inversion matrix.

Since $u = \pm 1$ are solutions of $u^n = 1$ for $n$ even, the operators $1 + u$ and $1 - u$ do not have exact inverses. However, if $n$ is odd, the operator $1 + u$ has an exact inverse but the operator $1 - u$ must be approximately inverted when required. This is necessary in the case of the integral operator.

When $n$ is odd the inverse of $x + yu$ is

$$(x + yu)^{-1} = (x^n + y^n)^{-1}(x^{n-1} - x^{n-2}yu + x^{n-3}y^2u^2 - \ldots - xy^{n-2}u^{n-2} + y^{n-1}u^{n-1})$$

or alternatively

$$(x + yu)^{-1} = x^{-1}(1 + a^n)^{-1}(1 - au + a^2u^2 - \ldots - a^{n-2}u^{n-2} + a^{n-1}u^{n-1})$$

where $a = y/x$.

The differential operator is $p = \dfrac{2}{\tau} \dfrac{(1 - u)}{(1 + u)}$ or

$$p = \frac{2}{\tau}(- u + u^2 - u^3 \ldots + u^{n-1})$$

The integral operator is $p^{-1} = \dfrac{\tau}{2} \dfrac{(1 + u)}{(1 - u)}$.

This can be approximately evaluated by only replacing $1 - u$ in the demominator by, say, $(1 - 0 \cdot 99u)$. This is quite an arbitrary choice, but one which is reasonable in that sufficient accuracy is obtainable for the ordinate spacings which have been employed and yet the coefficients of the resulting operator do not become too large. A number of integral operators based on this approximation are given in Section 9.2 for various values of $n$.

The application of the foregoing theory to linear and non-linear circuits with both sine-wave and arbitrary inputs is now considered.

## (4) APPLICATION TO LINEAR CIRCUITS

### (4.1) Circuit Analysis: Power and R.M.S. Values

In the application of the $u$-operator method to linear-circuit analysis in the steady-state, the general procedure is to form impedance, admittance and transfer-function operators by replacing $j\omega$ by $2(1 - u)/\tau(1 + u)$ throughout. The resulting expressions are arranged in ascending powers of $u$ in the numerator and denominator, and by inverting the denominator, a $u$-operator in the general form $A = \sum_{n-1} A_k u^k$ is obtained. This is operated on by the non-sinusoidal driving function, current or voltage as the case may be. In more complex circuits, the usual results for series and parallel combinations of operators apply.

In view of the waveform representation given by the method, particularly simple expressions for the r.m.s. values of voltages or currents are obtained, and also for the power supplied to a circuit. If the supply voltage and current in a circuit are given by $V = \sum_{n-1} V_k u^k$ and $I = \sum_{n-1} I_k u^k$, the r.m.s. voltage is

$$V = \left( \frac{1}{n} \sum_{n-1} V_k^2 \right)^{1/2}$$

and similarly for the current. The instantaneous power wave is

$$P = \sum_{n-1} V_k I_k u^k$$

of which the average value is

$$P = \frac{1}{n} \sum_{n-1} V_k I_k$$

This may be denoted by $P = (V \cdot I)/n$, the point signifying the scalar product of the $V$ and $I$ operators, i.e. the sum of products of corresponding components.

### (4.2) Linear Circuits

The two simple examples first given illustrate the procedure and accuracy to be expected from the method. The solution of a series-parallel circuit is then given, and it is suggested that 3- or 4-term demominators could be inverted by an alternative factorizing process. Finally, an example concerning the r.m.s. voltage generated in a distributed coil group moving through non-sinusoidal flux indicates a possible application in machine-theory calculations. In the first two examples, inputs have been chosen consisting of a fundamental and one harmonic; this has been done purely to facilitate checking by working out the

individual harmonic currents and by subsequent point-by-point calculation of the total value of the complex wave. So far as the present method is concerned, arbitrary periodic inputs may be handled with only a little extra labour, depending upon the frequency components present and the accuracy desired.

**(4.2.1) Simple *RL* and *RC* Circuits.**

Consider the impedance $R + pL$ to which the voltage shown in Fig. 4 is applied, the waveshape containing only odd harmonics. Dividing the half-cycle into, say, eight intervals, gives

$$V = 0 \cdot 4 + 0 \cdot 5358u + 0 \cdot 4243u^2 + 0 \cdot 5543u^3 + 1 \cdot 0u^4$$
$$+ 1 \cdot 2935u^5 + 0 \cdot 9899u^6 + 0 \cdot 2296u^7$$

The above figures are, in fact, the ordinates of $\sin \omega t + 0 \cdot 4 \cos 3\omega t$
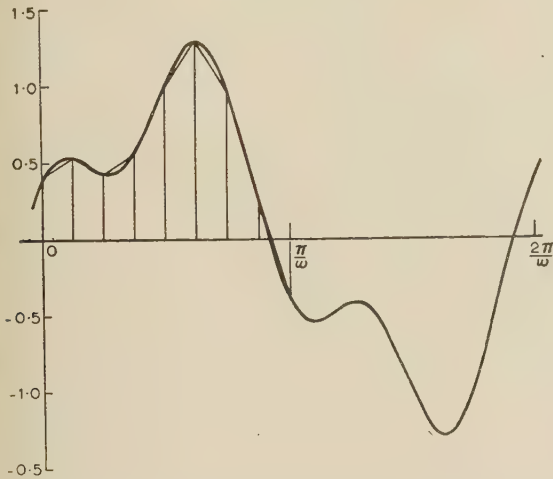


**Fig. 4.**—Periodic input to *RL* circuit and approximation.

calculated at $0, \tau, 2\tau, \ldots$, where $\tau = \pi/8\omega$. If the coil has $\omega L = 1$ and $R = 1$, say, the impedance operator is

$$Z = 1 + \frac{16}{\pi} \frac{(1 - u)}{(1 + u)} = \frac{6 \cdot 0930 - 4 \cdot 0930u}{1 + u}$$

Hence

$$Z^{-1} = \frac{1 + u}{6 \cdot 0930(1 - 0 \cdot 6718u)}$$

$$= 0 \cdot 1576(0 \cdot 9383 + 1 \cdot 6718u + 1 \cdot 1231u^2 + 0 \cdot 7545u^3$$
$$+ 0 \cdot 5069u^4 + 0 \cdot 3405u^5 + 0 \cdot 2278u^6 + 0 \cdot 1536u^7)$$

The current is $I = Z^{-1}V$, and the result is $I = -0 \cdot 468 - 0 \cdot 161u + 0 \cdot 050u^2 + 0 \cdot 194u^3 + 0 \cdot 385u^4 + 0 \cdot 635u^5 + 0 \cdot 802u^6 + 0 \cdot 739u^7$. The calculation using frequency components and evaluating at $0, \tau, 2\tau, \ldots$ gives

$$-0 \cdot 460, -0 \cdot 144, -0 \cdot 057, 0 \cdot 188, 0 \cdot 380, 0 \cdot 644, 0 \cdot 820, 0 \cdot 749$$

The error is nowhere greater than $0 \cdot 02$, and for all but two of the ordinates it is about half that value. Expressed as percentages of the ordinates, this represents about $12\%$ for the two lowest ordinates and between $1\%$ and $3\%$ for the remainder. If we consider the errors introduced by the polygonal approximation of the input (see Fig. 4), these are, in fact, $11\%$ at $\tau/2$ and $5\tau/2$, and about $7\%$ at $11\tau/2$. It may therefore be concluded that the accuracy of the answer is much the same as that of input representation. This is true, provided that sufficient figures are used in the calculation to bring computational errors to a low

figure in comparison with that due to the polygonal approximation, and this, in turn, depends on the number of ordinates used.

As a second example, consider the series *RC* circuit in which $R = 1$ and $1/\omega C = 1$, where $\omega$ is the fundamental angular frequency of the applied voltage wave $V = \sin \omega t + 0 \cdot 4 \cos 2\omega t$. It is necessary in this case to divide the whole cycle into $n$ parts. Since we are at the moment concerned more with procedure than in obtaining an accurate solution, we shall take $n = 9$ and hence $\omega\tau = 2\pi/9$. Therefore

$$V = 0 \cdot 4 + 0 \cdot 7122u + 0 \cdot 6089u^2 + 0 \cdot 6660u^3 + 0 \cdot 6484u^4$$
$$- 0 \cdot 0356u^5 - 1 \cdot 0660u^6 - 1 \cdot 3607u^7 - 0 \cdot 5734u^8$$

$$Z = 1 + \frac{\tau}{2C} \frac{(1 + u)}{(1 - u)} = \frac{1 \cdot 3491 - 0 \cdot 6509u}{1 - u}$$

$$I = Z^{-1}V = \frac{(1 - u)V}{1 \cdot 3491 - 0 \cdot 6509u}$$

$$= 0 \cdot 7423V(0 \cdot 9971 - 0 \cdot 5175u - 0 \cdot 2497u^2$$
$$- 0 \cdot 1205u^3 - 0 \cdot 0581u^4 - 0 \cdot 0280u^5$$
$$- 0 \cdot 0136u^6 - 0 \cdot 0065u^7 - 0 \cdot 0031u^8)$$

$$= 0 \cdot 841 + 0 \cdot 638u + 0 \cdot 231u^2 + 0 \cdot 154u^3$$
$$+ 0 \cdot 061u^4 - 0 \cdot 478u^5 - 0 \cdot 994u^6$$
$$- 0 \cdot 698u^7 + 0 \cdot 247u^8$$

The ordinates of the current, computed from frequency components, are

$$0 \cdot 820, 0 \cdot 602, 0 \cdot 242, 0 \cdot 162, 0 \cdot 049, -0 \cdot 499, -0 \cdot 982, -0 \cdot 652,$$
$$-0 \cdot 275$$

The lower accuracy is due to the coarse spacing of ordinates employed ($\omega\tau = 40°$) and to the relatively higher harmonic content of the current wave compared with the voltage wave. It is emphasized that this method of calculating linear-circuit responses to non-sinusoidal inputs is being advocated only when the input is of arbitrary form and of unknown Fourier content, and when the total waveform picture at the output is required. If the Fourier components are known and the output waveform is not required, it is manifestly simpler to proceed in the orthodox fashion.
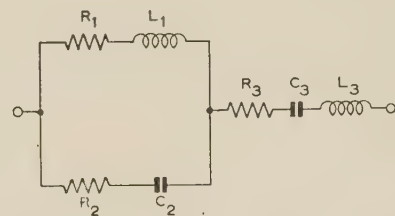


**Fig. 5.**—Illustrative series-parallel circuit.

**(4.2.2) Series-Parallel Circuit: Inverse of Quadratic or Cubic Denominator.**

The circuit shown in Fig. 5 has $R_1 = R_3 = 1$, $R_2 = 2$, $\omega L_1 = \omega L_3 = 0 \cdot 9818$, $1/\omega C_2 = 15 \cdot 2788$, and $1/\omega C_3 = 5 \cdot 0929$. Consider its response to the trapezoidal wave

$$V = 0 \cdot 0 + 0 \cdot 5u + 1 \cdot 0u^2 + 1 \cdot 0u^3 + 1 \cdot 0u^4$$
$$+ 1 \cdot 0u^5 + 1 \cdot 0u^6 + 0 \cdot 5u^7$$

the break-point of $V$ occurring at $\omega t = \pi/4$. The choice of $n = 8$ will give an exact input representation. The operators are

$$Z_1 = R_1 + \frac{2n\omega L_1}{\pi} \frac{(1-u)}{(1-u)} = \frac{6-4u}{1+u}$$

$$Z_2 = \frac{5+u}{1-u}$$

$$Z_3 = \frac{7-8u+5u^2}{1-u^2}$$

The admittance of the circuit is

$$Z^{-1} = \frac{Z_1+Z_2}{Z_1Z_2+Z_2Z_3+Z_3Z_1}$$

$$= \frac{11-4u-6u^2+4u^3-5u^4}{107(1-1\cdot2150u+0\cdot8224u^2-0\cdot4299u^3+0\cdot2710u^4)}$$

The inverse of the operator in the denominator is calculated by solving the set of equations given in Section 9.1, with $A_0 = 1$, $A_1 = -1\cdot2150$, etc., $A_5$, $A_6$ and $A_7$ being zero. This gives

$$A^{-1} = 1\cdot1398 + 1\cdot2206u + 0\cdot5661u^2 + 0\cdot0925u^3$$
$$- 0\cdot1374u^4 - 0\cdot3303u^5 - 0\cdot4021u^6 - 0\cdot3010u^7$$

and

$$Z^{-1} = \frac{1}{107}(9\cdot5554 + 7\cdot0183u - 6\cdot3006u^2 - 5\cdot5163u^3$$
$$- 6\cdot0946u^4 - 7\cdot4773u^5 - 4\cdot7380u^6 - 0\cdot7329u^7$$

The current is

$$VZ^{-1} = 0\cdot2522 + 0\cdot3036u + 0\cdot3258u^2 + 0\cdot2749u^3$$
$$+ 0\cdot1563u^4 + 0\cdot0450u^5 - 0\cdot0440u^6 - 0\cdot1492u^7$$

In the above example four decimal places were used throughout the calculation, although less than this number would probably do for practical purposes. It should be noted that each term in any product can be found in one machine operation (sums or differences or products) of a desk calculating machine. Similarly, the method of solving simultaneous equations given by Crout[11] is particularly suitable for machine calculation. Nevertheless, there is considerable work attached to calculating general inverses, but it should be borne in mind that the alternative method of procedure, given a numerical or graphical input, is to perform a Fourier analysis, calculate the components separately, add and subsequently evaluate the resultant waveform point by point.

An alternative method of obtaining the inverse of a quadratic or cubic denominator is to factorize it into real and, if necessary, complex factors. These may be inverted separately according to the rule

$$(1+au)^{-1} = (1+a^n)^{-1}(1-au+a^2u^2-\ldots \pm a_{n-1}u^{n-1})$$

where $n$ is odd or even, and the inverses then multiplied together, e.g.

$$(1+2u+5u^2)^{-1} = [1+(1+j2)u]^{-1}[1+(1-j2)u]^{-1}$$

$$[1+(1+j2)u]^{-1} = (-526+j336)^{-1}[1-(1+j2)u$$
$$+(-3+j4)u^2-(-11-j2)u^3+\ldots]$$

for $n = 8$.

The second inverse is the conjugate of the first, the product of the two being

$$(1+2u+5u^2)^{-1} = -0\cdot0018 + 0\cdot0014u + 0\cdot0061u^2$$
$$-0\cdot0192u^3 + 0\cdot0080u^4 + 0\cdot0802u^5 - 0\cdot2002u^6 + 0\cdot0004u^7$$

This technique is recommended for quadratic and cubic denominators, but there is no advantage for those of higher order unless

exact factors result, and this is most unlikely. Note that, in forming the product of the complex inverses, only the real part of each term in the product requires to be calculated, since the imaginary part is zero.

### (4.2.3) R.M.S. Voltage in Distributed-Coil Group moving in Non-Sinusoidal Flux.

The shift operator $u$ is designed primarily for operations such as addition and multiplication of arbitrary periodic functions displaced with respect to each other. Hence it is convenient for calculating the resultant e.m.f. in a distributed coil moving through non-sinusoidal flux.

Consider an a.c. machine having a 3-phase winding on the stator and d.c. excitation on the rotor, which may be of salient- or non-salient-pole construction. Let there be an integral number, $g$, of slots per pole. We shall consider the fluxes in the successive teeth $t_0, t, \ldots, t_{g-1}$ throughout one pole pitch at the successive instants $t = 0, \tau \ldots (n-1)\tau$, where $n\tau$ is equal to the half-period and $n$ is even. At $t = 0$ we have the set of tooth fluxes $\Psi_{0i} = \Psi_{00}, \Psi_{01}, \Psi_{02} \ldots \Psi_{0(g-1)}$; at $t = \tau$, the set $\Psi_{1i} = \Psi_{10}, \Psi_{11}, \Psi_{12} \ldots \Psi_{1(g-1)}$; and so on up to $t = (n-1)\tau$. These fluxes may be either those holding for the condition of open-circuit or those holding with some given load current (non-sinusoidal in general). If the second condition is envisaged, it is to be taken that the flux sets $\Psi_{0i}, \Psi_{1i} \ldots \Psi_{(n-1)i}$ are due to the resultant m.m.f. of the rotor and the stator coils, each coil current taking $n$ successive values throughout the half-period.

The flux linking a coil enclosing teeth $t_0-t_m$ takes in succession the values $\Phi_{k0} = \Psi_{k0} + \Psi_{k1} + \ldots + \Psi_{km}, k = 0, 1, 2, \ldots, n-1$. Similarly, the flux linking a coil enclosing teeth $t_1-t_{m+1}$ takes in succession the values $\Phi_{k1} = \Psi_{k1} + \Psi_{k2} + \ldots \Psi_{k(m+1)}, k = 0, 1, 2, \ldots, n-1$, and so on with the remaining coils. These flux-linkage waveforms in the successive coils may be written $N\Phi_0 = N\sum_{n-1}\Phi_{k0}u^k, N\Phi_1 = N\sum_{n-1}\Phi_{k1}u^k \ldots$, $N$ being the turns in each coil. The e.m.f.'s in these coils are then $V_0 = pN\Phi_0$, $V_1 = pN\Phi_1 \ldots$, where $p$ is the differential operator.

If $r$ coils are connected together to form a group, the e.m.f. of the coil group is $V = V_0 + V_1 + \ldots + V_{r-1}$. In terms of the ordinates, this is $\sum_{n-1} V_k u^k$, from which the waveform and r.m.s. value can be found.

The above procedure is of general application, except when the number of slots per pole is non-integral. In this case, if the slots per pole pair are integral, the analysis may be performed over a pole pair instead of a pole pitch. If the number of slots per pole is even, it is possible to choose $n = g$, with a consequent simplification in the analysis. In this case, with no stator current flowing, the flux sets $\Psi_{0i}, \Psi_{1i}, \ldots, \Psi_{(n-1)i}$ will repeat, apart from a displacement of one element to the right or left for each interval of $\tau$. If the first coil voltage is $v$, successive coils have the voltages $uv, u^2v, \ldots, u^{r-1}v$ and the e.m.f. of the coil group is $V = (1+u+u^2+\ldots+u^{r-1})v$.

A substantial simplification of the above can be effected if the common procedure is adopted of assuming a mean flux-density distribution round the air-gap, either on load or on no-load. Taking $n$ equal to the number of slots per pole, the flux-density wave may be expressed by the ordinates $B_k = B_0, B_1, \ldots, B_{n-1}$ throughout one pole pitch. The e.m.f. per coil side is then $v_c = \sum_{n-1} CB_k u^k$, $C$ being a constant of proportionality. If the coil spans $m$ slot pitches, the coil e.m.f. is $(1+u^m)v_c$. The e.m.f. of $r$ coils forming a group is then $V = \sum_{n-1} V_k u^k = (1+u^m)(1+u+u^2+\ldots+u^{r-1})v_c$.

At the moment, full investigation has not been made of the application of this type of analysis in machine theory. There would appear to be particular advantages in the method, however,

when the flux distributions in machines are known numerically from the results of experiments and are therefore, as yet, of unknown Fourier content.

## (5) APPLICATION TO NON-LINEAR CIRCUITS

### (5.1) Procedure

Since the method of generalized operators is capable of dealing with non-sinusoidal waveforms, it is immediately applicable, by a process of continued approximation, to the steady-state analysis of non-linear circuits, and it is chiefly with this objective in mind that the method has been evolved. It is clear that, for any one periodic input to a non-linear element, there corresponds an impedance or admittance operator for the element. This impedance, admittance or transfer-function operator may be obtained by considering the output which results on applying the input waveform to the static or d.c. characteristic of the non-linearity, or to the series of static characteristics in the case of more complex non-linearities such as hysteresis. The real problem is that the input waveform to the non-linearity is unknown when the non-linear element is part of a series circuit. While it is therefore evident that $u$-operators are an adequate tool for solving the problem, the solution has to be taken out by a number of approximations. This can be done in a simple manner.

Consider a linear impedance $Z_s$ in series with a non-linear element (Fig. 6). The information about the non-linear element
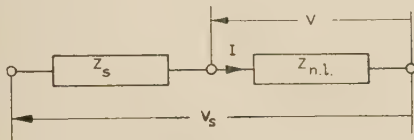


Fig. 6.—Non-linear impedance in series with linear impedance.

is given by its static characteristic or characteristics, and the waveform of the applied voltage—which is not necessarily sinusoidal—is given. The procedure is then as follows:

(a) Assume or calculate, using linear approximations, a first approximation of one of the variables, $V$, entering the non-linear relationship.

(b) Form the waveform, $I$, of the second variable entering into the non-linear relationship by considering the effect of $V$ on the static characteristic ($V/I$ relation) of the non-linearity.

(c) Calculate the waveform of the first variable from the known circuit equation, given $I$; this calculation of the first variable from the circuit relation will be denoted by $V'$.

(d) Average $V$ and $V'$, and use $V_{av}$ to repeat (b) and (c).

(e) Continue the calculation until $V = V' = V_{av}$; from this the final $I$ may be found.

This procedure is best shown schematically as

$V$————non-linear————$\rightarrow I$————circuit————$\rightarrow V'$
(assumed or    relation          equation
approximate)

$\frac{1}{2}(V + V') = V_{av(1)}$————non-linear————$\rightarrow$etc.
                           relation
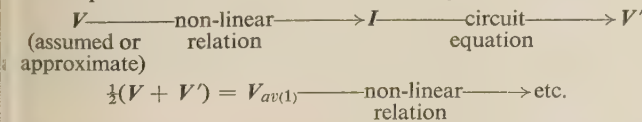
The circuit equation for Fig. 6 is $V' = V_s - IZ_s$. For the starting-point of the calculation the whole of the supply voltage may be taken as acting across the non-linearity (i.e. take supply voltage equal to $V$). If, however, any guidance can be obtained from the values of the circuit components as to the probable manner in which $V$ will develop, it should be used to reduce the number of approximations which have to be made. In the above scheme it will be realized that we have been thinking of the non-linear relationship as being of the nature of an impedance. This is not always the case, but the procedure remains substantially the same with other types of non-linearity.

A further point to note is that there are a variety of methods of carrying out the approximating process. Also, where possible, the circuit relation should be arranged to contain integrating (or smoothing) operators rather than differentiating operators. This will help the general accuracy of the computation. These principles are illustrated below.

### (5.2) Non-Linear Resistor in Series with a Capacitor: Non-Sinusoidal Applied Voltage

The problem of the steady-state analysis of a non-linear resistor in series with an impedance has received consideration by Moullin[8,9] and Slemon.[10] The work of Moullin has been directed mainly to the calculation and prediction of r.m.s. values rather than to waveform study. Slemon's method enables the fundamental and third-harmonic current components to be obtained, the first mentioned being dependent upon a correction estimated from the third-harmonic component. Both analyses are approximate. The method advanced here abandons the Fourier concept and instead deals with waveforms described by ordinates at regular intervals. Corrections are then applied to the waveforms by stages. It has an advantage in that complex applied-voltage waveforms may be handled with ease equal to that of sinusoidal waveforms.

The circuit for illustrative purposes is shown in Fig. 7 and the
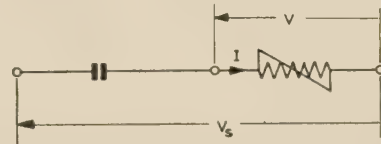


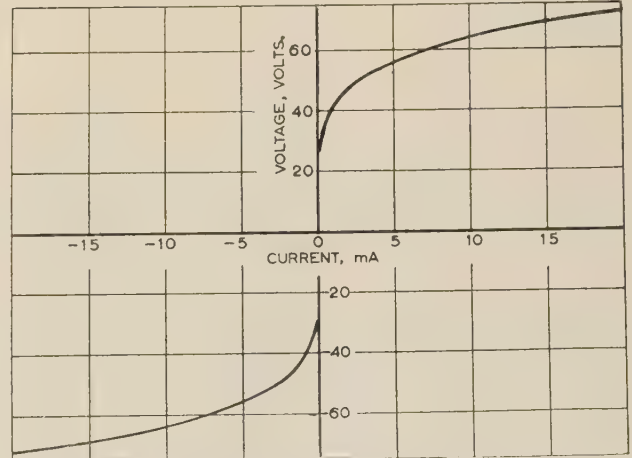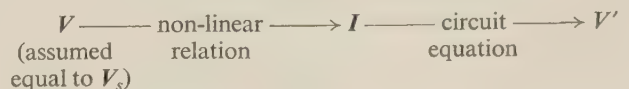Fig. 7.—Non-ohmic resistor in series with capacitor.



Fig. 8.—Voltage-current relation for non-ohmic resistor.

non-linear characteristic is given in Fig. 8. Since it is symmetrical about the origin, only odd harmonics will occur in the waveforms and the half-wave will be divided into eight parts ($n = 8$). The applied voltage is non-sinusoidal and given by

$$V_s = 68 \cdot 3 + 69 \cdot 1u + 33 \cdot 9u^2 + 14 \cdot 8u^3 - 30 \cdot 9u^4$$
$$- 50 \cdot 9u^5 - 62 \cdot 7u^6 - 66 \cdot 1u^7$$

It is shown in Fig. 9. The scheme of calculation is

$V$———— non-linear ————$\rightarrow I$———— circuit ————$\rightarrow V'$
(assumed      relation           equation
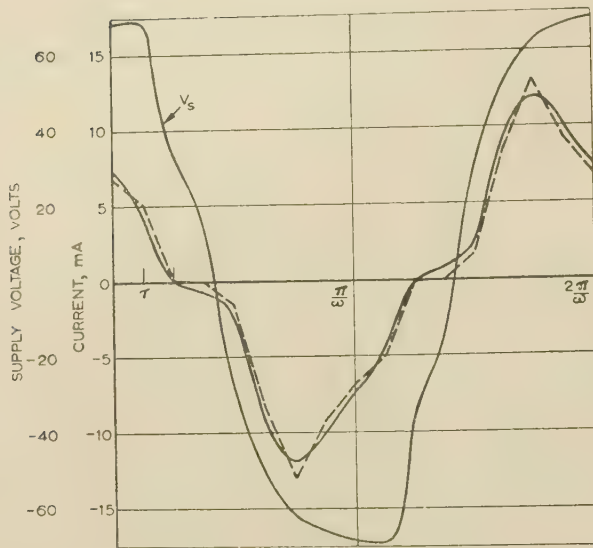equal to $V_s$)

$\frac{1}{2}(V + V') = V_{av(1)}$

Fig. 9.—Applied voltage wave and resultant current for circuit shown in Fig. 7.

————— Waveforms taken from oscillograms.
– – – – Calculated current waveform.

The circuit equation giving $V'$ in terms of $I$ is

$$V' = V_s - \frac{I}{pC}$$

where $\dfrac{1}{pC} = \dfrac{\tau}{2C}(u + u^2 + \ldots + u^7)$, with $\dfrac{\tau}{2C} = 0 \cdot 294\,8 \times 10^3$.

The calculation is given in Table 1 with the values of current expressed in milliamperes.

**Table 1**

| $t$ .. | .. | 0 | $\tau$ | $2\tau$ | $3\tau$ | $4\tau$ | $5\tau$ | $6\tau$ | $7\tau$ |
|---|---|---|---|---|---|---|---|---|---|
| $V$ | .. | 68·3 | 69·1 | 33·9 | 14·8 | −30·9 | −50·9 | −62·7 | −66·1 |
| $I$ | .. | 14·4 | 15·4 | 0·3 | 0 | −0·2 | −2·9 | −9·2 | −12·1 |
| $(1/pC)I$ | .. | 2·6 | 11·3 | 16·0 | 16·1 | 16·0 | 15·1 | 11·5 | 5·2 |
| $V'$ | .. | 65·7 | 57·8 | 17·9 | −1·3 | −46·9 | −66·0 | −74·2 | −71·3 |
| $V_{av(1)}$ | .. | 67·0 | 63·4 | 25·9 | 6·7 | −38·9 | −58·4 | −68·4 | −68·7 |
| $I$ .. | .. | 13·0 | 9·7 | 0·1 | 0 | —0·6 | −6·2 | −14·6 | −14·9 |
| etc. | | | | | | | | | |
| $V_{av(2)}$ | .. | 63·7 | 59·0 | 21·2 | 2·0 | −43·5 | −62·2 | −70·1 | −67·6 |
| $V_{av(3)}$ | .. | 60·9 | 56·6 | 19·1 | 0 | −45·4 | −63·3 | −69·4 | −65·3 |
| $V_{av(4)}$ | .. | 59·6 | 56·0 | 18·9 | −0·2 | −45·5 | −62·8 | −68·1 | −63·6 |
| $V_{av(5)}$ | .. | 59·6 | 56·4 | 19·5 | 0·4 | −44·8 | −61·9 | −67·0 | −62·9 |
| $I$ .. | .. | 6·8 | 5·1 | 0·02 | 0 | −1·6 | −8·4 | −13 | −9·2 |
| $I$ .. | .. | 7·4 | 4·5 | 0·1 | −0·7 | −2·3 | −9·3 | −11·9 | −10·1 |
| (experiment) | | | | | | | | | |

The calculated and measured current waveforms are shown in Fig. 9. There is a divergence of the order of 10% between the two, except at the low values of $2\tau$, $3\tau$ and $4\tau$. It should be borne in mind, however, that both $V_s$ and the measured current wave are obtained from oscillograms, where there is probably room for about 5% error. The rest may be debited to the errors incurred in representing the waveforms by a series of eight segments. Although the calculation may seem tedious, more so because the description in words is lengthy, the whole of the work in Table 1 can, with some familiarity and the aid of a desk calculator, be done in less than half an hour.

The r.m.s. current and power supplied may be easily calculated. We have

$$\text{R.M.S. current} = \left(\frac{1}{n}\sum_{n-1} I_k^2\right)^{1/2} = 7 \cdot 1\,\text{mA}$$

and

$$\text{Power} = \frac{1}{n}\sum_{n-1} V_{sk}I_k = 340 \cdot 3\,\text{mW}$$

### (5.3) More Complex Circuits with Non-Linear Impedances

The procedure only is indicated here. In the two cases given Figs. 10 and 11, the non-linearities are described by current/voltage relations of the instantaneous type or otherwise.
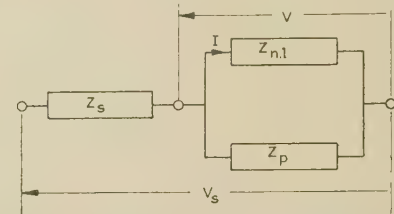


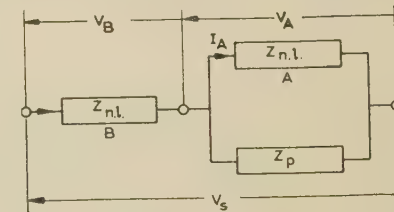Fig. 10.—Series-parallel circuit with non-linear impedance.



Fig. 11.—Series-parallel circuit with two non-linear impedances.

In Fig. 10 the calculating scheme would be as before, with $I = f(V)$ as the non-linear relation, and $V' = V_s - Z_s(I + VZ_p^{-1})$ as the circuit equation.

For a similar circuit with two non-linear elements (Fig. 11) $I_A = f(V_A)$ as the non-linear relation of $A$, and $V'_A = V_s - V_1$ as the circuit equation, where

$$V_B = g(I_A + V_A Z_p^{-1}) = g(I_B)$$

i.e. the non-linear relation of B.

Calculations would be carried out until $V = V'$ in the first case and $V_A = V'_A$ in the second.

### (5.4) Iron-Cored Coil in Series with Impedance: Non-Instantaneous Non-Linearity

The non-linear relationship introduced here is more complicated than before, because both saturation and hysteresis loss are present; nevertheless, the general method of procedure is the same. The information about the non-linearity is given by the series of flux/current relationships shown in Fig. 12. In the circuit considered here (Fig. 13) the series impedance is a simple resistor, although no difficulty arises if this is replaced by a general impedance or more complex circuit. Similarly, although a simple sine input was taken here to facilitate experimental checking, the applied voltage wave can be of any form. The scheme of calculation is

$$\Phi \xrightarrow{\text{non-linear relation}} I \xrightarrow{\text{circuit equation}} \Phi$$

(calculated from linear approximation)

$$\tfrac{1}{2}(\Phi + \Phi') = \Phi_{av(1)} \xrightarrow{\text{non-linear relation}} \text{etc.}$$

The circuit equation is

$$V_s = IR + Np\Phi'$$

arranged as

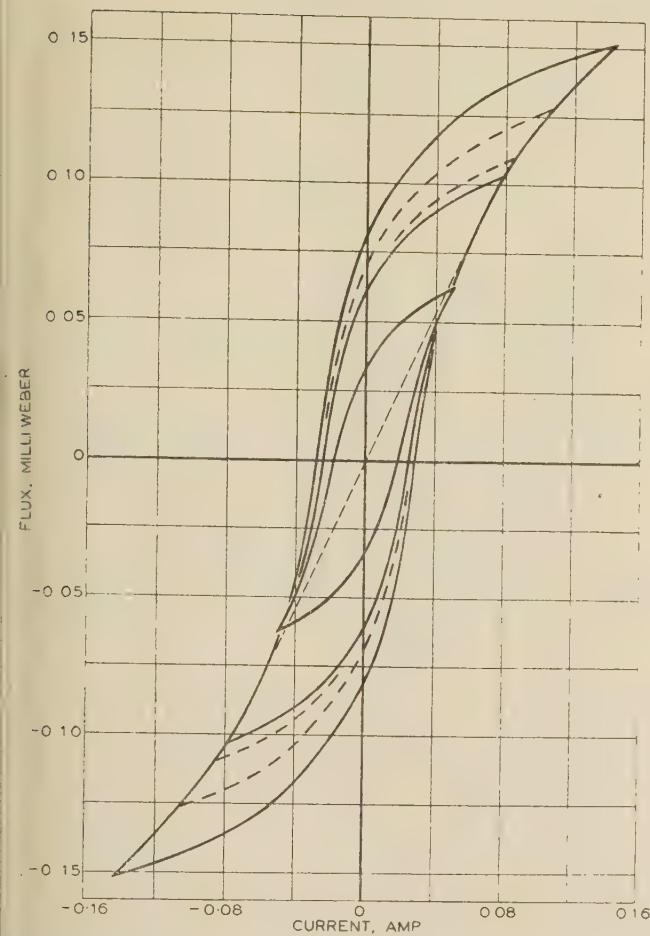$$\Phi' = \frac{1}{Np}(V_s - IR)$$
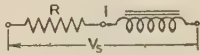
Fig. 12.—Flux/current relation for iron-cored coil.



Fig. 13.—Iron-cored coil in series with resistor.

For this example, $R = 334$ ohms, $N = 1\,000$ turns and the supply voltage is the waveform $50\cdot6 \sin 314t$. With a division of the half-wave into eight parts, we have

$$V_s = 19\cdot37u + 35\cdot78u^2 + 46\cdot75u^3 + 50\cdot60u^4$$
$$+ 46\cdot75u^5 + 35\cdot78u^6 + 19\cdot37u^7$$

and $1/Np = (u + u^2 + u^3 + \ldots + u^7)/(1\,600 \times 10^3)$.

In this particular example the calculation will be started by making a linear approximation to $\Phi$, taking a relation $\Phi/I = 0\cdot08 \times 10^{-3}/0\cdot06$ indicated by the broken line in Fig. 12. This gives

$$\Phi = 0\cdot126 \times 10^{-3} \sin (314t - 0\cdot895), \text{ i.e.}$$

$$\Phi = 10^{-3}(-0\cdot099 - 0\cdot061u - 0\cdot014u^2 + 0\cdot035u^3$$
$$+ 0\cdot079u^4 + 0\cdot110u^5 + 0\cdot125u^6 + 0\cdot121u^7)$$

The calculation is shown in Table 2, with the fluxes given in milliwebers.

In making the calculation, $\Phi/I$ relations for which experimental loops are not provided have to be sketched in as shown by the broken loops in Fig. 12. This, of course, is bound to introduce errors, which mean, in fact, that the calculation will have to be taken further before agreement between successive values of $\Phi_{av}$ is obtained. Furthermore, since the actual time at which maximum flux and current are reached will not necessarily coincide with a particular value of $\tau$, the shift of the maximum ordinate in $\Phi_{av(2)}$ from the time $6\tau$ to the time $7\tau$ in $\Phi_{av(3)}$ indicates that the limit of accuracy with this selected number of ordinates is being approached. The fact that the value of the maximum ordinate is not changing is more important.

Although the calculated values of current do not in some cases show very close agreement with those obtained experimentally, it should be remembered that quite a number of experimental errors may be accumulated in the process of obtaining the loops and in recording and abstracting from oscillograms. On this basis the figures are not unreasonable for a method of this nature. It should also be noted that if the impedance in series with the coil were more complex, the only requirement would be to evaluate its operator form, $Z = \sum_{n-1} A_k u^k$, for substitution in the circuit equation.

### (6) CONCLUSION

An approximate method has been given for the steady-state analysis of linear and non-linear circuits having sinusoidal or non-sinusoidal applied voltages. In short, the method is a periodic counterpart of the time-series technique. The general properties of the shift operator $u$, however, and the rules which have been found to govern the various manipulations required, indicate it to be more aptly described as an $n$-component algebra of generalized operators.

In its application to linear circuits there is one situation where the method will prove advantageous, namely when the non-sinusoidal input is known graphically or numerically but not in terms of Fourier components and a similar waveform picture of the output is desired. In these circumstances, the alternative procedure of performing a Fourier analysis, working out the harmonics and evaluating the total by subsequent point-by-point calculation would be more lengthy. Although this would appear

### Table 2

| $t$ | | | | $0$ | $\tau$ | $2\tau$ | $3\tau$ | $4\tau$ | $5\tau$ | $6\tau$ | $7\tau$ |
|---|---|---|---|---|---|---|---|---|---|---|---|
| $V_s$ | .. | .. | .. | $0$ | $19\cdot37$ | $35\cdot78$ | $46\cdot75$ | $50\cdot60$ | $46\cdot75$ | $35\cdot78$ | $19\cdot37$ |
| $\Phi$ | .. | .. | .. | $-0\cdot099$ | $-0\cdot061$ | $-0\cdot014$ | $0\cdot035$ | $0\cdot079$ | $0\cdot110$ | $0\cdot125$ | $0\cdot121$ |
| $I$ | .. | .. | .. | $-0\cdot033$ | $0\cdot007$ | $0\cdot024$ | $0\cdot035$ | $0\cdot059$ | $0\cdot085$ | $0\cdot103$ | $0\cdot081$ |
| $V_s - IR$ | .. | .. | .. | $11\cdot02$ | $17\cdot03$ | $27\cdot76$ | $35\cdot06$ | $30\cdot89$ | $18\cdot36$ | $1\cdot38$ | $-7\cdot68$ |
| $\Phi$ | .. | .. | .. | $-0\cdot077$ | $-0\cdot059$ | $-0\cdot031$ | $0\cdot008$ | $0\cdot049$ | $0\cdot080$ | $0\cdot092$ | $0\cdot088$ |
| $\Phi_{av(1)}$ | .. | .. | .. | $-0\cdot088$ | $-0\cdot060$ | $-0\cdot023$ | $0\cdot022$ | $0\cdot064$ | $0\cdot095$ | $0\cdot109$ | $0\cdot105$ |
| $I$ | .. | .. | .. | $-0\cdot028$ | $0\cdot003$ | $0\cdot020$ | $0\cdot029$ | $0\cdot050$ | $0\cdot072$ | $0\cdot084$ | $0\cdot067$ |
| | etc. | | | | | | | | | | |
| $\Phi_{av(2)}$ | .. | .. | .. | $-0\cdot090$ | $-0\cdot067$ | $-0\cdot034$ | $-0\cdot010$ | $0\cdot053$ | $0\cdot086$ | $0\cdot103$ | $0\cdot102$ |
| $\Phi_{av(3)}$ | .. | .. | .. | $-0\cdot092$ | $-0\cdot075$ | $-0\cdot045$ | $-0\cdot003$ | $0\cdot051$ | $0\cdot080$ | $0\cdot100$ | $0\cdot103$ |
| $I$ | .. | .. | .. | $-0\cdot042$ | $-0\cdot014$ | $0\cdot012$ | $0\cdot024$ | $0\cdot042$ | $0\cdot060$ | $0\cdot077$ | $0\cdot080$ |
| $I$ | .. | .. | .. | $-0\cdot035$ | $-0\cdot007$ | $0\cdot016$ | $0\cdot031$ | $0\cdot045$ | $0\cdot062$ | $0\cdot079$ | $0\cdot070$ |
| (experiment) | | | | | | | | | | | |

to be the only situation in normal linear-circuit analysis where the method would be justified, the application of the method to studies of torque and e.m.f. production in machine windings situated in non-sinusoidal flux has yet to be fully explored. It is felt that development on this and other similar lines is possible.

It may also be interesting to mention, before leaving consideration of linear problems, that should the applied wave be sinusoidal, the substitution of $u = \varepsilon^{-j\omega\tau}$ will reduce the theory to a 2-component operator theory similar to normal vector algebra but with the components measured in oblique instead of rectangular co-ordinates. At the moment the author cannot see any real advantage in this. Moreover, the theory for sinusoidal waveforms is none other than the theory of $n$ symmetrical components, of which the case $n = 3$ is well known.

For non-linear circuits having sinusoidal or non-sinusoidal applied voltages the theory has some very definite advantages, the first being its generality. It would be unwise to claim that the method could deal with all forms of non-linear steady-state response, but the nature of the method seems to indicate that there are few situations with which it could not deal. It is available for both instantaneous and non-instantaneous non-linearities, and for both sine and non-sine waveforms. Since it provides essentially information about waveform, it also provides values of r.m.s. currents and of powers. The method is also capable of dealing with circuits containing two non-linear elements in combination with linear impedances. The non-linear elements in this case do not necessarily have to be of the same nature, as for example two non-linear resistors, but may be of different types.

Against the method it might be said that it is complex and necessarily lengthy, if an accuracy within 1–2% is to be attained. This it cannot fail to be, in view of the amount of information which the method is providing. It is necessary to recognize that accurate waveform studies of non-linear circuits will require considerable labour. If, on the other hand, less information than a complete waveform study is sought, there are probably simpler methods available. This question would seem to be one of expediency.

Another point which at the moment has not been the subject of much investigation is the calculation of the response of non-linear circuits as an explicit function of frequency. The method here is essentially numerical and holds for an assigned frequency. The problem of waveform transmission in non-linear circuits as the frequency varies is certainly more complex.

Finally, accuracy depends—or should be made to depend—almost entirely on the number of ordinates used to represent the waveforms. While an appropriate choice can be made for the known input waveform, it is sometimes difficult to judge whether other waveforms occurring will not, in fact, require more ordinates for the same accuracy in description. It is impossible to reach a general conclusion on this question. It can only be said that the accuracy in general will increase as the number of ordinates used increases, and that the choice is a compromise between the desired accuracy and the amount of computational work which will have to be done. The calculations which have been performed so far without special effort, with eight ordinates in the half-cycle, indicate that an accuracy within about 5% of the maximum ordinate is attainable. The accuracy of r.m.s. value and power calculations is certainly greater than this, the error being seldom greater than 2%.

### (7) ACKNOWLEDGMENT

### (8) REFERENCES

(1) TUSTIN, A.: 'A Method of Analysing the Behaviour of Linear Systems in Terms of Time Series', *Journal I.E.E.*, 1947, **94**, Part IIA, p. 130.

(2) THOMSON, W. E.: 'A Theory of Time Series for Waveform Transmission Systems', *Proceedings I.E.E.*, Monograph No. 53 R, October, 1952 (**99**, Part IV, p. 397).

(3) LEWIS, N. W.: 'Waveform Computations by the Time-Series Method', *ibid.*, Paper No. 1382 R, September, 1952 (**99**, Part III, p. 294).

(4) MADWED, A.: 'Numerical Analysis by the Number Series Transformation Method', Proceedings of a Symposium on Nonlinear Circuit Analysis, Polytechnic Institute of Brooklyn, New York, 1953, p. 320 (Edwards, Ann Arbor, 1953).

(5) RAGAZZINI, J. R., and BERGEN, A. R.: 'A Mathematical Technique for the Analysis of Linear Systems', *Proceedings of the Institute of Radio Engineers*, 1954, **42**, p. 1645.

(6) CRUICKSHANK, A. J. O.: 'A Note on Time Series and the Use of Jump Functions in Approximate Analysis', *Proceedings I.E.E.*, Monograph No. 110 M, October, 1954 (**102** C, p. 81).

(7) BOXER, R., and THALER, S.: 'A Simplified Method of Solving Linear and Nonlinear Systems', *Proceedings of the Institute of Radio Engineers*, 1956, **44**, p. 89.

(8) MOULLIN, E. B.: 'The Problem of a Non-Ohmic Resistor in Series with an Impedance', *Proceedings I.E.E.*, Paper No. 1048, March, 1951 (**98**, Part I, p. 87).

(9) MOULLIN, E. B.: 'The Solution of a Certain Differential Equation', *ibid.*, Monograph No. 99, May, 1954 (**101**, Part IV, p. 290).

(10) SLEMON, G. R.: 'A Method of Approximate Steady-State Analysis for Non-Linear Networks', *ibid.*, Paper No. 1530, September, 1953 (**100**, Part I, p. 275).

(11) CROUT, P. D.: 'A Short Method for Evaluating Determinants and Solving Systems of Linear Equations with Real or Complex Coefficients', *Transactions of the American I.E.E.*, 1941, **60**, p. 1235.

### (9) APPENDICES

#### (9.1) Inverses of $U$-Operators

Consider first the case of only odd harmonics present in the waveform. Let $A = A_0 + A_1 u + A_2 u^2 + \ldots + A_{n-1} u^{n-1}$ be the operator whose inverse is required. Let the required inverse be $A^{-1} = B = B_0 + B_1 u + B_2 u^2 + \ldots + B_{n-1} u^{n-1}$. From the definitions $AA^{-1} = 1$ and the multiplication rule there results the set of linear equations in which the coefficients $B_k$ are regarded as the variables and the coefficients $A_k$ as the equation constants, namely

$$A_0 B_0 - A_{n-1} B_1 - A_{n-2} B_2$$
$$- \ldots - A_3 B_{n-2} - A_2 B_{n-2} - A_1 B_{n-1} = 1$$

$$A_1 B_0 + A_0 B_1 - A_{n-1} B_2$$
$$- \ldots - A_4 B_{n-3} - A_3 B_{n-2} - A_2 B_{n-1} = 0$$

$$A_2 B_0 + A_1 B_1 + A_0 B_2$$
$$- \ldots - A_5 B_{n-3} - A_4 B_{n-2} - A_3 B_{n-1} = 0$$

$$A_{n-2} B_0 + A_{n-3} B_1 + A_{n-4} B_2$$
$$+ \ldots + A_1 B_{n-3} + A_0 B_{n-2} - A_{n-1} B_{n-1} = 0$$

$$A_{n-1} B_0 + A_{n-2} B_1 + A_{n-3} B_1$$
$$+ \ldots + A_2 B_{n-3} + A_1 B_{n-2} + A_0 B_{n-1} = 0$$

The required coefficients $B_k$ are therefore given by $B_k = A_{1,k+1}/A$

where $A_{1,k+1}$ is the cofactor of the element in the first row and $(k + 1)$th column of the determinant

$$A = \begin{vmatrix} A_0 & -A_{n-1} & -A_{n-2} \ldots & -A_3 & -A_2 & -A_1 \\ A_1 & A_0 & -A_{n-1} \ldots & -A_4 & -A_3 & -A_2 \\ A_2 & A_1 & A_0 & \ldots -A_5 & -A_4 & -A_3 \\ & & & & & \\ A_{n-2} & A_{n-3} & A_{n-4} \ldots & A_1 & A_0 & -A_{n-1} \\ A_{n-1} & A_{n-2} & A_{n-3} \ldots & A_2 & A_1 & A_0 \end{vmatrix}$$

Although this formally demonstrates the result, it is better in practice to employ a short method of solving the equations, e.g. Crout's[11] method, rather than to evaluate the cofactors separately.

When even harmonics are present in the waveform, the expression for the inverse is formally the same as that given above. Since, however, the fundamental relation for $u$ is now $u^n = +1$, the negative signs of those elements above the principal diagonal in the above determinant are replaced by positive signs.

### (9.2) Approximate Integral Operators

The following operators are intended for use with waveforms having even harmonics only, or even and odd harmonics together. In all cases they are based on the approximation

$$p^{-1} \simeq \frac{\tau}{2} \frac{(1 + u)}{(1 - 0\cdot99u)}$$

The number of ordinates, $n$, by which the complete cycle is described is odd. Each column gives the operator in ascending powers of $u$ starting with $u^0$, apart from the factor $\tau/2$ by which each must be multiplied.

#### VALUES OF $n$

| Power of $u$ | 9 | 11 | 13 | 15 | 17 | 19 |
|---|---|---|---|---|---|---|
| 0 | 22·2278 | 18·1891 | 15·3992 | 13·3575 | 11·7849 | 10·5552 |
| 1 | 23·0058 | 19·0067 | 16·2450 | 14·2245 | 12·6671 | 11·4499 |
| 2 | 22·7757 | 18·8166 | 16·0825 | 14·0823 | 12·5405 | 11·3354 |
| 3 | 22·5480 | 18·6285 | 15·9217 | 13·9415 | 12·4151 | 11·2220 |
| 4 | 22·3226 | 18·4422 | 15·7625 | 13·8021 | 12·2910 | 11·1098 |
| 5 | 22·0994 | 18·2579 | 15·6050 | 13·6641 | 12·1681 | 10·9988 |
| 6 | 21·8786 | 18·0755 | 15·4490 | 13·5276 | 12·0465 | 10·8889 |
| 7 | 21·6601 | 17·8949 | 15·2948 | 13·3925 | 11·9292 | 10·7801 |
| 8 | 21·4428 | 17·7154 | 15·1413 | 13·2581 | 11·8065 | 10·6720 |
| 9 | | 17·5377 | 14·9895 | 13·1252 | 11·6881 | 10·5649 |
| 10 | | 17·3629 | 14·8401 | 12·9943 | 11·5717 | 10·4597 |
| 11 | | | 14·6915 | 12·8643 | 11·4558 | 10·3549 |
| 12 | | | 14·5446 | 12·7356 | 11·3412 | 10·2514 |
| 13 | | | | 12·6084 | 11·2279 | 10·1490 |
| 14 | | | | 12·4818 | 11·1153 | 10·0471 |
| 15 | | | | | 11·0045 | 9·9470 |
| 16 | | | | | 10·8944 | 9·8475 |
| 17 | | | | | | 9·7485 |
| 18 | | | | | | 9·6513 |

# A NOTE ON THE EVALUATION OF THE RESPONSE OF A NON-LINEAR ELEMENT TO SINUSOIDAL AND RANDOM SIGNALS

## By J. L. DOUCE, M.Sc., Ph.D., Graduate.

## SUMMARY

A simple method is developed for analysing the response of non-linear elements to sinusoidal and random signals. Special cursors are presented which enable the effective gain of the non-linear unit to be determined quickly.

For sinusoidal signals the technique provides a rapid means for finding the Fourier components of fundamental frequency of the output waveform, for both single-valued and for hysteretic forms of non-linearity. The gain of any single-valued non-linearity when subject to a random signal is also evaluated. The amplitude probability distribution of the signal can be any known function.

The method of analysis is invaluable for deriving the response of non-linear control systems subjected to random or sinusoidal inputs.

## (1) INTRODUCTION

Many cyclic control systems incorporate non-linear elements within the closed loop. These non-linear effects may be inherent in the system, e.g. motor saturation, hysteresis and backlash, or may be introduced intentionally to improve the performance of the system. In either case it is extremely difficult to derive an exact analysis of the behaviour of the system for a given input.[1] As a result, approximate techniques have been developed, giving results with a minimum of computation with sufficient accuracy for all engineering applications.[2,3]

All practical methods of evaluating the overall performance consider the complete system in two distinct parts. First there is the linear portion, whose response is frequency dependent but independent of amplitude, and can usually be determined accurately from theoretical information or by measurement. For completely linear systems, knowledge of the open-loop response enables the closed-loop response of the system for any input to be determined. Secondly there is the non-linear portion, whose response is assumed to be independent of frequency and entirely dependent on input amplitude; to obtain an approximate representation of its behaviour, all distortion introduced by this element is neglected. Thus, if a sinusoidal signal is applied to the non-linearity, only the output components of input frequency are considered. Similarly, if the input to the non-linearity consists of a random signal of known spectral density, its output is considered as a random signal with the same spectral density, intermodulation terms and harmonics[4] being small compared with the direct component. This neglect of the harmonic terms is legitimate in practice, since the response of the linear system must fall with increasing frequency. The approximation usually introduces an error of less than 10% between observed and theoretical performance of the overall system. Once the responses of the linear and non-linear parts of the system have been found, graphical techniques enable the overall performance to be evaluated quickly.

Frequently, the objection to carrying out the above calculation arises from the labour involved in determining the response of

the non-linear element for all possible inputs. Fourier analysi becomes complex when hysteretic effects are present in the non linearity, and graphical techniques are likewise laborious. The method of analysis presented in the paper enables the behaviou of a non-linearity to be evaluated extremely rapidly, so that it i feasible to analyse the system for many different non-linearitie with little additional labour. The mathematical technique ha been described previously by Lewis.[6]

## (2) SINUSOIDAL ANALYSIS

Consider a signal $v_i = x = a \sin \theta$ applied to the non-linearity defined by

$$v_0 = f(v_i)$$

The in-phase and quadrature components of the output are given by

$$A_1 = \frac{1}{\pi} \int_{-\pi}^{+\pi} f(a \sin \theta) \sin \theta \, d\theta \quad . \quad . \quad . \quad (1$$

$$B_1 = \frac{1}{\pi} \int_{-\pi}^{+\pi} f(a \sin \theta) \cos \theta \, d\theta \quad . \quad . \quad . \quad (2$$

Substituting $x = a \sin \theta$ in these equations gives

$$A_1 = \frac{2}{\pi} \int_{x=-a}^{x=a} f(x) \left(\frac{x}{a}\right) \frac{1}{\sqrt{\left(1 - \frac{x^2}{a^2}\right)}} d\left(\frac{x}{a}\right)$$

$$= \frac{2}{\pi} \int_{x=-a}^{a} f(x) d\sqrt{\left(1 - \frac{x^2}{a^2}\right)} \quad . \quad . \quad . \quad (3$$

and

$$B_1 = \frac{2}{\pi} \int_{x=-a}^{a} f(x) d\left(\frac{x}{a}\right) \quad . \quad . \quad . \quad (4$$

This expression shows that the first Fourier coefficient, $A$, is the area under the curve of $f(x)$ plotted against $\sqrt{[1 - (x^2/a^2)]}$ from $x = -a$ to $x = a$. This area can be evaluated conveniently from the known curve of $f(x)$ as a function of $x$.

Eqn. (3) is rewritten

$$A \simeq \frac{2}{\pi} \sum_{x_1=-a}^{x_N=+a} f(x_r) \delta \sqrt{\left[1 - \left(\frac{x_r}{a}\right)^2\right]}$$

Thus the coefficient $A$ is found by summing the values of $f(x)$ at values of $x$ which correspond to equal changes in the function $\sqrt{[1 - (x/a)^2]}$. Similarly, the out-of-phase component is determined by summing values of $f(x)$ for values of $x$ corresponding to equal intervals of the function $x/a$.

Taking ten spot values of $x/a$ in the range 0–1, Table 1 shows

he values of $x/a$ corresponding to variations of $0 \cdot 1$ for the function $\sqrt{[1 - (x/a)^2]}$.

For ease in determining the required values of $x$ at which $f(x)$ has to be found, a transparent cursor has been prepared (Fig. 1). The horizontal axis, $x$, is divided to give equal intervals to the function $\sqrt{[1 - (x^2/a^2)]}$, for all values of $a$. Thus, to find the in-phase component of a waveform produced when a signal $a_1 \sin \theta$ is passed into a non-linearity $f(x)$, the particular

Table 1 enables this integral to be evaluated approximately, giving

$$\int_{x=-1}^{x=1} x d\sqrt{(1 - x^2)} = 2 \sum_0^1 x\delta(1 - x^2) = 1 \cdot 572$$

Therefore $\qquad A_1 = \frac{2}{\pi} \times 1 \cdot 572 = 1 \cdot 00(1)$
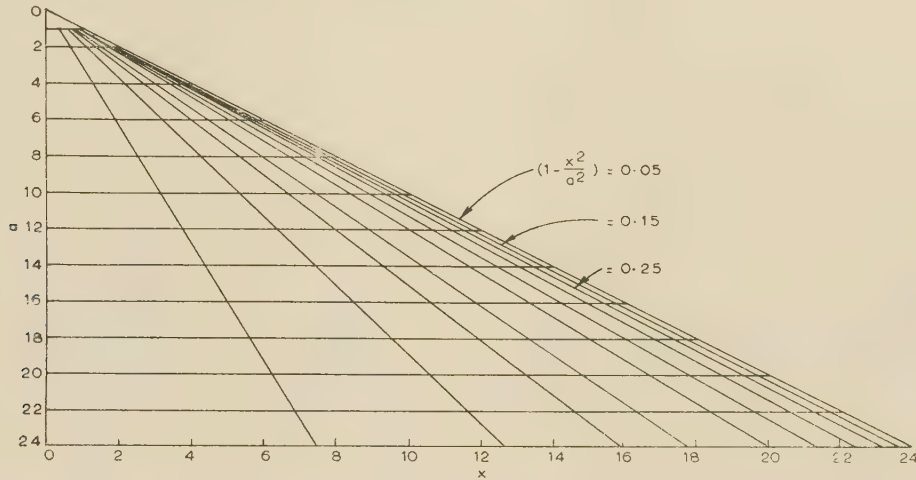


Fig. 1.—Cursor for deriving sinusoidal response.

value $a = a_1$ is taken on the cursor. The horizontal line $a = a_1$ is divided into segments, each corresponding to equal changes in the function $\sqrt{[1 - (x/a_1)^2]}$. Thus, at each value of $x$ the corresponding value of $f(x)$ is found, and the total $\Sigma f(x)$ is determined.

The out-of-phase component is proportional to the area enclosed by the hysteretic effect introduced by the non-linearity, and is zero in this case.

Proceeding in this manner, the response of several simple non-linearities has been determined for sinusoidal signals. The

### Table 1
#### DERIVATION OF RESPONSE TO SINUSOIDAL INPUT

| $\sqrt{\left(1 - \frac{x^2}{a^2}\right)}$ | 0·05 | 0·15 | 0·25 | 0·35 | 0·45 | 0·55 | 0·65 | 0·75 | 0·85 | 0·95 |
|---|---|---|---|---|---|---|---|---|---|---|
| $\frac{x}{a}$ | | 0·9987 | 0·9887 | 0·9683 | 0·9368 | 0·8930 | 0·8352 | 0·7399 | 0·6615 | 0·5268 | 0·3122 |

For a symmetrical non-linearity with no hysteresis, the waveform is an odd function and the Fourier coefficient is

$$A = \frac{1}{\pi} \int_{-\pi}^{+\pi} f(a \sin \theta) \sin \theta d\theta = \frac{4}{\pi} \int_0^{\pi/2} f(a \sin \theta) \sin \theta d\theta \quad (5)$$

$$= \frac{4}{\pi} \int_{x=0}^a f(x) d\sqrt{\left(1 - \frac{x^2}{a^2}\right)}$$

Hence, only one quadrant need be evaluated, giving ten spot values, and the required component is

$$A = \frac{4}{\pi} \times \frac{1}{10} \sum_{10} f(x)$$

As an illustration of the method, consider a signal $x = 1 \sin \theta$ applied to a linear element of unity gain, such that $f(x) = x$.

Substitution in eqn. (3) gives

$$A_1 = \frac{2}{\pi} \int_{x=-1}^{x=1} x d\sqrt{\left(1 - \frac{x^2}{1^2}\right)}$$

particular non-linearities were chosen since they have been encountered in non-linear servo mechanisms, and have previously been evaluated by Fourier analysis.

Fig. 2 shows the forms of non-linearity assumed, while the exact and approximate analyses of the output waveforms are compared in Figs. 3 and 4, the error being less than 5%. These approximate results were found with ten spot values for $f(x)$, and this is considered adequate for all practical applications.

#### (2.1) Hysteretic or Double-Valued Non-Linearities

When the non-linearity is double valued, such that the output corresponding to a given input depends on the previous input, the output waveform is no longer a purely odd function and so eqn. (5) no longer applies. It is now necessary to evaluate the coefficients over half a cycle of the waveform, for a symmetrical non-linearity, so that the expressions to be evaluated become

$$A = \frac{2}{\pi} \int_0^\pi f(a \sin \theta) \sin \theta d\theta$$

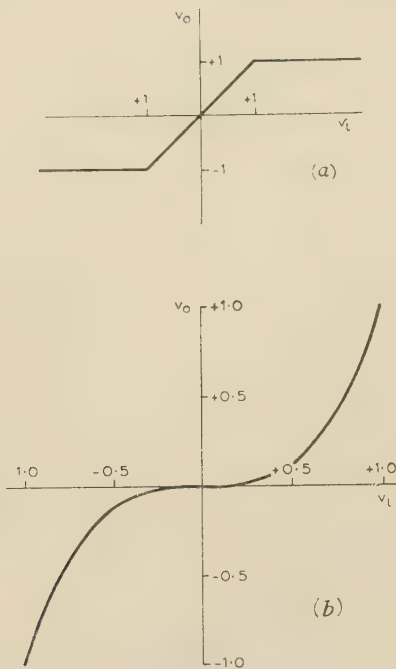$$B = \frac{2}{\pi} \int_0^\pi f(a \sin \theta) \cos \theta d\theta$$

Fig. 2.—Non-linear characteristics.
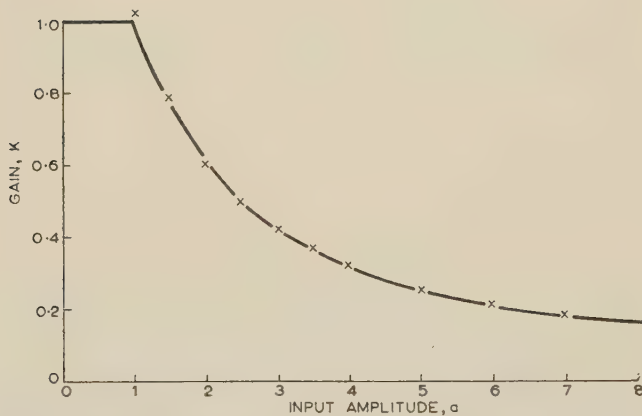
(a) Saturation.
(b) Cubic, $v_0 = v_i{}^3$.
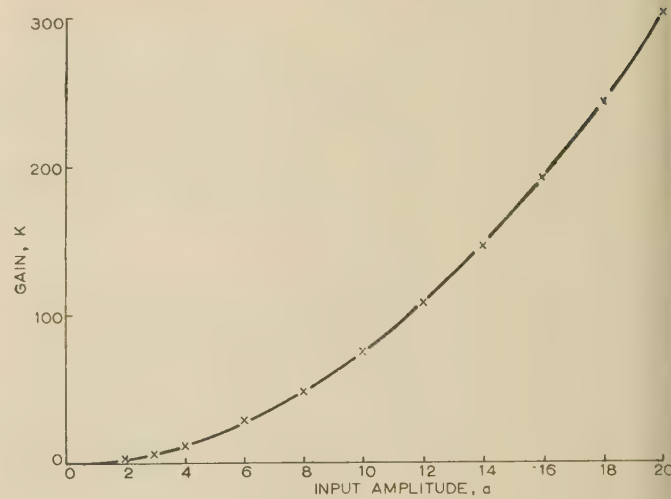


Fig. 4.—Response of non-linear characteristic shown in Fig. 2(b) t
sinusoidal input.

———— Exact analysis.
× × × Results from cursor.



Fig. 3.—Response of non-linear characteristic shown in Fig. 2(a)
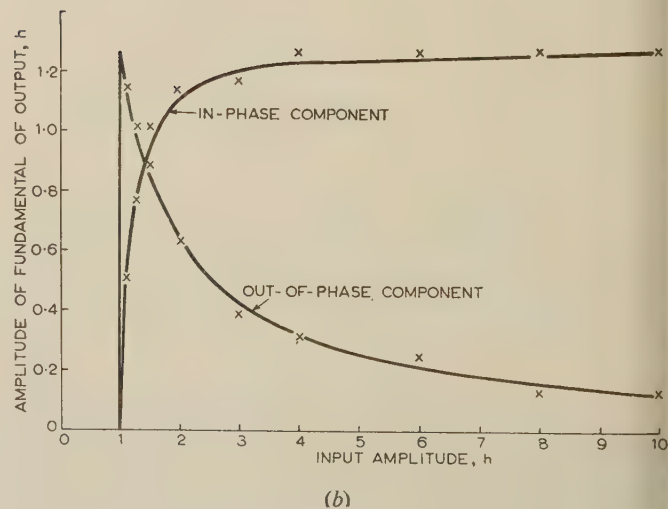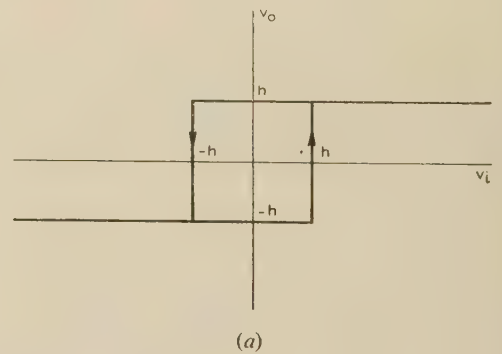to sinusoidal input.

———— Exact analysis.
× × × Results from cursor.

As an example, consider the non-linearity shown in Fig. 5(a). This gives zero output for inputs less than $|h|$, and for $v_i > h$ the output is constant at $+h$. As the input is reduced, the output remains at $+h$ until $v_i < -h$, when the output jumps to $-h$. For all sinusoidal inputs of magnitude greater than $h$ the output is a square wave. Since the square wave passes through zero after the input sinusoid, the fundamental of the output lags behind the input, the phase change being a function of input amplitude.

The in-phase component of the output is given by

$$A = \frac{2}{\pi} \int_0^\pi f(a \sin \theta) \sin \theta \, d\theta$$



Fig. 5.—Analysis of double-valued non-linear function.

(a) Non-linear characteristic.
(b) Response of non-linearity.

———— Exact analysis.
× × × Results from cursor.

Since $\sin \theta$ is positive for $0 < \theta < \pi$, this expression becomes, as before,

$$A \simeq \frac{2}{\pi} \Sigma \, f(x) \delta \sqrt{\left[1 - \left(\frac{x}{a}\right)^2\right]}$$

Thus the values of $f(x)$ are summed at values of $x$ corresponding to equal intervals of the function $\sqrt{[1 - (x^2/a^2)]}$. Where $f(x)$ is double valued the lower value is taken for the first quadrant of the input signal and the remaining value for the second quadrant, exactly as when constructing the output waveform graphically.

The out-of-phase component is given by

$$B = \frac{2}{\pi} \int_0^\pi f(a \sin \theta) \cos \theta d\theta$$

In the first quadrant of the input sinusoidal $\cos \theta$ is positive and so the partial sum is found to be

$$\frac{2}{\pi} \sum_{x=0}^{x=a} f(x) d\frac{x}{a}$$

Here again the lower value of $f(x)$ is taken, corresponding to an input $a \sin \theta$ for $0 < \theta < \pi/2$. For the second quadrant the term $\cos \theta$ is negative, and so the required sum is

$$-\frac{2}{\pi} \sum_{x=0}^{x=-a} f'(x) d\frac{x}{a}$$

Here $f'(x)$ represents the output corresponding to the input $w_i = a \sin \theta$ where $\pi/2 < \theta < \pi$. Hence, the resultant out-of-phase component is given by

$$B \simeq \frac{2}{\pi} \Sigma [f(x) - f'(x)] \delta \frac{x}{a}$$

A negative result indicates a phase lag for the output waveform. This shows that the out-of-phase component is directly related to the area enclosed by the non-linear characteristic, the latter being given by

$$B' = \int [f(x) - f'(x)] dx$$

For the hysteretic non-linearity shown, approximate and

$K_{eq}$ is chosen to minimize the mean-square error between the true output of the non-linearity and the calculated output waveform assuming an equivalent gain $K_{eq}$.

Calculation of $K_{eq}$ requires knowledge of the amplitude probability distribution $P(x)$ of the random signal and of the mean-square value, $\sigma^2$, of the input signal.

As shown in Reference 4, Booton's method gives the equivalent gain as

$$K_{eq} = \frac{1}{\sigma^2} \int_{-\infty}^{+\infty} x f(x) P(x) dx$$

where $f(x)$ is the non-linear characteristic.

Proceeding as before, this expression is rewritten as

$$K_{eq} = \frac{1}{\sigma^2} \int_{x=-\infty}^{x=+\infty} f(x) d \left[ \int x P(x) dx \right] \quad . \quad . \quad . \quad (6)$$

Thus, $K_{eq}$ is found approximately by summing $f(x)$ for values of $x$ corresponding to equal intervals of the function $\int x P(x) dx$. This integral is independent of the form of the non-linearity, and is simple to evaluate for typical forms of $P(x)$.

Two amplitude probability distributions have been considered, namely the Gaussian distribution, where

$$P(x) = \frac{1}{\sigma^2 \sqrt{2\pi}} \varepsilon^{-x^2/2\sigma^2} \quad . \quad . \quad . \quad . \quad (7)$$

and a uniform amplitude distribution such that

$$\left. \begin{array}{l} P(x) = \dfrac{1}{2a}, \quad |x| < a \\[2mm] P(x) = 0, \quad |x| > a \end{array} \right\} \quad . \quad . \quad . \quad . \quad (8)$$

For the Gaussian distribution, eqn. (6) becomes

$$K_{eq} = \frac{2}{\sigma \sqrt{2\pi}} \int_0^1 f(x) d\varepsilon^{-x^2/2\sigma^2}$$

Thus, $\Sigma f(x)$ is found for values of $x$ corresponding to equal variations in the function $\varepsilon^{-x^2/2\sigma^2}$. Table 2 shows the values of $x/\sigma$ corresponding to variations of $0 \cdot 1$ in the value of $\varepsilon^{-x^2/2\sigma^2}$.

### Table 2

#### DERIVATION OF RESPONSE TO RANDOM INPUTS

(a) *Gaussian Amplitude Probability Distribution.*

| $\varepsilon^{-x^2/2\sigma^2}$ | 0·05 | 0·15 | 0·25 | 0·35 | 0·45 | 0·55 | 0·65 | 0·75 | 0·85 | 0·95 |
|---|---|---|---|---|---|---|---|---|---|---|
| $\dfrac{x}{\sigma}$ | 2·450 | 1·950 | 1·665 | 1·450 | 1·263 | 1·093 | 0·930 | 0·758 | 0·570 | 0·327 |

(b) *Uniform Amplitude Probability Distribution.*

| $\dfrac{x^2}{a^2}$ | 0·05 | 0·15 | 0·25 | 0·35 | 0·45 | 0·55 | 0·65 | 0·75 | 0·85 | 0·95 |
|---|---|---|---|---|---|---|---|---|---|---|
| $\dfrac{x}{a}$ | 0·224 | 0·387 | 0·500 | 0·592 | 0·671 | 0·741 | 0·806 | 0·866 | 0·922 | 0·974 |

exact analysis gives the results shown in Fig. 5(b). It is seen that the errors introduced are sufficiently small to be neglected for all practical purposes.

### (3) THE RESPONSE TO RANDOM SIGNALS

When the input to the non-linearity is a random signal, the equivalent gain, $K_{eq}$, is determined by a method due to Booton.

As before, a cursor is constructed giving the values of $x$ at which $f(x)$ is to be determined, for all values of $\sigma$.

For the uniform-amplitude probability distribution eqn. (6) becomes

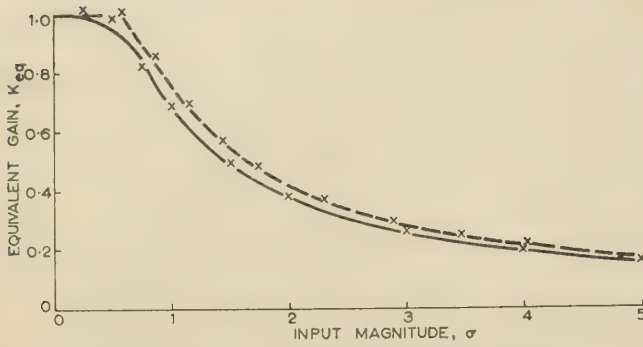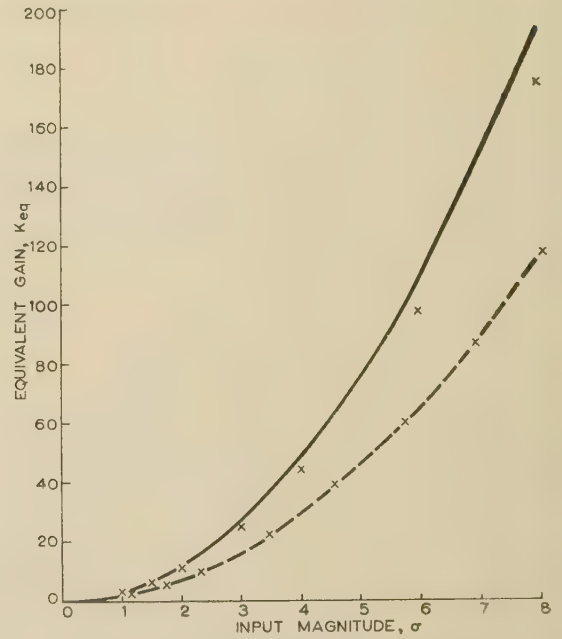$$K_{eq} = \frac{3}{2a} \int_0^{a^2} f(x) d\frac{x^2}{a^2}$$

Fig. 6.—Response of saturation to random inputs.

——— Exact, Gaussian amplitude distribution.
− − − − Exact, uniform-amplitude distribution.
× × × Results from cursor.

Hence, $f(x)$ is determined at values of $x$ corresponding to equal changes in $x^2/a^2$. With ten spot values, Table 2 gives the required values of $x/a$.

The gain of two non-linearities has been found for these different random signals and compared with the exact evaluation of eqn. (6). Fig. 6 shows the approximate and exact gain of the saturation characteristic, Fig. 2(a), and Fig. 7 shows that of the cubic non-linearity in Fig. 2(b) as a function of input magnitude, $\sigma$.

### (4) CONCLUSIONS

The method presented gives a rapid means of determining the response of non-linear elements to sinusoidal and random signals. Simple cursors can be constructed to give the effective gain of the non-linearity with sufficient accuracy for all practical purposes. The technique is considered invaluable for the analysis of non-linear systems.

### (5) REFERENCES

(1) TUSTIN, A.: 'A Method of Analysing the Effect of Certain Kinds of Non-Linearity in Closed-Cycle Control Systems', *Journal I.E.E.*, 1947, **94**, Part IIA, p. 152.
(2) KOCHENBERGER, R. J.: 'A Frequency-Response Method for Analysing and Synthesizing Contactor Servomechanisms', *Transactions of the American I.E.E.*, 1950, **69**, p. 270.

Fig. 7.—Response of cubic non-linearity to random inputs.

——— Exact, Gaussian amplitude distribution.
− − − − Exact, uniform amplitude distribution.
× × × Results from cursor.

(3) WEST, J. C., and DOUCE, J. L.: 'The Frequency Response of a Certain Class of Non-Linear Feedback Systems', *British Journal of Applied Physics*, 1954, **5**, p. 204.
(4) BARRETT, J. F., and COALES, J. F.: 'An Introduction to the Analysis of Non-Linear Control Systems with Random Inputs', *Proceedings I.E.E.*, Monograph No. 154 M, November, 1955 (**103** C, p. 190).
(5) BOOTON, R. C.: 'Non-Linear Control Systems with Statistical Inputs', Report No. 61, Dynamic Analysis and Control Laboratory, M.I.T., 1954.
(6) LEWIS, L. T.: 'Harmonic Analysis for Non-Linear Characteristics', *Transactions of the American I.E.E.*, 1954, **73**, Part 1, p. 673.

# THE DESIGN OF AUTOMATIC-GAIN-CONTROL SYSTEMS FOR AUTO-TRACKING RADAR RECEIVERS

By Lt.-Cdr. J. C. G. FIELD, R.N., B.Sc., Associate Member.

## SUMMARY

A survey is presented of the automatic-gain-control requirements for target-tracking radars of the conical-scanning type. A simple analysis of linear closed-loop a.g.c. systems is given, from which the required performance can be related to circuit parameters. Practical considerations regarding methods of controlling i.f. amplifier gain, number and position of controlled stages, and means of extracting the conical-scan modulation are briefly reviewed.

The frequency-response characteristics of the a.g.c. loop, as governed by the conflicting requirements of stability, speed of response, and faithful reproduction of the scan modulation, are discussed from the Bode and Nyquist-diagram points of view. A simple graphical method of allowing for the sampling process in a pulsed radar system is given.

The design methods are illustrated by a description of the development of an a.g.c. system for a particular naval fire-control radar. This system employs suppressor-grid i.f. amplifier control, the control voltage being developed by a special d.c. amplifier having an exponential characteristic obtained by negative feedback via a series of biased diodes. A filter embodying a twin-T network is employed to achieve maximum speed of response consistent with minimum modulation phase shift.

Target-tracking trials with this system demonstrated that a significant increase in aiming error can be produced by fast-acting automatic gain control unless the receiver noise level is sufficient to keep the loop closed during deep fades.

## LIST OF SYMBOLS

$v_1$ = Echo-signal voltage.
$N(t)$ = Fractional fading modulation.
$m$ = Fractional scan modulation.
$f_s$ = Conical scan frequency.
$f_r$ = Pulse recurrence frequency.
$\phi$ = Conical scan modulation phase.
$S$ = Target echoing area.
$R$ = Target range.
$K_1, K_2$, etc. = Arbitrary constants.
$K$ = Zero-frequency loop gain.
$Y$ = Loop frequency-response function, normalized to unity at zero frequency, i.e. $Y(0) = 1$.
$M$ = I.F. amplifier gain.
$G$ = I.F. amplifier gain, dB.
$v_2$ = I.F. amplifier video frequency output.
$V_c$ = A.G.C. 'set-point' or 'delay' voltage.
$v$ = A.G.C. error voltage = $V_c - v_2$.
$U$ = Ratio of dB change in $v_2$ to dB change in $v_1$.
$V$ = A.G.C. control voltage.
$B$ = Zero-frequency gain in the feedback path.
$P, Q, W$ = Arbitrary constants.
$g_m$ = Mutual conductance.
$V_0$ = Magnitude of projected suppressor cut-off voltage for a pentode.

## (1) INTRODUCTION

The automatic-gain-control system of a receiver associated with an auto-tracking radar system of the conical-scanning type should fulfil the following requirements:

(*a*) It should prevent the receiver output from rising to a saturation value, which would result in the loss of scan modulation.

(*b*) It should maintain the mean receiver output within specified limits of a set value, so that the scan-modulation output voltage always corresponds to a given beam misalignment, within the same limits. The limits are set by the permissible variations in loop gain that can be tolerated by the auto-aiming servo system.

(*c*) It should maintain an approximately constant receiver output, in order to limit the dynamic range of the succeeding strobing circuits. In this connection it should be noted that video-frequency pulses are inevitably lengthened and distorted to an approximately triangular form, and that any variation in peak amplitude therefore implies a corresponding alteration in pulse length.

(*d*) It should suppress variations in receiver output due to target fading at all frequencies up to the cut-off frequency of the auto-ranging servo loop, so that there is no contribution to range jitter from this cause.

(*e*) It should suppress variations in receiver output due to target fading over as large a frequency band as possible, in addition to the band specified by requirement (*d*), in order to reduce the possible effect of system non-linearities in generating higher-order product terms from the fading spectrum, which may fall within the servo bandwidths of the ranging or aiming servo loops, and thereby contribute jitter to the system.

(*f*) It should avoid shifting the phase of the scan modulation by more than some specified small angle.

(*g*) It should recover as rapidly as possible from a transient input signal which momentarily saturates the receiver.

### (1.1) Nature of the Received Signal

The echo signal, $v_e$, received from the target will have the general form

$$v_e = V_e[1 + N(t)][1 + m \sin(\omega_s t + \phi)] \quad . \quad . \quad (1)$$

where $V_e$ is the mean value, $N(t)$ is the fractional modulation due primarily to target fading, $m$ is the fractional scan modulation due to beam misalignment, $\omega_s/2\pi = f_s$ is the conical scan frequency, and $\phi$ is the phase of the scan modulation, defining the direction of the misalignment.

Eqn. (1) becomes, on multiplication,

$$v_e = V_e[1 + N(t) + m \sin(\omega_s t + \phi) + mN(t) \sin(\omega_s t + \phi)] \quad (2)$$

This indicates that the received signal is modulated at the range of frequencies given by the Fourier transform of $N(t)$, and at the scan frequency $f_s = \omega_s/2\pi$. In addition, there will be a further range of spectral components given by the sum and difference of $f_s$ and the spectral components of $N(t)$, although

these will be almost negligible while tracking, owing to the small value of $m$ which then obtains.

If any appreciable non-linearities exist in the system, a further range of higher-order terms will appear in the receiver output.

Experimental evidence seems to indicate that the fading spectrum from modern aircraft targets at S-band frequencies exhibits a maximum at about $0 \cdot 5 \, \text{c/s}$, and at $5 \, \text{c/s}$ has fallen to a relatively low and almost constant value. The r.m.s. value of $N(t)$ appears to be of the order of $5 \, \text{dB}$ (see Fig. 1).
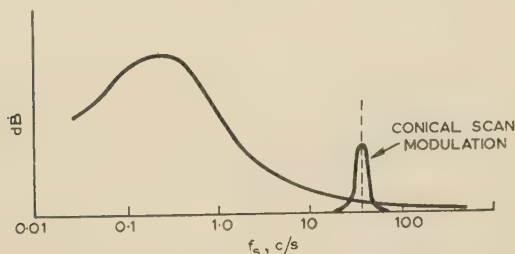


Fig. 1.—Typical fading spectrum from an aircraft target.

The mean value of the received signal, $V_e$, is given by the radar equation as

$$V_e^2 = \frac{K_1 S}{R^4}$$

where $K_1$ is a constant embracing the parameters of the radar, $S$ is the target mean echoing area, and $R$ is the target range. Values of $S$ range from about 1 to $100 \, \text{m}^2$, and for a typical medium-range anti-aircraft system, accurate tracking is required between ranges of 12 000 and 1 500 yd, say. Thus the variation in $V_e$ due to range variation will be $40 \log 8 = 36 \, \text{dB}$, and that due to target echoing area will be $10 \log 100 = 20 \, \text{dB}$, giving a total variation in mean received signal of $56 \, \text{dB}$ over the useful tracking range.

Although, in this case, $56 \, \text{dB}$ (plus an allowance of, say, $10 \, \text{dB}$ for fading) is the maximum range over which the a.g.c. system *need* meet the overall system requirements, it is nevertheless desirable to have a margin to allow for variations in $K_1$. Thus it would appear that $70$–$80 \, \text{dB}$ should be taken as the total dynamic range over which automatic gain control should operate effectively. (Similar calculations for other practical cases yield comparable figures.)

### (1.2) Types of A.G.C. System

There are two basic methods of achieving automatic gain control in radar receivers, namely

(a) Closed-loop error-actuated gain control of a linear i.f. amplifier (usually known as 'linear automatic gain control').
(b) Open-loop gain control according to a logarithmic law, i.e. by the use of an i.f. amplifier having logarithmic output/input characteristics.

Method (a) involves the selection of the 'wanted' echo, comparing its amplitude with a 'set-point' voltage, and feeding the resultant error signal back in the correct sense to control the i.f.-amplifier gain. In this way, variations in the level of the 'wanted' signal can be kept below an arbitrarily small amount. Other signals weaker than the 'wanted' one will normally be eliminated from the displays, while stronger ones will saturate.

Method (b) involves the provision of an i.f. amplifier whose output is proportional to the logarithm of its input. Such an amplifier can be constructed by arranging for each stage to saturate in turn, and adding together the rectified outputs of each stage. With a sufficient number of identical stages, each of a small dynamic range, the input/output curve is smooth and

logarithmic in form. A typical design might have ten stages an cater for an input range of $80 \, \text{dB}$. The output would vary ove a range of 10 : 1, i.e. $20 \, \text{dB}$, for this input variation.

The logarithmic system has the attraction of simplicity, an gives constant scan-modulation voltage per degree of misalign ment, without introducing any phase shift of the modulation It also gives a closer approach to a sinusoidal modulation wave form when the aerial polar diagram approximates to a Gaussia error function. In spite of these advantages, however, it has no yet found application in auto-tracking systems where the rang co-ordinate is important, owing to the practical difficulty c avoiding small range shifts when changes in echo amplitud occur. This effect, although small, is liable to result in a con siderable increase in range and range-rate jitter.

Further information on the design of logarithmic i.f. amplifier is given by Croney[1] and Rozenstein.[2] The remainder of th paper will be restricted to a discussion of linear a.g.c. systems.

### (2) LINEAR AUTOMATIC GAIN CONTROL

Fig. 2 is a block schematic of a linear a.g.c. system. The i.l amplifier, of gain $M$, produces a gated video-frequency outpu $v_2 = Mv_1$, which is compared with a fixed 'set-point' voltage, $V_c$
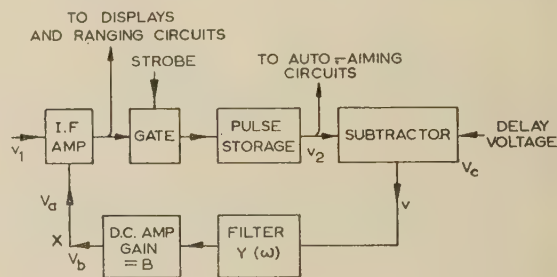


Fig. 2.—Block schematic of linear a.g.c. system.

The difference $(V_c - v_2)$ is the error signal $v$, which, after passin through a filter whose transfer function is taken to be unity a zero frequency, is amplified by a factor $B$ and fed to the i.l amplifier as a gain-control voltage. The arrangement is thu seen to be a servo system in which the input is $V_c$ and the outpu $v_2$. Variations in $v_1$ are of the nature of disturbing signals, an the criterion of effectiveness of the system as a servo mechanisn or regulator is the degree to which $v_2$ is kept equal to $V_c$ in spit of such disturbing signals.

In practice, $V_c$ is normally a 'delay' voltage, such that th error voltage is zero when $v_2$ is smaller than $V_c$. In other words the loop is broken when $v_1$ falls below $v_2/M_{max}$. (The loop will in any case, be broken when $v_1$ falls to zero, unless the inpu noise level is higher than $v^2/M_{max}$).

### (2.1) Static Control Characteristics

The following treatment is based on that of Oliver:[3]

The loop gain of the system can be determined by breaking th loop at a point such as X in Fig. 2. Then, with a constant signa $v_1$, the voltage $V_a$ is adjusted so that $v_2$ is at its normal controllec level, and the fed-back voltage, $V_b$, is equal to $V_a$—so that th loop could be closed again without disturbance. If $V_a$ is nov changed by a small amount $\Delta V_a$, $V_b$ will change correspondingl by an amount $\Delta V_b$. The loop gain of the system is defined a $\Delta V_b / \Delta V_a = K$ at zero frequency.

By analogy with feedback amplifier theory, it follows that an output $(v_2)$ variations due to any disturbing factor will be reducec by a factor $1/(1 + K)$. In particular, the fractional change in $v$

due to a fractional change $\Delta v_1/v_1$ in input signal will be given by

$$\frac{\Delta v_2}{v_2} = \frac{\Delta v_1}{v_1} \times \frac{1}{1+K}$$

Since $\frac{d}{dx}(\log x) = \frac{1}{x}$, we can write

$$\frac{d}{dv_2}(\log v_2) = \frac{1}{1+K}\frac{d}{dv_1}(\log v_1)$$

i.e. $\dfrac{\text{dB increase of } v_2}{\text{dB increase of } v_1} = U = \dfrac{1}{1+K}$

Thus if the ratio $U$ is specified, the required loop gain $K$ can be found, and is given by

$$K = \frac{1}{U} - 1 \quad . \quad . \quad . \quad . \quad . \quad . \quad (3)$$

For the typical medium-range system being considered, Section 1.1 showed that the expected range of $v_1$ would be of the order of 80 dB. It therefore only remains to specify the maximum tolerable range of $v_2$ to determine the necessary loop gain. In this respect it is advisable not to make the limits any smaller than really necessary. As will be seen later, a price has to be paid for high loop gain in terms of slow recovery from overload and tighter tolerances on components.

An average i.f. amplifier will overload at about twice its normal output level (operation at lower levels would tend to militate against linear second-detector operation), and therefore it would appear that a variation of $\pm 3$ dB about the mean level is the maximum that could be tolerated. A figure of $\pm 2$ dB would be reasonable, allowing modulation of 4 dB or 60% before positive clipping occurs.

Thus the required loop gain would be

$$K = \frac{80}{4} - 1 = 19, \quad \text{i.e. 26 dB approximately.}$$

This is therefore the minimum loop gain required to keep the output of the receiver sufficiently within its linear range. With this value a 10 dB fade would be reduced to 0·5 dB.

## (2.2) Calculation of Loop Gain from Circuit Parameters

Assuming, as before, that a constant input signal, $\bar{v}_1$, is applied to the amplifier, we have

$$v_2 = M\bar{v}_1$$

If we now open the loop, and change $V_a$ by a small amount $\Delta V_a$, $v_2$ will change correspondingly by a small amount $\Delta v_2$, where

$$\Delta v_2 = \bar{v}_1\left(\frac{dM}{dV}\right)_{V=V_a}\Delta V_a$$

We also have

$$\Delta V_b = BY(\omega)\Delta v_2$$

Therefore $\dfrac{\Delta V_b}{\Delta V_a} = BY(\omega)\bar{v}_1\left(\dfrac{dM}{dV}\right)_{V=V_a}$

But $$v_1 = \frac{v_2}{M}$$

Therefore

$$\frac{\Delta V_b}{\Delta V_a} = BY(\omega)v_2\frac{1}{M}\left(\frac{dM}{dV}\right)_{V=V_a}$$

Let $G$ be the amplifier gain, in decibels.

Then $G = 20\log_{10} M$ decibels

and $$\frac{1}{M}\frac{dM}{dV} = \frac{\log_\varepsilon 10}{20}\frac{dG}{dV} = 0\cdot115\frac{dG}{dV}$$

Thus the loop gain is given by

$$\frac{\Delta V_b}{\Delta V_a} = 0\cdot115 Bv_2\left(\frac{dG}{dV}\right)_{V=V_a}Y(\omega) \quad . \quad . \quad . \quad (4)$$

where $B =$ D.C. gain in the feedback path.

$v_2 =$ Output voltage.

$\dfrac{dG}{dV} =$ Rate of change of amplifier gain, dB/volt.

$Y(\omega) =$ Frequency-response function of the loop, normalized to unity at zero frequency, i.e. $Y(0) = 1$.

It is thus seen that, if $dG/dV$ is constant (i.e. if the amplifier has logarithmic control characteristics) and if $v_2$ is held approximately constant, the loop gain may be written

$$\frac{\Delta V_b}{\Delta V_a} = KY(\omega), \text{ where } K = 0\cdot115 Bv_2\frac{dG}{dV}$$

which is approximately constant.

The fact that $K$ is proportional to $v_2$ accounts for the well-known fact in relation to communication receivers that tight a.g.c. control results from the use of a large delay voltage, $V_c$, and also accounts for the comparative success of undelayed a.g.c. systems in simple receivers.

It should be noted that if $v_2$ is allowed to vary to a considerably greater extent than the 4 dB maximum quoted above, the exact calculations should take this into account, and a process of successive approximations will be necessary to compute the final performance curve.

## (3) METHOD OF CONTROLLING I.F. AMPLIFIER GAIN

The gain of a linear i.f. amplifier may be controlled, in principle, by applying the control voltage $V$ to any one or more electrodes of a number of valves. For practical reasons, the choice is limited to

(a) Control grid.
(b) Suppressor grid.
(c) Combination of (a) and (b).

### (3.1) Control-Grid Control

Method (a) depends on the relationship between grid voltage and mutual conductance of normal high-slope amplifying pentodes. Valve designers often endeavour to achieve an exponential control characteristic such that the anode current $i_a$ is given by an equation of the form

$$i_a = \varepsilon^{(P+QV)}, \quad \text{where } P \text{ and } Q \text{ are constants.}$$

Thus $$\frac{di_a}{dV} = g_m = Q\varepsilon^P\varepsilon^{QV}$$

Since the gain of a single stage is given by $M_1 = g_m Z_a$, where $Z_a$ is the anode load impedance, we have

$$M_1 = Q\varepsilon^P\varepsilon^{QV}Z_a = W\varepsilon^{QV}$$

and $$\log_\varepsilon M_1 = \log_\varepsilon W + QV$$

Let $G_1$ be the stage gain in decibels; then

$$G_1 = 20\log_{10} M_1 = \frac{20}{\log_\varepsilon 10}\log_\varepsilon M_1$$

i.e. $G_1 = 8\cdot68\log_\varepsilon M_1$.

Differentiating once more, we obtain finally

$$\frac{dG_1}{dV} = 8\cdot 68 Q \ . \ \ . \ \ . \ \ . \ \ . \ \ .(5)$$

Thus the rate of change of gain, expressed in decibels per volt, is constant. This fulfils the requirement of Section 2 for constancy of a.g.c. loop gain.

If the fractions $a$, $b$, $c$, etc., of the control voltage $V$ are applied to individual stages, we obtain for the control characteristic of the complete amplifier

$$\frac{dG}{dV} = 8\cdot 68 Q \, (a + b + c + \ldots)$$

If $a = b = c$, etc., are all equal to unity, $dG/dV = 8\cdot 68nQ$, where $n$ is the number of controlled stages.

In practice, owing to the close grid-cathode spacing and the necessity for making efficient use of cathode area imposed by the requirement for large gain-bandwidth products, valve characteristics are only very approximately exponential. Moreover, considerable variations from one sample to another of the same valve type are likely to be encountered—again owing to the small clearances which magnify the effects of manufacturing tolerances.

The author has no exact figures for actual valve samples, but would estimate that for an average type CV138 (EF91), $dG_1/dV$ varies by a factor of about 4 : 1 for a change in $G_1$ of 27 dB. Thus, in an amplifier having three similar controlled stages and handling a dynamic range of 80 dB, the a.g.c. loop gain could vary by 4 : 1 or 12 dB. Similar figures are found for the type 6AK5 pentode.

This variation can be reduced only by employing more controlled stages. However, it is generally desirable to restrict the number of controlled stages to three or four, except possibly in very wide-band systems.

There will be an additional variation in $dG_1/dV$ between valve samples at given values of $V$, of the order of $2\frac{1}{2}$ : 1. It thus appears that a variation of $\pm 10$ dB in a.g.c. loop gain should be expected and allowed for in design when using grid-bias control.

### (3.2) Suppressor-Grid Control

If the control voltage $V$ is applied to the suppressor grid of an amplifying stage, the mutual conductance is reduced by the mechanism of electrons being turned back and collected by the screen grid. Owing to the screening effect of the latter, the total cathode current remains constant, and is shared between the screen grid and the anode in proportions determined by $V$. One consequence of this is that stabilized power supplies are not essential, although it is still necessary that there should not be any large resistance in series with the screen grid. In practice, there is a danger of exceeding the maximum allowable screen dissipation with this method; in some cases this difficulty may be overcome by gating the i.f. amplifier so that it is operative only for the duration of the range scan.

The form of the suppressor-grid control characteristic is approximately linear, and can be expressed by

$$g_m = \frac{g_{m(max)}}{V_0}(V_0 + V) \ . \ \ . \ \ . \ \ . \ \ . \ (6)$$

where $V_0$ is the (negative) voltage required to produce anode-current cut-off and is a function of anode and screen voltages (Fig. 3).

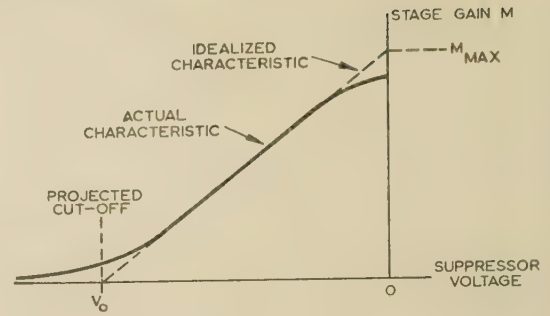Thus the stage gain $M_1$ is

$$\frac{M_{1\,max}}{V_0}(V_0 + V)$$

Fig. 3.—Stage gain of pentode as a function of suppressor voltage.

and for the whole amplifier, we have

$$M = \frac{M_{max}}{V_0}(V + V_0) \ . \ \ . \ \ . \ \ . \ \ . \ (7)$$

Thus $\dfrac{dM}{dV} = \dfrac{M_{max}}{V_0}$, and $\dfrac{1}{M}\dfrac{dM}{dV} = \dfrac{V_0}{M_{max}}\dfrac{1}{V + V_0}\dfrac{M_{max}}{V_0}$

i.e. 
$$\frac{d(\log M)}{dV} = \frac{1}{V + V_0} \ . \ \ . \ \ . \ \ . \ (8)$$

and 
$$\frac{dG}{dV} = \frac{20}{\log_e 10}\frac{d(\log M)}{dV} = 8\cdot 68\frac{1}{V + V_0}$$

This varies from $8\cdot 68/V_0$ to infinity as $V$ varies from 0 to $-V_0$.

Hence it is necessary to make $V$ some non-linear function of $v$, the error voltage, if constant a.g.c. loop gain is to be achieved. The required relationship between $V$ and $v$ is given by the differential equation

$$\frac{dV}{dv} = K_2(V + V_0) \ . \ \ . \ \ . \ \ . \ (9)$$

for, if we substitute for $dV = K(V + V_0)dv$ in eqn. (8), we obtain

$$\frac{d(\log M)}{K_2(V + V_0)dv} = \frac{1}{V + V_0}$$

i.e. 
$$\frac{d(\log M)}{dv} = K_2 \ . \ \ . \ \ . \ \ . \ \ . \ (10)$$

A solution of eqn. (9) is

$$V = V_0(\varepsilon^{K_2 v} - 1) \ . \ \ . \ \ . \ \ . \ (11)$$

The conclusion reached is therefore that, to make effective use of suppressor-grid control for a.g.c. purposes, the control voltage, $V$, must be produced from the error voltage, $v$, by means of an amplifier having an exponential characteristic of the type given by eqn. (11). There is no difficulty in principle in achieving such a characteristic to any desired accuracy by systems such as those shown in block form in Figs. 4 and 5.

Sources of error in practice are (a) departure of the suppressor-grid characteristic from strict linearity, and (b) variation of the
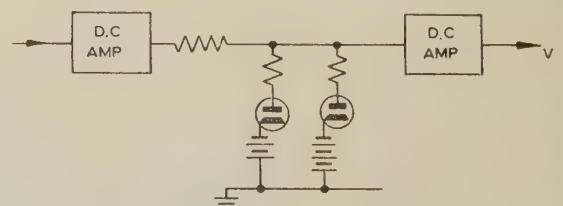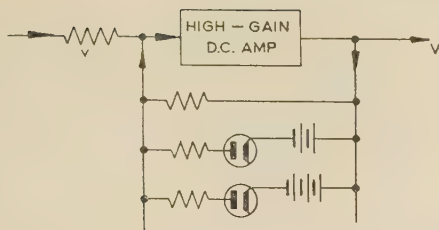
Fig. 4.—Curve-fitting circuit.

Fig. 5.—Alternative curve-fitting circuit.

cut-off voltage $V_0$ from valve to valve. With regard to (a), it is, in principle, relatively easy to achieve a reasonably linear spacing of the suppressor-grid coil. Clearances are relatively large in this region, thus making reproducibility in manufacture an easier problem. Against this, however, valve specifications seldom cover suppressor-grid characteristics in any detail.

Departures from linearity will, in any case, occur in the region $V = 0$, owing to space-charge effects in the screen-anode space, and near $V = V_0$ owing to the impossibility of achieving an abrupt cut-off. The non-linear region near $V = 0$ extends over a range of less than 1 dB, and can be neglected. The curvature at the other end starts when the stage gain has been reduced by about 20 dB, after which the gain/voltage curve is approximately exponential. Thus, in practice, the exponential characteristic of the a.g.c. amplifier will be arranged to change at this point to a linear characteristic. This is a fortunate circumstance, as it reduces the voltage-handling capacity required of certain stages in the a.g.c. amplifier.

With regard to variations in the projected suppressor-grid cut-off voltage, $V_0$, it is apparent that the effect will be most serious in the vicinity of the $-20$ dB point mentioned above. Detailed investigation leads to the conclusion that a variation in the numerical value of $V_0$ of $-10\%$ to $+20\%$ causes variations in loop gain of $+6$ dB to $-10$ dB. In the case of the type CV 1091, the spread in $V_0$ is such that in 90% of samples tested it lies between $-5\%$ and $+15\%$ of the nominal figure. It can therefore be concluded that the effect of valve variations with suppressor-grid control will not exceed, and will normally be appreciably less than, those associated with control-grid control.

In practice, a curve should be plotted from the actual amplifier it is proposed to control, under working conditions. If change of gain in decibels is plotted horizontally against control voltage $V$, as in Fig. 6, the shape of the curve is precisely the form of
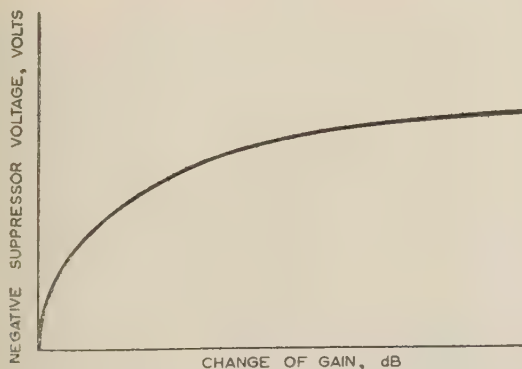


Fig. 6.—Typical i.f. amplifier gain-control characteristic.

characteristic required from the a.g.c. amplifier. A suitable linear scale for $v$ can therefore be marked alongside the decibel scale.

### (3.3) Combined Control-Grid and Suppressor-Grid Control

It is found that the variations in both the conductive and susceptive components of the input admittance of a pentode, such as the type CV 1091, at high frequencies vary in opposite directions with the application of control bias, according to whether the bias is applied to the control or suppressor grid. There is therefore a possibility of maintaining the input admittance approximately constant if the control bias is fed to both grids simultaneously in the correct proportions. This is very desirable, in order to avoid mistuning and change in bandwidth.

Considerable care is necessary if any useful improvement is to be obtained in practice, owing to the effect of the inductance of cathode leads and other small stray feedback couplings. However, this approach has been successfully applied in one particular naval radar equipment.

The relationship between gain and control voltage in this case is intermediate between an exponential and a linear law. A non-linear a.g.c. amplifier is therefore still required, although it may be rather easier to design, since it need not provide such large changes in gain as are required with pure suppressor-grid control.

There is no difficulty in avoiding excessive screen dissipation with this system; in fact, on the whole, it probably represents the optimum in design in cases where the highest performance is sought.

### (3.4) Number and Position of Controlled I.F. Stages

The gain of an i.f. stage does not become zero even when the valve transconductance vanishes, because there is an irreducible minimum coupling between grid and anode via the inter-electrode capacitance, apart from any extra stray coupling. It is found that the maximum gain reduction that can be obtained in a single stage when the valve is completely cut off is about 40 dB. Thus at least two stages must be controlled, and in practice three is usually the minimum number that can be controlled without excessive variation in a.g.c. loop gain.

At the same time it is desirable that the number of controlled stages, expressed as a fraction of the total number of stages, should be as small as possible, in order to reduce the effect of mistuning. Thus a compromise has to be reached between a large proportion of controlled stages, giving high consistency of a.g.c. loop gain, and a small proportion, giving a small mistuning effect. In practice, the compromise usually results in there being three controlled stages in amplifiers of about 4 Mc/s bandwidth, containing about seven amplifying stages. Amplifiers of about 10 Mc/s bandwidth, containing 12 or 14 stages, generally have a.g.c. voltages applied to four stages.

The actual stages to which control should be applied require to be chosen with care. The first stage (the one immediately following the mixer) should always operate at full gain, otherwise the noise factor of the amplifier will be increased. For the same reason, it is also prudent to allow the second stage to operate continuously at full gain. These two stages are normally located in a head amplifier close to the crystal mixer.

The maximum undistorted output of an amplifying stage is reduced when its gain is reduced by the application of a control voltage. For this reason, the last i.f. stage, and preferably the one before it, should not be controlled.

We can therefore summarize by saying that the third stage should be the earliest to be controlled, and that there should be at least two uncontrolled stages following the last controlled stage.

## (4) METHODS OF EXTRACTING THE SCAN MODULATION

Although the question of the frequency response of the a.g.c. loop is to be treated in more detail in Section 5, it will already be clear that, if the modulation at conical scan frequency is to

be extracted without distortion from the video-frequency output of the receiver, the a.g.c. loop gain must be much less than unity at the conical scan frequency. Thus a filter is necessary in the feedback loop which attenuates the conical scan frequency by a sufficient amount.

Alternatively, it is possible to maintain the a.g.c. loop gain up to frequencies much higher than the conical scan frequency, so that all scan modulation is effectively suppressed at the video-frequency output of the receiver. This output is then used only for the ranging circuits.

The a.g.c. voltage will now be modulated at scan frequency (as well as with the fading spectrum) and this modulation can be extracted via a band-pass filter and fed to the aiming circuits. If the control characteristic is intrinsically exponential, as is approximately realized with control-grid control, the scan modulation voltage per degree of target misalignment will be constant. With suppressor-grid control, or mixed control, the scan modulation must be derived from a point in the feedback loop ahead of the non-linear amplifier. In either case, the performance when the scan modulation is derived from the feedback voltage is equivalent to that of a logarithmic i.f. amplifier.

With regard to the merits of the two methods of extracting the scan modulation, the second should give a superior ranging performance, owing to the complete elimination of all frequencies in the bandwidth of the range servo loop—particularly if the latter has a short time-constant. On the other hand, there is perhaps more chance of increased cross-product noise being fed to the aiming servo mechanisms, as with logarithmic systems.

## (5) FREQUENCY-RESPONSE CHARACTERISTICS OF THE A.G.C. SYSTEM

If the input signal $v_1$ is modulated at an angular frequency $\omega$ with a percentage depth of modulation $m_1$, the corresponding percentage modulation of the output, $m_2$, is given by

$$\frac{m_2}{m_1} = \frac{1}{1 + KY(\omega)} \quad . \quad . \quad . \quad . \quad (12)$$

(This follows from normal feedback theory.)

Since $Y(\omega)$ is a complex quantity, $m_2$ will, in general, be complex also (assuming $m_1$ to be real). Eqn. (12) thus enables the amplitude and phase of the output modulation to be calculated as a function of $\omega$, when $K$ and $Y(\omega)$ are specified.

In a radar system in which the scan modulation is to be extracted from the receiver output, it is important that the phase shift of $m_2$ with respect to $m_1$ shall be less than some arbitrary figure, otherwise the co-ordinates into which the target misalignment is resolved will not coincide with the vertical and lateral co-ordinates of the auto-aiming system. Such a rotation of co-ordinate axes, or phasing error, has a deleterious effect on auto-aiming stability, owing to the cross-coupling it introduces between the vertical and lateral auto-aiming loops. The maximum tolerable phasing error will depend on the inherent stability of the auto-aiming loops, and may be as little as 2° in some applications. For a particular case of identical second-order aiming loops, it has been shown that the 'phase margin' of the loops is reduced precisely by the amount of phasing error. For a conventional auto-follow radar system, the maximum tolerable phasing error will be of the order of 10°.

It might be suggested that phasing errors produced by the a.g.c. system could be compensated elsewhere. Two factors prevent much advantage being taken of this fact; one is the variation of $K$ due to imperfect valve characteristics, discussed in Section 3; the other is the fact that, in many systems, it is a requirement that auto-following should be possible with signals below the a.g.c. threshold level. Provided that adequate

means are available for setting up a phase-correction circuit, however, there seems no reason why error should not be halved by arranging to correct for half the maximum a.g.c. phasing error, since this will normally be always in one direction. When the signal falls towards a.g.c. threshold level, the phasing error will fall to zero and then increase again with reversed sign.

### (5.1) Performance of a Simple $RC$ Filter

If the filter in the a.g.c. loop is a simple $RC$ low-pass structure,

$$Y(\omega) = \frac{1}{1 + j\omega T}$$

where $T$ is the filter time-constant ($T = CR$).

Therefore

$$\frac{m_2}{m_1} = \frac{1}{1 + \dfrac{K}{1 + j\omega T}}$$

At the conical-scan angular frequency $\omega_s$, $j\omega T$ will be numerically large compared with unity, and we can therefore write approximately

$$\frac{m_2}{m_1} = \frac{1}{1 - j\dfrac{K}{\omega_s T}}$$

The phase shift is given by

$$\tan \theta = \frac{K}{\omega_s T}$$

and since it is to be small,

$$\theta \simeq \frac{K}{\omega_s T}$$

The quantity $K/\omega_s T$ is the approximate value of the loop gain at the conical scan frequency. We can therefore say that if $\theta$ is not to exceed 10° or $\pi/18$ rad, the loop gain must have fallen to $\pi/18$ or $-15$ dB.

As the modulation angular frequency, $\omega$, falls, the loop gain increases at the rate of 6 dB per octave. Thus if $K = 27$ dB, a total of $(27 + 15)/6 = 7$ octaves must elapse before the loop gain is restored to its zero-frequency value. (This is an asymptotic approximation—actually it would then be within 3 dB of this value.)

It can therefore be seen that, if the scan frequency is, say, 32 c/s, full a.g.c. action will be obtained only for frequencies below 0·25 c/s. Fading at 2 c/s will be reduced by a factor of about two only. The time-constant $T$ is given by the relationship $T = 1$ at the $-3$ dB point—in this case 0·25 c/s. Hence $T = 1/(2\pi \times 0·25) = 0·64$ sec.

It is apparent from this example that fast a.g.c. action cannot be obtained with such a simple filter. For a constant phasing error, an increase in loop gain would call for an increased filter time-constant (double for each 6 dB increase) and the effective loop gain at fading frequencies would remain the same.

If, on the other hand, the scan modulation is to be derived from the a.g.c. voltage, the frequency response of the a.g.c. loop must be such that the loop gain is as high as possible at the conical scan frequency; above this frequency it must fall in such a manner that it is well below unity at half the pulse-repetition frequency (Section 6). If $f_r/f_s > f_s/f_a$, where $f_a$ is the highest fading frequency it is desired to suppress effectively, this condition will normally be easier to meet than in the alternative system.

By reasoning somewhat similar to that used in the previous

case, it can be shown that for the phasing error not to exceed 10°, the loop gain must not fall below 15 dB at the conical scan frequency. In the case of an American system described in the literature,[4] a filter time-constant of 0·02 sec is employed. Although full details are not available to the author, it seems likely that the design value of loop gain at half the repetition frequency, i.e. at 1 500 c/s, will be about −13 dB. Since the interval between this frequency and the conical scan frequency of 30 c/s is 5·7 octaves, the simple filter will allow the loop gain to have increased by 5·7 × 6 = 34 dB over this interval. Thus the loop gain at the scan frequency will be 21 dB, and the system is just satisfactory if variations in loop gain do not exceed about ±6 dB. The asymptotic 6 dB per octave line extends a further 1·9 octaves down to $f = 1/(2\pi \times 0\cdot02) = 8$ c/s at which frequency the loop gain, on the previous assumption, would be 3 dB down on its zero-frequency value of 21 + (1·9 × 6) = 32·5 dB.

It can be concluded that very fast a.g.c. action and high loop gain can be achieved when the scan modulation is derived from the a.g.c. control voltage, provided that the pulse-repetition frequency is about 100 times the conical scan frequency. It is probably true that the method is not feasible, even with complex filter networks, if the ratio of pulse-repetition frequency to scan frequency is less than 30.

On the other hand, when the scan modulation is derived from the receiver output, high loop gain requires large filter time-constants, resulting in slow recovery from overload. With a simple filter there will be little attenuation of fading above one or two cycles per second, unless the conical scan frequency can be considerably increased. It will be shown, however, that this situation can be substantially improved by the use of more complex filter networks.

### (5.2) Stability of the Feedback Loop

The a.g.c. system has the characteristics of a class-0 servo mechanism, the output being $v_2$ and the input $V_c$. The relationship between output and input is given by

$$\frac{v_2}{V_c} = \frac{KY(\omega)}{1 + KY(\omega)} \quad . \quad . \quad . \quad . \quad (13)$$

In common with all feedback systems, instability can occur if the phase shift round the loop reaches 180° at some frequency at which the gain is more than unity. More formally, in order that the system be stable, the roots of the equation $1 + KY(p) = 0$ must all have negative real parts. This condition may be illustrated by drawing a Nyquist diagram for the loop, i.e. a plot of the locus of $KY(\omega)$ expressed as a vector quantity on an Argand diagram. Nyquist's criterion is then that the locus must not enclose the point $(-1, j0)$.

For design purposes, these and other stability criteria are not particularly useful, since the problem is to synthesize an optimum system with an adequate margin of stability, rather than to determine whether an existing system is stable or not. For this purpose, the graphical method of Bode[5] is undoubtedly the most convenient, although the Nyquist diagram is advantageous when overall system phase shift is being examined.

In Bode's method, the loop gain in decibels is plotted against a logarithmic scale of frequency, and the loop phase-shift is separately plotted against the same frequency scale. This has the advantage that all common networks have simple, symmetrical response curves against a logarithmic scale of frequency, which can therefore be sketched after a minimum of computation; furthermore, a change of frequency or time-constant requires only a bodily shift of the whole curve along the frequency axis. Where a loop consists of several networks in tandem, the individual amplitude and phase curves can be added directly to give the overall response curves.

The problem of devising a suitable filter reduces to one of manipulating the Bode curves of 'likely' networks in such a way that the overall amplitude curve has the desired shape, consistent with an adequate phase margin at the frequency of gain cross-over. The overall phase and amplitude curves are, of course, related by the 'minimum phase theorem', so that the average rate of cut-off that can be employed in the region of the gain cross-over frequency cannot exceed about 9 dB per octave if a phase margin of the order of 45° is required.

For any filter other than the simple $RC$ structure there will be a frequency, normally somewhat higher than that of gain cross-over, at which the magnitude of $1 + KY(\omega)$ is less than unity. This means that the a.g.c. system will magnify variations in $v_1$ at this frequency. As a rough rule, this magnification will not exceed about 1·4 if the phase margin is 50°.

The existence of a peak of this nature in the system frequency-response curve is always associated with the presence of overshoots and possibly undershoots following the application of a step function. Again very roughly, the maximum overshoot will not usually exceed 40% if the phase margin is 45° or more.

### (6) DISCONTINUOUS NATURE OF THE DATA

In a pulse radar system, information about the amplitude of the 'wanted' signal is available only for a brief interval once in every pulse-repetition period. It follows that the a.g.c. loop is a pulse-monitored control system, operating on a 'periodic check-up' basis rather than as a continuous controller. This fact immediately brings it into the general class of *sampling servo mechanisms*.

It is intuitively obvious that, if the sampling rate is very high compared with the essential filter time-constant of the system, operation will be negligibly affected by the sampling process. With radar a.g.c. systems, however, it cannot be generally assumed that this will be the case, and the system characteristics may be considerably modified by the fact that the loop is only closed intermittently.

The classical approach to the problem is by linear difference equations, whose solution yields values of the output at successive sampling instants. Other mathematical approaches are the pulsed transfer function and the Z-transform, developed by Hurewicz, Ragazzini, and others.[6,7,8,9] These methods tend to suffer from the same limitations as the corresponding analytical methods for continuous servo mechanisms, in that they can be readily applied only to the analysis of an existing system. For design purposes, a presentation is required such that the effect of varying system parameters is made readily apparent, preferably with a minimum of calculation. In the author's opinion, the approach by Linvill[10] is by far the most satisfactory from this point of view.

Briefly, Linvill's method is to assume that the sampling process is equivalent to the inclusion within the servo loop of an *impulse modulator*. This is defined as a linear modulator whose 'carrier' is a uniform succession of unit impulses spaced at the sampling interval. (N.B. A unit impulse is a pulse of unit area but infinitesimal duration.) The output of such a modulator will be a succession of impulses of individual areas determined by the values of the input to the modulator at the successive sampling instants. Such a sequence of impulses will have a Fourier transform which is periodic in frequency, i.e. the spectrum will contain an exact replica of the input spectrum, centred on zero frequency, together with an infinite array of 'complementary' signals, each being a replica of the input spectrum, but centred on frequencies of $\pm f_r$, $\pm 2f_r$, etc., the complete spectrum extending between

frequencies of minus infinity and plus infinity. All the 'complementary' signals and the 'pure' signals are equal in amplitude at this point. The expression for the Fourier transform is

$$\frac{1}{t_r} \sum_{n=-\infty}^{n=+\infty} F(\omega + n\omega_r) \quad . \quad . \quad . \quad (14)$$

The output of the impulse modulator is now fed to low-pass filter elements, and after traversing the loop, it arrives back at the input with the 'complementary' signals attenuated with respect to the 'pure' signal. If the attenuation is sufficient for the complementary signals to be negligible at this point (and this implies that no frequencies higher than $f_r/2$ can pass the filters), the system operates essentially as if it were a continuous servo mechanism, except that the pulse-storage device introduces a lag that would not otherwise be present. If, however, appreciable amplitudes of 'complementary' signals remain at the input to the impulse modulator after traversing the loop, the modulator will operate on them to produce additional infinite periodic spectra, each containing terms centred round zero frequency, and thus contributing to the 'pure' signal. It follows from this that the performance of the loop will be modified as compared with its continuous counterpart, and moreover it is not possible to define a transfer function with which to multiply the continuous loop transfer function in order to obtain this modified performance. It is therefore impossible, unfortunately, to devise a simple modification to the Bode-diagram procedure for shaping loop transmission characteristics, unless one restricts oneself to the case in which the loop transmission is negligible at and above $f_r/2$. (N.B. By 'negligible' is meant less than $-30$ dB, say.)

Linvill's method of dealing with sampling servo mechanisms consists in the construction of a modified Nyquist diagram from the 'continuous' Nyquist diagram of the system. The performance of the sampling servo mechanism is then effectively the same as that of a continuous servo mechanism described by the modified Nyquist diagram. If $KY(\omega)$, expressed as a complex number, gives the point on the 'continuous' Nyquist diagram corresponding to the angular frequency $\omega$, the corresponding point on the modified diagram is obtained by the infinite summation

$$K \sum_{n=-\infty}^{n=+\infty} Y(\omega + n\omega_r), \text{ where } n \text{ is an integer.}$$

This sum can be obtained by writing down the values of $(\omega + n\omega_r)$ for $n = 0, 1, 2$, etc., and reading the resultant values of $Y(\omega + n\omega_r)$ from the continuous Nyquist locus. Since $Y(\omega)$ must have low-pass characteristics, the series will converge rapidly in all practical cases; a value of $n$ greater than 2 should seldom be necessary. The sums of real and imaginary parts give new co-ordinates for the angular frequency, $\omega$, on the modified locus. The process is repeated for other values of $\omega$, enabling the modified locus to be sketched in. It should be noted that $Y(-\omega)$ is the complex conjugate of $Y(\omega)$, i.e. to find $Y(\omega)$ for a negative frequency, look up the value for the same positive frequency and then reverse the sign of the imaginary part. Alternatively, the continuous locus of $Y(\omega)$ for negative frequencies can be drawn as the reflection in the real axis of the locus for positive frequencies. It will be observed that, when $\omega = \omega_r/2$, the summation becomes

$$Y\frac{\omega_r}{2} + Y\frac{3\omega_r}{2} + Y\frac{5\omega_r}{2} + \ldots$$
$$+ Y\frac{-\omega_r}{2} + Y\frac{-3\omega_r}{2} + Y\frac{-5\omega_r}{2} + \ldots$$

It is thus seen that the imaginary components cancel, leaving a real number. Thus the phase shift at $\omega_r/2$ will be 0° or 180°

(nearly always the latter, in practice) and the modified locus cuts the real axis at this frequency. This demonstrates the tendency of sampling servo mechanisms to oscillate at half the sampling frequency if the loop gain at this frequency exceeds unity.

The modified locus for negative values of $\omega$ is the mirror image of that for positive values of $\omega$, reflected in the real axis. There is therefore no need to plot this. There is also no need to work out the summation for values of $\omega$ greater than $\omega_r/2$, since the complete locus is retraced for such values. A typical example is given in Fig. 20.

### (6.1) Pulse Storage Devices

A practical pulsed system normally incorporates some form of pulse-to-pulse storage following the sampling switch or 'impulse modulator'. This storing process is often referred to as 'clamping', particularly when the device is such that each sample is held constant in the interval before the next one is available. In radar systems, the 'box-car' detector and other similar triggered clamp circuits are used to perform this function.

The Laplace transform of a circuit whose response to a unit impulse is a rectangle of unit height and duration $t_r$ is

$$\frac{1}{p}(1 - \varepsilon^{-pt_r})$$

For the purpose of frequency-response analysis, we can replace $p$ by $j\omega$, giving for the frequency-response function of the clamp

$$\frac{V_0}{v_i} = \frac{1}{j\omega}(1 - \varepsilon^{-j\omega t_r}) \quad . \quad . \quad . \quad . \quad (15)$$

In practice, a simpler storage device is often used; this consists essentially of a condenser which is charged to the peak value of the pulse through a diode, after which it discharges exponentially through a resistance to some fraction of its initial value, when it is recharged by the next pulse. Such a circuit is frequently known as the 'third detector'. The discharge time-constant is usually made equal to the repetition period, and the corresponding Laplace transform is then

$$\frac{1}{p + \dfrac{1}{t_r}}[1 - \varepsilon^{-(1+pt_r)}]$$

Again, on going over to the frequency domain, we have

$$\frac{v_0}{v_i} = \frac{1}{j\omega + \dfrac{1}{t_r}}[1 - \varepsilon^{-(1+j\omega t_r)}] \quad . \quad . \quad (16)$$

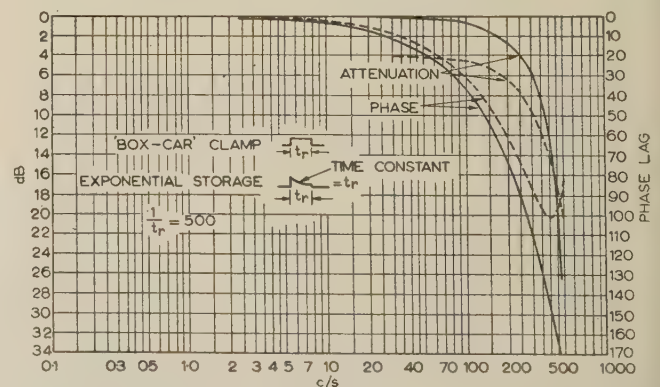Fig. 7 is a graph of the above frequency-response functions



Fig. 7.—Frequency-response functions for a pulse repetition frequency of 500 c/s.

————— 'Box-car' clamp. ———— Exponential storage. $1/t_r = 500$.

for a repetition frequency, $f_r$, of 500 c/s. The functions have been multiplied by $1/t_r$ to take account of this factor in the Fourier transform of the impulse modulator [eqn. (14)].

## (7) DESIGN OF A PRACTICAL A.G.C. SYSTEM

This section describes the steps that were taken in designing a new a.g.c. system for an existing naval fire-control radar. The procedure is given in some detail, as it is thought that a similar approach may be found useful in other design problems of the same type.

The design objective was to produce an a.g.c. system having the following characteristics:

(a) Maximum suppression of fading up to the highest practicable frequency, i.e. fast regulating action.
(b) Output not to vary more than 4 dB for an input variation of 80 dB.
(c) Peak magnification not to exceed 1·5.
(d) Phasing error not to exceed 5°.
(e) It must be easily checked and set up in service.

capacitor in parallel. This valve conducts heavily on the arrival of the lengthened pulse, and charges the capacitor to the peak value. This charge leaks away in the interval before the next pulse with a time-constant of 2·2 millisec, which is roughly equal to the repetition period. The circuit therefore provides exponential pulse storage. The output is fed away via a simple $RC$ filter of 1 millisec time-constant, which serves the dual purpose of reducing the peak ripple voltages to be handled by subsequent stages and of providing some integration for an auto-hold-rate relay circuit.

### (7.1) Experimental Equipment

In order to obtain the necessary data on which to base the design, the equipment illustrated schematically in Fig. 8 was assembled. The modulator consisted of a single type CV138 pentode with the modulation voltage applied to its suppressor grid. Careful screening and location of units was necessary, in order that attenuations of the order of 90 dB could be measured



Fig. 8.—Arrangement of the equipment for measuring the performance of an a.g.c. system.
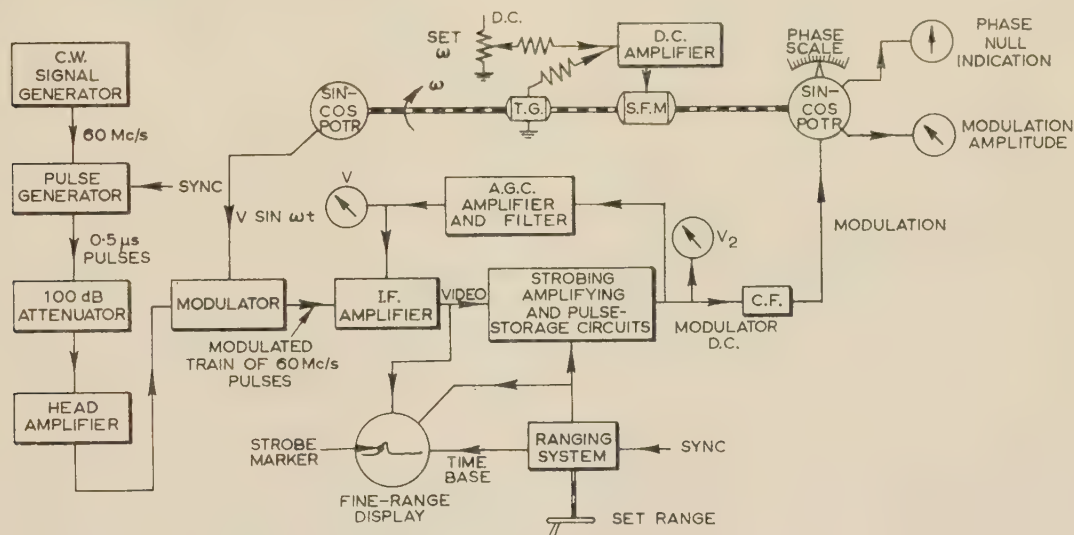
For economic and administrative reasons it was desirable to use as much of the existing equipment as possible, and so reduce the amount of modification to a minimum. Thus the final design became somewhat more complicated than might otherwise have been the case.

The radar in question operates at a nominal repetition rate of 500 c/s (determined by the frequency of the power supply) and has a conical scan frequency of 28 c/s, controlled by an electro-mechanical governor. The receiver consists of a crystal mixer followed by a 2-stage head amplifier, feeding a 5-stage i.f. amplifier, which operates at 60 Mc/s with a 4 Mc/s bandwidth. The first three stages of the main i.f. amplifier are arranged for gain control by variation of their suppressor voltage. The i.f. valves are all type CV1091.

The video-frequency output from the i.f. amplifier is fed to various displays via individual video-frequency amplifiers, and is also fed to an electronic gate, which is opened for 1 microsec by a strobe pulse generated by the ranging system, and occurring at a time corresponding to the range set. The output of this gate is thus the 'wanted' echo only, and is amplified and lengthened in subsequent video stages. The final pulse storage stage consists of a cathode-follower detector, whose cathode load consists of a 2·2-megohm resistor and 0·001 $\mu$F

with reliability. The attenuator actually consisted of a number of pushbutton units in series, so that the whole range could be covered in steps of 1 dB.

With this arrangement, an i.f. pulse of normal width and at some arbitrary 'range' could be injected into the system and strobed in the normal manner. Gain-control characteristics of i.f. amplifiers, and static control characteristics of a.g.c. systems, could then be obtained by varying the attenuator.

Dynamic characteristics could be checked by modulating the echo at varying frequencies.

At each frequency, the sine-cosine potentiometer was rotated to null the phase indicator, after which modulation amplitude and phase could be read off. The zero of the phase scale was set each time with the automatic gain control disconnected and replaced by a manual gain control.

### (7.2) Design Procedure

The first step was to determine a suitable value for the a.g.c. loop gain and devise a method of ensuring that it remained substantially constant for all signal levels above threshold. From consideration of the performance required, a figure of 20 (26 dB) was chosen [eqn. (3)].

It was necessary to retain the existing suppressor-grid control

of the i.f. amplifier, chiefly owing to the fact that the h.t. supplies were not stabilized. It was therefore necessary to include a logarithmic d.c. amplifier in the a.g.c. loop. In order to determine the characteristics required for this amplifier, measurements were made of the control characteristics of six sample i.f. amplifiers. These measurements were taken on pulsed inputs with the normal radar pulse duration of 0·5 microsec, using the equipment depicted in Fig. 8. The output from the pulse storage circuit was brought to a standard level for each measurement, in order to avoid errors due to system non-linearities. From the resultant graphs of gain in decibels against suppressor-grid voltage, values of $dG/dV$ were obtained by drawing tangents. Finally, curves of log $dG/dV$ against $V$ were drawn, and are reproduced in Fig. 9.

Hence, for a loop gain of 20,

$$B\frac{dG}{dV} = \frac{20}{0\cdot115 \times 80} = 2\cdot175 \text{ decibels per volt}$$

The following values were therefore required for $B$, corresponding to the mean values of $dG/dV$:

$B_a = 13\cdot7.$
$B_b = 6\cdot8.$
$B_c = 3\cdot84.$
$B_d = 2\cdot08.$
$B_e = 1\cdot14.$

The feedback arrangement shown in Fig. 5 was chosen, since it
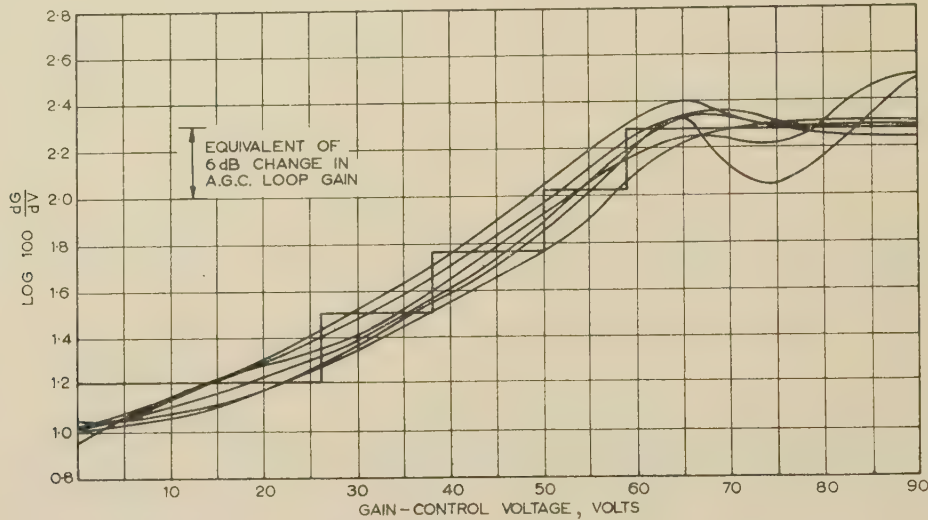


Fig. 9.—Sample i.f. amplifier characteristics, showing 'staircase' approximation.

(It should be noted in connection with work of this nature that simple measurements made with a c.w. signal generator are unlikely to yield sufficiently accurate results, owing to mistuning effects.)

An examination of the log $dG/dV$ curves, coupled with other information regarding the consistency of the suppressor characteristics of the type CV1091 valve, indicated that the maximum error if the mean curve were replaced by a 'staircase' of five sections would be unlikely to exceed 6 dB, but that a greater number of sections would not be justified. A 'staircase' of five sections was accordingly sketched in, giving the following set of values for $dG/dV$:

|     | Range of $V$ | Mean value of $dG/dV$ |
|-----|--------------|------------------------|
|     | volts        | dB/volt                |
| (a) | 0 to −26     | 0·16                   |
| (b) | −26 to −38   | 0·32                   |
| (c) | −38 to −50   | 0·58                   |
| (d) | −50 to −59   | 1·05                   |
| (e) | −59 to −100  | 1·90                   |

From the loop-gain formula [eqn. (4)], we have

$$K = 0\cdot115 \, Bv_2\frac{dG}{dV}$$

For the radar equipment in question, the d.c. output of the pulse storage circuit was 80 volts at a suitable working point.

avoids voltage-handling difficulties and the necessity for preset gain controls. The arrangement of the feedback networks is shown in Fig. 10, from which it can be seen that five feedback
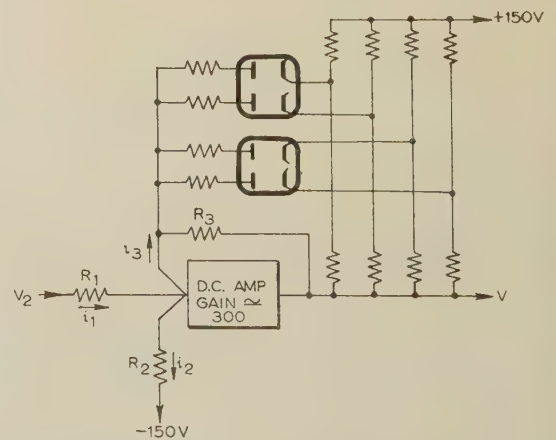


Fig. 10.—Basic curve-fitting amplifier.

networks provide the different values of $B$ required. These feedback paths are switched into circuit at the appropriate values of $V$ by the biased diodes.

Current is fed into the 'virtual earth' presented by the input terminal of the high-gain amplifier in the positive sense from $v_2$

via $R_1$, and in the negative sense via $R_2$ from a stabilized −150-volt supply. When $v_2$ is small, $i_2$ predominates and $V$ would become positive, except that it is prevented from doing so by a diode clamp, not shown. When $i_1 = i_2$, i.e. when $v_2 = 150\ R_1/R_2$, $i_3$ will be zero, and $V$ will be zero. As $v_2$ increases beyond this point, $V$ goes negative, and until the first diode conducts, the gain is given by $B_a = \dfrac{dV}{dv_2} = \dfrac{R_3}{R_1}$.

A convenient nominal value for $R_1$ is $0 \cdot 075$ megohm, giving $R_3 = 0 \cdot 075 \times 13 \cdot 7 = 1 \cdot 0$ megohm approximately. For a 'threshold' of 80 volts, $R_2 = 0 \cdot 14$ megohm. It is, in fact, necessary to be able to vary the threshold setting with this particular radar equipment, which is allowed for by making $R_1$ variable. This allows the threshold setting to be varied without varying the a.g.c. loop gain, since $R_1$ increases proportionally with $v_2$, so that the product $B_a v_2 = R_3 v_2/R_1$ remains constant. (N.B. In a completely new design the threshold would be fixed; there is no essential need for it to be variable, and a fixed setting eliminates one source of variation in the 'stiffness' of the auto-follow loops.)

It is now necessary to compute the values of the three resistors associated with each diode to satisfy simultaneously the following conditions:

    (*a*) The diode shall start to conduct when $V$ reaches the appropriate voltage.
    (*b*) The equivalent resistance of the circuit shall be such that, when placed in parallel with $R_3$ (and the equivalent resistance of diode circuits already conducting) the overall gain has the required value.

The detailed calculations will not be given. The general procedure is given by Burt and Lange[11] and is straightforward if the calculation is done in terms of conductance rather than resistance. Provided that the d.c. amplifier gain is adequate, and the +150 and −150-volt supplies are stabilized, the circuit can be relied on to perform as calculated. Grade 1 5%-tolerance resistors are used.

With regard to the d.c. amplifier itself, a gain of the order of 300 is obtainable with two stages of push-pull double-triode amplification. A cathode-follower output stage provides a low-impedance output for driving the diode feedback network. A diode connected between the cathode-follower grid and earth prevents the output from going more than 2 or 3 volts positive. The amplifier itself was designed to be capable of an output swing from +30 volts to −110 volts, giving a margin of 30 volts either side of the 0 to −80-volt range actually required. By using Grade 1 5% resistors, the need for a balance control is eliminated, and production models can be relied on to produce a given output with a variation in mean input level not exceeding ±0·25 volt. A simplified circuit is given in Fig. 16.

The loop gain round the d.c. amplifier is a maximum when all diodes are conducting, and is high enough for instability to occur, owing to phase shifts produced by the Miller input capacitances of the amplifying stages and other stray capacitances. A 'step' network is therefore included, to reduce the gain sufficiently before these phase shifts become large ($R_{20}$, $C_5$ in Fig. 16).

The steady-state a.g.c. characteristics measured with the final amplifier design are shown in Fig. 11. The gain calculations had, in fact, to be modified before this performance was achieved, owing to the non-linearity of the pulse storage system. Eqn. (4) was derived on the assumption that the overall characteristic is linear, whereas in this case Fig. 11 shows that it has a slope of 0·595. To compensate for this effect, the value of $B$ requires to be multiplied by approximately $(1/0 \cdot 595)^2$, i.e. about 2·8; it was necessary to fall back on experimental measurement, however, before the final adjustments to the calculated values could

be made. Given complete freedom in the design, this non-linearity would have been eliminated.

In Fig. 11, the ratio of the slopes above and below the threshold gives the value of $U$, from which loop gain actually achieved was $K = (1/U) - 1$, i.e. 19 and 17, respectively, for the two threshold levels.
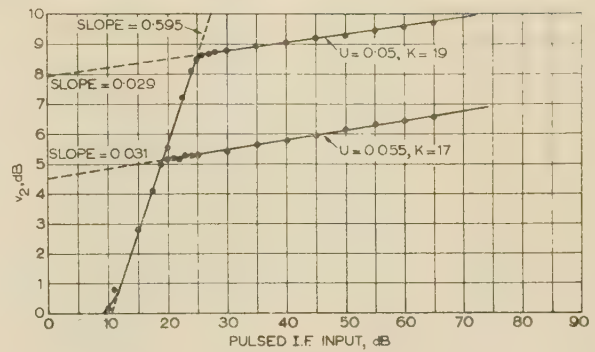


Fig. 11.—Measured static performance of a.g.c. system with two different threshold levels.

### (7.3) Choice of the Filter Network

The problem of network synthesis in this context is best solved by a 'cut and try' process, making use of the Bode type of decibel/log-frequency diagram to minimize the labour involved in sketching the individual response curves of filter sections.

The following typical sections were considered likely to be useful in synthesizing the complete filter:

    (*a*) Simple low-pass $RC$ structure.
    (*b*) Low-pass 'step' network.
    (*c*) 'Notch' network.
    (*d*) Symmetrical twin-T network.

Response curves of these networks are plotted in Figs. 12–15. Since a change in network parameters only requires simple horizontal and/or vertical shifts of the asymptotes, these 'master' curves can be readily used in building-up the complete filter.
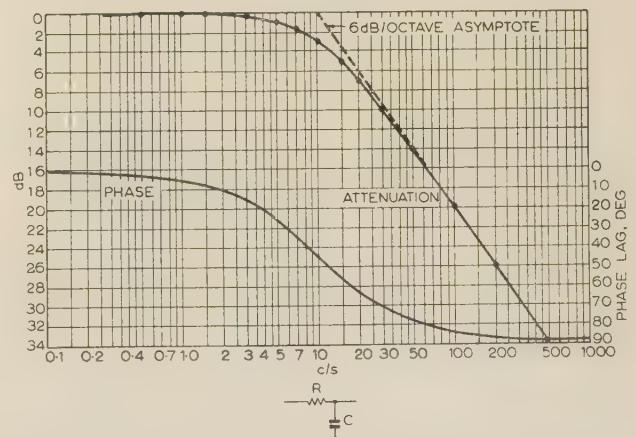


Fig. 12.—Response curves of the simple low-pass $RC$-structure.
$$f_0 = \omega_0/2\pi = 1/2\pi CR = 10\,\text{c/s}.$$
$$CR = 1/(2\pi \times 10) = 1/68 = 0 \cdot 0159\,\text{sec}.$$

As a general guide in arriving at the overall $Y(\omega)$ response in this way, the following principles were followed:

    (*a*) To keep phasing error below acceptable limits, the loop attenuation should be 20 dB at the conical scan frequency of 28 c/s. For a zero-frequency loop gain of 26 dB, this means that the $Y(\omega)$ function must produce an attenuation of 46 dB at 28 c/s.
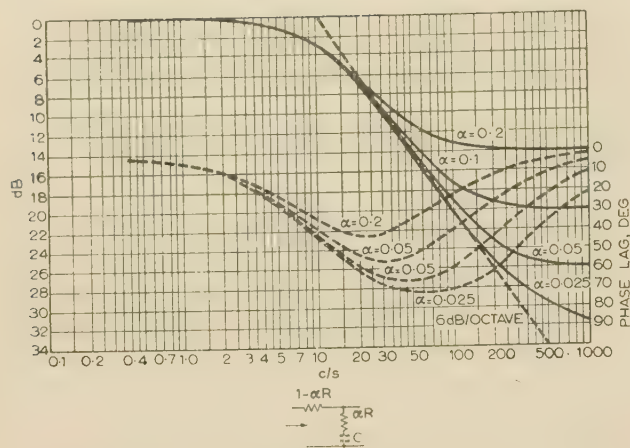
Fig. 13.—Response curves of the low-pass step network.
$$T = CR = 0.015\,9\,\text{sec.}$$
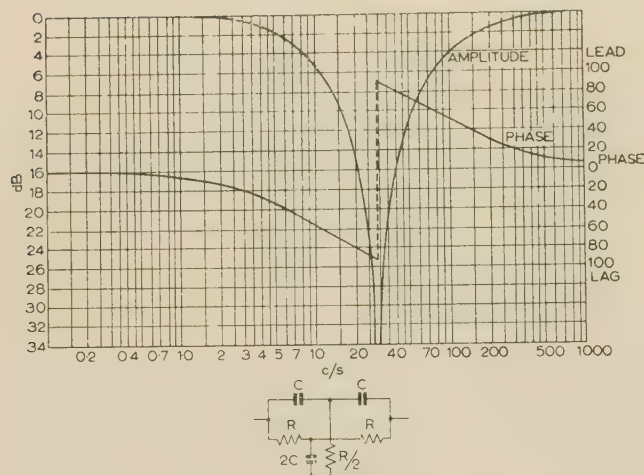$$f_0 = 1/2\pi T = 10\,\text{c/s.}$$



Fig. 14.—Response curves of the twin-T network.
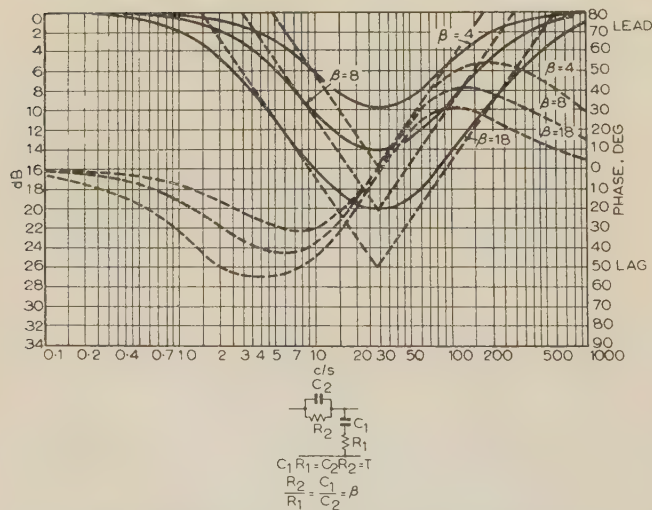$$f_0 = 1/2\pi CR = 28\,\text{c/s.}$$



Fig. 15.—Response curves of the 'notch' network.
$$T = 0.005\,69.$$
$$f_0 = 1/2\pi T = 28\,\text{c/s.}$$
——————— Attenuation.
– – – – – Phase.

(b) The loop attenuation at 250 c/s should not be less than 10 dB, i.e. $Y(\omega) = -36\,\text{dB}$, to avoid oscillation at half the sampling frequency.

(c) The phase margin at low-frequency gain cross-over should be of the order of 50°.

(d) In order to keep the phase margin as high as possible consistent with the maximum rate of cut-off, the attenuation at frequencies above the conical scan frequency should be no greater than necessary.

The last of these requirements strongly suggests the use of a twin-T null network centred on the conical scan frequency. By the use of very stable components and the provision of preset tuning adjustments, the required attenuation could be achieved by this network alone; however, the conical scan frequency would have to be maintained very accurately, and an additional rejection network would be required at 250 c/s to prevent instability. A more realistic approach is to regard the twin-T as a network which can be relied on in production equipment to introduce an attenuation of at least 26 dB over a bandwidth of ±5%, when constructed of randomly-selected Grade 1 components of ±5% tolerance. Production test specifications can then be easily devised to reject the occasional case where an unfavourable combination of tolerances is encountered. The remaining 20 dB of attenuation can now be provided by a low-pass 'step' network.

An alternative to the twin-T is the 'notch' network, of which at least two in tandem are required to achieve the necessary selectivity. The attenuation is under greater control with this arrangement, and the effect of component variations is less. On investigation, however, it was found that the improvement obtainable was only marginal, and in view of the greater number of components required, this solution was rejected in favour of the twin-T.

A further possibility is the inclusion within the loop of a Miller integrator with a resistor in series with the feedback capacitor. This would replace the simple 20 dB step network, and would have the effect of extending the 6 dB per octave slope of the step back to (theoretically) zero frequency; in other words, the system would become a Class 1 or zero-position-error servo mechanism. The advantages of this arrangement appear to be small; in view of its added complication and poorer overload characteristics, it was not considered for the present application.

The final arrangement decided on consisted of a 26 dB 'step' network of time-constant 0·16 sec, followed by a symmetrical twin-T network centred on 28 c/s. Cathode-follower stages were used to isolate the two networks, and to avoid loading the output of the twin-T. The actual arrangement is shown in Fig. 16, $v_2$ being derived from a cathode-follower in the pulse-storage chassis. The mean level of $v_2$ is about 30 volts positive in the absence of a signal, rising to about 120 volts with a signal at saturation level. The 'step' section was put ahead of the twin-T to reduce ripple currents in the first cathode-follower, which might otherwise have produced undesirable interaction effects via the power supply. The combined loop frequency-response characteristic is shown in Fig. 17. The characteristics of the exponential-decay pulse-storage circuit and of a 1 millisec low-pass section are included in this Figure.

### (7.4) Nyquist Diagram

Although the Bode diagram is the most useful during preliminary investigation, it is necessary to construct a Nyquist plot of the loop transmission in order to carry out a final check that the design is satisfactory. The required values can be read off the Bode diagram and transferred to the Nyquist diagram with the aid of tables of decibel equivalents. Having constructed the 'continuous' $Y(\omega)$ plot in this manner, it is then necessary to construct the $\Sigma Y(\omega + n\omega_r)$ plot to obtain the 'sampling servo-
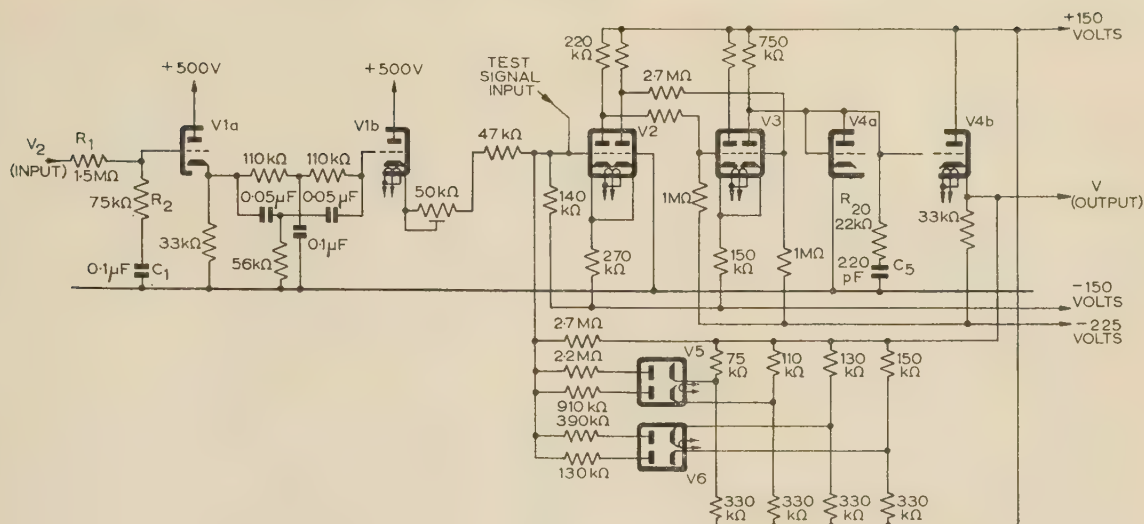
**Fig. 16.**—Simplified circuit diagram of the a.g.c. amplifier.

V1 and V4: Type CV455.    V5 and V6: Type CV140.
V2 and V3: Type CV492.

mechanism' locus, in accordance with Linvill's method (Section 6). This only involves the use of dividers and a parallel ruler, remembering that the vector response to a negative frequency is the complex conjugate of that for the same position frequency. An example of the construction is given in Fig. 20 for a frequency of 100 c/s, from which it is seen that values of $n$ of 0, 1, $-1$, 2 and $-2$ have been taken, corresponding to frequencies of 100, 600, $-400$, 1 100, and $-900$ c/s. In fact, the first three terms give a sufficiently accurate result.

With the 'sampled' locus sketched in, it is now possible to evaluate the performance of the system. Referring to Fig. 19, it is seen that a circle centred on the point $(-1, j0)$ just touches the locus at a point corresponding to 15 c/s when its radius is 0·71. This shows that the peak magnification is 1·4 at a frequency of 15 c/s. Owing to the fairly constant phase in this region, the peak magnification changes slowly with variation in loop gain—for example, if the loop gain is doubled, the peak magnification becomes 1·65 at 20 c/s.

An interesting point made evident in Figs. 19 and 20 is the fact that the loop gain is no longer zero at 28 c/s, in consequence of the sampling process. It has a value of about $-0·1$, so that the loop magnification has a value of 1·11 at this frequency, i.e. conical scan modulation is increased 11 % by the presence of the a.g.c. system. This was checked experimentally by switching the i.f. amplifier gain-control lead from a hand-controlled gain potentiometer to the output of the a.g.c. amplifier, when it was found that the modulation rose by the order of the predicted amount.

The loop transmission at 250 c/s is $-0·215$, indicating that the loop gain must increase by a factor of 4·65 or 13 dB for instability to occur at half the sampling frequency. This was checked experimentally by altering the attenuation of the 26 dB step network until oscillation was observed. This was also found to be a fairly reliable way of carrying out a quick check of loop gain variation over the working range of the system. The appearance of the fine range display when the system is oscillating at half the sampling frequency is shown in Fig. 21.

It will be noted from Fig. 20 that the relatively large margin of stability at half the sampling frequency is due to the fact that the 'continuous' phase shift at 250 c/s is not much greater than 90°. This suggests that, if the phase could be advanced to less
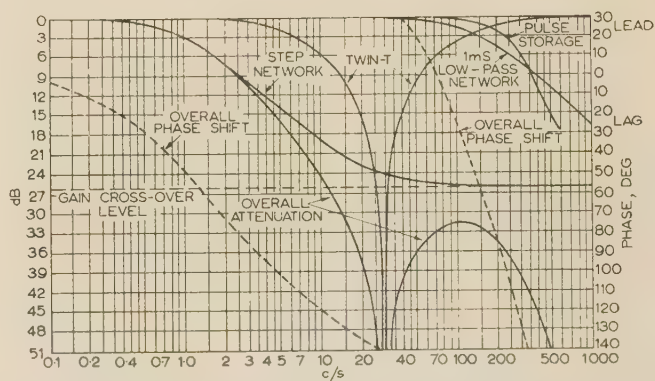


**Fig. 17.**—Overall attenuation and phase characteristics of a.g.c. loop.
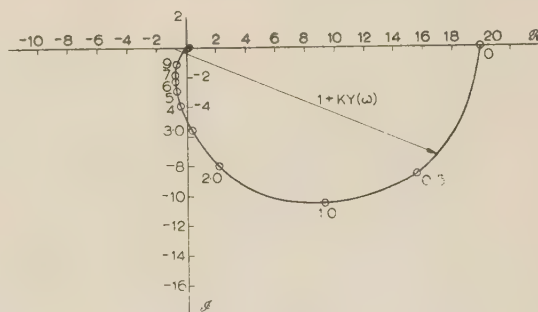


**Fig.**          of $KY(\omega)$ between 0 and 9 c/s.

than 90°, a sampling servo-mechanism could be made stable even if the gain at this frequency exceeded unity.

**(7.5) Overall System Frequency-Response Characteristic**

By drawing vectors from the $(-1, j0)$ point to the 'sampled' Nyquist locus, the vectors $1 + K\sum Y(\omega + n\omega_r)$ can be read off, and their reciprocals plotted in terms of amplitude and phase shift against a logarithmic frequency scale. The resultant
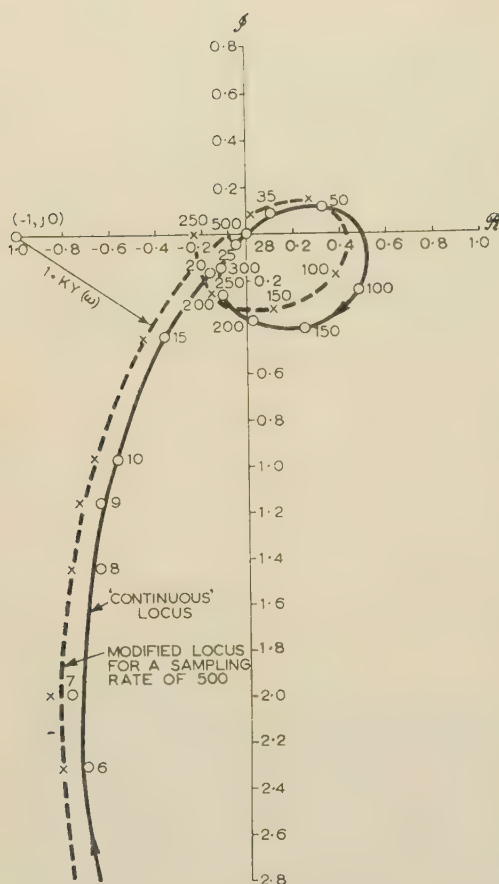
Fig. 19.—Locus of $KY(\omega)$ between 6 and 500 c/s.
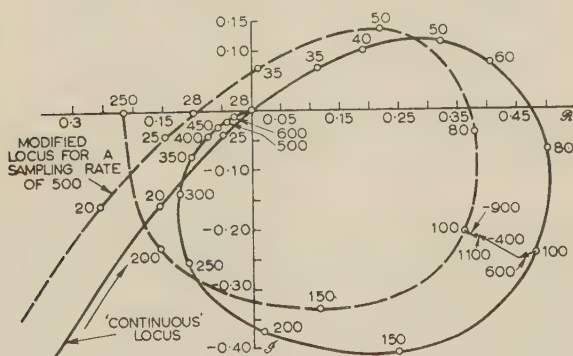


Fig. 20.—Locus of $KY(\omega)$ above 20 c/s.



Fig. 21.—Appearance of display when a.g.c. system is oscillating at half the repetition frequency.

characteristic shows the effect of the a.g.c. system on modulation at various frequencies, and is illustrated in Fig. 22.

It is seen from this characteristic that fading is suppressed by a factor of about 20 up to 1 c/s, and by a factor of 2 at 7 c/s.
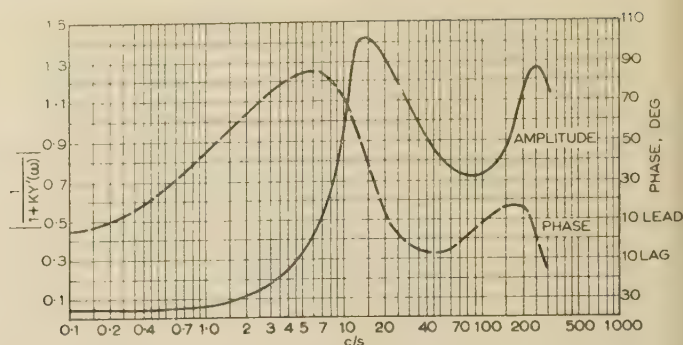


Fig. 22.—Overall frequency response of a.g.c. system.

The phasing error in the vicinity of the conical scan frequency is well within the required limits, and the peak magnification at 15 c/s is such that the response to a step function would show an overshoot of about 40% followed by one undershoot. The peak at 250 c/s indicates the tendency for a damped sawtooth oscillation at half the sampling frequency to follow the application of a step function, as is normal with sampling servo mechanisms.

This characteristic was checked experimentally at frequencies between 0·5 and 40 c/s with the equipment shown in Fig. 8, and satisfactory confirmation of the design calculations was obtained.

### (7.6) Provision of Test Facilities

In connection with the design of electronic equipment for the naval service, it is axiomatic that means shall be provided for enabling maintenance personnel to check that the equipment is, in fact, operating in accordance with the designer's intentions. In view of the limited maintenance effort available, the provision of built-in monitoring or testing equipment can with advantage be carried to an extent considerably beyond what might be considered economic under different conditions.

An appraisal of the problem indicated that, apart from obvious catastrophic failures, the a.g.c. system could be reasonably relied on to be working properly provided that the logarithmic d.c. amplifier could be shown to be operating correctly, and provided that no component in the filter network had developed an open-circuit.

On this basis, the test unit illustrated in Fig. 23 was designed for fitting on the front panel of the radar equipment. In normal operation, $v_2$ and $V$ are measured by the voltmeters, thus providing a rough check that the system is working whenever a target echo is within the strobe. In the case of complete failure, the voltmeters will indicate which major unit has failed (e.g. strobing circuits, a.g.c. amplifier or i.f. amplifier).

With the switch in position 2, $v_2$ is disconnected from the input to the a.g.c. amplifier and replaced by a variable voltage obtained from $RV_1$. This enables the threshold voltage to be checked.

With the switch in position 3, the voltage from $RV_1$ remains connected to the a.g.c. amplifier input, but a voltage from $RV_2$ is now connected via $R_4$ to the virtual earth of the logarithmic d.c. amplifier. The meter $M_1$ is also switched to read this voltage. The method of carrying out the test is as follows:

(a) Set $RV_2$ to zero.
(b) Set $RV_1$ to the threshold, as shown by $M_2$ just beginning to move.
(c) Adjust $RV_2$ to give the series of readings of $M_1$ specified in the instruction manual, and note the corresponding readings of $M_2$. Switch to position 4 as necessary.

In this way, the input/output curve is checked at selected points, so that, for example, the failure of one of the diodes
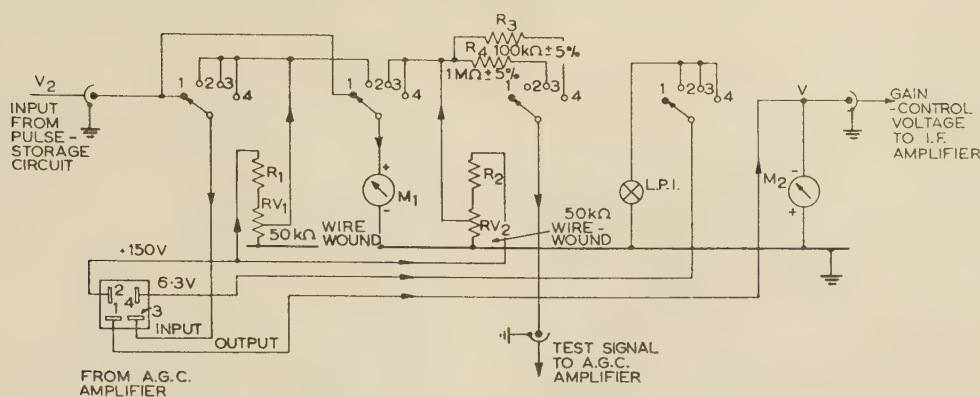
**Fig. 23.—A.G.C. test unit.**

*Voltmeter labels.*
M₁: Signal amplitude.
M₂: A.G.C. voltage.

*Switch positions.*
1. Normal.
2. Check threshold.
3. Inject test signal.
4. Inject test signal × 10.

R₁: 15 kΩ.
R₂: 15 kΩ.
R₃: 100 kΩ ± 5%.
R₄: 1 MΩ ± 5%.
RV₁: 50 kΩ (wire wound).
RV₂: 50 kΩ (wire wound).

M₁: 0–100 volts, 1 kΩ/volt, 2½ in.
M₂: 0–100 volts, 1 kΩ/volt, 2½ in.

would be detected. By feeding current into the virtual earth in this manner, readings are rendered independent of the setting of the a.g.c. amplifier threshold control.

Although the above test practically guarantees that the static performance of the system will be sufficiently close to the design figures, there remains the possibility of some derangement of the filter characteristics. However, a fairly good check can be made if a suitable fixed target echo can be found. If, for example, $R_2$ or $C_1$ became open-circuited, the system would oscillate at half the repetition frequency as soon as the strobe was moved over the echo. If a fault occurred in the twin-T network, there would be a large change in the misalignment outputs to the lateral and vertical auto-follow channels if the test unit were switched from 'normal' to position 4, and adjusted to give the same echo amplitude.

### (8) OPERATIONAL TRIALS

Prototype models of the a.g.c. amplifier and test unit described in the preceding Section were fitted to an operational radar system during a series of auto-follow tracking trials.

Arrangements were made so that the original slow-response a.g.c. system could be switched in, thus facilitating a comparison of the two under actual working conditions. Although the trials were far from exhaustive, there was every indication that the expected improvement in the range display, and consequent improvement in ranging accuracy, was in fact obtained; nevertheless, this improvement was small in the case of propeller-driven aircraft, being largely masked by high-frequency flutter and propeller modulation. The steady-state accuracy of regulation was greatly improved.

With respect to auto-aiming accuracy, no improvement could be detected as a result of the greater suppression of low-frequency fading; this would seem to indicate that cross-modulation noise at the conical scan frequency was negligible in comparison with the direct contribution from the fading spectrum, in spite of the non-linearity of the system characteristic. However, the trials were not very extensive, and this negative result can, at present, only be interpreted rather cautiously as evidence that cross-

modulation noise does not make a large contribution to jitter in aim.

One very important result was, however, obtained from the records of auto-aiming performance. This was the observation that a significant disturbance was injected into the auto-aiming system each time the echo amplitude crossed the a.g.c. threshold. During a typical run this would occur three or four times, owing to exceptionally deep fades; the resulting increase in the standard deviation of aim over the whole run often amounted to as much as 25%.

This was regarded as serious, and was checked with the simulator equipment shown in Fig. 8 by applying slow sinusoidal 'fading' modulation to the modulator, while allowing the velodyne to run at the conical scan frequency. In this way it was confirmed that a transient was produced in the auto-aiming channels each time the echo amplitude crossed the threshold. The effect can be explained in terms of the severe distortion of the fading modulation under these conditions, which can be regarded as equivalent to the generation of a whole series of higher harmonics of considerable amplitude. Some of these harmonics fall in the conical scan frequency band, and consequently produce spurious misalignment signals.

The effect can be reduced to negligible proportions by slowing down the rate of response of the a.g.c. system, or by 'rounding off' the knee of the characteristic so that the transition from the non-regulating to the fully-regulating region is made more gradual. Either expedient involves a considerable sacrifice in performance, and the correct approach is undoubtedly to arrange for the receiver noise level to be of sufficient amplitude to operate the a.g.c. system at all times, so that the a.g.c. loop remains closed even during a complete fade-out of the echo.

### (9) CONCLUSIONS

The design of a.g.c. systems for pulsed radar receivers has been shown to involve an interesting combination of the methods of pulse techniques, closed-loop regulators, electronic function-generators and sampling servo mechanisms. The particular example given represents a fairly difficult case, owing to the fact

that the repetition frequency is only about four octaves above the conical scan frequency.

The design of fast-acting automatic-frequency-control systems for pulsed radar receivers is an analogous problem, which can be approached in a similar manner.

The same general approach is, of course, applicable to c.w. systems, where the complications due to sampling do not arise. Alternatively, in the case of a range-only pulsed radar, the restriction due to the necessity for reproducing a band of modulation frequencies without distortion does not exist. In a television receiving system where automatic gain control is based on the amplitude of gated line synchronizing pulses, very rapid response can be achieved with simple circuits. However, care must be taken to avoid a significant change in output between sampling instants, otherwise the picture will suffer from left-to-right 'shading'.

## (10) ACKNOWLEDGMENTS

## (11) REFERENCES

(1) CRONEY, J.: 'A Simple Logarithmic Receiver', *Proceedings of the Institute of Radio Engineers*, 1951, **39**, p. 807.

(2) ROZENSTEIN, S.: 'Design of a Logarithmic Receiver', *Proceedings I.E.E.*, Paper No. 1733 R, January, 1955 (**102 B**, p. 69).

(3) OLIVER, B. M.: 'Automatic Volume Control as a Feedback Problem', *Proceedings of the Institute of Radio Engineers*, April, 1948.

(4) VAN VOORHIS, S. N. (Edit.): 'Microwave Receivers' (McGraw-Hill, New York, 1948), Chap. 5.

(5) BODE, H. W.: 'Network Analysis and Feedback—Amplifier Design' (Van Nostrand, New York, 1945).

(6) HUREWICZ, W.: 'Theory of Servo-Mechanisms' (McGraw-Hill, New York, 1947), Chap. 5.

(7) MACCOLL, L. A.: 'Fundamental Theory of Servo-mechanisms' (Van Nostrand, New York, 1945).

(8) BARKER, R. H.: 'The Pulse Transfer Function and its application to Sampling Servo Systems', *Proceedings I.E.E.*, Monograph No. 43, July, 1952 (**99**, Part IV, p. 302).

(9) McDONNEL, D., and PERKINS, W. R.: 'The Stability and Time Response of Fast-Operating Closed-Loop Pulsed Radar Circuits', *ibid.*, Monograph No. 121 R, March, 1955 (**102 C**, p. 191).

(10) LINVILL, W. K.: 'Sampled-Data Control Systems studied through Comparison of Sampling with Amplitude Modulation', *Transactions of the American I.E.E.*, 1951, **70**, p. 1779.

(11) BURT, E. G. C., and LANGE, O. H.: 'Function Generators based on Linear Interpolation with Applications to Analogue Computing', *Proceedings I.E.E.*, Monograph No. 137 M, June, 1955 (**103 C**, p. 51).

# A CONTRIBUTION TO THE THEORY OF PROBES IN WAVEGUIDES

## By L. LEWIN, Associate Member.

### SUMMARY

An account is given of some of the difficulties which beset the calculation of the impedance of the finite-size probe in a waveguide. In the particular case of a probe completely spanning a rectangular guide and fed by a coaxial line, a solution is set up in which the line is represented by an arbitrary loading impedance terminating the probe. An integral equation for the current in the probe is solved by a Fourier series in the waveguide modes, and an approximate summation of the double series involved is achieved using Poisson's formula. An expression is derived for the probe impedance from which an equivalent circuit with determinate parameters is obtained. The quasi-static antenna solution is derived as a limiting case for small probe radius, and an interpretation is attempted of the physical significance of the individual terms in the expression for the inductance of an inductive post in waveguide. This is a particular case of the probe for which the solution is well known but for which the meaning of the formula is not too clear.

## (1) INTRODUCTION

Recent years have seen the mathematical solution of a wide range of waveguide problems, including junctions, obstacles of various kinds, steps and other discontinuities, bends and twists, radiation from open ends and propagation in loaded or imperfect waveguide, to mention but a few. In most cases the problem has been formulated exactly and the mathematical solution has been either a rigorous one or has involved approximations of known type, e.g. the expansion in terms of a small parameter as in perturbation theory, or variational solutions in which only a second-order error appears as a result of first-order approximations made earlier. In contrast, problems involving coupling into a waveguide through a probe have been solved only in the case in which the probe is very small. This type of problem includes coaxial-line-to-waveguide coupling, either via an aerial or with a crossbar transducer, crystal pick-up probes, various types of waveguide-to-waveguide coupling, and many others. In general, it is not permissible to assume that the probe is small, and it may well be a quarter of a wavelength long or more. Under these circumstances, both the formulation of the problem and its solution become extremely difficult; the paper discusses the difficulties and presents in one particular case a solution which may help to indicate the way forward.

## (2) CONNECTION WITH SOME RELATED STRUCTURES

The configuration examined is shown in Fig. 1. A coaxial cable of impedance $Z_c$ feeds into a waveguide of cross-section $a \times b$ through a probe of radius $r$ and distance $d$ from the side wall, the probe being short-circuited at the far end. Alternatively, the waveguide may be considered as feeding via the probe into the cable. It does not matter which way the problem is tackled, and if the target of specifying an equivalent circuit with determinate parameters is achieved, the configuration may be used any way round that may be of use.

As seen from the cable, the probe represents a top-short-circuited aerial feeding into an enclosed structure, whose effects
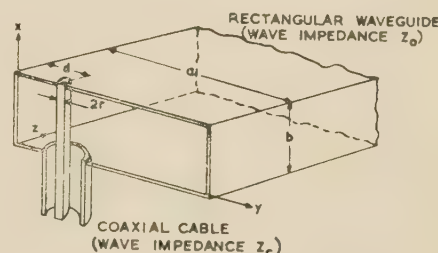


Fig. 1.—Half-section of waveguide and cable-fed top-short-circuited probe.

can be represented by a doubly infinite series of images whose mutual coupling with the aerial determines its input impedance. The association here is with ordinary aerial theory, but complicated by the mutual coupling. One can expect to meet all the problems of this theory, including the reactance effect which appears when the feed gap is improperly treated, and the difficulties which arise in solving the integral equation for the current. It is probably impossible to consider in any detail the hole in the waveguide wall at the entrance to the cable, with its effect on the multiple series of images; yet if the hole is ignored completely the cable becomes short-circuited.

A somewhat different aspect arises if we consider the probe from the point of view of the waveguide. First, take the simple case in which the cable is short-circuited. The probe is then just an inductive stub across the guide, for which the solution, in the main, is known.[1] If the cable is open-circuited the probe becomes a tuned post in the waveguide, and in this case, too, a partial solution is known.[1] This suggests that the problem be treated as that of a waveguide post terminated at one end by the cable impedance as shown diagrammatically in Fig. 2.
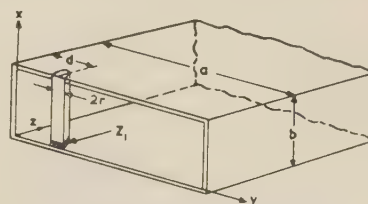


Fig. 2.—Half-section of waveguide and probe, terminated at $x = 0$ with an impedance, $Z_1$, representing the cable.

In the treatment of this configuration we must expect to meet, in addition to the points already mentioned, the aspects that arise in the treatment of the tuned post and the inductive stub. We will now consider the latter in a little more detail.

When an electromagnetic field is incident on a metal stub in a waveguide, surface currents are set up in the stub of such a nature as to cancel at the surface and interior of the stub the incident electric field. These currents radiate into the waveguide and are responsible for the reflected wave. When the stub radius is small, there is no appreciable phase change of the incident wave across the stub, and hence the effect of the surface

currents will be in phase all round the stub. Now a fictitious current filament at the centre of the stub would produce just such a field. Hence, so far as effects external to the stub are concerned, we can assume a current filament at the centre of the stub and of such amplitude as to cancel at the stub surface the incident field: the radiation from this filament then gives the disturbance in the waveguide due to the stub.

When the stub crosses the waveguide completely and the incident wave is in the dominant mode, there is no field variation across the waveguide. Accordingly, we take the current filament also to be constant. The radiation from such a current filament constitutes a straightforward problem and the solution is relatively simple. By utilizing, in addition, filamentous current dipoles and quadruples, it is possible in a similar way to produce a variation of the field round the stub surface of just such a form as to simulate the variation of the incident field when the stub radius is not so small as to give negligible phase change across it. In this way an exact solution can be built up, although the process becomes very complicated for the higher-order solutions.

When the stub does not cross the waveguide completely, the constancy of the field pattern across the guide is spoilt and it is no longer possible to take the current as constant. In fact, it must be zero at the open end, increasing approximately sinusoidally along the post, with a period given by the free-space wavelength. This last result follows from an application of transmission-line theory, which may be considered approximately valid, at least for very small post radii. The non-constant current gives rise to a complete set of modes, so that this problem involves a doubly infinite series of terms whose manipulation constitutes an appreciable part of the solution. There seems no question here of being able to go to higher-order solutions, so the stub radius must be presumed to be quite small. However, in this case the question of variation of field over the stub surface cannot be overlooked. Since the field pattern consists of a complete set of modes, an order of mode will exist for which the variation period across the waveguide is comparable to the post radius. From this point onward the higher-order mode terms cannot be significant, since they take into account an order of variation which has already been ignored elsewhere in the problem. Provided that the solution is sufficiently rapidly convergent, the modes beyond this point will contribute negligibly and their retention is irrelevant. But if for any reason the solution is not converging rapidly here, the higher modes must be discarded, although there may be no unique method of doing this. The justification for this procedure lies in the effects which must be presumed to arise from the hitherto ignored variation of field round the stub, and which would have to be investigated in detail if a more exact solution were required. This question of convergence is considered in more detail later.

In the case of the tuned stub the equivalent circuit will still represent a reactance across the waveguide. Hence the current along the stub will be co-phased, and although its exact form may not be known, a variational solution using a sinusoidal variation should be adequate. However, when the stub is to be terminated in a cable whose impedance may contain a resistive element, there will be a power flow along the stub and energy will be taken from the waveguide. A simple sinusoidal current distribution, which is essentially reactive, is now no longer adequate: a quadrature component is necessary, and the form for this can be found only through the use of the integral equation of aerial theory, as modified for a waveguide environment. It is apparent that the difficulties inherent in several different problems are here mounting up together, and this is, no doubt, one of the main reasons why the probe problems have proved so intractable. We shall now show, in the particular case of a probe across the waveguide, how an explicit solution of the aerial equation may

be found, and with its help the equivalent circuit and impedance parameters will be deduced.

### (3) THE TERMINATED PROBE

Fig. 2 shows a probe spanning the waveguide, with an impedance $Z_1$ at one end; this represents the input impedance of the cable, but is considered here as a small region of the probe having the property of causing a voltage drop $Z_1 I$ when a current $I$ flows at the end of the probe. Using Dirac's $\delta$-function, the corresponding electric field at the surface is therefore $E = Z_1 \delta(x)$, since this integrates to give a voltage $Z_1 I$. Accordingly, an incident field $E_{in} = \varepsilon^{-jk'z} \sin(\pi y/a)$ in the waveguide will cause currents to flow in the stub such that the field at the stub surface is $Z_1 \delta(x)$, this being zero everywhere except at $x = 0$, where it gives the correct voltage drop at $Z_1$. As before, when the stub radius is small enough, we can consider a fictitious filamentary current, $I$, in the stub of such a form and amplitude as to give rise to the necessary field.

Now the electric field produced by a current filament located at $y = d$ is[1]

$$E_x = \sum_{n=1}^{\infty} \sum_{m=0}^{\infty} (-j240\pi/k\Gamma_{mn}ab)$$
$$\epsilon_m \sin(n\pi y/a) \sin(n\pi d/a) \exp(-\Gamma_{mn}|z|)$$
$$\times (k^2 - m^2\pi^2/b^2) \cos(m\pi x/b) \int_0^b I(\xi) \cos(m\pi\xi/b)d\xi \quad . \quad (1)$$

where $$k = 2\pi/\lambda, \; k' = 2\pi/\lambda_g,$$
$$\Gamma_{mn} = (m^2\pi^2/b^2 + n^2\pi^2/a^2 - k^2)^{1/2} \quad \text{and} \quad \Gamma_{01} = jk'$$

If we put $z = 0$ and take $y = d \pm r$, this gives the field at the post due to the current. If to this be added the incident field, the resultant is to equal $Z_1 I\delta(x)$. This determines the following integral equation for the, as yet, unknown current:

$$\sin(\pi d/a) + \sum_{n=1}^{\infty} \sum_{m=0}^{\infty} \left(\frac{-j240\pi}{kab}\right)$$
$$\frac{\epsilon_m(k^2 - m^2\pi^2/b^2)}{\Gamma_{mn}} \sin\left(\frac{n\pi d}{a}\right) \sin\left[\frac{n\pi(d \pm r)}{a}\right] \cos\left(\frac{m\pi x}{b}\right)$$
$$\times \int_0^b I(\xi) \cos\left(\frac{m\pi\xi}{b}\right) dx = IZ_1 \delta(x) \quad . \quad . \quad . \quad . \quad (2)$$

Since $r$ is assumed to be small it is convenient later to ignore it, except in terms where its omission could cause divergence.

We note from eqn. (1) that the reflected wave ($m = 0$, $n = 1$) is given by

$$R = \frac{-j120\pi k}{ab} \frac{\sin(\pi d/a)}{jk'} \int_0^b I(\xi)d\xi \quad . \quad . \quad . \quad (3)$$

In order to obtain a variational expression for the impedance of the stub as presented to the waveguide, multiply eqn. (1) by $I(x)$ and integrate, and then divide through by $J^2$ where $J = \int_0^b I(x)dx$. This gives

$$\frac{\sin(\pi d/a)}{J} + \sum_{n=1}^{\infty} \sum_{m=0}^{\infty} \left(\frac{-j240\pi}{kab}\right)$$
$$\frac{\epsilon_m(k^2 - m^2\pi^2/b^2)}{\Gamma_{mn}} \sin\left(\frac{n\pi d}{a}\right) \sin\left[\frac{n\pi(d \pm r)}{a}\right]$$
$$\times \left[\int_0^b I(\xi) \cos(m\pi\xi/b)d\xi/J\right]^2 = \frac{I^2(0)Z_1}{J^2} \quad . \quad . \quad . \quad (4)$$

If we separate from the summation the term with $m = 0$, $n = 1$ (using a prime on the summation symbol to indicate the future omission of this term) and utilize eqn. (3) to eliminate $J$ from the initial term in eqn. (4), the first terms become simply

$$\frac{\sin(\pi d/a)}{J} - \frac{120\pi k}{k'ab}\sin^2(\pi d/a) = \frac{-j120\pi k}{abjk'}\sin^2(\pi d/a)\frac{1+R}{R}$$

$$\cdots \quad (5)$$

Now if the post acts as an impedance $Z$ across a waveguide of wave impedance $Z_0$, then $ZZ_0/(Z + Z_0) = (1 + R)/(1 - R)$, giving $Z/Z_0 = -(1 + R)/2R$—the form appearing in eqn. (5). Hence we can return to eqn. (4) and separate out the post impedance, thus obtaining

$$Z = \text{cosec}^2(\pi d/a)\left\{\frac{I^2(0)Z_1}{(J/b)^2} + jZ_0\sum_{n=1}^{\infty}\sum_{m=0}^{\infty}{}'\frac{k'(k^2 - m^2\pi^2/b^2)}{k^2\Gamma_{mn}}\epsilon_m\right.$$

$$\left.\times \sin\left(\frac{n\pi d}{a}\right)\sin\left[\frac{n\pi(d \pm r)}{a}\right]\left[\int_0^b I(\xi)\cos(m\pi\xi/b)d\xi/J\right]^2\right\}$$

$$\cdots \quad (6)$$

In this equation it has been convenient to define the waveguide wave impedance $Z_0$ by the relation

$$Z_0 = 240\pi(b/a)(\lambda_g/\lambda) \quad \cdots \quad (7)$$

which is consistent with the power-flow equation $P = V^2/Z_0$, where $V$ is the r.m.s. voltage across the waveguide centre.

It is readily verified[1] that eqn. (6) is in variational form, i.e. if the current departs from that implied by eqn. (2) by a first-order quantity, the impedance defined by eqn. (6) will differ from the correct impedance by a second-order quantity.

Before proceeding it is desirable to examine in closer detail the form of eqn. (2). Let us define a quantity $X_m(m > 0)$ by the equation

$$\sum_{n=1}^{\infty}\left(\frac{240\pi}{kab}\right)\frac{(m^2\pi^2/b^2 - k^2)}{\Gamma_{mn}}\sin\left(\frac{n\pi d}{a}\right)\sin\left[\frac{n\pi(d \pm r)}{a}\right] = 4X_m/b^2$$

$$\cdots \quad (8)$$

$X_m$ is closely related to the impedance of a short-circuited post as seen by the waveguide working in the $m$th mode (which is assumed to be evanescent).

Although the summation in eqn. (8) cannot be performed exactly, Poisson's formula[1] can be used to express it as a series of modified Bessel functions $K_0$. The arguments of these functions, which decay approximately exponentially, are all large, except the first, and it is easily verified numerically that only the first term need be retained to obtain an excellent agreement. The only exception to this statement is when the spacing $d$ of the post from the wall is so small as to be comparable with $r$, in which case a further term may be retained. The approximate summation is used in the form

$$\sum_{n=1}^{\infty}\frac{\cos(n\pi r/a) - \cos(2n\pi d/a)}{\Gamma_{mn}} = (a/\pi)[K_0(r\Gamma_m) - K_0(2d\Gamma_m)]$$

$$\cdots \quad (9)$$

where $\Gamma_m = (m^2\pi^2/b^2 - k^2)^{1/2}$. Eqn. (8) can now be replaced by

$$X_m = (30b/k)\Gamma_m^2[K_0(r\Gamma_m) - K_0(2d\Gamma_m)] \quad \cdots \quad (10)$$

This method fails when $m = 0$ because $\Gamma_m$ is imaginary, leading to a series of Hankel functions which do not decay rapidly. From eqn. (2) in this case the relevant terms (omitting the $n = 1$, $m = 0$ term, which is treated separately) are

$$\frac{-j120\pi k}{ab}\sum_{2}^{\infty}\frac{\sin\left(\frac{n\pi d}{a}\right)\sin\left[\frac{n\pi(d \pm r)}{a}\right]}{(n^2\pi^2/a^2 - k^2)^{1/2}} \quad \cdots \quad (11)$$

Now the equation for the reactance, $X_0$, of a short-circuited post in a waveguide gives[1]

$$X_0/Z_0 = (k'/4)\text{cosec}^2(\pi d/a)\sum_{2}^{\infty}\frac{\cos(n\pi r/a) - \cos(n\pi 2d/a)}{(n^2\pi^2/a^2 - k^2)^{1/2}} \cdot \quad (12)$$

and on comparison with eqn. (11) we get simply $-jX_0\sin^2(\pi d/a)/b^2$ for the $m = 0$ terms. [Eqn. (7) has been used for $Z_0$ and approximations involving small $r$ have been made.]

Eqn. (2) can now be written

$$\sin(\pi d/a) + B\int_0^b I(\xi)d\xi + b^{-2}\sum_1^{\infty}4jX_m\cos(m\pi x/b)$$

$$\int_0^b I(\xi)\cos(m\pi\xi/b)d\xi = IZ_1\delta(x) \quad \cdot \quad (13)$$

where $B = -\sin^2(\pi d/a)(\frac{1}{2}Z_0 + jX_0)/b^2$

In order to solve this equation, put

$$I(x) = A_0 + 2\sum_1^{\infty}A_n\cos(n\pi x/b)$$

Since the cosines are orthogonal over the range $0 < x < b$, eqn. (13) becomes

$$\sin(\pi d/a) + bBA_0 + \frac{4}{b^2}\sum_1^{\infty}jX_mbA_m\cos(m\pi x/b) = IZ_1\delta(x) \cdot (14)$$

Integrate with respect to $x$ from 0 to $b$, giving

$$b[bBA_0 + \sin(\pi d/a)] = I(0)Z_1 \quad \cdots \quad (15)$$

Multiply eqn. (14) by $\cos(n\pi x/b)$ and integrate from 0 to $b$, giving

$$2jX_nA_n = I(0)Z_1 \quad \cdots \quad (16)$$

From eqn. (16), $\quad A_n = \frac{1}{2}I(0)Z_1/jX_n \quad \cdots \quad (17)$

Since $I(0) = A_0 + 2\sum_1^{\infty}A_n$, we get

$$I(0) = \frac{I(0)Z_1}{b^2B} - \frac{\sin(\pi d/a)}{bB} + I(0)Z_1\sum_1^{\infty}1/jX_n \quad \cdot \quad (18)$$

This may be solved for $I(0)$:

$$I(0) = \frac{(b/B)\sin(\pi d/a)}{(Z_1/B) - b^2 + Z_1b^2\sum_1^{\infty}1/jX_n} \quad \cdot \quad (19)$$

Accordingly, the expression for $I(x)$ is

$$I(x) = \frac{b\sin(\pi d/a)}{BD}\left[1 - Z_1\sum_1^{\infty}\frac{1 - \cos(n\pi x/b)}{jX_n}\right] \cdot \quad (20)$$

where $D = (Z_1/B) - b^2 + Z_1\sum_1^{\infty}1/jX_n$

The quantity $J$ appearing in eqn. (6) is $\int_0^b I(x)dx$, whence

$$J = \frac{b^2\sin(\pi d/a)\left(1 - Z_1\sum_1^{\infty}1/jX_n\right)}{BD} \cdot \quad (21)$$

and $\quad [bI(0)/J]^2 = \left(1 - Z_1\sum_1^{\infty}1/jX_n\right)^{-2} \quad \cdots \quad (22)$

Similarly,

$$\left[\int_0^b I(x)\cos(m\pi x/b)dx/J\right]^2$$
$$= (bA_m/J)^2 = (Z_1/2jX_m)^2 \Big/ \left(1 - Z_1 \sum_1^\infty 1/jX_m\right)^2$$

and on substituting in eqn. (6) we get finally

$$Z = jX_0 + \operatorname{cosec}^2(\pi d/a) \Big/ \left(1/Z_1 - \sum_1^\infty 1/jX_m\right) \quad . \quad (23)$$

This formula leads to the equivalent circuit shown in Fig. 3, in which the waveguide is presented with a reactance $jX_0$ feeding
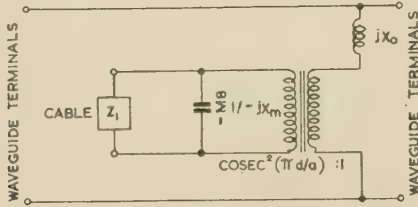


Fig. 3.—Equivalent circuit of waveguide and post shown in Fig. 2.

$$X_0 = Z_0\frac{a}{2\lambda_g}\left\{\operatorname{cosec}^2\frac{\pi d}{a}\left[\log\left(\frac{2a}{\pi r}\sin\frac{\pi d}{a}\right) + s\right] - 2\right\}$$

where $s$ is a small correction term.
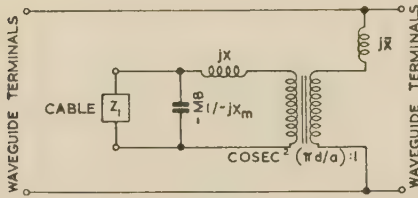


Fig. 4.—Preferred equivalent circuit of waveguide and terminated post.

$$\overline{X} = -2Z_0\frac{a}{2\lambda_g}$$

$$X = Z_0\frac{a}{2\lambda_g}\left[\log\left(\frac{2a}{\pi r}\sin\frac{\pi d}{a}\right) + s\right]$$

into a transformer of turns ratio $n = \operatorname{cosec}(\pi d/a)$ and with impedances $Z_1$ (representing the cable input) and all the $-jX_m$ in parallel at the secondary. An alternative form is shown in Fig. 4, in which the post reactance $jX_0$ is divided into a constant part and a part varying as $\operatorname{cosec}^2(\pi d/a)$, the latter being represented at the secondary of the transformer. This second part is recognizable as simply the inductance of a post of radius $r$ in a casing of mean radius approximately $2a/\pi$, a value which physically seems quite reasonable. No such simple explanation has been found for the constant part, which represents a negative inductance, and whose interpretation arises primarily from attempting to represent the simple short-circuited post itself.

The reactances $-jX_m$ are seen, from eqn. (10), to vary in the long-wavelength region inversely as $\omega$. They are therefore approximately capacitive, and a capacitance, $C$, may be defined by $\omega C = \sum_1^\infty 1/X_m$. It will vary somewhat with frequency. An interpretation of this capacitance is given in Section 6.

## (4) A DIVERGENT SERIES

The series for $C$ and that in eqn (20) for the current both contain the reciprocal of $X_m$, and it is now necessary to see how this quantity varies with $m$.

From eqn. (10) we have

$$X_m = \frac{30\pi^2}{kb}(m^2 - 4b^2/\lambda^2)[K_0(r\Gamma_m) - K_0(2d\Gamma_m)]$$

where

$$\Gamma_m = (m^2\pi^2/b^2 - k^2)^{1/2} \simeq m\pi/b$$

For $m$ small to moderate we can use the approximation $K_0(x) \simeq -(\gamma + \log\frac{1}{2}x)$ (where $\gamma$ is Euler's constant, $\simeq 0.5772$) in the term involving $r$. If $2d$ is comparable to $r$, the same approximation can also be made in the second term. In this case

$$X_m \simeq \frac{30\pi^2 m^2}{kb}\log\left(\frac{2d}{r}\right)$$

and the series for $1/X_m$ starts converging as $1/m^2$. However, when $m$ is large enough, $r\Gamma_m \simeq m\pi r/b$ will no longer be small. The function $K_0(x)$ behaves like $\varepsilon^{-x}x^{-\frac{1}{2}}$ for large values of $x$, so that it is obvious that the series diverges as $\varepsilon^{m\pi r/b}/m^{3/2}$. The function $1/x^2K_0(x)$ is shown in Fig. 5. It falls rapidly up to
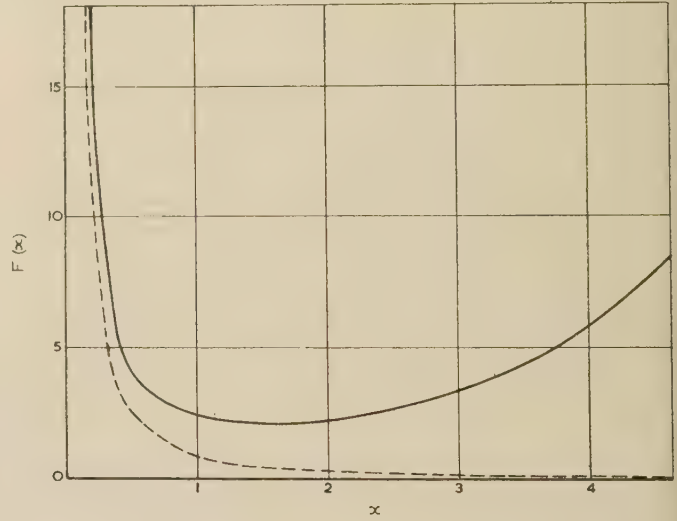


Fig. 5.—Curves illustrating convergence and divergence.

$$\text{———} \quad F(x) = \frac{1}{x^2K_0(x)}$$
$$\text{- - - -} \quad F(x) = \frac{\varepsilon^{-x}}{x^2K_0(x)}$$

the value $x \simeq \frac{1}{2}\pi$ and then increases. If we consider the equation $m\pi r/b = \frac{1}{2}\pi$ as determining a value of $m$ beyond which the series is unusable, it is seen to correspond to the case in which the mode considered is so high that a complete period could be encompassed in the wire diameter. Now the approximations implied at the beginning of Section 3, using a filamentary current to simulate the effect of the currents in the post, cannot be considered valid when the variation interval is comparable with the post radius, since other effects of this order have already been ignored. Hence, although eqn. (20) may be considered to hold with the correct values of $X_m$, these values cannot be obtained from eqn. (10) when $m$ is about $b/2r$ or greater. Probably the dominant effect invalidating eqn. (10) as it stands arises from propagation in the waveguide from the front edge to the side of the wire, an axial distance equal to the wire radius. The dominant incident wave first impinges on the front edge of the post and sets up currents there. As it propagates past the post it envelops it completely, and the overall effect is approximately positioned at the post centre. One would therefore expect from this source an error of the order of $\varepsilon^{-jk'r}$ : 1, which is negligible for small values of $r$. This is no longer so, however,

or an incident higher-order evanescent mode; in fact, if the mode number is high enough, the wave never reaches the back of the wire at all, only the front participating as a reflecting surface. Hence, an analysis based on a current positioned at the centre will lead to a result too small, by an amount given approximately by the attenuation of the wave from the front to the centre position of the post, namely $\varepsilon^{\Gamma_m r} \simeq \varepsilon^{m\pi r/b}$. Since the $\Gamma_m$ have been interpreted in terms of the impedance of the post to the $m$th mode, an additional factor $\varepsilon^{m\pi r/b}$ is called for with the present analysis. This is the dominant correction: a change of effective post radius is probably also required, but an accurate analysis would be needed to give this effect. It is seen that the factor $\varepsilon^{-m\pi r/b}$ restores the convergence in eqns. (10) and (20), the function $\varepsilon^{-x}/x^2 K_0(x)$ corresponding to it being shown dotted in Fig. 5. It is probable that, with this alteration, eqns. (10) and (20) can be used as accurate approximations, and the remainder of the paper will assume this modification.

When the above considerations are applied it is seen that the series converges ultimately as $\Sigma m^{-3/2}$. It is possible that a more rigorous analysis would lead to a further factor $m^{1/2}$ leading to a logarithmic divergence. Such a situation could be avoided by distributing the load impedance $Z_1$ over a small distance, $\delta$, leading to an additional factor $\sin(n\pi\delta/b)/(n\pi\delta/b)$. This would restore the convergence and give rise to a term in $\log \delta$, which could be interpreted in terms of a capacitance across the load. Such a form would indeed be expected from aerial theory, being the so-called 'gap capacitance' which short-circuits the aerial input impedance if not correctly taken into account. In the present analysis the load $Z_1$ is ultimately replaced by a physical coaxial cable and the question of a gap capacitance does not arise. Its place is taken by a 'junction capacitance', of an essentially similar nature, which is considered in a little more detail in Section 6.

## (5)  THE CURRENT IN THE POST

According to eqn. (20) and the remarks of the previous section the current in the post is taken proportional to

$$I = 1 - Z_1 \sum_1^\infty \frac{1 - \cos(n\pi x/b)}{jX_n}\varepsilon^{-n\pi r/b} \quad . \quad . \quad (24)$$

Using the approximation to $X_n$ which is valid when $r$ and $d$ are both very small, we get

$$I \simeq 1 + \frac{jZ_1 kb}{30\pi^2 \log(2d/r)} \sum_1^\infty \frac{1 - \cos(n\pi x/b)}{n^2 - 4b^2/\lambda^2} \quad . \quad (25)$$

This series may be summed, using the general result

$$\sum_1^\infty \frac{\cos n\theta}{n^2 - a^2} = \frac{1}{2a^2}\left[1 - \frac{\pi a}{\sin \pi a}\cos(a\pi - \overline{|\theta|})\right], \quad (0 < \theta < 2\pi)$$

leading to

$$I = 1 + \frac{jZ_1}{60 \log(2d/r)}\frac{\cos(kb - x) - \cos kb}{\sin kb} \quad . \quad (26)$$

From transmission line theory this current would be associated with a voltage $jZ_0'\partial I/\partial(kx)$ where $Z_0' = 60 \log(2d/r)$, i.e. $V = -Z_1\dfrac{\sin(kb - x)}{\sin kb}$, giving, as required, $V = -Z_1 I$ at $x = 0$ and $V = 0$ at $x = b$. Thus the assumption of $r$ and $d$ very small leads to the quasi-static aerial solution, with appropriate boundary conditions, based on a modification of simple line theory. Eqn. (24) can now be written, in the general case

$$I = 1 + \frac{jZ_1}{60 \log(2d/r)}\frac{\cos(kb - x) - \cos kb}{\sin kb} + \delta I . \quad (27)$$

where

$$\delta I = \frac{jZ_1 kb}{30\pi^2}\sum_1^\infty \frac{1 - \cos(n\pi x/b)}{n^2 - 4b^2/\lambda^2}$$

$$\left[\frac{e^{-n\pi r/b}}{K_0(\Gamma_n r) - K_0(\Gamma_n 2d)} - \frac{1}{\log(2d/r)}\right] . \quad (28)$$

This last expression gives the correction to the quasi-static formula for the current in the post.

## (6)  THE POST CAPACITANCE

The capacitance $C$ is defined by

$$\omega C = \sum_1^\infty \varepsilon^{-\Gamma_m r}/X_m$$

$$\simeq \frac{kb}{30\pi^2}\sum_1^\infty \frac{1}{m^2 - 4b^2/\lambda^2}\frac{\varepsilon^{-m\pi r/b}}{K_0(m\pi r/b) - K_0(2m\pi d/b)} . \quad (29)$$

where the amplitude correction factor has been included and the approximation $\Gamma_m \simeq m\pi r/b$ has been made.

When $r$ and $d$ are small enough this sums approximately to $(1/kb - \cot kb)/[60 \log(2d/r)]$. Denoting this value by $\omega C_0$ we get

$$C = C_0 + \delta C . \quad . \quad . \quad . \quad (30)$$

where

$$\omega\delta C = \frac{kb}{30\pi^2}\sum_1^\infty \frac{1}{m^2 - 4b^2/\lambda^2}$$

$$\left[\frac{\varepsilon^{-m\pi r/b}}{K_0(m\pi r/b) - K_0(2m\pi d/b)} - \frac{1}{\log(2d/r)}\right] . \quad (31)$$

$\delta C$ measures the departure of $C$ from its quasi-static value $C_0$.

In order to interpret this capacitance we return to the equivalent circuit, in which the impedance $Z_1$ is now replaced by its coaxial-cable equivalent. The circuit may, of course, be used any way round, and it is convenient to consider the junction as presented to the cable. The two waveguide terminals are now to be short-circuited at distances $\frac{1}{2}L$ from the post, so as to produce the circuit shown in Fig. 6: a coaxial cable of wave impedance $Z_c$
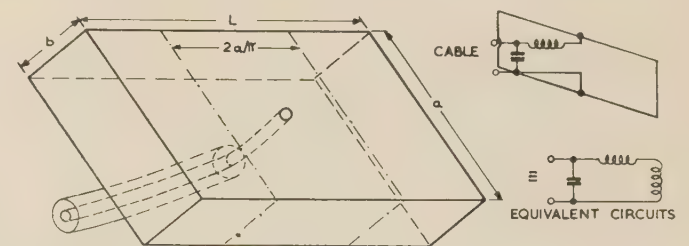


Fig. 6.—Short-circuited waveguide section fed by probe.

feeds into a short-circuited length of coaxial cable of rectangular cross-section, of sides $a$ and $L$ and length $b$. The probe is taken to be central, so that no transformer effect occurs from offsetting.

The total waveguide termination is

$$\frac{1}{2}jZ_0 \tan(\frac{1}{2}k'L) = j120\pi\frac{b}{a}\frac{\lambda_g}{\lambda}\tan\left(\frac{\pi L}{\lambda_g}\right)$$

If we seek a quasi-static interpretation, the waveguide should be worked in the neighbourhood of cut-off, so that $\lambda_g$ is very large, and the termination becomes $j120\pi(\pi bL/\lambda a)$ approximately. This is in series with $X_0 \simeq jZ_0(a/2\lambda_g)\left[\log(2a/\pi r) - 2\right] = j120\pi(b/\lambda)\left[\log(2a/\pi r) - 2\right]$, so that the total inductive reactance across

the capacitance is $j60kb\left[\log\left(2a/\pi r\right) - 2 + \pi L/a\right]$. The interpretation of the last two terms in this expression is bedevilled by the same difficulty that arises with the term $-2$ itself, a quantity giving a negative inductive component in the equivalent circuit of the simple short-circuited post.

The terms under consideration cancel at $L = 2a/\pi$. For smaller values than this the effect of the short-circuits on the higher-order modes cannot be negligible and the formula will not apply. For larger values of $L$ the formula seems to indicate an excess inductance, associated, perhaps, with the storage of energy in the waveguide extensions, which has no counterpart in a simple coaxial-line formula. If this interpretation is correct the $-2$ term has no other significance than that it sets an origin from which this excess inductance has to be computed, and below which the inductance contributes to the coaxial line—in other words it constitutes a demarcation between the coaxial line and waveguide aspects of the junction. In order to simulate a section of pure coaxial line we must on this basis take $L = 2a/\pi$, giving the post a resultant inductive reactance of $jkb60\log\left(2a/\pi r\right)$, or $jZ'kb$, where $Z'$ is the wave impedance of the post. Now the expression for $\omega C$ can be written $\left[1/kb - \cot\left(kb\right)\right]/Z'$, where $Z' = 60\log\left(2d/r\right)$ when the post is near the side of the waveguide but can be presumed to be given by the more general

expression $60\log\left[\dfrac{2a}{\pi r}\sin\left(\pi d/a\right)\right]$, taken from the formula for

the inductive post, when $d$ is not small. This gives the value $60\log\left(2a/\pi r\right)$ when the post is central.

The effect of $1/\omega C_0$ and the post inductance in parallel is at once seen to be an impedance $jZ'\tan kb$, which is just the form expected for a section of short-circuited coaxial line. Accordingly, $C$ is to be interpreted in terms of the capacitance between the post and the walls of the waveguide.

When the post-terminating impedance $Z_1$ is replaced by a physical coaxial line, some disturbance of the field must be expected, owing to the annular gap at the junction. An analysis of a stepped junction in a coaxial line shows that a junction capacitance, $C_j$, appears at the discontinuity.[2] This has not been allowed for in the formulae so far, so that a further capacitance across the post must be added. The complete equivalent circuit for this case is shown in Fig. 7. A formula for the junction capacitance is given in Reference 2.
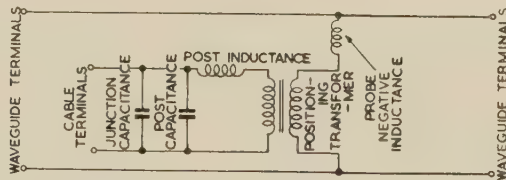


Fig. 7.—Equivalent circuit of cable-fed probe in waveguide.

### (7) THE TOP-LOADED PROBE

The nature of the solution investigated so far depends on the extension of the probe fully across the guide, but is applicable with any (finite) number of lumped impedances inserted in the probe. In particular, if the probe is terminated at its far end in other than a short-circuit the solution can be found. This generalization covers a number of configurations met in practice, including the case in which the termination constitutes a tuning plunger for matching the probe.

A dominant mode is incident in the waveguide and impinges on a probe which spans it at a distance $d < \frac{1}{2}a$ from the wall. The probe is terminated at its ends $x = 0$ and $x = b$ by impedances $Z_1$ and $Z_2$. The total electric field tangential to the surface of the probe must be zero except at the ends, where field

strengths exist to give the necessary voltage drops across $Z_1$ and $Z_2$. The field can be represented by $IZ_1\delta(x) + IZ_2\delta(b - x)$ since this expression is zero everywhere except at $x = 0$ and $x = b$, where it integrates to $I(0)Z_1$ and $I(b)Z_2$ as required.

The condition that the combination of incident field and the field set up by currents in the probe shall equal the prescribed form gives rise to an integral equation for the current. Apart from a term in $Z_2$, this is the same as eqn. (13) for the short-circuited probe, and quoting from there we get

$$\sin\left(\pi d/a\right) + B\int_0^b I(\xi)d\xi + b^{-2}\sum_1^\infty 4jX_m\cos\left(m\pi x/b\right)$$

$$\int_0^b I(\xi)\cos\left(m\pi\xi/b\right)d\xi = \left[Z_1\delta(x) + Z_2\delta(b - x)\right]I(x) \quad . \quad (32)$$

where the constant $B$ is given by $-\sin^2\left(\pi d/a\right)(\frac{1}{2}Z_0 + jX_0)/b^2$. The term $X_m(m \geqslant 1)$ is given by the expression

$$X_m \simeq (30b/k)\Gamma_m^2\left[K_0(r\Gamma_m) - K_0(2d\Gamma_m)\right]\varepsilon^{\Gamma_m r} \quad . \quad (33)$$

where the final exponential factor arises from considerations explained in Section 3: for convenience it has here been absorbed into the expression for $X_m$.

The radiation into the waveguide can be computed from the current in the probe, and from this the reflection and transmission coefficients are deduced. The impedance of the probe, as presented to the waveguide, follows, and can be put in variational form as in eqn. (6). This equation, modified to include the effect of $Z_2$ and rearranged in terms of $X_m$, can be written

$$Z = jX_0 + \mathrm{cosec}^2\left(\pi d/a\right)$$

$$\left\{\frac{I^2(0)Z_1 + I^2(b)Z_2}{(J/b)^2} - 4j\sum_1^\infty X_m\left[\int_0^b I(\xi)\cos\left(m\pi\xi/b\right)d\xi/J\right]^2\right\}$$

$$. \quad . \quad . \quad (34)$$

where $J = \displaystyle\int_0^b I(\xi)d\xi$

In order to complete the solution it is necessary to solve eqn. (32) for the current, substitute in eqn. (34) for the impedance and deduce an equivalent circuit for the latter.

### (8) THE PROBE CURRENT

The solution of eqn. (32) for $I(x)$ can be found by assuming a Fourier series for the current

$$I(x) = A_0 + 2\sum_1^\infty A_n\cos\left(n\pi x/b\right) \quad . \quad . \quad (35)$$

Since the cosines are orthogonal over $0 \leqslant x \leqslant b$, eqn. (32) can be written

$$\sin\left(\pi d/a\right) + bBA_0 + 4b^{-2}\sum_1^\infty jX_mbA_m\cos\left(m\pi x/b\right)$$

$$= \left[Z_1\delta(x) + Z_2\delta(b - x)\right]I(x) \quad . \quad (36)$$

Integration with respect to $x$ from 0 to $b$ gives

$$b\left[bBA_0 + \sin\left(\pi d/a\right)\right] = I(0)Z_1 + I(b)Z_2 \quad . \quad . \quad (37)$$

This equation determines $A_0$.

Multiplying eqn. (36) by $\cos\left(n\pi x/b\right)$ and integrating from 0 to $b$,

$$2jX_nA_n = I(0)Z_1 + \cos\left(n\pi\right)I(b)Z_2 \quad . \quad . \quad (38)$$

Since

$$I(0) = A_0 + 2\sum_1^\infty A_n$$

and

$$I(b) = A_0 + 2 \sum_1^\infty A_n \cos(n\pi)$$

we get, on substituting from eqn. (38), the following pair of equations for $I(0)$ and $I(b)$:

$$I(0) = A_0 + I(0)Z_1 Y + I(b)Z_2 Y' \quad . \quad . \quad . \quad (39)$$

$$I(b) = A_0 + I(0)Z_1 Y' + I(b)Z_2 Y \quad . \quad . \quad . \quad (40)$$

where $\quad Y = \sum_1^\infty 1/jX_n \quad$ and $\quad Y' = \sum_1^\infty \cos(n\pi)/jX_n \quad . \quad . \quad (41)$

It is not necessary to use eqn. (37) to eliminate $A_0$ unless the absolute value of the current is of interest; but since eqn. (34) for the probe impedance is presented in terms of current ratios only, eqns. (39) and (40) in their present form suffice. They are solved for $I(0)$ and $I(b)$, and eqn. (38) then gives $A_n$ in terms of $A_0$, whence the form for $I(x)$ is deduced from eqn. (35):

$$I(x) = A_0$$

$$\times \left\{ 1 + \sum_1^\infty \frac{Z_1[1 - Z_2(Y - Y')] + \cos(n\pi)Z_2[1 - Z_1(Y - Y')]}{jX_n D} \right.$$

$$\left. \times \cos(n\pi x/b) \right\} \quad . \quad (42)$$

where $\quad D = (1 - Z_1 Y)(1 - Z_2 Y) - Z_1 Z_2 Y'^2 \quad . \quad . \quad (43)$

## (9) THE PROBE IMPEDANCE

From eqns. (42) and (34),

$$J = \int_0^b I(\xi)d\xi$$

is just $bA_0$. Similarly the quantity $\int_0^b I(\xi) \cos(m\pi\xi/b)d\xi/J$ is equal to

$$\frac{Z_1[1 - Z_2(Y - Y')] + \cos(n\pi)Z_2[1 - Z_1(Y - Y')]}{jX_n 2D}$$

On substituting into (34) we get, after some reduction,

$$Z = jX_0 + \operatorname{cosec}^2(\pi d/a)\frac{2Z_1 Z_2(Y - Y') - Z_1 - Z_2}{Z_1 Z_2 Y'^2 - (1 - Z_1 Y)(1 - Z_2 Y)} \quad . \quad (44)$$

$$= jX_0 + \operatorname{cosec}^2(\pi d/a)\bar{Z} \quad \text{say}$$

This represents an inductance given by $jX_0$ in series with an impedance $\bar{Z}$ seen through a transformer of turns ratio cosec $(\pi d/a)$. As before the reactance $X_0$ may be split into two components, one of which can be placed at the secondary of the transformer in series with $\bar{Z}$, and the special points which arise when this is done have already been dealt with. It remains to interpret $\bar{Z}$.

## (10) AN EQUIVALENT CIRCUIT

The expression for $\bar{Z}$, on dividing through by $Z_1 Z_2$, can be put in the form

$$\bar{Z} = \frac{(1/Z_1 + Y' - Y) + (1/Z_2 + Y' - Y)}{(1/Z_1 - Y)(1/Z_2 - Y) - Y'^2} \quad . \quad (45)$$

If we make the substitution $Y_{1,2} = 1/Z_{1,2} + Y' - Y$ we get

$$\bar{Z} = \frac{Y_1 + Y_2}{Y_1 Y_2 - Y'(Y_1 + Y_2)} \quad . \quad . \quad . \quad . \quad (46)$$

Dividing through by $(Y_1 + Y_2)$ and inverting both sides gives

$$\frac{1}{\bar{Z}} = \frac{1}{1/Y_1 + 1/Y_2} - Y' \quad . \quad . \quad . \quad . \quad (47)$$

Thus $\bar{Z}$ consists of impedances represented by $Y_1$ and $Y_2$ in series, the whole shunted by $-Y'$. $Y_1$ and $Y_2$ themselves consist of the impedances $Z_1$ and $Z_2$ each shunted by $(Y' - Y)$. The equivalent circuit of $\bar{Z}$ itself is therefore as shown in Fig. 8, where all components are represented as impedances.
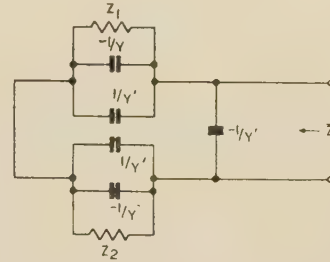


Fig. 8.—Equivalent circuit for $\bar{Z}$.

The quasi-static values of the parameters $Y$ and $Y'$ are easily found by taking the limiting value of zero for $r$ and $d$ in eqn. (32). Then

$$X_m \simeq Z'\frac{\pi^2}{2\theta}(m^2 - \theta^2/\pi^2)$$

where $Z' = 60 \log(2d/r)$ and $\theta = kb$, the electrical length of the probe. This gives

$$\left. \begin{array}{l} Y_{qs} \simeq -j\sum_1^\infty \frac{2\theta}{\pi^2 Z'}\frac{1}{m^2 - \theta^2/\pi^2} = \frac{1}{jZ'}\left(\frac{1}{\theta} - \cot\theta\right) \\[2ex] \text{and} \quad Y'_{qs} \simeq -j\sum_1^\infty \frac{2\theta}{\pi^2 Z'}\frac{\cos m\pi}{m^2 - \theta^2/\pi^2} = \frac{1}{jZ'}\left(\frac{1}{\theta} - \operatorname{cosec}\theta\right) \end{array} \right\} \quad (48)$$

Hence the impedance represented by $(Y' - Y)_{qs}$ is given by

$$\frac{jZ'}{\left[\left(\frac{1}{\theta} - \operatorname{cosec}\theta\right) - \left(\frac{1}{\theta} - \cot\theta\right)\right]} = -jZ' \cot(\tfrac{1}{2}\theta)$$

equal to the impedance of an open-circuited probe of half the full length, and therefore capacitive (for short probes).

Similarly, the impedance represented by $-Y'_{qs}$ is

$$-jZ'\bigg/\left(\frac{1}{\theta} - \operatorname{cosec}\theta\right)$$

For small values of $\theta$ this approximates to $jZ'(6/\theta)$ and hence behaves as a negative capacitance for short probe lengths. It is, of course, always associated with $Y' - Y$, which is a positive capacitance in this region.

As already discussed, the quasi-static values are those to be expected from transmission-line theory, using a suitable value for the wave impedance $Z'$. The expression $60 \log(2d/r)$ is obviously correct for a small-diameter probe close to the wall of the waveguide. Nearer the centre the form

$$Z' = 60 \log\left(\frac{2a}{\pi r}\sin\frac{\pi d}{a}\right)$$

which comes from the formula for the inductive post, is appropriate. If we multiply the parameters $Y' - Y$ and $Y'$ by $jZ'$ and subtract the quasi-static values, we obtain two correction terms $e$ and $e'$ as follows.

$$e = jZ'[(Y' - Y) - (Y' - Y)_{qs}]$$

$$- \frac{2\theta}{\pi^2} \sum_1^\infty \frac{1 - \cos m\pi}{m^2 - \theta^2/\pi^2} \left[ \frac{\varepsilon^{-m\pi r/b} \log \left( \frac{2a}{\pi r} \sin \frac{\pi d}{a} \right)}{K_0(m\pi r/b) - K_0(2m\pi d/b)} - 1 \right]$$

$$. \quad . \quad . \quad . \quad (49)$$

$$e' = jZ'[- Y' + Y'_{qs}]$$

$$- \frac{2\theta}{\pi^2} \sum_1^\infty \frac{\cos m\pi}{m^2 - \theta^2/\pi^2} \left[ \frac{\varepsilon^{-m\pi r/b} \log \left( \frac{2a}{\pi r} \sin \frac{\pi d}{a} \right)}{K_0(m\pi r/b) - K_0(2m\pi d/b)} - 1 \right]$$

$$. \quad . \quad . \quad . \quad (50)$$

These quantities express the departure of the circuit parameters from their quasi-static transmission line values. They are plotted in Fig. 9 for a central probe in a waveguide of width 2·5 times
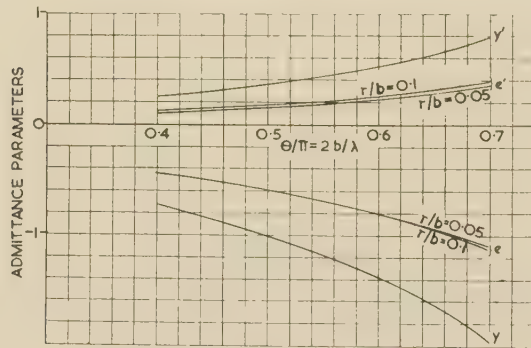
Fig. 9.—Variation of admittance parameters and correction terms with $2b/\lambda$.

its height for $r/b = 0.05$ and $0.1$. The abscissa is $2b/\lambda$, which is proportional to frequency. Also plotted is $y = jZ'(Y' - Y)_{qs} = - \tan \frac{1}{2}\theta$ and $y' = jZ'(- Y')_{qs} = - 1/\theta + \cosec \theta$. It is seen that in this example the correction terms are comparable with the quasi-static values—a strong indication of the inadequacy of making the usual approximations of aerial theory in dealing with probes in waveguides. The correction terms are insensitive to values of $r/b$ in the range considered, so that the main effect of $r$ on the circuit parameters is through the probe wave impedance $Z'$.

The complete representation of the terminated probe can now be given. As before we consider the terminations as being due to the loading of the probe ends by coaxial cable with arbitrary loading impedances. The replacement of lumped loads by cable introduces a junction capacitance $C_J$, and the probe inductance is broken down into two parts, one on each side of the transformer. In the present instance it is convenient to maintain symmetry by dividing the probe inductance appearing at the secondary into two halves, one at each terminal. The equivalent circuit is given in Fig. 10, the post capacitances being as shown in Fig. 8. When one end of the probe is short-circuited the circuit reduces to that given in Fig. 3, to which reference should be made for the details of the post inductance.

Using the basic circuit shown in Fig. 10, it is now possible to analyse combinations of waveguides coupled by probes. If the waveguide walls are contiguous, the length of connecting cable
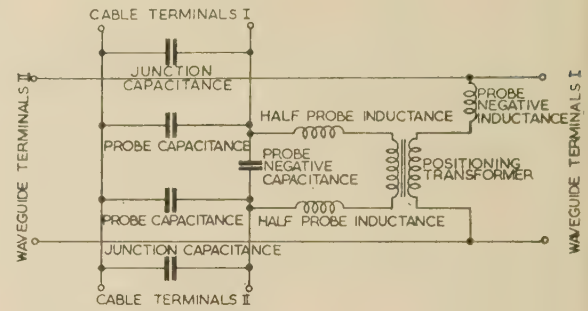
Fig. 10.—Waveguide-fed doubly-terminated probe and equivalent circuit.

is effectively that of the wall thickness and presumably may be lumped with the junction capacitances. However, the usual formula for the junction capacitance may here be inaccurate because of the close proximity of the next junction. This condition is very similar to that arising from taking the junction capacitance as being equal to half that of a diaphragm of the same dimensions; an estimate of the error arising in this instance is given by MacFarlane.[3]

## (11) CONCLUSIONS

The method of analysis seems a fruitful one and is probably capable of extension to a number of other useful and interesting configurations. Difficulties of convergence require closer attention, especially in relation to the impedance of stubs to high-order modes, for which the approximations used in more familiar cases may not be valid. Difficulties also arise in the interpretation of equivalent circuits, but here the crux of the matter seems to be contained in the simpler special case of the inductive post, and further work on this aspect would be worth while.

## (12) REFERENCES

(1) LEWIN, L.: 'Advanced Theory of Waveguides' (Iliffe, London, 1951), pp. 26, 27, 78–81 and 86.
(2) MARCUVITZ, N.: 'Waveguide Handbook' (McGraw-Hill, New York, 1951), p. 311.
(3) MACFARLANE, G. G.: 'Quasi-Stationary Field Theory and its Application to Diaphragms and Junctions in Transmission Lines and Waveguides', Journal I.E.E., 1946, 93, Part IIIA, p. 709.

# SOME TESTS ON A STATOR-FED POLYPHASE SHUNT COMMUTATOR MOTOR

## By C. S. JHA, B.Sc., Graduate.

### SUMMARY

Based on theory developed in earlier papers, equivalent circuits are established for a stator-fed 3-phase shunt commutator motor available for tests. Details are given of methods used in the measurement of equivalent-circuit parameters. The measurement and separation of motor no-load losses are discussed. Test results obtained in no-load and load tests are shown to give fairly good agreement with calculated behaviour.

### LIST OF PRINCIPAL SYMBOLS

$\alpha$ = Electrical angle by which the regulator shaft is rotated from its neutral position, electrical degrees.

$\theta$ = Brush shift angle, against the direction of rotation, electrical degrees.

$\gamma$ = Angle by which the auxiliary winding e.m.f. lags the stator e.m.f. (neglecting transformer effect).

$a$ = Pairs of parallel paths in the armature.

$i_1, i_r, i_2$ = Currents in the motor primary, machine secondary, and regulator primary circuits, respectively.

$k$ = Effective turns ratio (secondary/primary) of the component single regulators of the double regulator.

$k_m, k_x$ = Effective turns ratios, motor-secondary/motor-primary and motor-auxiliary/motor-primary, respectively.

$P_1, P_2$ = Wattmeter readings in the two-wattmeter method of measuring power.

$R_b$ = Carbon brush contact resistance for each brush set on the motor, also effective per phase value for the test-motor brush contact resistance.

$R_{om}, R_{11}$ = Loss component of the mutual and self-impedances of the primary winding, respectively.

$R_{s1}, R_{r1}, R_{s3}$ = Resistances of the motor primary, secondary and auxiliary windings, respectively.

$s$ = Slip.

$x_{s1}, x_{r1}, x_{s3}$ = Leakage reactances of the motor primary, secondary and auxiliary windings, respectively.

$X_{om}, X_{11}$ = Reactive components of the mutual and self-impedances, respectively.

$Z_{om}, Z_{11}$ = Mutual and self-impedances, respectively, of the motor primary winding.

$z_{11}$ = Leakage impedance of the motor primary winding.

$Z_o, Z_s$ = Mutual and self-impedances, respectively, of the component single regulator primary windings.

$z_r, z_s$ = Leakage impedances of the component single regulator secondary and primary windings, respectively.

All resistances, reactances and impedances are effective per phase values unless otherwise stated.

### (1) INTRODUCTION

Polyphase shunt commutator machines were developed to meet the need of alternating-current drives with induction motor characteristics but with provision for speed regulation and power-factor control. The basic principle of speed regulation and power-factor improvement of an induction machine lies in the injection of a suitable electromotive force into its secondary circuit at slip frequency. In the stator-fed machine, the main winding is on the stator, while the rotor carries a commutator winding. The e.m.f. injected in the rotor circuit is usually obtained at supply frequency from the combination of a double induction regulator and an auxiliary winding on the motor stator, and is converted into slip frequency by the commutator and fixed brushes.

The theory of the double induction regulator and of the stator-fed motor with regulator have been discussed in References 6 and 7, respectively. The present paper deals with some tests carried out in experimental verification of the theory proposed in Reference 7.

### (2) THE TEST MACHINE

The machine whose behaviour was tested has a simple (unbiased) double regulator for speed regulation and an auxiliary stator winding displaced 120° electrically from the main winding for power-factor improvement. A patented commutating winding in the rotor slots is in parallel with the main rotor winding to ease commutation troubles. The brushes are diametrical and two terminals per phase are brought out on the terminal board. The regulator is the same as that used in tests described in Reference 6. The manufacturer's rating for the machine is as follows:

Motor: 5·5/0·55 h.p.; 2 200/220 r.p.m.; 400 volts 50 c/s 3-phase 4-pole.
Regulator: 2-pole 3-phase. Input, 400 volts 9 amp; output, 4·13 kVA 30·6 volts, 45 amp.

The test machine connections are shown in Fig. 1.

### (3) THE IMPEDANCE TENSOR AND THE EQUIVALENT CIRCUITS OF THE TEST MACHINE

Using Reference 7, the final impedance tensor for the test machine can be shown to be

$$Z_{\mu\nu} =$$

| $\mu \backslash \nu$ | 1 | $r$ | 2 |
|---|---|---|---|
| 1 | $Z_{11}$ | $Z_{om}(k_m \varepsilon^{-j\theta} - k_x \varepsilon^{j\gamma})$ | |
| $r$ | $Z_{om}(k_m s \varepsilon^{j\theta} - k_x \varepsilon^{-j\gamma})$ | $Z_{rr}$ | $-k Z_o \cos \alpha$ |
| 2 | | $-k Z_o \cos \alpha$ | $Z_s/2$ |

. . . . . (1)

where $Z_{11} = R_{s1} + jx_{s1} + Z_{om}$

and $\quad Z_{rr} = R_{r1} + jsx_{r1} + R_{s3} + jx_{s3}$
$$+ \left\{ k_m^2 s + k_x^2 - k_m k_x [s\varepsilon^{j(\gamma+\theta)} + \varepsilon^{-j(\gamma+\theta)}] \right\} Z_{om}$$
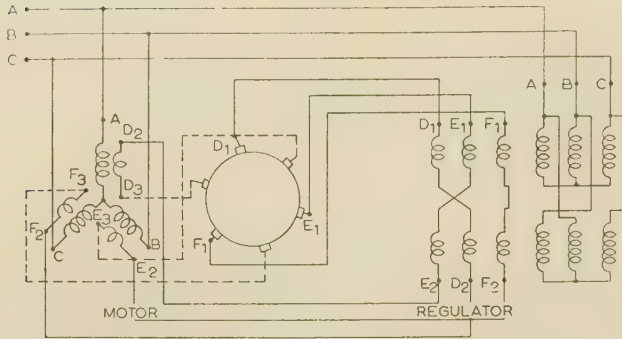$$+ 2z_r + 2k^2(Z_o/Z_s)z_s + 2k^2(Z_o^2/Z_s) \cos^2 \alpha \quad . \ (2)$$

**Fig. 1.**—General connections of test machine.
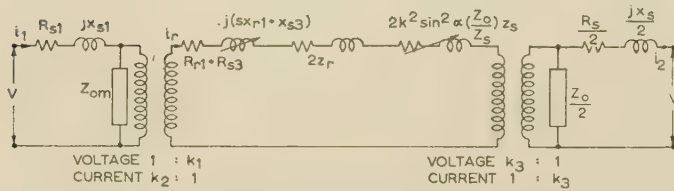


**Fig. 2.**—Orthodox equivalent circuit for test machine.

$k_1 = k_m s \varepsilon^{+j\theta} - k_x \varepsilon^{-jY}$; $k_2 = k_m \varepsilon^{-j\theta} - k_x \varepsilon^{+jY}$; $k_3 = 2k \cos \alpha$.
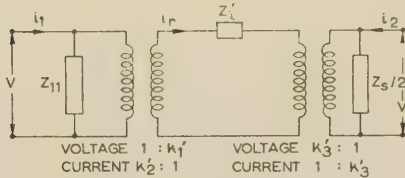


**Fig. 3.**—Exact practical equivalent circuit of test machine.

$k_1' = (k_m s \varepsilon^{+j\theta} - k_x \varepsilon^{-jY}) Z_{om}/Z_{11}$; $k_2' = (k_m \varepsilon^{-j\theta} - k_x \varepsilon^{+jY}) Z_{om}/Z_{11}$;

$k_3' = 2k(Z_0/Z_s) \cos \alpha$; $\qquad Z_l' = Z_{rr} - k_1' k_2' Z_{11} - k_3'^2 Z_s/2$.

The orthodox and the exact practical equivalent circuits representing eqn. (1) are shown in Figs. 2 and 3, respectively. Iron losses in the machine have been included by considering the mutual-impedance terms $Z_{om}$ and $Z_o$ to include resistive components.

## (4) MEASUREMENT OF PARAMETERS

In addition to the regulator parameters, the measurement of which has been discussed in detail in Reference 6, the following motor parameters must be known to enable theoretical calculation of machine performance:

(a) Effective turns ratios, $k_m$ and $k_x$.
(b) Brush shift angle $\theta$ and auxiliary winding displacement angle $\gamma$.
(c) Resistances $R_{s1}$, $R_{r1}$, and $R_{s3}$.
(d) Leakage reactances $x_{s1}$, $x_{r1}$, and $x_{s3}$.
(e) Reactive component of mutual impedance, $X_{om}$.
(f) Loss component of mutual impedance, $R_{om}$.

### (4.1) Effective Turns Ratios and the Displacement Angle

When design details of the motor windings and the configuration of the fixed brushes are available, the values of $k_m$, $k_x$, $\theta$ and $\gamma$ can be easily and accurately determined. In absence of these details the normal open-circuit test is used. Comparison of the magnitudes and the phase displacements of the secondary and auxiliary induced voltages with those of the primary supply voltage determines these four constants.

### (4.2) The Resistance Measurements

The measurement of primary and auxiliary winding resistance is straightforward, but that of the secondary resistance is complicated by the presence of carbon brushes. The carbon brush contact resistance forms a major part of the total secondary resistance, and its non-linearity makes it necessary for the resistance to be measured at different current densities. Moreover, the measured resistances must be converted to effective per phase values.

#### (4.2.1) Separation of Winding and Contact Resistances.

In a 2-pole 3-phase armature with a commutator winding, as shown in Fig. 4, if a direct voltage is applied to any pair (1–2) of diametric brushes, such that the current entering and leaving the brushes is $I$, then a current $I/2$ will flow through each conductor. If $r$ is the resistance of all conductors in the armature connected in series, the resistance measured across 1–2 is given by $2R_b + r/4$, where $R_b$ is the contact resistance of each brush set. If, instead of a 2-pole armature, there are $a$ pairs of parallel paths, the resistance across 1–2 will be

$$R_{12} = V_{12}/I = 2R_b/a + r/4a^2 \quad . \quad . \quad . \quad (3$$

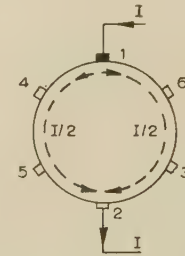If the current is passed as shown in Fig. 4, and voltages across



**Fig. 4.**—Two-pole armature with commutator fed across one pair of diametric brushes.

3–4 and across 5–6 are measured, $V_{34}$ and $V_{56}$, since they do not include contact drops, will be given by

$$V_{34} = V_{56} = (I/2a)(r/6a)$$

Hence $\qquad V_{34}/I = r/12a^2 \quad . \quad . \quad . \quad . \quad . \quad (4$

From eqns. (3) and (4), $R_b$ and $r$ can be easily separated.

#### (4.2.2) Conversion of Measured Values to Effective Per-Phase Values.

Consider a 2-pole 3-phase armature with diametric brushes being fed by a balanced 3-phase supply, and let the phase currents be $I_1$, $I_2$, and $I_3$. The armature shown in Fig. 5 is divided into six sections $a$, $b$, $c$, $d$, $e$ and $f$. The current flowing in any of these winding sections at any moment can be determined by adding the separate effects of the three currents. It can be seen that every section of the winding, and hence every conductor, takes a current equal in magnitude to the phase currents. If there are $a$ parallel paths on the armature, the current in every conductor will be $I/a$, where $I$ is the magnitude of the phase currents.

Hence,

$$\text{Total loss in the rotor winding} = (I/a)^2 r \quad . \quad . \quad (5$$

If the brushes are included, the total loss becomes

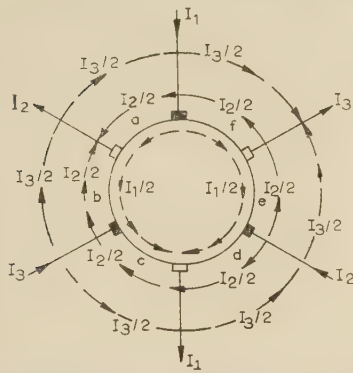$$(I/a)^2 (r + 6aR_b)$$

since the number of brushes is $6a$.

Fig. 5.—Two-pole armature with commutator fed from a 3-phase supply.

Total currents in the winding sections:

a, $-I_3$; b, $+I_1$; c, $-I_2$; d, $+I_3$; e, $-I_1$; and f, $+I_2$.

Therefore

$$\text{Loss per phase} = (I/a)^2(r/3 + 2aR_b) \quad . \quad . \quad . \quad (6)$$

from which

$$\text{Effective resistance per phase} = (r/3a^2 + 2R_b/a) \quad . \quad . \quad (7)$$

In the test motor, $a = 2$, giving

$$R_{r1} = r/12 + R_b \quad . \quad . \quad . \quad . \quad (8)$$

Since the carbon contact resistance is non-linear, $R_b$ was measured for a series of values of $I$. Because $R_b$ is very susceptible to outside influences such as temperature, humidity, etc., any exact reproduction of results over a long period is impossible, and the values of $R_b$ used for calculation of characteristics were the means of numerous values obtained over a long period. An investigation was carried out with a pair of carbon brushes mounted on a copper slip-ring to find if there was any difference between the a.c. and d.c. values of the contact resistances. It was shown that for all practical purposes the d.c. value measured across the brushes (i.e. the sum of the positive and negative polarity contact resistances in series) was equal to the a.c. value (two contact resistances in series).

Since the resistance is a function of temperature, the measurements should be carried out while the machine is hot and the hot values used in the calculation of machine characteristics. Copper resistances in the machine increase with temperature, but the carbon contact resistance has a negative temperature coefficient. The curves for $R_b$ obtained on the test motor (B-phase) when cold and hot are shown in Fig. 6. On the test machine, $R_b$ for the three different phases showed a difference of up to 20%. The mean hot value for the three phases is shown in Fig. 7, and this was used for performance calculation.

### (4.3) Leakage Reactance Measurements

In separating primary and secondary leakage reactances in induction machines an approximation is usually made that the reactances referred to the same voltage base are equal. However, in any machine where an auxiliary winding either on the stator or on the rotor is present, the individual leakage reactances of the three windings can easily be measured. The method involved is the same as that used in the determination of leakage reactances in 3-winding transformers. This method, with transformers, gives simultaneously the leakage reactances of the three windings and their effective a.c. resistances. In the case of the stator-fed motor, however, the presence of losses in short-circuited coils makes the resistances measured in the test very different from actual values.
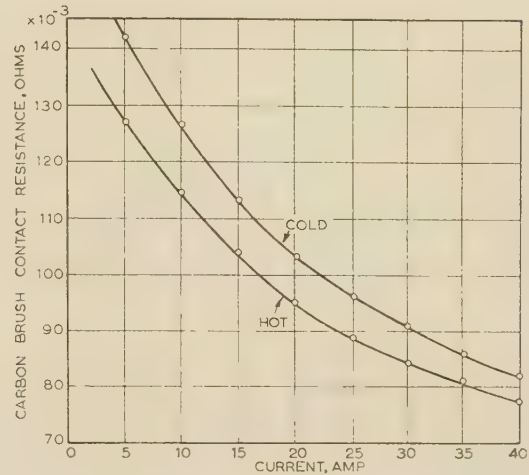


Fig. 6.—Variation of carbon-contact resistance with current and with temperature.
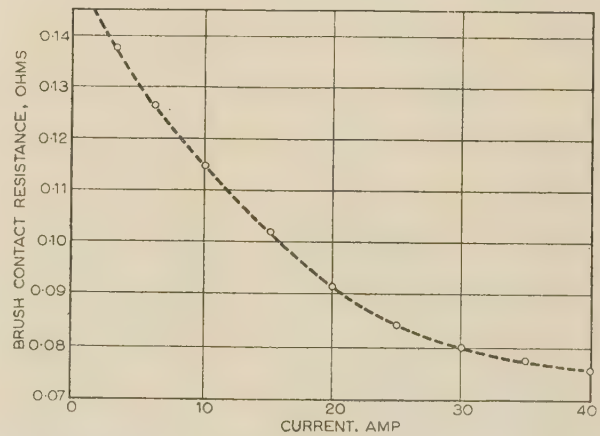
(Related to the B-phase of the test motor.)



Fig. 7.—Average hot values of carbon-contact resistance per phase plotted against current flowing through the contact.

The leakage reactances of the primary and auxiliary windings on the stator-fed motor are independent of the speed of the rotor. For normal induction machines the rotor leakage reactance is proportional to the slip of the rotor. But the leakage reactance of an armature with a commutator winding, measured across fixed brushes, is known to have a slip-independent portion in addition to the slip-dependent one. This necessitates the replacement of $sx_{r1}$ in eqn. (1) by $sx'_{r1} + x''_{r1}$. The behaviour of the secondary leakage reactance of a stator-fed commutator motor is of considerable interest, and the determination of the slip-independent component $x''_{r1}$ is essential for correct performance calculation.

#### (4.3.1) Determination of the Slip-independent Portion of the Secondary Leakage Reactance.

Let the motor be fed through the brushes, the primary kept on short-circuit and the auxiliary on open-circuit. The voltage equations for the primary and secondary circuits are then

$$\left.\begin{array}{l} 0 = i_1(R_{s1} + jx_{s1} + Z_{om}) + i_r k_m Z_{om}\varepsilon^{-j\theta} \\ V_r = i_1 k_m s Z_{om}\varepsilon^{+j\theta} + i_r(R_{r1} + sx'_{r1} + x''_{r1} + k_m^2 s Z_{om}) \end{array}\right\} \quad . \quad (9)$$

From which, on simplification, the short-circuit impedance is

$$V_r/i_r = R + jx \quad . \quad \quad . \quad (10)$$

where
$$R = R_{r1} + k_m^2 cs R_{s1}$$
$$x = x_{r1}'' + s(x_{r1}' + k_m^2 cx_{s1})$$
$$c = Z_{om}/Z_{11}$$
. . . (11)
and

$c$ being assumed approximately real.

If the rotor is driven in the direction of rotation of the field by an auxiliary drive, both $R$ and $x$ will vary linearly with speed and the value of $x$ at synchronous speed will give $x_{r1}''$. In actual test, $V_r/i_r$ can be measured over the entire speed range quite easily by noting the applied phase voltage and the phase current at different speeds. If the power lost per phase, $P$, is also recorded, $x$ can be calculated from the relation

$$x = \sqrt{[(V_r/i_r)^2 - (P/i_r^2)^2]} \quad . \quad . \quad . \quad (12)$$

Curve (a) in Fig. 8 shows the values of $x$ for the test motor obtained by this method, and at first sight suggests that the slip-independent portion of the armature leakage reactance changes sign as the rotor is driven through synchronism. If this were so, a study of the voltage and current oscillograms should show a sudden change of phase of the secondary current as the rotor is driven through synchronism. No such sudden change was, however, observed. The current was shown to be considerably lagging the voltage when the rotor was at standstill ($s = 1$), and, as the rotor speed was increased, the phase angle became gradually smaller and smaller, until near synchronous speed (approximately $s = 0$) no phase difference between the current and voltage waves could be ordinarily detected; and at speeds above synchronism the current started leading the voltage. It therefore became obvious that the measurement of $x$ by eqn. (12) is erroneous.

The above method will give an accurate value of reactance $x$ at the fundamental frequency, only if both the current and voltage in the test are sinusoidal. Under test conditions, although the current flowing could be kept sinusoidal and hence approximately free from harmonics, the voltage appearing at the brushes, $V_r$, usually contains higher harmonics (mainly due to commutation), the percentage of which becomes quite high near synchronous speeds.

Richter[2] has shown that in the case when either the voltage or the current is free from harmonics, the phase angle $\phi$ between the fundamental components of voltage and current can be easily measured from the relation

$$\tan \phi = \frac{\sqrt{3}(P_1 - P_2)}{P_1 + P_2} \quad . \quad . \quad . \quad (13)$$

Curve (b) in Fig. 8 shows the variation of $x$ with speed when $x$ is calculated from the relation

$$x = (V_r/i_r) \sin \phi \quad . \quad . \quad . \quad . \quad (14)$$

Although this method of measuring $x$ is more accurate than the previous one, the effect of harmonics is not altogether eliminated, since $V_r$ contains harmonic components. The best method of finding the slip-independent portion of the leakage reactance is to find the speed at which $P_1 = P_2$, giving $\tan \phi = 0$ and hence $x = 0$. A straight line is then drawn joining this point ($x = 0$) on the speed axis with the value of $x$ at zero speed, where the effect of harmonics is practically negligible. The ordinate of this straight line at synchronous speed ($s = 0$) gives $x_{r1}''$.

From Fig. 8 it is seen that for the test motor $P_1 = P_2$ at a speed slightly below synchronism, thus giving a very small negative value for $x_{r1}''$. It seemed unusual that $x_{r1}''$ was negative; its magnitude was, however, so small that experimental errors may have been responsible for this.

An open-circuit test with the secondary connected to normal-frequency supply (primary and auxiliary open-circuited) was
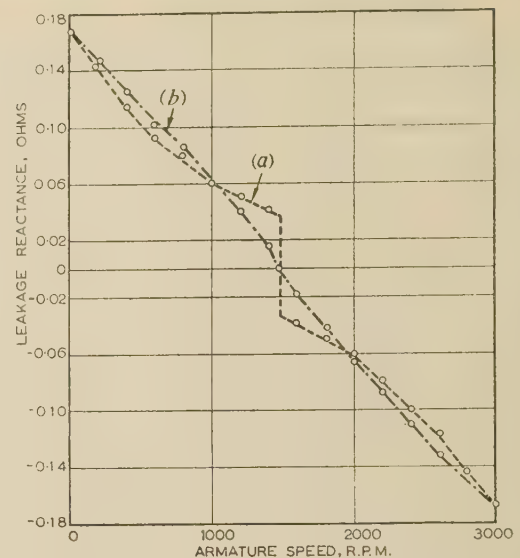


Fig. 8.—Variation of secondary short-circuit reactance with armature speed.

Curve (a) calculated from eqn. (12).
Curve (b) calculated from eqn. (14).

carried out to study the variation of the secondary self-reactance with speed. Results showed that in this experiment again $P_1 = P_2$ at a speed slightly less than synchronous. Since the slip-independent value of the secondary leakage reactance is equal to the secondary self-reactance at zero slip, this test confirmed that $x_{r1}''$ for the test motor should be negative.

There seems to be no explanation for this result, which is so contrary to the general idea[3] that the slip-independent portion is about a quarter of the standstill value of the secondary leakage reactance. Since $x_{r1}''$ is in any case very small, it has been assumed to be negligible in the subsequent calculation of characteristics.

### (4.4) Measurement of $X_{om}$

The self-impedance $Z_{11}$ of the primary winding can be easily measured in an open-circuit test, with the secondary and auxiliary on open-circuit. The measurement of power loss in the test enables $Z_{11}$ to be split into resistive and reactive components. The mutual impedance $Z_{om}$ is then obtained by subtracting the primary leakage impedance $z_{11}$ ($= R_{s1} + jx_{s1}$) from $Z_{11}$, i.e.

$$Z_{om} = Z_{11} - z_{11} = a + jb \text{ (say)}$$

If, in the magnetizing branch of the equivalent circuit, the resistive and reactive components are in parallel, $X_{om}$ is given by $(a^2 + b^2)/b$. The test should be carried out at the operating voltage to make the measured value approximate to the value under normal working conditions.

### (4.5) Measurement of $R_{om}$

The no-load mechanical losses (i.e. windage and friction) are usually omitted from machine equivalent circuits, these losses being considered to be part of the machine output. The electrical no-load losses, on the other hand, are lumped together and shown as part of the mutual-impedance branch of the primary winding. This lumping together of the losses is not quite justifiable as the losses occur in different parts of the machine, but experience over a number of years has shown that no serious errors are involved.

In the stator-fed motor, the no-load electrical losses are a complicated function of the motor speed and may vary within very wide limits. $R_{om}$ in the equivalent circuit must therefore be represented by a variable resistance expressed as a function of the slip of the machine.[7] One way of estimating $R_{om}$ is to record the total power lost in the no-load run of the motor with regulator and then to subtract from it the mechanical losses, the calculable $I^2R$ losses in the different circuits of the machine, and the regulator iron losses. Neglecting the voltage drop across the primary leakage impedance, $R_{om}$ is then obtained by $V^2$/loss-per-phase. Loss per phase being a function of speed, $R_{om}$ is thus expressed as an experimentally determined function of the machine slip.

In the test motor the no-load electrical losses measured in this way were very different from the estimated values of normal-frequency iron losses. An attempt was therefore made to separate the constituent no-load losses of the motor; this is discussed in the next Section.

### (4.6) Measurement and Separation of No-load Losses

Apart from the calculable $I^2R$ losses and easily determinable iron losses in the regulator, the no-load losses in the machine include the following:

(a) Brush friction loss, $P_b$.
(b) Bearing friction and windage loss, $P_f$.
(c) Fundamental-frequency stator iron losses (hysteresis and eddy-current losses), $P_{e1} + P_{h1}$.
(d) Rotor hysteresis loss, $P_{h2}$.
(e) Rotor eddy-current loss, $P_{e2}$.
(f) Surface and pulsation losses (including all losses due to the presence of stator and rotor slot openings), $P_p$.
(g) Losses in the coils short-circuited by the brushes, $P_{sc}$.

Except for (g), these losses have the same nature as in any polyphase induction machine.[4] In induction machines, however, the speed is more or less fixed, hence the variation of constituent no-load losses with speed is of no particular importance. The stator-fed commutator motor, on the other hand, has a wide speed range and the variation of losses with speed is thus of considerable interest from both design and operational points of view.

The method used for separating the losses of this machine is an extension of that used by Alger and Eksergian[1] for separating the iron losses of wound-rotor induction machines. If a constant voltage and frequency are applied to the stator and the rotor is driven by another motor at different speeds, the power taken from the line decreases and that taken by the driving motor increases abruptly when the rotor passes synchronous speed. This discontinuity in the power curves at synchronous speed, being due to the reversal of the rotor hysteretic torque as the rotor is driven through synchronism, is equal in magnitude to twice the standstill value of rotor hysteresis loss, $P_{h2}$.

If a driving motor is available and the brushes on the commutator can be easily lifted or removed, all the losses of the test motor can be separated by means of the following two tests:

*Test A*

In this test the commutator motor, with the brushes in their normal position, is driven by a d.c. driving motor in the direction of its normal rotation. Normal supply is connected to the stator terminals of the test motor, while the auxiliary and secondary windings are kept open-circuited. The power needed for the driving motor to drive the combination with the test motor unexcited is recorded for different speeds. The test motor is then excited and the power input to the driving motor and to the test motor at different speeds is recorded.

*Test B*

The same experiment is repeated with the brushes on the test motor lifted off the commutator surface.

From tests A and B, six sets of readings for power at different speeds are obtained, giving six curves plotted against speed. Fig. 9 shows the results obtained on the test motor. D.C.1
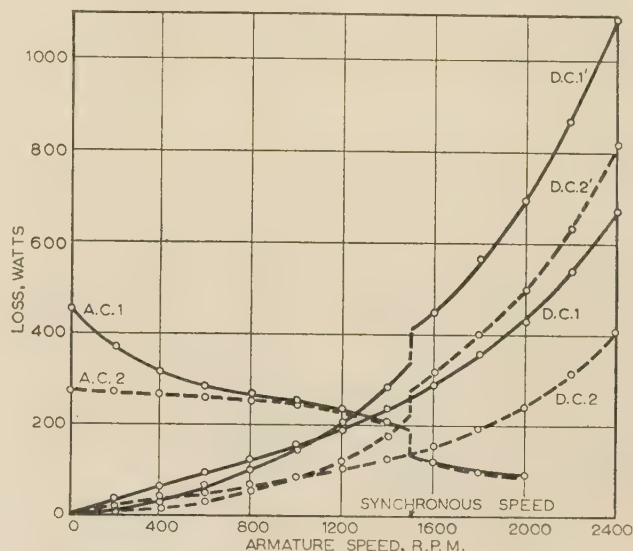


Fig. 9.—Separation of test motor no-load losses.

and D.C.2 represent the curves for the driving motor inputs (corrected for copper losses in the driving motor) with the test motor unexcited; D.C.1′ and D.C.2′, the driving motor inputs (corrected for copper losses) with the test motor excited; and A.C.1 and A.C.2 the total inputs to the test motor (corrected for copper losses in primary winding) in the two tests A and B, respectively.

From these six curves all the test motor losses can be separated and their variation with speed determined, as shown below:

(a) The brush friction loss, $P_b$, is given directly from the difference of the two curves D.C.1 and D.C.2.

(b) The bearing friction and windage loss, $P_f$, is given by subtracting $P_b$ and the driving motor no-load losses from D.C.1.

(c) The stator iron loss, $P_{e1} + P_{h1}$, is independent of the speed of the rotor and is given by the average value of the A.C.1 or A.C.2 curve at synchronous speed (i.e. midpoint of the discontinuity).

(d) The standstill value of the rotor hysteresis loss, $P_{h2}$, is given by half the amount of discontinuity in the A.C. curves at synchronous speed. The magnitude of this loss at any particular speed is obtained from the assumption that the loss is directly proportional to the rotor slip. It is to be remembered, however, that the loss is always positive even when the slip is negative.

(e) In test B, owing to the absence of parasitic brush losses, the ordinate of the A.C.2 curve at standstill represents the sum of the standstill values of stator and rotor eddy-current and hysteresis losses. Since the stator iron losses and the rotor hysteresis loss have been obtained from (c) and (d) above, $P_{e2}$ is easily determined. Using the assumption that the eddy-current loss in the rotor, $P_{e2}$, is directly proportional to the square of the rotor slip, the value of this loss at any motor speed can be obtained.

(f) In test B, the total input to the driving motor and test motor combination corrected for $I^2R$ losses is dissipated in the form of the driving motor no-load losses, the windage and friction losses in the test motor, the stator and rotor eddy-current

and hysteresis losses and the surface and pulsation losses in the test machine  Hence $P_p$ is obtained from

$$P_p = P_{AC2} + (P_{DC2'} - P_{DC2}) - (P_{e1} + P_{h1}) - (s^2 P_{e2} + s P_{h2})$$
$$\cdots \cdots (15)$$

(g) The difference between the A.C.1 and A.C.2 curves gives the electrical input to the short-circuited coils.  Part of this input comes back as useful torque in driving the motor.  The direction of the torque is reversed at super-synchronous speeds.  This part which does work is given by

$$P_m = (P_{DC2'} - P_{DC2}) - (P_{DC1'} - P_{DC1}) \quad . \quad (16)$$

Hence, $\qquad P_{sc} = (P_{AC1} - P_{AC2}) - P_m . \quad \cdots \quad (17)$

It is thus seen that the two tests A and B are sufficient for measuring and separating the no-load losses of the test motor at all speeds.  Though a d.c. drive was used in the test, any other drive may be used, provided that the no-load losses of the driving motor do not vary appreciably with small changes of load.  The d.c. motor used in the test was separately excited and the field current was kept constant throughout, the variation of speed being obtained by varying the armature voltage.  The variation of armature currents relating to the four curves D.C.1, D.C.1', D.C.2 and D.C.2' at any particular speed was small enough to enable the effect of armature reaction to be ignored.  Accurate metering is essential for the success of the test.

a predominant part of the parasitic brush current circuit.  Since the contact resistance is high at low current densities and hence low slips, and low at high current densities and hence high slips the parasitic-current circuit losses will vary apparently as a power higher than the square of the slip.

The losses in the coils short-circuited by the brushes therefore represent predominantly a contact loss.  When the machine is running normally there are two currents flowing through the contact, the main secondary current $i_r$ and the current in the short-circuited coils $i_b$.  The currents at the two ends of the contact are therefore $i_r + i_b$ and $i_r - i_b$.  This non-uniform distribution of current across the contact, which has a non-linear resistance, makes it difficult to estimate an average value of the contact resistance.  The losses $P_{sc}$ have been measured in the tests described above when $i_r = 0$.  The presence of $i_r$ in normal machine operation not only affects the contact resistance, and hence $P_{sc}$, but also increases the magnitude of $i_b$ to some extent (owing to the introduction of the reactance voltage due to commutation in the short-circuited coils).  In this paper it has been assumed that the two currents can be treated separately: the main current $i_r$ produces the usual contact loss $i_r^2 R_b$, where $R_b$ depends only on $i_r$, and the parasitic brush current $i_b$ produces a loss which is independent of $i_r$.  This assumption, though theoretically unjustifiable, does not introduce any serious error in practice.

<div align="center">

**Table 1**

Loss Separation Table

</div>

| Armature speed | Driving motor no-load losses | Separation of no-load losses of test motor | | | | | | | | | Test motor no-load losses from no-load run |
|---|---|---|---|---|---|---|---|---|---|---|---|
| | | $P_b$ | $P_f$ | $P_{e1} + P_{h1}$ | $P_{h2}$ | $P_{e2}$ | $P_p$ | $P_m$ | $P_{sc}$ | Total no-load losses | |
| r.p.m. | watts | watts | watts | watts | watts | watts | watts | watts | watts | watts | watts |
| 0 | 0 | 0 | 0 | 160 | 25 | 91 | 0 | 0 | 174 | 450 | — |
| 200 | 9 | 15 | 8 | 160 | 21·6 | 68 | 13·4 | 15·5 | 84·5 | 370·5 | — |
| 400 | 17 | 27 | 16 | 160 | 18·3 | 49 | 24·7 | 18 | 30 | 325 | 350 |
| 600 | 25 | 42 | 23 | 160 | 15 | 33 | 34 | 13 | 12 | 319 | 345 |
| 800 | 34 | 58 | 30 | 160 | 11·7 | 20 | 48·3 | 13 | 3 | 331 | 340 |
| 1 000 | 42 | 71 | 42 | 160 | 8·3 | 10 | 65·7 | 4 | 2 | 359 | 340 |
| 1 200 | 51 | 88 | 51 | 160 | 5·0 | 3·6 | 77·4 | — | — | 385 | 400 |
| 1 400 | 62 | 110 | 63 | 160 | 1·7 | 0·4 | 91·9 | — | — | 427 | 440 |
| 1 600 | 75 | 134 | 78 | 160 | 1·7 | 0·4 | 114·9 | — | — | 489 | 490 |
| 1 800 | 90 | 162 | 102 | 160 | 5·0 | 3·6 | 138·4 | — | — | 571 | 580 |
| 2 000 | 105 | 190 | 135 | 160 | 8·3 | 10 | 169·7 | —4 | 2 | 675 | 690 |
| 2 200 | 126 | 223 | 189 | 160 | 11·7 | 20 | 225 | —8 | 3 | 832 | 850 |
| 2 400 | 150 | 260 | 260 | 160 | 15·0 | 33 | 312 | —13 | 12 | 1 052 | 1 070 |

The separated values of the constituent no-load losses for the test motor are shown in Table 1.  In spite of best efforts the ill-conditioning of eqn. (16) makes the measurement of $P_m$ not very accurate.  To check that all the no-load losses have been located, the values of total no-load losses, obtained by synthesizing the separated losses, are compared with those obtained from a normal no-load run of the motor with regulator.  The comparison is given in the last two columns of Table 1 and shows good agreement.

One surprising result obtained in the test is the apparent evidence that the losses in short-circuited coils varied very nearly as the fourth power of the slip.  Since the parasitic brush losses are directly proportional to the square of the commutator segment voltage and the latter is a linear function of slip, the parasitic losses should be proportional to the square of the slip.

It is difficult to believe that experimental inaccuracies would be responsible for such a wide divergence from theoretical relationship.  The test result can, however, be explained if we consider the non-linearity of the contact resistance which forms

**(4.7) Measurement of Parameters of the Exact Equivalent Circuit**

The principle of the measurement of parameters of the practical circuit (Fig. 3) has been discussed in Reference 7.  In practice the measurement is slightly modified by separating the motor and regulator parameters, as shown in Fig. 10.  The regulator being a static piece of equipment, its parameters can
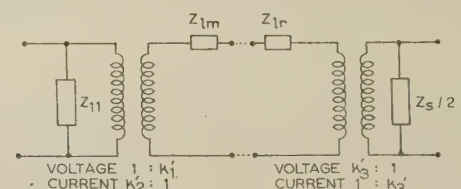


Fig. 10.—Splitting of equivalent circuit of Fig. 3 into motor and regulator constituents.

$$Z_{lm} = R_{r1} + R_{s3} + j(sx_{r1} + x_{s3})$$
$$\qquad\qquad + \{k_m^2 s + k_x^2 - k_m k_x [se^{j(\gamma+\theta)} + \varepsilon^{-j(\gamma+\theta)}](Z_{om}/Z_{11})z_{11}$$

$$Z_{lr} = 2z_r + 2k^2(Z_0/Z_s)z_s$$

measured with great accuracy and such measurement has been discussed in Reference 6. The remaining motor parameters be measured are

(a) $Z_{11}$
(b) $k_m s (Z_{om}/Z_{11}) \varepsilon^{+j\theta} - k_x (Z_{om}/Z_{11}) \varepsilon^{-j\gamma}$
(c) $k_m (Z_{om}/Z_{11}) \varepsilon^{-j\theta} - k_x (Z_{om}/Z_{11}) \varepsilon^{+j\gamma}$
(d) $Z_{lm}$

The open-circuit and short-circuit tests for the measurement the above parameters are now discussed.

*Open-circuit test.*

In this test the motor primary is connected to a normal-voltage normal-frequency supply, while the secondary and auxiliary windings are kept open-circuited with the rotor locked. The following symbols are used in the test:

$V$ = Supply voltage, volts per phase.
$i_1$ = Supply current, amperes per phase.
$V_r$ = Induced voltage across the secondary, volts per phase.
$V_x$ = Induced voltage across the auxiliary, volts per phase.

Then
$$Z_{11} = V/i_1 \text{ ohms}$$

$$k_m \frac{Z_{om}}{Z_{11}} \varepsilon^{+j\theta} = V_r/V$$

$$k_x \frac{Z_{om}}{Z_{11}} \varepsilon^{-j\gamma} = V_x/V$$

Hence $$k_m s \frac{Z_{om}}{Z_{11}} \varepsilon^{+j\theta} - k_x \frac{Z_{om}}{Z_{11}} \varepsilon^{-j\gamma} = sV_r/V - V_x/V$$

The phases of $i_1$, $V_r$ and $V_x$ with respect to $V$ must be measured express the parameters in complex forms.

Since $Z_{om}/Z_{11}$ can be regarded as approximately real,

$$k_m \frac{Z_{om}}{Z_{11}} \varepsilon^{-j\theta} - k_x \frac{Z_{om}}{Z_{11}} \varepsilon^{+j\gamma} = (V_r/V)^* - (V_x/V)^*$$

where $(V_r/V)^*$ and $(V_x/V)^*$ are complex conjugates of $V_r/V$ and $V_x/V$, respectively.

$X_{11}$, the reactive part of $Z_{11}$, is a constant at constant voltage, but the loss component as discussed earlier is a function of speed. the total no-load losses (electrical) in the motor, including the copper losses in the primary winding, are f(s), then $R_{11}$, the loss component of $Z_{11}$ when $R_{11}$ and $X_{11}$ are in parallel, is given by

$$R_{11} = V^2/f(s) \quad . \quad . \quad . \quad . \quad . \quad (18)$$

*Short-circuit test.*

In this test the auxiliary and secondary are connected in series (as in normal operation) and further connected to a normal-frequency supply, the primary terminals being on short-circuit. The supply voltage is so adjusted as to allow full-load current to flow in the primary winding. The leakage impedance term $Z_{lm}$ is then given by the input impedance measured in the test. To find its dependence on slip, the input impedance is measured at at least two speeds, the rotor being driven by an auxiliary drive. To avoid effects of harmonics, the impedance was measured at standstill where the voltage and current waves were nearly sinusoidal, and then the rotor was driven to the speed where $P_1 = P_2$, $P_1$ and $P_2$ being the wattmeter readings the two-wattmeter method of measuring power (see Section 9). This speed was noted. At this speed the circuit is purely resistive, and hence $x_{lm}$, the reactive portion of $z_{lm}$, must be zero. From knowledge of $x_{lm}$ at standstill and the speed at which it is zero, its slip-dependent and slip-independent parts are easily evaluated.

Determination of $R_{lm}$, the resistive portion of $Z_{lm}$, and its dependence on slip present considerable difficulty owing to the presence of the non-linear contact resistance, the iron losses in the test and the losses in the coils short-circuited by the brushes.

To eliminate the effect of non-linearity of contact resistance the secondary current in the short-circuit test is kept at a fixed value both at standstill and at the speed where $P_1 = P_2$. Corrections for parasitic and iron losses at these points are made by measuring these losses at the same input voltages in an open-circuit test (primary open-circuited). From the corrected values of resistance obtained at standstill and at a speed where $P_1 = P_2$, $R_{lm}$ is easily expressed as $R_b + sR + R'$, with $R_b$ remaining in the circuit as a non-linear parameter. Both for this test and for characteristics calculation the variation of $R_b$ with the secondary current must be known (Fig. 7).

(4.8) **Summarized Values of Motor Parameters**

The values of parameters for the test motor as measured in the preceding Sections are summarized below.

(a) *For the orthodox equivalent circuit:*

$k_m = 0.137$, $k_x = 0.0181$, $\theta = 5°$, $\gamma = 60°$, $R_{s1} = 2.0$ ohms, $R_{r1} = R_b + 0.015$ ohm, $R_{s3} = 0.0085$ ohm, $x_{s1} = 4.13$ ohms, $x_{r1} = 0.091$ ohm, $x_{s3} = 0.0065$ ohm, $x_{om}$ (parallel branch) = $78.3$ ohms; and $R_{om}$ (parallel branch) = $53.3/(90 - 75s + 125s^2)$ kilohms.

(b) *For the practical equivalent circuit:*

Voltage transformation ratio = $(0.130s - 0.0085) + j(0.0113s + 0.0148)$; current transformation ratio = $0.1215 - j0.0261$; $R_{11} = 53.3/(106 - 75s + 125s^2)$ kilohms; $X_{11} = 83.2$ ohms; $Z_{lm} = (R_b + 0.028 + 0.027s) + j(0.161s)$ ohms.

The above parameters and the variation of $R_b$ with secondary current, together with the regulator parameters, are sufficient to enable calculation of characteristics for the test motor to be carried out.

The parameters of the practical equivalent circuit can also be calculated from the known values of parameters of the orthodox circuit. Comparison of these calculated values with those obtained by tests shows very slight expected differences, the major difference being in the values of $Z_{lm}$, as can be seen from the following:

*Calculated.* $\quad Z_{lm} = (R_b + 0.013 + 0.043s)$
$$+ j(0.156s + 0.008) \text{ ohms} \quad . \quad (19)$$

*Test.* $\quad Z_{lm} = (R_b + 0.028 + 0.027s) + j(0.161s) \text{ ohms} . \quad (20)$

In the actual test for measuring $R_{lm}$ no correction was made for iron losses at the speed where $P_1 = P_2$, these being considered to be small. This may be why the slip-independent portion of $R_{lm}$ in eqn. (20) is higher and the slip-dependent portion lower than the corresponding quantities in eqn. (19). The slip-independent portion of $x_{lm}$ in eqn. (19) is small compared with the slip-dependent portion, and its absence in eqn. (20) may be due to experimental inaccuracies in measurement. In performance calculations eqn. (19) has been used.

(4.9) **Measured Values of Regulator Parameters**

The values of regulator parameters taken from Reference 6 are:

(a) *Orthodox circuit:*

$k = 0.068$, $Z_0 = 12.53 + j67.03$ ohms, $z_s = 1.47 + j1.85$ ohms and $z_r = 0.0178 + j0.0083$ ohm.

(b) *Practical circuit:*

$Z_s/2 = 7 + j34.44$ ohms, $2k(Z_o/Z_s) = 0.132$ and
$$Z_{lr} = 0.049 + j0.033 \text{ ohm.}$$

(5) **CHARACTERISTICS CALCULATION AND COMPARISON WITH TEST RESULTS**

Once the parameters are evaluated, either of the circuits of Fig. 2 or 3 or the tensor equations $i = Z^{-1}V$ can be used to

calculate the behaviour of the test motor under steady-state conditions. The orthodox and practical circuits given identical performance equations since both are exact representations of the impedance tensor [eqn. (1)]. Owing to the various approximations made in measurement of parameters, the two circuits using measured values as shown in Sections 4.8 and 4.9 give slightly different results under the same operating conditions. The difference, however, is usually small, as is illustrated by a sample below.

*Operating conditions*: $\cos \alpha = 0\cdot707$; slip $= 0\cdot673$; supply voltage $= 231$ volts per phase.

(a) From the orthodox circuit on calculation:

$$i_1 = (0\cdot44 - j2\cdot77) + (0\cdot12 - j0\cdot0264)i_r \quad . \quad . \quad . \quad (21a)$$

$$i_r = 231(- 0\cdot0146 + j0\cdot0226)/R_b + 0\cdot091 + j0\cdot146 \quad (21b)$$

$$i_2 = (1\cdot33 - j6\cdot45) - 0\cdot0932 i_r \quad . \quad . \quad . \quad . \quad . \quad (21c)$$

(b) From the exact practical circuit:

$$i_1 = (0\cdot48 - j2\cdot77) + (0\cdot1215 - j0\cdot026)i_r \quad . \quad . \quad . \quad (22a)$$

$$i_r = 231(- 0\cdot0142 + j0\cdot0224)/R_b + 0\cdot091 + j0\cdot146 \quad (22b)$$

$$i_2 = (1\cdot33 - j6\cdot45) - 0\cdot0932 i_r \quad . \quad . \quad . \quad . \quad . \quad (22c)$$

On comparison it is seen that $i_r$ and $i_2$ in eqns. (21) and (22) are almost identical. There is, however, a slight difference in

the loss component of current representing the no-load losses in the motor [eqns. (21a) and (22a)]. The difference is due to the approximation made in the orthodox circuit by neglecting the voltage drop across the primary leakage impedance in determining $R_{om}$. For all practical purposes the two circuits can be considered identical and hence, in subsequent calculation, only the practical circuit has been used. It will be appreciated that the practical circuit is easier to handle for numerical solutions.

### (5.1) No-Load and Load Tests

Using the equivalent circuit, the supply current and individual currents in the motor primary, regulator primary and the rotor circuit can be calculated for given values of $\cos \alpha$ and slip. In experimental verification of the theory a number of no-load and load tests were carried out on the test machine. Calculated and observed values of currents in the test are shown in Tables 2 and 3.

The temperature and other ambient conditions affect the current in the rotor circuit considerably. Variation in rotor circuit current in its turn affects, though to a lesser degree, the motor and regulator primary currents. Precautions were taken to allow the machine to run for a considerable time before any readings were taken, to ensure that the brush contacts had reached a steady temperature. In spite of this, there were variations of

### Table 2
#### COMPARISON OF NO-LOAD TEST RESULTS WITH CALCULATIONS FROM THE EQUIVALENT CIRCUIT

| cos α | Slip | $\lvert i_r \rvert$ | | $i_1$ | | $i_2$ | | $I = i_1 + i_2$ | |
|---|---|---|---|---|---|---|---|---|---|
| | | Calculated | Observed | Calculated | Observed | Calculated | Observed | Calculated | Observed |
| | | amp | amp | amp | amp | amp | amp | amp | amp |
| 0·707 | 0·673 | 26·8 | 28 | 1·61 + j0·33 | 0·95 + j0·2 | 1·0 − j8·93 | 1·75 − j9·2 | 2·61 − j8·6 | 2·7 − j9·0 |
| 0·582 | 0·574 | 25·8 | 26 | 1·64 + j0·2 | 0·95 + j0·2 | 0·99 − j8·4 | 1·63 − j8·8 | 2·63 − j8·2 | 2·58 − j8·6 |
| 0·442 | 0·446 | 25·2 | 25 | 1·57 + j0·13 | 1·05 + j0·2 | 1·09 − j7·91 | 1·52 − j8·5 | 2·66 − j7·78 | 2·57 − j8·3 |
| 0·291 | 0·314 | 24·0 | 23·5 | 1·59 − j0·02 | 1·06 + j0 | 1·15 − j7·36 | 1·50 − j7·8 | 2·74 − j7·38 | 2·56 − j7·8 |
| 0·131 | 0·173 | 23·0 | 21 | 1·61 − j0·18 | 1·05 − j0·2 | 1·24 − j6·84 | 1·45 − j7·3 | 2·85 − j7·02 | 2·50 − j7·5 |
| −0·033 | 0·0133 | 22·4 | 19·5 | 1·34 − j0·17 | 0·95 − j0·4 | 1·34 − j6·35 | 1·35 − j6·4 | 2·68 − j6·52 | 2·30 − j7·0 |
| −0·196 | −0·140 | 20·6 | 18 | 1·19 − j0·30 | 1·0 − j0·6 | 1·36 − j5·92 | 1·40 − j6·0 | 2·55 − j6·22 | 2·40 − j6·6 |
| −0·354 | −0·286 | 18·6 | 16 | 1·20 − j0·57 | 0·97 − j0·8 | 1·38 − j5·59 | 1·55 − j5·6 | 2·58 − j6·16 | 2·52 − j6·4 |
| −0·50 | −0·427 | 16·4 | 14 | 1·17 − j0·8 | 0·95 − j0·9 | 1·36 − j5·35 | 1·65 − j5·2 | 2·53 − j6·15 | 2·6 − j6·1 |
| −0·635 | −0·568 | 13·0 | 12 | 0·92 − j1·14 | 0·98 − j1·2 | 1·16 − j5·36 | 1·67 − j5·1 | 2·08 − j6·50 | 2·65 − j6·3 |
| −0·707 | −0·640 | 11·0 | 10 | 0·92 − j1·41 | 1·0 − j1·3 | 1·14 − j5·35 | 1·68 − j5·0 | 2·06 − j6·76 | 2·68 − j6·3 |

### Table 3
#### COMPARISON OF LOAD TEST RESULTS WITH CALCULATIONS FROM THE EQUIVALENT CIRCUIT

| cos α | Slip | $i_r$ | | $i_1$ | | $i_2$ | | $I = i_1 + i_2$ | |
|---|---|---|---|---|---|---|---|---|---|
| | | Calculated | Observed | Calculated | Observed | Calculated | Observed | Calculated | Observed |
| | | amp | amp | amp | amp | amp | amp | amp | amp |
| 0·707 | 0·673 | 26·8 | 28 | 1·61 + j0·33 | 0·95 + j0·2 | 1·0 − j8·93 | 1·75 − j9·2 | 2·61 − j8·6 | 2·7 − j9·0 |
| (sub- | 0·69 | 25·8 | 26 | 1·8 + j0·15 | 1·4 + j0 | 0·82 − j8·8 | 1·31 − j9·0 | 2·62 − j8·65 | 2·71 − j9·0 |
| synchronous) | 0·72 | 24 | 24 | 2·1 − j0·29 | 1·8 − j0·4 | 0·52 − j8·52 | 0·92 − j8·6 | 2·62 − j8·81 | 2·72 − j9·0 |
| | 0·76 | 22·4 | 22·5 | 2·54 − j0·85 | 2·3 − j1·0 | 0·14 − j8·18 | 0·5 − j8·2 | 2·68 − j9·03 | 2·8 − j9·2 |
| | 0·80 | 22·2 | 22 | 2·92 − j1·36 | 2·82 − j1·5 | −0·2 − j7·86 | 0·08 − j7·8 | 2·72 − j9·22 | 2·9 − j9·3 |
| −0·033 | 0·0133 | 22·4 | 19·5 | 1·34 − j0·17 | 0·95 − j0·4 | 1·34 − j6·35 | 1·35 − j6·4 | 2·68 − j6·52 | 2·30 − j7·0 |
| (near | 0·05 | 22·8 | 21 | 2·21 − j0·58 | 1·7 − j0·8 | 1·37 − j6·36 | 1·4 − j6·4 | 3·58 − j6·94 | 3·10 − j7·2 |
| synchronous) | 0·10 | 26 | 24 | 3·29 − j1·22 | 2·8 − j1·3 | 1·42 − j6·38 | 1·45 − j6·4 | 4·71 − j7·6 | 4·25 − j7·7 |
| | 0·13 | 29·8 | 27 | 3·93 − j1·64 | 3·7 − j1·8 | 1·44 − j6·39 | 1·46 − j6·4 | 5·37 − j8·03 | 5·16 − j8·2 |
| | 0·16 | 33·2 | 30 | 4·51 − j2·07 | 4·2 − j2·2 | 1·47 − j6·4 | 1·49 − j6·4 | 5·98 − j8·47 | 5·69 − j8·6 |
| −0·5 | −0·427 | 16·4 | 14 | 1·17 − j0·8 | 0·95 − j0·9 | 1·36 − j5·35 | 1·65 − j5·2 | 2·53 − j6·15 | 2·6 − j6·1 |
| (super- | −0·40 | 19·5 | 16·5 | 1·9 − j0·71 | 1·6 − j0·8 | 1·74 − j5·24 | 2·2 − j5·2 | 3·64 − j5·95 | 3·8 − j6·0 |
| synchronous) | −0·38 | 24 | 22 | 2·51 − j0·61 | 2·3 − j0·7 | 2·05 − j5·15 | 2·4 − j5·0 | 4·56 − j5·76 | 4·7 − j5·7 |
| | −0·36 | 27·4 | 25 | 3·28 − j0·63 | 3·4 − j0·7 | 2·47 − j5·05 | 2·4 − j5·1 | 5·75 − j5·68 | 5·8 − j5·8 |
| | −0·34 | 30·2 | 28 | 3·76 − j0·67 | 3·9 − j0·7 | 2·72 − j5·0 | 2·7 − j5·1 | 6·48 − j5·67 | 6·6 − j5·8 |
| | −0·32 | 37·2 | 33 | 4·82 − j0·77 | 5·2 − j0·9 | 3·29 − j4·95 | 3·3 − j5·1 | 8·11 − j5·72 | 8·5 − j6·0 |

bout 10–15% from day to day. The observed values for currents shown in Tables 2 and 3 are an average of numerous readings taken over a long period.

The small size of the machine and the loading generator (1 kW) limited the tests to a small range of loads, which is a serious disadvantage in any experimental verification of theory. In view of the inherent limitations of the theory, the dependence of some of the parameters supposed constant on the operating conditions (e.g. leakage reactances on current, mutual reactances on voltage, etc.) and many difficulties experienced in the measurement of parameters, the agreement between calculated and observed values shown in Tables 2 and 3 is very encouraging. The supply currents seem to agree best, but their division into motor and regulator currents shows considerable divergence in the calculated and observed values, particularly at subsynchronous speeds. The divergence is in the loss components of the currents, the quadrature components agreeing reasonably well, more power being supplied through the regulator and less through the motor than calculated. This is thought to be due to the regulator supplying part of the surface and parasitic losses of the motor at subsynchronous speeds.

Some tests were made on the machine with the auxiliary winding disconnected from the main machine circuit. The agreement reached between calculated behaviour and test results was of about the same order as in tests with the auxiliary winding in.

## (6) CONCLUSION

The evidence of fairly good agreement between experimental and theoretical results justifies the belief that not only is the theory within its inherent limitations basically sound but also that the methods used for measurement of machine parameters are fairly accurate. It is hoped that the information contained in this paper and in two earlier related papers[6, 7] will prove useful to those interested in the design and operation of the stator-fed 3-phase shunt commutator motor with induction regulator control.

## (7) ACKNOWLEDGMENTS

## (8) REFERENCES*

ALGER, P. L., and EKSERGIAN, R.: 'Iron Losses in Induction Motors', *Journal of the American I.E.E.*, 1920, **39**, p. 906.

RICHTER, R.: 'Elektrische Maschinen' (Springer-Verlag, Berlin, 1950), Vol. 5.

ADKINS, B., and GIBBS, W. J.: 'Polyphase Commutator Machines' (Cambridge University Press, 1951).

SAY, M. G.: 'The Performance and Design of Alternating Current Machines' (Pitman, 1952).

JHA, C. S.: 'Tensor Analysis of the Steady-State Behaviour of the Stator-Fed Polyphase Shunt Commutator Motor', Thesis for Fellowship, Heriot-Watt College, June, 1955.

JHA, C. S.: 'Theory and Equivalent Circuits of the Double Induction Regulator', *Proceedings I.E.E.*, Monograph No. 197 U, September, 1956 (**104** C, p. 96).

JHA, C. S.: 'Theory and Equivalent Circuits of the Stator-Fed Polyphase Shunt Commutator Motor', *ibid.*, Monograph No. 220 U, February, 1957 (**104** C, p. 305).

* For a comprehensive Bibliography see Reference 7.

## (9) APPENDIX: SPECIAL APPLICATION OF THE TWO WATTMETER METHOD OF MEASURING POWER AND THE PHASE ANGLE BETWEEN VOLTAGE AND CURRENT VECTORS IN A THREE-PHASE CIRCUIT

### (9.1) Three-phase Three-wire System

The two-wattmeter method of measuring power in a 3-phase 3-wire circuit is well known. If $P_1$ and $P_2$ be the two wattmeter readings,

$$\text{Total power} = P_1 + P_2 \quad . \quad . \quad . \quad (23)$$

The phase angle $\phi$ between voltage and current vectors is given by the relation

$$\tan \phi = \frac{\sqrt{3}(P_1 - P_2)}{P_1 + P_2} \quad . \quad . \quad . \quad (24)$$

### (9.2) When the Load is in the form of a Commutator Winding with Two Brushes per Phase

In this case, assuming a 3-phase 6-wire supply available, the wattmeter connections for measuring power and $\tan \phi$ are as shown in Fig. 11. For balanced conditions, the following relations can be easily derived:

$$\text{Total power} = 2(P_1 + P_2) \quad . \quad . \quad . \quad (25)$$

and

$$\tan \phi = \frac{\sqrt{3}(P_1 - P_2)}{P_1 + P_2} \quad . \quad . \quad . \quad (26)$$
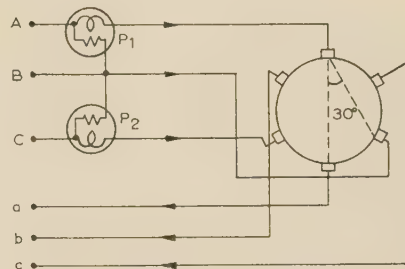


Fig. 11.—The two-wattmeter method when the load is in the form of a commutator winding with two brushes per phase.
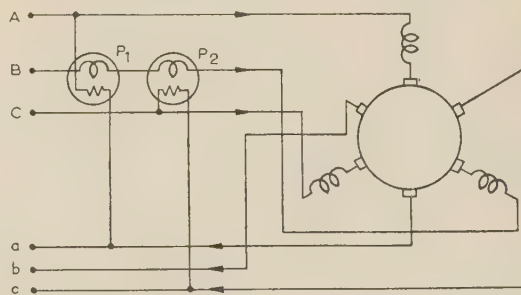


Fig. 12.—The two-wattmeter method when the load is in the form of a commutator winding with two brushes per phase and an extra balanced load connected to each phase.

### (9.3) When, in addition to the Commutator Winding with Two Brushes per Phase, extra Balanced Loads are present in each Phase

In this case, the measurement is slightly modified, the wattmeter connections being as shown in Fig. 12. It can be shown that for balanced conditions

$$\text{Total power} = 3(P_1 + P_2) \quad . \quad . \quad . \quad (27)$$

$$\tan \phi = \frac{P_1 - P_2}{\sqrt{3}(P_1 + P_2)} \quad . \quad . \quad . \quad (28)$$

# OUTLINE OF A THEORY OF NON-UNIFORM TRANSMISSION LINES

## By BORIS G. KAZANSKY.

### SUMMARY

Complex differential equations relating to non-uniform transmission lines are studied, and the corresponding two-parameter families of solution curves are investigated with the aim of establishing some important properties, e.g. the relationship which exists between the singular points of the differential equation for the normalized impedance and the non-reflective impedances of the corresponding non-uniform line. Because of this relationship it is possible to determine the non-reflective impedances of an arbitrary tapered line by a purely algebraic method and to construct the tangents to the impedance loci at a given point of the impedance plane. Moreover, reflection and transmission coefficients are uniquely determined by the singularities, and differential equations can be readily deduced for these coefficients. Methods of synthesis of non-uniform lines are also indicated.

### LIST OF PRINCIPAL SYMBOLS

$A = \sqrt{\left[\left(\dfrac{l}{K\lambda}\right)^2 - 1\right]}$ = Reduced length of exponential taper.

$K = \dfrac{1}{4\pi} \log_\varepsilon (Z_r/Z_t)$.

$k = |k| \angle \sigma$ = Outer parameter of a standard net.

$m = Z_0^-/Z_0 = n - js = \angle - \tau$ = Normalized non-reflective impedance for backward waves.

$n = \sqrt{(1 - s^2)} = \cos \tau$.

$p = Z_0^+/Z_0 = n + js = \angle \tau$ = Normalized non-reflective impedance for direct waves.

$q = \dfrac{Z_0'}{Z_0} = \dfrac{d \log_\varepsilon Z_0}{d\phi}$ = Logarithmic derivative of the nominal characteristic impedance.

$s = q/2 = \sin \tau$; with exponential lines $s = -v$.

$x$ = Distance from the transmitting end; imaginary part of $z$.

$y = l - x$ = Distance from the receiving end.

$Z = V/I$ = Equivalent impedance.

$Z_0 = \sqrt{(Z_s/Y_p)}$ = Nominal characteristic impedance.

$Z_0^+ = V^+/I^+$ = Actual characteristic impedance (non-reflective impedance) associated with direct waves.

$Z_0^- = -V^-/I^-$ = Non-reflective impedance for backward waves.

$Z_r$ = Value of $Z_0$ for $y = 0$.

$Z_t$ = Value of $Z_0$ for $y = l$.

$z = Z/Z_0 = r + jx$ = Normalized equivalent impedance.

$z_1, z_2$ = Invariant normalized impedances.

$z_L$ = Normalized load impedance.

*In Sections* 3 *and* 11.1.

$z = x + jy$ = General complex variable.

$z_0, z_p$ = Singular points.

$\Gamma = \Gamma_V$ = Voltage reflection coefficient.

$\Gamma_H$ = Overall voltage reflection coefficient of composite lines.

$\gamma = \sqrt{(Z_s Y_p)} = \alpha + j\beta$ = Nominal propagation coefficient.

$\delta = \dfrac{1}{l} \log_\varepsilon(Z_r/Z_t)$ (exponential lines).

$\theta$ = Phase angle of $z'$.

$v = \delta/2\beta$ for loss-free exponential lines.

$\sigma = \arg k$.

$\tau = \arg p = -\arg m$.

$\phi = \beta y$ = Angular distance along loss-free lines.

$z' = \dfrac{dz}{d\phi}$.

### (1) INTRODUCTION

The classical method of investigation of non-uniform transmission lines employing differential equations for voltage and current seems to have reached its natural limit of efficiency, and new approaches have been proposed by several authors. Thus Pierce[1] deduced a differential equation for impedance as early as 1943. Walker and Wax[14] derived a differential equation for the overall reflection coefficient of composite lines in 1946; this equation has been the basis of a long series of papers devoted to tapered lines.

On the other hand, the importance of the theory of non-uniform lines now reaches far beyond the scope of tapered electrical lines as such; analogies already existing or anticipated with the theory of propagation of electromagnetic or acoustic waves in non-homogeneous media, with some problems of electron optics,[1] etc., make it desirable to establish general methods enabling us to determine in a simple manner the most important properties and characteristic quantities of arbitrary non-uniform lines.

The objective of the present paper is to submit an elementary theory of non-uniform transmission lines based on the differential equation for normalized impedance. The theory is valid for all transmission lines and electrical systems obeying the 'transmission-line equations'. In close analogy with the theory of dynamic systems, transmission lines are subdivided into *autonomic* and *non-autonomic* lines; for a non-autonomic line the derivative of the characteristic impedance explicitly depends upon the distance along the line. Essentially new phenomena occur in the case of non-autonomic lines which cannot occur with the autonomic (uniform and exponential) lines. These phenomena can be treated by methods which are interesting and instructive in themselves without being difficult and which do not require the use of complicated mathematics.

It is seldom possible and scarcely ever useful, in the first stage of a new theory, to combine mathematical rigour with clarity of presentation, and it is hoped that the emphasis laid upon the physical and geometrical meaning of the new notions will compensate for the lack of rigour.

The basic differential equations are derived in Section 2 and a survey of properties of complex differential equations—some of which are published here for the first time—is given in Section 3, where the notion of 'standard nets' is also introduced. These are special two-parameter families of curves. In Section 4 the singular points of a non-autonomic differential equation are shown to be the local invariant impedances of the corresponding line which are intimately connected with the local non-reflective

impedances. Applications are condensed in Section 5, and differential equations for reflection and transmission coefficients are deduced in Section 6. Section 7 is concerned with the synthesis of non-uniform lines. The Appendices deal with more general properties of complex differential equations, with the optical inversor and anisotropic normalized impedances, respectively.

## (2) DIFFERENTIAL EQUATIONS FOR THE NORMALIZED IMPEDANCE

The line equations can be written in the form

$$\frac{dV}{dy} = Z_s I, \quad \frac{dI}{dy} = Y_p V \quad . \quad . \quad . \quad . \quad (1)$$

where $Z_s$ and $Y_p$ denote the series impedance and the parallel admittance per unit length of the non-uniform line at the point $y = l - x$.

The nominal characteristic impedance is defined as

$$Z_0(y) = \sqrt{(Z_s/Y_p)} \quad . \quad . \quad . \quad . \quad (2)$$

$Z_0$ is real for loss-free lines.

$$\gamma(y) = \sqrt{(Z_s Y_p)} = \alpha + j\beta \quad . \quad . \quad . \quad . \quad (3)$$

is the *nominal* propagation coefficient, which is purely imaginary for loss-free lines.

$Z_0$ and $\gamma$ are the characteristic impedance and the propagation coefficient of the uniform line having the same parameters, $Z_s$ and $Y_p$, as the non-uniform line at the given point. It is easy to see that

$$\gamma = Z_s/Z_0 = Y_p Z_0 \quad . \quad . \quad . \quad . \quad (4)$$

The normalized equivalent impedance at any point is

$$z = \frac{V}{Z_0 I} \quad . \quad . \quad . \quad . \quad . \quad (5)$$

Differentiating the logarithm of this quantity

$$\frac{1}{z}\frac{dz}{dy} = \frac{1}{V}\frac{dV}{dy} - \frac{1}{I}\frac{dI}{dy} - \frac{1}{Z_0}\frac{dZ_0}{dy} \quad . \quad . \quad (6)$$

The individual terms of the second member are, using eqns. (1), (2) and (5),

$$\frac{1}{V}\frac{dV}{dy} = \frac{Z_0 I}{V}\frac{1}{Z_0 I}\frac{dV}{dy} = \frac{1}{z}\frac{Z_s}{Z_0} = \frac{\gamma}{z}$$

$$\frac{1}{I}\frac{dI}{dy} = \frac{V}{Z_0 I}\frac{Z_0}{V}\frac{dI}{dy} = z Y_p Z_0 = z\gamma$$

Eqn. (6) can now be written

$$\frac{1}{z}\frac{dz}{dy} = \frac{\gamma}{z} - z\gamma - \frac{1}{Z_0}\frac{dZ_0}{dy} \quad . \quad . \quad . \quad (7)$$

or finally

$$\frac{dz}{dy} = \gamma(1 - z^2) - \frac{d \log_\varepsilon Z_0}{dy} z \quad . \quad . \quad (8)$$

This is the fundamental differential equation for all following discussions. It governs the normalized impedance of any non-uniform lines obeying eqns. (1). It is a Riccati equation and cannot be solved in general if the logarithmic derivative or $\gamma$ is variable. In many practical cases $\gamma$ is approximately constant.

Eqn. (8) can be rewritten in the form

$$\frac{dz}{dy} = -\gamma(z - z_1)(z - z_2) \quad . \quad . \quad . \quad (9)$$

where $z_1(y)$, $z_2(y)$ are the roots of the second member of eqn. (8).

For loss-free lines we obtain, introducing $d\phi = \beta dy$ and

$$q(\phi) = \frac{d \log_\varepsilon Z_0}{\beta dy} = \frac{d \log_\varepsilon Z_0}{d\phi} \quad . \quad . \quad . \quad (10)$$

the following equation:

$$\frac{dz}{d\phi} = j(1 - z^2) - q(\phi)z \quad . \quad . \quad . \quad (11)$$

This differential equation explicitly contains the rate of change of $Z_0$. Returning to $Z = zZ_0$, we obtain the equation of Pierce[1] which, in our notation, is

$$Z_0\frac{dZ}{dy} = j\beta(Z_0^2 - Z^2) \quad . \quad . \quad . \quad (12)$$

In this form, which does not contain the rate of change of $Z_0$, it is not very suitable for investigation of tapered lines.

Equations for admittances have the same form as eqns. (8) and (11). If desired, expressions for voltage and current can be obtained from the expression for impedance.

### (2.1) Types of Transmission Line Equations

For the sake of brevity we denote $dz/d\phi$ by $z'$.

If $q = 0$, eqn. (11) assumes the form

$$z' = j(1 - z^2) \quad . \quad . \quad . \quad . \quad (13)$$

corresponding to loss-free uniform lines ($Z_0 = $ constant).

If $q$ is constant we can write

$$z' = j(1 - z^2) - qz \quad . \quad . \quad . \quad (14)$$

which corresponds to exponential lines since, for constant $\beta$,

$$\frac{d \log_\varepsilon Z_0}{dy} = \text{constant} = -\delta \quad . \quad . \quad (15)$$

and

$$Z_0 = Z_r \varepsilon^{-\delta y} \quad . \quad . \quad . \quad . \quad (16)$$

The second member of eqns. (13) and (14) does not explicitly contain $\phi$, so that $z'$ is a function of $z$ only. In the qualitative theory of differential equations such equations are termed 'autonomic differential equations'. Equations of the form of eqn. (11) are termed 'non-autonomic', since the second member involves $q$, which is a given function of $\phi$. This terminology will also be applied to transmission lines.

## (3) SOME PROPERTIES OF COMPLEX DIFFERENTIAL EQUATIONS

The ever-increasing use of complex functions of a real variable is not accompanied by a corresponding development of the theory of differential equations of such functions. Some properties, essential for the theory of non-uniform lines, will be given in this Section; further details of more general interest will be considered in Appendix 11.1.

Throughout this Section and Appendix 11.1, we denote by $z = x + jy$ any complex function of the real variable $t$, which can be the geometrical or angular distance along the transmission line.

An autonomic differential equation

$$z' = f(z) = u(x, y) + jv(x, y) \quad . \quad . \quad (17)$$

represents a one-parameter family of oriented curves

$$\int \frac{dz}{f(z)} = F(z) = t + c \quad . \quad . \quad . \quad (18)$$

and the corresponding real differential equation is of the form

$$\frac{dy}{dx} = \frac{v(x, y)}{u(x, y)} = H(x, y) = \tan \theta \quad . \quad . \quad (19)$$

where $\theta = \arg z'$ is the angle between the tangent vector $z'$ and the real axis.

A non-autonomic differential equation

$$z' = f(z, t) = u(x, y, t) + jv(x, y, t) \quad . \quad . \quad (20)$$

represents in general (see Appendix 11.1) a two-parameter family of oriented curves which cannot be determined in the majority of cases by the integration of eqn. (20).

For different values of $t$, different solution-curves pass in this case through any given point $z$, thus forming a pencil of curves with its vortex at $z$. The corresponding values of $\theta$ are given by the equation

$$\frac{dy}{dx} = \frac{v(x, y, t)}{u(x, y, t)} = H_t(x, y, t) = \tan \theta \quad . \quad . \quad (21)$$

Singular points of a complex differential equation of the type of eqn. (17) or (20) and of the corresponding family of curves are as follows:

    (*a*) The points $z_0$ for which $z'$ is zero.
    (*b*) The points $z_p$ for which $z'$ is infinite (poles).

In both cases there exists no definite tangent to the solution-curve or curves (cf. Reference 2).

Singular points can be also termed stationary points or supports of the family of curves.

In the autonomic case the singularities are fixed while in the non-autonomic case we have moving singularities.

If $z$ denotes impedance, the stationary points $z_0$ of eqns. (17) and (20) are the invariant impedances of the transmission line in question. Thus, for uniform lines, $z' = j(1 - z^2)$ and the invariant impedances are $\pm 1$ [see eqn. (13)].

Isogonal trajectories of a family of curves given by $z' = f(z)$ are governed by the differential equation

$$z' = kf(z) \quad . \quad . \quad . \quad . \quad . \quad (22)$$

where $k = |k| \underline{/\sigma}$; since $|k|$ does not affect the direction of tangents we can also write $z' = \underline{/\sigma} f(z)$. Elementary arcs and tangents are rotated through the angle $\sigma = \arg k$, while the position of the supports is not affected by the rotation. $k$ is the 'outer' parameter determining a fixed family of isogonal trajectories.

For a given set of supports, say $z_{01}$, $z_{02}$ and $z_p$, the notion of the *standard net* SN is introduced by the differential equation

$$z' = k\frac{(z - z_{01})(z - z_{02})}{z - z_p} \quad . \quad . \quad . \quad (23)$$

which obviously governs a two-parameter family of all isogonal trajectories of the family of curves

$$z' = \frac{(z - z_{01})(z - z_{02})}{z - z_p}$$

This family corresponds to $k = 1$ and is the first basic family of the standard net [eqn. (23)]; for $k = j$ we obtain the second basic family orthogonal to the first. Complex values of $k$, $k = \underline{/\sigma}$, correspond to the diagonal families of SN.

We shall be interested here mainly in the polynomial SN having no poles, $z_p$. The degree of the polynomial (identical to the number of supports) will be denoted by a subscript and the supports can be indicated in parenthesis. Thus $SN_2(1, -1)$ denotes the standard net of the second degree with supports at $z = \pm 1$.

The most important types of standard net will be analysed in the next Section. Primarily, the standard nets are solutions of autonomic differential equations; nevertheless, the solutions of non-autonomic equations are often intimately connected with local standard nets corresponding to fixed values of the independent variable (see Section 4.4).

### (3.1) The Four Types of Standard Net

#### (3.1.1) SN$_0$. The Standard Net of Zero Degree.

$$z' = k, \ z = kt + C \ (C \text{ is complex}) \quad . \quad . \quad (2\ )$$

has no supports. The basic families $z' = 1$, $z' = j$ form the orthogonal co-ordinate network, the diagonal families $z' = \underline{/}$ consist of oblique parallel straight lines.
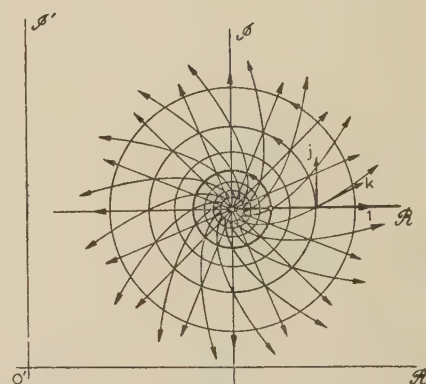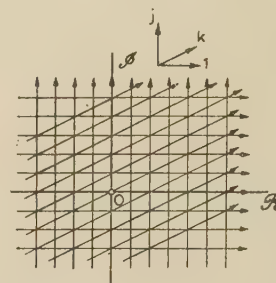




Fig. 1.—The standard net of the first degree.
$$z' = kz, (\mathcal{R}, I).$$
$$z' = k(z - z_1), (\mathcal{R}', I').$$

#### (3.1.2) SN$_1$. The Standard Net of the First Degree (see Fig. 1).

$$z' = k(z - z_1), \ z = z_1 + C\varepsilon^{kt} \quad . \quad . \quad . \quad (2\ )$$

has the single support $z_0 = z_1$. We shall discuss the SN$_1(0)$

$$z' = kz, \ z = C\varepsilon^{kt} \quad . \quad . \quad . \quad . \quad (2\ )$$

with the support at the origin. The basic families $z' = z$ and $z' = jz$ form the polar co-ordinate network; the diagonal families $z' = \underline{/\sigma} z$ are logarithmic spirals. SN$_1(0)$ thus represents the polar Smith chart for the reflection coefficient. The general SN$_1$ follows by translation.

#### (3.1.3) SN$_2$. The Standard Net of the Second Degree (see Fig. 2).

$$z' = k(z - z_1)(z - z_2) = kz^2 + Az^2 + B, \ z = \frac{z_1 - z_2 C\varepsilon^{(z_1-z_2)kt}}{1 - C\varepsilon^{(z_1-z_2)kt}}$$

$$. \quad . \quad . \quad (2\ )$$

is supported by the points $z_1, z_2$. We shall discuss SN$_2(1, -1)$

$$z' = k(1 - z^2), \ z = \tanh[k(t + t_0)] \quad . \quad . \quad (2\ )$$
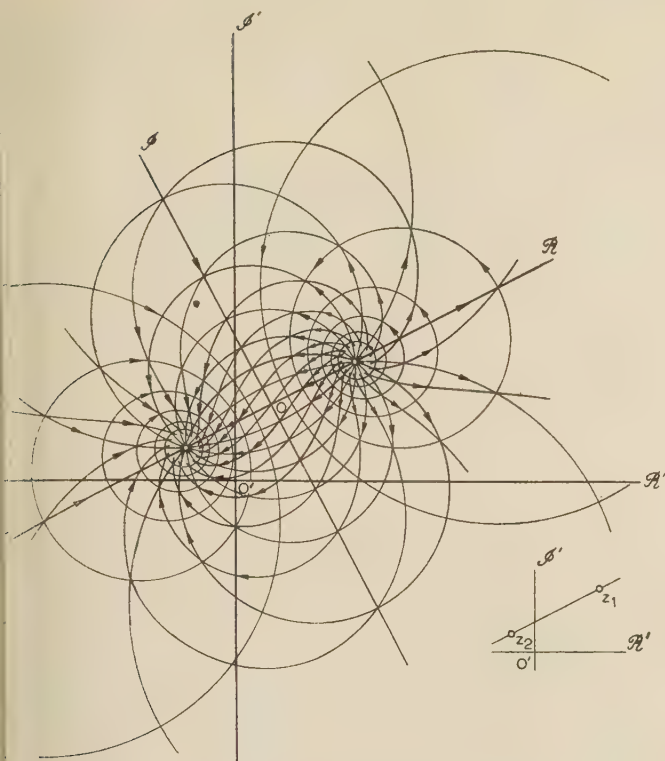
Feldtkeller,[3] among other authors, uses the basic families of the first and second degree in certain problems of the theory of four-terminal networks. With regard to the diagonal families, Feldtkeller vizualizes the transformation of impedances, in Fig. 33 of Reference 3, by means of vectors 'whirling out' of the point $-Z$ and 'whirling into' the point $Z$. These vectors seem to be tangential to our diagonal S-shaped curves.

The general standard net $SN_2$ occurs as the local impedance chart of non-autonomic lines (see Section 4.4).

**(3.1.4) $SN_{2p}$.  The Parabolic Standard Net of the Second Degree or the Generalized Dipole.**

$$z' = k(z - z_1)^2, \ z = z_1 - \frac{1}{kt + c} \quad . \quad . \quad . \quad (29)$$

has a *double* support $z_1$. As $z_2$ approaches $z_1$ in $SN_2(z_1, z_2)$ all component families of $SN_2$ become parabolic families of circles. (Circles of a parabolic family have a common tangent at the common point.)  For $z_1 = 0$ we have the special $SN_{2p}(0, 0)$:

$$z' = kz^2, \ z = -\frac{1}{kt + C} \quad . \quad . \quad . \quad . \quad (30)$$

with the double singularity at the origin.  The first basic family is $z' = z^2 = x^2 - y^2 + j2xy$, whence

$$\frac{dy}{dx} = \frac{2xy}{x^2 - y^2} \quad . \quad . \quad . \quad . \quad (31)$$

This is the parabolic family of circles

$$x^2 + y^2 - 2cy = 0$$

with a common horizontal tangent at the origin as can be seen by differentiation and elimination of $c$.  Other values of $\sigma = \arg k$ yield parabolic families with other directions of the common tangent, $z' = jz^2, \ z' = \underline{/\sigma} z^2$.  The two basic families form the familiar circles of constant resistances and reactances in the Smith chart.

Table 1 shows some of the substitutions which transform the differential equations and the corresponding standard nets of one type into those of other types.  It will be noted that analogous transformations of real differential equations are much more complicated.



Fig. 2.—The standard net of the second degree.
$$z' = k(1 - z^2), \ (\mathscr{R}, \ I).$$
$$z' = k(z - z_1)(z - z_2), \ (\mathscr{R}', \ I').$$

the supports are $(1, -1)$, the basic families $z' = 1 - z^2$, and $z' = j(1 - z^2)$ are the orthogonal elliptic and hyperbolic families of circles occurring in the rectangular impedance chart.  The diagonal families $z' = \underline{/\sigma}(1 - z^2)$ consist of S-shaped curves, corresponding to lossy lines.  The basic families also occur in the Smith chart as the curves of constant mod $z$ and arg $z$, respectively.

The general standard net $SN_2(z_1, z_2)$ follows by rotation, translation and extension, such that the supports $(1, -1)$ become $z_1, z_2$, respectively.

**Table 1**

| | $z' = k$ | $z' = kz$ | $z' = k(z - M)$ | $z' = k(1 - z^2)$ | $z' = kz^2$ |
|---|---|---|---|---|---|
| $w' = k$ | $z = w$ | $z = \varepsilon^w$ | $z = P + \varepsilon^w$ | $z = \tanh w$ | $z = -\dfrac{1}{w}$ |
| $w' = kw$ | $z = \log_\varepsilon w$ | $z = w$ | $z = P + w$ | $z = \tanh(\log_\varepsilon w) = \dfrac{w^2 - 1}{w^2 + 1}$ $\left[\text{also } z = \dfrac{1 + w}{1 - w}\right]$ | $z = -\dfrac{1}{\log_\varepsilon w}$ $w = \varepsilon^{-1/z}$ |
| $w' = k(w - P)$ | $z = \log_\varepsilon(w - P)$ | $z = w - P$ | $z = w$ | $z = \tanh[\log_\varepsilon(w - P)]$ | $z = -\dfrac{1}{\log_\varepsilon(w - P)}$ |
| $w' = k(1 - w^2)$ | $z = \text{arc tanh } w$ $z = \dfrac{1}{2}\log_\varepsilon \dfrac{1 + w}{1 - w}$ | $z = \sqrt{\dfrac{1 + w}{1 - w}} = \exp(\text{arc tanh } w)$ $\left[\text{also } z = \dfrac{w - 1}{w + 1}\right]$ | $z = P + \sqrt{\dfrac{1 + w}{1 - w}}$ | $z = w$ | $z = -\dfrac{1}{\text{arc tanh } w}$ |
| $w' = kw^2$ | $z = -\dfrac{1}{w}$ | $z = \varepsilon^{-1/w}$ | $z = P + \varepsilon^{-1/w}$ | $z = -\tanh \dfrac{1}{w}$ | $z = w$ |

## (4) NON-UNIFORM LINES

### (4.1) Notation and Definitions of Important Quantities

In this and all following Sections of the main text we denote by $z = r + jx$ the normalized impedance, by $y = l - x$ or by $\phi = \beta y$ the distance denoted in Section 3 by the general independent variable $t$.

We introduce the 'actual characteristic impedances' (cf. References 4, 5 and 6)

$$Z_0^+ = \frac{V^+}{I^+}, \; Z_0^- = -\frac{V^-}{I^-} \quad . \quad . \quad . \quad . \quad (32)$$

which are the local non-reflective impedances associated with the positive (decreasing $y$) and negative (increasing $y$) directions of propagation, respectively. The normalized actual characteristic impedances for the 'plus' and 'minus' waves will be denoted by

$$p = \frac{Z_0^+}{Z_0}, \; m = \frac{Z_0^-}{Z_0} \quad . \quad . \quad . \quad . \quad (33)$$

$Z_0^+$, $p$, $Z_0^-$, $m$ are complex functions of $y$ or $\phi$.

According to Schelkunoff[4] we can write for the voltage and current reflection coefficients associated with waves travelling in the positive direction

$$\left. \begin{array}{l} \Gamma_V = \dfrac{V_{ref}}{V_{inc}} = \dfrac{Z_0^-}{Z_0^+} \dfrac{Z - Z_0^+}{Z + Z_0^-} = \dfrac{m(z - p)}{p(z + m)} \\[3mm] \Gamma_I = \dfrac{I_{ref}}{I_{inc}} = \dfrac{Z_0^+}{Z_0^-} \dfrac{-Z}{+Z} = \dfrac{p - z}{m + z} \end{array} \right\} \quad . \quad . \quad (34)$$

Denoting $\Gamma_V$ by $\Gamma$ we can write for $z = p$ and $z = -m$

$$\Gamma(p) = 0, \; \Gamma(-m) = \infty \quad . \quad . \quad . \quad . \quad (35)$$

For reasons which will be clear in Section 6, the reflection coefficients [eqn. (34)] will be termed the 'intrinsic reflection coefficients'.

We introduce reflection coefficients for waves propagating in the *negative* direction ($p$ is interchanged with $m$)

$$\overleftarrow{\Gamma} = \overleftarrow{\Gamma}_V = \frac{p(z - m)}{m(z + p)}, \; \overleftarrow{\Gamma}_I = \frac{m - z}{p + z} . \quad . \quad . \quad (36)$$

Then we have

$$\overleftarrow{\Gamma}(m) = 0, \; \overleftarrow{\Gamma}(-p) = \infty \quad . \quad . \quad . \quad . \quad (37)$$

It is clearly seen that $m$ is the non-reflective impedance for backward waves. The infinite values of $\Gamma$ in eqns. (35) and (37) correspond to active loads or active equivalent impedances, i.e. to sources.

Schelkunoff and other authors,[5,6] using eqns. (34), did not indicate either a method for determination of the values of $Z_0^+$, $Z_0^-$ or a relation between $Z_0^+$ and $Z_0^-$. We shall give a simple algebraical method for determination of the local non-reflective impedances $p$ and $m$ directly from the differential equation for $z$. Since $p$ and $m$ are intimately connected with the local invariant impedances which are the 'moving singularities' of the differential equation, we shall first explain these notions.

### (4.2) The Local Invariant Impedances as Moving Singularities

The term 'local invariant impedance' seems to be contradictory; an example will clear the matter. One case of a single moving singularity is a circle rolling along a curve. The instantaneous centre of rotation is the moving stationary point, since for any value of $t$ its velocity is zero but its position changes with time along the supporting curve. This point could be termed the 'local invariant point'.

In the case of two moving singularities we should have two stationary points of zero velocity changing their positions with time, i.e. two local invariant impedances depending upon the distance $y$. $dz/dy$ is zero at these two points of the $z$-plane for this, and only this, value of $y$.

### (4.3) Determination of the Local Invariant Impedances from the Differential Equation for $z$

The singular points will be denoted henceforth by $z_1$, $z_2$. The differential equation for $z$ is of the form of eqn. (11):

$$\frac{dz}{d\phi} = j(1 - z^2) - q(\phi)z \quad . \quad . \quad . \quad . \quad (38)$$

We denote $q = 2s$, where $|s|$ is the ratio of the cut-off frequency to the working frequency

$$|s| = \left| \frac{q}{2} \right| = \frac{f_c}{f} \quad . \quad . \quad . \quad . \quad (39)$$

cf. Reference 7 for exponential lines. At any point of an exponential line we have a constant value of $s = q/2$ for a constant working frequency $f$. Thus the critical frequency $f_c = |s|f$ is constant all along the line. On the contrary, with non-autonomic lines, the logarithmic slope $s$ varies along the line; each elementary length $\Delta\phi = \beta\Delta y$ of the line can be considered as being replaced by an equivalent exponential length with the same value of $s$ as the non-autonomic line at the point in question. This local value of the logarithmic slope $s$ then determines the 'local cut-off frequency' valid for the chosen elementary length $\Delta\phi$, for constant working frequency. Since $f_c$ is proportional to $|s|$, it is possible that, while certain sections of the line (where $|s| < 1$) are working above the cut-off frequency ($f > f_c$), other sections, where $|s| > 1$, would simultaneously work under the cut-off frequency ($f < f_c$). The normal working condition is then as follows: the absolute value of the logarithmic slope should be $|s| < 1$ all along the line.

The invariant normalized impedances are the supports of eqn. (38) and are readily found by equating $dz/d\phi$ to zero:

$$z^2 - j2sz - 1 = 0 \quad . \quad . \quad . \quad . \quad (40)$$

whence

$$z_1 = js + \sqrt{(1 - s^2)} = js + n \quad . \quad . \quad (41)$$

$$z_2 = js - \sqrt{(1 - s^2)} = js - n \quad . \quad . \quad (42)$$

$s$ is real and $n$ is the arithmetic value of $\sqrt{(1 - s^2)}$.

If $|s| < 1$ the invariant impedances $z_1$, $z_2$ are complex and we can put

$$s = \sin\tau, \; n = \cos\tau \quad . \quad . \quad . \quad (43)$$

with $-90° < \tau < 90°$.

This corresponds to $f > f_c$, which is the normal working condition of the line; for $|s| \geqslant 1$ the invariant impedances become imaginary. We shall suppose that $|s| < 1$ all along the line.

The two local invariant normalized impedances of the non-autonomic line represented by eqn. (38) can thus be written as

$$z_1 = n + js = \underline{/\tau} \quad . \quad . \quad . \quad . \quad (44)$$

$$z_2 = -n + js = -\underline{/-\tau} \quad . \quad . \quad (45)$$

(above the cut-off frequency) and are given by the singular points of the differential equation (38). Here

$$\mathscr{R}z_1 > 0$$

$$\mathscr{R}z_2 < 0$$

$$s = \frac{d \log_\varepsilon Z_0}{2\beta dy}$$

$$n = +\sqrt{(1 - s^2)}$$

Moreover we have

$$z_1 z_2 = -1, \ z_2 = -z_1^* \quad . \quad . \quad . \quad . \quad (46)$$

In close analogy with $m$ and $\overleftarrow{\Gamma}$ we introduce $\overleftarrow{z_1}$, $\overleftarrow{z_2}$, the local invariant impedances associated with backward waves, for which the logarithmic derivative $q = 2s$ is of the opposite sign. Thus, replacing $+js$ by $-js$ in eqns. (44) and (45) we see that the two local invariant normalized impedances for backward waves of the non-autonomic line represented by eqn. (38) can be written in the form

$$\overleftarrow{z_1} = n - js = \underline{/-\tau} = z_1^* \quad . \quad . \quad . \quad (47)$$

$$\overleftarrow{z_2} = -n - js = -\underline{/\tau} = z_2^* \quad . \quad . \quad . \quad (48)$$

(above the cut-off frequency) and are given by the supports of the differential equation

$$z' = j(1 - z^2) + q(\phi)z \quad . \quad . \quad . \quad (49)$$

corresponding to the same transmission line as eqn. (38) but driven from the opposite end ($\phi = 0$).

Here again is

$$\overleftarrow{z_1}\overleftarrow{z_2} = -1, \ \overleftarrow{z_2} = -\overleftarrow{z_1}^* \quad . \quad . \quad . \quad . \quad (50)$$

If we wish to find the invariant impedances by classical methods it is necessary to determine expressions for $V$ and $I$, to obtain the transformation law $z = f(z_L, y)$ and then, putting $z = z_L = z_{inv}$, to solve the last equation for $z_{inv}$. Here we have a direct method for the determination of the invariant impedances without integration of eqn. (38).

## (4.4) Fundamental Property of Non-Reflective Impedances

The local non-reflective normalized impedances of the non-autonomic line [represented by eqn. (38)] associated with the
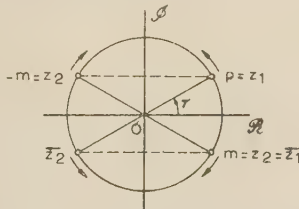


Fig. 3.—The four intrinsic impedances.

two directions of propagation are given by the relations (see Fig. 3)

$$p = z_1 \text{ or } p = \frac{Z_0^+}{Z_0} = n + js = \underline{/\tau} \quad . \quad . \quad (51)$$

and

$$m = -z_2 \text{ or } m = \frac{Z_0^-}{Z_0} = n - js = \underline{/-\tau} \quad . \quad (52)$$

respectively. Moreover we have

$$pm = 1, \ m = p^* \quad . \quad . \quad . \quad . \quad . \quad (53)$$

and

$$Z_0^+ Z_0^- = Z_0^2 \quad . \quad . \quad . \quad . \quad . \quad (54)$$

$s$, $\tau$ are functions of $q$ and consequently of $\phi$ or $y$.

*Proof of eqn.* (51).—Any non-reflective impedance $p$ is, at least locally, an invariant impedance, but not all invariant impedances $z_i$ are non-reflective. Thus, if a line has non-

reflective impedances, they must be found among the invariant impedances.

Since a non-reflective impedance is a passive (load) impedance its real part is positive, and since, by virtue of eqns. (44) and (45), only the 'first' invariant impedance $z_1$ has a positive real part, the non-reflective impedance $p$ is identical with the 'first' invariant impedance $z_1$.

The same argument holds for eqn. (52) if we replace $p$ and $z_i$ in eqns. (44) and (45) by $m$ and $\overleftarrow{z_i}$ in eqns. (47) and (48), respectively.

Since $pm = 1$ [eqn. (53)] the equations for the voltage reflection coefficients [eqns. (34) and (36)] assume the form

$$\Gamma = \Gamma_V = \frac{mz - 1}{pz + 1}, \ \overleftarrow{\Gamma} = \frac{pz - 1}{mz + 1} \quad . \quad . \quad . \quad (55)$$

It will be noted that $\overleftarrow{z_2} = -p$ and $z_2 = -m$ are exactly the 'active loads' causing 'infinite' reflections in the two respective directions [see eqns. (35) and (37)].

The four intrinsic impedances $p = z_1$, $m = -z_2 = \overleftarrow{z_1}$, $-p = \overleftarrow{z_2}$, $-m = z_2$ are represented by four points on the circumference of the unit circle centred at the origin. They move simultaneously, conserving their symmetrical arrangement as the logarithmic derivative $q$ varies along the non-autonomic line (see Fig. 3).

At any position $z_1 = p$ and $z_2 = -m$ are the supports of a 'local' standard net of the second degree $SN_2(p, -m)$ which is geometrically similar to $SN_2(1, -1)$ (see Section 3.1), with the exception of the S-shaped curves corresponding to lossy lines and requiring special investigation since the invariant impedances of lossy lines are not located on the unit circle.

The exact meaning of the local standard net and of the moving singular points $(p, -m)$ as compared to the fixed singularities $(1, -1)$ of the uniform line, is as follows. The fixed singularities determine the whole circle of constant $|\Gamma|$ passing through the given point $z$ as well as the whole circle of constant $\beta y \pm 90°$ passing through $z$; the moving singular points determine only the elementary arcs of the curves

$$|\Gamma| = \text{constant}: dz = f(z, \phi)d\phi = [j(1 - z^2) - q(\phi)z]d\phi \quad (56)$$

$$\beta y \pm 90° = \text{constant}: dz = [(1 - z^2) + jq(\phi)z]d\phi \quad . \quad . \quad (57)$$

(see Section 3.1).

The tangent to the curve $|\Gamma| = \text{constant}$ at a given point $z = A$ can be determined graphically (see Fig. 4) if we draw a line
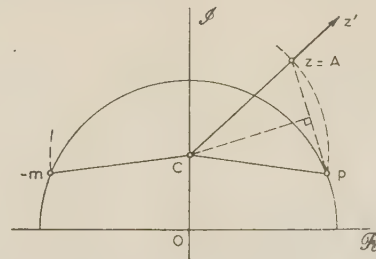


Fig. 4.—Graphical determination of the tangent to the impedance locus at the given point $z = A$, from the local non-reflective impedance $p$.

$CA = Cp$, the tangent to the curve $\beta y = \text{constant}$ is then perpendicular to $CA$. This construction is a generalization of a known construction used in connection with the uniform line. It is clear that for other values of the angular distance $\phi$ and consequently for other positions of the supports $(p, -m)$, we obtain other directions of tangents at the same point $z = A$.

This is one of the most characteristic properties of non-autonomic transmission lines (cf. Section 3).

## (5) APPLICATIONS OF THE GENERAL THEORY

### (5.1) The Uniform Line

Since the supports of eqn. (13) $z' = j(1 - z^2)$ are $(+1, -1)$ the orthogonal impedance chart is given by the standard net $SN_2(1, -1)$ (see Section 3.1). Furthermore, we have $p = 1$, $m = -z_2 = 1$. The transformation law for impedances is the solution of eqn. (13):

$$z = j \tan (\phi + c) = \frac{z_L + j \tan \phi}{1 + j z_L \tan \phi} \quad . \quad . \quad . \quad (58)$$

where $z_L = j \tan c$ is the load impedance.

Differentiating $\Gamma = (z - 1)/(z + 1)$, which follows from eqn. (55), and inserting $z'$ from eqn. (13) we obtain

$$\Gamma' = -j2\Gamma \text{ or } \frac{d\Gamma}{dy} = -j2\beta\Gamma \quad . \quad . \quad . \quad (59)$$

These classical relations are arrived at in a very simple manner by means of the new theory.

### (5.2) The Exponential Line

The supports of eqn. (14), $z' = j(1 - z^2) - qz$, where $q = 2s = \text{constant}$, are $z_1 = p = n + js$, $z_2 = -m = -n + js$ ($z_1$ and $z_2$ are constant). $p, m$ can be also obtained directly from eqns. (51) and (52). The orthogonal chart is given by $SN_2(p, -m)$

with $w_L = j \tan c$. The load impedance is $z_L = j(n \tan c - v$ and we obtain after some manipulation

$$z = \frac{(n \cot n\beta y + v)z_L + j}{n \cot n\beta y - v + jz_L} \quad . \quad . \quad . \quad (62$$

which is the known expression for $z$ (cf. Reference 9).

The substitution $w = (z + jv)/n$ can be regarded as a 'mapping' of the exponential line reducing it to a fictitious line [eqn. (60)]. This quasi-uniform line has the same support and the same remaining properties as the uniform line with the exception of the effective phase coefficient $\bar{\beta} = n\beta$ instead o $\beta$ (cf. Reference 7).

The voltage reflection coefficient is obtained from eqn. (55 with $p = n - jv = \underline{/-\rho}$, $m = \underline{/\rho}$:

$$\Gamma = \frac{z \underline{/\rho} - 1}{z \underline{/-\rho} + 1} \quad . \quad . \quad . \quad . \quad (63$$

Differentiating and substituting $z'$ from eqn. (14)

$$\Gamma' = -j2n\Gamma \text{ or } \frac{d\Gamma}{dy} = -j2n\beta\Gamma \quad . \quad . \quad . \quad (64$$

whence $\Gamma = \Gamma_r \varepsilon^{-j2n\beta y}, \Gamma_r = \Gamma$ at $y = 0$

These differential equations are of the type $\xi' = k\xi$ and correspond to $SN_1(0)$ (see Section 3). $SN_1(0)$ is in this case the poin $\Gamma$-diagram for the exponential line and can be readily con structed as the Smith chart for the quasi-uniform line of eqn. (60 (see Fig. 5). The circles of constant $r$ and $x$ are numbered



Fig. 5.—The polar chart for $\Gamma$ of a divergent exponential line.

$v = \frac{\delta}{2\beta} = 0.4, n = 0.916, \beta l = 100°, z_L = 0.39 + j0.8.$ The input impedance $z = 0.2 - j$ is obtained by rotation of $z_L$ through the angle $-2n\beta l = -183.2°$.

with the exception of the S-shaped curves. $SN_2(p, -m)$ is geometrically similar to $SN_2(1, -1)$ and can be found in Fig. 6 of Reference 8. The derivation of the orthogonal chart given in this Reference is very complicated.

Denoting $s$ by $-v$ (cf. Reference 7) we can solve the equation $z' = j(1 - z^2) + 2vz$ introducing $w = (z + jv)/n$. We obtain

$$w' = jn(1 - w^2) \quad . \quad . \quad . \quad . \quad (60)$$

and

$$\int \frac{dw}{1 - w^2} = jn d\phi$$

whence

$$w = i \tan (n\phi + c) = \frac{w_L + j \tan n\phi}{1 + jw_L \tan n\phi} \quad . \quad . \quad (61)$$

according to the substitution $w = (z + jv)/n$ so that the circ $r = 1$ does not pass through the centre, and the locus of $x =$ (the image of the real axis) is a circular arc orthogonal to th basic circle, since, for $z = 0$, we have $w = jv/n$, for $z =$ $w = (1 + jv)/n$ and for $z = \infty$ $w = \infty$. Since the circl $|\Gamma| = \text{constant}$ are concentric it is possible to determine th input impedance by rotating the load impedance through th angle $-2n\beta y$. The reflection coefficient of the quasi-unifor line $\Gamma_w$ is given by

$$\Gamma_w = \frac{w - 1}{w + 1} = \frac{p}{m} \frac{mz - 1}{pz + 1} = \Gamma \underline{/-2\rho} \quad . \quad . \quad (6$$

and differs from $\Gamma$ only in phase angle.

For variable length $l$ of an exponential line with constant characteristic impedances $Z_t$ at the transmission end and $Z_r$ at the receiving end, the input intrinsic reflection coefficient can be obtained as follows. At the output we have $z_L = 1$ and we obtain from eqn. (55)

$$\Gamma_r = \frac{\angle \rho - 1}{\angle -\rho + 1}, \quad |\Gamma_r| = \left| \tan \frac{\rho}{2} \right| \qquad . \quad . \quad (66)$$

For loss-free exponential lines we can write for the input $|\Gamma_t| = |\Gamma_r| = \left| \tan \frac{\rho}{2} \right|$. For variable taper length $l$ and $Z_r/Z_t = $ constant we have, from $Z_r = Z_t \varepsilon^{\delta l}$,

$$\delta = \frac{1}{l} \log_\varepsilon \frac{Z_r}{Z_t}; \sin \rho = \nu = \frac{\delta}{2\beta} = \frac{1}{4\pi} \frac{\lambda}{l} \log_\varepsilon \frac{Z_r}{Z_t} = K \frac{\lambda}{l},$$

where

$$K = \frac{1}{4\pi} \log_\varepsilon \frac{Z_r}{Z_t}$$

Using these relations we obtain

$$\tan \frac{\rho}{2} = \frac{1 - \cos \rho}{\sin \rho} = \frac{1}{\nu} - \frac{1}{\nu} \surd(1 - \nu^2) \quad . \quad . \quad (67)$$

and finally 
$$|\Gamma_t| = \frac{1}{K} \left\{ \frac{l}{\lambda} - \surd \left[ \left( \frac{l}{\lambda} \right)^2 - K^2 \right] \right\} . \quad . \quad . \quad (68)$$

This is an equation of a hyperbola having no zeros for finite $l/\lambda$. For $l/\lambda < K$, $|\Gamma_t|$ has no real values, $l_c = K\lambda$ being the critical length of taper for a given $\lambda$. If we compare this result with the 'reflection pattern' of Ragan [eqn. (4) of Reference 10], and Willis and Sinha[11] (with zeros at $k\lambda/2$), we see that these authors investigated the overall reflection pattern of a line composed of a uniform line and an exponential line instead of the exponential line as such (see Section 6).

### (5.3) Example of a Non-Autonomic Line

Eqn. (11) $z' = j(1 - z^2) - q(\phi)z$ can be solved in some special cases even if $q = 2s$ is variable.

Introducing $w = z - js$ we obtain

$$w' = j(1 - s^2 - s' - w^2) \quad . \quad . \quad . \quad (69)$$

$$s^2 + s' = a^2 = \text{constant} \quad . \quad . \quad . \quad (70)$$

Eqn. (69) can be solved, $s$ can be determined from the differential equation (70), and then $q = 2s$:

$$q = 2a \tanh (a\phi + \bar{c}) \quad . \quad . \quad . \quad (71)$$

Since $q = \frac{d \log_\varepsilon Z_0}{d\phi}$ we have $\log_\varepsilon Z_0 = \int q d\phi$

and 
$$Z_0 = C_1 \cosh^2 (a\phi + \bar{c}) = C_1 \cosh^2 a(\phi + \phi_L) \quad . \quad (72)$$

This is real if $C_1$ and $a$ are real.

We thus obtain a non-autonomic transmission line for which

$$z' = j(1 - z^2) - 2a \tanh (a\phi + \bar{c})z \quad . \quad (73)$$

The real constant $\bar{c}$ is determined by the location of the load: $\bar{c} = a\phi_L$. $\bar{c} = 0$ if the load is at the point of minimum $Z_0$.

We can integrate eqn. (69) written in the form

$$w' = j(b^2 - w^2) \quad . \quad . \quad . \quad . \quad (74)$$

where $b^2 = 1 - a^2$, $a < 1$. We have (with $w_L = jb \tan c$)

$$w = jb \tan (b\phi + c) = \frac{w_L + jb \tan (b\phi)}{1 + jw_L \dfrac{\tan (b\phi)}{b}} . \quad (75)$$

and finally

$$z = w + js = jb \tan (b\phi + c) + ja \tanh (a\phi + \bar{c}) . \quad (76)$$

The complex constant $c$ is determined by the load impedance $z_L = jb \tan c + ja \tanh \bar{c}$; $c = 0$ if $z_L = ja \tanh \bar{c}$.

This non-autonomic line is relatively simple, since the impedance $z$ is split into the autonomic part $w$ corresponding to the 'quasi-uniform' line [eqn. (74)] and the non-autonomic part $js$, which depends upon the position of the load $\phi$ but not upon the load impedance $z$ itself.

Fig. 6 represents $z$-curves for $a = 0.6$ and $b = 0.8$. The
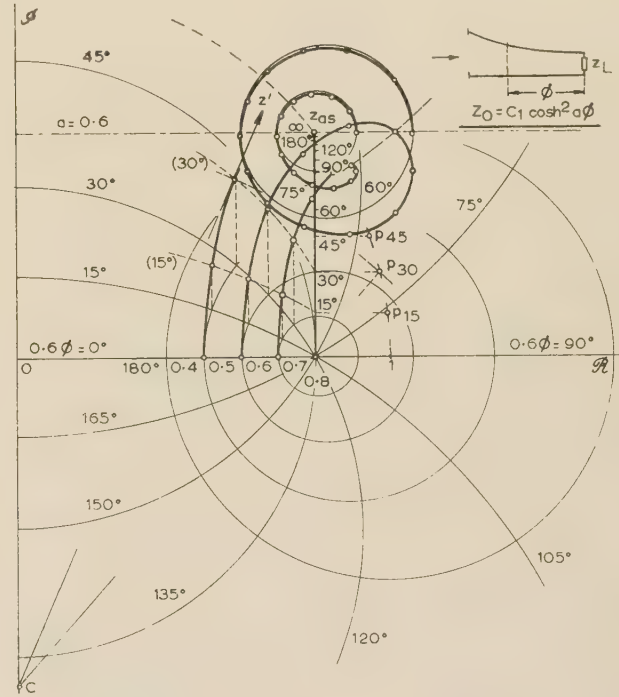


Fig. 6.—Impedance loci for real load impedances located at the minimum of $Z_0$ of the non-autonomic line $Z_0 = C \cosh^2 a\phi$.

load impedances are $z_L = 0.5, 0.6, 0.7$ and $0.8$, and are located at the minimum value of $Z_0$, $\bar{c} = 0$. The supports of the quasi-uniform line [eqn. (74)] are $w_{1,2} = \pm b = \pm 0.8$; the corresponding $SN_2(b, -b)$ is shown in Fig. 6 and is used for the construction of $z = w + js$. We start at $z_L = 0.6$ and follow the circle, adding to its points the vectors $js = ja \tanh (a\phi)$. The construction of Fig. 4 is also shown. The impedance loci are similar to trochoids, but have asymptotic circles for $\phi \to \infty$ belonging to the asymptotic standard net $SN_2(z_{as}, -z_{as}^*)$, where $z_{as} = b + ja = 0.8 + j0.6$. For $z_L = b = 0.8$ the fictitious 'line' is matched (the non-reflective 'impedance' is $w_1 = 0.8$) and $z = w_1 + js = 0.8 + ja \tanh (a\phi)$, so that $z$ transforms along the straight line parallel to the imaginary axis and ending at the asymptotical point $z_{as}$.

Fig. 7 represents a typical non-autonomic case. A fixed load impedance is placed at different points $\phi_L = 0°$, $30°/a$, $60°/a$ and $90°/a$ of the line [eqns. (72) and (73)] corresponding to different values of $\bar{c}$. The rest of the line is thought to be cut away. To each location of the load we obtain a separate $z$-locus constructed in the same manner as in Fig. 6, only the vectors to be added are $ja \tanh (a\phi + \bar{c}) - ja \tanh \bar{c}$, since $ja \tanh \bar{c}$ is already contained in $z_L$.

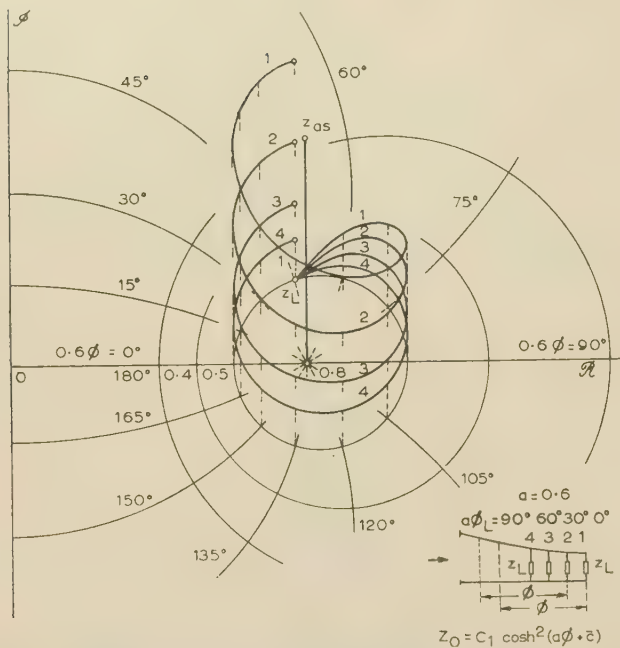This behaviour is typical for non-autonomic lines and is

Fig. 7.—Impedance loci for a fixed complex load impedance located at different points of the line $Z_0 = C \cosh^2 (a\phi + \bar{c})$.

caused by the fact that the impedance at a point $\phi$ depends upon both $\phi$ and $\phi_L$ (location of the load),

$$z = \mathrm{F}(z_L, \phi, \phi_L) \quad . \quad . \quad . \quad . \quad (77)$$

[cf. Reference 5, eqn. (37)] and not only upon the difference $\phi - \phi_L$ as in the case of the autonomic lines, where

$$z = \mathrm{F}(z_L, \phi - \phi_L) \quad . \quad . \quad . \quad . \quad (78)$$

Inserting

$$p = n + js = +\sqrt{[1 - a^2 \tanh^2 (a\phi + \bar{c})]} + ja \tanh (a\phi + \bar{c}),$$

$$m = n - js \quad . \quad . \quad . \quad . \quad . \quad . \quad . \quad . \quad . \quad (79)$$

into eqn. (55) we can obtain $\Gamma$ as a function of $\phi$.

The general equation (11) can be also solved if

$$j(1 - s^2 - s') = a\phi^\eta \quad . \quad . \quad . \quad . \quad (80)$$

The case $\eta = 0$ corresponds to eqn. (70); $\eta = -2$ and $\eta = -4h/(2h - 1)$, where $h$ is an integer, represent the remaining solvable cases (cf. Reference 12, p. 21).

### (5.4) Summary of Properties of Non-autonomic Lines

(a) The invariant impedances $z_1 = p$, $z_2 = -m$ as well as the non-reflective impedances $p$, $m$ are of a local character, since they depend upon $\phi$.

(b) The local character of the non-reflective impedances implies 'inner' reflections; $p(\phi_1)$ is non-reflective at the point $\phi_1$, but causes reflections at the neighbouring point $\phi_2 = \phi_1 + \Delta\phi$, since $p(\phi_2) \neq p(\phi_1)$.

(c) A pencil of impedance loci passes through any point of the impedance plane.

(d) An impedance locus can intersect itself or other impedance loci.

(e) For any point $\phi$ along the line there exists a field of directions $\arg z'$ readily constructed as shown in Fig. 4.

(f) Since the transformation formulae for $z$ involve both $\phi$ and $\phi_L$ [eqn. (77)], different locations $\phi_L$ of the same load impe-

dance along the line cause different transformed impedances a the distance $\beta l = \phi - \phi_L = $ constant.

(g) Anticipating eqn. (88), Section 6.1, the invariant reflectio coefficients of non-autonomic lines are in general neither zer nor infinity and do not correspond to the invariant impedance

## (6) DIFFERENTIAL EQUATIONS FOR REFLECTION AND TRANSMISSION COEFFICIENTS

Although $\Gamma_V$ can be readily determined for any given lin from eqn. (55), it is interesting to deduce differential equation for this quantity as well as for $\Gamma_I$ and the transmission coefficient of a non-uniform line.

It should be emphasized that in eqns. (34)–(37) as well a eqn. (55), $\Gamma$ is the intrinsic reflection coefficient of a tapere line as such and not the overall reflection coefficient of a lin composed of a uniform line and a non-uniform line.

The intrinsic reflection coefficient $\Gamma_V(y) = V_{ref}/V_{inc}$ describe reflections at any point on the tapered line, since eqns. (3 contain $Z_0^+$, $Z_0^-$ which are functions of $y$. On the contrar the overall reflection coefficient describes reflections at th junction of the input uniform line and the tapered line.

This difference seems to be completely neglected in th literature. For example, Reference 13 expressly states that th magnitudes of $\Gamma$ on both sides of the junction are equal.

### (6.1) Intrinsic Reflection and Transmission Coefficients of Non-Uniform Lines as Such

From eqn. (55) we obtain

$$z = \frac{1 + \Gamma_V}{m - p\Gamma_V} \quad . \quad . \quad . \quad . \quad (8$$

Differentiation and substitution into eqn. (38) yields [notin that all quantities in eqn. (81) are variable]

$$\frac{d\Gamma_V}{d\phi} = \frac{p}{p+m}[q^- + j(p-m)]\Gamma_V^2 + \frac{1}{p+m}(pq^- - mq^+ - j4)\Gamma_V$$
$$- \frac{m}{p+m}[q^+ + j(p-m)] = R\Gamma_V^2 + S\Gamma_V + W. \quad (8$$

where $q^+ = \dfrac{p'}{p} + q$, $q^- = \dfrac{m'}{m} + q$ (see Appendix 11.3) and th coefficients $R$, $S$ and $W$ are functions of $\phi$. All quantities a in general complex.

This equation can be simplified to

$$\Gamma_V' = -\frac{p'}{2n}\Gamma_V^2 - j\frac{1}{n}(s' + 2n^2)\Gamma_V + \frac{m'}{2n}$$
$$= \frac{s'}{2n}\left(\frac{s}{n} - j\right)\Gamma_V^2 - j\frac{1}{n}(s' + 2n^2)\Gamma_V - \frac{s'}{2n}\left(\frac{s}{n} + j\right) \quad (8$$

Similar differential equations for the current reflection coeffi cient $\Gamma_I$ and for the voltage and current transmission coefficien $T_V$, $T_I$ are readily obtained from the second equation (34) an the equations of Schelkunoff (Reference 4, p. 34):

$$T_I = (Z_0^- + Z_0^+)/(Z_0^- + Z), \quad T_V = (Z/Z_0^+)T_I$$

We obtain

$$\Gamma_I' = -\frac{m'}{2n}\Gamma_I^2 + j\frac{1}{n}(s' - 2n^2)\Gamma_I + \frac{p'}{2n}$$
$$= \frac{s'}{2n}\left(\frac{s}{n} + j\right)\Gamma_I^2 + j\frac{1}{n}(s' - 2n^2)\Gamma_I - \frac{s'}{2n}\left(\frac{s}{n} - j\right) \quad (8$$

$$T_V' = -\frac{p'}{2n}T_V^2 - \left(\frac{s}{n^2}s' + j2n\right)T_V + j2n \quad . \quad . \quad (8$$

$$T_I' = -\frac{m'}{2n}T_I^2 - \left(\frac{ss'}{n^2} + j2n\right)T_I + j2n \quad . \quad . \quad . \quad . \quad (86)$$

The four equations (83)–(86) are Riccati equations and cannot be solved in the general case; there are, however, cases (cf. Reference 12, p. 21), when Riccati equations can be solved.

If $p = m = 1$ (uniform lines) we have $R = 0$, $W = 0$, $S = -j2$, and eqn. (83) yields $\Gamma_V' = -j2\Gamma_V$.

If $p = \angle\tau = $ constant, $m = \angle-\tau = $ constant (exponential lines), we obtain $R = 0$, $W = 0$, $S = -j2n$ and eqn. (83) yields

$$\Gamma_V' = -j2n\Gamma_V \text{ or } \frac{d\Gamma_V}{dy} = -j2n\beta\Gamma_V.$$

Equating the second member of eqn. (82) to zero,

$$R\Gamma^2 + S\Gamma + W = 0 \quad . \quad . \quad . \quad . \quad . \quad (87)$$

we obtain the two 'local invariant reflection coefficients'

$$\Gamma_{1,2} = \frac{-S \pm \sqrt{(S^2 - 4RW)}}{2R} \quad . \quad . \quad . \quad (88)$$

The invariant reflection coefficients of the autonomic lines are either zero or infinity corresponding to the invariant impedances $z = p$ and $z = -m$ [see eqns. (35)]. In the case of non-autonomic lines the invariant reflection coefficients are, in general, neither zero nor infinity and do not correspond to $z_1$, $z_2$. This is one of the striking features of non-autonomic lines.

### (6.2) The Overall Reflection Coefficient of Composite Lines

Fig. 8 shows a tapered line between two uniform lines. The nominal characteristic impedance $Z_0$ varies continuously from
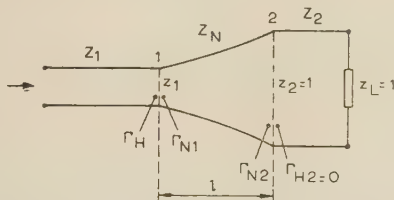


Fig. 8.—A composite transmission line.

The non-reflective normalized impedances at the junction 1 are $p_1$, $m_1$; the corresponding values at the junction 2 are $p_2$, $m_2$.

$Z_1$ to $Z_2$, but its logarithmic derivative changes *abruptly* at the junctions, which causes $\Gamma$ to be discontinuous at these points. $Z_N$ is the nominal characteristic impedance of the non-uniform section. Since the output line is matched, $\Gamma_{H2} = 0$, but $\Gamma_{N2} = (m_2 - 1)/(p_2 + 1)$ [cf. eqn. (55)]. We can thus refer to the transforming action of smooth junctions. We have

$$\Gamma_{N2} \neq \Gamma_{H2}$$

$$\Gamma_{N1} = \frac{m_1 z_1 - 1}{p_1 z_1 + 1} \neq \Gamma_H = \frac{z_1 - 1}{z_1 + 1} \quad . \quad . \quad (89)$$

We shall now deduce the differential equation for the overall reflection coefficient $\Gamma_H$. For any given $z_2$ the impedance $z_1$ is a function of the taper length $l$ and is governed by eqn. (38). We can write, dropping the subscript 1,

$$\Gamma_H = \frac{z - 1}{z + 1} \quad . \quad . \quad . \quad . \quad . \quad (90)$$

Differentiating and substituting for $z'$ from eqn. (38) we obtain

$$\frac{d\Gamma_H}{d\phi} = -j2\Gamma_H - s(1 - \Gamma_H^2) \quad . \quad . \quad . \quad (91)$$

$$\frac{d\Gamma_H}{dy} = -j2\beta\Gamma_H - \frac{1}{2}(1 - \Gamma_H^2)\frac{d\log_\varepsilon Z_0}{dy} \quad . \quad (92)$$

The last equation (92) is identical with the differential equation of Walker and Wax,[14] although these authors deduced it for $\Gamma$ of a non-uniform line as such, not mentioning any uniform line at the input. On the other hand, since these authors did not consider the $\Gamma$-transforming action of the junction, they could have meant the overall $\Gamma_H$ as well. All authors working with the equation of Walker and Wax use it on the tacit assumption that the equation governs the overall reflection coefficient $\Gamma_H$.

In deducing their equation, Walker and Wax state that $\Gamma$ is defined, in the notation of this paper, by

$$\Gamma = \frac{V/I - Z_0(x)}{V/I + Z_0(x)} \quad . \quad . \quad . \quad . \quad (93)$$

This formula is incorrect for the following reasons:

(a) If $\Gamma$ denotes the intrinsic voltage reflection coefficient of the non-uniform line as such (in the sense of Schelkunoff[4]), $\Gamma$ must vanish for $V/I = Z_0^+(x)$, which follows from eqns. (34) and from the definition of the local non-reflective impedance $Z_0^+$ [eqn. (32)]. Since $Z_0^+(x) \neq Z_0(x)$, $\Gamma$ as given by eqn. (93) does not vanish for $V/I = Z_0^+(x)$. On the other hand, the reflection coefficient $\Gamma$ given by eqn. (93) vanishes for $V/I = Z_0(x)$, which is the nominal characteristic impedance and for which reflections do occur in non-uniform lines, $Z_0$ being merely a parameter associated with the point $x$ on the line.

Moreover, since the notion of the reflection coefficient as the ratio $V_{ref}/V_{inc}$ is intimately connected with both the incident and reflected waves, any expression for $\Gamma$ as a function of $Z$ must necessarily contain the characteristic impedances associated with the two directions of propagation, $Z_0^+$, $Z_0^-$. This condition is satisfied by the formulae of Schelkunoff [eqns. (34) of this paper] as well as by the equation for $\Gamma$ of exponential lines deduced by Burrows (Reference 7, p. 559), whereas eqn. (93) does not satisfy the condition.

(b) If $\Gamma$ denotes the overall voltage reflection coefficient $\Gamma_H$, eqn. (93) is correct for $x = 0$ and only for this value of $x$, since $\Gamma_H$ is determined by the mismatch at the junction of the input uniform line and the non-uniform line.

It follows that the formula for $\Gamma$ of the uniform line, $\Gamma = (Z - Z_0)/(Z + Z_0)$, cannot be generalized for non-uniform lines by replacing the constant nominal characteristic impedance $Z_0 = \sqrt{(Z_s/Y_p)}$ by a variable $Z_0(x)$.

Willis and Sinha,[11] as well as many other authors, solve eqn. (92) in the case of the exponential line in the linearized form neglecting $\Gamma^2$. They arrive at the formula

$$|\Gamma| = \frac{1}{\pi}\log_\varepsilon\frac{Z_2}{Z_1}\left|\frac{\sin 2\pi l/\lambda}{4l/\lambda}\right| \quad . \quad . \quad . \quad (94)$$

Eqn. (92), however, can be solved (for exponential lines) without linearization; the resulting solution will be obtained more easily in the following manner:

The exponential taper is terminated by $z_L = 1$, the length of taper is $y = l$. Substituting these values into eqn. (62) we obtain

$$z = \frac{n + (\nu + j)\tan n\beta l}{n - (\nu - j)\tan n\beta l} \quad . \quad . \quad . \quad (95)$$

Then

$$\Gamma_H = \frac{z - 1}{z + 1} = \frac{\nu}{n\cot n\beta l + j} \quad . \quad . \quad (96)$$

For variable taper length we have (see Section 5.2)

$$n = \sqrt{(1 - \nu^2)} = \frac{K\lambda}{l}\sqrt{\left[\left(\frac{l}{K\lambda}\right)^2 - 1\right]} = \frac{K\lambda}{l}A$$

where $A$ is the 'reduced length';

$$A = \sqrt{\left[\left(\frac{l}{K\lambda}\right)^2 - 1\right]} \quad . \quad . \quad . \quad . \quad (97)$$

Denoting $C = 2\pi K$ we obtain the reflection coefficient

$$\Gamma_H = \frac{1}{A \cot CA + j\sqrt{(A^2 + 1)}} \quad . \quad . \quad . \quad (98)$$

whence

$$|\Gamma_H| = \frac{1}{+\sqrt{\left(\dfrac{A^2}{\sin^2 CA} + 1\right)}}$$

$$= \left\{\frac{\left(\dfrac{l}{K\lambda}\right)^2 - 1}{\sin^2 2\pi K\sqrt{\left[\left(\dfrac{l}{K\lambda}\right)^2 - 1\right]}} + 1\right\}^{-1/2} \quad (99)$$

or

$$|\Gamma_H| = \left|\frac{\sin CA}{\sqrt{(A^2 + \sin^2 CA)}}\right|$$

The asymptotic expression for $|\Gamma_H|$ (large values of the reduced length $A$, $A \gg \sin CA$) is then

$$|\Gamma_H|_{as} = C\left|\frac{\sin CA}{CA}\right| = \frac{1}{2}\log_\varepsilon \frac{Z_2}{Z_1}\left|\frac{\sin CA}{CA}\right| \quad . \quad (100)$$

which is exactly eqn. (94), since $CA = 2\pi l/\lambda$ for large values of $l/\lambda$. Thus eqn. (94) may be taken as an approximation of eqn. (99) for long tapers.

Putting $A = 0$ we obtain the critical length $l_c = K\lambda$; smaller values of $l$ correspond to imaginary values of $A$ and no propagation takes place [cf. eqn. (68)]. Eqn. (94) yields no information on this well-known fact.

It is interesting to note that Ragan (Reference 10, pp. 307, 308) distinguishes as many as three limiting values of $\Gamma$ at $l = 0$, which shows that the conventional theory does not hold for small taper lengths.

### (7) SYNTHESIS OF NON-UNIFORM LINES

The general differential equations (8), (11) or (38) can be solved in some exceptional cases only. Fortunately, it is possible to find non-autonomic lines, i.e. to determine $Z_0 = Z_0(y)$, for any desired function $z = z(y)$ or $Z = Z(y)$.

(a) It follows from eqn. (8) that

$$\frac{1}{z}\frac{dz}{dy} + \frac{d\log_\varepsilon Z_0}{dy} = \frac{d\log_\varepsilon(zZ_0)}{dy} = \gamma\left(\frac{1}{z} - z\right) \quad (101)$$

or

$$Z_0(y) = C\frac{1}{z}\exp\left[\int \gamma\left(\frac{1}{z} - z\right)dy\right] \quad . \quad . \quad (102)$$

In the case of loss-free lines this expression assumes the form

$$Z_0(\phi) = C\frac{1}{z}\exp\left[j\int\left(\frac{1}{z} - z\right)d\phi\right] \quad . \quad . \quad (103)$$

Differentiating eqn. (103), or directly from eqn. (11) or (38), we obtain

$$q(\phi) = j\left(\frac{1}{z} - z\right) - \frac{z'}{z} \quad . \quad . \quad . \quad . \quad (104)$$

For $z = j\tan(\phi + c)$ we obtain $Z_0 = $ constant and for

$$z = jb\tan(b\phi + c) + ja\tanh(a\phi + \bar{c})$$

we can write

$$Z_0(\phi) = C_1\cosh^2(a\phi + \bar{c})$$

in accordance with eqn. (72).

Beginning with equations of the form $z = f(\phi, c) + g(\phi, \bar{c})$ we obtain non-autonomic lines for which $z = f + g$ is the general

solution of the corresponding differential equation. However if we begin with $z = f(\phi, c)$ the line obtained will be also non-autonomic in the most cases, but $z = f(\phi, c)$ will be a particular solution of the corresponding differential equation valid for a definite location of the load.

(b) For a given $Z = Z(y)$ we can use eqn. (12) deduced by Pierce.[1] It follows immediately that

$$Z_0(y) = \frac{1}{2\beta}\left\{-j\frac{dZ}{dy} \pm \sqrt{\left[4\beta^2Z^2 - \left(\frac{dZ}{dy}\right)^2\right]}\right\} \quad (105)$$

In this case $Z_0$ is obtained without integration.

(c) The general solution of any Riccati differential equation is of the form

$$z = \frac{CF_1 + G_1}{CF_2 + G_2}, \Delta = \begin{vmatrix} F_1 & G_1 \\ F_2 & G_2 \end{vmatrix} \neq 0 \quad . \quad . \quad (106)$$

This is also the general solution of eqn. (38), if certain conditions are imposed on the four functions. Determining $C$ from eqn. (106) and differentiating we obtain, comparing the result with eqn. (38), the conditions

$$F_1G_1' - F_1'G_1 = G_2F_2' - G_2'F_2 = j(F_1G_2 - F_2G_1) = j\Delta \quad (107)$$

and

$$q\Delta = F_1G_2' - F_1'G_2 + F_2G_1' - F_2'G_1 \quad . \quad . \quad (108)$$

Thus, any four functions satisfying the conditions of eqn. (107) determine a non-uniform line; $q$ is given by eqn. (108) and

$$Z_0(\phi) = C_1\varepsilon^{\int q(\phi)d\phi} \quad . \quad . \quad . \quad . \quad (109)$$

It follows from eqn. (107) that the following four cases leading to $\Delta = 0$ are excluded:

  (i) All $F_{1,2}$, $G_{1,2}$ are simultaneously constants.
  (ii) $F_1$ and $G_1$ are constants.
  (iii) $F_2$ and $G_2$ are constants.
  (iv) $F_1G_2 = F_2G_1$.

The equation of Walker and Wax has been used in the sense specified in this paper by following authors: Ghose,[15] Scott,[16] Klopfenstein,[17] Collin,[18] Bolinder.[19] Ghose proposed a method of synthesis based on the linearized equation of Walker and Wax. The differential equation for the normalized impedance derived by Burkhardtmaier[20] is incorrect, and is not used by this author in the rest of his paper.

### (8) CONCLUSIONS

Introduction of families of complex differential equations corresponding to standard nets $[z' = kf(z)]$ makes it possible to analyse and transform two-parameter families of curves as a whole; transformations of individual component families within a standard net are effected simply by changing the phase angle of the outer parameter $k$. All component families have common singularities representing the invariant impedances. The non-reflective impedances of autonomic and non-autonomic lines can be determined algebraically; the field of directions of the impedance loci is readily obtained either graphically or analytically. 'Mapping' of transmission lines reduces more complicated lines to less complicated fictitious lines; approximative methods are also possible.

Reflection and transmission coefficients can be determined directly from the non-reflective impedances; the corresponding differential equations are derived from the differential equation for the normalized impedance. Furthermore, the equation for the overall voltage reflection coefficient is deduced and methods of synthesis of non-uniform lines are indicated.

Even the brief treatment of complex differential equations as given in the paper leads to interesting relationships, and it is

very probable that more detailed analysis would bring about further important results.

## (9) ACKNOWLEDGMENT

## (10) REFERENCES

(1) PIERCE, J. R.: 'A Note on the Transmission Line Equation in Terms of Impedance', *Bell System Technical Journal*, 1943, **22**, p. 263.

(2) STOKER, J. J.: 'Non-linear Vibrations in Mechanical and Electrical Systems' (Interscience Publishers, New York, 1950).

(3) FELDTKELLER, R.: 'Einführung in die Vierpoltheorie der elektrischen Nachrichtentechnik' (Hirzel, Leipzig, 1942), 2nd edition.

(4) SCHELKUNOFF, S. A.: 'The Impedance Concept and its Applications to Problems of Reflection, Refraction and Power Absorption', *Bell System Technical Journal*, 1938, **17**, p. 17.

(5) MONTGOMERY, C. G., DICKE, R. H., and PURCELL, E. M.: 'Principles of Microwave Circuits' (McGraw-Hill, 1948).

(6) MARCUVITZ, N.: 'Waveguide Handbook' (McGraw-Hill, 1951).

(7) BURROWS, C. R.: 'Exponential Transmission Line', *Bell System Technical Journal*, 1938, **17**, p. 555.

(8) RUHRMANN, A.: 'Die Energieausbreitung auf Leitungen mit exponentiell veränderlichem Wellenwiderstand', *Hochfrequenztechnik und Elektroakustik*, 1941, **58**, p. 61.

(9) ZINKE, O.: 'La ligne exponentielle comme transformateur', *La Radio Française*, 1950, No. 1, p. 9.

(10) RAGAN, G. L.: 'Microwave Transmission Circuits' (McGraw-Hill, 1948).

(11) WILLIS, J., and SINHA, N. K.: 'Non-uniform Transmission Lines as Impedance Transformers', *Proceedings I.E.E.*, Paper No. 1961 R, March, 1956 (**103 B**, p. 166).

(12) KAMKE, E.: 'Differentialgleichungen' (Geest and Portig, Leipzig, 1956).

(13) AJSENBERG, G. S.: 'Kurzwellen-Antennen' (Fachbuchverlag, Leipzig, 1954) Chapter 1, Section 3.

(14) WALKER, L. R., and WAX, N.: 'Non-uniform Transmission Lines and Reflection Coefficients', *Journal of Applied Physics*, 1946, **17**, p. 1043.

(15) GHOSE, R. N.: 'Non-uniform Transmission Line as a Matching Section', *Proceedings of the National Electronics Conference*, 1955, **11**, p. 959.

(16) SCOTT, H. J.: 'The Hyperbolic Transmission Line as a Matching Section', *Proceedings of the Institute of Radio Engineers*, 1953, **41**, p. 1654.

(17) KLOPFENSTEIN, R. W.: 'A Transmission Line Taper of Improved Design', *ibid.*, 1956, **44**, p. 31.

(18) COLLIN, R. E.: 'The Optimum Tapered Transmission Line Matching Section', *ibid.*, 1956, **44**, p. 539.

(19) BOLINDER, E. F.: 'Fourier Transforms and Tapered Transmission Lines', *ibid.*, 1956, **44**, p. 557.

(20) BURKHARDTMAIER, W.: 'Widerstandstransformation mit Leitungen', *Funk und Ton*, 1949, pp. 151 and 202.

## (11) APPENDICES

### (11.1) Further Properties of Complex Differential Equations

Since differential equations of complex functions of a real independent variable are very important, not only for the theory of non-uniform transmission lines but for many other branches too, further properties of complex differential equations will be discussed using the notation of Section 3.

The distinction between the autonomic and non-autonomic cases requires some more explanation. If the non-autonomic differential equation can be written in the form

$$z' = f(z)g(t) \quad . \quad . \quad . \quad . \quad (110)$$

where $\arg g(t) = \psi =$ constant, the solution curves constitute a one-parameter family. Separating the real and imaginary parts, we obtain with $f(z) = f_r + jf_i$

$$\tan \theta = \frac{dy}{dx} = \frac{f_i \cos \psi + f_r \sin \psi}{f_r \cos \psi - f_i \sin \psi} = H(x, y) \quad . \quad (111)$$

Thus, although $z'$ explicitly depends on $t$, the angle $\theta$ is not affected by $t$ and a unique solution-curve (or a finite number of them) passes through any given point $z$. This is a *quasi-autonomic* case or, more exactly, a *phase-autonomic* case; other quasi-autonomic cases will not be discussed.

If the differential equation cannot be solved or the solution is complicated, the construction of the solution curves can be facilitated by the use of isoclinals, i.e. curves of constant $\theta$. For a fixed value $\theta = \theta_1$ we readily obtain from eqns. (19) and (21) the equations of isoclinals

$$u(x, y) \tan \theta_1 - v(x, y) = 0 \quad . \quad . \quad . \quad (112)$$

$$u(x, y, t) \tan \theta_1 - v(x, y, t) = 0 \quad . \quad . \quad (113)$$

Given the family of curves $z' = f(z)$, the differential equation of its isoclinals can be shown to be of the form

$$z' = \frac{f}{\dfrac{df}{dz}} \quad . \quad . \quad . \quad . \quad (114)$$

Since there exist no definite directions of tangents at the singular points, they could be also defined as the points of 'intersection' of isoclinals pertaining to different values of $\theta$.

A singular point of the first kind, $z_0$, can be a 'centre', a 'nodal point' (of various types) or a 'spiral point'; the poles $z_p$ are termed 'saddle points'. The kind and character of singular points of complex differential equations can be determined more easily than those of real differential equations, for which the well-known criteria of Poincaré and Bendixson are used.

In rectangular impedance diagrams, the supports of the constant-$|\Gamma|$ circles are 'centres', and those of the phase circles are nodal points, whereas the supports of the S-shaped curves (for lossy lines) are focal points.

In the theory of plane electromagnetic fields, the configurations of the lines of force and of the equipotential lines are represented by standard nets of the form

$$z' = k \prod_{r=1}^{m} (z - A_r)^{a_r} \prod_{s=1}^{n} (z - B_s)^{b_s} \quad \left. \begin{array}{l} r = 1, 2, \ldots, m; \, a_r > 0 \\ s = 1, 2, \ldots, n; \, b_s < 0 \end{array} \right\} \quad (115)$$

(The analogy with the Schwarz–Christoffel transformation of a polygon may be noted.) In the case of electric fields the points $A_r$ correspond to the charged conductors (of very small diameter) and are the nodal points of the family of the lines of force and the 'centres' of the family of the equipotential lines; the poles $B_s$ are the points where the field vector $E$ vanishes, and are therefore the saddle points. A long thin magnet carrying current produces a field having spiral points of the magnetic lines of force.

The exponents $a_r$ are proportional to the charge densities, and the exponents $b_s$ correspond to multiple saddle points.

In the theory of four-terminal networks the singularities occur in many diagrams; see, for example, Reference 3, Fig. 40 (curves of constant working attenuation).
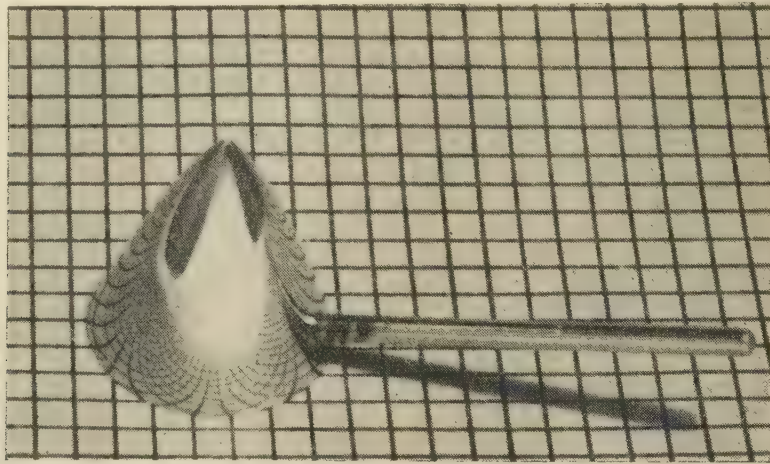
Fig. 9.—General view of the optical inversor.

In general, complex differential equations can be used with advantage in many problems involving families of curves; in addition to the branches mentioned we may mention aerodynamics, theory of vibrations and kinematics.

### (11.2) The Optical Inversor

Some transformations of standard nets (see Table 1), for example the transformations of $SN_1$ into $SN_2$, and $SN_0$ into $SN_{2p}$, as well as the converse transformations, can be visualized by means of an optical inversor. Many interesting relations were found by the author with the aid of this simple device, e.g. the polar $\Gamma$-diagram for exponential lines (Fig. 5). The inversor is a rotational body the generatrix of which is determined by the differential equation

$$y'^2 + \frac{2xy}{1-x^2}y' - 1 = 0 \quad . \quad . \quad . \quad . \quad (116)$$

and can be approximated by a hyperbola. If the inversor is put on a drawing its polished surface reflects the lines so that their inverted images can be seen from above (see Fig. 9).

### (11.3) Differential Equations for 'Anisotropic' Normalized Impedances

There is a type of normalized impedance used mainly in connection with the radial and spherical lines (cf. References 5

and 6). The impedances are normalized with respect to the actual characteristic impedances $Z_0^+$ and $Z_0^-$, which are different for the two directions of propagation. We denote the anisotropic normalized impedances by

$$z_+ = \frac{Z}{Z_0^+} = \frac{z}{p} \text{ and } z_- = \frac{Z}{Z_0^-} = \frac{z}{m} \quad . \quad . \quad (117)$$

Differentiating $z = pz_+$ and inserting into eqn. (38) we obtain with

$$q^+ = \frac{d\log_\varepsilon Z_0^+}{d\phi} = \frac{p'}{p} + q \quad . \quad . \quad . \quad (118)$$

the equation

$$\frac{dz_+}{d\phi} = j(m - pz_+^2) - q^+ z_+ \quad . \quad . \quad . \quad (119)$$

For $z_-$ we obtain correspondingly

$$\frac{dz_-}{d\phi} = j(p - mz_-^2) - q^- z_- \quad . \quad . \quad . \quad (120)$$

where

$$q^- = \frac{d\log_\varepsilon Z_0^-}{d\phi} = \frac{m'}{m} + q \quad . \quad . \quad . \quad (121)$$

# THERMAL NOISE IN MULTI-SECTION RADIO LINKS

## By B. B. JACOBSEN, B.Sc.(Eng.), Associate Member.

### SUMMARY

Microwave radio links are used for the long-distance transmission of large groups of telephone channels and for television signals. Thermal noise effects arise in each section of the link, and the magnitude of the resulting noise in the overall circuit is one of the major parameters of the overall transmission circuit.

The paper outlines methods of calculating the thermal noise in a long radio link when the individual radio-transmission sections are subject to fading. Various methods of expressing fading statistics are discussed, and it is proposed that the statistics of the individual path shall be expressed in terms of the three first hourly moments of the fading ratio and the statistics of these moments.

A technique is described for combining the effects of fluctuating fading in successive (tandem-connected) paths to obtain the hourly fading moments of the overall circuit. A method is given of converting the overall moments into an overall circuit fading distribution; this is expressed in terms of an 'augmented log-normal distribution', which can readily be translated into the distribution of thermal noise in the overall connection.

The noise requirements for long-distance telephone circuits are specified for a 2 500 km circuit, although any particular project will generally be much shorter. To avoid the difficulties involved in subdividing the noise permitted for 2 500 km, it is proposed instead to treat such path performance data as can be made available as if it were representative of all the sections which would enter into a 2 500 km circuit (synthetic overall circuit).

Thermal noise can be calculated for the synthetic circuit and compared with the requirements; this comparison will show whether the actual paths for which data are available are suitable to form part of an overall connection.

## (1) INTRODUCTION

Microwave radio relay links that provide large numbers of telephone channels and/or a television channel are coming into use. In current systems the useful signal (base-band signal) is transmitted as phase or frequency modulation of the carrier frequency, modulation taking place at the transmitting terminal, repeater stations being provided at spacings of about 30 miles. At these stations the received carrier signal is amplified and retransmitted along the route, usually with a change of carrier frequency. The carrier signal finally reaches the receiving terminal, where, after amplification and demodulation, it again provides the base-band signal. There may be terminal stations at several points along a long route.

The object of the paper is to give a method of calculating thermal-noise effects in multi-section radio links. This calculation would be very simple but for the fact that the radio paths between the stations have a transmission loss which is continually varying (fading).

In most systems the carrier-power outputs from the transmitting terminal and the repeater equipment are held at specified values, independent of effects in the preceding sections. (There may be occasions when this is not true, and these will need special consideration.)

The power is carried by the transmitting feeder to the aerial, and via the space path reaches the aerial of the next station. From this aerial the received signal is taken to the repeater or receiving equipment. The loss between the transmitting equipment and the receiving equipment at the next station is the gross path loss, and this will be referred to as path loss.

The path loss in each section will vary in time, owing to fading, and as a result so will the carrier power received at the end of the section. At these end-points the carrier signal is of relatively low level and may be considered here to be exposed to thermal-noise effects. The thermal-noise power is uniformly distributed over most of the significant part of the frequency spectrum; its density is approximately $-139$ dBm per 3 kc/s bandwidth for an ideal receiver, but in practice this value must be increased by the noise factor of the equipment. The thermal noise at the input remains constant, but its relative value is increased when there is fading in the preceding path. The input-circuit noise is added to the incoming wave, and is amplified and transmitted with it into the next sections, where further noise additions occur. In practice, the total noise power over the r.f. bandwidth of one repeater is small compared with the lowest carrier-signal power received, so that threshold effects do not occur.

In phase- and frequency-modulation systems it is normal to provide some limiting action in each repeater, to prevent the accumulation of noise which, after several sections, could produce threshold effects. The limiters have no useful effect otherwise on the amount of noise found in the output signal after detection at the receiving terminal. The limiters at repeater stations remove the amplitude effect of the noise but incorporate the phase-modulation effect into the carrier signal itself, which may then be said to consist of the original signal plus phase noise.

Each repeater produces a phase-noise signal, although it will be incorporated into the signal proper only where a limiter is present. The phase noise which is effective in the whole link will be the power sum of the phase-noise power produced at the end of each space-transmission section. The noise will therefore consist of many contributions, each of the same quality (white phase noise), but the scale of each contribution will vary with the path loss of the section. The structure of the total noise will nevertheless be that of white phase noise, but the scale of the total will depend on the combined effect of the varying path losses of the space sections. 'Noise' will therefore be taken to mean white noise; however, the fluctuations dealt with are not those of white noise *per se*, but rather are the fluctuations of the short-term mean power of the noise which arises from fading.

## (2) COMBINATION OF PATH-LOSS EFFECTS

A useful concept borrowed from carrier telephony is that of the equivalent single section, which has a transmission loss such that, used by itself, it would produce the same noise as the actual tandem-connected sections. Two equal sections connected in tandem would, for instance, have an equivalent loss 3 dB higher than the individual section, while for 50 equal sections it would be 17 dB higher than the loss of one section. If the losses in the

individual sections vary with time, so will the loss of the equivalent single section. The equivalent single-section loss is

$$A_e = 10 \log_{10} \sum_{r=1}^{r=n} 10^{A_r/10} \text{ decibels} \quad . \quad . \quad . \quad (1)$$

where $A_e$ is the equivalent single-section loss, $A_r$ is the loss of the $r$th section, and $n$ is the total number of paths connected in tandem (if diversity is used this will modify the $A_r$ functions for the sections having diversity).

It is, of course, possible to extract from the $A_r$ values a constant $A_0$; eqn. (1) then becomes

$$A_e - A_0 = 10 \log_{10} \sum_{r=1}^{r=n} 10^{(A_r - A_0)/10} \text{ decibels} \quad . \quad (2)$$

Each of the quantities after the summation sign in eqn. (2) will later be referred to as a 'fading ratio'—the factor by which the power-transfer factor of a section is divided when the path loss increases from $A_0$ to $A_r$, and also that by which the phase-noise power due to the $r$th section is increased when the loss of that section is $A_r$ instead of $A_0$.

Both equations imply that the $A$ values for each section are taken at the same time; they may be either actual values which have occurred at a particular instant or values which are expected to occur at a future instant. In the following work these quantities will be assumed to be only statistically defined, and then $A_e$ also will be statistically defined, but any instantaneous $A_e$ value will be the result of a set of $A_r$ values which by implicit assumption occur simultaneously.

### (2.1) Evaluation and Use of the Combined Path Loss

There are three distinct problems in evaluating and using the equivalent-single-section loss in eqns. (1) and (2). These are briefly stated here, and the discussion of them occupies the major part of the paper.

*First Problem.*—Express statistically the fading properties of each radio section (Sections 5 to 6.4).

Functions $A_r$ must be found which adequately describe in statistical terms the performance of each path at various times. In practice, this would mean making path-loss measurements over a long period and condensing the results without losing information in the process. It must be borne in mind that any test of path loss is, in effect, a sampling process, and only if the sample is large can it be relied upon to represent the path performance accurately.

*Second Problem.*—From the fading properties of individual sections, find the combined multi-section fading effect (Sections 8–10.2 and 13).

Given suitable functions $A_r$, a method must be found for effecting the summation of eqn. (2). This, in effect, is a further sampling process; each $A_r$ function describes a 'population', and the equivalent-single-section loss is the result of combining, according to eqn. (2), a sample from each of the $n$ populations. By repeating such sampling indefinitely the population $A_e$ may be inferred.

*Third Problem.*—Calculate the thermal noise in an overall connection and compare it with the noise requirements (Sections 6.5, 11 and 12).

The thermal noise in the base-band is readily calculated from $A_e$ and the parameters of the radio link, but the overall specification for noise is in terms of a 2 500 km circuit. An actual project for which fading data are available will, in general, have a shorter length; it will therefore be necessary to translate either the specification or the expected performance, so that they may be compared.

Only one part of the overall requirement has been agreed by the C.C.I.F., namely the maximum limit for the hourly mean noise power in a telephone channel during any hour. A further part, defining permissible values of noise during shorter periods is being studied[1] by the C.C.I.T.T. The permissible noise includes other effects, and the thermal noise is only a part of the total.

It is obviously desirable that the terms in which eqn. (2) is expressed should be compatible with those in which the complete noise specification will eventually be stated. It will be assumed in the absence of a final specification, that it is satisfactory to express the thermal-noise effect in terms of its statistical distribution during any hour.

### (3) SOURCES OF FADING BEHAVIOUR

The radio transmission paths used for microwave links are usually designed for line-of-sight transmission with first Fresnel zone clearance. There are three main sources of fading on such paths, namely

    (a) Atmospheric multi-path transmission.
    (b) Abnormal refraction gradient with height (beam bending).
    (c) Ground or water reflection multi-path transmission.

These effects have different statistics.

*Atmospheric multipath transmission* occurs during still air conditions, and increases in severity and frequency of occurrence as the path length increases. The incidence and amplitude of this type of fading show strong diurnal and seasonal variations, but diversity is effective in reducing it. This type of fading tends to make the third source of fading more troublesome.

*Abnormal refraction gradient with height* is particularly liable to cause trouble when the ground clearance of the path is small, since the beam then tends to be intercepted by the ground. Although this type of fading occurs less frequently when the path clearance is large, the clearance used in practice will rarely be sufficient to prevent occasional occurrence. This type of fading is not improved by diversity, and oversea paths may on rare occasions suffer severely from it. This form of fading starts gradually, but it may persist for a considerable time at a high value.

*Ground or water reflection*, when it is large, can give severe fading which on occasion can last for as long as an hour. When the ground reflection is small, it will be harmful only in the presence of the first type of fading. Diversity is very effective against these reflection effects.

### (4) CYCLIC EFFECTS

If the fading performance of a specific section is measured over many periods each of, say, an hour's duration, several different types of hourly distribution are obtained and diurnal and annual effects become noticeable. Cyclic effects are in some measure common to all the sections and constitute correlation between the fading events in the individual sections.

When the test results are subsequently sampled for the purpose of inferring the equivalent-single-section loss of a multi-section system, it is necessary that the 'populations' from which the samples representing each of the individual sections are drawn shall be typical of the actual path performance likely to apply at the time of day for which the sample is taken.

If cyclic effects are present it will be necessary to define 'populations' to represent different parts of the cycle; i.e. the fading statistics for the individual paths must be given for periods short enough to ensure that they are mutually at random inside the period.

### (4.1) Consequences of Ignoring Cyclic Effects

The statement that 'fading in all paths is liable to be high between the hours of 6 and 8 a.m.' expresses correlation between

the path losses. If only a single path were involved, it would not be completely unreasonable to give the distribution for a long period including the hours 6–8 a.m. This distribution would indicate that the path was liable to bad fading for a fraction of the time, and it might be considered a matter of indifference if this liability occurred at one time or another. But if several path performances are to be combined, as in eqn. (1), it would be wrong to use long-term distributions which do not explicitly include the important fact (in the example) that all paths are liable to fading at the same time of day and that, *per contra*, they are all less liable at other times. Even if it is a matter of indifference whether liability to high noise occurs at one time or another, the fact that all the sections are liable at the same time cannot be disregarded.

To illustrate this point more clearly, assume that, in fact, all of 50 sections have a fixed loss for 22 hours but have 6 dB extra loss (fading) for 2 hours. If the sections now have full fading correlation, the extra loss will occur in all sections simultaneously and the equivalent loss will be 23 dB for 2 hours and 17 dB for 22 hours. If, however, the losses are mutually at random, they will occur in each section at times which are quite independent of occurrences in other sections and without any restriction except that the total time of fading in each path is 2 hours; the equivalent loss will in this case be within 18 dB ± 1 dB (for 98% of the time).

If, in fact, the first assumption of correlation is correct, the consequence of ignoring the correlation would be to over-estimate the equivalent loss by 1 ± 1 dB most of the time; but for 2 hours the consequence would be to underestimate the loss by 5 ± 1 dB, which would be a serious error.

This example is a simplified version of correlation effects that may occur with real links, but it shows clearly that path performances must not be averaged if cyclic effects which are likely to be common to many paths are thereby concealed. Annual cyclic effects are well known and must be taken into account.

### (4.2) Non-Cyclic Co-Variation

It should be mentioned that non-cyclic co-variation between path losses could occur; it might, for instance, be caused by common weather conditions. This co-variation, however, is likely to be infrequent and small, and will hardly ever extend over groups of more than two sections. For this reason it is not likely to be significant when a large number of sections are to be considered together.

### (5) PATH PERFORMANCE DATA

The overall noise performance or expectation for a multi-section link is required to be in terms of the noise during any hour. In Section 4.1 it was apparent that cyclic effects make it necessary not to combine the path performance data for periods having cyclic differences. It is therefore proposed that all path-loss data shall be expressed on an hourly basis.

Collecting data is a sampling process, and unless sampling is carried on for a long time there will be uncertainty, particularly about the 'true' proportion of rare events. Rare events, in this connection, mean not only considerable fading in the hourly data, but also 'abnormal' average monthly fading for a period of the day during a particular month. The average may vary from year to year, but this cannot, of course, be seen from the results unless testing has been carried out over many years. Usually it will not be possible to collect data over very long periods, but in the preparation of condensed data all the available facts should be included.

Data may be presented in several ways, e.g. as level recordings against time (raw data), histograms giving for each hour the fraction of time during which the path loss falls within each of a number of ranges (frequency data) or a distribution curve derived from other data and expressing the probability of a certain level of fading being (or not being) exceeded. The data should be given for separate periods of an hour.

### (5.1) Path Performance in Terms of Fading Moments

A new method of presenting hourly path performance data will now be considered. It consists in calculating or measuring directly the hourly statistical moments of the fading ratio [defined in eqn. (2)].

The first hourly crude moment (about zero fading ratio) is the mean fading ratio over the hour, while the second is the mean-square fading ratio, and so on. The crude moments can be calculated from an hourly distribution curve or they may be measured directly (a practical method of measurement would have to be developed).

The hourly fading distribution is precisely defined by its moments. If only the three lowest moments are used, the definition is less precise and no longer unique. The lower moments contain less information than the hourly curve, but they contain the most essential information. It will be seen later that this statement is particularly accurate when the path data are required only for finding the overall effect of using several paths in tandem [addition according to eqn. (2)].

Section 18.2 shows a convenient method of computing the crude moments from the fading distribution curve. The sloping ordinate scale used for this computation is generally a useful one for presenting distribution functions of highly fluctuating quantities for which a logarithmic scale for the variant is appropriate. In Figs. 7 and 8 the data are plotted with reference to the sloping lines, which apply a weighting allowance for the relative frequency of occurrence of the various parts of the original distribution. The area under the curve when the logarithmic ordinate is allowed for is the first moment of the fading ratio distribution. The second and third moments are found in the same way, but by plotting double or treble the distribution-curve values. The performance of a path during an hour may therefore be given by three figures. Such figures must be obtained for a large number of hours and tests must be made over a whole year—ideally over several years.

The expression of path-loss data in terms of moments is a considerable advance over other methods which do not give a simple numerical result. It offers the possibility of making the hourly performance (in terms of moments) the subject for statistical treatment.

### (6) CLASSIFICATION AND CONDENSATION

The hourly results expressed by moments may be considered as a condensation of one hour's fading information into a set of three quantities. Before condensing the test results further it will be necessary to divide the totality of results into classes of results which belong to different parts of the diurnal cycle.

This could be done by averaging separately each of the three hourly moments or their logarithms for each hour of the day over, for instance, a month. If these (hour class) averages are plotted against the hour of day, the resulting curves will show the diurnal cyclic effect. Data for all periods of day having similar performance as shown by these curves may be provisionally classed together.

It is not desirable to have too many classes, and similar performance in the above should be interpreted rather broadly. It should, in particular, be remembered that the third moment depends on the third power of the fading ratio, so that a difference of 2 : 1 (3 dB) in third moments corresponds roughly to a fading

difference of only 1 dB. It may thus be convenient to plot the second and third moments in terms of their square and cube roots respectively.

### (6.1) Final Classification

The purpose of this Section is to determine the grouping of the path data into classes. The problem of expressing the class performance will be dealt with separately. While it is desirable to have only a few classes, it is also important not to class together data which have systematic differences.

Sets of 30 hourly results are 'small samples' and so liable to sampling error, and it is therefore very desirable to combine as many single-hour sets as appropriate. It may be quite proper in this case that the frequency of occurrence of a single bad hour is reduced. This may be an improvement in the data due to the larger (combined) sample, but in combining data in this way it is implicitly assumed that a very 'bad' event which actually occurred in only one part of the sample (hour class) did so by sampling effect, but that if testing could be extended it would be found in all parts of the data to the average extent. In other words, it is assumed that the hour classes which are put into one class are samples of the same population. This assumption should be borne in mind in selecting the hour classes for a class.

It is not easy to distinguish sampling differences between hour classes (which do not bar the hours from being classed together) from systematic differences between hour classes (which make it improper to put them into a class). To answer such questions, it will be desirable to consider the statistics of the moment distributions. In each particular hour-class there will be (for one month) 30 sets of crude hourly fading moments, the variates being $m_1'$, $m_2'$ and $m_3'$, each of which should be considered separately. When these distributions are very skew the comparison between hour classes is best carried out in terms of the logarithms of the moment rather than of the moments themselves. Two methods of comparison will now be described.

The distribution of $\frac{1}{2} \log m_1'$ has moments $t_{11}'$ and $t_{12}'$, which are its first and second crude moments. Each hour class defines such a set of parameters, and each set applies to a sample of 30 items from a parent (class) population. The problem is to decide which sets of parameters belong to the same parent population.

The individual hour class values, $t_{11}'$, have a theoretical variance which for a sample of 30 items will be approximately $1/30$ of the variance, $t_{12}$, of the sample (hour class) itself $[t_{12} = t_{12}' - (t_{11}')^2]$.

The standard error of the sample mean, $t_{11}'$, is the square root of the theoretical variance. The parent mean (which it is desired to find) and the sample mean are not likely to differ by more than three times the standard error. This rule is fully accurate only when $m_1'$ is log-normally distributed. Similarly, if two samples have been drawn from the same parent population, the theoretical variance of the difference of their mean will be $1/30$ of the sample variances. The difference should not exceed three times the square root of the theoretical variance of the difference.

To be more sure that two samples were taken from the same parent population it is also necessary to compare the parameters $t_{12}$, the sample variance of each hour class.*

What has been said about the distribution of $m_1'$ also applies to $m_2'$ and $m_3'$, but the higher moments arise largely from rare events and are therefore subject to large sampling effects. When the parent population is non-uniform or 'patchy', sampling variations will be particularly severe and this is likely to be the case with fading effects.

An alternative method of deciding which hour classes may be classed together consists in plotting the (discontinuous) log-moment distribution curve for each hour class on the special co-ordinate system described in Section 18.2. For 30 results the increments in $p$ may conveniently be taken as $3 \cdot 2\%$ per result.

The curve is a very unusual type of histogram which gives prominence to high values of the variate without giving them undue weight. By comparing the histograms of different hour classes it should be possible to decide which may be classed together.

If an overall fading problem which involves many sections is to be solved, the small errors in classification of the separate section data will not be serious. In Section 13, however, the data for a single path will be used to represent many sections and in such a case it is particularly important to classify correctly.

### (6.2) Class Performance

It would seem reasonable to express the result of the statistical summation in eqn. (2) in terms of overall moments. Such moments have been formulated, and it was found that all the expressions are simplified if both the individual section moments and the overall moments are expressed in terms of central moments rather than as crude moments. (The central moments are taken with respect to the mean of the hourly distribution.) The result is quoted without proof:* the moments of the sum are equal to the sum of the moments of the quantities being added. This is true for second and third central moments.

The central moments are very simply related to the crude moments.[2] The first moment is left as a crude moment but obeys the moment addition rule (the first central moment being always zero). The data for a class will consist of a set of crude hourly fading ratio moments for each individual test hour. In a class there will be 30 such sets for each hour class. The results for each single hour should now be translated from crude into central moments.

The next problem is to find suitable ways of condensing the central moment data for a class into a simple statement. One method is to plot the distribution of each central moment for the whole class, there being three such curves for each class. It should be noted that these curves contain no information about correlation between the three central moments, and in using them it will be assumed that there is a high degree of correlation between the three moments. This should be verified at this stage. Another method is to express each of the three moment distributions by its central moments. For clarity these moments of moments will be called central distribution parameters of the central fading ratio moments.

The method of parameters is preferred for general purposes; the path performance for a class will then be given by three groups of three figures. The first group describes the hourly first-moment distribution, $m_1'$, by its distribution parameters, i.e.

First moment (mean) . . . $x_{11}$.
Second central moment . . . $x_{12}$.
Third central moment . . . $x_{13}$.

The second group similarly describes the hourly second central-moment distribution, $m_2$, by its central parameters $x_{21}$, $x_{22}$ and $x_{23}$, while the third group describes the hourly third central moment distribution, $m_3$, by its central parameters $x_{31}$, $x_{32}$ and $x_{33}$. It will generally be found convenient to state the parameters logarithmically.

All the figures depend on the arbitrary quantity $A_0$ in eqn. (2), but they can readily be translated to be in terms of a different constant. If $A_0$ is reduced by $A_1$ decibels, for instance, the

---

* For a description of the necessary tests see, for instance, YULE and KENDALL: 'The Theory of Statistics', Chapter 22, 'The Analysis of Variance'.

* This rule is a special case of a more general rule, namely that the 'cumulants' of a summation equal the sum of the 'cumulants' of the quantities being added. The cumulants (or Thieles 'seminvariants') are described by Kendall.[2]

**Table 1**

INCREASE OF MOMENTS AND THEIR DISTRIBUTION PARAMETERS WHEN THE REFERENCE LOSS $A_0$ IN EQN. (2) IS REDUCED BY $A_1$ DECIBELS

| Quantity .. | .. | $m_1$ | $x_{11}$ | $x_{12}$ | $x_{13}$ |
|---|---|---|---|---|---|
| Increase, dB | .. | $A_1$ | $A_1$ | $2A_1$ | $3A_1$ |
| | | | | | |
| Quantity .. | .. | $m_2$ | $x_{21}$ | $x_{22}$ | $x_{23}$ |
| Increase, dB | .. | $2A_1$ | $2A_1$ | $4A_1$ | $6A_1$ |
| | | | | | |
| Quantity .. | .. | $m_3$ | $x_{31}$ | $x_{32}$ | $x_{33}$ |
| Increase, dB | .. | $3A_1$ | $3A_1$ | $6A_1$ | $9A_1$ |

moments and their distribution parameters will change as shown in Table 1.

The quantities $m_1'$, $m_2$ and $m_3$ are variates (hourly central moments), and a particular set of these values describe the hourly fading behaviour of one section for one class. The quantities $x_{11}$, $x_{12}$ and $x_{13}$ are the distribution parameters of the first hourly moment; similarly, the other $x$-values define the parameters of the higher hourly moment distribution. These parameters are characteristic of the fluctuation of the $m$-values of their class. More particularly it can be said that an $m_1'$-value is the mean fading ratio for an hour (this is the 'power mean', sometimes referred to as 'r.m.s. fade'). The following serves to clarify the significance of some of the parameters:

$x_{11}$ is the mean fading ratio for the whole class (period of day).
$x_{12}$ is the variance of the hourly mean fade for the whole class.
$x_{21}$ is the mean hourly fading variance for the whole class.
$x_{22}$ is the variance of the hourly fading variance for the whole class.

The variance is the second moment about the mean value of the variate and is equal to the square of the standard deviation. It may be appropriate to select only a few classes of data for further work. These might for instance include such classes as: the worst period of day during the worst month and the worst period of day which coincides with the busy hour. These may be used to represent the performance of the particular path when computing in Section 10 the equivalent-single-section loss distribution. It is, of course, essential that the classes taken for the individual paths shall be consistent, i.e. apply to the same time of day.

### (6.3) Validity of the Condensed Results

In using the condensed results for prediction, the implicit assumption is made that further tests, if they were made in subsequent years, would give results statistically equal. This assumption cannot be avoided, but the probability of the prediction being accurate becomes greater as the volume of results on which the prediction is based increases. But however carefully the available results are treated, they are only the results for a particular test period, and the possibility cannot be excluded that in the future there may be years when the statistical performance will be rather different from that of the test year. The overall error to which this may lead in practice is lessened by the fact that the single path is only one of a large number which go to make up the overall circuit. If, however, there are long-term effects common to all the paths, the error could be substantial. Other methods of reducing the volume of results are less appropriate than that described. It would, for instance, be incorrect to base the work on the fading performance for periods of several hours; such data would not necessarily be valid for prediction of hourly performance, but rather for the performance over several hours together.

The condensation method proposed includes all the available path information, provided that the extent of averaging is limited, as discussed in Section 6.1.

Although the discussion has been in terms of hourly results, the methods could be applied equally for other lengths of time, provided that cyclic effects were not concealed. Data expressed for a certain period of time can often be used for calculating performance over a greater length of time, but generally they cannot be used for accurate prediction of the performance over much shorter periods. It is therefore very important that the basic data should be available in terms that are closely related to the terms of the overall noise-performance specification.

### (6.4) Comparison between Different Radio Paths

An important advantage of the condensed form of path-performance statement (Section 6.2) is that it permits comparison of the performance of different paths on a realistic and numerical basis. It is expected that with experience of such data it may become possible to associate the various $x$-parameters with detailed properties of the individual paths, e.g. length, local climate, clearances and reflection factors. It may also be found possible to isolate the effect of aerial directivity on the path-loss performance. Knowledge of such effects would be a great help in planning future radio paths.

### (6.5) Recommendation for an Overall Noise Specification

The full benefit of such knowledge of path performance will be effective only if the overall noise requirements for a complete 2 500 km circuit are stated in such a form that they may be translated into terms of $x$-parameters for the overall permitted noise. These can then be subdivided to provide for various sources of noise and particularly to provide for thermal noise in terms of $x$-parameter requirements for a single path or for a few paths used in tandem.

With this in view it is recommended that the overall noise requirements for long-distance telephone circuits should be stated in terms of moment parameters.

### (7) TIME STRUCTURE OF FADING

The type of data discussed so far gives information about the distribution of fading, i.e. for what fraction of time certain values are exceeded. It does not give a complete and unambiguous answer to questions about the short-time structure of fading events, i.e. the length of time a fade remains in excess of a certain value or the number of occasions on which fading passes through a certain value. The time structure for very short periods may be of interest for the overall link with many paths connected in tandem, but the interest will mainly be in the time structure of high values of fading in the equivalent single section. These will arise largely from very high fading in a single link; only very rarely will they be caused by a combination of fading in several links.

When time-structure information is required, it may be sufficient to know the time structure of only the very highest fading in the individual paths and to measure the number and length of periods during which the path loss of individual sections exceeds a particular single large value.

An alternative way of obtaining more information about the time structure is to express the path performance in terms of the moments of fading for intervals much shorter than an hour. These moments will fluctuate much more than the hourly ones, but the overall result of using such data may give sufficient detail of the time structure.

### (8) A SIMPLE TANDEM-SECTION FADING PROBLEM

In this Section a method will be described of calculating the equivalent-single-section loss [eqn. (2)] when $n$ sections are

connected in tandem. All sections are assumed to have a log-normal fading-ratio distribution. This case is not likely to arise in practice, but its solution is a useful stage in the approach to the problem of finding a distribution function having specified moments.*

Log-normal fading ratio distribution means that the fading loss (in logarithmic measure) is normally distributed. The curve for $n = 1$ in Fig. 1 is an example of such a distribution when the standard deviation is 1 neper. These curves are always straight lines when plotted on the probability scale used in Fig. 1,
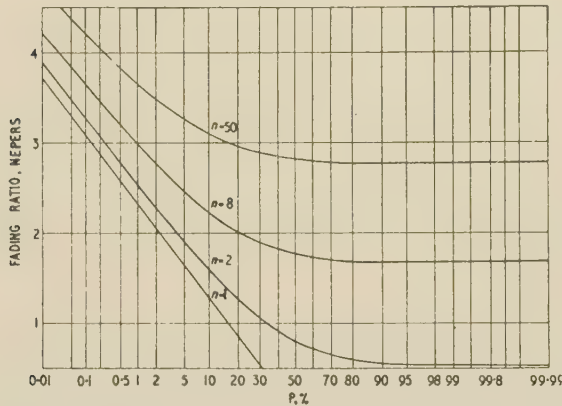


**Fig. 1.**—Addition of log-normal distributions for $\sigma = 1$ neper.
Curve ($n=1$) is the parent population; the other curves represent the sum of 2, 8 and 50 items from curve ($n=1$).

the slope of the curve indicating the standard deviation of the logarithmic quantity. The single-path loss, $A$, in this case is given by

$$A = A_0 + y\sigma \text{ nepers} \quad . \quad . \quad . \quad . \quad (3a)$$

where $A_0$ is the median path loss, $\sigma$ is the standard deviation and $y$ is the normalized variate common to all normal distributions. (In Fig. 1 the probability scale could be replaced by a linear $y$-scale having $y + 3 \cdot 72$ at the left-hand edge ($0 \cdot 01\%$), $y = 0$ in the middle at $50\%$ and $y = -3 \cdot 72$ at the right-hand edge ($99 \cdot 99\%$). The frequency function for this distribution is

$$dP = \frac{1}{\sqrt{2\pi}} \varepsilon^{-y^2/2} dy \quad . \quad . \quad . \quad (3b)$$

The fading ratio is $W$, where

$$W = \varepsilon^{2y\sigma} \text{ units} \quad . \quad . \quad . \quad . \quad (4)$$

It is required to find the equivalent-single-section loss, $A_e$, in eqn. (2) when $n$ sections are used in tandem (neper measure is used in order to simplify the formulae). Eqn. (2) can now be rewritten as

$$A_e - A_0 = \tfrac{1}{2} \log \sum_1^n W_r \text{ nepers} \quad . \quad . \quad . \quad (2a)$$

The $W$-values from the different sections are log-normally distributed and mutually independent, and the addition will be carried out in terms of the central moments of $W$ (see Section 6.2). It is easiest first to determine the crude moments.

The $r$th crude moment of $W$ is

$$m_r' = \int_0^1 W^r dP \quad . \quad . \quad . \quad . \quad (5a)$$

* The solution is also very useful in dealing with the addition of intermodulation noise products in multi-channel telephone systems.

Substituting from eqns. (3b) and (4) and rearranging gives

$$m_r' = \varepsilon^{2r^2\sigma^2} \frac{1}{\sqrt{2\pi}} \int_{-\infty}^{+\infty} \varepsilon^{-1/2(y - 2r\sigma)^2} dy \quad . \quad . \quad . \quad (5b)$$

$$= \varepsilon^{2r^2\sigma^2} \text{ or } r^2\sigma^2 \text{ nepers} \quad . \quad . \quad . \quad (5c)$$

The first moment is the mean fading ratio of the distribution ('r.m.s. fade'). Allowing now for the median value $A_0$, the first moment will be the median value plus the square of the standard deviation (in nepers). The second and third central moments, $m_2$ and $m_3$, are related to the crude moments by the following formulae:

$$m_2 = m_2' - (m_1')^2 \quad . \quad . \quad . \quad . \quad (6)$$

$$m_3 = m_3' - 3m_1'm_2' + 2(m_1')^3 \quad . \quad . \quad . \quad (7)$$

The sum moments, i.e. the moment of $\Sigma W_r$ in eqn. (2a), are $n$ times the moments for a single section. To simplify the expressions the following substitution is made:

$$\varepsilon^{4\sigma^2} - 1 = p \quad . \quad . \quad . \quad . \quad . \quad (8)$$

Table 2 shows the result.

**Table 2**

MOMENTS OF LOG-NORMAL DISTRIBUTIONS WITH ZERO MEDIAN

| Order of moment | Crude moments | Central moments | Central moments ($n$ combined) |
|---|---|---|---|
| 1 | $\varepsilon^{2\sigma^2}$ | — | $n\varepsilon^{2\sigma^2}$ |
| 2 | $\varepsilon^{8\sigma^2}$ | $\varepsilon^{4\sigma^2}p$ | $n\varepsilon^{4\sigma^2}p$ |
| 3 | $\varepsilon^{18\sigma^2}$ | $\varepsilon^{6\sigma^2}[p^3 + 3p^2]$ | $n\varepsilon^{6\sigma^2}[p^3 + 3p^2]$ |

The central moments of the sum distribution given in Table 2 may in some cases be a sufficient answer—at least when the overall noise specification can be expressed in moment form. It is particularly convenient to retain the moment form if other noise contributions have to be added. If these also are expressed in central-moment form, the addition is direct. It may, however, be required to find the distribution function for $A_e$ or other related variables of similar properties, and the following Section deals with this problem.

### (9) TO FIND A DISTRIBUTION FUNCTION HAVING SPECIFIED MOMENTS

Strictly speaking, all the moments should be taken into account to define a distribution function, but in practice it is often sufficient if the first three moments are correctly represented by the solution. A distribution function based on the first three moments is not unique and the higher moments are not necessarily correctly represented.

A function has been found which is particularly appropriate when $W$ is a log-normal quantity [eqn. (4)]. In selecting this function it has been borne in mind that the upper values of the distribution for the summation (2a) will be rather similar in general character to that of the original distribution, but with increased occurrence, and that the lower values are not required to be very exact.

The chosen function will be referred to as an 'augmented log-normal' distribution, defined by

$$W = (1 - a) + a\varepsilon^{2y\sigma_s - 2\sigma_s^2} \text{ units} \quad . \quad . \quad (9)$$

where $W$ is the variate (later to be used to represent the sum variate $W_n$), $\sigma_s$ and $a$ are auxiliary constants and $y$ has the

definition used in eqn. (3b). The central moments of this function are found to be

$$M_1' = 1$$

$$M_2 = a^2 p_s$$

$$M_3 = a^3[p_s^3 + 3p_s^2] \quad . \quad . \quad . \quad . \quad (10)$$

where $p$ is defined as before [eqn. (8)]. It should be noted that this formula is for a distribution function of unit mean power, and it will therefore be necessary to increase $W$ in eqn. (9) to obtain the required mean power; the second and third moments [eqn. (10)] must then be increased respectively by the square and cube of the multiplier $k$.

The required constants are obtained by equating the increased moments with the central sum-moments from Table 1. This gives

$$n\varepsilon^{2\sigma^2} = k \quad . \quad . \quad . \quad . \quad . \quad . \quad (11a)$$

$$n\varepsilon^{4\sigma^2}p = a^2 k^2 p_s \quad . \quad . \quad . \quad . \quad . \quad (11b)$$

$$n\varepsilon^{6\sigma^2}[p^3 + 3p^2] = a^3 k^3[p_s^3 + 3p_s^2] \quad . \quad . \quad (11c)$$

If eqn. (11a) is substituted in the others,

$$\frac{p}{n} = a^2 p_s \quad . \quad . \quad . \quad . \quad . \quad . \quad (12)$$

$$\frac{1}{n^2}[p^3 + 3p^2] = a^3[p_s^3 + 3p_s^2] \quad . \quad . \quad . \quad (13)$$

If eqn. (13) is divided by eqn. (12) raised to the power 3/2,

$$\frac{1}{n^{1/2}}C = \frac{p^{3/2} + 3p^{1/2}}{n^{1/2}} = p_s^{3/2} + 3p_s^{1/2} = C_s \quad . \quad (14)$$

This quantity has the advantage of being independent of $a$. (The quantities $C$ and $C_s$ indicate skewness of the distributions. $C$ is the square root of Pearson's $\beta_1$ coefficient.)

Eqn. (14) is conveniently solved by a graphical method. Fig. 2 shows $C$ and $p$ as functions of $\sigma$. The value of $C$ is found first by entering the graph with the value of $\sigma$ given in eqn. (3a). $C$ is then divided by $n^{1/2}$ to give $C_s$. By entering the graph with this value, $\sigma_s$ is found. Eqn. (12) then yields $a^2$ as the ratio $p/np_s$ (the $p$ values are read from Fig. 2 by using $\sigma$ and $\sigma_s$). $k$ is most conveniently found as $n\varepsilon^{2\sigma^2}$.

The required distribution of $W_n$ is obtained by combining the two parts of eqn. (9) each multiplied by $k$. It will generally be desired to express $W_n$ in log measure as $A_e$. The required sum distribution plotted to a scale of linear probability has an asymptote corresponding to each of the two components. The horizontal asymptote is

$$\tfrac{1}{2}\log(1-a) + \tfrac{1}{2}\log n + \sigma^2 \text{ nepers} \quad . \quad . \quad (15)$$

The other asymptote is a log-normal distribution, with median

$$\tfrac{1}{2}\log a + \tfrac{1}{2}\log n + \sigma^2 - \sigma_s^2 \quad . \quad . \quad . \quad (16)$$

and standard deviation $\sigma_s$.

The final curve may be calculated by plotting the two asymptotes and adding for each probability the power values corresponding to the asymptotes. Fig. 1 shows the result of a particular example in which $\sigma = 1$ neper; curves are shown for $n = 1$, 2, 8 and 50 sections, while Fig. 3 is for $\sigma = 0.5$ neper.

The statistical summation of log-normal distributions expressed in augmented log-normal form will in most cases be accurate at the higher levels of fading but less accurate at the lower and lowest levels.

Possibly a better function could be found for the special case of log-normal summation, but the augmented log-normal form
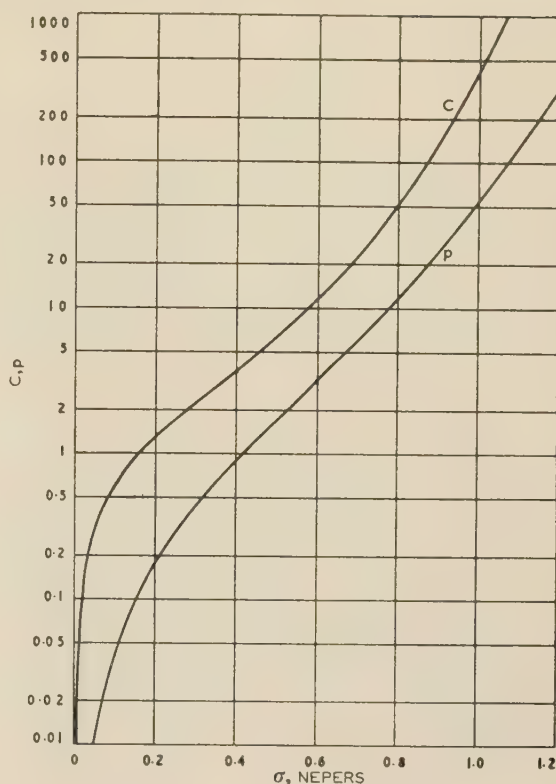


Fig. 2.—The constants $p$ and $C$ used for log-normal distributions.

$$p = \varepsilon^{4\sigma^2} - 1.$$
$$C = p^{3/2} + 3p^{1/2}.$$
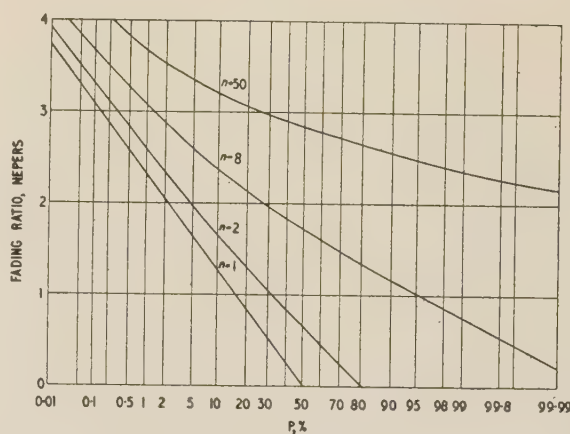


Fig. 3.—Addition of log-normal distributions for $\sigma = 0.5$ neper.

is very simple in use and, it is believed, sufficiently accurate where accuracy is needed.

### (9.1) Distribution Curve representing Moment Summations

The augmented log-normal distribution can be used more widely to find distribution functions corresponding to sets of statistical moments which are the result, not of the addition of log-normal distributions, but of other distributions which are approximately log-normal only in their upper ranges.

In the general case the path losses to be combined are unlikely to be log-normally distributed, but they may still be expressed in terms of their fading-ratio moments, and these may be added

and the sum distribution, $A_e$ [eqn. (2)], determined from the sum-moments.

If the three moment sums are $M_1'$, $M_2$ and $M_3$, then

$$
\left.
\begin{aligned}
M_1' &= k \\
M_2/(M_1')^2 &= a^2 p_s \\
M_3/(M_2^s)^{3/2} &= p_s^{3/2} + 3p_s^{1/2}
\end{aligned}
\right\} \quad . \quad . \quad (17)
$$

These correspond respectively to eqns. (11a), (12) and (14) and thus define an augmented log-normal distribution representing the three moments. In this case there is no restriction to addition of path losses all having the same distribution; the formulae apply quite generally where the sum-moments are available, but the result is, of course, an approximation to the true distribution curve.

## (10) CALCULATION OF MULTI-SECTION FADING EFFECTS

In Section 6.2 the path performance was expressed in terms of the distribution parameters of the hourly central moments of the section fading ratio. Each transmission section in a multi-section link has nine such parameters for each class of performance. In this Section the statistical addition of the fading effects in the individual tandem-connected sections will be carried out in terms of these parameters.

The first step is to determine nine parameters, $X_{rs}$, of the equivalent-single-section loss. These describe the hourly moment distributions of the equivalent-single-section loss (or overall fading ratio)

$$
X_{rs} = \sum_1^n {}_1x_{rs} + {}_2x_{rs} + \dots + {}_nx_{rs} \quad . \quad . \quad (18)
$$

By applying the $X$-values in eqn. (17) in place of $M$, augmented log-normal curves may be found describing the three first hourly moments of the equivalent single section (or overall circuit fading-ratio hourly moments) for a particular class of performance. The $X$-values themselves, or the moment distribution curves, may in some cases be a sufficient final answer; if this is not the case, a further stage of calculation is required.

In the next step it is necessary to determine levels of probability at which the overall moment distribution curves shall be read. If, for instance, the data apply for three hours of each day during a month, this particular prediction will cover nearly 100 hours in a month; and if the readings for a probability of 99% are taken on the sum-moment distribution curves, the sum-moments indicated will be exceeded for (on the average) one hour in the 100 hours for which the class is valid. The distribution of the equivalent-single-section loss is next found by using eqn. (17) again. The result is the hourly distribution which is likely to obtain for one hour in the class considered. This is one final answer. It will generally be appropriate to repeat this process for other assumed probability values and later to deal with other sets of data (classes) in the same way. The precise procedure will depend on the exact form in which the information is required.

When using the sum-moment distribution curves, the same probability value is taken for all three moments—a compromise necessary to make the method workable. It is not an exact procedure, because the three moments are somewhat independent of each other, but it is believed that the error resulting from this simplification will be very small, particularly when the sum-moments have many component moments, as will usually be the case.

The first sum-moment will show a relatively small fluctuation, and therefore will not vary very greatly with the level of probability taken. It has been found that the higher region of a loss-distribution curve as determined from the moments is not very sensitive to moderate changes in either the second or the third moment by itself. The assumption that the moments vary together is thus not likely to lead to serious errors.

### (10.1) Combination of Classes of Overall Performance

The sum-moment parameters $X$ may be used in a different way. Instead of considering $X$-values separately for each class, they may be combined into a single statement which covers many classes. Combination of this nature must be carried out in terms of crude parameters (of the central moments). The $X$-values for each moment distribution must therefore first be converted to the crude values, $X'$. Each separate type of $X'$-value must then be averaged over all classes, the individual values being weighted according to the size of the class. This results in nine parameters, $X'$, which should now be converted to central $X$-parameters. There will be nine such parameters similar to the $X$-parameters in Section 10, but in this case they describe the moment distribution over all the classes which have been combined.

They may conveniently cover the performance over a month, but could cover longer periods if the corresponding classes were included. The data for a month will thus cover about 700 hours, and the corresponding moment distribution curves may be determined as before by using eqn. (17).

These curves may now be read to determine the moments of the hourly overall fading distribution which is exceeded only during, for instance, the worst seven hours (1%). What was said in Section 10 about using the same probability values when reading the three moment curves applies here also, but probably the consequences are more serious in the present case, since the combined statistics contain classes of very different performance, whereas in Section 10 there was only a single class of relatively uniform performance.

### (10.2) A Practical Limitation

The practical value of the methods just described may be restricted for lack of the necessary data. As a rule, only a small number of transmission sections are installed at any one time, and test results can at best be obtained for only a few sections. It is nevertheless necessary to be able to check whether such sections as are available for test are suitable for forming part of an overall connection to the full 2 500 km planning length. The problem has received some attention,[4] and two methods of making the necessary comparisons will be dealt with in Sections 11 and 12 respectively.

## (11) SUBDIVISION OF OVERALL NOISE SPECIFICATION

One method is to find the equivalent specification for a fraction of the overall circuit (partial circuit). If the overall specification can be translated into terms of moments, there is little difficulty in defining the permissible moments for partial circuits or in translating these moments into limiting path-loss-distribution curves, but it is not possible to define fluctuation for the partial-circuit moments unless the overall criterion itself contains a moment-fluctuation allowance. In the absence of a fluctuation clause the requirements tend to become unnecessarily severe for the partial circuit.

It is therefore very desirable that the overall specification should contain a moment-fluctuation clause, at least for the third moment, which is most sensitive to high fading values of short duration. A more satisfactory form for the overall criterion would be one that specified a distribution curve for the hourly moments during the month, or the parameters of such a distribution as proposed in Section 6.5.

The present C.C.I.F. noise specification in effect gives a

maximum limit for the first moment in any hour; it would therefore remain necessary to define limits for the second and third moments, and it is for these that a specification in terms of hourly-moment distributions would be more suitable than mere maximum values.

## (12) SYNTHETIC OVERALL CIRCUIT BASED ON A PARTIAL CIRCUIT

According to the second method, a synthetic overall circuit is produced by imagining the real partial circuit in question to be tandem connected with itself a sufficient number of times to reach the full planning distance. This device is available only for statistical approach: it would be incorrect to make such a tandem connection on an actual circuit, for this would amount to the assumption that the path losses in the partial circuits are completely co-variant—an assumption that is quite unwarranted. But statistically it is possible to make proper use of this device. In the sampling process which is normally used for computing overall performance it is only necessary in eqn. (18) to take all $n$ items in the samples from the data of the actual partial-circuit sections instead of from $n$ different sets of path data. The data must, of course, apply to a particular class.

In an extreme case this can even be carried out for a single radio path. A procedure which can be carried out with so little data is more likely to find practical application than the more complete one, and it will therefore be described in more detail. A very convenient method has been found for calculating the sum-moment distributions for this special case.

## (13) SYNTHETIC OVERALL CIRCUIT BASED ON A SINGLE PATH

The path data consist of the moment distributions for various periods of the day (classes). The $r$th moment is represented by a function $M_r(p)$, where $p$ is the probability that $M_r(p)$ will not be exceeded. It is required to find the distribution of the sum of $n$ values chosen at random from $M_r(p)$. The resulting distribution is $M(z_n)$, for which the following approximate formula has been derived:

$$M(z_n) = (n - 1)\frac{1}{p_1}\int_0^{p_1} M(p)dp + M(p_1) \quad . \quad . \quad (19)$$

where $z_n = p^n$.

Fig. 4 shows $z_n$ in graphical form.
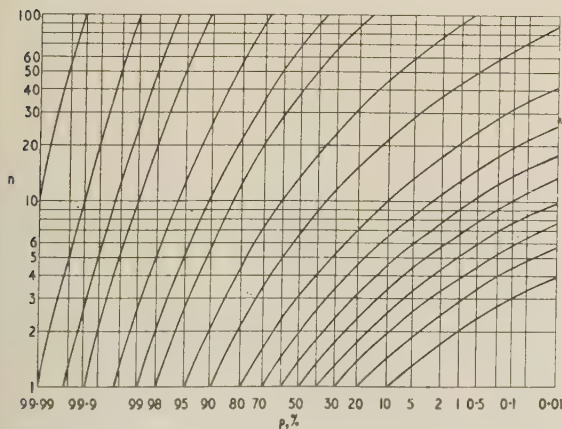
**Fig. 4.**—Curves for transforming probability scales.

Used in connection with eqn. (19) for statistical summation

$$z_n = p^n$$

In the special case of a distribution with unit first moment the function

$$\frac{1}{p_1}\int_0^{p_1} M(p)dp$$

goes from 0 to 1 as $p_1$ goes from 0 to 1, and the function shows promise of being important for the sampling of distributions. It may be said to indicate the running mean value of the distribution over the range 0 to $p$. This function is easily calculated either directly from the data or from $M(p)$ in graphical form; in the latter case the method described in Section 18.2 is useful for the integration process.

For the purpose of a check, eqn. (19) has been applied to the summation of log-normal distributions. It is more accurate than the augmented log-normal method, but the results of the two summations agree accurately at the higher levels. Fig. 5
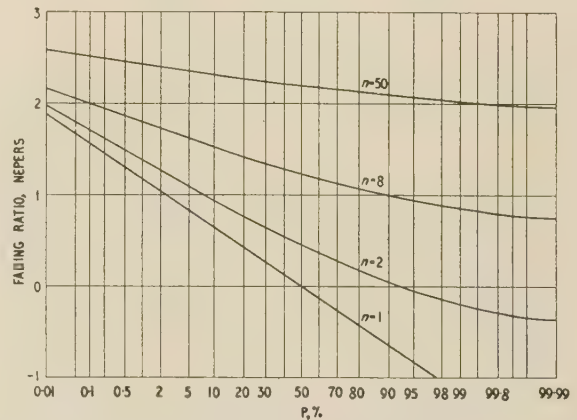


**Fig. 5.**—Addition of log-normal distributions for $\sigma = 1$ neper.

Addition carried out by eqn. (19).

shows the result of this computation, and should be compared with Fig. 1.

For the purpose of the present Section, $M(z_n)$ should be determined from eqn. (19) for each of the three moment distributions. If the final result is required in terms of equivalent-single-section distribution, eqn. (17) may be used as before (Section 10) to find augmented log-normal distribution for a number of levels of probability in the $M(z_n)$ functions. The distributions thus found describe the equivalent-single-section loss of the synthetic overall circuit, and from this the thermal agitation noise in any given system is readily calculated.

For an alternative calculation of synthetic overall circuit performance, the $x$ values in eqn. (18) may all be taken from the available single-path data instead of from $n$ separate paths; the work can then proceed exactly as in the general case (Section 10). However, the method just described is the more accurate.

## (14) ACCEPTANCE TEST FOR A RADIO PATH

The results of Sections 12 and 13 show what fading would result in an overall circuit if it were built up by using sections with fading statistics identical with those of the actual single section for which fading results are available. This is a very important result which would make it possible to decide whether the section in question was suitable to be one of the sections in an overall circuit.

The final step of comparing the noise calculated for the synthetic circuit and the specified overall noise cannot be taken until a complete overall noise specification is available. A recommendation for the form of such a specification is made in Section 6.5.

## (15) CONCLUSIONS

In calculations of the thermal noise for a multi-section radio link it is very important to take proper account of cyclic effects common to the fading statistics of many of the sections. It is recommended that fading data shall be expressed in terms of hourly performance, and that the hourly fading performance shall be expressed in terms of the first three statistical moments of the fading ratio.

The moments for a particular hour of the day (during, perhaps, a month) may be grouped into a class with the moments for other hours of the day which appear to have similar performance. In each class the moments of individual samples of hourly fading performance will fluctuate. It is therefore also necessary to calculate the statistics of the moments in each class. The path information for each class will then be specified by nine parameters. Separate classes will also be needed for different parts of the year.

When these parameters are available for all the sections of an overall circuit the hourly overall-circuit fading effect can be evaluated in terms of either the overall fading-ratio moments or the overall fading distributions which will not be exceeded for specified fractions of the periods covered by a class of fading behaviour.

The full data needed for such an overall computation will rarely be available, but in the light of the principles of this computation a synthetic overall circuit is proposed which may be based on the performance data of even a single path. The performance computed for this circuit makes it possible to judge whether the single path is suitable for use as one of the paths in the hypothetical reference circuit which is used to define the noise-performance objectives for long-distance transmission.

A formula is given for the summation of log-normal distributions as well as a more general sampling function. Methods are described for converting distribution data to moment form, and a formula is given for finding an approximate distribution function from the first three moments of a variant.

It is recommended that the overall noise specification for a long-distance circuit shall be expressed in terms of the distribution parameters of the hourly central moments of the noise.

## (16) ACKNOWLEDGMENTS

The author wishes to thank Mr. F. O. Roe for help in preparing the paper for publication, and Standard Telephones and Cables, Ltd., for permission to publish it.

## (17) REFERENCES

(1) 'Red Book' of the C.C.I.T.T., 1st Plenary Session (to be published shortly).
(2) KENDALL, M. G.: 'The Advanced Theory of Statistics' (Griffin, 1952), Fifth Edition, Volume 1, p. 60.
(3) KENDALL, M. G.: loc. cit., p. 290 et seq.
(4) JACOBSEN, B. B.: 'Probability Theory in Telephone Transmission' Teleteknik (English Edition), May, 1954, p. 83.
(5) DAWSON, G., HALL, L. L., HODGSON, K. G., MEERS, R. A., and MERRIMAN, J. H. H.: 'The Manchester–Kirk o'Shotts Television Radio-Relay Systems', Proceedings I.E.E., Paper No. 1623 R, May, 1954 (**101**, Part 1, p. 93).
(6) YULE, G. U., and KENDALL, M. G.: 'An Introduction to the Theory of Statistics' (Griffin), Fourteenth Edition.

## (18) APPENDICES

### (18.1) Phase Noise

Assume that the carrier frequency is $\omega_p$ rad/sec and consider as a noise element a sine wave differing by $\omega_q$ rad/sec in fre-

quency and of $a$ times the carrier-frequency power. The sum of these two voltages has the following approximate form when $a$ is very small:

$$[1 + (\sqrt{a}) \sin \omega_q t] \sin [\omega_p t + (\sqrt{a}) \cos \omega_q t]$$

The carrier frequency appears to be modulated in amplitude and phase. The effect of a limiter is to suppress the amplitude modulation, but the phase modulation becomes 'incorporated' and is equivalent to what could have been produced by a useful input signal of frequency $\omega_q$. The effect of the carrier noise element is therefore to produce 'phase noise'. In the example the phase noise is of r.m.s. amplitude $\sqrt{\frac{1}{2}a}$ rad. It is convenient to express the square of the phase noise amplitude in decibels referred to an amplitude of 1 rad r.m.s.

For the noise element of power $A = 10 \log a$ decibels referred to that of the carrier, the phase noise will be $(A - 3)$ decibels referred to 1 rad r.m.s. (0 dBrr).

If a number of single small noise elements are present, the phase noise effects will combine on a power basis when the noise elements are of differing frequencies.

If the carrier-frequency noise is of uniform spectral density, the phase noise also will be of uniform density (white noise). Since noise bands above and below the carrier frequency are operative, the phase noise density per unit bandwidth at base-band frequency will equal the r.f. noise density relative to the carrier power. If the r.f. noise density per unit bandwidth is $A$ decibels referred to the carrier level received, the phase noise per unit bandwidth at base-band frequency will be $A$ dBrr. This formula is true also when the carrier frequency is phase or frequency modulated.

Phase noise will be translated into base-band noise at the receiving terminal, but the exact translation will depend on the phase-modulation constant of the system at the various base-band frequencies. This constant is the phase signal (in dBrr) which results when a 0 dBm0 base-band signal is applied.*

If, for example, the phase-modulation constant for a particular telephone channel is $-16$ dBrr and the phase noise per 4kc/s bandwidth is $A$ dBrr, the circuit noise will be $(A + 16)$ dBm0. This is the noise power referred to a point of zero relative level, and in practice a psophometric weighting allowance may be required.

In a frequency-modulated system the phase-modulation constant will vary over the base-band: in a phase-modulated system it is constant. Actual systems tend to use frequency modulation at the lower frequencies but to approach phase modulation at the upper base-band frequencies.

The phase noise will in all systems tend to be of uniform density, and for this reason it is convenient to work in terms of phase noise.

### (18.2) Determination of Crude Moments from a Distribution Curve

When a logarithmic scale is used for the variate it is particularly easy to determine graphically the moments of a distribution function. The principle adopted is to weight the distribution curve by its own 'frequency'. When the variate is in logarithmic terms, this is done by subtracting from the log-variate a quantity proportional to the logarithm of the frequency of occurrence. The frequency of occurrence is the differential of the probability, and a suitable constant must be selected which will determine the scale of the crude moment integral.

The method will be explained with reference to Fig. 6, which shows a distribution curve (a). The variate is the fading with

---

\* The symbol dBm0 indicates a power level in a telephone circuit, expressed in decibels relative to 1 mW (or in dBm) at a point of zero relative level (0). This symbol is used in telephone transmission work when dealing with signal loading, pilot frequencies and noise.
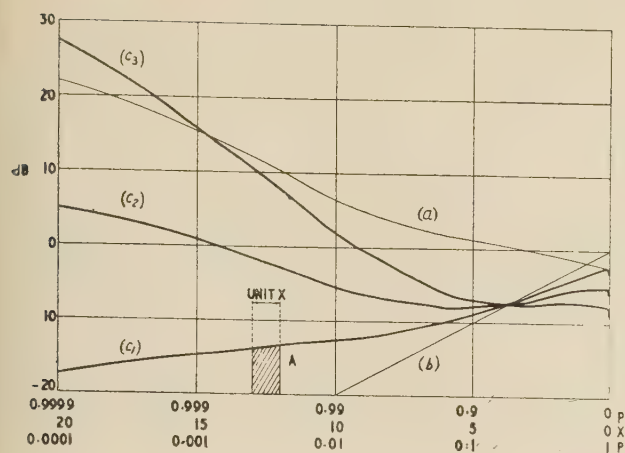
Fig. 6.—Graphical determination of moments and a special presentation of probability curves.

Multiply moment result by 0·461 (−3·36 dB).



Fig. 7.—Path-loss curves and their moments (250 hours).

4 000 Mc/s path, 40 miles long.   1 500–2 100 hours.

respect to free-space transmission. The probability scale is logarithmic; $p$ is the probability of the variate not being exceeded. The $x$-scale is a transformed probability scale, where $x = 5 \log_{10} (1 - p)$.

Curve (b) shows the weighting function used, and has a slope of 10 dB per decade in $(1 - p)$. For convenience, the curve applies zero weighting at $x = 0$. This introduces a scale error when the curve is integrated, but this is readily corrected by multiplying the moment results by 0·461 (−3·36 dB). This correction applies when the integration is made in terms of unit $x$-values.

The curve $(c_1)$ is obtained by adding the weighting values to curve (a). To determine the first moment of curve (a) the ordinates of curve $(c_1)$ should, in principle, be transformed into fading ratios, the area under the transformed curve then being the first moment. In practice, however, it is easier to proceed in a different way. Consider the column marked A. This is of unit width, and its moment contribution is therefore the mean fading ratio corresponding to the segment of curve $(c_1)$.

For small slopes of the segment its mean height is very nearly equal to the linear mean in log measure. For greater slopes it is recommended to make a table of the linear mean in log measure with respect to the upper-end point of the segment. The first moment is the sum of the mean fading ratios of all segments multiplied by 0·461. The second (third) crude moment is worked out in precisely the same way, except that the variate values of curve (a) must be doubled (trebled). The resulting curves corresponding to $(c_1)$ are marked $(c_2)$ and $(c_3)$. Fig. 7 shows a more convenient way of plotting curves (c) directly. Sloping weighting lines are drawn at 10 dB intervals and the fading distribution $(c_1)$ is plotted with respect to these lines, thereby applying the weighting automatically. The area under the resulting curve is determined as for Fig. 6, using the horizontal ordinate lines in Fig. 7. For the second (third) moment, two (three) times the fading distribution values have been plotted on the sloping co-ordinate system [curves $(c_2)$ and $(c_3)$].

The data actually used for Fig. 6 were obtained from Reference 5 over a 1 000-hour test in the Arncliffe Wood–Tinshill section of the Manchester–Kirk o'Shotts system in the course of a general check of path performance.

Those used for Fig. 7 were obtained for the same path and period, but taking the results for the hours 1500–2100 only. Fig. 8 applies to the same path, but covers only a single 6-hour period which showed exceptionally severe fading. Unfortunately,
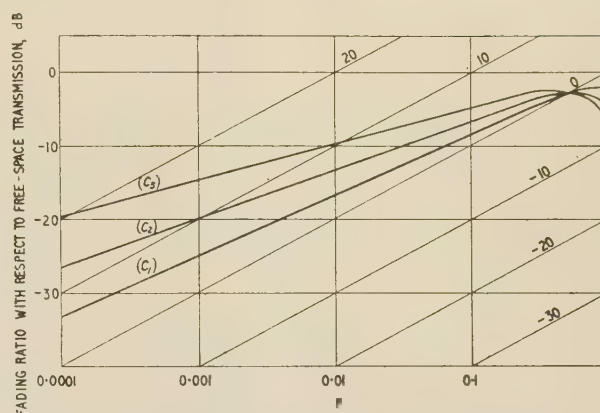
data are not available beyond 30 dB fading and the complete evaluation of the second and third moments, in particular, is impossible. The path in question is nearly 40 miles long and therefore particularly liable to abnormal refraction fading (see Section 3.2). Another difficulty is that the data are for a 6-hour period rather than for the 1-hour period proposed in the present paper. For 1-hour distributions the weighted curves would be more likely to bend over and so define the moments.

There are, however, distributions for which the moments are not finite: if 'complete' fading occurs for even a very short time
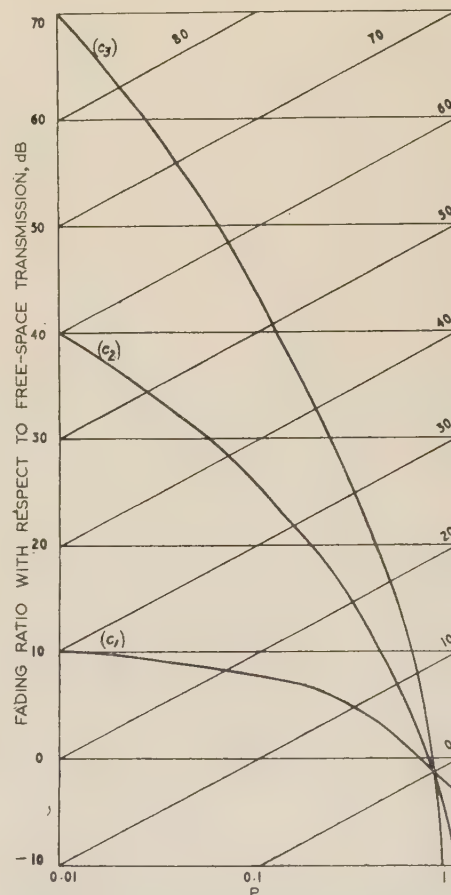


Fig. 8.—Path-loss curves and their moments (worst 6-hour period).

the moments will be infinite. Such distributions are not acceptable for long-distance links, or, at the worst, they can be accepted on only very few occasions. By determining hourly fading distributions separately and condensing each hour's performance into the first three crude moments, the way is open for dealing properly with rare effects. This is done in terms of the distribution of the hourly moments for a particular hour of the day over, for instance, a month.

In evaluating the higher moments, particularly the third, it should be remembered that an error in the third moment has less effect than might at first be expected. An error of 3 dB, for instance, will for many purposes correspond to an error of only 1 dB in the variate. Also there should not be too much concern about that part of the moment line which falls outside $p = 0 \cdot 01 \%$, and which in any case represents only a very small time ($2 \cdot 2$ sec in Fig. 8, but for an hourly curve only, $0 \cdot 36$ sec).

The first three moments can, in general, be adequately summed, provided that the distribution curves cover sufficiently short periods of time. The period of one hour seems suitable.

It is clear from curve ($c_1$) of Fig. 6 that the first moment arises largely from fading of less than 2 dB with respect to the free-space path loss. Curves ($c_2$) and ($c_3$) show that the second and third moments arise largely from fading which lasted for perhaps 10 min during a 1 000-hour test period. The presentation in Figs. 6–8 gives a better indication of the relative importance of various levels of fading than does an ordinary distribution curve.

Curves such as ($c_1$) in Fig. 6 can also be used to determine, for a particular fading distribution, the integral in eqn. (19). The integral is the moment up to a certain $p$-value on the curve divided by $p$ (the 'probability of not exceeding'). The resulting function may be said to represent the linear mean of all variate values below that for which the probability of its not being exceeded is $p$.

It should be noted that in Fig. 4 the probability figures are in terms of $p$, where $p = 1 - P$.

# AN IMPROVED ELECTROMAGNETIC ANALOGUE

## By W. T. J. ATKINS, B.Sc.(Eng.), Member.

### SUMMARY

The paper is concerned with the quantitative representation of symmetrical electromagnetic fields by analogue. An improved type of analogue is described, enabling dynamic as well as static effects to be studied. Possible applications are indicated.

### LIST OF SYMBOLS

*3-Dimensional System*

$E, E$ = Electric field strength, V/m.
$e, e$ = *External voltage gradient, V/m.
$J, J$ = Current density, A/m$^2$.
$H, H_x, H_y$ = Magnetic field strength, A/m.
$B, B_x, B_y$ = Magnetic flux density, Wb/m$^2$.
$\Phi$ = Magnetic flux per unit depth, Wb/m.
$\rho$ = Resistivity, ohm-m.
$\mu$ = Permeability, H/m.

*2-Dimensional System*

$V$ = *Electric potential of side of capacitance remote from surface, volts.
$v$ = Electric potential of surface, volts.
grad $v$ = Surface voltage gradient, V/m.
$I, I_x, I_y$ = Current density in surface, A/m.
div $I$ = Emergent current density, A/m$^2$.
$R$ = Surface resistivity, ohms.
$C$ = Shunted capacitance, F/m$^2$.

*Both Systems*

$x, y, z, s$ = Length, m.
$t$ = Time, sec.
$\theta$ = Angle, rad.
$\omega$ = Angular velocity, rad/s.

The units are rationalized M.K.S.
The suffixes denote axial components.
The quantities marked * are not functions of position.

### (1) BASIC PRINCIPLES

The mapping of extended fields in space, generally with a change of scale, is regularly practised for many engineering purposes. One such purpose is the study of the electric field, together with the resulting distribution of current or displacement, between boundaries held at differing equipotential levels. Where the field manifests some suitable kind of symmetry, a 2-dimensional model can be used in this way to represent a 3-dimensional configuration. Two principal forms of such analogues have been employed, namely:

(*a*) A continuous smooth sheet, usually a shallow electrolytic tank but sometimes an actual sheet of conductive material.
(*b*) An equivalent 2-dimensional network of discrete circuit elements arranged in some more or less regular mesh system.

The same devices can be used to represent the magnetic field due to electric currents by interchanging forces and potentials to take account of the fundamental differences between the electric and magnetic quantities. The practical usefulness of this development appears to have been pointed out in the first instance by Prof. Peierls[1] and it has since become a well-known technique.[2] The method is limited to static conditions, being valid only in relation to the steady fields produced by constant currents, though it still gives approximately correct results under varying conditions if secondary or eddy currents are either suppressed by insulation between laminations or are disregarded. Current flow-lines in the 2-dimensional sheet represent magnetic equipotentials in the 3-dimensional body, and the orthogonal equipotentials indicate flux direction. Currents injected into or withdrawn from the surface of the model correspond directly in the two cases. Surface resistivity represents permeability, and voltage differences on the model measure flux linkages in the original. The scheme may be regarded as an expression of Ampère's law.

### (2) INTRODUCTION OF TIME AS A VARIABLE

The present proposal is a generalization of the foregoing electromagnetic scheme, enabling allowance to be made for the effect of Faraday's law as well as that of Ampère's law.

Ignoring quantities which are insignificant for present purposes, the electromagnetic relations in a 3-dimensional region are as follows:

$$J = \operatorname{curl} H \quad \text{(Ampère's law)} \quad . \quad . \quad . \quad (1)$$

and

$$-\frac{\partial B}{\partial t} = \operatorname{curl} E \quad \text{(Faraday's law)} \quad . \quad . \quad . \quad (2)$$

with

$$E = \rho J + e, \text{ and } B = \mu H.$$

If we take rectangular co-ordinates $(x, y, z)$ and assume that there is axial symmetry—or more strictly, uniformity—in the sense that $E$ is everywhere parallel to $z$ and that $H$ is in the plane $(x, y)$, eqns. (1) and (2) reduce to

$$J = \frac{\partial H_y}{\partial x} - \frac{\partial H_x}{\partial y} \quad . \quad . \quad . \quad . \quad . \quad . \quad . \quad (1)$$

$$\left.\begin{aligned} -\frac{\partial B_x}{\partial t} &= \frac{\partial E}{\partial y} \\[2mm] \frac{\partial B_y}{\partial t} &= \frac{\partial E}{\partial x} \end{aligned}\right\} \quad . \quad . \quad . \quad . \quad . \quad . \quad . \quad (2)$$

$$E = \rho J + e$$

$$B_{x,y} = \mu H_{x,y}$$

Also

$$\left[\Phi\right]_a^b = \int_a^b B \, ds \quad (ds \text{ is perpendicular to } B).$$

For simplification in the first place only those parts of any cross-section which possess conductivity are considered, and it is assumed that they are subdivided into as many separate zones

as there are regions of conductivity bordered by insulation, one such zone being selected for study.

We now turn to the 2-dimensional structure, and, in particular, that portion of it corresponding to the zone just defined. The surface resistivity is, as in the elementary scheme, a measure of local permeability, but there is now to be appended to it a uniform distribution of capacitance, proportional to the effective conductivity of the 3-dimensional structure in the direction of symmetry, and bearing upon its remote side a uniform voltage which, in general, varies with time.

If we take rectangular co-ordinates $(x, y)$ in the surface, the relations for the electrical quantities are as follows:

$$C\frac{\partial}{\partial t}(V - v) = \operatorname{div} \boldsymbol{I} \quad . \quad . \quad . \quad . \quad . \quad (3)$$

and

$$-RI = \operatorname{grad} v \quad . \quad . \quad . \quad . \quad . \quad (4)$$

These may be rewritten as

$$C\left(\frac{dV}{dt} - \frac{\partial v}{\partial t}\right) = \frac{\partial I_x}{\partial x} + \frac{\partial I_y}{\partial y} \quad . \quad . \quad . \quad . \quad . \quad . \quad . \quad (3)$$

$$\left.\begin{aligned} -RI_x &= \frac{\partial v}{\partial x} \\[1em] -RI_y &= \frac{\partial v}{\partial y} \end{aligned}\right\} \quad . \quad . \quad . \quad . \quad . \quad . \quad . \quad (4)$$

with $\quad v_b - v_a = \displaystyle\int_a^b \operatorname{grad} v\, ds$ ($ds$ is parallel to grad $v$)

If the system of eqns. (1) and (2) is now compared with that of eqns. (3) and (4), and it is assumed, for the present, that the units of length and time are the same in both systems, it will be found by substitution that exact correspondences exist according to the following list of identifications, in which $m$ and $n$ are arbitrary multipliers:

| 2-*Dimensional System* | 3-*Dimensional System* |
|:---:|:---:|
| $I_x$ | $-mH_y$ |
| $I_y$ | $mH_x$ |
| div $\boldsymbol{I}$ | $-mJ$ |
| $\dfrac{dV}{dt}$ | $ne$ |
| $\dfrac{\partial v}{\partial t}$ | $nE\left(= n\dfrac{d\Phi}{dt}\right)$ |
| $R$ | $n\mu/m$ |
| $C$ | $m/n\rho$ |

So far, attention has been confined to a single zone of the cross-section, but it will be clear that the separate zones can be recombined and the group treated as a whole provided that the respective parts of $C$ are kept insulated from each other, so that $V$ can take values differing from one zone to another. Upon the surface of the sheet itself, $\boldsymbol{I}$ and $v$ are continuous; this corresponds to the continuity of $H$ and $\Phi$ in the 3-dimensional system.

In the majority of practical problems about parallel conductors it is required to determine the consequences of constraining $e$ to follow given variations in time and place, bearing in mind that the total cross-section is comprised of a number of zones, each carrying its own uniform $e$ differing from that of its neighbours from which it is insulated. Since the equivalent of $e$ is $(1/n)dV/dt$ the solution is immediately obtained through the application of $n\int e\,dt$, again varying in time and place, to the corresponding zones of the distributed capacitance.

$e$ need not be given expressly everywhere, but where it is not specified the effective impedance closing the external circuit must be known. That value will often be zero or infinity, but in no case is it permissible to omit the representative section of capacitance, because this would prevent the flow of eddy currents which are essential for the complete simulation of events.

An important case is that in which $e$ varies sinusoidally with time; the corresponding $V$ is $ne/\omega$ varying in the same way with time but lagging in phase by $\pi/2$.

Where $e$ is unidirectional the integration rule would require $V$ to increase without limit at an average rate of $ne$ volts per second. Since this is generally not practicable, an equivalent step-by-step procedure may be substituted, working in increments of time, $\delta t$. Each element of $C$ is replaced by the conductance $C/\delta t$. Before the commencement of a particular step $ne\delta t$ is calculated; this will be the increment $\delta V$. $v$ is measured everywhere, giving the accumulated results of all previous steps, and finally the conditions resulting from the step are found by applying $v + \delta V$ to the surface via $C/\delta t$. This technique resembles one which has been applied to the closely similar problem of thermal diffusion.[3] Where $e$ either is, or eventually becomes, constant the process degenerates to that of direct injection of div $\boldsymbol{I}$ at a voltage dependent only on $\rho$, in other words, to the elementary static form of analogue.

An interesting possibility is that of making automatic allowance for magnetic saturation where it occurs. This could be done by using semi-conducting material for the representation of regions of non-linear permeability, with an accuracy measured by the closeness of resemblance between grad $v/I$ and $nB/mH$ over the working range.

Changes in the scales of length and time (or frequency) within physical limitations, are available by operating with the multipliers $m$ and $n$.

## (3) EXTENSION TO CYLINDRICAL PROBLEMS

Some stationary groups of conductors have an alternative kind of symmetry for which the element of volume is a wedge-shaped sector of a solid of revolution. This cylindrical pattern is represented by making $R$ directly, and $C$ inversely, proportional to distance from the axis of revolution, and follows the practice described in Section 5 of Reference 2. Transformers and allied equipment may be so simulated, provided that the nature of any approximation this involves is borne in mind, i.e. that a transformer seldom has true cylindrical symmetry. In these problems, the voltage gradients are circumferential instead of rectilinear, and they vary inversely with distance from the axis of revolution. The voltage per turn is a convenient unit, so that $e$ in the formula represents (volts per turn)$/2\pi$ (radius).

## (4) APPLICATION TO ROTATING MACHINES

Another use for the analogue is in the study of certain types of rotating machines, notably the high-speed steam-turbine-driven synchronous alternator. A machine of this type has the first or rectilinear type of symmetry, and is essentially a 'long' machine, so that end effects are relatively unimportant.

To study the effects of rotation, we have to refer to the statements of fundamental principles.

Eqn. (1) and the relations involving $\rho$ and $\mu$ are unchanged, since they are independent of time. Eqn. (2) is affected by movement of $B$ relative to the medium which supports it. If that movement is measured by change of $\theta$, the instantaneous position angle of a point in the medium relative to the axis of rotation, the total rate of change of $B$ with time is

$$\frac{\partial B}{\partial t} + \frac{\partial B}{\partial \theta}\frac{d\theta}{dt}$$

By fixing the datum of $\theta$ in the rotor, or field member of the alternator, $d\theta/dt$ is maintained at zero for the rotor and is equal to the actual speed for the stator, or armature member.

In the analogue, therefore, the procedure previously laid down remains unaltered for dealing with the rotor, but for the stator it is necessary to replace $\partial/\partial t$ by

$$\frac{\partial}{\partial t} + \frac{\partial}{\partial \theta}\frac{d\theta}{dt} = \frac{\partial}{\partial t} + \omega\frac{\partial}{\partial \theta}$$

If we examine eqns. (3) and (4), we notice that $\partial/\partial t$ occurs in eqn. (3) only, which becomes

$$C\left(\frac{\partial}{\partial t} + \omega\frac{\partial}{\partial \theta}\right)(V - v) = \text{div } \boldsymbol{I}$$

This has no simple counterpart in the analogue, though it might, with some complication, be applied to problems involving unbalanced loading, waveform distortion, etc. It is not proposed to pursue these matters here, but to consider only the case of balanced polyphase sinusoidal loading, and to make the not unusual approximation of ignoring stator-conductor resistance.

These assumptions lead to the following modified statements:

$$C = \infty$$
$$V = v$$
$$e = E$$

and $e$ is represented by

$$\frac{1}{n}\left(\frac{\partial V}{\partial t} + \omega\frac{\partial V}{\partial \theta}\right)$$

i.e.

$$\frac{1}{n}\frac{\partial V}{\partial t} + \frac{\omega}{n}V'$$
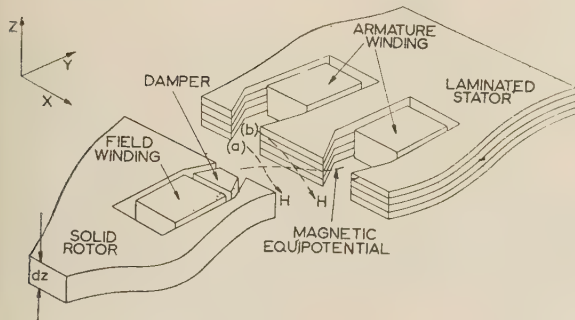


Fig. 1.—Volume element of part of alternator.
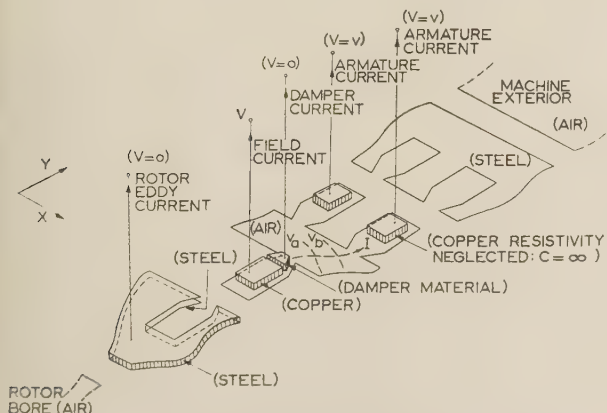


Fig. 2.—Exploded analogue corresponding to Fig. 1.

Machine running: axes fixed in rotor.

where $V'$ is the value of $V$ at the corresponding point 90° in advance round the stator periphery.

(The foregoing assumes that the rotor of the alternator is momentarily locked in some particular position. Any slight resulting error due to slot formation could, if desired, be eliminated by averaging the results of experiments made over a range of positions.)

The effect of the scheme described is to convert the study of the running synchronous alternator into that of the same machine at standstill but with special rules for computing quantities in the armature member.

Figs. 1 and 2 illustrate this particular case, as well as the essential features of the general theory.

## (5) PROSPECTIVE APPLICATIONS

### Stationary conductors: Axial symmetry.

Characteristics of transmission lines for power and communication purposes, aerial, underground and submarine.
Mutual impedance of earth-return circuits.
Sheath losses and screening effects.
Heavy-current conductor shapes and proximity effects.

### Stationary conductors: Cylindrical symmetry.

Characteristics of transformers, regulators, reactors, induction furnaces.
Effects of unbalance of windings and tappings.
Forces between conductors, transient and sustained.

### Rotating electromagnetic machines.

Characteristics of synchronous machines under steady and transient conditions, allowing for magnetic saturation and rotor eddy-currents.

## (6) REFERENCES

(1) PEIERLS, R. E.: *Nature*, 1947, **158**, p. 851.
(2) DIGGLE, H., and HARTILL, E. R.: 'Some Applications of the Electrolytic Tank to Engineering Design Problems', *Proceedings I.E.E.*, Paper No. 1627 M, February, 1954 (**101**, Part II, p. 349).
(3) 'Analogue Computer at Imperial College', *The Engineer*, 8th March, 1957, p. 376.

## (7) APPENDICES

### (7.1) Notes on Practical Realization

The paper was written with the object of establishing a theoretical principle, namely that the addition of a layer of distributed capacitance to the well-known conductive-sheet analogue will provide a great extension to the versatility of the latter in applications to electromagnetic problems. The practical aspects of the idea were regarded as a separate issue and have not been fully studied, but the broad indication is that the simple sheet and the electrolytic tank, although attractive at first glance, are not easily convertible to the more complex forms which are necessary.

The main difficulty arises through the relatively numerous electrodes required for current transference at boundaries. These unavoidably distort flow lines and gradients, with loss of accuracy. Furthermore, no satisfactory method has yet been found of making use of semi-conducting material, where this is required.

These troubles do not occur in the equivalent mesh network, which is likely, therefore, to be more adaptable in spite of its lower flexibility and relative complication. In this form the

technical problems which arise do not, in fact, differ from those of any other specialized kind of network analyser and hence do not stand in need of particular examination.

### (7.2) Simple Example

Two circular rings of square-section copper are disposed coaxially as shown in the dimensioned sketch (see Fig. 3).
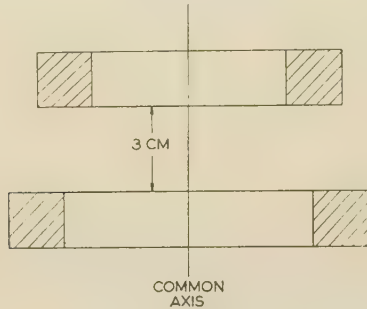


Fig. 3.—Cross-section of rings.
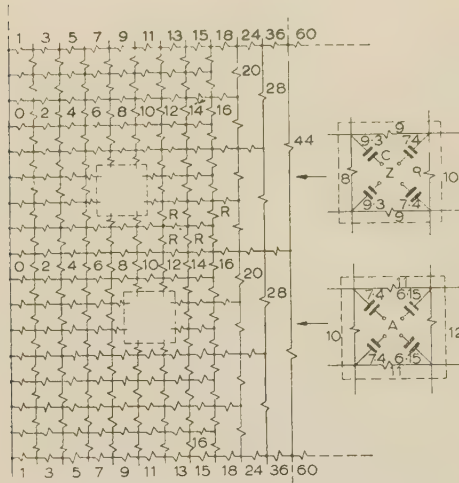Both rings are 2 cm square section.   One is 9 cm and the other is 11 cm mean diameter.



Fig. 4.—Analogue corresponding to Fig. 3.
Values of R are in kilohms.
Values of C are in microfarads.
Small meshes represent squares 1 cm × 1 cm.

A saw cut is made in the lower ring and 1 volt (r.m.s.) at 50 c/s is applied across the gap.  It is required to determine all the currents.

This is a case of cylindrical symmetry.  For copper, $\mu = 4\pi \times 10^{-7}$ and $\rho = 1\cdot7 \times 10^{-8}$, i.e. $\mu/\rho = 74$ and consequently $CR = 74$.  Convenient values (at radius 10 cm) are chosen as follows:

$$R = 1\,000 \text{ ohm}$$
$$C = 7\cdot4\,\mu\text{F/cm}^2$$

This sets          $m/n = 4\pi \times 10^{-10}$

The square-mesh network of Fig. 4 can now be constructed to represent a semi-infinite cross-section of the field of events.  For the sake of simplicity only a coarse mesh is used, but this could be subdivided locally to show fine detail where necessary, or enlarged in the less important regions as is done in Fig. 3.

At radius $0\cdot1$ m in the cross-section 1 volt per turn produces $10/2\pi$ volts/m, and $\int e\,dt = 10/(2\pi \times 100\pi)$ lagging by $90°$. Elsewhere, the gradient and its integral are inversely proportional to the radius.  At the terminals A of the analogue 50 c/s r.m.s. voltages are applied, having convenient values of, for example, 100 volts at a radius of 10 cm with suitably related values at other radii.  The terminals Z are to be maintained at zero voltage.

This gives          $n = 2\pi^2 \times 10^3$

and          $m = 8\pi^3 \times 10^{-7}$

Finally, the analogue currents are measured.  The actual currents will be the measured values multiplied by $10^7/8\pi^3$ and retarded in phase by $90°$.

Only the steady state has been considered, but any transient condition can equally well be studied.  For example, the consequences of switching on the alternating voltage for a few cycles and afterwards switching off would be correctly represented provided that the voltage applied to the analogue truly followed the time integral of the actual voltage and that measurements were sufficiently prolonged to cover the subsidence of transient effects.

If the original voltage has a substantial unidirectional component, practical considerations compel the use of the alternative step-by-step technique in the analogue.

One millisecond is chosen as the unit of time, and each capacitor is replaced by a resistor of $1/C$ kilohm ($C$ is in microfarads).

Take the simple case where $e$ is a 1-volt step-function.   $V$ in successive time intervals is $n/2, 3n/2, 5n/2 \ldots$, with equal increments, $\delta V$, of $n$ volts.

The first $\delta V$'s are applied to the terminals A with the terminals Z held at zero voltage.   Measurements are made of all currents and of the voltages of the network, $v$, where currents enter or leave it.  These voltages become the bases from which the next set of $\delta V$'s are reckoned, and the new total voltages produce in their turn a second set of currents.   This process is continued until the currents reach final values such that div $I(\delta t)/C = \delta V$ when the currents via terminals A become independent of the magnetic field and those via terminals Z subside to zero.  (In this final state $v$ has nothing to do with voltage, but is a measure of $\Phi$.)

### (7.2.1.) Remarks.

It is of interest that, if the two rings in this example were made of steel, the corresponding network components would have suitably modified values and, in particular, certain resistors would be replaced by non-linear elements having characteristics matched as closely as possible to the magnetic saturation curve of the steel.  This would incidentally restrict the choice of scale factors by virtually fixing the impedance level of the analogue.

The mechanical force (in newtons per cubic metre) on a current-carrying conductor in any steady or transient condition may be obtained directly from the analogue, since the force $J \times B = J$. grad $\Phi$ is represented by (div $I$) (grad $v$)/$mn$ in the direction of $I$.

Ⓒ

# THE MATHEMATICAL THEORY OF VIBRATORY ANGULAR TACHOMETERS

## By K. FEARNSIDE, M.A., Associate Member, and P. A. N. BRIGGS, B.A.

### SUMMARY

A mathematical theory for a vibratory rate-of-turn measuring device is developed in order to bring out the more important characteristics.

By using properties of Mathieu's equation it is shown how performance depends on the parameters of the system, particularly the resonant frequency and damping factor of the torsion mechanism. These results are compared with those obtained from the more simplified theory.

## (1) INTRODUCTION

In the evolution of aircraft control systems the rate gyroscope has been developed to a state where further improvement along the present lines is possible only with considerable mechanical elaboration. The manufacture of present rate gyroscopes is comparatively expensive and requires highly skilled labour. The use of these instruments in aircraft calls for very accurate measurement of space rates, and one of their more serious drawbacks is the presence of a datum error, which has an effect similar to the application of a steady rate of turn to the platform on which the instrument is mounted. In general, this error is temperature-sensitive, and in cases where the instrument is required for service over a wide range of temperature the reduction of datum error is one of the most difficult design problems.

The principle of the gyroscope depends on the provision of a large fixed angular momentum so that orientation of the gyroscope can be disturbed only by application to the instrument of considerable torques. Such torques do result from mechanical imperfections and are responsible for the datum errors. The possibility of their elimination, by using a moment of inertia having a component of alternating value about the axis of reference, has been previously investigated by a number of workers. An early instrument, based on the halteres of *Diptera*,[1] was developed by F. W. Meredith and is shown in Fig. 1. The instrument possessed remarkable sensitivity, but in practice it proved very difficult to define the plane of vibration of the tine and the long-term stability was considered to be unsatisfactory.

The advent of the guided weapon raised additional objections to the gyroscope. Its cost, as a percentage of the cost of an aircraft, was exceedingly small, and its life bore reasonable relation to the life of the vehicle in which it was carried. Considered as a component of the guided weapon, however, these relations were altogether altered, and the need for developing a space-rate measuring instrument, not necessarily so long-lived but capable of being produced in quantity by less highly skilled labour, became extremely pressing. Earlier investigations were therefore reviewed, and the theory of such instruments was examined in detail.

A second instrument of the same general type as that shown in Fig. 1, in which the plane of vibration is more accurately defined, is the double-tined tuning-fork type, shown in Fig. 2. This has been very thoroughly described,[2-4] but, in order to reduce the system equation for this type of instrument to one of simple harmonic motion, a number of simplifying assumptions
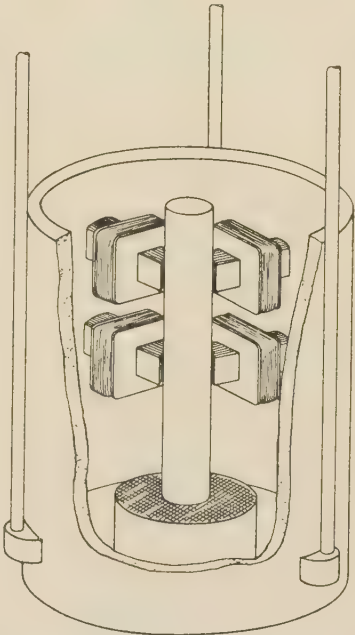


Fig. 1.—Experimental single-tine vibratory angular tachometer.

are made. The present paper demonstrates that the system can be better defined by Mathieu's equation, if more cautious simplifying assumptions are made.

Expressions based on the solutions of Mathieu's equation are derived for the response of the instrument, and from these it is shown how response and stability depend on the parameters of the system. The results suggest that some amendments must be made to the conclusions derived from the simplified methods of References 2–4.

## (2) DESCRIPTION OF THE 'TUNING FORK' INSTRUMENT

As described in References 2 and 3, the tuning-fork type of instrument consists (Fig. 2) of a 'tuning fork' mounted on a torsion bar, the axes of the two coinciding. The fork is electromagnetically maintained in a vibration of constant amplitude so that, in the absence of rotation, the fork prongs, or tines, vibrate radially with respect to the axis.

When the torsion bar is rotated, a torque is applied to the fork, which starts rotational oscillations about the instantaneous mean position, the fundamental frequency of these oscillations being the same as the driven frequency of the fork radial vibrations. Their amplitude depends on the angular velocity of the turning motion applied to the base.

An electromagnetic pick-off is used to measure the rate of change of the angle of the torsion-bar twist. The signal is in the form of a modulated carrier, and is passed through a demodulator, using the fork driving current as a reference, the output indicating the amplitude and sense of the rotational velocity.
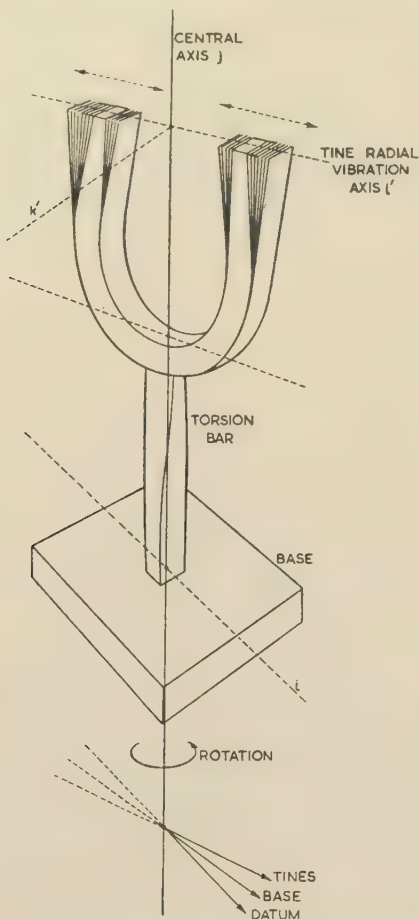
Fig. 2.—Double-tined vibratory angular tachometer.

On the basis of the simplified theory,[2,3] a number of advantages over conventional rate-of-turn instruments have been claimed, including the following:

(a) Robustness and probable lengthy life without any need of maintenance, owing to the solid construction of the fork and absence of bearings.
(b) Rapid response and wide range of rates measurable with good linearity.
(c) Sensitivity to motion about one axis only, with negligible acceleration effects.

A number of design requirements for good response and high output are stipulated:

(i) The fork motion must approximate to a pure sine wave.
(ii) Damping must be applied in order to obtain a suitable time-constant and bandwidth.
(iii) For high efficiency, the modulated inertia must be designed to be as high as possible.
(iv) Highest output will be obtained by operating with the resonant frequency of the torsion mechanism equal to the driven frequency of the fork.

All these statements are considered in the following discussion and some amendments are shown to be necessary to certain of them.

## (3) VECTOR NOTATION FOR THE SYSTEM

Because of the nature of the problem it is advantageous to use vector notation in forming the equations of the system, and the axes used are as shown in Fig. 3.

$i'$, $j$, $k'$ are unit vectors parallel to the principal axes of the system, where $i'$ is in the plane of vibration of the tines; $j$ is
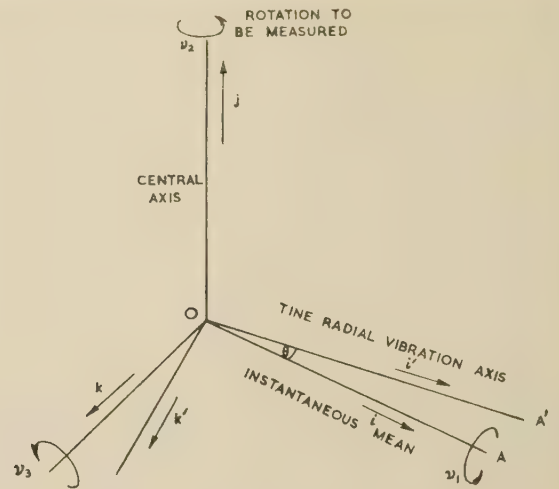


Fig. 3.—Axes for vector notation.

along the joint axis of the fork and torsion bar; and $k'$ completes a right-handed set.

$i$, $k$ are the vectors corresponding to $i'$, $k'$ if the torsion bar were in an unstrained state.

Thus the vectors $i$, $j$, $k$ may be called the axes of the instrument, and $i'$, $j$, $k'$ the axes of the tine motion.

The inertia tensor about the axes of the tines may be taken as

$$I = Ai'i' + (B_0 + B_1 \sin \omega t)jj + (C_0 + C_1 \sin \omega t)k'k' \quad . \quad (1)$$

where $\omega$ is the natural frequency of the tines.

The applied rate of turn is taken to be

$$\nu = \nu_1 i + \nu_2 j + \nu_3 k \quad . \quad . \quad . \quad . \quad (2)$$

about the instantaneous instrument axes, where $\nu_2$ is the angular velocity about axis $j$ to be measured. Hence the angular velocity of the tines about the same axes is

$$\nu' = \nu_1 i + (\nu_2 + \zeta)j + \nu_3 k \quad . \quad . \quad . \quad (3)$$

where $\zeta = d\theta/dt$ is the radial angular velocity of the tines, i.e. line OA′ of Fig. 3, within the instrument.

If OA′ moves through a small angle $\theta$, the following approximate relations hold:

$$\left. \begin{array}{l} i.i' = k.k' \simeq 1 \\ i.k' = -i'.k \simeq \theta \\ i \times i' = k \times k' \simeq \theta j \\ i \times k' = i' \times k \simeq -j \end{array} \right\} \quad . \quad . \quad . \quad (4)$$

### (3.1) The Vector Equations of the System

From the above, the angular momentum of the tines is given by

$$H = I . \nu' \quad . \quad . \quad . \quad . \quad . \quad . \quad (5)$$
$$= A(\nu_1 - \theta\nu_3)i' + (B_0 + B_1 \sin \omega t)(\nu_2 + \zeta)j$$
$$+ (C_0 + C_1 \sin \omega t)(\nu_3 + \theta\nu_1)k' \quad . \quad (6)$$

The rate of change of angular momentum is the time differential of $H$ in relation to a fixed space datum.

$$\Gamma = \frac{dH}{dt} \quad . \quad . \quad . \quad . \quad . \quad (7)$$

$$= \frac{\partial H}{\partial t} + \nu' \times H \quad . \quad . \quad . \quad . \quad (8)$$

where $\partial/\partial t$ refers to $i'$, $j$, $k'$ as fixed.

Thus

$$\Gamma = A(\dot{\nu}_1 - \theta\dot{\nu}_3 - \zeta\nu_3)i'$$
$$+ [(B_0 + B_1 \sin \omega t)(\dot{\nu}_2 + \dot{\zeta}) + B_1 \cos \omega t \, \omega(\nu_2 + \zeta)]j$$
$$+ [(C_0 + C_1 \sin \omega t)(\dot{\nu}_3 + \theta\dot{\nu}_1 + \zeta\nu_1) + C_1 \cos \omega t \, \omega(\nu_3 + \theta\nu_1)]k'$$
$$+ A(\nu_1 - \theta\nu_3)\nu_1\theta j - A(\nu_1 - \theta\nu_3)(\nu_2 + \zeta)k' + A(\nu_1 - \theta\nu_3)\nu_3 j$$
$$+ (B_0 + B_1 \sin \omega t)(\nu_2 + \zeta)\nu_1 k - (B_0 + B_1 \sin \omega t)(\nu_2 + \zeta)\nu_3 i$$
$$- (C_0 + C_1 \sin \omega t)(\nu_3 + \theta\nu_1)\nu_1 j$$
$$+ (C_0 + C_1 \sin \omega t)(\nu_3 + \theta\nu_1)(\nu_2 + \zeta)i'$$
$$+ (C_0 + C_1 \sin \omega t)(\nu_3 + \theta\nu_1)\nu_3\theta j \qquad . \quad . \quad . \quad . \quad . \quad (9)$$

### (3.2) The Reduced Equation

The couple about the central axis of the instrument is

$$\Gamma \cdot j = (B_0 + B_1 \sin \omega t)(\dot{\nu}_2 + \dot{\zeta}) + B_1 \cos \omega t \, \omega(\nu_2 + \zeta)$$
$$+ (A - C_0 - C_1 \sin \omega t)(\nu_1 - \theta\nu_3)(\nu_3 + \theta\nu_1) \quad . \quad (10)$$

The couple exerted by the torsion bar is assumed proportional to $\theta$. Including a torsion-damping term, the total couple about the axis is

$$R\theta + \epsilon\zeta + (B_0 + B_1 \sin \omega t)(\dot{\nu}_2 + \dot{\zeta}) + B_1 \cos \omega t \, \omega(\nu_2 + \zeta)$$
$$+ (A - C_0 - C_1 \sin \omega t)(\nu_1 - \theta\nu_3)(\nu_3 + \theta\nu_1) = 0 \quad . \quad (11)$$

This is zero since there is no external force.

The term $(A - C_0 - C_1 \sin \omega t)(\nu_1 - \theta\nu_3)(\nu_3 + \theta\nu_1) \simeq (A - C_0)\nu_1\nu_3$, which depends on motion about axes other than the one about which measurements are required, provides a limit to the accuracy of the instrument, since it will produce an output error of unknown, though limited, magnitude. This term is not found in the results obtained by the non-vector methods used in References 2–4. If this last term of eqn. (11) is ignored, there remains, upon differentiation once,

$$R\zeta + \epsilon\dot{\zeta} + (B_0 + B_1 \sin \omega t)(\ddot{\nu}_2 + \ddot{\zeta}) + 2B_1 \cos \omega t \, \omega(\dot{\nu}_2 + \dot{\zeta})$$
$$- \omega^2 B_1 \sin \omega t \, (\nu_2 + \zeta) = 0 \quad . \quad (12)$$

In the remaining discussion the subscript 2 will be dropped, since there is no ambiguity, and the normal symbol $I$ will be used for moment of inertia about the instrument axis.

The equation of the system is therefore

$$(I_0 + I_1 \sin \omega t)\ddot{\zeta} + (\epsilon + 2\omega I_1 \cos \omega t)\dot{\zeta} + (R - \omega^2 I_1 \sin \omega t)\zeta$$
$$= - (I_0 + I_1 \sin \omega t)\ddot{\nu} - 2\omega I_1 \cos \omega t \, \dot{\nu} + \omega^2 I_1 \sin \omega t \, \nu \quad (13)$$

and this is used as the basis for both the simplified theory of the instrument and the general theory presented here.

### (4) THE SIMPLIFIED THEORY

The methods used in References 1–3 are equivalent to taking $I_1/I_0$, $\omega I_1/\epsilon$ and $\omega^2 I_1/R$ all very much less than unity and disregarding the effects of derivatives of the applied angular rate. Eqn. (13) is then reduced to

$$I_0 \frac{d^2\zeta}{dt^2} + \epsilon \frac{d\zeta}{dt} + R\zeta = + \omega^2 I_1 \sin \omega t \, \nu \quad . \quad . \quad (14)$$

Because of a positive damping factor $\epsilon$, the complementary function solutions are damped out with increase of time, and only the particular integral of eqn. (14) is of importance in the response. For constant rate of turn, $\nu = \nu_0$, the response will be

$$\zeta \simeq \frac{- \nu_0\omega^2 I_1}{[(R - \omega^2 I_0)^2 + \epsilon^2\omega^2]^{1/2}} \cos (\omega t - \alpha) \quad . \quad (15)$$

where

$$\tan \alpha = \frac{R - \omega^2 I_0}{\epsilon\omega}$$

The response will be a maximum when the natural frequency of the torsion mechanism equals the driven frequency of the tines, i.e. when

$$R = \omega^2 I_0 \quad . \quad . \quad . \quad . \quad . \quad (16)$$

and this leads to

$$\zeta = - \frac{\nu_0\omega I_1}{\epsilon} \cos \omega t \, . \quad . \quad . \quad . \quad (17)$$

which is exactly 90° out of phase with the sinusoidal motion of the tines.

References 2–4 particularly consider the case where the rate of turn to be measured may be broken down into sinusoidal components, e.g. weathercocking effects.

Putting
$$\nu = \nu_0 \cos \eta t \, . \quad . \quad . \quad . \quad . \quad (18)$$

where it is assumed that $\eta \ll \omega$, the right-hand side of eqn. (14) becomes

$$f(t) = + \omega^2 I_1 \nu_0 \sin \omega t \cos \eta t$$
$$= + \frac{\omega^2 I_1 \nu_0}{2}[\sin (\omega + \eta)t + \sin (\omega - \eta)t] \quad . \quad (19)$$

The particular integral of eqn. (18) with this right-hand side is

$$\zeta = C_1 \cos [(\omega + \eta)t + \alpha_1] + C_2 \cos [(\omega - \eta)t + \alpha_2] \quad . \quad (20)$$

where
$$C_1 = \frac{- \nu_0\omega^2 I_1}{2[(R - (\omega + \eta)^2 I_0)^2 + \epsilon^2(\omega + \eta)^2]^{1/2}}$$

$$\tan \alpha_1 = \frac{R - (\omega + \eta)^2 I_0}{\epsilon(\omega + \eta)}$$

and $C_2$ and $\alpha_2$ are similarly defined with $-\eta$ for $+\eta$.

If the tine and torsion frequencies are equal, then, since $\eta/\omega$ is very small, $C_1 \simeq C_2$ and $\alpha_1 \simeq -\alpha_2$, and the equation reduces to

$$\zeta = \frac{- \nu_0\omega I_1}{2(4I_0^2\eta^2 + \epsilon^2)^{1/2}}\{\cos [(\omega + \eta)t + \alpha] + \cos [(\omega - \eta)t - \alpha]\}$$
$$. \quad . \quad . \quad . \quad (21)$$
$$= \frac{- \nu_0\omega I_1}{(4I_0^2\eta^2 + \epsilon^2)^{1/2}} \cos \omega t \cos (\eta t + \alpha) \quad . \quad . \quad . \quad (22)$$

where $\tan \alpha = - \frac{2I_0\eta}{\epsilon}$.

It is noted in References 2, 3 and 4 that the response as given by eqn. (21) is of the suppressed-carrier type of signal.

In order to compare with results which will be obtained from the more general theory, it is necessary to put those of this Section in terms of the special parameters, $a$ (corresponding to the ratio of frequencies), $q$ (corresponding to ratio of inertias), and $\kappa_0$ (corresponding to damping), these being defined as

$$a = \frac{4R}{\omega^2 I_0} \quad . \quad . \quad . \quad . \quad . \quad (23)$$

$$q = \frac{2RI_1}{\omega^2 I_0^2} \quad . \quad . \quad . \quad . \quad . \quad (24)$$

$$\kappa_0 = \frac{\epsilon}{(RI_0)^{1/2}} \quad . \quad . \quad . \quad . \quad . \quad (25)$$

Eqn. (15) can then be written

$$\frac{\zeta}{\nu_0} = \frac{16\frac{1}{\sqrt{a}}q\kappa_0 \cos \omega t - \frac{8q}{a}(a - 4) \sin \omega t}{(a - 4)^2 + 4\kappa_0^2 a} \quad . \quad . \quad (26)$$
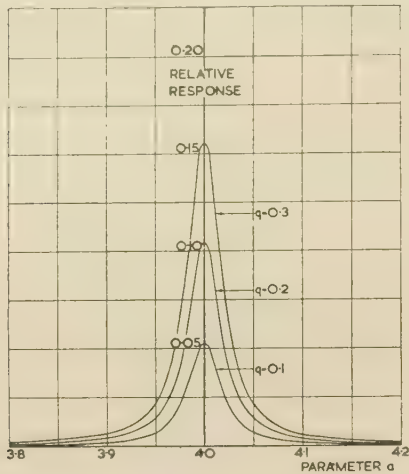
**Fig. 4.**—Response curve: simplified theory.
Quadrature component $\kappa_0 = 0 \cdot 01$.
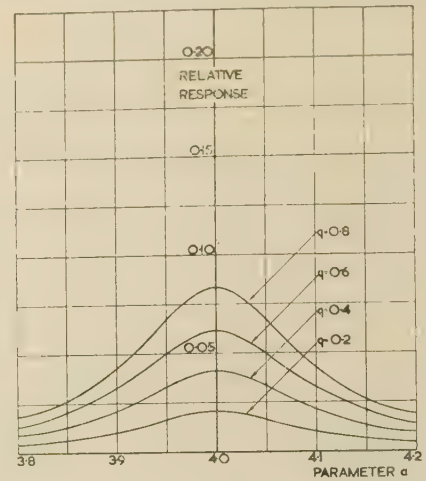


**Fig. 6.**—Response curve: simplified theory.
Quadrature component $\kappa_0 = 0 \cdot 05$.
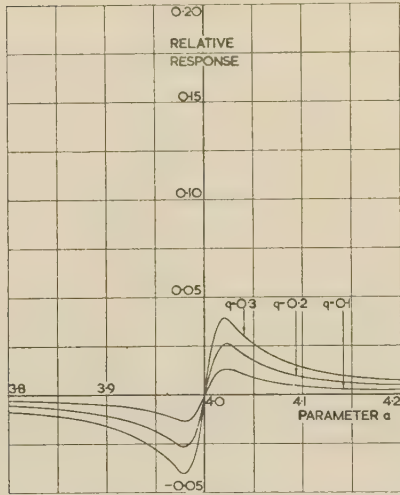


**Fig. 5.**—Response curve: simplified theory.
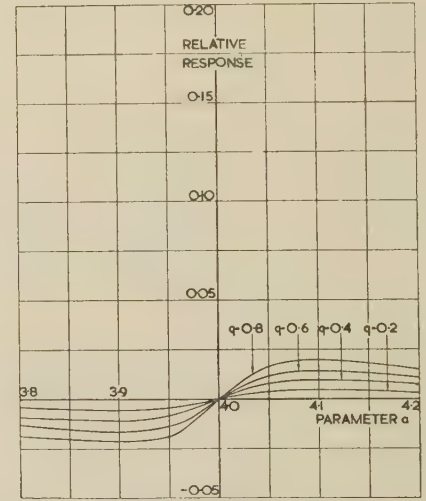In-phase component $\kappa_0 = 0 \cdot 01$.



**Fig. 7.**—Response curve: simplified theory.
In-phase component $\kappa_0 = 0 \cdot 05$.

Graphs of the two components (Figs. 4–7) show the variation of the amplitude of response with these parameters. All the graphs are linear in $q$, Figs. 4 and 6 indicating a maximum quadrature response at $a = 4$, i.e. with the tine and the torsion-system natural frequencies equal. From Figs. 5 and 7 the in-phase component is zero at $a = 4$ and has one peak on each side of zero. These peaks are considerably smaller than those of the quadrature component.

## (5) GENERAL THEORY OF TUNING-FORK-TYPE ANGULAR TACHOMETERS

The theory developed in the present paper differs from that described in Section 4 in retaining the first-order small terms omitted when the system is viewed as simple harmonic motion. Eqn. (13) may be written as

$$\frac{d^2\zeta}{dt^2} + \frac{\epsilon + 2\omega I_1 \cos \omega t}{I_0 + I_1 \sin \omega t} \frac{d\zeta}{dt} + \frac{R - \omega^2 I_1 \sin \omega t}{I_0 + I_1 \sin \omega t} \zeta$$

$$- \frac{d^2\nu}{dt^2} - \frac{2\omega I_1 \cos \omega t}{I_0 + I_1 \sin \omega t} \frac{d\nu}{dt} + \frac{\omega^2 I_1 \sin \omega t}{I_0 + I_1 \sin \omega t} \nu \quad . \quad (27)$$

The complementary functions for $\zeta$ are found by equating the left-hand side of eqn. (27) to zero.

Assuming that $I_1/I_0$ and $\epsilon/I_0$ are sufficiently small for second-order terms in them to be neglected, expanding the coefficients and retaining only first-order terms gives

$$\frac{d^2\zeta}{dt^2} + \frac{\epsilon + 2\omega I_1 \cos \omega t}{I_0} \frac{d\zeta}{dt}$$

$$+ \left(\frac{R - \omega^2 I_1 \sin \omega t}{I_0} - \frac{RI_1 \sin \omega t}{I_0^2}\right)\zeta = 0 \quad . \quad (28)$$

This equation can be changed to one of Mathieu type by using the substitution

$$\zeta = u \exp\left(-\frac{\epsilon t + 2I_1 \sin \omega t}{2I_0}\right) \quad . \quad . \quad . \quad (29)$$

Again retaining only first-order terms in $I_1/I_0$ and $\epsilon/I_0$, eqn. (28) becomes

$$\frac{d^2u}{dt^2} + \left(\frac{R}{I_0} - \frac{RI_1}{I_0^2} \sin \omega t\right)u = 0 \quad . \quad . \quad . \quad (30)$$
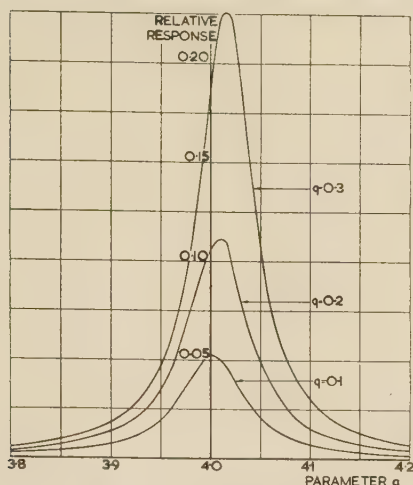
**Fig. 8.**—Response curve.
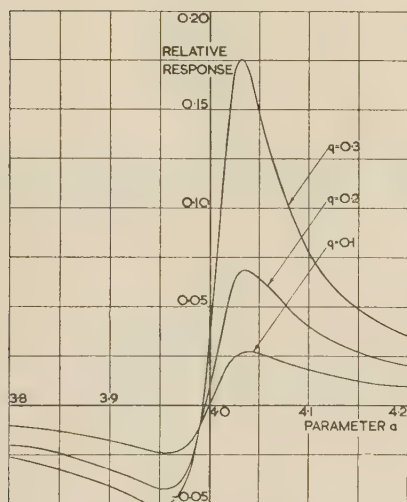
Quadrature component $\kappa_0 = 0 \cdot 01$.



**Fig. 10.**—Response curve.

Quadrature component $\kappa_0 = 0 \cdot 05$.
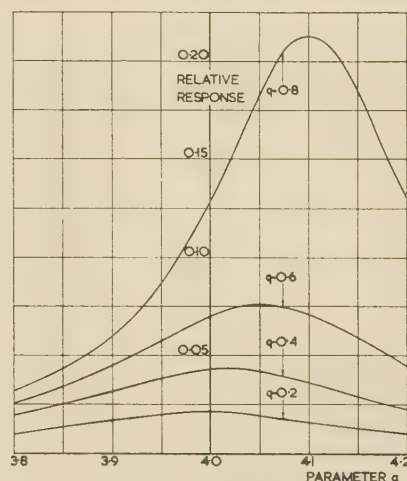


**Fig. 9.**—Response curve.

In-phase component $\kappa_0 = 0 \cdot 01$.
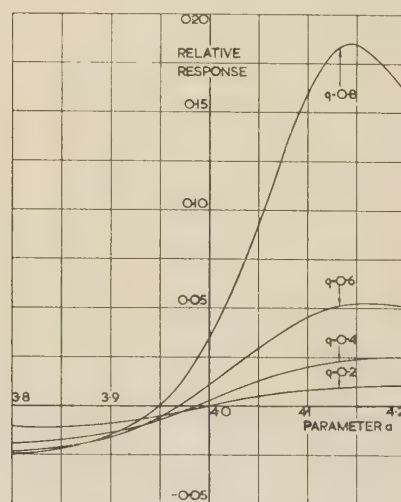


**Fig. 11.**—Response curve.

In-phase component $\kappa_0 = 0 \cdot 05$.

On changing the independent variable by the relation

$$2y = \frac{\pi}{2} - \omega t \quad . \quad . \quad . \quad . \quad . \quad (31)$$

and defining parameters $a$ and $q$ as in eqns. (23) and (24), eqn. (30) can be written

$$\frac{d^2u}{dy^2} + (a - 2q \cos 2y)u = 0 . \quad . \quad . \quad . \quad (32)$$

which is the standard form of Mathieu's equation.[5]

Eqn. (27) can then be written as

$$\frac{d^2u}{dy^2} + (a - 2q \cos 2y)u = f(y) \quad . \quad . \quad . \quad (33)$$

where $\quad f(y) = \exp\left[\frac{\epsilon}{\omega I_0}\left(\frac{\pi}{4} - y\right) + \frac{I_1}{I_0}\cos 2y\right]$

$$\times \left(-\frac{d^2v}{dy^2} + \frac{4I_1 \sin 2y}{I_0 + I_1 \cos 2y}\frac{dv}{dy} + \frac{4I \cos 2y}{I_0 + I_1 \cos 2y}\right) \quad (34)$$

If $u_1$ and $u_2$ are two independent solutions of eqn. (32), the particular integral of eqn. (33), since the coefficient of $du/dy$ is zero, is found by the method of parameters to be

$$u = -\frac{1}{W_0}\left[u_1(y)\int^y u_2(x)f(x)dx - u_2(y)\int^y u_1(x)f(x)dx\right] . \quad (35)$$

where

$$W_0 = \begin{vmatrix} u_1 & u_2 \\ \dfrac{du_1}{dy} & \dfrac{du_2}{dy} \end{vmatrix}_{y=0} \quad . \quad . \quad . \quad . \quad (36)$$

The appropriate solutions of Mathieu's equation for use in the above formula are considered in Section 9.1. It will be assumed, as in the simplified theory given in Section 4, that the driven frequency $\omega$ of the fork and the resonant frequency $\omega_T$ of the torsion mechanism are nearly equal.

Hence

$$\frac{R}{I_0} = \omega_T^2 \simeq \omega^2 . \quad . \quad . \quad . \quad . \quad (37)$$

so that

$$a = \frac{4R}{\omega^2 I_0} \simeq 4 . \quad . \quad . \quad . \quad . \quad (38)$$

and
$$q = \frac{2RI_1}{\omega^2 I_0^2} \simeq 2\frac{I_1}{I_0} \quad \ldots \quad \ldots \quad (39)$$

The ratio $I_1/I_0$ may be considered such that $q$ is sufficiently small for the solutions of Mathieu's equation in the region of $a = 4$ to be written

$$u_1 = \varepsilon^{\mu y} \sin(2y - \sigma) \quad \ldots \quad \ldots \quad (40)$$

$$u_2 = \varepsilon^{-\mu y} \sin(2y + \sigma) \quad \ldots \quad \ldots \quad (41)$$

where, from Section 9.1, the parameters $\mu$ and $\sigma$ are defined by

$$\mu = \frac{q^2}{16} \sin 2\sigma \, . \quad \ldots \quad \ldots \quad (42)$$

and
$$a = 4 + \frac{q^2}{12}(2 - 3\cos 2\sigma) \quad \ldots \quad \ldots \quad (43)$$

The output is taken to be the quantity $\zeta$, the angular velocity of the torsion mechanism. In terms of the solution of eqn. (34), this is

$$\zeta = u \exp\left(-\frac{\epsilon t + 2I_1 \sin \omega t}{2I_0}\right) \quad \ldots \quad \ldots \quad (44)$$

Using eqn. (31) and making

$$\kappa = \frac{\epsilon}{\omega I_0} \quad \ldots \quad \ldots \quad (45)$$

the output is

$$\zeta = u \exp -\left[\kappa\left(\frac{\pi}{4} - y\right) + \frac{I_1}{I_0}\cos 2y\right] \quad \ldots \quad (46)$$

The transients will include the exponential factors $\varepsilon^{(\kappa + \mu)y}$ and $\varepsilon^{(\kappa - \mu)y}$. Since $y$ decreases with time, the transients will be damped out if

$$\mathcal{R}(\kappa - \mu) > 0 \text{ and } \mathcal{R}(\kappa + \mu) > 0 . \quad \ldots \quad (47)$$

The response will therefore depend on the particular integral of eqn. (33):

$$u = -\frac{1}{W_0}\left[\varepsilon^{\mu y}\sin(2y - \sigma)\int^y \varepsilon^{-\mu x}\sin(2x + \sigma)f(x)dx\right.$$

$$\left. - \varepsilon^{-\mu y}\sin(2y + \sigma)\int^y \varepsilon^{\mu x}\sin(2x - \sigma)f(x)dx\right] \quad . \quad (48)$$

where $W_0 =$

$$\begin{vmatrix} \varepsilon^{\mu y}\sin(2y - \sigma) & \varepsilon^{-\mu y}\sin(2y + \sigma) \\ \varepsilon^{\mu y}[\mu\sin(2y - \sigma) & \varepsilon^{-\mu y}[-\mu\sin(2y + \sigma) \\ \quad + 2\cos(2y - \sigma)] & \quad + 2\cos(2y + \sigma)] \end{vmatrix}_{y=0}$$

$$= -2\sin\sigma(2\cos\sigma - \mu\sin\sigma) \quad \ldots \quad \ldots \quad (49)$$

The second term will be small, so that $W_0 \simeq -2\sin 2\sigma$.
In Section 9.2 eqn. (48) is integrated and $u$ becomes

$$u = b\varepsilon^{\kappa\left(\frac{\pi}{4} - y\right)}\left[-\frac{\kappa}{\kappa^2 - \mu^2}\sin 2y - \frac{\mu\tan\sigma}{\kappa^2 - \mu^2}\cos 2y\right]\nu$$

$$+ b\varepsilon^{\kappa\left(\frac{\pi}{4} - y\right)}\begin{bmatrix}\left[\dfrac{\mu\cot\sigma}{\kappa^2 - \mu^2} - \dfrac{(\kappa^2 + \mu^2)}{(\kappa^2 - u^2)^2}\right]\sin 2y \\ + \left[\dfrac{\kappa}{\kappa^2 - \mu^2} - \dfrac{2\kappa\mu\tan\sigma}{(\kappa^2 - \mu^2)^2}\right]\cos 2y\end{bmatrix}\frac{d\nu}{dy} \quad . \quad (50)$$

and terms in higher-order differentials of $\nu$, where $\kappa = \epsilon/\omega I$ and $b = I_1/I_0$.

Thus the expression for $\zeta$ in terms of $t$ becomes, on using eqns. (29) and (31),

$$\zeta = -\nu\frac{I_1}{I_0}\frac{\kappa\cos\omega t + \mu\tan\sigma\sin\omega t}{\kappa^2 - \mu^2}\exp\left(-\frac{I_1}{I_0}\sin\omega t\right) \quad . \quad (51)$$

together with the terms which are much smaller in magnitude depending on the successive derivatives of $\nu$.

The largest of these is

$$-\frac{2}{\omega}\frac{d\nu}{dt}\frac{I_1}{I_0}\frac{[(\kappa^2 - \mu^2)\mu\cot\sigma - (\kappa^2 + \mu^2)]\cos\omega t + [(\kappa^2 - \mu^2)\kappa - 2\kappa\mu\tan\sigma]\sin\omega t}{(\kappa^2 - \mu^2)^2}\exp\left(-\frac{I_1}{I_0}\sin\omega t\right) \quad . \quad (52)$$

If the operating frequency $\omega$ is sufficiently high this may be neglected in comparison with the first term.

Thus the response is proportional to the rate of turn. This response can be split into two parts, in phase and out of phase with the motion of the fork.

### (5.1) Components of Response

Disregarding the term $\exp\left[-(I_1/I_0)\sin\omega t\right]$, which impresses a slight periodic variation, the amplitudes of the two components of $\zeta$ in eqn. (51) are:

*In quadrature to the tine motion.*

$$A = \nu\frac{I_1}{I_0}\frac{\kappa}{\kappa^2 - \mu^2} \quad \ldots \quad \ldots \quad (53)$$

*In phase with the tine motion.*

$$B = \nu\frac{I_1}{I_0}\frac{\mu\tan\sigma}{\kappa^2 - \mu^2} \quad \ldots \quad \ldots \quad (54)$$

Let
$$h = a - 4 \, . \quad \ldots \quad \ldots \quad (55)$$

Then
$$h \simeq \frac{2 - 3\cos 2\sigma}{12}q^2$$

or, putting $\sigma$ in terms of $q$ and $h$,

$$\cos 2\sigma = \frac{2q^2 - 12h}{3q^2} \quad \ldots \quad \ldots \quad (56)$$

From eqns. (42) and (56),

$$\mu^2 = \frac{q^4 \sin^2 2\sigma}{256}$$

$$= \frac{(5q^2 - 12h)(q^2 + 12h)}{2\,304} \quad \ldots \quad \ldots \quad (57)$$

Further,
$$\mu\tan\sigma = \frac{q^2 \sin^2 \sigma}{8}$$

$$= \frac{q^2 + 12h}{48} \, . \quad \ldots \quad \ldots \quad (58)$$

Also $\kappa$ can be related to the parameter $\kappa_0$ defined by eqn. (25):

$$\kappa = \frac{\epsilon}{\omega I_0}$$

$$= \frac{\epsilon}{(RI_0)^{1/2}}\left(\frac{R}{\omega^2 I_0}\right)^{1/2}$$

$$= \kappa_0\frac{a^{1/2}}{2} \, . \quad \ldots \quad \ldots \quad (59)$$

The ratio of inertias in terms of $a$ and $q$ is

$$\frac{I_1}{I_0} = 2\frac{2RI_1}{\omega^2 I_0^2} \bigg/ \frac{4R}{\omega^2 I_0}$$

$$= \frac{2q}{a} \quad . \quad . \quad . \quad . \quad . \quad . \quad . \quad (60)$$

Using these relations the components of the response can be written:

*Quadrature response.*

$$\frac{A}{} = \frac{2q}{a}\kappa_0\frac{a^{1/2}}{2}\frac{1}{\dfrac{\kappa_0^2 a}{4} - \dfrac{(5q^2 - 12h)(q^2 + 12h)}{2\,304}}$$

$$= \frac{2\,304\kappa_0 q}{(4 + h)^{1/2}(2\,304\kappa_0^2 - 5q^4 + (576\kappa_0^2 - 48q^2)h + 144h^2)} \cdot (61)$$

*In-phase response.*

$$\frac{B}{} = \frac{2q}{a}\frac{q^2 + 12h}{48}\frac{1}{\dfrac{\kappa_0^2 a}{4} - \dfrac{(5q^2 - 12h)(q^2 + 12h)}{2\,304}}$$

$$= \frac{96q(q^2 + 12h)}{(4 + h)(2\,304\kappa_0^2 - 5q^4 + (576\kappa_0^2 - 48q^2)h + 144h^2)} \cdot (62)$$

Graphs of eqns. (61) and (62), as response against parameter $a$, have been drawn in Figs. 8–11 for the cases of

$$\kappa_0 = 0\cdot01, \; q = 0\cdot1, \; 0\cdot2 \text{ and } 0\cdot3$$

and

$$\kappa_0 = 0\cdot05, \; q = 0\cdot2, \; 0\cdot4, \; 0\cdot6 \text{ and } 0\cdot8$$

with parameter $a$ varying between $3\cdot8$ and $4\cdot2$ (cf. Figs. 4–7). The behaviours of the quadrature (Figs. 8 and 10) and the in-phase (Figs. 9 and 11) components to variations in $a$ and $q$ differ from the behaviours of these components (shown in Figs. 4–7) obtained from the simplified theory. It may be noted, in particular, that in no case is the maximum quadrature response exactly at $a = 4$, corresponding to the fork and torsion frequencies being equal, neither is the in-phase component of the response zero for this value of $a$.
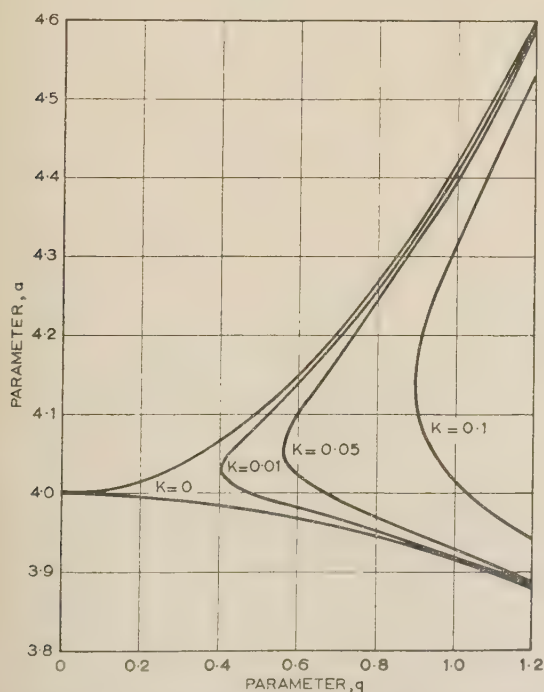
The deviations from the simplified system become much greater as $q$ is increased. The graphs are not linear with $q$, the maximum response becomes increasingly large as $q$ increases, and, in particular, the known stability conditions for solutions of Mathieu's equation (see Reference 5 and Figs. 12 and 13)
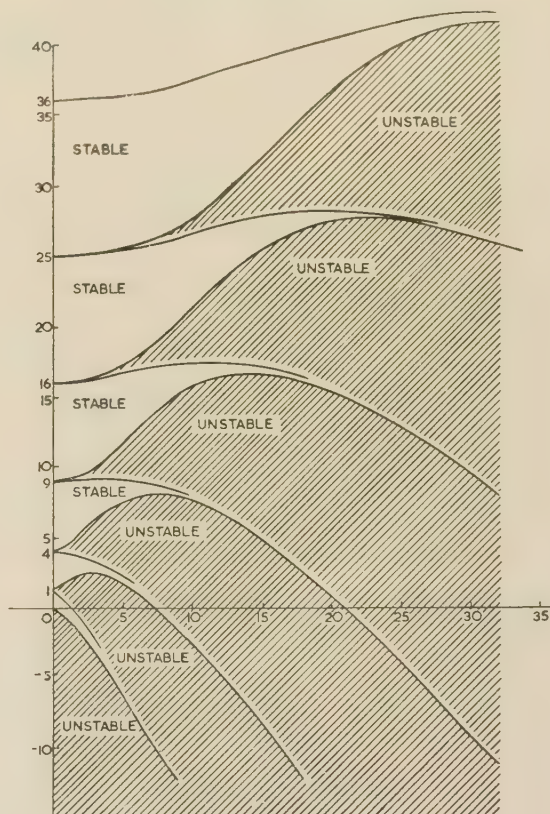


Fig. 13.—Stable and unstable regions for solutions of Mathieu's equation.

predict instability (infinite response), which will occur if $q$ is taken at or beyond a limiting value depending on $a$ and $\kappa$.

Referring to the stability diagram of Fig. 12, solutions for the system will be stable so long as the point $(a, q)$ lies to the left of the stability line for the appropriate value of $\kappa_0$. This stability diagram is part of the full Mathieu-equation-solution stability diagram of Fig. 13. This shows that the resonance already found near $a = 4$ is only one of a number to be found near any square integer. However, the amplitude of response is likely to be less in these cases.

The parameter $\kappa_0$ varies the boundary in the stability diagram and the shape of the response curves.

### (6) CONCLUSIONS

In the light of the foregoing discussion, it is now possible to comment on some of the statements made in References 2 and 3 and summarized at the end of Section 2.

Referring to advantage (a) in Section 2, there is the possibility of slight changes in the parameters during the life and operation of the equipment. Thus the changes in amplitude and frequency



Fig. 12.—Stability boundaries for solutions of Mathieu's equation.
The area to the left of the line for a value of $\kappa$ is the stable area with that value of $\kappa$.

of the fork radial motion would affect $q$ and $a$, changes in damping would affect $\kappa_0$, and changes in the spring constant of the torsion mechanism would affect all three parameters. It follows that the tuning-fork-type angular tachometer must be so constructed that any changes in the system constants over a period are sufficiently small for the required accuracy to be maintained. This should not prove difficult, owing to the general simplicity of the device.

The rapidity of response, advantage (b), depends on a suitable selection of the damping factor, and restrictions on the permitted value of this factor are considered later in this Section.

One lower limit for linearity of response is provided by signals due to motion about axes other than that about which the measurement is required, while the upper limit will be due to power loss in torsional oscillations of large amplitude. Altogether there should be a wide range of linear response.

With regard to advantage (c) of Section 2, error effects exist due to motion about the other axes mentioned above, and to acceleration, and they give rise to the terms in eqns. (11) and later omitted. These errors, and those due to periodically varying inputs, may be made negligibly small by the choice of an operating frequency sufficiently high in relation to velocities, accelerations and frequencies likely to be met with in any particular application of the instrument, and also by keeping the torsional displacement suitably small under the same conditions.

Although a pure sinusoidal fork motion has been assumed, [cf. requirement (i) of Section 2], any periodic motion could be substituted. By using a Fourier series approximation, an equation of Hill's type is reached instead of Mathieu's. Thus the solution would include larger terms at the harmonic frequencies, but would otherwise be similar. Substantially the same response characteristics might be obtained with suitable filtering of the output.

The simplified theory does not bring out the full effect of the damping coefficient, requirement (ii), which not only secures a suitable time-constant to eliminate transients but also affects the stability of the system, the accuracy and the response in general. Hence the damping coefficient must be chosen carefully having regard to the requirements of these characteristics in any application.

The fact that the ratio between modulated and static inertias should be as large as possible in order to secure increased response, requirement (iii) of Section 2, follows naturally from the response formulae. However, the general theory shows that stability of the system depends on $q \simeq 2I_1/I_0$, so that there is a limit to the value of the inertia ratio which can be used.

Reference to the graphs of response against parameter $a$ shows that the statement that highest output is obtained with the torsion and fork frequencies equal, requirement (iv), is misleading. While the two frequencies should be approximately equal, the maximum response is not at $a = 4$, corresponding to exact equality: as $q$ is increased the approximation gets steadily worse. The design must be considered carefully in order to arrive at the correct relation for the two frequencies.

It is seen that, while the simplified theory appears to give a useful basic approach to the operation, the properties of the system are not explored fully.

In particular, the Mathieu-equation approach shows, in far more detail, the correct relationship of the driven and torsion frequencies and the effect of damping, and also indicates that there are design limits beyond which the instrument is unstable.

## (7) ACKNOWLEDGMENTS

## (8) REFERENCES

(1) MEREDITH, F. W.: 'Control of Equilibrium in the Flying Insect', *Nature*, 1949, **163**, p. 74.
(2) LYMAN, J.: 'A New Space Rate Sensing Instrument', *Aeronautical Engineering Review*, 1953, **12**, No. 11, p. 24.
(3) BARNABY, R. E., CHATTERTON, J. B., and GERRING, F. H.: 'General Theory and Operating Characteristics of the Gyrotron Angular Rate Tachometer', *ibid.*, 1953, **12**, No. 11, p. 31.
(4) CHATTERTON, J. B.: 'Some General Comparisons between the Vibratory and Conventional Rate Gyro', *Journal of Aeronautical Science*, September, 1955, p. 633.
(5) McLACHLAN, N. W.: 'Theory and Application of Mathieu Functions' (Oxford University Press, 1951).

## (9) APPENDICES

### (9.1) Mathieu's Equation

(9.1.1) **Solutions of non-integral order in the region $a = 4$.**

The standard form of Mathieu's equation [eqn. (32)] is

$$\frac{d^2u}{dy^2} + (a - 2q\cos 2y)u = 0$$

Since $a \simeq 4$ let

$$a = 4 + qf_1(\sigma) + q^2f_2(\sigma) + q^3f_3(\sigma) + \dots \quad . \quad (63)$$

where $\sigma$ is a parameter depending on $a$ and $q$.

Define a further parameter $\mu$ as

$$\mu = qg_1(\sigma) + q^2g_2(\sigma) + q^3g_3(\sigma) + \dots \quad . \quad (64)$$

so that Mathieu's equation has the solutions

$$u = \varepsilon^{\mu y}\phi(y, \sigma) \quad \text{and} \quad \varepsilon^{-\mu y}\phi(y, -\sigma) . \quad . \quad (65)$$

where the function $\phi(y, \sigma)$ is a periodic function

$$\phi = \sin(2y - \sigma) + qh_1(y, \sigma) + q^2h_2(y, \sigma) + q^3h_3(y, \sigma) . \quad (66)$$

If

$$u = \varepsilon^{\mu y}\phi$$

then

$$\frac{du}{dy} = \varepsilon^{\mu y}(\phi' + \mu\phi)$$

and

$$\frac{d^2u}{dy^2} = \varepsilon^{\mu y}(\phi'' + 2\mu\phi' + \mu^2\phi)$$

Substituting these values, Mathieu's equation [eqn. (32)] is thus transformed to

$$\varepsilon^{\mu y}[\phi'' + 2\mu\phi' + (\mu^2 + a - 2q\cos 2y)\phi] = 0 \quad . \quad (67)$$

By removing the $\varepsilon^{\mu y}$ factor and substituting eqns. (63), (64) and (66) into eqn. (67), the following information is obtained:

$$-4\sin(2y - \sigma) + qh_1'' + q^2h_2'' + q^3h_3'' + \dots$$
$$+ 2(qg_1 + q^2g_2 + q^3g_3 \dots)$$
$$\times [2\cos(2y - \sigma) + qh_1' + q^2h_2' + q^3h_3' + \dots]$$
$$+ [(qg_1 + q^2g_2 + q^3g_3 + \dots)^2$$
$$+ 4 + qf_1 + q^2f_2 + q^3f_3 \dots - 2q\cos 2y]$$
$$\times [\sin(2y - \sigma) + qh_1 + q^2h_2 + q^3h_3 + \dots] = 0$$
$$. \quad . \quad . \quad (68)$$

Taking this expression to be an identity, the coefficients of powers of $q$ can be equated to zero.

Successively this gives

$$q^0: -4 \sin(2y - \sigma) + 4 \sin(2y - \sigma) = 0 \text{ (an identity)} \quad . \quad (69)$$

$$q^1: h_1'' + 4g_1 \cos(2y - \sigma) + 4h_1 + f_1 \sin(2y - \sigma)$$
$$- 2\cos 2y \sin(2y - \sigma) = 0 \quad . \quad (70)$$

Writing $2 \cos 2y \sin(2y - \sigma) = \sin(4y - \sigma) - \sin \sigma$,

$$h_1'' + 4h_1 = \sin(4y - \sigma) - \sin \sigma - 4g_1 \cos(2y - \sigma)$$
$$- f_1 \sin(2y - \sigma) \quad . \quad (71)$$

In this differential equation the terms in $\cos(2y - \sigma)$ and $\sin(2y - \sigma)$ would give rise to non-periodic particular integrals.

Hence $\qquad\qquad f_1 = 0 \qquad . \quad . \quad . \quad . \quad . \quad (72)$

and $\qquad\qquad g_1 = 0 \qquad . \quad . \quad . \quad . \quad . \quad (73)$

So the equation reduces to

$$h_1'' + 4h_1 = \sin(4y - \sigma) - \sin \sigma \quad . \quad . \quad . \quad (74)$$

The particular integral of this is

$$h_1 = -\tfrac{1}{12} \sin(4y - \sigma) - \tfrac{1}{4} \sin \sigma \quad . \quad . \quad (75)$$

$$q^2: h_2'' + 2g_1 h_1' + 4g_2 \cos(2y - \sigma) + g_1^2 \sin(2y - \sigma)$$
$$+ 4h_2 + f_1 h_1 + f_2 \sin(2y - \sigma) - 2h_1 \cos 2y = 0 \quad . \quad (76)$$

Putting into eqn. (76) the values already obtained,

$$h_2'' + 4g_2 \cos(2y - \sigma) + 4h_2 + f_2 \sin(2y - \sigma)$$
$$+ \tfrac{1}{6} \sin(4y - \sigma) \cos 2y + \tfrac{1}{2} \sin \sigma \cos 2y = 0 \quad . \quad (77)$$

Writing $\cos 2y = \cos \sigma \cos(2y - \sigma) - \sin \sigma \sin(2y - \sigma)$

$$2 \sin(4y - \sigma) \cos 2y = \sin(6y - \sigma) + \sin(2y - \sigma)$$

we have

$$h_2'' + 4h_2 = (-f_2 - \tfrac{1}{12} + \tfrac{1}{2} \sin^2 \sigma) \sin(2y - \sigma)$$
$$+ (-4g_2 - \tfrac{1}{2} \cos \sigma \sin \sigma) \cos(2y - \sigma) - \tfrac{1}{12} \sin(6y - \sigma)$$
$$. \quad . \quad . \quad (78)$$

To eliminate non-periodic terms from the particular integral, put

$$f_2 = -\tfrac{1}{12} + \tfrac{1}{2} \sin^2 \sigma$$
$$= \frac{(2 - 3 \cos 2\sigma)}{12} \quad . \quad . \quad . \quad (79)$$

and $\qquad\qquad g_2 = -\tfrac{1}{8} \sin \sigma \cos \sigma$
$$= -\frac{\sin 2\sigma}{16} \quad . \quad . \quad . \quad . \quad . \quad (80)$$

The differential equation for $h_2$ is now

$$h_2'' + 4h_2 = -\tfrac{1}{12} \sin(6y - \sigma) \quad . \quad . \quad . \quad (81)$$

The particular integral of this is

$$h_2 = \frac{1}{384} \sin(6y - \sigma) \quad . \quad . \quad . \quad (82)$$

$$q^3: h_3'' + 2g_1 h_2' + 2g_2 h_1' + 4g_3 \cos(2y - \sigma)$$
$$+ g_2^2 h_1 + 2g_1 g_2 \sin(2y - \sigma) + 4h_3 + f_1 h_2$$
$$+ f_2 h_1 + f_3 \sin(2y - \sigma) - 2h_2 \cos 2y = 0 \quad . \quad . \quad (83)$$

Putting the values already obtained into eqn. (80),

$$h_3 + \frac{\sin 2\sigma}{24} \cos(4y - \sigma) + 4g_3 \cos(2y - \sigma) + 4h_3$$
$$- \frac{(2 - 3 \cos 2\sigma)}{144} \sin(4y - \sigma) - \frac{(2 - 3 \cos 2\sigma)}{48} \sin \sigma$$
$$+ f_3 \sin(2y - \sigma) - \frac{1}{192} \sin(6y - \sigma) \cos 2y = 0 \quad . \quad (84)$$

Writing $2 \sin(6y - \sigma) \cos 2y = \sin(8y - \sigma) + \sin(4y - \sigma)$

Then $\quad h_3'' + 4h_3 = \dfrac{(2 - 3 \cos 2\sigma) \sin \sigma}{48} - f_3 \sin(2y - \sigma)$

$$- 4g_3' \cos(2y - \sigma) + \left(\frac{2 - 3 \cos 2\sigma}{144} + \frac{1}{384}\right) \sin(4y - \sigma)$$

$$- \frac{\sin 2\sigma}{24} \cos(4y - \sigma) + \frac{1}{384} \sin(8y - \sigma) \quad . \quad . \quad . \quad (85)$$

As before, the coefficients of $\sin(2y - \sigma)$ and $\cos(2y - \sigma)$ must be zero.

$$f_3 = 0 \qquad . \quad . \quad . \quad . \quad . \quad (86)$$

$$g_3 = 0 \qquad . \quad . \quad . \quad . \quad . \quad (87)$$

The differential equation for $h_3$ is

$$h_3'' + 4h_3 = \frac{(2 - 3 \cos 2\sigma) \sin \sigma}{48} + \frac{19 - 24 \cos 2\sigma}{1152} \sin(4y - \sigma)$$

$$- \frac{\sin 2\sigma}{24} \cos(4y - \sigma) + \frac{1}{384} \sin(8y - \sigma) \quad . \quad (88)$$

This leads to a particular integral of

$$h_3 = \frac{2 - 3 \cos 2\sigma}{192} \sin \sigma - \frac{19 - 24 \cos 2\sigma}{13824} \sin(4y - \sigma)$$

$$+ \frac{\sin 2\sigma}{288} \cos(4y - \sigma) - \frac{1}{23040} \sin(8y - \sigma) \quad . \quad (89)$$

$$q^4: h_4'' + 2g_1 h_3' + 2g_2 h_2' + 2g_3 h_1' + 4g_4 \cos(2y - \sigma)$$
$$+ g_1^2 h_2' + 2g_1 g_2 h_1' + (g_2^2 + 2g_1 g_3) \sin(2y - \sigma) + 4h_4$$
$$+ f_1 h_3 + f_2 h_2 + f_3 h_1 + f_4 \sin(2y - \sigma) - 2h_3 \cos 2y = 0$$
$$. \quad . \quad . \quad (90)$$

Replacing the known symbols,

$$h_4'' - \frac{\sin 2\sigma}{512} \cos(6y - \sigma) + 4g_4 \cos(2y - \sigma)$$

$$+ \frac{\sin^2 2\sigma}{256} \sin(2y - \sigma) + 4h_4$$

$$+ \frac{(2 - 3 \cos 2\sigma)}{4608} \sin(6y - \sigma) + f_4 \sin(2y - \sigma)$$

$$- \frac{(2 - 3 \cos 2\sigma) \sin \sigma}{96} \cos 2y$$

$$+ \frac{(19 - 24 \cos) 2\sigma}{6912} \sin(4y - \sigma) \cos 2y$$

$$- \frac{\sin 2\sigma}{144} \cos(4y - \sigma) \cos 2y$$

$$+ \frac{1}{11520} \sin(8y - \sigma) \cos 2y = 0 \quad . \quad . \quad . \quad (91)$$

Writing $\cos 2y = \cos \sigma \cos(2y - \sigma) - \sin \sigma \sin(2y - \sigma)$

$$2 \sin(4y - \sigma) \cos 2y = \sin(6y - \sigma) + \sin(2y - \sigma)$$

$$2 \cos(4y - \sigma) \cos 2y = \cos(6y - \sigma) + \cos(2y - \sigma)$$

and $\quad 2 \sin(8y - \sigma) \cos 2y = \sin(10y - \sigma) + \sin(6y - \sigma)$

Then

$$h_4'' + 4h_4 = \left[ -\frac{\sin^2 2\sigma}{256} - f_4 - \frac{19 - 24\cos 2\sigma}{13824} \right.$$
$$\left. - \frac{(2 - 3\cos 2\sigma)\sin^2 \sigma}{96} \right] \sin (2y - \sigma)$$

$$+ \left[ -4g_4 + \frac{(2 - 3\cos 2\sigma)\sin \sigma \cos \sigma}{96} + \frac{\sin 2\sigma}{288} \right] \cos (2y - \sigma)$$

$$+ \left[ -\frac{(2 - 3\cos 2\sigma)}{4608} - \frac{(19 - 24\cos 2\sigma)}{13824} - \frac{1}{23040} \right] \sin (6y - \sigma)$$

$$+ \left( \frac{\sin 2 \sigma}{512} + \frac{\sin 2\sigma}{288} \right) \cos (6y - \sigma) - \frac{1}{23040} \sin (10y - \sigma)$$
$$\qquad \qquad \cdots \cdots \quad (92)$$

As before, the coefficients of $\cos (2y - \sigma)$ and $\sin (2y - \sigma)$ must be zero.

Therefore

$$f_4 = - \left[ \frac{\sin^2 2\sigma}{256} + \frac{19 - 24\cos 2\sigma}{13824} + \frac{(2 - 3\cos 2\sigma)\sin^2 \sigma}{96} \right]$$

$$= - \left[ \frac{145}{13824} - \frac{1}{36} \cos 2\sigma + \frac{3}{256} \cos^2 2\sigma \right] \quad \cdots \quad (93)$$

and

$$y_4 = \frac{(2 - 3\cos 2\sigma)\sin \sigma \cos \sigma}{384} + \frac{\sin 2\sigma}{1152}$$

$$= \frac{1}{288} \sin 2\sigma - \frac{1}{512} \sin 4\sigma \quad \cdots \cdots \quad (94)$$

The differential equation for $h_4$ is

$$h_4'' + 4h_4 = \left( -\frac{1}{540} + \frac{11}{4608} \cos 2\sigma \right) \sin (6y - \sigma)$$

$$+ \frac{25}{4608} \cos (6y - \sigma) - \frac{1}{23040} \sin (10y - \sigma) \quad \cdot \quad (95)$$

So that the particular integral is

$$h_4 = \left( \frac{1}{17280} - \frac{11}{147456} \cos 2\sigma \right) \sin (6y - \sigma)$$

$$- \frac{25}{147456} \cos (6y - \sigma) + \frac{1}{2211840} \sin (10y - \sigma) \quad \cdot \quad (96)$$

The solution of Mathieu's equation may therefore be written as

$$u = A\varepsilon^{\mu y}\phi(y, \sigma) + B\varepsilon^{-\mu y}\phi(y, -\sigma) \quad \cdots \quad (97)$$

where $\sigma$ is connected with $a$ and $q$ by

$$a = 4 + q^2 \left( \frac{2 - 3\cos 2\sigma}{12} \right)$$

$$+ q^4 \left( \frac{145}{13824} + \frac{1}{36} \cos 2\sigma - \frac{3}{256} \cos^2 2\sigma \right), \text{ etc.} \quad \cdot \quad (98)$$

$\mu$ is given by

$$\mu = - \frac{q^2}{16} \sin 2\sigma + q^4 \left( \frac{1}{288} \sin 2\sigma - \frac{1}{512} \sin 4\sigma \right), \text{ etc.} \quad \cdot \quad (99)$$

and $\phi$ is given by

$$\phi(y, \sigma) = \sin (2y - \sigma) + q \left[ -\frac{1}{12} \sin (4y - \sigma) - \frac{1}{4} \sin \sigma \right]$$

$$+ q^2 \left[ \frac{1}{384} \sin (6y - \sigma) \right]$$

$$+ q^3 \left[ \frac{2 - 3\cos 2\sigma}{192} \sin \sigma - \frac{19 - 24\cos 2\sigma}{13824} \sin (4y - \sigma) \right.$$
$$\left. + \frac{\sin 2\sigma}{288} \cos (4y - \sigma) - \frac{1}{23040} \sin (8y - \sigma) \right]$$

$$+ q^4 \left[ \left( \frac{1}{17280} - \frac{11}{147456} \cos 2\sigma \right) \sin (6y - \sigma) \right.$$

$$- \frac{25}{147456} \sin 2\sigma \cos (6y - \sigma)$$

$$\left. + \frac{1}{2211840} \sin (10y - \sigma) \right] \text{ etc.} \quad \cdots \quad (100)$$

We can write

$$\phi(y, \sigma) = \sin \sigma \left( -\frac{q}{4} + \frac{2 - 3\cos 2\sigma}{192} q^3 \ldots \right)$$

$$+ \sin (2y - \sigma)$$

$$+ \sin (4y - \sigma) \left( \frac{q}{12} - \frac{19 - 24\cos 2\sigma}{13824} q^3 \ldots \right)$$

$$+ \cos (4y - \sigma) \left( \frac{\sin 2\sigma}{288} q^3 \ldots \right)$$

$$+ \sin (6y - \sigma) \left[ \frac{1}{384} q^2 + \left( \frac{1}{17280} - \frac{11\cos 2\sigma}{147456} \right) q^4 \right]$$

$$+ \cos (6y - \sigma) \left( -\frac{25\sin 2\sigma}{147456} q^4 \ldots \right)$$

$$+ \sin (8y - \sigma) \left( -\frac{1}{23040} q^3 \ldots \right)$$

$$+ \sin (10y - \sigma) \left( \frac{1}{2211840} q^4 \ldots \right) \quad \cdots \quad (101)$$

Taking only the fundamental, assuming that $q$ is small, the solution of Mathieu's equation is approximately

$$u = A\varepsilon^{+\mu y} \sin (2y - \sigma) + B\varepsilon^{-\mu y} \sin (2y + \sigma) \quad \cdot \quad (102)$$

This is used in Section 5 [eqn. (40)].

### (9.1.2) Stability.

From eqn. (47), the response will be stable if

$$\mathscr{R}(\kappa - \mu) > 0 \quad \cdots \cdots \quad (103)$$

Since $k$ is real and positive, consider the condition

$$\mathscr{R}\mu < \kappa \quad \cdots \cdots \quad (104)$$

where $\mu = -\frac{q^2}{16} \sin 2\sigma$

In the region under consideration it can be shown that $\sigma$ is negative, i.e. $-\frac{1}{2}\pi \leqslant \sigma \leqslant 0$, so that $\mu$ is real and positive. A chart connecting the $a$ and $q$ parameters can be plotted;

$$a = 4 + q^2 \left( \frac{1}{6} - \frac{1}{4} \cos 2\sigma \right) \quad \cdots \cdots \quad (105)$$

with $\sigma$ obtained from $\sin 2\sigma = -\frac{16\kappa}{q^2}$

This may be written

$$a = 4 + \frac{q^2}{6} \pm \frac{q^2}{4}\left(1 - \frac{256\kappa^2}{q^4}\right)^{1/2} \quad . \quad . \quad . \quad (106)$$

which is plotted in Fig. 9 for various values of the parameter $\kappa$. The area for stable solutions is that to the left of the curve for a particular value of $\kappa$. This corresponds to $\mu < \kappa$.

### (9.2) Evaluation of Particular Integral

Writing $\kappa = \epsilon/\omega I_0$, $b = I_1/I_0$, and assuming that second order terms in $\kappa$ and $b$ can be neglected, eqn. (34) reduces to the standard Mathieu equation form

$$\frac{d^2u}{dy^2} + (a - 2q\cos 2y)u = \varepsilon^{\kappa(\pi/4-y)}\left[ -(1 + b\cos 2y)\frac{d^2v}{dy^2}\right.$$

$$\left. + 4b\sin 2y\frac{dv}{dy} + 4b\cos 2y\,v \right] = f(y)\text{ say} \quad . \quad (107)$$

If the torsion system is in approximate resonance, $R/I_0 \simeq 4\omega^2$, and therefore $a \simeq 4$.

Thus the complementary function solutions of Mathieu's equation are approximately

$$u = \varepsilon^{\mu y}\sin(2y - \sigma)$$

$$u = \varepsilon^{-\mu y}\sin(2y + \sigma)$$

where $\mu$ and $\sigma$ are the parameters as previously defined.

Solving the differential equation by 'the method of variation of parameters', we arrive at the solution

$$u = \frac{1}{2\sin 2\sigma}\left[\begin{array}{l}\varepsilon^{\mu y}\sin(2y - \sigma)\displaystyle\int \varepsilon^{-\mu x}\sin(2x + \sigma)f(x)dx \\ -\varepsilon^{-\mu y}\sin(2y + \sigma)\displaystyle\int \varepsilon^{\mu x}\sin(2x - \sigma)f(x)dx\end{array}\right]$$

$$. \quad . \quad . \quad . \quad (108)$$

Thus

$$2\sin 2\sigma\, u\varepsilon^{-\pi\kappa/4} = \varepsilon^{\mu y}\sin(2y - \sigma)\int^y \varepsilon^{-(\kappa+\mu)x}\sin(2x + \sigma)\left[\begin{array}{l}-(1 + b\cos 2x)\dfrac{d^2v}{dx^2} \\ + 4b\sin 2x\dfrac{dv}{dx} + 4b\cos 2x\,v\end{array}\right]dx$$

$$-\varepsilon^{-\mu y}\sin(2y + \sigma)\int^y \varepsilon^{-(\kappa-\mu)x}\sin(2x - \sigma)\left[\begin{array}{l}-(1 + b\cos 2x)\dfrac{d^2v}{dx^2} \\ + 4b\sin 2x\dfrac{dv}{dx} + 4b\cos 2x\,v\end{array}\right]dx. \quad . \quad . \quad . \quad . \quad . \quad (109)$$

$$= \tfrac{1}{2}\varepsilon^{\mu y}\sin(2y - \sigma)\int^y \varepsilon^{-(\kappa+\mu)x}\left[\begin{array}{l}\sin\sigma\left(-b\dfrac{d^2v}{dx^2} + 4bv\right) + \cos\sigma\left(4b\dfrac{dv}{dx}\right) \\[4pt] + \sin(2x + \sigma)\left(-2\dfrac{d^2v}{dx^2}\right) + \sin(4x + \sigma)\left(-b\dfrac{d^2v}{dx^2} + 4bv\right) \\[4pt] + \cos(4x + \sigma)\left(-4b\dfrac{dv}{dx}\right)\end{array}\right]dx$$

$$-\tfrac{1}{2}\varepsilon^{-\mu y}\sin(2y + \sigma)\int^y \varepsilon^{-(\kappa-\mu)x}\left[\begin{array}{l}-\sin\sigma\left(-b\dfrac{d^2v}{dx^2} + 4bv\right) + \cos\sigma\left(4b\dfrac{dv}{dx}\right) \\[4pt] + \sin(2x - \sigma)\left(-2\dfrac{d^2v}{dx^2}\right) + \sin(4x - \sigma)\left(-b\dfrac{d^2v}{dx^2} + 4bv\right) \\[4pt] + \cos(4x - \sigma)\left(-4b\dfrac{dv}{dx}\right)\end{array}\right]dx \quad . \quad . \quad (110)$$

The $\sin(2x \pm \sigma)$, $\frac{\sin}{\cos}(4x \pm \sigma)$ terms will, on integration, be reduced in proportion to $\frac{1}{2}\kappa$, $\frac{1}{4}\kappa$ approximately, and will give terms in $u$ either in the harmonics or in non-periodic terms, but not the fundamental. It will be assumed, therefore, that they may be neglected.

Now

$$\int^y \varepsilon^{\alpha x}g(x)dx = \frac{\varepsilon^{\alpha y}g(y)}{\alpha} - \int^y \frac{\varepsilon^{\alpha x}}{\alpha}\frac{dg}{dx}dx = \varepsilon^{\alpha y}\left\{\frac{g}{\alpha} - \frac{1}{\alpha^2}\frac{dg}{dy} + \frac{1}{\alpha^3}\frac{d^2g}{dy^2} - \frac{1}{\alpha^4}\frac{d^3g}{dy^3} + \text{etc.}\right\} \quad . \quad . \quad . \quad . \quad (111)$$

the differential coefficients with respect to $y$ are converted back to functions of time, it will be seen that, in the integral expansion, the differentials are multiplied by a factor $1/(\kappa \pm \mu)\omega$ to a power equal to the order of the differential. If $\omega$ is sufficiently large, this factor is much less than unity. Hence differential coefficients as far as the second order only need be retained, and eqn. (110) becomes

$$4\sin 2\sigma u\varepsilon^{-\pi\kappa/4} = b\varepsilon^{-\kappa y}\sin(2y - \sigma)\left[\begin{array}{l}\sin\sigma\left[-\dfrac{1}{\kappa + \mu}\left\{-\dfrac{d^2v}{dy^2} + 4v\right\} - \dfrac{4}{(\kappa + \mu)^2}\dfrac{dv}{dy} - \dfrac{4}{(\kappa + \mu)^3}\dfrac{d^2v}{dy^2}\right] \\[8pt] + \cos\sigma\left[-\dfrac{4}{\kappa + \mu}\dfrac{dv}{dy} - \dfrac{4}{(\kappa + \mu)^2}\dfrac{d^2v}{dy^2}\right]\end{array}\right]$$

$$- b\varepsilon^{-\kappa y} \sin(2y + \sigma) \left[ \begin{array}{l} - \sin\sigma \left[ -\dfrac{1}{\kappa - \mu}\left\{ -\dfrac{d^2v}{dy^2} + 4v \right\} - \dfrac{4}{(\kappa - \mu)^2}\dfrac{dv}{dy} - \dfrac{4}{(\kappa - \mu)^3}\dfrac{d^2v}{dy^2} \right] \\ + \cos\sigma \left[ -\dfrac{4}{\kappa - \mu}\dfrac{dv}{dy} - \dfrac{4}{(\kappa - \mu)^2}\dfrac{d^2v}{dy^2} \right] \end{array} \right] \quad . \quad . \quad (112)$$

$$= b\varepsilon^{-\kappa y} \left[ \begin{array}{l} \sin 2y \sin\sigma \cos\sigma \left[ -\left\{ \dfrac{1}{\kappa + \mu} + \dfrac{1}{\kappa - \mu} \right\}\left\{ -\dfrac{d^2v}{dy^2} + 4v \right\} - \left\{ \dfrac{4}{(\kappa + \mu)^2} + \dfrac{4}{(\kappa - \mu)^2} \right\}\dfrac{dv}{dy} \right. \\ \qquad\qquad\qquad \left. -\left\{ \dfrac{4}{(\kappa + \mu)^3} + \dfrac{4}{(\kappa - \mu)^3} \right\}\dfrac{d^2v}{dy^2} \right] \\[6pt] + \cos 2y \sin\sigma \cos\sigma \left[ +\left\{ \dfrac{4}{\kappa + \mu} + \dfrac{4}{\kappa - \mu} \right\}\dfrac{dv}{dy} + \left\{ \dfrac{4}{(\kappa + \mu)^2} + \dfrac{4}{(\kappa - \mu)^2} \right\}\dfrac{d^2v}{dy^2} \right] \\[6pt] + \sin 2y \cos^2\sigma \left[ -\left\{ \dfrac{4}{\kappa + \mu} - \dfrac{4}{\kappa - \mu} \right\}\dfrac{dv}{dy} - \left\{ \dfrac{4}{(\kappa + \mu)^2} - \dfrac{4}{(\kappa - \mu)^2} \right\}\dfrac{d^2v}{dy^2} \right] \\[6pt] + \cos 2y \sin^2\sigma \left[ \left\{ +\dfrac{1}{\kappa + \mu} - \dfrac{1}{\kappa - \mu} \right\}\left\{ -\dfrac{d^2v}{dy^2} + 4v \right\} + \left\{ \dfrac{4}{(\kappa + \mu)^2} - \dfrac{4}{(\kappa - \mu)^2} \right\}\dfrac{dv}{dy} \right. \\ \qquad\qquad\qquad \left. + \left\{ \dfrac{4}{(\kappa + \mu)^3} - \dfrac{4}{(\kappa - \mu)^3} \right\}\dfrac{d^2v}{dy^2} \right] \end{array} \right] \quad . \quad . \quad (113)$$

$$= b\varepsilon^{-\kappa y} \left[ \begin{array}{l} \sin 2y \left[ \begin{array}{l} v\left[ 4\sin\sigma\cos\sigma\left\{ -\dfrac{1}{\kappa + \mu} - \dfrac{1}{\kappa - \mu} \right\} \right] \\ + \dfrac{dv}{dy}\left[ +4\cos^2\sigma\left\{ -\dfrac{1}{\kappa + \mu} + \dfrac{1}{\kappa - \mu} \right\} - 4\sin\sigma\cos\sigma\left\{ \dfrac{1}{(\kappa + \mu)^2} + \dfrac{1}{(\kappa - \mu)^2} \right\} \right] \\ + \dfrac{d^2v}{dy^2}\left[ \begin{array}{l} +\sin\sigma\cos\sigma\left\{ \dfrac{1}{\kappa + \mu} + \dfrac{1}{\kappa - \mu} \right\} - 4\cos^2\sigma\left\{ \dfrac{1}{(\kappa + \mu)^2} - \dfrac{1}{(\kappa - \mu)^2} \right\} \\ + 4\sin\sigma\cos\sigma\left\{ -\dfrac{1}{(\kappa + \mu)^3} - \dfrac{1}{(\kappa - \mu)^2} \right\} \end{array} \right] \end{array} \right] \\[12pt] + \cos 2y \left[ \begin{array}{l} v\left[ +4\sin^2\sigma\left\{ \dfrac{1}{\kappa + \mu} - \dfrac{1}{\kappa - \mu} \right\} \right] \\ + \dfrac{dv}{dy}\left[ +4\sin\sigma\cos\sigma\left\{ \dfrac{1}{\kappa + \mu} + \dfrac{1}{\kappa - \mu} \right\} + 4\sin^2\sigma\left\{ \dfrac{1}{(\kappa + \mu)^2} - \dfrac{1}{(\kappa - \mu)^2} \right\} \right] \\ + \dfrac{d^2v}{dy^2}\left[ \begin{array}{l} -\sin^2\sigma\left\{ \dfrac{1}{\kappa + \mu} - \dfrac{1}{\kappa - \mu} \right\} + 4\sin\sigma\cos\sigma\left\{ \dfrac{1}{(\kappa - \mu)^2} + \dfrac{1}{(\kappa + \mu)^2} \right\} \\ + 4\sin^2\sigma\left\{ \dfrac{1}{(\kappa + \mu)^3} - \dfrac{1}{(\kappa - \mu)^3} \right\} \end{array} \right] \end{array} \right] \end{array} \right] \quad . \quad (114)$$

Therefore the equation for $u$ is

$$u = b\varepsilon^{\kappa\left(\frac{\pi}{4} - y\right)}\left[ -\dfrac{\kappa}{\kappa^2 - \mu^2}\sin 2y - \dfrac{\mu\tan\sigma}{\kappa^2 - \mu^2}\cos 2y \right]v + b\varepsilon^{\kappa\left(\frac{\pi}{4} - y\right)}\left[ \begin{array}{l} \left\{ \dfrac{\mu\cot\sigma}{\kappa^2 - \mu^2} - \dfrac{\kappa^2 + \mu^2}{(\kappa^2 - \mu^2)^2} \right\}\sin 2y \\ + \left\{ \dfrac{\kappa}{\kappa^2 - \mu^2} - \dfrac{2\kappa\mu\tan\sigma}{(\kappa^2 - \mu^2)^2} \right\}\cos 2y \end{array} \right]\dfrac{dv}{dy} \quad . \quad . \quad (115)$$

and terms in higher order differentials of $v$.

# A SIMPLIFIED DERIVATION OF THE FOURIER COEFFICIENTS FOR CHEBȲSHEV PATTERNS

## By J. L. BROWN, Jr., Ph.D.

### SUMMARY

In the design of linear arrays containing an odd number of elements with constant element spacing of less than a half wavelength, the mathematical problem reduces to that of finding explicitly the coefficients, $b_m$, in the expansion

$$T_n(ax + b) = \sum_{m=0}^{n} b_m T_m(x)$$

where $a$ and $b$ are constants, $n > 0$, and $T_m(x)$ is defined as cos $(m$ arc cos $x)$ for $m \geqslant 0$. Such a problem was initially solved by DuHamel and later given by Salzer in a form more convenient for computation. The purpose of this paper is to give an alternative derivation of Salzer's result, making use of the orthogonality properties of the Chebȳshev polynomials in order to obviate the fairly elaborate series manipulations required in the previous derivation.

### (1) INTRODUCTION

A brief summary of the use of Chebȳshev polynomials in the design of linear broadside arrays is given in Salzer's paper[1] and will not be repeated here. For an odd number of elements in the super-directive case (constant element spacing of less than a half wavelength), the mathematical problem is that of expanding $T_n(ax + b)$ as a series in terms of $T_m(x)$, where $T_m(x)$ is the $m$th Chebȳshev polynomial defined by $T_m(x) =$ cos $(m$ arc cos $x)$ for $m \geqslant 0$. Salzer[1] provided an explicit formula for the calculation of the coefficients of such an expression, his formula being much simpler and computationally more tractable than the one previously given by DuHamel.[2] In essence, Salzer's method of derivation consists of expanding $T_n(ax + b)$ in powers of $x$, expanding each power of $x$ in terms of the Chebȳshev polynomials, $T_m(x)$, and then identifying the coefficients $b_m$ from his final expansion. In the process, several rearrangements of the (finite) series are necessitated, and these are complicated enough to require diagrams explaining the new forms.

Since the Chebȳshev polynomials are orthogonal with respect to the weight function $(1 - x^2)^{-1/2}$ on the interval $(-1, 1)$, it is easily seen that the $b_m$'s in the equation

$$T_n(ax + b) = \sum_{m=0}^{n} b_m T_m(x), (n > 0) \quad . \quad . \quad (1)$$

are given by

$$
\begin{cases}
b_m = \dfrac{2}{\pi} \displaystyle\int_{-1}^{1} \dfrac{T_n(ax + b) T_m(x)}{\sqrt{(1 - x^2)}} dx; \; m \geqslant 1 \\[3mm]
b_0 = \dfrac{1}{\pi} \displaystyle\int_{-1}^{1} \dfrac{T_n(ax + b)}{\sqrt{(1 - x^2)}} dx
\end{cases}
$$

This result is used to obtain a simple alternative derivation of Salzer's result which eliminates the need for involved series operations.

Correspondence on Monographs is invited for consideration with a view to publication.

Dr. Brown is at the Ordnance Research Laboratory, The Pennsylvania State University, Pennsylvania, U.S.A.

### (2) DERIVATION

Let $T_m(x)$ be defined as follows:

$$T_m(x) = \cos (m \text{ arc cos } x) \quad \text{for } m \geqslant 0 \quad . \quad . \quad (2)$$

This definition employs the normalization given by Bateman.[3] Salzer[1] makes the special definition $T_0(x) \equiv 1/2$ in order to give a consistent representation for $x^k$ in terms of $T_m(x)$.

Replacing $x$ by $ax + b$ in the expression

$$T_n(x) = n \sum_{m=0}^{[n/2]} \frac{(-1)^m}{m} \binom{n - m - 1}{m - 1} 2^{n-2m-1} x^{n-2m}, (n > 0)(3)$$

[Reference 3, eqn. (22)]

and then using the binomial formula to expand the various powers of $ax + b$ we have

$$T_n(ax + b) = \sum_{r=0}^{[n/2]} \sum_{k=0}^{n-2r} c_{rk} x^k \quad . \quad . \quad . \quad (4)$$

where

$$c_{rk} = (-1)^r 2^{n-2r-1} \left[ 2 \binom{n - r}{r} - \binom{n - r - 1}{r} \right] \binom{n - 2r}{k} a^k b^{n-2r-k} \quad (5)$$

In this equation, $\binom{m}{k}$ denotes the binomial coefficient $\dfrac{m!}{k! \, (m - k)!}$ and $[x]$ denotes the greatest integer not exceeding $x$. Thus far, the derivation is identical to Salzer's, but at this point the orthogonality property of the polynomials is invoked rather than expanding $x^k$ in terms of the polynomials and then matching coefficients with eqn. (1). The orthogonality property is

$$\int_{-1}^{1} \frac{T_n(x) T_m(x)}{\sqrt{(1 - x^2)}} dx = \begin{cases} 0, \; m \neq n \\ \pi/2, \; n = m \neq 0 \\ \pi, \; n = m = 0 \end{cases} \quad . \quad . \quad (6)$$

[See Reference 4, eqn. (4); the result has been altered by the factor $2^{2n}$ to conform to the normalization adopted here.]

From eqn. (1), therefore,

$$
\left.
\begin{cases}
b_m = \dfrac{2}{\pi} \displaystyle\int_{1}^{1} \dfrac{T_n(ax + b) T_m(x)}{\sqrt{(1 - x^2)}} dx; \; m \geqslant 1 \\[3mm]
b_0 = \dfrac{1}{\pi} \displaystyle\int_{-1}^{1} \dfrac{T_n(ax + b)}{\sqrt{(1 - x^2)}} dx
\end{cases}
\right\} \quad . \quad . \quad (7)
$$

Using eqn. (4) for $T_n (ax + b)$ in eqn. (7),

$$b_m = \frac{2}{\pi} \sum_{r=0}^{[n/2]} \sum_{k=0}^{n-2r} c_{rk} \int_{1}^{1} \frac{T_m(x) x^k}{\sqrt{(1 - x^2)}} dx; \; m \geqslant 1 \quad . \quad (8)$$

[Since $T_m(1) = 1$ for $m \geqslant 0$, eqn. (1) gives

$$T_n(a + b) = \sum_{m=0}^{n} b_m$$

Thus, $b_0$ can be found easily if the $b_m$'s for $m = 1, 2, \ldots, n$ are known; eqn. (7) may therefore be used without special consideration for the case $m = 0$.]

The integral appearing in eqn. (8) is well known [see Reference 4, eqn. (6), again taking into account the different normalizations]:

$$\int_{-1}^{1} \frac{T_m(x)x^k}{\sqrt{(1 - x^2)}} dx = \begin{cases} 0 & \text{if } (k - m) \text{ is odd} \\ 0 & \text{if } k < m \\ \dfrac{\pi}{2^k} \begin{pmatrix} k \\ \dfrac{k - m}{2} \end{pmatrix} & \text{if } (k - m) \text{ is even or zero} \end{cases} \quad (9)$$

Using this result in eqn. (8), the expression for $b_m$ becomes

$$b_m = \sum_{r=0}^{[n/2]} \sum_{k=m}^{n-2r}\!\!{}^{*}\; c_{rk} \frac{1}{2^{k-1}} \begin{pmatrix} k \\ \dfrac{k - m}{2} \end{pmatrix}; \; m \geqslant 1 \quad . \quad . \quad (10)$$

The notation $\Sigma^*$ has been introduced to mean that the sum is extended over odd integers only if the lower summation limit is odd and over even integers only if the lower summation limit is even. Substituting for $c_{rk}$, eqn. (10) gives

$$b_m = (2b)^n \sum_{r=0}^{[n/2]} \frac{(-1)^r \left[ 2\begin{pmatrix} n - r \\ r \end{pmatrix} - \begin{pmatrix} n - r - 1 \\ r \end{pmatrix} \right]}{(2b)^{2r}}$$
$$\times \sum_{k=m}^{n-2r}\!\!{}^{*} \begin{pmatrix} n - 2r \\ k \end{pmatrix} \begin{pmatrix} k \\ \dfrac{k - m}{2} \end{pmatrix} \left( \frac{a}{ab} \right)^k \quad \text{for } m = 1, 2, \ldots \quad (11)$$

The upper limit in eqn. (11) may be replaced by $[(n - m)/2]$ since values of $r$ larger than $[(n - m)/2]$ result in the second sum being zero.

Thus

$$b_m = (2b)^n \sum_{r=0}^{\left[ \frac{n-m}{2} \right]} \frac{(-1)^r \left[ 2\begin{pmatrix} n - r \\ r \end{pmatrix} - \begin{pmatrix} n - r - 1 \\ r \end{pmatrix} \right]}{(2b)^{2r}}$$
$$\times \sum_{k=m}^{n-2r}\!\!{}^{*} \begin{pmatrix} n - 2r \\ k \end{pmatrix} \begin{pmatrix} k \\ \dfrac{k - m}{2} \end{pmatrix} \left( \frac{a}{2b} \right)^k \quad . \quad (12)$$

which is the desired formula. That this is equivalent to Salzer's form may be seen by introducing a new index of summation, $j$, in the second sum, where $j$ is given by the equation $k - m = 2j$. Eqn. (12) becomes

$$b_m = (2b)^{n-m} a^m \sum_{r=0}^{\left[ \frac{n-m}{2} \right]} \left( \frac{-1}{4b^2} \right)^r \left[ 2\begin{pmatrix} n - r \\ r \end{pmatrix} - \begin{pmatrix} n - r - 1 \\ r \end{pmatrix} \right]$$
$$\times \sum_{=0}^{[(n-m)/2]-r} \begin{pmatrix} n - 2r \\ m + 2j \end{pmatrix} \begin{pmatrix} m + 2j \\ j \end{pmatrix} \left( \frac{a^2}{4b^2} \right)^j; \; m \geqslant 1 \quad (13)$$

which is identical with Salzer's formula for $m \geqslant 1$. The single term $b_0$ may be computed from the other $b_m$'s as indicated above, or may also be obtained by taking half the result predicted by eqn. (13) when $m$ is equal to zero. Equivalently, eqn. (13) may be used for all values of $m \geqslant 0$ if $T_0(x)$ is taken to be one-half rather than unity—a device introduced in Reference 1.

### (3) CONCLUSION

By employing the orthogonality properties of the Chebyshev polynomials, a simplified derivation of the Fourier coefficients in the expansion

$$T_n(ax + b) = \sum_{m=0}^{n} b_m T_m(x)$$

has been given. The final result is equivalent to that obtained earlier by Salzer,[1] as seen by a simple change of summation index. The derivation suggests that the orthogonality concept may also be useful in other pattern investigations involving Chebyshev polynomials.

### (4) REFERENCES

(1) SALZER, H. E.: 'Note on the Fourier Coefficients for Chebyshev Patterns', *Proceedings I.E.E.*, Monograph No. 166 R, February, 1956 (**103** C, p. 286).

(2) DuHAMEL, R. H.: 'Optimum Patterns for Endfire Arrays', *Proceedings of the Institute of Radio Engineers*, 1953, **41**, p. 652.

(3) BATEMAN, H.: 'Higher Transcendental Functions' (McGraw-Hill, 1953), Vol. 2, p. 185.

(4) GRÖBNER, W., and HOFREITER, N.: 'Integraltafel—Zweiter Teil—Bestimmte Integrale' (Springer-Verlag, 1950), p. 27.

# VARIATIONS OF CHARACTERISTIC IMPEDANCE ALONG SHORT COAXIAL CABLES

## By J. ALLISON, B.Sc.(Eng.), Ph.D., Graduate.

### SUMMARY

A method is described for determining the local characteristic impedance at any point on a high-frequency coaxial cable. Measurements are made of the deviations from a harmonic series of the resonant frequencies of a short length of open- or short-circuited cable. It is shown how these deviations can be used to calculate the coefficients of a Fourier series describing the impedance variations along the length. Since the measurements are performed at microwave frequencies, the resolution of the impedance changes is considerably better than for lower-frequency methods.

Measurements on an artificially discontinuous cable have allowed the experimental accuracy of the method to be determined, and close agreement has been obtained between the experimentally predicted and the actual impedance changes.

Results from short cable samples indicate that the local variations of characteristic impedance are largely due to changes in the diameter over the dielectric filling.

### LIST OF PRINCIPAL SYMBOLS

$l$ = Length of line.
$Z_m$ = Mean characteristic impedance of line.
$x$ = Distance from end of line.
$Z(x)$ = Local characteristic impedance at the point $x$.
$S(x)$ = Deviation of local characteristic impedance from $Z_0$.
$A_n$ = $n$th coefficient of Fourier series describing $S(x)$.
$\delta$ = Deviation of input impedance from $Z_0$.
$\lambda_l$ = Spatial wavelength of periodic variation of $Z(x)$ along the line.
$V_1$ = Peak voltage applied to line at $x = 0$.
$V$ = Voltage at any point on the resonant line.
$I$ = Corresponding current at any point on the resonant line.
$C_0$ = Capacitance per unit length of transmission line.
$L_0$ = Inductance per unit length of transmission line.

### (1) INTRODUCTION

The effects of impedance irregularities on the input impedance and transmission characteristics of high-frequency coaxial cables have been studied frequently during recent years. Work on the subject can be divided into two main groups. These are the statistical treatment of impedance irregularities and methods for measuring their effects.

Theoretical studies which involve statistical methods[1-5] yield results which are applicable to families of lines. Whereas general conclusions can be drawn as to the electrical behaviour of a group of similar cables, precise information about any specific member of the group is not an objective of this type of theory.

A comprehensive review of methods for ascertaining the form of the impedance irregularities of a specific cable and their effect on its electrical performance has been given by Parcé.[6] The methods reviewed, together with subsequently published techniques, can be divided into four subsidiary groups, as follows:

(*a*) *Determination of the impedance deviation from image-impedance measurements.*—The impedance deviation, $\delta$, is defined as the difference between the input impedance of the cable and its mean characteristic impedance when terminated by the mean characteristic impedance. The real part of the impedance deviation, $\delta_r$, can be found by determining the difference between the two image impedances of the cable at even-harmonic frequencies.[6]

(*b*) *Input-impedance methods.*—Didlaukis and Kaden's[1] measurements were performed at even-harmonic frequencies, the cable being terminated in a resistance $R$ near to $Z_0$. The difference between the measured input impedance and the mean characteristic impedance when measured under these conditions provides a value for $\delta_r$. Parcé[6] shows how this value can be modified to take account of small line attenuations. Cotte[7, 8] shows how the measurement of input impedance at even-harmonic frequencies of a line terminated in its mean characteristic impedance allows the construction of a Fourier series which represents the change of local impedance from the mean characteristic impedance along the length of the cable. He has determined the first ten coefficients of such a series from measurements at frequencies between 300 kc/s and 6 Mc/s on a 75-ohm coaxial cable of length 240 m. A variable-impedance bridge was used for the impedance measurements.

(*c*) *Resonant-frequency methods.*—These techniques involve the determination of the resonant frequencies of a cable which is terminated by an open- or short-circuit. If the line were perfectly uniform, the measured frequencies would form a harmonic series, and the slight deviations from such a series for an actual cable provide a measurement of the irregularities present. Kaden[9] has shown that the mean-square value of the input-impedance changes $\overline{|\delta|^2}$ can be calculated from the mean-square deviations of the resonant frequencies from a true harmonic series. He has measured the frequency deviations on a cable of length 285 m, at frequencies up to 4 Mc/s, using a differential bridge method, thus providing 16 harmonics for the calculation of $\overline{|\delta|^2}$.

(*d*) *Pulse techniques.*—Pulse test sets enable the relative magnitudes of irregularities to be measured in terms of the return loss of echo pulses reflected from the irregularities when short pulses of carrier frequency are fed into the cable. Roberts[10] has used a method which employs pulses 0·3 microsec long, of a carrier frequency of 20 Mc/s, to investigate the impedance changes in drum lengths and longer jointed lengths of high-frequency coaxial cable. The accuracy of location of an irregularity in such a system is estimated to be within $\pm 15$ m.

The work described here began with the aim of providing additional information for a study of input-impedance variations of cables over frequency bands around 3 000 and 10 000 Mc/s which was already in progress. Some indication was required of the changes of impedance to be expected along the length of the cables being examined by this other technique. Thus a method which does not provide statistical results concerning a family of cables but gives information about a particular cable was required. Also, because of the high operating frequency, it

would be preferable if the impedance deviations could be ascertained over quite small lengths—of the order of a few wavelengths at these frequencies.

The method evolved for determining the form and position of irregularities has the following features:

(i) Information is provided about the changes of impedance along a relatively short length, which allows a graph of $S(x)$ against distance along this specific cable to be drawn.

(ii) Since the measurements are performed at microwave frequencies, the linear resolution of $S(x)$ is considerably better than for lower-frequency methods.

(iii) The only parameters to be measured are changes in resonant frequency. This eliminates the necessity for a slotted line and associated equipment, which would be required at high frequencies if input-impedance changes were to be measured.

On the other hand, the method has the disadvantage that several signal generators may be required to provide sufficient harmonic frequencies. Also, when the frequency deviations are found, their conversion to give a graph of $S(x)$ against $x$ is rather long and arduous.

## (2) DETERMINATION OF IMPEDANCE VARIATIONS ALONG AN IRREGULAR TRANSMISSION LINE BY MEASUREMENT OF THE RESONANT FREQUENCIES OF THE OPEN- AND SHORT-CIRCUITED LINE

Consider a lossless, uniform transmission line of length $l$, which is short-circuited at the far end and has a sinusoidal voltage applied to it [see Fig. 1(a)]. When the line is an integral number
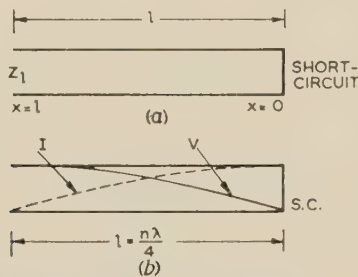


Fig. 1.—Resonant short-circuited transmission line.

of quarter wavelengths long, it will resonate, and the voltage and current relationships are, as in Fig. 1(b):

$$V = -2jV_1 \sin(n\pi x/2l) . \quad . \quad . \quad . \quad . \quad (1)$$

$$I = (2V_1/Z_m) \cos(n\pi x/2l) \quad . \quad . \quad . \quad . \quad (2)$$

When $n$ is odd, there will be an open-circuit at $x = l$, and when $n$ is even there will be a short-circuit there.

The energy stored under these conditions is given by

$$W = \frac{1}{4} \int_0^l (C_0|V|^2 + L_0|I|^2)dx \quad . \quad . \quad . \quad . \quad (3)$$

Hence, from eqns. (1), (2) and (3),

$$W = V_1^2 C_0 l = V_1^2 L_0 l / Z_m^2 \quad . \quad . \quad . \quad . \quad (4)$$

Now consider the line to be non-uniform, the irregularities being assumed very small. The local values of $C$ and $L$ are changed such that

$$\begin{matrix} C(x) = C_0 + \Delta C(x) \\ L(x) = L_0 + \Delta L(x) \end{matrix} \Bigg\} \quad . \quad . \quad . \quad . \quad (5)$$

And

$$\int_0^l \Delta C dx = \int_0^l \Delta L dx = 0 \quad . \quad . \quad . \quad . \quad (6)$$

Also, since the irregularities are assumed to be small,

$$\frac{\Delta C}{C_0} \ll 1 \text{ and } \frac{\Delta L}{L_0} \ll 1 . \quad . \quad . \quad . \quad (7$$

If the line is imagined to be lossless and initially uniform with no connections to external sources, and is subsequently deformed infinitely slowly into the non-uniform line with very small irregularities just described, the work done will be equal to the change of stored energy and can be shown to be

$$\Delta W = \frac{1}{4} \int_0^l (\Delta C|V|^2 + \Delta L|I|^2)dx \quad . \quad . \quad (8$$

Hence, using eqns. (1), (2) and (6),

$$\Delta W = \frac{1}{2} \int_0^l V_1^2 \left(\frac{\Delta L}{Z_m^2} - \Delta C\right) \cos\left(\frac{n\pi x}{l}\right) dx \quad . \quad . \quad (9$$

The fractional change in stored energy is then, from eqns. (4) and (9),

$$\frac{\Delta W}{W} = \frac{1}{2l} \int_0^l \left(\frac{\Delta L}{L_0} - \frac{\Delta C}{C_0}\right) \cos\left(\frac{n\pi x}{l}\right) dx \quad . \quad . \quad (10$$

Also, because of the assumption given in eqn. (7),

$$\frac{S(x)}{Z_m} \simeq \frac{1}{2}\left(\frac{\Delta L}{L_0} - \frac{\Delta C}{C_0}\right) \quad . \quad . \quad . \quad . \quad (11$$

Hence

$$\frac{\Delta W}{W} = \frac{1}{l} \int_0^l \frac{S(x)}{Z_m} \cos\left(\frac{n\pi x}{l}\right) dx \quad . \quad . \quad (12$$

We now apply the theorem of adiabatic invariance of action, which has been proved for electromagnetic resonators by Maclean.[11] Action in this context is defined as the product of stored energy and period of oscillation, and is constant under the assumed conditions of 'slow' deformation. It follows that the fractional change in energy resulting from such a deformation is accompanied by the same fractional change in resonant frequency.

Hence, from eqn. (12) we can write at once

$$\frac{\Delta f_n}{f_n} = \frac{1}{l} \int_0^l \frac{S(x)}{Z_m} \cos\left(\frac{n\pi x}{l}\right) dx \quad . \quad . \quad (13$$

It can be shown that, subject to certain assumptions, $S(x)/Z_m$ is real and independent of frequency.[7] This quantity can be represented by a Fourier half-range series for values of $x$ defined by $0 \leqslant x \leqslant l$ as follows:

$$\frac{S(x)}{Z_m} = \sum_{n=1}^{\infty} A_n \cos\frac{n\pi x}{l} \quad . \quad . \quad . \quad . \quad (14$$

Thus, from eqns. (13) and (14) and the usual formula for the Fourier coefficients, we see that

$$\frac{S(x)}{Z_m} = \sum_{n=1}^{\infty} \frac{2\Delta f_n}{f_n} \cos\left(\frac{n\pi x}{l}\right) \quad . \quad . \quad (15$$

If the same length of transmission line is now considered short-circuited at $x = l$, the voltage and current relationships are given by

$$V = 2V_1 \cos\left(\frac{n\pi x}{2l}\right) \quad . \quad . \quad . \quad (16$$

$$I = (2jV_1/Z_m) \sin\left(\frac{n\pi x}{2l}\right) \quad . \quad . \quad . \quad (17$$

When $n$ is odd there will be an open-circuit at $x = 0$, and when $n$ is even there will be a short-circuit there. Proceeding as before, the fractional change in resonant frequency is found to be

$$\frac{\Delta f_n^{(2)}}{f_n} = -\frac{1}{l} \int_0^l \left[ \frac{S(x)}{Z_m} \cos\left(\frac{n\pi x}{l}\right) \right] dx \quad . \quad . \quad (18)$$

Comparing eqns. (17) and (13) it is seen that

$$\Delta f_n^{(2)} = -\Delta f_n^{(1)}$$

and

$$A_n^{(2)} = -A_n^{(1)} \quad . \quad . \quad . \quad . \quad . \quad (19)$$

Thus the resonant frequencies of an irregular line of length $n\lambda/4$ when supporting a voltage sine wave (i.e. short-circuited at $x = 0$ and open-circuited at $x = l$ for $n$ odd, or short-circuited at both ends for $n$ even) are given by

$$f_n^{(1)} = f_n + \Delta f_n \quad . \quad . \quad . \quad . \quad . \quad (20)$$

where $f_n$ is the resonant frequency for a uniform line. Also, the resonant frequencies of the same line when supporting a voltage cosine wave (i.e. short-circuited at $x = l$ and open-circuited at $x = 0$ for $n$ odd, or open-circuited at both ends for $n$ even) are given by

$$f_n^{(2)} = f_n - \Delta f_n \quad . \quad . \quad . \quad . \quad (21)$$

Substituting eqns. (21) and (20) into eqn. (15) gives

$$\frac{S(x)}{Z_m} = \sum_{n=1}^{\infty} \frac{2(f_n^{(1)} - f_n^{(2)})}{f_n^{(1)} + f_n^{(2)}} \cos\left(\frac{n\pi x}{l}\right) \quad . \quad . \quad (22)$$

Thus, by measuring the pairs of resonant frequencies $f_n^{(1)}$ and $f_n^{(2)}$ of an irregular transmission line, it is possible, using eqn. (22), to calculate the local characteristic impedance at any point on the line.

### (2.2) Periodic Variation of $S(x)$

It is possible for the variation of $S(x)$ to be of a cyclic nature. When this occurs, then, at a frequency such that the irregularity is repeated at half-wavelength intervals, successive reflections become additive causing very large input-impedance deviations. Suppose that the periodicity is such that $m$ complete spatial wavelengths, $\lambda_i$, plus a fraction of a spatial wavelength are included in the line of length $l$. If the distances from the extremities of the line to the nearest positive maximum values of $S(x)$ are $a\lambda_i$ and $b\lambda_i$, the fundamental component of the irregularity can be defined as

$$S(x)/Z_m \propto \cos\left[2\pi(x/\lambda_i - a)\right] \quad . \quad . \quad . \quad (23)$$

The Fourier coefficients of the series defining $S(x)$ as given by eqn. (23) are found to be

$$A_n = \frac{4l[-\sin(2\pi a) \pm \sin 2\pi(l/\lambda_i - a)]}{\lambda_i \pi (n^2 - 4l^2/\lambda_i^2)} \quad . \quad (24)$$

It is evident from this equation that there will be a maximum value of $A_n$ when

$$\lambda_i \simeq 2l/n \quad . \quad . \quad . \quad . \quad . \quad (25)$$

If the value of $n$ which gives the coefficient with the largest magnitude is $n^1$, there will be further maxima when $n = 2n^1$, $3n^1$, etc., due to the harmonic components of the irregularity.

It is therefore possible to find whether any cyclic variation of $S(x)$ is present in a sample simply by inspection of the magnitudes of the experimentally-derived Fourier coefficients. Also, knowing the order of the coefficient with maximum magnitude $n^1$, the spatial wavelength of the fundamental of the irregularity can be calculated from eqn. (25). For example, if a line, containing

a sinusoidal variation of $S(x)$ including five complete spatial wavelengths in its length, were examined by the resonant-frequency technique, then, assuming $a = 0 \cdot 01$ and $b = 0 \cdot 2$, the Fourier coefficients obtained would have the following relative magnitudes:

| $n$ | 1 | 2 | 3 | 4 | 5 | 6 | 7 |
|---|---|---|---|---|---|---|---|
| $A_n$ | $-0 \cdot 04$ | $+0 \cdot 08$ | $-0 \cdot 04$ | $+0 \cdot 09$ | $-0 \cdot 05$ | $+0 \cdot 11$ | $-0 \cdot 07$ |

| $n$ | 8 | 9 | 10 | 11 | 12 | 13 | 14 |
|---|---|---|---|---|---|---|---|
| $A_n$ | $+0 \cdot 19$ | $-0 \cdot 15$ | $+0 \cdot 84$ | $+0 \cdot 39$ | $-0 \cdot 25$ | $+0 \cdot 07$ | $-0 \cdot 10$ |

The periodicity of the cyclic variation of $S(x)$ is thus apparent without having to sum the Fourier series describing $S(x)$.

### (3) EXPERIMENTAL PROCEDURE FOR MEASURING THE FREQUENCY DEVIATIONS

A schematic of the measuring apparatus is shown in Fig. 2. Three signal generators, each having a calibration accuracy better than 1%, supply a series of about 20 harmonic frequencies
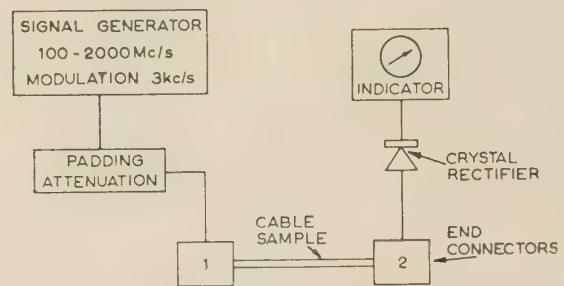


Fig. 2.—Block schematic of the measuring equipment.
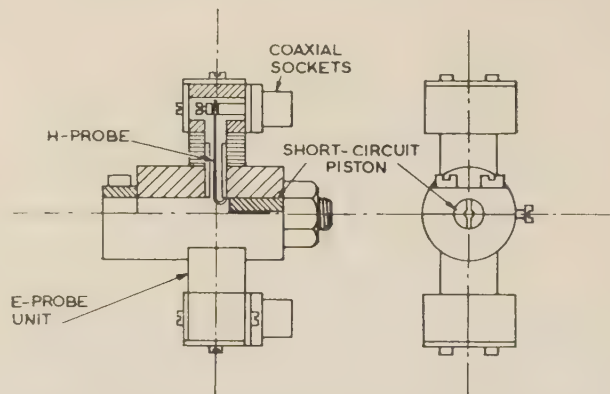


Fig. 3.—End connectors, showing arrangement of probes.

from 100 to 2000 Mc/s. The signal is modulated by a square wave whose frequency is 3000 c/s, and fed into the cable by either an H-probe for a short-circuited input or an E-probe if the input is open-circuited. The arrangement of the end connectors and probes is shown in detail in Fig. 3. The cable sample is arranged to have an electrical length of a quarter of the wavelength corresponding to the fundamental frequency. At its far end the signal is again received by an E- or H-probe, depending on the termination, detected by a crystal, the arrangement of which is shown in Fig. 4, and displayed on a selective amplifier indicator.
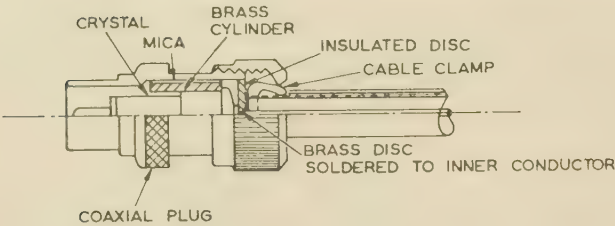
Fig. 4.—Arrangement of crystal detector.

The technique for determination of the frequency deviations is dependent on whether the resonant frequency is close to an odd or even harmonic of the fundamental. For the odd harmonics, end 1 is open-circuited whilst end 2 is short-circuited and the signal generator is tuned until the meter at end 2 indicates resonance. End 1 is then short-circuited whilst end 2 is open-circuited, different probes, of course, being employed, and the signal generator is again tuned to resonance. The fractional difference between the frequencies for the two resonance conditions gives, from eqn. (22), a value for the Fourier coefficient corresponding to the particular harmonic used. For even resonant frequencies, when the line is an integral number of half-wavelengths long, a similar procedure is followed, but this time the difference in resonant frequencies is found with the cable originally open-circuited at both ends and then short-circuited at both ends.

This measuring technique requires that the open- and short-circuited lengths of air-filled line at the ends of the cable can be represented by the same equivalent length of open- or short-circuited homogeneous line having the same properties as those of the cable. If one end of the cable is open- or short-circuited as in Fig. 5, it can be shown that this condition is satisfied if

$$l_2' = \left[ \frac{\log_{10} (r_3/r_1)}{\log_{10} (r_2/r_1)} \right]^2 \epsilon_r l_1 \quad . \quad . \quad . \quad . \quad (26)$$

where $l_2'$ is the equivalent length of $l_2$, which allows for the fringing field at its end, and $\epsilon_r$ is the relative permittivity of the dielectric in the cable.
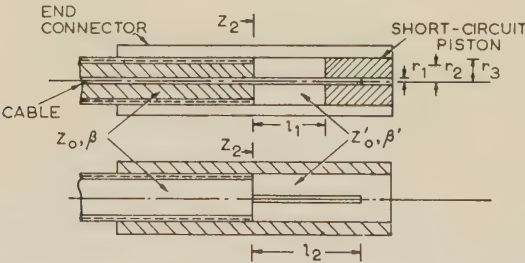


Fig. 5.—Open- and short-circuited termination of the transmission line.

Thus, to determine $l_1$ corresponding to a chosen open-circuited length $l_2$, the equivalent shunt capacitance of the fringing field which is a function of $r_1$ and $r_3$ must first be calculated.[12] The distributed capacitance of the air-filled line is then deduced[13] and the shunt capacitance is transformed to an equivalent length of the same line. This length, when added to $l_2$, gives the length $l_2'$. Knowing $l_2'$, the required short-circuited length $l_1$ can be calculated immediately from eqn. (26).

## (4) EXPERIMENTAL VERIFICATION OF METHOD AND RESULTS ON CABLE SAMPLE

To provide a standard by which the accuracy of the method could be ascertained, an artificial discontinuity of known magni-
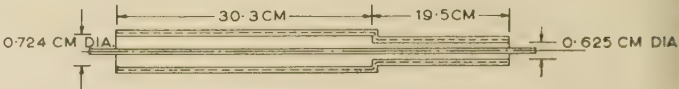


Fig. 6.—Cable with artificial discontinuity.

tude was introduced into a dielectric-filled cable (Fig. 6). The step in the line was formed by turning down the dielectric to the required diameter and then binding the braiding back into place. The resulting line had a uniform characteristic impedance $Z_{m1}$ over one section of its length and another constant characteristic impedance $Z_{m2}$ over the rest. The position of the sudden change of characteristic impedance was chosen in an arbitrary manner.

On testing the cable, as described in the previous Section, at 20 harmonic frequencies ranging from 100 to 2 000 Mc/s, the frequency deviations obtained yield values of $A_n$ shown in Table 1. The function $S(x)$ is now completely defined for this

### Table 1

FOURIER COEFFICIENTS OBTAINED FOR ARTIFICIALLY STEPPED CABLE

| $n$ | 1 | 2 | 3 | 4 | 5 | 6 | 7 |
|---|---|---|---|---|---|---|---|
| $A_n$, % | 4·92 | −1·68 | −0·87 | 1·29 | −0·18 | −0·75 | 0·57 |

| $n$ | 8 | 9 | 10 | 11 | 12 | 13 | 14 |
|---|---|---|---|---|---|---|---|
| $A_n$, % | −0·22 | −0·58 | 0·18 | 0·37 | −0·37 | −0·07 | −0·36 |

| $n$ | 15 | 16 | 17 | 18 | 19 | 20 |
|---|---|---|---|---|---|---|
| $A_n$, % | −0·18 | −0·20 | −0·29 | 0 | −0·25 | +0·16 |

particular line, and values of $S(x)$ for any specific value of $x$ can be obtained by summing the series as in eqn. (20). This has been done to give graphs of $S(x)$ along the line length for summations of 5, 10 and 20 terms of the series (Fig. 7). It is evident from the graphs that, provided that sufficient terms of the summation are obtained, the method provides a very good approximation to the change of impedance along the line length. Whereas the summation of five terms of the series gives evidence as to the approximate magnitude of impedance changes, more terms are required to determine the form and position of the changes. For instance, if 20 coefficients are found, then, neglecting end effects, the amplitude of the irregularity is given to better than $\pm 1\%$ and its position is located to within $2\%$ of the cable length. Errors which arise through taking a series with a finite number of terms to represent an infinite Fourier series will be discussed more fully in Section 5.

After these errors, together with others which will be discussed in more detail in the next Section, had been reduced to a minimum, actual samples of polythene cable were examined by the frequency-deviation method. Thus, the frequency deviations of a length of UR65 type cable when tested as 12 harmonics of 150 Mc/s yield coefficients $A_n$, as shown in Table 2. The change in impedance along the length of this cable as calculated from the coefficients $A_n$ and eqn. (20) is shown in Fig. 8(a), whilst the change of impedance along the same length as calculated from mean diameter measurements over the polythene, assuming a uniform inner-conductor diameter, is given in Fig. 8(b).
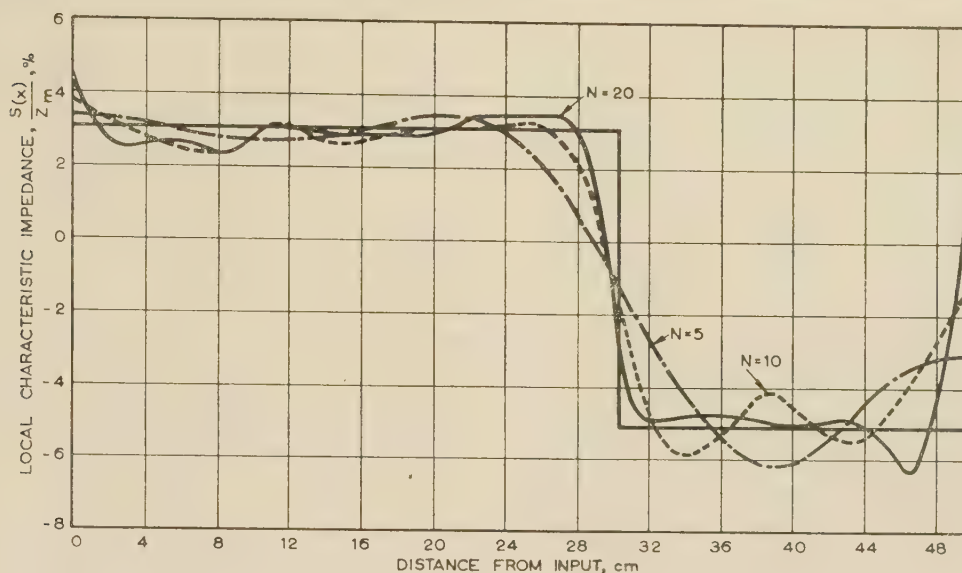
Fig. 7.—Variation of local characteristic impedance along the artificially discontinuous cable.

**Table 2**

FOURIER COEFFICIENTS OBTAINED FOR CABLE TYPE UR65

| $n$ | 1 | 2 | 3 | 4 | 5 | 6 |
|---|---|---|---|---|---|---|
| $A_n$, % | 0·11 | 0·14 | 0 | 0·12 | 0·04 | 0·04 |

| $n$ | 7 | 8 | 9 | 10 | 11 | 12 |
|---|---|---|---|---|---|---|
| $A_n$, % | 0·02 | 0·01 | 0·03 | −0·03 | 0 | 0·02 |

Fig. 8(a) is typical of results obtained on several cables of type UR65. There appears to be no impedance deviation as great as $\frac{1}{2}$% along the short lengths examined. Thus, if these deviations are taken to represent a typical section of a random deviation along a longer length of cable, it can be shown[9] that the r.m.s. input-impedance deviation for a family of cables is of the order of 0·2%.

On the other hand, the particular specimens examined were taken from a longer length which gave input-impedance deviations over a frequency band around 3 000 Mc/s much greater than the expected value, when measured by a technique due to Blackband.[14] The large input-impedance variations over this particular frequency band are due to components of the cable irregularity which have a spatial wavelength between 4·35 and 5·0 cm. However, any periodicity of $S_{(x)}$ is not apparent from the magnitude of the Fourier coefficients as given in Table 2. This is because the impedance deviations are so small that it would be very difficult to select any one coefficient whose maximum magnitude could definitely be attributed to a periodic variation of $S_{(x)}$.

The impedance deviation for the cable length as measured [Fig. 8(a)] bears some resemblance to that calculated from diameter measurements over the polythene dielectric [Fig. 8(b)]. The r.m.s. impedance changes calculated from the two graphs are 0·001 8 and 0·001 3, respectively. This seems to support the argument that the impedance changes along the cable sample measured are mainly due to variations in the diameter over the polythene dielectric. This assumption has been substantiated by measurements made on other samples of the same cable.
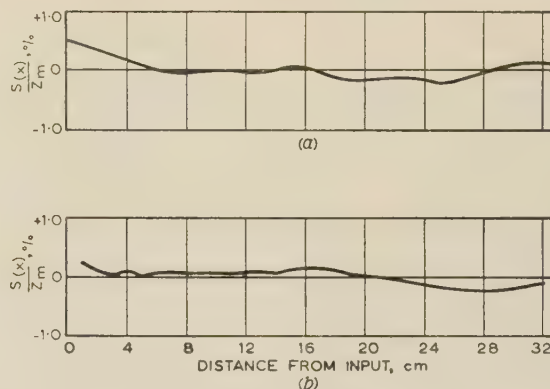


Fig. 8.—Variation of local characteristic impedance along sample of cable, type UR65.

(a) From resonant-frequency measurements.
(b) From measurements of diameters over the dielectric.

## (5) ERRORS AND LIMITATIONS OF THE METHOD

### (5.1) Effects of Probe Penetration on Resonant Frequency

Consider a uniform line of length $l$ terminated by an open-circuit. The line will resonate at a frequency given by

$$f_n = nv/4l$$

If an E-probe is introduced into the plane of the open-circuit it will act, for small penetrations, as a shunt susceptance $C_1$, and the resonant frequency of the combination of line and probe will change from $f_n$ by a value $\Delta f'_n$.

If the probe were introduced very slowly into a supposedly lossless ideal line, the action theorem[11] would give

$$\frac{\Delta f'_n}{f_n} = \frac{\Delta W'}{W} \qquad . \quad . \quad . \quad . \quad (27)$$

where $\Delta W'$ = Change in stored energy due to $C_1$.

$W$ = Initial stored energy.

The right-hand side of eqn. (27) is independent of frequency for a particular value of $C_1$. Hence, for constant probe penetrations,

$$\Delta f'_n \propto f_n \qquad . \quad . \quad . \quad . \quad . \quad (28)$$

Also, for a particular value of $f_n$,

$$\Delta f_n' \propto C_1 \quad . \quad . \quad . \quad . \quad . \quad (29)$$

since the stored energy of the probe, $\Delta W'$, is proportional to its equivalent capacitance.

Let us consider the measuring circuit to be approximately
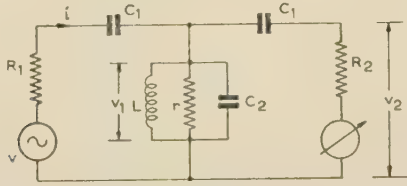
**Fig. 9.**—Equivalent circuit of measuring apparatus.

represented by Fig. 9. The probes at either end of the resonant line are assumed to have the same capacitance $C_1$.

Then

$$\frac{|v_2|}{v} = \omega R_2 Q \frac{C_1^2}{C_2} \quad . \quad . \quad . \quad . \quad (30)$$

It is evident from this equation that

$$\frac{\text{Power to indicator}}{\text{Power from generator}} \propto C_1^4 \quad . \quad . \quad . \quad . \quad (31)$$

The change in resonant frequency indicated by eqn. (29) will, to the first order, be independent of frequency deviations due to impedance irregularities and is only a function of the probe penetration. Thus, for large probe penetrations, it is possible for the frequency deviations due to the probes to be of the same order of magnitude as those corresponding to the irregularity content of the cable. This could cause considerable error in the experimental results. The probe coupling should therefore be as light as possible to reduce such errors to a minimum. Unfortunately, as the probe is withdrawn the signal to the indicator is reduced very considerably, as shown by eqn. (31). Again, the amplification of the indicator is limited by noise in the system. Thus the choice of the optimum probe penetration is a compromise between minimum probe intrusion and adequate power to the indicator.

The change in resonant frequency due to the changing penetration of one probe, the others remaining at constant depths, can be found experimentally. Fig. 10(a) shows the changes which occur at frequencies near to 300 Mc/s, whilst Fig. 10(b) shows the effect around 900 Mc/s. It will be seen that these curves agree fairly well with the relationship given in eqn. (28) that, for constant probe penetrations, the change in resonant frequency is proportional to the frequency. It is also evident that, for the particular test arrangement employed, the probes should be at least $0\cdot13$ in from the inner conductor if they are to have a negligible effect on the resonant frequency. Again, since the E- and H-probes alter the resonant frequency in different directions, frequency deviations due to probes will tend to cancel for the odd harmonics when the measurement involves the use of an E-probe at end 1 and an H-probe at end 2 to be used alternately with an H-probe at end 1 and an E-probe at end 2. Probe errors will be very pronounced at even harmonics, however, since E-probes at ends 1 and 2 are used alternatively with H-probes at ends 1 and 2.

### (5.2) Validity of the Approximate Formula for $S(x)$ with a Finite Number of Fourier Coefficients

If measurements are performed at $N$ harmonic frequencies, allowing only $N$ Fourier coefficients to be calculated, the value
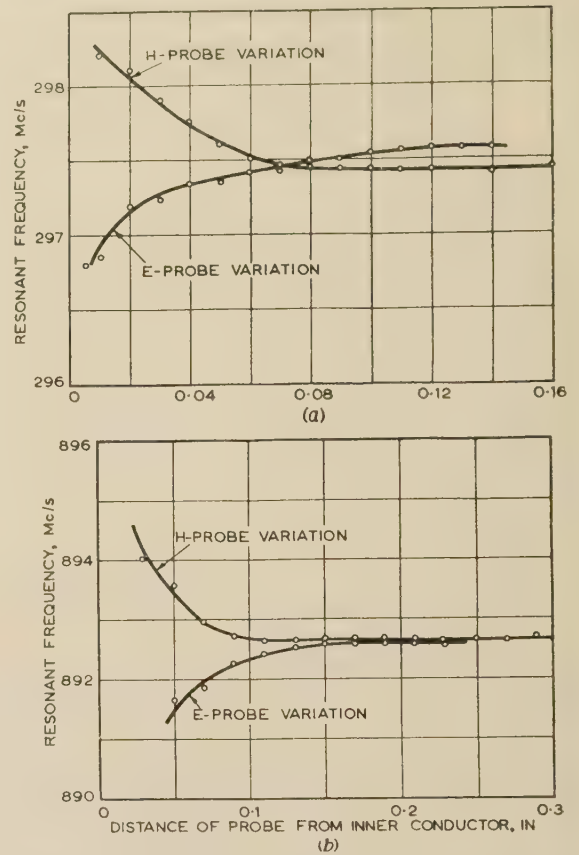
**Fig. 10.**—Effect of probe intrusion on resonant frequency.

(a) Frequencies around 300 Mc/s.
(b) Frequencies around 900 Mc/s

$S^N(x)$ obtained by summing $N$ terms of the series describing the impedance irregularities is only approximately equal to $S(u)$, the actual local impedance deviation. The nearness of the approximation is found as follows:

$$\frac{S^N(x)}{Z_m} = \frac{2}{l} \sum_{n=1}^{n=N} \int_0^l \frac{S(u)}{Z_m} \cos\left(\frac{n\pi u}{l}\right) du \cos\left(\frac{n\pi x}{l}\right) \quad . \quad (32)$$

Interchanging the integral sign and the summation sign and summing gives

$$\frac{S^N(x)}{Z_m} = \frac{1}{2l} \int_0^l \left( \frac{S(u)}{Z_m} \left\{ \frac{\sin\left[\frac{2N+1}{2}\left(\frac{\pi u}{l} + \frac{\pi x}{l}\right)\right]}{\sin\left[\frac{1}{2}\left(\frac{\pi u}{l} + \frac{\pi x}{l}\right)\right]} \right.\right.$$
$$\left.\left. + \frac{\sin\left[\frac{2N+1}{2}\left(\frac{\pi u}{l} - \frac{\pi x}{l}\right)\right]}{\sin\left[\frac{1}{2}\left(\frac{\pi u}{l} - \frac{\pi x}{l}\right)\right]} \right\} \right) du \quad (33)$$

Consider the specific case of a line with a local characteristic impedance which is defined by

$$S(u) = A \text{ when } 0 \leqslant u \leqslant l/2$$
$$= 0 \text{ elsewhere}$$

If this condition is substituted in eqn. (33) it can be shown that, for values of $x$ near to $l/2$,

$$\frac{S^N(x)}{Z_m} = \frac{2A}{(2N+1)\pi}\left[\sin\frac{2N+1}{4}\left(\frac{2\pi x}{l}+\frac{\pi}{2}\right)\sin\frac{2N+1}{4}\frac{\pi}{2}\right]$$

$$+\frac{A}{\pi}\left\{Si\left[\frac{2N+1}{2}\left(\frac{\pi}{2}-\frac{\pi x}{l}\right)\right]+Si\left(\frac{2N+1}{2}\frac{\pi x}{l}\right)\right\}$$

$$\cdots\quad(34)$$

This equation has been evaluated for various values of $N$, and graphs of $S^N(x)/Z_m$ versus distance along the line are shown in
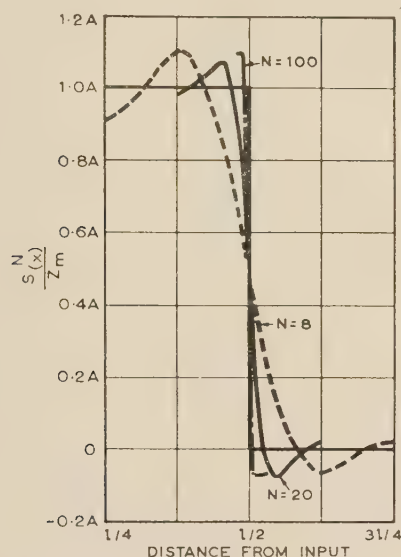
Fig. 11.—Nearness of the approximate formula for the local characteristic impedance.

Fig. 11. These indicate the nearness of the approximate value to the actual local impedance for finite numbers of coefficients of the Fourier series.

**(5.3) Conditions at Short-Circuited Termination of Line and their Effect on the Resonant Frequency**

During preliminary investigations on a cable sample open-circuited at one end and short-circuited at the other and resonating at a frequency of 300 Mc/s, it was found that rotation of the short-circuit plunger could cause changes greater than $0\cdot1\%$ in the measured resonant frequency. Further, it was possible for these changes to be doubled when the line resonated at an even harmonic and was short-circuited at either end. The changes were thought to be due either to non-contact of the plunger with the inner conductor or to contact of the inner conductor with the plunger in a plane different from that of the short-circuit. Analysis indicates that the latter possibility is most likely to cause errors of the same magnitude as those encountered experimentally.

The method used to eliminate errors of this type is shown in detail in Fig. 3. The short-circuiting piston is slotted longitudinally and a set-screw compresses it slightly to ensure good contact with the inner conductor at the plane of the short-circuit. It can be shown that changes in resonant frequency due to the narrow slots in the piston are less than $0\cdot01\%$, and errors due to this cause are therefore entirely negligible.

**(5.4) Frequency Drifts of the Signal Generators**

The difference between the frequencies for the two resonance conditions of each Fourier coefficient, as described in Section 3, was measured using the calibrated vernier of the slow-motion drive controlling the signal generator. The signal generator was tuned to one resonant frequency, the line terminations were altered as described and the vernier was adjusted until resonance was again indicated. In this way, it was possible to detect frequency changes of less than $0\cdot03\%$ of the mean frequency. This operation at each near harmonic could be carried out very quickly. Since the frequency drift of each signal generator used is claimed to be better than $\pm0\cdot005\%$ in 15 min once fully warmed up, negligible error due to this cause is to be expected.

Another source of error is frequency pulling of the main signal generator by the different load impedances presented to it at each resonant frequency. This is eliminated in the actual test equipment by connecting a long length of coaxial cable between the oscillator and the test length which acts as a padding attenuator and virtually isolates the signal generator from impedance changes during the test.

**(6) CONCLUSIONS**

The method described in Sections 2 and 3 can provide a very good approximation to the impedance changes along a length of coaxial cable, provided that the errors discussed in Section 5 are reduced to a negligible level.

Whilst the actual experimental determination of the frequency deviations at one particular harmonic is quite simple, the evaluation of a series of Fourier coefficients and the interpretation of the results into a graph of impedance deviations, $S(x)$, along the length of the cable is long and tedious. A harmonic synthesizer would be found invaluable for summation of the Fourier series.

Since the errors described previously are not entirely eliminated and because of the various assumptions made in the theory, the smallest impedance change which can be measured by the present techniques is limited to the order of $0\cdot2\%$. Whereas, in theory, this performance is capable of improvement by reduction of errors and a more precise theory of probe effects, it is doubtful whether the effort would be justified.

**(8) REFERENCES**

(1) DIDLAUKIS, M., and KADEN, H.: 'Die inneren Ungleichmässigkeiten von koaxialen Breitbandkabeln', *Elektrische Nachrichten-Technik*, 1937, **14**, p. 13.
(2) METZ, P., and PFLEGER, W.: 'Irregularities in Broad-Band Wire Transmission Circuits', *Bell System Technical Journal*, 1937, **16**, p. 541.
(3) BRILLOUIN, L.: 'Irregularities in Telephone and Television Coaxial Cables', *Electrical Communication*, 1938, **17**, p. 164.
(4) CLARKE, W. W. H., and HINCHLIFFE, J. D. S.: 'The

Evaluation of Cable Irregularities at Very High Frequencies', *Proceedings I.E.E.*, Monograph No. 75 R, September, 1953 (**101,** Part IV, p. 55).

(5) ROSEN, A.: 'The "Unit" Treatment of Impedance Irregularities and its Application to Long Lines', *ibid.*, Monograph No. 98, May, 1954 (**101,** Part IV, p. 271).

(6) PARCÉ, L.: 'Paires concentrique pour hautes fréquences', *Annales des Postes, Télégraphes et Téléphones*, 1939, **28,** p. 362.

(7) COTTE, M.: 'La détermination des écarts d'impédance locale dans un câble et de la function de correlation de ces écarts', *Bulletin de la Société Française des Électriciens*, 1948, **8,** p. 16.

(8) COTTE, M.: 'Étude d'une longueur de fabrication de câble par des mesures d'impédance terminale', *Câbles et Transmission*, 1955, **9,** p. 161.

(9) KADEN, H.: 'Über ein Verfahren zer Messung von Breit-band-kabeln', *Telegraph und Fernsprechtechnik*, 1936, **25,** p. 322.

(10) ROBERTS, F. F.: 'A Pulse Test Set for the Measurement of Small Impedance Irregularities in High Frequency Cables', *Proceedings I.E.E.*, Paper No. 736 R, January, 1949 (**96,** Part III, p. 17).

(11) MACLEAN, W. R.: 'The Resonator Action Theorem', *Quarterly of Applied Mathematics*, 1945, **2,** p. 329.

(12) WHINNERY, R., and JAMIESON, H. W.: 'Coaxial Line Discontinuities', *Proceedings of the Institute of Radio Engineers*, 1944, **32,** p. 695.

(13) JACKSON, W.: 'High Frequency Transmission Lines' (Methuen, 1945).

(14) BLACKBAND, W. T., and BROWN, D. R.: 'The Two-Point Method of Measuring Characteristic Impedance and Attenuation of Cables at 3 000 Mc/s', *Journal I.E.E.*, 1946, **93,** Part IIIA, p. 1383.

# TRANSFORMATION OF THE SMITH CHART THROUGH LOSSLESS JUNCTIONS

## By H. V. SHURMER, M.Sc., Ph.D., Associate Member.

### SUMMARY

It is frequently necessary, when using microwave transmission systems, to determine the impedance on one side of a lossless junction in terms of a known impedance on the other side. The paper provides a rigorous analysis of the relation between Smith charts for the two sides of the junction by utilizing the theory of a complex variable. Pairs of reference planes are chosen so that an open-circuit at the first plane corresponds to an open-circuit at the second, which is on the other side of the junction. The transforming section is described in terms of the reflection coefficient at the first plane when the line containing the other is matched. The circles of constant reflection coefficient, etc., which constitute a Smith chart corresponding to the first plane, are transformed mathematically into corresponding circles at the second plane. A universal chart is derived which enables circles of constant voltage standing-wave ratio (or reflection coefficient) to be transformed readily from one plane to the other.

### LIST OF SYMBOLS

$\rho, \sigma$ = Complex reflection coefficient for planes 1 and 2, respectively.

$k$ = Radius when vector $\rho$ varies in such a manner as to describe a circle.

$K$ = Radius when vector $\sigma$ varies in such a manner as to describe a circle.

$a$ = Vectorial displacement of centre from origin when vector $\rho$ varies in such a manner as to describe a circle.

$A$ = Vectorial displacement of centre from origin when vector $\sigma$ varies in such a manner as to describe a circle.

$l = \varepsilon^{j2\phi}$.

$\phi$ = Argument (phase) of $\rho$.

$z_1$ = Normalized impedance, plane 1.

$Z_{01}$ = Characteristic impedance, plane 1.

$z_2$ = Normalized impedance, plane 2.

$Z_{02}$ = Characteristic impedance, plane 2.

$Z_{12}$ = Value of $z_2$ corresponding to iconocentre.

$r_1$ = Normalized resistance, plane 1.

$r_2$ = Normalized resistance, plane 2.

$x_1$ = Normalized reactance, plane 1.

$x_2$ = Normalized reactance, plane 2.

$\left. \begin{array}{l} b, c \\ \beta, \gamma \end{array} \right\}$ = Complex constants.

$r_{12}, x_{12}$ = Co-ordinates of iconocentre, plane 2.

$\Delta r_1, \Delta x_1$ = Displacements of $r_1$ and $x_1$, respectively.

The complex conjugate is denoted by the bar, e.g. $\bar{a}$, $\bar{b}$, etc.

### (1) INTRODUCTION

The paper is concerned with the problem of the transformation of impedance through lossless networks. Whereas previous treatments of a more general nature by Deschamps,[1] Storer et al.[2] and by Dukes[3,4] use rather tedious studies in plane geometry with elaborate graphical constructions, in the present work the theory of the complex variable is applied to the graphical representation of reflection coefficient in the well-known Smith chart.[5,6] The results appear in a particularly clear and easily applicable form if the reference planes on either side of the network are chosen appropriately.

The practical application of these results is illustrated by examples relating to the design of microwave crystal valves. The r.f. impedance of a crystal is measured in the coaxial line, but is controlled by the contact between the whisker and the semi-conductor. The circuit in the crystal body between the contact and the coaxial line may be represented as a lossless network whose parameters are measured or calculated from the dimensions. The analysis then enables the contact impedance to be calculated easily in terms of impedance measurements in the coaxial line.

Coaxial-line crystal valves are often used in conjunction with waveguide/coaxial-line transformers which are by no means matched although their properties can be measured and specified. The analysis shows a simple way of calculating the impedance of a crystal valve as 'seen' through one transformer in terms of its impedance measured through another.

### (2) THE SMITH CHART: DERIVATION OF LOCI OF CONSTANT NORMALIZED RESISTANCE AND REACTANCE

The Smith chart is a co-ordinate system representing reflection coefficient as a complex variable.

For a reflection coefficient of constant amplitude and varying phase the plot is a circle centred at the origin. The angle subtended by the radius vector to a point on the circle and a reference axis through the origin of the diagram represents the phase angle of the reflection coefficient. One complete rotation about the origin represents a distance of one half-wavelength.

The circle representing unit-amplitude reflection coefficient contains the entire diagram. The general equation of circles of constant-amplitude reflection coefficient is written in the notation of complex variables as

$$\rho\bar{\rho} = k^2 \quad . \quad . \quad . \quad . \quad . \quad . \quad (1)$$

where $\rho$ represents the reflection coefficient, $\bar{\rho}$ its complex conjugate, and $k$ is the radius ($< 1$).

Certain of these circles are selected and marked on the chart. They are usually labelled as circles of constant voltage standing-wave ratio, this being related to the modulus of the reflection coefficient by the formula

$$\text{V.S.W.R.} = \frac{1 + \sqrt{(\rho\bar{\rho})}}{1 - \sqrt{(\rho\bar{\rho})}} \quad . \quad . \quad . \quad (2)$$

The radial lines representing reflection coefficients of constant phase and varying amplitude are written in the form

$$\frac{\rho}{\bar{\rho}} = l \quad . \quad . \quad . \quad . \quad . \quad . \quad (3)$$

If $\rho$ is written in the form $\sqrt{(\rho\bar{\rho})}\varepsilon^{j\phi}$, $l = \varepsilon^{j2\phi}$.

The normalized impedance $z$, at any plane in a transmission line, is related to the reflection coefficient at the plane by

$$z = \frac{1 + \rho}{1 - \rho} \qquad . \quad . \quad . \quad . \quad . \quad (4)$$

Writing $z = r + jx$, where $r$ and $x$ are, respectively, the normalized resistance and reactance, and separating $z$ into its real and imaginary parts,

$$r = \frac{1 - \rho\bar{\rho}}{1 + \rho\bar{\rho} - \rho - \bar{\rho}} \qquad . \quad . \quad . \quad . \quad (5)$$

$$jx = \frac{\rho - \bar{\rho}}{1 + \rho\bar{\rho} - \rho - \bar{\rho}} \qquad . \quad . \quad . \quad . \quad (6)$$

eqn. (5) may be written in the form

$$\rho\bar{\rho} - \frac{r}{(1 + r)}\rho - \frac{r}{(1 + r)}\bar{\rho} - \frac{(1 - r)}{(1 + r)} = 0 \quad . \quad . \quad (7)$$

The general equation of the circle described by the vector $\rho$ measured from the origin, having radius $k$ and with centre displaced from the origin by the vector $a$, is

$$(\rho - a)(\bar{\rho} - \bar{a}) = k^2$$

or

$$\rho\bar{\rho} - a\bar{\rho} - \bar{a}\rho + a\bar{a} = k^2 \quad . \quad . \quad . \quad (8)$$

If $r$ is constant, eqn. (7) represents a circle for which

$$a = \frac{r}{(1 + r)} \qquad . \quad . \quad . \quad . \quad (9)$$

$$k = \frac{1}{(1 + r)} \qquad . \quad . \quad . \quad . \quad (10)$$

Similarly eqn. (6) may be rewritten

$$\rho\bar{\rho} - \left(1 - \frac{j}{x}\right)\rho - \left(1 + \frac{j}{x}\right)\bar{\rho} + 1 = 0 \quad . \quad . \quad (11)$$

If $x$ is constant, eqn. (11) represents a circle for which

$$a = 1 + \frac{j}{x} \qquad . \quad . \quad . \quad . \quad (12)$$

$$k = \frac{1}{x} \qquad . \quad . \quad . \quad . \quad . \quad (13)$$

Eqns. (7) and (11) thus represent the circles for constant $r$ and $x$ loci, respectively.

## (3) TRANSFORMATION OF CIRCLES OF CONSTANT V.S.W.R.

It is well known that the reflection coefficients at any two planes in a transmission line are bilinear functions, related by an equation of the general form

$$\sigma = \frac{a\rho + b}{c\rho + 1} \text{ or } \rho = \frac{-\sigma + b}{c\sigma - a} \qquad . \quad . \quad (14)$$

where $a$, $b$ and $c$ are, in general, complex constants.[1]

Circles of constant v.s.w.r. at the one plane satisfying the equation $\rho\bar{\rho} = k^2$ transform, therefore, at the second plane into circles satisfying the equation

$$\left(\frac{-\sigma + b}{c\sigma - a}\right)\left(\frac{-\bar{\sigma} + \bar{b}}{\bar{c}\bar{\sigma} - \bar{a}}\right) = k^2 \qquad . \quad . \quad (15)$$

Writing eqn. (15) in the form of eqn. (8) gives

$$\sigma\bar{\sigma}(1 - k^2 c\bar{c}) - \sigma(\bar{b} - k^2\bar{a}c) - \bar{\sigma}(b - k^2 a\bar{c})$$
$$+ (b\bar{b} - k^2 a\bar{a}) = 0 \quad . \quad (16)$$

If $A$ represents the vector by which the centre of this circle i displaced from the origin, and $K$ represents the radius,

$$A = \frac{b - k^2 a\bar{c}}{1 - k^2 c\bar{c}} \qquad . \quad . \quad . \quad . \quad (17$$

$$K^2 = A\bar{A} - \frac{b\bar{b} - k^2 a\bar{a}}{1 - k^2 c\bar{c}} \qquad . \quad . \quad . \quad (18$$

The conditions for which eqns. (17) and (18) are solved are:

(a) The transforming section is lossless and is specified in term of the reflection coefficient at the one plane under conditions which give a match at the other.

(b) The reference planes are 'corresponding planes', i.e. an open circuit at the one plane gives an open-circuit at the other.

It is shown in Section 13.1 that when these conditions ar applied eqns. (17) and (18) become, respectively,

$$A = \frac{b(1 - k^2)}{1 - k^2 b\bar{b}} \qquad . \quad . \quad . \quad . \quad (19$$

and

$$K = \frac{k(1 - b\bar{b})}{1 - k^2 b\bar{b}} \qquad . \quad . \quad . \quad . \quad (20$$

Circles representing constant v.s.w.r. may thus be trans formed from the $\rho$- to the $\sigma$-plane by means of eqns. (19) and (20). It will be noted that the right-hand side of eqn. (19) represent a scalar multiplied by the vector $b$. The direction of $A$ is there fore that of $b$, which implies that the centres of the family o circles represented by eqn. (16) all lie on the radius which is ir the direction of $b$, i.e. which passes through the iconocentre.

## (4) TRANSFORMATION OF LINES OF CONSTANT PHASE ANGLE

Substitution of eqn. (14) into eqn. (3) gives the equation o the loci in the $\sigma$-plane of the radial lines in the $\rho$-plane which represent reflection coefficients of constant phase and varying amplitude:

$$\left(\frac{-\sigma + b}{c\sigma - a}\right)\left(\frac{\bar{c}\bar{\sigma} - \bar{a}}{-\bar{\sigma} + \bar{b}}\right) = l \quad . \quad . \quad . \quad (21$$

Eqn. (21) may be rewritten in the following form:

$$\sigma\bar{\sigma} - \left(\frac{la - b\bar{c}}{lc - \bar{c}}\right)\bar{\sigma} - \left(\frac{l\bar{b}c - \bar{a}}{lc - \bar{c}}\right)\sigma + \left(\frac{la\bar{b} - \bar{a}b}{lc - \bar{c}}\right) = 0$$
$$. \quad . \quad . \quad (22$$

It may readily be shown that the coefficients of $\sigma$ and $\bar{\sigma}$ are conjugate terms, so that eqn. (22) represents a circle for which

$$A = \frac{la - b\bar{c}}{lc - \bar{c}} \qquad . \quad . \quad . \quad . \quad (23$$

$$K^2 = A\bar{A} - \left(\frac{la\bar{b} - \bar{a}b}{lc - \bar{c}}\right) \qquad . \quad . \quad . \quad (24$$

It is shown in Section 13.2 that, when the relevant condition are applied, eqns. (23) and (24) become, respectively,

$$A = \frac{l(1 - b)^2 - b^2(1 - \bar{b})^2}{l\bar{b}(1 - b)^2 - b(1 - \bar{b})^2} \qquad . \quad . \quad . \quad (25$$

$$K = \frac{(1 - b\bar{b})}{\sqrt{\left[2b\bar{b} - l\bar{b}^2\left(\frac{1 - b}{1 - \bar{b}}\right)^2 - b^2 l\left(\frac{1 - \bar{b}}{1 - b}\right)^2\right]}} \qquad . \quad (26$$

The radial lines representing constant phase angle in the $\rho$-plane may thus be transformed into corresponding circular tracks in the $\sigma$-plane by means of eqns. (25) and (26). Since

he radial lines in the $\rho$-plane all pass through the origin, it ollows that the family of circles represented by eqn. (22) all pass hrough the iconocentre, as may also be shown by substituting $r = b$ in eqn. (22).

An important result is obtained by applying the above equaions to the axis of the diagram, which is done by substituting $= 1$ in eqns. (25) and (26).

This leads to the result

$$A = \frac{b\bar{b} - 2b + 1}{\bar{b} - b} \qquad \cdots \quad \cdots \quad (27)$$

$$K = \frac{(1 - b)(1 - \bar{b})}{(b - \bar{b})} \qquad \cdots \quad \cdots \quad (28)$$

The same results are obtained by substituting $\rho = b$ in eqn. (11) nd applying eqns. (12) and (13). This indicates that the axis f the diagram in the $\rho$-plane transforms in the $\sigma$-plane into the ircular track representing the line of constant reactance in the -plane which passes through the point $\rho = b$.

## (5) TRANSFORMATION OF CIRCLES OF CONSTANT RESISTANCE AND REACTANCE

Consider a pair of corresponding planes 1 and 2, the nor-nalized impedances at which are $z_1$ and $z_2$ and the reflection ⊃ufficients $\rho$ and $\sigma$, respectively. The form of eqn. (4) indicates nat the normalized impedance and reflection coefficient at any lane are bilinearly related, and since $\rho$ and $\sigma$ are bilinear unctions so also are $z_1$ and $z_2$.

Thus

$$z_2 = \frac{\alpha z_1 + \beta}{\gamma z_1 + 1} \qquad \cdots \quad \cdots \quad (29)$$

There $\alpha$, $\beta$ and $\gamma$ are, in general, complex constants.

Since $\sigma = 1$ when $\rho = 1$, it follows by application of eqn. (4) nat $z_2 = \infty$ when $z_1 = \infty$. This implies that $\gamma = 0$.

Thus $z_2$ is a linear function of $z_1$, i.e.

$$z_2 = \alpha z_1 + \beta \qquad \cdots \quad \cdots \quad (30)$$

When $z_1$ is purely imaginary, $z_2$ is also purely imaginary. This implies that $\alpha$ is real and $\beta$ is imaginary.

When $z_1 = 1$,

$$z_2 = Z_{12} = r_{12} + jx_{12} = \alpha + \beta \quad \cdots \quad (31)$$

hus

$$\alpha = r_{12}$$
$$\beta = jx_{12}$$

qn. (30) may therefore be written

$$z_2 = r_{12}z_1 + jx_{12} \qquad \cdots \quad \cdots \quad (32)$$

Substituting
$$\left. \begin{array}{l} z_1 = r_1 + jx_1 \\ z_2 = r_2 + jx_2 \end{array} \right\}$$

e have

$$r_2 + jx_2 = r_{12}(r_1 + jx_1) + jx_{12}$$

ence

$$r_2 = r_{12}r_1 \cdot \qquad \cdots \quad \cdots \quad (33)$$

$$x_2 = r_{12}x_1 + x_{12} \qquad \cdots \quad \cdots \quad (34)$$

⊃ ircles of constant $r_2$ and $x_2$ are defined by replacing $r$ and ⊃ by $r_2$ and $x_2$, respectively, in eqns. (9), (10), (12) and (13) and ⊃i⊃g the values for $r_2$, $x_2$ given by eqns. (33) and (34).

When these substitutions are made and eqns. (33) and (34) re used to define the circles in the $\sigma$-plane which correspond to ⊃nstant $r_1$ and $x_1$ circles, respectively, in the $\rho$-plane, the results e is follows:

*Constant r.*

$$a = \frac{r_{12}r_1}{1 + r_{12}r_1} \qquad \cdots \quad \cdots \quad (35)$$

$$K = \frac{1}{1 + r_{12}r_1} \qquad \cdots \quad \cdots \quad (36)$$

*Constant x.*

$$a = 1 + \frac{j}{r_{12}x_1 + x_{12}} \qquad \cdots \quad \cdots \quad (37)$$

$$K = \frac{j}{r_{12}x_1 + x_{12}} \qquad \cdots \quad \cdots \quad (38)$$

## (6) TRANSFORMATION OF SINGULAR POINTS

Let the normalized impedance $z_1$ exceed unity by $\Delta r_1 + j\Delta x_1$, where $\Delta r_1$, $\Delta x_1$ can have any value.

Applying eqn. (32),

$$z_2 = r_{12}(1 + \Delta r_1 + j\Delta x_1) + jx_{12}$$

Now

$$z_{12} = r_{12} + jx_{12}$$

Hence

$$z_2 = z_{12} + r_{12}(\Delta r_1 + j\Delta x_1) \quad \cdots \quad \cdots \quad (39)$$

Eqn. (39) gives a convenient means of transforming singular points.

## (7) THEORY OF GRAPHICAL METHOD FOR TRANSFORMING CIRCLES OF CONSTANT V.S.W.R.

A set of plots are drawn on the Smith chart to provide a simple geometrical construction for the circle corresponding to any given iconocentre and any value of v.s.w.r.

Examination of eqns. (19) and (20) shows that the family of circles in the $\sigma$-plane corresponding to circles of constant v.s.w.r. in the $\rho$-plane have centres which all lie on the radius through the iconocentre, and also that the radii and radial distances from the origin of the centres of these circles depends only on the radial distance of the iconocentre from the origin.

Consider two such families of circles in the $\sigma$-plane, one associated with an iconocentre at some arbitrary point on the diagram and the other associated with an iconocentre having the same radial displacement from the origin but lying on the axis.

The centre of each circle of the one family will then be rotated by a fixed angle about the origin of the diagram with respect to the centre of the corresponding circle of the other family.

If the family of circles corresponding to an iconocentre on the axis is determined, it is a simple matter to find the corresponding circles with any other iconocentre which is the same radial distance from the origin.

Consider an iconocentre at a point P on the axis and apply eqn. (39) to the two points of intersection of each circle of constant v.s.w.r. in the $\rho$-plane with the axis. The two points thus derived define the corresponding circle in the $\sigma$-plane.

Referring to Fig. 1, these pairs of points have been found corresponding to a succession of points P along the axis. Each of these pairs of points has then been rotated anticlockwise about P through a right angle. Plots have been drawn through the points so derived which correspond to the same value of v.s.w.r. in the $\rho$-plane. For any such value of v.s.w.r. there are clearly two plots, one on each side of the axis. The diameter of the unit circle which is perpendicular to the axis intersects the plots at points on the corresponding v.s.w.r. circles in the $\rho$-plane.

The distance perpendicular to the axis from any point P to two corresponding plots represents the radial displacements
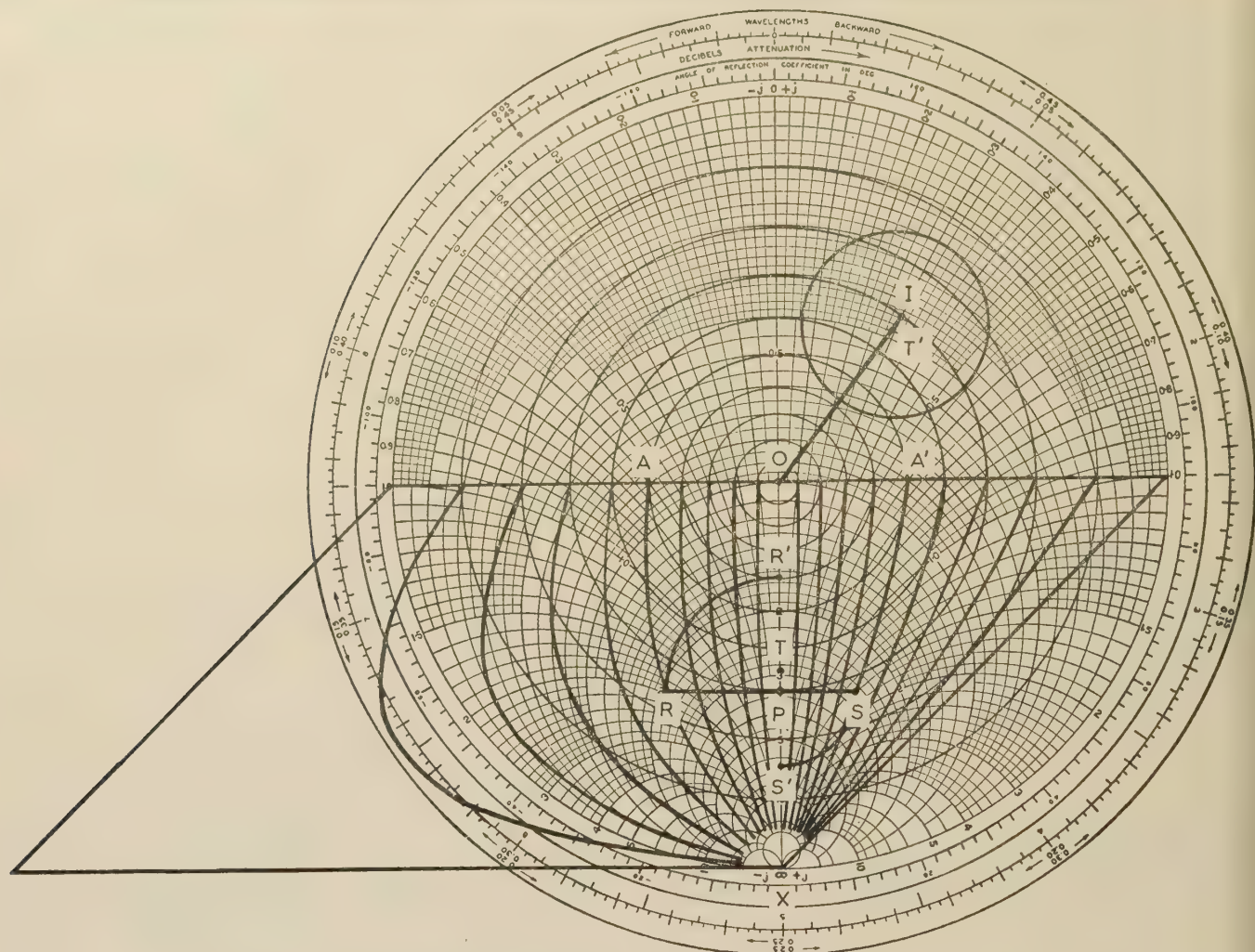
Fig. 1.—Chart for transforming circles of constant v.s.w.r.

| | | | |
|---|---|---|---|
| O | Centre. | R, S | Intersections of line through P parallel to AA′ with curves AX, A′X, respectively. |
| X | Pole. | | |
| I | Iconocentre. | R′, S′ | Points on axis such that PR′ = PR, PS′ = PS. |
| P | Point on axis such that OP = OI. | T | Midpoint of R′S′. |
| AA′ | Point of intersection with 0·5 v.s.w.r. circle of diameter which is perpendicular to axis. | T′ | Point on OI such that OT′ = OT. |

The circle with T′ as centre and radius equal to TR′ represents the 0·5 v.s.w.r. circle transformed with respect to the iconocentre I.

from P of the diametrical points of intersection with the axis of a circle in the $\sigma$-plane corresponding to a constant v.s.w.r. circle in the $\rho$-plane. In Fig. 1, plots on the left-hand side of the axis represent displacements in the direction of the centre of the diagram and those on the right-hand side represent displacements in the opposite direction.

The chart therefore defines the whole family of circles in the $\sigma$-plane corresponding to circles of constant v.s.w.r. in the $\rho$-plane when the iconocentre lies on the axis. If the iconocentre lies in some other direction, the corresponding family of circles is obtained by rotating each circle of the previous family about the origin of the diagram so that its centre now lies on the radius through the iconocentre.

## (8) APPLICATION OF GRAPHICAL METHOD FOR TRANS-FORMING CIRCLES OF CONSTANT V.S.W.R.

Fig. 1 enables circles of constant v.s.w.r. on a Smith chart relating to any plane on one side of a lossless junction to be transformed into the corresponding circles on a diagram relating to a corresponding plane on the other side of the junction. The

two planes must correspond, in that an open-circuit at the one plane produces an open-circuit at the other, in the case of an impedance diagram, and similarly for a short-circuit with an admittance diagram. Also, the point on the diagram relating to the second plane which corresponds to matched conditions on the other side of the junction must be known. This point is called the iconocentre.

Fig. 1 is used as follows:

To transform the 0·5 v.s.w.r. circle, for instance, from the first diagram to the second, assuming an iconocentre I, the point P on the axis OX is found such that OP = OI. The line through P perpendicular to OX is drawn to intersect the plots AX and A′X at R and S, respectively.

The point R′ is then marked off on PO such that PR′ = PR, and similarly S′ is marked off on PX such that PS′ = PS. The point T midway between R′ and S′ is then found. The distance OT′ is marked off along OI such that OT′ = OT.

With T as centre, a circle is drawn with radius TR′. This circle represents the 0·5 v.s.w.r. circle transformed with reference to the iconocentre I.

## Table 1

### Formulae for defining Circles

| Constant parameter | ρ-plane | | σ-plane | |
|---|---|---|---|---|
| | $a$ | $k$ | $A$ | $K$ |
| $r_1$ | $\dfrac{r_1}{1+r_1}$ | $\dfrac{1}{1+r_1}$ | $\dfrac{r_{12}r_1}{1+r_{12}r_1}$ | $\dfrac{1}{1+r_{12}r_1}$ |
| $x_1$ | $1+\dfrac{j}{x_1}$ | $\dfrac{1}{x_1}$ | $1+\dfrac{j}{r_{12}x_1+x_{12}}$ | $\dfrac{1}{r_{12}x_1+x_{12}}$ |
| $\rho$ | $0$ | $\sqrt{(\rho\bar\rho)}$ | $\dfrac{b(1-k^2)}{1-k^2 b\bar b}$ | $\dfrac{k(1-b\bar b)}{1-k^2 b\bar b}$ |
| $l$ | $\infty$ | $\infty$ | $\dfrac{l(1-b)^2-b^2(1-\bar b)^2}{l\bar b(1-b)^2-b(1-\bar b)^2}$ | $\dfrac{(1-b\bar b)}{\sqrt{\left[2b\bar b - l\bar b^2\left(\dfrac{1-b}{1-\bar b}\right)^2 - b^2 l\left(\dfrac{1-\bar b}{1-b}\right)^2\right]}}$ |

## (9) SUMMARY OF FORMULAE

A summary of the formulae defining all the various circles which have been considered in the paper is given in Table 1.

## (10) THEOREM

Consider an arbitrary reference plane in a transmission line which is initially matched. It is clear that by inserting a series reactance which is variable in magnitude and position between the reference plane and the matched termination any value of reflection coefficient may be produced at the reference plane.

It has been shown that the properties of a lossless junction are uniquely defined by the complex value of reflection coefficient at a reference plane in the measuring line corresponding to matched conditions at the load. Any such lossless system may therefore be represented by an equivalent system of a matched line with a reactance inserted at some particular plane. The matching of such a system is then equivalent to removing his reactance.

## (11) ACKNOWLEDGMENTS

## (12) REFERENCES

) DESCHAMPS, G. A.: 'Determination of Reflection Coefficients and Insertion Loss of a Waveguide Junction', *Journal o, Applied Physics*, 1953, **24**, No. 8, p. 1046.

) STORER, G. E., SHEINGOLD, L. S., and STEIN, S.: 'A Simple Graphical Analysis of a Two-Port Waveguide Junction', *Proceedings of the Institute of Radio Engineers*, 1953, **41**, No. 8, p. 1004.

) DUKES, J. M. C.: 'Waveguides and Waveguide Junctions', *Wireless Engineer*, 1955, **32**, No. 3, p. 65.

) DUKES, J. M. C.: 'Transmission-Line Termination', *ibid.*, 1955, **32**, No. 10, p. 266.

) SMITH, P. H.: 'Transmission Line Calculator', *Electronics*, January, 1939, **12**, p. 29.

) SMITH, P. H.: 'An Improved Transmission Line Calculator', *ibid.*, January, 1944, **17**, p. 130.

## (13) APPENDICES

### (13.1) Transformation of Circles of Constant V.S.W.R.

The solution of eqns. (17) and (18) for the three specified conditions is obtained in the following manner:

*Condition* 1.

The transforming section is lossless. This implies that with a purely reactive termination of the line the modulus of the reflection coefficient is unity at all planes.

Thus, for
$$k = 1,$$
$$\left.\begin{array}{c} K = 1 \\ A = 0 \end{array}\right\} \quad \ldots \ldots \quad (40)$$

Substituting these values in eqn. (17) gives

$$b = a\bar c \quad . \quad . \quad . \quad . \quad . \quad (41)$$

and hence
$$\bar b = \bar a c \quad . \quad . \quad . \quad . \quad . \quad (42)$$

*Condition* 2.

The reference planes are chosen such that an open-circuit at the one plane gives an open-circuit at the other. This may be written:

For
$$\rho = 1$$
$$\sigma = 1$$

Substituting these values in eqn. (14) gives

$$a + b = c + 1 \quad . \quad . \quad . \quad . \quad (43)$$

$$\bar a + \bar b = \bar c + 1 \quad . \quad . \quad . \quad . \quad (44)$$

*Condition* 3.

The transforming section is specified in terms of the reflection coefficient at the one plane under conditions which give a match at the other, i.e. the value of $\sigma$ corresponding to $\rho = 0$ is known.

Substituting $\rho = 0$ in eqn. (14) gives $\sigma = b$. Thus $b$ and $\bar b$ are known constants. The point whose affix is $b$ is called the iconocentre.[1]

Using the above results, eqn. (17) may be solved as follows:

Substituting eqn. (41) into eqn. (17) gives

$$A = \frac{b(1-k^2)}{1-k^2 c\bar c} \quad . \quad . \quad . \quad . \quad (45)$$

The term $c\bar{c}$ may be evaluated as follows:

$$b\left(1 + \frac{c}{c\bar{c}}\right) = c + 1$$

or

$$c = \frac{1 - b}{\dfrac{b}{c\bar{c}} - 1} \qquad \ldots \quad \ldots \quad (46)$$

Hence

$$\bar{c} = \frac{1 - \bar{b}}{\dfrac{\bar{b}}{c\bar{c}} - 1} \qquad \ldots \quad \ldots \quad (47)$$

Multiplying eqns. (46) and (47) and simplifying the resulting equation gives

$$(c\bar{c})^2 - (1 + b\bar{b})c\bar{c} + b\bar{b} = 0 \ . \quad \ldots \quad . \quad (48)$$

or

$$(c\bar{c} - 1)(c\bar{c} - b\bar{b}) = 0 \quad \ldots \quad . \quad (49)$$

Thus, $c\bar{c} = 1$ or $b\bar{b}$.

If $c\bar{c} = 1$ is substituted into eqn. (45) the result is $A = b$, which is the solution when $\rho = 0$. The general solution of eqn. (27) is

$$c\bar{c} = b\bar{b} \ . \quad \ldots \quad . \quad \ldots \quad . \quad (50)$$

Eqn. (45) may now be written in terms of the known values $b$, $\bar{b}$ and $k$, which gives eqn. (19).

Returning to eqn. (18) for the solution of $K$, it is seen that the only term not evaluated above is the product $a\bar{a}$. Substituting eqns. (40) and (50) into eqn. (18) gives

$$a\bar{a} = 1 \ . \quad \ldots \quad . \quad \ldots \quad . \quad (51)$$

Substituting for the various terms of eqn. (18) which are now known in terms of $b$, $\bar{b}$ and $K$ gives eqn. (20).

### (13.2) Transformation of Lines of Constant Phase Angle

Eqns. (25) and (26) are derived from eqns. (23) and (24), respectively, as follows:

The value given by eqn. (41) for $a$ in terms of $b$ and $\bar{c}$ is substituted into eqns. (23) and (24).

The terms $c$ and $\bar{c}$ are evaluated by substituting eqn. (41) into eqn. (43) and using eqn. (50), whence

$$\bar{c} = \frac{b(1 - \bar{b})}{1 - b} \quad \ldots \quad . \quad \ldots \quad (52)$$

and

$$c = \frac{\bar{b}(1 - b)}{1 - \bar{b}} \quad \ldots \quad . \quad \ldots \quad (53)$$

Substituting for $a$ from eqn. (41) in eqn. (23) gives

$$A = \frac{b\left(\dfrac{l}{\bar{c}} - \bar{c}\right)}{lc - c}$$

and applying eqns. (52) and (53), gives eqn. (25).

Substituting eqn. (25) into eqn. (24) and putting $ll = 1$ gives eqn. (26).

# THE CONDUCTIVITY OF OXIDE CATHODES

## Part 3.—Movements of Electrolytic Oxygen in a Conventional Diode System

### By G. H. METSON, M.C., Ph.D., M.Sc., B.Sc.(Eng.), Associate Member.

## SUMMARY

A conventional form of oxide-cathode diode can, in appropriate circumstances, evolve a continuous current-dependent stream of electrolytic oxygen. This oxygen emerges from the cathode surface as a negative ion and passes to the anode, where it may or may not be chemically absorbed. If absorption is incomplete, a proportion of the oxygen can be returned to the cathode and give rise to a number of characteristic reactions. These reactions are studied and shown to be analogous to the electrolytic actions of the S-type assembly described in Part 2 of the paper.

### LIST OF PRINCIPAL SYMBOLS

$I_A$ = Flectron current through matrix.
$V_A$ = Potential difference between anode and cathode.
$i_{out}$ = Rate at which oxygen ions leave matrix.
$i_{ret}$ = Rate at which oxygen atoms return to matrix.
$S$ = Gas return factor = $i_{ret}/i_{out}$.
$A$ = Cathode area.
$b$ = Distance from matrix surface to anode in a diode.
$V_H$ = Voltage applied to cathode heater.
$T_C$ = Absolute temperature of cathode.
$R_d$ = Matrix resistance.

## (1) INTRODUCTION

### (1.1) Purposes of Present Part

The movements and effects of ions in an oxide matrix sandwiched between two core pieces have been shown in Part 2 to be complex but systematic. Of the two forms of gas action studied the *residual* component is found to be transitory in a well-processed system—a technological by-product which can be eliminated by further processing improvement. The *electrolytic* component, however, is fundamental to the operation of a matrix, and the generation of electrolytic oxygen will continue so long as the matrix passes the useful electron stream which is its sole reason for existence. The purpose of the present Part is to extend the study of electrolytic oxygen to a practical form of valve—the oxide-cathode diode with a finite spacing between the anode and the electron-exit boundary of the matrix.

### (1.2) The Gas Return Factor

If the anodic core of an S-type valve is withdrawn from the matrix by a distance $b$, as in Fig. 1, the system changes into the conventional form of oxide-cathode diode. For vanishingly small values of $b$ the two systems become indistinguishable, and it seems possible that they are members of a common system whose qualitative behaviour is independent of $b$. If such an hypothesis is justified we might expect to find close parallels between the reactions of an S-type valve and a conventional diode to electrolysis.
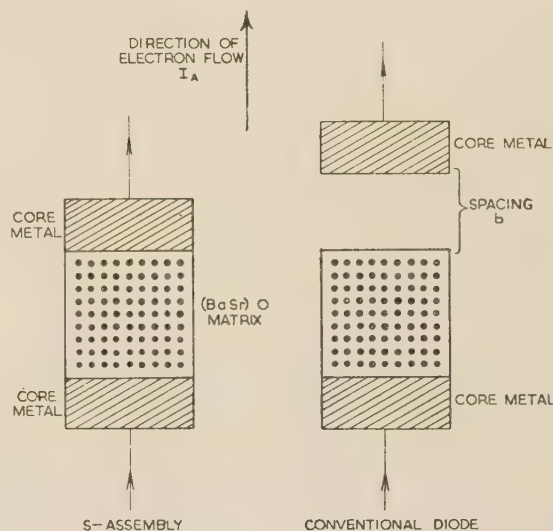
Fig. 1.—Cross-section of S-type assembly and conventional diode.

Consider the two systems shown in Fig. 1 fitted with platinum cores or electrodes. An electron flow, $I_A$, in either system is coincident with a p.d., $V_A$, across the matrix which induces an electrolytic flow of oxygen ions. These ions will cross the electron-exit boundary of either matrix at some rate $i_{out}$. In the S-type valve the ions will discharge on the anodic core and be returned intact to the matrix at a rate $i_{ret}$. Thus,

$$i_{out} = i_{ret}$$

or

$$S = \frac{i_{ret}}{i_{out}} = 1 \cdot 0$$

where $S$ is the gas return factor. In the conventional diode shown in Fig. 1 the oxygen ions will pass the electron-exit boundary, cross the intervening vacuum gap and discharge on the platinum anode. Since the oxygen atoms cannot congregate indefinitely on the platinum surface, they will pass back into the vacuum gap and, if the anode envelops the system, all will re-enter the matrix. Thus the above equations again apply. Both systems, with a unity return factor, will therefore build up their oxygen concentrations in identical manner, and their resistance reactions should follow in similar fashion.

Suppose now that the two systems have chemically active electrodes capable of removing electrolytic oxygen as fast as it is generated. In each case the ion stream on to the anodic electrode is $i_{out}$, but the returning atom stream is zero. The return factor is therefore $0/i_{out}$, i.e. zero, and no oxygen concentrations build up in the matrix.

The resistance reaction of a system to ion flow is thus deter-

mined by its chemical activity and is qualitatively independent of its mechanical arrangement. The activity is conveniently defined by the return factor, $S$: an inert system, with $S = 1$, showing the maximum resistance reaction and an active system, with $S = 0$, showing no response whatever. The magnitude of the return factor in an inert system is largely a matter of geometry.

In a parallel-plate system with cathode area $A$ and spacing $b$, the factor will approach unity as the ratio $A/b$ becomes large. The resistance reaction should, of course, be observed for any finite value of $S$, but it will be convenient experimentally to make it sufficiently great to ensure easy detection.

### (1.3) System Activity

It has been assumed so far that the activity of a system is localized at the anodic core surface. This simple picture has been adequate up to the present, but a more sophisticated view will now be required. Consider the case of an S-type valve fitted with one core of platinum and the other of active nickel. If the electron stream passes from the inert to the active core, the system is clearly active; if the electron stream is reversed, the system would logically seem to be inert, since the platinum anode is unable to accept the electrolytic oxygen. In fact, the assembly behaves as an active system in both directions of transmission and the idea of a purely localized anodic absorption of oxygen must be modified.

The activity of a core is a measure of its ability to reduce barium oxide chemically and inject a stream of metallic barium into the matrix. If, for example, the rate of chemical reduction by the cathodic core is equal to or greater than the rate of electrolytic oxygen generation at the anodic core, then, in an equilibrium state, no build-up of oxygen is possible: the barium metal will diffuse under a concentration gradient into the trailing section of the matrix as fast as or faster than the anodic discharge rate of oxygen. Such a system will therefore be active, whether or not its anodic core is itself active or inert.

### (2) CURRENT-DEPENDENT DECAY PHENOMENA

#### (2.1) Experimental Valve

The valve used in the present work is the experimental Post Office diode type 6D15—a 2-watt rectangular-box indirectly-heated cathode and a collector consisting of a fine molybdenum-wire grid structure supported on copper or nickel support rods. The structure is, in fact, identical in general form with the cathode and control-grid arrangement in a typical high-slope pentode.

The 6D15 has been extensively studied* in respect of its long-term emission stability when fitted with active and inert core materials, and this accumulation of experience makes it a useful starting-point for the present endeavour. The valves are processed on a high-grade bench pump and emerge with a total or temperature-limited emission of 3–6 amp/cm$^2$ at $1\,020°$ K—an emission level which is largely independent of the activity of the core metal employed.

The collector or anode of the 6D15 is essentially inert at its operating temperature and the activity of the system is therefore determined by the choice of core metal. The return factor of an inert system should be about $0 \cdot 5$, since there is a roughly equal geometrical probability of an oxygen atom, on leaving the collector, escaping into the outer vacuum or being returned to the matrix. This value of $S$ is adequate for easy experimental detection.

The current/voltage characteristic of a typical 6D15 at $1\,020°$ K is shown in Fig. 2.

* METSON, G. H.: 'A Study of the Long-Term Emission Behaviour of an Oxide-Cathode Valve', *Proceedings I.E.E.*, Paper No. 1790 R, April, 1955 (**102 B**, p. 657).
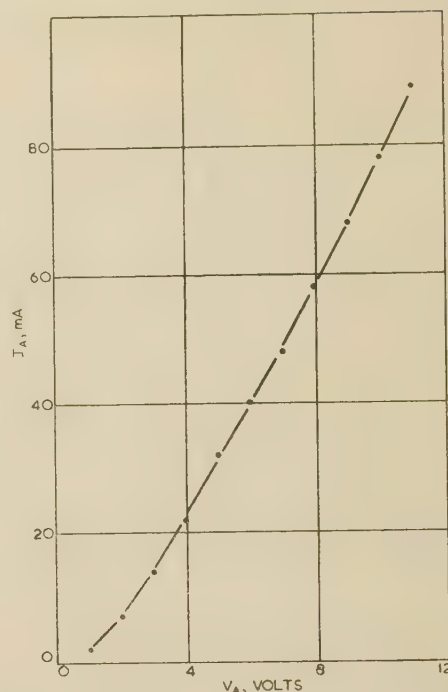


Fig. 2.—Typical voltage/current characteristic of the type 6D15 diode.

#### (2.2) Characteristics of $I_A$/Time at Constant $V_A$

A typical experiment is carried out on the following lines. A group of ten 6D15 valves is selected for reasonable uniformity of total emission and is set up on a test rack under the following conditions:

$$V_H = \phantom{0}6 \cdot 0 \text{ volts.}$$
$$V_A = 10 \cdot 0 \text{ volts.}$$
$$T_C = 1\,020° \text{ K.}$$

The voltage conditions are maintained constant for a test period of 12 000 hours and regular measurements made of the anode current, $I_A$. Fig. 3 shows the characteristics of $I_A$/time for three groups of valves—each curve being the mean of ten samples and referring to a different cathode-core material.
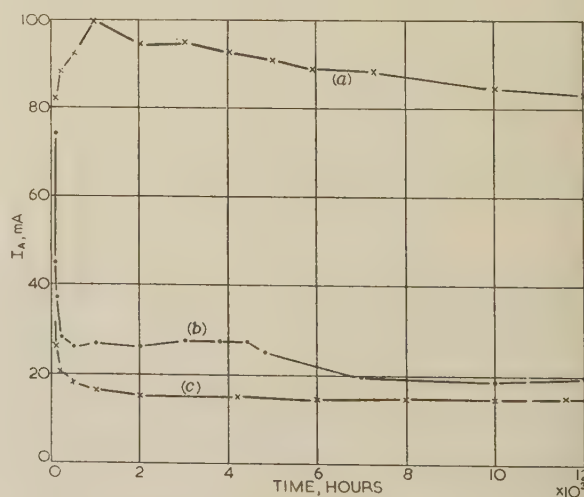


Fig. 3.—Characteristics of conductance decay in 6D15 diode.

(a) Active-nickel cathode core.
(b) Pure-nickel cathode core.
(c) Platinum cathode core.

The significance of the results seems to be in the level of anode current which can be supported by the (BaSr)O matrix on a particular core metal. The two essentially inert cores of pure nickel and platinum are only able to maintain some 15–20 mA; the conventional active nickel changes its normal space-charge-limited current but little over the whole test period.

The low steady conditions achieved by the inert cores after a few hundred hours of operation will be described as the 'decayed state'.

### (2.3) Properties of the Decayed State

2.3.1) **Uniformity of the Decay Effect.**

The decay of the platinum-cored system shown in Fig. 3 involves a fall from the space-charge-limited level of about 50 mA to the steady level of about 17 mA which hardly varies over a period of 10 000 hours. This constancy is notable, but even more so is the small spread in individual level amongst samples. Fig. 4 shows the distribution of $I_A$ in a group of 60



Fig. 5.—Reversibility of current-dependent decay (6D15 diode).



Fig. 4.—Distribution of anode currents of 6D15 diodes in decayed state.

samples of platinum-cored valves after a 1 000-hour run under the standard conditions given in Section 2.2. The whole of the group is included in the range $17 \pm 7$ mA. Such uniformity can hardly be fortuitous.

2.3.2) **Current Dependence of the Decay.**

A group of ten 6D15 platinum-cored valves was set up on the test rack to run at $V_H = 6 \cdot 0$ volts but under zero-current load condition. $I_A$ at $V_A = 10 \cdot 0$ volts was explored at suitable intervals, but showed no signs of decay from its initial high level of about 80 mA. At the end of a 35 000-hour run the mean current/voltage characteristic was essentially that shown in Fig. 2. Similar results were obtained for 6D15 valves fitted with pure nickel cathodes.

A first conclusion can now be drawn, namely that the decay effects in the inert systems shown in Fig. 3 are wholly current-dependent.

2.3.3) **Complete Reversibility of the Decay.**

A 6D15 valve fitted with a platinum core was set up at $1\,020°$ K and run with $V_A = 8 \cdot 0$ volts for 250 hours. The initial anode current of 55 mA decayed during the test to 23 mA. The valve was then subjected to the following sequence of measurements: $V_A$ was removed from the valve, which ran for 5 min under zero-current load except for 2 sec pulse tests at $V_A = 8 \cdot 0$ volts applied at 1 min intervals. For the next 5 min the potential $V_A = 8 \cdot 0$ volts was continuously applied, and so on until three complete cycles had been traversed. The result is set out in Fig. 5, and shows that the current-dependent decay of $I_A$ is completely reversible on zero-load running. The phenomenon is shown in another different way in Fig. 6. A group of ten 6D15 tubes with



Fig. 6.—Mean voltage/current characteristic of 6D15 diode after recovery from decayed state.
——— Platinum core after recovery.
– – – – Typical active-nickel core.

pure nickel cores was run for 3 000 hours in the decayed state with $V_H = 6 \cdot 0$ and $V_A = 10 \cdot 0$ volts. At the end of the run the group was allowed to recover under zero load, and was then measured for current/voltage characteristic by a 2 sec pulse application of voltage. The mean characteristic of the recovered group is compared in Fig. 6 with that of a typical active-nickel-core valve.

2.3.4) **Temperature Dependence of the Decay.**

Temperature dependence of conductance decay is simple to demonstrate. A platinum-cored 6D15 is aged for a few hundred hours into the decayed stage under current load; the variation of $I_A/V_H$ at constant $V_A$ is then measured, a typical example being shown in Fig. 7. The valve is now allowed to recover for an hour at $1\,020°$ K under zero-current load and the characteristic measurement is repeated, using only pulse application of $V_A$ for current measurement. The value of $V_A$ for both sets of measurements shown in Fig. 7 is $8 \cdot 0$ volts.
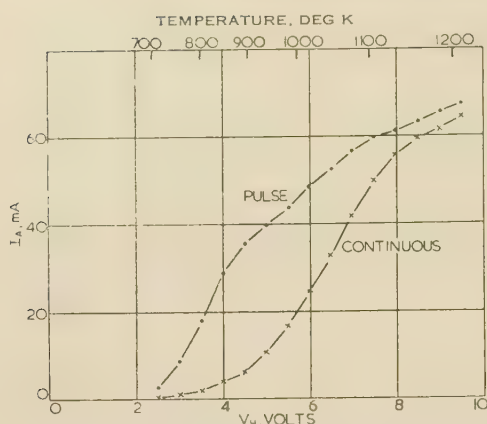
Fig. 7.—Temperature dependence of the decay phenomenon of 6D15 diode at $V_A = 8$ volts.

The results show that the conductance decay—or the difference in level of the two characteristics at a common heater voltage—decreases as the cathode temperature increases.

### (2.3.5) Current Limitation in the Decayed State.

The factor limiting $I_A$ in the decayed state appears to be a straightforward lack of emission from the cathode. Fig. 8
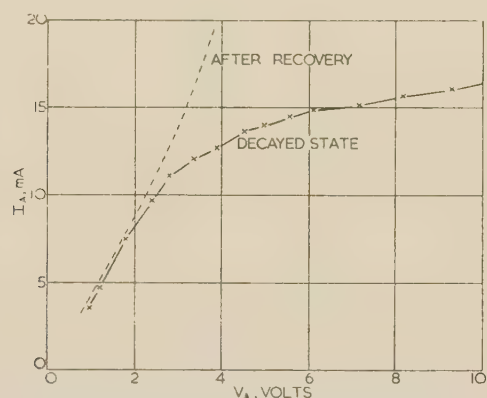


Fig. 8.—Voltage/current characteristic of diode in decayed state.

shows the mean current/voltage characteristic at $1\,020°\,K$ of a group of ten platinum-cored valves which have run for $1\,000$ hours in the decayed state. The characteristic is typically that of an oxide-cathode diode running into saturation at about $10\,mA$. The broken line sketched into Fig. 8 is the mean characteristic after recovery under zero-current load.

Fig. 9 shows the variation of $\log I_A$ with reciprocal of cathode temperature for a tube in the decayed state. The characteristic is similar to a Richardson plot with a work function of about $1\cdot3\,eV$.

### (2.3.6) Influence of an Ionizing Voltage on the Decayed State.

The magnitude of the applied potential, $V_A$, seems to have little effect on the stable level of the decayed state until an ionization potential is reached. The experimental result set out in Fig. 10 illustrates the reaction. A group of eight 6D15 valves with platinum cores was set up for test at $1\,020°\,K$ with $V_A = 10$ volts. The whole test period of $1\,200$ hours showed a normal decay reaction with the exception of an intercept of 160 hours under an ionizing potential of 15 volts. It is clear that ionization depressed the normal decayed level of $I_A$ by a substantial amount.
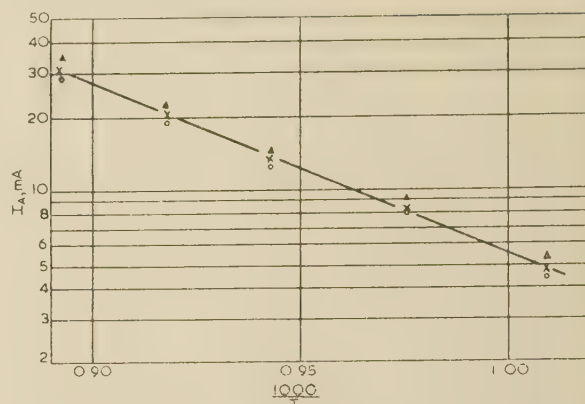


Fig. 9.—Variation of $\log I_A$ with the reciprocal of absolute temperature for 6D15 diode in the decayed state.

$\triangle$  $V_A = 10$ volts.
$\times$  $V_A = 9$ volts.
$\bigcirc$  $V_A = 8$ volts.
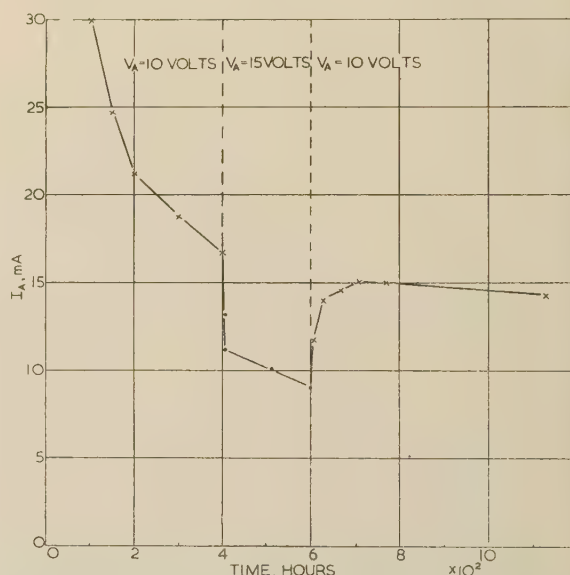


Fig. 10.—Influence of an ionizing potential on a normal decay characteristic of a diode.

### (2.4) Correlation of Decay Phenomena and Changes of Total Emission

#### (2.4.1) Measurement of Total Emission in the 6D15 Valve.

The total or temperature-limited emission in the 6D15 diode is conveniently measured by the low-temperature technique, i.e. the temperature of the cathode is lowered to $700°\,K$ and the total emission is measured with the collector at a saturating potential of $5\cdot0$ volts. It is not practicable to use temperature as a basis of accurate and reproducible measurement, and it is therefore customary to make the measurement on the basis of cathode heater power. The 6D15 cathode takes about $1\cdot5$ watts at $1\,020°\,K$. The measurement of total emission is therefore undertaken at $400\,mW$ of heater power and an applied collector potential of $5\cdot0$ volts.

New 6D15 valves have total emission in the range $0\cdot5$–$8\cdot0\,mA$, but values outside the range 2–6 mA have been rejected for the present work. The conversion factor relating total emission at $700°\,K$ and at the normal operating temperature of $1\,020°\,K$ is about $1\,000$, i.e. a total emission of $1\,mA$ at $700°\,K$ is equivalent to a normal-temperature emission of $1$ amp.

2.4.2) **Variation of Total Emission with Time for Zero-Load Running at 1 020° K.**

Groups of 6D15 diodes fitted with pure-nickel, active-nickel and platinum cores were run under zero-current load at 1 020° K for 12 000 hours. At intervals the valves were measured for low-temperature total emission, and the mean variations of total emission with time for ten samples of each type are set out in
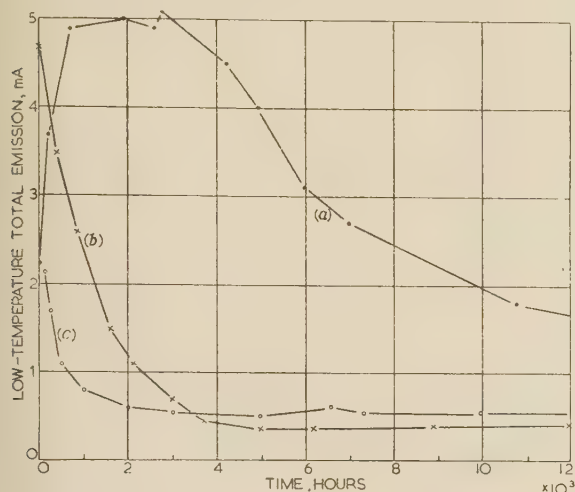


Fig. 11.—Variation of total emission with time under zero load at 1 020° K.

(a) Active-nickel core.
(b) Pure-nickel core.
(c) Platinum core.
Low-temperature total emission measured at 700° K.

Fig. 11. The cause of the several behaviours of the emission has been considered elsewhere* and the characteristics need be regarded here only as phenomenological information. A comparison of the total-emission characteristics with those of conductance decay in Fig. 3 brings out the following points:

(a) The two sets of characteristics have a general resemblance to each other.
(b) The decayed level of $I_A$ at any time might be correlated to the emission level at that time.
(c) When the total emission ceases to vary with time, so also does the decayed level of $I_A$.

From such observations it is concluded that the decayed level of $I_A$ is a direct function of the total emission of the cathode. The conclusion is supported by Fig. 12, which shows the decay characteristics at 1 020° K of two platinum-cored tubes of widely different total emissions.

2.4.3) **Total-Emission Transitions.**

A group of ten 6D15 platinum-cored diodes was run at 1 020° K and collector potential of 10 volts for 1 400 hours, the mean decayed level of $I_A$ at the end of the run being 17 mA. At this stage the power was removed from the valves in such a way that an electric stress remained across the matrix during the cooling period, i.e. $V_H$ was switched off before $V_A$. This switching sequence prevented any zero-load recovery of the valve during cooling down. A low-temperature total-emission measurement showed the group to have a mean value of 10 µA—equivalent by the conversion factor of Section 2.4.1 to an emission of 10 mA at 1 020° K. The group was next run at 1 020° K under zero load for 300 min with intermittent measurements of low-temperature emission. This operation resulted in a steady increase of total emission up to a constant value of 0·73 mA—equivalent to 0·73 amp at 1 020° K. The sequence is set out in Fig. 13 and

* See footnote on page 184.
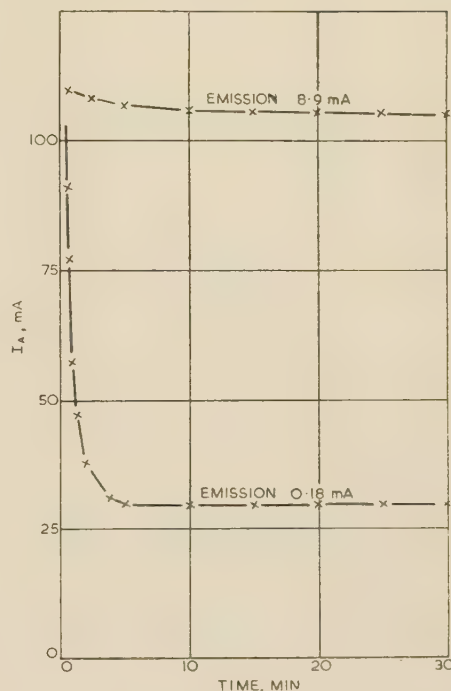


Fig. 12.—Dependence of decayed level of $I_A$ on total emission.
Low-temperature total emission measured at 700° K.
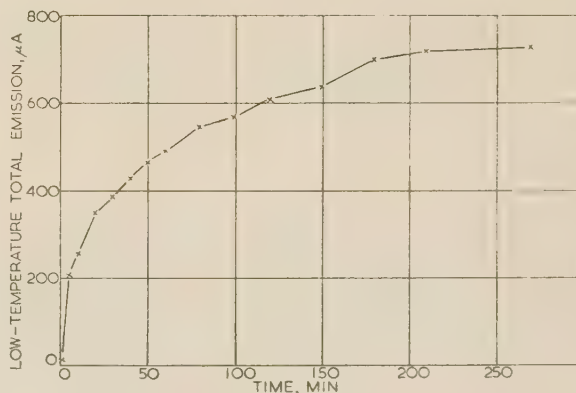


Fig. 13.—Recovery of low-temperature total emission under zero load at 1 020° K.
Low-temperature total emission measured at 700° K.

shows a remarkable dependence of total emission on current load.

The following conclusions may now be set down:

(a) A cathode gives its maximum emission on zero-current load. The level of the emission is then a function of the excess barium concentration in the matrix.
(b) A current, $I_A$, passing through the system reduces the total emission.
(c) As $I_A$ is increased, the total emission decreases until a state of equilibrium is established and $I_A$ becomes equal to the total emission at 1 020° K (which can be calculated from the measurements at 700° K).
(d) The actual level at which the equilibrium or stable decayed state is established is a function of the zero-load total emission, i.e. of the excess barium concentration in the matrix.

These conclusions, of course, refer to a particular valve—the inert 6D15—which has a substantial gas return factor.

(2.5) **Comparative Behaviour of the 6D15 Diode and the S-Type Assembly**

It will have been noticed that the general lines of examination of the 6D15 diode have followed those applied to the S-type assembly in Part 2 of the paper. Comparison of the various characteristics of the two systems, in both active and inert forms, are set out in Table 1.

**Table 1**

COMPARISON OF CHARACTERISTICS OF THE 6D15 AND S-TYPE VALVES

| Characteristic | S-Valve | | 6D15 | |
|---|---|---|---|---|
| | Active | Inert | Active | Inert |
| $I_A$/time at constant $V_A$ | No decay | Decay | No decay | Decay |
| Resistance reversibility on zero-load running | Not applicable | Completely reversible | Not applicable | Completely reversible |
| Dependence of decayed level of $I_A$ with temperature | Not applicable | $I_A$ increases with temperature | Not applicable | $I_A$ increases with temperature |

In the three principal characteristics examined it seems that, in both active and inert forms, the S-valve and 6D15 diode are qualitatively identical in performance. The conductance stability or otherwise is thus independent of the existence of a spacing distance, $b$, and is determined only by the magnitude of the gas return factor.

## (3) DISCUSSION OF RESULTS

Experimental results are summarized in the following form:

(a) The active system shows a high level of conductivity which is independent of time.

(b) The two inert systems show a high initial level of conductivity, but this decays rapidly with time under current load.

(c) The low conductivity or decayed state is constant over prolonged periods of operation and represents an equilibrium condition.

(d) Conductance decay is wholly dependent on current load and disappears completely on removal of the load.

(e) The decayed current level is a function of matrix temperature.

(f) The decayed current level is a function of the zero-load total emission of the matrix.

The interpretation of the results follows an identical course to that put forward in Part 2 for electrolytic action in the S-valve. Both cases are explained in terms of a gas return factor which feeds back and accumulates electrolytic oxygen in the vacuous pores of the matrix.

The only novel point arising in the present work is the sudden reduction of the decayed level of $I_A$ when $V_A$ reaches an ionizing potential. The action is clearly that of returning a proportion of the electrolytic oxygen atoms, which would otherwise have escaped into outer space, to the matrix in positive ion form, i.e. the effect is equivalent to a sudden increase in return factor.

The implied assertion in (a) above, that the active-nickel system has a zero return factor, is, of course, only a partial truth. As the activators perform their chemical work they will exhaust themselves, and the activity of the system will diminish with time. This slow activity decay is clear in the active-nickel cases depicted in Figs. 3 and 11.

## (4) ACKNOWLEDGMENT

# THE CONDUCTIVITY OF OXIDE CATHODES

## Part 4.—Electron Transfer Mechanisms

### By G. H. METSON, M.C., Ph.D., M.Sc., B.Sc.(Eng.), Associate Member.

#### SUMMARY

The present Part considers the mechanisms of electron transfer through the oxide-cathode matrix. In the temperature range 850–1100° K it is shown experimentally that, effectively, the whole of the electron stream passes through the vacuum interstices of the matrix. Progression is on a start-stop basis, with the electrons dissipating energy in the form of heat by successive non-elastic collisions with impeding oxide particles. The whole electron current is emitted thermionically at the cathodic core surface, where the theoretically predicted cooling effect is localized and observed. In the temperature range 290–600° K, electron transfer is on a purely resistive basis and involves no act of thermionic emission, i.e. the electron never emerges from the solid oxide into vacuum.

The results of the experimental work are in complete harmony with the hypothesis put forward in 1949 by Loosjes and Vink.

#### LIST OF PRINCIPAL SYMBOLS

$I_A$ = Current through matrix, mA.
$P_{H1}$ = Cathodic-core heater power, mW.
$P_{H2}$ = Anodic-core heater power, mW.
$P_{E1}$ = Equivalent cathodic-core power, mW.
$P_{E2}$ = Equivalent anodic-core power, mW.
$P_F$ = Emission cooling power, mW/mA.
$R$ = Resistance of solid matrix, ohms.
$T_C$ = Cathodic-core temperature, deg K.
$T_A$ = Anodic-core temperature, deg K.
$V_A$ = P.D. across matrix, volts.

The following difference symbols are used:

$$\Delta P_H = P_{H2} - P_{H1}$$
$$\Delta T = T_A - T_C$$
$$\Delta P_E = P_{E2} - P_{E1}$$

$a$, $b$, and $k$ are constants.

## (1) INTRODUCTION

It is proposed in the present Part to examine the mechanisms of electron transfer through the oxide cathode. It is known, of course, that the matrix has an open porous structure and that only one-fifth of its volume is filled with solid (BaSr)O particles. An electron crossing the matrix therefore has a choice in the path that it selects: it may proceed down a continuous but irregular chain of particles on the basis of a solid semi-conduction, or it may travel freely *in vacuo* down a series of hollow passages or pores.

Loosjes and Vink* in 1949 examined the complex nature of the conductivity/temperature characteristic of an oxide cathode and put forward the novel view that complexity was due to the

* LOOSJES, R., and VINK, H. J.: *Philips Research Reports*, 1949, **4**, p. 449.

existence of two forms of transfer mechanism—a solid semi-conduction at low temperature and a vacuum flight through the pores at higher temperature. The present work examines this hypothesis with the aid of a new experimental technique which seems capable of a rigorous and quantitative assessment of a conduction mechanism.

The experimental valve used in the work was the standard S-type assembly described in Part 1 of the paper. The essential features of the matrix are shown in Fig. 1, together with the
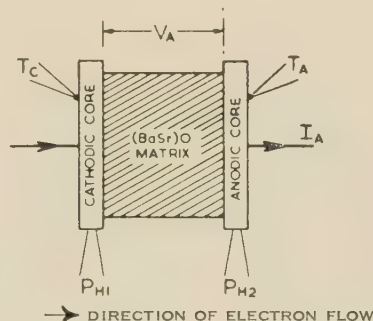


Fig. 1.—Schematic of S-type assembly.

basic symbols employed in subsequent Sections. To avoid the ion effects described in Part 2, the assemblies were fitted with active-nickel cores and were run for sufficient time to achieve the stable-characteristic-resistance, $R_0$, state. Mechanical dimensions and vacuum processing techniques for the valve were described in Part 1. All valves for the present work had independent heater-power sources and individual thermocouples fitted to each core.

## (2) POSSIBLE TRANSFER MECHANISMS

### (2.1) Preliminary Considerations

It is possible to visualize an electron traversing the matrix of an S-type valve in two distinct physical ways—the path may be through the crystal lattice of a solid chain of activated oxide particles, or it may be a wholly vacuum flight through hollow pores.

First suppose that the transmission path is a uniform solid semi-conductor of resistance $R$. An electron current, $I_A$, under an applied potential, $V_A$, will dissipate power $V_A I_A$ and result in a uniform generation of heat throughout the matrix on an $I^2R$ basis. The temperature of the system as a whole will increase, but no temperature gradient will arise between the two core pieces, since power dissipation is symmetrical in an essentially symmetrical system.

Suppose now that the transmission path is a vacuum which is traversed by current $I_A$ under potential $V_A$. Owing to the random tortuosity of the vacuum path, the electrons will collide

at frequent intervals with the solid walls of the passage, but, after each rebound, will travel in the same overall direction set by the applied electric field. These collisions may be elastic or non-elastic. In the elastic case the electrons will show a mean acceleration throughout their passage and will deliver the whole power, $V_A I_A$, for thermal dissipation at the anodic core surface. In the non-elastic case a start-stop method of progression will occur, mean acceleration will be zero and the power, $V_A I_A$, will be uniformly dissipated throughout the matrix.

The three cases of $V_A I_A$ dissipation are summarized in Table 1.

### Table 1

DISSIPATION OF POWER $V_A I_A$

| Case | Transfer mechanism | Location of power dissipation $V_A I_A$ |
|------|--------------------|-----------------------------------------|
| (a) | Solid semi-conduction | Uniform dissipation throughout matrix |
| (b) | Vacuum flight with successive non-elastic collisions | Uniform dissipation throughout matrix |
| (c) | Vacuum flight with successive elastic collisions | Dissipation wholly at surface of anodic core |

A further and different aspect of power transfer must now be considered. Cases (b) and (c) involve the free flight of electrons *in vacuo*, and both cases imply an act of thermionic emission at the cathodic core surface. Energy will therefore be extracted from the cathodic core, carried intact* through the body of the matrix, and delivered for local dissipation on the surface of the anodic core. If the coefficient of cooling power is $P_F$ milliwatts per milliampere, then in both cases there will be a loss of power, $P_F I_A$, at the cathodic core and a gain of power $P_F I_A$ by the anodic core.

Three different mechanisms of electron transfer have now been postulated, and it seems that to each can be assigned a unique distribution of power dissipation. If these distributions can be recognized experimentally, the actual transfer mechanism at any particular temperature can be determined. It is probable, of course, that different operating temperatures may involve different transfer mechanisms, and experimental success will be possible only if temperatures can be selected at which a particular mechanism is in absolute ascendancy over others.

### (2.2) Distribution of Power Dissipation

#### (2.2.1) Assumptions and Nomenclature.

The reactangular slab of oxide matrix sandwiched between the two core pieces of the S-type assembly is such that the slab thickness is small compared with its other two dimensions. Almost all the power generated within the slab must therefore cross the two core-matrix boundaries, to be lost by radiation from the backs of the two cores. A small fraction of power will, in fact, be lost by direct radiation from the narrow edges, but this is assumed, on dimensional grounds, to be inconsiderable and will be disregarded. Such an assumption leads to the following useful result: if power $V_A I_A$ is uniformly dissipated throughout the matrix, it will produce the same core-temperature distribution as would a direct addition of $\frac{1}{2} V_A I_A$ to each core-heater power. Various modes of power dissipation in the matrix or at its boundaries can thus be compounded with the core-heater powers to give equivalent core-temperature distributions.

* No element of the power $P_F I_A$ is dissipated within the body of the matrix, since the individual oxide particles cannot accumulate electrons, i.e. an impacted particle will gain an element of the energy $P_F I_A$ on the arrival of an electron but must lose it when the electron departs.

For the particular case of uniform dissipation of power within the matrix it follows that

$$P_{E1} = P_{H1} + \tfrac{1}{2} V_A I_A$$
$$P_{E2} = P_{H2} + \tfrac{1}{2} V_A I_A$$

and

$$\Delta P_E = \Delta P_H = 0$$

for the condition of equal core-heater powers and for all values of $I_A$. On grounds of symmetry it follows that $\Delta T = 0$ for all values of $I_A$.

A second assumption will now be introduced, to the effect that differences in equivalent core powers, $\Delta P_E$, result in proportional differences in core temperatures, $\Delta T$, provided that the temperature range $T_A - T_C$ is sufficiently limited. This assumption

$$\Delta P_E = k \Delta T$$

will be justified over the working temperature range in Section 2.2.6.

#### (2.2.2) Case A.—Semi-Conduction Mechanism.

This simple case postulates the dissipation of power $V_A I_A$ in a uniform semi-conductive resistance. The equivalent core powers are therefore written

$$P_{E1} = P_{H1} + \tfrac{1}{2} V_A I_A$$
$$\underline{P_{E2} = P_{H2} + \tfrac{1}{2} V_A I_A}$$
$$\Delta P_E = \Delta P_H$$

For the case of equal core-heater powers we can therefore write

$$\Delta P_E = k \Delta T = 0$$

for all values of $I_A$. The semi-conducting case is therefore defined by the condition $\Delta T = 0$ for all values of $I_A$. It should perhaps be mentioned that, if $P_{H1} \gtrless P_{H2}$, then $\Delta T$ is a positive or negative constant for all values of $I_A$.

#### (2.2.3) Case B.—Free Flight with Non-Elastic Collisions.

This case postulates the thermionic emission of the whole electron stream $I_A$ at the cathodic core–matrix boundary and its subsequent free flight through the vacuous pores of the matrix. During flight the electrons suffer successive impacts with the walls of impeding oxide particles, and these impacts are regarded as non-elastic. Each electron therefore accelerates from rest to some velocity at which it strikes a particle and loses the whole of its kinetic energy. After impact, the performance is successively repeated until the electron finally arrives at the anodic core surface. Assuming uniformity of matrix structure, the power $V_A I_A$ therefore suffers uniform dissipation and, so far as core temperatures are concerned, is equivalent to increasing each core-heater power by $\frac{1}{2} V_A I_A$. The distribution of power dissipation is now similar to that of case (a), but the picture is not yet complete. The thermionic emission of current $I_A$ at the cathodic-core surface results in a cooling effect which is equivalent to a decrease of cathodic-core power by $P_F I_A$ and a corresponding increase of anodic core power by $P_F I_A$.

The equivalent core powers are therefore written

$$P_{E1} = P_{H1} + \tfrac{1}{2} V_A I_A - P_F I_A$$
$$\underline{P_{E2} = P_{H2} + \tfrac{1}{2} V_A I_A + P_F I_A}$$
$$\Delta P_E = \Delta P_H + 2 P_F I_A$$

It follows that, for the case of equal core heater powers,

$$\Delta P_E = 2 P_F I_A = k \Delta T$$

or

$$\Delta T \propto I_A$$

for all values of $I_A$.

The case of thermionic emission at the cathodic core and subsequent free flight with non-elastic collisions is therefore defined by a direct proportionality between the function $\Delta T$ and $I_A$ for all values of $I_A$. The case can, of course, be generalized for unequal core-heater-powers in the form

$$\Delta T = a + bI_A$$

where $a$ and $b$ are constants.

**(2.2.4) Case C.—Free Flight with Elastic Collisions.**

This case is similar to the previous one, with the exception that the electrons lose none of their kinetic energy on colliding with the oxide particles. Each electron therefore experiences a progressive increase of velocity during transit and arrives at the anodic core boundary surface with energy $eV_A$. The whole of the power $V_AI_A$ is therefore delivered to the anodic core and not, as in the two previous cases, equally divided between the two cores. The equivalent core powers are therefore written

$$P_{E1} = P_{H1} - P_FI_A$$
$$P_{E2} = P_{H2} + V_AI_A + P_FI_A$$

$$\overline{\Delta P_E = \Delta P_H + V_AI_A + 2P_FI_A}$$

It follows that, for equal core-heater powers,

$$\Delta P_E = V_AI_A + 2P_FI_A$$
$$= k\Delta T$$
$$\Delta T \propto (V_AI_A + 2P_FI_A)$$

for all values of $I_A$.

The case of thermionic emission at the cathodic core and subsequent free flight with elastic collisions at the oxide particles is therefore defined by a proportionality between the functions $\Delta T$ and $(V_AI_A + 2P_FI_A)$. The case can be generalized for unequal core heater wattages in the form

$$\Delta T = a + b(V_AI_A + 2P_FI_A)$$

**(2.2.5) Summary of Cases.**

The characteristics of $\Delta T = f(I_A)$ for the three postulated transfer mechanisms are summarized in Table 2.

**Table 2**

$\Delta T = f(I_A)$ FOR TRANSFER MECHANISMS

| Electron transfer mechanism | $\Delta T = f(I_A)$ |
|---|---|
| Solid semi-conduction .. .. <br> Thermionic emission from cathodic- core surface and free flight with non-elastic collisions | $\Delta T = a$ <br> $\Delta T = a + bI_A$ |
| Thermionic emission from cathodic- core surface and free flight with elastic collisions | $\Delta T = a + b(V_AI_A + 2P_FI_A)$ |

The quantities $a$ and $b$ are constants, with $a$ always zero for the special case of equal core-heater powers, i.e. $\Delta P_H = 0$. Fig. 2 shows the flow patterns of power for the three cases. It now remains to determine the form of $\Delta T/I_A$ for a practical tube, and to attempt to relate it to one or other of the above characteristics. Before attempting this task, however, it will be useful to justify the assumption $\Delta P_E = k\Delta T$ and to consider the matrix temperature ranges into which experimental effort may be most profitably directed.
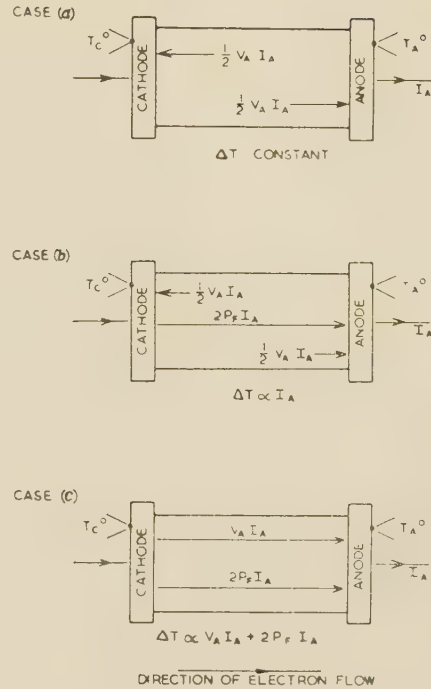


Fig. 2.—Power distribution patterns.

(a) Solid semi-conduction.
(b) Vacuum flight with non-elastic collisions.
(c) Vacuum flight with elastic collisions.

**(2.2.6) Justification of the Assumption $\Delta P_E = k\Delta T$.**

With zero current, $I_A$, in the matrix the quantities $\Delta P_E$ and $\Delta P_H$ are identical and the task reduces itself to that of justifying the condition

$$\Delta P_H = k\Delta T$$

over the working range of temperature. The task is a simple one and involves the initial setting-up of a standard S-type assembly with accurately measured core-heater powers $P_{H1}$ and $P_{H2}$ with $I_A = 0$. Either one or both heater powers are then changed by successive small amounts and the corresponding core temperatures are recorded. A plot of $(P_{H2} - P_{H1})/(T_A - T_C)$ is finally made over a temperature range of 60°. A typical result for tube S-103 is shown in Fig. 3 for the special case of equal
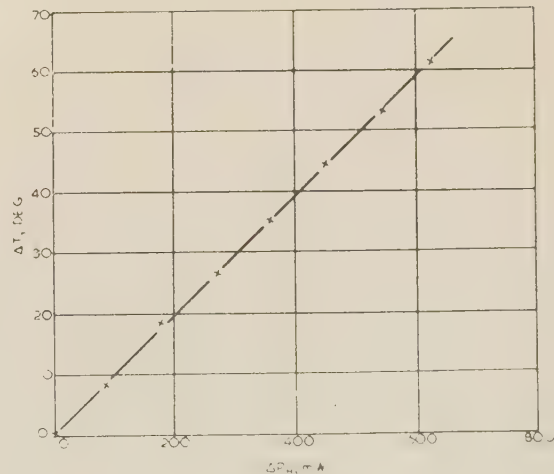


Fig. 3.—$\Delta P_H/\Delta T$.

initial core-heater powers. If the initial value of $\Delta P_H$ is not zero but some small quantity, the slope of the characteristic remains unchanged but it acquires positive or negative intercepts on the two axes.

Within the limits of experimental error it has always been found that the relationship $\Delta P_H = k\Delta T$ is observed over the temperature range of 60°. Some curvature of the characteristic must, of course, exist, but it is less than 1° in 60° and any systematic trend is not detectable by the adopted method of core temperature measurement. The quantities $T_C$ and $T_A$ were actually measured by platinum/platinum–rhodium thermo-couples connected to a high-grade potentiometer standardized against a standard cell. These thermocouples were readily able to detect core-temperature changes of 0·2° at 800° C when the thermocouple cold junctions were held constant. Random variations from linearity were thought to be due to second-order mechanical instabilities in the core-matrix system rather than to power-law radiation effects or measurement errors.

#### (2.2.7) Selection of Suitable Temperature Ranges.

We can hope to recognize an electron transfer mechanism by examination of the $\Delta T/I_A$ characteristic, provided that only one mechanism is present. Fig. 4 shows a plot of the logarithm of
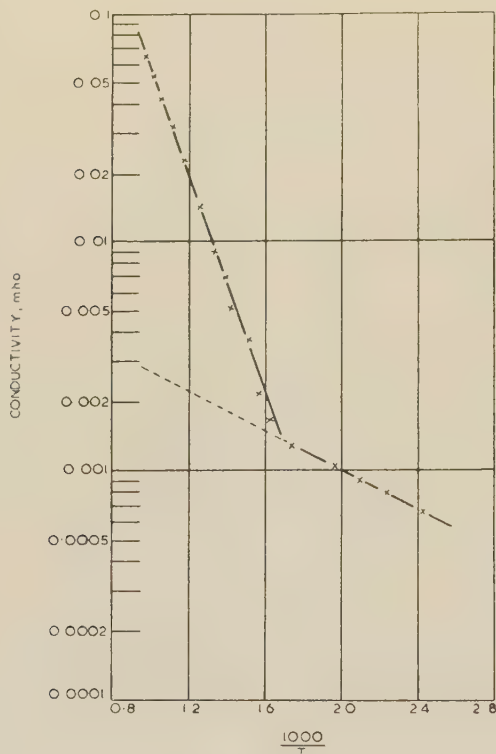


Fig. 4.—Conductivity/temperature characteristic.

matrix conductivity against the reciprocal of absolute tempera-ture for a typical S-type assembly. The result is very similar to those of Loosjes and Vink, who propose that the two straight parts of the characteristic are due to two different transfer mechanisms. The curved part of the characteristic is therefore likely to cover a temperature range over which two mechanisms coexist in varying proportions. Measurements of the $\Delta T/I_A$ characteristic must accordingly be directed into temperature ranges corresponding to the linear sections, namely 290–600° K and 850–1 100° K.

### (3) TRANSFER MECHANISM IN TEMPERATURE RANGE 850–1 100° K

#### (3.1) Characteristic of $\Delta T/I_A$ with $\Delta P_H = 0$

Determination of the $\Delta T/I_A$ characteristic is a straightforward affair using a standard S-type assembly. The core-heater powers are first adjusted to equality to give core temperatures of about 1 000° K. With these powers, $P_{H1}$ and $P_{H2}$, accurately constant and equal, the current, $I_A$, through the matrix is increased from zero to about 150 mA. The core temperatures, $T_C$ and $T_A$, are measured with the d.c. potentiometer for each current setting. The resulting characteristic of $\Delta T/I_A$ for valve S-43 is shown in Fig. 5, and the variation of core temperature with matrix current is shown in Fig. 6.

The results show an unequivocal option for case (b) as the
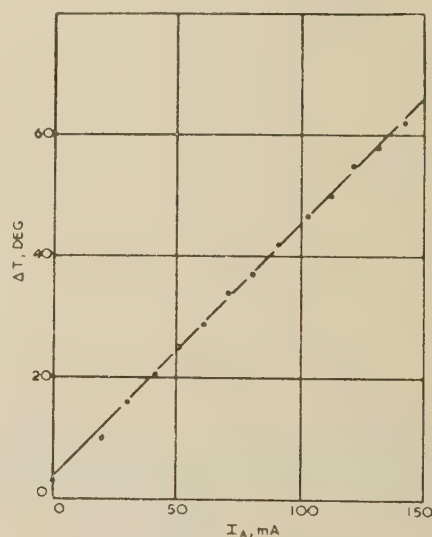


Fig. 5.—$\Delta T/I_A$ for valve S-43.
Slope = 0·410 deg/mA.
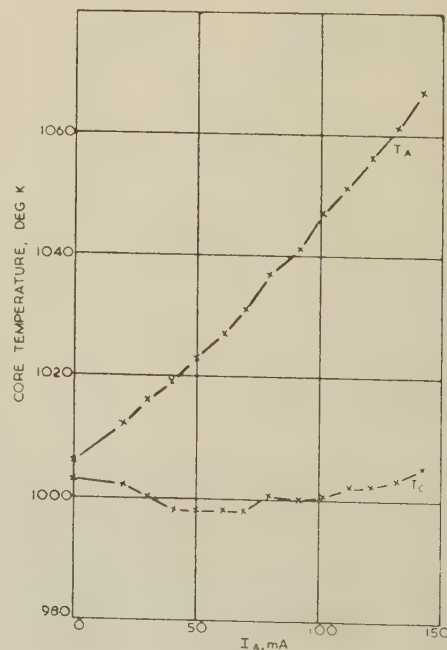


Fig. 6.—$T_A/I_A$ and $T_C/I_A$ for valve S-43.

electron transfer mechanism at $1\,000°$ K, i.e. the electron stream is thermionically emitted at the cathodic-core surface and thereafter travels by way of porous passages, suffering regular non-elastic collisions with the impeding matrix particles. Apart from the linearity of the $\Delta T/I_A$ characteristic, perhaps the most interesting feature of the results is the relative change with $I_A$ of the two core temperatures. While $T_A$ rises continuously in a regular manner over a range of $60°$, $T_C$ falls slowly by about $5°$ and has gained only $3°$ over its initial level when $T_A$ has reached its highest value—a spectacular demonstration of the cooling effect at the cathodic-core surface.

Under the condition $\Delta P_H = 0$ we should achieve the state $\Delta T = 0$ for $I_A = 0$, but this can never be realized in practice, owing to a small unavoidable asymmetry introduced during assembly of the S-type device. This is the reason why the $\Delta T/I_A$ characteristic misses the origin by about $3°$ in Fig. 5. The phenomenon is, however, without significance to the general conclusions.

Attempts were made to fit the experimental data to the criterion of case (c), but without success. With various values of the cooling factors, $P_F$, in the predicted range of $1\cdot0$–$2\cdot0$ mW/mA, a series of characteristics of $\Delta T/(V_A I_A + 2P_F I_A)$ were obtained, but these showed an increasing departure from linearity as $I_A$ increased. Case (c) has therefore been abandoned as inapplicable in the range $850°$–$1\,100°$ K.

### (3.2) Characteristic of $\Delta T/I_A$ with $\Delta P_H \gtrless 0$

To illustrate the generality of the technique, a further example is shown for valve S-103 in Figs. 7 and 8. $P_{H1} > P_{H2}$ to the extent that, with zero matrix current, $T_C$ exceeds $T_A$ by about $30°$. With the initial core powers constant, increasing $I_A$ results in $T_A$ exceeding $T_C$ by $30°$. Comparison of the characteristics for valves S-43 and S-103 will show that they are identical in all essential respects.

Fig. 8.—$T_A/I_A$ and $T_C/I_A$ for valve S-103.

### (3.3) Characteristic of $\Delta P_{H1}/I_A$ at Constant $\Delta T$

The power-flow diagram in Fig. 2 for case (b) shows that the anodic core has an excess of power of $2P_F I_A$ over that of the cathodic core. This results in a difference of core temperature $\Delta T = bI_A$ for the condition $\Delta P_H = 0$. It will be obvious that additions of power $\Delta P_{H1}$ to the initial cathodic-core heater power, $P_{H1}$, can be made in such a way that the two core temperatures remain equal for all values of $I_A$. Both $T_C$ and $T_A$ will, of course, increase with each addition to $I_A$, but $\Delta T$ will remain zero so long as $\Delta P_{H1} = 2P_F I_A$. The power balance for $\Delta T = 0$ is thus defined by the following equations:

$$P_{H1} = P_{H2}$$
$$\Delta P_{H1} = 2P_F I_A$$

and is shown diagrammatically in Fig. 9. The case can be generalized for finite values of $\Delta P_H$ by substituting a constant for the zero value of $\Delta T$.
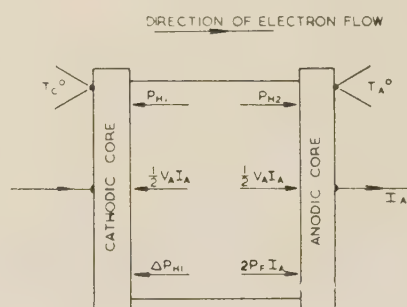
Fig. 9.—Power-flow diagram for $\Delta T = 0$.

Flow conditions:  $P_{H1} = P_{H2}$
$\Delta P_{H1} = 2P_F I_A$
$T_A - T_0 = \Delta T = 0$

The experimental characteristic $\Delta P_{H1}/I_A$ at constant $\Delta T$ is readily available from the standard S-type assembly. The valve is set up initially with equal core-heater powers. As the matrix current $I_A$ is then progressively increased, so an element $\Delta P_{H1}$ is added to the cathodic-core heater power to maintain $T_C$ at the same level as $T_A$. A typical result is set out in Fig. 10, which shows that the predicted linearity of $\Delta P_{H1}/I_A$ is experimentally realized. The slope of the characteristic is given by $2P_F$, and we have now for the first time in the paper given to

Fig. 7.—$\Delta T/I_A$ for valve S-103.

Slope = $0\cdot342$ deg/mA.

7
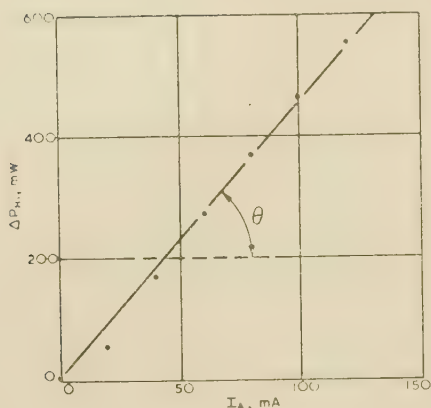
Fig. 10.—$\Delta P_{H1}/I_A$ for constant $I_A$.
Tan $\theta = 2P_F = 4 \cdot 6$ mW/mA.

the coefficient of cooling power a numerical value, namely $2 \cdot 3$ mW/mA.

$P_F$ can be calculated from the basic thermionic constants and will probably be in the range $1 \cdot 5$–$2 \cdot 5$ mW/mA, depending on the actual numerical values assigned to the constants. The measurement taken from the characteristic in Fig. 10 is therefore in good agreement with the theoretical prediction. Two direct determinations of $P_F$ were made in the laboratory on a conventional form of oxide-cathode diode. The core cooling effect was derived from a knowledge of the rate of change of core temperature with cathode-heater power and on the observed rate of change of core temperature with cathode current. The two samples gave $P_F = 1 \cdot 8$ and $2 \cdot 4$ mW/mA respectively.

### (3.4) Conclusions

Experiments on the lines described above have been carried out over the temperature range 900–1 100° K, and the conclusions set out below refer to this range:

(a) The whole of the matrix current $I_A$ is thermionically emitted at the cathodic-core boundary, at which it causes the theoretically predicted cooling effect.
(b) The whole of the current $I_A$ travels in vacuum through the matrix by way of porous passages.
(c) During the vacuum flight through the uniform matrix the electrons suffer successive non-elastic collisions with impeding oxide particles, as a result of which the power $V_A I_A$ is uniformly dissipated throughout the matrix and the average electron velocity during transit remains constant.

## (4) TRANSFER MECHANISM IN TEMPERATURE RANGE 290–600° K

### (4.1) Characteristic of $\Delta T/I_A$ with $\Delta P_H = 0$

Determination of $\Delta T/I_A$ in the range 290–600° K is somewhat difficult, on account of the restricted temperature range. $P_{H1}$ and $P_{H2}$ must therefore be set as low as is consistent with obtaining a reasonable range of matrix current with a reasonable voltage. If, for example, $P_{H1} = P_{H2} = 300$ mW, then, without any power, $V_A I_A$, in the matrix, the core temperatures will be about 600° K and we are already entering the inadmissible temperature region. It is clear, then, that the condition

$$(P_{H1} + P_{H2} + V_A I_A) < 600 \text{ milliwatts}$$

must be observed. Furthermore, if a reasonable range of $V_A I_A$ is to be obtained,

$$V_A I_A > P_{H1} + P_{H2}$$

These conditions seem to be onerous, but in fact they turn out to be simple: the S-type assembly with active nickel cores is

quite ready to start up from cold under the matrix power $V_A I_A$ alone. The core-heater powers can therefore be maintained at zero and the whole power range of 600 mW is available for use as $V_A I_A$.

A practical measurement is taken in the following manner: The core-heater powers are set either to zero or some small equal value (say 50 mW). A voltage, $V_A$, is then applied across the cores, and this results in a current $I_A$ and a power dissipation $V_A I_A$; this in turn leads to a general temperature rise, and the values of $T_C$ and $T_A$ are noted as functions of $V_A I_A$. $V_A$ is then increased and the sequence is repeated until the required range is covered. Results on a typical valve for the two conditions $P_{H1} = P_{H2} = 0$ and 50 mW are set out in Fig. 11, which shows
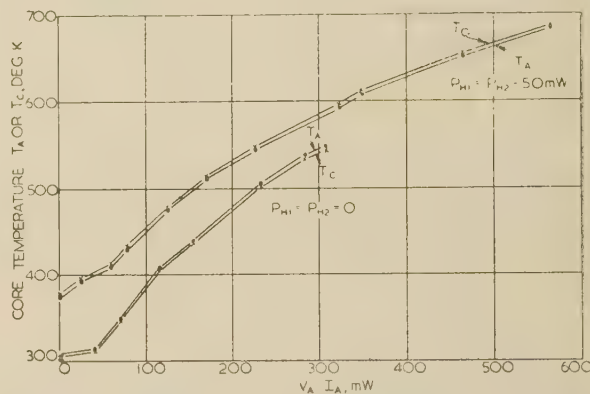


Fig. 11.—Variation of $T_C$ and $T_A$ with matrix power $V_A I_A$.

that, over a range of 500 mW, the two core temperatures move almost exactly together over the absolute temperature range 300–680° K, i.e. a span of nearly 400°. The $\Delta T/I_A$ characteristic over a current range corresponding to a core-temperature span of 320° K is shown in Fig. 12. After discounting the initial
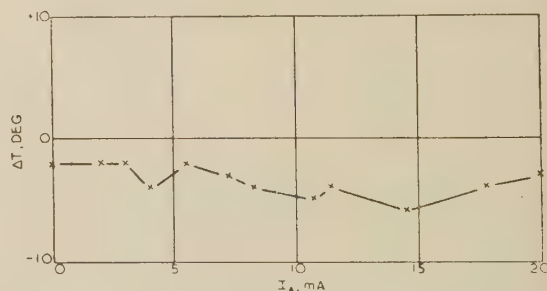


Fig. 12.—Variation of $\Delta T/I_A$ over temperature range 360–680° K.

difference of 2° for zero current, the average value of $\Delta T$ over the whole core-temperature range is $1 \cdot 6$°, i.e. about $0 \cdot 5$% of the range. Such variations are regarded as experimental errors, and it is concluded that, for the condition $P_{H1} = P_{H2}$ in the temperature range 300–600° K, $\Delta T$ is zero for all values of $I_A$. The electron-transfer mechanism below 600° K therefore follows case (a) as a purely resistive process involving no act of thermionic emission.

### (4.2) Experimental Note

It may surprise some engineers to learn that the oxide cathode sandwiched between active-nickel cores has sufficient solid conductivity at room temperatures to start up on the dissipated power $V_A I_A$ alone. The action appears to take the following course: on application of $V_A$ a small power, $V_A I_A$, is dissipated

in the matrix. This raises the matrix temperature and lowers its resistance, which leads to a further power increase. At constant applied voltage the system therefore tends naturally to rise in temperature up to a point where radiation losses bring the system into thermal equilibrium. A further increase in $V_A$ then sets the process going again until a matrix temperature is reached at which thermionic emission occurs, whereafter the system becomes progressively unstable. A typical example of the behaviour is shown in Fig. 13, where an S-type valve has been
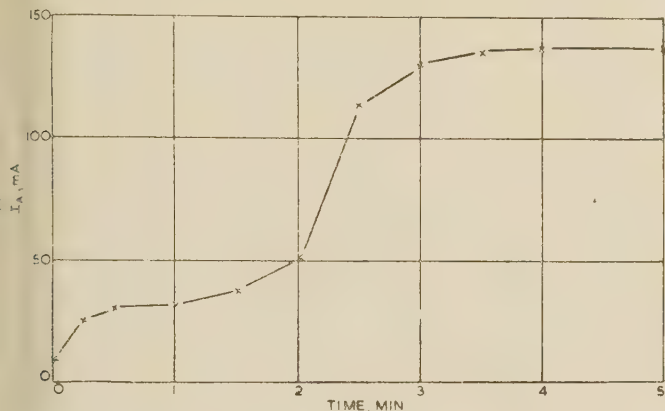


Fig. 13.—Cold-self-starting property of oxide matrix under power $V_A I_A$.

placed in series with a 25-volt battery and a ballast resistor of 00 ohms.

This self-starting property has been mentioned because it has a bearing on the practical determination of the characteristic shown in Fig. 11. Since the system is dynamic, one precaution must be taken to ensure that the core temperatures change slowly during the operation and that $T_C$ and $T_A$ are measured simultaneously. In practice, this proves a simple task if $V_A$ is advanced by small increments and the temperatures are measured on direct-reading moving-coil-type pyrometers.

### (4.3) Solid Conduction at $1000°$ K

In Section 3 it was concluded that the whole of the current $I_A$ at $1000°$ K was emitted thermionically at the cathodic core and travelled through the vacuum pores of the matrix. This view must now be modified to include a small element of $I_A$ which may travel by way of a solid semi-conduction process. The magnitude of this element can be estimated from Fig. 4 by extrapolation of the solid-conductivity characteristic; at $1000°$ K the solid resistance is about 350 ohms, compared with the total resistance of about 15 ohms. The current travelling vacuum-wise is therefore more than $95\%$ of the total current $I_A$. Thus, for practical purposes the conclusions set out in Section 3.4 remain unaffected.

### (5) CONCLUSIONS

The results set out above are in complete agreement with the hypothesis of Loosjes and Vink. In the examined range 900–$1100°$ K, effectively the whole current $I_A$ is thermionically emitted at the cathodic-core surface and travels in vacuum through the matrix. During passage the electrons progress on a start-stop basis, dissipating energy uniformly by successive non-elastic collisions with the solid oxide particles. The cooling effect at the cathodic-core surface is similar to that predicted theoretically.

In the examined range, 300–$700°$ K, the transmission mechanism is essentially one of solid semi-conduction and no act of thermionic emission is involved.

### (6) ACKNOWLEDGMENTS

# ON THE AMPLIFICATION FACTOR OF A TRIODE VALVE: PART 2

By Professor E. B. MOULLIN, M.A., Sc.D., Past President.

## SUMMARY

A recent paper showed that in the well-known relation $I = f(V_a + \mu V_g)$, the parameter $\mu$ (commonly called the 'amplification factor') should be a constant, and thus independent of the magnitude of $I$. Though long experience has shown that $\mu$ is substantially independent of $I$, yet the derivation, used in that paper, for calculating the value of $\mu$, appeared to show that it ought to be completely independent of $I$. The classic derivation of $\mu$, e.g. that used by H. J. Van der Bijl, appeared to show that the classic formula for $\mu$ was exact only in the limit when $I$ was vanishingly small.

This paper describes measurements designed to test whether $\mu$ really is independent of $I$. A balance method was devised which was capable of measuring $\mu$ to an accuracy of about 1%. The valve which was tested consisted of a separately heated disc cathode, 8 mm in diameter and an anode (also 8 mm in diameter) 0·55 mm distant from it. The distance between the grid plane and the cathode was 0·15 mm.

Fig. 3 shows the measured values of $\mu$ plotted as a function of $V_g$ for three different constant values of anode current. It shows that, for a given value of $V_g$, $\mu$, in fact, increases by some 20% as $I$ is increased from 3 to 11 mA. It also shows that, in fact, $\mu$ decreases by about 20% when $I$ is constant, as the negative value of $V_g$ is increased from about 2 to 8 volts.

Fig. 4 shows that, for constant $I$, the effect of changing $V_g$ is removed by a substantial reduction of cathode temperature; but this reduction does not remove the increase of $\mu$ with increase of $I$. This means that the increase of $\mu$ with $I$ is due to the increase of distance between grid-plane and barrier—an increase which must be significant for a valve in which the distance between grid plane and cathode is only 0·15 mm. It is argued, it is thought conclusively, that the effect of $V_g$ is due to the periodic fluctuations, across the plane of the barrier, of the current density crossing it. The author is convinced that, if a valve had been used in which the pitch of the grid wires was small compared with their distance from the barrier plane, $\mu$ would be independent of both $I$ and $V_g$. In other words, $\mu$ was constant in the early separately-heated cathode valves.

Section 5 points out that the necessary and sufficient condition for constant anode current is that any change in $V_g$ must not cause any change on the positive charge on the cathode. Accordingly the positive charge, extracted from the grid to make it more negative, must be handed on, unchanged, to the anode, thereby increasing its potential. If the electric force due to the space charge between grid and anode is ignored as unimportant, and it is shown that this must be true, $\mu$ is equal to the product of the capacitance between grid and anode and the capacitance between grid and the barrier plane, both in the absence of space charge—a form which has long been known but whose meaning has always seemed rather obscure. Its validity depends only on (*a*) ignoring any striation in the stream of anode current, and (*b*) ignoring the effect of the presence of space charge between grid plane and anode.

Section 6 explores the dependence of $\mu$ on the ratio of peak grid-swing to mean grid potential. Experiment shows that $\mu$ is constant, within about 1%, for all peak grid swings which do not exceed the grid bias.

## (1) INTRODUCTION

About the year 1915, H. J. Van der Bijl discovered experimentally that, with a given current to the anode of a triode valve,

if the observed voltage of the anode and of the grid were plotted as rectangular co-ordinates, the points of observation lay on what appeared to be a straight line. This observed fact is often expressed by the familiar equation $I = f(V_a + \mu V_g)$, where $\mu$ was a constant, and one which was approximately independent of $I$.

Within a few years of the discovery of this remarkable property of a triode, Van der Bijl published a study relating to the electric field of a charged grating of wires, and likened it, very plausibly, to the problem of the triode. By this means he obtained an algebraic formula for the constant $\mu$. Numerical evaluation of this formula yielded results which evidently were approximately correct. But his formula for $\mu$ explicitly ignored the electric forces arising from the electrons in transit from cathode to anode. Thus his expression for $\mu$ appeared to be the limiting value for a vanishingly small current. His exposition seems to have been accepted, rather blindly, for the next 40 odd years. Experience showed that, in fact, the measured values of $\mu$ were substantially independent of current over a very wide range. This experience might well have given the clue that the value of $\mu$, valid only in the limit when the current was vanishingly small, could scarcely have been derived on a basis which really was sound; but, in fact, it did not give the clue.

In a recent paper[1] the present author has shown that the force urging the electrons to proceed to the anode arises only from the electrons which are in transit. Consequently, any derivation of $\mu$ which assumes explicitly that the current is vanishingly small must, *ipso facto*, not be a sound representation of a triode. In the correct development, $\mu$ turns out to be independent of the current, and this constant value happens to agree with that calculated by Van der Bijl for the limiting value when the current is zero. A crucial experimental test of the soundness of the present writer's treatment must be to find by observation that $\mu$ is, in fact, independent of $I$. Accordingly the present author set up some apparatus by which $\mu$ could be measured, using a balance method, with considerable accuracy. This paper is concerned chiefly with the result of these measurements. The experimental method of measuring $\mu$ is described.

The familiar formula for $\mu$ contains the distance $g$ between the plane of the grid wires and the barrier plane, which is a small distance from the cathode. If $\mu$ is to be independent of $I$, it is essential that a change of $I$ shall not cause a change of the distance $g$; in other words, the inescapable approach of the barrier towards the cathode, as the anode current increases, must not cause an appreciable increase in $g$. Until some ten years ago, the mechanical method of constructing the grid of a triode was such that it was obviously unimportant to the calculated value of $\mu$ whether $g$ was taken as the distance from grid plane to cathode or as the slightly smaller distance from grid plane to the barrier plane, wherever the barrier might reasonably be assumed to be. But in more recent times, the methods of mechanical manufacture have improved so markedly that the distance between grid plane and cathode may well be no more than $\frac{1}{8}$ mm. In such circumstances the inevitable small movements of the barrier, caused by changes of $I$, will certainly be significant in the calculated value of $\mu$. Hence, in triodes

which $g$ is only a small fraction of a millimetre, it is clear that $\mu$ will not be independent of $I$—not because the force due to the moving electron was changing, as such, but because in effect the geometry of the triode was changing significantly with $I$.

The three curves in Fig. 3 show the measured values of $\mu$ plotted as a function of $V_g$ for three constant values of anode current. Ignoring, for the present, the finite effect of changes of $V_g$, it is evident that $\mu$ increases with anode current, in fact from about 25 to 30 as the current increases from 3 to 11 mA. The cathode temperature being constant, an increase in anode current must cause the barrier to move closer to the cathode surface and thus increase the distance $g$ between grid plane and barrier; and evaluation of the formula for $\mu$ shows that an increase of $g$ does tend to cause an increase in $\mu$.

Fig. 4 shows $\mu$ plotted as a function of $V_g$ for two different anode currents when the temperature of the cathode was very much reduced. This decrease of temperature has resulted in $\mu$ increasing from 24 to 35 when the anode current was about 4 mA. Figs. 3 and 4 are in accordance in showing that $\mu$ is appreciably a function of anode current in this valve, not because $\mu$ was a function of anode current, *per se*, as an effect of space charge, *per se*, but because the change of current in effect changed the geometry on which $\mu$ depends. The valve was being made to function as a variable-mu valve, in the most accurate sense of the term.

Accordingly the measured results do not conflict with the main finding of Reference 1, namely the argument showing that $\mu$ should not be a function of anode current, as follows implicitly from the work of Van der Bijl onward. To make direct observations on an old type of triode, with large spacing between grid plane and cathode, seemed accordingly to be ill-judged and irrelevant.

Fig. 3 shows that when the barrier is very close indeed to the grid plane, then $\mu$ is a function (to a small degree) of $V_g$. The inference is pretty clear that this is due to a considerable concentration of density of anode current in the spaces between the grid wires—an effect which was ignored in the argument set out in Reference 1.

Thus these accurate measurements of $\mu$ appear to show that the treatment of a triode developed in Reference 1 is both valid and complete for the old pattern of triode, for which, in fact, the whole concept of $\mu$ was developed. It is only with triodes in which the grid-cathode clearance is exceedingly small that the original concept of a constant $\mu$ may possibly need to be treated with a small amount of reserve.

The present paper describes some experimental work which has been done to extend and test the analytical work described in Reference 1. In 1913 and 1920 H. J. Van der Bijl[2,3] described the experimental discovery that (at least provided that the grid of the triode was negative) the anode current $I$ was a function of $V_a + \mu V_g$), where $\mu$ was a constant depending on the geometry of the valve. Within this period an analytical description of this property was developed and the numerical value of the factor $\mu$ was calculated in terms of the geometry of the valve. However, the derivation was said explicitly to be valid only in the limiting case when the current was vanishingly small—in other words, the effect of space charge was ignored. The present author has pointed out[1] that it is absurd to ignore the effect of space charge, since it is the space charge alone which causes the electrons to move from the 'barrier region' to the anode. Taking into account this basic principle of operation, he showed that the classic and limiting value of the constant $\mu$ should be correct for all values of anode current, from zero upwards. The experimental work, to be described here, was undertaken to determine whether or not the factor $\mu$ was independent of current in the triodes used in engineering practice.

The Van der Bijl principle is perhaps described more accurately as follows: for any given anode current ($V_a + \mu V_g$) is constant and $\mu$ is substantially independent of this current. Accordingly if, for any given current, $V_a$ is plotted as a function of $V_g$, the result should be a straight line and the family of such lines (for various constant currents) should be very nearly parallel. This is illustrated in Fig. 1. The experiments, now to be described,
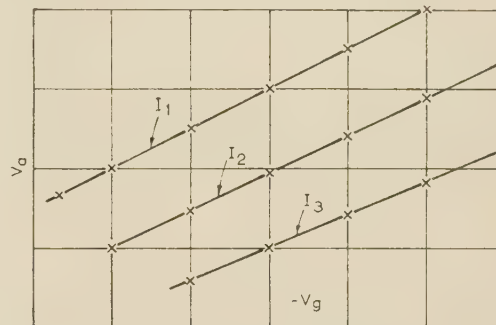
**Fig. 1.**—Graphical display of the equation $I = \mathrm{f}(V_a + \mu V_g)$.
The lines should be straight and parallel.

were designed to test accurately whether (*a*) the lines typified by Fig. 1 really are straight, and (*b*) if so, they are parallel.

The method used was to make an accurate measurement of the slope of any one line at many points along its length. This was done by applying small anti-phase sinusoidal fluctuations of $V_a$ and $V_g$ and adjusting their ratio until the consequent sinusoidal fluctuations of anode current passed through their zero value. The diagram of connections for the test is shown in Fig. 2, in which I is a d.c. 0–10 mA milliammeter, and D is a
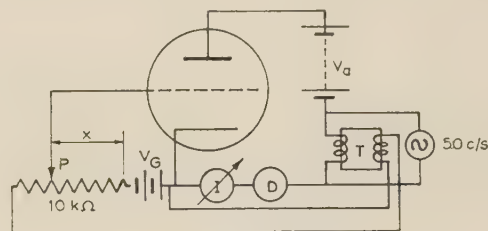
**Fig. 2.**—Circuit diagram to describe the balance method used for measuring $\mu$ in terms of $x$ and $T$.

reflecting dynamometer instrument whose fixed coils are excited from the 50 c/s mains supply. Its sensitivity was 160 mm per mA (r.m.s.) at 50 c/s. For successive values of $V_g$, $V_a$ was adjusted until $I$ attained its assigned value. Then the wander point P on the 10-kilohm voltage divider was adjusted until the deflection of D passed through zero, at an observed value of $x$. The sensitivity was such that it was possible to ascertain that the alternating component of anode current was less than 10 $\mu$A.

If the turns ratio of the transformer T was $k$, the value of $\mu$ was $k/x$ when $x$ had been adjusted so that the deflection of D was zero. The voltage divider was constructed from ten resistors in series, each of 1 kilohm, its switch system being such that the wander point P could be set at any tenth of any one of the ten resistors. It often happened that a setting of, say, $x = 0.76$ produced a small right-hand deflection of D whereas $x = 0.77$ produced a small left-hand deflection. In such circumstances the correct value of $x$ would be recorded as, say, $x = 0.763$. Thus $\mu$ could usually be determined to closer than 1%. Since the tests were concerned with changes of $\mu$ as a

function of $V_g$, for assigned values of $I$, the value of $k$ was unchanged during a given test. Hence, so far as the changes of $\mu$ are concerned, an inaccuracy in the various possible turns ratios, available on the transformer, would have been of no importance.

## (2) DETAILS OF TRIODE AND TESTS AT CONSTANT CATHODE TEMPERATURE

An appropriate triode for the test was a pattern D.E.T. valve. It is similar in design to, but larger than, the type CV273 (illustrated in Fig. 27 of Reference 4), and was chosen largely because it is a very close approximation to a planar triode. The anode and the cathode are circular discs 8 mm in diameter. The distance between the cathode and grid planes is approximately $0 \cdot 15$ mm, and the distance between the anode and grid plane is $0 \cdot 4$ mm. Thus

$$\frac{d}{g} = z = \frac{4}{1 \cdot 5} = 2 \cdot 66$$

The grid wires are $0 \cdot 05$ mm in diameter and their pitch is $0 \cdot 21$ mm. The factor $B$ is defined by the equation

$$-B = \frac{s}{\pi} \left[ \log \sinh \frac{\pi x}{s} - \frac{\pi x}{s} \right]_c^g$$

In this valve $c/s = 2 \cdot 5/20$, whence $\pi c/s = 0 \cdot 4$. Moreover, since the distance between grid plane and barrier must be less than $0 \cdot 15$ mm, the value of $g/s$ must be less than $15/20$. Accordingly this is a valve in which the pitch of the grid wires is inevitably larger than the distance between grid plane and barrier. Taking $g/s$ as $\frac{3}{4}$, $\pi g/s = 2 \cdot 35$. Then

$$-B = \frac{s}{\pi} \left[ \log \frac{\sinh 2 \cdot 35}{\sinh 0 \cdot 4} - (2 \cdot 35 - 0 \cdot 4) \right] = \frac{s}{\pi} \left( \log \frac{5 \cdot 19}{0 \cdot 41} - 1 \cdot 95 \right)$$

$$= \frac{s}{\pi}(2 \cdot 6 - 1 \cdot 95) = 0 \cdot 65 \frac{s}{\pi}$$

whence

$$\mu_1 = \frac{2\pi d}{0 \cdot 65 s} = 1 \cdot 54 \times \frac{2\pi d}{s} = 1 \cdot 54 \times \frac{2\pi 0 \cdot 4}{0 \cdot 21} = 18 \cdot 5$$

Suppose that the distance between the cathode and the barrier is $0 \cdot 1$ mm; then $g/s = 5/20$ and $\pi g/s = 0 \cdot 8$, and

$$-B = \frac{s}{\pi} \left( \log \frac{\sinh 0 \cdot 8}{\sinh 0 \cdot 4} - 0 \cdot 4 \right) = \frac{s}{\pi}(0 \cdot 77 - 0 \cdot 4)$$

whence

$$\mu_2 = 2 \cdot 7 \times \frac{2\pi d}{s} \quad \text{and} \quad \mu_2/\mu_1 = \frac{2 \cdot 7}{1 \cdot 54} = 1 \cdot 75$$

Hence for a given current it might well be expected that $\mu$ would increase very considerably with the temperature of the cathode. Since $c/s = 0 \cdot 125$, it is clear[1] that these calculated values of $B$ cannot be invalidated appreciably by the finite diameter of the grid wires. Moreover, for a given cathode temperature $g$ must increase with $I$, thus involving a diminution in the value of the geometrical factor $B$. Thus it is to be expected that, in this valve, $\mu$ may well increase appreciably with increase of anode current. The heater current was about 1 amp at 6 volts. The anode voltage should not exceed 400 volts or the anode dissipation 20 watts; the grid conductance was expected to be about 10 mA/V.

Fig. 3 shows curves of measured values of $\mu$ as a function of $V_g$ for three values of constant anode current, the heater voltage being 6 volts. It shows that $\mu$ tends to about 23 (which is about halfway between the calculated values of $\mu_1$ and $\mu_2$ above). Even for constant $I$, $\mu$ is not precisely constant but passes through
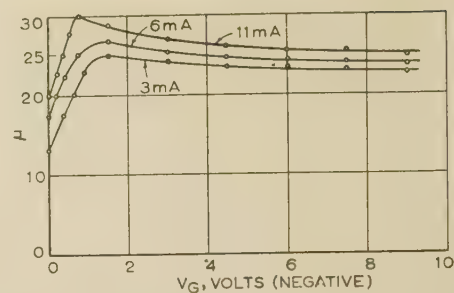


Fig. 3.—Typical test of $\mu$ as a function of $V_g$ with $I$ constant, for three different values of $I$.

$V_f = 6$ volts.

a maximum at $V_g \simeq 1$ volt (negative). Moreover $\mu$ increases slightly with $I$—from about 23 to 26 as $I$ increases from 3 to 11 mA. Accordingly the lines typified by Fig. 1 (Van der Bij relationship) are neither precisely straight nor parallel.

That $\mu$ should increase slightly with $I$ for a constant cathode temperature is to be expected, since an increase of $I$ will force the barrier to move towards the cathode and thus increase the distance $g$. But that, for constant $I$, $\mu$ should decrease slightly as the grid is made more negative is surprising, and a rational explanation of this effect must now be sought.

## (3) TESTS OF EFFECT OF CATHODE TEMPERATURE

The tests recorded in Fig. 4 differ only from those of Fig. 3 in that they were obtained at a reduced cathode temperature, in
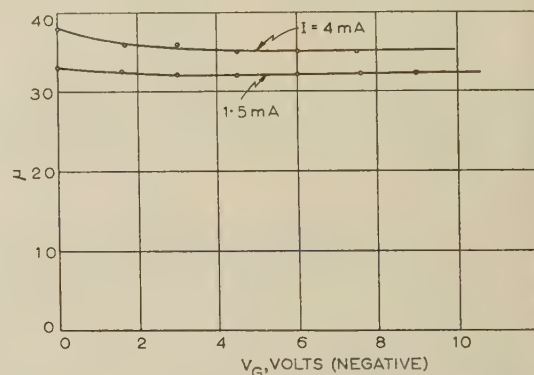


Fig. 4.—Typical test result as in Fig. 3, but with much reduced cathode temperature.

$V_f = 3 \cdot 3$ volts.

that the potential difference across the cathode heater was reduced from 6 to $3 \cdot 3$ volts. Fig. 4 shows that, for a given anode current, the measured values of $\mu$ are now independent of $V_g$, provided that $V_g$ is more negative than about 1 volt. The observed value of $\mu$ still increases with $I$, as is to be expected. But now $\mu$ has increased from about 25 to about 35. The cathode emission in Fig. 4 must have been considerably less than in Fig. 3, with the result that the barrier must have been brought much nearer to the cathode, with consequent considerable increase of $g$. And thereby a substantial increase in $\mu$ is to be expected. In fact, $\mu$ has increased in a ratio of about $35/25 = 1 \cdot 4$. We have seen earlier that, if the barrier-to-cathode distance decreased from $0 \cdot 1$ mm to zero, this would be expected to increase $\mu$ in the ratio $1 \cdot 75$. Accordingly an observed increase of $1 \cdot 4$ times is not unreasonable. We appear now to have found that the dependence of $\mu$ on $V_g$ can be removed by decreasing the cathode temperature, even though it is not yet apparent why this should be.

Curves corresponding to Fig. 4 were plotted when the potential ifference across the heater was 3·6 and 3·8 volts, respectively, ut without introducing a dependence of $\mu$ on $V_g$; but it did nuse a reduction of $\mu$ for a given current. This last is in ccordance with expectation, since increasing temperature will ecrease $g$. But when the heater voltage was increased to 4·1, ne measured values of $\mu$ decreased appreciably and progressively ith increase of $-V_g$. This implies that the dependence of $\mu$ n $V_g$ does not occur until $g$ is less than some definite size.

The presence of the grid will cause the current density to oncentrate somewhat in a succession of planes normal to the arrier, and it would seem as though the overall effect of this henomenon is not significant until $g$ is less than some definite alue. This leads us to consider more closely the formation of barrier surface in the presence of a grid.

### (4) THE BARRIER SURFACE IN A TRIODE

Fig. 5 serves to describe a planar triode having an anode A, cathode C and grid G. Between G and C there must be some
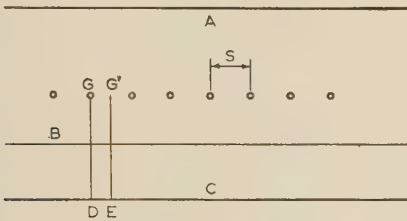


Fig. 5.—Diagram showing anode A, grid GG', barrier plane B and cathode C, for planar triode.

urface at which the normal component of electric force passes urough zero, in the process of changing sign; it is commonly lled the 'barrier surface'. Below B electrons are moving out-ards from the cathode and returning back to it. Between B nd G electrons are moving outwards only, and, provided that is sufficiently negative, all will continue to move outwards ntil they collide with the anode. The barrier surface must cist, since it provides the mechanism which permits the anode urrent to be less than the rate of emission from the cathode, hich depends only on the temperature of the cathode. All ectrons which reach the barrier surface, against the electric rce (which is in the direction B to C) at all points between B ld C, will cross the barrier and proceed onwards under the tion of the electric force (which is directed towards A at all ints between B and A), even those whose outward velocity ls fallen just to zero when they reach B. Since the region tween B and C is occupied by a gas of negatively charged rticles, it follows that the charge on the cathode plate must be sitive in order that it can be possible for the normal electric rce across B to be zero. When the charge on the grid is gative, there must be an equal positive charge on the anode. the grid were a continuous flat sheet, the net electric force tween C and B would be zero. Let the charge on the wires of e grid be negative. There is a gas of electrons (therefore aring a negative charge) between the anode plate A and the rrier surface B, where the force is zero by definition. Conse-ently, A must bear a positive charge equal in amount to the tal negative charge on the grid wires together with the total nount of negative charge in the electron gas which is in transit tween B and A. It is convenient to think of this total positive arge as consisting of a charge $Q$ equal to the total negative arge on the grid wires together with a charge $q$ equal to that ne by the electron gas in transit between B and A. If the arge $Q$ on the grid wires were smeared uniformly over the

grid plane, the net resultant force due to $-Q$ on this grid plane and $+Q$ on the anode would be zero at all points between the grid plane and the barrier. However, the charge $-Q$ is not smeared uniformly over the grid plane but is concentrated into filaments, namely the thin grid wires. Because of this concentration the force near these thin wires is much greater than it would be if $Q$ were smeared uniformly, as indeed $+Q$ is smeared uniformly over A. This excess of force will continue all along a line typified by GD in Fig. 5, the excess diminishing asymptotically towards zero as D is approached. The net resultant force along GD is equal to the difference between the attraction on an electron due to the positive charge on A and the slightly greater repulsion due to the charge concentrated on the filamentary grid wires. Accordingly the net electric force at any point on the line typified by GD must be in the direction GD, with respect to an electron proceeding from D towards G.

The force at the point typified by G', midway between two consecutive wires, must be zero with respect to the charges on the wires. Also the force at G' due to the positive charge smeared uniformly over A is such as to attract an electron towards A. Continuation of this argument will show that the net resultant force on an electron must be in the direction EG' at any and every point along the line EG', this force being a maximum at G' and tending asymptotically towards zero at E. Accordingly, where the lines GD and G'E cross B, the force on an electron must be downwards where GD crosses B and upwards where G'E crosses B.

But, by definition, the normal force at all points of B is to be zero. How, then, can these two contradictory requirements be met?

Since the emission per unit area of C is controlled purely by its temperature, it seems almost certain that the positive charge on C must have a uniform density. Thus this charge on C must produce an attractive force on an electron which is constant in magnitude at all points between B and C.

Since, as we have seen, the combined effect of the charge $-Q$ on the grid and $+Q$ on the anode produce a resultant force across B, which changes sign in passing from the intersection, with B, of the lines GD and G'E, the total net force from all charges (be they the uniform smearing on the cathode C, from the electron gas, from the filaments of charge on the grid wires and the uniform smearing of positive charge on the anode A) can be brought to zero only by periodic fluctuations (in space, not in time) of density of the electron gas between C and B.

We now presume the barrier surface remains a plane, although this may not be true since it may possibly be undulating.

Consider the normal component of electric force at distance $x$ from a plane sheet, of thickness $\delta x$, of charge density $q = a_n \cos n\pi y/s$, and at a point in the plane $y = 0$. Then

$$E = 4a_n\delta x \int_0^\infty \frac{x}{x^2 + y^2} \cos \frac{n\pi y}{s} \delta y$$

$$= \frac{4a_n\delta x}{x} \int_0^\infty \frac{1}{1 + \frac{y^2}{x^2}} \cos \frac{n\pi y}{s} \delta y$$

$$= 4a_n\delta x \int_0^\infty \frac{\cos \frac{n\pi x}{s}k}{1 + k^2} dk, \quad \text{where } \frac{y}{x} = k$$

$$= \frac{2\pi a_n\delta x}{\varepsilon^{n\pi x/s}}, \text{ by a well-known integral.}$$

Consideration will show that in the normal plane $y$

$$E \quad \frac{2\pi a_n \delta x}{\varepsilon^{n\pi x/s}} \cos \cdot \frac{n\pi y}{s}$$

Take

$\frac{x}{s} = 0\cdot1$, then $\varepsilon^{-0\cdot31} = 0\cdot73$, $\varepsilon^{-0\cdot93} = 0\cdot39$, $\varepsilon^{-1\cdot55} = 0\cdot212$

if $\quad \frac{x}{s} = 1$, then $\varepsilon^{-\pi} = 0\cdot0434$, $\quad \varepsilon^{-3\pi} = \frac{1}{12\,400}$

In Fig. 6, let B be the barrier plane and let the charge density at distance $x$ below it be $-a_n \cos 2\pi y/s$. If $x/s = 1/20$ the force at the point F will be $0\cdot73 \times 2\pi a_n \delta x$. Hence consideration will
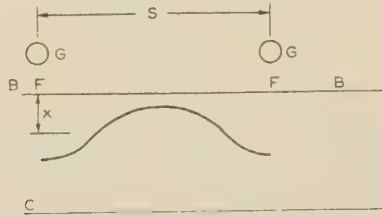


Fig. 6.—Diagram to describe fluctuation of current density across a typical plane between barrier and cathode.

show that if the gas density between B and C varied with $x$ in the manner which would cause the force all over B to be zero and a superposed density fluctuation typified diagrammatically in Fig. 6, the force at F would be upwards. The effect at F of fluctuations in density at increasing levels of $x$ will decrease exponentially with $x$. To put this slightly differently, the residue of upward force at F arises mainly from the fluctuations of density which are only slightly below B. The residue of force at F can be made to balance the downward force arising from the grid wire G by appropriate choice of $a_n$. Thus a barrier can be maintained in the presence of a grid, and with a uniform charge density on the cathode, if the gas density between B and C tends to be greater than the average over the middle half of the intervals between successive wires. And it does look as though the barrier surface can be a plane.

The force at a distance $x$ below the centre of a grid wire in Fig. 6 is

$$E = \frac{2\pi v}{s}\left(\coth \frac{\pi x}{s} - 1\right) = \frac{2\pi v}{s} \times 0\cdot78$$

if $x/s = \frac{1}{5}$. At the same distance above the centre of the wire the force would be $(2\pi v/s) \times 2\cdot78$. To balance the force at the barrier plane, the decrease of gas density must be of the order of $2\pi a_n \delta x \simeq (2\pi v/s) \times 0\cdot78$, or $a_n \delta x \simeq 0\cdot78v/s$. From the previous paper[1] $q/s = y$ times the charge in transit from barrier to grid plane, where $y$ is a number larger than, say, 5. Accordingly the charge below the barrier and under a grid wire must be diminished by about $y$ times the average amount of charge in transit, per unit area, between barrier and grid. This must surely mean a very marked concentration of current through the middle half of the grid spaces. If $x/s = 0\cdot7$, i.e. the barrier is almost at the cathode, the figure which has been $0\cdot78$ previously becomes $0\cdot025$—a diminution of about thirtyfold. Thus it is clear that a considerable reduction of cathode temperature can and will have a marked effect in making the anode current much more uniform across the grid plane.

It is now clear that for a given anode voltage, and thus an ostensibly given position of the barrier, the anode current will become progressively more non-uniform in density as the negative charge on the grid is increased; is this directly associated with the observed progressive small diminution of $\mu$? Moreover, and as a second effect, the fluctuations in density over the barrier may well be equivalent to a small change in the position of the barrier. If this change is towards the grid, it alone would result in a progressive diminution of $\mu$; if the movement is in the other sense, the two suspected effects will operate in opposite directions.

## (5) FURTHER CONSIDERATION OF GRID POTENTIAL AND THE RELATION BETWEEN $V_a$ AND $V_b$ FOR CONSTANT $I$

The various points raised in the paper appear to make it worth while to develop the relation $(V_a + \mu V_g) = $ constant by quite another method, as follows, and for this purpose the schematic of the triode shown in Fig. 7 will be helpful.
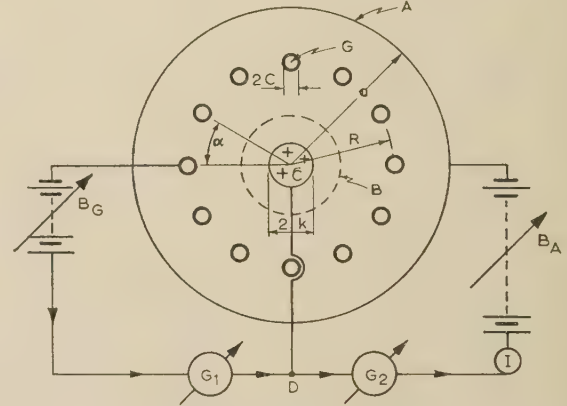


Fig. 7.—Diagram of cylindrical triode, designed to describe passage of charge from grid to anode.

Inside the cylindrical anode A there is the grid G, which it is helpful to show as squirrel cage in construction. This grid is connected to the cathode C by means of a battery $B_G$, shown variable in voltage, the connection being made through a ballistic galvanometer $G_1$. Similarly the anode A is connected to the cathode C through a battery $B_A$ of variable voltage, through the ballistic galvanometer $G_2$. It is proposed to change the voltage $B_G$, as the independent variable, and then to make the increase in $B_A$ which is necessary to restore the anode current $I$ to the value it had before the change in $B_G$ was made.

It must be remembered that the charge on the cathode C is necessarily positive (see Section 2 of Reference 1) in order that the barrier B (a surface across which the normal force is zero) can exist.

When the voltage of $B_G$ is increased, the negative charge on the grid G must increase by some amount $Q$; and thus positive charge $Q$ must pass through $G_1$ in the direction of the arrow marked on the diagram. When $Q$ reaches the point marked there are two paths open to it: (a) up to the cathode C and (b) through $G_2$ up to the anode A. Any part of $Q$ which reaches C will increase the positive charge on C and thereby reduce the current $I$ which crosses the barrier. But any such increase of positive charge on C is forbidden to occur.

Accordingly the adjustment of $B_A$ requisite to maintain $I$ constant may be expressed, in other words, by saying that the charge $Q$ which came from the grid and reached the point then all passed on, through $B_A$, and increased the positive charge on the anode by an amount $Q$. The meaning of the condition $I$ constant is, in essence, the statement that any increase of negative charge on the grid is transferred to the anode as an increase of positive charge on it. These changes need not be infinitesimal, they may be of any size.

Since the electric force produced by the charge on the squirrel-cage grid is extremely small at the cathode, and alternates in direction from point to point around it, any change of charge on the grid is very unlikely, *per se*, to have any appreciable effect on the current leaving the barrier. But this change has increased the amount of negative charge within the valve by an amount $Q$. The electric force due to it at points between G and A will be almost the same as if $Q$ were smeared with uniform density round a continuous metal cylinder having the same radius as the squirrel cage.

Since the anode is a metal cylinder, the radial electric force must be zero, through its radial thickness, and beyond it. This means that the total positive charge on the inside surface of the anode must equal the total negative charge between anode and barrier; i.e. the negative charge on the grid wires together with the total charge on all the electrons in transit. The current leaving the barrier is maintained constant, by hypothesis. Moreover, as we have just seen, the change of charge on the grid wires cannot alter appreciably the motion of electrons from barrier up to the cage radius and thus will not change the negative charge in transit between barrier and cage radius. In the notation of Reference 1, it will not change the transit time denoted there by the symbol $t_1$.) Electrons in transit between cage radius and anode will be accelerated considerably by the increased negative charge on the grid and will thereby arrive more quickly at the anode. Hence, even with a constant current leaving the barrier, the total space charge in transit above the squirrel cage will be decreased as the result of the increase $Q$ of negative charge on the grid. Accordingly the requisite increase of positive charge on the anode must tend to be less than $Q$. But the condition that $I$ should be constant is that the anode charge should increase by an amount $Q$. Hence the two conditions are not identical. In fact, this means that the requisite increase of $V_a$ (for a given current) is slightly less than in proportion to the increase of negative charge on the grid. Inevitably this will mean that $V_a + \mu V_g$ is not precisely constant for a given $I$. The imprecision will turn out to be the space charge between grid and anode.

But it was shown in Section 8 of Reference 1 that, in order to prevent grid current, $Q$ must be at least of the order of $\frac{1}{2}\mu I t_1$. It is also shown that the charge in transit between cage radius and anode is much smaller than $I t_1$, roughly in the order of $^{-1/3}$. Hence the charge in transit between cage radius and anode is very small compared to $Q$; the more so as the grid is made more and more negative. All this emerges from Tables 5 and 6 of Reference 1, where it is shown that $t'/t_1$ is much less than unity and changes slowly as $y$ increases from, say, 6. In these Tables, the parameter $y$ is proportional to $Q$, from the relation $Q = yIt_1$; the space charge above this plane grid is $It'$, whence the total negative charge on grid plus the space charge above it is

$$Q + It' = It_1\left(y + \frac{t'}{t_1}\right) = It_1 y\left(1 + \frac{1}{y}\frac{t'}{t_1}\right)$$

Table 1 is derived from Table 4 of Reference 1. This serves to show that, with $z = 1$, the positive charge on the anode is only

### Table 1

| $y$ | 6 | 10 | 27·3 |
|---|---|---|---|
| $1 + \dfrac{1}{y}\dfrac{t'}{t_1}$ | 1·025 | 1·014 | 1·003 |

of the order of 1% greater than the charge on the grid. This is equivalent to the statement at the end of Section 12.2 of Reference 1, that the effect of the electrons in transit between grid and anode is negligible.

The negative potential of the grid is equal to the difference between (a) the work done in bringing unit charge from the barrier up to the surface of a grid wire, against the force arising from the charge on the grid wires, and (b) the work done by the space charge in moving unit charge from the barrier up to the radius of the grid. Clearly (a) does not depend on the existence of space charge, and hence $V' = qB$, where $B$ is a purely geometrical constant having the nature of a capacitance. Case (b), which arises from the space charge, is obviously a function of current. Hence $V_G = qB - f(I)$. When $I$ is maintained constant, it now follows that any change of $q$ is proportional to any change of $V_G$. This is true provided that (b) is a function of $I$ only; just what that function is does not matter. Accordingly, the relation between changes of $V_G$ and changes of $q$ does not involve space charge. As discussed in the previous Section, large changes of $q$, even with a given current, may cause the streams of current flow to become more and more striated, and in that case (b) will not be a function of $I$ only. But it is only in this way that space charge behind the grid can affect the relation between changes of $q$ and changes of $V_G$. Thus the existence of space charge can, at the most, have only a second-order effect on this relationship.

We have seen that the space charge between grid and anode is negligible compared with the charge on the grid, and hence the electric force in this region must differ insensibly from what would obtain if the electrons in transit *in this region* did not exist. Hence if the charge on the grid increases by $\delta Q$ the anode voltage must be increased by $\delta V_a$, where

$$\delta V_a = C_{GA}\delta Q$$

and

$$C_{GA} = \frac{1}{2\log\dfrac{a}{R}} = C_{GA}C_{GB}\delta V_G$$

whence we have obtained the relation $\delta V_a + \mu\delta V_g = $ constant, where $\mu = C_{GA}C_{GB}$, valid for all currents. Thus $\mu$ has been obtained in terms of capacitances and is derived in the general form which was done in early days. But it has now been obtained in a way which explicitly ignores space charge only to the extent (i) that the striation of the flow of a given current does not change appreciably as the negative charge on the grid is increased, and (ii) the well-justified simplification that the presence of space charge between grid and anode is unimportant. It is clear that $\mu$ will not depend on $I$, as such, though it does leave a loop-hole for $\mu$, at a given current, being slightly dependent on $V_g$.

Now

$$V_1 = \frac{2Q}{N}\left\{\log\frac{R}{NC} + \log\left[1 - \left(\frac{b}{R}\right)^N\right]\right\}$$

from Section 7 of Reference 1. Whence

$$\mu \equiv C_{GA}C_{GB}$$

$$= \frac{\log\dfrac{a}{R}}{\dfrac{1}{N}\left\{\log\dfrac{R}{NC} \div \log\left[1 - \left(\dfrac{b}{R}\right)^N\right]\right\}}$$

This agrees with eqn. (22).

### (6) μ AS A FUNCTION OF VOLTAGE SWINGS

It is perhaps worth while to remember that, following Van der Bijl, the parameter $\mu$ has been defined as the ratio of corresponding changes of anode and grid voltage required to maintain the anode current at a given value. The presumption is

that any given line in Fig. 1 is straight. If this be really true, the observed value of $\mu$ should be independent of the absolute value of $V_a$ and $V_g$. In the method of measurement used in this paper, it should follow that the measured values of $\mu$ are independent of the applied alternating voltage swings applied to the grid and anode, provided only that they have been adjusted to be in the ratio which does not produce any a.c. component of anode current. But the measurements recorded in Fig. 3 show that, for a given mean anode current, $\mu$ is not entirely independent of $V_g$ when the voltage swings are very small. Accordingly it would be expected to follow that $\mu$ would be a function of voltage swing; at least, when these swings are large. Therefore it seemed worth while to observe the range of $\mu$ which occurred when the swing of anode voltage was comparable with the mean anode voltage. Accordingly the swing was increased progressively up to 120 volts (r.m.s.), i.e. about 170 volts (peak), in circumstances when the mean anode voltage was within the range 210–330 volts, thus causing the anode voltage to fall, instantaneously, to some 40 volts. The corresponding grid swings were up to $7\frac{1}{2}$ volts (peak), with a mean grid potential of 8 volts; thus the grid did not become positive. When the heater voltage was 6 volts, $\mu$ was measured at anode currents of $11 \cdot 3$, 8 and 4 mA. In these circumstances the observed values of $x$ (see Fig. 2) required to make the a.c. component of anode current zero were certainly constant to within less than 2%. With a given current meter, the sensitivity of the balance obviously increased with the voltage swings. The 10-kilohm voltage divider (again see Fig. 2) had only 100 steps on it, and thus no intermediate setting was obtainable between, say, $0 \cdot 46$ and $0 \cdot 47$. Thus it was not practicable to measure $\mu$ precisely to closer than within some 2%. But to this limit of accuracy it was certain that $\mu$ was not a function of voltage swing when the heater voltage was 6 volts. In fact, the results recorded in Fig. 3 show that $\mu$ must have varied slightly during a cycle of voltage swing. Even though this effect must, in fact, have obtained, experience shows that the net effect of such changes is not sufficiently apparent to affect $\mu$ to within $2\frac{1}{2}\%$.

Admittedly the a.c. galvanometer responded only to the fundamental component of current, and thus at intervals during the cycle there could have been a higher harmonic of anode current

Though measurements with a very small grid swing show that $\mu$ decreases measurably with increasing mean $V_g$, the measurements just described show that the general results of the paper are valid at least up to peak grid swings nearly equal to the grid bias.

The results recorded in Fig. 4 show that this must be still more nearly true when the triode is operated with an appreciably reduced cathode temperature. For example, the heater voltage was reduced from 6 to 4 volts, and $\mu$ was measured with constant anode currents of 10 and 4 mA. When the anode swing was increased progressively up to 120 volts (r.m.s.) again, $\mu$ remained constant to within less than 2%, with 8 volts bias on the grid. Hence, even if the valve was being operated intentionally in circumstances such as to make use of the variable-mu properties of this particular triode (having a clearance of only $\frac{1}{4}$ mm between grid and cathode), it would still operate (in any arranged value of $\mu$) with a value of $\mu$ which was constant over a peak grid swing almost equal to the grid-bias voltage. In short, the variable-mu properties are not confined to vanishingly small grid swings. This is in accordance with the arguments set out in Reference 1.

## (7) REFERENCES

(1) MOULLIN, E. B.: 'On the Amplification Factor of the Triode', *Proceedings I.E.E.*, Monograph No. 211 R, November 1956 (**104 C**, p. 222).
(2) VAN DER BIJL: 'Initial Energies of Photoelectrically-Liberated Electrons', *Verhandlungen der Deutschen Physikalischen Gesellschaft*, 1913, **15**, p. 330.
(3) VAN DER BIJL: 'The Thermionic Vacuum Tube and its Applications' (McGraw-Hill, New York, 1920).
(4) BELL, J., GAVIN, M. R., JAMES, E. G., and WARREN, G. W.: 'Triodes for Very Short Waves—Oscillators', *Journal I.E.E.*, 1946, **93**, Part IIIA, p. 833.

# THE SLIDING CONTACT OF GRAPHITE AND COPPER

By W. DAVIES, Ph.D., B.Sc., Associate Member.

## SUMMARY

Experiments with well-developed sliding contacts of graphite and copper have shown the marked influence of atmospheric and electrical conditions on the kinetic friction and contact resistance.

Dry oxygen at low pressures appears to be lubricating for currents of any magnitude flowing in either direction through the contact. However, at higher pressures of this gas it is no longer lubricating and its effect on the friction and resistance is markedly dependent upon the direction of the current.

Water vapour alone is found to be lubricating, but in company with oxygen its action is complex and it modifies the effect of oxygen profoundly. It lubricates currentless and negative brushes, but increases the kinetic friction of positive brushes, probably as a result of its stabilization of the contact interface.

Increase in the pressure of dry oxygen always increases the contact resistance of positive brushes, but an initial increase at moderate pressure with negative brushes is followed by a marked decrease at higher pressures.

Water vapour alone has only a slight effect on contact resistance, but it modifies the effect of oxygen quite remarkably, especially in the case of positive brushes. Again its action is complex, but in the main it tends to reduce the contact resistance of positive brushes and to increase that of negative brushes.

## (1) INTRODUCTION

The sliding contact of graphite and copper is one of very great technological importance, and it is not surprising to find that it has been the subject of a good deal of investigation since its inception more than half a century ago. However, within the last decade the advent of high-altitude flight has led to much more intensive investigations of the contact. Renewed activity in this field derives from the fact that under low-moisture conditions the rate of wear of plain graphite brushes mounted in boxes in the usual manner in electrical machines is abnormally high. The atmospheric conditions which lead to brush wear in this case are well known, and the use of adjuvants such as barium fluoride to reduce the rate of wear is well established. The fundamental cause of this rapid wear and the true function of the adjuvants are, however, the subject of some speculation and of conflicting opinion. It seems to the author that this speculation and divergence of opinion almost certainly stem from our lack of knowledge of the physics and chemistry of the contact interface.

The electrical and frictional characteristics of the sliding contact are, of course, determined by the nature and structure of the interfacial region and by its chemical and mechanical stability under mechanical, thermal and electrical stresses. Consequently a satisfactory explanation of the contact characteristics requires in the first place fairly complete knowledge of the essential features of the interfacial region.

The present state of our knowledge of the interfacial region of the graphite-copper contact may perhaps be summarized briefly as follows. In the first place, the black film on the copper

is stratified with a layer of graphite flakes overlying one of cuprous oxide, and the well-known non-linearity and asymmetry of the contact are due almost entirely to this film. Secondly, at the rubbing surface of the graphite the surface crystallites lie with their slip planes almost always at a trailing angle to the plane of sliding, the angle of trail being anything up to 90°. The slip planes, it seems, are not everywhere parallel with the plane of sliding, as Bragg has supposed.

Explanation of observed phenomena such, for example, as the effect of dry oxygen on the contact resistance, and of condensible vapours on the kinetic friction, has so far been based on the assumption that the graphite layer of the black film is continuous and that the powerful intra-planar valence forces 'exposed' at the edges of the tilted slip planes of the brush-face crystallites can be neutralized by certain gases and condensible vapours. The second of these assumptions is particularly well founded as a result of the work of Bowden and Savage, but the author feels that the first assumption is by no means well founded.

It seems hardly to be expected that simply by rubbing a graphite brush on a copper slip-ring a layer of graphite would be laid down such that it would cover entirely the surface of the metal or its oxide film. It is rather to be expected that such a layer would be discontinuous at the summits of the higher asperities on the surface of the metal. This is a point of some importance because it implies that at the true areas of contact the graphite of the brush makes contact with the metal of the slip-ring via a film of cuprous oxide. Electrical conduction and sliding take place at these higher asperities; consequently the contact characteristics should be explained in terms of the structure and stability of this interface and not in terms of a graphite-graphite interface.

The experiments to be described were designed to provide information on the contact behaviour not so far available, and in the main this was obtained by simultaneous measurement of contact resistance and kinetic friction under various operating conditions.

It is hoped that examination of the results of these experiments may reveal a little of the fundamental processes taking place in the contact, while a theoretical explanation in terms of the interfacial structure already mentioned may perhaps provide a stimulus for further investigation.

## (2) EXPERIMENTAL METHOD

### (2.1) Apparatus

#### (2.1.1) Friction Measurement.

The brushes under test were mounted in a friction-measuring device so designed that the distribution of nominal pressure between a brush and the copper disc was always uniform over the arc of contact. This secured, on the average, a uniform distribution of contact spots over the brush arc. The arrangement is shown diagrammatically in Fig. 1, while Fig. 2 indicates the mechanical forces acting in the system.

Two graphite brushes were used, but since they were made to carry equal currents in the same direction and operated under

Correspondence on Monographs is invited for consideration with a view to publication.
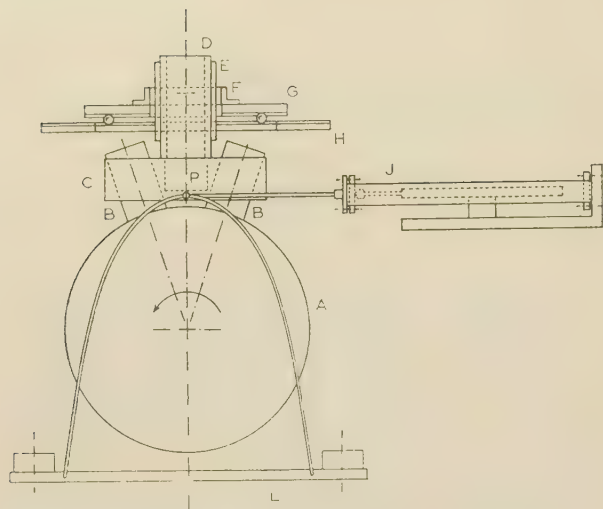W. Davies is at University College, Cardiff.

[ 203 ]

Fig. 1.—Apparatus for measurement of kinetic friction.

A     Copper slip-ring.
B, B    Carbon brushes.
C     Insulated brush-clamping plates.
D     Brass tube solidly connected to clamping plates.
E     Pivoted brass guide tube.
F     Flanged bush carrying pivots for E.
G     } Ball and plate assembly.
H    
J     Proving-ring and dial gauge.
L     Dead-weight loading platform.
P     Spindle through brush-holder, to which the proving ring is attached, and from which the loading platform is suspended. P is the effective point of application of the resultant friction force.
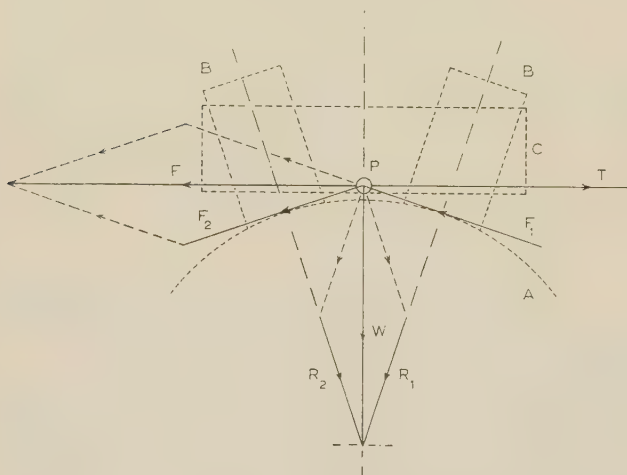


Fig. 2.—Force diagram for friction-measuring apparatus.

A     Copper slip-ring.
B, B    Carbon brushes.
C     Clamping plate.
F     Resultant friction force.
$F_1$
$F_2$ } Individual friction forces on brushes.
P     Effective point of application of resultant force F.
$R_1$
$R_2$ } Reaction forces between brushes and slip-ring.
T     Force applied by proving ring (T = F).
W     Dead weight applied by loading platform.

identical mechanical conditions, they really constituted a single brush.

The stiffness of the proving ring used to measure the friction force was such that the maximum displacement of the brush-gear was extremely small—of the order of $0 \cdot 5°$ round the surface of the disc.

## (2.1.2) Electrical Connections.

Current was led to and from the contact via the usual flexible braids on the brushes and the steel shaft carrying the copper disc.

The p.d. across the contact interface was measured by means of phosphor-bronze probes attached to the brushes at about $\frac{1}{8}$ in from the interface and by a graphite probe rubbing on a graphite disc attached to the copper ring. A graphite-graphite connection was considered essential at this point in the circuit to avoid spurious thermal e.m.f.'s.

## (2.1.3) Control of Atmospheric Conditions.

In order that tests might be carried out under controlled conditions, the apparatus described above was placed in a vacuum-tight test chamber and driven by an external motor.

Cleanliness of the atmosphere was secured by using only alcathene, polythene or mica as insulators within the chamber, and by careful cleaning of all gases admitted to the test space. In the auxiliary gas-cleaning apparatus, water vapour was removed by calcium chloride and phosphorous pentoxide, dust was removed by a tightly packed column of resinized wool fibres, and grease by a column of shavings of high-melting-point paraffin wax.

## (2.1.4) Oscillographic Traces of the 'Waveform' of Contact Potential Difference.

Continuous observation was made of the variation of p.d. across the interface at constant current as a brush moved over a selected portion of the surface of the copper disc. For this purpose a synchronizing contact was mounted on the driving shaft, and selection of a portion of interface could be made by adjustment of this contact. For photographic recording an associated single-shot technique was used for triggering the oscilloscope. These observations proved to be of considerable interest.

## (2.2) Preparation of Contact Surfaces

### (2.2.1) The Surface of the Copper Disc.

The cylindrical surface of the copper disc was prepared by lathe turning with a clean dry cutting tool, the disc being run in its own bearings to avoid any undue eccentricity.

Experience showed that the quality of surface finish was markedly affected by the speed of cutting and the depth of cut; the higher the speed and shallower the depth of cut the better was the result. In order to standardize the preparation of the surface of the copper, a cutting speed of 750 ft/min and a depth of cut of $0 \cdot 001$ in were adopted.

Following the final bedding of the graphite brushes onto the copper disc and just prior to the installation of the apparatus in the test chamber, the surface of the copper was carefully wiped with swabs of clean cotton-wool soaked in pure benzene. Using this method of preparation the surface of the metal proved to be quite reproducible.

### (2.2.2) The Surfaces of the Graphite Brushes.

Before their assembly in the brush-gear the graphite brushes were thoroughly baked-out in air at about 200° C, and then in vacuum ($0 \cdot 1$ mm Hg) at about the same temperature for at least one hour. The object of this process was to remove all traces of grease or oil on or in the brushes. For final bedding of the brushes the very finest grade of emery paper was used.

Reproducibility of the contact surfaces was in all cases verified by actual operation of the contact under selected conditions.

Freshly prepared contact surfaces of copper and graphite were always developed, naturally, by causing them to slide on one another for some hours. Experiment showed that full development took place in about eight hours; however, to ensure

that full development had been reached prior to any tests on the contact, it was operated under standardized conditions (current, 10 amp per brush; vacuum, 0·1 mm Hg) for about 30 hours.

### (2.2.3) Contact Materials.

The copper disc was cut from a slab of hot-rolled tough-pitch copper having the following composition:

| | | | | |
|---|---|---|---|---|
| Copper | .. | .. | .. | 99·92% |
| Arsenic | .. | .. | .. | Nil |
| Tin | .. | .. | .. | Trace |
| Lead | .. | .. | .. | Trace |
| Bismuth | .. | .. | .. | 0·001% |
| Oxygen | .. | .. | .. | 0·06% |

### (3) EXPERIMENTAL RESULTS

In all the experiments the contact was operated under a constant mechanical load of 500 g per brush and the speed of sliding was maintained constant at 500 cm/s. Here it is worth noting that preliminary tests revealed that an increase in the speed of sliding generally resulted in an increase in the (average) contact p.d. and a decrease in the coefficient of kinetic friction. This effect was rather more noticeable at higher atmospheric pressures but was observable even in vacuum. These results suggest that the effect was due in part to aerodynamically induced gas films under the brushes and in part to some unavoidable eccentricity of the copper disc.

In the presentation of the results a brush is described as positive if the conventional current flowed from it to the disc.
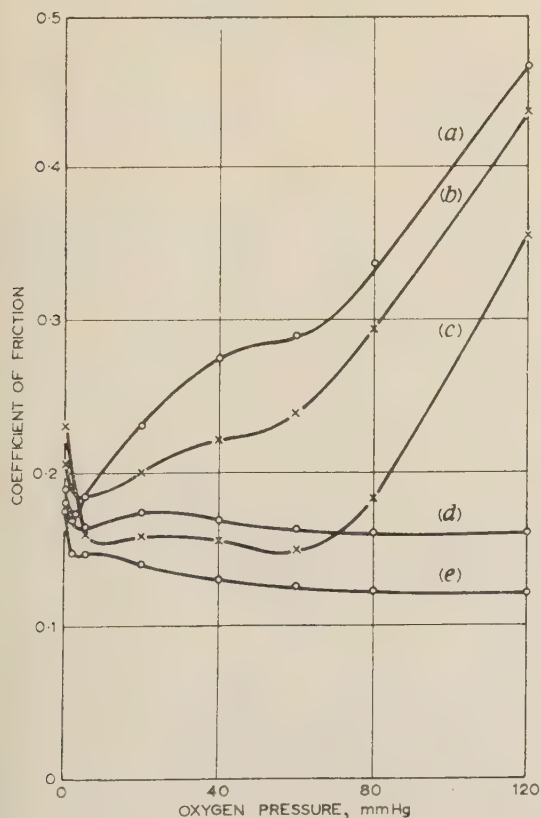
### (3.1) The Effects of Dry and Moist Oxygen

The ways in which dry and moist oxygen were found to affect the coefficient of friction and the average value of the contact p.d. are shown in Figs. 3–9. The general conclusion here is that oxygen must play a most important part in the structure of the film on the copper disc as well as having some effect on the surface forces of the graphite brushes. Furthermore, it seems clear that the direction of flow of current through the contact has a profound effect on the mechanical and electrical characteristics, possibly as a result of its effect on the stability of the film on the metal. The magnitude of the current seems to be of rather less importance in this connection.

The effect of water vapour seems to be one of lubrication in the case of the comparatively stable interfacial structure which corresponds to currentless and negative brushes, and one of stabilization in the case of the otherwise unstable structure which corresponds to positive brushes (see later).

The oscillograms of Fig. 10 refer to the variation of contact resistance with movement of a brush over a certain portion of the surface of the copper disc, the current remaining constant all the while. These oscillograms are for a positive brush; the corresponding oscillogram for a negative brush operating at the higher oxygen pressure is in its general form similar, but the average value of the resistance is less. Each point on these oscillograms refers, of course, to the brush in a certain position on the surface of the disc. Incidentally, the traces in Fig. 10 are those for a brush movement of 7·5 cm.

A brush in any one position on the disc makes contact at three points at least, and in general at a rather greater number. Under
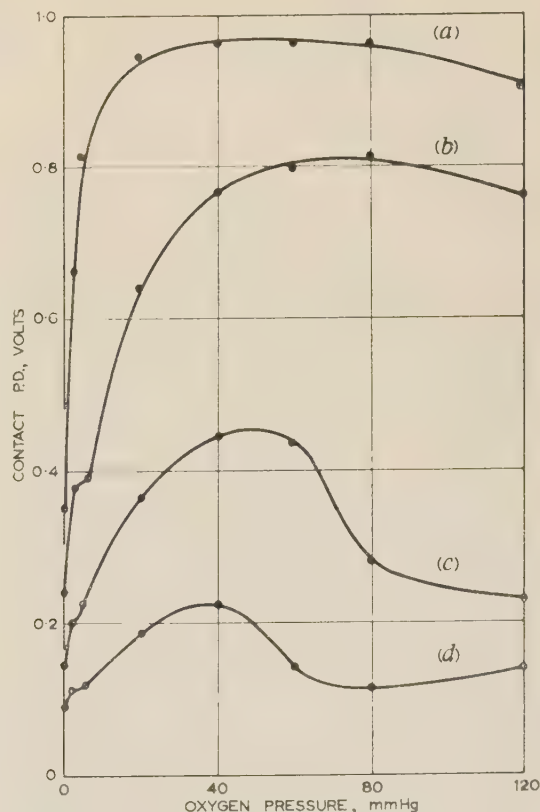


Fig. 3.—Dependence of kinetic friction on pressure of ambient dry oxygen.

(a) Zero current.
(b) Negative brush, 10 amp.
(c) Negative brush, 20 amp.
(d) Positive brush, 10 amp.
(e) Positive brush, 20 amp.



Fig. 4.—Dependence of contact resistance (contact p.d. at constant current) on pressure of ambient dry oxygen.

(a) Positive brush, 20 amp.
(b) Positive brush, 10 amp.
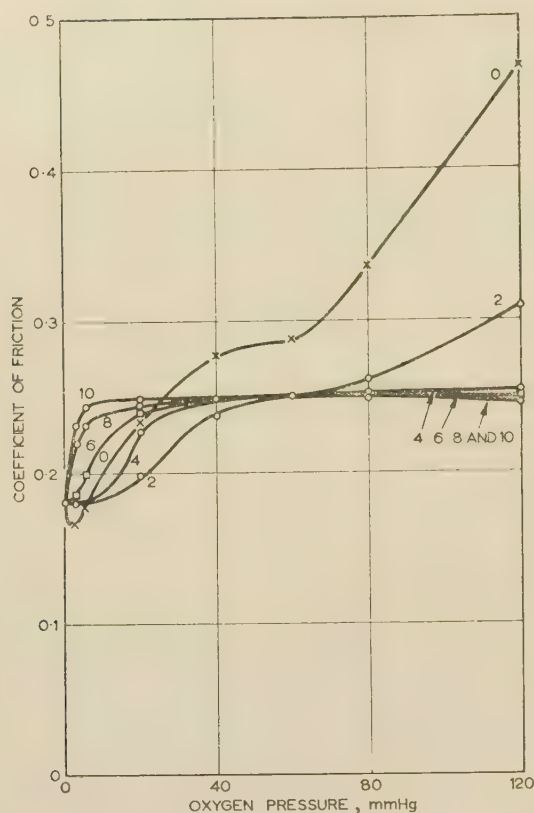(c) Negative brush, 20 amp
(d) Negative brush, 10 amp

Fig. 5.—Influence of water vapour on friction/oxygen-pressure characteristic of currentless brush.

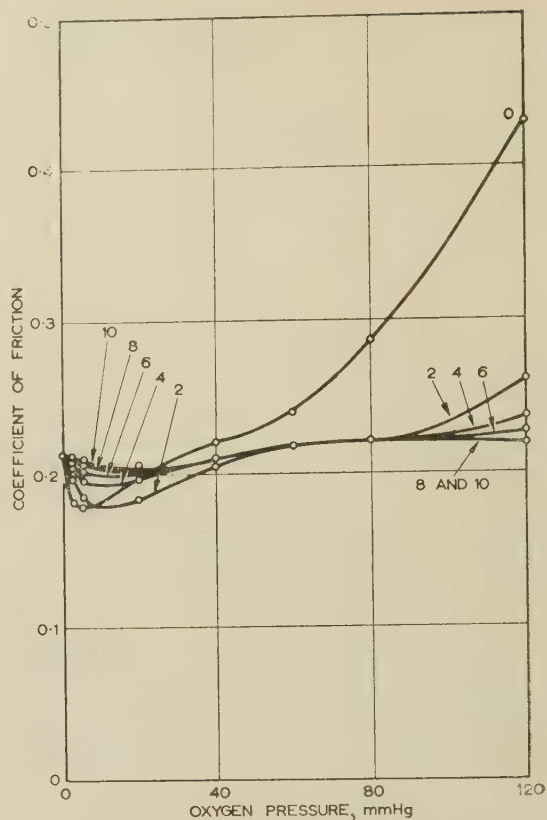Numerals on curves refer to water-vapour pressure, mm Hg.



Fig. 7.—Influence of water vapour on friction/oxygen-pressure characteristic of negative brush carrying 10 amp.

Numerals on curves refer to water-vapour pressure, mm Hg.



Fig. 6.—Influence of water vapour on friction/oxygen-pressure characteristic of positive brush carrying 10 amp.

Numerals on curves refer to water-vapour pressure, mm Hg.

given atmospheric conditions, then, if the topography of the film on the copper is stable the oscillographic trace for a selected portion of the disc should repeat more or less exactly for each revolution of the disc and should appear as a relatively stationary pattern on the screen of the oscilloscope. This proved in large measure to be the case; continuous observation of the trace showed fairly rapid change of fine detail in the trace—especially with positive brushes—but relatively slow change of major features. The higher peaks of the trace refer to contact of a brush at a few large spots, and such peaks persisted in dry oxygen for as many as 700 repeated contacts (700 revolutions of the disc) or more before suffering very serious change. In moist oxygen the 'life' of a group of such large spots was of the order of 10 000 repeated contacts. It must be pointed out, however, that at no time in the experiments, with dry oxygen in particular, could it be said that the trace of contact p.d. (or resistance) remained unchanged for longer than a fraction of a second, actually for more than two or three revolutions of the disc. In other words, it appears that a given group of contact spots on the brush and disc did not on the average remake in their entirety a second or possibly a third time under these conditions. In this connection there was greater stability with negative than with positive brushes.

Finally it is perhaps worth noting that the variation of contact resistance with movement of a brush was far more violent with positive brushes than with negative brushes.

It is interesting to see that, when water vapour acted as a lubricant of the comparatively stable interfacial region of current-less brush contacts, its action was virtually complete when its partial pressure exceeded about 3 mm Hg. This agrees almost
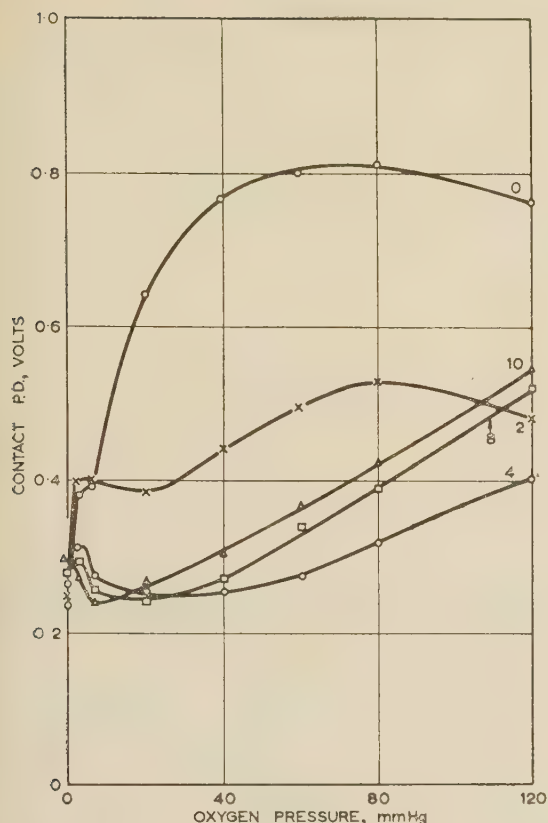
Fig. 8.—Influence of water vapour on contact-resistance/oxygen-pressure characteristic of positive brush carrying 10 amp.

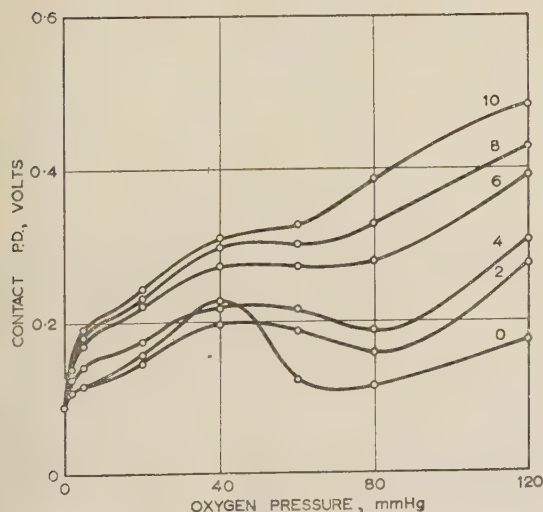Numerals on curves refer to water-vapour pressure, mm Hg.



Fig. 9.—Influence of water vapour on contact-resistance/oxygen-pressure characteristic of negative brush carrying 10 amp.

Numerals on curves refer to water-vapour pressure, mm Hg.

...ctly with an observation made by Savage,[20] namely that in ...paratus used by him rapid brush-wear occurred whenever the ...tial pressure of water vapour in the atmosphere was less ...n about 3 mm Hg.
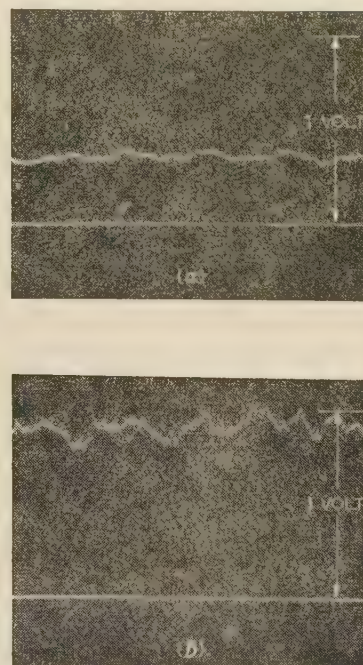


Fig. 10.—Oscillograms of contact p.d. of positive brush carrying 20 amp.

(a) Oxygen pressure, 0·1 mm Hg.
(b) Oxygen pressure, 60 mm Hg.
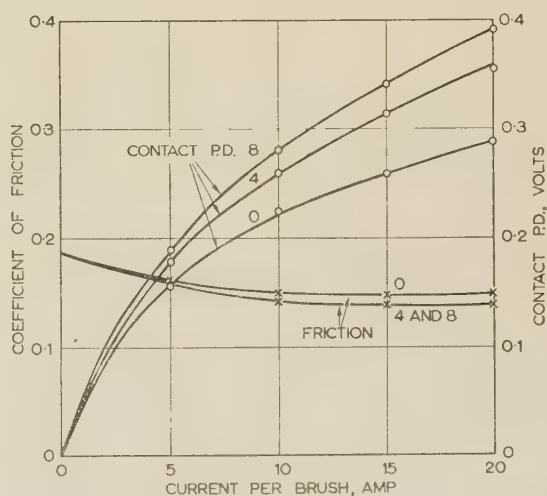


Fig. 11.—Influence of magnitude of current on friction and contact resistance.

Positive brush; oxygen pressure, 0·1 mm Hg.
Numerals on curves refer to water-vapour pressure, mm Hg.

## (3.2) The Effect of the Magnitude of the Current

Some indication of the effect of the magnitude of the current on the coefficient of friction and contact resistance is provided by the results already mentioned; however, more complete information on these points is provided by Figs. 11–16.

It will be seen that, in general, an increase in the magnitude of the current resulted in a decrease in friction, the variation with current being greatest at the higher oxygen pressures. With positive brushes there appears to be a complex result deriving from the tendency of water vapour to stabilize the interface—

an action modified somewhat by higher surface temperatures at higher currents.

The form of the voltage/current characteristic was of the now familiar form in practically every case.

### (3.3) The Effect of an Inert Gas

The effect of dry nitrogen on the average value of the contact resistance was found to be almost completely negligible; however, its effect on the friction was appreciable. In this connection an increase in gas pressure from 0·1 to 760 mm Hg resulted in a
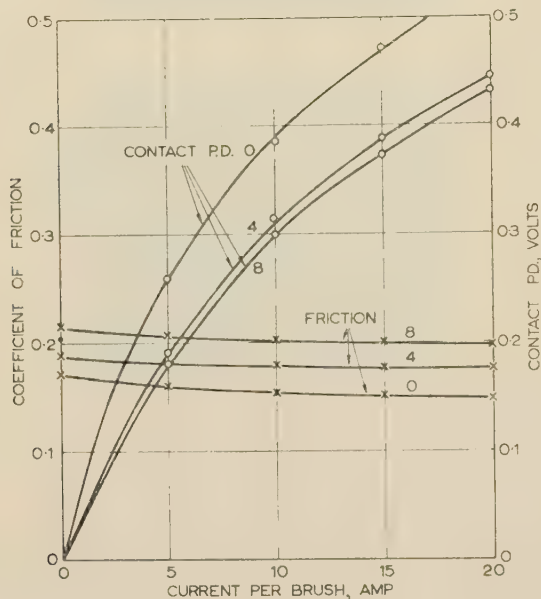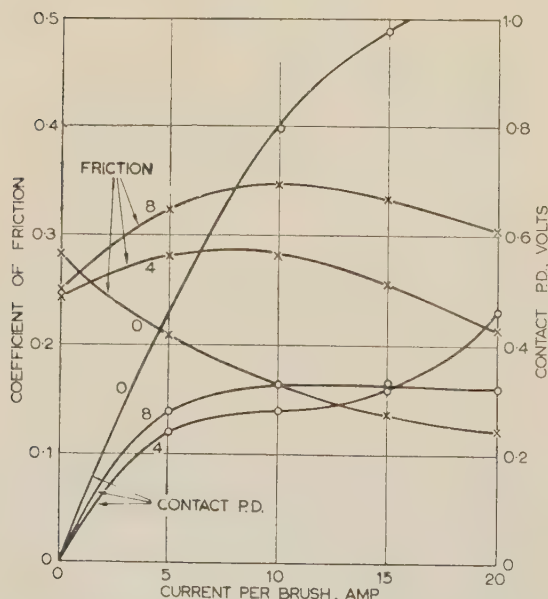


Fig. 12.—Influence of magnitude of current on friction and contact resistance.

Positive brush; oxygen pressure, 2 mm Hg.
Numerals on curves refer to water-vapour pressure, mm Hg.



Fig. 13.—Influence of magnitude of current on friction and contact resistance.

Positive brush; oxygen pressure, 60 mm Hg.
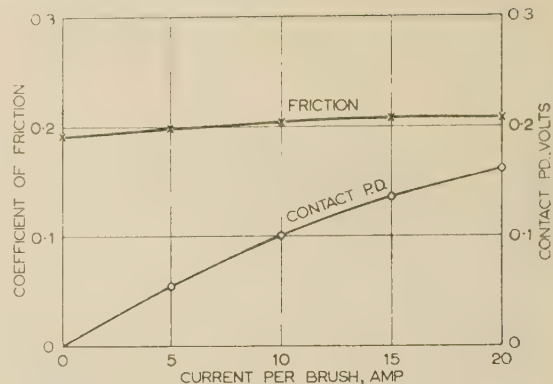Numerals on curves refer to water-vapour pressure, mm Hg.



Fig. 14.—Influence of magnitude of current on friction and contact resistance.

Negative brush.
Oxygen pressure, 0·1 mm Hg.
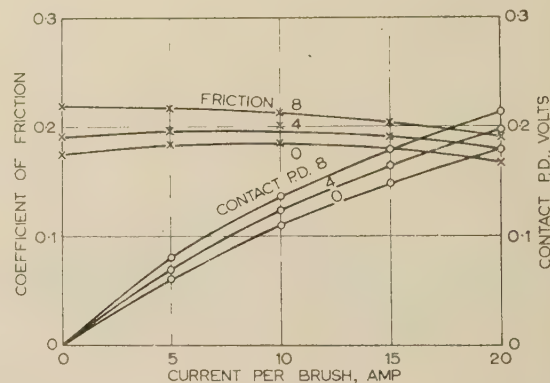Water-vapour pressure, 0, 4 and 8 mm Hg.



Fig. 15.—Influence of magnitude of current on friction and contact resistance.

Negative brush; oxygen pressure, 2 mm Hg.
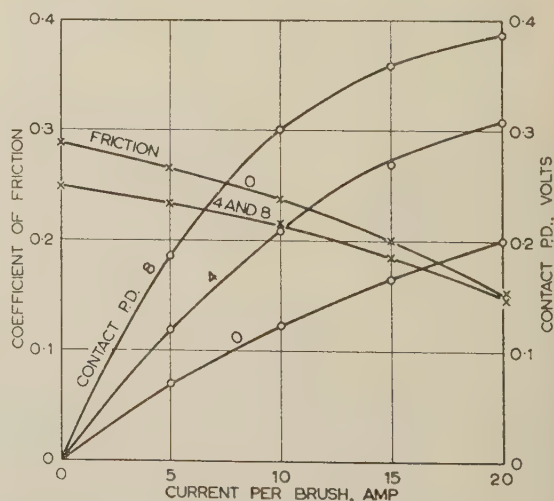Numerals on curves refer to water-vapour pressure, mm Hg.



Fig. 16.—Influence of magnitude of current on friction and contact resistance.

Negative brush; oxygen pressure, 60 mm Hg.
Numerals on curves refer to water-vapour pressure, mm Hg.

decrease of the coefficient of friction from about 0·2 to 0·16 for currentless and positive and negative brushes. This effect was evidently due to very thin gas films aerodynamically induced beneath the brushes.

Finally it must be reported that the wear of brushes used in the experiments, although not measured accurately, was found to be of the same order of magnitude in vacuum, in dry air and in dry oxygen, as is generally experienced in normal atmospheres. This was our experience with brushes operating as described earlier for some hundreds of hours in these moisture-free conditions. We shall return to this point later.

## (4) CONCLUSIONS

### (4.1) Structure of the Black Film

The most probable form of the black film on the copper disc has already been described; a fully developed film is illustrated by Fig. 17. The film in this state is to be regarded as fully deve-
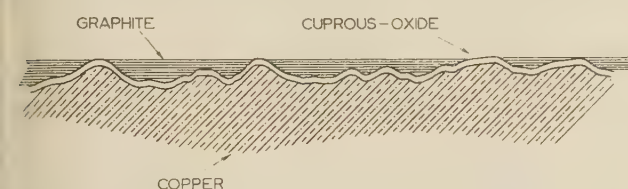


Fig. 17.—Structure of black film on brush track of copper disc.

loped, for it seems that no amount of additional rubbing is likely to change its character or to increase the thickness of the graphite stratum.

The higher asperities on the surface of the copper are evidently the spots of real contact of the brush and metal (or its oxide); consequently the small holes or gaps in the graphite stratum, to which these asperities inevitably give rise, are the most important regions of the whole film. Compared with the existence of these gaps, the continuity of the remainder of the graphite stratum would seem to be of secondary importance.

Evidence in support of the essential features of our model of the black film derives from several sources. In the first place, the average thickness of the film should correspond to the average depth of surface irregularities on the copper disc. Savage and Van Brunt[14] reported that this is of the order of $\times 10^{-5}$ mm. This corresponds fairly well with the results of Talysurf measurements of machined surfaces made recently by Deare, Robinson and Wolfe.[24] Again from the results of our experiments there appears to be no doubt that the resistance of the contact is very largely attributable to oxide film on the copper, and furthermore this resistance changes rapidly and reversibly with changes in the pressure of ambient dry oxygen. Now, the patches of cuprous oxide which matter in this connection are those on the summits of the highest asperities on the metal. It follows, then, that the rapidity of response of the contact resistance to changes in oxygen pressure must be due to the rapid adjustment in the thickness of these patches of oxide and possibly to changes in the degree of adsorption of the gas. This can only mean that the summits of the higher asperities to which we have referred must be free of any overlying film of graphite.

Since the contact resistance increases and decreases with rise and fall of oxygen pressure, conditions at the oxide caps of the higher asperities must be in a continual state of change. With positive brushes these caps are almost certainly torn away by the graphite brush, and they re-form afterwards and attain a thickness which is primarily determined by the pressure of the ambient oxygen. If this were not so, the oxide once formed

would remain in position and lead to a contact resistance of a more or less permanent value corresponding to the highest pressure of the oxygen attained in any cycle of variation.

A simple experiment was carried out to test this proposition concerning the formation and removal of oxide caps with positive-brush operation. In the first place with the brushes positive the contact was operated in dry oxygen at a pressure of 120 mm Hg. At a sliding speed of 500 cm/s and with a current of 10 amp per brush, the p.d. was 0·7 volt. The disc was then stopped and the p.d. fell immediately to 0·4 volt for the same current. With the disc stationary the oxygen pressure was reduced to 0·1 mm Hg. The disc was then turned very slowly and the p.d. was found to be 0·38 volt, for a current of 10 amp, until the disc had completed almost one revolution. Further rotation to complete one revolution caused the p.d. to fall to 0·2 volt, at which value it remained irrespective of further movement of the disc. Finally with the disc at rest, increase of oxygen pressure to 120 mm Hg caused only a very slight increase in p.d.; the original values of 0·4 and 0·7 volt were attained only after the disc had been rotated for a second or so at the original speed.

Much the same results were observed in a similar experiment with negative brushes, except that the p.d. for a given current and oxygen pressure was practically the same for the stationary as for the sliding contact. This observation confirms that of Soper.[11] In this case the oxide caps are not removed—this point will be discussed later.

### (4.2) The Role of Cuprous Oxide in the Electrical and Frictional Characteristics of the Contact

It seems at this stage to be beyond question that the cuprous oxide on the contact asperities of the copper disc plays a very important part in the determination of the electrical and frictional characteristics of the contact.

During the stick phase of the stick-slip process of sliding, the graphite brush makes contact with the cuprous oxide on the higher asperities on the metal. The oxide therefore constitutes a layer intermediate between the two primary members, and we have therefore to recognize the existence of two distinct forces of adhesion, namely that between the oxide and the copper base and that between the oxide and the graphite. At the instant when the slip phase commences, the adhesion which is significant is the lesser of these two forces.

The composition of a cuprous-oxide film when this is more than a few molecular layers in thickness departs from strict stoichiometric proportions. The lattice imperfections correspond in this case to the absence of copper ions, and the oxide behaves as a deficit semi-conductor.

The edge atoms of a shingled crystallite of graphite in a brush face are in an excellent position to supply the 'deficit' electrons to the oxide lattice; consequently an electric field would readily be set up across the oxide-graphite boundary, and this could account for a strong force of adhesion in this region. A similar explanation may be put forward for the adhesion at the oxide-metal boundary, but possibly other factors also contribute to the adhesion here.

It seems, then, that in the absence of any applied electric field the copper and the graphite will each be positive with respect to the oxide.

The strengths of the boundary fields are determined by the concentration and mobility of the lattice imperfections of the oxide, the concentration depending upon the crystallinity and heterogeneity of the oxide, and the mobility upon the temperature and the effect of oxygen adsorbed on to the outer surface of the oxide.

It appears, then, that a p.d. applied to the contact serves to weaken the field at one boundary and to strengthen that at the other; the forces of adhesion will be correspondingly weakened and strengthened.

In order that we may attempt to explain the experimental results in terms of this hypothesis we need to make one further assumption, namely that in the absence of any applied electric field the force of adhesion at the graphite-oxide boundary is less than that at the oxide-metal boundary.

On the basis of these assumptions, then, for the contact operating in dry oxygen, sliding should take place at the graphite-oxide boundary in the case of currentless and negative brushes, and the oxygen and friction relationship should be of much the same form for such brushes. This is in fact borne out by experiment (see Fig. 3). On the other hand, with positive brushes, if the applied electric field is strong enough, the adhesion at the oxide-metal boundary can be reduced to such a value that the oxide caps at the contact asperities are torn away by the graphite brush. These oxide caps are crushed together with some disturbed graphite flakes from the graphite stratum on the black film, and the dust serves to lubricate the contact during the slip phase of sliding. This dust would also increase the contact resistance. In this way we might explain the relatively low coefficient of friction and high resistance of positive brushes in dry oxygen.

### (4.3) The Effect of Oxygen on the Contact Characteristics

It is apparent from Fig. 3 that, with the contact operating in dry oxygen, the kinetic friction decreases in all cases when the oxygen pressure is raised from 0·1 to about 2 mm Hg. This is almost certainly due to adsorption of the gas on to the active areas of the brush face. This adsorption would partly neutralize the strong valence forces of the shingled crystallites of graphite and so reduce the adhesion at the graphite-oxide boundary. At such low pressures of oxygen the semi-conductivity of the oxide caps would be little affected.

It is worth noting that Bowden and Young[23] have found that saturated adsorption of oxygen on graphite occurs at about 0·1 mm Hg. In their experiment—graphite sliding on graphite—the speed of sliding was very low; at higher speeds of the order of 500 cm/s we might expect that rather higher gas pressures would be required to secure such complete adsorption.

With currentless and negative brushes the oxide caps on the contact asperities are not removed during sliding, so that an increase in oxygen pressure beyond that needed for saturated adsorption on the graphite brush might be expected to increase the forces of adhesion and thence the friction. This would arise owing to an increase in semi-conductivity of the oxide resulting from some increase in thickness, or more probably increased adsorption of the gas. This increase was in fact observed.

With positive brushes the contact is lubricated by crushed oxide caps and graphite, and it might be expected that at higher oxygen pressures the thicker caps of oxide would lead to a decrease in kinetic friction and to an increase in resistance. This was observed, though the effect on the friction was small, probably owing to the less rapid growth of the oxide as it thickens. This latter effect might explain the 'levelling-off' of the resistance of the positive brush contact at the higher oxygen pressures.

The resistance of negative brush contacts changes in a remarkable way with change in oxygen pressure, as Fig. 4 shows. It is interesting to note that an inflection in the friction curve corresponds to a peak value of the resistance, and a rapid increase in friction thereafter is associated with a rapid decrease in resistance. It is not easy to provide an explanation of this phenomenon, but the following remarks may be worth noting. In the first

place, conduction through the oxide under a negative brush is by way of filamentary coherer bridges of copper formed as result of electrical rupture of the oxide. The bridges when formed have a temperature approximating to the melting point of the metal, and being freshly reduced the metal of these bridges is in an activated condition. When a bridge ceases to conduct it is re-oxidized to an extent determined by the pressure of ambient oxygen. However, we should not expect the electrical characteristics of such oxide and its copper base to be the same as those of oxide formed at lower temperatures on unactivated copper. Williams and Thompson[25] have reported that the temperature at which the oxide is formed is an important factor in determining the characteristics of copper/copper-oxide rectifiers. It is possible that with activated copper the pressure of ambient oxygen also has a marked effect on the characteristics of the oxide-copper pair—as regards reverse resistance for instance, and the semi-conductivity of the oxide itself. On this latter point Wagner[18] has shown that at room temperature the conductivity of cuprous oxide increases with increase in the pressure of ambient dry oxygen. The effect is apparently small, but might be more marked at higher temperatures.

It does seem, then, to be just possible that with negative brushes increasing the oxygen pressure from a low value will give increasingly more complete oxidation of coherer bridges and an increase in resistance. When the pressure is such that the bridges are completely oxidized in one revolution of the disc a further increase in pressure causes no further increase in resistance. This may in part explain the occurrence of the peak resistance referred to earlier. It seems from our results that increase of the gas pressure beyond this stage increases semi-conductivity and friction but in some way reduces the rupture strength of the oxide.

Incidentally, the coherer bridges are thicker the greater the current, so we might expect that complete oxidation within a revolution and hence the resistance peak would correspond to a higher oxygen pressure. This is confirmed by the curves for negative brushes in Fig. 4.

The friction of negative brushes is expected to be of much the same order as it is with currentless brushes for the reasons I have given earlier; however, the fact that it is smaller may be due to the formation of the molten metallic bridges at the contact spots.

### (4.4) The Effect of Water Vapour

The effect of dry oxygen alone arises partly from its adsorption on the powerfully adsorptive areas of the graphite brush face and partly by its adsorption on, or its chemical reaction with, the copper or cuprous oxide of the disc surface. Water vapour can modify both of these effects, first by competing with oxygen in the process of adsorption on the graphite, and secondly by modifying the interactions of oxygen and cuprous oxide. The first of these is probably the more important action of the adsorbed water.

It would seem that, in general, the effect of water adsorbed on the active areas of the graphite would be to reduce the adhesion at the graphite-oxide boundary. Consequently increasing pressures of water vapour, up to that point which corresponds to saturated adsorption on the active areas of the graphite, should result in a decrease in friction of currentless and negative brushes. This was observed to be the case at partial pressures of oxygen greater than about 25 mm Hg, and saturation was reached at a water-vapour pressure of approximately 3 mm Hg with currentless brushes, and 6 mm Hg with negative brushes. A higher vapour pressure in this latter case was probably necessary because of the tendency to some desorption

on of vapour due to electrical heating. For partial pressures of xygen below about 25 mm Hg the slight increase in friction ith increase in vapour pressure is difficult to explain.

If the thin film of adsorbed water weakens the oxide-to-raphite adhesion to such an extent that even with positive rushes this adhesion is less than that at the oxide-metal boundary, en the oxide caps at the contact asperities will not be torn way. This would lead to a reduction of the coefficient of static iction and to an increase in the coefficient of kinetic friction, e latter effect being due to the absence of the lubricating 'film' oxide and graphite dust. This stabilization of the contact terface becomes more and more complete as the vapour essure is increased with corresponding increase in kinetic iction. Saturation in this case was found to occur at a vapour essure of approximately 8 mm Hg, a pressure again in excess that for the currentless brush owing to the desorption conse-ent upon electrical heating.

The adsorbed film of water serves to increase the resistance of gative brushes as we might expect, but it reduces the resistance positive brushes by virtual elimination of the 'film' of crushed ide and graphite. This is a general tendency which begins to e way to newly increasing resistance at vapour pressures ater than about 6 or 7 mm Hg (see Fig. 8).

### (4.5) The Rate of Wear of the Graphite Brushes

Measurement of the wear of brushes was not one of the jects of the investigations described earlier; however, it was dily observed that under the conditions of the experiments e amount of wear was very small. This experience is at riance with the well-established fact that brushes in electrical achines operating under high-altitude conditions wear away ite rapidly.

Now, the essential differences between the conditions of the periments and those of high-altitude operation are the atmo-heric temperature and the mechanical freedom of the brushes. e first difference is possibly of no great importance as a parate factor, but the second may be so. In the apparatus ed in the experiments the brushes had no freedom whatever cept that the whole of the brush-gear could move in the plane rotation of the disc), but a brush located in the usual type of ash box in an electrical machine has some freedom of movement thin the box. In this case the comparatively great differences ween the coefficients of static and kinetic friction under low-isture conditions might cause a brush to tilt first one way d then the other as a result of this variable force—the oscil-ng tilt taking place in the plane of rotation of the slip-ring commutator, of course. Crushing and wear might then take ce at a rate not much affected by the current. This conclusion orne out by observations reported by Sims.[26]

xperiments with adjuvant-loaded brushes are continuing are as yet incomplete; but it is possible to report that brushes taining barium fluoride show the same characteristics as in graphite brushes if they carry no current from the commence-nt. However, such brushes have very greatly diminished fficients of friction when once they have carried an appre-ble current for a short time, and low friction is thereafter erved even when the brushes carry no current. These obser-ions appear to correspond to Sims's observation of the rate wear of such brushes (loc. cit.).

The low friction may perhaps arise in this case from the interaction of barium fluoride with the cuprous oxide on the contact asperities, the fluoride reacting with the oxide to give a new stable compound which has comparatively small adhesion at its boundary with the graphite.

### (5) ACKNOWLEDGMENT

### (6) BIBLIOGRAPHY

(1) HOLM, R.: 'Electric Contacts' (Gebers, Stockholm, 1946).
(2) BAILY, F. G., and CLEGHORNE, W. S. H.: 'Some Phenomena of Com-mutation', Journal I.E.E., 1907, 38, p. 150.
(3) HUNTER-BROWN, P.: 'Carbon Brushes: considered in relation to the Design and Operation of Electrical Machinery', ibid., 1919, 57, p. 193.
(4) HUNTER-BROWN, P., and HEWS, C. J.: 'A Practical Investigation into the Design of Brushes and Brush-Holders', ibid., 1932, 71, p. 799.
(5) TAYLOR, H. G.: 'Phenomena connected with the Collection of Current from Commutators and Slip-Rings', ibid., 1930, 68, p. 1356.
(6) BAKER, R. M.: 'Voltage Drop in Sliding Contacts', Electrical Journal, 1934, 31, p. 448.
(7) HESSLER, V. P.: 'The Effect of Various Operating Conditions upon Electrical Brush Wear and Contact Drop', Bulletin 122, Iowa Engineering Experimental Station, Ames, Iowa, 1935.
(8) HESSLER, V. P.: 'Electrical Brush Wear', Transactions of the American I.E.E., 1935, 54, p. 1050.
(9) HESSLER, V. P.: 'Abrasion—a Factor in Electrical Brush Wear', Electrical Engineering, 1937, 56, pp. 8–12, and p. 16.
(10) HESSLER, V. P.: 'Probe Studies of Collector-Ring Films', General Electric Review, 1937, 40, p. 358.
(11) SOPER, P. F.: 'Carbon-Brush Contact Phenomena in Electrical Machinery', Proceedings I.E.E., Paper No. 826, August, 1949 (96, Part II, p. 645).
(12) SCHLIEPHAKE, A.: 'Experiments on the Influence of the Ambient Atmosphere on the Brush Contact Voltage', Elektrotechnische Zeitschrift, 1950, 71, p. 32.
(13) HAYES, M. E.: 'Current-Collecting Brushes in Electrical Machines' (Pitman, London, 1947).
(14) VAN BRUNT, C., and SAVAGE, R. H.: 'Carbon Brush Contact Films—I', General Electric Review, 1944, 47, p. 16.
(15) VAN BRUNT, C.: 'Carbon Brush Contact Films—II', ibid., 1944, 47, p. 28.
(16) SAVAGE, R. H., and FULLAM, E. F.: 'Carbon Film Formation and Commutator Brush Wear as revealed by the Electron Microscope', Journal of Applied Physics, 1948, 19, No. 1, p. 654.
(17) HESSLER, V. P., and SAVAGE, R. H.: 'Collector-Ring Films; For-mation and Influence', General Electric Review, 1939, 42, p. 192.
(18) KUBASCHEWSKI, O., and HOPKINS, B. E.: 'Oxidation of Metals and Alloys' (Butterworth, London, 1953).
(19) TYLECOTE, R. F.: 'A Review of Published Information on the Oxidation and Scaling of Copper and Copper-Base Alloys', Journal of the Institute of Metal, 1950, 78, Part 3, p. 259.
(20) SAVAGE, R. H.: 'Graphite Lubrication', Journal of Applied Physics, 1948, 19, No. 1, p. 1.
(21) SAVAGE, R. H.: 'Physically and Chemically Adsorbed Films in the Lubrication of Graphite Sliding Contacts', Annals of the New York Academy of Sciences, 1951, 53, p. 862.
(22) BRAGG, W. H.: 'An Introduction to Crystal Analysis' (Bell, London, 1928), p. 64.
(23) BOWDEN, F. P., and YOUNG, J. E.: 'Friction of Diamond, Graphite and Carbon, and the Influence of Adsorbed Films', Proceedings of the Royal Society, A, 1951, 208, p. 444.
(24) SPEARE, P., ROBINSON, I. R., and WOLFE, K. J. B.: 'The Influence of Machining and Grinding Methods on the Mechanical and Physical Condition of Metal Surfaces', Institute of Metals, 1953, Symposium on Properties of Metallic Surfaces.
(25) WILLIAMS, A. L., and THOMPSON, L. E.: 'Metal Rectifiers', Journal I.E.E., 1941, 88, Part I, p. 353.
(26) SIMS, R. F.: 'The Wear of Carbon Brushes at High Altitudes', Pro-ceedings I.E.E., Paper No. 1505, July, 1953 (100, Part I, p. 183).

# THE VARIATION WITH CURRENT AND INDUCTANCE OF METAL TRANSFER BETWEEN CONTACTS OF PALLADIUM AND SILVER

By R. I. B. COOPER, M.A., Ph.D., and JANET RIDDLESTONE, B.A.

## SUMMARY

The work on transfer between platinum contacts, published by one of the authors in previous papers, has been extended to palladium and silver. Curves of the net transfer in 6-volt d.c. circuits are given for currents of a few amperes and inductances ranging from less than $0 \cdot 1 \mu H$ up to $110 \mu H$. Some measurements have also been made in 12- and 24-volt circuits for palladium. The general nature of the transfer for palladium is both qualitatively and quantitatively similar to that for platinum, but in the case of silver, neither residual nor reversed short-arc transfer has been demonstrated. Theoretical analysis of the results shows that the quantity determining transfer in an inductive circuit is the ratio of the charge passed in the arc to the volume of residual transfer at the same break current. Under conditions of constancy of this ratio, transfer is found to be proportional to the square of the break current up to $6 \cdot 5$ amp.

## LIST OF PRINCIPAL SYMBOLS

$A, n =$ Constants.
$C =$ Capacitance of by-pass capacitor C.
$c =$ Local contact capacitance.
$d =$ Mean diameter of craters.
$h =$ Pip height.
$I_b =$ Break current.
$I_e =$ Arc-extinction current.
$L =$ Total inductance of circuit.
$L_b =$ Inductance of battery leads.
$L_c =$ Self-inductance of C.
$L_d =$ Self-inductance of wiring.
$N =$ Number of switchings.
$Q =$ Charge.
$R =$ Current-controlling resistor.
$r =$ Pip base radius.
$V =$ Supply voltage.
$V_0 =$ Arc voltage.
$V_b =$ Boiling voltage of metal.
$\rho_0 =$ Resistivity at room temperature.
$\rho_m =$ Resistivity at melting temperature.
$\tau =$ Arc duration.

## (1) INTRODUCTION

The variation of metal transfer between separating contacts of platinum in 6-volt d.c. circuits under certain conditions has been described in two previous papers.[1,2] Investigations with the same apparatus and under similar conditions have been carried out for palladium and silver, and results for these metals are given here. The results for palladium are similar to those for platinum, but for silver only 'short-arc' and 'long-arc' transfer are apparent.

The behaviour of palladium was also investigated in 12- and

24-volt circuits. The results for 12 volts, which is below th arc voltage of contacts in air, are similar to those for 6 volts In 24-volt circuits, however, the duration of the discharge whic follows opening of the contacts depends upon various factors as yet imperfectly understood, in addition to the circuit para meters and cannot be predicted, except for currents below $2 \cdot 7$ amp. Although measurements were made of discharg durations in 24-volt circuits they can only be regarded a indicative and not necessarily as of general application. Palla dium suffered severe erosion from the negative contact in t 24-volt 5 amp circuit.

The results for palladium have been analysed with a view t solving some of the problems resulting from the earlier work.[1] Whilst no further light has been shed on the various specia mechanisms of arc transfer and their interdependence, som indicative generalizations have emerged. In particular, it shown that arc-transfer phenomena are similar if the values the ratio of charge passed in the arc to a standard volun dependent only on the break current are equal.
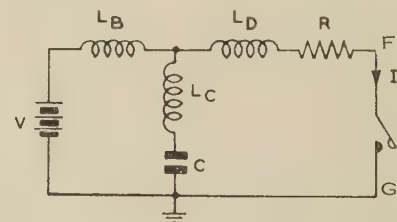


Fig. 1A.—Diagram of standard circuit.

The standard circuit arrangement is shown in Fig. 1A and w as in Reference 2: the volumes transferred were assessed by th optical method described in Reference 1.

## (2) RESULTS FOR PALLADIUM AND SILVER IN A 6-VOLT CIRCUIT

### (2.1) Transfer Measurements

Results were obtained for palladium for break currents of 1· $2 \cdot 7$, $3 \cdot 6$ and $6 \cdot 5$ amp, and for silver for break currents of 3· $7 \cdot 0$ and $14 \cdot 5$ amp. The numbers of switchings made in ead test was $5 \times 10^4$ for palladium at $1 \cdot 6$ amp, $1 \cdot 5 \times 10^5$ f palladium at higher currents, and $7 \cdot 5 \times 10^3$ for silver: the values were chosen in each case to give a reasonable ratio pip height to base radius (between $0 \cdot 3$ and $1 \cdot 0$). The effecti circuit inductance, $L$, was varied from a residual value of abo $0 \cdot 07 \mu H$ up to $77 \mu H$.

In order to attain for some tests a still smaller residual indu tance, a modified circuit was used (Fig. 1B) with the curren controlling resistor R inserted between the battery and the by-p capacitor C. This removes the self-inductance of R from t contact circuit, and the residual inductance is now made up or of the self-inductance, $L_c$, of the by-pass capacitor and the se
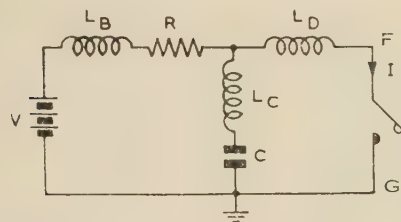
Fig. 1B.—Diagram of modified circuit for very low residual inductance.

inductance, $L_d$, of the wiring.   The sum of $L_d$ and $L_c$ ($=L$) could be reduced to as little as $0 \cdot 025\,\mu\text{H}$.   There is, however, a difficulty with this circuit in measuring the break current.   As the contacts open, the voltage across FG (Fig. 1B) rises to $V_b$, the boiling voltage of the metal under test, in a time of a few hundred microseconds for most of these tests.   The time-constant $CR$ is of the same order.   Thus, current flows into C during the opening and the current through FG is appreciably reduced.   As the form of the variation with time of the opening voltage varies from one switching to the next as well as with the experimental conditions, it is an uncertain procedure to make a theoretical allowance for the effect.   The break current must be measured directly by observing on an oscilloscope the voltage developed across a very short length of resistance wire inserted in FG.

After the circuit is broken, the discharge phenomena will differ slightly from those in the circuit of Fig. 1A.   However, it can be shown that the discharge energy will still be approximately $\frac{1}{2}LI_b^2$, where $I_b$ is the break current, since $RC \gg \sqrt{(Lc)}$, where $c$ is the local capacitance at the contacts, and $L/R \ll CR$.   Thus continuity would be expected with the results obtained in the circuit used earlier.   This was checked by adding to $L_d$ artificially in the modified circuit to increase $L$ to the least value attainable in the original circuit.   The results were the same in both arrangements.
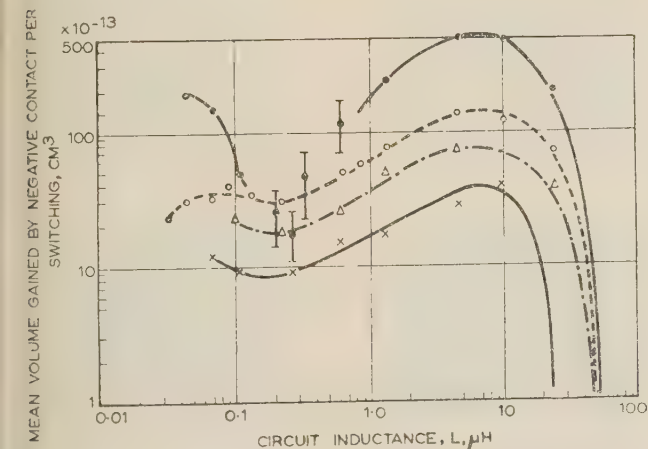


Fig. 2.—Variation with inductance and current of mean volume gained per switching by negative contact: palladium contacts in 6-volt circuit.

<table>
<tr><td>×</td><td>1·6 amp.</td><td>○</td><td>3·6 amp.</td></tr>
<tr><td>△</td><td>2·7 amp.</td><td>●</td><td>6·5 amp.</td></tr>
</table>

Negative values at higher values of inductance are not shown.

The results are displayed graphically for palladium in Fig. 2 and for silver in Fig. 3.   For palladium at 6·5 amp the transfer was cylindrical in shape rather than a pip and was spread over rather a large radius compared with that of the wire used for the contact.   The estimate of volume was accordingly possible only
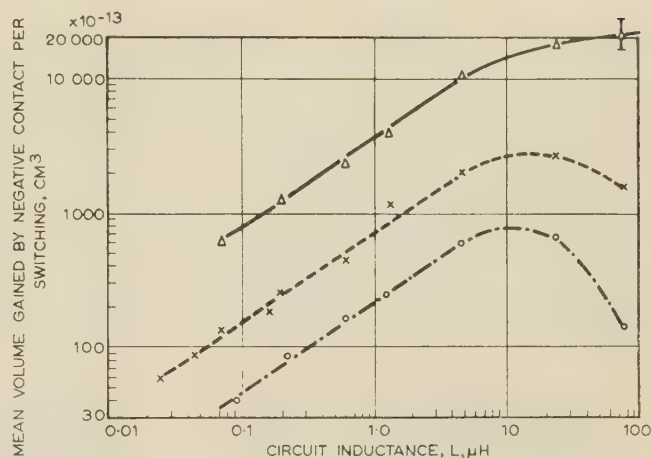


Fig. 3.—Variation with inductance and current of mean volume gained per switching by negative contact: silver contacts in 6-volt circuit.

<table>
<tr><td>○</td><td>3·7 amp.</td></tr>
<tr><td>×</td><td>7·0 amp.</td></tr>
<tr><td>△</td><td>14·5 amp.</td></tr>
</table>

between rather wide limits, as shown on the curve.   The positive contact showed a tendency to 'bed in' to fit the shape of the negative contact.   It is apparent that, except at values of inductance less than $0 \cdot 1\,\mu\text{H}$, the transfer of silver is several times greater than that of palladium under the same conditions.   There is an indication that residual transfer is reached in palladium at 3·6 amp, but for the other currents there are insufficient measurements to establish residual transfer.   The 'reversed short arc' and 'short arc' regions are also clearly recognizable.   Transfer for silver diminishes with inductance down to the lowest value used: it would be expected that residual transfer for silver would be many times less than for palladium, since the bridges are much smaller.[4]   Empirical relations can be fitted to the mean cathode gain as a function of current at constant inductance within the experimental range.   For both metals and both for the least inductance used and for an inductance of $4 \cdot 5\,\mu\text{H}$, the relation

$$\text{Volume per switching} = AI_b^n$$

is satisfied by a value of $n$ between 1·8 and 2·2.

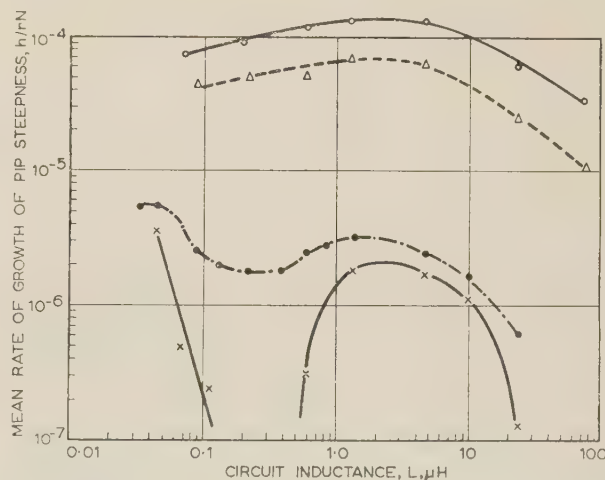The manner of growth of the pips is shown in Fig. 4.   This



Fig. 4.—Mean rate of growth of pip steepness for silver and palladium.

Silver. 14·5 amp, $N = 7\cdot5 \times 10^3$ switchings.
△ Silver. 3·7 amp, $N = 7\cdot5 \times 10^3$ switchings.
× Palladium. 6·5 amp, $N = 1\cdot5 \quad 10^5$ switchings.
● Palladium. 3·5 amp, $N = 1\cdot5 \times 10^5$ switchings.

(a)

(b)

(c)

(d)

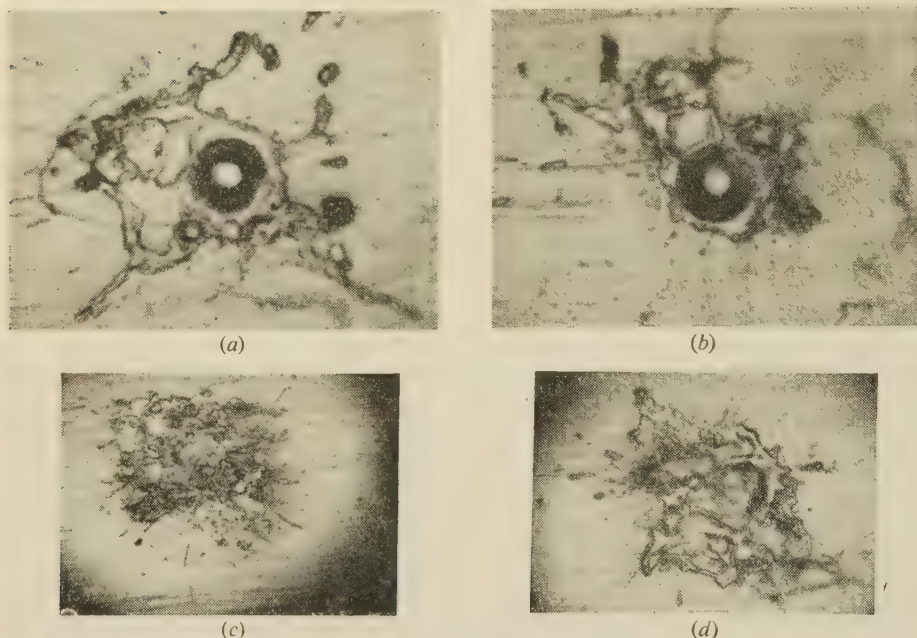Fig. 5.—Electrode marks left after a single switching: palladium.

All tests in a 6-volt circuit.    Magnification: (a) and (b), ×780; (c) and (d), ×300.

(a) $I_B = 5 \cdot 9$ amp, $L = 0 \cdot 07 \mu$H.    Negative contact.
(b) $I_B = 5 \cdot 9$ amp, $L = 0 \cdot 07 \mu$H.    Positive contact.
(c) $I_B = 5 \cdot 9$ amp, $L = 4 \cdot 5 \mu$H.    Negative contact.
(d) $I_B = 5 \cdot 9$ amp, $L = 4 \cdot 5 \mu$H.    Positive contact.

shows the mean rate of growth of pip-steepness, $h/rN$, where $h$ is the pip height, $r$ the pip base radius and $N$ the number of switchings, as a function of current and inductance for both metals. It can be seen that silver pips grow very rapidly in steepness compared with palladium pips.

Observations of transfer for palladium and silver have also been made by W. B. Ittner.[3] Although his experiments were carried out in a 3-volt circuit, it is possible to compare his results for residual transfer with the present work. It appears that his results for palladium are in general about half as great as ours at the same current, and his results for silver about twice as great. Since the minimum inductance he was able to attain was about $0 \cdot 25 \mu$H, it can be seen from Figs. 2 and 3 that this was to be expected.

### (2.2) Results of a Single Switching

To obtain records of the surface damage caused by a single switching, a circuit was designed to supply a single opening-current pulse to the relay, of shape very similar to that used when the relay was operating continuously. The opening velocity was measured and found to be not more than 50% higher than under running conditions. Photographs of the contact surfaces after single switchings are shown in Figs. 5 and 6.

It can be seen that, for palladium with minimal inductance, single round craters of closely similar diameters are left in each contact and a certain amount of molten metal is splashed on both contacts. The mean diameter, $d$, of the craters is related to the break current by the empirical relation

$$d = 2 \times 10^{-4} I_b \text{ centimetres } (1 \cdot 6 \text{ amp} < I_b < 6 \cdot 5 \text{ amp})$$

The factor is rather low compared with the figures given by Pfann,[4] $2 \cdot 44 \times 10^{-4}$, and Ittner,[5] $2 \cdot 70 \times 10^{-4}$. The theoretical factor given by Lander and Germer[6] is $2 \cdot 28 \times 10^{-4}$; their formula is stated to refer to 'maximum bridge diameter,' but it can be found that this means the diameters of the craters left

behind after rupture of a single bridge, assuming them to be hemispherical. Their formula is based on the assumption that the appropriate mean resistivity to be taken for the solid metal of the contacts is $(\rho_0 + 2\rho_m)/3$, where $\rho_0$ is the resistivity at room temperature, and $\rho_m$ the resistivity at the melting temperature. It can be shown on reasonable assumptions that a better mean to take is $(\rho_0 + \rho_m)/2$. With this correction, the theoretical factor becomes $1 \cdot 67 \times 10^{-4}$. The fact that all measured values exceed the theoretical figure may be due either to the effects of discharges or to the craters being, not of hemispherical form, but shallower.

At $4 \cdot 5 \mu$H the single round craters are no longer in evidence. Melting is on a much larger scale at both contacts, and the impression is gained that several separate pits have been occupied by the discharge at the anode, while the cathode has been pitted and also covered by fine drops of metal scattered on it at random. Either the arc has moved about on the surface or interruptions may have occurred. These could be short-circuits caused by bridging of the gap by melted metal or open-circuits due to extinction of the arc as the conditions in the gap change with time. A discussion of interruptions of the latter type has been given by Boyle and Germer.[7]



(a)

(b)

(c)

(d)
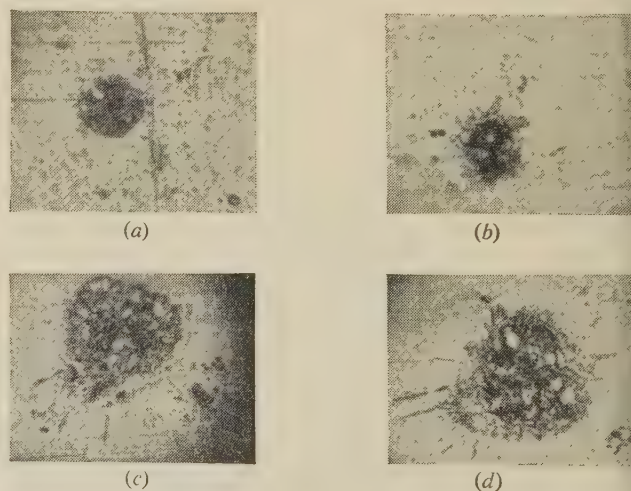
Fig. 6.—Electrode marks left after a single switching: silver.

All tests in a 6-volt circuit.    Magnification: (a) and (b), ×550; (c) and (d), × 300.

(a) $I_B = 6 \cdot 7$ amp, $L = 0 \cdot 07 \mu$H.    Negative contact.
(b) $I_B = 6 \cdot 7$ amp, $L = 0 \cdot 07 \mu$H.    Positive contact.
(c) $I_B = 6 \cdot 2$ amp, $L = 4 \cdot 5 \mu$H.    Negative contact.
(d) $I_B = 6 \cdot 2$ amp, $L = 4 \cdot 5 \mu$H.    Positive contact.

The craters in the anode surface of silver contacts at $0 \cdot 07 \mu$H are too large to be the sites of a ruptured bridge and are probably caused by the discharge following rupture of a smaller bridge. The cathode surface shows little sign of erosion but only of condensed metal. At $4 \cdot 5 \mu$H, silver anodes show multiple pitting, but the cathodes still show very little sign of erosion.

This differs from the case of palladium, where the cathode seems to have suffered erosion at the higher inductance. These facts seem to be in line with the explanations advanced recently by workers at the Bell Telephone Laboratories.[8, 9, 10]

## (3) RESULTS FOR PALLADIUM IN 12- AND 24-VOLT CIRCUITS

Results were obtained for palladium for break currents of $1 \cdot 9$ and $3 \cdot 5$ amp in a 12-volt circuit and $1 \cdot 3$, $2 \cdot 4$ and $5 \cdot 0$ amp in a 24-volt circuit. The number of switchings in each test was $5 \times 10^4$.* Only a few values of $L$ were used as the results were intended only to be indicative. The circuit used was the standard one of Fig. 1A. The results in a 12-volt circuit are displayed in Fig. 7, and in a 24-volt circuit in Fig. 8.
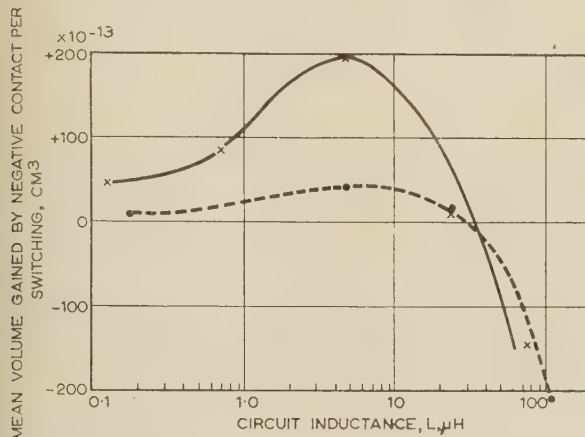


**Fig. 7.**—Variation with inductance and current of mean volume gained per switching by negative contact: palladium contacts in 12-volt circuit.

$\times \; I_B = 3 \cdot 6 \, \text{amp}.$
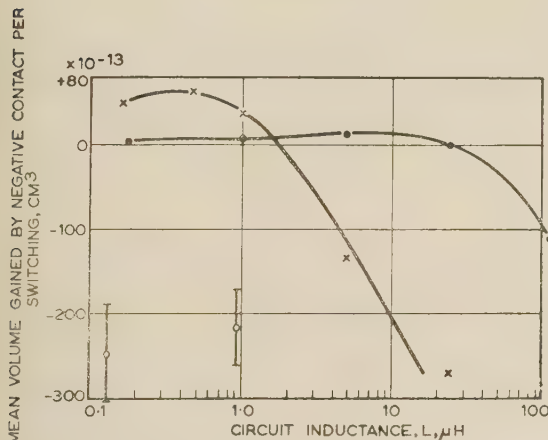$\bullet \; I_B = 1 \cdot 9 \, \text{amp}.$



**Fig. 8.**—Variation with inductance and current of mean volume gained per switching by negative contact: palladium contacts in 24-volt circuit.

$\bullet \; I_B = 1 \cdot 3 \, \text{amp}.$
$\times \; I_B = 2 \cdot 4 \, \text{amp}.$
$\circ \; I_B = 5 \cdot 0 \, \text{amp}.$

It can be seen that the general trend of the variation of transfer with inductance is similar at 12 volts to that at 6 volts, but that at 24 volts considerable cathode erosion appears at quite low

*This was because the original reason for making these measurements was to compare the behaviour of palladium and tungsten in 12- and 24-volt circuits and the tests on tungsten had already been carried out using $5 \times 10^4$ switchings. Possible departures from proportionality between transfer and number of switchings are unlikely to be large enough to invalidate the conclusions reached here.

inductances when the current is increased to $2 \cdot 4$ amp or more. This is because the mean arc voltage lies between 12 and 24 volts[11] so that the arc duration in circuits of the latter voltage is governed by considerations different from those in the case of 6- and 12-volt circuits. On this account, direct oscillographic measurements of arc duration were made in a 24-volt circuit; the results are given in Table 1.

### Table 1

DURATION OF DISCHARGES BETWEEN PALLADIUM CONTACTS IN 24-VOLT CIRCUITS

| Closed circuit current | Inductance | $L/R$ | Arc duration |
|---|---|---|---|
| amp | μH | μsec | μsec |
| $1 \cdot 3$ | 77 | $4 \cdot 0$ | $2 \cdot 65$ |
| $2 \cdot 7$ | $4 \cdot 77$ | $0 \cdot 54$ | $2 \cdot 9$ |
| $2 \cdot 7$ | 77 | $8 \cdot 7$ | 21 |

An indication of the dependence of arc duration on the supply voltage can be obtained by considering the equivalent circuit for the arc current shown in Fig. 1(c) of Reference 2. The following expression can be derived for the duration of an arc from the instant at which it starts to burn at a voltage $V_0$ in a circuit of supply voltage $V$:

$$\tau = \frac{L}{R} \log \frac{V_0 - V_b}{V_0 - V + RI_e} \quad \cdot \quad \cdot \quad \cdot \quad \cdot \quad (1)$$

provided that $V_0$ may be taken as constant while the contacts continue to separate. This assumption is valid here, as the opening speed is only about 1 cm/sec: the oscillograms also confirm that the arc voltage is approximately constant. The value of $I_e$ depends on the history of the arc as much as on the initial conditions but increases, in general, as the contacts continue to separate. There is at present no theoretical account of the values of $I_e$ observed, which are in the neighbourhood of $1 \cdot 0$ amp for palladium arcs at minimum separation. (Atalla.[12])

When $V > V_0$, as is the case for 24-volt circuits, $\tau$ is indeterminate unless

$$V_0 - V + RI_e > 0$$

i.e.
$$V - V_0 < RI_e (< V) \quad \cdot \quad \cdot \quad \cdot \quad \cdot \quad \cdot \quad (2)$$

Inserting the values $V = 24$ volts, $V_0 = 15$ volts and $I_e = 1$ amp, the result is $R > 9$ ohm. Thus, for circuits carrying more than $24/9 = 2 \cdot 7$ amp the arc duration will be determined by the rise of extinction current due to the continued separation of the contacts. Such an arc may conveniently be described as a 'ruptured' arc, and the type whose duration is determined by the exhaustion of the inductive energy stored in the circuit, to which eqn. (1) applies, an 'inductive' arc.

Referring to Table 1, it will be seen that the arc duration in the test at $1 \cdot 3$ amp is $0 \cdot 66 L/R$. From eqn. (1) it is found that $I_e = 0 \cdot 86$ amp, a not unreasonable value. But for the tests at $2 \cdot 7$ amp, the observed arc durations are large multiples of $L/R$ and eqn. (1) becomes very sensitive to $I_e$ and much less sensitive to $L/R$. This marks the transition condition between inductive and ruptured arcs.

The consequences are apparent in the transfer measurements of Fig. 8. At 24 volts, $1 \cdot 3$ amp, cathode erosion will not set in until $L$ is increased to $24 \, \mu H$, whereas at $5 \cdot 0$ amp it is already heavy at minimal inductance. Intermediate behaviour is shown at $2 \cdot 4$ amp.

The data are not available from which to calculate the arc durations in 24-volt circuits where the arc is ruptured (i.e. $R > 9$ ohms in the case of palladium), and it does not seem

possible that useful predictions of transfer can be made for these conditions. The difficulty arises because the arc is modifying the surfaces between which it is burning and will be extinguished ultimately by chance. A high opening speed should favour reduced transfer: in the apparatus available for these experiments, opening speed could not readily be varied so that this conclusion could not be checked.

## (4) ANALYSIS OF RESULTS FOR PALLADIUM

### (4.1) The Variation of Transfer with Arc Charge

From the general similarity of the curves of Figs. 2, 7 and 8 it seemed likely that the data could be reduced to a single curve of general application. A natural hypothesis to test is that the amount of transfer, expressed as a fraction of some standard volume depending only on the current, should depend in a unique way on the ratio of the charge passed in the arc to the standard volume. The latter quantity is conveniently referred to as the specific charge. The question arises as to what to take as the standard volume. Ideally it would be the volume of residual transfer, i.e. the transfer at zero specific charge. However, in only one case have experiments been conducted at low enough inductances for a reasonable assumption to be made that residual transfer is being measured. Extrapolation in the other cases would be hazardous. For this reason the standard volume was taken to be the volume of transfer measured at a standard specific charge of $10^4$ C/cm$^3$.

The data were treated in the following manner. For each individual measurement the charge passed was calculated from the following expression, assuming $V_0 = 15$ volts and $I_e = 1 \cdot 0$ amp constant throughout:

$$Q = \frac{L}{R}(I_b - I_e) - \frac{(V_0 - V)}{R}\tau \quad . \quad . \quad . \quad (3)$$

where $\tau$ is given by eqn. (1). For each given value of $I_b$ the data of Figs. 2, 7 and 8 were replotted, using $Q$ as abscissa. From each curve it was possible to determine the standard volume corresponding to a specific charge of $10^4$ C/cm$^3$. All specific charges and reduced volumes (ratio of volume transferred to standard volume) could then be calculated for each current and all the inductances used. This procedure was followed for all currents and voltages used in the complete series of tests, where eqn. (2) applied. The results are shown in Fig. 9.

It can be seen that the observations under all conditions are reduced in this way to one general curve, of form resembling that previously found for platinum.[2] One of the 24-volt observations, for a high specific charge, is seen to depart from the curve in a way which suggests that the charge actually passed was greater than that calculated. This could indicate a lower extinction current than $1 \cdot 0$ amp and would not be surprising. Three useful conclusions may be drawn from Fig. 9:

(a) The hypothesis that transfer phenomena are similar at equal specific charges receives support. This conclusion does not involve any special assumptions about the mechanisms of arc transfer.

(b) Residual transfer in palladium can be observed, provided that the specific charge does not exceed about $7 \times 10^3$ C/cm$^3$.

(c) Zero net transfer due to a combination of residual and arc processes is attained for a specific charge of about $4 \times 10^6$ C/cm$^3$.

The specific total heat of evaporation of palladium is about 16 kcal/cm$^3$. For a mean arc voltage of 15 volts, this figure is equivalent to $4 \cdot 4 \times 10^3$ C/cm$^3$. It is thus clear that the discharge energy in the balanced transfer condition must be almost entirely conducted away into the body of the solid contacts during the time of the discharge. In the case of the extremely short arcs of less than $10^4$ C/cm$^3$ specific charge, of duration less than $10^{-7}$ sec, there is insufficient time for this conduction,
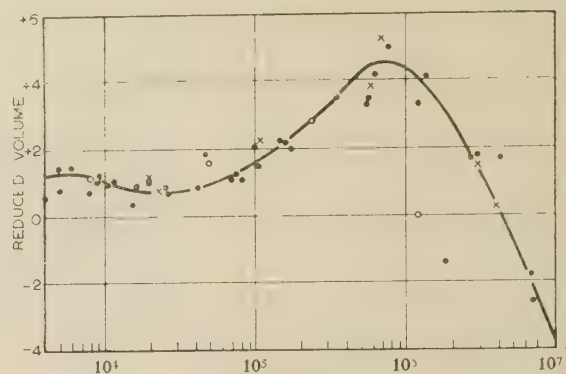


Fig. 9.—Variation with specific charge of reduced volume gained by negative contact: palladium contacts.

● $V = 6$ volts.
× $V = 12$ volts.
○ $V = 24$ volts.

so that it is not until the specific charge is reduced to be comparable with the figure equivalent to the specific total heat of evaporation that residual transfer can be observed. The thermal-diffusion time-constant of a palladium bridge carrying $3 \cdot 16$ amp would be $4 \times 10^{-7}$ sec.

It is of interest to treat the data obtained previously on platinum in the same way. The corresponding figures indicate that platinum is slightly more resistant to arcing than palladium but the difference is unimportant. The specific total heat of evaporation of platinum is about 18 kcal/cm$^3$.

### (4.2) The Variation of Transfer with Current

The empirical relations for constant inductance noted in Section 2.1 are of doubtful significance in view of the foregoing. Reliable generalizations will only be obtained from observations at different break currents but constant specific charge. The standard volumes referred to in Section 3.1 were found to fit very accurately the relation:

Transfer (at specific charge $10^4$ C/cm$^3$) = $3 \times 10^{-13}I_b^2$ cubic centimetres per switching.
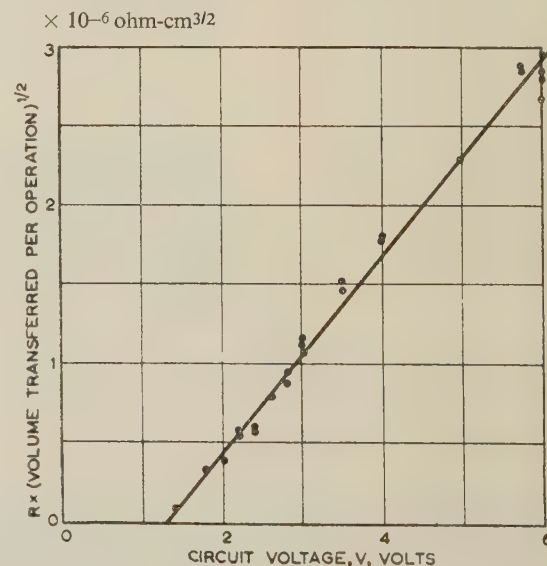


Fig. 10.—Variation with circuit voltage of mean volume gained per switching by negative contact: palladium contacts.

Specific charge less than $7 \times 10^3$ C/cm$^3$.

It seemed desirable to find the relation for a specific charge of less than $7 \times 10^3$ C/cm³ in a separate series of tests, as some confidence could be placed in the contention that this would represent true residual transfer. To do this, it is necessary to use minimal inductance and to decrease the supply voltage, $V$, as the break current is decreased. In this way the factor by which $L/R$ is multiplied in eqn. (1) is made smaller as the break current, and hence the standard volume, becomes less and approximate constancy of specific charge at a low value is preserved.

In the tests, $V$ was varied from 0·6 to 6·0 volts and $I_b$ from 0 to 3·2 amp: $1·5 \times 10^5$ switchings were used throughout. The quantity $R \times$ (volume per switching)$^{1/2}$ is shown plotted against $V$ in Fig. 10. The linear relation establishes that a square law is being followed, and the intercept of 1·3 volts on the $V$-axis is equal to the boiling voltage, as expected. From the slope of the line the result is obtained:

Residual transfer = $4·1 \times 10^{-13} I_b^2$ cubic centimetres per switching.

## (5) CONCLUSIONS

The general nature of transfer between separating contacts of palladium is similar to that in the case of platinum: neither residual transfer nor 'reversed short arc' transfer can be demonstrated in silver. Palladium is slightly less resistant to arcing than platinum, but the difference is not important. Residual transfer is rather less for palladium. Transfer for silver is greater than for either palladium or platinum except at inductances less than about 0·1 μH. Silver transfer tends to assume a spiky form, which would make it unsuitable over the current range in these experiments for some applications.

Transfer in palladium in both 6- and 12-volt circuits may be calculated for any conditions within the range of these experiments from a single curve relating the reduced volume to the specific charge associated with the arc. At constant specific charge, transfer is found to be proportional to the square of the break current and residual transfer is equal to $4·1 \times 10^{-13} I_b^2$ cubic centimetres per switching. These conclusions apply to 24-volt circuits in which the current is less than about 2·7 amp, but otherwise reliable predictions of transfer in 24-volt circuits cannot be made. This is because the expected arc durations depend strongly on the value assumed for the extinction current.

## (7) REFERENCES

(1) WARHAM, J.: 'The Effect of Inductance on Fine Transfer between Platinum Contacts', *Proceedings I.E.E.*, Paper No. 1504, July, 1953 (**100**, Part I, p. 163).

(2) RIDDLESTONE, J.: 'The Variation with Current and Inductance of Metal Transfer between Platinum Contacts', *ibid.*, Monograph No. 103, July, 1954 (**102** C, p. 29).

(3) ITTNER, W. B.: 'Bridge and Short Arc Erosion of Copper, Silver and Palladium Contacts on Break', *Journal of Applied Physics*, 1956, **27**, p. 382.

(4) PFANN, W. G.: 'Bridge Erosion of Electrical Contacts and its Prevention', *Transactions of the American I.E.E.*, 1948, **67**, p. 1528.

(5) ITTNER, W. B.: 'Bridging and Arc Formation at Separating Tungsten Contacts', Proceedings of the Electrical Contacts Seminar, Pennsylvania, July, 1954.

(6) LANDER, J. J., and GERMER, L. H.: 'Bridge Erosion of Electrical Contacts, Part 1', *Journal of Applied Physics*, 1948, **19**, p. 910.

(7) BOYLE, W. S., and GERMER, L. H.: 'Arcing at Electrical Contacts on Closure: Part VI—The Anode Mechanism of Extremely Short Arcs', *ibid.*, 1955, **26**, p. 571.

(8) ATALLA, M. M.: 'Arcing of Electrical Contacts in Telephone Switching Circuits: Part V—Mechanism of the Short Arc and Erosion of Contacts', *Bell System Technical Journal*, 1955, **34**, p. 1081.

(9) GERMER, L. H., and BOYLE, W. S.: 'Anode and Cathode Arcs', *Nature*, 1955, **176**, p. 1019.

(10) GERMER, L. H., and BOYLE, W. S.: 'Two Distinct Types of Short Arcs', *Journal of Applied Physics*, 1956, **27**, p. 32.

(11) RIDDLESTONE, J.: 'Short Duration Discharges between Separating Contacts in a 6 V Circuit', *British Journal of Applied Physics*, 1957, **8**, p. 105.

(12) ATALLA, M. M.: 'Arcing of Electrical Contacts in Telephone Switching Circuits: Part II—Characteristics of the Short Arc', *Bell System Technical Journal*, 1953, **32**, p. 1493.

# ELECTROMAGNETIC FIELDS IN A FERROMAGNETIC MEDIUM, WITH PARTICULAR REFERENCE TO HARMONIC DISTORTION DUE TO HYSTERESIS

## By V. G. WELSBY, Ph.D., B.Sc.(Eng.), Associate Member.

### SUMMARY

As a result of magnetic hysteresis, the propagation of electromagnetic waves through a ferromagnetic medium is accompanied by the generation of harmonic-frequency fields. An approximate theoretical method of treating the problem is developed and applied to study the third-order voltage distortion factor of an inductor as a function of frequency. An analogue method is also described which enables the study to be extended experimentally to cases where the theoretical analysis is not applicable; e.g. for large flux densities or for complex input waveforms.

### LIST OF SYMBOLS

$\mu_0$ = Universal magnetic constant.
$\epsilon_0$ = Universal electric constant.
$\mu$ = Permeability.
$\epsilon$ = Permittivity.
$\sigma$ = Conductivity.
$Z$ = Field impedance.
$Z_c$ = Circuit impedance.
$\gamma$ = Propagation coefficient.
$E$ = Electric field intensity.
$H$ = Magnetic field intensity.
$B$ = Magnetic flux density.
$V$ = Voltage.
$I$ = Current.
$\delta$ = Depth of penetration.
$a$ = Radius of cylindrical core or half-thickness of lamination.
$\theta = 2a/\delta$.
$\alpha_1, \alpha_2$ = Constants defining the hysteresis loop of a material.
$k$ = Voltage distortion factor.
$I_0, I_1, K_0, K_1$ = Bessel functions.

### (1) INTRODUCTION

It is well known that, because of magnetic hysteresis, the waveform of the alternating e.m.f. induced in the winding of an iron-cored inductor carrying a sinusoidally alternating current will be distorted, and can be expressed as the sum of a sinusoidal component at the fundamental frequency and a series of harmonic components at integral multiples of the fundamental frequency. As a result of power losses in the core and the winding, the fundamental-frequency e.m.f. component will not be in exact phase-quadrature with the current, as it would be in the case of an ideal loss-free inductor, but can be split into two parts, of which one is in phase-quadrature with the current and the other, representing the total power dissipated, is in phase with the current.

The ratio of the $n$th-harmonic e.m.f. to the part of the fundamental-frequency e.m.f. which is in quadrature with the current

is defined as the $n$th-order voltage distortion factor. Although the value of the distortion factor varies with the amplitude of the current, it is a property of the inductor itself, and is independent of the external circuit into which the latter is connected.

At low frequencies, where the form of the alternating electromagnetic field in the core of the inductor remains practically the same as it would be for direct current flowing in the winding, it is generally fairly simple to predict the voltage distortion factor in terms of the geometrical shape and size of the inductor and the known magnetic properties of its core material. As the frequency is progressively raised, however, the electromagnetic field distribution in the core begins to change so that the greatest intensity appears near its surface, whilst, at the same time, phase differences begin to appear between the alternating field values measured at various points in the core. This effect, which becomes more and more marked as the frequency rises, can be explained in terms of interaction between the original field and a superimposed induced field associated with eddy currents in the core. The concentration of field near the surface at the expense of that in its interior is therefore sometimes referred to as the 'eddy-current shielding effect'. This method of attempting to explain, in terms of circuit theory, a problem which is essentially one of electromagnetic wave propagation is, however, extremely cumbersome, particularly when the question of hysteresis distortion has to be considered.

From a field-theory aspect, the so-called eddy-current shielding effect, or 'magnetic skin-effect', appears as a natural result of the attenuation of the electromagnetic field as it penetrates from the surrounding dielectric into the conducting core material. At very high frequencies, the depth of penetration is relatively small and the field is effectively confined to a thin layer just below the surface of the core. If the frequency is now reduced, the depth of penetration becomes greater and greater until the attenuation and phase-shift of the field eventually become negligible and the low-frequency 'stationary' alternating field conditions is again reached.

In the present paper the problem of electromagnetic fields in a ferromagnetic medium will be investigated, and the results applied to predict the way in which the voltage distortion factor of an iron-cored inductor is likely to vary with frequency. No attempt is made to obtain a rigorous mathematical solution to the Maxwell field equations in a non-linear medium, but the problem is approached by means of several simplifying assumptions, each of which is justified within certain definite limits. The results obtained, although not exact, are likely to be within the practical limits set by lack of homogeneity of the magnetic material, and serve as a useful guide to the sort of effects which can be expected.

### (1.1) Assumptions upon which the Analysis is Based

It is first assumed that the flux density at all points in the medium is relatively small, so that the maximum permeability only slightly exceeds its 'initial' value (i.e. the limiting value to which it tends as the flux density is reduced indefinitely). In

[ 218 ]

practice, this means that the results will not be greatly in error provided that the rise in permeability with flux density does not exceed about 10%, a condition which is usually met in tele-communication problems where hysteresis distortion is of importance. It is also assumed, of course, that the intrinsic magnetic properties of the material are themselves independent of frequency. Under these conditions, the hysteresis loop can be represented with sufficient accuracy for the present purpose by the Rayleigh equations.

It should be pointed out that the theoretical analysis described can be applied only to cases where the geometry of the electro-magnetic field is accurately known and can be expressed in relatively simple mathematical terms. Generally, this implies that the method is confined to 'closed' magnetic circuits, which, apart from possible small air-gaps, have no appreciable magnetic field outside the core. Typical examples are ferrite or laminated iron cores. Care must be taken in attempting to apply the results obtained to dust-cores (other than toroids), in which the magnetic field distribution may be complicated.

A further fundamental assumption which has to be made is that the application of a purely sinusoidal current to the ener-gizing winding which produces the field results in a purely sinusoidal magnetizing force throughout the material. This cannot be strictly true, but it can be shown that, for the low flux densities already specified, the error produced is likely to be within the practical limits set by uncertainties about the homo-geneity of the material.

## (2) CIRCUIT AND FIELD IMPEDANCES

Consider an ideal infinitely-long transmission line formed by two thin air-spaced conducting strips of width $b$ and uniform separation $d$. Neglecting any edge effects, the distributed induc-tance $L$ and capacitance $C$ per unit length of the line are

$$L = \mu_0 \frac{d}{b} \text{ henrys per metre}$$

$$C = \epsilon_0 \frac{b}{d} \text{ farads per metre}$$

where $\mu_0$ and $\epsilon_0$ are universal constants.

The characteristic impedance of the transmission line is

$$Z_0 = \sqrt{\frac{L}{C}}$$

$$= \frac{d}{b}\sqrt{\frac{\mu_0}{\epsilon_0}} \text{ ohms} \quad . \quad . \quad . \quad . \quad . \quad (1)$$

If the potential difference between the conductors at any point is denoted by $V$, the electric field intensity at that point in the transmission line is

$$E = \frac{V}{d} \text{ volts per metre}$$

and the magnetic field intensity is

$$H = \frac{I}{b} \text{ amperes per metre}$$

where $I$ is the current flowing in the conductors. By definition, the characteristic impedance is equal to the ratio $V/I$ at any point, so that

$$Z_0 = \frac{V}{I} = \frac{d}{b}\frac{E}{H} \quad . \quad . \quad . \quad . \quad . \quad (2)$$

Comparison of eqns. (1) and (2) shows that the ratio $E/H$ has the dimensions of an impedance and

$$\frac{E}{H} = \sqrt{\frac{\mu_0}{\epsilon_0}} = Z \quad . \quad . \quad . \quad . \quad . \quad (3)$$

A ratio of this type is called a field impedance.

In general, the idea of a field impedance is associated with any surface in a region in which an electromagnetic field exists, but it is of particular interest wherever it is possible to choose surfaces which meet the following requirements:

(*a*) The tangential electric and magnetic field components at any point on the surface are mutually perpendicular.
(*b*) The field impedance is uniform over the surface.

Under these conditions, the direction of propagation of energy through the field will be perpendicular to the surface chosen. In the present case the required conditions are met by any plane perpendicular to the axis of the transmission line.

A ratio between a voltage and a current, e.g. the characteristic impedance of a transmission line, is called a circuit impedance. For the simple transmission line under consideration, the electro-magnetic field may be defined in terms of the circuit parameters $V$, $I$ and $Z_0$ or of the field parameters $E$, $H$ and $Z$. There is little to choose between the two methods here, but the advantage of the field-impedance idea lies in the fact that it applies generally to any plane-polarized electromagnetic field, even if it exists in the absence of the guiding conductors, which were introduced above merely to make the explanation simpler. Furthermore, this method is not confined to plane-polarized systems; it can be adapted to deal with any field in which surfaces fulfilling the necessary conditions can be defined in simple geometrical terms.

## (3) THE CURRENT-SHEET AND VOLTAGE-SHEET CONCEPTS

The 'current sheet' forms a convenient link between circuit theory and electromagnetic field theory. Fig. 1 represents a
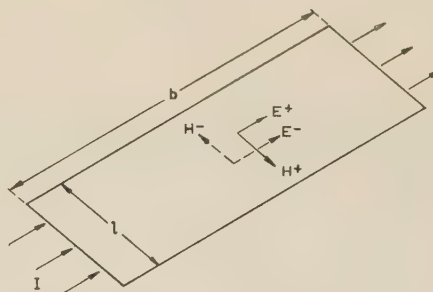


Fig. 1.—Current sheet.

The diagram indicates the relative directions of the field components at the surface of a current sheet.

straight strip of width $l$ and negligible thickness, made of a material of infinite conductivity and carrying an alternating current $I$ uniformly distributed across its width. The current must be assumed to be maintained by an externally-applied potential difference $V$. The current in the strip and the voltage drop along its length are related to the electromagnetic fields at the two surfaces of the strip by the two fundamental equations

$$V = \int E dl$$

$$I = \oint H dl$$

which may be expressed in words as follows:

(a) The potential difference between two points is equal to the line integral of the electric field intensity along any path joining the two points.

(b) The line integral of the magnetic field intensity around any closed path is equal to the current which links the path.

Applying these equations to the current sheet gives

$$E^+b = E^-b = V$$
$$H^+l + H^-l = I$$

where the plus and minus signs refer, respectively, to the upper and lower surfaces of the sheet. The circuit impedance presented by the current sheet to the source of e.m.f. which maintains the current is $Z_c$, where

$$\left.\begin{aligned}
\frac{1}{Z_c} \cdot \frac{I}{V} &= \frac{H^+l}{E^+b} + \frac{H^-l}{E^-b} \\
&= \frac{l}{b}\left(\frac{1}{Z^+} + \frac{1}{Z^-}\right) \\
Z^+ &= \frac{E^+}{H^+} \\
Z^- &= \frac{E^-}{H^-}
\end{aligned}\right\} \quad . \quad . \quad . \quad (4)$$

Eqn. (4) shows that, apart from a numerical factor, the circuit impedance of an ideal current sheet is equal to the parallel combination of the two field impedances $Z^+$ and $Z^-$. The current sheet can be regarded as the electromagnetic field equivalent of the infinite-impedance generator in circuit theory.

The voltage sheet, which forms the field-theory analogue of a zero-impedance source of e.m.f. in circuit theory, must be imagined to be composed of a material of zero conductivity which has e.m.f.'s induced in it from some external source. These e.m.f.'s will be uniformly distributed within the sheet and will produce potential differences along the upper and lower surfaces, corresponding to the electric field vectors $E^+$ and $E^-$
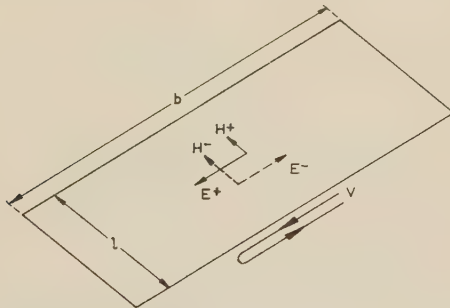
Fig. 2.—Voltage sheet.

The diagram indicates the relative directions of the field components at the surface of a voltage sheet.

respectively (see Fig. 2). The total applied e.m.f. will be equal to $V$, where

$$V = b(E^+ + E^-)$$

and the current taken from the generator will be

$$I = H^+l = H^-l$$

The circuit impedance presented to the external generator is thus

$$\begin{aligned}
Z_c = \frac{V}{I} &= \frac{b}{l}\left(\frac{E^+}{H^+} + \frac{E^-}{H^-}\right) \\
&= \frac{b}{l}(Z^+ + Z^-) \quad . \quad . \quad . \quad . \quad (5)
\end{aligned}$$

which is proportional to the series combination of the two field impedances $Z^+$ and $Z^-$.

It is fairly easy to visualize the similarity between the idea of inserting an isolated current or voltage sheet into an infinite medium and that of injecting energy into an infinitely-long transmission line by inserting either an infinite-impedance current generator in parallel with the line or a zero-impedance e.m.f. generator in series with it, respectively.

### (3.1) Application of the Current Sheet to an Inductor

An example of the purpose of the current-sheet idea will be given by using it to study the circuit impedance of a single-turn solenoidal coil and also the field conditions inside the coil.[3]

Suppose that the current sheet shown in Fig. 1 is formed into a single-turn coil with a rectangular cross-section of width $\frac{1}{2}l$ and thickness $2a$, where $a \ll b$ [see Fig. 3(a)]. The length of the
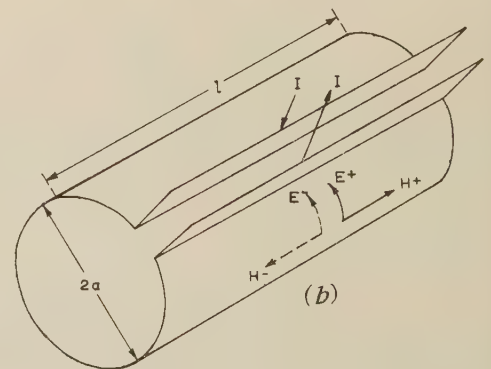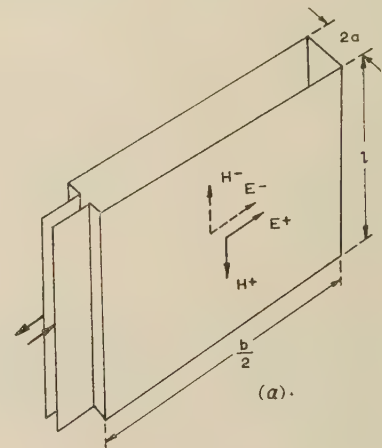
Fig. 3.—Current tubes.

The diagram indicates the relative directions of the field components at the inner and outer surfaces of a current tube.

(a) Rectangular cross-section.
(b) Circular cross-section.

resulting current tube is assumed to be sufficiently great for end effects to be neglected. Considerations of symmetry show that the electric field intensity must be zero over a plane situated midway between the two surfaces formed by the current sheet, so that conditions would be unchanged if a perfectly conducting sheet were introduced at this position. The field impedance $Z$ relating to electromagnetic waves emanating from the inner surface of the rectangular current tube corresponds to the sending-end impedance of a short-circuited transmission line

length $a$. From the usual theory of uniform transmission lines, therefore, it follows that

$$Z^- = Z_0 \tanh \gamma a \quad . \quad . \quad . \quad . \quad (6)$$

where $Z_0$ and $\gamma$ are, respectively, the intrinsic field impedance and propagation coefficient of the medium within the current tube. If the latter is air, complete reflection will occur at the mid-plane, and a stationary alternating field will exist within the tube similar to that associated with the standing waves in a short-circuited transmission line. In this case,

$$\gamma = j\omega\sqrt{(\mu_0\epsilon_0)} = j\frac{2\pi}{\lambda}$$

$$Z_0 = \sqrt{\frac{\mu_0}{\epsilon_0}}$$

$$Z^- = jZ_0 \tan \frac{2\pi a}{\lambda} \quad . \quad . \quad . \quad . \quad (7)$$

Assuming that $a$ is small compared with the wavelength $\lambda$, eqn. (6) becomes

$$Z^- = Z_0\gamma a$$

$$= j\omega a\mu_0. \quad . \quad . \quad . \quad . \quad (8)$$

The 'outward' wave impedance $Z^+$ will generally be so much greater than $Z^-$ that its shunting effect can be neglected, with the result that the circuit impedance of the current-sheet loop will be

$$Z_c = \frac{b}{l}Z^-$$

$$= j\omega\mu_0\frac{ab}{l}$$

The loop then has an inductance of $\mu_0 ab/l$.

Suppose now that, instead of air, the current tube is filled with a non-magnetic conducting medium having conductivity $\sigma$ and permittivity $\epsilon$. Eqn. (6) will still apply, but the propagation coefficient and intrinsic impedance will now be given by

$$\gamma = \sqrt{[j\omega\mu_0(\sigma + j\omega\epsilon_0\epsilon)]} \quad . \quad . \quad . \quad (9)$$

$$Z_0 = \sqrt{\frac{j\omega\mu_0}{\sigma + j\omega\epsilon_0\epsilon}} \quad . \quad . \quad . \quad . \quad (10)$$

For the present it will be assumed that $\sigma$ is sufficiently large for the term $j\omega\epsilon_0\epsilon$ to be neglected in comparison with it, so that these expressions reduce to

$$\gamma = \sqrt{(j\omega\mu_0\sigma)} \quad . \quad . \quad . \quad . \quad (11)$$

$$Z_0 = \sqrt{\frac{j\omega\mu_0}{\sigma}} \quad . \quad . \quad . \quad . \quad (12)$$

The propagation coefficient $\gamma$ will be a complex quantity with a phase angle of $\frac{1}{4}\pi$ radians, and the electromagnetic waves propagated inwards towards the central plane will be attenuated. The quantity $\delta$, defined by

$$\gamma\delta = (1 + j) \quad . \quad . \quad . \quad . \quad . \quad (13)$$

is called the depth of penetration of the field into the core:

$$\delta = \sqrt{\frac{2}{\omega\mu_0\sigma}} \quad . \quad . \quad . \quad . \quad (14)$$

so that

$$\gamma a = \frac{a}{\delta}(1 + j) \quad . \quad . \quad . \quad . \quad (15)$$

$$= \frac{\theta}{2}(1 + j)$$

where

$$\theta = \frac{2a}{\delta} \quad . \quad . \quad . \quad . \quad . \quad (16)$$

Eqn. (6) can be written

$$Z^- = Z_0\gamma a \frac{\tanh \gamma a}{\gamma a} \quad . \quad . \quad . \quad . \quad (17)$$

Substituting for $Z_0$ and $\gamma$ from eqns. (11) and (12) gives

$$Z^- = j\omega\mu_0 a \frac{\tanh \gamma a}{\gamma a} \quad . \quad . \quad . \quad . \quad (18)$$

The circuit impedance of the current sheet is then

$$Z_c = \frac{b}{l}Z^-$$

$$= j\omega\mu_0\frac{ab}{l} \frac{\tanh \gamma a}{\gamma a} \quad . \quad . \quad . \quad . \quad (19)$$

The introduction of the conducting core thus has the effect of multiplying the circuit impedance by the factor $(\tanh \gamma a)/\gamma a$. Substituting $\gamma a = \frac{1}{2}\theta(1 + j)$, and expanding into real and imaginary parts,

$$\frac{\tanh \gamma a}{\gamma a} = \frac{1}{\theta}\left[\left(\frac{\sinh \theta + \sin \theta}{\cosh \theta + \cos \theta}\right) - j\left(\frac{\sinh \theta - \sin \theta}{\cosh \theta + \cos \theta}\right)\right] \quad . \quad (20)$$

Thus, if $Z_c$ is expressed as a series combination of inductance and resistance,

$$Z_c = R + j\omega L . \quad . \quad . \quad . \quad . \quad (21)$$

$$R = \frac{1}{\theta}\left(\frac{\sinh \theta - \sin \theta}{\cosh \theta + \cos \theta}\right)\frac{\omega\mu_0 ab}{l} \quad . \quad . \quad . \quad (22)$$

$$L = \frac{1}{\theta}\left(\frac{\sinh \theta + \sin \theta}{\cosh \theta + \cos \theta}\right)\frac{\mu_0 ab}{l} \quad . \quad . \quad . \quad (23)$$

The important thing to note, from the point of view of the present investigation, is the close analogy between the field distribution in each half of the core and that along an equivalent short-circuited transmission line.

## (4) ELECTROMAGNETIC FIELDS IN A FERROMAGNETIC MEDIUM

The properties of an alternating magnetic field can be expressed in terms of two vector quantities: the magnetic field intensity or magnetizing force $H$, relating to the equivalent current required to produce the field, and the magnetic flux density $B$, relating to the e.m.f. which would be induced in a conductor by the field. The directions of the $H$ and $B$ vectors will coincide in any homogeneous medium which does not exhibit magnetic polarity. In free space, the $B/H$ ratio is a universal constant denoted by $\mu_0$. For a homogeneous ferromagnetic medium of infinite extent, the $B/H$ ratio is increased by a factor defined as the permeability of the medium. If the ferromagnetic medium is limited in extent, the effective magnetizing force will be the vector sum of $H$ and an induced component $H'$, the existence of which is characterized by the appearance of magnetic polarity at the boundary surface of the material. The direction of $H'$ tends to oppose that of $H$ within the medium, with the result that the

effective magnetizing force $H + H'$ is less than $H$. The general relationship between the applied magnetizing force $H$ and the resulting flux density is thus

$$B = \mu(H + H')$$

The induced field $H'$ may still be negligible, even when the ferromagnetic medium is of finite extent; if the latter takes the form of a long thin rod with a solenoidal winding, for example, the separation of the induced poles at the ends of the rod may be sufficiently large for $H'$ to be negligibly small compared with $H$. Similar conditions exist in a toroidal core which forms a closed magnetic circuit having no polarity and no induced field.

Suppose now that the rectangular current tube discussed in Section 3 is filled with a ferromagnetic medium, and assume that the ratio $l/b$ is made sufficiently large for the induced field associated with the magnetic polarity at the ends of the tube to be neglected. Eqn. (6) will then apply, but the propagation coefficient and intrinsic field impedance will be, respectively,

$$\gamma = \sqrt{[j\omega\mu_0\mu(\sigma + j\omega\epsilon_0\epsilon)]} \quad . \quad . \quad . \quad (24)$$

and

$$Z = \sqrt{\frac{j\omega\mu_0\mu}{\sigma + j\omega\epsilon_0\epsilon}} \quad . \quad . \quad . \quad . \quad (25)$$

so that

$$Z^- = j\omega\mu_0\mu a\left(\frac{\tanh \gamma a}{\gamma a}\right) \quad . \quad . \quad . \quad (26)$$

The general case, in which $\gamma$ is a complex quantity with a phase angle varying with frequency, will be omitted for the present and attention confined to conducting materials for which $\sigma$ is large enough for $j\omega\epsilon_0\epsilon$ to be neglected. This assumption is justified for all magnetic alloys but will not necessarily apply to ferrites, which tend to have low conductivities and high permittivities.

For ferromagnetic conducting materials, therefore,

$$\gamma = \sqrt{(j\omega\mu_0\mu\sigma)} = \frac{1}{\delta}(1 + j) \quad . \quad . \quad . \quad (27)$$

$$Z_0 = \sqrt{\frac{j\omega\mu_0\mu}{\sigma}} \quad . \quad . \quad . \quad . \quad (28)$$

where $\delta$ is the depth of penetration, so that

$$\delta = \sqrt{\frac{2}{\omega\mu_0\mu\sigma}} \quad . \quad . \quad . \quad . \quad (29)$$

### (4.1) Effect of Hysteresis

In a non-magnetic material, the instantaneous value of the flux density $B$ at any point is always proportional to the instantaneous magnetizing force $H$ at that point. A sinusoidally varying $H$ is accompanied by a $B$ which varies sinusoidally in phase with it. So far, it has been assumed that the same will apply to a magnetic material, i.e. that the permeability is a simple numerical ratio. In fact, of course, this is not true and the instantaneous relationship between $B$ and $H$ is rather more complicated. At the relatively low flux densities to which the present discussion refers, it can be represented by a hysteresis loop of the form

$$\frac{B}{\mu_0 H} = (\mu + \alpha_1 \hat{H}) \pm \frac{\alpha_2}{2}(\hat{H}^2 - H^2) \quad . \quad . \quad (30)$$

where $\alpha_1$, $\alpha_2$ and $\mu$ are constants for the material and $\hat{H}$ denotes the peak value of $H$. The positive sign applies when $H$ is

increasing and the negative sign when it is decreasing. Then $H$ is varying sinusoidally with time, so that

$$H = \hat{H} \cos \omega t$$

$$\frac{B}{\mu_0} = (\mu + \alpha_1\hat{H})\hat{H} \cos \omega t \pm \frac{\alpha_2}{2}\hat{H}^2(1 - \cos^2 \omega t)$$

$$= (\mu + \alpha_1\hat{H})\hat{H} \cos \omega t \pm \frac{\alpha_2}{2}\hat{H}^2 \sin^2 \omega t$$

The second term of this expression represents a periodic function with positive half-cycles proportional to $+ \sin^2 \omega t$ and negative half-cycles proportional to $- \sin^2 \omega t$. Expanding this term in a Fourier series and neglecting higher-order terms gives

$$\frac{B}{\mu_0} = (\mu + \alpha_1\hat{H})\hat{H} \cos \omega t + 4\frac{\alpha_2\hat{H}}{3\pi} \hat{H} \sin \omega t - \frac{4\alpha_2\hat{H}}{15\pi} \hat{H} \sin 3\omega t$$

$$. \quad . \quad . \quad (31)$$

For a uniform plane-polarized electromagnetic field in a homogeneous hysteresis-free medium, the rate of change of the instantaneous electric field intensity with distance in a direction perpendicular to the plane of polarization is

$$dE = \frac{dB}{dt}dx \quad . \quad . \quad . \quad . \quad . \quad . \quad . \quad (32)$$

$$= \mu_0\mu\frac{dH}{dt}dx$$

$$= \mu_0\mu\frac{d}{dt}(\hat{H} \cos \omega t)dx$$

$$= \mu_0\mu\omega\hat{H} \cos \left(\omega t + \frac{\pi}{2}\right)dx$$

$$= j\mu_0\mu\omega H dx$$

or

$$\frac{1}{\mu_0}dE = j\mu\omega H dx \quad . \quad . \quad . \quad . \quad . \quad . \quad (33)$$

(using the '$j$' operator to denote that the time-phase of $dE$ leads that of $H$ by $\frac{1}{2}\pi$ radians).

To take hysteresis into account, it is necessary to substitute in eqn. (32) the value of $B$ given by eqn. (31):

$$\frac{1}{\mu_0}\frac{dE}{dx} = \frac{d}{dt}\left(\frac{B}{\mu_0}\right)$$

$$= (\mu + \alpha_1\hat{H})\omega\hat{H} \cos \left(\omega t + \frac{\pi}{2}\right) + 4\frac{\alpha_2\hat{H}}{3\pi}\omega\hat{H} \cos \omega t$$

$$- \frac{4\alpha_2\hat{H}}{5\pi} \omega\hat{H} \cos 3\omega t$$

or $dE = j\omega\mu_0\mu H dx + j\omega\mu_0\mu H \left(\frac{\alpha_1\hat{H}}{\mu} - j\frac{4\alpha_2\hat{H}}{3\pi\mu}\right) + \delta E_3$ . (34)

The change in electric field in the interval $dx$ now contains not only a fundamental-frequency term whose value depends on the peak magnetic field intensity $\hat{H}$, but includes also a series of odd-order harmonic-frequency components of which the third-order one is represented by $\delta E_3$.

Since, by hypothesis, $H$ is purely sinusoidal in the interval, the harmonic-frequency electric field component $\delta E_3$ must appear alone without any accompanying magnetic field component; in other words, it must be imagined to be injected into the system from some source external to the medium. As far as the remaining portion of the medium outside the elemental slab of thickness is concerned, the situation is just as if a voltage sheet, carrying

n e.m.f. $\delta E_3$ per unit length, exists within the slab and generates harmonic-frequency electromagnetic field which is propagated utwards in both directions throughout the medium. One esult will be that the waveform of $H$ cannot be sinusoidal anyhere except within the slab $dx$, so that eqn. (34) cannot apply xactly to any similar interval $dx$ elsewhere. The error produced y neglecting this effect is small, however, and can be ignored rovided $\alpha_2 \hat{H}/\mu$ is small compared with unity.

This condition, which implies that the magnetic flux density in ne medium is relatively small, is one which is likely to be tisfied in many cases where harmonic distortion is of interest, nd even if the condition is not satisfied, the approximate method f analysis to be described provides some indication of the results be expected.

The method of solution consists first in finding an expresson for $H$, at the fundamental frequency, as a function of istance. The fact that the flux density has been assumed to be mall leads to a further simplification, because it means that $\hat{H}/\mu$ will also be sufficiently small to enable the variation of ermeability with $\hat{H}$ to be neglected, so that $H$ can be calculated y normal transmission theory based on a constant permeability. The next step is to derive the field equations relating to the armonic-frequency field generated in an elemental slab of thickess $dx$. Finally, the total harmonic-frequency field, due to all uch elemental slabs, can be obtained by integrating between ppropriate limits.

The modulus of $\delta E_3$ is obtained from eqn. (34):

$$|\delta E_3| = \frac{4\alpha_2 \hat{H} \mu_0}{5\pi}\omega|H|dx$$

$$= \frac{4\alpha_2 \hat{H} \mu_0}{5\pi\mu}\omega\mu|H|dx \quad . \quad . \quad . \quad (35)$$

his can be changed into a more convenient form by introducing e field parameters.

$$Z_0 = \sqrt{\frac{j\omega\mu_0\mu}{\sigma}}$$

$$\gamma = \sqrt{(j\omega\mu_0\mu\sigma)}$$

that

$$Z_0\gamma = j\omega\mu_0\mu \quad . \quad . \quad . \quad . \quad (36)$$

$$|\omega\mu| = \frac{1}{\mu_0}|Z_0\gamma| \quad . \quad . \quad . \quad . \quad (37)$$

ubstituting in eqn. (35) gives

$$|\delta E_3| = \frac{4\alpha_2 \hat{H}}{5\pi\mu}|Z_0 H\gamma|dx \quad . \quad . \quad . \quad (38)$$

rovided that the frequency remains constant, $\gamma$ is also a constant nd $|\delta E_3|$ can be expressed in terms of a dimensionless paraeter $\gamma x$:

$$|\delta E_3| = \frac{4\alpha_2 \hat{H}}{5\pi\mu}|Z_0 Hd(\gamma x)| \quad . \quad . \quad . \quad (39)$$

he magnetic field intensity $H$ is also a function of $x$ and can us be expressed in terms of the parameter $\gamma x$.

Using the suffixes $a$ and $x$ to denote, respectively, values at stances $a$ and $x$ from a reference plane along a direction erpendicular to the plane of polarization, it is seen that

$$\left|\frac{\delta E_{3x}}{\delta E_{3a}}\right| = \left|\frac{H_x}{H_a}\right|^2$$

$$|\delta E_{3x}| = \frac{4\alpha_2 \hat{H}_a}{5\pi\mu}\left|Z_0 H\left(\frac{H_x}{H_a}\right)^2 d(\gamma x)\right|$$

$$|\delta E_{3a}| = \frac{4\alpha_2 \hat{H}_a}{5\pi\mu}|Z_0 H_a d(\gamma x)| \quad . \quad . \quad . \quad (40)$$

Since the important thing here is the *relative* phase of $\delta E_3$ at various distances from the reference plane, it will be convenient to take the phase angle $\delta E_3$ as zero when $x = a$.

Then

$$\delta E_{3a} = \frac{4\alpha_2 \hat{H}_a}{5\pi\mu}Z_0 H_a d(\gamma x) \quad . \quad . \quad . \quad (41)$$

The modulus of $\delta E_3$ is proportional to the square of the fundamental-frequency field intensity, but its phase angle is always fixed relative to that of $H$ at the point concerned. Since $\delta E_3$ has a frequency equal to three times that of $H$, however, its phase-angle will change three times as rapidly as that of $H$. Thus

$$\frac{\delta E_{3x}}{\delta E_{3a}} = \frac{f_1(\gamma x)}{f_1(\gamma a)} \quad . \quad . \quad . \quad . \quad (42)$$

where $f_1(\gamma x)$ represents a complex function of $\gamma x$ whose modulus is $|H_x|^2$ and whose phase-angle is three times that of $H_x$.

## (5) DISTORTION FACTOR OF A SOLENOIDAL COIL OF RECTANGULAR CROSS-SECTION

In Section 3 it was shown that the circuit impedance of a single-turn solenoid is given by

$$Z_c = j\omega\mu_0\mu\frac{ab}{l}\frac{\tanh\gamma a}{\gamma a}$$

and that the electromagnetic field within each half of the coil cross-section is analogous to that in a short-circuited transmission line. Suppose that such a coil is fed with a sinusoidal current from an infinite-impedance source, and that the above method is used to determine the extent to which the resulting voltage waveform is distorted as a result of hysteresis if the coil is filled with a ferromagnetic core. Making use again of the transmission line analogy and taking the reference plane midway between the two main surfaces of the core, the ratio $H_x/H_a$ is given by

$$\frac{H_x}{H_a} = \frac{\cosh\gamma x}{\cosh\gamma a} \quad . \quad . \quad . \quad . \quad (43)$$

so that

$$f_1(\gamma x) = r^2\varepsilon^{3j\phi} \quad . \quad . \quad . \quad . \quad (44)$$

where

$$r\varepsilon^{j\phi} = \cosh\gamma x \quad . \quad . \quad . \quad . \quad (45)$$

The harmonic-frequency electric field component $\delta E_{3x}$, injected into the elemental slab of the core of thickness $dx$ at a distance $x$ from the reference plane, will produce a corresponding electric field component $\delta E'_{3x}$ at the surface of the core, i.e. at a distance $a$ from the reference plane. The problem of determining $\delta E'_{3x}$ is somewhat similar to that of calculating the voltage which will appear at the open end of a length of transmission line which is short-circuited at the other end and has an e.m.f. injected at some point along its length. An injected field component $\delta E$ will generate electromagnetic fields in which the direction of energy flow is respectively towards the points $x = 0$ and $x = a$. The relative amplitudes of the two fields at the point $x$ will be determined by the field impedances $Z_x^+$ and $Z_x^-$ (calculated here, of course, for the harmonic frequency concerned). The electric component, at the point $x$, of the field directed towards $x = a$, will be

$$\delta E\left(\frac{Z^+}{Z^+ + Z^-}\right)_x$$

If the medium extended to $x = \infty$, $Z^+$ would be equal to the intrinsic field impedance $Z$ of the medium, and the resulting field at $x = a$ would be

$$\delta E\left(\frac{Z}{Z + Z^-}\right)\varepsilon^{-\gamma(a-x)}$$

$$-\delta E\left(\frac{Z}{Z+Z^{-}}\right)\frac{\varepsilon^{\gamma x}}{\varepsilon^{\overline{\gamma a}}}$$

The replacement of the medium beyond $x = a$ by space with an intrinsic impedance which is much greater than $Z_a^{+}$ has the effect of multiplying the electric field at $x = a$ by a factor $(Z + Z^{-})/Z$. Finally, therefore, the electric field at the surface of the core is

$$\delta E\left(\frac{Z}{Z+Z^{-}}\right)_x\left(\frac{Z+Z^{-}}{Z}\right)_a\frac{\varepsilon^{\gamma x}}{\varepsilon^{\gamma a}}$$

The harmonic-frequency electric field at the surface of the core, due to the injected field $\delta E_{3x}$ at $x$, is thus given by

$$\delta E_{3x}' = \delta E_{3x}\frac{f_2(\sqrt{3}\gamma x)}{f_2(\sqrt{3}\gamma a)} \quad . \quad . \quad . \quad (46)$$

where

$$\frac{1}{f_2(\gamma x)} = \left(1 + \frac{Z^{-}}{Z}\right)_x\varepsilon^{-\gamma x}$$

$$= (1 + \tanh\gamma x)\varepsilon^{-\gamma x}$$

$$= \frac{1}{\cosh\gamma x}$$

or

$$f_2(\gamma x) = \cosh\gamma x$$

and

$$f_2(\sqrt{3}\gamma x) = \cosh(\sqrt{3}\gamma x) \quad . \quad . \quad . \quad . \quad (47)$$

(The factor $\sqrt{3}$ is introduced here because we are dealing with the third-harmonic frequency and $\gamma$ is proportional to $\sqrt{\omega}$.)

Combining eqns. (42) and (46) gives

$$\delta E_{3x}' = \delta E_{3a}\frac{f_1(\gamma x)}{f_1(\gamma a)}\frac{f_2(\sqrt{3}\gamma x)}{f_2(\sqrt{3}\gamma a)} \quad . \quad . \quad (48)$$

$$= \frac{4\alpha_2\hat{H}_a}{5\pi\mu}ZH_a\frac{f_1(\gamma x)}{f_1(\gamma a)}\frac{f_2(\sqrt{3}\gamma x)}{f_2(\sqrt{3}\gamma a)}d(\gamma x) \quad (49)$$

But

$$ZH_a = E_a\frac{Z}{Z_a^{-}} = E_a\coth\gamma a \quad . \quad . \quad (50)$$

therefore

$$\frac{\delta E_{3x}'}{E_a} = \frac{4\alpha_2\hat{H}_a}{5\pi\mu}\coth\gamma a\frac{f_1(\gamma x)}{f_1(\gamma a)}\frac{f_2(\sqrt{3}\gamma x)}{f_2(\sqrt{3}\gamma a)}d(\gamma x) \quad . \quad (51)$$

The total harmonic-frequency electric field at the surface of the core is obtained by integrating this expression between limits $\gamma x = 0$ and $\gamma x = \gamma a$:

$$\frac{E_3}{E_a} = \frac{4\alpha_2\hat{H}_a}{5\pi\mu}\coth\gamma a\int_0^{\gamma a}\frac{f_1(\gamma x)}{f_1(\gamma a)}\frac{f_2(\sqrt{3}\gamma x)}{f_2(\sqrt{3}\gamma a)}d(\gamma x) \quad . \quad (52)$$

The ratio $E_3/E_a$ is equal to the ratio between the harmonic-frequency e.m.f. induced in the coil and the fundamental-frequency voltage, and is referred to as the third-order open-circuit distortion factor, $k_3$.

As the fundamental frequency $\omega$ is reduced indefinitely, the distortion factor tends to the limit

$$k_{3LF} = \frac{4\alpha_2\hat{H}_a}{5\pi\mu} \quad . \quad . \quad . \quad . \quad (53)$$

At higher frequencies the distortion factor is then of the form

$$k_3 = k_{3LF}Y(\gamma a) \quad . \quad . \quad . \quad . \quad (54)$$

where $Y(\gamma a)$ is a function of $(\gamma a)$ such that

$$Y(\gamma a) = \coth\gamma a\int_0^{\gamma a}\frac{f_1(\gamma x)}{f_1(\gamma a)}\frac{f_2(\sqrt{3}\gamma x)}{f_2\sqrt{(3\gamma a)}}d(\gamma x) . \quad . \quad (55)$$

where

$$f_1(\gamma x) = r^2\varepsilon^{3j\phi}$$
$$r\varepsilon^{j\phi} = \cosh\gamma x$$
$$f_2(\sqrt{3}\gamma x) = \cosh(\sqrt{3}\gamma x)$$

As already stated, $Y(\gamma a)$ tends to unity for small values of $\gamma$. For large values of $\gamma a$, the asymptotic value of $Y(\gamma a)$ can be obtained as follows:

In this case,

$$\frac{H_x}{H_a} \to \frac{\varepsilon^{\gamma x}}{\varepsilon^{\gamma a}}$$

$$= \exp[-\gamma(a - x)]$$

$$= \exp(-\gamma d)$$

$$= \exp[-pd(1 + j)]$$

where $\gamma = p(1 + j)$ and $d$ represents distances measured from the surface of the core instead of from its centre.

$$f_1(\gamma x) \to \exp[-pd(2 + 3j)]$$
$$f_2(\sqrt{3}\gamma x) \to \exp[-\sqrt{3}pd(1 + j)]$$
$$\coth\gamma a \to 1$$

$$Y(\gamma a) \to \int_0^{\gamma a}\exp\{-pd[(2 + \sqrt{3}) + j(3 + \sqrt{3})]\}d(\gamma x)$$

$$= \int_{\gamma a}^0\exp\left\{-\gamma d\left[\frac{(2 + \sqrt{3}) + j(3 + \sqrt{3})}{(1 + j)}\right]\right\}d(\gamma d)$$

$$= \frac{1 + j}{(2 + \sqrt{3}) + j(3 + \sqrt{3})}$$

whence

$$|Y(\gamma a)| = 0\cdot235 \quad . \quad . \quad . \quad . \quad (56)$$

As the frequency increases indefinitely, therefore, the third-order distortion factor tends theoretically to a constant value which is about a quarter of that measured at low frequencies.

The function $Y(\gamma a)$ has been computed by graphical integration for the intermediate range of frequencies where the depth of penetration is comparable with the dimensions of the core. The results have been plotted in Fig. 4.
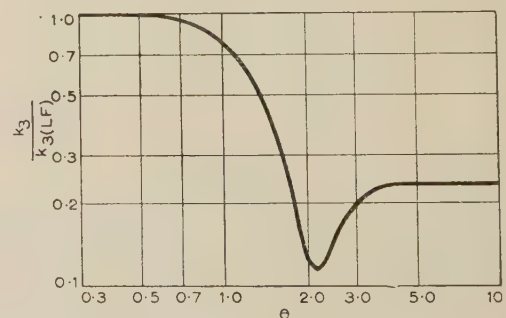


Fig. 4.—Variation of third-order distortion factor with frequency.
Curves of $k_3/k_{3(LF)}$ are plotted as a function of the parameter $\theta$ for a core of rectangular cross-section.

### (5.1) Effect of Laminating the Core

So far, we have been dealing with the somewhat unrealistic case of a single-turn solenoidal winding on a thin strip of ferromagnetic material. The results can be applied, however, to the more practical problem of a coil consisting of many turns of wire wound on a core composed of a stack of laminations. Leaving aside complications such as the question of the self-capacitance of a multi-turn coil, the only effect will be to multiply the circuit impedance of the winding by the square of the number of turns, while the distortion factor will remain unchanged for a given

amination thickness and a given flux density in the core, i.e. for a given number of ampere-turns in the winding. The variation of the distortion factor with frequency will be determined by the thickness $2a$ of each lamination, and will be independent of the number of laminations in the stack forming the core. It should be pointed out, however, that this theoretical study has been based on several simplifying assumptions which may not always be justified in practice.

It has been assumed, for example, that the laminations are all perfectly insulated from each other and, above all, it has been assumed that each lamination is perfectly homogeneous. At high frequencies, where the depth of penetration into the lamination is small, the result will be greatly influenced by any lack of uniformity in the properties of the material. A thin surface skin of relatively low permeability, for instance, would have a considerable effect on the high-frequency performance of the core. On the other hand, the theoretical analysis is of value in showing the results which should be obtained under ideal conditions.'

## (6) DISTORTION FACTORS OF COILS OF OTHER CROSS-SECTIONS

The method used above to derive an expression for the distortion factor of a coil with a core of rectangular cross-section can be applied to cores of any cross-section. A solution generally of the form of eqn. (54) will exist in each case, except that the functions $f_1(\gamma x)$, $f_2(\sqrt{3}\gamma x)$ and $\coth \gamma a$ will have to be replaced by other functions appropriate to the geometrical configuration of the electromagnetic field in the core concerned. The asymptotic values of the expression which replaces $Y(\gamma a)$ will still be unity at low frequencies and $0 \cdot 235$ at high frequencies, irrespective of the shape of the core, the latter having an effect only over the critical frequency range, where the depth of penetration of the field is comparable with the dimensions of the core cross-section.

### (6.1) Core of Circular Cross-Section

In this case the electromagnetic field is cylindrical in form, with a circumferential direction of polarization and a radial direction of energy flow, and is generated by an equivalent cylindrical current sheet tube [see Fig. 3(b)].

It is shown in Section 12 that the variation of field in a radial direction is given by

$$\frac{H_x}{H_a} = \frac{I_0(\gamma x)}{I_0(\gamma a)} \quad . \quad . \quad . \quad . \quad (57)$$

$$\frac{E_x}{E_a} = \frac{I_1(\gamma x)}{I_1(\gamma a)} \quad . \quad . \quad . \quad . \quad (58)$$

where the suffixes refer to radial distances from the centre of the cross-section, $a$ is the radius at the surface of the core, and $I_0$ and $I_1$ are modified Bessel functions. For outward-travelling waves originating at the centre, the functions are replaced by the corresponding Bessel K functions, in particular the electric field being given by

$$\frac{E_x}{E_a} = \frac{K_1(\gamma x)}{K_1(\gamma a)} \quad . \quad . \quad . \quad . \quad (59)$$

Generally, for a circumferentially-polarized cylindrical field in an infinite medium, the impedance offered at a radius $x$ to waves travelling radially inwards and outwards are $Z_x^-$ and $Z_x^+$, respectively, where

$$Z_x^- = \frac{I_1(\gamma x)}{I_0(\gamma x)} Z \quad . \quad . \quad . \quad . \quad (60)$$

$$Z_x^+ = \frac{K_1(\gamma x)}{K_0(\gamma x)} Z \quad . \quad . \quad . \quad . \quad (61)$$

An induced electric field component $\delta E$ at a radius $x$ in an infinite medium will generate inward- and outward-travelling waves, the amplitude of the latter being $\delta E\left(\dfrac{Z_x^+}{Z_x^+ + Z_x^-}\right)$ at $x$.

From eqn. (59) the amplitude of the electric field at radius $a$ would then be

$$\delta E\left(\frac{Z^+}{Z^+ + Z^-}\right)_x \frac{K_1(\gamma a)}{K_1(\gamma x)} \quad . \quad . \quad . \quad (62)$$

The replacement of the medium beyond $x = a$ by space having a much higher intrinsic field impedance will have the effect of multiplying the electric field intensity at $x = a$ by a factor

$$\left(\frac{Z^+ + Z^-}{Z}\right)_a$$

so that the electric field at the surface of the cylindrical core, due to induced electric field component $\delta E$ at a radius $x$ will be

$$\delta E\left(\frac{Z^+ + Z^-}{Z^+}\right)_a \left(\frac{Z^+}{Z^+ + Z^-}\right)_x \frac{K_1(\gamma a)}{K_1(\gamma x)} \quad . \quad . \quad (63)$$

The harmonic-frequency electric field at the surface of the core, due to the injected field at $x$, is thus given by

$$\delta E'_{3x} = \delta E_x \frac{f_4(\sqrt{3}\gamma x)}{f_4(\sqrt{3}\gamma a)} \quad . \quad . \quad . \quad . \quad (64)$$

where

$$\frac{1}{f_4(\sqrt{3}\gamma x)} = K_1(\sqrt{3}\gamma x)\left(1 + \frac{Z_x^-}{Z_x^+}\right)$$

$$= K_1(3\gamma x)\left(1 + \frac{I_1 K_0}{I_0 K_1}\right)(\sqrt{3}\gamma x)$$

$$= I_1(\sqrt{3}\gamma x)\left(\frac{K_1}{I_1} + \frac{K_0}{I_0}\right)(\sqrt{3}\gamma x) \quad . \quad (65)$$

Following the same reasoning as for the rectangular core, it can be concluded that eqns. (54) and (55) will still hold, except that

$$\coth (\gamma a) \text{ is replaced by } \frac{I_0}{I_1}(\gamma a)$$

$$f_1(\gamma x) \text{ is replaced by } f_3(\gamma x)$$

where

$$f_3(\gamma x) = r^2 \varepsilon^{3j\phi} \quad . \quad . \quad . \quad . \quad . \quad (66)$$

and

$$r\varepsilon^{j\phi} = I_0(\gamma x) \quad . \quad . \quad . \quad . \quad . \quad (67)$$

$$f_2(\sqrt{3}\gamma x) \text{ is replaced by } f_4(\sqrt{3}\gamma x)$$

where

$$\frac{1}{f_4(\sqrt{3}\gamma x)} = I_1(\sqrt{3}\gamma x)\left(\frac{K_1}{I_1} + \frac{K_0}{I_0}\right)(\sqrt{3}\gamma x)$$

The resulting Y-function defining the variation of the third-order distortion factor with the frequency-dependent variable $\gamma a$ can then be computed by graphical integration in the same way as that for the rectangular core. To do this it is necessary to obtain numerical values for the Bessel $I_0$ and $I_1$ functions and for the ratios $K_0/I_0$ and $K_1/I_1$ of the K and I functions of a 'semi-imaginary' complex variable (i.e. one of the form $zj^{1/2}$ where $z$ is real). These can be obtained from the Bessel J functions and the Hankel $H^{(1)}$ functions tabulated by Jahnke and Emde.

$I_0$ is $J_0$ with the phase angle reversed in sign.
$I_1$ is $-jJ_1$ with the phase angle reversed in sign.
$[K_0/I_0 + K_1/I_1]$ is $j\frac{1}{2}\pi[H_0^{(1)}/J_0 - H_1^{(1)}/J_1]$ with the phase angle reversed in sign.

The curve of $k_3/k_{3(LF)}$ as a function of $\theta$ will be found to have the same general form as that relating to a core of rectangular cross-section (see Fig. 4).

## (7) FERRITE CORES

Although the method described above was used to study the case of a ferromagnetic conducting material in which the conductivity was high enough for the parameter $\gamma a$ to have a fixed phase-angle of $\frac{1}{4}\pi$ radians, it applies equally well to a ferrite core in which the effect of permittivity cannot be neglected. In such a case, eqn. (52) would still apply, but the phase angle of $\gamma a$ would vary with the frequency—thus making computation more difficult. Furthermore, $Y(\gamma a)$ would not be uniquely defined for a given value of $|\gamma a|$, and another parameter would have to be introduced to take into account the varying phase angle of $\gamma a$.

The change in the distortion factor of a coil with a ferrite core, due to phase-shift of the electromagnetic field within the core, is, however, not likely to have much practical significance, because other design considerations generally limit the maximum working frequency of a given core to a value for which the wavelength in the material is still large compared with its linear dimensions. Large variations in the value of the distortion factor would be expected on approaching frequencies at which 'dimensional resonance' occurs in a given core, i.e. where the wavelength is comparable with its dimensions.

## (8) THE TRANSMISSION-LINE ANALOGUE OF AN INDUCTOR

Not only can the relationship between the field inside a coil and the distribution of current and voltage along an equivalent transmission line be used to assist in obtaining an analytical solution to the problem of coil design, but it can be taken a step further and used to design a physical analogue for investigating cases which do not lend themselves to mathematical treatment. This is done by building up a ladder network of series inductors and shunt resistors, the number of sections being chosen to give a satisfactory approximation to the smooth transmission line. The measured sending-end impedance of the equivalent network is then proportional to the circuit impedance of the coil under consideration, and the measured currents and voltages in the various sections of the network are proportional to the magnetic and electric field components respectively at appropriate points in the core. Hysteresis distortion can be taken into account by arranging that the series inductors of the network themselves have ferromagnetic cores with the correct magnetic properties. By suitable choice of the network component values, the required range of values of $\gamma a$ can be attained at a very much lower value of $\omega$ than would be the case for the real core. This means that the high-frequency behaviour of the latter can be investigated by means of low-frequency measurements on the transmission-line analogue, so that, if desired, the inductors used in constructing the analogue can be wound on cores which are identical with the one under investigation and yet can be worked at frequencies for which $k_3 = k_{3(LF)}$. This experimental method is not restricted to small flux densities or to metallic core materials. It can be used, for example, to study the high-frequency properties of a ferrite core, the equivalent network in this case having its parallel resistance arms shunted by capacitors to represent the effect of the permittivity of the material.

The use of an equivalent ladder network to study hysteresis distortion in laminated cores was first suggested by Feldtkeller[4] and Kämmerer.[5] They, however, used ladder networks with relatively small numbers of sections to obtain approximate theoretical solutions by a step-by-step method, rather than as experimental analogues.

### (8.1) Core of Rectangular Cross-Section

Apart from a numerical ratio whose value depends on the geometry of the system, the circuit impedance of a rectangular

solenoid is equal to the sending-end impedance of a short-circuited transmission line whose propagation coefficient and characteristic impedance are

$$\gamma = \sqrt{(j\omega\mu_0\mu\sigma)} = \sqrt{\left[ j\omega\mu_0\mu p\left(\frac{\omega}{\omega_1}\right) \frac{\sigma}{p\left(\frac{\omega}{\omega_1}\right)} \right]} \quad . \quad (68)$$

and

$$Z_0\sqrt{\frac{j\omega\mu_0\mu}{\sigma}} = p\left(\frac{\omega}{\omega_1}\right)\sqrt{\frac{j\omega\mu_0\mu p\left(\frac{\omega}{\omega_1}\right)}{\dfrac{\sigma}{p}\left(\dfrac{\omega}{\omega_1}\right)}} \quad . \quad . \quad (69)$$

In general, if a uniform transmission line has a series impedance $Z$ and shunt admittance $Y$ per unit length,

then

$$\gamma = \sqrt{(ZY)} \quad . \quad . \quad . \quad . \quad (70)$$

and

$$Z_0 = \sqrt{\frac{Z}{Y}} \quad . \quad . \quad . \quad . \quad (71)$$

An equivalent short-circuited line whose impedance at a frequency $\omega_1$ represents that of the rectangular solenoid at a frequency $\omega$ will thus have a total series inductance $\mu_0\mu ap(\omega/\omega_1)$ and a total shunt conductance $\sigma a/[p(\omega/\omega_1)]$. The frequency conversion factor $\omega/\omega_1$ and the numerical constant $p$ can be chosen to give a convenient frequency range and convenient values for the analogue network. Fig. 5(a) shows the component values for $n$-section networks using either T or $\pi$ basic sections. An even closer approximation to the ideal smooth line can be obtained, for a given number of sections, by taking the mean of measurements made with T and $\pi$ arrangements respectively.

### (8.2) Core of Circular Cross-Section

It is shown in Section 12 that the equations determining the electromagnetic field in the core of a cylindrical solenoid are

$$\frac{d}{dx}\left(\frac{x}{a}E\right) = j\omega\mu_0\mu\left(\frac{x}{a}\right)H \quad . \quad . \quad . \quad (72)$$

$$\frac{dH}{dx} = \left(\frac{x}{a}E\right)\left(\frac{a}{x}\sigma\right) \quad . \quad . \quad . \quad (73)$$

Comparison with the equations for the voltage and current along a transmission line,

$$\frac{dV}{dx} = ZI$$

$$\frac{dI}{dx} = YV$$

shows that the equivalent line in this case will not be uniform but will be tapered, in the sense that both the series impedance and the reciprocal of the shunt admittance per unit length will change with distance at a uniform rate, both becoming zero at a distance $a$ from the sending end. The total series inductance of the equivalent ladder network will be $\frac{1}{2}\mu_0\mu ap(\omega/\omega_1)$ and the total shunt resistance will be $p(\omega/\omega_1)/(2\sigma a)$. Fig. 5(b) shows the alternative T and $\pi$ forms of the tapered network.

### (8.3) Effect of an Air-Gap

Fig. 6 represents a side view of the basic current tube [Fig. 3(a)], but instead of being filled with magnetic material, the latter must now be imagined to extend only over a length $l - g$ of the tube, the remaining length $g$ being filled with a non-magnetic insulant representing a relatively narrow 'air-gap' in
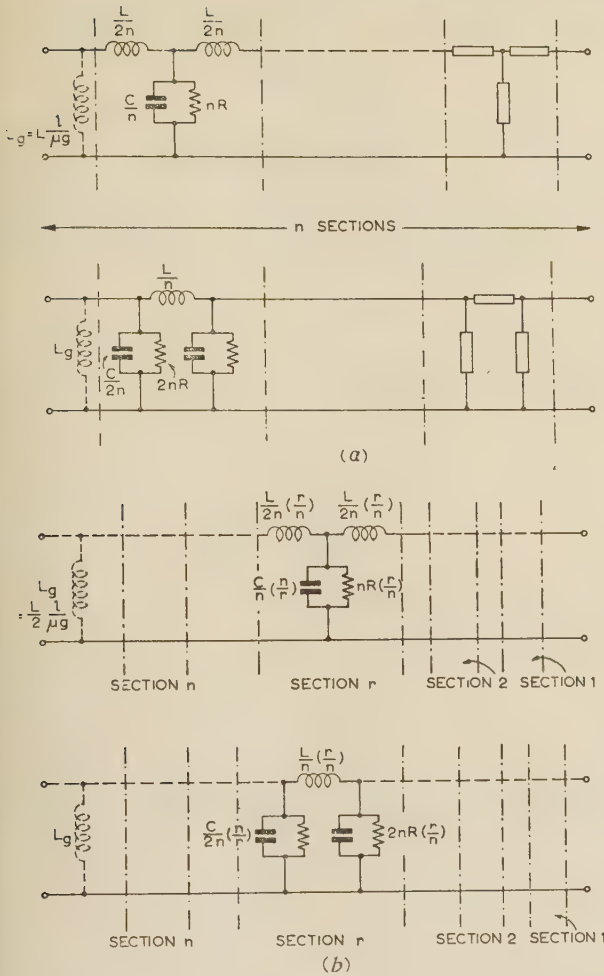
**Fig. 5.**—Equivalent T and π networks for solenoidal cores.

      (a) Rectangular cross-section.
      (b) Circular cross-section.

In both cases the element values are given by

$$L = \mu_0 \mu a p \left(\frac{\omega}{\omega_1}\right)$$

$$C = \frac{\epsilon_0 \epsilon a}{p}\left(\frac{\omega_1}{\omega}\right)$$

$$R = \frac{p}{a\sigma}\left(\frac{\omega}{\omega_1}\right)$$

the core. There will be two 'inward' field impedances $Z_m^-$ and $Z_g^-$, relating respectively to the field in the magnetic material and in the gap. The total circuit impedance is the parallel combination of two components

$$Z_{cm} = \frac{b}{l-g}Z_m^- \simeq \frac{b}{l}Z_m^-$$

and

$$Z_{cg} = \frac{b}{g}Z_g^-$$

where

$$Z_m^- = j\omega\mu_0\mu a\left(\frac{\tanh \gamma a}{\gamma a}\right)$$

$Z_g^-$ will be given by a similar expression in which $\mu = 1$ and $\gamma$ has the appropriate value for the dielectric material in the gap. This value will generally be so small that $Z_g^-$ will be given by

$$Z_g^- = j\omega\mu_0 a$$

An air-gap can thus be taken into account in the analogue network by shunting across its sending-end terminals an air-cored
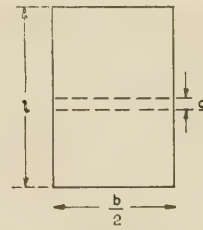


**Fig. 6.**—Effect of an air-gap.

Side view of a current tube of rectangular cross-section. [As Fig. 3(a), except that an air-gap of length g is included.]

inductor whose inductance is $l/\mu g$ times the total series inductance of the network (see Fig. 5). Looked at from this point of view, it can be seen that the air-gap will not only reduce the effective impedance of an inductor but will also reduce its hysteresis distortion factor. If the applied potential difference is kept constant, the current flowing in the equivalent network will be unchanged by the gap, and the harmonic-frequency e.m.f. appearing at the sending end will also be the same as if the gap were not present. Owing to the shunting effect of the inductor representing the gap, however, the actual harmonic-frequency voltage appearing at the sending-end terminals will be multiplied by a quantity

$$\frac{b/g}{\frac{b}{g} + \left(\frac{b}{l}\mu \frac{\tanh \gamma a}{\gamma a}\right)} = \frac{1}{1 + \frac{\mu g}{l}\left(\frac{\tanh \gamma a}{\gamma a}\right)} \quad . \quad . \quad (74)$$

The distortion factor will be multiplied by the same amount. Fig. 7 shows how the distortion-factor curve for a gapped rectangular solenoid depends on the gap factor, $\mu g/l$.
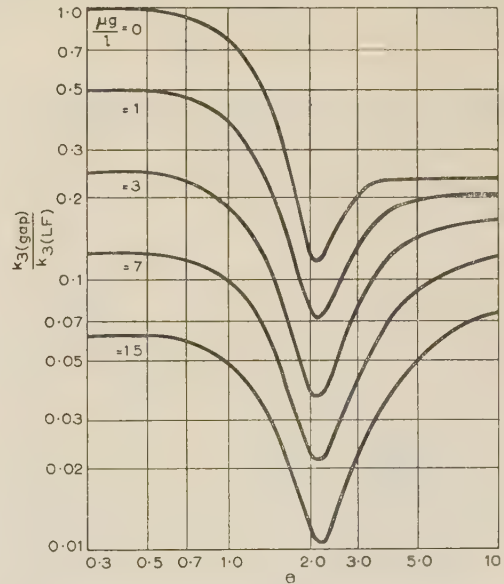


**Fig. 7.**—Effect of an air-gap on the third-order distortion factor.

Curves of $k_{3(gap)}/k_{3(LF)}$ are plotted as a function of $\theta$ for various values of the gap factor $\mu g/l$.

## (9) CONCLUSIONS

The third-order distortion factor of an inductor with a ferro-magnetic core will vary at high frequencies as a result of attenuation and phase shift of the electromagnetic field as it penetrates into the core from the surrounding dielectric material. It has been shown theoretically that, at low flux densities, the distortion

factor of a metallic core passes through a minimum and finally settles down to a constant value as the frequency is increased indefinitely. An analogue method has been described which enables the frequency response of the distortion factor to be determined in cases where theoretical analysis is difficult or impossible. The experimental method can be applied, for example, to ferrite cores, to metallic cores at high flux densities or to study the effect of hysteresis distortion on complex input waveforms. A simple modification of the analogue circuit enables the effect of an air-gap in the ferromagnetic core of an inductor to be taken into account.

## (10) ACKNOWLEDGMENTS

The permission of the Engineer-in-Chief of the Post Office to make use of the information contained in the paper is acknowledged. The author would also like to thank his former colleagues in the Post Office for their assistance and advice during the preparation of the paper.

## (11) REFERENCES

(1) CARTER, G. W.: 'The Electromagnetic Field in its Engineering Aspects' (Longmans, London, 1954).
(2) BOOKER, H. G.: 'The Elements of Wave Propagation using the Impedance Concept', *Proceedings I.E.E.*, 1947, **94**, Part III, p. 171.
(3) COOPER, W. H. B.: 'An Approach to the Operation of Inductors and Transformers in Terms of the Field Impedance', *ibid.*, Paper No. 836 M, June, 1949 (**96**, Part II, p. 509).
(4) FELDTKELLER, R.: 'Spulen und Übertrager' (Hirzel, Stuttgart, 1949).
(5) KÄMMERER, H.: 'Die Frequenzabhängigkeit des Spannungsklirrfaktors', *FTZ*, 1949, **2**, p. 201.

## (12) APPENDIX: Equations Defining the Electromagnetic Field Inside a Solenoid of Circular Cross-Section

Fig. 8 represents a portion of a single-turn solenoid of radius $a$ and length $l$.
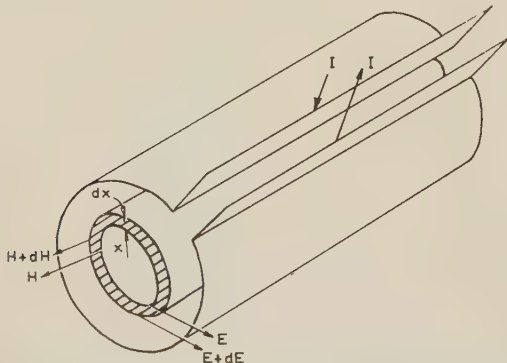


**Fig. 8.**—Field conditions in a solid core.

The diagram illustrates the field conditions inside a cylindrical core.

The magnetic field intensity in the shaded tube of radius $x_1$ and thickness $dx$ is $H$, and the flux density there is thus

$$B = \mu_0\mu H$$

The total magnetic flux enclosed by the elemental tube is

$$\int_0^{x_1} 2\pi x B dx$$

$$= \mu_0\mu \int_0^{x_1} 2\pi x H dx \quad . \quad . \quad . \quad . \quad (75)$$

The induced e.m.f. is equal to the rate of change of magnetic flux, so that, for a sinusoidally-varying $H$, the induced e.m.f. is

$$j\omega\mu_0\mu \int_0^{x_1} 2\pi x H dx \quad . \quad . \quad . \quad . \quad (76)$$

This must be equal to the electric field intensity $E$ multiplied by the path length, so that

$$2\pi x E = j\omega\mu_0\mu \int_0^{x_1} 2\pi x H dx$$

or $$xE = j\omega\mu_0\mu \int_0^{x_1} x H dx . \quad . \quad . \quad . \quad (77)$$

Differentiating both sides with respect to $x$,

$$E + x\frac{dE}{dx} = j\omega\mu_0\mu x H \quad . \quad . \quad . \quad (78)$$

or $$\frac{dE}{dx} = j\omega\mu_0\mu H - \frac{E}{x} . \quad . \quad . \quad . \quad (79)$$

The line integral of $H$ around the shaded tube in an axial direction is equal to the total circumferential current in the tube, so that

$$l(H + dH - H) = E(\sigma + j\omega\epsilon_0\epsilon)l dx$$

$$\frac{dH}{dx} = E(\sigma + j\omega\epsilon_0\epsilon) . \quad . \quad . \quad . \quad (80)$$

Differentiating, $$\frac{d^2H}{dx^2} = \frac{dE}{dx}(\sigma + j\omega\epsilon_0\epsilon)$$

Substituting for $dE/dx$ and rearranging,

$$\frac{d^2H}{dx^2} + \frac{1}{x}\frac{dH}{dx} - j\omega\mu_0\mu(\sigma + j\omega\epsilon_0\epsilon)H = 0$$

or $$\frac{d^2H}{dx^2} + \frac{1}{x}\frac{dH}{dx} - \gamma^2 H = 0$$

where $$\gamma = \sqrt{[j\omega\mu_0\mu(\sigma + j\omega\epsilon_0\epsilon)]}$$

Or, expressed with $\gamma x$ as the independent variable,

$$\frac{d^2H}{d(\gamma x)^2} + \frac{1}{\gamma x}\frac{dH}{d(\gamma x)} - H = 0 \quad . \quad . \quad . \quad (81)$$

Differentiating eqn. (75) gives

$$x\frac{d^2E}{dx^2} + 2\frac{E}{x} = j\omega\mu_0\mu\left(x\frac{dH}{dx} + H\right)$$

$$= j\omega\mu_0\mu(\sigma + j\omega\epsilon_0\epsilon)xE + \frac{1}{x}\left(x\frac{dE}{dx} + E\right)$$

which, when rearranged, becomes

$$\frac{d^2E}{d(\gamma x)^2} + \frac{1}{\gamma x}\frac{dE}{d(\gamma x)} - \left[1 + \frac{1}{(\gamma x)^2}\right]E = 0 . \quad . \quad (82)$$

Eqns. (81) and (82) are modified Bessel equations of order

nd 1, respectively, so that their solution can be written down terms of Bessel I and K functions.

$$H = AI_0(\gamma x) + BK_0(\gamma x) \quad . \quad . \quad . \quad . \quad (83)$$

$$E = CI_1(\gamma x) + DK_1(\gamma x) \quad . \quad . \quad . \quad (84)$$

The I and K functions represent wave systems with radially-inward and radially-outward directions of propagation, respectively. For the inward-directed field, therefore,

$$H = AI_0(\gamma x)$$

$$E = CI_1(\gamma x)$$

$$\frac{dH}{dx} = A\gamma I_1(\gamma x)$$

$$= E(\sigma + j\omega\epsilon_0\epsilon)$$

o that

$$\frac{C}{A} = \frac{\gamma}{\sigma + j\omega\epsilon_0\epsilon} = Z$$

where

$$Z = \sqrt{\frac{j\omega\mu_0\mu}{\sigma + j\omega\epsilon_0\epsilon}}$$

The 'inward' field impedance at a radius $x$ is thus

$$Z^- = \frac{E}{H} = \frac{C}{A}\frac{I_1(\gamma x)}{I_0(\gamma x)}$$

$$= Z\frac{I_1(\gamma x)}{I_0(\gamma x)} \quad . \quad . \quad . \quad . \quad . \quad (85)$$

Similarly, the 'outward' field impedance is found to be

$$Z^+ = Z\frac{K_1(\gamma x)}{K_0(\gamma x)} \quad . \quad . \quad . \quad . \quad (86)$$

By slight rearrangement, eqns. (78) and (80) can be presented in a form which is more convenient for deriving the equivalent transmission line representing a solenoid of circular cross-section:

$$\frac{d}{dx}\left(\frac{x}{a}E\right) = j\omega\mu_0\mu\left(\frac{x}{a}\right)H$$

$$\frac{dH}{dx} = \left(\frac{x}{a}E\right)\left[\left(\frac{a}{x}\right)(\sigma + j\omega\epsilon_0\epsilon)\right] \quad . \quad . \quad . \quad (87)$$

# A THEORETICAL INVESTIGATION OF THE FORM ASSUMED BY A SUBMARINE CABLE DURING LAYING OR RECOVERY

By V. G. WELSBY, Ph.D., B.Sc.(Eng.), Associate Member.

## SUMMARY

The increasing use of submerged repeaters and the introduction of new cable types have drawn attention to the hydrodynamic problems involved in the laying and recovery of deep-sea cables. The paper deals with the case of a uniform cable being laid or picked up at a constant speed. A method is described whereby the shape of the curve assumed by the cable under given conditions can be estimated and the maximum tension in the cable predicted.

## (1) INTRODUCTION

During the last 100 years, telegraph cables totalling many thousands of miles in length have been laid across the oceans, often at depths of two or three miles below the surface of the water. Although the danger of damage to such cables on the sea bed is normally very small, the need does nevertheless arise from time to time for part of a cable to be recovered from deep water to enable a faulty section to be repaired or replaced. Changing conditions may also make it desirable to be able to pick up a cable which has served its original purpose so that it may be relaid and used again in a new position. The problem of picking up a deep-sea cable without damaging or breaking it is one which has always presented a considerable difficulty. To explain this it will be assumed that the cable on the sea bed has been successfully hooked by the repair ship and cut, and that one of the severed ends has been brought to the surface. The ship now has to haul in the cable, stowing it in its own storage tanks as it does so, until the required length has been picked up. Two difficulties are immediately encountered, an obvious one being that the tension at the top end of the suspended cable is due not only to its own weight but also to the drag of the water as the cable moves through it. The other difficulty is due to the fact that, up to the present, it has been the practice to surround the electrical structure of the cable by a helical lapping of steel armouring wires which serve the double purpose of protecting the cable from accidental damage and of providing it with the required tensile strength. The application of tension to a helically-armoured cable of this type introduces a twisting moment tending to unlay the armour wires. This unlaying effect will either strain the cable torsionally so that it becomes impossible to coil it properly in the tanks in the ship or, alternatively, perhaps cause it to kink and break before the recovery operation has proceeded very far. The danger of damage to the cable from this cause can be minimized by using the rolling action of the cable against the bow sheave of the cable ship to apply an equal and opposite twisting effect.[1] This is why cables are normally picked up with a small starboard lead, i.e. with the cable leaving the water at a point which is displaced laterally with respect to the axis of the ship.

The paper is concerned with the former of these questions, i.e. with the way in which the tension in the cable depends on the pick-up conditions, and also with the rather simpler problem of cable-laying under steady-state conditions.

Lord Kelvin showed, as long ago as 1857,[2] that a cable laid at a uniform speed eventually assumed the form of a straight line extending from the ship to the sea bed, and empirical formulae have been in use for many years to calculate the laying tension in terms of the speed of the cable ship and the percentage of slack cable laid.[3] The exact conditions during the recovery of a cable from the bottom of the sea have not been so well understood, however, and the success of such operations has always depended on the practical experience and intuition of the officer in charge rather than on theory.

The introduction of deep-sea submerged repeaters and the proposed use in the future of armourless cables have drawn attention once again to the problem of cable recovery. Although the economical use of submerged repeaters has been made possible only by the development of electronic components possessing an extremely high degree of reliability, the fact remains that the presence of possibly a hundred or more such devices in a single cable link is bound to increase the chance of a fault occurring, which may make it necessary to cut the cable at a convenient point and then to pick it up until the fault is reached. An armourless cable, in which the tensile strength is produced by central steel strands rather than by external armour wires, is free from the danger of kinking due to torsional stresses. On the other hand, its lightness and lower breaking tension, compared with the conventional armoured cable, make it necessary to control the pick-up tension with great care. The theoretical analysis which follows appears to show that the optimum conditions for the recovery of armourless cable may differ considerably from those hitherto applied to armoured cables.

The problem will be introduced by dealing first of all with the case of a length of cable, fixed to the ship at one end and towed at a constant speed with its bottom just clear of the sea bed. It will then be shown that the resulting cable curve is not affected if instead of being towed, the cable is paid out uniformly. Following the same technique, the general case of a towed cable with force applied to the lower end will then be dealt with and the results applied to the steady-state recovery of a laid cable.

## (2) RESISTANCE TO MOTION OF CABLE THROUGH WATER

The resistance experienced by a body moving through a fluid is due partly to skin friction and partly to the inertia of the fluid swept aside by the moving body. For the range of velocities which are of interest in connection with the laying and recovery of submarine cables (0·5–10 knots, say), the resistance to transverse motion perpendicular to the axis of the cable is predominantly due to fluid inertia, with a small contribution from skin friction. The resistance to motion in an axial direction, on the other hand, is due to skin friction alone, since no change in fluid displacement is involved.

The force exerted, per unit length, on a cable when its motion through the fluid is wholly in a direction perpendicular to its axis can be expressed in the form[4]

$$F_p = \frac{C_D}{2} \rho v_p^2 d \quad . \quad . \quad . \quad . \quad . \quad (1)$$

where $\rho$ is the density of the fluid, $v_p$ is the velocity of motion, $d$ is the diameter of the cable, and $C_D$ is a factor whose value can be taken as $1 \cdot 2$ for the range of velocities quoted above, so that

$$F_p = 0 \cdot 6 \rho v_p^2 d \quad . \quad . \quad . \quad . \quad . \quad (2)$$

Inserting the appropriate value of $\rho$ for sea water and expressing $d$ in inches gives

$$F_p = 0 \cdot 6 \times \frac{64}{32 \cdot 2} \times \frac{1}{12} v_p^2 d$$

$$= 0 \cdot 097 v_p^2 d \text{ pounds per foot} \quad . \quad , \quad . \quad (3)$$

where $v_p$ is expressed in feet per second.

Consider next the force exerted, per unit length, on a cable whose motion is entirely in a direction parallel to its axis. The skin friction, in a case of this type, was established by Froude as being proportional both to the square of the relative velocity between the moving surface and the fluid, and also to the wetted area of the moving body. He found that, for surfaces ranging from smooth wax to coarse sand, the friction force varied between 0·25 and 0·50 pound per square foot of wetted area.[4] If the cable diameter is $d$, the area is $\pi d/12 \text{ ft}^2$ per foot length, and taking the higher value quoted as being the one most likely to apply to a cable with armour wires and a rough tarred-jute outer covering, the force is thus given by

$$F_q = \frac{0 \cdot 5 \pi d v_q^2}{12 \times 100}$$

$$= 0 \cdot 0013 v_q^2 d \text{ pounds per foot} \quad . \quad . \quad . \quad (4)$$

where $v_q$ is the axial velocity of the cable in feet per second.

It has also been confirmed experimentally[6] that the transverse and axial resistance forces when a cable moves through a fluid are due to effects which are practically independent of each other. In other words, when a cable moves in any direction through water the total force on it may be taken as the resultant of the component forces obtained from eqns. (3) and (4) by substituting in them the component velocities of the cable, resolved respectively in directions perpendicular and parallel to its axis.

### (2.1) Definition of Settling Velocity

There will be some value of $v_p$ such that the transverse force due to its motion through the water is just equal to the immersed weight of the cable. This is evidently the speed at which a straight horizontal section of the cable would fall freely through the water and is defined as the transverse settling velocity, $\bar{v}_p$.

Thus

$$w = 0 \cdot 097 \bar{v}_p^2 d$$

$$\bar{v}_p = 3 \cdot 2 \sqrt{\frac{w}{d}} \text{ feet per second} \quad . \quad . \quad . \quad (5)$$

where $w$ is the weight of the cable (in water) in pounds per foot. This enables the transverse force on the cable to be expressed in the form

$$F_p = w \frac{v_p^2}{\bar{v}_p^2} \quad . \quad . \quad . \quad . \quad . \quad (6)$$

where the same units are used for $F_p$ and $w$. The two velocities $v_p$ and $\bar{v}_p$ are, of course, also expressed in the same units.

In the same way, it is possible to define the axial settling velocity, $\bar{v}_q$, as that at which a straight section of the cable would sink freely with its axis vertical (neglecting end-effects). Taking the values assumed above for an armoured cable, we get

$$w = 0 \cdot 0013 v_q^2 d$$

and

$$F_q = w \frac{v_q^2}{\bar{v}_q^2} \quad . \quad . \quad . \quad . \quad . \quad (7)$$

Note that there is a fixed relationship between $\bar{v}_p$ and $\bar{v}_q$ which is independent of the cable diameter and weight but depends to some extent on the surface texture.

An armourless cable having a smooth surface would be likely to have an axial friction coefficient tending to the lower limit quoted by Froude for smooth wax surfaces. This would have the effect of increasing the value of $\bar{v}_q$ by a factor of $\sqrt{2}$ compared with that for an armoured cable with a relatively rough exterior surface. Thus, approximately,

$$\left. \begin{array}{l} \bar{v}_q = 8 \cdot 7 \bar{v}_p \text{ for armoured cables} \\ \bar{v}_q = 12 \cdot 3 \bar{v}_p \text{ for armourless cables} \end{array} \right\} \quad . \quad . \quad (8)$$

### (3) FORM OF TOWED CABLE WITH BOTTOM END FREE

Consider first of all the relatively simple case of a fixed length of cable which is attached to a ship at the top end and simply towed through the water with its bottom end free. When towed at a constant horizontal velocity $v_s$, the cable curve will be a straight line inclined at an angle $\phi$ to the horizontal. A mathematical proof of this will be given later, but it can be shown to be true by the following reasoning. First, suppose that a uniform straight rod is hinged at the top end and towed through the water in place of the cable. Provided that the lower end is free, the rod will take up a position of equilibrium such that the three forces acting on it, namely its weight, the water resistance and the reaction at the hinge, have directions which all intersect at a common point. Since the water resistance can be represented by a single force acting through the centre of gravity of the rod, it follows that the reaction at the hinge must also be directed through the centre of gravity and therefore along the rod. The introduction of another hinge at any point in the rod can have no effect on its equilibrium. Following this argument to its logical conclusion, it is seen that a uniform flexible cable will also assume the form of a straight line when towed at a uniform speed with bottom end free. It is still theoretically possible for the cable to remain in a straight line, even when the bottom end is not free, but this can occur only in the special case where the force happens to be directed along the straight line which would be assumed by the cable if the force were absent. In general, the application of any tension to the bottom end will cause the shape of the cable to deviate from a straight line. This general case will be dealt with later.

If $T$ is the tension at the top end of a cable of length $s$, whose bottom end is free, and $v_s$ is the speed of the ship which tows it through the water, the following equations can be obtained by resolving forces respectively along the cable and perpendicular to it:

$$T - F_q s = w s \sin \phi \quad . \quad . \quad . \quad . \quad (9)$$

$$F_p s = w s \cos \phi \quad . \quad . \quad . \quad . \quad (10)$$

$F_p$ and $F_q$ are, respectively, the transverse and axial forces exerted on the cable per unit length as a result of its motion through the water.

$F_p$ can be expressed in terms of the actual transverse component velocity of the cable, $v_p$, and its transverse settling velocity, $\bar{v}_p$:

$$F_p = w \frac{v_p^2}{\bar{v}_p^2}$$

The transverse component velocity of the cable is given by

$$v_p = v_s \sin \phi$$

so that

$$F_p = w \frac{v_s^2}{\bar{v}_p^2} \sin^2 \phi$$

Substituting this value of $F_p$ in eqn. (10),

$$\cos \phi = \frac{v_s^2}{\bar{v}_p^2} \sin^2 \phi$$

or

$$\sin \phi = k \sqrt{\cos \phi} \quad . \quad . \quad . \quad . \quad (11)$$

where

$$k = \frac{\bar{v}_p}{v_s} \quad . \quad . \quad . \quad . \quad . \quad (12)$$

Eqns. (11) and (12) can be used to determine the angle of inclination of the cable, $\phi$, in terms of the speed of the ship and the transverse settling velocity of the cable.

The solution to eqn. (11) is

$$\sin \phi = \left[ k^2 \left( 1 + \frac{k^4}{4} \right)^{1/2} - \frac{k^4}{2} \right]^{1/2} \quad . \quad . \quad . \quad (13)$$

which gives $\phi$ exactly for all permissible values of $k$. If $k$ does not exceed about 45°, however, an approximate solution can be obtained by applying the binomial theorem to the right-hand side of eqn. (13):

$$\sin \phi \simeq k \left( 1 - \frac{k^2}{4} \right) \quad . \quad . \quad . \quad . \quad (14)$$

The tension at the top end of the towed cable is given by eqn. (9) as

$$T = w s \sin \phi + F_q s$$

$$= w s \sin \phi + w s \frac{v_q^2}{\bar{v}_q^2}$$

But

$$v_q = v_s \cos \phi$$

so that

$$T = w s \sin \phi + w s \frac{v_s^2}{\bar{v}_q^2} \cos^2 \phi$$

$$= w s \sin \phi \left( 1 + \frac{v_s^2}{\bar{v}_q^2} \frac{\cos^2 \phi}{\sin \phi} \right)$$

$$= w h \left( 1 + \frac{v_s^2}{\bar{v}_q^2} \frac{\cos^2 \phi}{\sin \phi} \right) \quad . \quad . \quad . \quad . \quad (15)$$

$$= w h \left( 1 + \frac{\bar{v}_p^2}{\bar{v}_q^2} \cot^3 \phi \right) \quad . \quad . \quad . \quad . \quad (16)$$

where $h$ is the vertical distance from the surface of the water to the bottom end of the cable.

## (4) APPLICATION TO STEADY-STATE PAY-OUT OF CABLE FROM SHIP

The results obtained above can be applied quite simply to the case of a cable which is paid out continuously from a ship travelling at a uniform speed, provided that the tension at the bottom end of the suspended cable remains negligible. Eqn. (11) shows that the angle of inclination of the cable curve depends only on the resistance of transverse motion of the cable as a whole. On the other hand, the axial water-resistance force depends on the actual axial velocity of the cable relative to the water. The only effect of starting to pay out the cable instead of merely towing it will be to superimpose an additional axial velocity component, which, as stated above, will have no effect on the angle of inclination.

If the paying-out speed of the cable relative to the ship is $u$, the axial velocity of the cable relative to the water changes from $v_s \cos \phi$ to $(v_s \cos \phi - u)$. Since $u$ will normally be greater than $v_s \cos \phi$, the direction of the axial motion will be reversed, so that it is more correct to write $-(u - v_s \cos \phi)$ instead of $(v_s \cos \phi - u)$. The change in the direction of $F_q$ must be taken into account by reversing the appropriate sign of eqn. (15), so that the tension at the ship is now given by

$$T = w h \left[ 1 - \frac{(u - v_s \cos \phi)^2}{\bar{v}_q^2 \sin \phi} \right]$$

$$= w h \left[ 1 - \frac{v_s^2}{\bar{v}_q^2} \frac{(1 + e - \cos \phi)^2}{\sin \phi} \right]$$

where $e$ is the slack factor.

$$e = \frac{\text{Percentage slack}}{100}.$$

Substituting

$$k = \frac{\bar{v}_p}{v_s}$$

this becomes

$$T = w h \left[ 1 - \frac{\bar{v}_p^2}{\bar{v}_q^2} \frac{(1 + e - \cos \phi)^2}{k^2 \sin \phi} \right] \quad . \quad . \quad (17)$$

where $\bar{v}_p^2 / \bar{v}_q^2$ is a factor whose value is independent of the diameter or weight of the cable but depends to some extent on the roughness of its surface. The angle $\phi$ is given by

$$\sin \phi = \left[ k^2 \left( 1 + \frac{k^4}{4} \right)^{1/2} - \frac{k^4}{2} \right]^{1/2} \quad . \quad . \quad (18)$$

Eqns. (17) and (18) enable the relationship between cable tension and percentage slack to be worked out for various laying speeds, assuming that positive slack is being laid so that the tension in the cable at the point of contact with the sea bed is either zero or negligibly small.

### (4.1) Numerical Example

Suppose that the ship is travelling at six knots and paying out, with 5% slack, an armoured cable whose diameter is 1·21 in and weight 35·5 cwt/1 000 fathoms.

Then

$$v_s = \frac{6 \times 6080}{3600} = 10 \cdot 2 \, \text{ft/s}$$

$$e = 0 \cdot 05$$

$$w = 35 \cdot 5 \, \text{cwt per 1 000 fathoms}$$

$$= \frac{35 \cdot 5 \times 112}{6000} = 0 \cdot 66 \, \text{lb/ft}$$

$$d = 1 \cdot 21 \, \text{in}$$

$$\bar{v}_p = 3 \cdot 20 \sqrt{\frac{w}{d}}$$

$$= 2 \cdot 36 \, \text{ft/s}$$

$$k = \frac{2 \cdot 36}{10 \cdot 2} = 0 \cdot 231$$

$$\sin \phi = \left[ k^2 \left( 1 + \frac{k^4}{4} \right)^{1/2} - \frac{k^4}{2} \right]^{1/2}$$

whence

$$\phi = 13 \cdot 3°$$

and

$$T = w h [1 - 0 \cdot 088]$$

It will be noted that the cable tension at the ship is slightly less than the weight of a length of cable equal to the depth of water. This is the normal laying condition for any type of cable and any speed; the tension is roughly equal to the 'weight of the depth of water', even though the suspended length of cable may be several times greater than the depth.

### (4.2) Approximate Formulae

The following formulae have been in use for a number of years:[3]

$$\sin \phi = \frac{1}{v_s}\sqrt{\frac{w}{P}}\left[\left(1 - \frac{1}{4v_s^2}\frac{w}{P}\right)\right] \qquad . \quad . \quad (19)$$

$$T = wh\left[1 - \frac{v_sQ}{w}\left(1 + \frac{e - \cos\phi}{\sin\phi}\right)\right] \qquad . \quad . \quad (20)$$

where $v_s$ = Speed of the ship in knots.

$w$ = Weight of the cable in hundredweight per 1 000 fathoms.

$P = 20 \cdot 7d$

$Q = 1 \cdot 55d$

The remaining symbols have the same meaning as before.

Comparison of eqns. (19) and (14) shows that $1/v_s\sqrt{(w/P)}$ is identical with the parameter $k$, i.e. $\sqrt{(w/P)}$ is the transverse settling velocity, expressed in knots. Substituting the given value of $P$,

$$\sqrt{\frac{w}{P}} = \sqrt{\frac{w}{20 \cdot 7d}} \text{ knots } (w \text{ in hundredweight per 1 000 fathoms})$$

$$= \sqrt{\frac{w}{20 \cdot 7d}} \times \sqrt{\frac{6\,080}{112}} \text{ knots } (w \text{ in pounds per foot})$$

$$= 2 \cdot 68\sqrt{\frac{w}{d}} \text{ feet per sec } (w \text{ in pounds per foot})$$

Turning to eqn. (20), it is clear that this is of the same form as eqn. (17), except that it appears to have been derived on the assumption that the axial friction force on the cable is directly proportional to the axial velocity instead of to its square.

The reason why this assumption was made, in contradiction to accepted experimental evidence,[4] is not clear. It is a curious fact, however, that, although fundamentally unsound, eqn. (20) does give results which are very nearly correct over the range of values of $v_s$ and $e$ which are likely to be of interest in cable-laying work, the agreement being even closer if the angle $\phi$ used in eqn. (20) is calculated from eqn. (19) rather than from eqn. (18). This suggests that eqns. (19) and (20) should be regarded merely as empirical formulae which are sufficiently accurate for most practical purposes but which should be applied with caution. It is better to use the more correct formulae given by eqns. (17) and (18), because these are not restricted to any particular range of speeds and slack factors.

### (4.3) Numerical Example

To illustrate the degree of agreement between the results obtained from the two sets of equations, suppose that the empirical formulae had been used to work out the example already considered above.

$v_s = 6 \cdot 0$ knots

$e = 0 \cdot 05$

$w = 35 \cdot 5$ cwt per 1 000 fathoms

$$\frac{1}{v_s}\sqrt{\frac{w}{P}} = \frac{1}{6}\sqrt{\frac{35 \cdot 5}{20 \cdot 7}} = 0 \cdot 218$$

$$\sin \phi = 0 \cdot 218(1 - \tfrac{1}{4} \times 0 \cdot 218^2) = 0 \cdot 215$$

whence $\phi = 12 \cdot 4°$

and $T = wh(1 - 0 \cdot 108)$

Comparison of these results with those obtained from eqns. (17) and (18) shows a discrepancy of about 1° in the angle of inclination and of 2% in the cable tension, both these amounts being within the limits of accuracy to which the respective values are likely to have been measured in the past.

### (5) FORM ASSUMED BY TOWED CABLE WITH FORCE APPLIED AT BOTTOM END

Although the formulae derived above apply strictly to the case of a cable which is being laid under steady-state conditions, they cannot be used to deal with cable recovery where the tension at the bottom end of the suspended cable is not zero. As a first step towards the solution of the latter problem, the general case will be considered of a cable which is towed at a uniform horizontal speed but which has some device attached to its bottom end which exerts a constant force in a fixed direction. The cable curve will then no longer be a straight line, and eqns. (9) and (10) must be replaced by differential equations which are valid for small incremental lengths of cable. Resolving forces respectively parallel and perpendicular to the cable, we obtain the differential equations defining the cable curve:

$$dT - F_q ds = w \sin \phi ds \qquad . \quad . \quad . \quad . \quad (21)$$

or $$\frac{dT}{ds} = F_q + w \sin \phi \qquad . \quad . \quad . \quad . \quad (22)$$

and $$T\frac{d\phi}{ds} = w \cos \phi - F_p \qquad . \quad . \quad . \quad . \quad (23)$$

Substituting for $F_p$ and $F_q$ gives

$$\frac{dT}{ds} = w\left(\frac{v_s^2}{\bar{v}_q^2}\cos^2\phi + \sin\phi\right)$$

$$= w\left(\frac{\bar{v}_p^2}{\bar{v}_q^2}\frac{\cos^2\phi}{k^2} + \sin\phi\right) \qquad . \quad . \quad (24)$$

and $$T\frac{d\phi}{ds} = w\left(\cos\phi - \frac{\sin^2\phi}{k^2}\right) \qquad . \quad . \quad . \quad (25)$$

$d\phi/ds = 1/R$, where $R$ is the radius of curvature.

A problem very similar to this has been studied in connection with the towing of an object suspended from an aircraft by a flexible rope.[5] A solution was obtained in this case by neglecting the effect of axial friction altogether and taking into account only the transverse aerodynamic resistance to the motion of the rope. It will therefore be of interest to consider to what extent the same assumption would be justified for a submarine cable moving through water. The two cases are, in fact, more closely comparable than might appear at first sight, because although the water is so much denser than air the lower speeds concerned bring the problem into the same general region of fluid-flow conditions. From eqn. (24) it can be seen that it would be justifiable to neglect the effect of axial friction only if

$$\sin \phi \gg \frac{v_s^2}{\bar{v}_q^2}\cos^2\phi$$

For small values of $\sin \phi$, $\cos \phi \simeq 1$, so that the condition reduces to

$$\sin \phi > \frac{v_s^2}{v_q^2} \quad \cdot \quad \cdot \quad \cdot \quad \cdot \quad \cdot \quad (26)$$

Substituting typical values of $v_s$ and $v_q$, it is found that the required condition is likely to be met over by far the larger part of the cable curve. The errors involved in neglecting the axial water friction are very unlikely to have any practical significance, and, in any case, are probably less than the errors introduced by unknown factors, e.g. differing ocean drift speeds at various depths.

$F_q$ will therefore be neglected, so that eqns. (24) and (25) become

$$\frac{dT}{ds} = w \sin \phi \quad \cdot \quad \cdot \quad \cdot \quad \cdot \quad \cdot \quad \cdot \quad (27)$$

$$T \frac{d\phi}{ds} = w \left( \cos \phi - \frac{1}{k^2} \sin^2 \phi \right) \quad \cdot \quad \cdot \quad \cdot \quad (28)$$

The object now is to derive a general series of possible curves which will satisfy these differential equations. The particular curve can then be selected which satisfies also the given boundary conditions.

Eqns. (27) can be written as

$$dT = w \sin \phi ds$$

$$= w dy$$

Integrating gives $\qquad T = wy + T_0 \quad \cdot \quad \cdot \quad \cdot \quad \cdot \quad (29)$

where $T_0$ is the value of $T$ at $y = 0$.

[It is interesting to note that eqn (29) gives the simple rule that the difference in tension between any two points in the cable is always equal to the weight of a piece of cable whose length is equal to the vertical distance between the two points.]

A particular solution to eqn. (28) is $d\phi/ds = 0$ and, in this case,

$$\cos \phi - \frac{1}{k^2} \sin^2 \phi = 0$$

The condition $d\phi/ds = 0$ means that the radius of curvature is infinite at all points, i.e. the curve is a straight line. The resulting relationship between $k$ and $\phi$ corresponds to eqn. (11).

The first step towards finding a general solution to eqn. (28) is to substitute in it the value of $T$ obtained from eqn. (29). Then

$$(T_0 + wy) \frac{d\phi}{ds} = w \left( \cos \phi - \frac{1}{k^2} \sin^2 \phi \right)$$

or $\qquad (T_0 + wy) \frac{\sin \phi d\phi}{dy} = w \left( \cos \phi - \frac{1}{k^2} \sin^2 \phi \right)$

Rearrangement gives

$$\left( \frac{\frac{w}{T_0} dy}{1 + \frac{wy}{T_0}} \right) = \frac{k^2 \sin \phi d\phi}{k^2 \cos \phi - \sin^2 \phi} \quad \cdot \quad \cdot \quad \cdot \quad (30)$$

After replacing $k$ by a subsidiary parameter $\alpha$, where $k^2 = 2 \tan \alpha$, eqn. (30) can be integrated to give

$$\log_\varepsilon \left[ 1 + 2 \tan \alpha \left( \frac{wy}{k^2 T_0} \right) \right]$$

$$= \sin \alpha \log_\varepsilon \left[ \pm \frac{\cos \alpha + (1 - \sin \alpha) \cos \phi}{\cos \alpha - (1 + \sin \alpha) \cos \phi} \right]$$

or

$$\log_\varepsilon \left[ 1 + 2 \tan \alpha \left( \frac{y}{\lambda} \right) \right]$$

$$= \sin \alpha \log_\varepsilon \left[ \pm \frac{\cos \alpha + (1 - \sin \alpha) \cos \phi}{\cos \alpha - (1 + \sin \alpha) \cos \phi} \right] \quad (31)$$

where

$$\lambda = \frac{k^2 T_0}{w}$$

The quantity $\lambda$ is defined as the characteristic length of the particular cable under consideration. It is the length of a piece of the cable which, if towed laterally through the water at a speed $v_s$, will experience a transverse force equal to $T_0$. It will be explained later how the characteristic length is used to fix the scale of the portion of a general curve which will satisfy the given boundary conditions.

The ambiguity of sign in eqn. (31) can be removed by specifying that $y/\lambda$ is positive when $\cos \phi$ is positive.

Care must be taken to ensure that both sides of the equation are integrated between the same limits. This has already been simplified by arranging that $y/\lambda = 0$ when $\cos \phi = 0$, so that no constant of integration is required in eqn. (31). It applies for both positive and negative values of $\cos \phi$; the curve is continuous in the vicinity of $\phi = 90°$, the sign of $y/\lambda$ becoming negative for values of $\phi$ between $90°$ and $180°$. A difficulty arises, however, because there is a critical value of $\phi$, between 0 and $90°$, for which $y/\lambda$ becomes infinite. Denoting this by $\phi_0$, we have

$$\cos \alpha - (1 + \sin \alpha) \cos \phi_0 = 0$$

Comparison with eqns. (13) and (11) shows that the angle $\phi_0$ is, in fact, the inclination of the straight line which the cable takes up when the tension at the bottom end is zero.

The general curve is discontinuous when $\phi = \phi_0$, so that when $\phi$ lies between 0 and $\phi_0$ it is no longer permissible to take $\phi = 90°$ as one of the limits of integration, and a constant of integration must be introduced.

Let $y_1$ be the value of $y$ when $\cos \phi = 1$; then

$$\log_\varepsilon \left[ 1 + 2 \tan \alpha \left( \frac{y_1}{\lambda} \right) \right] = \sin \alpha \log_\varepsilon \left[ \frac{(1 - \sin \alpha) + \cos \alpha}{(1 + \sin \alpha) - \cos \alpha} \right]$$

$$\cdot \quad \cdot \quad \cdot \quad \cdot \quad (32)$$

Integrating between limits $y_1/\lambda$ and $y/\lambda$ gives

$$\log_\varepsilon \left[ 1 + 2 \tan \alpha \left( \frac{y}{\lambda} \right) \right]$$

$$= \sin \alpha \log_\varepsilon \left[ \frac{\cos \phi (1 - \sin \alpha) + \cos \alpha}{\cos \phi (1 + \sin \alpha) - \cos \alpha} \right]$$

$$- \sin \alpha \log_\varepsilon \left[ \frac{(1 - \sin \alpha) + \cos \alpha}{(1 + \sin \alpha) - \cos \alpha} \right] \quad (33)$$

This equation must be used, instead of eqn. (31), when $\phi$ lies between 0 and $\phi_0$. Eqns. (31) and (33) enable the vertical ordinates of the general curve to be computed in terms of the angle $\phi$, i.e. in terms of $dy/dx$.

A further integration is necessary before the cable curve itself can be plotted:

$$\frac{dy}{dx} = \tan \phi$$

so that $\qquad \dfrac{x}{\lambda} = \displaystyle\int \cot \phi d \left( \frac{y}{\lambda} \right)$

Unfortunately, this integration cannot be performed analytically, so that it is necessary to carry it out graphically by plotting the curve of $y/\lambda$ against $\cot\phi$ and then computing the integral by measuring the area under the curve.

Fig. 1 shows diagrammatically the form of the complete curve of $y/\lambda$ against $x/\lambda$ for a given value of the parameter $\alpha$. Both parts of the curve become asymptotic to a straight line with a slope of $\phi_0$ as $x/\lambda$ or $y/\lambda$ increases indefinitely.

The solution of the original differential equations can be represented by a family of curves drawn for various values of $\alpha$.

For any steady-state condition involving uniform horizontal movement of a suspended cable relative to the water, the shape assumed by the cable must be an arc of the general curve corresponding to the appropriate value of $\alpha$ (and therefore of $k$). For example, a towed cable with a weight attached to the lower end might be represented by the arc AB in Fig. 1 while the arc
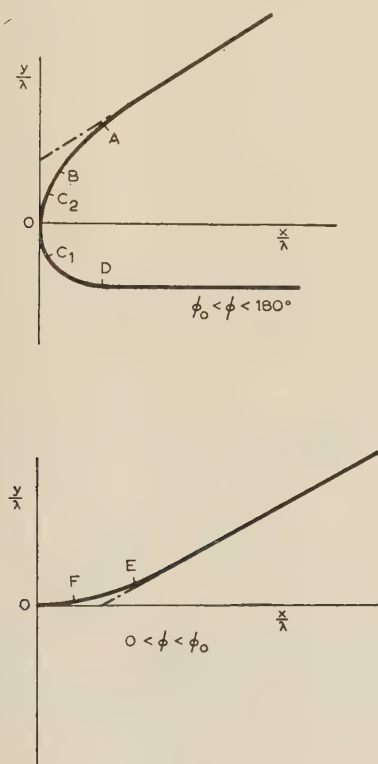
sea bed is brought to rest. In the case of the equivalent towed cable, its axial velocity relative to the water is zero at the top of the curve and a maximum at the bottom, whilst, during recovery of a cable, its axial velocity is zero at the point where it leaves the bottom of the sea and rises to a maximum at the top end. In the latter case, the reasoning which led to the neglecting of the axial friction when deriving eqns. (24) and (25) will apply even more clearly, so that the shape of the suspended cable must be represented by the general curves obtained above. For example, it may follow the arc $DC_1$ (Fig. 1) if the ship is 'holding back', the arc DO if the cable leaves the water vertically, or even an arc such as $DC_2$ if the ship is over-running the cable. The direction of motion of the ship would be from left to right in Fig. 1.

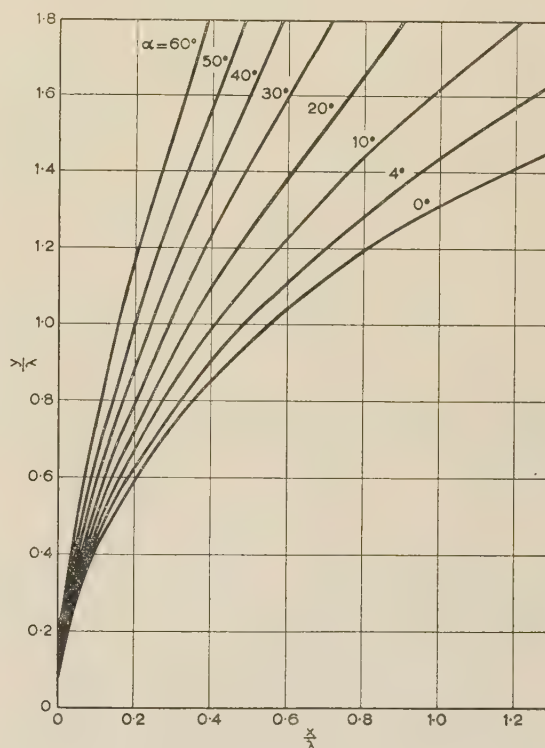Some general cable curves are shown, plotted to scale, in Figs. 2 and 3, for various values of the parameter $\alpha$. The curves



Fig. 1.—Form of the general cable curves.



Fig. 2.—Shape of cable curves.

$$\phi_0 < \phi < 90°$$
$$\tan\alpha = \tfrac{1}{2}k^2$$

EF might give the shape of a towed cable carrying at its lower end some object producing a horizontal drag force in addition to its own weight. In the special case where the tension applied to the lower end of the cable happens to have a direction making an angle $\phi_0$ with the horizontal, the cable curve becomes a straight line.

## (6) APPLICATION TO STEADY-STATE CABLE RECOVERY

An imaginary observer recording the shape of the suspended cable would not be able to distinguish whether it was being laid uniformly or merely being towed with its bottom end just clear of the sea bed. Applying the same argument to the recovery operation, the cable will behave as if the bottom of the suspended part were being pulled along the sea bed in the direction in which the ship is travelling and at a speed equal to that of the ship. The true conditions can be obtained by superimposing a purely axial velocity of the whole cable such that the portion on the

are continuous through $y/\lambda = 0$, but, for convenience, they have been drawn separately for positive and negative values of $y/\lambda$. To determine the shape of the suspended cable for any given steady-state pick-up conditions the procedure is as follows: First of all, the value of $\alpha$ must be calculated for the given pick-up speed, $v_s$, and the transverse settling velocity of the cable concerned:

$$\tan\alpha = \frac{k^2}{2} = \frac{\bar{v}_p^2}{2v_s^2}$$

The appropriate curve can then be selected from Figs. 2 and 3, interpolating if necessary. The top end of the suspended cable will be represented by the point on the curve where its slope corresponds to the given slope of the cable at the point where it leaves the water. The bottom end is given by the point where the slope of the curve becomes zero. Finally, the scale of the resulting arc of the curve must be adjusted so that its vertical height represents the depth of water. Suppose, for example, the
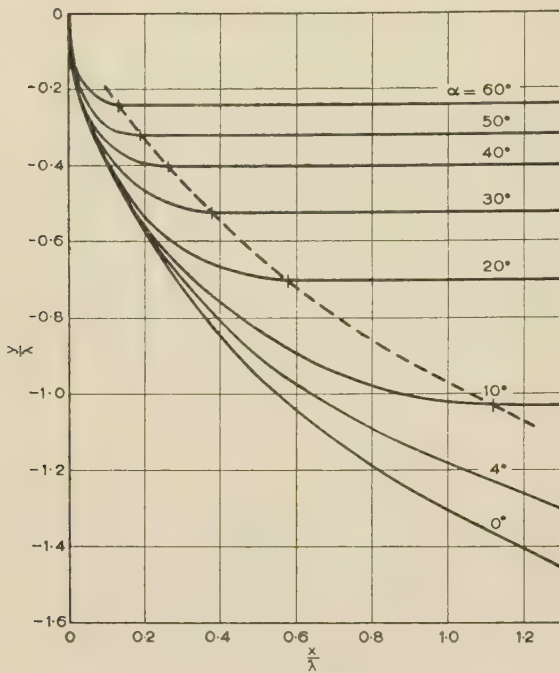
Fig. 3.—Shape of cable curves.

$90° < \phi < 180°$

The dotted line indicates the locus of the point at which the curve becomes horizontal.

value of $\phi$ at the surface of the water is denoted by $\phi_1$ and the corresponding value of $y/\lambda$ by $y_1/\lambda$. Let $y_2/\lambda$ be the value of $y/\lambda$ representing the bottom end of the suspended part of the cable. Then

$$\left(\frac{h}{\lambda}\right) = \left(\frac{y_1}{\lambda}\right) - \left(\frac{y_2}{\lambda}\right) \qquad . \quad . \quad . \quad . \quad (34)$$

where $h$ is the depth of water.

The typical cable curves shown in Figs. 4 and 5 were obtained by the above method.
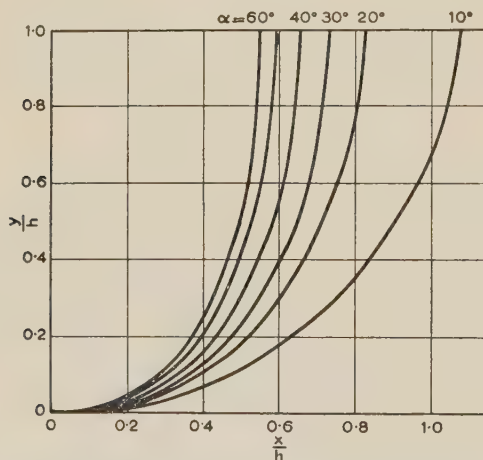


Fig. 4.—Shape of cable curve during pick-up.

$\tan \alpha = \frac{1}{2}k^2$

Plotted for $\phi = 90°$, showing the effect of changing speed at constant angle of lead.

### (6.1) Calculation of Cable Tension

The tension of the cable can be calculated directly without making use of the general curve. By combining eqns. (29) and
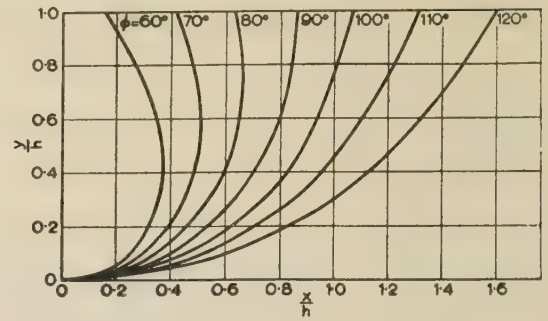


Fig. 5.—Shape of cable curve during pick-up.

$\tan \alpha = \frac{1}{2}k^2$

Plotted for $\alpha = 20°$ ($k = 0·85$), showing the effect of changing angle of lead a constant speed.

(32), the tension at any point along the cable can be expressed in the form

$$T = \frac{w\lambda}{k^2} + wy$$

In particular, the tension $T_1$ at the surface is

$$T_1 = w\left(\frac{\lambda}{k^2} + y_1\right)$$

$$= wh\frac{1}{\left(\frac{h}{\lambda}\right)}\left(\frac{1}{k^2} + \frac{y_1}{\lambda}\right)$$

Substituting for $h/\lambda$ from eqn. (34), this becomes

$$T_1 = wh\left[\frac{\frac{1}{k^2} + \left(\frac{y_1}{\lambda}\right)}{\left(\frac{y_1}{\lambda}\right) - \left(\frac{y_2}{\lambda}\right)}\right] \qquad . \quad . \quad . \quad (35$$

The quantity in the bracket is defined as the 'tension factor' It is the factor by which the tension at the surface exceeds the weight of a straight piece of cable having a length equal to the depth of water. In the special case where the cable leaves the water vertically, $y_1/\lambda = 0$ and the tension factor is given by

$$-\frac{1}{k^2\left(\frac{y_2}{\lambda}\right)}$$

[Note that $y_2/\lambda$ is always negative, so that this expression i positive.]

The tension $T_2$ at the point where the cable leaves the sea be is given by eqn. (29) as

$$T_2 = T_1 - wh$$

$$= wh\left[(\text{tension factor}) - 1\right]$$

The tension factor, $T_1/(wh)$, has been computed for various value of $\phi_1$ and $\alpha$, and the results are shown in Figs. 6 and 7. Bot sets of curves contain the same information presented in differer ways.

The use of the curves may be illustrated by a practical example Suppose a ship is picking up, at a speed of $1·64$ knots, a cab whose diameter is $1·21$ in and weight $35·5$ cwt/$1 000$ fathoms.
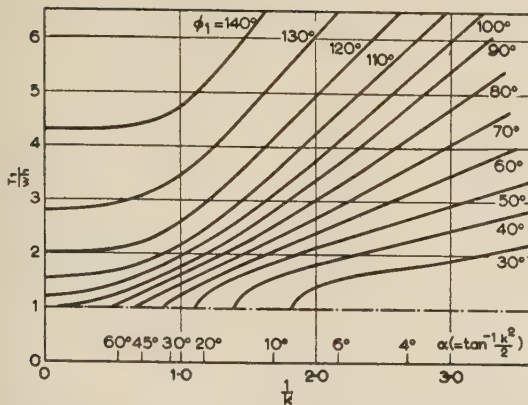
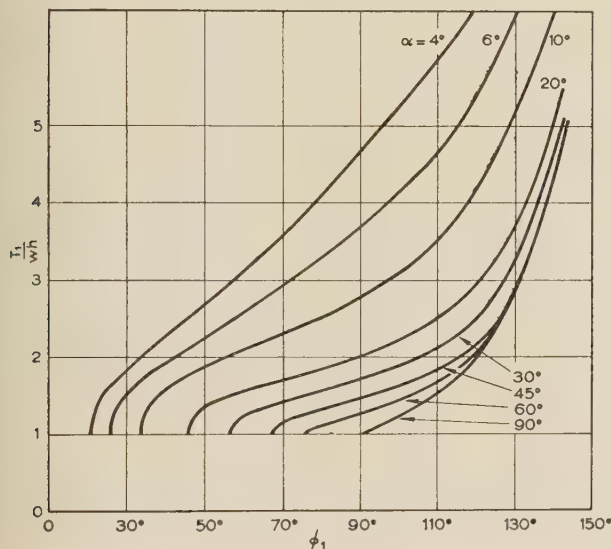Fig. 6.—Tension factor as a function of speed for various angles of lead.



Fig. 7.—Tension factor as a function of angle of lead for various ship speeds.

The transverse settling velocity of the cable is given by eqn. (5) as

$$v_p = 3 \cdot 2 \sqrt{\frac{w}{d}}$$

$$= 3 \cdot 2 \sqrt{\left(\frac{35 \cdot 5 \times 112}{1 \cdot 21 \times 6000}\right)}$$

$$= 2 \cdot 36 \,\text{ft/s}$$

$$v_s = \frac{1 \cdot 64 \times 6080}{3600} = 2 \cdot 78 \,\text{ft/s}$$

$$k = 0 \cdot 85 \quad \frac{1}{k} = 1 \cdot 18$$

From Fig. 6, it is found that, when $\phi_1 = 90°$ and $1/k = 1 \cdot 18$, the tension factor is $2 \cdot 3$.

At this particular speed, therefore, water resistance has caused the tension to rise to more than twice what it would have been with the ship stationary, even though the cable is leaving the water vertically and appears to be coming straight up from the bottom. The true shape of the suspended cable when $k = 0 \cdot 85$ is shown in Fig. 5. It is seen that, when the cable is

vertical at the surface ($\phi_1 = 90°$), it leaves the sea bed at a point about $0 \cdot 85$ times the depth of water ahead of the ship. Fig. 5 also indicates the way in which the curve assumed by this particular cable changes if the tension at the surface is varied while the speed of the ship is kept constant. If the tension is raised by allowing the ship to 'fall back', so that it is tending to pull itself along by the cable, the angle $\phi_1$ will increase. On the other hand, the tension can be reduced by driving the ship forward until the cable is leading aft, i.e. trailing back from the bows. For the particular value of $\alpha$ for which the curves of Fig. 5 have been drawn, for example, the angle $\phi_1$ will have fallen to about $60°$ when the ship maintains a position roughly vertically above the point at which the cable leaves the sea bed. Reference to Fig. 6 shows that this will reduce the tension factor to about $1 \cdot 7$ instead of $2 \cdot 3$.

### (6.2) Restrictions on a Minimum Tension

In the example, the tension factor will fall practically to unity as the angle $\phi_1$ approaches the limiting value of about $48°$ (at which the cable would simply trail back in a straight line from the bow-sheaves). This condition would certainly reduce the cable tension at the ship to its minimum possible value for a given cable and depth of water, but other considerations must be taken into account.

The tendency for a conventional armoured cable to twist under tension has already been mentioned in Section 1, where it is pointed out that the use of the correct amount of starboard lead can theoretically avoid a build-up of torque in the suspended cable. It is difficult in practice, however, to control the process sufficiently accurately to ensure that no torque will occur at any time during pick-up. The worst possible condition, as far as kinking of the cable is concerned, will occur if any part of the cable is ever subjected to torque in the absence of tension. For this reason, therefore, it is undesirable that the tension at the point where the cable leaves the sea bed should approach zero. Since the tension at this point and at the surface must differ by an amount $wh$, this means that the tension factor, given by eqn. (35), must not approach unity if the danger of kinks forming near the bottom of the suspended cable is to be avoided.

The accepted practice when picking up armoured cable is to work with it leaving the water either vertically or with a slight forward lead (i.e. $\phi_1 = 90°$–$95°$), and then to allow the pick-up speed to be dictated by the maximum tension which may safely be applied to that particular cable. With an unarmoured cable, on the other hand, the danger of damage due to kinking is very much less, so that there is no longer any need to maintain such a high relative tension at the point where the cable leaves the sea bed. This suggests, on theoretical grounds alone, that when picking up an unarmoured cable there may be some advantage in departing from the usual procedure by allowing the cable to lead aft from the bow-sheave. This would have the effect of reducing the pick-up tension for a given speed.

### (6.3) Effect of Vertical Motion of the Ship

The maximum tension to which the cable is subjected will depend not only on the pick-up speed but also on the weather conditions, because the vertical movement of the ship in response to the sea swell will cause the instantaneous velocity of the cable to vary with time. To obtain some idea of the magnitude of this effect it will be supposed that the ship has stopped and that the cable is simply hanging vertically to the sea bed. It will be assumed that the vertical motion of the bow-sheave is sinusoidal with respect to time, and can be expressed in the form

$$r = \hat{r} \sin \omega t$$

where $r$ is the vertical displacement from the mean position, $\hat{r}$

is the amplitude of oscillation and $\omega = 2\pi f$, where $f$ is the frequency of oscillation.

The velocity of propagation of longitudinal elastic waves down the cable will be so great that the motion of all points in the hanging cable can be assumed to be in time-phase, so that the instantaneous vertical velocity at any point in the cable is

$$v_q = \omega \hat{r} \cos \omega t$$

and its instantaneous acceleration is

$$a = -\omega^2 r \sin \omega t$$

The tension component due to axial water friction will be given by eqn. (7) as

$$wh\frac{v_q^2}{\bar{v}_q^2}$$

$$= \pm\, wh\frac{\omega^2 r^2}{\bar{v}_q^2} \cos^2 \omega t$$

the ambiguity of sign being taken to mean that the modulus of the alternating force is proportional to $\cos^2 \omega t$ but that its direction alternates so that it always opposes the motion of the cable. The tension component due to the inertia of the cable will be

$$-\frac{wh}{g}\omega^2 \hat{r} \sin \omega t$$

Adding these values to the static tension $wh$ gives the total instantaneous tension as

$$wh\left(1 - \frac{\omega^2 \hat{r}^2}{\bar{v}_q^2} \cos^2 \omega t - \frac{\omega^2 \hat{r}}{g} \sin \omega t\right)$$

when $\omega t$ is between 0 and $\pi$

and

$$wh\left(1 + \frac{\omega^2 \hat{r} \cos^2 \omega t}{\bar{v}_q^2} - \frac{\omega^2 \hat{r}}{g} \sin \omega t\right)$$

when $\omega t$ is between $\pi$ and $2\pi$.

($t = 0$ is the instant when the bow-sheave is moving downwards through its mid-position.) The relative magnitudes of the friction and inertia forces can be illustrated by an example.

*Numerical Example.*

Suppose that the periodic time of the bow sheave motion is 10 sec, and that the amplitude is $\pm 10$ ft. Assume that the cable is armoured and has a transverse settling velocity of 2·36 ft/s. From eqn. (8), the axial settling velocity is

$$\bar{v}_q = 8\cdot 7\bar{v}_p = 20 \text{ ft/s}$$

The tension is then $wh(1 \pm 0\cdot10 \cos^2 \omega t - 0\cdot12 \sin \omega t)$. In this case, therefore, the contributions made by axial water friction and inertia to the alternating tension component would be roughly equal. The ratio between the friction and inertia effects depends on $\hat{r}/v_q$ only. It is independent of the periodic time and depends only on the amplitude of motion and on the settling velocity of the cable. The friction force will tend to predominate for light cables, while the inertia force will be more important for heavy cables. It will be noted that both components of the alternating tension are proportional to $\omega^2$ and therefore to the vertical acceleration of the bow-sheave. They have different waveforms, however, and could probably be separated experimentally by recording and subsequently analysing the waveform of the tension in a practical case.

During an actual recovery operation, of course, the cable would not be hanging vertically and an exact theoretical treatment would be very much more difficult. Although, as far as is known, no systematic attempt has ever been made to collect experimental data on the relationship between the instantaneous tension in a cable and the vertical motion of the ship, there is some evidence to suggest that the alternating tension component during cable recovery is roughly of the same order as it would have been if the cable had been hanging vertically. This was shown in a case where a cable, which was being recovered from deep water, suddenly broke at a point whose distance along the cable from the ship was roughly equal to the depth of water. Although the average tension fell almost immediately to about half its original value, the amplitude of the alternating tension component remained practically unchanged. An estimate of the vertical acceleration of the bow-sheave (by noting the maximum and minimum readings of a spring balance supporting a suitable mass), showed that the alternating tension was roughly the same as that which would have been required to impart the observed acceleration to a vertical piece of cable hanging freely to the sea bed.

### (6.4) Comparison of Measured and Predicted Cable Tensions

Table 1 gives some typical average tension figures, measured during actual cable recovery. In each case pick-up had con-

### Table 1

#### MEASURED VALUES OF TENSION

| Type of cable | $w$ | $h$ | $d$ | $\bar{v}_p$ | $v_s$ | $k$ | $T_1/wh$ | |
|---|---|---|---|---|---|---|---|---|
| | | | | | | | Measured | Predicted |
| | cwt/1 000 fathoms | fathoms | in | knots | knots | | | |
| 600/340 GP telegraph type, 18/14 armour wires | 22 | 600 | 1·0 | 1·22 | 1·6 | 0·76 | 2·0 | 2·2 |
| | | 1 850 | | | 1·4 | 0·87 | 2·3 | 1·9 |
| | | 1 850 | | | 1·1 | 1·10 | 2·1 | 1·7 |
| 0·620 in polythene coaxial telephone cable, 24/14 armour wires | 35·5 | 700 | 1·25 | 1·40 | 1·0 | 1·4 | 1·5 | 1·4 |
| | | 700 | | | 0·7 | 2·0 | 1·2 | 1·2 |
| | | 2 700 | | | 0·8 | 1·75 | 1·6 | 1·3 |

tinued long enough for steady-state conditions to be reached and the cable was leaving the water with a slight starboard lead but practically no fore-and-aft lead.

Much more experimental evidence, including results of tests with armourless cables, would be required to obtain a real check of the accuracy of the theoretical tension curves. Accepting the few figures recorded in Table 1 as representative, however, it appears that the measured tension is somewhat greater than that predicted by theory, particularly at the greater water depths. One possible cause of the apparent discrepancy might be error

in the observations of the angle at which the cable leaves the water. As mentioned in Section 1, an armoured cable is picked up with a deliberately applied starboard lead, which means that the cable curve cannot ever be truly vertical at the surface of the water. In calm weather and with no surface tide, the ship should move bodily along the cable track but with its axis making a small angle with the track, corresponding to the starboard lead. Under adverse wind and tide conditions, however, the ship might be forced to follow a path parallel to the cable track but not exactly coinciding with it. In this case, even though the cable were observed to be leaving the water almost vertically, the suspended portion would follow a 3-dimensional curve which would tend to cause a rise in tension. Reference to Fig. 7 shows that the differences between the respective tension-factor results in Table 1 could be explained by relatively small errors in observation of $\phi_1$.

## (7) CONCLUSIONS

A theoretical analysis of the motion of submarine cables during steady-state laying conditions has confirmed that simplified formulae already in use give results which are sufficiently accurate for practical purposes. General curves have been computed and plotted which enable the form assumed by the suspended portion of a cable during steady-state pick-up conditions to be predicted, and also enable an estimate to be made of the increase in cable tension during pick-up due to the resistance of the water to the motion of the cable. Experimental evidence is scanty, but that which is available suggests that the actual tensions are somewhat higher than predicted, particularly in very deep water. The theory shows, however, that these discrepancies may possibly be due to the difficulty of obtaining accurate observations of the angle at which the cable leaves the water.

The relationship between the vertical motion of the ship and the resulting alternating tension component has also been investigated. It appears that the latter is mainly due to inertia effects in the case of an armoured cable but that water friction effects might predominate for a light armourless cable.

## (9) REFERENCES

(1) BESLY, J. C., and HIGGITT, H. V.: 'The Recovery of Deep-Sea Cable', *Journal I.E.E.*, 1933, **72**, p. 160.
(2) LORD KELVIN: 'On Machinery for Laying Submarine Telegraph Cables', *Engineer*, 16th October, 1857, **4**, p. 280.
(3) 'Cable Engineering Notes', Eastern and Associate Telegraph Co., No. 50, p. 33.
(4) GOLDSTEIN, S.: 'Modern Development in Fluid Dynamics' (Clarendon Press, 1938).
(5) GLAUERT, H.: 'The Form of a Heavy Flexible Cable Used for Towing a Heavy Body Below an Aeroplane', Aeronautical Research Committee Reports and Memoranda, No. 1952, February, 1933.
(6) McLEOD, A. R.: 'The Action of Wind on Flexible Cables', *ibid.*, No. 554, October, 1918.
(7) ZAJAC, E. E.: 'Dynamics and Kinematics of the Laying and Recovery of Submarine Cable', *Bell System Technical Journal*, 1947, **36**, p. 1129.

# TWO THEOREMS CONCERNING GROUP DELAY WITH PRACTICAL APPLICATION TO DELAY CORRECTION

## By G. G. GOURIET, Associate Member.

### SUMMARY

Two theorems are stated which enable properties of group delay to be expressed directly in terms of the transfer function of a linear transmission system. Examples are given to show how the results might be usefully applied to certain problems of delay correction.

### (1) INTRODUCTION

Most generally, the differential equation of a linear 4-terminal communication system with fixed parameters may be written

$$a_0 R + a_1 \frac{dR}{dt} + a_2 \frac{d^2 R}{dt^2} + \ldots a_n \frac{d^n R}{dt^n}$$

$$= b_0 + b_1 \frac{dE}{dt} + b_2 \frac{d^2 E}{dt^2} + \ldots b_m \frac{d^m E}{dt^m}$$

where $R(t)$ is the response of the system to an arbitrary excitation $E(t)$, and all coefficients are real constants. The transfer function of such a system may be defined as

$$f(p) = \frac{R[p]}{E[p]} = \frac{b_0 + b_1 p + b_2 p^2 \ldots b_m p^m}{a_0 + a_1 p + a_2 p^2 \ldots a_n p^n}$$

where $E[p]$ and $R[p]$ are the complex Fourier transforms of $E(t)$ and $R(t)$ respectively. A knowledge of $f(p)$ is sufficient to determine completely the linear behaviour of the system in all circumstances, using well-known operational methods.

When dealing with systems for which the 'shape' of the transmitted signal is of interest, it is normal practice to use this direct approach, which does not require the concepts of frequency and phase. For certain purposes, however, particularly where signals use specified frequency bands, the steady-state behaviour continues to be of interest, and this is expressed by the transfer function with $p$ replaced by $j\omega$, giving

$$f(j\omega) = \frac{b_0 + b_1(j\omega) + b_2(j\omega)^2 + \ldots b_m(j\omega)^m}{a_0 + a_1(j\omega) + a_2(j\omega)^2 + \ldots a_n(j\omega)^n}$$

Thus we recognize that $f(j\omega)$ is a particular case of the more general characteristic $f(p)$, and it is in this connection that we propose to discuss group delay.

In terms of its real and imaginary parts, the steady-state transfer function may be written

$$f(j\omega) = P(\omega) + jQ(\omega)$$

where

$$P(\omega) = \tfrac{1}{2}[f(j\omega) + f(-j\omega)]$$

$$jQ(\omega) = \tfrac{1}{2}[f(j\omega) - f(-j\omega)]$$

The characteristic known as group delay, which expresses the dispersive behaviour of a system, is defined as

$$\tau(\omega) = \frac{d\theta*}{d\omega}$$

where

$$\theta = \tan^{-1} \frac{Q(\omega)}{P(\omega)}$$

By its very definition, group delay demands the frequency concept, but with advantage it may be derived directly from the transfer function, $f(p)$, as defined above.

### (2) RELATIONSHIP BETWEEN GROUP DELAY AND GAIN SLOPE

In the following we shall state two theorems which do not appear to have been previously published:

*Theorem* (i).—If $f(p)$ is a transfer function and $f'(p)$ its first derivative with respect to $p$, the real part of $-f'(p)/f(p)$ is the group delay, $\tau(\omega)$, and the imaginary part is the gain slope $dG/d\omega$, where $G$ is the gain in nepers. (It is to be understood that the real and imaginary parts are obtained after substitution of $j\omega$ for $p$.)

*Proof.*—The proof follows directly from the fact that

$$\frac{f'(p)}{f(p)} = \frac{d}{dp}[\log f(p)] \quad . \quad . \quad . \quad . \quad (1)$$

Writing $j\omega$ for $p$ we have

$$-\frac{f'(j\omega)}{f(j\omega)} = -\frac{d}{d(j\omega)}[\log |f(j\omega)| \varepsilon^{j\theta}]$$

$$= j\frac{d}{d\omega}[\log |f(j\omega)| + j\theta]$$

$$= -\frac{d\theta}{d\omega} + j\frac{dG}{d\omega} \quad . \quad . \quad . \quad . \quad (2)$$

where $G(\omega) = \log |f(j\omega)|$ and $\theta(\omega)$ is the phase of $f(j\omega)$. The attenuation is of course $-G(\omega)$, whilst $-d\theta/d\omega$ is by definition the group-delay, $\tau(\omega)$. We note that being the real and imaginary parts of a function of $j\omega$, $\tau(\omega)$ and $dG/d\omega$ are even and odd functions of $\omega$, respectively.[1]

The fact that $\tau(\omega)$ and $G'(\omega)$ are derived directly from the transfer function, $f(p)$, would suggest that these parameters may be more fundamental than attenuation and phase. As will be shown later, the relationship between them is somewhat simpler than that between attenuation and phase.

In passing, it is perhaps worth stating the condition for distortionless transmission in terms of this theorem; this is simply

---

\* The negative sign is not at variance with the usual definition $d\beta/d\omega$ which applies in transmission theory, where $\beta$ is the phase-change coefficient. As defined, the propagation coefficient of a transmission system is the natural logarithm of the complex ratio, input/output, for a cisoidal excitation, whereas the transfer function, somewhat more logically, is concerned with the reciprocal of this ratio.

that $f'(p)/f(p)$ must be a real constant. The only realizable transfer function satisfying this condition over an infinite range of $p$ is the delay function $\varepsilon^{-p\tau}$.

The following corollaries to this theorem are also of interest.

(*a*) *Group-delay in terms of products and quotients of transfer functions.*—Because of the logarithmic form of $f'(p)/f(p)$ the group delay corresponding to the products and quotients of transfer functions becomes the sums and differences of the respective component group-delays.

Thus if
$$f(p) = g(p)h(p)$$

$$\tau(\omega) = -\mathscr{R}\left[\frac{h'(p)}{h(p)} + \frac{g'(p)}{g(p)}\right]_{p=j\omega} \quad . \quad . \quad . \quad (3)$$

Also if
$$f(p) = \frac{g(p)}{h(p)}$$

$$\tau(\omega) = \mathscr{R}\left[\frac{h'(p)}{h(p)} - \frac{g'(p)}{g(p)}\right]_{p=j\omega} \quad . \quad . \quad . \quad (4)$$

In general if
$$f(p) = \frac{\psi_0(p)\psi_1(p)\psi_2(p)\ldots\psi_m(p)}{\Omega_0(p)\Omega_1(p)\Omega_2(p)\ldots\Omega_n(p)}$$

$$\tau(\omega) = \mathscr{R}\left[\sum_0^n \frac{\Omega_k'(p)}{\Omega_k(p)} - \sum_0^m \frac{\psi_k'(p)}{\psi_k(p)}\right]_{p=j\omega} \quad . \quad . \quad (5)$$

(*b*) *Group-delay in terms of zeros and poles of* $f(p)$.—Let $f(p)$ have zeros at $\alpha_1, \alpha_2, \alpha_3, \ldots \alpha_m$, and poles at $\beta_1, \beta_2, \beta_3, \ldots \beta n$, so that

$$f(p) = \frac{(p - \alpha_1)(p - \alpha_2)(p - \alpha_3)\ldots(p - \alpha_m)}{(p - \beta_1)(p - \beta_2)(p - \beta_3)\ldots(p - \beta_n)}$$

From (5),

$$\tau(\omega) = \mathscr{R}\left[\sum_1^n \frac{(p - \beta_r)'}{(p - \beta_r)} - \sum_1^m \frac{(p - \alpha_r)'}{(p - \alpha_r)}\right]_{p=j\omega}$$

which gives

$$\tau(\omega) = \sum_1^m \frac{\alpha_r}{\alpha_r^2 + \omega^2} - \sum_1^n \frac{\beta_r}{\beta_r^2 + \omega^2} \quad . \quad . \quad . \quad (6)$$

There is no need to insert $\mathscr{R}$ ($=$ real part) in the above expression, since the imaginary terms due to complex conjugate roots will cancel in the summation.

At zero frequency ($\omega = 0$),

$$\tau(0) = \sum_1^m \frac{1}{\alpha_r} - \sum_1^n \frac{1}{\beta_r} \quad . \quad . \quad . \quad . \quad (7)$$

For $f(p)$ to be physically realizable, all poles will be in the left half of the $p$-plane, i.e. all $\beta_r$ will have negative real parts, whence the contribution

$$-\sum_1^n \frac{\beta_r}{\beta_r^2 + \omega^2}$$

which is due to the denominator, $h(p)$, will be positive for all values of $\omega$. If, in addition, $f(p)$ is free from zeros in the right half of the $p$-plane, which will be true for a minimum phase system, all $\alpha_r$ will have negative real parts, so that the contribution

$$\sum_1^m \frac{\alpha_r}{\alpha_r^2 + \omega^2}$$

due to the numerator, $g(p)$, will be negative for all values of $\omega$. An important conclusion is that if $f(p)$ is expressed as the ratio of two polynomials, $g(p)/h(p)$, a necessary condition* for $f(p)$

---

\* For orders up to a cubic this is also a sufficient condition, but this is a limiting and does not apply to higher orders.

to be physically realizable (i.e. free from poles in the right half of the $p$-plane) is that

$$\mathscr{R}\frac{h'(p)}{h(p)} > 0 \text{ for all values of } p = j\omega$$

A negative group delay may be produced by a realizable transfer characteristic over a finite frequency band, but it will always be due to the numerator of $f(p)$. For example,

$$f(p) = \frac{a + p}{b + p}$$

can be realized over a finite frequency band extending upwards from zero frequency.

In this case, by eqn. (6),

$$\tau(\omega) = \frac{b}{b^2 + \omega^2} - \frac{a}{a^2 + \omega^2}$$

and this will be a negative quantity if $a > b$ and $\omega^2 > ab$, or alternatively, if $a < b$ and $\omega^2 < ab$.

A second theorem will now be stated which relates gain slope $G'(\omega)$ with group delay $\tau(\omega)$.

*Theorem* (ii).—If $f(p)$ is free from poles and zeros in the right half of the $p$-plane, then $G'(\omega)$ and $\tau(\omega)$ are a pair of Hilbert transforms. Thus

$$\left.\begin{array}{l} G'(\omega) = \dfrac{1}{\pi}\displaystyle\int_{-\infty}^{\infty} \dfrac{\tau(\lambda)}{\lambda - \omega}d\lambda \\[2em] \tau(\omega) = -\dfrac{1}{\pi}\displaystyle\int_{-\infty}^{\infty} \dfrac{G'(\lambda)}{\lambda - \omega}d\lambda \end{array}\right\} \quad . \quad . \quad . \quad (8)$$

This is another way of stating the relationship between attenuation and phase given by Lee,[2] but is somewhat more simple and direct in that it avoids the use of circular functions.

*Proof.*—The real and imaginary parts of any transfer function $\phi(p)$, $[\equiv \phi(j\omega)]$ are a pair of Hilbert transforms provided that $\phi(p)$ is free from poles in the right half of the $p$-plane, and that $|\phi(j\omega)|$ tends uniformly to zero as $\omega \to \infty$. A simple proof of this is given in the Appendix.

Consider now a transfer function

$$f(p) = \frac{g(p)}{h(p)} = \frac{a_0 + a_1p + a_2p^2 \ldots a_mp^m}{b_0 + b_1p + b_2p^2 \ldots b_np^n}$$

which is free of poles and zeros in the right half of the $p$-plane. By the previous theorem,

$$-\frac{f'(p)}{f(p)} = \frac{h'(p)}{h(p)} - \frac{g'(p)}{g(p)} = -\frac{d\theta}{d\omega} + j\frac{dG}{d\omega}$$

Now, since $h'(p)$ will always be of a lower order than $h(p)$, and similarly $g'(p)$ will be of a lower order than $g(p)$,

$$\left|\frac{f'(j\omega)}{f(j\omega)}\right|$$

will tend uniformly to zero as $\omega \to \infty$. Also, since both $h(p)$ and $g(p)$ are free from zeros in the right half of the $p$-plane, $f'(p)/f(p)$ will be free from poles in the right half, and the real and imaginary parts of $f'(j\omega)/f(j\omega)$ will thus be a pair of Hilbert transforms. Hence, by Theorem (i), $G'(\omega)$ and $\tau(\omega)$ are a pair of Hilbert transforms.

We shall illustrate the use of this theorem with an elementary example. The group delay which results from the transfer function

$$f(p) = \frac{a}{a + p}$$

is

$$\tau(\omega) = \frac{a}{a^2 + \omega^2} \quad . \quad . \quad . \quad . \quad (9)$$

Also

$$|f(j\omega)| = \frac{a}{\sqrt{(a^2 + \omega^2)}} \quad . \quad . \quad . \quad (10)$$

Suppose we are given $\tau(\omega)$ and wish to deduce $|f(j\omega)|$ consistent with the minimum phase condition. For the gain slope we have

$$\frac{dG}{d\omega} = \frac{1}{\pi} \int_{-\infty}^{\infty} \frac{\tau(\lambda)}{\lambda - \omega} d\lambda = \frac{1}{\pi} \int_{-\infty}^{\infty} \frac{a}{a^2 + \lambda^2} \frac{1}{\lambda - \omega} d\lambda \quad (11)$$

This integral may be readily evaluated by contour integration to give

$$\frac{dG}{d\omega} = -\frac{\omega}{a^2 + \omega^2}$$

Thus

$$G(\omega) = \log_\varepsilon |f(j\omega)| = -\int \frac{\omega}{a^2 + \omega^2} d\omega + c$$

$$= \log_\varepsilon \frac{k}{\sqrt{(a^2 + \omega^2)}}$$

where $k$ is an arbitrary constant.

Thus

$$|f(j\omega)| = \frac{k}{\sqrt{(a^2 + \omega^2)}} \quad . \quad . \quad . \quad (12)$$

which is, of course, correct and identical with (10) if $k = a$.

### (3) SERIES EXPANSION

Using the expression $f'(p)/f(p)$, it is a simple matter to express either group delay or gain slope as a series in ascending powers of $\omega$. This can prove particularly useful in determining the circuit parameters required for delay correction. To illustrate this point, we shall consider the normalized transfer function

$$\frac{1}{f(p)} = \frac{1}{1 + p\tau_1 + p^2\tau_2 + p^3\tau_3 + p^4\tau_4} \quad . \quad . \quad (13)$$

and establish the values that the coefficients of $p$ must have in order that the group delay shall be constant in the maximally-flat[3] sense.

For this particular case we have

$$\frac{f'(p)}{f(p)} = \frac{\tau_1 + 2p\tau_2 + 3p^2\tau_3 + 4p^3\tau_4}{1 + p\tau_1 + p^2\tau_2 + p^3\tau_3 + p^4\tau_4} \quad . \quad . \quad (14)$$

Straightforward division gives

$$\frac{f'(p)}{f(p)} = a + bp + cp^2 + dp^3 + ep^4 \ldots \text{etc.}$$

where $a = \tau_1$
$b = -(\tau_1^2 - 2\tau_2)$
$c = (\tau_1^3 - 3\tau_1\tau_2 + 3\tau_3)$
$d = -(\tau_1^4 - 4\tau_1^2\tau_2 + 4\tau_1\tau_3 - 4\tau_4 + 2\tau_2^2)$
$e = (\tau_1^5 - 5\tau_1^3\tau_2 + 5\tau_1^2\tau_3 - 5\tau_1\tau_4 + 5\tau_1\tau_2^2 - 5\tau_2\tau_3)$
$f = -(\tau_1^6 - 6\tau_1^4\tau_2 \ldots)$

Substituting $j\omega$ for $p$ and collecting even terms, we obtain for the normalized group delay

$$\omega_0\tau(\omega) = 1 - (1 - 3k_2 + 3k_3)\left(\frac{\omega}{\omega_0}\right)^2$$
$$+ (1 - 5k_2 + 5k_3 - 5k_4 + 5k_3^2 5k_2 k_3)\left(\frac{\omega}{\omega_0}\right)^4$$
$$- (1 - 7k_2 \ldots)\left(\frac{\omega}{\omega_0}\right)^6 \quad . \quad . \quad . \quad . \quad (15)$$

where

$$\omega_0 = \frac{1}{\tau_1}$$

$$k_n = \omega_0^n \tau_n$$

On equating to zero the coefficients of $\omega^2$ and $\omega^4$ we obtain

$$\left. \begin{array}{l} k_3 = k_2 - \dfrac{1}{3} \\[2mm] k_4 = \dfrac{1}{3}\left(k_2 - \dfrac{2}{5}\right) \end{array} \right\} \quad . \quad . \quad . \quad (16)$$

so that

$$\tau_1 = 1/\omega_0$$

$$\tau_2 = k_2/\omega_0^2$$

$$\tau_3 = \left(k_2 - \frac{1}{3}\right)\Big/\omega_0^3$$

$$\tau_4 = \frac{1}{3}\left(k_2 - \frac{2}{5}\right)\Big/\omega_0^4$$

Substitution of these values in (13) gives

$$f(p) = 1 + \frac{p}{\omega_0} + K\left(\frac{p}{\omega_0}\right)^2 + \left(K - \frac{1}{3}\right)\left(\frac{p}{\omega_0}\right)^3 + \frac{1}{3}\left(K - \frac{2}{5}\right)\left(\frac{p}{\omega_0}\right)^4$$
$$\quad . \quad . \quad . \quad . \quad (17)$$

where $k_2$ has been replaced by $K$, which is now an arbitrary constant.

Eqn. (17) expresses the most general quartic transfer function with maximally flat group delay in the sense that the first five derivatives with respect to $\omega$ are zero at $\omega = 0$.

We note that $f(p)$ now has only two degrees of freedom, one of which is $\omega_0$, which determines the frequency scale, and the other, the arbitrary constant $K$, which will control the behaviour of the group delay beyond the maximally flat region.

For $1/f(p)$ to be physically realizable, a first condition is that all coefficients of $p$ must be positive; this is satisfied if $K > \frac{2}{5}$. As a second condition, $f(p)$ must satisfy the stability criterion for a quartic,[4, 5] namely that if

$$F(p) = a + bp + cp^2 + dp^3 + ep^4$$

$1/F(p)$ will be stable (i.e. all poles in the left half of the $p$-plane) only if $bcd > ad^2 + eb^2$.

Applying this to $f(p)$ as expressed by (17), we obtain the result

$$(K^2 - K/3) > \left(K^2 - K/3 - \frac{1}{45}\right)$$

which is true and independent of the value of $K$. We therefore conclude that $1/f(p)$ is physically realizable for all values of $K > \frac{2}{5}$.

The corresponding normalized group delay is

$$\omega_0\tau(\omega) = 1 + \left(\frac{7}{45}K - \frac{1}{15}\right)\left(\frac{\omega}{\omega_0}\right)^6 + \text{higher powers of } \left(\frac{\omega}{\omega_0}\right)^{2r}$$
$$\quad . \quad . \quad . \quad (18)$$

The following cases are of interest:

(i) $K = \frac{3}{7}$. Here the coefficient of $(\omega/\omega_0)^6$ is also zero.

(ii) $K = \frac{1}{2}$, for which case

$$f(p) = 1 + \left(\frac{p}{\omega_0}\right) + \frac{1}{2}\left(\frac{p}{\omega_0}\right)^2 + \frac{1}{6}\left(\frac{p}{\omega_0}\right)^3 + \frac{1}{30}\left(\frac{p}{\omega_0}\right)^4$$

This corresponds to $\varepsilon^{p\tau_1}$ over a substantial range of $p$, since f($p$) differs from the first five terms of the expansion of $\varepsilon^{p/\omega_0}$ by only $\frac{1}{120}\left(\frac{p}{\omega_0}\right)^4$.

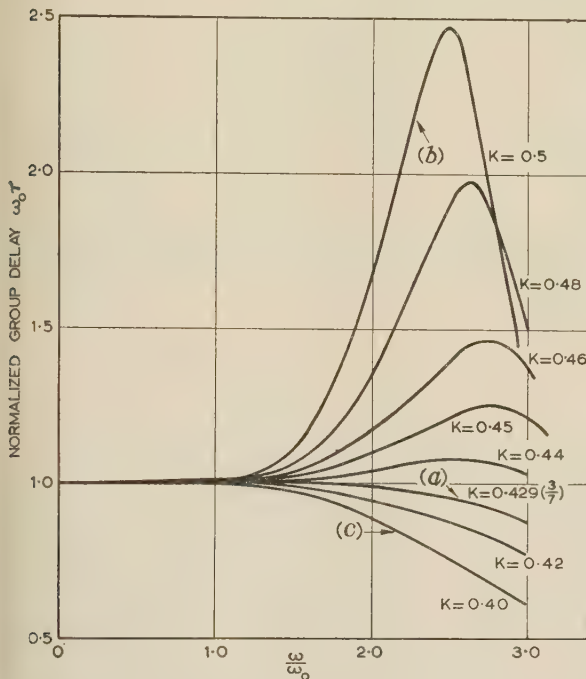(iii) $K = \frac{2}{5}$. For this value f($p$) reduces to a cubic.



Fig. 1.—Maximally flat delay characteristics of the quartic transfer function given in eqn. (17).

(a) First 7 derivatives zero at $\omega = 0$.
(b) Eqn. (17) approximates to $\varepsilon^{p/\omega_0}$.
(c) Eqn. (17) reduces to a cubic.

The group delay for these and some other values of $K$ is shown in Fig. 1. These results may be usefully employed in certain problems of delay equalization in the following manner:

The transfer function

$$\frac{f(-p)}{f(p)} = \frac{1 - p\tau_1 + p^2\tau_2 - p^3\tau_3 + p^4\tau_4}{1 + p\tau_1 + p^2\tau_2 + p^3\tau_3 + p^4\tau_4} \quad . \quad (19)$$

produced by a pair of 6-element constant-resistance all-pass lattice filters or bridged-T equivalents. With the coefficients chosen to make the group delay maximally flat, f($-p$)/f($p$) still has two degrees of freedom, which means that there is a double infinity of such pairs of filters which will produce the maximally flat delay characteristics of Fig. 1, multiplied by a factor of 2, because of the conjugate numerator. These combinations can prove useful in many problems of delay correction where phase error is occurring mainly at high frequencies; for example, phase correction of low-pass filter characteristics.

There are a number of known methods of obtaining the

numerical roots of a quartic, and values for $K$ and $\omega_0$ having been chosen, f($p$) in (19) can be expressed as the product of two quadratic factors from which can be determined the actual values of the filter elements for each all-pass section. Thus, each of the quadratic factors will be of the form

$$\phi(p) = 1 + \lambda_1 p + \lambda_2 p^2$$

and the corresponding all-pass filter sections will each have a transfer function of the form

$$\frac{\phi(-p)}{\phi(p)} = \frac{1 - \lambda_1 p + \lambda_2 p^2}{1 + \lambda_1 p + \lambda_2 p^2} \quad . \quad . \quad . \quad (20)$$

This may be written

$$\frac{\phi(-p)}{\phi(p)} = \frac{1 - q\frac{p}{\omega_c} + \left(\frac{p}{\omega_c}\right)^2}{1 + q\frac{p}{\omega_c} + \left(\frac{p}{\omega_c}\right)^2} \quad . \quad . \quad . \quad (21)$$

where $q = \lambda_1/\sqrt{\lambda_2}$
$\omega_c^2 = 1/\lambda_2$

The values of the filter elements for the appropriate bridged-T sections may be readily determined from the following design equations with reference to Fig. 2:

$$\left.\begin{array}{l} L = q\dfrac{R}{\omega_c} \\[2mm] C = q/\omega_c R \end{array}\right\} \quad . . . . . . (22)$$

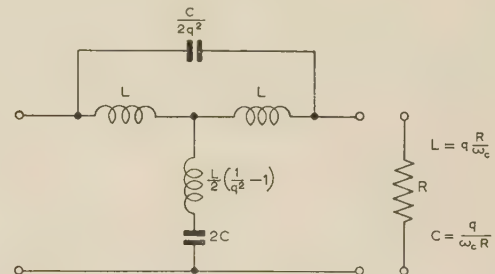where $R$ is the termination resistance.



Fig. 2.—Bridged-T all-pass filter with transfer function of eqn. (21).

For values of $q > 1\cdot0$ the shunt inductance in Fig. 2 is negative and may be provided by arranging for mutual coupling between the two series inductances using a coupling factor $(q^2 - 1)/(q^2 + 1)$.

### (4) ACKNOWLEDGMENTS

### (5) REFERENCES

(1) GOURIET, G. G.: 'Spectrum Equalization: Use of Differentiating and Integrating Circuits', Wireless Engineer, 1953, 30, p. 112.
(2) LEE, Y. W.: 'Synthesis of Electric Networks by means of the Fourier Transforms of Laguerre's Functions', Journal of Mathematics and Physics, 1931–1932, 11, p. 88.
(3) THOMSON, W. E.: 'Networks with Maximally Flat Delay', Wireless Engineer, 1952, 29, p. 256.

(4) ROUTH, E. J.: 'Advanced Rigid Dynamics' (Macmillan), Vol. 2.

(5) CARTER, G. W.: 'Simple Calculations of Electrical Transients' (Cambridge University Press, 1944).

### (6) APPENDIX

*Proof that the real and imaginary parts of* $f(j\omega)$ *are Hilbert transforms if* $f(j\omega)$ *is free from poles in the lower half of the* $\omega$*-plane (right half of the p-plane) and* $|f(j\omega)|$ *tends uniformly to zero as* $\omega \to \infty$.

By Cauchy's integral theorem,

$$f(j\omega) = \frac{1}{2\pi j} \int_C \frac{f(j\lambda)}{\lambda - \omega} d\lambda \quad . \quad . \quad . \quad (23)$$

where the contour C encloses the pole at $\omega$, and $f(j\lambda)$ is analytic within and on the contour.

Now if $f(j\lambda)$ is analytic in the lower half of the $\lambda$-plane including the real axis, the contour C may be an infinite semicircle in the lower half-plane enclosing only the single pole at $\omega$ on the real axis (see Fig. 3). Furthermore, if $|f(j\lambda)|$ tends uniformly to zero as $\lambda \to \infty$, the semicircle will not contribute to the integral and we may write

$$f(j\omega) = -\frac{1}{\pi j} \int_{-\infty}^{\infty} \frac{f(j\lambda)}{\lambda - \omega} d\lambda \quad . \quad .. \quad . \quad . \quad (24)$$

The negative sign arises because the direction of integration is the reverse of that for the closed contour in Fig. 3. The coefficient $1/\pi j$ replaces the coefficient $1/2\pi j$ [eqn. (23)] since the path of integration is now strictly along the real axis and therefore includes only one half of the contribution of the pole at $\omega$.
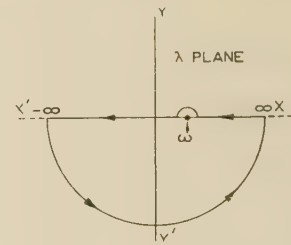


Fig. 3

Now let $f(j\omega)$ be expressed as

$$P(\omega) + jQ(\omega)$$

where $P(\omega)$ and $Q(\omega)$ are both real.

We then have

$$P(\omega) + jQ(\omega) = -\frac{1}{\pi j} \int_{-\infty}^{\infty} \frac{P(\lambda) + jQ(\lambda)}{\lambda - \omega} d\lambda$$

$$= \frac{j}{\pi} \int_{-\infty}^{\infty} \frac{P(\lambda)}{\lambda - \omega} d\lambda - \frac{1}{\pi} \int_{-\infty}^{\infty} \frac{Q(\lambda)}{\lambda - \omega} d\lambda \quad (25)$$

Since both of the integrands in (25) are real, we may equate the real and imaginary parts and thus obtain the pair of Hilbert transforms

$$P(\omega) = -\frac{1}{\pi} \int_{-\infty}^{\infty} \frac{Q(\lambda)}{\lambda - \omega} d\lambda$$

$$Q(\omega) = \frac{1}{\pi} \int_{-\infty}^{\infty} \frac{P(\lambda)}{\lambda - \omega} d\lambda$$

# CONDITIONS FOR THE IMPEDANCE AND ADMITTANCE MATRICES OF $n$-PORTS WITHOUT IDEAL TRANSFORMERS

## By I. CEDERBAUM, Ph.D.

### SUMMARY

The matrices relating two adequate systems of simple network co-ordinates of the same network, e.g. node-pair voltages or loop currents, are shown to have all their elements and subdeterminants equal to $+1$, $-1$ or $0$. Any $n$-port may be looked upon as a part of an adequate system of independent node pairs described on the network or loops inscribed into the network. In the former case the additional node pairs, not included in the $n$-port, ought to be considered as open-circuited and in the latter case the additional loops ought to be looked on as short-circuited. The conditions for cut-set and loop-incidence matrices are discussed, and then the conditions for impedance and admittance matrices of $n$-ports without ideal transformers are defined in terms of those incidence matrices. The discussion of the conditions thus derived leads, among other things, to a conclusion that matrices representing pure-resistance $n$-ports are necessarily such that each principal minor of such a matrix is greater than the modulus of any minor built from the same rows (or columns).

## (1) INTRODUCTION

Most of the works on multi-port networks use the artifice of the ideal transformer to solve the realization problem. On the other hand, most of them, as observed by Darlington,[1] fit a pattern called by him the 'classical model'. One of the characteristic concepts of this model is the canonical configuration. The existence of the canonical configuration, or more than one such configuration, means that a small group of the networks considered may be taken as representatives of the whole class with regard to their terminal properties.

It seems that these two features are most closely interconnected. The admission of mutual inductances simplifies the problem of network synthesis by removing a part of the topological constraints inherent in any configuration of network elements. By suitable arrangement of transformers one is able to get combinations of currents and voltages which otherwise would be impossible. If, in addition, this removal of topological constraints is necessary for all frequencies, including zero and infinity, without affecting the flow of currents, the ideal transformer (like the *deus ex machina* in classical tragedies) appears to be an indispensable element.

Therefore it seems that, if one aims at elimination of ideal transformers, another approach to network synthesis is needed. In such an approach the configuration of the network should not be assumed in anticipation but should be derived from its mathematical characterization, say from its impedance or admittance matrix.* There is little likelihood that the structure which will arise as a result of this method will be one of the known canonical configurations. In a general case it will be a complex connection of elements, a network in the true sense of the word.

The simplest characterization of such a complex network con-

* See, for example, Reference 2, p. 356.

figuration seems to be its node incidence matrix. Thus the ultimate end in this kind of synthesis procedure should be the derivation of that matrix. If this task is accomplished the evaluation of network elements does not furnish in general any further major difficulty.

The following is *not* a paper on synthesis of $n$-ports without ideal transformers. Although a set of necessary and sufficient conditions for matrices representing such networks are here given, further efforts are required to find a procedure for testing whether a given matrix belongs to this class and to produce a comprehensive method of synthesis of the corresponding $n$-port.

Although the derivation of the conditions is straightforward, the author prefers to postpone it until Section 7, and first to build up some knowledge on cut-set and loop matrices in terms of which those conditions are expressed.

## (2) THE RELATIONS BETWEEN TWO SYSTEMS OF INDEPENDENT NODE-PAIR VOLTAGES

Let us consider some connected network with $t$ nodes and $b$ branches, and let us choose on it two arbitrary systems of independent node-pair voltages $U$ and $V$. As is well known,[3] each set of independent node-pairs may contain at most $s = t - 1$ such pairs, and since each node-pair from such a set may play the role of a port in a multi-port based on the network, at most an $s$-port may be described on the considered network. The relation between two sets of $s$ independent voltages $U$ and $V$ may be alternatively regarded as a relation between the voltages of an $s$-port and the voltages of some system of independent node-pairs, or as a relation between the voltages of two $s$-ports described on the same network.

Since the voltages of each system are independent, regarded as branches they cannot form closed circuits, and since the number of voltages in each system is less by one than the number of nodes, they necessarily form tree-like structures,[4] although, of course, there need not exist the network branches which correspond to all or some of those voltages. In a paper published recently[5] it has been shown that the transformation from some adequate system of node-pair voltages to another calls for a unimodular matrix all of whose elements are 1, $-1$ or 0. Thus if

$$V = AU \quad . \quad . \quad . \quad . \quad . \quad (1)$$

is the relation between $V$ and $U$ then the $(s \times s)$ matrix A and its inverse $A^{-1}$ are unimodular matrices with all their elements equal to 1, $-1$ or 0. This shows that, all minors of order $s - 1$ of the matrix A being, apart from the sign, equal to the elements of $A^{-1}$, are also equal to 1, $-1$ or 0. Moreover, it can be proved that all subdeterminants of A are equal to 1, $-1$ or 0.

*Proof.*—Let us assume that some subdeterminant of A of order $p$, say, $D^{(p)}$ is not equal to zero. By a suitable numeration of the node-pairs in both systems this determinant can be brought into the top left position in the transformation matrix; therefore, without loss of generality, we can assume that it does occupy this position. Let us short-circuit the node-pairs $p + 1$, $p + 2$, ..., $s$

of the system $U$. The new voltages $\bar{V}$ may be obtained from eqn. (1) if we put there

$$U_{p+1} = U_{p+2} = \ldots = U_s = 0$$

or from the relation $\qquad \bar{V} = \bar{A}\bar{U}$ . . . . . . . (2)

where the $(s \times p)$ matrix $\bar{A}$ consists of the first $p$ columns of $A$ and the $(p \times 1)$ column vector $\bar{U}$ is the vector of the $p$ voltages of the $U$ node-pairs not short-circuited. By this action we have reduced the number of the nodes of the network to $p + 1$ and the voltages $\bar{U}$ (having a tree-like structure) form a system of $p$ independent node-pair voltages on the reduced network. The reduction of the number of the nodes may have caused also short-circuiting of some node-pairs of the system $\bar{V}$, but certainly none of the first $p$ node-pairs is short-circuited, since this would mean that in the matrix $\bar{A}$ one of the first $p$ rows is zero, contrary to the hypothesis that $D^{(p)} \neq 0$. Also the 'new' voltages $\bar{V}_1, \bar{V}_2, \ldots, \bar{V}_p$ can form no closed circuit, since this would result in linear dependence between the first $p$ rows of $\bar{A}$ leading to $D^{(p)} = 0$. Therefore these voltages form another set of independent node-pair voltages on the reduced network, and $D^{(p)}$, being the determinant of the matrix relating two systems of independent node-pair voltages, must be equal to 1 or $-1$. Thus we have:

(i) The transformation matrix relating two vectors of $s$ independent node-pair voltages described on the same network with $s + 1$ nodes is unimodular with all its elements and all sub-determinants equal to 1, $-1$ or 0.

In the following we shall refer to a matrix having all its sub-determinants (elements being the subdeterminants of order 1) equal to 1, $-1$ or 0 as an E-matrix, extending this definition also to the case of rectangular matrices.

Let us now consider the more general case of an $n$-port with $n \leqslant s$ based on a connected network with $s + 1$ nodes and let

$$V_1 = A_1 U \quad . \quad . \quad . \quad . \quad . \quad (3)$$

be the relation between the $(n \times 1)$ vector of port voltages $V_1$ and the $(s \times 1)$ vector of independent node-pair voltages $U$. Since it is always possible to augment an $n$-port by addition of $s - n$ ports to form an $s$-port described on the same network,* we can look on $A_1$ as an $(n \times s)$ submatrix of some transformation matrix $A$. Taking into account that the voltages of an $n$-port are independent, $A_1$ must be of rank $n$, and since a submatrix of an E-matrix is an E-matrix we have a more general result:

(ii) The matrix relating the vector of the voltages of an $n$-port $(n \leqslant s)$ described on some network to the vector of any $s$ independent node-pair voltages of that network is an E-matrix of rank $n$.

### (3) THE RELATIONS BETWEEN TWO SYSTEMS OF INDEPENDENT CURRENTS

There is another, dual, possibility of deriving a multi-port from a network. Let us choose some arbitrary tree on the network and cut some $n$ (or all) of the $f = b - s$ links corresponding to that tree. Taking apart the cut ends we may look on them as an $n$-port inscribed into the network. The currents of the links form a set of independent currents and at most an $f$-port can be inscribed in such a way into the network.†

The relation between two $(f \times 1)$ vectors of link currents $I$ and $J$ corresponding to two trees on the same network

$$J = BI \quad . \quad . \quad . \quad . \quad . \quad . \quad (4)$$

* See Reference 2, lemma 1.3.
† See Reference 3, p. 10.

calls for a unimodular $(f \times f)$ matrix with all elements equal to 1, $-1$ or 0,* and by an exactly dual reasoning to that for the voltage transformation we arrive at the following theorem:

(i) The matrix relating the vector of the currents of an $n$-port $(n \leqslant f)$ inscribed into the network to the vector of any $f$ independent link currents of that network is an E-matrix of rank $n$.

### (4) SOME PROPERTIES OF E-MATRICES

The more detailed study of algebraic and structural properties of E-matrices will, it is hoped, be published in a separate paper. Here we refer only to those properties which are of immediate importance for the following discussion.

(i) The transpose, the matrix obtained by any permutation of rows and columns, and any submatrix of an E-matrix are E-matrices.

The proof of these properties follows immediately from the definition of an E-matrix.

(ii) The matrix obtained by changing the signs of all elements of some rows or columns of an E-matrix is an E-matrix.

This is evident, since any element or subdeterminant of the 'new' matrix is equal numerically to the corresponding element or subdeterminant of the original matrix.

(iii) The inverse of a non-singular E-matrix is an E-matrix.

This is evident since the elements of the inverse matrix are, apart from the sign, the minors of the original matrix, and the subdeterminants are, by Jacobi's theorem,[6] equal to the complementary signed subdeterminants of the transpose of the original matrix divided by its determinant.

### (5) CUT-SET AND LOOP MATRICES

The $(t \times b)$ node (or vertex) incidence matrix† and any of its $(s \times b)$ submatrices obtained by deleting one of its rows will be referred to in the following shortly as the IM and RIM's respectively. Similarly the $(f \times b)$ incidence matrix of a system of $f$ loops and the $(s \times b)$ incidence matrix of a system of $s$ cut-sets‡ will be for simplicity denoted by LM and CSM respectively.

An RIM of a connected network is a special case of a CSM which corresponds to the system of node voltages of any $s$ nodes with respect to the remaining node (node-to-datum system of voltages). As may be readily seen, such a system of voltages corresponds to a system of cut-sets each of which contains all branches incident at one node.

For the IM, Veblen and Franklin[7] have shown that it has the characteristic properties of an E-matrix. We shall now prove the more general theorem:

(i) The CSM of any system of $s$ independent node-pair voltages is an E-matrix, and dually,

(ii) The LM of any system of $f$ independent link currents is an E-matrix.

*Proof.*—The proof of the first theorem follows readily if we transform the given network $N$ with $t$ nodes and $b$ branches into a tree. One way to do this is to choose an arbitrary tree and to cut off all the $f = b - s$ links at one node from the tree. The 'new' network $\bar{N}$ has $b + 1$ nodes and $b$ branches and it is a tree. If a system $U$ of $s$ independent node-pair voltages has been chosen on $N$, then, together with the 'new' $b - s$ node-pair voltages between the nodes from which the links have been separated and the free ends of the links, it forms a system $\bar{U}$ of $b$ independent node-pair voltages on $\bar{N}$. Another system on $\bar{N}$ is, for example, the system $V$ of all branch voltages, since $\bar{N}$ is a tree.

Let $\qquad\qquad\qquad V = A\bar{U}$ . . . . . . . (5)

* See Reference 5, p. 237.
† See Reference 4, definition 18.
‡ See Reference 5, p. 240.

Since $V$ and $\bar{U}$ are both adequate systems of node-pair voltages the transformation matrix A is according to (i) of Section 2 an E-matrix. It may be partitioned in the form

$$A = [A_1, A_2] \quad . \quad . \quad . \quad . \quad . \quad (6)$$

where $A_1$ corresponds to the 'old' voltages $U$ (considered to occupy the first $s$ places in $\bar{U}$). Short-circuiting the 'new' node-pairs is equivalent to putting the last $b - s$ co-ordinates of $\bar{U}$ equal to zero, which gives

$$V = [A_1, A_2]\begin{bmatrix} U \\ 0 \end{bmatrix} = A_1 U \quad . \quad . \quad . \quad . \quad (7)$$

On the other hand, short-circuiting those node-pairs leaves us with the original network $N$. Thus the relation (7) gives the branch voltages $V$ of the network $N$ expressed by the node-pair voltages $U$, and $-A_1$ may be identified as the transpose of the CSM corresponding to the chosen system $U$.* Applying the properties (ii) and (i) of Section 4 to the E-matrix A we see that the CSM is an E-matrix.

For the proof of the dual theorem let $I$ be the vector of $f$ independent link currents corresponding to some tree $T$ on the given network $N$. Let us put a 'new' branch parallel to each of the $s$ branches of the tree $T$ and let $\bar{N}$ be the augmented network with $b + s$ branches. The 'old' tree $T$ is a tree on $\bar{N}$, and therefore the system of the old links $(I)$, together with the 'new' $s$ branches, forms an adequate system $\bar{I}$ of $s + b$ links on $\bar{N}$. Another such system of links is the system $J$ of all branches of $N$, which corresponds to the tree of the 'new' branches added to $N$. Therefore we have:

$$J = B\bar{I} \quad . \quad . \quad . \quad . \quad . \quad (8)$$

where B, according to (i) of Section 3, is a non-singular $(b \times b)$ E-matrix.

The matrix B can be partitioned:

$$B = [B_1, B_2] \quad . \quad . \quad . \quad . \quad . \quad (9)$$

according to the 'old' and 'new' links. Open-circuiting the 'new' branches gives

$$J = [B_1, B_2]\begin{bmatrix} I \\ 0 \end{bmatrix} = B_1 I \quad . \quad . \quad . \quad (10)$$

On the other hand, open-circuiting those links leaves us with the original network. Therefore $B_1'$ may be identified with the LM corresponding to the chosen set $I$. This proves according to (i) of Section 4 that the LM is an E-matrix.

**(6) THE CONDITIONS ON RIM's OF CONNECTED NETWORKS AND TREES, AND LM's AND CMS's CORRESPONDING TO SOME SIMPLE SYSTEMS OF NETWORK CO-ORDINATES**

In this Section, for the sake of convenience and uniformity of formulation, we have collected those theorems on RIM's, LM's and CMS's which are relevant to the further discussion. The proofs of these theorems, or slightly differing versions of them, can be found in the quoted literature.

(i) The necessary and sufficient conditions for an $(s \times b)$ matrix Q to be an RIM of a connected network with $t = s + 1$ nodes and $b$ branches are that†

(*a*) All elements of Q are 1, $-1$ or 0.

(*b*) In each column of Q there are at most two non-zero elements.

(*c*) Q is of rank $s$.

* The relation between the $(b \times 1)$ vector $V$ of the branch voltages and the $(s \times 1)$ vector of cut-set voltages involving the $(s \times b)$ CSM W is here and throughout the paper adopted in the form $V = -W'U$ and not $V = W'U$ as in Reference 5, eqn. (8). This convention is made so as to distinguish between the voltage drop caused by a current in a branch and voltage rise caused by a source.
† See Reference 2, proof of theorem 9.

*Corollary.*—The necessary and sufficient condition for an $(s \times s)$ matrix K to be an RIM of a tree network with $t = s + 1$ nodes (and $s$ branches) is that K is a non-singular matrix satisfying conditions (*a*) and (*b*).*

(ii) The necessary and sufficient condition for an $(s \times b)$ matrix W to be a CSM of a network with $t = s + 1$ nodes and $b$ branches corresponding to a system of tree-branch voltages $(U)$ is that, possibly after some permutation of its columns, W may be presented in the form

$$W = [S, -I] = -K^{-1}[L, K] \quad . \quad . \quad (11)$$

where K and $[L, K]$ are RIM's of a tree and a connected network respectively. The RIM of the network and the tree of $U$ voltages 'realizing' W are then $[L, K]$ and K respectively.†

(iii) The necessary and sufficient condition for an $(f \times b)$ matrix C to be the LM of a network with $t = b - f + 1$ nodes and $b$ branches corresponding to a system of link currents is that, possibly after some permutation of its columns, C may be presented in the form

$$C = [I, R] = [K', L'](K^{-1})' \quad . \quad . \quad . \quad (12)$$

where K and $[L, K]$ are RIM's of a tree and a connected network respectively. The RIM of the network and the system of links 'realizing' C are $[L, -K]$ and L respectively.‡

(iv) The necessary and sufficient condition for an $(s \times b)$ matrix W to be a CSM of a network with $t = s + 1$ nodes and $b$ branches corresponding to a system $(U)$ of node pairs is that

$$W = -K^{-1}Q \quad . \quad . \quad . \quad . \quad (13)$$

where K and Q are RIM's of a tree and a connected network respectively. The RIM's of the network and of the tree of the node-pair voltages $U$ 'realizing' W are then Q and K respectively.

For the proof it suffices to add to the network the 'branches' of the system $U$ which form a tree and then apply (ii) to the augmented network.

**(7) THE IMPEDANCE AND ADMITTANCE MATRICES OF *n*-PORTS**

The relation

$$V = -W'U \quad . \quad . \quad . \quad . \quad . \quad (14)$$

between the $(b \times 1)$ vector $V$ of branch voltages and the $(s \times 1)$ vector $U$ of some system of independent node-pair voltages involving the CSM W leads to the relation[8]

$$Y_s = WGW' \quad . \quad . \quad . \quad . \quad . \quad (15)$$

where $Y_s$ is the admittance matrix of the $s$-port corresponding to the chosen system of $s$ node pairs, and G is the branch admittance matrix of the network. Both matrices W and G should, of course, correspond to the same ordering of branches. From eqn. (15) the impedance matrix $Z_s$ of that $s$-port is

$$Z_s = (WGW')^{-1} \quad . \quad . \quad . \quad . \quad (16)$$

In the case where an $n$-port with $n < s$ is described on the network we can look upon it as if in the $s$-port including this $n$-port§ the remaining $s - n$ ports have been open-circuited. Its impedance matrix $Z_n$ is therefore the $(n \times n)$ principal sub-matrix of $Z_s$ obtained after crossing out the rows and columns corresponding to the open-circuited ports.

If the network under consideration is without mutual couplings, G is diagonal and its elements are the elementary admittances $1/R$, $1/pL$ and $pC$. But, conversely, suppose that an $(n \times n)$

* See Reference 4, theorem 12.
† See Reference 2, p. 360, matrix $A_1$.
‡ See Reference 2, theorem 12.
§ See Reference 2, lemma 1.3.

matrix Z can be presented as a principal submatrix of a matrix $(WGW')^{-1}$ with G diagonal and having as elements the elementary admittances, and W satisfying condition (iv) of Section 6. Then, after building the graph and the $s$-port 'realizing' W, as has been indicated in (iv) of Section 6, we introduce the values of the elementary admittances given by G into the branches of the graph and finally open-circuit those ports which do not enter into the submatrix Z. The $n$-port obtained in this way has for its impedance matrix the given matrix Z. Thus the above conditions are also sufficient.

Similarly the relation

$$J = C'I \quad . \quad . \quad . \quad . \quad . \quad (17)$$

between the $(b \times 1)$ vector $J$ of the branch currents and the $(f \times 1)$ vector $I$ of independent link currents involving the LM C leads to the relation

$$Z_f = CDC' \quad . \quad . \quad . \quad . \quad . \quad (18)$$

where $Z_f$ is the impedance matrix of the $f$-port inscribed into the network, and D is the branch impedance matrix. The admittance matrix of the same $f$-port is then

$$Y_f = (CDC')^{-1} \quad . \quad . \quad . \quad . \quad (19)$$

Similarly to the previous case, if an $n$-port with $n < f$ is inscribed into the network, we can consider it as being obtained by short-circuiting in the $f$-port containing it the remaining $f - n$ ports. Its admittance matrix $Y_n$ is thus the $(n \times n)$ principal submatrix of $Y_f$ after deleting the rows and columns corresponding to the short-circuited ports.

Exactly as in the previous case, if a matrix Y can be presented as a principal submatrix of a matrix $(CDC')^{-1}$ with D diagonal and having for elements the elementary impedances $R$, $pL$, and $1/pC$ and the matrix C satisfying condition (iii) of Section 6, then, after building the graph and the inscribed $f$-port 'realizing' C, as indicated in (iii) of Section 6, we insert into the branches of the graph the values of the elementary impedances given by the matrix D and short-circuit those ports which do not enter into Y. The $n$-port obtained in this way has for its admittance matrix the given matrix Y. Thus the above conditions also are sufficient.

It must, however, be pointed out that the distinction between multi-ports described on and inscribed into a network is rather a formal one. Any $n$-port inscribed into a network $N$ may be looked on as an $n$-port described on the network which can be obtained from $N$ if the $n$ links carrying the ports are cut off from one node and remain hinged at the other one. Similarly any $n$-port described on a network $N$ may be looked on as an $n$-port inscribed into the network augmented by $n$ short-circuiting links corresponding to the ports of the $n$-port. Thus the terms 'described' or 'inscribed' are meaningful only in relation to the network from which the multi-port has been derived, but if the 'parent' network is unknown any multi-port may be looked on as belonging to both those kinds.

Combining thus the results of this Section we have:
(i) The necessary and sufficient conditions for a matrix to be an impedance or an admittance matrix of an RLC $n$-port without mutual inductance are that it is a principal submatrix of a matrix $(WGW')^{-1}$ or $(CDC')^{-1}$, where G and D are diagonal matrices with elements $a$, $bp$, $c/p$ ($a, b, c > 0$), and W and C satisfy the conditions for CSM or LM corresponding to an adequate system of node-pair voltages or link currents respectively.

Grouping together in G and D the branches of the same kind we have

$$G = G_1 + pG_2 + \frac{1}{p}G_3 \quad . \quad . \quad . \quad . \quad (20)$$

and

$$D = D_1 + \frac{1}{p}D_2 + pD_3 \quad . \quad . \quad . \quad (21)$$

where $(G_1, D_1)$, $(G_2, D_2)$ and $(G_3, D_3)$ correspond to the resistive capacitive and inductive branches respectively.*

As a corollary of (i) we have:
(ii) The necessary and sufficient condition for a matrix t represent an $R$, $RL$ or $LC$ $n$-port without mutual inductance is that a presentation of that matrix satisfying (i) may be foun where, in addition, in the direct sums (20) or (21) the onl matrices present are those with the suffixes 1, 1 and 2, 1 and or 2 and 3 respectively.

Where the network contains mutual inductances the matrice $G_3$ and $D_3$ in eqns. (20) and (21) cease to be diagonal. $G_3$ an $D_3$, however, are always symmetric and positive definite. Con versely, having a matrix, say, $CDC'$ with C being the LM a link system and D presentable in the form (21), where $D_1$ an $D_2$ are positive diagonal and $D_3$ symmetric and positive definit we can construct the graph together with the inscribed $f$-po corresponding to C. Let us then introduce the impedanc corresponding to the diagonal elements of D into the branche of the graph. Any non-zero element $d_{kj}$ ($k \neq j$) of the matrix (which may occur only in $D_3$) can be afterwards realized as mutual inductance between the branches $k$ and $j$, and since $D$ is positive definite, this will in all cases lead to physically possib couplings. Thus we have:

(iii) The necessary and sufficient condition for a matrix t be an impedance or admittance matrix of an RLCM $n$-po without ideal transformers is that it is a principal submatr of a matrix $(WGW')^{-1}$ or $(CDC')^{-1}$, where G and D are dire sums (20) and (21) with $G_1$, $G_2$ and $D_1$, $D_2$ positive diagon and $G_3$ and $D_3$ symmetric and positive definite, and W and satisfy the same conditions as in (i).

Remark.—The given $(n \times n)$ impedance or admittance matr of an $n$-port may be a principal submatrix of many matrices the form $(WGW')^{-1}$ or $(CDC')^{-1}$. The networks correspondir to all such presentations are equivalent with respect to the por of the $n$-port.

Example.—Synthesis of a pure resistance 3-port with th impedance matrix

$$Z_3 = \frac{1}{24} \begin{bmatrix} 12 & 6 & 0 \\ 6 & 13 & 8 \\ 0 & 8 & 16 \end{bmatrix}$$

According to (i) and (ii), this matrix should be presented as principal submatrix of some matrix $(WGW')^{-1}$ with G positiv diagonal (with constant elements).

Let us take, for example,

$$(WGW')^{-1} = Z_4 = \begin{bmatrix} 12 & 6 & 0 & 0 \\ 6 & 13 & 8 & -4 \\ 0 & 8 & 16 & -8 \\ 0 & -4 & -8 & 16 \end{bmatrix} \frac{1}{24}$$

After inversion we obtain

$$WGW' = Y_4 = \begin{bmatrix} 3 & -2 & 1 & 0 \\ -2 & 4 & -2 & 0 \\ 1 & -2 & 3 & 1 \\ 0 & 0 & 1 & 2 \end{bmatrix}$$

* The sign $+$ denotes the direct sum of two matrices defined by
$$A + B = \begin{vmatrix} A, & 0 \\ 0, & B \end{vmatrix}$$

This matrix may be decomposed as follows

$$WGW' = Y_4 = \begin{bmatrix} -1 & 0 & 0 & 0 & 1 & 1 & 0 \\ 0 & -1 & -1 & 0 & -1 & -1 & 0 \\ 0 & 1 & 0 & 0 & 1 & 0 & 1 \\ 0 & 0 & 0 & -1 & 0 & 0 & 1 \end{bmatrix} \text{diag } (1, 1, 1, 1, 1, 1, 1) \begin{bmatrix} -1 & 0 & 0 & 0 \\ 0 & -1 & 1 & 0 \\ 0 & -1 & 0 & 0 \\ 0 & 0 & 0 & -1 \\ 1 & -1 & 1 & 0 \\ 1 & -1 & 0 & 0 \\ 0 & 0 & 1 & 1 \end{bmatrix}$$

with the identification

$$W = \begin{bmatrix} -1 & 0 & 0 & 0 & 1 & 1 & 0 \\ 0 & -1 & -1 & 0 & -1 & -1 & 0 \\ 0 & 1 & 0 & 0 & 1 & 0 & 1 \\ 0 & 0 & 0 & -1 & 0 & 0 & 1 \end{bmatrix} \text{ and } G = \text{diag.} (1, 1, 1, 1, 1, 1, 1)$$

The matrix W, according to (iv) of Section 6, is then presented as

$$W = \begin{bmatrix} 1 & 1 & 0 & 0 \\ 0 & 0 & 1 & -1 \\ 0 & -1 & -1 & 0 \\ -1 & 0 & 0 & 0 \end{bmatrix}^{-1} \times \begin{bmatrix} -1 & -1 & -1 & 0 & 0 & 0 & 0 \\ 0 & 1 & 0 & 1 & 1 & 0 & 0 \\ 0 & 0 & 1 & 0 & 0 & 1 & -1 \\ 1 & 0 & 0 & 0 & -1 & -1 & 0 \end{bmatrix}$$

where the first and the second factor in this product satisfy the conditions of Section 6 for an RIM of a tree and a connected network respectively. The graph and the 4-port corresponding to the CSM W may be immediately constructed (Fig. 1). Open-circuiting the port 4 corresponding to the row and column which do not appear in $Z_3$, and introducing the values of the
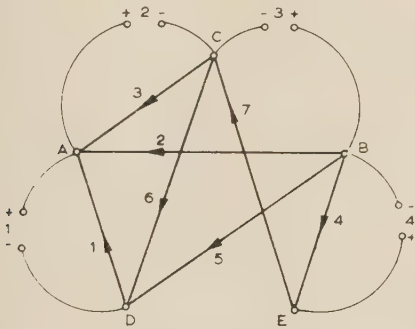


**Fig. 1.**—The linear graph and the 4-port described on it corresponding to the given CSM.
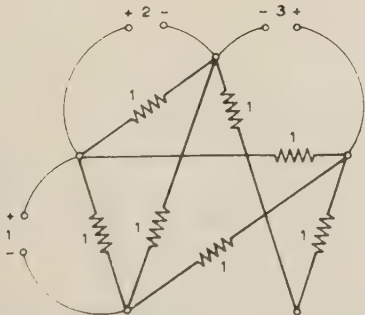


**Fig. 2.**—The 3-port network with the impedance matrix $Z_3$.

branch admittance matrix G leaves us with the 3-port Fig. 2, whose impedance matrix is the given matrix $Z_3$.*

Although no procedure can yet be given for tackling a given matrix to test whether it can be presented in one of the forms required by the above theorems, nevertheless they lead to important conclusions which will be the subject of the following discussion.

## (8) DUAL NETWORKS

Suppose that a matrix M fulfils the conditions for the impedance matrix of an *n*-port without mutual couplings being a principal submatrix of a matrix $(WGW')^{-1}$, and let W correspond to a set of tree-branch voltages of a planar network N. On the geometrically dual network $\bar{N}$ the matrix $W = \bar{C}$, where $\bar{C}$ is the LM corresponding to the system of links dual to the tree on N (provided that the dual branches of N and $\bar{N}$ have the same indices and appropriate orientations). If the duality is both geometrical and electrical, the dual branches have reciprocal values and the branch impedance matrix $\bar{D}$ on $\bar{N}$ is equal to G. Thus we have

$$WGW' = \bar{C}\bar{D}\bar{C}'$$

and M, being a submatrix of $(\bar{C}\bar{D}\bar{C}')^{-1}$, is also an admittance matrix of the *n*-port obtained on the dual network $\bar{N}$ by short-circuiting the $s - n$ ports which do not belong to the *n*-port considered.

This discussion shows that the impedance matrix of an *n*-port based on a network which remains planar if all the *n*-ports are short-circuited is the admittance matrix of the dual *n*-port. Thus the class of matrices which may be the impedance as well as the admittance matrices of multi-ports is not empty.

In the case where the *n*-port realizing W is based on a non-planar network N, there does not exist the geometric dual[9] of N, and although an electrical dual may be constructed,[10] it requires in general the use of ideal transformers. But it is an unsolved problem if, among all networks equivalent to N with respect to the *n*-ports, there cannot exist some network remaining planar when the ports are short-circuited and which does not contain ideal transformers. If such a network exists then the matrix M, as before, will be the admittance matrix of the dual network. There are, however, strong indications that there exist impedance matrices which are not admittance matrices, and vice versa.

## (9) M-MATRICES

The family of matrices K which may be presented in the form

$$K = ADA' \quad . \quad . \quad . \quad . \quad . \quad (22)$$

* From Fig. 2 it can be readily observed that branches 4 and 7 may be replaced by one branch or that $Z_3$ may be presented in the form $(W_1G_1W_1')^{-1}$ by putting

$$W_1 = \begin{bmatrix} -1 & 0 & 0 & 0 & 1 & 1 \\ 0 & -1 & -1 & 0 & -1 & -1 \\ 0 & 1 & 0 & 1 & 1 & 0 \end{bmatrix} \text{and } G_1 = \text{diag } (1, 1, 1, 1/2, 1, 1)$$

where the decomposition

$$W_1 = -\begin{bmatrix} -1 & -1 & 0 \\ 0 & 1 & 1 \\ 0 & 0 & -1 \end{bmatrix}^{-1} \times \begin{bmatrix} -1 & -1 & -1 & 0 & 0 & 0 \\ 0 & 1 & 0 & -1 & 0 & 1 \\ 0 & 1 & 0 & 1 & 1 & 0 \end{bmatrix}$$

shows that $W_1$ satisfies the conditions (iv) of Section 6. In this simpler solution, however, not all steps of the general procedure would be illustrated.

where D is diagonal with constant and positive elements and A is an E-matrix, is of considerable interest. As follows from the previous results, the impedance and admittance matrices of purely resistive networks are necessarily submatrices of matrices whose inverses belong to that family. We shall prove that:

(i) Each principal minor of the matrix K = ADA', with D diagonal with constant and positive elements and A an E-matrix, is not less in magnitude than any other minor built from the same rows (or columns).

*Proof.*—Let us call a symmetric matrix with constant real elements each of whose principal minors is not less than the modulus of any other minor built from the same rows (or columns) an M-matrix.*

Let the $(n \times s)$ matrix A be equal to $(a_{ij})$, where $i = 1, 2, 3, \ldots, n$ and $j = 1, 2, \ldots, s$; let $D = \mathrm{diag}\,(d_1, d_2, \ldots, d_s)$; and let $K = (k_{ij})$, where $i, j = 1, 2, \ldots, n$. Then, as can be readily seen, we have

$$k_{11} = a_{11}^2 d_{11} + a_{12}^2 d_2 + \ldots + a_{1s}^2 d_s \quad . \quad . \quad . \quad (23)$$

$$k_{12} = a_{11}a_{21}d_1 + a_{12}a_{22}d_2 + \ldots + a_{1s}a_{2s}d_s \quad . \quad . \quad (24)$$

and generally

$$k_{ij} = a_{i1}a_{j1}d_1 + a_{i2}a_{j2}d_2 + \ldots + a_{is}a_{js}d_s \quad . \quad . \quad (25)$$

By comparing eqns. (23) and (24), taking into account that all $a_{ij}$ are equal to 1, −1 or 0, and all $d_i$ are positive, we see that all terms of (23) are not less than the moduli of the corresponding terms of (24); therefore we have $k_{11} \geqslant |k_{12}|$. Applying the same arguments to other elements of the matrix K, we obtain

$$k_{ii} \geqslant |k_{ij}| \text{ for } i, j = 1, 2, \ldots, n \quad . \quad . \quad . \quad (26)$$

Since, by the Binet–Cauchy theorem,† the compound of a product of matrices is equal to the product of their compounds, we have for the $h$th compound, from eqn. (22),

$$K^{(h)} = A^{(h)}D^{(h)}A^{(h)\prime} \quad . \quad . \quad . \quad (27)$$

Since A is an E-matrix, all elements of $A^{(h)}$ are 1, −1 or 0, while all elements of $D^{(h)}$ are positive. Thus, by the same reasoning as above, each element on the main diagonal of $K^{(h)}$ is not less than the modulus of any other element of the same row (or column). But the element on the main diagonal of $K^{(h)}$ is a principal minor of order $h$ of K, while other elements in the same row (or column) of $K^{(h)}$ are equal to other minors of order $h$ built from the same rows (or columns) of K. Thus the proof is complete.

Of course, we have evidently:

(ii) Any principal submatrix of an M-matrix is an M-matrix.

By application of Jacobi's theorem to the inverse of a non-singular M-matrix, and noting that the complementary minors of principal minors are themselves principal, and the complements of non-principal minors occupy similar non-principal positions, we have:

(iii) The inverse of a non-singular M-matrix is an M-matrix.

If K is a non-singular M-matrix the set of equations

$$KX = Y \quad . \quad . \quad . \quad . \quad . \quad (28)$$

where X and Y are $(n \times 1)$ column vectors with the co-ordinates

$x_i$ and $y_i$ respectively, exhibits a feature which may be called the 'no-amplification property'. Namely:

(iv) If we choose some $r$ $y$'s, say, $y_{i1}, y_{i2}, \ldots, y_{i(r)}$ and some $n - r - l$ $x$'s, say, $x_{i(r+2)}, x_{i(r+3)}, \ldots, x_{i(n)}$ equal to zero and $x_{i(r+1)} > 0$, the indices $i_1, i_2, \ldots, i_n$ being some permutation of $1, 2, \ldots, n$, then we have

(a) $|x_{i(j)}| \leqslant x_{i(r+1)}$ \qquad for $j = 1, 2, \ldots, r$

(b) $y_{i(r+1)} > 0$

(c) $|y_{i(j)}| \leqslant y_{i(r+1)}$ \qquad for $J = r + 2, r + 3, \ldots, n.$‡

## (10) NECESSARY CONDITIONS FOR MATRICES REPRESENTING $n$-PORTS WITHOUT IDEAL TRANSFORMERS

In a paper quoted above[11] the author has obtained necessary conditions for a matrix representing an $n$-port without ideal transformers using physical arguments (the no-amplification property of pure-resistance networks). Here similar conditions (in a sharper form*) are deduced by means of analytical reasoning.

Since any CSM and LM of the simple systems discussed are E-matrices (cf. Section 5), from (i), (iii) and (ii) of the previous Section there follows immediately:

(i) A necessary condition for a matrix to be an impedance or admittance matrix of a pure-resistance $n$-port is that it is a non-singular $(n \times n)$ M-matrix.

Since an $RLC$ network without mutual inductances has, for positive real values of the complex variable, the same properties as an $R$-network[12, 13] we have:

(ii) A necessary condition for a matrix to be an impedance or admittance matrix of an $RLC$ $n$-port without mutual inductances is that it is a symmetric, rational in $p$, positive real $(n \times n)$ matrix, which for all real positive values of $p$ fulfils the condition of (i).

Finally, a general linear reciprocal network which may contain mutual inductances but does not contain ideal transformers behaves at zero frequency like an $R$-network. Since, however, some (or all) elements of the impedance or admittance matrix may have a pole at zero frequency, by applying the same reasoning as in Reference 11, we have:

(iii) A necessary condition for a matrix to be the impedance or admittance matrix of a general linear reciprocal $n$-port without ideal transformers is that it is a symmetric, rational in $p$, positive real $(n \times n)$ matrix which for $p = 0$ has the property that all its finite non-singular principal submatrices fulfil the condition of (i).

*Remark* 1.—Since the impedance and admittance matrices (Z, Y) of an $R$ $n$-port are necessarily non-singular M-matrices, the equations

$$ZI = V \text{ and } YV = I$$

are of the type discussed under (iv) of the previous Section. The results of (iv) show that if a current or voltage is applied to some port $(r + 1)$ while the other ports are either short- or open-circuited, then the current in the short-circuited ports, or the voltage at the open-circuited ports, cannot be greater than the current or voltage at the port where the excitation is applied. The no-amplification property of pure-resistance networks is thus proved by our discussion.

*Remark* 2.—The necessary conditions given in this Section do not distinguish between the impedance and admittance matrices as do the necessary and sufficient conditions of Section 7.

## (11) CONCLUSION

The work given in this paper suggests that further research is needed if a comprehensive method of $n$-port synthesis without

---

* See Reference 11. In that paper we have called an M-matrix a matrix any principal minor of which is not smaller than the modulus of any minor obtained by replacing only one of its rows (or columns) by another row (or column) of that matrix. Here the conditions for an M-matrix are sharper, since more than one (or even all) rows (or columns) of the principal minor may be replaced by other rows (or columns) of the matrix.

† See Reference 6, p. 93.

‡ For proof see Reference 11, p. 181.

ideal transformers is to be found. First a procedure for testing whether a matrix with constant elements may be presented as a principal submatrix of a matrix $(ADA')^{-1}$ should be found. Then we should be able to answer the question whether the matrix A satisfies the conditions for a CSM or LM corresponding to the simple co-ordinate systems (Section 6), which requires further decompositions in terms of RIM's. This solves the simplest problem of $R$ *n*-ports. The practical solution of *RC*, *RL*, *RLC* and *RLCM n*-ports requires still greater efforts. The author feels, however, that by the approach presented in this paper those difficult problems can be attacked with some hope of a final solution.

## (12) ACKNOWLEDGMENTS

## (13) REFERENCES

(1) DARLINGTON, S.: 'A Survey of Network Realization Techniques', *Transactions of the Institute of Radio Engineers Professional Group on Circuit Theory*, 1955, CT–2, p. 291.

(2) SESHU, S.: 'Topological Considerations in the Design of Driving-Point Functions', *ibid.*, 1955, CT–2, p. 356.

(3) GUILLEMIN, E. A.: 'Introductory Circuit Theory' (Wiley, New York, 1953), p. 10.

(4) REED, M. B., and SESHU, S.: 'On Topology and Network Theory', *Proceedings of the University of Illinois Symposium on Circuit Analysis*, 1955, p. 2–1.

(5) CEDERBAUM, I.: 'Invariance and Mutual Relations of Electrical Network Determinants', *Journal of Mathematics and Physics*, 1956, **34**, p. 236.

(6) AITKEN, A. C.: 'Determinants and Matrices' (Oliver and Boyd, Edinburgh and London, 1951), p. 99.

(7) VEBLEN, O., and FRANKLIN, PH.: 'On Matrices whose Elements are Integers', *Annals of Mathematics*, 1921–22, **23**, p. 1.

(8) KRON, G.: 'Tensor Analysis of Networks' (Wiley, New York, 1939), p. 102.

(9) WHITNEY, H.: 'Non-Separable and Planar Graphs', *Transactions of the American Mathematical Society*, 1932, **34**, p. 339.

(10) BLOCH, A.: 'On Methods for the Construction of Networks Dual to "Non-Planar" Networks', *Proceedings of the Physical Society*, 1946, **58**, p. 677.

(11) CEDERBAUM, I.: 'On Networks Without Ideal Transformers', *Transactions of the Institute of Radio Engineers Professional Group on Circuit Theory*, 1956, CT–3, p. 179.

(12) REZA, F. M., and LEWIS, P. M.: 'A Note on the Transfer Voltage Ratio of Passive *RLC* Networks', *Proceedings of the Institute of Radio Engineers*, 1954, **42**, p. 1452.

(13) TALBOT, A.: 'Some Fundamental Properties of Networks without Mutual Inductance', *Proceedings I.E.E.*, Monograph No. 118 R, January, 1955 (**102** C, p. 168).

# EXCITATION OF SURFACE WAVES

## By B. FRIEDMAN and W. ELWYN WILLIAMS.

### SUMMARY

It is shown how to locate a dipole source above a dielectric surface so as either to produce as pure a surface wave as possible or to maximize the amount of energy carried by the surface wave.

### LIST OF SYMBOLS

$A$ = Amplitude of the direct plane wave.
$E$ = Electric field intensity.
$F(\phi)$ = Radiation pattern.
$H$ = Magnetic field intensity.
$H_y$ = Field component.
$H_y^*$ = Complex conjugate of $H_y$.
$H_\phi$ = Field component.
$h_1$ = Optimum height above the surface.
$h_2$ = Height of source.
$k_0$ = Wave number.
$L$ = Differential operator.
$q(z)$ = Function depending on permittivity of the medium.
$R$ = Radial distance.
$u(z)$ = Representation of waves in vertical direction.
$X(k)$ = Reactance of the guiding surface.
$Z$ = Impedance at interface.
$Z(k)$ = Impedance of the guiding surface.
$Z_0$ = Characteristic impedance of free space.
$\gamma$ = Phase change on reflection from interface.
$\epsilon$ = Permittivity.
$\epsilon_0$ = Permittivity of free space.
$\mu$ = Permeability.
$\rho(k)$ = Reflection coefficient.

### (1) INTRODUCTION

Since the appearance of Sommerfeld's classical paper[1] on the field produced by a dipole above a plane dielectric earth, a considerable amount of attention has been devoted to the problem of the excitation of surface waves over dielectric surfaces. The two questions which are of practical importance are these: to determine under what conditions a surface wave exists, and, if it exists, to determine the type of source which is its most efficient generator.

These problems have been considered both by Kay[2] and one of the present authors,[3] and it has been shown that the surface wave and the radiation field terms may be obtained from a knowledge of the far-field radiation pattern of the original source distribution. From these results it is theoretically possible to combine sources with different far-field patterns in order to determine the most suitable source distribution for generating surface waves. Since this approach requires a large amount of tedious numerical work, it seems desirable to attack the problem in a more analytic manner.

This has been done by Cullen,[4] Brick,[5] and Fernando and Barlow[6] in a series of recent papers. Cullen considers the excitation of surface waves by a horizontal slot placed above a plane surface on which an impedance type of boundary condition holds. For a reactive-type boundary condition it is known that a surface wave exists. Cullen discusses two different criteria for determining that height of source above the ground plane which is most efficient in exciting the surface wave. By the first criterion the most efficient source is that which produces an almost pure surface wave (this concept will be explained later) near the guiding surface. By the second criterion the most efficient source is the one which produces a field such that the ratio of energy per unit area of wavefront in the surface wave to the sum of energy per unit area of wavefront in the radiated field and the surface wave is a maximum. Cullen obtains values of the optimum source height for each of these criteria. However, when discussing the second criterion, he finds it necessary to use numerical methods and thus obtains the optimum source height only for one particular value of the surface impedance.

The present work was suggested by Cullen's paper, but it is more general than the previous work in that both 2- and 3-dimensional problems are investigated and a more general type of guiding surface is employed. The surface is assumed to be a slab of dielectric resting on a ground plane on which an impedance-type boundary condition holds. The dielectric need not be homogeneous; in fact, it may consist of layers of different materials, but we assume that the permittivity of the dielectric varies only in the direction perpendicular to the ground plane. When investigating the field produced by a source above this guiding surface, we find it desirable to expand the source into plane waves of all wavelengths in a direction *perpendicular* to the ground plane and not in a *parallel* direction, as Cullen does. With our type of expansion we find that the only property of the guiding surface we need is its impedance $Z(k)$ to an incoming normally incident plane wave of wave number $k$. The optimum height $h_1$ above the surface at which a slot must be placed to provide a nearly pure surface wave is then determined to be

$$h_1 = \frac{Z_0}{k_0 X(0)}$$

where $k_0$ is the wave number, $Z_0$ the characteristic impedance of free space, and where we put

$$Z(k) = R(k) + jX(k)$$

so that $X(k)$ is the reactance of the guiding surface. This result is a generalization of that obtained by Cullen.

We consider also a second criterion for launching efficiency which differs from that proposed by Cullen. The criterion is as follows: that height of source, $h_2$, is most efficient for which the energy in the radiated field per unit area of wavefront is a minimum. If $Z(k)$ is purely reactive we find that $h_2$ is given by the following formula:

$$h_2 = \frac{\sqrt{2}}{k_0} \operatorname{arc\,cot}\left[\frac{\sqrt{2}}{jZ_0} Z\left(\frac{k_0}{\sqrt{2}}\right)\right]$$

In the case considered by Cullen these two criteria give practically the same results for $h_2$ as those he obtained.

The formula for finding the most efficient launching height $h_2$ may be given the following physical interpretation: consider a plane wave with wave number $k_0$ travelling toward the interface in a direction making an angle of 45° with the vertical; then $h_2$ is that height at which the total field produced by this wave and the reflected wave is a minimum.

## (2) MATHEMATICAL FORMULATION

Consider a ground plane at $z = -z_0$ and suppose that the permittivity of the medium above it depends on the $z$-co-ordinate only. For example, the medium might be a dielectric slab from $z = -z_0$ to $z = 0$ and then free space from $z = 0$ to $z = \infty$; or the medium might be composed of layers of dielectric of arbitrary thickness and permittivity from $z = -z_0$ to $z = 0$ and free space above; or the permittivity of the medium might vary continuously with height from $z = -z_0$ to $z = 0$ and again have free space above. In all cases we shall assume that the medium between $z = 0$ and $z = \infty$ is free space and that it contains a source of electromagnetic radiation. Finally, we assume that the electromagnetic field satisfies an impedance-type boundary condition at the ground plane $z = -z_0$.

We shall treat both a 2- and 3-dimensional problem simultaneously with the help of the following co-ordinate systems:

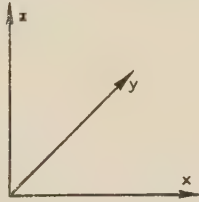In Fig. 1 the source of the electromagnetic field is a magnetic



Fig. 1.—Co-ordinate system for Case I.

line dipole placed at $z = h$, $x = a$ and extended parallel to the $y$-axis. Because of the geometry, the field produced will be independent of $y$. We shall call this the 2-dimensional problem and denote it by Case I.

In Fig. 2 the source is a circular magnetic dipole located at $z = h$, $r = a$. Because of the geometry, the field produced will be independent of $\phi$. We shall call this the 3-dimensional problem and denote it by Case II. In both cases we shall assume a time factor of the form $\epsilon^{j\omega t}$.

The simple-harmonic form for Maxwell's equations is

$$\text{curl } H = -j\omega\epsilon E$$

$$\text{curl } E = j\omega\mu H$$

where $E$, $H$ are the electric and magnetic field intensities and $\epsilon$ and $\mu$ are the permittivity and magnetic permeability. Note that, by assumption, $\epsilon$ is a function of $z$ and $\mu$ is a constant.

In Case I, because the source is a magnetic line dipole, the field is completely determined by the value of $H_y$. We have

$$H_x = E_y = H_z = 0$$

and

$$E_x = (-j\omega\epsilon)^{-1}\frac{\partial H_y}{\partial z}$$

$$E_z = (-j\omega\epsilon)^{-1}\frac{\partial H_y}{\partial z}$$

The field component $H_y$ satisfies the equation

$$\frac{\partial^2 H_y}{\partial x^2} + \epsilon\frac{\partial}{\partial z}\left(\frac{1}{\epsilon}\frac{\partial H_y}{\partial z}\right) + \omega^2\epsilon\mu H_y = \delta(z - h)\delta(x - a) \quad (1)$$
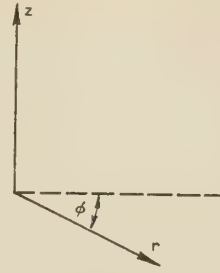


Fig. 2.—Co-ordinate system for Case II.

Put $H_y = \epsilon^{1/2}H_y'$ and eqn. (1) becomes

$$\frac{\partial^2 H_y'}{\partial x^2} + \frac{\partial^2 H_y'}{\partial z^2} + \omega^2\epsilon'\mu H_y' = \frac{1}{\sqrt{\epsilon}}\delta(z - h)\delta(x - a) \quad (2)$$

where

$$\omega^2\epsilon'\mu = \omega^2\epsilon\mu + \frac{1}{2\epsilon}\left[\frac{d^2\epsilon}{dz^2} - \frac{3}{2}\left(\frac{d\epsilon}{dz}\right)^2\right] \quad (3)$$

In Case II, because of our assumption about the source, the field will be completely determined by the value of $H_\phi$. We have

$$H_z = H_r = E_\phi = 0$$

and

$$E_r = (j\omega\epsilon)^{-1}\frac{\partial H_\phi}{\partial z}$$

$$E_z = (j\omega\epsilon)^{-1}r^{-1}\frac{\partial}{\partial r}(rH_\phi)$$

The field component $H_\phi$ will satisfy the equation

$$\frac{\partial^2 H_\phi}{\partial r^2} + \frac{1}{r}\frac{\partial H_\phi}{\partial r} + \left(\omega^2\epsilon\mu - \frac{1}{r^2}\right)H_\phi + \epsilon\frac{\partial}{\partial z}\left(\frac{1}{\epsilon}\frac{\partial H_\phi}{\partial z}\right)$$
$$= \frac{\delta(z - h)\delta(r - a)}{2\pi r} \quad (4)$$

Put $H_\phi = \epsilon^{1/2}H_\phi'$ and the following equation is obtained:

$$\frac{\partial^2 H_\phi'}{\partial z^2} + \frac{\partial^2 H_\phi'}{\partial r^2} + \frac{1}{r}\frac{\partial H_\phi'}{\partial r} + \left(\omega^2\epsilon'\mu - \frac{1}{r^2}\right)H_\phi = \frac{\delta(z - h)\delta(r - a)}{2\pi r\epsilon^{1/2}} \quad (5)$$

where $\epsilon'$ is defined by eqn. (3).

We set $\omega^2\epsilon'\mu = \omega^2\epsilon_0\mu - q(z) = k_0^2 - q(z)$

where $\epsilon_0$ is the permittivity of free space. Note that, by our assumption, $q(z) = 0$ if $z > 0$. If we denote the operator $q(z) - \partial^2/\partial z^2$ by $L$, the formal solution of eqn. (2) is

$$H_y' = \epsilon^{-1/2}\frac{\exp\left[j\sqrt{(k_0^2 - L)}|x - a|\right]}{2j\sqrt{(k_2^2 - L)}}\delta(z - h) \quad (6)$$

and the corresponding formal solution of eqn. (5) is

$$H_\phi' = \frac{\epsilon^{-1/2}}{4j}J_1[\sqrt{(k_0^2 - L)}a]H_1^{(1)}[\sqrt{(k_0^2 - L)}r]\delta(z - h), r > a \quad (7)$$

These results will be interpreted in the following Section.

## (3) INTERPRETATION OF SOLUTION

To interpret eqns. (6) and (7) it is necessary to express $\delta(z - h)$ in terms of the eigenfunctions of the operator $L$.

Consider the eigenvalue problem

$$Lu(z) = -\frac{d^2u}{dz^2} + q(z)u = \lambda u \quad (8)$$

where $u(z)$ satisfies the given impedance-type boundary condition at $z = -z_0$. If $q(z)$ and the impedance-type boundary condition at $z = -z_0$ are real, there may exist negative values of $\lambda$ such that eqn. (8) has a non-zero solution satisfying the given boundary condition at $z = -z_0$. If $q(z)$ (or the impedance-type boundary condition) is not real, there may exist complex values of $\lambda$ with negative real parts such that eqn. (8) has a non-zero solution satisfying the given boundary condition at $z = -z_0$. In either case we shall denote these values of $\lambda$ by $\lambda_n$ and the corresponding normalized solution of eqn. (8) by $u(z, \lambda_n)$. Note that $u(z, \lambda_n)$ vanishes exponentially as $z \to \infty$.

Every positive value of $\lambda$ will be in the continuous spectrum of the operator $L$. Put $\lambda = k^2$ and denote by $u(z, k)$ that solution of eqn. (8) which satisfies the boundary condition at $z = -z_0$ and which as $z \to \infty$ has the asymptotic form

$$u(z, k) \simeq \varepsilon^{-jkz} + \rho(k)\varepsilon^{jkz} \quad . \quad . \quad . \quad (9)$$

Here $\rho(k)$ is the reflection coefficient for the incoming plane wave $\varepsilon^{-jkz}$ incident on the dielectric at $z = 0$. Since $q(z) = 0$ for $z > 0$, formula (9) is an equality for $z > 0$. We have[7]

$$\delta(z - h) = \sum_n u(z, \lambda_n)u(h, \lambda_n) + \frac{1}{2\pi}\int_0^\infty u(z, k)\overline{u(h, k)}dk \quad (10)$$

Here $\overline{u(z, k)}$ is that solution of eqn. (8) satisfying the boundary condition at $z = -z_0$, which for $z > 0$ has the form

$$\overline{u(z, k)} = \varepsilon^{jkz} + \rho(-k)\varepsilon^{-jkz} \quad . \quad . \quad . \quad (11)$$

If $q(z)$ and the impedance-type boundary condition at $z = -z_0$ are real, the value of $\rho(-k)$ is the complex conjugate of the value of $\rho(k)$ and hence $\overline{u(z, k)}$ is the complex conjugate of $u(z, k)$. However, in all cases, comparison of eqns. (9) and (11) shows that $\rho(-k) = \rho(k)^{-1}$.

If the expression (10) is substituted in eqns. (6) and (7), and if we use the fact that $u$ satisfies eqn. (8), we get the following:

$$H'_y = \frac{\varepsilon^{-1/2}}{2j}\sum_n \frac{\exp\left[j\sqrt{(k_0^2 - \lambda_n)}|x - a|\right]}{\sqrt{(k_0^2 - \lambda_n)}}u(z, \lambda_n)u(h, \lambda_n)$$

$$+ \frac{\varepsilon^{-1/2}}{4\pi j}\int_0^\infty \frac{\exp\left[j\sqrt{(k_0^2 - k^2)}|x - a|\right]}{\sqrt{(k_0^2 - k^2)}}u(z, k)\overline{u(h, k)}dk \quad . \quad (12)$$

$$H'_\phi = \frac{\varepsilon^{-1/2}}{4j}\sum_n J_1[\sqrt{(k_0^2 - \lambda_n)}a]H_1^{(1)}[\sqrt{(k_0^2 - \lambda_n)}r]u(z, \lambda_n)u(h, \lambda_n)$$

$$+ \frac{\varepsilon^{-1/2}}{8\pi j}\int_0^\infty J_1[\sqrt{(k_0^2 - k^2)}a]H_1^{(1)}[\sqrt{(k_0^2 - k^2)}r]u(z, k)\overline{u(h, k)}dk$$

$$\quad . \quad . \quad . \quad (13)$$

The first term on the right-hand side of eqn. (12) or (13) represents the surface wave, whereas the integral term in these equations represents the radiation field. These formulae show that the existence of a surface wave depends on the existence of eigenvalues of eqn. (18) with negative real parts. Thus existence depends only on the value of $q(z)$ and the impedance-type boundary condition at the ground plane, i.e. only on the electromagnetic properties of the medium in the $z$-direction and not on the type of source.

### (4) ASYMPTOTIC BEHAVIOUR OF THE FIELD

We shall obtain the asymptotic behaviour of the integrals in eqns. (12) and (13) and from these obtain the asymptotic value of the electromagnetic field components.

Using eqns. (9) and (11), we see that

$$u(z, k)\overline{u(h, k)} = \varepsilon^{-jk(z-h)} + \varepsilon^{jk(z+h)}$$
$$+ \rho(k)\varepsilon^{jk(z+h)} + \rho(-k)\varepsilon^{-jk(z+h)}$$

Putting this expression into eqns. (12) and (13), we find that in Case I the integral term becomes

$$\int_{-\infty}^\infty \frac{\exp\left[j\sqrt{(k_0^2 - k^2)}|x - a|\right]}{\sqrt{(k_0^2 - k^2)}}\left[\varepsilon^{+jk(z-h)} + \rho(k)\varepsilon^{jk(z+h)}\right]dk$$
$$\quad . \quad . \quad . \quad (12a)$$

whereas in Case II it is

$$\int_{-\infty}^\infty J_1[\sqrt{(k_0^2 - k^2)}a]H_1^{(1)}[\sqrt{(k_0^2 - k^2)}r]\left[\varepsilon^{+jk(z-h)}\right.$$
$$\left. + \rho(k)\varepsilon^{jk(z+h)}\right]dk \quad . \quad . \quad . \quad (13a)$$

The method of stationary phase will be used to obtain asymptotic expressions for these integrals. In Case I we put

$$x - a = R\cos\theta \qquad z = R\sin\theta$$

but in Case II we put

$$r = R\cos\theta \qquad z = R\sin\theta$$

For large values of $R$, the integral in eqn. (12) is asymptotically

$$\frac{\varepsilon^{-1/2}}{\sqrt{(8\pi)}}\frac{\varepsilon^{j\left(k_0R - \frac{\pi}{4}\right)}}{\sqrt{(k_0R)}}\left[\varepsilon^{-ik_0h\sin\theta} + \rho(k_0\sin\theta)\varepsilon^{+ik_0h\sin\theta}\right] \quad . \quad (14)$$

and the integral in eqn. (13) is asymptotically

$$\frac{\varepsilon^{-1/2}}{4\pi}\frac{\varepsilon^{j\left(k_0R - \frac{3\pi}{4}\right)}}{k_0R}J_1(k_0a\cos\theta)\left[\varepsilon^{-jk_0h\sin\theta} + \rho(k_0\sin\theta)\varepsilon^{+jk_0h\sin\theta}\right]$$
$$\quad . \quad . \quad . \quad (15)$$

Expressions (14) and (15) are essentially the radiation field parts of $H_y$ and $H_\phi$, respectively. We now consider the value of the radiation field on the surface of the slab, at large distance from the source, i.e. at $z = 0$ but $R \gg 0$. In this case $\theta$ approaches zero and we can show that the expression in brackets in eqns. (14) and (15) approaches zero. This indicates that at $z = 0$ the asymptotic expression for the radiation field is no longer given by eqns. (14) and (15).

We shall obtain the correct asymptotic formula for the radiation field on the surface of the slab for $R$ large by evaluating the integrals in eqns. (12) and (13) in a different manner. However, first we evaluate $\rho(k_0\sin\theta)$.

At the interface $z = 0$, between the dielectric slab and free space, the ratio $E_x/H_y$ or $E_r/H_\phi$ must be continuous. Denote this ratio by $Z(k)$;

then

$$(j\omega\epsilon)^{-1}\frac{\partial H_y}{\partial z}\bigg/ H_y = Z(k)$$

or

$$\frac{1}{u}\frac{du}{dz}\bigg|_{z=0} = j\omega\epsilon Z(k) = \frac{ik_0}{Z_0}Z(k) \quad . \quad . \quad . \quad (16)$$

where $Z_0$ is the characteristic impedance of free space. Note that $Z(k)$ is the impedance at the interface to an incoming wave $\varepsilon^{-jkz}$. For convenience, we shall sometimes write this impedance as $Z$. For $z > 0$ we have

$$u(z, k) = \varepsilon^{-jkz} + \rho(k)\varepsilon^{jkz}$$

Then by (16),

$$\frac{1 - \rho}{1 + \rho} = -\frac{k_0Z}{kZ_0}$$

$$\rho = \cfrac{\dfrac{k}{k_0} + \dfrac{Z}{Z_0}}{\dfrac{k}{k_0} - \dfrac{Z}{Z_0}}$$

Finally  $\qquad \rho(k_0 \sin \theta) = \cfrac{\sin \theta + \dfrac{Z(k_0 \sin \theta)}{Z_0}}{\sin \theta - \dfrac{Z(k_0 \sin \theta)}{Z_0}}$   . . . . (17)

From this formula it is clear that if $Z(0) \neq 0$, the value of $\rho(k_0 \sin \theta)$ approaches $-1$ as $\theta$ approaches zero and therefore the bracketed expression in eqns. (14) and (15) approaches zero. Also, from (17),

$$\rho(k_0 \sin \theta) = -1 - \frac{2Z_0}{Z(0)} \sin \theta$$

for small values of $\theta$.   Then

$$u(z, k_0 \sin \theta) = \varepsilon^{-jk_0 z \sin \theta} + \rho(k_0 \sin \theta)\varepsilon^{jk_0 z \sin \theta}$$

$$= -\frac{2 \sin \theta}{k_0}\left[\frac{Z_0}{Z(0)} + jk_0 z\right]$$

We shall denote the bracketed expression in this formula by $u_1(z)$.

Let us return to the integrals in eqns. (12) and (13) and consider their asymptotic behaviour for large values of $x$ or $r$. When we make the change of variables

$$k^2 = k_0^2 - \beta^2$$

we have

$$\frac{dk}{\sqrt{(k_0^2 - k^2)}} = \frac{d\beta}{\sqrt{(k_0^2 - \beta^2)}}$$

Therefore the resulting integrand becomes infinite at $\beta = k_0$, i.e. at $k = 0$.   This indicates that the asymptotic behaviour of the integrals in eqns. (12) and (13) can be obtained by expanding the integrand in powers of $k$.   In this way we find that the integral in Case I is

$$\sqrt{\frac{2}{\pi}} \frac{Z_0}{Z(0)} \frac{\varepsilon^{j\left(k_0|x-a| - \frac{\pi}{4}\right)}}{k_0|x - a|^{3/2}} u_1(z)u_1(h) \quad . \quad . \quad . \quad (18)$$

and in Case II it is

$$\frac{1}{4\pi} \frac{J_1(k_0 a)}{k_0^2} \frac{Z_0}{Z(0)} \frac{\varepsilon^{j\left(k_0 r - \frac{3\pi}{4}\right)}}{r^2} u_1(z)u_1(h)$$

If we choose $u_1(h)$ such that $u_1(h) = 0$, then clearly both expressions for the radiation field will vanish. This means that, to obtain as pure a surface wave as possible on the interface, we must require the height $h$ of the source to be such that

$$k_0 h = \frac{jZ_0}{Z(0)} \quad . \quad . \quad . \quad . \quad . \quad (19)$$

Since the source is always above the interface, i.e. $h > 0$, formula (19) shows that a surface wave will exist only if $Z$ is a positive reactance. If $Z$ is complex, formula (19) gives a complex value for $h$, which means that at no real height will $u_1(h) = 0$. However, if we put $Z = R + jX$, a surface wave can exist only if $X > 0$ and we see that $|u_1(h)|$ will be a minimum at that height $h$ for which

$$k_0 h = +\frac{Z_0}{X(0)} \quad . \quad . \quad . \quad . \quad . \quad (20)$$

### (5)  COMPARISON  OF  POWER

In this Section we compare the radiated power to that in the surface wave. For simplicity we shall restrict ourselves to Case I. Similar results can be obtained for Case II.

From eqn. (12) the amplitude of one surface wave term in $H_y$ is

$$(2j)^{-1}\frac{\varepsilon^{j\sqrt{(k_0^2 - \lambda_1)}|x - a|}}{\sqrt{(k_0^2 - \lambda_1)}} u(z, \lambda_1)u(h, \lambda_1) \quad . \quad . \quad (21)$$

Note that

$$u(z, \lambda_1) = (2j\sqrt{\lambda_1})^{1/2}\varepsilon^{j\sqrt{(\lambda_1)}z} \qquad (z > 0) \quad . \quad . \quad (22)$$

The $x$-component of the average power is

$$\tfrac{1}{2}\mathscr{R}(j\omega\epsilon)^{-1}\int_0^\infty \frac{\partial H_y}{\partial x}H_y^* dz \quad . \quad . \quad . \quad . \quad (23)$$

where $H_y^*$ is the complex conjugate of $H_y$.

Since power orthogonality between surface wave and radiated field occurs only when $\lambda_1$ is real, we shall assume henceforth that $\lambda_1$ is real. Then, applying (23) to (21), we find that the average power in the surface wave is

$$\frac{\beta}{8\sqrt{(k_0^2 + \beta^2)}}\varepsilon^{-2\varrho h} \quad . \quad . \quad . \quad . \quad (24)$$

if $\lambda_1 = -\beta^2$.

To find the radiated power per unit area of wavefront we must evaluate

$$\tfrac{1}{2}\mathscr{R}\int_0^{\pi/2} H_y^* E_\theta d\theta$$

or, since

$$E_\theta = (j\omega\epsilon)^{-1}\frac{\partial H_y}{\partial r}$$

we must evaluate $\quad \tfrac{1}{2}\mathscr{R}(j\omega\epsilon)^{-1}\int_0^{\pi/2}\frac{\partial H_y}{\partial r}H_y^* d\theta$

Using eqn. (14) multiplied by $\epsilon^{1/2}$ for the amplitude of the radiated field in $H_y$, we find that the radiated power per unit width of wavefront is

$$\frac{(\omega\epsilon)^{-1}}{16\pi k_0}\int_0^{\pi/2}\left[\varepsilon^{-jk_0 h \sin \theta} + \rho(k_0 \sin \theta)\varepsilon^{jk_0 h \sin \theta}\right]$$

$$\left[\varepsilon^{jk_0 h \sin \theta} + \rho(-k_0 \sin \theta)\varepsilon^{-jk_0 h \sin \theta}\right]d\theta$$

$$. \quad . \quad . \quad . \quad (25)$$

If we assume $Z$ is purely reactive and constant for all $k$, we shall get Cullen's results. Put $Z = j\alpha Z_0$;

then, from (17), $\qquad \rho(k_0 \sin \theta) = \dfrac{j \sin \theta - \alpha}{j \sin \theta + \alpha}$

and eqn. (25) becomes $\qquad (16\pi\omega\epsilon k_0)^{-1}I(h, h)$

where $\quad I(h, h) = \displaystyle\int_0^{\pi/2}\left[\varepsilon^{-jk_0 h \sin \theta} - \frac{\alpha - j \sin \theta}{\alpha + j \sin \theta}\varepsilon^{jk_0 h \sin \theta}\right]$

$$\left[\varepsilon^{jk_0 h \sin \theta} - \frac{\alpha + j \sin \theta}{\alpha - j \sin \theta}\varepsilon^{jk_0 h \sin \theta}\right]d\theta \quad . \quad . \quad (26)$$

It is easy to show that

$$I(h, h') = 2\int_0^{\pi/2}\left\{\cos\left[k_0(h - h')\sin \theta\right]\right.$$

$$\left. + 2\,\mathscr{R}\frac{j \sin \theta + \alpha}{j \sin \theta - \alpha}\varepsilon^{-jk_0 \sin \theta(h + h')}\right\}d\theta$$

$$= \pi J_0[k_0(h - h')] + \pi J_0[k_0(h + h')]$$

$$-\pi \int_0^\infty 2k_0\alpha\varepsilon^{-k_0\alpha t}J_0\{k_0[t-(h+h')]\}dt$$

$$=\pi\left\{J_0[k_0(h-h')]+J_0[k_0(h+h')]\right.$$

$$\left.-\frac{2\alpha\varepsilon^{-2k_0\alpha k}}{\sqrt{(1+\alpha^2)}}-2\alpha\varepsilon^{-2k_0\alpha h}\int_0^{2k_0\alpha h}\varepsilon^t J_0\left(\frac{t}{\alpha}\right)dt\right\}\quad . \quad . \quad (27)$$

The last integral is fairly easy to compute numerically for various values of $\alpha$ and $\beta = 2k_0\alpha h$. It was found that the values of $I(h, h)$ so obtained are very closely approximated by the $\pi/2$ times the value of the integrand at $\pi/4$.
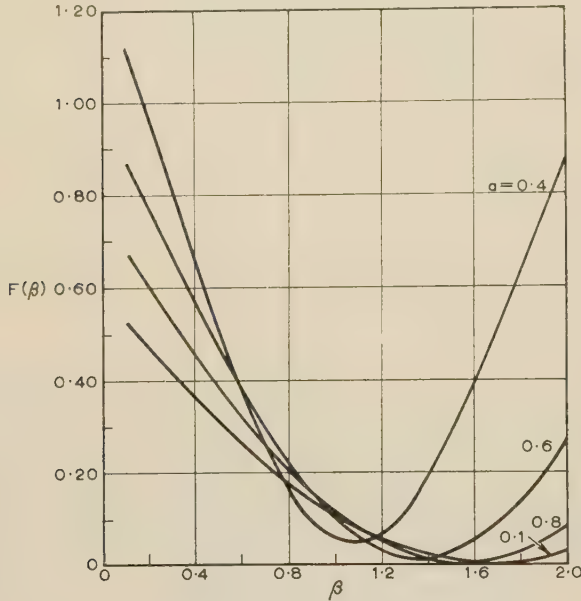


Fig. 3.—Graph of $F(\beta)$.

In Figs. 3 and 4 we have graphed for various values of $\alpha$ the functions

$$F(\beta) = 1 + J_0\left(\frac{\beta}{\alpha}\right) - \frac{2\alpha\varepsilon^{-\beta}}{\sqrt{(1+\alpha^2)}} - 2\varepsilon^{-\beta}\int_0^\beta \varepsilon^t J_0\left(\frac{t}{\alpha}\right)d\alpha$$

and $\quad g(\beta) = \dfrac{1}{\pi}\left[\dfrac{2(1-2\alpha^2)}{1+2\alpha^2}\cos\left(\dfrac{\beta}{\alpha\sqrt{2}}\right) - \dfrac{4\alpha\sqrt{2}}{1+2\alpha^2}\sin\left(\dfrac{\beta}{\alpha\sqrt{2}}\right)\right]$

Here $\beta = 2k_0\alpha h$, $F(\beta) = \dfrac{1}{\pi}I(h, h)$, and $2 + \pi g(\beta)$ is the value of the integrand in eqn. (26) for $\theta = \pi/4$. By our approximation, we should have

$$F(\beta) = 1 + \frac{\pi}{2}g(\beta)$$

The graphs show that this relation is satisfied very closely.

When this approximation is used in eqn. (25), the radiated power per unit area of wavefront becomes

$$(16\pi k_0\omega\epsilon)^{-1}[2 + 2\cos 2(k_0\sin h + \gamma)]$$

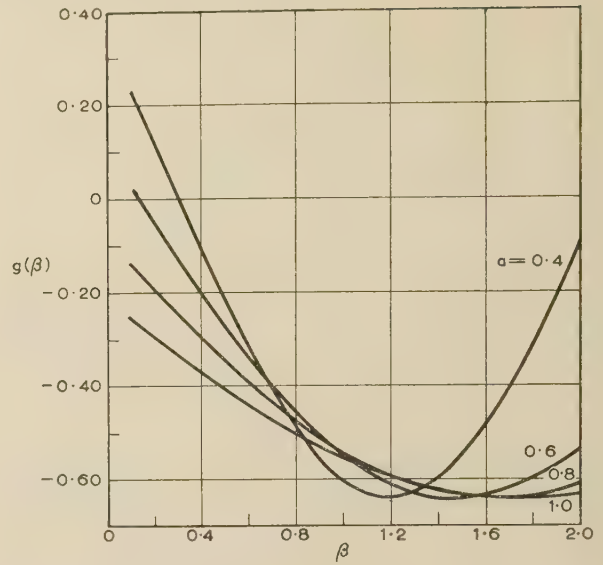where $\quad\tan\gamma = \dfrac{\alpha}{\sin\pi/4} = (\sqrt{2})\alpha$



Fig. 4.—Graph of $g(\beta)$.

Note that $\gamma$ is the phase change on reflection from the interface. From this formula we see that the radiated power will be a minimum if $k_0\sin h + \gamma = \pi/2$,

i.e. if $\qquad k_0h = \sqrt{2}\cot^{-1}(\sqrt{2})\alpha$ . . . . . (28)

For $\alpha = \frac{1}{2}$, this formula gives $k_0h = 1\cdot35$, which agrees fairly well with the value $1\cdot26$ found by Cullen. Table 1 compares the value for $k_0h$ found by using eqn. (28) with those found by numerical integration of eqn. (27).

Table 1

| $\alpha$ | 0·2 | 0·4 | 0·6 | 0·8 | 1·0 |
|---|---|---|---|---|---|
| $k_0h$ from (27) | 1·62 | 1·37 | 1·13 | 0·94 | 0·82 |
| $k_0h$ from (28) | 1·83 | 1·47 | 1·23 | 1·02 | 0·88 |

We conclude that for values of $\alpha \geqslant 0\cdot4$, the value $h$ of the most efficient launching height as computed from the approximate formula (28) is within $10\%$ of the height as computed exactly from eqn. (27).

## (6) PHYSICAL INTERPRETATION AND CONCLUSIONS

Suppose that the dielectric material extends from $z = -z_0$ to $z = 0$ and that there is free space for $z > 0$. The field produced by a horizontal magnetic slot parallel to the $y$-axis and passing through the point $z = h$, $x = a$ can be expressed in terms of $H_y$ as follows:

$$\left.\begin{aligned} H &= (0, H_y, 0)\\ E &= (j\omega\epsilon)^{-1}\left(\frac{\partial}{\partial z}, 0, -\frac{\partial}{\partial x}\right)H_y \end{aligned}\right\}\quad . \quad . \quad (29)$$

There are two methods for obtaining $H_y$. One, which Cullen uses, is to expand the source in terms of waves travelling along the $x$-axis. The other, which is used in this paper, is to expand the source in terms of waves which come in and are reflected along the $z$-axis.

Suppose that a wave $\varepsilon^{-jkz}$ comes in along the $z$-axis. Because of the presence of the dielectric, this will produce a reflected wave $\rho(k)\varepsilon^{jkz}$ for $z > 0$. Here $k$ will be any real number from

0 to ∞. However, if the source is oscillating with frequency $\omega$, thus producing waves whose wave number in free space is $k_0$, then the incoming wave will be

$$\varepsilon^{-jkz} \exp\left[j\sqrt{(k_0^2 - k^2)}|x - a|\right]$$

and the reflected wave will be

$$\rho(k)\varepsilon^{jkz} \exp\left[j\sqrt{(k_0^2 - k^2)}|x - a|\right]$$

Notice that this may be interpreted as a wave coming in at an angle $\theta$ to the $x$-axis and then reflected (Fig. 5). Here $\sin\theta = k/k_0$.
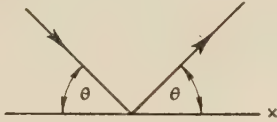


**Fig. 5.**—Reflection of waves from $x$-axis.

When we take into account the fact that the source produces plane waves travelling in all directions we find [see eqn. (12a)] that $H_y$ contains a term proportional to

$$\int_{-\infty}^{\infty} \frac{\exp\left[j\sqrt{(k_0^2 - k^2)}|x - a|\right]\varepsilon^{jk(z-h)}}{\sqrt{(k_0^2 - k^2)}}dk$$

$$+ \int_{-\infty}^{\infty} \rho(k)\frac{\exp\left[j\sqrt{(k_0^2 - k^2)}|x - a|\right]\varepsilon^{jk(z+h)}}{\sqrt{(k_0^2 - k^2)}}dk \quad . \quad (30)$$

The first integral is just the field that would be produced by the source in free space if the dielectric were not present, and the second is the reflected field that is produced by the dielectric. The sum of these two integrals will give the radiation field.

Let us consider $\rho(k)$. For $k = k_1$, a complex number with a positive imaginary part, it may happen that $\rho(k_1)$ is infinite. This value of $k$ produces a surface wave and we have in $H_y$ [see eqn. (12)] a term proportional to

$$\exp\left[j\sqrt{(k_0^2 - k_1^2)}|x - a|\right]\varepsilon^{jk_1z}\varepsilon^{jk_1h} \qquad (z > 0)$$

Notice that, because the imaginary part of $k_1$ is positive, this expression represents a wave which travels along the $x$-axis more slowly than light and is exponentially attenuated in the $z$-direction. This behaviour is typical of surface waves.

From eqn. (14) the radiation field at large distances $R$ from the source and in the direction $\theta$ to the $x$-axis is proportional to

$$\frac{\varepsilon^{jk_0R}}{\sqrt{(k_1R)}}\left[\varepsilon^{-jk_0h\sin\theta} + \rho(k_0\sin\theta)\varepsilon^{jk_0h\sin\theta}\right]$$

Using this we find [see eqn. (25)] that the radiated power per unit area of wavefront is proportional to

$$\int_0^{\pi/2} |1 + \rho(k_0\sin\theta)\varepsilon^{2jk_0h\sin\theta}|^2 d\theta \quad . \quad . \quad (31)$$

This formula may be given a simple physical interpretation. The field produced by the source may be decomposed into plane waves travelling in all directions. Those which travel in the direction $-\theta$ are reflected back to the height $h$ of the source with a reflection factor $\rho(k_0\sin\theta)\varepsilon^{2jk_0h\sin\theta}$. The total field at a distance $R$, then, is the sum of the direct plane wave whose amplitude is $A$, say, and the reflected plane wave with amplitude $A\rho(k_0\sin\theta)\varepsilon^{2jk_0h\sin\theta}$. The total energy power in the wavefront is the integral of the square of the absolute value of the field, and in this way we get eqn. (31).

Put $\rho = |\rho|\varepsilon^{+2j\gamma}$, where $|\rho|$ and $\gamma$ are real. Using this, we find that the radiation pattern $F(\theta)$ is given by

$$F(\theta) = |\varepsilon^{-jk_0h\sin\theta} + |\rho|\varepsilon^{j(k_0h\sin\theta + 2\gamma)}|$$

$$= [1 + |\rho|^2 + 2|\rho| \cos 2(k_0h\sin\theta + \gamma)]^{1/2} \quad . \quad (32)$$

Note that the value of the reflection coefficient can be obtained from the impedance of the dielectric to an incoming wave $\varepsilon^{-jkx}$. We have, from eqn. (17),

$$\rho(k_0\sin\theta) = \frac{\sin\theta + \dfrac{Z(k_0\sin\theta)}{Z_0}}{\sin\theta - \dfrac{Z(k_0\sin\theta)}{Z_0}} \quad . \quad . \quad . \quad (33)$$

If $Z$ is a pure reactance, this formula shows that $|\rho| = 1$, and a knowledge of the far-field pattern $F(\theta)$ enables us to obtain $\gamma$ and thus also $\rho(k_0\sin\theta)$. Theoretically, this information about $\rho$ permits us to obtain the values of $\theta$ for which $\rho(k_0\sin\theta) = \infty$, i.e. for which surface waves exist. This agrees with the results in References 2 and 3. However, in practice it is very difficult to find the surface wave in this way because the far-field pattern gives the values of $\rho(k_0\sin\theta)$ for real angles $\theta$, whereas a surface wave corresponds to complex angles $\theta$.

A glance at the diagrams will show that, at least in the case where $Z$ is a constant reactance, the radiated power per unit area of wavefront is approximately proportional to $F(\theta)^2$ evaluated at $\theta = \pi/4$. Using this approximation, we can determine the height $h_2$ for which the radiated power per unit area of wavefront is a minimum. We find

$$k_0h_2 \sin\frac{\pi}{4} + \gamma = \frac{\pi}{2}$$

or

$$h_2 = \frac{\sqrt{2}}{k_0}\left(\frac{\pi}{2} - \gamma\right)$$

Since, with a pure reactance, $\gamma = \tan^{-1}\dfrac{X}{Z_0 \sin\dfrac{\pi}{4}}$, we get [see eqn. (28)]

$$h_2 = \frac{\sqrt{2}}{k_0}\cot^{-1}\left(\sqrt{2}\frac{X}{Z_0}\right)$$

Going back to the physical interpretation of eqn. (31), we can interpret $h_2$ as follows:

*The height of source $h_2$ at which the radiated power per unit area of wavefront is a minimum is approximately the height at which there is complete interference, i.e. zero amplitude for the sum of the direct and reflected waves travelling in the 45°-direction to the interface.*

For experimental purposes it is useful to be able to produce a field which is as pure a surface wave as possible. Since the surface wave attenuates exponentially in a direction perpendicular to the interface, we consider the field at a point on the interface at a distance $x$ from the source. From eqn. (12) the $H_y$-component produced by the surface wave is

$$\frac{1}{2j}\frac{\varepsilon^{j\sqrt{(k_0^2 - \lambda_1)}x}}{\sqrt{(k_0^2 - \lambda_1)}}u(0, \lambda_1)u(h, \lambda_1)$$

whereas from eqn. (18) the $H_y$ component produced by the radiation field is

$$\sqrt{\frac{2}{\pi}\frac{Z_0}{Z(0)}}\frac{\exp\left[j\left(k_0|x| - \dfrac{\pi}{4}\right)\right]}{k_0|x|^{3/2}}u_1(0)u_1(h)$$

plus terms of order $|x|^{-5/2}$.

By proper choice of the launching height, the above term in

the radiation field of order $|x|^{-3/2}$ can be made zero, and therefore the total field, which is the sum of the surface wave and the radiation field, becomes, at least at large distances from the source, very nearly a pure surface wave. The height at which this term in the radiation field vanishes is given by eqn. (19) as

$$h = \frac{jZ_0}{k_0 Z(0)} \qquad . \qquad . \qquad . \qquad . \qquad (34)$$

### (7) REFERENCES

(1) SOMMERFELD, A.: 'Über die Ausbreitung der Wellen in der drahtlosen Telegraphis', *Annalen der Physik*, Fourth Series, 1909, **28**, p. 665, and Fourth Series, 1926, **81**, p. 1135.
(2) KAY, A.: 'The Excitation of Surface Waves in Multilayered Media', Final Report Section No. 1, Technical Research Group, New York, October, 1954.
(3) WILLIAMS, W. E.: 'Reflection and Refraction of Electromagnetic Waves by a Dielectric Slab between Dielectric Media', New York University, Institute of Mathematical Sciences, Division of Electromagnetic Research, Research Report No. EM-70, November, 1954.
(4) CULLEN, A. L.: 'The Excitation of Plane Surface Waves', *Proceedings I.E.E.*, Monograph No. 93 R, February, 1954 (**101**, Part IV, p. 225).
(5) BRICK, D. B.: 'The Radiation of a Hertzian Dipole over a Coated Conductor,' *ibid.*, Monograph No. 113 R, December, 1954 (**102** C, p. 392).
(6) FERNANDO, W. M. G., and BARLOW, H. E. M.: 'An Investigation of the Properties of Radial Cylindrical Surface Waves launched over Flat Reactive Surfaces', *ibid.*, Paper No. 2009 R, May, 1956 (**103** B, p. 307).
(7) FRIEDMAN, B.: 'Principles and Techniques of Applied Mathematics' (Wiley, 1956), Chap. 4.

# THE NETWORK SYNTHESIS ON THE INSERTION-LOSS BASIS

## By J. ZDUNEK, Dipl.Ing.

### SUMMARY

A unified and concise exposition is provided of the general insertion-loss filter theory. Methods of synthesis of most important network functions are derived in terms of the prescribed steady-state network performance; also realization procedures are explained and expressed in terms of explicit formulae for direct application to the design of conventional ladder structures with an arbitrary number of branches.

Two particular cases are solved in detail, namely the symmetrical and the inverse-impedance, low-pass networks, which are both unified in a single mathematical treatment. Such unification enables one to consider both of them as one general case of a low-pass analogue ladder structure.

Special emphasis is given to the Cauer–Darlington method of synthesis of networks whose insertion-loss response approximates, in Chebyshev's sense, to that of the ideal wave filter; however, Taylor's approximation (maximally flat response) and the constant-$k$ filters are also included.

In the case of the maximally flat and the Chebyshev pass-band approximation, important explicit formulae for the ladder components are derived for a network with an arbitrary number of branches and an arbitrary termination ratio. These components (ladder coefficients) are thus directly computable from the required discrimination characteristics or the reflection factor, and from the bandwidth specifications.

### LIST OF PRINCIPAL SYMBOLS

$\mathrm{T}, \Pi$ = The two main classes of network structure (also used as subscripts).

$\mathscr{P}, V, I,$ = Power, voltage, current (these occur with subscripts).

$D$ = Discrimination (also with subscripts).

$\mathrm{A}_a, \mathrm{A}_p$ = Insertion loss at extremal points.

$\mathrm{B}_a, \mathrm{B}_p$ = Bandwidth at extremal points.

$u = u_{\pm s}, u_{os}, u_{ns}, u'_{e(n)}.$
 = Arguments of Jacobi's elliptic functions.

$t$ = Transformer ratio.

$r$ = Resistance ratio.

$H, L, a, b, c, d, h$ = Arbitrary constants.

$q, q_L$ = Elliptic modular constants.

$A, B, A', B', \bar{A}, \bar{B}, N,$
$N', P, S, T, U$ = Polynomials in $p$ or in $\Omega$. ($p = j\Omega$, $p_{\pm s} = -\alpha_s \pm j\Omega_s$).

$G, R, Q = 1/d, L, C$ = Network elements and their properties.

$s, n, [n/2], k, r, q$ = Integers.

$u_0, u_\infty, u_{qr}, v_{qr}, w_{qr}$ = Auxiliary quantities occurring in the calculation of network elements.

$\bar{U}_r, \bar{V}_r, \overline{W}_r$ = Auxiliary constants defining ladder coefficients occurring in Section 3.6 only.

$W_{e(n)}, \vartheta_{e(n)}$ = Auxiliary quantities.

$I_{e(n)}$ = An integral defined in eqns. (268) and (269).

$F(\Omega)$ = Function or polynomial in $\Omega$.

$f$ = Frequency.

$\mathbf{A}, \mathbf{B}, \mathbf{C}, \mathbf{D}$ = Chain matrix parameters.

$\nu$ = Number of sections.

$n$ = Number of branches.

$\delta_{qr}$ = Kronecker's delta.

$\vartheta_0 = \alpha_0$ = Real root of the discrimination function.

$\rho_s, \alpha_s$ = Modulus and real part of roots of insertion-loss function.

$\gamma_s$ = Poles of design impedance or admittance.

$\zeta_s$ = Reciprocals of poles of insertion-loss function.

$\theta$ = Arguments of circular and hyperbolic functions.

$\eta$ = Efficiency.

$\Phi, \phi, \psi, \Xi, \Lambda$ = Network characteristic functions.

$\Gamma$ = Reflection factor.

$\Omega, \bar{\Omega}, \tilde{\Omega}$ = Normalized frequencies.

$\check{\Omega} = \omega/\omega_0$.

$\mathscr{F}, \mathscr{A}, \mathscr{B}, \mathscr{R}$ = Polynomials in $\zeta = -1/p^2$.

$\mathscr{A}_s, \mathscr{B}_s, \mathscr{R}_s, \mathscr{D}_s$ = Coefficients of polynomials in $\zeta$.

$\mathscr{H}_{qr}, \mathscr{U}_s, \mathscr{W}_s, \mathscr{V}_s$ = Parameters derived from $\mathscr{F}(\zeta)$.

$\mathfrak{M}, \mathfrak{T}$ = Operators.

$\mathbf{R}, \mathbf{I}$ = Real and imaginary parts of complex quantities.

$o(n) = \frac{1}{2}[1 - (-1)^n].$

$e(n) = \frac{1}{2}[1 + (-1)^n].$

### (1) INTRODUCTION

Among the many engineering problems of to-day, the synthesis of electric networks is an outstanding one of great importance in both heavy and light-current engineering. From the early days of electrical engineering science, the analysis of electric circuits was the only known way of attacking electrical engineering problems. Since the last war, however, the advance of the art of synthesis has been so marked that it appears that further study in this field may well result eventually in adding to the art of network synthesis a consistent procedure whereby the cut-and-try methods of yesterday will be replaced by well-systematized experiment and computation.

The synthesis problem consists in finding the network itself when its performance is specified. This broad definition resolves itself into two separate problems: to find the mathematical form of the network response function; and to find the network itself. The second problem has no unique solution; it is usually possible to find several networks that will yield the same performance. However, with additional stipulations regarding, say, the phase response or the minimum number of elements to be used or the particular network pattern, e.g. the ladder structure, the lattice, etc., the problem is susceptible of a straightforward solution by known methods. The first problem, that of finding the network function when the performance of the network is specified, is less straightforward,[1] although an approximate solution may be obtained experimentally by means of the potential analogue method.

The network performance can be specified in many ways, but

Correspondence on Monographs is invited for consideration with a view to publication.

Mr. Zdunek is with Marconi's Wireless Telegraph Co. Ltd.

all of them reduce to the following statements. In the case of two-terminal networks, the performance is completely specified by one network function, i.e. the network impedance function defined over the whole frequency range. In the case of four-terminal networks, three functions must be specified in order that the structure may be uniquely determined. In the special case of symmetrical four-terminal networks, only two functions are required.

In all the above cases the network impedance functions (self and transfer) are uniquely specified by their real, or by their imaginary, parts alone, the two parts being Hilbert transforms of one another, and each can be calculated in terms of the other.[2] Since all impedance functions representing lumped-parameter structures are meromorphic, the potential analogue (electrolytic tank) permits of an experimental determination of the real part (or the imaginary part) of an impedance function. The same applies, of course, to the insertion-loss function.

The potential-analogue method (e.g. the electrolytic tank) is of great importance when the performance of the synthesized network cannot be simply identified with any known analytic function of the generalized complex frequency. However, in the case of ordinary filter responses, the empirical search for suitable poles and zeros, and the associated measurements on such a device as an electrolytic tank, can be replaced by known analytic methods, such as those introduced by Cauer,[3] Norton,[4] Darlington,[5] Cocci[6] and others. The present work is based on these methods.

Up to now most of the authors have treated the synthesis of symmetrical and unsymmetrical filter networks as two separate cases. In fact the latter (with Chebýshev's approximation in both the pass band and the attenuation band of the insertion-loss function) are hardly treated in English, except for a few useful lines in Darlington's paper.[5] In the present work the problem of ladder-filter synthesis is treated in such a way that the symmetrical and the inverse-impedance (antimetric) ladders may be designed from common definitions following directly a given procedure. The principal aim is to present a powerful insertion-loss method of network synthesis in a consistent but also directly useful general form. It is believed that the methods of derivation are as important as the final formulae themselves, and for this reason many derivations of formulae are included to display the method of attacking the problem.

The present work is divided into four parts (Sections 2–5) and is followed by an Appendix (Section 9). Section 2 includes the general insertion-loss theory and its relation to the well-known ladder structures regarded as four-terminal networks. In Section 3 important operations, formulae and definitions are derived for use in practical filter computations. Section 4 gives an outline of one of the methods of accounting for the ohmic losses distributed between the inductors and the capacitors of a ladder. Several practical insertion-loss functions are discussed in Section 5; in particular, complete and explicit design formulae for an actual low-pass ladder are given in the case of the maximally-flat and the Chebýshev's approximation in the pass band alone.

Section 9.1 includes the derivation and formulation of the special network functions, namely the Cauer–Darlington insertion-loss functions; this method of derivation can be applied to other functions. The important transformations in the complex-frequency plane also are discussed.

In Section 9.2 some aspects of the derivation of the formulae for ladder coefficients are outlined.

## (2) INSERTION-LOSS THEORY

Insertion-loss theory may be defined as a system of mathematical and physical relations which can be shown to exist between prescribed insertion-loss or discrimination or other related data and the electrical network whose performance or response satisfies these data. Such relations can be demonstrated most readily by recalling the well-known conventional four-terminal network theory, from which useful information concerning the network and its insertion-loss function can be simply established.

### (2.1) General Aspects

A four-terminal (quadripole) network can be defined most concisely by a chain matrix of the form

$$\begin{Vmatrix} A & B \\ C & D \end{Vmatrix} = \frac{1}{Z_{12}} \begin{Vmatrix} Z_{11} & \Delta \\ 1 & Z_{22} \end{Vmatrix} \quad . \quad . \quad . \quad (1)$$

The quadripole under consideration is assumed to be purely reactive, obeying Maxwell's law of reciprocity, i.e. $Z_{12} = Z_{21}$ so that the determinant of the chain matrix (1) is unity.

$$AD - BC = 1 \quad . \quad . \quad . \quad . \quad (2)$$

The impedances $Z_{11}$, $Z_{22}$ and $Z_{12}$ are the self- and transfer impedances of the quadripole and $\Delta$ in eqn. (1) is the determinant of the impedance matrix, defined by $\Delta = Z_{11}Z_{22} - Z_{12}^2$. The quadripole impedances can be identified with the open-circuit impedances. Using the clockwise convention of the loop currents, the open-circuit and the short-circuit impedances are given in terms of the chain-matrix parameters $A$, $B$, $C$ and $D$ by

$$\begin{aligned} Z_{11} &= Z_{1,oc} = \frac{A}{C} & Z_{1,sc} &= \frac{\Delta}{Z_{22}} = \frac{B}{D} \\[2mm] Z_{22} &= Z_{2,oc} = \frac{D}{C} & Z_{2,sc} &= \frac{\Delta}{Z_{11}} = \frac{B}{A} \\[2mm] Z_{12} &= -Z_{12,oc} = \frac{1}{C} & Z_{12,sc} &= \frac{\Delta}{Z_{12}} = B \end{aligned} \Biggr\} \quad . \quad (3)$$

Important relations concerning the conditions of realizability can be derived from eqns. (1), (2) and (3) in the following way

$$\frac{AD-1}{C^2} = \frac{B}{C} = \frac{A}{C}\frac{B}{A} = \frac{D}{C}\frac{B}{D} \quad . \quad . \quad . \quad (4)$$

so that

$$Z_{1,oc}Z_{2,oc} - Z_{12,oc}^2 = Z_{1,oc}Z_{2,sc} = Z_{1,sc}Z_{2,oc} = -Z_{12,oc}Z_{12,sc}$$

The formulae giving the insertion power and voltage ratio are derived by considering in Fig. 1 the quadripole defined in
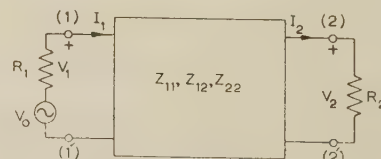


Fig. 1.—Terminated reactive quadripole.

eqn. (1), terminated by prescribed resistances $R_1$ and $R_2$ on the input and the output sides respectively, with one source or generator of e.m.f. $V_0$ in series with $R_1$, so that $R_1$ can be regarded as the internal resistance of the generator subject to the reciprocity theorem. The set of equations for this arrangement may be written in the matrix form

$$\begin{Vmatrix} V_0 \\ 0 \end{Vmatrix} = \begin{Vmatrix} R_1 + Z_{11} & -Z_{12} \\ -Z_{12} & R_2 + Z_{22} \end{Vmatrix} \cdot \begin{Vmatrix} I_1 \\ I_2 \end{Vmatrix} \quad . \quad . \quad (5)$$

The quantities $V_2$ and $V_{20}$ are defined as

$$V_2 = R_2 I_2 = |V_2| \angle \beta_2$$

and

$$V_{20} = \frac{V_0 R_2}{R_1 + R_2} = \frac{R_2}{R_1 + R_2} |V_0| \angle \beta_0 \Bigg\} \quad . \quad (6)$$

From eqns. (1), (5) and (6) the insertion-loss voltage ratio can be expressed in the form

$$\frac{V_{20}}{V_2} = \frac{(R_1 Z_{22} + R_2 Z_{11}) + (R_1 R_2 + Z_{11} Z_{22} - Z_{12}^2)}{(R_1 + R_2) Z_{12}}$$

$$= \left| \frac{V_{20}}{V_2} \right| \angle (\beta_0 - \beta_2). \quad (7)$$

and the fundamental definitions for the power and the efficiency of an electrical network are given by

$$\mathcal{P}_{20\,max} = \frac{|V_0|^2}{4R_1}; \quad \mathcal{P}_{20} = \frac{|V_{20}|^2}{R_2}; \quad \mathcal{P}_2 = \frac{|V_2|^2}{R_2} \leqslant \mathcal{P}_{20\,max}$$

and

$$\frac{\mathcal{P}_{20}}{\mathcal{P}_{20\,max}} = \eta_G - \frac{4R_1 R_2}{(R_1 + R_2)^2} = \frac{4r}{(1 + r)^2}$$

where

$$r = \frac{R_1}{R_2} \text{ or } \frac{R_2}{R_1}; \quad \eta = \frac{\mathcal{P}_2}{\mathcal{P}_{20}} \quad . \quad . \quad . \quad (8)$$

The power must obviously be a positive real function of the frequency. The impedances $Z_{11}$, $Z_{22}$ and $Z_{12}$ are purely reactive and, as follows from Foster's reactance theorem, are odd functions of frequency.

Here, only the low-pass analogue filters will be discussed, so it will be convenient to adopt the use of the normalized frequency variable, $\Omega$, say. The use of this variable is well known, but to avoid any ambiguity we shall now define this variable for particular systems. Thus, for a low-pass system, we define $\Omega$ by

$$\Omega = (\Omega)_{LP} = \frac{\omega}{\omega_B} = \frac{f}{f_B} \quad . \quad . \quad . \quad . \quad (9)$$

where $\omega = 2\pi f$ and $f_B$ may be the cut-off frequency, or any other frequency convenient for normalization. (This factor is discussed in Section 3.1.) In cases other than the low-pass, networks are obtained by means of frequency or, more accurately, impedance transformations. Thus:

for a high-pass, $\quad \Omega = (\Omega)_{HP} = \dfrac{-f_B}{f} \quad . \quad . \quad . \quad . \quad (10)$

for a band-pass, $\quad \Omega = (\Omega)_{BP} = Q_B\left(\dfrac{f}{f_0} - \dfrac{f_0}{f}\right) \quad . \quad . \quad (11)$

for a band-stop, $\quad \Omega = (\Omega)_{BS} = -Q_B^{-1}\left(\dfrac{f}{f_0} - \dfrac{f_0}{f}\right)^{-1}. \quad (12)$

where $f_0$ is the mid-band frequency and $Q_B = f_0/f_B$.

In the band-pass and the band-stop cases we shall restrict our investigations to the responses symmetrical about the mid-band frequency on a logarithmic scale. Thus we shall replace $j\omega$, occurring in the low-pass impedance functions or other low-pass functions, by $j\Omega$, or more simply by $p$, where

$$p = j\Omega \quad . \quad . \quad . \quad . \quad . \quad (13)$$

Defining $\qquad V_{20}/V_2 = \Lambda(p) \quad . \quad . \quad . \quad . \quad (14)$

the insertion-loss power ratio can be written immediately in the form

$$\frac{\mathcal{P}_{20}}{\mathcal{P}_2} = \left| \frac{V_{20}}{V_2} \right|^2 = \Lambda(p)\Lambda(-p) = |\Lambda(p)|^2 = \frac{1}{\eta} \quad . \quad (15)$$

where $|\Lambda(p)|^2$ must be an even, positive and real function for all real frequencies, since $\eta \leqslant \eta_G \leqslant 1$ at all real frequencies and $\mathcal{P}_2 \leqslant \mathcal{P}_{20\,max}$. Hence

$$\frac{\mathcal{P}_{20}}{\mathcal{P}_2} \geqslant \frac{\mathcal{P}_{20}}{\mathcal{P}_{20\,max}}$$

or $\qquad |\Lambda(p)|^2 = \eta^{-1} \geqslant \eta_G \quad . \quad . \quad . \quad . \quad (16)$

must be satisfied at all real frequencies. It is thus logical to try to express the insertion-loss power ratio in eqn. (15) in terms of limiting constant such as $\eta_G$, defined in eqn. (8), which depends only on the termination ratio, and in terms of some even function of frequency, $|\Phi|^2$ say, or $|\Xi(p)|^2$. The logical relation, satisfying eqn. (16), may be written

$$\frac{\mathcal{P}_{20}}{\mathcal{P}_2} = \eta_G + |\Phi|^2 \quad \text{or} \quad \frac{\mathcal{P}_{20}}{\mathcal{P}_2} = \eta_G |\Xi(p)|^2 \quad . \quad . \quad (17)$$

The insertion-loss theory must now be developed in such a way as to give a satisfactory guide to the proper choice of either the function $\Phi$ or $\Xi$, and must provide necessary relations between these functions and the actual network whose power ratio takes the form of eqn. (17). This is the basis for Darlington's method, which has now become classical and is most clear and simple. Following Darlington, we may separate the insertion-loss voltage ratio (7) into two parts, of which one is an even and the other is an odd function. (This can be clearly seen when one remembers that the impedance functions are odd, as shown by Foster, Brune and others.) Thus

$$\left. \begin{array}{l} \dfrac{R_1 Z_{22} + R_2 Z_{11}}{(R_1 + R_2) Z_{12}} = \dfrac{A}{P} \quad \text{an even function} \\[3mm] \dfrac{R_1 R_2 + Z_{11} Z_{22} - Z_{12}^2}{(R_1 + R_2) Z_{12}} = \dfrac{pB}{P} \quad \text{an odd function} \end{array} \right\} . \quad (18)$$

where $A$, $B$ and $P$ are even polynomials in $p$, with real coefficients. The insertion-loss voltage ratio (7) is now given by

$$\frac{V_{20}}{V_2} = \frac{A + pB}{P} = \Lambda(p) \quad . \quad . \quad . \quad (19)$$

$$\beta_0 - \beta_2 = \text{arc tan} \frac{\Omega B}{A} \quad . \quad . \quad . \quad (20)$$

The numerator of $\Lambda(p)$, namely $(A + pB)$, is a Hurwitz polynomial, whose roots have negative real parts and thus lie in the left half of the complex-frequency $p$-plane. From eqns. (7), (18) and (19), the insertion-loss power ratio in eqn. (15) becomes

$$\frac{\mathcal{P}_{20}}{\mathcal{P}_2} = \frac{(R_1 Z_{22} + R_2 Z_{11})^2 - (R_1 R_2 + Z_{11} Z_{22} - Z_{12}^2)^2}{(R_1 + R_2)^2 Z_{12}^2} = \frac{N}{P^2} . \quad (21)$$

where $\qquad N = A^2 - p^2 B^2 \quad . \quad . \quad . \quad . \quad (22)$

It should be recalled here that the $Z$-impedances in eqn. (1) are purely reactive, so that $Z(-p) = -Z(p)$, and hence $N = (A + pB)(A - pB)$. It is not difficult now to cast the power ratio into a form like eqn. (17) by adding and subtracting $\eta_G$ in eqn. (21). Thus

$$\frac{\mathcal{P}_{20}}{\mathcal{P}_2} = \frac{N}{P^2} = \eta_G + \frac{N - \eta_G P^2}{P^2} = \eta_G + \frac{N'}{P^2} = \eta_G + |\Phi|^2 \quad . \quad (23)$$

where $\qquad N' = N - \eta_G P^2 \quad . \quad . \quad . \quad . \quad (24)$

The rational function $N'/P^2$ in eqn. (23) can be expressed readily in terms of network impedances in the form

$$|\Phi|^2 = \frac{N'}{P^2} = \frac{(R_1 Z_{22} - R_2 Z_{11})^2 - (R_1 R_2 - Z_{11} Z_{22} + Z_{12}^2)^2}{(R_1 + R_2)^2 Z_{12}^2}$$

$$\quad . \quad . \quad . \quad (25)$$

This form is very similar to that occurring in the power ratio (21) except for the signs, and hence we may define $N'$ analogously to $N$ by

$$N' = A'^2 - p^2 B'^2 = (A' + pB')(A' - pB') \quad . \quad . \quad (26)$$

from which $A'/P$ and $pB'/P$ can be identified readily in the manner of eqn. (18) with even and odd functions

$$\left. \begin{array}{l} \dfrac{A'}{P} = \dfrac{R_1 Z_{22} - R_2 Z_{11}}{(R_1 + R_2) Z_{12}} \quad \text{an even function} \\[3mm] \dfrac{pB'}{P} = \dfrac{R_1 R_2 - Z_{11} Z_{22} + Z_{12}^2}{(R_1 + R_2) Z_{12}} \quad \text{an odd function} \end{array} \right\} \quad . \quad (27)$$

where $A'$ and $B'$ are even polynomials in $p$ similar in form to the polynomials $A$ and $B$. As these polynomials are derived from quadratic functions it will be necessary to establish the proper signs. The signs, as will be shown in Section 3.2, will depend upon the configuration and the termination of the network. The relation between the function occurring in eqn. (17) and quadripole impedances (i.e. open- or short-circuit impedances) is seen through eqns. (23) and (25); thus

$$|\Phi|^2 = \frac{N'}{P^2} = \frac{A'^2 - p^2 B'^2}{P^2} = \eta_G H^2 |\phi|^2 \quad . \quad . \quad (28)$$

where $H$ is an arbitrary real constant and $\phi$ will be called the insertion-loss characteristic function. Hence

$$\frac{\mathscr{P}_{20}}{\mathscr{P}_2} = \eta_G + |\Phi|^2 = \eta_G(1 + H^2 |\phi|^2) = \eta_G |\Xi(p)|^2 \quad . \quad (29)$$

and

$$1 + H^2 |\phi|^2 = |\Xi(p)|^2 = \Xi(p)\Xi(-p) \quad . \quad . \quad (30)$$

where $\Xi$ defines the discrimination function, i.e. $\Xi(p) = 1 + H\phi(p)$.

The insertion-loss power ratio can thus be defined in any of the following forms:

$$\frac{\mathscr{P}_{20}}{\mathscr{P}_2} = \frac{1}{\eta} = \left|\frac{V_{20}}{V_2}\right|^2 = |\Lambda(p)|^2 = \frac{N}{P^2} = \eta_G + \frac{N'}{P^2}$$

$$= \eta_G(1 + H^2 |\phi|^2) = \frac{A^2 - p^2 B^2}{P^2} = \eta_G |\Xi(p)|^2 \quad . \quad (31)$$

All these definitions are important and we shall often return to them in the further development of the theory.

The quadripole open- and short-circuit impedances must also be related to insertion-loss polynomials. The relations can be obtained by making use of eqns. (3), (18) and (27), from which it follows that

$$\left. \begin{array}{l} Z_{1,oc} = \dfrac{A}{C} = R_1 \dfrac{A - A'}{p(B + B')}; \\[3mm] Z_{1,sc} = \dfrac{B}{D} = R_1 \dfrac{p(B - B')}{A + A'} \\[3mm] Z_{2,oc} = \dfrac{D}{C} = R_2 \dfrac{A + A'}{p(B + B')}; \\[3mm] Z_{2,sc} = \dfrac{B}{A} = R_2 \dfrac{p(B - B')}{A - A'} \\[3mm] Z_{12,oc} = \dfrac{-1}{C} = \dfrac{-2R_1 R_2}{R_1 + R_2} \dfrac{P}{p(B + B')}; \\[3mm] Z_{12,sc} = B = \dfrac{R_1 + R_2}{2} \dfrac{p(B - B')}{P} \end{array} \right\} \quad . \quad . \quad (32)$$

This is the important set of design impedances which must satisfy the conditions of realizability; the design impedances must be odd functions of frequency and $Z_{1,oc}$, $Z_{2,oc}$, $Z_{1,sc}$ and $Z_{2,sc}$-impedances must be separately realizable as two-terminal network reactances. Also, the design impedances must satisfy the condition stated in eqn. (4), following from $\mathbf{AD} - \mathbf{BC} = 1$. The important relations between the chain-matrix and the insertion-loss polynomials can be expressed in the following concise form:

$$\left\| \begin{array}{cc} \mathbf{A} & \mathbf{B} \\ \mathbf{C} & \mathbf{D} \end{array} \right\| = \frac{R_1 + R_2}{2 R_1 R_2 P} \left\| \begin{array}{cc} R_1(A - A') & R_1 R_2 p(B - B') \\ p(B + B') & R_2(A + A') \end{array} \right\| . \quad (33)$$

and the determinant of the chain matrix, from eqn. (2), can be expressed by

$$\mathbf{AD} - \mathbf{BC} = 1 = \frac{N - N'}{\eta_G P^2}. \quad . \quad . \quad . \quad (34)$$

From eqn. (34) useful relations concerning reflection factors can be derived in the following way:

$$N' = N - \eta_G P^2 = N(1 - \eta_G \eta) \quad . \quad . \quad (35)$$

as

$$\eta_G \eta = \mathscr{P}_2 / \mathscr{P}_{20\,max}$$

and hence $\quad 1 - \eta_G \eta = (\mathscr{P}_{20max} - \mathscr{P}_2)/\mathscr{P}_{20max} = |\Gamma|^2 \quad . \quad (36)$

where $(\mathscr{P}_{20\,max} - \mathscr{P}_2)$ is the reflected power and $\Gamma$ is the reflection factor. Since the network is loss-free,

$$|\Gamma_1|^2 = |\Gamma_2|^2 = |\Gamma|^2 = \frac{N'}{N} = \frac{A'^2 - p^2 B'^2}{A^2 - p^2 B^2} \quad . \quad (37)$$

from which it can be readily shown that the reflection factors can be expressed by

$$\left. \begin{array}{l} \Gamma_1 = \dfrac{R_1 - Z_{1\,in}}{R_1 + Z_{1\,in}} = \dfrac{A' + pB'}{A + pB} \\[3mm] \Gamma_2 = \dfrac{R_2 - Z_{2\,in}}{R_2 + Z_{2\,in}} = \dfrac{-A' + pB'}{A + pB} \end{array} \right\} \quad . \quad . \quad (38)$$

where $Z_{1,2\,in}$ are the input impedances of the terminated network as seen from the proper ends, and are defined by $Z_{1\,in} = Z_{11} - Z_{12}^2/(R_2 + Z_{22})$ and $Z_{2\,in} = Z_{22} - Z_{12}^2/(R_1 + Z_{11})$. It is important to note that $(R_{1,2} - Z_{1,2\,in})$ are non-physical impedances. Hence, it follows that the roots of corresponding polynomials $(\pm A' + pB')$ may be non-physical, i.e. the single real root and the real parts of the complex roots may have positive signs. We shall return to this important point in Section 3. At present we need only mention that the sign of the real root depends on the termination ratio.

### (2.2) Basic Symmetrical and Inverse-Impedance Networks

In general, the insertion-loss theory for symmetrical, equally terminated networks, and for the inverse-impedance, loss-free networks, calls for special consideration.* More detailed discussion about these networks is required, because the present methods of filter design are more or less based, at least initially on these two cases, which will be referred to as basic, since they serve as a starting-point for the design of filters with arbitrary terminations with or without losses.

### (2.2.1) Symmetrical, Equally Terminated, Basic Four-terminal Networks

Electrical symmetry of a network requires that $Z_{11} = Z_{22}$ and hence

$$\mathbf{A} = \mathbf{D} \quad . \quad . \quad . \quad . \quad . \quad (39)$$

* Some aspects of the lattice and ladder symmetrical structures were treated in an earlier paper.[8]

(In the case of the image parameters, the image impedances must of course be the same.) If a network is to be equally terminated then $R_1 = R_2$ and $\eta_G = 1$, so that, from eqn. (33),

$$A' \equiv 0; \quad N' = -p^2 B'^2 = \Omega^2 B'^2 \quad . \quad . \quad (40)$$

From eqn. (31), the power-ratio function for $\eta_G = 1$ is that of the discrimination, so that

$$\frac{\mathscr{P}_{20}}{\mathscr{P}_2} = |\Lambda(p)|^2 = |\Xi(p)|^2 = 1 + \frac{N'}{P^2} = 1 - \left(\frac{pB'}{P}\right)^2 = 1 + H^2\phi^2$$
$$. \quad . \quad . \quad (41)$$

It is seen that the insertion-loss characteristic function must be an odd rational function and is defined by*

$$H'\phi = -j\frac{pB'}{P} = \frac{\Omega B'}{P} \quad . \quad . \quad . \quad (42)$$

where $B'$ and $P$ are even polynomials in $p$ or $\Omega$, and $\phi$ is clearly an odd rational function. The constant $H'(= \sqrt{H^2} = \pm H)$ may have arbitrary sign; it will be shown later that the sign of $H'$ depends upon the configuration (mid-series or mid-shunt) of the first ladder branch.

### (2.2.2) Inverse-Impedance Basic Four-Terminal Network Parameters.

In the case of an inverse-impedance network, the short-circuit design impedance of one end must be the inverse of the open-circuit impedance of the other, i.e.

$$\frac{Z_{1,oc}}{R_1} = \frac{R_2}{Z_{2,sc}} \quad . \quad . \quad . \quad . \quad (43)$$

from which it follows that

$$Z_{1,oc} Z_{2,sc} = R_1 R_2 = R_0^2 \quad . \quad . \quad . \quad (44)$$

(In the case of image-parameter filters, $R_0$ is the so-called characteristic resistance which, for a constant-$k$ filter, can be defined by $R_0^2 = Z_{Tk} Z_{\Pi k}$).

From inspection of eqns. (43) and (32) it is found that

$$Z_{1,oc} Z_{2,sc} = R_1 R_2 = \frac{\mathbf{B}}{\mathbf{C}} = R_1 R_2 \frac{B - B'}{B + B'} \quad . \quad . \quad (45)$$

It can be seen that eqn. (45) is satisfied when $B'$ is identically zero; hence, for an inverse-impedance basic network, it can be stated that

$$B' \equiv 0; \quad N' \equiv A'^2 \quad . \quad . \quad . \quad . \quad (46)$$

The insertion-loss power ratio can be defined for this case by

$$\frac{\mathscr{P}_{20}}{\mathscr{P}_2} = \eta_G |\Xi(p)|^2 = \eta_G\left(1 + \frac{N'}{\eta_G P^2}\right)$$
$$= \eta_G\left(1 + \frac{A'^2}{\eta_G P^2}\right) = \eta_G(1 + H^2\phi^2) \quad . \quad (47)$$

* A symmetrical basic network can be decomposed into two, defined by the matrices
$$\left\| \begin{matrix} \mathbf{A} & \mathbf{B} \\ \mathbf{C} & \mathbf{D} \end{matrix} \right\| = \left\| \begin{matrix} \mathbf{A'} & \mathbf{B'} \\ \mathbf{C'} & \mathbf{D'} \end{matrix} \right\| \cdot \left\| \begin{matrix} \mathbf{D'} & \mathbf{B'} \\ \mathbf{C'} & \mathbf{A'} \end{matrix} \right\|$$
Thus, from eqns. (3) and (7),
$$\frac{V_{20}}{V_2} = \mathbf{A} + \frac{R\mathbf{D}}{2} + \frac{\mathbf{B}}{2R} = (\mathbf{A'D'} + \mathbf{B'C'}) + \left(\mathbf{C'D'}R + \frac{\mathbf{A'B'}}{R}\right)$$
and hence
$$\left|\frac{V_{20}}{V_2}\right|^2 = (\mathbf{A'D'} + \mathbf{B'C'})^2 - \left(\mathbf{C'D'}R + \frac{\mathbf{A'B'}}{R}\right)^2 = 1 - \left(\mathbf{C'D'}R - \frac{\mathbf{A'B'}}{R}\right)^2$$
If the input terminals (11′) are associated with the mid-point between the two networks then the mid-point input impedances can be defined by
$$Z'_{1,\text{in}} = \frac{\mathbf{B'} + R\mathbf{D'}}{\mathbf{A'} + R\mathbf{C'}} = \frac{R + \mathbf{A'B'} - \mathbf{D'C'}R^2}{\mathbf{A'^2} - R^2\mathbf{C'^2}} = R'_{1,\text{in}} + jX'_{1,\text{in}}$$
... the insertion-loss power ratio is expressible as $\left|\frac{V_{20}}{V_2}\right|^2 = 1 + \left(\frac{X'_{1,\text{in}}}{R'_{1,\text{in}}}\right)^2$, which ... ves J. Reed's statement,[7] from which it follows that the association of a real ... stant multiplier with $Z'_{1,\text{in}}$ does not change the insertion-loss characteristic (i.e. the ... rimination function) but only adds constant reflection loss. This theorem will ... ound useful later.

and the characteristic insertion-loss function is given by

$$H'\phi = A'/\eta_G^{1/2}P \quad . \quad . \quad . \quad . \quad (48)$$

where $H'$ as before may have an arbitrary sign and $\phi$ must be an even function. It may be observed in eqn. (47) that, if the free term of the polynomial $A'$ is zero, it is implied that the termination must be equal, i.e. $\eta_G = 1$. Otherwise $\eta_G < 1$.

### (2.3) Special Case of Open- or Short-Circuit Termination

A special case of termination occurs when one of the network terminations is made zero or infinite. Such a case is often of interest when a constant-current or voltage-driven network is to operate as an inter-stage coupling between valves, or when groups of filters are to be combined at one end.[4] Thus, when putting

$$1/G_2 = R_2 = 0 \text{ or } R_2 = \infty; \quad \eta_G = 0 \quad . \quad . \quad (49)$$

then, from eqn. (33), $N \equiv N'$ and hence

$$A^2 \equiv A'^2; \quad B^2 \equiv B'^2 \quad . \quad . \quad . \quad . \quad (50)$$

By giving $A'$ and $B'$ the proper signs which follow from inspection of the $\Gamma$-factor, it can be found that the open-circuit design impedance simplifies to the form

$$Z_{1,oc} = R_1 A/pB \text{ for } R_2 = \infty; \quad R_{\text{in }2,oc} = R_1 \eta \quad . \quad (51)$$

$R_{\text{in }2,oc}$ is the resistance measured at the open-circuited end of the terminated network. Similarly, the short-circuit design impedance takes the form

$$Z_{1,sc} = R_1 pB/A \text{ for } 1/G_2 = R_2 = 0; \quad G_{\text{in }2,sc} = \eta/R_1 \quad . \quad (52)$$

where $G_{\text{in }2,sc}$ is the conductance measured at the short-circuited end of the terminated network.

In the above cases the design impedances are particularly simple when losses are to be considered; this is because the polynomials $A'$ and $B'$, which require most labour in computation when losses are accounted for, need not be evaluated. The procedure concerning the design with or without losses will be described in Section 3. It may be added that the designed open- or short-circuit network for normal termination is very insensitive to variation of the finite resistance $R_2$ (or conductance $G_2$ of current source); the design resistance $R_1$, on the other hand, must be kept within reasonable accuracy.

### (2.4) General Ladder and Ladder Coefficients

The design impedance, from which some or all of the ladder coefficients are to be computed, is assumed to be known in the form of an odd rational function. This may be any one of the design impedances given in eqn. (32), formed in the proper way for a particular ladder structure and termination. For purposes of illustration, we shall refer mostly to the design impedances seen from end (11′) of the network of Fig. 1, i.e. $Z_{1,oc}$ or $Z_{1,sc}$.

To distinguish the network configuration such as mid-series or mid-shunt, and the character of the ladder, e.g. symmetrical or inverse-impedance, we shall introduce an additional subscript, i.e. T or $\Pi$, defining the basic structure mid-series T or mid-shunt $\Pi$. In the case of an inverse-impedance network, as can be observed in Fig. 2, there is, in addition to the basic structure, a constant-$k$-like half-section; the character of this half-section, which may correspond to a T- or $\Pi$-configuration, will be indicated by a second subscript. Thus, the usual design impedances of networks illustrated in Fig. 2 will be defined from the end (11′) as $Z_{1,sc,\text{T}}$, $Z_{1,oc,\Pi}$ for symmetrical odd numbers of branches and $Z_{1,oc,\text{T}\Pi}$, $Z_{1,sc,\Pi\text{T}}$ for the inverse-impedance or an even number of branches. Similarly, the design impedance from the other end will be defined as $Z_{2,sc,\text{T}}$, $Z_{2,oc,\Pi}$ and $Z_{2,sc,\Pi\text{T}}$ and
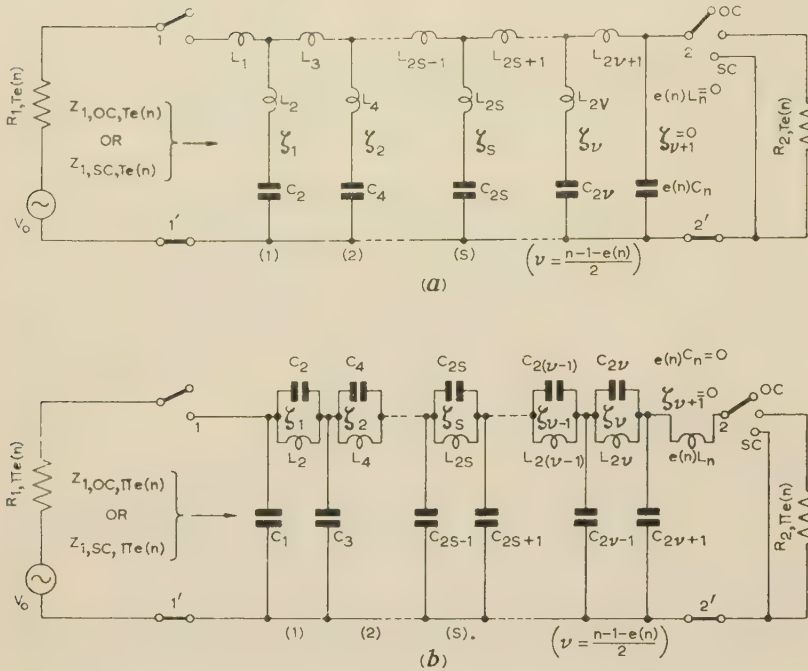
**Fig. 2.**—General ladder structures and performance characteristics.

(a) Mid-series $T_{e(n)}$-structure.     (b) Mid-shunt $\Pi_{e(n)}$-structure.     (c) Performance characteristics:

MF = Maximally flat ($\zeta_s = 0$, see Fig. 4).       C = Cauer–Darlington [symmetrical, see Fig. 6(a)].
T = Chebyshev pass-band ($\zeta_s = 0$, see Fig. 5).     $\bar{C}$ = Cauer–Darlington (antimetric, $R_1/R_2 = 1$, see Fig. 7).
Hyp = Hypothetical [$n$ even, see Fig. 6(b)].       $\tilde{C}$ = Cauer–Darlington (inverse-impedance, $R_1/R_2 \neq 1$, see Fig. 8).

These curves, plotted for $D_p = 1$ dB, can be read directly; for other values of $D_p$, the insert scale slide should be used. To read $D_a$ for other values of $D_p$ the scale slide should be placed parallel to the $D_a$ axis with its reference line coinciding with the curve at the required value $k_B$. (Example: for $n = 5$, $k_B = 0.5$ and $D_p = 0.3$ dB, the $D_a$ are read; for MF, $D_a \simeq 18.5$ dB; for T, $D_a \simeq 39.5$ dB; and for C, $D_a \simeq 63.5$ dB.)

$Z_{2,oc,\tau\Pi}$. Other design impedances also can be used. However, we shall limit most of our discussion to the impedances from end (11′) mentioned above. It must be stressed that ladder coefficients should be computed whenever possible from both ends independently, as this provides the best check of results. Sometimes the termination resistances $R_1$ and $R_2$ will be specified by the network structure, if it is found to be useful.

In addition to the symbols defined above, we shall also introduce a further very important one which will be used throughout the paper, namely $e(n) = \frac{1}{2}[1 + (-1)^n]$, which is zero for $n$ odd and unity for $n$ even, where $n$ will refer to the number of branches. By means of these and other similar symbols we shall specify the general ladder; e.g. $T_{e(n)}$ means a basic T-structure with an even or odd number of branches. Thus, for an odd number of branches we shall have $T_0$, or simply T, while for an even number of branches we shall have $T_{II}$, which may be $T_{II}$ or $_{II}T$. Similarly, we shall have $\Pi_{e(n)}$, which for $n$ odd is $\Pi_0$, or simply $\Pi$, and for $n$ even may be $\Pi_T$ or $_T\Pi$. These symbols, especially $e(n)$, will play an important part in the concise presentation of the theory. The branch reactances will be denoted by $X$ and will be numbered from the design end; thus, such a branch reactance for $T_{e(n)}$- or $\Pi_{e(n)}$-structures will be defined by $X_{r,Te(n)}$ or $X_{r,\Pi e(n)}$, where $r = 1, 2, 3, \ldots$ In a way similar to that used for the design impedances, the branch reactances will be characterized by the corresponding design resistance $R_1$ or $R_2$.

Fig. 2 illustrates mid-series and mid-shunt ladder structures of $m$-derived-like low-pass configurations with two elements in the even branches (these are duals when $R_{1,\Pi e(n)} = R_{2,Te(n)}$). It

can be seen clearly that the simplest configuration such as constant-$k$ can be obtained by assigning $C_{2s,\Pi e(n)} = 0$ or $L_{2s,Te(n)} = 0$. If all these constants are made zero, such a structure will correspond to constant-$k$, or Taylor approximation, or Chebyshev pass-band approximation, or any such filter which has no infinite attenuation at finite frequencies.*

The impedances of odd branches in a $T_{e(n)}$ mid-series structure can be written as

$$jX_{(2s\mp1),Te(n)} = j\omega L_{(2s\mp1),Te(n)} = R_{1,Te(n)}j\frac{\omega}{\omega_B}\frac{\omega_B L_{(2s\mp1),Te(n)}}{R_{1,Te(n)}}$$

$$= R_{1,Te(n)}pa_{2s\mp1} = pa_{(2s\mp1),Te(n)} \quad . \quad (53)$$

where $a_{(2s\mp1),Te(n)}$ are the actual ladder coefficients for an arbitrarily terminated mid-series $T_{e(n)}$-structure, while $a_{2s\mp1}$ are the normalized ladder coefficients defining, in a mid-series structure, the quantity

$$a_{2s\mp1} = \frac{\omega_B L_{(2s\mp1),Te(n)}}{R_{1,Te(n)}} = \frac{a_{(2s\mp1),Te(n)}}{R_{1,Te(n)}} \quad . \quad (54)$$

where $\omega_B$ and $R_{1,Te(n)}$ are usually the specified frequency and termination resistance (in the special case of equal termination ladder coefficients with a bar will be used, e.g. $\bar{a}_r$). If $a_{2s\mp1}$ are

---

* Reduction of the proper element in the even branch in the general structure in Fig. 2 corresponds to a shift of infinite loss from finite frequency to infinity in the appropriate general insertion-loss function used for filtering purpose. Such function will be discussed in detail in Section 5. It may be mentioned that the structure illustrated may also be preserved, even if mutual inductances occur (these will be signified by negative ladder coefficients).

given, then the inductances $L_{(2s\mp1),\mathrm{T}e(n)}$ can be readily computed. Similarly, the relation of the ladder coefficients for a mid-shunt structure is given by

$$jX_{2s\mp1),\Pi e(n)} = \frac{1}{j\omega C_{(2s\mp1),\Pi e(n)}} = R_{1,\Pi e(n)}\frac{1}{pa_{2s\mp1}} = \frac{1}{pa_{(2s\mp1),\Pi e(n)}}$$

$$. \quad . \quad . \quad (55)$$

where normalized ladder coefficients are defined as

$$a_{2s\mp1} = \omega_B C_{(2s\mp1),\Pi e(n)}R_{1,\Pi e(n)} = R_{1,\Pi e(n)}a_{(2s\mp1),\Pi e(n)} \quad . \quad (56)$$

The resonant frequencies of the elements of the even branches of a ladder structure $\mathrm{T}_{e(n)}$ or $\Pi_{e(n)}$ are defined by

$$L_{2s}C_{2s} = \frac{1}{\omega_{\infty r}^2} = \frac{1}{\omega_B^2\Omega_{\infty r}^2} = \frac{\zeta_s}{\omega_B^2}; \quad \zeta_s = \frac{1}{\Omega_{\infty r}^2} \quad . \quad (57)$$

(for the present let $r = s$)

where $\Omega_{\infty r}$ is the normalized frequency corresponding to infinite loss and $\omega_B$ is the normalizing constant. The impedance of the even branches for a mid-series structure can be written as

$$jX_{2s,\mathrm{T}e(n)} = j\omega L_{2s,\mathrm{T}e(n)} + \frac{1}{j\omega C_{2s,\mathrm{T}e(n)}}$$

$$= R_{1,\mathrm{T}e(n)}\frac{1+p^2\zeta_s}{pa_{2s}} = \frac{1+p^2\zeta_s}{pa_{2s,\mathrm{T}e(n)}} \quad . \quad (58)$$

where $a_{2s} = \omega_B C_{2s,\mathrm{T}e(n)}R_{1,\mathrm{T}e(n)}$ from which $C_{2s,\mathrm{T}e(n)}$ is readily found and $L_{2s,\mathrm{T}e(n)}$ follows from eqn. (57). It is clear that, when $\zeta_s = 0$, $\omega_{\infty s} = \infty$, then $L_{2s,\mathrm{T}e(n)} = 0$ and the branch is reduced to one element.

The mid-shunt ladder coefficient for the even branches are related by

$$jX_{2s,\Pi e(n)} = R_{1,\Pi e(n)}\frac{pa_{2s}}{1+p^2\zeta_s} = \frac{pa_{2s,\Pi e(n)}}{1+p^2\zeta_s} \quad . \quad . \quad (59)$$

from which

$$L_{2s,\Pi e(n)} = \frac{a_{2s}R_{1,\Pi e(n)}}{\omega_B} \quad \text{and} \quad C_{2s,\Pi e(n)} = \frac{\zeta_s}{a_{2s}\omega_B R_{1,\Pi e(n)}}$$

where, for $\zeta_s = 0$, $\omega_{\infty s} = \infty$ and $C_{2s,\Pi e(n)} = 0$.

Band-pass, band-stop or high-pass elements can be found by well-known frequency transformations (10) to (13). Such a transformation, e.g. from low-pass to band-pass, is simply accomplished by adding to every inductance in the low-pass ladder configuration a series capacitance such that $LC = \omega_0^{-2}$, and to every capacitance a parallel inductance such that, correspondingly, $LC = \omega_0^{-2}$, where $f_0$ is the mid-band frequency. Similarly, for the band-stop, a capacitance is added in parallel with every inductance and an inductance in series with every capacitance.

Details of a method of deriving ladder coefficients are given in Sections 3 and 9.2. Here we give only the important formulae for computing ladder coefficients. The importance of these formulae lies in the fact that, by proper expansion of certain determinants involved in them, it is possible to derive another set of design formulae which are more suitable for the actual computations.[3, 5]

An open- or short-circuit ladder can be treated as a two-terminal network from which ladder coefficients can be evaluated from design impedances, by continued-fraction expansion. However, Darlington has found very concise general formulae for ladder coefficients. The appropriate function $\mathscr{F}(\zeta)$ for the computation of the ladder coefficients by Darlington formulae formed from design impedances in eqn. (32) will be discussed with details in Section 3. For the present, consider a rational even function in $p^2$, obtained from suitable impedance or admittance $Z_\mathrm{T}$ or $1/Z_\Pi$ normalized by its corresponding resistance, $R_\mathrm{T}$ or $R_\Pi$, and divided by $p$. By replacing the variable $p^2$

by $-1/\zeta$ (which will be found more convenient for further operations), one obtains from this function

$$\mathscr{F}(\zeta) = \left(\frac{Z_\mathrm{T}}{pR_\mathrm{T}} \quad \text{or} \quad \frac{R_\Pi}{pZ_\Pi}\right)_{p^2 = -1/\zeta} \quad . \quad . \quad (60)$$

The subscripts T and $\Pi$ in eqn. (60) indicate only the input character of the ladder. (See Fig. 2.) The design impedances which can be used for $\mathscr{F}(\zeta)$ may be $Z_{1,sc,\mathrm{T}}$; $Z_{1,oc,\mathrm{T}\Pi}$; $Z_{1,oc,\Pi}$ or any other suitable impedance. It should also be noted that

$$\zeta_s = 1/\Omega_{\infty r}^2$$

In addition, we define $\zeta_0 = \zeta_{\nu+1} = 0$, where $\nu$ is the number of T- or $\Pi$-sections. It is also important to note that the $\zeta_s$ for $s = 1, 2, \ldots [\nu + e(n)]$ are associated with the network branches (see Fig. 2), while the $\Omega_{\infty r}$ for $r = 1, 2, \ldots \nu$, are associated with the insertion-loss function ($\Omega_{\infty r}$ are the finite frequencies of infinite loss, see Figs. 6, 7 and 8). In connection with eqn. (57) we said that $s = r$; which is always possible. In some cases, however, a relation other than $s = r$ may be needed: this will be discussed in Section 3.6.1.

The quantities $\mathscr{H}_{qr}$, by means of which ladder coefficients can be computed, are defined as

$$\mathscr{H}_{qr} = \mathscr{H}_{rq} = \frac{(1-\delta_{oq})\mathscr{F}(\zeta_q) - (1-\delta_{or})\mathscr{F}(\zeta_r)}{\zeta_q - \zeta_r} \quad . \quad (61)$$

for $q = 0, 1, 2, \ldots$, and $r = 0, 1, 2, \ldots$, where $\delta_{os}$ is Kroenecker's delta; $\delta_{os} = 1$ for $s = 0$ and $\delta_{os} = 0$ for $s \neq 0$. (This notation is introduced only to make the formulae for $\mathscr{H}_{qr}$ consistent for $r = 0$ or $q = 0$.) We also define $\mathscr{H}_{oo} \equiv 1$.

In the limiting case, when $q = r \neq 0$, the formulae for $\mathscr{H}_{qq}$ are found from

$$\mathscr{H}_{qq} = \lim_{q\to r}\frac{\mathscr{F}(\zeta_q)-\mathscr{F}(\zeta_r)}{\zeta_q-\zeta_r} = \frac{d}{d\zeta}\mathscr{F}(\zeta)\bigg|_{\zeta=\zeta_q} = \mathring{\mathscr{F}}(\zeta_s) \quad . \quad (62)$$

$$q = r = 1, 2, \ldots$$

The law of forming ladder coefficients may be written in a form

$$\left.\begin{array}{l} a_{2s+1} = (\zeta_{s+1}-\zeta_s)\dfrac{\mathscr{U}_s\mathscr{W}_s}{\mathscr{V}_s\mathscr{V}_{s+1}}; \quad s = 0, 1, 2, \ldots, \nu \\[2ex] a_{2s} = \dfrac{-\mathscr{V}_s^2}{\mathscr{U}_{s-1}\mathscr{U}_s}; \quad s = 1, 2, \ldots [\nu+e(n)] \end{array}\right\} \quad . \quad (63)$$

Some of the coefficients can be computed from special formulae given in Section 3. (These formulae reduce a great deal of otherwise tedious computation, or can serve as check of result.)

The factors $\mathscr{U}_s$, $\mathscr{V}_s$ and $\mathscr{W}_s$ formed by $\mathscr{H}_{qr}$, whose determinant form was discovered by Darlington,[5] are given by

$$\mathscr{U}_k = \begin{vmatrix} \mathscr{H}_{11} & \mathscr{H}_{12} & \cdots & \mathscr{H}_{1(k-1)} & \mathscr{H}_{1k} \\ \mathscr{H}_{21} & \mathscr{H}_{22} & \cdots & \mathscr{H}_{2(k-1)} & \mathscr{H}_{2k} \\ \cdot & \cdot & \cdot & \cdot & \cdot \\ \mathscr{H}_{k1} & \mathscr{H}_{k2} & \cdots & \mathscr{H}_{k(k-1)} & \mathscr{H}_{kk} \end{vmatrix}$$

where $\mathscr{U}_0 = \mathscr{H}_{00} = 1$ and $\mathscr{U}_1 = \mathscr{H}_{11}$;

$$\mathscr{V}_k = \begin{vmatrix} \mathscr{H}_{11} & \mathscr{H}_{12} & \cdots & \mathscr{H}_{1(k-1)} & 1 \\ \mathscr{H}_{21} & \mathscr{H}_{22} & \cdots & \mathscr{H}_{2(k-1)} & 1 \\ \cdot & \cdot & \cdot & \cdot & \cdot \\ \mathscr{H}_{k1} & \mathscr{H}_{k2} & \cdots & \mathscr{H}_{k(k-1)} & 1 \end{vmatrix} \quad \left.\right\} \quad . \quad (64)$$

where $\mathscr{V}_0 = \mathscr{V}_1 = 1$; and

$$\mathscr{W}_k = \begin{vmatrix} \mathscr{H}_{11} & \mathscr{H}_{12} & \cdots & \mathscr{H}_{1(k-1)} & \mathscr{H}_{1(k+1)} \\ \mathscr{H}_{21} & \mathscr{H}_{22} & \cdots & \mathscr{H}_{2(k-1)} & \mathscr{H}_{2(k+1)} \\ \cdot & \cdot & \cdot & \cdot & \cdot \\ \mathscr{H}_{k1} & \mathscr{H}_{k2} & \cdots & \mathscr{H}_{k(k-1)} & \mathscr{H}_{k(k+1)} \end{vmatrix}$$

where $\mathscr{W}_0 = \mathscr{H}_{01} = \mathscr{F}(\zeta_1)/\zeta_1$ and $\mathscr{W}_1 = \mathscr{H}_{12}$.

The $\mathcal{H}_{qr}$ are defined as in eqn. (61). Formulae (61)–(64) are the design formulae which can be used in actual computation. Usually, however, great precision is required, and for this reason the formulae in the form presented here may find a practical application only to ladder networks of up to seven branches without much difficulty (except, perhaps, the open- or short-circuit-terminated networks, which do not allow for computation from both ends of the ladder). It is important to note that normalized ladder coefficients must be related to the termination resistance by which the function $\mathscr{F}(\zeta)$, and hence also the actual ladder coefficients, were normalized.

## (3) FUNDAMENTAL DEFINITIONS AND OPERATIONS IN FILTER SYNTHESIS ON AN INSERTION-LOSS BASIS

We shall endeavour to formulate the principal operations involved in forming the design impedance of ladder filters from a prescribed insertion loss, with special emphasis upon symmetrical and inverse impedances with an arbitrary number of branches involved in the ladder. Conventional symmetrical and inverse-impedance ladders can be distinguished by the number of ladder branches; this number of branches should somehow enter into the characteristic function; then, once the relation of the number of branches is established, the derivation of general design formulae should be possible. It should also be possible to formulate a general synthesis procedure with or without losses and for an arbitrary number of branches and termination ratios. If such a general formulation is achieved, the formulae should also be consistent for the special cases of basic networks. Such a general method would involve the determination of all the insertion-loss polynomials such as $A$, $B$, $P$, and $A'$ and $B'$, some of which may vanish or may reduce to simple values in special cases. In our investigation of networks, we shall be concerned most with conventional symmetrical and inverse-impedance ladders, whose insertion-loss function will be zero at zero frequency and infinity at infinite frequency when the network is of purely reactive elements. The most commonly quoted configurations will be of the forms obtainable from Fig. 2.

### (3.1) Determination of Insertion-Loss Polynomials

Before we begin formulation of the general synthesis procedure, let us first adopt several important definitions.

(a) The transducer loss is defined by

$$10 \log \frac{\mathscr{P}_{20 \max}}{\mathscr{P}_2} = \text{insertion loss} + \text{reflection loss in decibels.}$$

(b) The insertion loss is defined by

$$10 \log \frac{\mathscr{P}_{20}}{\mathscr{P}_2} = 10 \log |\Xi(p)|^2 + 10 \log \eta_G + \text{dissipation loss in decibels.}$$

The extremal values will be denoted by $A_p$ and $A_a$.

If the insertion loss becomes negative, then we have an insertion gain. In the case of an inverse-impedance network, the insertion gain is given by $A_p = 10 \log \eta_G$, provided no losses exist, and $\eta_G |\Xi(p)|^2 = 1$, $\eta_G < 1$.

In the case of no dissipation and equal termination, the insertion loss equals the discrimination loss. The discrimination in general is defined in decibels by $D$, where:

(c) $D = 10 \log |\Xi(p)|^2 = 10 \log (1 + H^2 |\phi|^2)$ decibels.

The discrimination loss can also be related to the reflection factor $\Gamma$ by $D = -10 \log (1 - |\Gamma|^2)$ or $|\Gamma|^2 = 1 - 10^{-D/10}$.

In the u.h.f. techniques, the measurable quantity called the voltage standing-wave ratio (abbreviated v.s.w.r.), is often of interest and sometimes serves as a design specification. The

v.s.w.r. is given in terms of a reflection factor and is related to the discrimination data by

$$\text{v.s.w.r.} = \frac{1 + |\Gamma|}{1 - |\Gamma|} = \coth^2 \left[ \tfrac{1}{2} \operatorname{arc sinh} (10^{D/10} - 1)^{-1/2} \right]$$

The discrimination and insertion-loss functions have, in fact, the same character and can be given the same graphical shape, only differing in scale. Usually, design specifications do not imply wholly either the discrimination or the insertion-loss function, but only specify their maximum or minimum values in the pass-band or attenuation-band domains.

The discrimination function $\Xi$, or the characteristic function $\phi$ for filtering purposes, is usually an approximation to an ideal filter in the Taylor or Chebyshev sense, and may behave within the pass-band domain in an oscillatory fashion, or increase continuously. Also, in the attenuation band, it may have infinite loss at finite frequencies, or it may increase continuously, as in the case of constant-$k$ or maximally-flat filter response. At present we shall not specify what the approximation in the specified domain should be. We shall only require that the function in the transition band (between the pass band and the attenuation band) be continuous, as illustrated in Fig. 3 (where,
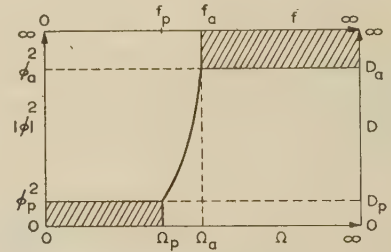


Fig. 3.—Discrimination function with specifications.

also, the specified domains are indicated by shaded areas). We assume that the function satisfies the specification and is realizable by means of minimum-phase-shift, four-terminal networks.

The specification of a filter may be given by the insertion loss $A_p$, $A_a$, or discrimination levels $D_p$, $D_a$, or by the corresponding reflection factors $|\Gamma_p|$, $|\Gamma_a|$, or v.s.w.r., specified at the extremal pass- and attenuation-band frequencies $f_p$, $f_a$, or normalized frequencies $\Omega_p$, $\Omega_a$. Sometimes, however, the maxima of discrimination within the pass band may be of interest and these will be denoted by $D_{\cap s}$, occurring at corresponding frequencies $\Omega_{\cap s}$. $D_{\cap s}$ is usually required to be less than or equal to $D_p$. Similarly, the discrimination minima $D_{\cup s}$ occur within the attenuation band at corresponding frequencies $\Omega_{\cup s}$. Thus $0 \leqslant \Omega_{\cap s} < \Omega_p$ while $\infty > \Omega_{\cup s} > \Omega_a$.

The extremal pass-band discrimination is defined by

$$D_p = 10 \log |\Xi(\Omega_p)|^2 = 10 \log (1 + H^2 \phi_p^2)$$

$D_p \geqslant D_{\cap s}$ at $\Omega \, (= \Omega_{\cap s}) \leqslant \Omega_p$; for $\eta_G = 1$, $D_p = A_p$ .   (65)

The extremal suppression-band discrimination is defined by

$$D_a = 10 \log |\Xi(\Omega_a)|^2 = 10 \log (1 + H^2 \phi_a^2)$$
$$\text{for } \eta_G = 1, \quad D_a = A_a, \quad . \quad . \quad (66)$$

where $\Omega_p$ and $\Omega_a$ are the extremal pass-band and attenuation-band normalized frequencies, and the specified bandwidth ratio, or filter selectivity factor $k_B$, and the normalizing factor $f_B$, necessary for network design are given by

$$k_B = \frac{\Omega_p}{\Omega_a} = \frac{B_p}{B_a} < 1; \quad \sqrt{(\Omega_p \Omega_a)} = \Omega_B; \quad f_B = \frac{\sqrt{(B_p B_a)}}{\Omega_B} \quad . \quad (67)$$

where $B_p$ and $B_a$ are the effective bandwidths at the levels $D_p$ and $D_a$ respectively, and for low-pass filters $B_p = f_p$ and $B_a = f_a$. [The relation between $k_B$, $n$, $D_p$ and $D_a$ is given in Fig. 2(c).]

For band-pass filters $B_p = f_{p2} - f_{p1}$, and $B_a = f_{a2} - f_{a1}$, where $f_B = \sqrt{(B_p B_a)}/\Omega_B$, $f_0^2 = f_{p1}f_{p2} = f_{a1}f_{a2}$ and where $f_{a1} < f_{p1} < f_0 < f_{p2} < f_{a2}$, and $k_B = B_a/B_a < 1$; while for band-stop, $k_B = B_a/B_p < 1$; $f_B = \sqrt{(B_p B_a)}/\Omega_B$, $f_{p1} < f_{a1} < f_0 < f_{a2} < f_{p2}$.

To facilitate network synthesis for an arbitrary number of branches let us adopt the definitions

$$n = \text{number of branches in the ladder}$$
$$\text{and} \quad \nu = \text{number of T- or } \Pi\text{-sections} \quad \rbrace \quad . \quad (68)$$

The relations between branches and section are given by

$$\nu = \frac{n-1}{2} = \left[\frac{n}{2}\right] \text{ for } n \text{ odd (symmetrical ladders)}$$
$$\text{and } \nu = \frac{n}{2} - 1 \text{ for } n \text{ even (inverse-impedance ladders)} \quad \rbrace \quad . \quad (69)$$

where $[n/2]$ is an integral number (lower integral for $n$ odd). $\nu$, $[n/2]$, $n$, $m$, $q$, $r$, $k$ and $s$ will be used as integers. Also, $\delta_{qr} = 0$ for $q \neq r$, 1 for $q = r$, and is a conventional Kroenecker delta.

$$\tfrac{1}{2}[1 + (-1)^n] = e(n) \quad . \quad . \quad . \quad . \quad (70)$$

is a function of $n$ even (this may be thought of as an operator); unity for $n$ even and zero for $n$ odd.

$$\tfrac{1}{2}[1 - (-1)^n] = o(n) \quad . \quad . \quad . \quad . \quad (71)$$

is a function* for $n$ odd (operator); unity for $n$ odd and zero for $n$ even. Thus

$$\nu = [n/2] - e(n) = \frac{n - 1 - e(n)}{2} \quad . \quad . \quad . \quad (72)$$

With the above definitions we can demonstrate the general aspect of the functions and the operations involved in network synthesis on an insertion-loss basis.

### (3.1.1) Insertion-Loss Polynomials.

From eqns. (23) and (31), it follows that the general insertion-loss characteristic function is

$$H^2|\phi|^2 = \frac{N'}{\eta_G P^2} = \frac{(R_1 Z_{22} - R_2 Z_{11})^2 - (R_1 R_2 - Z_{11}Z_{22} + Z_{12}^2)^2}{4R_1 R_2 Z_{12}^2}$$
$$. \quad . \quad . \quad (73)$$

which can also be expressed for a low-pass analogue system† in a general factorized form, that is in terms of poles and zeros, thus:

$$H^2|\phi|^2 = (-1)^n h \frac{(p - p_0')^{o(n)} \prod\limits_{s=1}^{\nu + e(n)} (p^2 - p_{+s}'^2)(p - p_{-s}'^2)}{\prod\limits_{s=1}^{m} (p^2 - p_{+\infty s}'^2)(p^2 - p_{-\infty s}'^2)} \quad . \quad (74)$$

where $h$ is an arbitrary real constant, $p_0'$ (the real root) and $p_{\pm s}'$ (the complex conjugate roots) will be called zeros of the characteristic insertion-loss function, and $p_{\pm\infty s}'$ are the complex conjugate poles, or frequencies of peak losses. In general, the number of finite poles will be fixed by an integer $m$ limited to

$$0 \leqslant m \leqslant \nu \quad . \quad . \quad . \quad . \quad . \quad (75)$$

As our quadripole is taken to be purely reactive, it is obvious that the peaks of the attenuation will be at infinity; hence poles will occur at real frequencies and must be purely imaginary conjugate quantities. In fact, the elements of a physical network have finite $Q$-values ($Q$ = resistance/reactance or conductance/susceptance ratio), and the real parts will exist; in such a case $p_{\pm\infty s}'$ will be a complex conjugate quantity given by

$$p_{\pm\infty s}' = -\alpha_{\infty s}' \pm j\Omega_{\infty s}' \quad . \quad . \quad . \quad . \quad (76)$$

With a reasonable $Q$, the $\alpha_{\infty s}'$ are usually much smaller than unity, while the $\Omega_{\infty s}'$ are greater than unity, since the attenuation at the peaks is usually great. Thus, in our investigation, we shall neglect $\alpha_{\infty s}'$ for filters, even if losses will be considered and, generally, the poles will be defined by

$$p_{\pm\infty s} = \pm j\Omega_{\infty s} \quad . \quad . \quad . \quad . \quad (77)$$

An assumption of purely imaginary poles $p_{\pm\infty s} = \pm j\Omega_{\infty s}$ is also necessitated by the method of evaluating the ladder coefficients.

For ordinary low-pass analogue filters, infinite loss at finite frequency is required to occur at frequencies greater than the extremal frequency $\Omega_a$. With this and also the restrictions on the poles we can express eqn. (74) as

$$H^2|\phi|^2 = \frac{N'}{\eta_G P^2} = H^2 \frac{(p_0'^2 - p^2)^{o(n)} \prod\limits_{s=1}^{\nu + e(n)} (p^2 - p_s'^2)(p^2 - p_{-s}'^2)}{\prod\limits_{s=1}^{m} \left(\dfrac{p^2}{\Omega_{\infty s}^2} + 1\right)^2}$$
$$= H^2 \frac{\sum\limits_0^n N_s' p^{2s}}{\left(\sum\limits_0^m P_s p^{2s}\right)^2} \quad . \quad (78)$$

where $H$ is an arbitrary real constant. For filters of our type the polynomial in the denominator, containing poles, can be identified with the polynomial $P$; thus

$$P = \prod\limits_{s=1}^{m} \left(\frac{p^2}{\Omega_{\infty s}^2} + 1\right) = \sum\limits_{s=0}^{m} P_s p^{2s}, \text{ where } 0 \leqslant m \leqslant \nu \quad . \quad (79)$$

This definition limits slightly the general character of the insertion-loss theory, but it will be found to be convenient in application to filters of our type. For the present we shall retain the zeros $p_{\pm s}'$ in complex conjugate form. (It is always possible to equate either part of a complex number to zero without loss of consistency in notation.) Hence the real and imaginary parts of the roots of eqn. (78) are defined in general by

$$|\mathbf{R} p_{\pm s}'| = \alpha_s'; \quad |\mathbf{I} p_{\pm s}'| = \Omega_s'; \quad \Omega_s' < \Omega_p; \quad \Omega_0' \equiv 0 \quad . \quad (80)$$
$$s = e(n), 1, 2, \ldots [n/2].$$

For the present we shall leave undetermined the position of the zeros, i.e. the sign of the real parts. For filtering purposes $\Omega_s'$ is required to be smaller than the extremal pass-band frequency $\Omega_p$ and hence, when losses are taken into account, the real parts $\alpha_s'$ play an important part, because attenuation in the pass band is usually very small and $\Omega_p$ is usually smaller than or equal to unity. Hence $\alpha_s'$ cannot be neglected, as in the case of $\alpha_{\infty s}'$, in relation to the very high attenuation peaks. In the case of the characteristic function for basic networks without losses, $\alpha_s'$ is obviously zero. For such basic networks, on which insertion-loss theory and design procedure of any filter network are based, we shall use a special notation for the zeros, emphasizing their purely imaginary character. Such zeros (and poles) are defined by

$$p_{\pm s}' = p_{\pm os} = \pm j\Omega_{os}, \text{ where } 0 \leqslant \Omega_{os} < \Omega_p; \quad \Omega_{00} \equiv 0$$
$$\text{and} \quad p_{\pm\infty s} = \pm j\Omega_{\infty s}, \text{ where } \Omega_a < \Omega_{\infty s} \leqslant \infty \quad \rbrace \quad . \quad (81$$

---

* Eqns. (70) and (71) can be conveniently defined by circular functions, namely the even one $c(n) = \cos^2 n\pi/2$, while the odd one $s(n) = \sin^2 n\pi/2$.
† A model system from which low-pass, band-pass, band-stop or high-pass networks can be obtained by the frequency transformation given in (9)–(13).

Then the insertion-loss characteristic function (78) for basic (loss-free) networks becomes

$$H^2\phi^2 = (-1)^n H^2 \frac{p^{2o(n)} \prod\limits_{s=1}^{\nu+c(n)} (p^2 + \Omega_{os}^2)^2}{\prod\limits_{s=1}^{m} \left(\dfrac{p^2}{\Omega_{\infty s}^2} + 1\right)^2}$$

$$= H^2 L^2 F^2(\Omega) = \frac{e(n)A'^2 - o(n)p^2 B'^2}{\eta_G^{e(n)} P^2} \quad . \quad (82)$$

where $L$ is a real constant arising from the properties of $F(\Omega)$ which may be any suitable rational function or polynomial.

The definitions (81) and (82) are very important because filter design is based on symmetrical and inverse-impedance basic networks, even if losses are to be considered, since a suitable function $F(\Omega)$ can be found and handled analytically for eqn. (82), while a suitable function of the form of eqn. (78) cannot be found easily without special devices (an electrolytic tank for example). However, the form of eqn. (78) can be constructed for networks with dissipative elements by a properly predistorted insertion-loss voltage ratio. The construction of numerator $N'$ for eqn. (78), for a symmetrical unequally terminated network, for example, can be obtained simply from the basic function in the following way:

$$\frac{\mathscr{P}_{20}}{\mathscr{P}_2} = 1 + (H^2\phi^2)_{\eta_G=1} = 1 - \left(\frac{p^2 B'^2}{P^2}\right)_{\eta_G=1} = \eta_G + \frac{(N')_{\eta_G \leqslant 1}}{P^2}$$

from which follows that

$$(N')_{\eta_G \leqslant 1} = (1 - \eta_G)P^2 - p^2(B'^2)_{\eta_G=1} = (A'^2)_{\eta_G<1} - p^2(B'^2)_{\eta_G \leqslant 1}$$

At present we shall assume that the characteristic function $\phi$ is given in the form of either eqn. (78) or eqn. (82). [It may be noted that eqn. (82) is a special case of eqn. (78) with the real root and real parts of complex roots equated to zero; also $(-j)^{o(n)}\phi(p) = \phi(\Omega)$ and $\phi(-p) = (-1)^{o(n)}\phi(p)$.] In network design from specifications (65)–(67), it is necessary to evaluate the polynomials $A'$, $B'$, $A$ and $B$, defining solely the design network impedances. The polynomials $A'$ and $B'$ can be evaluated from the characteristic functions (78)–(82); thus

$$N' = \eta_G^{e(n)} H^2 \sum_{s=0}^{n} N'_s p^{2s}$$

$$= \eta_G^{e(n)} H^2 (p_0'^2 - p^2)^{o(n)} \prod_{s=1}^{\nu+e(n)} (p^4 + 2\xi'_s p^2 + \rho_s'^4) = A'^2 - p^2 B'^2$$
$$. \quad . \quad . \quad (83)$$

where

$$\rho_s'^2 = p'_s p'_{-s} = \Omega_s'^2 + \alpha_s'^2; \quad \xi'_s = -\tfrac{1}{2}(p_s'^2 + p_{-s}'^2) = \Omega_s'^2 - \alpha_s'^2;$$
$$\rho_s'^2 \geqslant \xi'_s \quad . \quad . \quad . \quad . \quad (84)$$

We may note that $N' = (A' + pB')(A' - pB')$ and $\sqrt{H^2} = \pm H = H'$. The sign of the real root and of the real part of the complex roots are left arbitrary as yet. (Complex roots must be in conjugate pairs, and if $\alpha'_s = 0$ then $\rho'_s = \Omega'_s = \Omega_{os}$.) We can thus identify the polynomial $(A' + pB')$ with the expression given by

$$A' + pB' = \sqrt{[\eta_G^{e(n)}]}H'(p - p_0')^{o(n)} \prod_{s=1}^{\nu+e(n)} (p^2 - 2p\mathbf{R}p'_{\pm s} + \rho_s'^2)$$
$$. \quad . \quad . \quad (85)$$

from which the polynomials $A'$ and $B'$ can be obtained in the form

$$A' = \sqrt{[\eta_G^{e(n)}]}H' \sum_{s=0}^{\nu+e(n)} A'_s p^{2s}; \quad B' = \sqrt{[\eta_G^{e(n)}]}H' \sum_{s=0}^{\nu} B'_s p^{2s} \quad . \quad (86)$$

From eqns. (85) and (86) some of the real coefficients $A'_s$ and $B'_s$ can be defined in general terms of the zero parameters. Thus

$$\left.\begin{array}{l} A'_0 = (-p_0')^{o(n)} \prod\limits_{s=1}^{\nu+e(n)} \rho_s'^2; \quad A'_{\nu+e(n)} = \left(-p_0' - 2\sum\limits_{s=1}^{\nu} \mathbf{R}p'_{\pm s}\right)^{o(n)} \\[3mm] B'_{\nu} = \left(-2\sum\limits_{s=1}^{\nu+e(n)} \mathbf{R}p'_{\pm s}\right)^{e(n)} \quad B'_{[n/2]} = o(n) \end{array}\right\} \quad (87)$$

For a particular $n$, formulae for $A'_s$ and $B'_s$ in terms of $\alpha'_s$ and $\rho_s'^2$ can be readily formed, provided the signs of the real root and the real parts of complex roots are properly chosen. The proper sign of $H'$ and $p_0'$ will be discussed in Section 3.2. This problem only exists for non-basic networks, which include also dissipative networks.

Reductions of poles or zeros in eqn. (82) lead also to special cases and are also consistent with general formulae. It will be shown in Section 5.2 that, if all poles are shifted to infinity and all zeros to the origin of the frequency axis, a maximally flat characteristic function is obtained; the corresponding network, as is well known, will be of constant-$k$ configuration. A constant-$k$ filter has its poles at infinity, $\Omega_{\infty s} = \infty$, and some of its zeros at zero frequency; e.g. when terminated at equal resistances $p_0' = p'_{\pm 1} = 0$ and all $p_{\pm\infty s} = \pm j\infty$. This will be discussed in Section 5.1. Other types of filter may have some zeros reduced to zero and some poles at infinity, but the general formulae only simplify in particular cases. Other important polynomials which need to be evaluated are the $A$ and $B$ ones, defining the insertion-loss voltage ratio. These polynomials are derived as follows. Consider first the rational function $|\Xi(p)|^2$ formed from

$$|\Xi(p)|^2 = 1 + H^2|\phi|^2 = \frac{N'/\eta_G^{e(n)} + P^2}{P^2}$$

$$= H^2 \frac{\sum\limits_{s=0}^{n} N'_s p^{2s} + H^{-2} \sum\limits_{s=0}^{2m} S_s p^{2s}}{P^2} \quad . \quad (88)$$

where
$$P^2 = \prod_{s=1}^{m} \left(\frac{p^2}{\Omega_{\infty s}^2} + 1\right)^2 = S = \sum_{s=0}^{2m} S_s p^{2s} \quad . \quad . \quad (89)$$

(The coefficients $N'_s$ and $S_s$ are all real.) Equating $|\Xi(p)|^2$ to zero and factorizing the numerator, one obtains the following form:

$$H^{-2}P^2|\Xi(p)|^2 = \sum_{s=0}^{n} N'_s p^{2s} + H^{-2} \sum_{s=0}^{2m} S_s p^{2s}$$

$$= \sum_{s=0}^{n} N_s p^{2s} = (p_0^2 - p^2)^{o(n)} \prod_{s=1}^{[n/2]} (p^4 + 2\xi_s p^2 + \rho_s^4) \quad . \quad (90)$$

where
$$\rho_s^2 = p_s p_{-s} = \Omega_s^2 + \alpha_s^2 \text{ and } \xi_s = -\tfrac{1}{4}(p_s^2 + p_{-s}^2) = \Omega^2 - \alpha_s^2$$
$$. \quad . \quad . \quad (91)$$

from which $2\alpha_s = \sqrt{[2(\rho_s^2 - \xi_s)]}$. The quantities $\alpha_s$, $\rho_s^2$ and $\Omega_s$, as will be shown below, are the root parameters of insertion loss as well as of the discrimination function. Now $|\Xi(p)|^2$ can be expressed in an alternative, factorized form

$$|\Xi(p)|^2 = \frac{H^2 \sum\limits_{s=0}^{n} N_s p^{2s}}{P^2} = H^2 \frac{(p_0^2 - p^2)^{o(n)} \prod\limits_{s=1}^{[n/2]} (p^2 - p_s^2)(p^2 - p_{-s}^2)}{P^2}$$
$$. \quad . \quad . \quad (92)$$

Recalling eqn. (31), which states that $\mathscr{P}_{20}/\mathscr{P}_2 = \eta_G^{e(n)}|\Xi(p)|^2 = N/P$ while $N = \eta_G^{(e)n} H^2 \sum\limits_{s=0}^{n} N_s p^{2s} = (A + pB)(A - pB)$, and

noting that the voltage ratio $V_{20}/V_2$ corresponds to a minimum phase system, i.e. a system whose phase, and consequently the location of roots, is uniquely defined in the left half-plane, e.g. $p_{\pm s} = -\alpha_s \pm j\Omega_s$. The above-stated condition, together with eqns. (31) and (92), enables us to form the voltage ratio directly, by means of the roots, with negative real parts, selected from eqn. (92) or more clearly from

$$|\Xi(p)|^2 = (-1)^n H^2$$

$$\frac{[(p-p_0)(p+p_0)]^{o(n)} \prod_{s=1}^{[n/2]} (p-p_s)(p+p_s)(p-p_{-s})(p+p_{-s})}{P^2}$$

$$= \Xi(p)\,\Xi(-p) \quad . \quad (93)$$

from which we may form

$$\frac{V_{20}}{V_2} = \Lambda(p) = \frac{A+pB}{P}$$

$$= \sqrt{[\eta_G^{e(n)}]} H(p-p_0)^{o(n)} \frac{\prod\limits_{s=1}^{[n/2]} (p-p_s)(p-p_{-s})}{P}$$

$$= \sqrt{[\eta_G^{e(n)}]} H(p+\alpha_0)^{o(n)} \frac{\prod\limits_{s=1}^{[n/2]} (p^2+2\alpha_s p+\rho_s^2)}{P} \quad . \quad (94)$$

The $A$- and $pB$-polynomials are found by identification with the even and the odd polynomials in the numerator of eqn. (94).*

The voltage-ratio zeros (also called natural modes, or free oscillations, i.e. values of $p$ at which the output voltage $V_2$ can exist in the absence of a driving source) will be defined by

$$\left.\begin{aligned} p_{\pm s} &= -\alpha_s \pm j\Omega_s \text{ for } s = e(n), 1, 2, \ldots, [n/2] \\ \text{and also} \qquad \Omega_0 &\equiv 0 \text{ and } p_0 = -\alpha_0 \end{aligned}\right\} \quad . \quad (95)$$

The real constant $H$, which we can take as a positive real quantity, should satisfy the relation

$$\left.\frac{V_{20}}{V_2}\right|_{p=0} = 1 \quad \text{and} \quad \sqrt{[\eta_G^{e(n)}]} H = A_0^{-1} \quad . \quad (96)$$

(In the case of a dissipative network $\left.\dfrac{V_{20}}{V_2}\right|_{p=0} > 1$, and hence eqn. (94) requires an additional constant.) The polynomials $A$ and $B$ can be evaluated from eqn. (94) in the form

$$A = \sqrt{[\eta_G^{e(n)}]} H \sum_{s=0}^{\nu+e(n)} A_s p^{2s}; \quad B = \sqrt{[\eta_G^{e(n)}]} H \sum_{s=0}^{\nu} B_s p^{2s} \quad . \quad (97)$$

Similarly, as in eqns. (85) to (87), some of the real and, in this case, positive coefficients $A_s$ and $B_s$ can be determined in general by the voltage-ratio root parameters

$$A_0 = \alpha_0^{o(n)} \prod_{s=1}^{\nu+e(n)} \rho_s^2; \quad A_{\nu+e(n)} = \left(\alpha_0 + 2\sum_{s=1}^{\nu} \alpha_s\right)^{o(n)};$$

$$B_\nu = \left(2\sum_{s=1}^{\nu+e(n)} \alpha_s\right)^{e(n)}; \quad B_{(n/2)} = o(n) \quad . \quad . \quad (98)$$

* The other approach in obtaining $A$ and $pB$, or $2\alpha_s$ and $\rho_s^2$ which define the voltage ratio $\Lambda(p)$ is by equating $\Xi(p)$ to zero. For the case of eqn. (82) and for odd $n$, $\Xi(p) = 1 + jH\phi = 0 = P + pB'$. The roots of $(P + pB')$ will occur in the left as well as in the right half-plane; the quantities $2\alpha_s$ and $\rho_s^2$, however, are the same in $\Xi(p)$ and $\Lambda(p)$. (The sign of the real parts of the roots of $\Xi(p)$ for odd $n$ provides important information where lattice structure is concerned. The roots located in the left half-plane can be used, for example, for the determination of series-lattice branch impedance, or its dual, while those in the right half-plane will determine the diagonal branch, or vice versa.) Once the roots of $\Xi$ are determined the $2\alpha_s$ and $\rho_s^2$ can be used directly for the formation of $\Lambda(p)$ and hence $A$ and $B$. In case of $n$ even, $\Xi(p) = 0$ can also be used for the determination of $2\alpha_s$ and $\rho_s^2$, thus $\Xi(p) = 1 + jH\phi = 0 = \sum_{s=0}^{n/2} A_s' p^{2s} + jP/H = \prod_{s=1}^{n/2}(p^2 - x_s)$ where, $|\mathbf{R}x_s| = \xi_s$ and $|\mathbf{I}x_s| = 2\Omega_s\alpha_s$, from which $\rho_s^2 = \sqrt{(\xi_s^2 + 4\alpha_s^2\Omega_s^2)}$ and $2\alpha_s = \sqrt{[2(\rho_s^2 - \xi_s)]}$. In this case, however, the polynomial to be factorized is in $p^2$ with complex coefficients, but the degree is lower than that of $|\Xi(p)|^2$, used for eqns. (88) to (91).

The coefficients $A_s$ and $B_s$ are determined uniquely because they correspond to a minimum phase-shift network function. However, the coefficients of the $A'$- and $B'$-polynomials depend on the signs of $p_0'$, $\mathbf{R}p_{\pm s}'$ and $H'$. These signs must be determined before the impedance function can be formed. It will be shown that the signs of $p_0'$ and $H'$ can be determined uniquely for particular ladder configurations and terminations while the sign of $\mathbf{R}p_{+s}'$ is arbitrary and thus leads to multiplicity of solutions, which result in networks with the same insertion loss but different component values. The possibility of positive real parts of $p_{\pm s}'$ arises from non-physical roots, which occur in $(\pm A' + pB')$, defining the numerator of the reflection factors. This corresponds to a non-physical impedance $(R - Z_{in})$, as mentioned in eqn. (38) and the following discussion. The signs of $p_0'$ and $H'$ will be discussed in the following Section.

### (3.2) Sign Determination of $H'$ and $p_0'$ and Relation of the Termination for Design Procedure

Inspection of the reflection factor $\Gamma$ to determine the signs of $H'$ and $p_0'$ gives

$$\left.\Gamma_{1,\mathrm{T}e(n)}\right|_{p=\infty} = \left.\frac{R_1 - Z_{1,\mathrm{in\,T}}}{R_1 + Z_{1,\mathrm{in\,T}}}\right|_{p=\infty} = -1 = \left.\frac{A'+pB'}{A+pB}\right|_{p=\infty} = \frac{H'}{H}$$

$$\quad . \quad . \quad . \quad . \quad (99)$$

where $H' = -H$, for T- or $\mathrm{T}_{\Pi}$-configurations. It is observed that the sign is determined by the reactance of the first branch only. Similarly, for a $\Pi_{e(n)}$-structure,

$$\left.\Gamma_{1,\Pi e(n)}\right|_{p=\infty} = \left.\frac{R_1 - Z_{1,\mathrm{in\,\Pi}}}{R_1 + Z_{1,\mathrm{in\,\Pi}}}\right|_{p=\infty} = 1 = \frac{H'}{H} \quad . \quad (100)$$

Thus $H' = H$ for $\Pi$- or $\Pi_T$-configurations. The relation between the termination and the sign of the real root which exists for odd $n$ is found from the following. Considering a T- or $\mathrm{T}_{\Pi}$-configuration:

$$\left.\Gamma_{1,\mathrm{T}e(n)}\right|_{p=0} = \frac{R_1-R_2}{R_1+R_2} = \left.\frac{A'+pB'}{A+pB}\right|_{p=0}$$

$$= \frac{-A_0'}{A_0} = \frac{-(-p_0')^{o(n)} \prod\limits_{s=1}^{\nu+e(n)} \rho_s'^2}{A_0} \quad . \quad (101)$$

as $A_0$ is positive real, and all $\rho_s'$ and $\alpha_s'$ are also positive real, the sign of $p_0'$ is given by

$$p_0' = \frac{R_1 - R_2}{|R_1 - R_2|} \alpha_0' \quad . \quad . \quad . \quad . \quad (102)$$

and normal termination for a T-configuration will be assumed, $R_1 \geqslant R_2 \geqslant 0$, while for an even $n$ and $\mathrm{T}_{\Pi}$-configuration $R_1 \leqslant R_2 \leqslant \infty$. Similarly, for a $\Pi$- or $\Pi_T$-configuration,

$$\left.\Gamma_{1,\Pi e(n)}\right|_{p=0} = \frac{R_1-R_2}{R_1+R_2} = \frac{A_0'}{A_0}, \quad \text{hence} \quad p_0' = \frac{R_2-R_1}{|R_2-R_1|} \alpha_0'$$

$$\quad . \quad . \quad . \quad . \quad (103)$$

and normal termination for a $\Pi$-configuration is $R_1 \leqslant R_2 \leqslant \infty$, while for an even $n$ for $\Pi_T$-configuration it is $R_1 \geqslant R_2 \geqslant 0$. All these illustrated cases refer to design end (1); by similar reasoning it is possible to define conditions from end (22'). [The sign of $H'$ other than that following from eqn. (99) or (100) implies the use of an ideal transformer or perfectly coupled inductances.] A useful relation concerning the termination, the coefficients of the design polynomials $A_0$ and $A_0'$, and the

transformer primary/secondary turns ratio $t$ for even or odd $n$ is given by

$$\eta_G = 1 - \frac{A_0'^2}{A_0^2}; \quad t = \mathbf{A}(0)\big|_{R_1 = R_2} = \frac{1}{\mathbf{D}(0)}\bigg|_{R_1 = R_2}$$

$$\frac{R_2}{R_1} = \frac{1 - \Gamma_1(0)}{1 + \Gamma_1(0)} = \frac{A_0 - \dfrac{R_1 - R_2}{|R_1 - R_2|}|A_0'|}{A_0 + \dfrac{R_1 - R_2}{|R_1 - R_2|}|A_0'|} = (t^2)_{R_2 = R_1}$$

$$= \tanh^2\left[\tfrac{1}{2}\operatorname{arc\,sinh}\frac{1}{H\phi(0)}\right] \quad . \quad (104)$$

These formulae can be derived from eqns. (31), (36) and the above discussion.

### (3.3) Multiplicity of Solutions

At this stage a multiplicity of solutions in filter design can be limited to the real parts of the complex conjugate roots, which can be taken arbitrarily. However, it is expedient to choose a certain order of signs, e.g.

$$\mathbf{R}p'_{\pm s} = (\_+)^{e(n)}(-1)^s\left(\frac{p_0'}{\alpha_0'}\right)^{o(n)}\alpha_s'$$

or still more simply

$$\mathbf{R}p_{\pm s} = (\_+)^{e(n)}\left(\frac{p_0'}{\alpha_0'}\right)^{o(n)}\alpha_s$$

which would yield realizable design impedances and also simplify the general formulation (for even $n$ either of the signs $+$ or $-$ may be taken). The efficient choice of $\mathbf{R}p'_{\pm s}$ is perhaps of importance only when the required filter, computed with losses (or, in general, unequally terminated) for a certain bandwidth, produces critical components too small or too large for the requirements. Then a proper alteration of signs will lead to different component values. There are existing methods which permit design for prescribed decrements, and some of these methods will be illustrated in simple cases. It may be mentioned here that there exists another type of multiplicity of solutions, resulting from the fact that, to a certain extent, $\Omega_{\infty s}$ can be distributed arbitrarily between the proper branches, i.e. $\zeta_s = 1/\Omega_{\infty r}^2$. In the general case still another multiplicity of solutions may arise from the possibility of attributing constant factors to $N$ and $P^2$, which, within our case of low-pass analogue, is eliminated by definition of $P$. The advantage of the choice of signs in $\mathbf{R}p'_{\pm s} = (\_+)^{e(n)}(p_0'/\alpha_0')^{o(n)}\alpha_s'$ is merely that the formulation of a design-impedance procedure can be defined uniquely. This choice of sign also serves well as an illustration. Once this idea is comprehended the computation of a particular case can be handled without difficulty. We shall illustrate some of the effects of the choice of signs in Section 5.2 in a simple maximally flat case.

### (3.4) Formation of Design-Impedance Functions

All the impedances given in eqn. (32) must lead to the same network once $A'$ and $B'$ and the sequence of $\Omega_{\infty r}$ or $\zeta_s$ have been chosen. For illustration, it is expedient to choose one such impedance from which all the ladder coefficients can be computed. The ladder structure under consideration, as shown in Fig. 2, consists of $T_{e(n)}$ and $\Pi_{e(n)}$, i.e. T-, $\Pi$-, $T_\Pi$- and $\Pi_T$-configurations.

It was demonstrated that the ladder coefficients are evaluated from 2-terminal networks which represent corresponding open- or short-circuit design impedances. The short- or open-circuit impedances are formed in terms of the insertion-loss polynomials $A$, $B$, $A'$ and $B'$ and the arbitrary termination resistances

$R_1$ and $R_2$, according to eqn. (32). The $A'$-, $B'$-, $A$- and $B$-polynomials are formed according to eqns. (85)–(87) and (97). The constants $H$ and $H'$ reduce to unity, leaving the sign as determined in Section 3.2. From Fig. 2 it may be observed that T- or $\Pi_T$-configurations provide 2-terminal networks with all the elements when short-circuited; on the other hand, $\Pi$- and $T_\Pi$-configurations do so when open-circuited. It is thus expedient to choose these impedances for computation of ladder coefficients. To simplify the problem we shall examine a case where all roots of $(A' + pB')$ lie in the same half-plane, which can be defined by

$$\mathbf{R}p'_{+s} = (\_+)^{e(n)}\left(\frac{p_0'}{\alpha_0'}\right)^{o(n)}\alpha_s'; \quad s = e(n), 1, 2, \ldots [n/2] \quad . \quad (105)$$

where, for even $n$, either of the signs $+$ or $-$ may be taken. This case gives a unique solution of $A'$ and $B'$ for odd $n$ and hence enables a unique determination of the design impedance. Let us relate symbolically the quantities $A \_+ A' \propto \bar{A}$ and $B \_+ B' \propto \bar{B}$, which, with the conditions of eqn. (105) and Section 3.2, can be determined uniquely for a chosen configuration, number of branches in the ladder, and termination. Once the idea is understood it can be easily extended to other impedances, with an arbitrary distribution of signs in each case, which arises from the multiplicity of solutions and can be handled systematically if required.

Considering eqn. (105), we can state that

$$A_s' = (-p_0/\alpha_0)^{o(n)}|A_s| \quad \text{and} \quad B_s' = (\_+)^{e(n)}|B_s'|$$

while $A_s$ and $B_s$ are positive real coefficients. It can be checked that, in such a case, for odd $n$, the sign of $B'$ will only depend on $H'$, while that of $A'$ will depend on $H'$ and $p_0'$. On the other hand, for even $n$, $A'$ depends on $H'$ while $B'$ may have arbitrary sign. Hence, for eqn. (105), the $A'$- and $B'$-polynomials are defined by

$$A' = \sqrt{[\eta_G^{e(n)}]}\left(\frac{-p_0'}{\alpha_0'}\right)^{o(n)}H'\sum_{s=0}^{\nu + e(n)}|A_s|p^{2s};$$

$$B' = (\_+)\sqrt{\eta_G})^{e(n)}H'\sum_{s=0}^{\nu}|B_s'|p^{2s} \quad . \quad . \quad . \quad (106)$$

and the signs of $H'$ and $p_0'$ are determined as described in Section 3.2. For the condition stated in eqn. (105) for even $n$ all $A_s'$ will be positive, while for odd $n$ they will have the same sign as $-p_0'$; hence $|A_s'|$ can be computed by means of $\alpha_0'$, $2\alpha_s'$ and $\rho_s'^2$, which are positive real quantities, in exactly the same way as $A_s$ by means of $\alpha_0$, $2\alpha_s$ and $\rho_s^2$. The $B_s'$ will all be positive for odd $n$, and for even $n$ all may have the sign which was chosen in eqn. (105). For the design impedances and normal termination the design formulae takes the following form:

For $R_1 \leqslant R_2 \leqslant \infty$,

$$Z_{1,oc,\Pi} \text{ or } Z_{1,oc,T_\Pi} = Z_{1,oc} = R_1\frac{A - A'}{p(B + B')} = R_1\frac{\bar{A}}{p\bar{B}} \quad . \quad (107)$$

while, for $R_1 \geqslant R_2 \geqslant 0$,

$$Z_{1,sc,T} \text{ or } Z_{1,sc,\Pi T} = Z_{1,sc} = R_1\frac{p(B - B')}{A + A'} = R_1\frac{p\bar{B}}{\bar{A}} \quad . \quad (108)$$

where $\bar{A} = \sum_{s=0}^{\nu + e(n)}\bar{A}_s p^{2s}$     where $\bar{A}_s = A_s + |A_s'|$

and $\quad \bar{B} = \sum_{s=0}^{\nu}\bar{B}_s p^{2s}$     where $\bar{B}_s = B_s + B_s'$    . (109)

In the case of open- or short-circuit termination, special formulae are given in Section 2.3, but these are also consistent

with eqn. (109), with the only restriction that the $B'_s$ must all be taken with positive sign, i.e. in eqns. (107) and (108) $p'_{\pm s} = -p_{\pm s}$. These formulae can be checked by using Section 3.2. It may be observed that $\sqrt{\eta_G}$ and $H'$, $H$ cancel, in effect, leaving only the proper sign. The inversion of the normal resistance ratio amounts to designing from the other end; in fact, a similar set of design formulae can be derived from the other end (except the open- or short-circuit-termination case), where in effect the polynomials $\bar{A}$ and $\bar{B}$ will be defined by the coefficients $\bar{A}_s = A_s + (-1)^n|A'_s|$, while $\bar{B}_s = B_s - (-1)^n B'_s$, where $A_s$, $B_s$, $A'_s$ and $B'_s$ are the same as in eqns. (107)–(109). It is thus seen that the ladder coefficients derived for one configuration can be related in a proper way to its dual. It may be mentioned again that $\bar{A}$ and $\bar{B}$ are symbolic notations, and must be related in the way illustrated in eqns. (107)–(109) to the configuration and number of branches. In general, we can write for any such expression in the design impedances in eqn. (32)

$$\frac{A \_{\pm} A'}{B \_{\pm} B'} = \frac{\bar{A}}{\bar{B}} \quad \ldots \quad (110)$$

Proper sign is, of course, fixed in any particular case. For the design impedances chosen in eqns. (107)–(109) for eqn. (105), the $\bar{A}$- and $\bar{B}$-polynomials will be of the same degree and character as $A$ and $B$, and for open- or short-circuit $\bar{A}/\bar{B} = A/B$. The realizability requirements, which follows from Brune's realizability theory, are that $(\bar{A} + p\bar{B})$ must be a Hurwitz polynomial with negative real parts of complex conjugate roots (and a negative real root). (For other design impedances $\bar{A}$ and $\bar{B}$ may be of reduced degree.) $\bar{A}$ and $\bar{B}$ are obviously even polynomials in $p$ or $\Omega$, and for symmetrical and inverse-impedance networks can be expressed in the form, for the impedances chosen in eqns. (107)–(109),

$$\left.\begin{array}{l} \bar{A} = \sum_{s=0}^{\nu+e(n)} \bar{A}_s p^{2s} = \bar{A}_{\nu+e(n)} \prod_{s=1}^{\nu+e(n)} (p^2 + \Omega_{As}^2) \\[2mm] \text{and} \quad \bar{B} = \sum_{s=0}^{\nu} \bar{B}_s p^{2s} = \bar{B}_\nu \prod_{s=1}^{\nu} (p^2 + \Omega_{Bs}^2) \end{array}\right\} \quad . \quad (111)$$

where $\bar{A}_s$ and $\bar{B}_s$ can be computed for any particular case and are given in eqn. (109) for the particular conditions (105). It should be observed that, for a reactive network, the roots of $\bar{A}$ and $\bar{B}$ are real quantities; hence $\Omega_{As}$ and $\Omega_{Bs}$ correspond to real frequencies. The $\Omega_{Bs}$ represent natural oscillation frequencies of the network when its terminals are short-circuited (i.e. when the driving voltage is zero), while $\Omega_{As}$ represent that when the terminals are open-circuited (driving current is zero). If $\Omega_{As}$ and $\Omega_{Bs}$ are all smaller than $\Omega_{\infty m}$, the ladder coefficients will all turn positive for any distribution of $\Omega_{\infty s}$ between the branches; thus

$$a_s > 0 \text{ when } (\Omega_{As})_{max} < \Omega_{\infty m} > (\Omega_{Bs})_{max} \quad . \quad (112)$$

### (3.5) Determination of Design Function $\mathscr{F}(\zeta)$, enabling the Computation of Ladder Coefficients

As follows from the previous investigation, the design function $\mathscr{F}(\zeta)$ can be formed most conveniently for even or odd $n$ from the design impedances in eqns. (107) and (108).

For odd $n$,

$$\mathscr{F}(\zeta) = \frac{Z_{1,sc,\mathrm{T}}}{pR_{1,\mathrm{T}}}\Big|_{p^2=-1/\zeta} = \frac{R_{1,\Pi}}{pZ_{1,oc,\Pi}}\Big|_{p^2=-1/\zeta} = \frac{\bar{B}}{\bar{A}}\Big|_{p^2=-1/\zeta} \quad . \quad (113)$$

where $R_{1,\mathrm{T}} = R_{2,\Pi}$ and $R_{1,\Pi} = R_{2,\mathrm{T}}$

and, for even $n$,

$$\mathscr{F}(\zeta) = \frac{Z_{1,oc,\mathrm{T}\Pi}}{pR_{1,\mathrm{T}\Pi}}\Big|_{p^2=-1/\zeta} = \frac{R_{1,\Pi\mathrm{T}}}{pZ_{1,sc,\Pi\mathrm{T}}}\Big|_{p^2=-1/\zeta} = \frac{\bar{A}}{p^2\bar{B}}\Big|_{p^2=-1/\zeta} \quad . \quad . \quad (114)$$

where $R_{1,\mathrm{T}\Pi} = R_{2,\mathrm{T}\Pi}$ and $R_{1,\Pi\mathrm{T}} = R_{2,\Pi\mathrm{T}}$

In general, for even or odd $n$ and for the above chosen impedances,

$$\mathscr{F}(\zeta) = \left[\frac{1}{p}\left(\frac{\bar{A}}{p\bar{B}}\right)^{(-1)^n}\right]_{p^2=-1/\zeta} = \left(\frac{\bar{A}_0}{\bar{B}_0}\frac{\mathscr{A}}{\mathscr{B}}\right)^{(-1)^n}$$

$$= \left(\frac{\bar{A}_0}{\bar{B}_0}\frac{\sum_{s=0}^{\nu+e(n)}\mathscr{A}_s\zeta^s}{\sum_{s=0}^{\nu}\mathscr{B}_s\zeta^s}\right)^{(-1)^n} \quad . \quad (115)$$

where $\mathscr{A}$ and $\mathscr{B}$ are polynomials in $\zeta$ and their coefficients $\mathscr{A}_s$ and $\mathscr{B}_s$ are formed by means of $\bar{A}_s$- and $\bar{B}_s$-coefficients from the relation

$$\mathscr{A}_s = (-1)^s\frac{\bar{A}_{\nu+e(n)-s}}{\bar{A}_0} \quad \text{and} \quad \mathscr{B}_s = (-1)^s\frac{\bar{B}_{\nu-s}}{\bar{B}_0} \quad . \quad (116)$$

Having defined $\mathscr{F}(\zeta)$, the ladder coefficients can be computed according to eqns. (61)–(64)* or by a method which will now be given.

### (3.6) Procedure and Formulae for the Computation of Ladder Coefficients

The following method, originated by Darlington,[5] is also of great service in the computation of ladder coefficients. The operations are simple but, unfortunately, have many stages, differing for symmetrical and inverse-impedance networks in such a way that the complete design procedure for these networks cannot be formulated in a simple manner. For this reason we shall break from general formulae at a certain stage and refer to particular cases for even or odd $n$; for each of these a special set of formulae will be added. Design impedances other than those given for illustration can be handled in much the same way: however, these are rarely needed.

#### (3.6.1) Design Procedure.

The approach to the design of an actual network from chosen design impedance requires preparation of the same $\mathscr{F}(\zeta)$ design function as for the general method, (Section 2.4), and in addition, in this case, it is necessary to factorize one of the polynomials, either $\mathscr{A}$ or $\mathscr{B}$, according as $n$ is even or odd. The polynomials $\mathscr{A}$ or $\mathscr{B}$ must be generally expressed in the factorized form

$$\left.\begin{array}{l} \mathscr{A} = \sum_{s=0}^{\nu+e(n)}\mathscr{A}_s\zeta^s = (-1)^{\nu+e(n)}\prod_{s=1}^{\nu+e(n)}(\zeta-\zeta_{As}) \\[2mm] \mathscr{B} = \sum_{s=0}^{\nu}\mathscr{B}_s\zeta^s = (-1)^\nu\prod_{s=1}^{\nu}(\zeta-\zeta_{Bs}) \end{array}\right\} \quad . \quad (117)$$

In the further procedure, this method differs from the general one only in form. $\mathscr{F}(\zeta)$ for this method is to be expanded as the sum of partial fractions, which may be defined generally for even or odd $n$ by

$$\mathscr{F}(\zeta) = \left(\frac{\bar{A}_0}{\bar{B}_0}\frac{\mathscr{A}}{\mathscr{B}}\right)^{(-1)^n} = -\zeta u_0 + u_\infty + \sum_{q=1}^{\nu}\frac{u_{q0}}{(\zeta-\gamma_q)} \quad . \quad (118)$$

* $\mathscr{F}(\zeta)$ can be formed from impedances other than those given in eqns. (113) and (114) in much the same way. $\mathscr{H}_{qq}$ for eqn. (62) can be evaluated for even or odd $n$ from

$$\overset{\circ}{\mathscr{F}}(\zeta) = o(n)\left[\frac{\bar{B}_0}{\bar{A}_0}\overset{\circ}{\mathscr{B}}(\zeta) - \mathscr{F}(\zeta)\overset{\circ}{\mathscr{A}}(\zeta)\right]/\mathscr{A}(\zeta) + e(n)\left[\frac{\bar{A}_0}{\bar{B}_0}\overset{\circ}{\mathscr{A}}(\zeta) - \mathscr{F}(\zeta)\overset{\circ}{\mathscr{B}}(\zeta)\right]/\mathscr{B}(\zeta)$$

where $u_0$, $u_\infty$, $u_{q0}$ and $\gamma_s$ are real positive constants derived in slightly different ways for even or odd $n$. The poles of the design impedance are defined by $\gamma_s$. These quantities must be obtained from proper polynomials; thus, for odd $n$, $\gamma_s$ are the roots of the $\mathscr{A}$-polynomial, defined by

$$\gamma_s = \zeta_{As} = 1/\Omega_{As}^2 \quad . \quad . \quad . \quad . \quad (119)$$

For even $n$, $\gamma_s$ are the roots of the $\mathscr{B}$-polynomial, defined by

$$\gamma_s = \zeta_{Bs} = 1/\Omega_{Bs}^2 \quad . \quad . \quad . \quad . \quad (120)$$

The sufficient conditions for ladder coefficients to be positive are stated below. (For this, roots of $\mathscr{A}$- and $\mathscr{B}$-polynomials are needed.)

$$a_r > 0 \begin{cases} \text{when} \quad \zeta_1 \leqslant (\zeta_{Bs})_{\min} \geqslant \zeta_{[n/2]} \quad . \quad . \quad (121) \\ \text{and} \quad (\zeta_{As})_{\min} > 1/\Omega_{\infty\nu}^2 = (\zeta_s)_{\max} \quad (122) \end{cases}$$

For calculations it is expedient to choose $\zeta_1 = 1/\Omega_{\infty 1}^2$ and $\zeta_{[n/2]} = o(n)/\Omega_{\infty 2}^2$, which provides the smallest possible chance for ladder coefficients to appear negative. We assume also that $\zeta_{\nu+1} = 0$ for even or odd $n$.

If the general (Section 2.4) method is used, factorization of neither $\mathscr{A}$- nor $\mathscr{B}$-polynomials is needed. The condition for $a_r > 0$ is seen from $\mathscr{A}(\zeta_s) > 0$ and $\mathscr{B}(\zeta_1) > 0 < \mathscr{B}(\zeta_{[n/2]})$. For open- or short-circuited network design $\zeta_1 \leqslant (\zeta_{Bs})_{\min}$ suffice for eqn. (121). Negative ladder coefficients which sometimes occur, especially in open- or short-circuit design (e.g. when $k_B$ approach unity and $D_p$ is chosen too small), often turn out to be positive with equal or inverse termination, owing to the addition of the $A'$- or $B'$-polynomial. A ladder with a negative coefficient can also be turned into one with a positive one by

### Table 1

THE CONSTANTS $u_0$, $u_\infty$, $u_{q0}$

| $n$ odd; $\frac{n-1}{2} = \left[\frac{n}{2}\right] = \nu$ | $n$ even; $\frac{n}{2} - 1 = \nu$ |
|---|---|
| $u_\infty = \dfrac{\bar{B}_0}{\bar{A}_0}$; $u_0 = 0$ | $u_0 = \dfrac{\bar{A}_0}{\bar{B}_0}$; |
| | $u_\infty = (-1)^\nu u_0 (\mathscr{A}_\nu + \mathscr{B}_{\nu-1}) > 0$ |
| $\mathscr{F}(\zeta) = u_\infty \dfrac{\mathscr{B}}{\mathscr{A}} = u_\infty \left(1 + \dfrac{\mathscr{R}}{\mathscr{A}}\right)$ | $\mathscr{F}(\zeta) = u_0 \dfrac{\mathscr{A}}{\mathscr{B}}$ |
| | $= -\zeta u_0 + u_\infty + \dfrac{u_\infty \mathscr{R}}{(-1)^\nu \mathscr{B}}$ |
| $= u_\infty + \sum\limits_{q=1}^{\nu} \dfrac{u_{q0}}{(\zeta - \zeta_{Aq})}$ | $= -\zeta u_0 + u_\infty + \sum\limits_{q=1}^{\nu} \dfrac{u_{q0}}{(\zeta - \zeta_{Bq})}$ |
| where $\mathscr{R}$ is the remainder polynomial defined by | where $\mathscr{R}$ is the remainder polynomial defined by |
| | $\mathscr{R} = \sum\limits_{s=0}^{\nu-1} \mathscr{R}_s \zeta^s$; |
| $\mathscr{R} = \sum\limits_{s=0}^{\nu-1} \mathscr{R}_s \zeta^s$; $\mathscr{R}_s = \mathscr{B}_s - \mathscr{A}_s$ | $\mathscr{R}_s = \mathscr{D}_s + (-1)^{[n/2]} \mathscr{B}_s$ |
| | $\mathscr{D}_s = \dfrac{\mathscr{A}_s + \mathscr{B}_{s-1}(1 - \delta_{os})}{\mathscr{A}_\nu + \mathscr{B}_{\nu-1}}$ |
| and the residues $u_{q0}$ can be computed from | and the residues $u_{q0}$ can be computed from |
| $u_{q0} = \dfrac{u_\infty (\zeta - \zeta_{Aq}) \mathscr{R}(\zeta)}{(-1)^\nu \prod\limits_{s=1}^{\nu} (\zeta - \zeta_{As})} \bigg|_{\zeta = \zeta_{Aq}}$ | $u_{q0} = \dfrac{u_\infty (\zeta - \zeta_{Bq}) \mathscr{R}(\zeta)}{\prod\limits_{s=1}^{\nu} (\zeta - \zeta_{Bs})} \bigg|_{\zeta = \zeta_{Bq}}$ |
| $q = 1, 2, 3, \ldots \nu$ | $q = 1, 2, 3, \ldots \nu$ |

proper predistortion, described in Section 4. Another more general method leading, however, to a more complicated network was found by R. Bott and R. J. Duffin.[9]

The constants $u_0$, $u_\infty$ and $u_{q0}$ are derived for even or odd $n$ as given in Table 1.

The further procedure may now be formulated for even or odd $n$. The quantities, which must be evaluated by the aid of $u_{q0}$ for particular cases, are $u_{qs}$, $v_{qs}$ and $w_{qs}$, given by

$$\left. \begin{array}{l} q = 1, 2 \ldots, \nu \\ v_{qs} = \dfrac{u_{q(s-1)}}{\gamma_q - \zeta_s}; \quad u_{qs} = \dfrac{v_{qs}}{\gamma_q - \zeta_s}; \quad w_{qs} = \dfrac{v_{qs}}{\gamma_q - \zeta_{s+1}} \\ s = 1, 2 \ldots, \nu + e(n) \quad s = 1, 2, \ldots, \nu \quad s = 1, 2, \ldots, \nu - o(n) \end{array} \right\} \quad . \quad (123)$$

In the next step it is necessary to evaluate another set of related quantities, namely $\bar{U}_s$, $\bar{V}_s$, and $\bar{W}_s$, formed in the following way,[3,5] noting that $\nu = [n - 1 - e(n)]/2$:

$$\left. \begin{array}{l} \bar{V}_1 = 1; \quad \bar{V}_2 = \sum\limits_{q=1}^{\nu} v_{q2}; \quad \bar{V}_3 = \sum\limits_{q=1}^{\nu-1} \sum\limits_{r=2}^{\nu} v_{q3} v_{r3} (\gamma_q - \gamma_r)^2 \\ \\ \bar{V}_4 = \sum\limits_{q=1}^{\nu-2} \sum\limits_{r=2}^{\nu-1} \sum\limits_{k=3}^{\nu} v_{q4} v_{r4} v_{k4} (\gamma_q - \gamma_r)^2 (\gamma_q - \gamma_k)^2 (\gamma_r - \gamma_k)^2 \\ \\ \bar{U}_0 = 1; \quad \bar{U}_1 = u_0 + \sum\limits_{q=1}^{\nu} u_{q1}; \\ \\ \bar{U}_2 = u_0 \sum\limits_{q=1}^{\nu} u_{q2} + \sum\limits_{q=1}^{\nu-1} \sum\limits_{r=2}^{\nu} u_{q2} u_{r2} (\gamma_q - \gamma_r)^2 \\ \\ \bar{U}_3 = u_0 \sum\limits_{q=1}^{\nu-1} \sum\limits_{r=2}^{\nu} u_{q3} u_{r3} (\gamma_q - \gamma_r)^2 \\ \qquad + \sum\limits_{q=1}^{\nu-2} \sum\limits_{r=2}^{\nu-1} \sum\limits_{k=3}^{\nu} u_{q3} u_{r3} u_{k3} (\gamma_q - \gamma_r)^2 (\gamma_q - \gamma_k)^2 (\gamma_r - \gamma_k)^2 \\ \\ \bar{W}_1 = u_0 + \sum\limits_{q=1}^{\nu} w_{q1}; \\ \\ \bar{W}_2 = u_0 \sum\limits_{q=1}^{\nu} w_{q2} + \sum\limits_{q=1}^{\nu-1} \sum\limits_{r=2}^{\nu} w_{q2} w_{r2} (\gamma_q - \gamma_r)^2 \\ \\ \bar{W}_3 = u_0 \sum\limits_{q=1}^{\nu-1} \sum\limits_{r=2}^{\nu} w_{q3} w_{r3} (\gamma_q - \gamma_r)^2 \\ \qquad + \sum\limits_{q=1}^{\nu-2} \sum\limits_{r=2}^{\nu-1} \sum\limits_{k=3}^{\nu} w_{q3} w_{r3} w_{k3} (\gamma_q - \gamma_r)^2 (\gamma_q - \gamma_k)^2 (\gamma_r - \gamma_k)^2 \end{array} \right\} \quad (124)$$

The ladder coefficients can then be computed from

$$\left. \begin{array}{l} a_1 = u_\infty - u_0 \zeta_1 - \sum\limits_{q=1}^{\nu} v_{q1} \\ \\ a_{2s} = \dfrac{\bar{V}_s^2}{\bar{U}_{s-1} \bar{U}_s}; \quad a_{2s+1} = \dfrac{\bar{U}_s \bar{W}_s}{\bar{V}_s \bar{V}_{s+1}}; \quad s = 1, 2, \ldots, \nu \end{array} \right\} \quad . \quad (125)$$

The last ladder coefficient for even or odd $n$ is given by

$$a_n = a_{2[\nu+e(n)]+o(n)} = \frac{\bar{B}_0}{\bar{A}_0} - \sum\limits_{s=1}^{\nu} a_{2s-o(n)} \quad . \quad . \quad (126)$$

This coefficient can be calculated by means of the general procedure, i.e. by using $\zeta_{\nu+1} = 0$ and by extending the limits of $s$ in eqns. (123) and (124), so that $\bar{W}_\nu$ and $\bar{V}_{\nu+1}$ for $n$ odd or $\bar{U}_{\nu+1}$ for $n$ even can be computed either by eqns. (123) and (124) or (63) and (64).

For ladders with or without losses or arbitrarily terminated, the sum of even or odd ladder coefficients, according as $n$ is even or odd, is given by:

$$\sum_{s=1}^{\nu+1} a_{2s-o(n)} = \frac{\bar{B}_0}{\bar{A}_0} = \frac{\dfrac{o(n)}{\alpha_0}\left(1 + \prod_{s=1}^{\nu}\dfrac{\rho_s'^2}{\rho_s^2}\right) + \displaystyle\sum_{s=1}^{\nu+e(n)}\dfrac{2\alpha_s}{\rho_s^2} + \left(\dfrac{p_0'}{\alpha_0}\right)^{o(n)}\left[\prod_{s=1}^{\nu+e(n)}\dfrac{\rho_s'^2}{\rho_s^2}\right]\displaystyle\sum_{s=1}^{\nu+e(n)}\dfrac{2\mathbf{R}(p_s')}{\rho_s'^2}}{1 + \left(\dfrac{p_0'}{\alpha_0}\right)^{o(n)}\displaystyle\prod_{s=1}^{\nu+e(n)}\dfrac{\rho_s'^2}{\rho_s^2}} \quad \dots \quad (127)$$

For loss-free equally-terminated symmetrical and for inversely or equally-terminated inverse-impedance basic networks, $\mathbf{R}(p_s') = 0$ and $\rho_s'^2 = \Omega_{os}^2$. In the limiting case of open- or short-circuit-terminated networks, $\bar{B}_0/\bar{A}_0 = B_0/A_0$ and thus $\mathbf{R}(p_s') = \alpha_s$, $p_0' = \alpha_0$ and $\rho_s'^2 = \rho_s^2$. In the case of networks with losses, the predistorted values for $\alpha_0$, $\alpha_s$ and $\rho_s^2$, discussed in Section 4, should be used.

$\Sigma a_{2s-e(n)}$ is also found explicitly for finite termination from $(B_0 - B_0')/(A_0 - A_0')$; however, the general form consistent with the open- and short-circuit-termination cases seems too complicated.

For inverse-impedance networks ($n$ even) $a_n$ can be found explicitly; e.g. from end (11′) this is

$$a_n = \left(1 - \prod_{s=1}^{\nu+1}\frac{\Omega_{os}^2}{\rho_s^2}\right)\Bigg/\left[\left(1 + \prod_{s=1}^{\nu+1}\frac{\Omega_{os}^2}{\rho_s^2}\right)\sum_{s=1}^{\nu+1}\alpha_s\right]$$

which, for $R_1 = R_2$, simplifies to

$$a_n = \left(\sum_{s=1}^{\nu+1}\alpha_s\right)^{-1}$$

Eqns. (124), (125), (127) and the information following make the computation possible for $n$ as high as 15 and 16 [from ends (11′) and (22′)].

### (3.7) Special Formulae for Ladder Coefficients for Single-Branch-Element Ladders

The ladder coefficients of a low-pass network structure with an arbitrary number of branches, each consisting of one element only (e.g. $\Omega_{\infty s} = \infty$ or $\zeta_s = 0$, hence $P \equiv 1$), can be expressed by means of $\bar{A}_s$- and $\bar{B}_s$- coefficients of $\bar{A}$- and $\bar{B}$-polynomials. The formulae are given in terms of remainder coefficients rather than in terms of $\bar{A}_s$ and $\bar{B}_s$:

$$a_{2s+1} = \frac{^{(2s-1)}\mathscr{R}_{[n/2]-s}}{^{(2s)}\mathscr{R}_{[n/2]-s}};$$

$$a_{2s} = \frac{^{(2s-2)}\mathscr{R}_{[n/2]-s+1}}{^{(2s-1)}\mathscr{R}_{[n/2]-s}}; \quad s = 0, 1, 2, \dots, \leqslant [n/2]. \quad (128)$$

where $^{(q)}\mathscr{R}$ for $q = 1, 2, \dots$, is the $q$th remainder polynomial resulting from the expansion of the design impedance [or admittance into continued fraction of the form of eqn. (281)], and $^{(q)}\mathscr{R}_r$, for $r = 1, 2, 3, \dots$, are the coefficients of the corresponding $q$th remainder polynomial. To keep the notation consistent, we have also identified the polynomials $\bar{A}$ and $\bar{B}$ with the polynomials $^{(-1)}\mathscr{R}$ and $^{(0)}\mathscr{R}$ defined explicitly for even or odd $n$,

Thus
and
where
$$\left.\begin{aligned}^{(-1)}\mathscr{R} &= e(n)\bar{A} + o(n)\bar{B} \\ ^{(-1)}\mathscr{R}_r &= e(n)\bar{A}_r + o(n)\bar{B}_r \\ ^{(0)}\mathscr{R} &= e(n)p^2\bar{B} + o(n)\bar{A} \\ ^{(0)}\mathscr{R}_r &= e(n)\bar{B}_{r-e(n)} + o(n)\bar{A}_r\end{aligned}\right\} \quad \dots \quad (129)$$

The recursion formulae for the $^{(q)}\mathscr{R}_r$ coefficients in general are given by

$$^{(q)}\mathscr{R}_r = {}^{(q-2)}\mathscr{R}_r - a_q{}^{(q-1)}\mathscr{R}_{r-e(q)} \quad \dots \quad (130)$$

where $e(q)$ is zero for $q$ odd and unity for $q$ even, as defined in

eqn. (70). In the above expression all the quantities with negative subscripts are identically zero, thus

$$\bar{A}_{-r} \equiv \bar{B}_{-r} \equiv {}^{(\pm q)}\mathscr{R}_{-r} \equiv 0 \quad \text{also} \quad a_0 \equiv a_{-r} \equiv 0 . \quad (131)$$

[Relations (125)–(127) hold also in this case.] Eqns. (128)–(131) are the design formulae for any ladder with one branch element, either with or without losses.

### (4) CONSIDERATION OF DISSIPATION IN LADDER NETWORKS

One of the methods enabling the computation of filters with equally dissipative elements is based on the predistortions of the insertion-loss voltage-ratio numerator $(A + pB)$ of a basic network by a known constant, say $d$. This predistortion amounts to a shift of the natural modes by a fraction of a distance $(\alpha_s)_{\min}$ towards the imaginary axis, and for such new distribution of the roots the design impedance, and hence the ladder coefficients, are found exactly as in the case of loss-free network. Finally, the known losses in the form of resistances are added in series with the computed inductances and in parallel with the capacitances; the added resistances, in effect, bring back the insertion-loss natural modes to their initial positions (approximately), thus producing closely the prescribed discrimination characteristic (the insertion loss being raised only by a constant loss, i.e. the loss of dissipation and reflection).

#### (4.1) Procedure of Predistortion

The computation of the corresponding insertion-loss predistorted characteristic function is obtained by forming and solving the $N'$-polynomial in order to obtain $A'$- and $B'$-polynomials. To illustrate the procedure and operations associated with such computation, we shall consider losses equally distributed between coils and capacitors; thus $R_L/L = G_c/C$, where $R_L$ and $G_c$ are the resistance and conductance associated with the coil and capacitor respectively. Normalized low-pass system losses are defined by

$$\Delta_L = \frac{R_L}{\omega_B L} = \Delta_c = \frac{G_c}{\omega_B C} = d \quad \dots \quad (132)$$

(It may be observed that $d$ is the inverse of $Q$ of the corresponding element.) The magnitude of $d$ is restricted to values smaller than the smallest real part of insertion-loss voltage-ratio zeros, this being necessitated by the requirement that the predistorted voltage-ratio numerator $(A + pB)_d$ must still remain a Hurwitz polynomial with negative real parts of its roots. For this reason

$$d < (\alpha_s)_{\min} \quad \dots \quad \dots \quad (133)$$

[In the case of functions discussed in the paper, $(\alpha_s)_{\min} = \alpha_{[n/2]}$.] In practice, however, it is desirable to keep $d$ well below the limiting value, say $d \leqslant \frac{1}{2}(\alpha_s)_{\min}$. For a narrow pass-band filter it is not essential for $R_L/L$ and $G_c/C$ to be equal, because in band-pass networks of not too great bandwidth $B_p$, it is not important, so far as attenuation distortion with frequency is concerned, how the losses are distributed between the elements. For band-pass (or band-stop) networks the constant $d$ may be estimated from $d = (d_L + d_c)Q_B \leqslant \frac{1}{2}(\alpha_s)_{\min}$, where $Q_B = f_0/f_B \gg 1$ and $f_0$ is the mid-band frequency, while $f_B = \sqrt{(B_pB_a)}/\Omega_B$, $d_L = R_L/\omega_0 L$ and $d_c = G_c/\omega_0 C$. The predistortion of the voltage

ratio is accomplished by replacing $p$ in the polynomial $(A + pB)$ by $(p - d)$, thus giving $(A + pB)_d$. The denominator polynomial $P$ is left in its original form, as the polynomial is real at the real frequencies and $\Omega_{\infty s}$ is considerably larger than the losses $d$; hence the effect of losses on the insertion-loss response will be marked at the poles only, producing finite peaks. The realization method also requires that $P$ be unchanged.

As a result of predistortion we obtain new root parameters of the polynomial $(A + pB)_d$, defined by

$$\alpha_{s,d} = \alpha_s - d; \quad \rho^2_{s,d} = \rho^2_s - 2\alpha_s d + d^2$$
$$s = e(n), 1, 2, 3, \ldots [n/2] \quad . \quad . \quad (134)$$

With these predistorted root parameters, we can form new coefficients $A_{s,d}$ and $B_{s,d}$ and the predistorted $(N)_d$-polynomial from

$$\left(\sum_{s=0}^{[n/2]} A_{s,d}p^{2s}\right)^2 - p^2\left(\sum_{s=0}^{[n/2]} B_{s,d}p^{2s}\right)^2 = \sum_{s=0}^{n} N_{s,d}p^{2s} \quad . \quad (135)$$

This predistortion also provides a method of transforming a negative ladder coefficient into a positive one; this is also an important aspect of the method. The most laborious part is to form and factorize the $(N')_d$-polynomial, which is expressed (with the constant multiplier removed) by

$$\sum_{s=0}^{n} N'_{s,d}p^{2s} = \sum_{s=0}^{n} N_{s,d}p^{2s} - \eta_G A^2_{0,d}P^2 \quad . \quad . \quad (136)$$

It may be observed that, in this equation, the only unknown is the limit of $\eta_G$. However, $\eta_{Gmax}$ can be found by several methods; the analytic one starts with computation of

$$p'^2_{\pm[n/2],d} = -\Omega'^2_{[n/2],d}$$

from

$$\frac{P^4}{H^2}\frac{d}{dp}\left[\frac{(N)_d}{P^2}\right] = M = \sum_{s=0}^{n+2\nu-1} M_s p^{2s}$$

where $M_s = \sum_{q=1}^{s+1} q(N_q S_{s+1-q} - S_q N_{s+1-q})$; in this expression $N_{r>n} \equiv 0$ and $S_{r>2\nu} \equiv 0$. One real negative root, i.e. $-\Omega'^2_{[n/2],d}$, is extracted from the polynomial $M/M_{n+2\nu-1}$ most readily by the division method, i.e. dividing the $M/M_{n+2\nu-1}$ by $p^2 + \Omega^2_p$, as a first approximation, then approximating further until the remainder vanishes. Once $\Omega'^2_{[n/2],d}$ is evaluated, the other roots of $(N')_d$ can be found more readily from the polynomial $(\Sigma N'_{s,d}p^{2s})/(p^2 + \Omega'^2_{[n/2],d})^2$. If $n$ is odd there will still be one real, and in this case positive, root, i.e. the $\alpha'^2_{0,d}$, which can also be extracted by the division method. (When $P = 1$ all these processes simplify.) In all the cases where $\Omega'_{[n/2],d}$ is known the $\eta_G = \eta_{Gmax}$ can readily be found. Analytic solution leads to a minimum number of solutions. That for which $\eta_G > \eta_{Gmax}$ is excluded, as this leads to non-physical roots in $(N')_d$. When $\eta_G < \eta_{Gmax}$ all roots $p'_{\pm s,d}$ will become complex conjugate except one for odd $n$, namely $p'^2_{0,d} = \alpha'^2_{0,d}$. Another method for estimation of $\eta_{Gmax}$ is semi-graphical. First, $\Sigma N_{s,d}p^{2s}$ and $A^2_{0,d}P^2$ are plotted against the square of the frequency, $\Omega^2$ (or $-p^2$), close to $\Omega^2_p$. Then it will be found that, for certain values of $\eta_G < 1$, the quantity $\Sigma N_{s,d}p^{2s} - \eta_G A^2_{0,d}P^2$ can be made positive and real at all real frequencies. The maximum efficiency is found from

$$\left.\frac{\sum_{s=0}^{n} N_{s,d}p^{2s}}{A^2_{0,d}P^2}\right|_{min} = \left.\frac{\sum_{s=0}^{n} N_{s,d}p^{2s}}{A^2_{0,d}P^2}\right|_{p^2 = -\Omega'^2_{[n/2],d}} = \eta_{Gmax} \quad . \quad (137)$$

If $\eta_{Gmax}$, found graphically, is to be used for further design, great precision in computation of the roots of $(N')_d$ is required, and for this reason it is often preferable to take $\eta_G$ smaller than $\eta_{Gmax}$, although this leads to lower efficiency.

For $n = 3, 5$ and perhaps 7, and for $0\cdot3 \leqslant k_B \leqslant 0\cdot98$, the simplest first approximation to $\eta_G$ may be found from an empirical formula given by*

$$\eta_G \simeq (\chi - nk_B d)^{2(\nu!)}, \text{ where } \chi = \frac{A_{0,d}}{A_0} = \frac{\alpha_{0,d}\prod\limits_{s=1}^{\nu}\rho^2_{s,d}}{\alpha_0\prod\limits_{s=1}^{\nu}\rho^2_s}$$

If $\eta_G$ has been properly estimated, the coefficients of $(N')_d$ can be formed in the following way:

$$N'_{s,d} = N_{s,d} - \eta_G A^2_{0,d}S_s \quad . \quad . \quad . \quad (138)$$

where $S = P^2$ and $S_s$ are the coefficients of $S$ as defined in eqn. (89); the solution should take the form†

$$(-1)^n\sum_{s=0}^{n} N'_{s,d}p^{2s} = (p^2 - p'^2_{0,d})^{o(n)}\prod_{s=1}^{[n/2]}(p^4 + 2\xi'_{s,d}p^2 + \rho'^4_{s,d}) \quad . \quad (139)$$

From this we find $p'^2_{0,d} = \alpha'^2_{0,d}$ and $2\alpha'_{s,d} = \sqrt{[2(\rho'^2_{s,d} - \xi'_{s,d})]} \geqslant 0$. The check upon accuracy of solution for roots of $(N')_d$ can be obtained from the relation

$$A'_{0,d}/A_{0,d} = \sqrt{(1 - \eta_G)} \quad . \quad . \quad . \quad (140)$$

If eqn. (140) is satisfied, further design can safely proceed.

The required resistance termination ratio for the final filter may be computed from

$$\frac{R_2}{R_1} = \frac{1 \mp \sqrt{(1 - \eta_G)}}{1 \pm \sqrt{(1 - \eta_G)}} \quad . \quad . \quad . \quad (141)$$

When the proper signs corresponding to the chosen configuration (see Section 3.2) are established, the design procedure can be carried on in exactly the same way as for the general case described. Predistorted polynomials $A'$ and $B'$ and the proper design impedance are formed, and then the ladder coefficients can be computed in the usual way. Finally, when the actual network is built, proper losses or $Q$-factors must be ensured. As is seen, the computation is very laborious when losses are taken into account, especially for $n > 5$. In the case of open- or short-circuit termination, the whole procedure simplifies considerably. In such cases only the predistorted polynomials $(A)_d$ and $(B)_d$ and consequently $A_{s,d}$ and $B_{s,d}$ are sufficient, and the design impedance is formed according to Section 2.3, from which the ladder coefficients can be evaluated in the usual way, and the proper $Q$-factor ensured in the actual network. The transducer loss of a dissipative network at zero or mid-band frequency can be computed from

$$10 \log \left.\frac{\mathscr{P}_{20max}}{\mathscr{P}_2}\right|_{\Omega=0} = -10 \log(\eta_G\chi^2)$$
$$= 20 \log A_0 - 10 \log(A^2_{0,d} - A'^2_{0,d}) \quad . \quad (142)$$

There are many other methods taking into account losses[10-13] but, unfortunately, all are complicated and laborious. The essential approach to problems of unequally distributed losses between inductors and capacitors is also outlined in Darlington's paper.[5] However, his design formulae require substantial modification.

---

* More accurate empirical formulae are much too complicated to be included here. So also are those which allow an estimation of $d$ (which renders the negative ladder coefficient a positive one).

† When $\eta_G \simeq \eta_{Gmax}$ is used for the formation of $(N')_d$, the $(\alpha_s)_{min}$ usually becomes very small. However, it must be noticed that if, say, $A_{s,d}$ and consequently all the other coefficients, and $\alpha'_{s,d}$ and $\rho'^2_{s,d}$ are computed with, say, $l$ digits and $(\rho'^2_{s,d} - \xi'_{s,d})$ results in a figure in the last one or two places, then, after root extraction, this inaccurate figure will be in the $\frac{1}{2}l$th place. Such inaccuracy may lead to very inaccurate or even inconsistent ladder coefficients.

Where the specifications of $D_p$, $D_a$ and $k_B$ need be only approximately satisfied, it is often the practice to compute a loss-free filter with initial discrimination $D_{pi} \ll D_p$ and $D_{ai} > D_a$ and $k_{Bi} > k_B$. It is possible to form empirical formulae involving mostly $d$, $k_B$, $n$ and $D_p$, which permit proper estimation of initial data, often with a satisfactory result. It can be mentioned that the effect of losses may also be corrected in the pass band by the use of a proper equalizer; in fact, this method is favoured by many filter specialists.

## (5) CHARACTERISTIC INSERTION-LOSS FUNCTIONS FOR FILTERING PURPOSES

Characteristic insertion-loss functions for filtering purposes must have their zeros within the effective pass band and their poles (finite frequencies of infinite loss) within the effective suppression band. These are necessary but not sufficient conditions which are imposed on an insertion-loss function. The poles and zeros must be so distributed within the appropriate bands that the specification of discrimination is satisfied. We shall illustrate some of the methods leading to a proper distribution of poles and zeros, satisfying most of the discrimination specifications. There are many of these methods.[1, 3, 5, 6, 10, 12-18] The Laurent template method is widely used; there are special formulae which permit of a proper choice of $m$-values for the well-known Darlington reference filters; and perhaps most interesting of all is the potential analogue method using single- or double-layer electrolytic tanks. This somewhat empirical method is a very powerful tool for designing such special functions as, for example, networks working under vestigial conditions, or other network responses with special pass and transition bands. However, in ordinary filters, suitable functions are those obtained by the use of Chebyshev or Taylor approximations or $m$-derived-like or constant-$k$ filters. An ordinary filter is required to produce as low distortions as possible in the pass band and maximally high attenuation in the suppression band (usually the transition-band shape is of no importance). These general requirements suggest that the effective characteristic function in the attenuation band can be the inverse of that in the pass band. Such specific functions, introduced to filter theory by Cauer and employed more successfully by Darlington and Cocci, are certainly superior to any other known functions; hence time will be spared in the derivation and description of a typical number of such a class of functions, which will be referred to as Chebyshev pass-band and attenuation-band parameter functions.

Before investigating the very important functions of Chebyshev parameters, let us illustrate some better-known and simpler characteristic functions, e.g. constant-$k$ or maximally flat responses.

### (5.1) Characteristic Insertion-Loss Function for a Constant-$k$ Equally Terminated Filter

Constant-$k$ filters designed from the image parameter theory are very common and still of great service for waveguide systems and in u.h.f. techniques generally. The filters considered here consist of $n$ branches or $(n-1)$ half-sections, each half-section consisting of an inductance $L$ and a capacitance $C$. Thus, the ladder filter has $L$ or $C$ terminal elements and $2L$ and $2C$ inside elements, and may be in $T_{e(n)}$ or $\Pi_{e(n)}$ configurations, where $\zeta_s = 0$. The characteristic resistance and the cut-off frequency are defined by $R_0 = \sqrt{(L/C)}$ and $\omega_c = 1/\sqrt{(LC)}$, and the characteristic insertion-loss function can be expressed generally as

$$H^2\phi^2 = (-1)^n 4^{n-3} p^{2[2-o(n)]} \prod_{s=1}^{[n/2]-1} (p^2 + \Omega_{0s}^2)^2 \quad . \quad (143)$$

where

$$\Omega_{os} = \sin\left\{\frac{[e(n)+1]s - e(n)}{(n-1)[e(n)+1]}\pi\right\}$$

Comparing eqn. (143) with the general insertion-loss characteristic function (82), it is clearly seen that a constant-$k$ filter is a special case obtainable from the general function by reducing some of the zeros and by assigning all poles to be at infinity. The power ratio can be expressed simply in terms of the Chebyshev polynomials of the first and second kind,* defined by

$$\left.\begin{array}{l} T_s(\Omega) = \cos(s \arccos \Omega) \\ U_s(\Omega) = \dfrac{\sin(s \arccos \Omega)}{\sin(\arccos \Omega)} \end{array}\right\} \quad . \quad . \quad . \quad (144)$$

Using the Chebyshev polynomials, the characteristic function and the polynomials $A$ and $\Omega B$ can be expressed in terms of $\Omega$ rather than $p$ as

$$H^2\phi^2 = (-1)^n \tfrac{1}{4}\Omega^4 U_{n-1}^2 = e(n)A'^2 + o(n)\Omega^2 B'^2 \quad . \quad (145)$$

and

$$\mathscr{P}_{20}/\mathscr{P}_2 = 1 + H^2\phi^2 = A^2 + \Omega^2 B^2$$

The insertion-loss voltage ratio is given by $V_{20}/V_2 = A + pB$, where $B$ and $A$ are in terms of $\Omega$ rather than of $p$:

$$\left.\begin{array}{l} A = (-1)^{[n/2]}[o(n)T_{n-1} + \tfrac{1}{2}e(n)(\Omega^2 - 2)U_{n-1}] \\ \Omega B = (-1)^{[n/2]}[\tfrac{1}{2}o(n)(\Omega^2 - 2)U_{n-1} - e(n)T_{n-1}] \end{array}\right\} \quad . \quad (146)$$

The component values in constant-$k$ filters are determined in a well-known way and the method described here for determining ladder coefficients can be used when function is predistorted for losses. The formulae given here can be found serviceable when the insertion loss or delay of an $n$-branched filter is to be investigated within a prescribed bandwidth. The formulae for phase, delay and v.s.w.r. are easily derived, e.g.

$$\beta_0 - \beta_2 = \arctan\frac{\Omega B}{A};$$

$$\text{delay} = \frac{d(\beta_0 - \beta_2)}{d\omega} = \frac{AB + \Omega\left(A\dfrac{dB}{d\Omega} - B\dfrac{dA}{d\Omega}\right)}{A^2 + \Omega^2 B^2}\frac{d\Omega}{d\omega}$$

### (5.2) Filter with Maximally Flat Pass-Band Response

A maximally flat insertion-loss characteristic function belongs to the Taylor approximation class; it is given by the expansion of the $F(\Omega)$ polynomial by Taylor's series about $\Omega = 0$. These functions are most simply obtained from the general insertion-loss characteristic function (82) by assigning all poles to infinity and all zeros to zero frequency, i.e.

$$p'_{\pm s} = 0 \text{ and } p_{\pm \infty s} = \pm j\infty \quad \text{for} \quad s = e(n), 1, 2, \ldots$$
$$\text{Thus } P = 1, \text{ and for } \eta_G = 1$$
$$H^2\phi^2 = (N')_{\eta_G = 1} = (-1)^n H^2 p^{2n} \quad . \quad . \quad (147)$$

It can be observed in Fig. 4 that the characteristic function is zero at zero frequency and infinity at infinite frequency, and it is clear that the network can always be terminated in equal resistances for an arbitrary number of branches. The ladder coefficients are always positive; hence no ideal transformer or mutual inductances are required for arbitrary termination. If $\eta_G = 1$, the power ratio for a maximally flat response can be expressed as

$$\frac{\mathscr{P}_{20}}{\mathscr{P}_2} = |\Xi(p)|^2 = 1 + H^2\phi^2 = 1 + (-1)^n H^2 p^{2n} \quad . \quad (148)$$

---

* The first two polynomials for $s = 0, 1$, are given from eqn. (144) as $T_0(\Omega) = 1$ and $T_1(\Omega) = \Omega$ and $U_0(\Omega) = 0$, $U_1(\Omega) = 1$. Further polynomials can be formed from the recursion formulae $T_{r+q} = 2T_r T_q - T_{r-q}$ and $U_{r+q} = 2U_r T_q - U_{r-q}$, where the argument is understood.
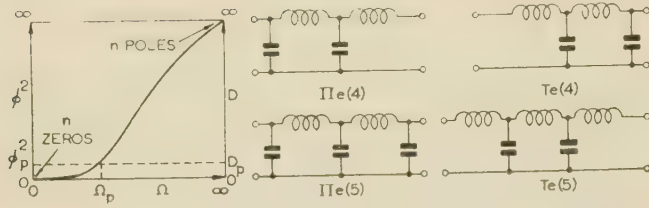
**Fig. 4.**— Maximally flat structure ($n = 4$ and $5$) and the general response shape.

Employing $\quad (-1) \equiv \varepsilon^{\pm j[n + e(n) - 2s]\pi}; \; (-1)^n \equiv j^{2n}$

and for the time being letting $\eta_G = 1$, i.e. $R_1 = R_2$, the discrimination function can be expressed as

$$|\Xi(p)|^2 = 1 + (-1)^n H^2 p^{2n}$$

$$= (-1)^n H^2 \{ p^{2n} - j^{2n} H^{-2} \varepsilon^{\pm j[n + e(n) - 2s]\pi} \}$$

$$= H^2 (H^{-2/n} - p^2)^{o(n)} \prod_{s=1}^{n - o(n)} \{ p + jH^{-1/n}\varepsilon^{\pm j[n + e(n) - 2s]\pi/2n} \}$$

$$\{ p - jH^{-1/n}\varepsilon^{\pm j[n + e(n) - 2s]\pi/2n} \} \quad . \quad (149)$$

Selecting from this expression that half of the complex roots which can be related to the discrimination function in the way described in eqns. (92)–(95), $\Xi$ can be written as

$$\Xi(p) = H'(p + H^{-1/n})^{o(n)} \prod_{s=1}^{\nu + e(n)} \{ p - (-1)^s H^{-1/n} j\varepsilon^{j[n + e(n) - 2s]\pi/2n} \}$$

$$\{ p - (-1)^s H^{-1/n}(-j)\varepsilon^{-j[n + e(n) - 2s]\pi/2n} \}$$

$$= H'(p - p_0)^{o(n)} \prod_{s=1}^{\nu + e(n)} [p - (-1)^s p_s][p - (-1)^s p_{-s}]$$

$$\quad . \quad . \quad . \quad . \quad (150)$$

From which the voltage ratio is given by

$$\frac{V_{20}}{V_2} = A + pB = H(p - p_0)^{o(n)} \prod_{s=1}^{\nu + e(n)} (p - p_s)(p - p_{-s})$$

$$= H(p + \alpha_0)^{o(n)} \prod_{s=1}^{\nu + e(n)} (p^2 + 2\alpha_s p + \rho_s^2) \quad . \quad (151)$$

where the root parameters of the insertion-loss voltage ratio are given by

$$\rho_s^2 = \rho^2 = H^{-1/n}$$

$$p_{+s} = \pm j\rho_s \varepsilon^{\pm j[n + e(n) - 2s]\pi/2n} = -\alpha_s \pm j\Omega_s \quad . \quad (152)$$

Hence $\qquad \alpha_s = \rho_s \sin \{ [n + e(n) - 2s]\pi/2n \}$

for $\qquad\qquad s = e(n), 1, 2, \ldots, [n/2]$

where $\qquad\qquad \Omega_{\infty s} \equiv \infty, \quad \text{thus} \quad \zeta_s \equiv 0$

In most cases the network components or ladder coefficients can be expressed explicitly for an arbitrary number of branches and termination. Some of the formulae will be given in this Section. We shall now indicate the procedure leading to an arbitrary termination. It can be noted that the power ratio is

$$\frac{\mathscr{P}_{20}}{\mathscr{P}_2} = 1 + (H^2\phi^2)_{\eta_G = 1} = \eta_G + (N')_{\eta_G \leqslant 1} = N = A^2 - p^2 B^2$$

$$\quad . \quad . \quad . \quad . \quad (153)$$

In this case $(H^2\phi^2)_{\eta_G = 1} = (-1)^n H^2 p^{2n}$ and hence is known; therefore $(N')_{\eta_G \leqslant 1}$ is found from eqn. (153). Noting that

$$1 - \eta_G = \left( \frac{1 - r}{1 + r} \right)^2 = \Gamma^2(0) = H^2 A_0'^2, \text{ where } r = \frac{R_1}{R_2} \text{ or } \frac{R_2}{R_1}$$

and $(N')_{\eta_G \leqslant 1} = (A'^2 - p^2 B'^2)_{\eta_G \leqslant 1} = 1 - \eta_G + (H^2\phi^2)_{\eta_G = 1}$

$$= H^2 (p_0'^2 - p^2)^{o(n)} \prod_{s=1}^{\nu + e(n)} (p^4 + 2\xi_s' p^2 + \rho_s'^4) \quad . \quad (154)$$

from inspection it follows that

$$\rho_s' = \rho' = \rho(1 - \eta_G)^{1/2n} = \rho \Gamma^{1/n}(0) = \rho\mu \quad . \quad (155)$$

and $\qquad \alpha_s' = \rho' \sin \{ [n + e(n) - 2s]\pi/(2n) \} = \mu\alpha_s$

and hence

$$A' + pB' = H'(p - p_0')^{o(n)} \prod_{s=1}^{\nu + e(n)} (p^2 - 2p\mathbf{R}\,p_{\pm s}' + \rho_s'^2) \quad . \quad (156)$$

where the signs of $p_0'$ and $H'$ can be determined in the usual manner for a chosen $n$ and the termination ratio, while $p_{\pm s}'$ for $s > 0$ is left arbitrary. From the distribution of the roots of $\mathbf{R}\,p_{\pm s}' = (-1)^s (p_0'/\alpha_0')^{o(n)} \alpha_s'$, the ladder coefficients, given in this Section, can be found explicitly in a simple manner for odd $n$, while $\mathbf{R}\,p_{\pm s}' = (p_0'/\alpha_0')^{o(n)} \alpha_s'$ leads to another solution of the prescribed decrement ratio, for which explicit formulae will also be given in this Section.

The design procedure of a maximally flat filter response is simple, and most of the satisfactory solutions require very little computation. In design, the first step is to estimate the number of branches for a ladder network to satisfy the specification, namely $k_B = B_p/B_a$, and discrimination $D_p$, $D_a$, or prescribed reflection factor $\Gamma_p$ in the pass band. By means of these data we may compute the constant $H$ from $D = 10 \log (1 + H^2\Omega^{2n})$: by letting $\Omega_p = 1$,

$$H = \sqrt{(10^{D_p/10} - 1)} = \frac{|\Gamma_p|}{\sqrt{(1 - |\Gamma_p|^2)}};$$

$$k_B = \frac{B_p}{B_a} = \frac{1}{\Omega_a} < 1; \quad f_B = B_p \quad . \quad . \quad . \quad (157)$$

then the number of branches is found from

$$n > \frac{D_a/20 + \log H^{-1}}{\log \Omega_a} \quad . \quad . \quad . \quad (158)$$

The relation between $n$, $k_B$, $D_p$ and $D_a$ for $n = 3, 5, 7$ and $9$ is given in Fig. 2(c). If, instead of $\Omega_p = 1$, we assume $\sqrt{(\Omega_p\Omega_a)} = \Omega_B = 1$, then $H^2 = \sqrt{[(10^{D_p/10} - 1)(10^{D_a/10} - 1)]}$ and $f_B = \sqrt{(B_p B_a)}$.

The normalized ladder coefficients for equal termination are given by

$$\left. \begin{array}{c} \bar{a}_s = 2H^{1/n} \sin \dfrac{2s - 1}{2n}\pi = \bar{a}_{n+1-s} = 2\rho^{-2}\alpha_{[n/2]+1-s} \\[2mm] s = 1, 2, \ldots (\nu + 1); \quad \nu = \tfrac{1}{2}[n - 1 - e(n)]; \\[2mm] R_1 = R_2 = R_0 \end{array} \right\} \quad . \quad (159)$$

Actual ladder coefficients, e.g. for $T_{e(n)}$-configuration $\bar{a}_{s, Te(n)}$ and for $\Pi_{e(n)}$-configuration $\bar{a}_{s, \Pi e(n)}$, are given by

$$\bar{a}_{s, Te(n)} = \bar{a}_s R_1^{(-1)^{s+1}} \text{ and } \bar{a}_{s, \Pi e(n)} = \bar{a}_s R_1^{(-1)^s} \quad . \quad (160)$$

for end $(11')$ in Fig. 2. For a symmetrical and arbitrarily terminated network, where $\nu = (n - 1)/2$, the arbitrary termination resistance is $R$, defined by

$$R = rR_0 \quad . \quad . \quad . \quad . \quad . \quad (161)$$

where $r$ is an arbitrary multiplier and $\eta_G \leqslant 1$. For a root distribution defined by $\mathbf{R}\,p_{\pm s}' = (-1)^s (p_0'/\alpha_0')\alpha_s$, the ladder coefficients are found[7, 19] for T-configuration from

$$\bar{a}_{s, T} = \bar{a}_s R_0^{(-1)^{s+1}}; \quad a_{(n+1-s), T} = \bar{a}_s r R_0^{(-1)^{s+1}}$$

$$s = 1, 2, 3, \ldots \nu \quad . \quad . \quad . \quad . \quad (162)$$

the ladder coefficients in the centre of the symmetrical T-structure being

$$a_{(v+1),\mathrm{T}} = \tfrac{1}{2}[1 + r^{(-1)^v}]R_0^{(-1)^v}\bar{a}_{v+1} \quad . \quad . \quad (163)$$

For $\Pi$-configurations,

$$\left.\begin{aligned}a_{s,\Pi} &= \bar{a}_s R_0^{(-1)^s}, \quad a_{(n+1-s),\Pi} = \bar{a}_s(rR_0)^{(-1)^s}; \\ &\quad s = 1, 2, 3, \ldots v\end{aligned}\right\} \quad . \quad (164)$$

$$\text{and} \quad a_{(v+1),\Pi} = \tfrac{1}{2}[1 + r^{(-1)^{v+1}}]R_0^{(-1)^{v+1}}\bar{a}_{v+1}$$

It is also possible to formulate ladder coefficients for even or odd $n$ for an arbitrary decrement ratio from the relations given in Section 3.7. In the case of a prescribed decrement ratio $\delta$, the roots $p'_{\pm s}$ are to be in the same half-plane. The approach to such a design is simple and easily found. Explicit formulae for quantities relating ladder coefficients for the maximally flat and the Chebyshev (pass-band) filters are given by Green.[20]

We shall now give essential information concerning the design of prescribed-decrement ladder filters. The root distribution may be chosen in the general form

$$\mathbf{R}\,p'_{\pm s} = (\underset{\_}{+})^{e(n)}(p'_0/\alpha'_0)^{o(n)}\alpha'_s$$

e.g. taking positive signs for even $n$, we shall have

$$\mathbf{R}\,p'_{\pm s} = (p'_0/\alpha'_0)^{o(n)}\alpha'_s \quad . \quad . \quad . \quad (165)$$

Then the required $\rho'$, which is necessary for formation of $A'$ and $B'$ and consequently $\bar{A}$ and $\bar{B}$ for a prescribed decrement ratio $\delta$, is defined by

$$\delta = {}^n\delta_1 = \frac{a_n}{ra_1} = \frac{\rho + \rho'}{\rho - \rho'} = \frac{1 + \mu}{1 - \mu} \quad . \quad . \quad . \quad (166)$$

Therefore

$$\frac{\delta - 1}{\delta + 1} = \mu \text{ for } 1 \leqslant \delta \leqslant \infty.$$

The proper termination ratio is then found from

$$r = \frac{1 - \mu^n}{1 + \mu^n} = \frac{1 - \Gamma(0)}{1 + \Gamma(0)} \quad . \quad . \quad . \quad (167)$$

The first and last ladder coefficients, which are often of primary interest, can be evaluated simply from $a_1 = (\bar{A}_{v+e(n)}/\bar{B}_v)^{(-1)^n}$ as follows from Section 3.7, thus

$$a_1 = \frac{\bar{a}_1}{1 + \mu} \text{ and } a_n = \frac{\bar{a}_1}{1 - \mu}r^{(-1)^{n+1}} \text{ where } \bar{a}_1 = 2H^{1/n}\sin\frac{\pi}{2n}$$

$$. \quad . \quad . \quad (168)$$

If eqn. (165) is taken with negative sign for even $n$, the signs in the subsequent formulae need to be properly reversed. (For odd $n$ the sign of $p'_0$ is determined from Section 3.2.) The first and the last ladder coefficients are:

$$a'_1 = \frac{\bar{a}_1}{1 - \mu} \text{ and } a'_n = \frac{\bar{a}_1}{1 + \mu}r^{(-1)^n}$$

These are the same as if evaluated from the other end.

The general formulae for ladder coefficients as derived from Section 3.7 for prescribed decrement ratio $\delta$ are given in terms of $\bar{a}_s$ as defined in eqn. (159), as well as $\delta$ and the quantities $\lambda'_k$ defined by

$$\lambda'_k = 4\frac{\delta - 1}{\delta + 1}\left(\frac{1}{\delta^2 - 1} + \cos^2\frac{k\pi}{2n}\right); \quad k = 1, 2, 3, \ldots (n-1)$$

$$. \quad . \quad . \quad (169)$$

and the ladder coefficients for the root distribution $\mathbf{R}\,p'_{\pm s} = (p'_0/\alpha'_0)^{o(n)}\alpha'_s$ and the termination ratio $r = \dfrac{(\delta + 1)^n - (\delta - 1)^n}{(\delta + 1)^n + (\delta - 1)^n}$ are given by

$$\left.\begin{aligned}a_{2s+1} &= \frac{\delta + 1}{2\delta}\bar{a}_{2s+1}\prod_{q-1}^{s}\frac{\lambda'_{2q-1}}{\lambda'_{2q}} \\ a_{2s} &= \frac{2\delta}{\delta + 1}\bar{a}_{2s}\frac{\displaystyle\prod_{q=1}^{s-1}\lambda'_{2q}}{\displaystyle\prod_{q=1}^{s}\lambda'_{2q-1}}\end{aligned}\right\} \quad . \quad . \quad (170)$$

$s = 0, 1, 2, \ldots, [n/2]$. Observe that $\prod\limits_{r=1}^{0}\lambda_r = 1$.

On the other hand, for $\mathbf{R}\,p'_{\pm s} = -(p'_0/\alpha'_0)^{o(n)}\alpha'_s$,

$$a'_s = a_{n+1-s}r^{(-1)^s} \quad . \quad . \quad . \quad . \quad (171)$$

For odd $n$ the coefficients $a'_s$ correspond to the other end of the ladder and the actual ladder coefficients will be expressed in terms of $R_2$ if normal termination is considered. In case of open- or short-circuit termination, $\delta = \infty$, and eqn. (170) is also consistent.

## (5.3) The Filter with Chebyshev's Pass-Band Parameters

Filters with a Chebyshev response are well known, and the derivation procedure will be only briefly outlined here. A model derivation will be given in Section 9 for a filter with Chebyshev pass and attenuation bands which is more general and of more importance. The filter with Chebyshev pass-band parameters is of the same type of complexity as the constant-$k$ or the maximally flat filters; its advantage lies in the more efficient distributions of the values of elements. Its discrimination oscillates between equal maxima and minima within the pass band with differing periodicity, and outside the pass band the function rises continuously, in a similar manner as in maximally flat or constant-$k$ filters. The even and odd functions are illustrated in Fig. 5. This function, like any
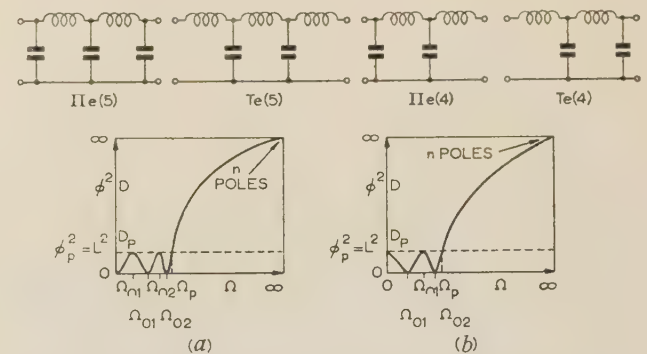


Fig. 5.—Characteristic functions and the corresponding ladder structures for Chebyshev pass-band parameters.

(a) $n$ odd ($n = 5$).
(b) $n$ even ($n = 4$).

others considered, is the special case of a general insertion-loss characteristic function [eqn. (78)] and is obtained by taking $\alpha'_s = 0$, $p_{\pm\infty s} = \pm j\Omega_{\infty 0} = \pm j\infty$, and $p'_{\pm s} = \pm j\Omega_{0s}$, where the $\Omega_{0s}$ are so distributed within the pass band that the effective maxima and minima of $\phi$ at the frequencies $\Omega_{ns}$ have equal amplitudes. Hence the problem is only to find the proper distribution of $\Omega_{0s}$. In general we shall require a $\phi$-function to satisfy

$$\left.\begin{aligned}\phi &= LF(\Omega) = \Omega^{o(n)}\prod_{s=1}^{v+e(n)}(\Omega^2 - \Omega_{0s}^2) \\ \text{where} \quad &|\phi(\Omega)|_{0\,\leqslant\,\Omega\,\leqslant\,\Omega_p} \leqslant L\end{aligned}\right\} \quad . \quad . \quad (172)$$

The aim is to find an analytical function $F(\Omega)$, which turns out to be a Chebyshev polynomial. The important resultant formulae are derived from the differential equation $d\phi = \pm n\sqrt{(L^2 - \phi^2)}d\Omega/\sqrt{(\Omega_p^2 - \Omega^2)}$, of which one of the solutions, namely $\phi = L\cos n\theta$, $\Omega = \Omega_p \cos\theta$, leads to a characteristic insertion-loss function defined by

$$H^2\phi^2 = H^2L^2T_n^2(\Omega) = (-1)^n H^2 p^{2o(n)} \prod_{s=1}^{v+e(n)}(p^2 + \Omega_{0s}^2)^2. \quad (173)$$

where $p = j\Omega_p \cos\theta$, $L = 2^{(1-n)}$; assuming $\Omega_p = 1$, $HL = \sqrt{(10^{D_p/10} - 1)}$.

Defining the complex arguments by $\theta_{\pm s} = \theta_{0s} \pm j\theta'_{e(n)}$, one obtains

$$p_{\pm s} = -\alpha_s \pm j\Omega_s = \pm j\cos\theta_{\mp s}$$
$$= -\sinh\theta'_{e(n)}\sin\theta_{0s} \pm j\cosh\theta'_{e(n)}\cos\theta_0.$$

The important frequencies of the maxima and zeros are given by

$$\left.\begin{array}{l}\Omega_{\cap s} = \cos\theta_{\cap s} = \cos\left[n - 1 + e(n) - 2s\right]\dfrac{\pi}{2n} \\[2mm] \Omega_{0s} = \cos\theta_{0s} = \cos\left[n + e(n) - 2s\right]\dfrac{\pi}{2n}\end{array}\right\} \quad (174)$$

By the usual general procedure described in eqns. (81)–(98) and illustrated in Section 9 for the more involved case of Chebyshev pass-band and attenuation-band parameters, one can obtain the roots for the insertion-loss voltage-ratio function from

$$|\Xi(p)|^2 = 1 + H^2L^2\cos^2 n\theta_{\mp s} = 1 - H^2L^2\sinh^2 n\theta'_{e(n)} = 0$$

Thus

$$\frac{V_{20}}{V_2} = \sqrt{[\eta_G^{e(n)}]}H(p + \alpha_0)^{o(n)}\prod_{s=1}^{v+e(n)}(p^2 + 2\alpha_s p + \rho_s^2) \quad (175)$$

where $\alpha_s = \vartheta_{e(n)}\sqrt{(1 - \Omega_{0s}^2)} = \vartheta_{e(n)}\sin\left[\dfrac{n + e(n) - 2s}{2n}\pi\right]$

$$\rho_s^2 = \vartheta_{e(n)}^2 + \Omega_{0s}^2 = \vartheta_{e(n)}^2 + \cos^2\left[\frac{n + e(n) - 2s}{2n}\pi\right]$$
$$s = e(n), 1, 2, \dots v + e(n)$$

and $\qquad \vartheta_{e(n)} = \sinh\theta'_{e(n)} = \sinh\left(\dfrac{1}{n}\text{arc sinh}\dfrac{1}{HL}\right) \quad (176)$

Obviously $\alpha_0 = \vartheta_0$, and exists only for odd $n$.

As will be shown, the ladder coefficients can be expressed explicitly in most cases by means of eqn. (128). Where losses are taken into account the general methods of forming $\bar{A}$ and $\bar{B}$ and eqn. (128) must be applied. The explicit formulae for ladder coefficients will be given for symmetrical and for inverse-impedance basic networks. Other cases, e.g. with losses or a prescribed decrement ratio, may be worked, if desired, in the general manner. In order to obtain explicit formulae for ladder coefficients for an inverse-impedance network, initially an ideal transformer is inserted in the ladder between the $\frac{1}{2}n$th and the $(\frac{1}{2}n + 1)$th elements to preserve equal termination. In this way half the ladder coefficients can be evaluated explicitly and the corresponding half on the other side of the transformer then have the same values. It is only necessary to transfer one-half of the network impedances, including the termination, to one side of the transformer, in order that the transformer may be removed.[21]

The transformer ratio, and in effect the termination ratio, enabling determination of all the network elements, is found from Section 3.2. The general design procedure for the design of basic networks follows.

(5.3.1) Design Procedure.

By specifying the discrimination or reflection factor, or associated data, we can compute, for $\Omega_p = 1$,

$$HL = \sqrt{(10^{D_p/10} - 1)} = |\Gamma_p|/\sqrt{(1 - |\Gamma_p|^2)};$$
$$k_B = \frac{B_p}{B_a} = \frac{1}{\Omega_a}; \quad f_B = B_p \quad . \quad . \quad . \quad (177)$$

by means of which we can find the necessary number of branches to satisfy $D_a$ at $\Omega_a$ from Fig. 2(c) or from the power ratio given by

$$\left.\begin{array}{l}\dfrac{\mathscr{P}_{20}}{\mathscr{P}_2} = \eta_G^{e(n)}[1 + H^2L^2\cos^2(n\,\text{arc}\cos\Omega)], \quad \Omega < 1 \\[3mm] \dfrac{\mathscr{P}_{20}}{\mathscr{P}_2} = \eta_G^{e(n)}[1 + H^2L^2\cosh^2(n\,\text{arc}\cosh\Omega)], \quad \Omega > 1\end{array}\right\} \quad (178)$$

Thus $\qquad D_a = 10\log\left[(1 + H^2L^2\cosh^2(n\,\text{arc}\cosh\Omega_a)\right]$

Then, if $n$ is known, we can compute the constant

$$\vartheta_{e(n)} = \sin\left(\frac{1}{n}\text{arc sinh}\frac{1}{HL}\right) \quad . \quad . \quad . \quad (179)$$

The next step is to evaluate the root parameters $\alpha_s$ and $\rho_s^2$, or in general, $\alpha_s$ and $\lambda_s$. The quantities $\lambda_s$ are defined by $\rho_s^2$ and $\Omega_{\cap s}^2$, the squares of the frequencies of the maxima of $\phi^2$ (in this case the zeros of the insertion-loss function). Design parameters are given in general by eqn. (179), and

$$\left.\begin{array}{l}\lambda_s = o(n)\rho_s^2 + e(n)[\vartheta_{e(n)}^2 + \Omega_{\cap s}^2] = \vartheta_{e(n)}^2 + \cos^2\dfrac{n - 2s}{2n}\pi \\[3mm] \alpha_s = \vartheta_{e(n)}\sin\dfrac{n + e(n) - 2s}{2n}\pi\end{array}\right\} \quad (180)$$

The transformer ratio $t$ and termination ratio $r$ are found from Section 3.2, thus

$$r = \left[\tanh^2\left(\frac{1}{2}\text{arc sinh}\frac{1}{HL}\right)\right]^{e(n)} = (t)_{R_2 = R_1}^{e(n)} \quad . \quad (181)$$

and one set of the ladder coefficients for even or odd $n$ is given by

$$\nu = \frac{n - 1 - e(n)}{2}$$

$$\left.\begin{array}{l}a_{2s+1} = \dfrac{2\alpha_{[v+e(n)-2s]}}{\vartheta_{e(n)}^2}\displaystyle\prod_{q=1}^{s}\dfrac{\lambda_{2q-1}}{\lambda_{2q}} = \left[o(n) + \dfrac{e(n)}{r}\right]a_{n-2s} \\[4mm] a_{2s} = 2\alpha_{[v+e(n)+1-2s]}\dfrac{\displaystyle\prod_{q=1}^{s-1}\lambda_{2q}}{\displaystyle\prod_{q=1}^{s}\lambda_{2q-1}} = [o(n) + e(n)r]a_{n+1-2s}\end{array}\right\} \quad (182)$$

$$s = 0, 1, 2, \dots\left[\frac{n + o(n)}{4}\right]$$

It can be observed that, in case of odd $n$, only $(\nu + 1)$ ladder coefficients need be evaluated, as the rest are symmetrically distributed about $a_{\nu+1}$, i.e. $\bar{a}_r = \bar{a}_{n+1-r}$. In the case of even $n$, half of the ladder coefficients are evaluated directly, while the other half are found by multiplying the evaluated coefficients by the proper resistance ratio $r$, as indicated in eqns. (182). Other solutions, e.g. for prescribed decrement ratio or for symmetrical and unequally terminated networks, can be found in a similar manner as indicated in a maximally flat-response filter. [For $n$ odd unequally terminated networks, it is necessary only to replace $\bar{a}_s$ in eqn. (162) or (164) by that of eqn. (182).] Evaluation of ladder coefficients with losses should be treated as indi-

cated for the general case in Sections 3.7 and 4. It may be mentioned again that, in the case of filters not having infinite loss at finite frequencies, the problem of the evaluation of the ladder coefficients is comparatively simple. It may be added that the so-called multiplicity of solutions can be systematically analysed without great labour, as it is necessary only to investigate half of the distribution of possible signs.

### (5.4) Design Formulae for Chebÿshev-Type Pass-Band Attenuation-Band Parameters for Symmetrical and Inverse-Impedance Networks

An insertion-loss response with frequencies corresponding to natural modes and infinite attenuation, distributed in the pass and attenuation bands in the Chebÿshev sense, provides an effective approximation to an ideal filter. The method of deriving this function and its parameters is illustrated in Section 9. Here we shall give only a brief outline of the essential points and indicate the necessary formulae for network design. For the derivation of the characteristic insertion-loss function $\phi$ for even or odd number of branches, we have been using a hypothetical filter characteristic function $\psi$, which is identical with $\phi$ for one case of symmetrical filter, while in the case of an inverse-impedance filter, $\psi$ requires suitable transformation. One class of such transformations, which we shall use for even $n$, is illustrated in Sections 5.4.1 and 5.4.2. In general, any required insertion-loss characteristic function $\phi$ can be obtained from

$$\psi = \Omega^{o(n)} \prod_{s=1}^{\nu+e(n)} \frac{\Omega^2 - \Omega_{0s}^2}{\Omega^2 \Omega_{0s}^2 - 1} \quad . \quad . \quad . \quad (183)$$

by suitable transformations, i.e. $\mathfrak{T}_{e(n)}\psi = \phi$, where $\mathfrak{T}_{e(n)}$ denotes transformation operations. From inspection of eqns. (183) and (82) it can be seen that, for odd $n$, $\phi \equiv \psi$; thus $\psi$ can be identified with one of the insertion-loss characteristic functions which gives prescribed $k_B$, $D_p$ and $D_a$ directly by the identical transformation. For further illustration we shall require suitable transformations for $n$ even, where even the simplest transformation must involve the reduction of at least one finite pole, i.e. shift of finite pole to infinite frequency. We shall illustrate some of the bilinear (Möbius) transformations, denoted by $\mathfrak{M}_{e(n),\tau}$ and limited to $\tau = (2, 1)e(n)$, where $\tau$ indicates the number of reductions (shifts) of at least one finite pole (i.e. $\tau = 1$), or pole and zero (i.e. $\tau = 2$). If, for odd $n$, $\mathfrak{M}_{0,0}$ denotes the identical transformation (i.e. $\mathfrak{M}_{0,0} \equiv 1$), then illustrated solutions giving prescribed insertion-loss response will be limited to one symmetrical and two inverse-impedance networks, whose characteristic insertion-loss function are given by

$$\phi = \mathfrak{M}_{e(n),\tau}\psi; \quad \tau = (2, 1)e(n); \quad \mathfrak{M}_{0,0} \equiv 1 \quad . \quad (184)$$

(Maximally flat or Chebÿshev pass-band, etc., filters are other cases of $\mathfrak{T}_{e(n)}$-transformation.)

The poles and zeros of the $\psi$-function are defined by means of Jacobi's elliptic sn functions. Thus

$$\Omega_{0s} = \frac{1}{\Omega_{\infty s}} = \sqrt{k} \, \text{sn} \left[ \frac{2s - e(n)}{n} K, k \right] \quad . \quad . \quad (185)$$

where $k(< 1)$ is the elliptic modulus and $K = K(k)$ is the corresponding complete elliptic integral. The frequencies of the maxima of the $|\psi|^2$-function, which are in the pass band, will be denoted by $\Omega_{\cap s}$, and those of the minima in the attenuation band by $\Omega_{\cup s}$. These parameters, sometimes called Cauer parameters, are given in similar form to eqn. (185):

$$\Omega_{\cap s} = \frac{1}{\Omega_{\cup s}} = \sqrt{k} \, \text{sn} \left[ \frac{2s - o(n)}{n} K, k \right] \quad . \quad . \quad (186)$$

The important design quantities are defined by

$$HL = \sqrt{(10^{D_p/10} - 1)}; \quad L = \sqrt{\left[ k^{o(n)} \prod_{s=1}^{\nu+e(n)} [e(n)\Omega_{0s}^2 + o(n)\Omega_{\cap s}^2] \right]}$$
$$. \quad . \quad . \quad (187)$$

$$\Omega_p = \frac{1}{\Omega_a} = \sqrt{k}; \quad \Omega_B = \sqrt{(\Omega_p \Omega_a)} = 1$$

where $L$ is the amplitude of the pass-band variation of $\psi$. The relation of the discrimination data, the bandwidth ratio and the number of branches can be found from the following consideration. Let us define the prescribed effective low-pass bandwidth ratio for any transformation by

$$k_B = \frac{B_p}{B_a} = k\mathfrak{G}_{e(n)} < 1 \quad \text{where} \quad \mathfrak{G}_{e(n)} \gtrless 1 \quad . \quad (188)$$

where for Möbius transformation, i.e. $\mathfrak{M}_{e(n),\tau}$, the $\mathfrak{G}_{e(n)}$ is given by

$$\mathfrak{G}_{e(n)} = \sigma_{e(n)}^\tau \quad \text{where} \quad \sigma_{e(n)} = \text{sn} \left[ \frac{n - 2 + e(n)}{n} K, k \right];$$
$$\tau = (2, 1)e(n) \quad . \quad . \quad . \quad (189)$$

Thus, the modulus $k$ can be found from

$$k_B = k \, \text{sn}^\tau \left[ \frac{n - 2 + e(n)}{n} K, k \right] = k\sigma_{e(n)}^\tau; \quad \tau = (2, 1)e(n) \quad . \quad (190)$$

by iterative method (for $n$ even). We shall consider $\tau = 0$ for symmetrical odd-$n$ networks, i.e. $k_B = k$; and for even $n$, $\tau = 2$, which results in a network permitting equal termination, and $\tau = 1$, leading to inverse termination. Thus,

$$\left. \begin{array}{l} k_B = k; \quad n \text{ odd}, \quad \tau = 0, \quad \dfrac{R_1}{R_2} = 1 \\[2mm] \tilde{k}_B = \sqrt{(k)}\Omega_{0\,n/2}; \quad n \text{ even}, \quad \tau = 1, \dfrac{R_1}{R_2} \neq 1 \\[2mm] \bar{k}_B = \Omega_{0\,n/2}^2; \quad n \text{ even}, \tau = 2, \quad \dfrac{R_1}{R_2} = 1 \end{array} \right\} \quad . \quad (191)$$

For $n = 4$ and 6, the modulus $k$ can be found from the bandwidth ratio from Fig. 2(c) or from special tables of $\Omega_{0s}$. $K(k)$ can be evaluated from the magnitude of $k$, which is conventionally defined by Mag $(1 + k, 1 - k) = M$; thus $K(k) = \frac{1}{2}\pi/M$. Defining $1 + k = b_0$ and $1 - k = c_0$, $M$ can be evaluated in the following steps:

$$b_1 = \tfrac{1}{2}(b_0 + c_0), \quad c_1 = \sqrt{(b_0 c_0)}$$
$$. \quad . \quad . \quad . \quad . \quad . \quad . \quad . \quad .$$
$$b_q = \tfrac{1}{2}(b_{q-1} + c_{q-1}) = c_q$$
where $\quad c_q = \sqrt{(b_{q-1}c_{q-1})} = M, \quad q = 1, 2, 3, \ldots$

Usually a few terms give sufficient accuracy. Once $k$ is known the relation of $D_a$, $D_p$ and $n$ can be found from

$$D_a = 10[\log(10^{D_p/10} - 1) - n \log q(k) - 1 \cdot 2] \text{ dB} \quad . \quad (192)$$

where $q_{(k)}$ is the elliptic modular constant and can be computed by means of $k$ from formulae given in eqn. (240). $K(k)$ and $\log q$ (arc sin $k$) are tabulated in Jahnke and Emde 'Tables of Functions'. The relation (192) is also given in graphical form in Fig. 2(c). Such graphs, with attached separate scale-slide of $D_p$, constructed for practical use, provide essential and quick information concerning the performance and complexity of suitable filters which often constitute only part of a more complex

system involving many selective networks. Zeros and poles and the frequencies of the maxima and minima of the $\psi$-function can be computed approximately from

$$\Omega_r \simeq \tanh \frac{\pi \, u_r}{2K'} \tanh \left[ \left( \frac{n+r}{n} K - u_r \right) \frac{\pi}{K'} \right] \leqslant \Omega_p \quad . \quad (193)$$

where $u_r \,(= u_{0s}, \, u_{ns})$ for $\Omega_r \,(\simeq \Omega_{0s}, \, \Omega_{ns})$ are defined in eqns. (253) and (255).

It is, of course, possible to establish the quantities from tables such as Milne Thomson's tables of Jacobian elliptic functions. More suitable tables for this purpose are being prepared for publication. An effective method of computing 'sn' was suggested by Orchard,[22] using the Landon (Gauss) transformation.

If the zeros $\Omega_{0s}$ are found, then the coefficients of the polynomials $A'$ and $B'$ for basic networks can be evaluated from

$$e(n)A' + o(n)B' = \mathfrak{T}_{e(n)} \sqrt{[\eta_G^{e(m)}]} H' \prod_{s=1}^{\nu + e(n)} (p^2 + \Omega_{0s}^2) \quad . \quad (194)$$

In our case

$$\mathfrak{T}_{e(n)} \equiv \mathfrak{M}_{e(n),\tau}, \quad \tau = (2,\,1)e(n); \quad \mathfrak{M}_{0,0} \equiv 1$$

The root parameters of the discrimination function can be evaluated from the following relations. The constant $\vartheta_{e(n)}$ is defined by

$$\vartheta_{e(n)} = \sqrt{k} \,\operatorname{tn}\,[u'_{e(n)}, \, k'] \quad . \quad . \quad . \quad (195)$$

where

$$k' = \sqrt{(1 - k^2)}$$

and where the constant $u'_{e(n)}$ can be computed from eqns. (267)–(272) or from the following approximate formulae:

$$\left. \begin{aligned} u'_{e(n)} &\simeq \frac{2K}{n\pi} (-\tfrac{1}{4} 10^{-D_a/10} + \operatorname{arc\,tanh} 10^{-D_p/20}) \\ &\simeq \frac{2K}{n\pi} \operatorname{arc\,sinh} (10^{D_p/10} - 1)^{-1/2} \end{aligned} \right\} \quad . \quad (196)$$

If $u'_{e(n)}$ is computed from either of the above formulae it is necessary only to evaluate sn $(u'_{e(n)}, \, k')$ and to identify it with, say, $\sin \theta'_{e(n)}$, where $\sin \theta'_{e(n)} = \operatorname{sn} (u'_{e(n)}, \, k')$; then if $\theta'_{e(n)}$ is known, $\vartheta_{e(n)}$ is readily found from eqn. (195), which may be written as $\vartheta_{e(n)} = \sqrt{k} \tan \theta'_{e(n)}$. The root parameters of voltage-ratio numerator, for an actual symmetrical ($n$-odd) and for hypothetical ($n$-even) networks (or in other words for $\mathfrak{M}_{e(n),0} \equiv 1$), are given by

$$\left. \begin{aligned} \alpha_s &= \vartheta_{e(n)} \frac{\sqrt{[1 - \Omega_{0s}^2(k + k^{-1} - \Omega_{0s}^2)]}}{1 + \vartheta_{e(n)}^2 \Omega_{0s}^2} \\ \rho_s^2 &= \frac{\vartheta_{e(n)}^2 + \Omega_{0s}^2}{1 + \vartheta_{e(n)}^2 \Omega_{0s}^2}; \quad s = e(n), \, 1, \, 2, \, \dots \, [n/2] \end{aligned} \right\} \quad . \quad (197)$$

It may be observed that $\Omega_{00} \equiv 0$ and that $\alpha_0 = \vartheta_0$ exists for odd $n$ only. The insertion-loss voltage ratio for an actual $n$-odd symmetrical $\nu$-section filter (i.e. $\nu = \tfrac{1}{2}(n-1)$ is given by

$$\frac{V_{20}}{V_2} = \frac{A + pB}{P} = \frac{H(p + \alpha_0) \displaystyle\prod_{s=1}^{\nu} (p^2 + 2\alpha_s p + \rho_s^2)}{\displaystyle\prod_{s=1}^{\nu} (p^2 \Omega_{0s}^2 + 1)} \quad . \quad (198)$$

from which the even polynomials $A$ and $B$ can be established. The positive real coefficients $A_s$ and $B_s$ can be formed according to eqn. (98), and for a basic network $A' \equiv 0$ and $B' = H' \prod_{s=1}^{\nu} (p^2 + \Omega_{0s}^2)$, which follows from eqn. (194) and Section 2.2. The ladder coefficients for this type of voltage-ratio network for arbitrary termination, and with predistortion for losses, can be

found in the general way described previously. The normalizing constant $f_B = \sqrt{(B_p B_a)}$ and $k_B = k$.

In the case of a symmetrical equally terminated network, however, the ladder coefficients can be found explicitly[3, 5, 8] in terms of $\alpha_s$, $\rho_s^2$ and $\Omega_{0s}^2$. One of the methods leading to explicit formulae makes use of the location of the roots of the discrimination function, which, in this case, takes the form of

$$\Xi(p) = H'(p + \alpha_0) \prod_{s=1}^{\nu} \left[ \frac{p^2 + (-1)^s 2\alpha_s p + \rho_s^2}{p^2 \Omega_{0s}^2 + 1} \right]$$

where also $\quad \alpha_0 \left( \prod_{s=1}^{\nu} \rho_s^2 \Omega_{0s}^2 - 1 \right) = 2 \sum_{s=1}^{\nu} (-1)^s \alpha_s$

Here the sum of odd ladder coefficients is determined by the roots of $\Xi(p)$ in the left half-plane,

$$\sum_{s=1}^{\nu+1} a_{2s-1} = \frac{\bar{B}_0}{\bar{A}_0} = 2 \left( \frac{1}{\alpha_0} + \sum_{s=1}^{[\nu/2]} \frac{2\alpha_{2s}}{\rho_{2s}^2} \right)$$

and the sum of even ladder coefficients by those in the right half-plane,

$$\sum_{s=1}^{\nu} a_{2s} = 2 \sum_{s=1}^{[(\nu+1)/2]} \frac{2\alpha_{2s-1}}{\rho_{2s-1}^2} \quad .$$

These formulae apply also to symmetrical maximally flat and Chebyshev pass-band response filters.

The hypothetical filter function $\psi$ for $n$ even, illustrated in Fig. 6(b), is of theoretical interest only, and for this and other good reasons we call $\psi$ a hypothetical characteristic function. However, the actual characteristic function $\phi$ can be obtained from $\psi$ by the following transformations.
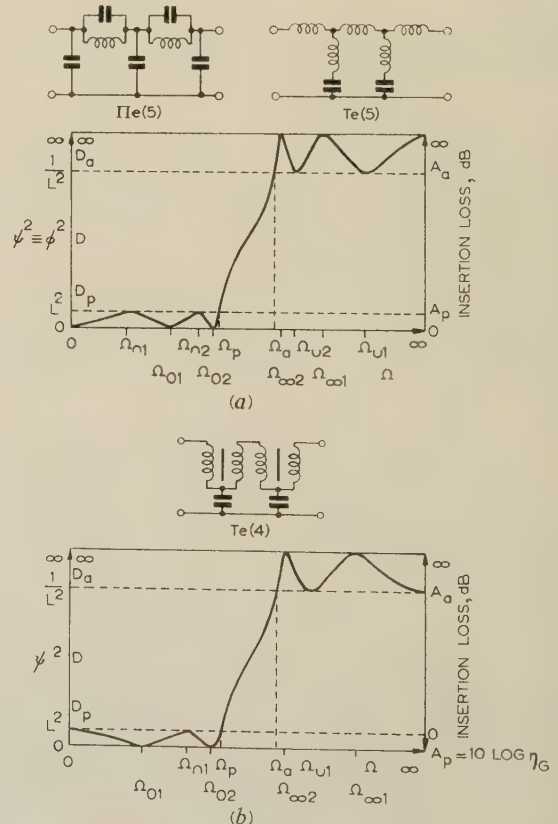


Fig. 6.—Characteristic functions and the corresponding ladder structures for Chebyshev pass-band and attenuation-band parameters.

(a) Actual ladder structure and characteristic function for odd $n$ ($n = 5$).
(b) Hypothetical structure and characteristic function for even $n$ ($n = 4$).

(5.4.1) **Special Case of an Inverse-Impedance (Antimetric) Network with Prescribed Insertion Loss and Equal Termination.**

The characteristic $\phi$-function is obtained from $\psi$ given in eqn. (183), by setting $\Omega_{01}^2 = 0$, i.e. by moving one of the zeros (e.g. $\mp\,\Omega_{01}$) to the origin and one of the poles (e.g. $\mp\,\Omega_{01}^{-1}$) to infinity (thus $\tau = 2$) and by adjustment of the remaining parameters to yield the same minima and maxima, $D_a$, $D_p$, in the discrimination function.
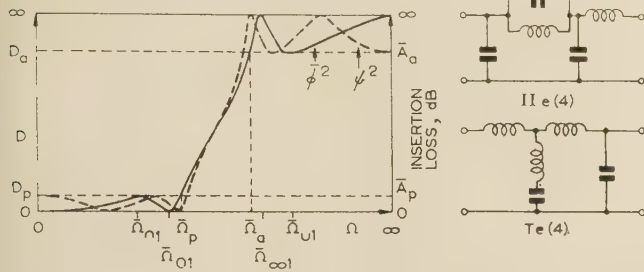


**Fig. 7.**—Special case of inverse impedance, equally-terminated (antimetric) network with Chebyshev pass-band and attenuation-band parameters ($n = 4$).

The result of this transformation is illustrated in Fig. 7 (for $n = 4$) and is specified by

$$\mathfrak{M}_{1,2}\left\{\begin{array}{l} H\psi = H\prod_{s=1}^{n/2}\left[\dfrac{\Omega^2 - \Omega_{0s}^2}{\Omega^2\Omega_{0s}^2 - 1}\right] \\[3mm] k, D_p, D_a, n, \eta_G < 1 \end{array}\right.$$

$$\rightleftharpoons \left\{\begin{array}{l} \bar{H}\bar\phi = -\,\bar{H}\bar\Omega^2\prod_{s=1}^{\nu}\dfrac{\bar\Omega^2 - \bar\Omega_{0s}^2}{\bar\Omega^2\bar\Omega_{0s}^2 - 1} \\[3mm] \bar{k}_B < k, D_p, D_a, n, \bar\eta_G = 1, \bar{H} = H \end{array}\right\} \quad . \quad (199)$$

or $\qquad \mathfrak{M}_{1,2}H\psi = H\phi = Hp^2\prod_{s=1}^{\nu}\dfrac{p^2 + \bar\Omega_{0s}^2}{p^2\bar\Omega_{0s}^2 + 1}$

Once the transformation formulae are obtained, the bar over the variable $\Omega$, $\phi$ or $p$ can be neglected as inessential. However, this bar may be preserved in the constants as it indicates a new parameter related to the parameters of the hypothetical function. The results stated in eqn. (199) are obtained from the Möbius transformation $\mathfrak{M}_{e(n),\tau} = \mathfrak{M}_{1,2}$ of the frequency variable, specified by

$$\Omega^2 = \frac{a\bar\Omega^2 + b}{c\bar\Omega^2 + d} \quad . \quad . \quad . \quad . \quad (200)$$

where
$$\Omega^2 - \Omega_{01}^2 \rightleftharpoons \bar\Omega^2 - 0$$
$$\Omega^2 = \Omega_{01}^{-2} \rightleftharpoons \bar\Omega^2 = \infty$$
$$\Omega^2 - k \rightleftharpoons \bar\Omega^2 - \bar{k}_B$$
$$\tau = 2$$

hence $\qquad \bar\Omega_p = \sqrt{\bar{k}_B}; \quad \bar\Omega_a = 1/\bar\Omega_p$

and
$$\bar\Omega = \frac{\Omega^2 - \Omega_{01}^2}{1 - \Omega^2\Omega_{01}^2} \quad . \quad . \quad . \quad . \quad (201)$$

from which the prescribed bandwidth ratio $\bar{k}_B$ is given in terms of parameters of the hypothetical filter as follows:

$$\bar{k}_B = \frac{\bar{B}_p}{\bar{B}_a} = \frac{k - \Omega_{01}^2}{1 - k\Omega_{01}^2} = k\,\mathrm{sn}^2\left(\frac{n-1}{n}K, k\right) = k\sigma_{e(n)}^2 = \Omega_{0\,n/2}^2$$
$$. \quad . \quad . \quad . \quad (202)$$

Since $\mathrm{sn}\,u \leqslant 1$ for real values of $u$, the actual bandwidth ratio will be smaller than the corresponding bandwidth ratio of the hypothetical filter as defined by the elliptic modulus $k$. The design for a prescribed bandwidth ratio for filters with an even number of branches should start by evaluating $\Omega_{0\,n/2}$ and hence modulus $k$ from the elliptic-function relation; for this purpose a semi-graphical method is advocated, or $k$ can be found from suitable graphs, e.g. Fig. 2(c), or tables.[23] Once the modulus $k$ is found, further design is straightforward. It must be observed in eqn. (199) that the discrimination levels and the number of sections are the same for hypothetical and for actual network. It will be shown that all parameters of actual networks can be computed in terms of the parameters of the hypothetical network. Thus the new finite zeros and poles of the function for the actual filter are found by means of eqn. (201) as follows:

$$\bar\Omega_{0s}^2 = \frac{1}{\bar\Omega_{\infty s}^2} = \frac{\Omega_{0(s+1)}^2 - \Omega_{01}^2}{1 - \Omega_{0(s+1)}^2\Omega_{01}^2}$$
$$= k\,\mathrm{sn}\left(\frac{2s}{n}K, k\right)\mathrm{sn}\left[\frac{2(s+1)}{n}K, k\right] = \Omega_{ns}\Omega_{n(s+1)} \quad . \quad (203)$$

and the frequencies corresponding to the maxima and minima are given by

$$\bar\Omega_{ns}^2 = \frac{1}{\bar\Omega_{ns}^2} = \frac{\Omega_{ns}^2 - \Omega_{01}^2}{1 - \Omega_{ns}^2\Omega_{01}^2}$$
$$= k\,\mathrm{sn}\left(\frac{2s-1}{n}K, k\right)\mathrm{sn}\left(\frac{2s+1}{n}K, k\right) = \Omega_{0s}\Omega_{0(s+1)} \quad . \quad (204)$$

Once the parameters of the characteristic function $\phi$ are determined, the roots of the power or voltage ratio are found from eqns. (253), (255), (273) and (201) extended to the complex-frequency plane and by simple elliptic-function transformations. Thus

$$\bar{p}_{\pm s}^2 = \frac{p_{\pm s}^2 + \Omega_{01}^2}{1 + p_{\pm s}^2\Omega_{01}^2} - k\frac{\mathrm{sn}^2(u_{\pm s}, k) - \mathrm{sn}^2(u_{01}, k)}{1 - k^2\,\mathrm{sn}^2(u_{\pm s}, k)\,\mathrm{sn}^2 u_{01}, k)}$$
$$= -k\,\mathrm{sn}(u_{n s} \pm ju_1', k)\,\mathrm{sn}(u_{n(s-1)} \pm ju_1', k) \quad . \quad . \quad (205)$$

As follows from the general theory, eqns. (83), (90) and (94), the necessary parameters for formation of the insertion-loss voltage ratio are $\bar\rho_s^2$ and $2\bar\alpha_s$. From eqn. (205) and further transformation of elliptic functions with complex arguments, as illustrated in eqn. (274), it follows that

$$\bar{p}_{\pm s}^2 = -\frac{(\Omega_{ns}W_1 \mp j\vartheta_1 cd_{ns})[\Omega_{n(s-1)}W_1 \mp j\vartheta_1 cd_{n(s-1)}]}{(1 + \vartheta_1^2\Omega_{ns}^2)[1 + \vartheta_1^2\Omega_{n(s-1)}^2]}$$
$$= -\bar\xi_s \pm j2\bar\alpha_s\bar\Omega_s \quad . \quad (206)$$

where $W_1$, $\vartheta_1$ and $cd_{nr}$ are as defined in eqn. (275). Hence the root parameters $\bar\rho_s^2$ and $2\bar\alpha_s$, for the voltage or power ratio, are evaluated from

$$\left.\begin{array}{l} \bar\xi_s = -\frac{1}{2}(\bar{p}_s^2 + \bar{p}_{-s}^2) = \dfrac{\Omega_{ns}\Omega_{n(s-1)}W_1^2 - \vartheta_1^2 cd_{ns}cd_{n(s-1)}}{(1 + \vartheta_1^2\Omega_{ns}^2)[1 + \vartheta_1^2\Omega_{n(s-1)}^2]} \\[4mm] \bar\rho_s^4 = \bar{p}_s^2\bar{p}_{-s}^2 = \dfrac{(\vartheta_1^2 + \Omega_{ns}^2)[\vartheta_1^2 + \Omega_{n(s-1)}^2]}{(1 + \vartheta_1^2\Omega_{ns}^2)[1 + \vartheta_1^2\Omega_{n(s-1)}^2]} \end{array}\right\} \quad (207)$$

from which $2\bar\alpha_s = \sqrt{[2(\bar\rho_s^2 - \bar\xi_s)]}$.

The insertion-loss voltage ratio is finally given for $n$, $\bar{k}_B = \bar{B}_p/\bar{B}_a$, $D_p$ and $D_a$ by

$$\frac{V_{20}}{V_2} = \frac{A + pB}{P} = H\frac{\prod\limits_{s=1}^{n/2}(p^2 + 2\bar\alpha_s p + \bar\rho_s^2)}{\prod\limits_{s=1}^{(n-2)/2}(p^2\bar\Omega_{0s}^2 + 1)} \quad . \quad (208)$$

from which the polynomials $A$ and $B$ can be evaluated. For basic networks $B' \equiv 0$, while

$$A' = H'p^2 \prod_{s=1}^{(n-2)/2} (p^2 + \bar{\Omega}_{0s}^2); \quad \text{hence } A_0' = 0 \qquad (209)$$

The further procedure to evaluate ladder coefficients is that given in the general theory. The actual filter configuration is of $\Pi_T$- or $T_\Pi$-type (see Figs. 2 and 7), with equal termination $R_1 = R_2$, therefore $\bar{\eta}_G = 1$, $f_B = \sqrt{(\bar{B}_p \bar{B}_a)}$.

### (5.4.2) Inverse-Impedance Filter.

Another type of derived function which is sometimes of interest results from moving only $\mp \Omega_{\infty 1}$ to infinity (i.e. $\tau = 1$) and by adjusting the remaining parameters. This transformation is shown in Fig. 8 and is stated by

$$\mathfrak{M}_{1,1} \left\{ \begin{array}{l} H'\psi = H' \displaystyle\prod_{s=1}^{n/2} \dfrac{p^2 + \Omega_{0s}^2}{p^2\Omega_{0s}^2 + 1} \\[2mm] k, D_p, D_a, n, \eta_G < 1 \end{array} \right\}$$

$$\rightleftharpoons \left\{ \begin{array}{l} \tilde{H}'\phi = \tilde{H}' \dfrac{\displaystyle\prod_{s=1}^{n/2} (p^2 + \tilde{\Omega}_{0s}^2)}{\displaystyle\prod_{s=1}^{(n-2)/2} \left(\dfrac{p^2}{\tilde{\Omega}_{\infty s}^2} + 1\right)} \\[4mm] \tilde{k}_B < k, D_p, D_a, n, \tilde{\eta}_G < 1; \\[2mm] \tilde{H} = HL \displaystyle\prod_{s=1}^{n/2} \tilde{\Omega}_{0s}^{-2} \end{array} \right\} \qquad (210)$$

The filter response obtained by this transformation will have a better bandwidth ratio than that of eqn. (199). However, the termination cannot be made equal without an ideal transformer. The bilinear transformation, from which the resultant function is obtained, is specified by

$$\Omega^2 = \frac{a\tilde{\Omega}^2 + b}{c\tilde{\Omega}^2 + d} \qquad (211)$$

for
$$\begin{array}{l} \Omega^2 = 0 \rightleftharpoons \tilde{\Omega}^2 = 0 \\[1mm] \Omega^2 = \Omega_{01}^{-2} \rightleftharpoons \tilde{\Omega}^2 = \infty \\[1mm] \Omega^2 = k \rightleftharpoons \tilde{\Omega}^2 = \tilde{k}_B \\ \qquad\quad \tau = 1 \end{array}$$

The new bandwidth ratio, in terms of hypothetical filter parameters or elliptic functions is given by

$$\tilde{k}_B = \sqrt{\left(k\frac{k - \Omega_{01}^2}{1 - k\Omega_{01}^2}\right)} = k \operatorname{sn}\left(\frac{n-1}{n}K, h\right) = k\sigma_{e(n)} = \sqrt{(k)}\Omega_{0\,n/2} \qquad (212)$$

and $\tilde{\Omega}_p = \sqrt{\tilde{k}_B} = \sqrt{(k^{1/2}\Omega_{0\,n/2})}$, while $\tilde{\Omega}_a = 1/\tilde{\Omega}_p$.

For a prescribed bandwidth ratio, $k$ should be found in a similar manner as stated in the previous case. For $n = 4$, and 6, $\tilde{k}_B$ can be estimated from Fig. 2(c). The new variable $\tilde{\Omega}$ can be expressed in the form

$$\tilde{\Omega}^2 = \frac{\Omega^2 cd_{01}}{1 - \Omega^2\Omega_{01}^2} \qquad (213)$$

where $cd_{01}$ is defined generally in eqn. (275). Finite poles and zeros of the characteristic function are found with the aid of eqn. (213) in a manner similar to that used in the previous case; so also the frequencies of maxima and minima of the derived

function can be found. These quantities, in terms of hypothetical filter parameters, are defined as

$$\left. \begin{array}{ll} \tilde{\Omega}_{0s}^2 = \dfrac{\Omega_{0s}^2 cd_{01}}{1 - \Omega_{0s}^2\Omega_{01}^2}, & \tilde{\Omega}_{\infty s}^2 = \dfrac{cd_{01}}{\Omega_{0(s+1)}^2 - \Omega_{01}^2} - \tilde{\Omega}_{01}^2 \\[4mm] \tilde{\Omega}_{\cap s}^2 = \dfrac{\Omega_{\cap s}^2 cd_{01}}{1 - \Omega_{\cap s}^2\Omega_{01}^2}, & \tilde{\Omega}_{\cup s}^2 = \dfrac{cd_{01}}{\Omega_{\cap s}^2 - \Omega_{0s}^2} \end{array} \right\} \qquad (214)$$

($\tilde{\Omega}_{\cap s}$ are now the zeros of the insertion-loss function while $\tilde{\Omega}_{0s}$ are the maxima of its gain. See Fig. 8.)
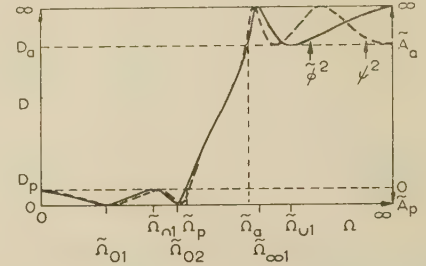


Fig. 8.—Inverse-impedance network and characteristic function with Chebȳshev pass-band and attenuation-band parameters ($n = 4$).

It must be observed that poles are no longer the reciprocals of zeros as in the previous case; and also that the frequencies of the maxima are no longer the reciprocals of those of minima. This should be obvious, as the number of finite poles is smaller than that of zeros. The root parameters for the insertion-loss voltage ratio are found in a manner similar to that used in the previous case:

$$\tilde{\xi}_s = \frac{(\xi_s - \Omega_{01}^2\rho_s^4)cd_{01}}{1 + \Omega_{01}^4\rho_s^4 - 2\xi_s\Omega_{01}^2}, \quad \tilde{\rho}_s^2 = \frac{\rho_s^2 cd_{01}}{\sqrt{(1 + \Omega_{01}^4\rho_s^4 - 2\xi_s\Omega_{01}^2)}} \qquad (215)$$

from which
$$2\tilde{\alpha}_s = \sqrt{[2(\tilde{\rho}_s^2 - \tilde{\xi}_s)]}$$

The insertion-loss voltage ratio and the polynomial $A'$ required for formation of the basic network are given for $n$, $\tilde{k}_B = \tilde{B}_p/\tilde{B}_a$, $D_p$ and $D_a$ by

$$\left. \begin{array}{l} \dfrac{V_{20}}{V_2} = \dfrac{A + pB}{P} = \sqrt{\tilde{\eta}_G}\,\tilde{H}\,\dfrac{\displaystyle\prod_{s=1}^{n/2} (p^2 + 2\tilde{\alpha}_s p + \tilde{\rho}_s^2)}{\displaystyle\prod_{s=1}^{(n-2)/2} (p^2/\tilde{\Omega}_{\infty s}^2 + 1)} \\[6mm] A' = \sqrt{\tilde{\eta}_G}\,\tilde{H}' \displaystyle\prod_{s=1}^{n/2} (p^2 + \tilde{\Omega}_{0s}^2) \\[4mm] \tilde{H} = HL \displaystyle\prod_{s=1}^{n/2} \tilde{\Omega}_{0s}^{-2} = \dfrac{HL}{A_0'}; \\[4mm] HL = \sqrt{(10^{D_p/10} - 1)}; \\[2mm] \tilde{\eta}_G = 1 - \left(\dfrac{A_0'}{A_0}\right)^2; \quad f_B = \sqrt{(\tilde{B}_p\tilde{B}_a)} \end{array} \right\} \qquad (216)$$

This network has exactly the same configuration as that of the previous case and the ladder coefficients can be evaluated in the general way. One of the merits of this type of network is a better bandwidth ratio, but lower possible allowance for the predistortion for losses. The actual resistance ratio is found by means of $A_0$ and $A_0'$ from Section 3.2.

### (6) CONCLUSION

The insertion-loss methods were introduced in various publications almost at the same time some twenty years ago, in Italy, the United States, and Germany.

Those who contributed most to this field of network synthesis are also those who were the first to introduce it, namely Darlington, Cauer, Cocci, Piloty and Bader. It is evident that the method owes its strong basis to many previous works on the subject, such as those of Foster, Brune, Cauer, Bode, Laurent, Norton, Zobel and Campbell and many others.

Opinion is that the method is superior to any other known. The precision and computational labour required for the design by the insertion-loss method is such that the method of image parameters is often preferred. So far as conventional filters are concerned, the image-parameter method can satisfy the requirements with only a few more network elements.

The necessary accuracy in the intermediate stages of evaluation of ladder coefficients is often high, except perhaps in the case of one-branch-element ladders (e.g. when $\zeta_r = 0$) or, in general, for a small number of branches. This high accuracy is especially important when some of the real parts of natural modes (i.e. $\alpha_s$) and those of a characteristic function (i.e. $\alpha'_s$) are found to be very small. However, the computational labour can be circumvented to some extent. It has been shown that the design is of such a nature that the ladder coefficients, and other required data for normalized low-pass ladder structures, can be completely formulated allowing programming for automatic computation and tabulation of the result for wide ranges of $k_B$, $D_p$ and $n$.

Such work is already being undertaken by the author, with Mr. J. K. Skwirzynski, on behalf of the company with which they are associated. It has been learned that similar work is being carried out in Germany by Dr. Glowatzki.[25]

Some results were published in the United States by Bedrosian, Luke and Putschi, giving normalized components for some cases of one- and two-section Cauer–Darlington symmetrical filters, and many tables concerning chain matrix parameters, including those of a hypothetical chain matrix (i.e. Tables IV, V, VI, X, XII, and XIII).[26]

Ladder coefficients for one- and two-section Darlington symmetrical filters are also published in graphical forms.[8] After the completion of the manuscript of this paper the author's attention was drawn to useful tables concerning maximally flat and Chebȳshev pass-band parameter filters by L. Weinberg.[27]

The only necessary computation which then remains for the user is the evaluation of the network elements $L_r$ and $C_r$, from given ladder coefficients $a_r$ and $\zeta_r$, for frequencies $f_0$ and $f_B$ and resistances $R_1$ or $R_2$, for a particular specification of $k_B$, $D_p$, $D_a$ and $n$. It is hoped that such a solution, though necessarily limited, will attract many engineers to employ this effective method of network synthesis for immediate practical purposes, which can be satisfied exactly with even less labour and fewer elements than are required for the Zobel or the Laurent filters. However, the element tolerances, the particular character of the insertion-loss responses, the network configuration, etc., are more restricted. The insertion-loss method given here can be readily extended beyond the low-pass analogue. Cauer, Fetzer, and later other authors, have developed a technique for the design of more general band-pass, etc., filters. Darlington's reference-filter method is also of more general type. All these methods can be completely formulated; in fact they need only a few additional statements concerning the ladder structure shown in Fig. 2 and definitions (18), (27) and (33).

Fetzer[15, 17] gives several explicit formulae for more general band-pass characteristic functions [e.g. $\phi$ given in eqn. (256), in which some poles and zeros are reduced or shifted or cancelled].

However, all the known methods seem still to be lacking in the required generality, simplicity and engineering technique characterizing the Zobel or even the Laurent method of design. Besides this, the complete solution of filter functions requires still further development of suitable mathematics, e.g. hyper-elliptic functions. The desired solution would be of practical application if it led in the manner of the Cauer–Darlington method to any prescribed specification, e.g. to any transformation $\mathbb{T}$ by analytic means. (Note that in operating on band-pass $\phi$ or band-stop $\hat{\phi}$ functions, the transformation $\mathbb{T}$ may involve not only shifts but also cancellations of poles and zeros.) Empirically, this problem is partly solved by potential analogue devices. However, empirical and graphical methods belong more to art than science. As to a method of network realization from a given function, in spite of Cauer, Brune, Gevertz, Cocci, Darlington, Piloty, Bader and other authors, only a very limited number of solutions are employed, and with a few exceptions, even these are limited to idealized simple cases. Talbot[28] made an attempt to solve the important part of the realization problem which, it seems, was partly successful.

Returning now to ladder coefficients and to the available data already published, or to be published shortly, the formulae for the elements of lattice, bridged-T or other useful structures can be found, and for some cases have been found, in terms of ladder coefficients and the frequencies of infinite loss. Lattice and bridged-T structures are especially useful when piezo-electric crystals are used.[29] Crystals may be cut according to design, or available crystals can be used in a suitably modified network (some such networks have been successful). Negative ladder coefficients, which occur sometimes and cannot be avoided by interchanges of $\Omega_{\infty s}$, can often be made positive by the predistortion method. Negative ladder coefficients can also be realized in a suitably chosen configuration by mutual inductances or by the appropriate use of transformers (e.g. Norton impedance transformation), or by the use of the Bott and Duffin realization method. The insertion-loss method is not restricted to low-pass analogue filters only. The material in this paper is thought to be of value in using another, more general, Darlington method of network synthesis,[1] application of which, with the insertion-loss and the potential-analogue techniques, provides a powerful means of constructing special network functions with particular amplitude, phase and transient responses. Thus, networks with specified $k_B$, $D_p$ and $D_a$ and, say, resulting rise time, or over-shoot due to particular input signal, and networks working under vestigial conditions (e.g. linear voltage change in the transition band about, say, 6 dB level), and particular phase networks, have been constructed successfully by the methods discussed.

## (7) ACKNOWLEDGMENTS

## (8) REFERENCES

(1) DARLINGTON, S.: 'Network Synthesis using Tchebycheff Polynomial Series', *Bell System Technical Journal*, 1952, **31**, p. 284.

(2) MORSE, P. M., and FESHBACH, H.: 'Methods of Theoretical Physics' (McGraw-Hill, 1953), Vol. 1, p. 373.

(3) CAUER, W.: 'Theorie der linearen Wechselstromschaltungen' (Akademie-Verlag, 1954).

(4) NORTON, E. L.: 'Constant Resistance Networks with Application to Filter Groups', Bell System Technical Journal, 1937, 16, p. 178.

(5) DARLINGTON, S.: 'Synthesis of Reactance Four-Poles', Journal of Mathematics and Physics, 1939, 18, p. 257.

(6) COCCI, G.: 'Filtri con numero minimo di elementi', Alta Frequenza, 1942, 11, p. 804.

(7) REED, J.: 'Low-Q Microwave Filters', Proceedings of the Institute of Radio Engineers, 1950, 38, p. 793.

(8) SKWIRZYNSKI, J. K., and ZDUNEK, J.: 'Design Data for Symmetrical Darlington Filters', Proceedings I.E.E., Monograph No. 227 R, March, 1957 (104 C, p. 366).

(9) BOTT, R., and DUFFIN, R. J.: 'Impedance Synthesis without use of Transformers', Journal of Applied Physics, 1949, 20, p. 816.

(10) CAUER, W.: 'Siebschaltungen' (V.D.I.-Verlag, 1931).

(11) MAYER, H. F.: 'Ueber die Daempfung von Siebketten in Durchleissigkeitsbereich', Elektrische Nachrichtentechnik, 1925, 2, p. 335.

(12) LAURENT, T.: 'Vierpoltheorie und Frequenztransformation' (Springer-Verlag, 1956).

(13) MING, N.-T.: 'Verwirklichung linearer Vierpolschaltungen vorgeschriebener Frequenz abhängigkeit unter Berücksichtigung gleicher Spulenverluste und gleicher Kondensatorenverluste', Archiv für Elektrotechnik, 1949, 39, p. 452.

(14) LINKE, J. M.: 'A Graphical Approach to the Synthesis of General Insertion Attenuation Function', Proceedings I.E.E., Paper No. 965 R, May, 1950 (97, Part III, p. 179).

(15) FETZER, V.: 'Die numerische Berechnung von Filterschaltungen mit allgemeinen Parametern nach der modernen Theorie unter besonderer Berücksichtigung der Cauerschen Arbeiten', Archiv der Elektrischen Übertragung, 1951, 5, p. 499.

(16) FETZER, V.: 'Die numerische Berechnung von Filterschaltungen mit Tschebyscheffschem Verhalten der Betriebsdämpfung nach der Methode von W. Cauer', ibid., 1952, 6, p. 419.

(17) FETZER, V.: 'Explizite Berechnungsformeln für Filterschaltungen mit allgemeinen Parametern', ibid., 1954, 8, p. 31.

(18) FETZER, V.: 'Vergleich von Filtern nach der Wellenparametertheorie mit den Filtern der Betriebsparametertheorie und die neuzeitlichen Methoden der Filterberechnung', ibid., 1956, 10, p. 225.

(19) McSKIMIN, H. J.: 'Transducer Design for Ultrasonic Delay Line', Journal of the Acoustical Society of America, 1955, 27, p. 307.

(20) GREEN, E.: 'Synthesis of Ladder Networks to give Butterworth or Chebyshev Response in the Pass Band', Proceedings I.E.E., Monograph No. 88 R, January, 1954 (101, Part IV, p. 192).

(21) BELEVITCH, V.: 'Tchebyshev Filters and Amplifier Networks', Wireless Engineer, 1952, 29, p. 106.

(22) ORCHARD, H. T.: 'Synthesis of Wideband Two-Phase Networks', ibid., 1950, 27, p. 72.

(23) ZDUNEK, J., and SKWIRZYNSKI, J. K.: 'Tables of Ladder Coefficients and Related Data for Symmetrical and Inverse-Impedance Filters' (to be published).

(24) CAYLEY, A.: 'An Elementary Treatise on Elliptic Functions' (Bell, 1895).

(25) GLOWATZKI, E.: 'Katalogisierte Filter', Nachrichtentechnik, 1956, 9, p. 11.

(26) BEDROSIAN, S. D., LUKE, E. L., and PUTSCHI, H. N.: 'On the Tabulation of Insertion Loss Low-Pass Chain Matrix Coefficients and Network Element Values', Proceedings of the National Electrical Conference, 1955, 11, p. 697.

(27) WEINBERG, L.: 'Network Design by Use of Modern Synthesis Techniques and Tables', Hughes Research Laboratory, Culver City, California, Technical Memorandum No. 427, 1956.

(28) TALBOT, A.: 'A New Method of Synthesis of Reactance Networks', Proceedings I.E.E., Monograph No. 77 R, October, 1953 (101, Part IV, p. 73).

(29) FABIJANSKI, F.: 'Próba Zastosówania Metody Cauera do Szerokopasmowych Filtrów Piezoelektryczynch', Prace P.I.T., 1955, 5, No. 15.

## (9) APPENDIX

### (9.1) Hypothetical Filter Characteristic Insertion-Loss Function with Chebyshev Pass- and Attenuation-Band Parameters, and Related Topics

Let us consider the function illustrated in Fig. 6. It can be shown that the most effective insertion loss that will satisfy required specifications can be derived from these functions. For these functions we shall require the same number of finite poles and finite zeros, all distributed within appropriate bands in the Chebyshev sense. This is most simply illustrated by inverting the Chebyshev pass-band type into the attenuation band, or in other words, by requiring the attenuation band to be the inverse of the pass-band about $\sqrt{(\Omega_p \Omega_a)}$. The frequency properties in such functions can be defined by the relations

$$0 < \Omega < 1 \rightleftharpoons \frac{1}{1 \leqslant \Omega \leqslant \infty}; \quad \sqrt{(\Omega_p \Omega_a)} = \Omega_B = 1 \quad . \quad (217)$$

from which it follows that

$$\Omega_p = \frac{1}{\Omega_a}, \quad \Omega_{0s} = \frac{1}{\Omega_{\infty s}} \quad \text{and} \quad \Omega_{\cap s} = \frac{1}{\Omega_{\cup s}} \quad . \quad (218)$$

Consequently the characteristic function $\psi$ (identical with $\phi$ for odd $n$ and transformable to $\phi$ for even $n$), is defined by

$$\psi(\Omega) = \Omega^{0(n)} \prod_{s=1}^{[n/2]} \frac{\Omega^2 - \Omega_{0s}^2}{\Omega^2 \Omega_{0s}^2 - 1} = \frac{1}{\psi(\Omega^{-1})}$$

i.e. $\quad |\psi(\Omega_p)| = |\psi(\Omega_{\cap s})| = L = \frac{1}{|\psi(\Omega_a)|} = \frac{1}{|\psi(\Omega_{\cup s})|} \quad . \quad (219)$

where the numbers of poles in $P$ in this case is extended to $m = [n/2]$.

Multiplying this function by the constant $H'$ does not change its form but only its magnitude and sign, if such are associated with $H'$. The poles and zeros and frequencies of maxima and minima will retain the same positions, i.e. $H$ only multiplies the $\psi$-function; hence Fig. 6 may represent $H^2\psi^2$, as well as the discrimination $D$ or insertion loss on a suitable chosen scale.

Let us consider the hypothetical insertion-loss functions $\psi$, defined in eqns. (217), (218) and Fig. 6, and related to eqn. (82), in which $1/\Omega_{\infty s}$ should be replaced in the extended $P$-polynomial by $\Omega_{0s}$, which follows from eqn. (217). We should note that, in the $\psi$ the absolute values of maxima and minima correspond to $L$ and its inverse $1/L$. The derivation of a suitable function corresponding to the $F(\Omega)$ is perhaps most simply illustrated by the following approach. [The same approach can be used for the Chebyshev pass-band parameters of eqn. (172).] By the aid of Fig. 6, eqns. (82) and (218), we can form

$$\psi^2 - L^2 = \frac{\Omega^{2o(n)} \prod\limits_{s=1}^{[n/2]} (\Omega^2 - \Omega_{0s}^2) - L^2 P^2}{P^2}$$

and $\quad \psi^2 - \dfrac{1}{L^2} = \dfrac{\Omega^{2\,o(n)} \prod\limits_{s=1}^{[n/2]} (\Omega^2 - \Omega_{0s}^2) - P^2/L^2}{P^2}$ $\quad$ . (220)

where the $P$-polynomial is similar to that in eqn. (79), namely

$$P = \prod_{s=1}^{[n/2]} (\Omega^2 \Omega_{0s}^2 - 1)$$

Inspection of Fig. 6 reveals that the expression (220) must have zeros when the function is tangential to the levels $L^2$ and $L^{-2}$, i.e. at $\pm\Omega_{\cap s}$ and $\pm\Omega_{\cup s}$, and also where it cuts these levels, i.e. at the extremal frequencies $\pm\Omega_p$ and $\pm\Omega_a$ (in Fig. 6 only positive frequencies are shown). It is obvious that these frequencies are the zeros of $(\psi^2 - L^2)$ and $(\psi^2 - L^{-2})$ in the positive- as well as in the negative $\Omega$-range. It must also be observed that the even $\psi^2$-function is tangential to the levels $L^2$ and $L^{-2}$ at the origin and at infinity. These last conditions imply some necessity of transformation for resistive termination.

Considering all these properties in Fig. 6, it is clear that eqn. (220) can be written as

$$\psi^2 - L^2 = \frac{(h_1\Omega^2)^{e(n)}(\Omega^2 - \Omega_p^2) \prod\limits_{s=1}^{\nu} (\Omega^2 - \Omega_{\cap s})^2}{P^2} ;$$

$$\nu - \frac{n-1-e(n)}{2} \qquad . \quad (221)$$

where $h_1$ is a real constant (this constant is of no immediate importance), and

$$\psi^2 - L^{-2} = \frac{h_2^{e(n)}(\Omega^2 - \Omega_a^2) \prod\limits_{s=1}^{\nu} (\Omega^2 - \Omega_{\cup s}^2)^2}{P^2} \qquad . \quad (222)$$

where $h_2$ is a real constant similar to $h_1$. A very important equation can be obtained by multiplying eqns. (221) and (222):

$$(\psi^2 - L^2)(\psi^2 - L^{-2}) =$$
$$\frac{(h_1 h_2 \Omega^2)^{e(n)}(\Omega^2 - \Omega_p^2)(\Omega^2 - \Omega_a^2) \prod\limits_{s-1}^{\nu} (\Omega^2 - \Omega_{\cap s}^2)^2(\Omega^2 - \Omega_{\cup s}^2)^2}{P^4}$$

$$\qquad . \quad . \quad . \quad (223)$$

The relation is self-evident, following from the properties of the functions illustrated in Fig. 6, extended to arbitrary $n$. Let us consider now the derivative of the functions $\psi$ defined in eqn. (219). For our purposes it is only necessary to consider the highest power of the variable $\Omega$, which will reveal sufficient information. The derivative will take the form

$$\frac{d\psi}{d\Omega} = \frac{d}{d\Omega}\left(\Omega^{o(n)} \prod_{s=1}^{[n/2]} \frac{\Omega^2 - \Omega_{0s}^2}{\Omega^2 \Omega_{0s}^2 - 1}\right) = \frac{h_4^{o(n)}(h_3\Omega)^{e(n)}(\Omega^{4\nu} + \ldots)}{P^2}$$

$$\qquad . \quad . \quad . \quad (224)$$

where $h_3$ and $h_4$ are real constants.

Let us now inspect the derivative and its relation to Fig. 6. The derivative is zero where $\psi$ is tangential to the levels $\pm L$ and $\pm L^{-1}$, which follows from the fundamental properties of the derivative. The points at which these zeros occur are at $\Omega_{\cap s}$ and $\Omega_{\cup s}$, and for an even function also at zero and at

infinite frequency. We can thus write eqn. (224) in the factorized form

$$\frac{d\psi}{d\Omega} = \frac{h_4^{o(n)}(h_3\Omega)^{e(n)} \prod\limits_{s=1}^{\overset{\vee}{}} (\Omega^2 - \Omega_{\cap s}^2)(\Omega^2 - \Omega_{\cup s}^2)}{P^2} \qquad . \quad (225)$$

By inspection of eqns. (223) and (225), eqn. (223) can be expressed in terms of a derivative $d\psi/d\Omega$ given in eqn. (225); i.e.

$$(\psi^2 - L^2)(\psi^2 - L^{-2})$$
$$= (h_1 h_2 h_3^{-2})^{e(n)}(h_4^{-2})^{o(n)}(\Omega^2 - \Omega_p^2)(\Omega^2 - \Omega_a^2)\left(\frac{d\psi}{d\Omega}\right)^2 \quad . \quad (226)$$

defining the constants as

$$h_1 h_2 h_3^{-2} = c_1'^2 \quad \text{and} \quad h_4^{-2} = c_0'^2 \qquad . \quad . \quad . \quad (227)$$

In general we can express eqn. (226) as

$$(\psi^2 - L^2)(\psi^2 - L^{-2}) = c_{e(n)}'^2(\Omega^2 - \Omega_p^2)(\Omega^2 - \Omega_a^2)\left(\frac{d\psi}{d\Omega}\right)^2 . \quad (228)$$

from which we can form the most important relations for further analysis defined by the differential equation

$$\frac{\pm \, c_{e(n)}' d\psi}{\sqrt{[(\psi^2 - L^2)(\psi^2 - L^{-2})]}} = \frac{d\Omega}{\sqrt{[(\Omega^2 - \Omega_p^2)(\Omega^2 - \Omega_a^2)]}} \qquad . \quad (229)$$

The problem remains to find a suitable solution that will satisfy this differential equation for a prescribed specification. To investigate more closely the differential equation (229), it is expedient to use a conventional substitution leading to a conventional form. Let us then define

$$\frac{\Omega}{\Omega_p} = x \quad \text{and} \quad \frac{\psi}{L} = y \quad . \quad . \quad . \quad . \quad (230)$$

recalling that $\Omega_p \Omega_a = 1$. Thus, as $\Omega_p/\Omega_a = k_B = k$,

$$\Omega_a = \frac{1}{\Omega_p} = \frac{1}{\sqrt{k}}$$

We can now express eqn. (229) (considering only the positive sign) in the conventional form

$$\frac{dx}{\sqrt{[(1 - x^2)(1 - k^2 x^2)]}} = \frac{c_{e(n)} dy}{\sqrt{[(1 - y^2)(1 - L^4 y^2)]}} = du \quad . \quad (231)$$

where $c_{e(n)} = Lc_{e(n)}'/\Omega_p$.

The differential equation (231) is recognizable as consisting of elliptic integrands of the first kind with elliptic moduli $k$ and $L^2$, and it may be expected that the solution satisfying the differential equation will be one involving elliptic functions. (Thus further information leading to the solution of this equation should be gathered from the theory of elliptic functions, of which we shall only mention the essentials concerning our problem here.) Further important information may be obtained by integrating eqn. (229) or (231) between the limits $0 \leqslant \Omega \leqslant \infty$ and $-\infty \leqslant \psi \leqslant \infty$. It should be observed that, as $\Omega$ changes between zero and $\Omega_p$, and $x$ changes between $x = 0$ and $x = 1$, within the same frequency limit, the $\psi$- or $y$-function oscillates $n$ times between $\psi = \pm L$ and hence between $y = \pm 1$, which necessitates the integration between $y = 0$ and $y = 1$, $n$ times. As integration between zero and unity yields the complete elliptic integral of the corresponding modulus, we have

$$\int_0^1 \frac{dx}{\sqrt{[(1 - x^2)(1 - k^2 x^2)]}} \qquad K(k) = K \quad . \quad . \quad (232)$$

where $k$ is the modulus and $K$ denotes the complete elliptic integral. Similarly

$$nc_{e(n)} \int_0^1 \frac{dy}{\sqrt{[(1-y)(1-y^2 L^4)]}} = nc_{e(n)} K(L^2); \quad K(L^2) = K_L$$
$$\dots \quad (233)$$

As both integrals define the same function within the same limits, we obtain the relation

$$K = nc_{e(n)} K_L . \quad . \quad . \quad . \quad (234)$$

This gives important relations between the bandwidth ratio and band-pass level (e.g. between $k$, $c_{e(n)}$, $n$ and $L$); and owing to the reciprocal character of the function, they also provide information about the attenuation band [i.e. replacing $x$ by $1/kz$, it can be shown that eqn. (232) integrated between $1/k$ and $\infty$ also gives $K$]. To obtain further information in the remaining transition zone (i.e. between $\Omega_p$ and $\Omega_a$), it should be observed that

$$\left.\begin{array}{c}\Omega_p \leqslant \Omega \leqslant \Omega_a \\ 1 \leqslant x \leqslant 1/k\end{array}\right\} \quad \text{and} \quad \left.\begin{array}{c}L \leqslant \psi \leqslant 1/L \\ 1 \leqslant y \leqslant 1/L^2\end{array}\right\}$$

It is then necessary to integrate eqn. (231) within these limits:

$$\int_1^{1/k} \frac{dx}{\sqrt{[(1-x^2)(1-x^2 k^2)]}} - c_{e(n)} \int_1^{1/L^2} \frac{dy}{\sqrt{[(1-y^2)(1-y^2 L^4)]}}$$
$$\dots \quad (235)$$

Integration within the indicated limits can be achieved easily if we perform the usual mathematical substitutions. Defining the quantities

$$k' = \sqrt{(1-k^2)}, \cdot \; (L^2)' = \sqrt{(1-L^4)} \quad . \quad . \quad (236)$$

which are referred to as the complementary modulus to $k$ and $L^2$, expressing $x$ and $y$ by a substitution of the form

$$x^{-1} = \sqrt{(1-z^2 k'^2)} \quad \text{and} \quad y^{-1} = \sqrt{[1-z^2(1-L^4)]}$$

and changing the limits of integration of eqn. (235) according to the new variable $z$, related by $x = 1 \rightleftharpoons z = 0$ and $x = 1/k \rightleftharpoons z = 1$ and also $y = 1 \rightleftharpoons z = 0$ and $y = 1/L^2 \rightleftharpoons z = 1$, then eqn. (235) reverts to the familiar form

$$\int_0^1 \frac{dz}{\sqrt{[(1-z^2)(1-z^2 k'^2)]}} = c_{e(n)} \int_0^1 \frac{dz}{\sqrt{\{(1-z^2)[1-z^2(1-L^4)]\}}}$$
$$\dots \quad (237)$$

This yields complete elliptic integrals of complementary moduli $k'$ and $\sqrt{(1-L^4)}$, and hence

$$K' = c_{e(n)} K_L' \quad . \quad . \quad . \quad . \quad (238)$$

where $K' = K(k')$ and $K_L' = K[\sqrt{(1-L^4)}]$. Combining eqns. (238) and (234), another important relation between $k$, $n$, and $L$ is obtained:

$$\frac{K'}{K} = \frac{K_L'}{nK_L} \quad . \quad . \quad . \quad . \quad (239)$$

These quantities are very well-defined in the theory of elliptic functions by the modular function $q$ (Jacobi's nome) in terms of the modulus given by

$$q = q(k) = \varepsilon^{-\pi K'/K}$$

$$= \frac{k^2}{16}\left[1 + 2\left(\frac{k}{4}\right)^2 + 15\left(\frac{k}{4}\right)^4 + 150\left(\frac{k}{4}\right)^6 + \dots\right]^4 \quad . \quad (240)$$

while
$$q(L^2) = q_L = \exp(-\pi K_L'/K_L) \quad . \quad . \quad (241)$$

It can be clearly seen that $q$ and $q_L$ are related by the number $n$ in the following way:

$$q_L = \exp(-\pi K_L'/K_L) = \exp(-\pi n K'/K) = q^n \; . \quad (242)$$

Up to this point we have been gathering the information provided by specifications. To find the pass-band and attenuation-band parameters, we still have to solve the differential equation (229). The mathematics and notation in the following analysis will mostly concern a special type of elliptic function, more details of which the reader can find in any elementary treatise on the subject. In our investigation we shall limit our discussion to the use of the Jacobian elliptic functions and their transformations.

### (9.1.1) Solution of Differential Equation (231).

Solving the differential equation (231) amounts to finding that function* $u$ that will satisfy the differential equation simultaneously. This may be obtained most simply by integrating eqn. (231) between arbitrary limits. Integrating the eqn. (231)-function of modulus $k$ we obtain

$$\int_0^x \frac{dt}{\sqrt{[1(-t^2)(1-t^2 k^2)]}} = u(t,k)|_0^x = u(x,k) \; . \quad (243)$$

Using the conventional notation of Jacobian elliptic functions, the inverse function $x$ can be defined by $x = \text{sn}(u, k)$. Since $x = \Omega/\sqrt{k}$,

$$\Omega = \sqrt{k}\,\text{sn}(u, k) \quad . \quad . \quad . \quad . \quad (244)$$

The values of $u$ which would correspond to zeros of the characteristic $\psi$-function will be denoted by $u_{0s}$, and hence the zeros of the characteristic function will be defined by

$$\Omega_{0s} = \sqrt{k}\,\text{sn}(u_{0s}, k) \quad . \quad . \quad . \quad . \quad (245)$$

The values $u_{0s}$ are not yet determined, and before they can be obtained we must find a solution for $y$ or $\psi$ from which, when expressed in terms of the frequency-variable $\Omega$, the zeros $\Omega_{0s}$ can be determined. The solution of eqn. (231) containing the $y$-function is not so straightforward because, as may be observed, the zeros are differently distributed for even and for odd $n$. However, integration of that part corresponding to $\psi$ reveals that

$$\int_{e(n)}^y \frac{dt}{\sqrt{[(1-t^2)(1-t^2 L^4)]}}$$
$$= \frac{1}{c_{e(n)}} u(t, L^2)\Big|_{e(n)}^y = \frac{o(n)}{c_0} u(t, L^2)\Big|_0^y + \frac{e(n)}{c_1} u(t, L^2)\Big|_1^y$$
$$= \frac{u(y, L^2)}{c_{e(n)}} - e(n) K_L \; . \quad . \quad . \quad . \quad . \quad . \quad (246)$$

hence
$$\int_0^y \frac{dt}{\sqrt{[(1-t^2)(1-t^2 L^4)]}} = \frac{u(y, L^2)}{c_{e(n)}} + e(n) K_L \; . \quad (247)$$

and the $y$-function is given by

$$y = \text{sn}\left[\frac{u}{c_{e(n)}} + e(n) K_L, L^2\right] \quad . \quad . \quad . \quad (248)$$

from which
$$\psi = L\,\text{sn}\left[\frac{u}{c_{e(n)}} + e(n) K_L, L^2\right] \quad . \quad . \quad (249)$$

* $\text{sn}(u, k)$ for real values of $u$ has a similar character to a circular sine, except that its period is $4K$, while that of the circular function is $4(\pi/2)$. In a sn $u$-function the zeros on the real axis occur at $0$, $2K$, $4K \dots 2sK$, while the analogous zeros in the circular sines occur at $0$, $2(\pi/2)$, $4(\pi/2) \dots 2s(\pi/2)$. For real values of $u$, sn $u$ varies, between $\pm 1$ at $K$, $3K$; a circular sine has similar maxima and minima at $(\pi/2)$, $3(\pi/2) \dots$ For imaginary values of $u$, however, sn $u$ is also periodic, having zeros on the imaginary axis at $2sK'$ and poles at $(2s-1)K'$; whereas a circular sine is continuous for all finite values of $u$.

As the constant $c_{e(n)} = K/nK_L$, eqn. (249) can be expressed

$$\psi = Ly = L \operatorname{sn}\left\{K_L\left[\frac{nu}{K} - e(n)\right], L^2\right\} \quad . \quad . \quad (250)$$

However, neither of the formulae (248) or (249) reveals its zeros directly, except perhaps the trivial zero for odd $n$. To obtain a more suitable form, from which the positions of the zeros on the frequency axis can be determined, it is necessary to express the $\psi$- or $y$-function in terms of the frequency $x$ or $\Omega$, i.e. to transform the $y$-function of modulus $L^2$ into a corresponding function of modulus $k$. Such a transformation of functions of one modulus of that of another, related modulus is called a modular transformation. Cayley gives the whole theory of such and similar transformations in his treatise on elliptic functions.[24] Unfortunately, Cayley only discusses odd functions in detail, and for these he gives ready formulae in art. 372 of his book. However, the general transformation seems to take the form

$$\frac{\psi}{L} = y = \operatorname{sn}\left[\frac{u}{c_{e(n)}} + e(n)K_L, L^2\right]$$

$$= (-1)^{[n/2]}\frac{\sqrt{k^n}}{L}\prod_{s=-[n/2]}^{s=[n/2]} \operatorname{sn}\left\{[1 - e(n)\delta_{0s}]u + u_{0s}, k\right\}$$

$$\quad . \quad . \quad . \quad (251)$$

where $\quad u_{0s} = \dfrac{sK}{n}\left\{2 + \dfrac{e(n)}{|s|}[(n+1)\delta_{0s} - 1]\right\}$

for $\quad s = -[n/2], \ldots -2, -1, 0, 1, 2, \ldots, [n/2]$

The transformation can be illustrated by the following graphical exercise. The contour (or relief) of sn $n$ (such as illustrated in Jahnke and Emde 'Tables of Functions', page 92) is considered. For simplicity let us assume that $c_{e(n)}$ is made unity, so that $K_L = K/n$ and $K'_L = K'$ and $K_L$ is an integral part of $K$. Then it can be seen that the general pattern of sn $(u, L^2)$ or sn $(u + K'_L, L^2)$ can be reproduced exactly by shifting sn $(u, k)$ along the real axis $n$ times, from the origin in the case of odd $n$ and from the distance $K/n$ from the origin in the case of even $n$.

Further transformations are simple. Making use of formulae

$$\operatorname{sn} K = 1, \quad \operatorname{sn}(u + K) = \operatorname{sn}(K - u)$$

and $\operatorname{sn}(u + v)\operatorname{sn}(u - v) = (\operatorname{sn}^2 u - \operatorname{sn}^2 v)/(1 - k^2\operatorname{sn}^2 u\operatorname{sn}^2 v)$

noting that $u_{00}$ reduces to $e(n)K$, the transformation (251) can be expressed as

$$y = (-1)^{[n/2]}\frac{\sqrt{k^n}}{L}(\operatorname{sn} u, k)^{o(n)}\prod_{s=1}^{[n/2]}\operatorname{sn}(u + u_{0s}, k)\operatorname{sn}(u - u_{0s}, k)$$

$$= \frac{1}{L}(\sqrt{k}\operatorname{sn} u, k)^{o(n)}\prod_{s=1}^{[n/2]}\frac{k\operatorname{sn}^2(u, k) - k\operatorname{sn}(u_{0s}, k)}{k^2\operatorname{sn}^2(u, k)\operatorname{sn}^2(u_{0s}, k) - 1} \quad . \quad (252)$$

and the corresponding argument $u_{0s}$ is defined from eqn. (251) in a simpler form by

$$u_{0s} = \frac{2s - e(n)}{n}K \quad . \quad . \quad . \quad . \quad (253)$$

for $s = e(n), 1, 2, 3, \ldots [n/2]$.

As follows from eqn. (252), the characteristic function (and its zeros and poles) is given by

$$\psi = Ly = \Omega^{o(n)}\prod_{s=1}^{[n/2]}\frac{\Omega^2 - \Omega_{0s}^2}{\Omega^2\Omega_{0s}^2 - 1}$$

where $\quad \Omega = \sqrt{k}\operatorname{sn}(u, k) \quad . \quad . \quad . \quad . \quad (254)$

thus $\quad \Omega_{0s} = \dfrac{1}{\Omega_{\infty s}} = \sqrt{k}\operatorname{sn}(u_{0s}, k) = \sqrt{k}\operatorname{sn}\left[\dfrac{2s - e(n)}{n}K, k\right]$

$$s = e(n), 1, 2, 3, \ldots [n/2]$$

The frequency of the maxima in the pass-band $\Omega_{\cap s}$ and the minima $\Omega_{U s}$ in the attenuation band, are given by

$$\Omega_{\cap s} = \frac{1}{\Omega_{U s}} = \sqrt{k}\operatorname{sn}(u_{\cap s}, k) = \sqrt{k}\operatorname{sn}\left[\frac{2s - o(n)}{n}K, k\right] . \quad (255)$$

$$s - o(n), 1, 2, 3, \ldots \nu$$

[It may be noted in Fig. 6 and eqns. (251) and (252), that the maxima are situated $(-1)^n K/n$ apart from the corresponding zeros.] The level $L$ being given by

$$L = \sqrt{k^n}\prod_{s=1}^{[n/2]}\operatorname{sn}^2\left(\frac{2s-1}{n}K, k\right) = \sqrt{k^{o(n)}}\prod_{s=1}^{[n/2]}[e(n)\Omega_{0s}^2 + o(n)\Omega_{\cap s}^2]$$

$$\quad . \quad . \quad . \quad (256)$$

**(9.1.2) Relations between Insertion Loss, Discrimination and the Hypothetical Filter Functions.**

Up to now, we have completely defined the pass and attenuation band of hypothetical characteristic $\psi$-functions, and all their parameters; however, complete solution of the problem requires determination of the roots of the discrimination function and a proper relation to voltage and power ratio, from which the polynomials $A$ and $B$ can be evaluated in the usual manner, and proper impedances and ladder coefficients found, as described in the general theory. The discrimination function can be formed according to the general theory, provided there exists a suitable transformation $\mathbb{T}_{e(n)}$ from $\psi$ to $\phi$. It may be observed in Fig. 6 that one such odd transformation results in $\psi$ being always identical with $\phi$ (this we have named the identical transformation). However, for even $n$, other transformations apart from the identical one must exist if the prescribed insertion-loss ladder network with resistive termination is to be realizable by reactive elements, implying infinite insertion loss at infinite frequency. It was shown in Section 5.4 that a bilinear transformation of the frequency variable gives some satisfactory results. Hence the discrimination function can be written as

$$|\Xi(p)|^2 = 1 + H^2\phi^2 = 1 + \mathbb{T}_{e(n)}H^2\psi^2$$

$$= 1 + \mathbb{T}_{(e)n}H^2L^2\operatorname{sn}^2\left[\frac{u}{c_{e(n)}} + e(n)K_L, L^2\right] . \quad (257)$$

where one $\mathbb{T}_{e(n)} \equiv 1$, and $\mathbb{T}_{e(n)}$ exists. It can also be shown that existence of transformations $\mathbb{T}_{e(n)}$ permits us to state the discrimination levels $D_{\cap s} = D_p$ and $D_{U s} = D_a$ as if $\mathbb{T}_{e(n)} = 1$; we shall assume this for further investigations. Thus, for $\mathbb{T}_{e(n)} = 1$ and $\mathbb{T}_0 \equiv 1$, we have

$$|\Xi(p)|^2_{max\, 0 \leqslant \Omega \leqslant \Omega_p} = 1 + H^2L^2 \quad . \quad . \quad (258)$$

The attenuation band can be analysed as the reciprocal of the pass band, which was postulated in eqn. (219). Making use of transformation such as sn $(u, k) = 1/[k\operatorname{sn}(u + jK', k)]$ we can express eqn. (257) explicitly for $\mathbb{T}_{e(n)} = 1$ in the suppression range:

$$|\Xi(p)|^2 = 1 + \frac{H^2L^2}{L^4\operatorname{sn}^2\left\{\frac{nK_L}{K}\left[u + e(n)\frac{K}{n} + jK'\right], L^2\right\}} . \quad (259)$$

where $\quad \Omega = \dfrac{1}{\sqrt{k}\operatorname{sn}(u + jK', k)}$

Thus, for real values of $(u + jK')$ and neighbouring complex

values, $\operatorname{sn}(u + jK', L^2)$ varies between $\pm 1$ for small $L$, which is the case of an ordinary filter with small variations within the pass band. From eqn. (259) it follows that minimum discrimination within the suppression band is given by

$$|\Xi(p)|^2_{min\,\Omega > \Omega_a} = 1 + \frac{H^2}{L^2} \quad . \quad . \quad . \quad (260)$$

and, as follows from eqns. (65), (66), (258) and (260),

$$\left. \begin{aligned} D_{Us} &= D_a = 10 \log\left(1 + \frac{H^2}{L^2}\right) \text{ dB}, \\ \frac{H^2}{L^2} &= 10^{D_a/10} - 1 \\ D_{\cap s} &= D_p = 10 \log\left(1 + H^2 L^2\right) \text{ dB} \\ H^2 L^2 &= 10^{D_p/10} - 1 \end{aligned} \right\} \quad . \quad . \quad (261)$$

thus

thus

The relations between the discrimination levels $D_p$, $D_a$, the level $L$ and the constant $H$ are given by

$$L^2 = \sqrt{\left(\frac{10^{D_p/10} - 1}{10^{D_a/10} - 1}\right)}; \quad H^2 = \sqrt{[(10^{D_p/10} - 1)(10^{D_a/10} - 1)]}$$

$$. \quad . \quad . \quad (262)$$

Since $L$ is usually very small, it follows from the definition of $q$ given in eqns. (240) to (242) that $q^n = q_L \simeq L^4/16$ and hence that $n \log q \simeq \log(L^4/16)$. From this relation very useful formulae concerning the discrimination $D_a$ and $D_p$ and the number of branches can be derived, e.g.

$$D_a = 10[\log(10^{D_p/10} - 1) - n \log q_{(k)} - 1\cdot 2] \text{ dB} \quad . \quad (263)$$

where $q_{(k)}$ is found either from tables or from eqn. (240) for known $k$. [Eqn. (263) is given also in graphical form in Fig. 2(c), for $n = 3, 4, 5, 6$ and 7.]

### (9.1.3) Determination of Root Parameters of the Discrimination Function and hence of the Power and Voltage Ratio.

The advantage of the Chebýshev pass-band and the attenuation-band parameters lies not only in the superior insertion-loss characteristic function, but also in the mathematical form, which permits of fairly automatic extraction of the roots for the power or voltage ratio. The roots are obtained by a general scheme, from equating the $|\Xi(p)|^2$-function to zero. Thus for $\mathfrak{T}_{e(n)} = 1$,

$$|\Xi(p)|^2 = 1 + H^2 L^2 \operatorname{sn}^2\left[\frac{u_{\pm s}}{c_{e(n)}} + e(n)K_L, L^2\right] = 0 \quad . \quad (264)$$

where $p_{\pm s} = \pm j\sqrt{k}\,\operatorname{sn}(u_{\pm s}, k)$ for $s = e(n), 1, 2, \ldots [n/2]$.

The complex roots of the power ratio or the discrimination function must be somewhat related to the roots of the characteristic function, and it is therefore logical to define $u_{\pm s}$ in complex conjugate form as

$$u_{\pm s} = u_{0s} \pm ju'_{e(n)} \quad . \quad . \quad . \quad . \quad (265)$$

where $u'_{e(n)}$ is some real constant which must be determined in such a way as to satisfy the physical conditions for the roots for even or odd $n$. Replacing $u_{\pm s}$ by $[u_{0s} \pm ju'_{e(n)}]$ in eqn. (264), it can be observed that the argument takes the form

$$\frac{u_{0s}}{c_{e(n)}} + e(n)K_L \pm j\frac{u_{e(n)}}{c_{e(n)}}$$

Since $\quad c_{e(n)} = \dfrac{K}{nK_L}$ and $u_{0s} = \dfrac{2s - e(n)}{n}K$

the argument becomes

$$\frac{u_{\pm s}}{c_{e(n)}} + e(n)K_L = 2sK_L \pm j\frac{u'_{e(n)}}{c_{e(n)}}$$

Noting that

$$\operatorname{sn}(v + 2sK) = (-1)^s \operatorname{sn} v \text{ and } \operatorname{sn}(jv, k) = j\operatorname{tn}(v, k')$$

we have

$$|\Xi(p)|^2 = 0 = 1 + H^2 L^2 \operatorname{sn}^2\left[j\frac{u'_{e(n)}}{c_{e(n)}}, L^2\right]$$

$$= 1 - H^2 L^2 \operatorname{tn}^2\left[\frac{u'_{e(n)}}{c_{e(n)}}, \sqrt{(1 - L^4)}\right] \quad . \quad (266)$$

From which it follows that

$$\frac{1}{H^2 L^2} = \operatorname{tn}^2\left[\frac{u'_{e(n)}}{c_{e(n)}}, \sqrt{(1 - L^4)}\right]$$

Thus $\quad \operatorname{sn}\left[\frac{u'_{e(n)}}{c_{e(n)}}, \sqrt{(1 - L^4)}\right] = \dfrac{1}{\sqrt{(1 + H^2 L^2)}} \cdot \quad . \quad (267)$

One of the methods of determining $u'_{e(n)}$ will be illustrated in the following analysis. The inverse function $u'_{e(n)}/c_{e(n)}$ is defined, according to the theory of elliptic functions, by the expression (267), from which

$$\frac{u'_{e(n)}}{c_{e(n)}} = \int_0^{1/\sqrt{(1 + H^2 L^2)}} \frac{dt}{\sqrt{\{(1 - t^2)[1 - (1 - L^4)t^2]\}}}$$

$$= \int_0^{1/\sqrt{(1 + H^2 L^2)}} \frac{dt}{(1 - t^2)\sqrt{\left(1 + \dfrac{L^4 t^2}{1 - t^2}\right)}} = I_{e(n)} \quad . \quad (268)$$

Inspection of the term under the square root in the integral reveals that

$$\frac{L^4 t^2}{1 - t^2} \leqslant \left.\frac{L^4 t^2}{1 - t^2}\right|_{t = 1/\sqrt{(1 + H^2 L^2)}} = \frac{L^2}{H^2} \simeq 10^{-D_a/10}$$

since $D_a$ is usually large, say 20 or more decibels, this term is considerably smaller than unity, and the square root can be expanded and approximate integration performed retaining, say, three terms, so that

$$\left(1 + \frac{L^4 t^2}{1 - t^2}\right)^{-1/2} = 1 - \frac{L^4 t^2}{2(1 - t^2)} + \frac{3}{8}\frac{L^8 t^4}{(1 - t^2)^2} + O(L^{12})$$

where $O(L^{12})$ is the order of the neglected terms. Approximate integration gives the following formula:

$$I_{e(n)} \simeq \left(1 - \frac{L^4}{4}\right)\operatorname{arc\,tanh}\left[\frac{1}{\sqrt{(1 + H^2 L^2)}}\right]$$

$$+ \frac{L^2\sqrt{(1 + H^2 L^2)}}{4H^2} + \frac{3L^4\sqrt{(1 + H^2 L^2)}}{32H^2} \quad . \quad (269)$$

[Observe that $\operatorname{arc\,tanh} 1/\sqrt{(1 + H^2 L^2)} = \operatorname{arc\,sinh} 1/HL$.]

For practical purposes, for small $D_p$, this can be approximated further

$$\left. \begin{aligned} I_{e(n)} &\simeq \operatorname{arc\,tanh}\left[\frac{1}{\sqrt{(1 + H^2 L^2)}}\right] + \frac{L^2\sqrt{(1 + H^2 L^2)}}{4H^2} \\ &\simeq \operatorname{arc\,sinh}\frac{1}{HL} \end{aligned} \right\} \; L \ll 1$$

$$. \quad . \quad . \quad . \quad (270)$$

Since
$$u'_{e(n)} = c_{e(n)}I_{e(n)} = KI_{e(n)}/nK_L \quad . \quad . \quad . \quad (271)$$

and for small $L$, $K_L \simeq \frac{1}{2}\pi(1 + L^4/4)$ or, approximating still further, $K_L \simeq \frac{1}{2}\pi$ giving

$$u'_{e(n)} \simeq \frac{2KI_{e(n)}}{n\pi} \quad . \quad . \quad . \quad . \quad (272)$$

We have thus determined the constant $u'_{e(n)}$, at least approximately in term of known quantities such as $H$, $L$, $K$ and $n$. [$u'_{e(n)}$ can be determined by several other methods derivable from eqn. (267).] Once this constant is calculated the roots of the discrimination function and hence of the power and voltage ratio can be determined.

Noting that
$$p_{\pm s} = -\alpha_s \pm j\Omega_s = \pm j\sqrt{k}\,\text{sn}\,(u_{\pm s}, k)$$
$$= \pm j\sqrt{k}\,\text{sn}\,(u_{0s} \pm ju'_{e(n)}, k) \quad . \quad (273)$$

and making use of the addition formulae for sn $u$ of complex argument, given by

$$\text{sn}\,(u_{0s} \pm ju'_{e(n)}, k) =$$

$$\frac{\text{sn}\,(u_{0s}, k)\dfrac{\text{dn}\,(u'_{e(n)}, k')}{\text{cn}^2(u'_{e(n)}, k')} \pm j\,\text{tn}\,[u'_{e(n)}, k']\,\text{cn}\,(u_{0s}, k)\,\text{dn}\,(u_{0s}, k)}{1 - k^2\,\text{sn}^2(u_{0s}, k)\,\text{tn}^2(u'_{e(n)}, k')}$$

$$. \quad . \quad . \quad (274)$$

Defining the quantities occurring in these formulae by
$$\vartheta_{e(n)} = \sqrt{k}\,\text{tn}\,[u'_{e(n)}, k'];$$
$$W_{e(n)} = \frac{\text{dn}\,(u'_{e(n)}, k')}{\text{cn}^2(u'_{e(n)}, k')} = \sqrt{[1 + \vartheta_{e(n)}^2(k + k^{-1} + \vartheta_{e(n)}^2)]} \quad . \quad (275)$$

and in general
$$cd_r = \text{cn}\,(u_r, k)\,\text{dn}\,(u_r, k) = \sqrt{[1 - \Omega_r^2(k + k^{-1} - \Omega_r^2)]}$$

the general expression for the root parameters of the discrimination function, the voltage-ratio function or power ratio are given, from eqns. (273) to (275), as

$$p_{\pm s} = -\alpha_s \pm j\Omega_s = \frac{-\vartheta_{e(n)}cd_{0s} \pm j\Omega_{0s}W_{e(n)}}{1 + \vartheta_{e(n)}^2\Omega_{0s}^2}$$
Hence
$$\alpha_s = \frac{\vartheta_{e(n)}\sqrt{[1 - \Omega_{0s}^2(k + k^{-1} - \Omega_{0s}^2)]}}{1 + \vartheta_{e(n)}^2\Omega_{0s}^2}, \quad \rho_s^2 = \frac{\vartheta_{e(n)}^2 + \Omega_{0s}^2}{1 + \vartheta_{e(n)}^2\Omega_{0s}^2}$$
$$\left.\right\} (276)$$
for $s = e(n), 1, 2, \ldots [n/2]$.

The real root for odd $n$ is obtained for $s = 0$, i.e. $\Omega_{00} = 0$ and
$$\alpha_0 = \rho_0 = \vartheta_0$$

The prescribed insertion-loss voltage ratio in terms of given root parameters takes the general form of

$$\frac{V_{20}}{V_2} = \frac{A + pB}{P}$$

$$= \mathbb{T}_{e(n)}\left[\sqrt{\eta_G^{e(n)}}H(p + \alpha_0)^{o(n)}\prod_{s=1}^{[n/2]}\left(\frac{p^2 + 2\alpha_s p + \rho_s^2}{p^2\Omega_{0s}^2 + 1}\right)\right]$$
$$. \quad . \quad . \quad . \quad (277)$$

Note that $k_B = \Omega_p/\Omega_a = B_p/B_a < 1$, for low-pass and band-pass, while for high-pass and band-stop $k_B = B_a/B_p < 1$. The normalizing constant for all the cases is defined by $f_B = \sqrt{(B_pB_a)}/\Omega_B$, where we assumed $\Omega_B = \sqrt{(\Omega_p\Omega_a)} = 1$.

For a symmetrical filter there is always one transformation

such that $\mathbb{T}_{e(2\nu+1)} \equiv 1$. Once the parameters of the insertion-loss voltage ratio are known, the design impedance function, and hence the ladder coefficients can be evaluated in the usual way. It may be observed that $A'$ or $B'$ for basic networks are obtained from

$$e(n)A' + o(n)B' = \mathbb{T}_{e(n)}[\sqrt{\eta_G^{e(n)}}H'\prod_{s=1}^{[u/2]}(p^2 + \Omega_{0s}^2)]$$

while the sign of $H'$ is determined as described in the general theory. The actual inverse-impedance network with a prescribed response for equal or unequal terminations is treated in Section 5.4, where two suitable Möbius transformations of the frequency variable are included. It may be added that $\mathbb{T}_1 = 1$ leads to a hypothetical filter, realization of which implies some sort of physical transformation; the response of such a filter will no longer be that prescribed for the hypothetical filter. The conventional band-pass characteristic insertion-loss function (which may be of interest for construction of special filters), defined by, say, $\breve{\phi}$, can be readily formed from any low-pass $\phi$-function by frequency transformation. This is, in general, given by

$$\breve{H}\breve{\phi} = \mathbb{T}_{e(n)}(H\psi)|_{\Omega = (\Omega)_{BP}} \quad . \quad . \quad . \quad (278)$$

where
$$\Omega = (\Omega)_{BP} = Q_B\left(\frac{f}{f_0} - \frac{f_0}{f}\right) = Q_B\left(\frac{\breve{\Omega}^2 - 1}{\breve{\Omega}}\right)$$

and
$$\breve{\Omega} = \frac{f}{f_0} \quad \text{and} \quad Q_B = \frac{f_0}{f_B}$$

[see also eqn. (11)] and for eqn. (82) $\breve{H}\breve{\phi}$ will take the form

$$\breve{H}\breve{\phi} = \breve{H}\left(\frac{\breve{\Omega}^2 - 1}{\breve{\Omega}}\right)^{o(n)}\frac{\prod\limits_{s=1}^{[n/2]}(\breve{\Omega}^2 - \breve{\Omega}_{0s,1}^2)(\breve{\Omega}^2 - \breve{\Omega}_{0s,2}^2)}{\breve{\Omega}^{2[\nu + e(n) - m]}\prod\limits_{s=1}^{m}(\breve{\Omega}^2 - \breve{\Omega}_{\infty s,1}^2)(\breve{\Omega}^2 - \breve{\Omega}_{\infty s,2}^2)}$$
$$. \quad . \quad . \quad . \quad (279)$$

where
$$\breve{H} = HQ_B^{\{o(n) + 2[\nu + e(n) - m]\}}\prod_{s=1}^{m}\Omega_{\infty s}^2$$

where also
$$(\breve{\Omega}_{\infty s,1}^2\breve{\Omega}_{\infty s,2}^2) = 1$$

and the particular frequencies $\Omega_{r,1,2}$ must satisfy the relations

$$0 \leqslant \breve{\Omega}_{\infty s,1} < \breve{\Omega}_{a1} < \breve{\Omega}_{p1} < \breve{\Omega}_{0s,1} \leqslant 1 \leqslant \breve{\Omega}_{0s,2}$$
$$< \breve{\Omega}_{p2} < \breve{\Omega}_{a2} < \breve{\Omega}_{\infty s,2} \leqslant \infty$$

Any one of these or other wanted frequencies can be computed by means of known low-pass normalized frequencies $\Omega_r$, the mid-band frequency $f_0$ and the normalizing constant $f_B$. Thus

$$\breve{\Omega}_{r,1,2} = \frac{f_{r,1,2}}{f_0} = \sqrt{\left[1 + \left(\frac{\Omega_r}{2Q_B}\right)^2\right]} \mp \frac{\Omega_r}{2Q_B} \quad . \quad (280)$$

Hence, for given normalized low-pass frequency, i.e.

$$\mp \Omega_r(= \mp \Omega_{0s}; \mp \Omega_p; \mp \Omega_a; \mp \Omega_{\infty s}; \mp \Omega_{\cap s}; \mp \Omega_{Us}; \mp \Omega_s)$$

the corresponding band-pass frequencies

$$f_{r,1,2}(= f_{0s,1,2}; f_{p1,2}; f_{a1,2}; f_{\infty s,1,2}; f_{\cap s,1,2}; f_{Us,1,2}; f_{s,1,2})$$

can be computed and the model function $\breve{H}\breve{\phi}$ readily formed. Similarly, the band-stop conventional function can be modelled from which another unconventional filter can be formed. The problem of more general band-pass, band-stop networks can also be solved by application of special frequency transformations such as $\Omega = (a\omega^2 + b)/(c\omega^2 + d)$ into eqn. (278).[3] The

10

realization procedure for these and other unconventional band-pass networks is not so straightforward as those given in this paper.

### (9.2) Derivation of General Ladder Coefficients

To demonstrate the way in which formulae for ladder coefficients can be obtained, consider an appropriate impedance $Z_T$ or admittance $Y_\Pi = 1/Z_\Pi$. This may be any one design impedance given in eqn. (32). Expanding such a normalized impedance or admittance into continued fractions, one obtains the following relation:

$$\left(\frac{Z_T}{R_T} \text{ or } Y_\Pi R_\Pi\right)$$

$$= a_1 p + \cfrac{1}{\cfrac{a_2 p}{1+p^2\zeta_1} + \cfrac{1}{a_3 p + \cfrac{1}{\cfrac{a_4}{1+p^2\zeta_2} + \cfrac{1}{a_5 p + \ldots}}}}$$

$$. \quad . \quad . \quad . \quad (281)$$

in which $\zeta_s = 1/\Omega_{\infty r}^2$, and particularly $\zeta_0 = 1/\Omega_{\infty 0}^2 = 0$. Dividing eqn. (281) by $p$, and for further convenience replacing $p^2$ in the even function and in the continued-fractions expansion by $-1/\zeta$, the $\mathscr{F}(\zeta)$ function is obtained, given by

$$\left(\frac{Z_T}{pR_T} \text{ or } \frac{Y_\Pi R_\Pi}{p}\right)_{p^2 = -1/\zeta}$$

$$= \mathscr{F}(\zeta) = a_1 + \cfrac{1}{\cfrac{a_2}{\zeta_1 - \zeta} + \cfrac{1}{a_3 + \cfrac{1}{\cfrac{a_4}{\zeta_2 - \zeta} + \cfrac{1}{a_5 + \ldots}}}}$$

$$. \quad . \quad . \quad . \quad (282)$$

(These continued-fractions expansions serve here only to derive the ladder coefficients for the ladders, e.g. in Fig. 2.)

Obviously, when $\zeta = \zeta_1$, the denominator in the continued-fractions expansion is infinite and

$$a_1 = \mathscr{F}(\zeta_1) . \quad . \quad . \quad . \quad . \quad (283)$$

The next ladder coefficient, $a_2$, can be obtained by dividing eqn. (282) by $(\zeta_1 - \zeta)$ and transferring $a_1/(\zeta_1 - \zeta)$ to the left side of the equation. Thus

$$\frac{\mathscr{F}(\zeta) - \mathscr{F}(\zeta_1)}{\zeta_1 - \zeta} = \cfrac{1}{a_2 + \cfrac{1}{\cfrac{a_3}{\zeta_1 - \zeta} + \cfrac{1}{a_4(\zeta_1 - \zeta) + \cfrac{1}{\cfrac{a_5}{\zeta_1 - \zeta} + \ldots}}}}$$

$$. \quad . \quad . \quad . \quad (284)$$

Thus, again,

$$\frac{1}{a_2} = \frac{\mathscr{F}(\zeta) - \mathscr{F}(\zeta_1)}{\zeta_1 - \zeta}\bigg|_{\zeta = \zeta_1} . \quad . \quad . \quad . \quad (285)$$

using now the notation given in eqn. (61), $a_2$ can be defined in terms of $\mathscr{H}_{qr}$

$$a_2 = -1/\mathscr{H}_{11} \quad . \quad . \quad . \quad . \quad (286)$$

To determine the coefficients beyond $a_2$, we write

$$\hat{\mathscr{F}}(\zeta) = a_3 + \cfrac{1}{\cfrac{a_4}{\zeta_2 - \zeta} + \cfrac{1}{a_5 + \ldots}} \quad . \quad . \quad . \quad (287)$$

and these ladder coefficients are found in exactly the same manner as $a_1$ and $a_2$, namely

$$\hat{a}_1 \equiv a_3 = \hat{\mathscr{F}}(\zeta_2) . \quad . \quad . \quad . \quad . \quad . \quad (288)$$

$$\hat{a}_2 \equiv a_4 = \frac{\hat{\mathscr{F}}(\zeta) - \hat{\mathscr{F}}(\zeta_2)}{\zeta_2 - \zeta}\bigg|_{\zeta = \zeta_2} = \frac{-1}{\hat{\mathscr{H}}_{22}} \quad . \quad (289)$$

It is now only necessary to express $\hat{\mathscr{F}}(\zeta)$ in terms of known quantities $\mathscr{F}(\zeta)$ and $\mathscr{H}_{qr}$. From inspection of eqns. (282) and (289), $\hat{\mathscr{F}}(\zeta)$ can be written as

$$\hat{\mathscr{F}}(\zeta) = \frac{[\mathscr{F}(\zeta) - a_1](\zeta_1 - \zeta)}{\zeta_1 - \zeta - a_2[\mathscr{F}(\zeta) - a_1]} \quad . \quad . \quad (290)$$

Rearranging this expression and using the notation $\mathscr{H}_{qr}$ defined in eqn. (61) we obtain

$$\hat{\mathscr{F}}(\zeta_2) = a_3 = (\zeta_2 - \zeta_1)\frac{\cfrac{1}{a_2}\cfrac{\mathscr{F}(\zeta_2) - \mathscr{F}(\zeta_1)}{\zeta_2 - \zeta_1}}{\cfrac{1}{a_2} + \cfrac{\mathscr{F}(\zeta_2) - \mathscr{F}(\zeta_1)}{\zeta_2 - \zeta_1}}$$

$$= (\zeta_2 - \zeta_1)\frac{\mathscr{H}_{11}\mathscr{H}_{12}}{\mathscr{H}_{11} - \mathscr{H}_{12}} \quad . \quad (291)$$

Now

$$a_4 = \frac{\zeta_2 - \zeta}{\hat{\mathscr{F}}(\zeta) - a_3}\bigg|_{\zeta = \zeta_2}$$

This undetermined quantity can be evaluated by de l'Hôpital's rule; thus

$$a_4 = \frac{\frac{d}{d\zeta}(\zeta_2 - \zeta)}{\frac{d}{d\zeta}\left\{\frac{[\mathscr{F}(\zeta) - a_1](\zeta_1 - \zeta)}{\zeta_1 - \zeta - a_2[\mathscr{F}(\zeta) - a_1]} - a_3\right\}}\Bigg|_{\zeta = \zeta_2}$$

$$= \frac{-\{\zeta_1 - \zeta - a_2[\mathscr{F}(\zeta) - a_1]\}^2}{(\zeta_1 - \zeta)^2\frac{d\mathscr{F}(\zeta)}{d\zeta} + a_2[\mathscr{F}(\zeta) - a_1]^2}\Bigg|_{\zeta = \zeta_2}$$

$$= \frac{-(\mathscr{H}_{11} - \mathscr{H}_{12})^2}{\mathscr{H}_{11}(\mathscr{H}_{11}\mathscr{H}_{22} - \mathscr{H}_{12}^2)} \quad . \quad (292)$$

Proceeding in the manner illustrated by $a_1$, $a_2$ and $a_3$, $a_4$, after considerable manipulation with known quantities and the reduced network functions, one can evaluate, step by step, further ladder coefficients in terms of $\mathscr{H}_{qr}$ and $\zeta_s$.

The actual problem is to find the law by which $\mathscr{H}_{qr}$ and $\zeta_s$ determine these ladder coefficients in general. This problem is already solved by Darlington.[5] Here we shall demonstrate some aspects of this solution.

Writing expressions for, say, $a_7$, $a_6$, $a_5$, etc., in terms of $\zeta_s$ and $\mathscr{H}_{qr}$ as found by a step-by-step method, we can readily detect the characteristic relation

$$a_{2s+1} = (\zeta_{s+1} - \zeta_s)\frac{(\quad y \quad)(\ldots\ldots)}{(\ldots\ldots)(\quad x \quad)}$$

$$a_{2(s+1)} = \frac{-(\quad x \quad)^2}{(\quad y \quad)(\ldots\ldots)}$$

This holds true down to $a_3$. Procuring an artificial consistency down to $a_1$, one can write

$$a_1 = \mathscr{F}(\zeta_1) = (\zeta_1 - \zeta_0)\frac{\mathscr{H}_{00}\mathscr{H}_{01}}{1 \times 1} = (\zeta_1 - \zeta_0)\frac{\mathscr{U}_0\mathscr{W}_0}{\mathscr{V}_0\mathscr{V}_1};$$

where $\mathscr{H}_{00} = \mathscr{U}_0 = 1$; $\mathscr{W}_0 = \mathscr{H}_{01} = \dfrac{\mathscr{F}(\zeta_1)}{\zeta_1}$ and $\mathscr{V}_0 = \mathscr{V}_1 = 1$

$$a_2 = \frac{-1}{\mathscr{H}_{11}} = \frac{-\mathscr{V}_1^2}{\mathscr{U}_0\mathscr{U}_1}; \quad \text{where} \quad \mathscr{H}_{11} = \mathscr{U}_1$$

$$a_3 = (\zeta_2 - \zeta_1)\frac{\mathscr{H}_{11}\mathscr{H}_{12}}{\mathscr{H}_{11} - \mathscr{H}_{12}} = (\zeta_2 - \zeta_1)\frac{\mathscr{U}_1\mathscr{W}_1}{\mathscr{V}_1\mathscr{V}_2};$$

where $\mathscr{H}_{12} = \mathscr{W}_1$ and $\mathscr{V}_2 = \mathscr{H}_{11} - \mathscr{H}_{21}$,

$$a_4 = \frac{-(\mathscr{H}_{11} - \mathscr{H}_{12})^2}{\mathscr{H}_{11}(\mathscr{H}_{11}\mathscr{H}_{22} - \mathscr{H}_{12}^2)} = \frac{-\mathscr{V}_2^2}{\mathscr{U}_1\mathscr{U}_2};$$

where $\mathscr{U}_2 = \mathscr{H}_{11}\mathscr{H}_{22} - \mathscr{H}_{12}^2$,

$$a_5 = (\zeta_3 - \zeta_2)\frac{\mathscr{U}_2(\mathscr{H}_{11}\mathscr{H}_{23} - \mathscr{H}_{13}\mathscr{H}_{12})}{\mathscr{V}_2^2(\mathscr{U}_2 - \mathscr{W}_2 + \Delta_2)} = (\zeta_3 - \zeta_2)\frac{\mathscr{U}_2\mathscr{W}_2}{\mathscr{V}_2\mathscr{V}_3};$$

where $\Delta_2 = \mathscr{H}_{12}\mathscr{H}_{23} - \mathscr{H}_{13}\mathscr{H}_{22}$,

$$a_6 = \frac{-\mathscr{V}_3^2}{\mathscr{U}_2(\mathscr{H}_{13}\Delta_2 + \mathscr{H}_{33}\mathscr{U}_2 - \mathscr{H}_{23}\mathscr{W}_2)} = \frac{-\mathscr{V}_3^2}{\mathscr{U}_2\mathscr{U}_3}$$

$$a_7 = (\zeta_4 - \zeta_3)\frac{\mathscr{U}_3(\mathscr{H}_{14}\Delta_2 - \mathscr{H}_{24}\mathscr{W}_2 + \mathscr{H}_{34}\mathscr{U}_2)}{\mathscr{V}_3(\mathscr{U}_3 - \mathscr{W}_3 + \Delta_3)}$$

$$= (\zeta_4 - \zeta_3)\frac{\mathscr{U}_3\mathscr{W}_3}{\mathscr{V}_3\mathscr{V}_4};$$

where
$$\begin{aligned}
\Delta_3 = -\Big\{ &\mathscr{H}_{41}[\mathscr{H}_{33}(\mathscr{H}_{22} - \mathscr{H}_{12}) + \mathscr{H}_{23}(\mathscr{H}_{13} - \mathscr{H}_{23})] \\
+ &\mathscr{H}_{42}[\mathscr{H}_{33}(\mathscr{H}_{11} - \mathscr{H}_{12}) + \mathscr{H}_{13}(\mathscr{H}_{23} - \mathscr{H}_{13})] \\
+ &\mathscr{H}_{43}[\mathscr{H}_{23}(\mathscr{H}_{21} - \mathscr{H}_{11}) + \mathscr{H}_{13}(\mathscr{H}_{12} - \mathscr{H}_{22})] \Big\}
\end{aligned}$$

· · · · · · · · · · · · · · · · · · · · · ·

$$a_{2s} = \frac{-\mathscr{V}_s^2}{\mathscr{U}_{s-1}\mathscr{U}_s}$$

$$a_{2s+1} = (\zeta_{s+1} - \zeta_s)\frac{\mathscr{U}_s\mathscr{W}_s}{\mathscr{V}_s\mathscr{V}_{s+1}}$$

$$a_{2(s+1)} = \frac{-\mathscr{V}_{s+1}^2}{\mathscr{U}_s\mathscr{U}_{s+1}}$$

The actual solution, i.e. general form of $\mathscr{U}_s$, $\mathscr{V}_s$ and $\mathscr{W}_s$, implies a knowledge of how to express the sum of products in a fairly concise and a logical form. Once this stage is achieved, even if only formulated up to $a_6$, $a_5$, $a_4$, etc., the general law and the formulae can be induced. The determinant forms of $\mathscr{U}_s$, $\mathscr{V}_s$ and $\mathscr{W}_s$ are given in eqn. (64).

# THE EFFECT OF THE GROUND CONSTANTS, AND OF AN EARTH SYSTEM, ON THE PERFORMANCE OF A VERTICAL MEDIUM-WAVE AERIAL

By G. D. MONTEATH, B.Sc., A.Inst.P., Associate Member.

## SUMMARY

The compensation theorem is used to determine the effect of finite ground conductivity, and of an earth system, on the performance of a vertical aerial, such as is used for medium-frequency broadcasting. The characteristics affected are the input impedance, the ground-wave field strength for a given aerial current and the vertical radiation pattern. The first two of these together determine the efficiency, which is the most important consideration in the design of earth systems. When the effective height of the aerial exceeds $0 \cdot 1\lambda$, little can be gained by the use of an earth system exceeding $0 \cdot 2\lambda$ in radius when the ground is highly conducting and $0 \cdot 3$ or $0 \cdot 4\lambda$ when it is poorly conducting. The effect of the earth system on the vertical radiation pattern is shown to be unimportant practically, but results are given for one case in order to compare with experimental radiation patterns. The agreement is quite good.

## LIST OF PRINCIPAL SYMBOLS

$A$ = Terminals of the aerial under investigation.

$B$ = A second pair of terminals.

$F_{AB}$ = Ground-wave attenuation factor between A and B.

$f$ = Complex height-gain factor.

$G$ = Ratio in which the ground-wave field for a given aerial current is changed by the presence of the earth system.

$H_A, H_A', H_{0A}$ = Tangential magnetic field due to unit current into terminals A when surface impedance is $\eta$, $\eta'$, and 0, amp/m.

$H_B, H_B'$ = Tangential magnetic field due to unit current into terminals B when surface impedance is $\eta$ and $\eta'$, amp/m.

$I_0 = H_{0A}/2\pi r$ = Total surface current at radius $r$ when surface impedance is zero, amp.

$J_1$ = Bessel function of the first kind and the first order.

$r$ = Radial distance from base of aerial, m.

$r_0$ = Radius of earth system, m.

$R', R_0$ = Input resistance of aerial when surface impedance is $\eta'$ and 0, ohms.

$Z', Z_0$ = Input impedance of aerial when surface impedance is $\eta'$ and 0, ohms.

$Z_{AB}, Z_{AB}'$ = Mutual impedance between A and B when surface impedance is $\eta$ and $\eta'$, ohms.

$z_c$ = Height of centroid of aerial, m.

$\alpha$ = Angular height of top of vertical aerial, rad.

$\beta = 2\pi/\lambda$.

$\gamma$ = Intrinsic propagation coefficient of the ground.

$\eta$ = Surface impedance in simple system whose properties are known, ohms.

$\eta'$ = Surface impedance in a more complex system under investigation, ohms.

$\eta_g$ = Intrinsic impedance or surface impedance of the ground, ohms.

$\eta_w$ = Surface impedance of radial-wire earth system, ohms.

$\eta_p$ = Parallel combination of $\eta_g$ and $\eta_w$, ohms.

$\eta_0$ = Intrinsic impedance of free space, ohms.

$\theta$ = Angle to the vertical, rad.

$\theta_0$ = Value of $\theta$ for minimum radiation, rad.

$\epsilon_0$ = Permittivity of free space, farads/m.

$\epsilon = \epsilon_r\epsilon_0$ = Complex permittivity of the ground, farads/m.

$\lambda$ = Wavelength in free space, m.

$\mu_0$ = Permeability of free space, henrys/m.

$\xi$ = Efficiency, as defined in Section 6.1.

$\rho = \beta r$ = Angular distance from the base of the aerial, rad.

$\rho_0$ = Angular radius of earth system, rad.

$\sigma$ = Conductivity of the ground, mhos/m.

$\psi, \psi_0$ = Angular distances defined in Fig. 5, rad.

Ei = Exponential integral, defined in eqn. (12).

## (1) INTRODUCTION

This paper is concerned with vertical aerials* for medium-wave broadcasting, of which the simplest is a vertical mast-radiator, usually driven between its base and earth. Where fading is important, the effective height[1,2] is usually about $\frac{1}{2}\lambda$, since this gives the optimum vertical radiation pattern; but a slightly smaller physical height may be made to give the same result by the addition of top capacitance, by series loading or by a combination of these methods. The adverse effect of feed current on the vertical radiation pattern may be avoided by loop feeding, i.e. by inserting an insulator near the current antinode and energizing it at that point while the base is earthed through a reactance.[3] Double feeding,[2] in which a power higher than that radiated is supplied at the current antinode, the excess being recovered at the base, may be used to overcome the effect of imperfect reflection at the ground. Where fading is not important the principal consideration affecting the height is the efficiency, since the radiation resistance of a very short aerial may be comparable with the resistance associated with losses. It is therefore usual to increase the radiation resistance of a short aerial by adding a considerable amount of top capacitance, so that the aerial takes the form of a T.

If the ground were a perfect conductor, its influence could readily be determined by the method of images, but each of the principal characteristics of the aerial is influenced—in general, for the worse—by the fact that the ground conductivity is imperfect. These effects may be mitigated to varying extents by the use of an earth system, which effectively improves the conductivity in the area it covers.

Both the resistance and reactance of an aerial will be affected by the ground constants and earth system, but the resistance is the more important component, since it determines the

* In the paper the term 'vertical aerial' will be restricted to aerials in which the lower end is at ground level.

power required to maintain a given current. The attenuation of the ground wave depends on the ground constants over an area including the entire path of propagation, but the regions near the transmitter and receiver are of particular importance.[4] It therefore seems reasonable to expect that an extensive earth system could cause an appreciable reduction in the attenuation, even though the proportion of the path it occupies is small.

The vertical radiation pattern,[2] which determines the degree of fading caused by reflection at the ionosphere, is adversely affected by imperfect ground conductivity. A mast radiator with an effective height greater than $0 \cdot 5\lambda$ has a vertical radiation pattern with a minimum at an angle depending on the height. Imperfect conductivity results in a reduction in the reflection coefficient at the ground, and the minimum field is thereby increased. It has commonly been supposed that the installation of an earth system about $\frac{1}{2}\lambda$ in radius would result in a radiation pattern substantially the same as that corresponding to a perfectly conducting earth, but this belief has proved unfounded.

Until recently, little has been published on earth systems, and several of the early theoretical papers, which are reviewed in Sections 4.1 and 6.3, appear to be erroneous, probably because of the complexity of the methods of analysis used. However, a preceding paper[5] outlined an extension of the compensation theorem to 3-dimensional systems and proposed its application to the problems under consideration. The comparative simplicity of this method enables the physical significance of approximations to be appreciated so that their validity can be assessed. One of the results enables the change in the mutual impedance between two aerials, or in the self-impedance of one aerial, due to a change in surface impedance, to be expressed as a surface integral. This work has provided a basis for investigations carried out by Wait, Surtees and Pope,[6-8] and by the author respectively. Wait, Surtees and Pope have shown that it is possible to derive some individual results from the wave equation, but their derivations are less simple. Although some of the expressions derived below have already been published, there appears to be scope for a more unified treatment of earth systems. Moreover, the validity of the approximations used requires more discussion than it has hitherto received, while the physical significance of some aspects of the results requires explanation.

The input impedance and the ground-wave field for a given input current are considered separately in Sections 4 and 5, and the results are combined to obtain the efficiency in Section 6. The effect of the earth system on the vertical radiation pattern is discussed in Section 7. Some numerical results are given for illustration, but to save space only one frequency, 1 Mc/s, will be considered.

Rationalized M.K.S. units will be used, and the time factor, $\varepsilon^{j\omega t}$, will be suppressed.

## (2) BOUNDARY CONDITIONS

### (2.1) General

In order to determine the characteristics of an aerial above an imperfectly conducting surface partly covered by an earth system, use is made of the concept of surface impedance. This is an approximate procedure, analogous to the use of circuit impedance in the analysis of networks. The application of surface impedance to the ground was considered briefly in Reference 5, but further discussion of the validity of this procedure is required, particularly in the presence of an earth system.

If the components of electric and magnetic field tangential to a surface are mutually perpendicular, and if their ratio is substantially independent of the sources, being peculiar to the surface, the ratio is termed the surface impedance. It is necessary

to show that in the present problem the properties of the ground can be adequately described by assigning a surface impedance, modified locally by the presence of the earth system, to its surface. Consideration will be given first to the boundary condition at the surface of homogeneous ground, and earth systems will then be considered in increasing order of complexity.

The ground may be specified in terms of its permeability, $\mu$, and permittivity, $\epsilon$; $\mu$ takes its free-space value, $\mu_0$, and $\epsilon$ may be written as $\epsilon = \epsilon_0 \epsilon_r$, where $\epsilon_0$ is the permittivity of free space. Conduction will be taken into account by assigning to $\epsilon_r$ an imaginary part, equal to $-j60\lambda\sigma$.

In Great Britain the conductivity usually varies between $10^{-3}$ and $10^{-2}$ mho/metre, so that at 1 Mc/s the imaginary part of $\epsilon_r$ lies between $-j18$ and $-j180$. The real part is not easily determined, but for the low and high values of conductivity quoted it seems reasonable to assume values of 5 and 20 respectively.

The intrinsic impedance and propagation coefficient, i.e. the field impedance and the propagation coefficient in the direction of propagation of uniform plane waves, are given by

$$\eta_g = \sqrt{(\mu_0/\epsilon)} \quad . \quad . \quad . \quad . \quad . \quad (1)$$

$$\gamma = j\omega\sqrt{(\mu_0\epsilon)} \quad . \quad . \quad . \quad . \quad . \quad (2)$$

For the extreme conductivities quoted and at 1 Mc/s, the quantities considered are given in Table 1.

**Table 1**

TYPICAL GROUND CONSTANTS

| $\sigma$ | For 1 Mc/s | | | |
|---|---|---|---|---|
| | $\epsilon_r$ | $\eta_g$ | $\gamma$ | $|\gamma|$ |
| mho/m | | ohms | $m^{-1}$ | |
| $10^{-3}$ | $5 - j18$ | $69 + j53$ | $0 \cdot 05 + j0 \cdot 07$ | $0 \cdot 09$ |
| $10^{-2}$ | $20 - j180$ | $20 + j18$ | $0 \cdot 19 + j0 \cdot 21$ | $0 \cdot 29$ |

For uniform plane waves propagated within the ground, $\mathscr{I}(\gamma)$ and $\mathscr{R}(\gamma)$ represent respectively the rate of phase retardation in radians per metre and the attenuation in nepers per metre.

Suppose that the $xy$-plane represents the surface of the earth, and let the electric and magnetic fields have components $E_x$, $E_y$, $H_x$ and $H_y$ tangential to it. If all sources are above ground, and if $H_x$ and $H_y$ do not vary too rapidly over the surface, there is a surface impedance $\eta_g$, so that*

$$\left. \begin{array}{l} E_x = \eta_g H_y \\ E_y = -\eta_g H_x \end{array} \right\} \quad . \quad . \quad . \quad . \quad (3)$$

The standard of length by which the rate of change of $H_x$ and $H_y$ over the surface is to be judged is $|\gamma|^{-1}$.

In so far as eqns. (3) are true, the surface behaves as an impedance sheet having an impedance $\eta_g$ between opposite edges of any square, backed by a slab of material of infinite permeability. $H_x$ and $H_y$ may be associated with components of surface current density flowing in the sheet, perpendicular to the tangential magnetic field and (using rationalized units) equal to it in magnitude. The fact that the electrical properties of the ground will generally vary with depth may be ignored, since a surface impedance can nevertheless be assigned it, although it may not be equal to the intrinsic impedance of the uppermost layer.

---

\* In ground-wave propagation theory a more accurate approximation is often used; it is applicable when the fields are set up by plane waves at grazing incidence. The effect of this is the same as if $\epsilon_r$ were increased by unity, and is negligible in the present application.

## (2.2) Perfectly Conducting Earth System

Fig. 1(a) shows a vertical aerial with an idealized circular earth system, a circular cylinder of perfectly conducting metal embedded in the ground. The surface of the earth system will
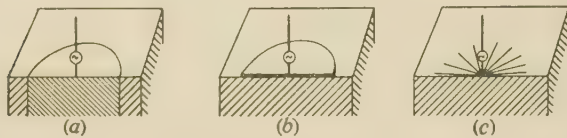


**Fig. 1.—Earth systems.**

(a) Perfectly conducting earth system.
(b) Metal disc.
(c) Radial-wire earth system.

clearly exhibit zero surface impedance, since the electric field cannot possess a component tangential to it. It remains to show that the ground outside the earth system will also exhibit a surface impedance, equal to that which it would possess if the system were absent. This proposition has not been established by the arguments so far advanced, which were applicable only when the properties of the ground were uniform. A further difficulty arises from the fact that if the radius of the earth system is small the tangential magnetic field will vary rapidly from point to point in its neighbourhood.

Eqns. (3) are exact if the fields within the earth correspond to any type of transverse electromagnetic waves travelling vertically downward. Let the magnetic field at a point on the surface whose distance from the axis is $r$ be $H$; if $H$, which will be tangential to circles centred on the axis of symmetry, is associated with a radial surface current, we may write $I = 2\pi r H$ for the total surface current crossing a circle of radius $r$. Now the fields within the ground would correspond exactly to TEM waves if $I$ were independent of $r$. It follows that the condition for the approximate validity of eqns. (3) is that $I$ should vary but slowly as a function of $r$; as before, the standard of length by which the slowness of variation is to be judged is $|\gamma|^{-1}$. Reference to Table 1 shows that, even in the case of the poorly conducting ground, $|\gamma|^{-1}$ is equal to only $10\,\text{m}$, i.e. to $0 \cdot 033\lambda$. The total surface current is found to vary quite slowly in this distance.

The circular sheet-metal disc laid upon the ground, shown in Fig. 1(b), may be thought of as a radial-wire earth system with an infinite number of wires; it is a convenient arrangement for small-scale models (see Section 7). The sharp edge leads to a difficulty that did not arise with the system shown in Fig. 1(a). In its vicinity the tangential magnetic field and the total surface current must vary rapidly with the radial distance, since all field components must be small at points under the disc and not too close to the edge. An alternative view is that the radial current flowing in the metal sheet must leave it near the boundary and spread out into the ground; within the region in which the spreading out occurs the tangential electric field will be greater than it would be if the earth system were cylindrical. As a result, the assignment of a surface impedance to the ground outside the earth system will lead to an error.

By using the dual integral equation method[9] to investigate the fields in the vicinity of the edge, it is found that, in addition to the surface impedance, $\eta_g$, of the ground outside the earth system, a line impedance, $s$, should be assigned to the edge: this is given by

$$s = \frac{\eta_g}{2\gamma} = \frac{1}{2j\omega\epsilon} \quad \cdots \cdots \quad (4)$$

Whatever the property of the aerial being studied, the error associated with the edge effect is equal in magnitude, but not in phase, to the change associated with a change of $1/2|\gamma|$ in

the radius of the earth system. In practice, the error is negligible for systems exceeding $0 \cdot 05\lambda$ in radius.

## (2.3) Radial-Wire Systems

Fig. 1(c) shows the type of earth system usually installed, comprising a number of radial wires buried a few inches below the surface. It will be taken into account by assigning to it a reactive surface impedance $\eta_w$, varying with the distance from the centre, and combining this in parallel with the surface impedance of the ground. It will be assumed that the surface impedance at any particular radial distance is the same as that of an infinite grating of parallel wires at the same spacing. This is given by the well-known formula[10]

$$\eta_w = \frac{j\eta_0 d}{\lambda} \log_\epsilon \frac{d}{2\pi a} \quad \cdots \cdots \quad (5)$$

where $d$ is the spacing and $a$ is the wire radius.

Eqn. (5), and its application to a radial earth system, is based on the following five assumptions:

(a) $d \gg 2\pi a$. This is always true in practical systems.
(b) In a lossless medium in which the wavelength is $\lambda_1$, $d \ll \lambda_1$. In a dissipative medium this condition may be generalized to $d \ll 2\pi/|\gamma|$. By deriving a more accurate expression for the surface impedance of a grating in the interface between two media, it is found that eqn. (5) is applicable to practical systems if $d < \pi/|\gamma|$. There will be an appreciable error only when $d$ is so large that the earth system has little effect.
(c) The fields must not vary too rapidly from point to point of the grating. Eqn. (5) will be sufficiently accurate provided that $I(r)$ does not vary rapidly with $r$, taking $d$ as the standard of length by which the rate of change is judged.
(d) The angle between adjacent wires must be a small fraction of a radian. It is believed that sufficient accuracy will be obtained if there are at least 36 equally spaced wires.
(e) Any small area of a radial earth system behaves like part of an infinite grating. This will not be true near to the ends of the wires, where the current must fall to zero. The ends may be thought of as giving rise to reflected waves of current, which will be propagated backwards with a propagation coefficient $\gamma$. Appreciable error will therefore occur only within a distance $1/\mathscr{R}(\gamma)$ of the ends. The effect should usually be negligible in Great Britain, but might be appreciable where the soil behaves substantially like a lossless dielectric.

Fig. 2 shows the surface reactance of the earth system as a function of the wire radius and the spacing, both expressed in wavelengths. The wire radius is not important, and corrosion is normally the major consideration in specifying it. Fig. 3 shows the surface impedance of the combination of the earth system and the surface of the ground in parallel, assuming a frequency of 1 Mc/s and No. 12 s.w.g. wires.

## (3) METHOD OF ANALYSIS

### (3.1) Basic Formula

The problem is to determine the effect of a finite surface impedance $\eta'$, in general varying from point to point, on the properties of an aerial. The procedure will be to begin with a simpler system in which the surface impedance of the ground is uniform, and then to determine approximately the effect of a change in the surface impedance over part of the surface.

In Fig. 4, A represents the input terminals of the aerial, and B a second pair of terminals, whose significance will be considered later. Let unit current impressed between terminals A, terminals B being open-circuited, result in a component of magnetic field $H_A$ tangential to the surface of the ground. Let the corresponding magnetic field for unit current impressed between terminals B be $H_B$. Let the mutual impedance between A and B be $Z_{AB}$. Now suppose that the surface impedance of the ground is
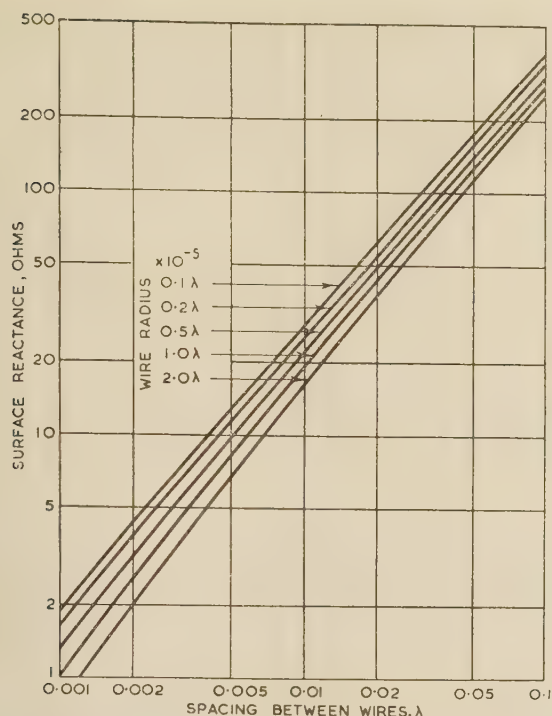
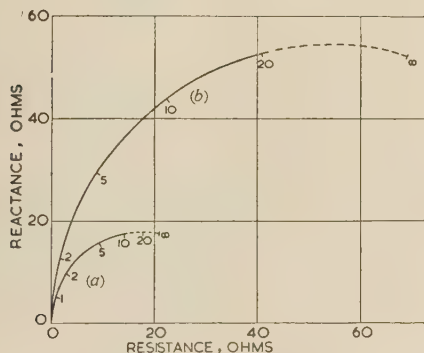Fig. 2.—The surface reactance of a radial earth system.



Fig. 3.—Surface impedance of the ground and earth system in parallel at 1 Mc/s.

Broken curves indicate regions where approximations fail. The numbers on the curves indicate the spacing, in wavelengths, between the 12 s.w.g. earth wires.

(a) $\sigma = 10^{-2}$ mhos/m; $\epsilon_r = 20 - j180$.
(b) $\sigma = 10^{-3}$ mhos/m; $\epsilon_r = 5 - j18$.



Fig. 4

changed from $\eta$ to $\eta'$ (in general $\eta$ and $\eta'$ may be functions of position) and that, in consequence, $H_A$, $H_B$ and $Z_{AB}$ change to $H'_A$, $H'_B$ and $Z'_{AB}$. Eqn. (7) of Reference 5 is essentially

$$Z'_{AB} - Z_{AB} = \int\int (\eta' - \eta)H'_A \cdot H_B dS \quad . \quad . \quad (6)$$

where $dS$ is an element of the surface, the integration being extended over all parts of the earth's surface making appreciable contributions to the integral. The use of this result is referred to as the compensation-theorem method.

Eqn. (6) will be used to determine the effect of a change in surface impedance from $\eta$ to $\eta'$ on the input impedance, the ground-wave field and the vertical radiation pattern. When considering the ground wave, B will be regarded as the terminals of a short dipole placed near the ground in order to measure field strength. Similarly, when considering the vertical radiation pattern, B will be supposed to be the terminals of an aerial which is raised to each angle of elevation in turn. Self-impedance will be regarded as a special case of mutual impedance, and terminals B will be regarded as a second pair of terminals connected in parallel with A. The mutual impedance between A and B will then be equal to the self-impedance at either.

#### (3.2) Approximation

Eqn. (6) is exact, apart from the approximation inherent in surface impedance. But in its exact form it is useless, since the right-hand side contains $H'_A$, a primed quantity applicable to the more complex system whose properties are under investigation. However, if $\eta' - \eta$ is small, $Z'_{AB} - Z_{AB}$ will be small, so that a small error in it can be tolerated. It follows that $H'_A$ may be replaced by an approximation, the resulting error in $Z'_{AB}$ being a second-order small quantity. The approximation that will be made is to replace $H'_A$ by $H_{0A}$, the magnetic field that would exist if the ground were everywhere perfectly conducting. In other words, ground-wave attenuation, as modified by the earth system, will be neglected in computing $H'_A$.

Eqn. (6) becomes

$$Z'_{AB} - Z_{AB} \simeq \int\int (\eta' - \eta)H_{0A} \cdot H_B dS \quad . \quad . \quad (7)$$

The fact that it is necessary to use an approximation for $H'_A$ in eqn. (6) renders it important to make the best choice of $\eta$, the surface impedance in the simple system, the characteristics of which can be evaluated by known methods. Only two alternatives are practicable: in the first, $\eta$ is taken as zero, so that $Z'_{AB} - Z_{AB}$ is the change in mutual impedance due to finite ground conductivity; in the second, $\eta$ is constant and equal to $\eta_g$, so that $Z'_{AB} - Z_{AB}$ is then the change in mutual impedance due to the presence of the earth system.

When considering the input impedance the first alternative will be adopted, since the impedance over imperfectly conducting ground cannot be determined by elementary methods. It is permissible to neglect ground-wave attenuation and use eqn. (7) instead of eqn. (6), because the input impedance depends on the conductivity only in the immediate neighbourhood of the aerial, where the horizontal magnetic field (the quantity measured by conventional field-strength measuring equipment) is not greatly affected by conductivity.

A similar approach cannot be made when considering the ground-wave field strength, because significant contributions to the integral would be made by regions of the surface in the vicinity of the entire path of propagation, and over most of this area ground-wave attenuation is too important to be neglected. The second alternative is therefore adopted; $\eta$ is taken to be $\eta_g$ and eqn. (7) is used to determine the change in the ground-wave field strength caused by the presence of the earth system. Since the integration is confined to the area covered by the system (elsewhere $\eta' - \eta$ is zero), it is again permissible to ignore ground-wave attenuation.

Either of the alternative starting-points may be used in computing the vertical radiation pattern.

#### (3.3) The Surface Current

In eqn. (7), $H_{0A}$ is the tangential component of magnetic field due to unit current impressed between the terminals of the vertical aerial when the ground is perfectly conducting. It is convenient

to replace $H_{0A}$ by $I_0/2\pi r$, where $I_0$ may be regarded as the total surface current crossing a circle of radius $r$.

In the first place it will be assumed that the aerial is sufficiently thin for the current distribution to correspond to a sinusoidal standing-wave pattern. Since $I_0$ is the total surface current for unit input current, it is necessary to specify the position of the input terminals, and these will be assumed to be placed at the current loop or antinode. This arrangement is sometimes used for an anti-facing mast-radiator,[3] whose base is then earthed through an appropriate reactance. The fact that loop feeding is impossible on an aerial less than $0 \cdot 25\lambda$ high is unimportant, since the results can be scaled for any feed point. In any case, it is customary to refer radiation resistance to the loop, whether or not it exists; results relating to other properties of the aerial may be expressed in a form independent of the feed point.

The total surface current is given by[11]

$$I_0 = j[(\varepsilon^{-j\psi} - \cos \alpha \varepsilon^{-j\rho}] \quad . \quad . \quad . \quad . \quad (8)$$

where $\alpha$, $\rho$ and $\psi$ are defined in Fig. 5.
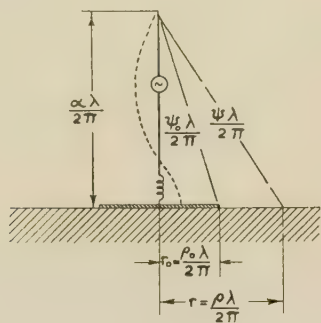


**Fig. 5**

In the limit, as $\rho \to 0$, $I_0 \to \sin \alpha$, which equals the current in the aerial at the base. At great distances its magnitude tends to a constant value proportional to the moment of the aerial, i.e. the line integral of the current along it.

The total surface current near to an anti-fading mast radiator is smaller than that at a great distance, but the reverse is true of an aerial less than $0 \cdot 25\lambda$ high. It follows that the surface impedance of the ground in the immediate vicinity of the aerial (at distances less than $0 \cdot 1\lambda$) will have most effect on its performance if the aerial is short.

### (3.4) Aerials of Finite Thickness

Up to this point consideration has been restricted to aerials of infinitesimal thickness, on which the current distribution is a sinusoidal standing-wave pattern. The different current distribution on a practical aerial will modify the distribution of surface current over the ground, and will therefore influence the effect of the ground constants and the earth system. If extremely thick aerials, such as self-supporting towers, are excluded, the effect of finite thickness may be ignored for heights less than $0 \cdot 3\lambda$. The remainder of this Section will therefore be concerned only with anti-fading mast radiators having a height of about $0 \cdot 5\lambda$. An approximate approach will be outlined briefly, and some numerical results will be given in Sections 5–7.

It is well known that finite thickness modifies the current distribution approximately as follows:[2,12]

(a) The standing-wave pattern is vertically compressed, corresponding to a velocity less than that of light (a factor of $0 \cdot 9$ is typical).

(b) In addition to the co-phased standing-wave pattern, which may be termed the primary current, there is a component of current, known as the feed current, in phase quadrature with it.

When the aerial is loop-fed, feed current may be neglected. On a typical base-fed anti-fading mast-radiator the feed-current distribution resembles—sufficiently closely for practical purposes—the current on a thin base-fed $\frac{1}{4}\lambda$ aerial, being a maximum at the base and tapering to zero near to the antinode of the primary current distribution. (The loop value of the feed current is typically about 25% of the loop value of the primary current.) Feed current may therefore be taken into account by combining results computed separately for a loop-fed anti-fading aerial and a $\frac{1}{4}\lambda$ aerial. The fields of the two component aerials are added as vectors, and the powers radiated are added in order to obtain the effective resistance of the combination. Feed current on a doubly-fed aerial may be treated similarly, but with a reversal of sign.

The vertical compression of the primary current distribution due to reduced velocity may be taken into account by assigning a fictitious height to the aerial. It is believed that the best choice for this is the height of a thin aerial having a similar vertical radiation pattern (the usual criterion is the angle to the vertical of minimum radiation). This v.r.p. height is usually known, since it is the first consideration in the design of an anti-fading aerial. Where numerical results for anti-fading aerials are given later in the paper, the heights quoted should be regarded as the v.r.p. heights rather than the physical heights.

### (3.5) Loaded Aerials

Various modifications are commonly made to the simple vertical aerial in order to reduce the vertical height required. Anti-fading mast radiators are frequently fitted with capacitive tops and may be series loaded. These forms of loading will be taken into account automatically, with sufficient accuracy for practical purposes, if the computation is performed for an equivalent thin unloaded aerial having the same v.r.p. height.

Short aerials are often heavily loaded with top capacitance, usually to form a T aerial, in order to increase the radiation resistance. In this case the vertical radiation pattern is unaffected by the loading, being insignificantly different from that of a very short vertical doublet. A simple method of treating this case is to consider an equivalent simple vertical aerial having the same total moment for a given current at the base. The total surface currents for the loaded and equivalent aerials will then be the same both near to the base, and at infinity.

### (4) THE INPUT IMPEDANCE

### (4.1) Previous Work

Barrow[13] considered an infinitely-thin vertical half-wave dipole, fed at the centre and elevated above ground. In the limit, when one end of the dipole approached ground level, the dipole corresponded to a vertical aerial without an earth system. The analysis was very involved, and the result appears to be wrong, having incorrect dimensions. Since much of the working is omitted from the paper, it is not possible to determine how the errors have arisen.

Hansen and Beckerley[14,15] have calculated the radiation resistance of an aerial above imperfectly conducting ground by expanding the fields in an orthogonal series of wave functions. There appears to be an error* equivalent to the neglect of the interaction of the aerial's local storage fields with the ground. Among aerials for which numerical results are given is a vertical quarter-wave. Now since the analysis can take no

---

* In eqn. (11) of Reference 14 the upper limit of the integral should be $\infty$, not $k$. In the subsequent paragraph it is explained that for $l > k$ the time-average of the Poynting vector is zero; in other words, the complex Poynting vector is imaginary. This is not true for the cross-product terms containing the reflection coefficients $\alpha_2$ and $\alpha_3$.

In eqns. (15) and (16) of Reference 15 the upper limit of the integrals should be $i\infty$, as in eqn. (14), not $\pi/2$.

account of an earth system, it must be supposed that current is forced into the earth at a point on the surface. But the power dissipated in the neighbourhood of this point would be infinite, and the input resistance of the aerial would therefore be infinite also. Nevertheless, Hansen and Beckerley show it to be finite and considerably less than it would be if the earth were a perfect conductor. Another case treated numerically is that of a very short vertical doublet placed just above the ground, and again the finite conductivity of the ground is wrongly supposed to cause a reduction in the radiation resistance. (This case of a doublet has also been considered by Sommerfeld and Renner.[16] Their result disagrees with that of Hansen and Beckerley, but agrees with a result obtained by the compensation-theorem method.[5]) Norton[18] has applied the results to the determination of the field set up by a $0.25\lambda$ aerial for a given input power. It is thus made to appear that, at a distance of $2\lambda$, the fields for a given input power can be *increased* by as much as 15% through the imperfect conductivity of the ground. In fact, there would be a decrease.

Bekefi[19] has employed a variational method to derive an approximation to the input resistance of a vertical aerial above a conducting circular disc laid on the ground, and has compared the results with those obtained by the compensation-theorem method. The complexity of the analysis was such that it was necessary to restrict consideration to very large earth systems and to ground behaving as a lossless dielectric. Bekefi considered the two methods to be in satisfactory agreement, although the agreement was good only for small values of $\epsilon_r$, being perfect for $\epsilon_r = 1$ (the ground then behaving like air). In this condition the approximations inherent in the use of the compensation-theorem method [the replacement of eqn. (6) by eqn. (7) and the use of surface impedance] break down, so that the agreement must have been fortuitous. For large values of $\epsilon_r$, the discrepancy between the two methods is believed to be due to a bad choice of trial function in the variational method. The choice made implies propagation along the ground with a velocity considerably greater than that of light.

Wait[6, 7, 8] and his collaborators have carried out extensive computations based on eqn. (9). Their results are particularly useful in connection with long-wave aerials which are short in comparison with the wavelength.

### (4.2) The General Result

It will be assumed that the impedance of the aerial over perfectly conducting ground is known. The object is to determine the change in impedance resulting from a change in surface impedance from zero to $\eta'$. The analysis is therefore based on eqn. (7), with $\eta = 0$ and $H_B$ replaced by $H_{0B}$. Since A and B will be regarded as terminals connected in parallel (see Section 3.1) $H_{0A}$ and $H_{0B}$ are identical, so that the equation may be written as

$$Z' - Z_0 \simeq \iint \eta' H_{0A}^2 \, dS - \int_0^\infty \frac{\eta' I_0^2 \, dr}{2\pi r} \quad . \quad . \quad (9)$$

For values of $r$ equal to a few wavelengths the integrand in eqn. (9) will decrease with distance approximately as $1/r$ and will be retarded in phase approximately as $\varepsilon^{-j\beta r}$. It follows that the integral will converge rapidly, and that the precise value of the integrand at distances exceeding a few wavelengths will not be important, provided that any error varies slowly. This fact justifies the approximation inherent in the use of eqn. (7) rather than eqn. (6).

Eqn. (9), which is accurate to the first order in $\eta'$, has a simple physical significance: $\eta' dr/2\pi r$ is the impedance of an annulus

of the surface between radii $r$ and $r + dr$. $Z' - Z_0$ is obtained by adding the impedance of all the elementary annuli, weighted in both amplitude and phase in proportion to the squares of the currents flowing across them.

### (4.3) Perfectly Conducting Earth Systems

Attention will first be directed to the idealized earth system shown in Fig. 1(*a*). The correction necessary to apply the results to the sheet-metal system in Fig. 1(*b*), which is discussed in Section 2.2, is negligible in most practical cases.

In eqn. (9), $\eta' = 0$ for $r < r_0$, but at greater radii it is constant and equal to $\eta_g$, so that the equation becomes

$$Z' - Z_0 \simeq \eta_g \int_{r_0}^\infty \frac{I_0^2 \, dr}{2\pi r} \quad . \quad . \quad . \quad (10)$$

For a sinusoidal current distribution on the aerial, $I_0$ may be obtained from eqn. (8), and the integral can then be evaluated in closed form. The result, expressed in terms of $\alpha$, $\rho_0$, and $\psi_0$ (defined in Fig. 5), is

$$Z' - Z_0 = \frac{\eta_g}{4\pi} \{ \varepsilon^{-2j\alpha} \operatorname{Ei} [-j(2\psi_0 - 2\alpha)] + \varepsilon^{2j\alpha} \operatorname{Ei} [-j(2\psi_0 + 2\alpha)]$$
$$- 4 \cos \alpha \varepsilon^{-j\alpha} \operatorname{Ei} [-j(\psi_0 - \alpha + \rho_0)]$$
$$- 4 \cos \alpha \varepsilon^{j\alpha} \operatorname{Ei} [-j(\psi_0 + \alpha + \rho_0)] + 4 \cos \alpha \operatorname{Ei} [-j(\psi_0 + \rho_0)]$$
$$+ 2 \cos^2 \alpha \operatorname{Ei} (-2j\rho_0) \} \quad . \quad . \quad . \quad (11)$$

where

$$\operatorname{Ei} (-jx) = \int_\infty^x \frac{\varepsilon^{-jt}}{t} \, dt = \operatorname{Ci} (x) - j \operatorname{Si} (x) + j\pi/2 . \quad (12)$$

Wait and Surtees[6] have published a more general and more complex result taking account of loading with top capacitance.

In Fig. 6, $(Z' - Z_0)$ is plotted on the Argand diagram as a function of $\rho_0/2\pi$, the radius of the earth system in wavelengths,
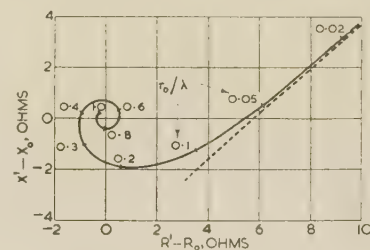


Fig. 6.—$Z' - Z_0$ for a $0.25\lambda$ aerial over highly conducting ground ($\epsilon_r = 20 - j180$).

Perfectly conducting earth system.

for a $0.25\lambda$ aerial over highly conducting ground at 1 Mc/s ($\epsilon_r = 20 - j180$). In order to convert this result for different ground constants or frequency, the Figure may be expanded in proportion to $|\eta_g|$, and rotated according to the change in arg $(\eta_g)$.

Owing to the complexity of eqn. (11), its physical significance cannot be appreciated on inspection, and it is instructive to consider limiting cases. For large radii it may be shown that $Z' - Z_0$ is inversely proportional to the radius of the earth system, and suffers a phase retardation which increases by $2\pi$ for an increase of $\frac{1}{2}\lambda$ in the radius. The nature of this result suggests that $Z' - Z_0$ may be regarded as a measure of the reaction upon the aerial of waves reflected from the boundary of the earth system. This view is discussed in Reference 5 in relation to an elevated doublet.
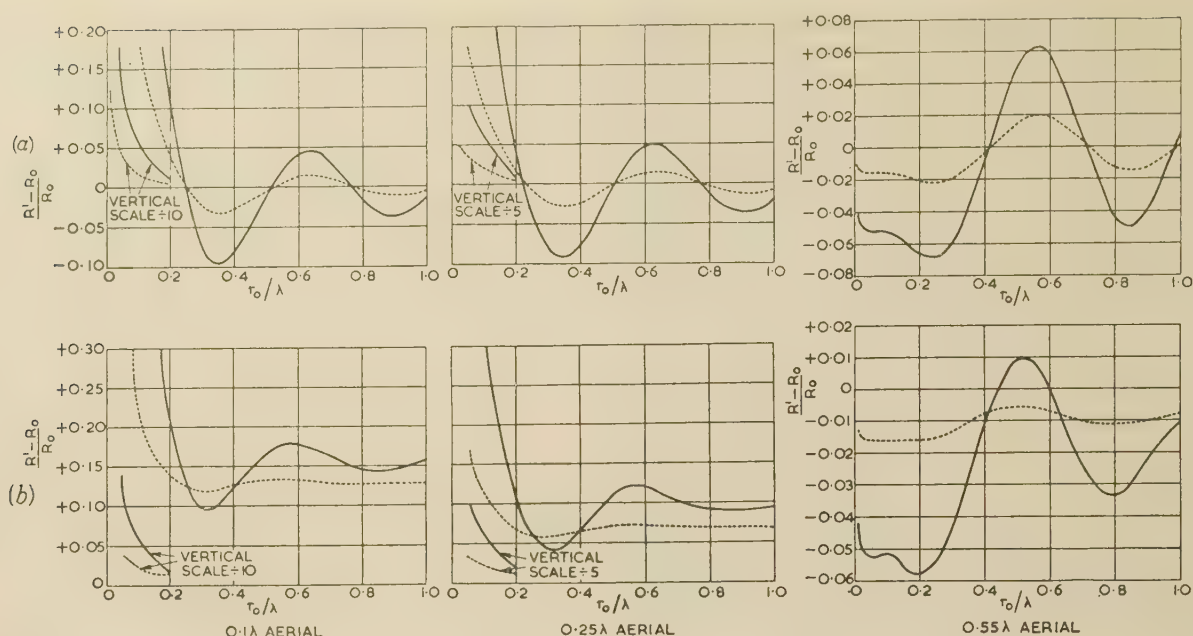
Fig. 7.—Relative increase in resistance due to finite ground conductivity.

——— Poorly conducting ground ($\epsilon_r = 5 - j18$).          - - - - Highly conducting ground ($\epsilon_r = 20 - j180$).

(a) Perfectly conducting earth system.          (b) 72 radial wires.

For small radii it may be shown that $Z' - Z_0$ varies logarithmically with the radius, so that the curve in Fig. 6 exhibits a tail extending to infinity. In this region each annulus of the ground behaves like an impedance connected in series with the base of the aerial.

The component of the impedance having most practical importance is the resistance, which determines the power required to maintain a given current. The most convenient method of expressing the effect of imperfect ground conductivity on the resistance is in terms of $(R' - R_0)/R_0$, which is independent of the choice of feed point. Curves giving $R_0$, the loop radiation resistance for perfectly conducting ground, assuming a sinusoidal current distribution, are given in Reference 20. In Fig. 7(a) $(R' - R_0)/R_0$ is shown as a function of $r_0/\lambda$ for highly conducting and poorly conducting ground and for aerials of three heights, $0\cdot1\lambda$, $0\cdot25\lambda$ and $0\cdot55\lambda$. A striking feature of these results is that the imperfect conductivity of the ground outside the earth system can sometimes cause a reduction in the resistance of the aerial. An increase in the radius of the system may then increase the power required to maintain a given current.

#### (4.4) Radial-Wire Earth Systems

For a radial-wire earth system the integral in eqn. (9) must be evaluated from zero to infinity, but it is convenient to divide this range into two parts, so that $Z' - Z_0$ is obtained as the sum of two contributions. One of these, due to the ground outside the earth system ($r > r_0$), is obtained from eqn. (11). The contribution due to the region covered by the earth system ($0 < r < r_0$) is obtained by substituting $\eta_p$, the surface impedance of the ground and the earth system in parallel, for $\eta'$ and carrying out the integration numerically. The integral converges at $r = 0$ in spite of the factor $1/r$, since $\eta_p$ diminishes more rapidly than $r$.

$(R' - R_0)/R_0$ is shown in Fig. 7(b) for the same ground constants applicable to Fig. 7(a). The number of radial wires is 72, so that the intervals are 5°; this provides a compromise between cost and performance in most cases. The wire size is No. 12 s.w.g., but the results may be applied without appreciable error to any

size between Nos. 18 and 6 s.w.g. Results for a $0\cdot25\lambda$ aerial and various numbers of wires have been published by Wait and Pope.[7]

Comparing Fig. 7(b) with Fig. 7(a), it will be seen that the radial-wire system behaves substantially like a perfectly conducting system for radii up to $0\cdot1$ or $0\cdot15\lambda$, being effective out to a greater radius when the ground is poorly conducting. If its radius exceeds about $0\cdot25\lambda$, the input resistance is very nearly the same for conductivities of $10^{-2}$ and $10^{-3}$ mho/m, even though it may differ appreciably from the resistance for perfectly conducting ground.

### (5) THE GROUND-WAVE FIELD STRENGTH FOR A GIVEN INPUT CURRENT

#### (5.1) General

The theory governing ground-wave propagation is not simple, but it has been made easy to compute the field strength at the surface of the earth, provided that the transmitting aerial is short, the current distribution on it is known and the ground is homogeneous. The field strength is obtained as the product of two factors: the field strength for a plane and perfectly conducting earth and the attenuation factor, which depends upon the ground constants, the distance and the radius of curvature. The attenuation factor may be obtained conveniently from numerical results such as those published by Norton.[17, 18, 21] Unfortunately, this procedure is not applicable to a high aerial, such as an anti-fading mast radiator, or an aerial having an extensive earth system. In order to extend it, it is convenient to express the vertically polarized component, $E$, of field strength in terms of four factors as

$$E = E_0 F_{AB} f G \quad . \quad . \quad . \quad . \quad . \quad (13)$$

where $E_0$ is the field strength that would exist if the earth were plane and perfectly conducting, $F_{AB}$ is the ground-wave attenuation factor for a short aerial, $f$ is the ratio in which the field strength is increased by the finite height in the absence of an extensive earth system, and $G$ is the ratio in which the field

strength for a given aerial current is increased by the presence of the earth system.

The merit of eqn. (13) is that $F_{AB}$, which depends on the ground constants in the vicinity of the entire path of propagation, is independent of the characteristics of the aerial or earth system. Its determination will be regarded as a propagation problem outside the scope of the paper. On the other hand, $f$ and $G$, which depend on the height of the aerial, are affected by the ground constants only in the vicinity of the aerial. These last two factors will therefore be regarded as properties of the aerial system, affecting its efficiency.

### (5.2) Height Gain

#### (5.2.1) The Height-Gain Factor of an Elevated Doublet.

There has been a tendency for the use of height-gain factors at medium frequencies to be discouraged by doubt regarding the conditions under which this procedure is valid. For example, Norton's[21] expression and curves for the height-gain factor of an elevated doublet are equivalent to those derived below, but the prescribed conditions render them almost useless at medium frequencies.* This difficulty is believed to have been occasioned by the complexity of the method of derivation.

A considerable simplification can be effected by considering a receiving aerial in the first instance, and then using the reciprocity principle, which implies that the height-gain factor is the same whether the aerial is used for transmission or reception. The problem is then reduced to the determination of the variation of vertical electric field with height, supposing the fields to be set up by a distant transmitter. It will be shown that this can be done without entering into the complexities of ground-wave propagation theory. The compensation-theorem method will not be used in the derivation.



Fig. 8

In Fig. 8, P and Q are two short doublets, P being near the ground while Q is at a height $z$. It will be supposed that radiation takes place from P. In order to determine the height-gain factor for Q, it is necessary to investigate the variation with the height of the vertical component of field, $E_z$. Now by combining eqn. (3) with Maxwell's equations, and eliminating all field components other than $E_z$, it is found that

$$\left(\frac{\partial E_z}{\partial z}\right)_{z=0} = \frac{j\beta\eta_g}{\eta_0}(E_z)_{z=0} \quad . \quad . \quad . \quad . \quad (14)$$

Eqn. (14) is well known as a boundary condition; it states the rate at which $E_z$ begins to change as $z$ increases from zero. In order to use it one must show that the rate of change $\partial E_z/\partial z$ remains constant up to a sufficient height, i.e. that $\partial^2 E_z/\partial z^2$ is sufficiently small. Now the second derivatives of any Cartesian field-component with respect to $x$, $y$ and $z$ are related by the wave equation, and it can be deduced that $\partial^2 E_z/\partial z^2$ must be small if the phase velocity in horizontal directions is close to the velocity of light and the attenuation per wavelength is small. These conditions are satisfied if the ground is flat and homogeneous for a distance of many wavelengths round the aerial under consideration, and if the second aerial is not too close.

* Reference 21, eqn. (18). The most severe restriction is $p > 20$. For a conductivity of $10^{-2}$ mho/m at 1 Mc/s, this implies that the distance must exceed 350 km.

(As already stated, the earth system is assumed to be absent when considering height-gain.)

The error resulting from the neglect of $\partial^2 E_z/\partial z^2$ has been assessed by deriving the horizontal phase velocity and attenuation from the complex attenuation factor. It was found that, for heights corresponding to an anti-fading mast radiator, the error in the height-gain factor does not exceed 2%, provided that the distance exceeds $25\lambda$. At shorter distances $\partial^2 E_z/\partial z^2$ would effectively increase the height-gain factor.

Neglecting $\partial^2 E_z/\partial z^2$, it follows from eqn. (14) that

$$E_z = E_{z0}(1 + j\beta\eta_g z/\eta_0) = E_{z0}(1 + j\beta z\epsilon_r^{-1/2}) \quad . \quad (15)$$

where $E_{z0}$ is the value of $E_z$ when $z = 0$. It follows that

$$f(z) = E_z/E_{z0} = 1 + j\beta z\epsilon_r^{-1/2} \quad . \quad . \quad . \quad (16)$$

In order to avoid confusion, $f(z)$ will be termed the 'complex height-gain factor', while the term 'height-gain factor' will be reserved for its magnitude. Although $f(z)$ is linear, $|f(z)|$ is not.
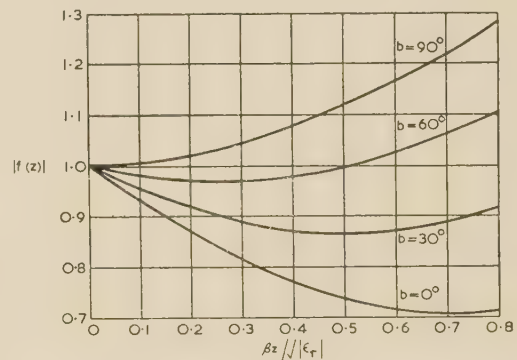


Fig. 9.—The height-gain factor for a vertical doublet.

In Fig. 9 $|f(z)|$ is given as a function of $\beta z|\epsilon_r|^{-1/2}$ and $b$. The parameter $b$ has the same significance as in Norton's papers,[17, 18, 21] being defined by

$$\epsilon_r = |\epsilon_r| \exp(jb - j\pi/2) \quad . \quad . \quad . \quad . \quad (17)$$

#### (5.2.2) Height-Gain Factor of a Vertical Aerial.

The fact that the complex height-gain factor of an elevated doublet varies linearly with the height enables that of an aerial of finite length to be expressed very simply: it is equal to $f(z_c)$, where $z_c$ is defined by

$$z_c \int_0^h I(z)dz = \int_0^h zI(z)dz \quad . \quad . \quad . \quad (18)$$

where $I(z)$ is the current in the aerial at a height $z$, and $h$ is the total height. The height-gain factor is therefore the same as that for a doublet placed at the centroid of the current distribution.

For a sinusoidal standing-wave pattern with a velocity equal to that of light, the height of the centroid is given by

$$\beta z_c = \frac{\beta h - \sin\beta h}{1 - \cos\beta h} \quad . \quad . \quad . \quad . \quad (19)$$

In Fig. 10 $z_c/\lambda$ is plotted against $h/\lambda$.

For an anti-fading mast radiator, departures from the idealized current distribution assumed above may be taken into account by the methods outlined in Section 3.4. If the current distribution is co-phased (loop feeding), the height of the centroid is closely correlated with the vertical radiation pattern. A scale
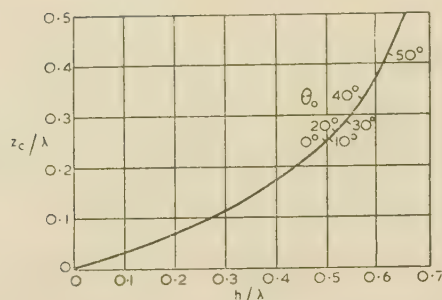
Fig. 10.—The height of the centroid of a vertical aerial with sinusoidal current distribution.



Fig. 11

of $\theta_0$, the angle to the vertical of minimum radiation, has therefore been marked on Fig. 10. If this scale is used, reduced velocity may be ignored.

When feed current has to be considered, it is convenient to calculate the moments of the primary- and feed-current distribution, and the heights of their centroids, separately; $z_c$ is then obtained in a manner similar to the calculation of the position of the centre of gravity of two unequal weights. Since the moments of the two distributions are in phase quadrature, $z_c$ is complex, so that it does not, in fact, represent a physical height.

Height-gain factors are given in Table 2. With double feeding

### Table 2

#### HEIGHT-GAIN FACTORS

| $\epsilon_r$ | $0.25\lambda$ aerial | $0.55\lambda$ aerial | | |
|---|---|---|---|---|
| | | Base fed | Loop fed | Doubly fed |
| 20 − j180 (high-conductivity ground) | 0.973 | 0.926 | 0.911 | |
| 5 − j18 (low-conductivity ground) | 0.927 | 0.868 | 0.816 | 0.766 |

of the $0.55\lambda$ aerial it is assumed that the feed current is the same as for a base-fed aerial but reversed in sign.

Feed current increases the height-gain factor, and reversed feed current obtained by double feeding reduces it. This fact is of importance only when the conductivity is low, but it does imply that the use of double—as opposed to base—feeding in order to improve the vertical radiation pattern may entail some sacrifice of field strength. This effect is associated with wave tilt; over imperfectly conducting ground energy is propagated obliquely downwards at a small angle to the horizontal. Now the presence of the feed current when transmitting implies that a base-fed vertical aerial behaves to some extent as a travelling-wave aerial, so that it is particularly well suited to receive waves tilted downwards. The reverse is true of a doubly-fed aerial; although this too is a travelling-wave aerial, the direction of travel is unfavourable.

### (5.3) The Effect of an Earth System

#### (5.3.1) General.

In Fig. 11, A and B represent respectively the terminals of the transmitting aerial under consideration and those of a distant receiving aerial at ground level. The problem is to determine the ratio in which mutual impedance between A and B is changed when the transmitting aerial is provided with an earth system. For this purpose eqn. (7) is used, and $Z_{AB}$ and $Z'_{AB}$ are respectively taken to be the mutual impedance in the absence of an
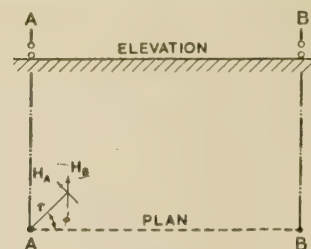
earth system, when the surface impedance in the neighbourhood of A is $\eta_g$, and that in the presence of one, when the surface impedance is $\eta'$. The integration may be restricted to the area, S, occupied by the earth system.

The reduction of eqn. (7) to a form suitable for computation will be outlined briefly. If B is sufficiently distant from A, then, at all points within S, $H_B$ will be very nearly perpendicular to AB and constant in magnitude, its phase variation from point to point corresponding almost exactly to propagation with the velocity of light. Taking polar co-ordinates $(r, \phi)$ as shown in Fig. 11, and writing $H_B(A)$ for the value of $H_B$ at $A$, we have

$$H_{0A} \cdot H_B = H_{0A} H_B(A) \varepsilon^{j\beta r \cos \phi} \cos \phi \quad . \quad . \quad (20)$$

In this equation $H_{0A}$, which is equal to $I_0(r)/2\pi r$, is a function of $r$ only, while $H_B(A)$, the magnetic field at A due to unit current in aerial B, is independent of both $r$ and $\phi$. It is convenient to express $H_B(A)$ in terms of the mutual impedance, $Z_{AB}$, between A and B in the absence of the earth system. In doing so, small corrections for wave tilt and height gain will be neglected, since any error resulting will be a second-order small quantity. Eqn. (7) becomes

$$Z'_{AB} - Z_{AB} = -\frac{Z_{AB}}{2\pi l \eta_0} \iint_S (\eta' - \eta_g) I_0(r) \varepsilon^{j\beta r \cos \phi} \cos \phi \, dr \, d\phi \quad (21)$$

where $l$ is the effective length of the aerial, i.e. the line integral of the current for unit input current. Since the mutual impedance is proportional to the ground-wave field at B due to unit current in A, eqn. (21) may be expressed in the form

$$G - 1 = -\frac{1}{2\pi l \eta_0} \iint_S (\eta' - \eta_g) I_0(r) \varepsilon^{j\beta r \cos \phi} \cos \phi \, dr \, d\phi \quad (22)$$

where $G$ is the complex ratio in which the ground-wave field is changed by the installation of an earth system, the current in the aerial being held constant.

#### (5.3.2) Circular Earth Systems.

If the earth system has circular symmetry, the integration with respect to $\phi$ in eqn. (22) can be performed, when the equation becomes

$$G - 1 = -\frac{j}{l\eta_0} \int_0^{r_0} (\eta' - \eta_g) I_0(r) J_1(\beta r) \, dr \quad . \quad . \quad (23)$$

where $r_0$ is the radius of the system. The integration with respect to $r$ must be performed numerically.

The first-order Bessel function provides a clue to the physical significance of eqn. (23), since it occurs also in the expression for the field of a circular loop carrying a uniform current. Considering an elementary annulus of the surface having radii $r$ and $r + dr$, the effect of reducing the surface impedance from $\eta_g$ to $\eta'$ is to reduce the series impedance presented to the surface current by $(\eta_g - \eta')dr/2\pi r$. The compensation theorem for networks suggests that a similar result would be achieved by cutting a
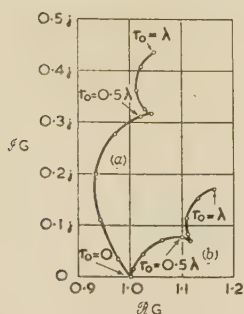
**Fig. 12.**—Variation of complex ground-wave field with radius of earth system. Perfectly conducting earth system and poorly conducting ground ($\epsilon_r = 5 - j18$).

    (a) 0·1λ aerial.
    (b) 0·55λ aerial.

Points are plotted at 0·1λ intervals but in (b) the points for $r_0 = 0$ and $r_0 = 0·1λ$ are coincident.

which would not radiate in its own plane. The cycloidal form of the curves suggests that the change in ground-wave field caused by the earth system is the sum of two components, one increasing steadily as the radius of the system increases, the other decreasing slowly in magnitude while its phase becomes progressively more retarded. The first component is associated with the elimination of ground-wave attenuation along that part of the path of propagation passing over the earth system; the second is the result of reflection from the discontinuity occurring at the boundary of the system behind the aerial. This explanation is confirmed in Section 5.3.3 by considering a semi-circular earth system oriented to produce either component separately.

The general trend of the locus of $G$ as a function of $r$ is connected with the way in which the ground-wave attenuation factor varies with distance at short distances. As might be expected, the earth system tends to overcome the attenuation and phase retardation caused by finite ground conductivity.



**Fig. 13.**—Variation of magnitude of ground-wave field with the radius of the earth system.

——— Poorly conducting ground ($\epsilon_r = 5 - j18$).      ---- Highly conducting ground ($\epsilon_r = 20 - j180$).
    (a) Perfectly conducting earth system.      (b) 72 radial wires.

narrow annular slot and connecting generators across it so as to assist the flow of surface current by maintaining the appropriate potential difference. Now the radiation field resulting from the excitation of this slot may be calculated by treating it as a magnetic conductor carrying a magnetic current.[22] In this way the right-hand side of eqn. (23) may be thought of as the summation of the fields of a large number of elementary annular slots simulating the effect of the earth system.

Although the magnitude of the field strength is of greater practical importance, consideration of the phase in a simple case assists in understanding the results. In Fig. 12, $G$ is plotted on the Argand diagram as a function of the radius of a perfect earth system, for 0·1λ and 0·55λ aerials and poorly conducting ground. The most striking result is the fact that the ground-wave field strength does not change steadily as the radius of the earth system is increased; in fact, $G$ traces out a locus resembling a cycloid, becoming stationary at each cusp. The radius corresponding to each cusp is equal to the radius of a loop aerial

Fig. 13 shows $|G|$ as a function of $r_0$ for three aerial heights, poorly conducting and highly conducting ground, and both perfectly conducting and radial earth systems. The way in which positive and reversed feed currents influence the variation of $|G|$ with the radius of the system is illustrated in Fig. 14, but to save space only the case of a perfectly conducting system and poorly conducting ground is considered.

The oscillatory component evident in the curves of Figs. 13 and 14 is due to reflection at the boundary. If it is ignored, the way in which the general trend of the curves varies from one aerial to another is found to be related to the height-gain factor. The earth system tends to overcome the effect of height gain; this might be expected, since the height-gain factor depends on the ground constants in the immediate vicinity. Thus $|G|$ increases with $r$ more rapidly for a high aerial than for a low one, and more rapidly when a mast radiator is doubly fed than when it is base fed. If the phase of the radiated field is considered, the earth system is again found to offset height gain.
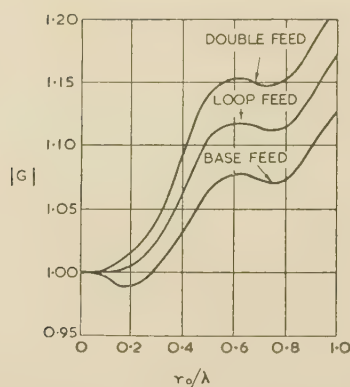
**Fig. 14.—The effect of feed current.**

Aerial height $0.55\lambda$.
Perfectly conducting earth system and poorly conducting ground ($\epsilon_r = 5 - j18$).

Thus Fig. 12 shows that the earth system advances the phase of the field of a high aerial less than that of a short one.

#### (5.3.3) Semicircular Earth Systems.

There are three reasons for considering semicircular earth systems. First it was desired to test a possible explanation, discussed in Section 5.3.2, for the cycloidal shape of the curves in Fig. 12. Secondly, an experiment with a semicircular system enabled theoretical and experimental results to be compared. Finally, it has been suggested that on a site of limited area it might be desirable to favour particular directions by means of an asymmetrical earth system.

In eqn. (23), which is applicable to a system with circular symmetry, the Bessel function $J_1(\beta r)$ was introduced as a result of integration from 0 to $2\pi$ with respect to $\phi$. It is not difficult to restrict the integration to any range of angles, so as to obtain a result for a sectoral earth system, but the first-order Bessel function is replaced by an infinite series. In the particular case
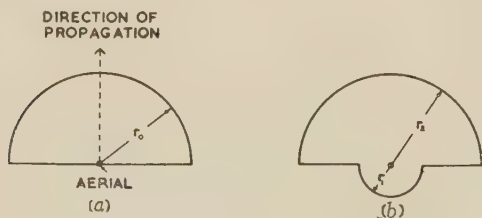


**Fig. 15.—Semicircular earth systems.**

of a semicircular system oriented as shown in Fig. 15(a), $J_1(\beta r)$ is replaced by the function $L(\beta r)$, defined by

$$L(x) = \tfrac{1}{2}J_1(x) - \frac{j}{\pi}\left[ J_0(x) - 2\sum_1^\infty \frac{J_{2m}(x)}{4m^2 - 1} \right]. \quad . \quad (24)$$

If the earth system shown in Fig. 15(a) is rotated through 180°, so that the initial portion of the path of propagation no longer passes over it, the sign of $\mathscr{I}L(\beta r)$ is reversed.

If $J_1(\beta r)$ is replaced by $L(\beta r)$ in eqn. (23), the integral may be evaluated numerically. As an example, Fig. 16 shows $G$ on the Argand diagram for an aerial $0.1\lambda$ high with a perfectly conducting semicircular earth system. The ground is assumed to be poorly conducting ($\epsilon_r = 5 - j18$), so that the result may be compared with that for a circular earth system shown in Fig. 12. This result confirms the tentative explanation given in Section 5.3.2 for the cycloidal form of the curves in Fig. 12. It is seen that the contribution to the total field caused by the forward
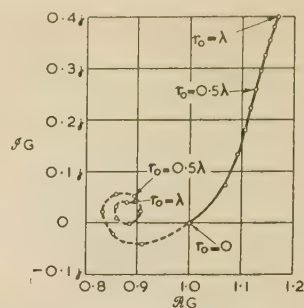


**Fig. 16.—The complex ground-wave field strength as a function of the radius of a semicircular earth system.**

$0.1\lambda$ aerial.
Poorly conducting ground ($\epsilon_r = 5 - j18$).
—— Earth system oriented as shown in Fig. 15(a).
---- Earth system oriented in reverse direction.   Points plotted at $0.1\lambda$ intervals.

half of a circular earth system increases steadily in magnitude with the radius. The spiral form of the broken curve, corresponding to the backward half of a circular earth system, is consistent with reflection at the boundary.

A more practical form of asymmetrical system is shown in Fig. 15(b). The effect of this may be obtained by adding the complex values of $(G - 1)$ for the two semicircular portions. One of these, corresponding to the portion extended in the forward direction, is read from the continuous curve in Fig. 16; the other is read from the broken curve. An earth system of this type was investigated experimentally at 500 Mc/s, the ground being simulated by a $0.6\%$ salt-water solution having a complex relative permittivity of $80 - j36$ at the operating frequency. The large real part of the permittivity had the advantage of causing a rapid initial rate of ground-wave attenuation. Hence the effect of the earth system on the ground-wave field was greater than for a typical broadcasting site.

Two heights of aerial were used, $0.55\lambda$ and $0.1\lambda$, $r_1$ and $r_2$ being $0.1\lambda$ and $0.5\lambda$ respectively. The earth system was made up of a cylindrical box $0.1\lambda$ in radius, which formed a mounting for the aerial and a container for the matching circuits, and a semicircular sheet $0.5\lambda$ in radius. The latter could be screwed to the cylindrical box in either of two opposite orientations, without causing any other change in the system. The object was to determine the forward/backward ratio, i.e. the ratio of the field strength obtained with the orientation as in Fig. 15(b) to that obtained with the reverse orientation. The results are compared with the theoretical forward/backward ratios below:

|             |    |    |    | $0.1\lambda$ Aerial | $0.55\lambda$ Aerial |
|-------------|----|----|----|--------------------|----------------------|
| Theoretical | .. | .. | .. | $1.05$             | $1.015$              |
| Measured    | .. | .. | .. | $1.07$             | $1.00$               |

It is possible that errors of $2\%$ could occur in the measurements, and the result is therefore inconclusive as a test of the method of analysis. Nevertheless, the practical conclusions reached theoretically are confirmed, namely that an asymmetrical earth system tends to favour the direction in which it is extended furthest, but that the effect is too small to be of practical importance.

#### (6) EFFICIENCY

#### (6.1) Definition

In spite of the fact that aerials extending down to ground level have been in use for 60 years, no satisfactory definition of their efficiency appears to have been laid down. The difficulty is to distinguish between ground losses associated with the aerial, which reduce the efficiency, and losses asso-

ciated with the path of propagation, which do not.* Williams[20] has suggested a definition giving 100% efficiency for a lossless aerial with a perfectly conducting circular earth system $0 \cdot 5\lambda$ in radius. This definition is, however, arbitrary, and it does not facilitate the calculation of field strengths. An alternative definition is proposed below:

The efficiency is equal to the square of the ratio in which the field strength at a distant point for a given input power is reduced by finite ground conductivity and other losses, divided by the square of the ground-wave attenuation factor, i.e. the ratio in which the field strength of a short vertical doublet near to the surface and carrying a given current would be reduced by finite ground conductivity in the absence of an earth system.

This definition makes a convenient distinction between the effect of earth losses on the efficiency of the aerial and their effect on the characteristics of the path of propagation. Moreover, it enables the ground-wave field strength, $E$, to be computed as the product of three factors, as follows:

$$E = E_0 F_{AB} \xi^{1/2} \quad . \quad . \quad . \quad . \quad . \quad (25)$$

* B.S. 204: 1943, No. 4225 defines 'radiation efficiency' as the ratio of the power radiated to the total power supplied. The meaning of 'radiated' is, however, obscure when earth loss can occur very near the aerial.

where

$E_0$ = The field strength that would obtain if the ground were perfectly conducting and the aerial were lossless, the input power being unchanged.

$F_{AB}$ = The ground-wave attenuation factor, defined above. For homogeneous ground this may be obtained from Norton's papers.[17,18,21]

$\xi$ = Efficiency.

The definition proposed can lead to an efficiency in excess of 100% if the earth system is sufficiently large. It would not be practicable to define efficiency so as to make this impossible, since the field at a sufficiently distant point could in principle be increased almost without limit by extending the earth system.

### (6.2) From the Impedance and the Ground-Wave Field

If losses in the aerial conductors, insulators, etc., which fall outside the scope of the paper, are ignored, the efficiency, as defined in Section 6.1, may be deduced from the height-gain factor, the ratio in which the ground-wave field for a given input current is increased by the presence of the earth system, and the ratio in which the input resistance in the presence of the earth system is increased by imperfect conductivity. It is given by

$$\xi = |fG|^2 R_0/R' \quad . \quad . \quad . \quad . \quad . \quad (26)$$
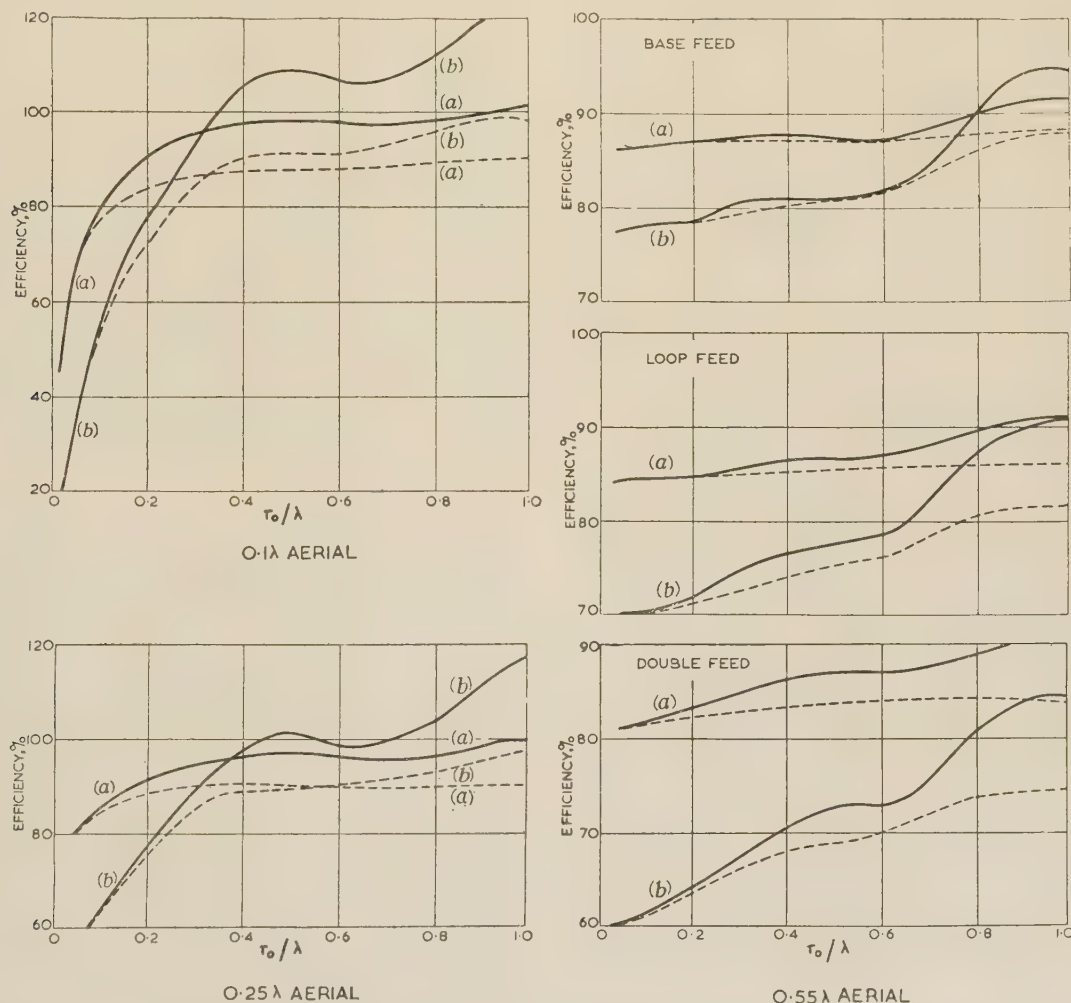


Fig. 17.—The efficiency as a function of the radius of the earth system.

——— Perfectly conducting earth system.
- - - - - 72 radial wires.
(a) Highly conducting ground ($\epsilon_r = 20 - j180$).
(b) Poorly conducting ground ($\epsilon_r = 5 - j18$).

$f$, $G$ and $R'/R_0$ have been considered in Sections 5.2, 5.3 and 4 respectively.

In Fig. 17 the efficiency is shown as a function of the radius of the earth system for aerials of three heights, one with three methods of feeding. The feed current on the doubly-fed aerial is assumed to be equal in magnitude but opposite in sign to that on the base-fed aerial.

It will be seen that it is sometimes possible for the efficiency to be reduced by a small extension of the earth system, and it is believed that this effect is associated with a small change in the vertical radiation pattern.

### (6.3) The Absorbed-Energy Method

Brown and his collaborators,[11, 23, 24] and later Abbott,[25] have assessed the efficiency of earth systems in terms of the extent to which they reduce the absorption of energy. They assumed that, if an improvement in earth system reduced the absorption of energy in the region covered by it by 1 kW, the resulting increase in field strength would correspond to an increase of 1 kW in the transmitter power. Even if this assumption were justified, the absorbed-energy approach could not lead to an estimate of the efficiency, but it would permit the calculation of the change in efficiency resulting from a given change in the earth system.

The absorbed-energy method can be justified by the conservation of energy provided that the earth system has little effect on the vertical radiation pattern, or on the way in which the surface current varies with distance outside it. Since its use would reduce the labour of computation in certain problems, it is desirable to check its accuracy.

The power, $dP$, absorbed in an elementary annulus of ground having inner and outer radii $r$ and $r + dr$ is given by

$$dP = (1/4\pi r)|I(r)|^2 \mathscr{R}(\eta_g)dr \quad . \quad . \quad . \quad (27)$$
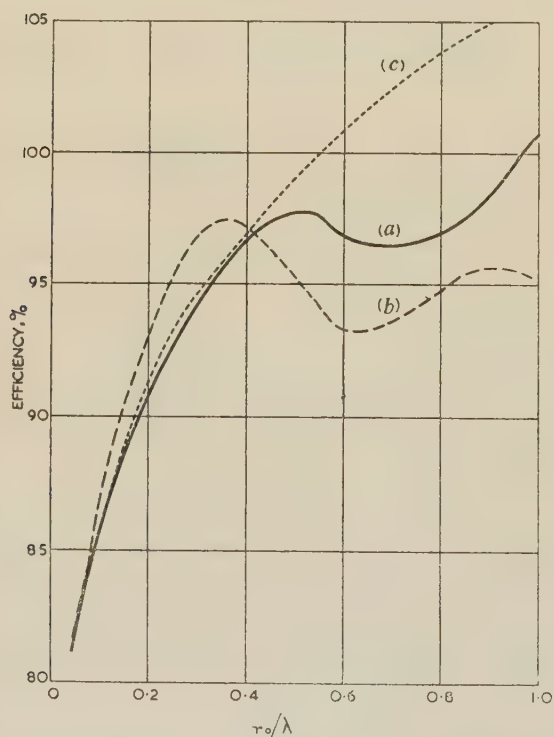


Eqn. (27) agrees with Brown's method if the real part of the permittivity is neglected in computing $\eta_g$.

In order to take account of a radial-wire earth system, Brown[23] used a formula (derived in an unpublished thesis) whose accuracy is suspect. The correct procedure is believed to be to replace $\eta_g$ in eqn. (27) by the surface impedance of the ground and the earth system in parallel. This method was proposed in Reference 5 and has also been put forward independently by Abbott.[25]

Fig. 18 shows the variation of the efficiency of a $0.25\lambda$ aerial with the radius of a perfectly conducting earth system. The efficiency has been computed by three methods, namely

(a) From the impedance and the ground-wave field [eqn. (26)].
(b) By ignoring the effect of the system on the ground-wave field for a given current, and considering only its effect on the input impedance.
(c) By the absorbed-energy method. Since this method gives only relative rather than absolute efficiencies, the curves have been scaled for the best fit with curve (a) at small radii.

Methods (a) and (b) agree to 1% for radii up to $0.13\lambda$ and (a) and (c) agree to 1% for radii up to $0.4\lambda$. Consideration of a $0.55\lambda$ aerial leads to approximately the same conclusions. Since, however, practical earth systems have far less effect near their outer edges than have perfectly conducting ones, it is considered that the absorbed-energy method can safely be employed for radii up to $0.5\lambda$ at least, i.e. to all systems at present used for medium-wave broadcasting in Great Britain. It would, however, be necessary to use the method given in Section 6.2 to calculate the efficiency for one earth system. This should preferably be perfectly conducting and of small radius—say $0.05\lambda$—so that its effect on the ground-wave field can be neglected. Once the absolute efficiency for one earth system has been obtained in this way, the efficiency for others may be derived by using the absorbed-energy method to compute differences in efficiency.

Abbott[25] used this method to deduce the number and length of the radial earth-wires that would be desirable on economic grounds, neglecting the cost of land and balancing the cost of buried copper against that of r.f. power. This approach indicated an optimum radius exceeding one wavelength in some cases, but the failure of the method at large radii is believed to have led to an over-estimate. In any case, it would be necessary to take the value of land into account in Great Britain.

### (7) VERTICAL RADIATION PATTERN

This Section will be concerned mainly with anti-fading mast-radiators having an effective height slightly greater than $0.5\lambda$. The vertical radiation pattern exhibits a minimum at an angle to the vertical depending upon the height. The imperfect conductivity of the ground affects the field in the neighbourhood of this minimum in two ways: the minimum is moved to a greater angle from the vertical, and the minimum field is increased. The latter effect is undesirable, and it is of interest to know to what extent it is reduced by the earth system.

Before this problem was approached theoretically, an experimental investigation with small-scale models had shown that a useful improvement could not be effected by the use of an earth system of practicable size. In any case, it was found in practice that the unevenness of the ground contours in the neighbourhood of the station had a far more serious effect than imperfect conductivity. Nevertheless, it is desirable to compare theoretical and experimental results in order to check the compensation theorem in its application to earth systems.

The method of analysis employed in Section 5.3.2 can be extended so as to obtain the effect of the earth system on the radiation pattern, the principal modification being the replacement of $J_1(\beta r)$ by $J_1(\beta r \sin \theta)$, where $\theta$ is the angle to the vertical.

Fig. 18.—The efficiency of a $0.25\lambda$ aerial computed by three methods.
Perfectly conducting earth system and highly conducting ground ($\epsilon_r = 20 - j180$).
(a) Complete theory.
(b) Considering input impedance only.
(c) Absorbed-energy method [scaled to fit (a) at small radii].
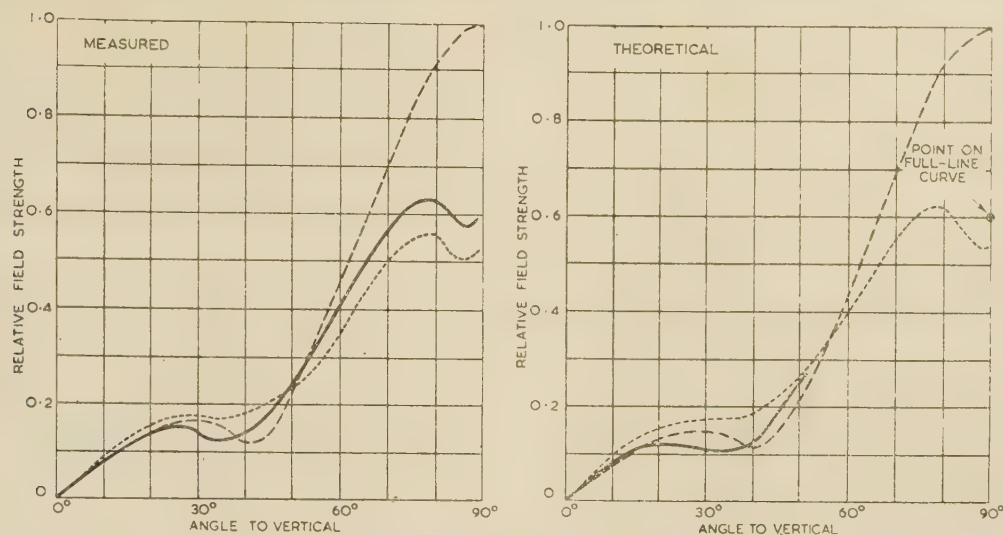
**Fig. 19.**—The effect of an earth system on the vertical radiation pattern.

0·55λ base-fed aerial of characteristic impedance 245 ohms.
– – – – Perfectly conducting ground.
- - - - - Imperfectly conducting ground, $\epsilon_r = 80 - j36$.
———— Imperfectly conducting ground with perfectly conducting earth system of λ radius.

This change is almost self-evident, since $J_1(\beta r \sin \theta)$ corresponds to the vertical radiation pattern of a horizontal loop of radius $r$. Some simplifying approximations can be made if consideration is restricted to perfectly conducting earth systems at least one wavelength in radius, and angles to the vertical less than 50°. An isolated point on the vertical radiation pattern can also be obtained at 90° (horizontal) by using the results obtained for the ground-wave field in Section 5.3.2. To save space the analysis will be omitted.

In Fig. 19 theoretical and experimental vertical radiation patterns are compared for a 0·55λ aerial with a perfectly conducting earth system of λ radius. In the experiments, which have already been described,[2] imperfectly conducting ground was simulated by a solution of salt in water having a relative permittivity of $80 - j36$. At angles exceeding 70° to the vertical the measured pattern was affected by the finite distance (9·4λ). A correction for this effect has therefore been applied to the theoretical curves.

The three theoretical patterns are scaled for the same aerial current, and the experimental patterns are scaled to fit the theoretical patterns exactly at 90°.

The agreement between the theoretical and experimental results is quite good. It will be seen that the effect of the earth system is beneficial, since the sky-wave field strength is reduced over the important range of angles (20°–40°) while the ground-wave field has been increased. It must, however, be borne in mind that an earth system which is perfectly conducting to a radius of λ is hardly practicable in Great Britain. The effect of a system 0·5λ in radius has been found to be insignificant.

## (8) CONCLUSIONS

In practice, the importance of the earth system at a medium-wave transmitting station resides solely in its effect on the efficiency of the radiating system. A system extensive enough to effect a useful improvement in the vertical radiation pattern would not be practicable in Great Britain.

Efficiency is difficult to measure accurately, and direct experimental evidence in support of the theoretical results is therefore lacking at present. Nevertheless, such experiments as have been carried out have confirmed the general order of magnitude of the predicted increase in efficiency resulting from an extension of the earth system. Moreover, an extension of the theory to the vertical radiation pattern has enabled the method to be checked experimentally.

The results of most practical importance are contained in Fig. 17, which shows the effect of the radius of the system on the efficiency. Although only three heights of aerial are considered, it should be possible to determine the earth system required in most cases.

It is always beneficial to erect a transmitting aerial on a site of high conductivity, say $10^{-2}$ mho/m. In this case, at low-power stations where the effective height of the aerial is between 0·1 and 0·25λ, there is little to be gained by installing an earth system more than 0·2λ in radius. Should it be possible to reduce the area of the site required, by curtailing the length of some of the earth wires to, say, 0·1λ, the saving of land would justify the small loss of efficiency. An earth system of 72 wires is believed to offer a reasonable compromise between cost and efficiency in the majority of cases.

For low-power stations on sites of low conductivity $(10^{-3}$ mho/m), an earth system 0·3λ in radius is sufficient.

At high-power stations with anti-fading mast radiators it has been the usual practice to install an earth system about 0·5λ in radius. Fig. 17 shows that this radius is unnecessarily great on a site of high conductivity, where there is little to be gained by a radius greater than 0·2λ. A radius of 0·4λ is, however, desirable for a site of low conductivity, particularly if loop feeding or double feeding is adopted.

## (9) ACKNOWLEDGMENTS

## 10) REFERENCES

(1) BALLANTINE, S.: 'High Quality Radio Broadcast Transmission and Reception', *Proceedings of the Institute of Radio Engineers*, 1934, **22**, p. 564.

(2) PAGE, H., and MONTEATH, G. D.: 'The Vertical Radiation Patterns of Medium-Wave Broadcasting Aerials', *Proceedings I.E.E.*, Paper No. 1714 R, May, 1955 (**102** B, p. 279).

(3) METZLER, E.: 'Sur un récent développement de l'antenne-pylône antifading', *Journal des Télécommunications*, 1940, **7**, p. 61.

(4) MILLINGTON, G.: 'Ground-Wave Propagation over an Inhomogeneous Smooth Earth', *Proceedings I.E.E.*, Paper No. 794, January, 1949 (**96**, Part III, p. 53).

(5) MONTEATH, G. D.: 'Application of the Compensation Theorem to Certain Radiation and Propagation Problems', *ibid.*, Monograph No. 3, October, 1951 (**98**, Part IV, p. 23).

(6) WAIT, J. R., and SURTEES, W. J.: 'Impedance of a Top-Loaded Antenna of Arbitrary Length over a Circular Grounded Screen', *Journal of Applied Physics*, 1954, **25**, p. 553.

(7) WAIT, J. R., and POPE, W. A.: 'The Characteristics of a Vertical Antenna with a Radial Conductor Ground System', *Applied Scientific Research*, 1954, B, **4**, p. 177.

(8) WAIT, J. R., and POPE, W. A.: 'Input Resistance of L.F. Unipole Aerials', *Wireless Engineer*, 1955, **32**, p. 131.

(9) CLEMMOW, P. C.: 'A Method for the Exact Solution of a Class of Two-Dimensional Diffraction Problems', *Proceedings Royal Society*, 1951, A, **205**, p. 286.

(10) WESSEL, W.: 'On the Passage of E.M. Waves through a Wire Grid', *Hochfrequenztechnik*, 1939, **54**, p. 62.

(11) BROWN, G. H.: 'The Phase and Magnitude of Earth Currents Near Radio Transmitting Antennas', *Proceedings of the Institute of Radio Engineers*, 1935, **23**, p. 168.

(12) WELLS, N.: 'Aerial Characteristics', *Journal I.E.E.*, 1942, **89**, p. 106.

(13) BARROW, W. L.: 'On the Impedance of a Vertical Half-Wave Antenna above an Earth of Finite Conductivity', *Proceedings of the Institute of Radio Engineers*, 1935, **23**, p. 150.

(14) HANSEN, W. W., and BECKERLEY, J. G.: 'Radiation from an Antenna over a Plane Earth of Arbitrary Characteristics', *Physics*, 1936, **7**, p. 220.

(15) HANSEN, W. W., and BECKERLEY, J. G.: 'Concerning New Methods of Calculating Radiation Resistance, either with or without Ground', *Proceedings of the Institute of Radio Engineers*, 1936, **24**, p. 1594.

(16) SOMMERFELD, A., and RENNER, F.: 'Radiation Energy and Earth Absorption for Dipole Antennae', *Wireless Engineer*, 1942, **19**, pp. 351, 409, 457.

(17) NORTON, K. A.: 'The Propagation of Radio Waves over the Surface of the Earth, and in the Upper Atmosphere, Part 1: Groundwave Propagation from Short Antennas', *Proceedings of the Institute of Radio Engineers*, 1936, **24**, p. 1367.

(18) NORTON, K. A.: 'The Propagation of Radio Waves over the Surface of the Earth and in the Upper Atmosphere, Part II: The Propagation from Vertical, Horizontal and Loop Antennas over a Plane Earth of Finite Conductivity', *ibid.*, 1937, **25**, p. 1203. (Note Table 1 on p. 1222.)

(19) BEKEFI, G.: 'The Impedance of an Antenna above a Circular Ground Plate Laid upon a Plane Earth', *Canadian Journal of Physics*, 1954, **32**, p. 205.

(20) WILLIAMS, H. PAUL: 'Antenna Theory and Design' (Pitman, London, 1950).

(21) NORTON, K. A.: 'The Calculation of Groundwave Field Intensity over a Finitely Conducting Spherical Earth', *Proceedings of the Institute of Radio Engineers*, 1941, **29**, p. 623.

(22) BOOKER, H. D.: 'Slot Aerials and their Relation to Complementary Wire Aerials (Babinet's Principle)', *Journal I.E.E.*, 1946, **93**, Part IIIA, p. 620.

(23) GIHRING, H. E., and BROWN, G. H.: 'General Consideration of Tower Antennas for Broadcast Use', *Proceedings of the Institute of Radio Engineers*, 1935, **23**, p. 311.

(24) BROWN, G. H., LEWIS, R. F., and EPSTEIN, J.: 'Ground Systems as a Factor in Antenna Efficiency', *ibid.*, 1937, **25**, p. 753.

(25) ABBOTT, F. R.: 'Design of Optimum Buried-Conductor R.F. Ground System', *ibid.*, 1952, **40**, p. 846.

# A RAPID METHOD OF ANALYSING THE M.M.F. WAVE OF A SINGLE OR POLYPHASE WINDING

By R. F. BURBIDGE, B.Sc., Graduate.

## SUMMARY

The usual method of evaluating the harmonic components of the m.m.f. wave of a polyphase winding is to perform a Fourier analysis. This can, however, be a long and tedious process, especially for stepped waveforms, and further it is common practice to perform the analysis for two limiting current-vector positions, to provide a check on the results.

The method described here is exceptionally simple to apply, and makes use of the well-known standard winding factors. It is shown that, by simple substitution, the magnitudes of the Fourier fundamental and harmonic components of the m.m.f. in the air-gap can be found directly, although no indication is given of their relative phase angles. The mathematics of the proof has been fitted as closely as possible to the conditions prevailing in a real machine winding, whilst at the same time maintaining generality of treatment.

The value of the method is exemplified in the last Section of the paper, by carrying out the analysis for an m.m.f. wave of some complexity. The ease of the method is at once apparent.

## LIST OF SYMBOLS

$C$ = Number of coils per phase.

$c$ = A particular coil of a winding (used as a suffix).

$N_c$ = Number of turns comprising coil $c$.

$2\alpha_c$ = Span of coil $c$.

$\beta_c$ = Angular displacement of axis of coil $c$ from arbitrary datum.

$2\epsilon$ = Small angular spread of each coil.

$a$ = Number of similar parallel paths into which each phase is divided.

$r$ = Radius of armature.

$\theta$ = General electrical angle measured from arbitrary datum.

$m$ = Order of a harmonic in armature m.m.f. distribution and conductor distribution.

$n$ = Order of a harmonic in resultant flux distribution.

$F(\theta)$ = M.M.F. distribution as a function of $\theta$.

$f(\theta)$ = Conductor distribution as a function of $\theta$.

$B$ = Flux density.

$B_{on}$ = Peak magnitude of $n$th harmonic component of air-gap flux density.

$\omega$ = Angular velocity of fundamental flux component.

$v_n$ = Instantaneous e.m.f. induced in a phase winding by $n$th harmonic component of flux density.

$V_{om}$ = Peak value of the e.m.f. induced in a phase winding by $m$th harmonic component of flux density.

$V'_{om}$ = Peak value of e.m.f. induced by the $m$th harmonic component of flux density in a hypothetical phase winding, consisting of a single concentrated coil with an equivalent span equal to the $m$th harmonic pole pitch, and with the same total number of turns and parallel paths as the actual winding.

$k_{wm}$ = $m$th harmonic winding factor.

$i_p$ = Instantaneous phase current.

$N_p$ = Turns in series per phase per pole pair.

$F_{omp}$ = Peak value of $m$th harmonic component of m.m.f. for one phase alone.

$F_{om}$ = Peak value of $m$th harmonic component of m.m.f. for a complete 3-phase winding.

$k_{dm}$ = Distribution factor.

$k_{pm}$ = Coil-pitch factor.

$k_{cm}$ = Connection factor.

*Note.*—This analysis is performed for a hypothetical winding of one pole-pair per phase. As the purpose of the analysis is to calculate a factor which will apply to each pole, whatever the number of poles, the ultimate result will not be affected, but a constant multiplier in the proof is avoided.

## (1) INTRODUCTION

By the orthodox method of Fourier analysis, both the magnitudes and the relative phase angles of the harmonic components of an m.m.f. wave can be found, but in practice it is usually only the magnitudes which are significant, because a study of the relative values of these will indicate, for example, whether or not an induction motor is likely to crawl or to be noisy in operation. This method gives the magnitudes in a very simple manner, as follows.
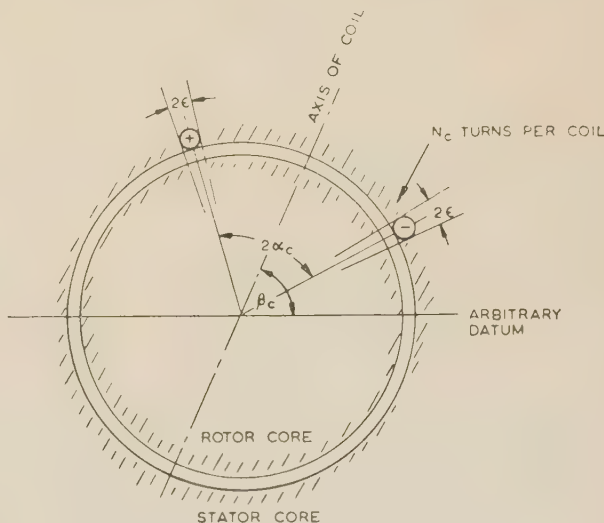


Fig. 1.—Typical coil of phase winding.

Suppose that each phase winding is represented by a finite number of coils, $C$, each of $N_c$ turns of pitch $2\alpha_c$, and displaced by an angle $\beta_c$ from an arbitrary zero, as shown in Fig. 1, where $\beta_c$ is different for each coil. The coils are assumed to be connected in series-parallel with $a$ similar parallel paths.

To obtain the required results, expressions are first derived for two related quantities. One quantity is the space distribution of the magnetizing force exerted by the conductors when carrying current, which is directly related to the waveform of flux in the air-gap; the other is the space distribution of the conductors themselves. The resultant e.m.f.'s induced in the conductors by the component fluxes are next deduced, and this enables the winding factors of the machine, for the various harmonic components, to be derived. These are then combined with the first two expressions to calculate the various component m.m.f.'s in terms of the winding factors.

The result for one phase-winding having been obtained, the last Section of the paper shows how to analyse the resultant m.m.f. wave of three phase-windings when combined to form a single polyphase winding.

Some previous authors have been aware of the methods of calculation developed in this paper, a leading example being Alger.* In all cases of which the present author knows, however, the result has been obtained or quoted under some restricting condition, such as dealing specifically with 3-phase windings, or ignoring harmonics of even order or triple harmonics. This proof is believed to be the first logical treatment in general terms, starting from first principles.

## (2) FOURIER SERIES FOR THE M.M.F. DISTRIBUTION AND CONDUCTOR DISTRIBUTION OF A PHASE WINDING

It is proposed to derive an expression for the m.m.f. distribution and conductor distribution of the winding in terms of a Fourier series, developing this from the series for a single coil.

The m.m.f. distribution of a single coil is shown in Fig. 2(a).



(a)



(b)
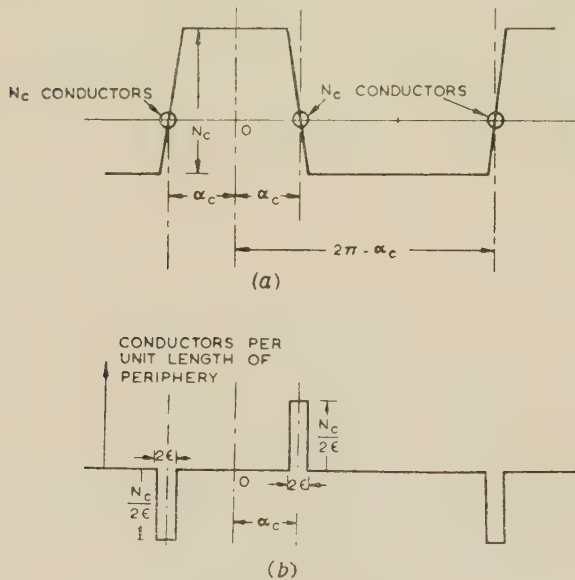
Fig. 2.—M.M.F. distribution and conductor distribution of a phase winding.

(a) M.M.F. distribution (with unit conductor current).
(b) Conductor distribution.

The vertical scale of this graph is arbitrary, since it depends on the current flowing in the coil. The corresponding conductor distribution is shown in Fig. 2(b). The coil sides are assumed to be spread over a small angle $2\epsilon$ which tends to zero in the limiting case.

* ALGER, P. L.: 'The Nature of Polyphase Induction Machines' (Wiley, 1920), pp. 68–79.

The Fourier series for the m.m.f. distribution of a particular coil c, when carrying unit current and when $2\epsilon \to 0$, can be shown by the usual methods to be

$$F_c(\theta) = \frac{2N_c}{\pi} \sum_{m=1}^{\infty} \left( \frac{\sin m\alpha_c}{m} \right) \cos m(\theta - \beta_c)$$

where $\beta_c$ is the angular displacement of this coil from the datum position. The m.m.f. distribution will so set itself about the horizontal axis that the positive and negative areas are equal, and therefore no constant term appears in this equation.

The corresponding expression for the conductor distribution can be shown to be

$$f_c(\theta) = \frac{2N_c}{\pi} \sum_{m=1}^{\infty} \sin m\alpha_c \sin m(\theta - \beta_c)$$

Making a summation for all the coils, the Fourier series for the m.m.f. distribution of the complete phase winding becomes

$$F(\theta) = \frac{2N_c}{\pi} \sum_{c=1}^{C} \sum_{m=1}^{\infty} \left( \frac{\sin m\alpha_c}{m} \right) \cos m(\theta - \beta_c) \quad . \quad (1)$$

and that for the corresponding conductor-distribution becomes

$$f(\theta) = \frac{2N_c}{\pi} \sum_{c=1}^{C} \sum_{m=1}^{\infty} \sin m\alpha_c \sin m(\theta - \beta_c) \quad . \quad . \quad (2)$$

## (3) E.M.F.'S INDUCED IN A PHASE WINDING BY THE COMPONENT FLUXES

To simulate the actual conditions present in an induction machine, each harmonic flux component will be supposed to have a synchronous speed inversely proportional to the order of the harmonic, i.e. the nth harmonic will rotate at $1/n$th of the synchronous speed of the fundamental flux wave.

Only the magnitudes of the e.m.f.'s due to the component harmonic fluxes are required, so that the directions of rotation assigned to the component fluxes are unimportant. For simplicity, therefore, they will all be assumed to have the same direction of rotation, although in a real induction motor the direction of rotation depends on the order of the harmonic.

Let the nth harmonic of the rotating flux be represented by

$$B_n = B_{on} \cos (n\theta + \omega t + \psi_n) \quad . \quad . \quad . \quad . \quad (3)$$

where $\psi_n$ is arbitrary and $n$ can have any one integral value. (The flux wave contains an infinite number of harmonic components, of peak magnitudes $B_{on}$, each rotating at its own angular velocity $\omega/n$.)

Using the flux-cutting rule, and assuming unit length of conductor, the total instantaneous e.m.f. induced by the nth harmonic flux component in a small segment ($\delta\theta$) of the conductor distribution, containing $[f(\theta)]\delta\theta$ conductors, is

$$\Delta v_n = B_n\left(\frac{\omega}{n}\right) r f(\theta) \delta\theta \quad . \quad . \quad . \quad . \quad (4)$$

where $B_n$ is the magnitude of the nth harmonic flux density at angle $\theta$; $\omega/n$ is the angular velocity of this component of flux density; and $r$ is the radius of the armature.

Substituting in eqn. (4) for $B_n$ from eqn. (3), and for $f(\theta)$ from eqn. (2), it follows that

$$\Delta v_n =$$

$$\frac{2B_{on}\omega r}{n\pi} \sum_{c=1}^{C} \sum_{m=1}^{\infty} N_c \sin m\alpha_c \sin m(\theta - \beta_c) \cos (n\theta + \omega t + \psi_n) d\theta$$

$$. \quad . \quad . \quad (5)$$

Now, the conductors in each phase are series-parallel con-

nected with $a$ similar parallel paths, and so the net instantaneous e.m.f. induced in the complete phase winding by the $n$th harmonic component of flux density is obtained by integrating with respect to $\theta$ right round the armature.

Therefore

$$v_n = \frac{1}{a} \int_{\theta=0}^{\theta=2\pi} \Delta v_n d\theta \quad . \quad . \quad . \quad . \quad . \quad (6)$$

Substituting for $\Delta v_n$ from eqn. (4) and rearranging, it follows in general, that

$$v_n = \frac{2B_{on}\omega r}{an\pi} \sum_{c=1}^{C} \sum_{m=1}^{\infty} N_c \sin m\alpha_c$$

$$\int_{0}^{2\pi} \sin m(\theta - \beta_c) \cos(n\theta + \omega t + \psi_n)d\theta \quad . \quad (7)$$

When $n$ is given one particular value, numerically equal to $m$, this can be reduced to

$$v_n = -\frac{2B_{on}\omega r}{am} \sum_{c=1}^{C} N_c \sin m\alpha_c \sin(m\beta_c + \omega t + \psi_n)$$

When $n$ is not equal to $m$, $v_n$ is always zero, as simple integration will show.

This establishes, in the most general terms, the very important fundamental principle that only the $m$th harmonic component of flux can induce a net e.m.f. in the $m$th harmonic component of conductor distribution. The remaining harmonic components of the flux, of orders other than $m$, will induce zero net e.m.f. in the $m$th harmonic component of conductor distribution.

Where $n$ is equal to $m$, the instantaneous e.m.f., $v_n$, can be rewritten as

$$v_n = -\frac{2B_{on}\omega r}{am} \sum_{c=1}^{C} N_c \sin m\alpha_c \sin m\beta_c \cos(\omega t + \psi_n)$$

$$- \frac{2B_{on}\omega r}{am} \sum_{c=1}^{C} N_c \sin m\alpha_c \cos m\beta_c \sin(\omega t + \psi_n)$$

The peak value of this is given by

$$V_{om} = -\frac{2B_{on}\omega r}{am}\left[\left(\sum_{c=1}^{C} N_c \sin m\alpha_c \sin m\beta_c\right)^2\right.$$

$$\left. + \left(\sum_{c=1}^{C} N_c \sin m\alpha_c \cos m\beta_c\right)^2\right]^{1/2} \quad . \quad (8)$$

### (4) THE HARMONIC WINDING FACTORS OF A PHASE WINDING

The winding factor of a machine, as the term will be understood here, is the product of its pitch (or chord) factor and its distribution (or spread) factor and a further factor, which is unity in most common cases, and which can be called the 'connection factor'. This latter factor is exemplified in Section 7.

The $m$th harmonic winding factor, $k_{wm}$, of a phase winding can thus be defined as the ratio

$$k_{wm} = \frac{V_{om}}{V'_{om}} \quad . \quad . \quad . \quad . \quad . \quad (9)$$

where these terms have the exact meanings defined in the list of symbols.

The total number of turns in the winding is $\sum_{c=1}^{C} N_c$ since there are $N_c$ turns per coil; and therefore there are $2\sum_{c=1}^{C} N_c$ conductors in all, and $\frac{2}{a}\sum_{c=1}^{C} N_c$ conductors in series.

The denominator, $V'_{om}$, of eqn. (9) can therefore be written as

$$V'_{om} = B_{om}\left(\frac{\omega}{m}\right)r\frac{2}{a}\sum_{c=1}^{C} N_c$$

or, rearranging,

$$V'_{om} = \frac{2B_{om}\omega r}{am}\sum_{c=1}^{C} N_c \quad . \quad . \quad . \quad . \quad (10)$$

Substituting from eqns. (8) and (10) in eqn. (9), the expression for the harmonic winding factor becomes

$$k_{wm} = \frac{1}{\sum_{c=1}^{C} N_c}\left[\left(\sum_{c=1}^{C} N_c \sin m\alpha_c \sin m\beta_c\right)^2\right.$$

$$\left. + \left(\sum_{c=1}^{C} N_c \sin m\alpha_c \cos m\beta_c\right)^2\right]^{1/2} \quad . \quad (11)$$

### (5) THE COMPONENTS OF M.M.F. DUE TO ONE PHASE-WINDING

Assuming an instantaneous phase current, $i_p$, the conductor current will be $i_p/a$ and the product of this current and the m.m.f. distribution, eqn. (1), gives an expression for the m.m.f. wave, i.e.

$$F(\theta) = \frac{2i_p}{a\pi}\sum_{c=1}^{C}\sum_{m=1}^{\infty} N_c \frac{\sin m\alpha_c}{m}\cos m(\theta - \beta_c) \quad . \quad (12)$$

The $m$th harmonic component of m.m.f. is therefore

$$F_m(\theta) = \frac{2i_p}{a\pi}\sum_{c=1}^{C} N_c \frac{\sin m\alpha_c}{m}\cos m(\theta - \beta_c) \quad . \quad . \quad (13)$$

The peak value of this m.m.f. component is given by

$$F_{omp} = \frac{2i_p}{ma\pi}\left[\left(\sum_{c=1}^{C} N_c \sin m\alpha_c \sin m\beta_c\right)^2\right.$$

$$\left. + \left(\sum_{c=1}^{C} N_c \sin m\alpha_c \cos m\beta_c\right)^2\right]^{1/2} \quad . \quad (14)$$

By substituting the expression for the winding factor, $k_{wm}$, given in eqn. (11), eqn. (14) can be reduced to

$$F_{omp} = \frac{2}{m\pi}i_p\frac{\sum_{c=1}^{C} N_c}{a}k_{wm} \quad . \quad . \quad . \quad . \quad (15)$$

But $\dfrac{\sum_{c=1}^{C} N_c}{a}$ are the total turns in series per phase $= N_p$; and

$\dfrac{\sum_{c=1}^{C} N_c}{2a}$ are the turns acting on the centre of a single pole $= N_p/2$.

Therefore

$$F_{omp} = \frac{4}{m\pi}k_{wm}\frac{N_p i_p}{2} \quad . \quad . \quad . \quad . \quad (16)$$

But $N_p i_p/2$ is a constant, equal to the space maximum of the m.m.f. of one phase, in ampere-turns, which acts on the centre of each pole; and the corresponding values of the fundamental and the harmonic m.m.f.'s can thus be obtained by determining the product $4k_{wm}/n\pi$. This quantity is always easy to calculate, $k_{wm}$ in the commoner cases being merely the product of the spread and chord factors.

### (6) THE RESULTANT M.M.F. OF A SYMMETRICAL 3-PHASE WINDING

All phases of a symmetrical 3-phase winding are identical, and each is ordinarily displaced from the adjacent phases by $2\pi/3$ electrical radians. It will be shown here that the magnitudes of

the fundamental and harmonic components of the m.m.f. wave of the complete winding when supplied with a balanced 3-phase current, and their directions of rotation, can be simply determined from the magnitude of the fundamental and harmonic components of the m.m.f. wave of one phase of the winding.

The distribution of the magnetizing turns, $N$, due to the phases $A$, $B$ and $C$ respectively, acting at any angular position $\theta$ around the air-gap, may be represented by the expressions

$$N \begin{Bmatrix} A \\ B \\ C \end{Bmatrix} = \sum_{m=1}^{\infty} N_m \cos m \begin{Bmatrix} 0 \\ \theta - 2\pi/3 \\ 4\pi/3 \end{Bmatrix} \quad . \quad . \quad (17)$$

and the current in each phase may be represented by

$$i \begin{Bmatrix} A \\ B \\ C \end{Bmatrix} = I_0 \cos \begin{Bmatrix} 0 \\ \omega t - 2\pi/3 \\ 4\pi/3 \end{Bmatrix} \quad . \quad . \quad (18)$$

Now the m.m.f. of each phase is found from the product of eqns. (17) and (18), taking each phase separately, i.e.

$$iN \begin{Bmatrix} A \\ B \\ C \end{Bmatrix} = I_0 \cos \begin{Bmatrix} 0 \\ \omega t - 2\pi/3 \\ 4\pi/3 \end{Bmatrix} \sum_{m=1}^{\infty} N_m \cos m \begin{Bmatrix} 0 \\ \theta - 2\pi/3 \\ 4\pi/3 \end{Bmatrix}$$
$$. \quad . \quad . \quad (19)$$

The resultant m.m.f., $(iN)_m$, is found by summing the three separate phase m.m.f.'s of eqn. (19), i.e.

$$(iN)_m = \sum_{A,\,B,\,C} \left[ iN \right] \begin{matrix} A \\ B \\ C \end{matrix} = i_A N_A + i_B N_B + i_C N_C$$

$$= \frac{I_0}{2} \Big\{ \sum N_m \cos(m\theta + \omega t) + \sum N_m \cos(m\theta - \omega t)$$
$$+ \sum N_m \cos[m\theta + \omega t - (m+1)2\pi/3]$$
$$+ \sum N_m \cos[m\theta - \omega t - (m-1)2\pi/3]$$
$$+ \sum N_m \cos[m\theta + \omega t - (m+1)4\pi/3]$$
$$+ \sum N_m \cos[m\theta - \omega t - (m-1)4\pi/3] \Big\}$$

Since $\cos\phi + \cos(\phi \pm 2\pi/3 + 2\pi\sigma) + \cos(\phi \pm 4\pi/3 + 2\pi\sigma)$ where $\sigma$ is any whole number, is always identically zero for all values of $\phi$, it follows that terms involving $m\theta + \omega t$ vanish where $m = 1, 3, 4, 6$, etc.; and that terms involving $m\theta - \omega t$ vanish where $m = 2, 3, 5, 6$, etc.

The harmonic components of the resultant m.m.f. can thus be expressed in terms of those of the phase m.m.f.:

$$\begin{aligned} [iN]_1 &= \tfrac{3}{2}[I_0 N_1] \cos(m\theta - \omega t) \\ [iN]_2 &= \tfrac{3}{2}[I_0 N_2] \cos(m\theta + \omega t) \\ [iN]_3 &= 0 \\ [iN]_4 &= \tfrac{3}{2}[I_0 N_4] \cos(m\theta - \omega t) \\ [iN]_5 &= \tfrac{3}{2}[I_0 N_5] \cos(m\theta + \omega t) \\ [iN]_6 &= 0 \end{aligned} \right\} \quad . \quad . \quad (20)$$

with a similar sequence of results for all higher-order harmonics.

Thus all the harmonics of orders 1, 4, 7, 10, 13 . . . $(3\lambda + 1)$ . . . rotate in the forward direction; those of orders 2, 5, 8, 11 . . . $(3\lambda - 1)$ . . . rotate in the backward direction; and the triplen harmonics, of orders 3, 6, 9 . . . $3\lambda$ are completely absent. $(\lambda = 1, 2, 3, 4,$ etc.$)$ Further, those harmonics (except triplen) which are present in the phase m.m.f. waveform are also present in the resultant 3-phase m.m.f. wave, but each is increased in magnitude by the factor $3/2$.

It ought to be added that all even harmonics are commonly absent from phase m.m.f. waveforms; but in the uncommon cases when they are present, they are reproduced in the resultant m.m.f. waveforms to the same scale, except where their order is a multiple of 6. These last harmonics, of order $6\lambda$, vanish completely from resultant m.m.f. waveforms.

Using the result already obtained in eqn. (16) for the harmonic components of a single phase-winding, it follows from this Section that the harmonic m.m.f. components of the resultant of three phase-windings, forming a single 3-phase winding, are given by

$$F_{om} = \frac{6}{\pi} \frac{k_{wm}}{m} \frac{N_p I_p}{2} \quad . \quad . \quad . \quad . \quad (21)$$

with the restriction that for $m = 3$, or any multiple of 3, the corresponding harmonic component is always zero.

## (7) EXAMPLE OF ANALYSIS BY THIS METHOD

One of a number of unorthodox windings which the author has recently had occasion to analyse will be used to exemplify the method. The arrangement and directions of the coils in one phase of the winding are shown, together with the corresponding m.m.f. wave, in Fig. 3. It will be observed that this is one phase of an orthodox 8-pole 60°-spread 120°-coil-pitch winding in a 48-slot stator, but with the second four consecutive coil-groups reversed in direction. The winding would, of course, occupy parts of two layers; it is shown diagrammatically in one layer.
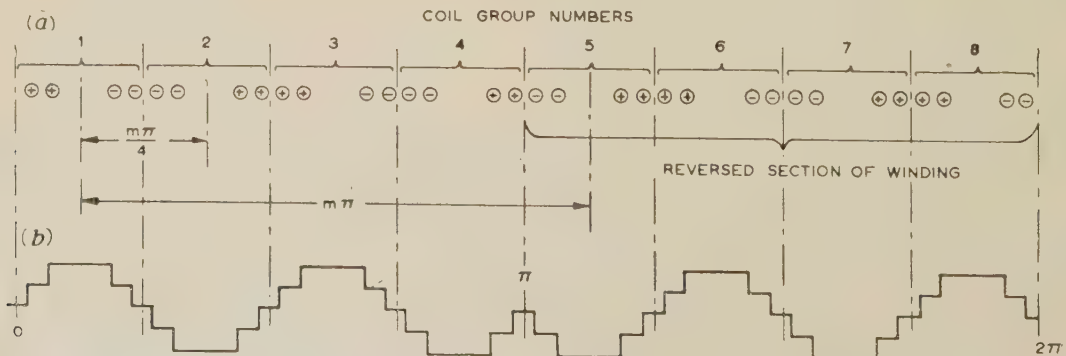


Fig. 3.—Example of m.m.f. analysis.
(a) Coil groups and winding directions of one phase-winding, shown in one layer.
(b) Air-gap m.m.f. wave of one phase-winding.

The wavelength of the winding, after which it repeats itself, is equivalent to an electrical angle of $2\pi$, and is thus equal to the length of the complete section shown. It follows therefore that calculations have to be made on a 2-pole basis rather than on an 8-pole basis; i.e. a 6-pole m.m.f. is a 3rd harmonic, and so on.

On this basis, the chord factor or coil-pitch factor for the $m$th harmonic is

$$k_{pm} = \sin\left[\frac{m}{4}\left(\begin{array}{c}\text{Half the fundamental}\\ \text{coil-pitch angle}\end{array}\right)\right] = \sin\frac{m\pi}{12}$$

and, since there are 2 slots per coil group, the spread or distribution factor is

$$k_{dm} = \frac{\sin\dfrac{m\pi}{24}}{2\sin\dfrac{m\pi}{48}} = \cos\frac{m\pi}{48}.$$

These two factors, $k_{pm}$ and $k_{dm}$, are common to all polyphase motor windings and their product normally constitutes the winding factor. In this example, however, an additional term arises owing to the unusual method of connection of the coil groups; this connection factor can be derived in a manner similar to the familiar derivation of the spread factor.

Let the maximum e.m.f. per coil be $v$. Then the resultant e.m.f., $v_{1234}$, for the first four coil groups is $v_1 - v_2 + v_3 - v_4$ having regard to the directions of the coils. Rearranging this in the form $(v_1 + v_3) - (v_2 + v_4)$, it can at once be seen from the vector diagram, Fig. 4, that it is equal to $4v\sin\dfrac{m\pi}{8}\cos\dfrac{m\pi}{4}$.

Now, $v_{1234}$ and the resultant e.m.f. for the second four coil groups, $v_{5678}$, are separated by an angle $m\pi$ and are in opposition. They are thus additive for odd flux harmonics and of opposite sign for even harmonics, so that the resultant e.m.f. for all the coils is

$$v_r = 8v\sin\frac{m\pi}{8}\cos\frac{m\pi}{4}\sin\frac{m\pi}{2}$$

($v_r$ will be zero for $m = 2, 4, 6$, etc., and equal to $2v_{1234}$ for $m = 1, 3, 5$, etc.)

The connection factor is therefore

$$k_{cm} = \left(\frac{v_r}{8v}\right) = \sin\frac{m\pi}{8}\cos\frac{m\pi}{4}\sin\frac{m\pi}{2}.$$

The complete winding factor, then, is

$$k_{wm} = k_{pm}k_{dm}k_{cm} = \sin\frac{m\pi}{12}\cos\frac{m\pi}{48}\sin\frac{m\pi}{8}\cos\frac{m\pi}{4}\sin\frac{m\pi}{2}.$$

With $N_p$ turns in series per phase and a peak phase current of $I_p$, the space-maximum of the $m$th harmonic component of air-gap m.m.f. for one phase alone is, by substitution in eqn. (16),

$$F_{omp} = \frac{4}{m\pi}\frac{I_pN_p}{2}\sin\frac{m\pi}{12}\cos\frac{m\pi}{48}\sin\frac{m\pi}{8}\cos\frac{m\pi}{4}\sin\frac{m\pi}{2}.$$
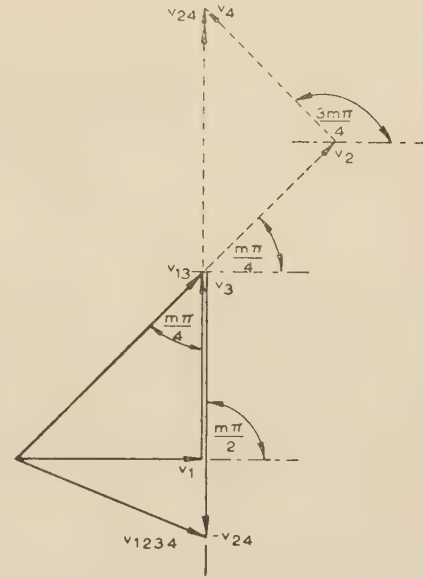


Fig. 4.—Vector diagram of coil e.m.f.'s in winding used as an example.

$$v_{1234} = 4v\sin\frac{m\pi}{8}\cos\frac{m\pi}{4}$$

where $v = v_1 = v_2 = v_3 = v_4$

Further, if the spacing between the three phase-windings were $2\pi/3$ the space maxima of the harmonic components of the resultant air-gap m.m.f. could be found by substitution in eqn. (21).

Simple substitution from trigonometrical tables in this formula will show that the Fourier coefficients of the m.m.f. wave of one phase of this winding are

Fundamental (2 pole) $= 0\cdot0446I_pN_p$
3rd harmonic (6 pole) $= 0\cdot0967I_pN_p$
5th harmonic (10 pole) $= 0\cdot0764I_pN_p$
7th harmonic (14 pole) $= 0\cdot0216I_pN_p$
9th harmonic (18 pole) $= 0\cdot0114I_pN_p$
11th harmonic (22 pole) $= 0\cdot0076I_pN_p$
13th harmonic (26 pole) $= 0\cdot0057I_pN_p$

etc.

These results have been verified by orthodox methods.

With a spacing of $2\pi/3$ between phase windings, measured on the fundamental 2-pole scale, those of the above harmonics which are multiples of 3 will not appear in the resultant m.m.f. wave. The rest will each be increased by the factor 3/2, remaining unchanged in relative magnitude.

### (8) ACKNOWLEDGMENTS

# DIFFRACTION BY CYLINDRICAL REFLECTORS

## By Professor ROBERT PLONSEY, Ph.D.

### SUMMARY

The electromagnetic diffraction problem is formulated in terms of the determination of the currents induced on a reflector-scatterer by a primary source. All field quantities are readily determined therefrom.

An approximate solution ignores the interaction of currents on the reflector-scatterer in that it relates the surface current to the incident magnetic field. This is the geometrical-optics current. For the strip and circular reflector with line source at its centre, corrections to the geometrical-optics currents are obtained by an approximate analytic technique. In each case this yields an equivalent line current at the edges.

The field of the line current is non-isotropic; its directional gain is determined by appealing to the Sommerfeld half-plane solution. The line currents do not greatly affect the total pattern; this indicates that the main character of the diffraction can be obtained from the geometrical-optics currents.

Measurements of the diffracted field of a circular cylindrical reflector with line feed at its centre were made in a parallel-plane device. A description of some of the features of the equipment is given. The results confirm that geometrical-optics currents are themselves satisfactory, but are inconclusive with respect to the correction line currents.

## (1) INTRODUCTION

The usual procedure for the calculation of scattered fields is first to determine the currents induced on the scatterer by the primary sources, and then to calculate the scattered field from these induced sources. Suitable approximations are often resorted to in order to simplify the work.

In the design of cylindrical reflectors, if the surface current densities be taken as equal to twice the tangential incident magnetic field, and the secondary field be evaluated by the principle of stationary phase, the final result is identical with a ray-optics treatment.[1] Indeed, geometrical optics is widely employed as a basis for reflector design. However, improvements on the geometrical-optics result are often required. Clearly, this may be achieved by means of corrections to the approximate value of induced current, by improved evaluation of the field integral, or both.

It is a matter of interest to learn the seriousness of the above-mentioned approximations. The field integral can always be evaluated rigorously, although numerical techniques may have to be resorted to. However, determination of the currents set up on a reflector normally leads to an integral equation[2] which cannot be solved. We are usually forced to make the geometrical-optics approximation, and this leads to the question of the error involved.

Moullin and Phillips[3] provide an answer to this question for the case of an infinite strip. They discovered that, for a strip $\lambda$ or greater in width, the current distribution due to a normally incident plane wave is very nearly the geometrical-optics value except near the edge. In that region the exact solution compares very closely with the Sommerfeld solution for a half-plane.

Although the current at the edge becomes infinite it exceeds the geometrical-optics value only within $\frac{1}{25}\lambda$ of the edge. This result led to an improved characterization of the surface currents in terms of geometrical-optics currents everywhere plus a line current at each edge. The field set up by these currents is predominantly determined by the geometrical-optics currents, provided that the field integral is evaluated rigorously. The 'edge line currents' contribute only a minor modification.

The strip is re-examined here by a method suggested in the Moullin–Phillips paper; a more general mathematical technique, however, is used. Extension to arbitrary incidence and to the circular strip, with a line feed at its centre, is then readily accomplished. In addition, the spatial character of those currents which contribute to the edge line currents is taken into account, its far-field directional gain being thus determined.

An attempt is made to connect the equivalent edge line current of the plane or circular strip with the Sommerfeld distribution at a half-plane edge. This is analogous to the supposition that the Sommerfeld half-plane solution would approximate the currents in the vicinity of an arbitrary edge. Such an approach was originally suggested by Braunbek.[4] In his solution to the problem of the scalar diffraction by an aperture of a plane wave he obtains a value for the induced sources on the screen by applying the Sommerfeld theory as if the screen had locally a straight edge. The resulting expressions for the circular aperture are more accurate than the Kirchhoff formulae. This assumption should be even more accurate when applied at a 2-dimensional edge. Some papers making use of this or an analogous approach are given in Reference 5.

Measurements were made of the near-zone field of a circular cylindrical reflector with a line source at the centre. This was performed in a parallel-plate device of the type described by Row and others.[6] The plate spacing is chosen less than $\frac{1}{2}\lambda$; this insures TEM propagation only, so that the fields are 2-dimensional in character. Close tolerance in plate spacing is required, and this was achieved by using a bonded honeycomb material which is very light yet requires no stiffeners. The device comprises a large turntable set flush with the lower surface; this permits of field measurements along circular arcs or the taking of azimuthal field patterns.

The measurements confirm that good results can be achieved by the use of geometrical-optics currents for the type of problem considered. The equivalent line currents somewhat improve the agreement between the calculated and measured fields, but not sufficiently to be conclusive.

## (2) DERIVATION OF EDGE CURRENTS

### (2.1) Edge Currents for Half-Plane Diffraction by an Incident Plane Wave

Consider a plane wave incident on a half-plane as shown in Fig. 1. The origin is chosen in the half plane $a/k$ from the edge; $k = 2\pi/\lambda$. If the entire plane were present the surface current would be given everywhere by $\bar{K}_{g.o.} = 2(\bar{n} \times \bar{H}_{inc})$. This is the geometrical-optics condition.
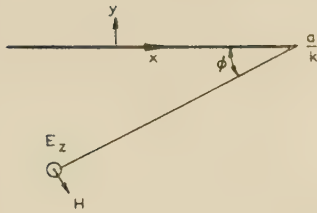
Fig. 1.—Plane wave incident on half-plane.

The half-plane of Fig. 1 is then thought of as resulting from removal of that portion of the full plane for which $x > a/k$. This operation produces a change in the currents on the remaining half-plane; we call this change $K_D$ (deviation from geometrical optics). If the electric field is to vanish over the conducting surface it is clear that the field, $E^0$, produced by the 'deviation currents' must be the same as that which was produced by the geometrical-optics currents on the removed half-plane. For any $a$, $E^0$ is related to the sources producing it as follows:

$$E^0 = \frac{-\omega\mu}{4} \int_{-\infty}^{a/k} K_D H_0^{(2)}(k|x|) dx = \frac{-\omega\mu}{4} \int_{a/k}^{\infty} K_{g.o.} H_0^{(2)}(kx) dx \quad . \quad (1)$$

Substitution of the value of $K_{g.o.}$ from its related value of incident magnetic field yields

$$E^0 = \frac{1}{k} \int_a^{\infty} C_a \varepsilon^{-jv\cos\phi} H_0^{(2)}(v) dv \quad . \quad . \quad . \quad (2)$$

where

$$C_a = \frac{-\omega\mu}{2} \sin\phi \varepsilon^{ja\cos\phi}, \quad kx = v$$

We now make use of an integral representation for the Hankel function:

$$H_0^{(2)}(v) = \frac{-2}{j\pi} \int_0^{\infty} \varepsilon^{-jv\cosh t} dt \quad . \quad . \quad . \quad (3)$$

Eqn. (3) is inserted in eqn. (2) and the order of integration interchanged. By considering $k$ as having a vanishingly small negative imaginary part, the upper limit in the $v$ integration contributes nothing. The result is

$$E^0 = \frac{2C_a}{\pi k} \int_0^{\infty} \frac{\varepsilon^{-ja(\cosh t + \cos\phi)}}{\cosh t + \cos\phi} dt \quad . \quad . \quad (4)$$

This integral can be evaluated in terms of an asymptotic expansion (see Appendix). The result is

$$E^0 = \frac{2C_a}{\pi k} \varepsilon^{-ja\cos\phi} \frac{\varepsilon^{-ja}\varepsilon^{-j\frac{\pi}{4}}}{\sqrt{a}} \sqrt{\frac{\pi}{2}} \frac{1}{1 + \cos\phi}$$

$$\left\{ 1 + \frac{j}{2a(1 + \cos\phi)} - \frac{3}{2[a(1 + \cos\phi)]^2} \cdots \right\} \quad . \quad (5)$$

If we impose the condition

$$\sqrt{a} \cos\frac{\phi}{2} > \sqrt{3} \quad . \quad . \quad . \quad . \quad (6)$$

higher terms in eqn. (5) may reasonably be neglected. This restriction can similarly justify use of the leading term in the asymptotic expansion of $H_0^{(2)}(a)$ for large $a$. If the latter operations are carried out with respect to eqn. (5) we finally have

$$E^0 = \frac{-\omega\mu}{4} \frac{-j2}{k} \tan\frac{\phi}{2} H_0^{(2)}(a) = \frac{-\omega\mu}{4} \int_{-\infty}^{a/k} K_D H_0^{(2)}(k|x|) dx \quad . \quad (7)$$

$E^0$ is consequently equal, asymptotically, to the field of a line current at the edge of strength $-j(2/k) \tan(\phi/2)$. Put another way, the deviation currents, $K_D$, can be replaced by an equivalent line current $I\delta(x - a/k)$, so that eqn. (7) is satisfied if $I = -j(2/k) \tan(\phi/2)$. $\delta(x - a/k)$ is a normalized impulse function that vanishes everywhere except at the edge. A more useful form results if we put

$$\frac{2}{k} = 0 \cdot 159 K_{g.o.}^0 \lambda$$

$K_{g.o.}^0$ is the geometrical-optics current that would result if the incidence were normal (i.e. $K_{g.o.}^0$ is a function not of $\phi$ but of $H_{inc}$ only). Then:

$$I = -j0 \cdot 159\lambda K_{g.o.}^0 \tan\frac{\phi}{2} \quad . \quad . \quad . \quad (8)$$

If $\phi \to 180°$, then $I \to \infty$ from eqn. (8), but note that under these conditions the maximum value of $a$ from eqn. (6) also becomes infinite.

### (2.2) Edge Currents for Half-Plane Diffraction by Incident Wave due to a Line Source

The above procedure may be followed for the case where the incident field is set up by a line source (see Fig. 2). If the
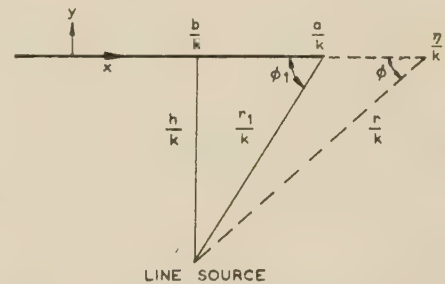


Fig. 2.—Half-plane in presence of line source.

restriction that $h \geqslant 10$ be imposed, the field at the origin due to the currents on the 'removed half-plane', asymptotically for large $a$, will be

$$E^0 = \frac{-j}{k} \frac{1}{1 + \cos\phi_1} K_{g.o.} H_0^{(2)}(\alpha) = \int_{-\infty}^{a/k} K_D H_0^{(2)}(k|x|) dx \quad . \quad (9)$$

As before, the criterion for sufficiently large $a$ is the satisfaction of

$$\sqrt{a} \cos\frac{\phi_1}{2} > \sqrt{3} \quad . \quad . \quad . \quad . \quad (10)$$

Again we may consider $K_D$ to be a line current of strength $I'$ at $a$, where

$$I' = -j0 \cdot 159\lambda K_{g.o.}' \tan\frac{\phi_1}{2} \quad . \quad . \quad . \quad (11)$$

$K_{g.o.}'$ is the geometrical-optics current at the edge, if the line source were located on a perpendicular to the edge. That is, $K_{g.o.}'$ is related to an incident field at the edge which is locally plane and at normal incidence. But this is precisely the definition of $K_{g.o.}^0$; the results are consequently identical. It is thus reasonable to believe that the actual surface currents in the vicinity of the edge as produced by a line source are given to a good approximation by the Sommerfeld currents due to a plane wave whose angle of incidence at the edge is the same as that of the cylindrical wave from the line source.

## (2.3) Diffraction by a Circularly Curved Strip due to a Line Source at its Centre

The techniques used for the half-plane problem can be applied equally well to a circular cylindrical reflector illuminated by a line source at its centre. The current that would flow on a complete cylinder is denoted by the constant $K_u$; we take the incident electric field at the cylinder to be $\sqrt{(\mu/\epsilon)}$. In this case $K_D$ is the 'deviation current' from $K_u$, i.e. $(K_u + K_D)$ is the
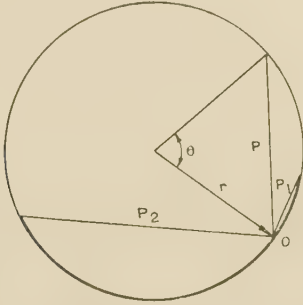


Fig. 3.—Circular strip with line source at its centre.

actual current on the reflector. Referring to Fig. 3, the boundary conditions at the origin will be satisfied if

$$-\frac{1}{4}\sqrt{\frac{\mu}{\epsilon}}\left\{\int_{a_1}^{R}\frac{K_u H_0^{(2)}(v)}{\sqrt{\left[1-\left(\frac{v}{R}\right)^2\right]}}dv + \int_{a_2}^{R}\frac{K_u H_0^{(2)}(v)}{\sqrt{\left[1-\left(\frac{v}{R}\right)^2\right]}}dv\right\}$$

$$=-\frac{1}{4}\sqrt{\frac{\mu}{\epsilon}}\left\{\int_{0}^{a_1}\frac{K_D H_0^{(2)}(v)}{\sqrt{\left[1-\left(\frac{v}{R}\right)^2\right]}}dv + \int_{0}^{a_2}\frac{K_D H_0^{(2)}(v)}{\sqrt{\left[1-\left(\frac{v}{R}\right)^2\right]}}dv\right\}$$

$$\cdots \cdots (12)$$

where $\rho = 2r\sin\theta/2$, $v = k\rho$, $2kr = R$, $a_1 = k\rho_1$, $a_2 = k\rho_2$.

We can show that asymptotically for large $a$ and small $a/R$

$$\int_{0}^{a}\frac{H_0^{(2)}(v)}{\sqrt{\left[1-\left(\frac{v}{R}\right)^2\right]}}dv \simeq 1 + \frac{jH_0^{(2)}(a)}{\sqrt{\left[1-\left(\frac{a}{R}\right)^2\right]}} \quad \cdot \quad (13)$$

By definition:

$$-\frac{1}{4}\sqrt{\frac{\mu}{\epsilon}}\int_{0}^{R}\frac{K_u H_0^{(2)}(v)}{\sqrt{\left[1-\left(\frac{v}{R}\right)^2\right]}}dv = -\frac{1}{2}E_{inc} = -\frac{1}{2}\sqrt{\frac{\mu}{\epsilon}} \quad \cdot \quad (14)$$

If, now, we assume $K_D$ to be the sum of a constant current $K_C$ and a line current at each edge $J_a$, eqn. (12) will be satisfied by separately satisfying two identical equations, one in $a_1$ and the other in $a_2$. If we let $a$ represent either of these, and the substitution of eqns. (14) and (13) into (12) is made, this equation can be written

$$-K_c\left\{1 + \frac{jH_0^{(2)}(a)}{\sqrt{\left[1-\left(\frac{a}{R}\right)^2\right]}}\right\} - \frac{kJ_a H_0^{(2)}(a)}{\sqrt{\left[1-\left(\frac{a}{R}\right)^2\right]}}$$

$$= -2 + K_u + j\frac{K_u H_0^{(2)}(a)}{\sqrt{\left[1-\left(\frac{a}{R}\right)^2\right]}} \quad \cdot \quad (15)$$

This leads to

$$K_c = 2 - K_u; \quad J_a = j0\cdot159\lambda K_{g.o.} \quad \cdots \quad (16)$$

The final result is thus of the same form as for the half-plane. That is, the boundary conditions, except near the edge, are satisfied asymptotically by geometrical-optics currents everywhere plus a 'line current' at each edge. Here again there is a strong suggestion that the actual current distribution near the edge is that given by the Sommerfeld solution for the half-plane.

In order for the error implied by the use of the asymptotic expression of eqn. (13) to be reasonably small, the following criteria is suggested:

$$\frac{a}{R} \leqslant \frac{1}{2}, \quad a \geqslant 6 \quad \cdots \cdots (17)$$

This is related to the criterion of eqn. (6), but in addition involves a restriction on the maximum central angle for the circular reflector ($\simeq 60°$).

## (3) ANALYSIS OF THE SOMMERFELD SOLUTION

The restriction imposed by eqn. (6) suggests that the deviation currents which are responsible for the 'line current' are substantially localized in the region of the edge of width $\sqrt{3}/\cos(\phi/2)$. If this were true, then the requirement that $a \geqslant \sqrt{3}/\cos(\phi/2)$ simply assures that the field point is sufficiently far from the detailed structure of $K_D$ in order that $K_D$ may simulate a line current.

This concept can be examined for the half-plane by an analysis
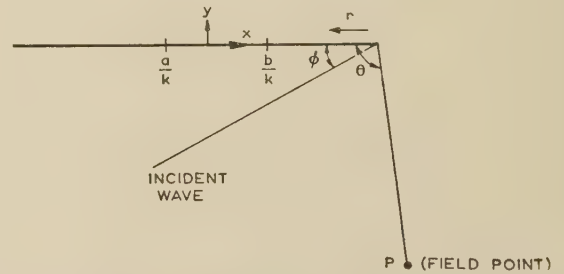


Fig. 4.—Sommerfeld half-plane geometry.

of the Sommerfeld solution. For the geometry of Fig. 4, the current distribution can be expressed as[7, 8]

$$K = \frac{4}{\sqrt{\pi}}\sin\phi\, \varepsilon^{j\left(\frac{4}{\pi}-kr\cos\phi\right)}\left[\frac{\sqrt{\pi}}{2}\varepsilon^{-j\frac{\pi}{4}} - \int_{\sqrt{(2kr)}\cos(\phi/2)}^{\infty}\varepsilon^{-jt^2}dt\right]$$

$$+ 2\left(\frac{2}{\pi}\right)^{1/2}\sin\frac{\phi}{2}\frac{\varepsilon^{-j\left(kr+\frac{\pi}{4}\right)}}{\sqrt{(kr)}} \quad \cdot \quad (18)$$

The geometrical-optics current can be separated out, being essentially the first term of eqn. (18). The remaining expression for $K_D$, if evaluated by means of asymptotic expansions, is

$$K_D \simeq -\frac{\sin\frac{\phi}{2}\varepsilon^{-j\left(kr-\frac{4}{\pi}\right)}}{\sqrt{(2\pi)(kr)^{3/2}\cos^2(\phi/2)}} \cdot \left[\sqrt{(kr)}\cos(\phi/2) \geqslant 6\right] \quad \cdot \quad (19)$$

The field at $a/k$ can be found by summing the contribution of $K_D$ from the edge to $b/k(M_0)$, from $b/k$ to $a/k(M_1)$, from $a/k$ to $\infty$ ($M_2$). Calculation of $M_1$ and $M_2$ yields the following approximate results:

$$M_1 \simeq \frac{E_{LC}\varepsilon^{-j\frac{\pi}{4}}}{\pi\cos(\phi/2)}\sqrt{\frac{\pi}{2}}\sqrt{\frac{a-b}{ab}} \quad \cdots \quad (20)$$

$$M_2 \simeq E_{LC}\left[\frac{j}{2\pi a\cos(\phi/2)}\right] \quad \cdots \quad (21)$$

where $E_{LC}$ is the field of an edge line current.

If $a \gg b$, $\sqrt{(b_{min})} \cos(\phi/2) = \sqrt{3}$, then the current contributing to the field of the equivalent line current lies substantially within $b_{min}$, to an error of approximately 16%. $b_{min}$ is the smallest distance of a field point from the edge in the sense of the condition imposed by eqn. (6). It is thus fairly reasonable to link the fictitious edge line current with the actual deviation currents over the $b_{min}$ region including the edge.

The far field of the equivalent line current should then be related to the field of the Sommerfeld deviation currents integrated from the edge to an appropriate $b \simeq b_{min}$. If the more accurate form for $K_D$ is used [eqn. (18)] the far field is given by

$$E_D = E_{LC}$$

$$\left[ \frac{2 \cos \frac{\phi}{2} \left( \cos \frac{\phi}{2} - \sin \frac{\phi}{2} \right)}{\cos \theta + \cos \phi} - \frac{\varepsilon^{j\frac{\pi}{4}}}{2\sqrt{(\pi)}(2b)^{3/2}} \frac{\varepsilon^{-j2b \sin^2 \frac{\theta}{2}}}{\cos \frac{\phi}{2} \sin^2 \frac{\theta}{2}} \right]$$

$$. \quad . \quad . \quad . \quad (22)$$

to a small error, provided that

$$\sqrt{b} \cos \frac{\phi}{2} \geqslant \sqrt{3}, \quad \sqrt{b} \sin \frac{\theta}{2} \geqslant \sqrt{3} \quad . \quad . \quad . \quad (23)$$

If $R$ is the distance to the field point from the edge, then $R \geqslant 8\pi^2 b^2 \lambda$ for the field point to lie in the far zone.

The quantity in the bracket of eqn. (22) is the directional gain for the equivalent line currents of the previous work. Eqn. (23) actually implies very little restriction on $\theta$ and $\phi$ since we normally take $R$ very large. However, eqn. (22) cannot be used when $\theta = 0$; $\phi = \pi$. It is of interest to note that the region about $\theta = \pi \pm \phi$ must be avoided in the asymptotic solution of the total field as obtained directly from the Sommerfeld solution,[8] thus differing from the result obtained here.

## (4) EXPERIMENTAL EQUIPMENT

### (4.1) General Description

The parallel-plate device consists of 5 ft × 5 ft plates spaced 0·5 in apart. Operation is at $X$-band. A turntable, 28 in diameter, is located at the centre of the lower plate; with the help of spring contacts it forms a portion of the lower electrical surface. The turntable is a machined aluminium casting and rides on a 3-point ball-bearing support.

Pick-up devices can be inserted into the rotating plate at four different radii. One may, alternatively, locate reflectors at these points; this permits rotation of the reflector with respect to its incident field. For the latter case, a fixed detector, located in the stationary part of the lower surface, measures the secondary field pattern. Devices for measuring either magnetic or electric fields are available.

A probe feed is attached to the upper plate through a double eccentric mechanism; this permits the probe to be adjusted so that it is concentric with the turntable axis. The probe itself is interchangeable, thereby allowing for variation in shape or size.

Details of some features of this device follow; other parallel-plane devices which have been constructed involve differences in design according to their special needs.[6]

### (4.2) Absorbers

In order to eliminate reflections from the edge of the parallel-plate region, radially oriented wedge-shaped resistor cards were placed around the circumference of a 2·5 ft radius circle. To facilitate the design, experiments were first conducted in a 2 ft diameter parallel-plate model. A waveguide feed was located at
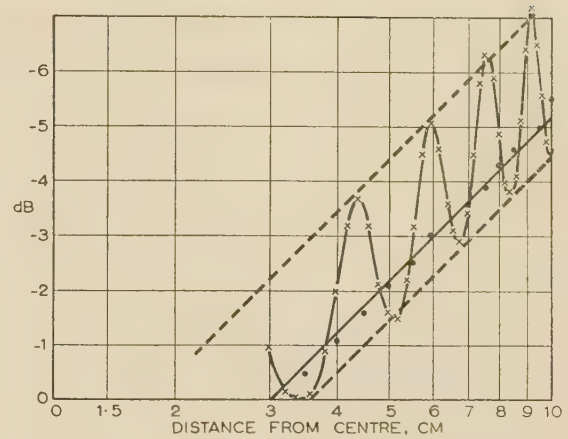


Fig. 5.—Electric field between round parallel plates, along a radius, with an open waveguide feed at the centre.

● Microwave absorbers placed round edges of parallel plates.
× Radiation into free space from parallel plates.

the centre, and the absorbers were arranged along a radial and spaced over a large arc of the outer circle.

Fig. 5 shows the results of such measurements with and without absorbers. As can be noted, a v.s.w.r. of 1·40 was obtained without absorbers. This compares with a calculated value of 1·47 for infinitely thick plates, i.e. radiation into half-space.[9] The curve satisfies the prescribed $1/\rho$ variation and proper wavelength spacing.

With wedges 6 in long, tapered over 5 in of their length, and a circumferential spacing of 0·8 in, a v.s.w.r. of 1·035 is measured. This value remains unchanged if the feed is moved off centre along a radius. However, if the absorbers are set skew to the radial direction the v.s.w.r. increases, as would be expected. For a rotation of about 15° a v.s.w.r. of 1·07 results.

### (4.3) Discontinuity due to Turntable

A clearance of $\frac{3}{16}$ in was allowed between the turntable and the lower sheet opening in which it rotates, spring contacts being employed to cover this gap. The springs were cut out of long strips, bent and cut as shown in Fig. 6. A metal tape was run
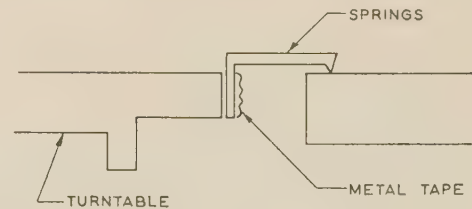


Fig. 6.—Detail of spring contacts at turntable.

around the circumference of the turntable to hold the springs in place. The spring material consisted of 0·003 in shim stock; this made it possible to achieve a very smooth transition. The turntable support is adjustable for vertical movement, thus facilitating proper levelling of the turntable.

In the parallel-plate model a step of 0·032 in was introduced by insertion of a concentric plate. This produced a measured reflection coefficient of 5%; a calculation yields $3\frac{1}{2}$%.[9] This makes clear the necessity for close tolerance in the turntable assembly.

The overall result is revealed in Fig. 7. This shows the magnetic field along a fixed radius in the parallel-plane device. The
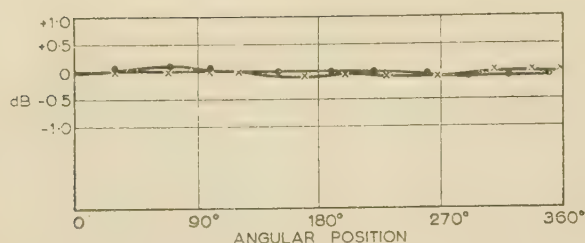
**Fig. 7.**—Measurement of magnetic field between parallel plates with dipole feed at centre.

For 360° rotation of 5·5 in radius pick-up.
Frequency, 9 375 Mc/s.
Maximum deviation, approximately 0·09 dB.
Accuracy of readings, 0·03 dB.
×   No tension in strongback.
●   Tension in strongback.

combined effects of the absorbers, turntable transition, etc., cause a field variation of no greater than ±0·09 dB, and even this perturbation is caused, mostly, by variation in plate spacing.

### (4.4)  The Plates and their Spacing

The plates must be spaced less than $\frac{1}{2}\lambda$ in order to attenuate modes other than TEM. A spacing of 0·50 in allows insertion of X-band guide (and horns), and with a tolerance of 0·500 + 0·100 and −0·000 the attenuation is greater than 12 dB per wavelength to the next higher mode.

A closer tolerance in spacing is desired for some other reasons. First, if a reflector is fixed to the upper plate and makes sliding contact with the turntable, close tolerance in spacing results in greater uniformity of contact. Secondly, since the value of the field is a function of the spacing, significant errors may develop with too wide a tolerance. If the change in spacing is not too abrupt, a perturbation of 0·012 inch in 0·500 inch causes a 0·1 dB change in the field. This effect is probably the major cause of the field variation in Fig. 7.

The parallel sheets are made of 0·030 in seamless aluminium sheet bonded to a 1 in thick aluminium honeycomb. The sandwich is very light and at the same time extremely strong. There is no perceptible sag when supported at its edge and consequently no stiffening members are required. The upper sheet is easily removed for access to the interior; indeed the entire set-up is readily assembled or disassembled.

The sheets arrived reasonably flat (within 0·030 in over the entire sheet). A strongback was used to vary the spacing, somewhat, in the region of the reflector. As indicated by Fig. 7 the overall result is satisfactory.

Metal pins located around the edge have 0·500 in shoulders and are responsible for the spacing. At the same time the pins fit through holes in the upper plate so as to index the upper sheet relative to the lower. This feature is important since it ensures that the probe in the upper plate will remain concentric with the turntable, once an initial adjustment has been made.

### (4.5)  Field Detection Devices

Two pick-ups were constructed, one for electric and the other for magnetic field measurements. The former is simply an adaptor for holding a standard electric probe in one of the four mounting holes located in the turntable.

The magnetic pick-up consists of a small slit in the surface of a plug that fits one of the turntable pick-up holes. This couples magnetic field parallel to the slit into a waveguide behind the slit. Since the slit is in the centre of the guide with its long dimension parallel to the long dimension of the guide, $TE_{10}$ is favourably excited in the pick-up guide. A slit dimension of

0·280 × 0·025 × 0·060 in deep is used. This was designed on the basis of Bethe's[10] formula in conjunction with Cohn's[11] experimental value for the equivalent magnetic polarizability of a rectangular slot; a value of 36·6 dB coupling was calculated and 33·9 dB measured.

The above results are for a matched load as is required in the Bethe theory. The thickness of the slot is taken into account by assuming it equivalent to a corresponding length of guide operating beyond cut-off. For the dimensions given, this results in at least 6 dB separation between the interior of the parallel-plate region and the detector for the dominant mode. Because of this isolation it is permissible to tune the effective shunt susceptance on the detector side of the slit and thereby obtain a larger power output; i.e. in this manner a conjugate load is presented to the slit. This procedure improved the output by as much as 21 dB. Field patterns were not affected by the presence or the degree of tuning. The disadvantage of such tuning is the increased frequency sensitivity of measurements, and close monitoring of signal-generator frequency is required.

A fixed standard electric probe pick-up is located in the stationary part of the lower surface. This is used for obtaining azimuth patterns when the scatterer is fixed to the turntable.

### (4.6)  Reflectors

For the measurements described in the first part of the paper several types of reflector were considered. Their cross-sections appear in Fig. 8. No significant difference was detected in the
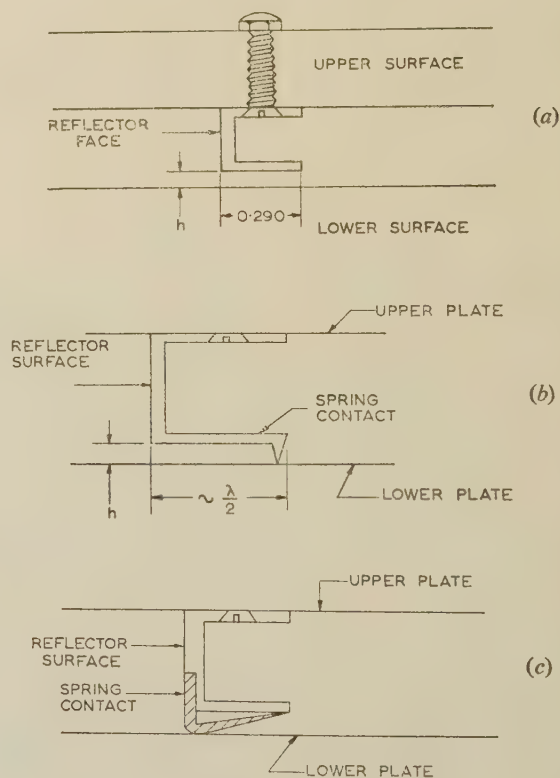


**Fig. 8.**—Types of reflector considered.

(a) Non-contacting reflector.
(b) Choke reflector.
(c) Contacting reflector.

fields they produce, except that with the contacting type of Fig. 8(c) the field along the reflector was somewhat erratic due to mechanical unevenness in the spring contacts.

By means of a special tool, the radius of the reflector relative

to the centre of rotation can be checked. In this manner the reflector can be correctly positioned before being tightened in place.

### (5) EXPERIMENTAL RESULTS

Measurements were made of the magnetic field due to a circular cylindrical reflector fed by a line current at its centre, with field points taken along a circle of the same radius as that of the reflector.

Fig. 9 shows the magnetic field plotted as a function of the indicated angle *a*, as computed both with and without inclusion
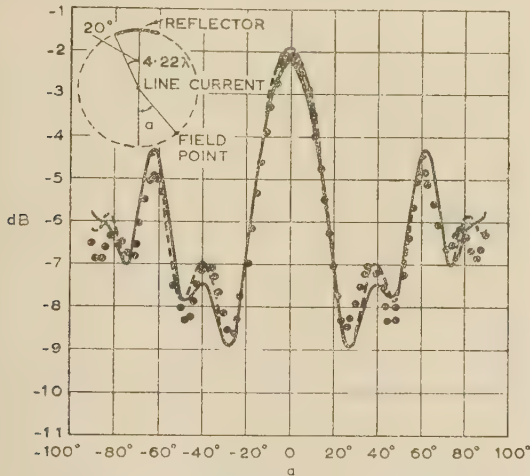


Fig. 9.—Tangential magnetic field for circular reflector and line feed at its centre: frequency, 9100 Mc/s.

——— Calculated from geometrical optics.
– – – Includes equivalent line current at edge.
O O O Measured points.
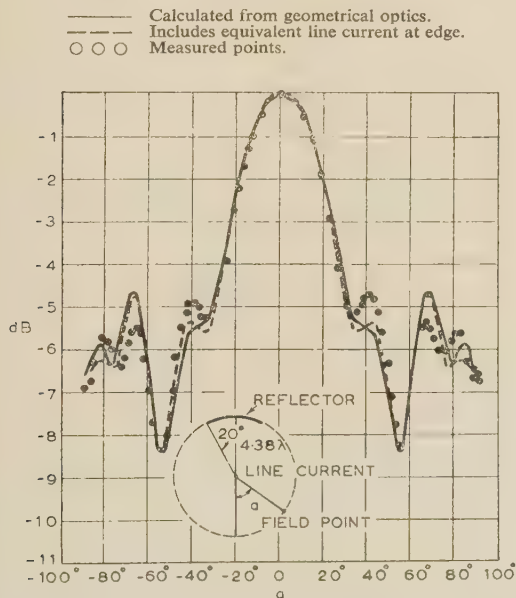


Fig. 10.—Tangential magnetic field for circular reflector and line feed at its centre: frequency, 9375 Mc/s.

——— Calculated from geometrical optics.
– – – Includes equivalent line current at edge.
O O O Measured points.

of the edge line currents, and as measured. Fig. 10 is similar but for a different frequency. The computed field was obtained in terms of Fresnel integrals; the integral evaluation is exact.

A measurement of the magnetic field for a complete 360° traverse is given in Fig. 11 and includes the interesting region in front of the reflector. The moderately smooth response tends to

bear out the notion of the predominance of the geometrical-optics currents. If the edge behaved like its tangent plane the magnetic field would change by 6 dB in going from a point in the aperture to the asymptotic value along the reflector. The measurement in Fig. 11 shows a value of about 5·7 dB, which
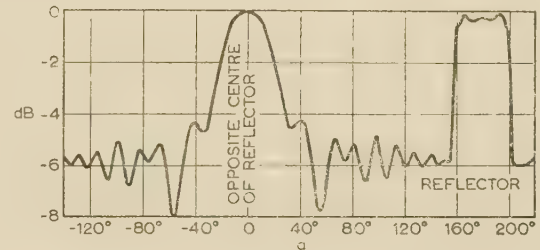


Fig. 11.—Resultant magnetic field for circular reflector and line feed at its centre.

bears out fairly well that the edge of the reflector does behave locally like a plane surface with an incident plane wave.

The reference signal level for Figs. 9, 10 and 11 was chosen as the average field strength just off the edge of the reflector in the aperture. This was arbitrarily assigned a −6 dB level. The previous paragraph provides a rationale for this procedure.

The main character of the field is quite adequately given by the geometrical-optics currents. Furthermore, the edge line currents as corrections to the geometrical-optics current appear to have some validity, since the shape of the calculated field is brought into closer agreement with the measured values. This would tend to confirm the results of the analysis pertaining to circumstances under which geometrical optics assumptions should be satisfactory, i.e. where correction currents are small. But the corrections introduced by the edge currents are smaller than the remaining difference between measured and calculated values, so that the above conclusions must be considered as tentative.

### (6) ACKNOWLEDGMENT

### (7) REFERENCES

(1) DUNBAR, A. S.: 'On the Theory of Antenna Beam Shaping', *Journal of Applied Physics*, 1952, **23**, p. 847.
(2) A general discussion of techniques available for the solution of diffraction problems, in addition to a discussion of the integral equation solution, may be found in
BOUWKAMP, C. J.: 'Diffraction Theory', *Reports on Progress in Physics*, 1954, **17**, p. 35.
(3) MOULLIN, E. B., and PHILLIPS, F. M.: 'On the Current Induced in a Conducting Ribbon by the Incidence of a Plane Electromagnetic Wave', *Proceedings I.E.E.*, Monograph No. 26 R, March, 1952 (**99**, Part IV, p. 137).
MOULLIN, E. B.: 'On the Current Induced in a Conducting Ribbon by a Current Filament Parallel to it', *ibid.*, Monograph No. 71 R, August, 1953 (**101**, Part IV, p. 7).
(4) BRAUNBEK, W.: 'Neue Näherungsmethode für die Beugung am ebenen Shirm', *Zeitschrift für Physik*, 1949–50, **127**, p. 381. 'Zur Beugung an der Kreisscheibe', *ibid.*, p. 405.

(5) MILLAR, R. F.: 'An Approximate Theory of the Diffraction of an Electromagnetic Wave by an Aperture in a Plane Screen', *Proceedings I.E.E.*, Monograph No. 152 R, October, 1955 (**103** C, p. 177).

KARP, S. N., and RUSSEK, A.: 'Diffraction by a Wide Slit', New York University, Institute of Mathematical Sciences, Division of Electromagnetic Research, Research Report No. EM-75 (1955).

(6) ROW, R. V.: 'Microwave Diffraction Measurements in a Parallel Plate Region', *Journal of Applied Physics*, 1953, **24**, p. 1448.

EL-KHARADLY, M. M. Z.: 'Some Experiments on Artificial Dielectrics at Centimetre Wavelengths', *Proceedings I.E.E.*, Paper No. 1700 R, January, 1955 (**102** B, p. 17).

SOLLOM, P. H., and BROWN, J.: 'A Centimetre-Wave Parallel-Plate Spectrometer', *ibid.*, Paper No. 2008 R, May, 1956 (**103** B, p. 419).

(7) SOMMERFELD, A.: 'Optics' (Academic Press, 1954), p. 259.

(8) BAKER, B. B., and COPSON, E. T.: 'The Mathematical Theory of Huyghens's Principle' (Oxford University Press, 1950), pp. 142–6.

(9) MARCUVITZ, N.: 'Waveguide Handbook', M.I.T. Radiation Laboratory Series, Vol. 10 (McGraw-Hill Book Co.).
The effect of curvature is considered in:
BRACEWELL: 'Step Discontinuities in Disk Transmission Lines', *Proceedings of the Institute of Radio Engineers*, 1954, **42**, p. 1543.

(10) BETHE, H. A.: 'Theory of Diffraction by Small Holes', *Physical Review*, 1944, **66**, p. 165.

(11) COHN, S. B.: 'Electrolytic Polarizability of Apertures of Arbitrary Shape', *Proceedings of the Institute of Radio Engineers*, 1952, **40**, p. 1069.

(12) ERDELYI, A.: 'Asymptotic Expansions' (Dover Publications).

## (8) APPENDIX

An integral of the form:

$$I = \int_a^b g(x) \varepsilon^{j\omega f(x)} dx$$

can be evaluated asymptotically for large $\omega$. The theory of asymptotics shows that $I$ is asymptotically equal to the asymptotic residue at the critical points. In this case the critical points are the end points and the stationary phase point, $f'(x) = 0$. The expansion at the latter point is in inverse odd half-powers of $\omega$, while the expansion at the end points is in inverse integral powers of $\omega$.

When $f'(x) \neq 0$, for $a \leqslant x \leqslant b$, the expansion is readily generated by integrating successively by parts. When $f'(x) = 0$ in the interval the technique is more complicated and Reference 12 should be consulted.

The general result is that

$$I = \varepsilon^{j\omega f(a)}\left[\frac{jg(a)}{\omega f'(a)} + \frac{1}{\omega^2}\frac{g(a)f''(a) - g'(a)f'(a)}{[f'(a)]^3} + \cdots\right]$$

$$- \varepsilon^{j\omega f(b)}\left(\frac{jg(b)}{\omega f'(b)} + \frac{1}{\omega^2}\left\{\frac{g(b)f''(b) - g'(b)f'(b)}{[f'(b)]^3}\right\} + \cdots\right)$$

$$+ (\sqrt{2})\varepsilon^{j\frac{\pi}{4}}\varepsilon^{j\omega f(u)}\left(\frac{g(u)\Gamma(\frac{1}{2})}{\omega^{1/2}[f''(u)]^{1/2}} - \frac{j}{\omega^{3/2}}\left\{\frac{g(u)f^{IV}(u)\Gamma(\frac{5}{2})}{6[f''(u)]^{5/2}}\right.\right.$$

$$\left.\left. - \frac{g(u)[f'''(u)]^2\Gamma(\frac{7}{2})}{9[f''(u)]^{7/2}} + \frac{2g'(u)f'''(u)\Gamma(\frac{5}{2})}{3[f''(u)]^{5/2}} - \frac{g''(u)\Gamma(\frac{3}{2})}{[f''(u)]^{3/2}}\right\} \cdots\right)$$

where $f'(u) = 0$.

---

## DISCUSSION ON

# 'THE EFFECT OF MAGNETIC SATURATION ON THE D.C. DYNAMIC BRAKING CHARACTERISTICS OF A.C. MOTORS'*

**Professor F. G. Heymann** (*South Africa: communicated*): An alternative way of calculating the maximum torque for a particular value of $I_m$, the magnetizing current, is presented below.

Eqn. (19) may be rewritten in terms of $I_m\frac{dX_m}{dI_m} = \frac{dV_0}{dI_m} - X_m$:

$$-I_m\frac{dX_m}{dI_m} = \frac{Z_2^4 - Z_2^2(X_m^2 + 2X_mX_2 + 2X_2^2)}{2X_2^3 - Z_2^2(X_m + 3X_2)}$$

The factor $-I_m\frac{dX_m}{dI_m}$ is equivalent to a reactance $X$. Insertion of this value yields the following equation:

$$Z_2^4 - Z_2^2 A - 2X_2^3 X = 0$$

where $A = X_m^2 + 2X_mX_2 + 2X_2^2 - X_mX - 3X_2X$

$Z_2^2$ must be positive, so that

$$Z_2^2 = \tfrac{1}{2}[A + \sqrt{(A^2 + 8X_2^3 X)}]$$

This is the value of $Z_2^2$ at maximum torque and may be obtained by plotting $X_m$ and $X$ as functions of $I_m$.

The currents $I_2$ and $I_1$ are easily found:

$$I_2 = \frac{V_0}{Z_2} = \frac{I_m X_m}{Z_2^2}$$

$$I_1^2 = I_m^2\left(1 + \frac{X_m^2 + 2X_mX_2}{Z_2^2}\right)$$

The maximum torque will be

$$T = mI_2^2\sqrt{(Z_2^2 - X_2^2)}$$

where $\sqrt{(Z_2^2 - X_2^2)} = R_2/S$

This method seems to involve a little less labour than the method of the paper, but of course the underlying idea is the same.

**Dr. O. I. Butler** (*in reply*): The modification proposed by Prof. Heymann for establishing the maximum torque conditions is an alternative to the use of eqn. (24) of the paper. In both cases, $I_m$ must be known or assumed.

In general, the solution is obtained most directly by tabular computation, which does not require the plotting of $X_m$ and $X$ as functions of $I_m$. Bearing this in mind, it appears that a worthwhile reduction in the labour of computation is obtained by using the proposed modification.

It may be of interest to note that when the calculation of running-down time is the main objective, a much simplified procedure is permissible.*

# THE INHERENT INSTABILITY OF INDUCTION MOTORS UNDER CONDITIONS OF DOUBLE SUPPLY

By Prof. J. C. PRESCOTT, D.Eng., Member, and B. P. RAJU, M.Sc., Ph.D.

## SUMMARY

A polyphase induction motor provided with balanced windings on both stator and rotor can operate as a synchronous motor at a certain specified speed if each of these windings is connected to a balanced polyphase supply. Under the conditions of such double supply it can maintain this specified speed over a range of mechanical power output, thus exhibiting a synchronizing torque similar to that associated with the conventional synchronous machine.

In addition to this synchronizing torque, there are present also torques which, being proportional to the speed of rotation, may be regarded as damping torques and which under certain circumstances may be negative, i.e. they may act in such a direction that a deviation from synchronous speed, though initially very small, will increase exponentially, thus making synchronous operation impossible. It is to the investigation of these damping torques that the discussion in this paper is directed, and they are considered in relation to the case which seems to present the greatest practical interest—that in which the stator and rotor are connected to the same busbars and in such sense as to give a synchronous speed which is twice that corresponding to the busbar frequency. Operating in this way the machine exhibits a negative damping torque which, in general, decreases with increase in rotor or stator leakage reactance but becomes positive over a small range of values of the coupling coefficient. It appears from the investigation that it is possible to design a motor for operation at the double synchronous speed which shall have a large positive damping torque and which will therefore be stable in operation.

## LIST OF PRINCIPAL SYMBOLS

$L_S$ = Cyclic total inductance of stator per phase, henrys.
$L_R'$ = Cyclic total inductance of rotor per phase, henrys.
$L$ = Inductance per phase connected in series between rotor and points where $V_R$ is kept constant, henrys.
$L_R = L_R' + L$.
$M$ = Stator-rotor or rotor-stator cyclic mutual inductance per phase, henrys.
$p$ = Number of pairs of poles.
$R_S$ = Stator circuit resistance per phase (measured from terminals where $V_S$ is kept constant), ohms.
$R_R'$ = Rotor circuit resistance per phase, ohms.
$R$ = Resistance in series with rotor per phase to the points where $V_R$ is kept constant, ohms.
$R_R = R_R' + R$.
$s = (\omega_S - \omega)/\omega_S$ = Slip with reference to stator field.
$s_1 = (\omega_R + \omega)/\omega_R$ = Slip with reference to rotor field.
$\quad s = s_1$ for $\omega_R = -\omega_S$.
$\quad s = s_1 = -1$ for $\omega = 2\omega_S$.
$V_S$ = Stator applied voltage per phase, volts (r.m.s.).
$V_R$ = Rotor applied voltage per phase, volts (r.m.s.).
$X_S = L_S\omega_S$ = Cyclic total reactance of stator per phase at stator frequency, ohms.

$X_{SR} = L_S\omega_R$ = Cyclic total reactance of stator per phase at rotor frequency, ohms.
$X_R = L_R\omega_S$ = Cyclic total reactance of rotor circuit per phase at stator frequency, ohms.
$X_{RR} = L_R\omega_R$ = Cyclic total reactance of rotor circuit per phase at rotor frequency, ohms.
$X_m = M\omega_S$ = Cyclic mutual reactance per phase at stator frequency, ohms.
$X_{mR} = M\omega_R$ = Cyclic mutual reactance per phase at rotor frequency, ohms.
$-\alpha$ = Angle between geometric axes of homologous phases on stator and rotor at instant when $t = 0$, electrical rad.
$\alpha_m = \alpha/p$, mechanical rad.
$\beta = -\alpha + \omega t$ = Angle between geometric axes of homologous phases on stator and rotor at any instant $t$, electrical rad.
$\omega_S$ = Angular velocity of rotating field caused by stator currents, with reference to stator winding, electrical rad/s.
$\omega_R$ = Angular velocity of rotating field caused by rotor currents with reference to rotor winding, electrical rad/s.
$\omega$ = Angular velocity of rotor in space, electrical rad/s.
$\omega_m$ = Angular velocity of rotor, mechanical rad/s.

## (1) INTRODUCTION

The performance of induction machines under conditions of double supply presents certain features of practical and theoretical interest. By suitably arranging the supply connections it is possible to obtain a speed of synchronous operation equal to the sum, or the difference, of the synchronous speeds corresponding to the supply frequencies. Thus, for instance, a machine with both stator and rotor connected to the same supply could have a synchronous speed equal to twice that corresponding to the frequency of the supply, and operating at this speed would have, for given conditions of electric and magnetic loading, a shaft output double that which it could give with the stator, or the rotor, supplied alone. The higher synchronous speed appears to answer two particular needs at the present time, namely as a generator where gas turbines are the prime movers and as a motor for centrifugal-pump drive. Experience shows, however, that the machine, operating at a synchronous speed higher than that corresponding to the supply frequencies, is likely to be unstable, and this instability may be traced to the presence of large negative damping torques—torques which act in such a direction as to increase any deviation from the synchronous speed.

The behaviour of machines under conditions of double supply has been studied for steady-state conditions by Kassjanow,[1] Messing[2] and Arnold.[3] Later Herschdorfer,[4] Tscherdanzev,[5] and Leonhard[6] analysed the steady state, and also considered the pulling-in phenomena. Kloss[7] and Steudel[8] studied steady-state as well as oscillatory conditions. Hannakam[9] considered suppression of oscillations using a starting motor. All the earlier

workers, including Kron, Concordia and Crary,[10] who used tensorial methods have employed leakage reactances in their analyses.

In the present paper the general equations for the machine are derived using the principle of superposition, and may be applied with relevant modifications to treat all conditions of operation under double supply, but special attention is directed to the case in which the machine operates synchronously at a speed twice that corresponding to the supply frequency.

This condition is achieved by feeding both stator and rotor from the same supply but with dissimilar phase sequences. In such a case, were the rotor stationary, the stator and the rotor would produce two fields rotating in opposite directions at the speed corresponding to the supply frequency. Rotation of the rotor at twice this speed in the direction of the stator field would then cause the field due to the rotor supply to rotate at synchronous speed in space in the same direction as that of the field due to the stator supply, thus bringing these two rotating fields to rest relative to each other, which is the condition for synchronous operation.

In applying the principle of superposition it is necessary to assume that the circuit equations are linear and contain only constant coefficients. This requirement might seem to impose a disabling limitation when circuits containing iron are to be considered, but the difficulty can be overcome if the equations are expressed in terms of constants which can be measured under conditions of saturation closely analogous to those obtaining under operating conditions. For this reason, and also because of the difficulties which present themselves when attempts are made to measure separately the rotor and stator leakage reactances, the constants which have been chosen are the total inductance of the stator and of the rotor and the mutual inductance between stator and rotor. The constants are expressed as cyclic quantities which in the case of self-inductance relate the stator (or rotor) current per phase to the total flux linkage produced in the stator (or rotor) phase by the rotating field generated by all the stator (or rotor) phases acting together; and in the case of mutual inductance, relating the rotor (or stator) current per phase to the total flux linkage produced in a stator (or rotor) phase by the rotating field generated by all the rotor (or stator) phases acting together.

## (2) THEORETICAL CONSIDERATIONS

### (2.1) Analysis

The analysis is developed for the general case where the rotor, the field due to the stator supply, and the field due to the rotor supply, considered relative to the rotor, all rotate in the same direction; i.e. $\omega_S$ (angular velocity in space of field due to stator supply), $\omega$ (angular velocity of rotor in space) and $\omega_R$ (angular velocity of field due to rotor supply relative to rotor) are all assumed to be positive.

Certain other assumptions are necessary. Harmonics, both of time and space, are neglected, which implies that voltages and currents as well as field distribution are sinusoidal. Variations in saturation over the working range are neglected. It is assumed that hysteresis and eddy-current losses in stator and rotor are met by their respective supplies, and hence are independent of rotation. The pulsation loss depends on the speed of rotation, but the torque due to the eddy-loss part of it, which affects damping, is small compared with the main developed torque due to induction-motor action and is neglected.

The operation of the machine is treated as the result of the superposition of two hypothetical conditions of operation, one with the stator supplied and the rotor short-circuited, the other with the rotor supplied and the stator short-circuited, the same speed and direction of rotation being maintained in each case.

In the first case let the stator be given a supply which produces a field rotating with an angular velocity $\omega_S$. If, then, the rotor is rotating with angular velocity $\omega$, the angular velocity effective in the rotor is $(\omega_S - \omega)$. The current in the A-phase of the stator can be written as

$$i_S = I_{S1} \sin(\omega_S t - \phi_S) . \quad . \quad . \quad . \quad (1)$$

where $\phi_S$ is the angle of lag of $i_S$ behind the voltage $v_S$ applied to the A-phase, namely

$$v_S = V_S \sin \omega_S t . \quad . \quad . \quad . \quad . \quad (2)$$

The relative magnitudes of the stator and rotor e.m.f.'s $e_{S1}$ and $e_{R1}$ induced in the corresponding A-phases due to $i_s$ are given by

$$\frac{e_{S1}}{e_{R1}} = \frac{L_S \omega_S}{M(\omega_S - \omega)} = \rho_1 \quad . \quad . \quad . \quad (3)$$

To define the phase angle between $e_{S1}$ and $e_{R1}$, it is assumed that at time $t = 0$, the A-phase of the rotor is geometrically behind that of the stator by an angle $\alpha$ as shown in Fig. 1. At
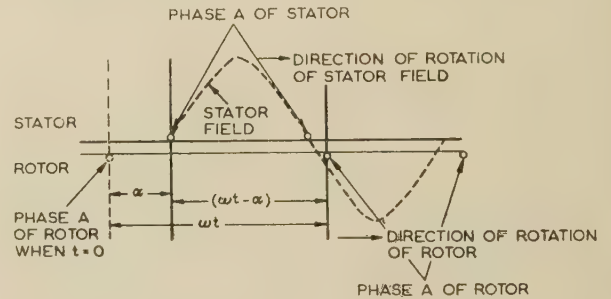


Fig. 1.—Relative angular positions of rotor and stator windings.

any subsequent time the angle between the A-phases is therefore $(\omega t - \alpha)$, and this represents the time lag between $e_{S1}$ and $e_{R1}$ corresponding to any rotor position defined by $t$. Hence

$$e_{S1} = - L_S \frac{d}{dt}[I_{S1} \sin(\omega_S t - \phi_S)]$$

$$= - L_S \omega_S I_{S1} \cos(\omega_S t - \phi_S) \quad . \quad . \quad (4)$$

and

$$e_{R1} = - \frac{1}{\rho_1} L_S \omega_S I_{S1} \cos[\omega_S t - \phi_S - (\omega t - \alpha)]$$

$$= - M(\omega_S - \omega)I_{S1} \cos[(\omega_S - \omega)t - \phi_S + \alpha] \quad . \quad (5)$$

The rotor current is driven by $e_{R1}$ and lags behind it by $\phi_R$ and behind $v_S$ by some angle $\theta + \omega t$ (say), thus giving

$$i_R = I_{R1} \sin[(\omega_S - \omega)t - \theta] . \quad . \quad . \quad (6)$$

where $\theta$ and $\phi_R$ are related by $\phi_R = \theta - (\phi_S - \alpha + \pi/2)$, which is independent of time. This is made clearer with the help of a vector diagram for the A-phases (Fig. 2). The angle $\theta$ represents the amount by which $I_{R1}$ would lag behind $V_S$ if $I_{R1}$ were given an additional speed $\omega$. Thus $\theta$ varies with $\alpha$, i.e. the position of the A-phase on the rotor relative to that on the stator.

Directing attention now to the e.m.f.'s $e_{R2}$ and $e_{S2}$ induced in the rotor and stator due to the rotor currents, it will be noticed that the ratio of e.m.f.'s becomes

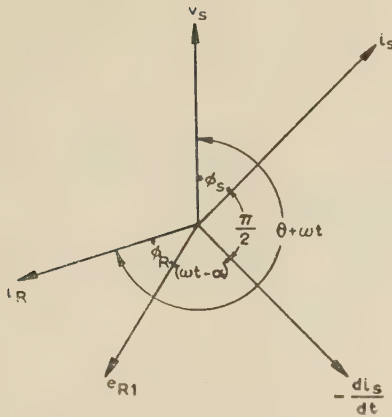$$\frac{e_{R2}}{e_{S2}} = \frac{L_R(\omega_S - \omega)}{M\omega_S} = \rho_2 \quad . \quad . \quad . \quad (7)$$

Fig. 2.—Vector diagram of rotor and stator quantities.

while $e_{S2}$ leads $e_{R2}$ by $(\omega t - \alpha)$. Thus

$$e_{R2} = - L_R \frac{d}{dt}\{I_{R1} \sin [(\omega_S - \omega)t - \theta]\}$$

$$= - L_R(\omega_S - \omega)I_{R1} \cos [(\omega_S - \omega)t - \theta] \qquad (8)$$

and

$$e_{S2} = - \frac{1}{\rho_2} L_R I_{R1}(\omega_S - \omega) \cos [(\omega_S - \omega)t - \theta + (\omega t - \alpha)]$$

$$= - M(\omega_S - \omega)I_{R1} \cos (\omega_S t - \theta - \alpha) \quad . \quad . \quad . \quad (9)$$

The Kirchhoff's law equations can now be written with reference to $v_S$:

$$V_S \sin \omega_S t = \left(R_S + L_S \frac{d}{dt}\right) I_{S1} \sin (\omega_S t - \phi_S)$$

$$+ M \frac{d}{dt}[I_{R1} \sin (\omega_S t - \theta - \alpha)] \quad (10)$$

and $\quad 0 = \left(R_R + L_R \frac{d}{dt}\right) I_{R1} \sin [(\omega_S - \omega)t - \theta]$

$$+ M \frac{d}{dt}\{I_{S1} \sin [(\omega_S - \omega)t - \phi_S + \alpha]\} \quad (11)$$

Writing them in complex form yields

$$V_S \varepsilon^{j\omega_S t} = \left(R_S + L_S \frac{d}{dt}\right) I_{S1} \varepsilon^{j(\omega_S t - \phi_S)} + M \frac{d}{dt}\{I_{R1} \varepsilon^{j(\omega_S t - \theta)}\}\varepsilon^{-j\alpha}$$

$$. \quad . \quad . \quad . \quad (12)$$

$$0 = \left(R_R + L_R \frac{d}{dt}\right) I_{R1} \varepsilon^{j[(\omega_S - \omega)t - \theta]} + M \frac{d}{dt}\{I_{S1} \varepsilon^{j[(\omega_S - \omega)t - \phi_S]}\}\varepsilon^{j\alpha}$$

$$. \quad . \quad . \quad . \quad (13)$$

or

$$V_S \varepsilon^{j\omega_S t} = (R_S + j\omega_S L_S)I_{S1}\varepsilon^{j(\omega_S t - \phi_S)} + jM\omega_S I_{R1}\varepsilon^{j(\omega_S t - \theta)}\varepsilon^{-j\alpha}$$

$$. \quad . \quad . \quad . \quad (14)$$

$$0 = [R_R + j(\omega_S - \omega)L_R]I_{R1}\varepsilon^{j[(\omega_S - \omega)t - \theta]}$$

$$+ jM(\omega_S - \omega)I_{S1}\varepsilon^{j[(\omega_S - \omega)t - \phi_S]}\varepsilon^{j\alpha} \quad (15)$$

If (15) is multiplied by $\varepsilon^{j\omega t}$ it yields

$$0 = [R_R + j(\omega_S - \omega)L_R]I_{R1}\varepsilon^{j(\omega_S t - \theta)}$$

$$+ jM(\omega_S - \omega)I_{S1}\varepsilon^{j(\omega_S t - \phi_S)}\varepsilon^{j\alpha} \quad (16)$$

where $I_{R1}\varepsilon^{j(\omega_S t - \theta)}$ as a vector is the result of giving the vector represented by $I_{R1}\varepsilon^{j[(\omega_S - \omega)t - \theta]}$ an additional speed of rotation $\omega$.

Eqns. (14) and (16) can now be written in vectorial form giving

$$V_S = (R_S + j\omega_S L_S)I_{S1} + jM\omega_S I_{R1}\varepsilon^{-j\alpha} \quad . \quad . \quad (17)$$

$$0 = [R_R + j(\omega_S - \omega)L_R]I_{R1} + jM(\omega_S - \omega)I_{S1}\varepsilon^{j\alpha} \quad (18)$$

which when solved give

$$I_{S1} = \frac{[R_R + j(\omega_S - \omega)L_R]V_S}{[R_S R_R - L_S \omega_S L_R(\omega_S - \omega) + M^2(\omega_S - \omega)\omega_S] + j[R_R L_S \omega_S + R_S L_R(\omega_S - \omega)]} \quad . \quad . \quad . \quad (19)$$

and $\quad I_{R1} = \frac{-jM(\omega_S - \omega)V_S\varepsilon^{j\alpha}}{[R_S R_R - L_S \omega_S L_R(\omega_S - \omega) + M^2(\omega_S - \omega)\omega_S] + j[R_R L_S \omega_S + R_S L_R(\omega_S - \omega)]} \quad . \quad . \quad . \quad (20)$

In the second case, when the rotor is supplied and the stator short-circuited, let the rotor be fed from a supply producing a rotating field having an angular velocity $\omega_R$ relative to the rotor. If $\omega$ is the angular velocity of the rotor, the angular velocity operative in the stator will be $(\omega_R + \omega)$. Reasoning similar to the above yields for the vectorial equations, if the stator and rotor applied voltages are in phase,

$$0 = [R_S + j(\omega_R + \omega)L_S]I_{S2} + jM(\omega_R + \omega)I_{R2}\varepsilon^{-j\alpha} \quad (21)$$

$$V_R = jM\omega_R I_{S2}\varepsilon^{j\alpha} + (R_R + j\omega_R L_R)I_{R2} \quad . \quad . \quad (22)$$

which give on solution

$$I_{S2} = \frac{-jM(\omega_R + \omega)V_R\varepsilon^{-j\alpha}}{[R_S R_R - L_S(\omega_R + \omega)L_R \omega_R + M^2(\omega_R + \omega)\omega_R] + j[R_R L_S(\omega_R + \omega) + R_S L_R \omega_R]} \quad . \quad . \quad . \quad (23)$$

$$I_{R2} = \frac{[R_S + j(\omega_R + \omega)L_R]V_R}{[R_S R_R - L_S(\omega_R + \omega)L_R \omega_R + M^2(\omega_R + \omega)\omega_R] + j[R_R L_S(\omega_R + \omega) + R_S L_R \omega_R]} \quad . \quad . \quad . \quad (24)$$

By the principle of superposition the total currents are

$$I_S = I_{S1} + I_{S2} . \quad . \quad . \quad . \quad . \quad (25)$$

and $\qquad I_R = I_{R1} + I_{R2} \quad . \quad . \quad . \quad . \quad (26)$

If $E'_{R1}$ and $E'_{R2}$ are the vectors of induced e.m.f.'s in the rotor due respectively to $I_{S1}$ and $I_{S2}$, the total generating torque per phase is given by

$$T_G = - \frac{1}{9\cdot81}\mathscr{R}\left[\frac{pE'^*_{R1}}{(\omega_S - \omega)} + \frac{pE'^*_{R2}}{\omega_R}\right]\left[I_{R1} + I_{R2}\right] \text{ kg-metres}$$

$$. \quad . \quad . \quad . \quad (27)$$

as suggested by Lyon and Edgerton,[11] where $E'^*_{R1}$ and $E'^*_{R2}$ are conjugates of $E'_{R1}$ and $E'_{R2}$ respectively.

11

Eqn. (27) yields general expressions for the four component torques which are shown in the Appendix.

Attention is drawn particularly to the double-synchronous-speed operation, the condition for which is

$$\omega_R = -\omega_S$$

For this case the general expressions given in the Appendix take a more compact form since

$$s = (\omega_S - \omega)/\omega_S = (\omega_R + \omega)/\omega_R$$

Thus, if $T_G = T_1 + T_2 + T_3 + T_4$ in kilogramme-metres, then

$$T_1 = -\frac{3pV_S^2}{9\cdot81\omega_S}\frac{sR_RX_m^2}{(R_SR_R - sX_SX_R + sX_m^2)^2 + (R_RX_S + sR_SX_R)^2}$$
$$\qquad\qquad\qquad\qquad\qquad\qquad (28)$$

$$T_2 = -\frac{3pV_R^2}{9\cdot81\omega_S}\frac{sR_SX_m^2}{(R_SR_R - sX_SX_R + sX_m^2)^2 + (R_SX_R + sR_RX_S)^2}$$
$$\qquad\qquad\qquad\qquad\qquad\qquad (29)$$

Or, writing

$$A = R_SR_R - sX_SX_R + sX_m^2$$

$$B = R_RX_S + sR_SX_R$$

and $\qquad D = R_SX_R + sR_RX_S$

$$T_1 = -\frac{3pV_S^2sR_RX_m^2}{9\cdot81\omega_S(A^2 + B^2)} \qquad \cdots \qquad (28a)$$

$$T_2 = -\frac{3pV_R^2sR_SX_m^2}{9\cdot81\omega_S(A^2 + D^2)} \qquad \cdots \qquad (29a)$$

$$T_3 = -\frac{3pMV_SV_R}{9\cdot81(A^2 + B^2)(A^2 + D^2)}$$

$$\{s(R_RX_S + R_SX_R)[(A^2 + BD)\cos\alpha - (AD - AB)\sin\alpha]$$

$$+ [R_SR_R - s^2X_SX_R][(AD - AB)\cos\alpha + (A^2 + BD)\sin\alpha]\}$$
$$\qquad\qquad\qquad\qquad\qquad\qquad (30)$$

and

$$T_4 = -\frac{3pMV_SV_R}{9\cdot81(A^2 + B^2)(A^2 + D^2)}$$

$$\{s^2X_m^2[(AD - AB)\cos\alpha + (A^2 + BD)\sin\alpha]\} \qquad (31)$$

$T_3$ and $T_4$ can be grouped together into the form

$$T_3 + T_4 = -\Delta\frac{(a_1 + a_2s + a_3s^2 + a_4s^3 + a_5s^4)\cos\alpha + (b_1 + b_2s + b_3s^2 + b_4s^3 + b_5s^4)\sin\alpha}{(d_1 + d_2s + d_3s^2 + d_4s^3 + d_5s^4)} \qquad \cdots \qquad (32)$$

as shown in the Appendix, where the meanings of all the constants are explained, and

$$\Delta = \frac{3pMV_SV_R}{9\cdot81}$$

the coefficient 3 referring to a 3-phase machine.

### (2.2) Stability

When discussing the oscillations of synchronous machines it is usual to assume that the total electrical torque can be divided into two parts, one directly proportional to the angular displacement of the rotor from a reference vector rotating synchronously, another directly proportional to the velocity of this displacement. On this assumption the equation of motion of the machine when acted upon by a small increment of mechanical torque, $\Delta T_q$, may be written

$$I\ddot{\alpha}_m + C_1\dot{\alpha}_m + C_2\alpha_m = \Delta T_q \qquad \cdots \qquad (33)$$

where $I$ = Polar moment of inertia of rotating parts, kg-m².
$\alpha_m$ = Mechanical angular displacement with respect to a steady-state reference vector, rad.
$C_1$ = Electrical torque opposing velocity, kg-m per mechanical rad/s.
$C_2$ = Electrical torque opposing displacement, kg-m per mechanical rad.

The solution of eqn. (33) is of the form

$$\alpha_m = P + Q\varepsilon^{-\lambda t}\sin(\psi t + \beta) \qquad \cdots \qquad (34)$$

where

$$\lambda = \frac{C_1}{2I} \qquad \cdots \qquad (35)$$

and

$$\psi = \sqrt{\left[\frac{C_2}{I} - \left(\frac{C_1}{2I}\right)^2\right]} \qquad \cdots \qquad (36)$$

and $P$, $Q$ and $\beta$ are constants.

If $C_1$ is positive, $\lambda$ is positive and the machine is stable since any oscillating displacement decays exponentially. If $C_1$ is negative any oscillating displacement, however small, will increase exponentially and the machine is unstable. This form of instability is generally described as being due to the presence of negative damping.

It is to be noted that $C_1$ and $C_2$ can be regarded as constants only if $\alpha_m$ is so small as to make $\alpha_m \simeq \sin\alpha_m$; and $\dot{\alpha}_m$ so small as to make the ratio $\dot{\alpha}_m/\omega_m$ small compared with unity.

For the machine under conditions of double supply and operating at double synchronous speed the total electrical generating torque is given by

$$T_G = T_1 + T_2 + T_3 + T_4$$

$T_1$ and $T_2$ are complicated functions of the slip and therefore of $\dot{\alpha}_m$, while $T_3$ and $T_4$ are functions of $\dot{\alpha}_m$, and are also sine and cosine functions of $\alpha_m$.

Plotted to a base of $\omega_m$, $T_G$ can be represented, in the region of the operating speed, by a family of curves such as those shown in Fig. 3, for various values of $\alpha_m$. If the excursion $\dot{\alpha}_m$ is small the curves to be considered lie close together and may be assumed to be equally spaced for equal increments $\alpha_m$ and may also be assumed to be sensibly parallel to each other where they cut the ordinate defining the operating speed. Further, if $\dot{\alpha}_m$ is small the curves at the operating speed may be replaced by their tangents at that point. On these assumptions

$$C_2 = -\frac{\partial T_G}{\partial\alpha_m} \qquad \cdots \qquad (37)$$

and

$$C_1 = \frac{\partial T_G}{\partial\omega_m} \qquad \cdots \qquad (38)$$

The case treated here is that in which $s = -1$, so that

$$C_1 = \frac{\partial T_G}{\partial\omega_m} = \frac{\partial}{\partial\omega_m}(T_1 + T_2 + T_3 + T_4) \qquad \cdots \qquad (39)$$

and, in kilogramme-metres per mechanical radian per second,

$$T_{d1} = \frac{\partial T_1}{\partial \omega_m} = -\frac{p}{\omega_S}\frac{\partial T_1}{\partial s} = -\frac{3p^2 V_S^2 X_m^2 R_R}{9 \cdot 81 \omega_S^2} \frac{\left[ R_S^2 X_R^2 + (X_m^2 - X_S X_R)^2 - \dfrac{R_R^2 Z_S^2}{s^2} \right]}{\left\{ \dfrac{R_R^2 Z_S^2}{s} + 2X_m^2 R_S R_R + s[R_S^2 X_R^2 + (X_m^2 - X_S X_R)^2] \right\}^2} \quad \cdots \cdots \quad (40)$$

where $Z_S^2 = R_S^2 + X_S^2$

$$T_{d2} = \frac{\partial T_2}{\partial \omega_m} = -\frac{p}{\omega_S}\frac{\partial T_2}{\partial s} = -\frac{3p^2 V_R^2 X_m^2 R_S}{9 \cdot 81 \omega_S^2} \frac{\left[ R_R^2 X_S^2 + (X_m^2 - X_S X_R)^2 - \dfrac{(R_R^2 + X_R^2)R_S^2}{s^2} \right]}{\left\{ \dfrac{(R_R^2 + X_R^2)R_S^2}{s} + 2X_m^2 R_S R_R + s[R_R^2 X_S^2 + (X_m^2 - X_S X_R)^2] \right\}^2} \quad \cdots \quad (41)$$

$$T_{d(3+4)} = \frac{\partial (T_3 + T_4)}{\partial \omega_m} = -\frac{p}{\omega_S} \cdot \frac{\partial (T_3 + T_4)}{\partial s}$$
$$= \frac{3p^2 M V_S V_R}{9 \cdot 81 \omega_S}\left\{ \left[ \frac{(a_2 + 2a_3 s + 3a_4 s^2 + 4a_5 s^3)\cos\alpha + (b_2 + 2b_3 s + 3b_4 s^2 + 4b_5 s^3)\sin\alpha}{(d_1 + d_2 s + d_3 s^2 + d_4 s^3 + d_5 s^4)} \right] \right.$$
$$\left. - (d_2 + 2d_3 s + 3d_4 s^2 + 4d_5 s^3)\left[ \frac{(a_1 + a_2 s + a_3 s^2 + a_4 s^3 + a_5 s^4)\cos\alpha + (b_1 + b_2 s + b_3 s^2 + b_4 s^3 + b_5 s^4)\sin\alpha}{(d_1 + d_2 s + d_3 s^2 + d_4 s^3 + d_5 s^4)^2} \right] \right\} \quad (42)$$

It is difficult to generalize when the winding constants such as $L$, $R$ and $M$ have a wide range of values, but for normal values of these quantities and for the double synchronous operation it may be said that $\partial T_1/\partial \omega_m$ and $\partial T_2/\partial \omega_m$ are large and negative, while $\partial (T_3 + T_4)/\partial \omega_m$ may be positive or negative. At or near no load the value of $\partial (T_3 + T_4)/\partial \omega_m$ is negative, and hence this is the worst condition so far as stability is concerned, but the actual magnitude of this negative value is negligibly small compared with the sum of $\partial T_1/\partial \omega_m$ and $\partial T_2/\partial \omega_m$. Thus at no-load the damping characteristics are mainly deter-
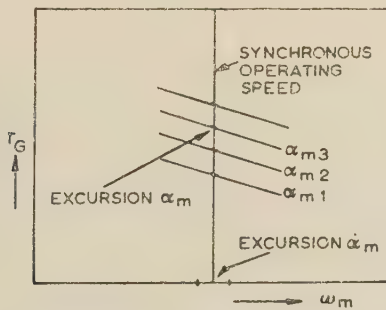


Fig. 3.—Diagram illustrating assumptions made in deriving synchronizing and damping-torque coefficients.

mined by $\partial T_1/\partial \omega_m$ and $\partial T_2/\partial \omega_m$, and it may be worth while to examine these expressions more closely. Considering $\partial T_1/\partial \omega_m$, for instance,

$$T_{d1} = \frac{\partial T_1}{\partial \omega_m} = -\frac{3p^2 V_S^2 R_R X_m^2}{9 \cdot 81 \omega_S^2}$$

$$\frac{\left[ R_S^2 X_R^2 + (X_m^2 - X_S X_R)^2 - \dfrac{R_R^2 Z_S^2}{s^2} \right]}{\left\{ \dfrac{R_R^2 Z_S^2}{s} + 2X_m^2 R_S R_R + s[R_S^2 X_R^2 + (X_m^2 - X_S X_R)^2] \right\}^2}$$

Putting $\Delta_1 = \dfrac{3p^2 V_S^2 X_m^2}{9 \cdot 81 \omega_S^2}$ and $y = X_R$, writing $T_{d1}$ as a function of $y$, and noting $s = -1$,

$$T_{d1} = -\Delta_1 R_R$$
$$\frac{y^2 Z_S^2 - y(2X_m^2 X_S) + (X_m^4 - R_R^2 Z_S^2)}{[y^2 Z_S^2 - y(2X_m^2 X_S) + (X_m^4 + R_R^2 Z_S^2 - 2X_m^2 R_S R_R)]^2} \quad (43)$$

Putting $D$ for the denominator and differentiating $T_{d1}$ with respect to $y$, the result is

$$\frac{\partial T_{d1}}{\partial y} = -\Delta_1 R_R \frac{D^2(2yZ_S^2 - 2X_m^2 X_S) - [y^2 Z_S^2 - y(2X_m^2 X_S) + (X_m^4 - R_R^2 Z_S^2)](2D)(2yZ_S^2 - 2X_m^2 X_S)}{D^4} \quad \cdots \quad (44)$$

Equating $\partial T_{d1}/\partial y$ to zero yields the conditions for maxima and minima for $T_{d1}$, as the total reactance $X_R$ of the rotor is varied. The conditions are

$$(yZ_S^2 - X_m^2 X_S)[y^2 Z_S^2 - y(2X_m^2 X_S)$$
$$+ X_m^4 - 3R_R^2 Z_S^2 + 2X_m^2 R_S R_R] = 0 \quad (45)$$

The values of $y$ are obtained from

$$yZ_S^2 - X_m^2 X_S = 0 \quad \cdots \cdots \quad (46)$$

and $y^2 Z_S^2 - y(2X_m^2 X_S) + X_m^4 - 3R_R^2 Z_S^2 + 2X_m^2 R_S R_R = 0 \quad (47)$

This equation gives two negative maxima of $y$, while eqn. (46) gives a positive maximum and the shape of variation of $T_{d1}$ with $X_R$ would be of the form of the full line in Fig. 4. The results are perhaps most easily studied in relation to a practical case. Taking reasonable values for a small induction motor as

$$R_S = 3 \text{ ohms}; \; R_R = 0 \cdot 3 \text{ ohm}$$

$$X_S = 132 \cdot 4 \text{ ohms}; \; X_m = 28 \cdot 18 \text{ ohms}$$

$$X_R = 6 \cdot 62 \text{ ohms (inherent)}.$$

$$V_S = 400 \text{ volts and } V_R = 150/\sqrt{3} = 86 \cdot 7 \text{ volts}$$

$$y_3 = \frac{X_m^2 X_S}{Z_S^2} = \frac{(28 \cdot 18)^2(132 \cdot 4)}{(132 \cdot 4^2 + 3^2)} \simeq 6 \text{ ohms}$$

$$y^2(132 \cdot 4^2 + 3^2) - y[2(28 \cdot 18)^2(132 \cdot 4)] + [(28 \cdot 18)^4$$
$$- 3(0 \cdot 3)^2(132 \cdot 4^2 + 3^2) + 2(28 \cdot 18)^2(3)(0 \cdot 3)] = 0$$

i.e. $$y^2 - 12y + 35 \cdot 81 \simeq 0$$

or $$y \simeq 6 \pm 0 \cdot 436 \text{ ohms}$$

or $$y_1 \simeq 5 \cdot 564 \text{ ohms}$$

$$y_2 \simeq 6 \cdot 436 \text{ ohms}$$
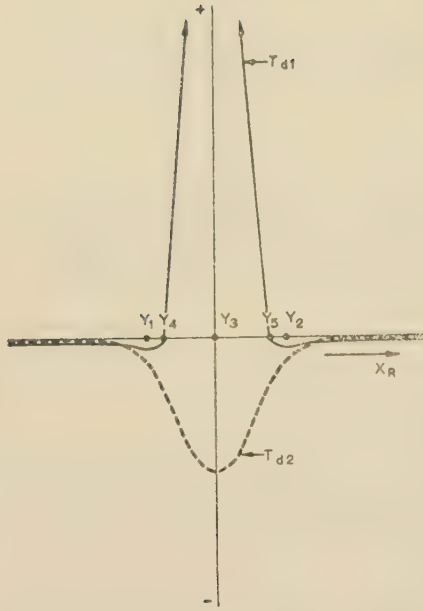
**Fig. 4.**—Variation of inherent damping-torque coefficients with total rotor reactance.

These values substituted for $y$ in eqn. (43) give

$$\left.\begin{array}{l} (T_{d1})_{y=y_1} \simeq -0\cdot153 \\ (T_{d1})_{y=y_2} \simeq -0\cdot153 \\ (T_{d1})_{y=y_3} \simeq +9\cdot442 \end{array}\right\} \text{ kg-m per mechanical rad/s.}$$

It may be noticed in passing that the inherent total rotor reactance for the machine considered is $6\cdot62$ ohms, which is beyond the second negative maximum.

Also, portions of Fig. 4 corresponding to $X_R < y_3$ have no physical significance, since when $X_R = y_3$ the coefficient of coupling $k$ is unity, where $k = M^2/L_S L_R = X_m^2/X_S X_R$.

The values $y_4$ and $y_5$ for which $T_{d1}$ is zero are obtained by equating eqn. (47) to zero. Thus

$$y^2 Z_S^2 - y(2X_m^2 X_S) + (X_m^4 - R_R^2 Z_S^2) = 0$$

$$y^2(132\cdot4^2 + 3^2) - y[2(28\cdot18)^2(132\cdot4)]$$
$$+ [(28\cdot18)^4 - (0\cdot3)^2(132\cdot4^2 + 3^2)] = 0$$

Therefore
$$y \simeq 6\cdot0 \pm 0\cdot3 \text{ ohms}$$
$$y_4 \simeq 5\cdot7 \text{ ohms}$$
$$y_5 \simeq 6\cdot3 \text{ ohms}$$

The approximate value of $y_5$ indicates the limit for the value of the total rotor reactance below which the damping is positive and the coefficient of coupling, $k$, is less than unity. The shape of the curve suggests that

(a) The negative damping could be greatly reduced by putting reactance in series with the rotor windings.

(b) By designing the machine in such a way that the rotor reactance lies within the range defined by $y_3$ and $y_5$ it should be possible to avoid the negative damping effects altogether.

Point (a) is illustrated by the right-hand curve of Fig. 5, which was obtained by adding algebraically $T_{d1}$ and $T_{d2}$. The variation of $T_{d2}$ for the same region of variation of $X_R$ can be shown by similar reasoning.

Eqn. (41) can be written, at $s = -1$,



**Fig. 5.**—Variation of total inherent damping-torque coefficient with total rotor reactance.

Writing $\Delta_2$ for $3p^2 V_R^2 X_m^2/9\cdot81\omega_s^2$, neglecting $R_S^2$ in comparison with $X_S^2$, and differentiating with respect to $y$,

$$\frac{\partial T_{d2}}{\partial y} = -\frac{\Delta_2 R_S}{D^4}\{D^2[2yX_S^2 + (-2X_S X_m^2)]$$
$$- (2D)[y^2 X_S^2 + y(-2X_S X_m^2)$$
$$+ R_R^2 X_S^2 + X_m^4][2yX_S^2 + (-2X_S X_m^2)]\}$$

Equating this expression to zero yields the maxima and minima of $T_{d2}$ with variation in $y$:

$$[2yX_S^2 - 2X_S X_m^2][-y^2 X_S^2 + y(2X_S X_m^2)$$
$$- R_R^2 X_S^2 - X_m^4 - 2X_m^2 R_S R_R] = 0$$

Therefore
$$2yX_S^2 - 2X_S X_m^2 = 0$$

or
$$y = \frac{X_m^2}{X_S}$$

which is the same value as $y_3$ in the first case.

$$y^2 X_S^2 - y(2X_S X_m^2) + R_R^2 X_S^2 + X_m^4 + 2X_m^2 R_S R_R = 0$$

i.e. $y^2(132\cdot4)^2 - y[2(132\cdot4)(28\cdot18)^2]$
$$+ (0\cdot3)^2(132\cdot4)^2 + (28\cdot18)^4 + 2(28\cdot18)^2(3)(0\cdot3) = 0$$

or, approximately,

$$y^2 - 12y + 36\cdot17 = 0$$

so that
$$y \simeq 6\cdot0 \pm \sqrt{-0\cdot17} \text{ ohms}$$

The values of $y$ are complex. Thus $T_{d2}$ has one maximum at the value $y_3$ and this is obtained from eqn. (37) and gives a negative maximum as shown below.

At a rotor reactance of $6\cdot00$ ohms

$$T_{d2} = -3\cdot796 \text{ kg-m per mechanical rad/s.}$$

The parts of the curves for values of $X_R < 6\cdot00$ ohms have no physical meaning since the coefficient of coupling for $X_R = 6\cdot00$ ohms is unity. In an actual machine, therefore, attention must be directed to the region between points represented by $y_3$ and $y_5$ in Fig. 4.

Fig. 6 indicates the nature of variation of $T_{d1}$, $T_{d2}$ and $T_{d1} + T_{d2}$ in the range of values of $X_R$ of $5\cdot8$ to $6\cdot7$ ohms. The curve of $T_{d1} + T_{d2}$ suggests the possibility of eliminating the negative damping by choosing a value of $X_R$ between $6\cdot0$

$$T_{d2} = \frac{\partial T_2}{\partial \omega_m} = -\frac{3p^2 V_k^2 X_m^2 R_S}{9\cdot81\omega_S^2} \frac{[y^2(X_S^2 - R_S^2) + y(-2X_m^2 X_S) + R_R^2(X_S^2 - R_S^2) + X_m^4]}{[y^2(X_S^2 + R_S^2) + y(-2X_m^2 X_S) + R_R^2(X_S^2 + R_S^2) + X_m^4 - 2X_m^2 R_S R_R]^2}$$

and 6·180 ohms. The coefficient of coupling for $X_R = 6·0$ ohms is unity and for $X_R = 6·180$ ohms is 0·97. Fig. 6, taken together with eqns. (40) and (41), shows an interesting possibility. These equations show that $T_{d1}$ is directly proportional to $R_R$ and that $T_{d2}$ is directly proportional to $R_S$. Fig. 6 suggests
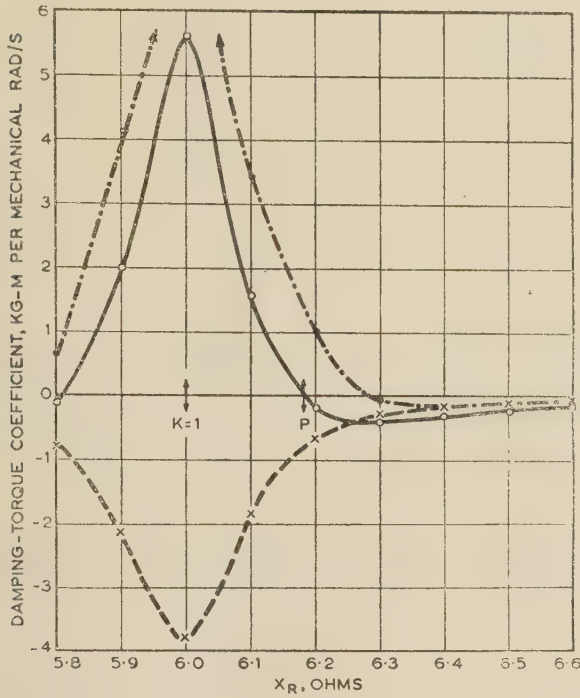


Fig. 6.—Damping torque coefficients in the region of positive maximum for $\alpha = 0$.

● $T_{d1}$.
× $T_{d2}$.
○ $T_{d1} + T_{d2}$.

that, if the ordinates of the $T_{d1}$ curve are increased and/or the ordinates of the $T_{d2}$ curve are decreased in magnitude, then the point P at which the ordinate of the $T_{d1} + T_{d2}$ curve is zero could be made to shift away from $X_R = 6·0$ ohms. In other words, stability could be achieved at a slightly lower coefficient of coupling by increasing rotor resistance and reducing stator resistance, thus making the design problem easier. Experiment has borne this point out, in that an originally unstable machine could be stabilized by introduction of external rotor resistance.

#### (2.3) Elimination of Inherent Negative Damping

To be of use to the designer of a double-synchronous-speed machine, the points noticed above need to be put in a more general form.

Eqns. (40) and (41) give the damping-torque coefficients, $T_{d1}$ and $T_{d2}$, due to the induction-motor torques. The total damping-torque coefficient in the region of no-load, which would be the worst condition for stability, is the algebraic sum of $T_{d1}$ and $T_{d2}$. It is instructive to notice the effect of various parameters on the sign of $T_{d1} + T_{d2}$ when $s = -1$. An analysis developed below seems to possess just this advantage, as it clearly displays the effects of variations in any of the constants, $R_S$, $R_R$, $X_S$, $X_R$ and $X_m$.

In eqns. (40) and (41) make the substitutions $R_S/X_S = \phi$; $R_R/X_R = \psi$, and assume that $V_S/V_R = \beta$ and $X_S/X_R = \beta^2$. Further let $X_m^2/X_S X_R = \theta < 1$. Dividing both numerator and denominator by $X_S^4 X_R^4$

$$T_{d1} = -\left(\frac{3p^2 V_S^2 \theta \psi}{9·81 \omega_S^2 X_S}\right) \frac{\left[\phi^2 + (1-\theta)^2 - \frac{\psi^2(\phi^2+1)}{s^2}\right]}{\left\{\frac{\psi^2(\phi^2+1)}{s} + 2\theta\phi\psi + s[\phi^2+(1-\theta)^2]\right\}^2}$$

. . . . (48)

and

$$T_{d2} = -\left(\frac{3p^2 V_R^2 \theta \phi}{9·81 \omega_S^2 X_R}\right) \frac{\left[\psi^2 + (1-\theta)^2 - \frac{\phi^2(\psi^2+1)}{s^2}\right]}{\left\{\frac{\phi^2(\psi^2+1)}{s} + 2\theta\phi\psi + s[\psi^2+(1-\theta)^2]\right\}^2}$$

. . . . (49)

since $V_S^2/X_S = V_R^2/X_R$, the sign of $T_{d1} + T_{d2}$ is determined by the sign of the expression

$$\left[-\frac{\psi\left[\phi^2 + (1-\theta)^2 - \frac{\psi^2(\phi^2+1)}{s^2}\right]}{\left\{\frac{\psi^2(\phi^2+1)}{s} + 2\theta\phi\psi + s[\phi^2+(1-\theta)^2]\right\}^2}\right.$$
$$\left. + \frac{\phi\left[\psi^2 + (1-\theta)^2 - \frac{\phi^2(\psi^2+1)}{s^2}\right]}{\left\{\frac{\phi^2(\psi^2+1)}{s} + 2\theta\phi\psi + s[\psi^2+(1-\theta)^2]\right\}^2}\right] \quad (50)$$

When $s = -1$, both denominators are equal to

$$[\phi^2(\psi^2+1) - 2\theta\phi\psi + \psi^2 + (1-\theta)^2]^2$$
$$= [\psi^2(\phi^2+1) - 2\theta\phi\psi + \phi^2 + (1-\theta)^2]^2 \quad (51)$$

Hence the sign of $T_{d1} + T_{d2}$ at $s = -1$ is determined by the sign of

$$-\psi[\phi^2 + (1-\theta)^2 - \psi^2(\phi^2+1)]$$
$$- \phi[\psi^2 + (1-\theta)^2 - \phi^2(\psi^2+1)] \quad (52)$$
$$= -(\psi+\phi)(1-\theta)^2 + \psi^3\phi^2 + \psi^3$$
$$- \psi\phi^2 + \phi^3\psi^2 + \phi^3 - \phi\psi^2 \quad (53)$$
$$= (\psi+\phi)[-(1-\theta)^2 + \psi^2\phi^2 + (\phi-\psi)^2] \quad (54)$$

and this is $\geqslant 0$ if

$$(1-\theta)^2 \leqslant \psi^2\phi^2 + (\phi-\psi)^2 \quad . \quad . \quad . \quad (55)$$

i.e. if

$$(1-\theta) \leqslant +\sqrt{[\psi^2\phi^2 + (\phi-\psi)^2]} \quad \text{(as } 0 \leqslant \theta \leqslant 1) \quad (56)$$

Now if $\phi$ and $\psi$ are very small, this condition is approximately

$$(1-\theta) \leqslant \phi - \psi \quad \text{if } \phi > \psi \quad . \quad . \quad . \quad (57)$$
or
$$(1-\theta) \leqslant \psi - \phi \quad \text{if } \psi > \phi \quad . \quad . \quad . \quad (58)$$
i.e.
$$\theta \geqslant 1 - (\phi - \psi) \quad \text{if } \phi > \psi \quad . \quad . \quad . \quad (59)$$
or
$$\theta \geqslant 1 - (\psi - \phi) \quad \text{if } \psi > \phi \quad . \quad . \quad . \quad (60)$$

In other words, $T_{d1} + T_{d2}$ is positive if

$$1 \geqslant \frac{X_m^2}{X_S X_R} \geqslant 1 - \frac{R_S}{X_S} + \frac{R_R}{X_R} \quad \text{if } \frac{R_S}{X_S} > \frac{R_R}{X_R} \quad . \quad (61)$$
or
$$1 \geqslant \frac{X_m^2}{X_S X_R} \geqslant 1 - \frac{R_R}{X_R} + \frac{R_S}{X_S} \quad \text{if } \frac{R_R}{X_R} > \frac{R_S}{X_S} \quad . \quad (62)$$

This result is helpful in that, given $X_S$ and $X_R$, it not only gives the limits for $X_m$ which would keep $T_{d1} + T_{d2}$ positive but also shows how these limits could be widened by manipulating

the stator and rotor resistances. Thus, in a case in which $R_R/X_R > R_S/X_S$, increase of the rotor resistance or decrease of the stator resistance gives a wider range for positive $T_{d1} + T_{d2}$, thus making a design with a smaller coefficient of coupling possible. A value of $R_R$ which would give positive damping could be found for any given values of $X_R$, $X_S$ and $X_m$. Thus, for the machine considered earlier, a value for $R_R$ could be found which would stabilize it. This has been verified by stabilizing a machine, the constants of which have been used as an example, by inserting external resistance in the rotor phases.

From the designer's standpoint it is suggested that eqns. (61) and (62) could be put into a different form. To do this let it be assumed that all quantities are referred to the stator; then if

$$X_M = \text{Mutual reactance,}$$

$$x_S, x_R = \text{Stator and rotor leakage reactances,}$$

$$r_S, r_R = \text{Stator and rotor resistances,}$$

eqns. (61) and (62) expressed together yield

$$\frac{X_M^2}{(X_M + x_S)(X_M + x_R)} \geqslant 1 - \left| \frac{r_R}{(X_M + x_R)} - \frac{r_S}{(X_M + x_S)} \right| \quad (62a)$$

i.e. $$1 - \frac{X_M^2}{(X_M + x_S)(X_M + x_R)} \leqslant \left| \frac{r_R}{(X_M + x_R)} - \frac{r_S}{(X_M + x_S)} \right| \quad (62b)$$

or $$\frac{x_S x_R + X_M(x_S + x_R)}{(X_M + x_S)(X_M + x_R)} \leqslant \left| \frac{r_R}{(X_M + x_R)} - \frac{r_S}{X_M + x_S} \right| \quad (62c)$$

As $x_S$ and $x_R$ are very small relative to $X_M$, $x_S x_R$ can be neglected in comparison with $X_M(x_S + x_R)$ and also $X_M + x_S \simeq X_M$ and $X_M + x_R \simeq X_M$.

The condition will thus approximate to

$$(x_S + x_R) \leqslant |r_R - r_S| \quad . \quad . \quad . \quad (62d)$$

which means that, referred to the stator, the total leakage reactance per phase should be less than the difference between the stator and rotor resistances. This way of expressing the result shows that this requirement is not dependent on the coupling coefficient.

### (3) EXPERIMENTAL WORK

In order to test the results obtained by mathematical analysis a series of measurements were made on a 7·5 h.p. 3-phase induction motor, the rotor and stator of which were supplied from the same 50 c/s busbars (Fig. 7). The machine had six poles and was operated with rotor and stator voltages, $V_R$ and $V_S$, of 150 and 400 volts. These voltages were maintained constant by means of Variac transformers (not shown in the
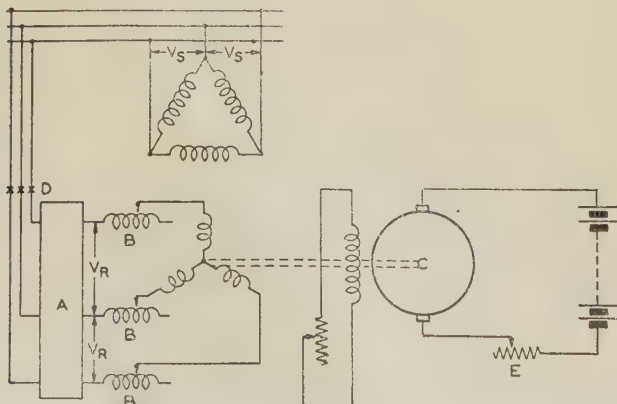
diagram). An adjustable phase-shifting transformer (A) connected in the rotor circuit was used to maintain the rotor and stator voltages in phase with each other, phase alignment being checked by means of a Lissajou figure. Three variable air-cored inductances (B) were connected between the transformer and the rotor terminals, and the phase sequences of rotor and stator were so arranged that the rotor would operate at a 'synchronous' speed of 2 000 r.p.m.

The induction machine was connected mechanically through a rigid coupling to a direct-current machine (C) having a rating of 6·5 h.p. at 1 000 r.p.m. The field of this machine was separately excited, and its armature was supplied from a battery.

The rotor cyclic self-reactance was measured as the ratio of rotor voltage to rotor current when the stator was on open-circuit and the rotor at rest. For this test the rotor was supplied at a line voltage of 150 volts. The stator cyclic self-reactance was measured in a similar manner with the stator supplied at a line voltage of 400 volts. The mutual reactance, measured 3-phase, as the ratio of stator phase voltage to rotor phase current with a line voltage of 150 volts applied to the rotor was found to differ slightly from the value obtained when the stator was supplied at a line voltage of 400 volts, by taking the ratio of rotor phase voltage to stator phase current. For the purposes of calculation the mean of these two values was used.

The rotor and stator resistances were measured by voltmeter and ammeter on direct current after the windings had been brought up to the operating temperature. No difficulty was encountered so far as the measurement of stator resistance was concerned, but it was found that the effective rotor resistance was a complicated function of the rotor current, and a series of readings had to be taken with the rotor driven at 2 000 r.p.m. by means of the d.c. motor over a range of values of the rotor current. This precaution was necessary as the damping torque is very sensitive to variations in rotor and stator resistance.
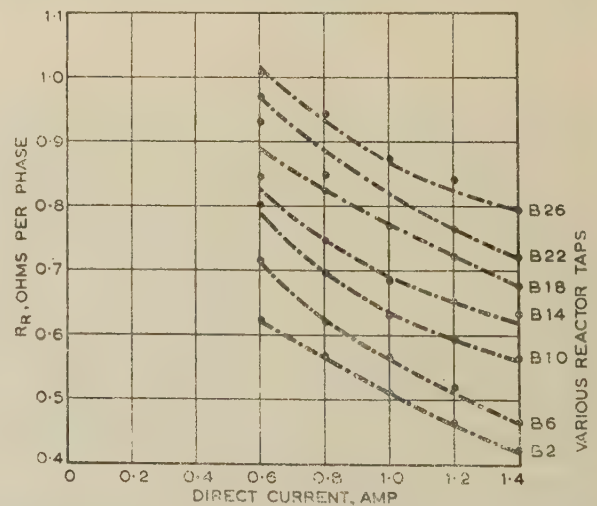
Fig. 8.—Variation of rotor circuit resistance with rotor current.

The results of the measurements which have been described are given in Fig. 8. Typical values for the various quantities are:

|        |     | Resistance | Total self-reactance | Mutual reactance |
|--------|-----|-----------|----------------------|------------------|
| Stator | .. .. | 2·58 ohms | 132·4 ohms | 28·18 ohms |
| Rotor  | .. .. | 0·4–1·0 ohm | 6·62 ohms |  |

### (3.1) Estimation of Negative Damping

The method used, which has been described previously,[12] depends on the ability of a d.c. machine to provide a positive

Fig. 7.—Diagram of connections used in experimental work.

damping torque the values of which can be easily calculated. For such a machine operating with constant excitation on a controlled applied armature voltage, $V$, the generating armature current is given by

$$i_a = \frac{F\omega - V}{R_a} \qquad . \quad . \quad . \quad . \quad . \quad (63)$$

where $\omega$ is the angular velocity of rotation, $F$ is a constant defined as generated volts per radian per second, and $R_a$ is the total resistance in the armature circuit. The generating torque may be written as

$$T_q = \frac{Fi_a}{9\cdot81} = \frac{F(F\omega - V)}{9\cdot81 R_a} \text{ kg-m} \quad . \quad . \quad . \quad (64)$$

The damping torque is given by

$$T_d = \frac{\partial T_q}{\partial \omega} = \frac{F^2}{9\cdot81 R_a} \text{ kg-m per mechanical rad/s} \quad . \quad (65)$$

This is a positive damping torque as it represents a retarding torque acting in such a direction as to oppose any increase in angular velocity. The total damping torque provided by the d.c. machine is arrived at by adding the contribution made by the eddy-current loss in the core. It is assumed that the loss current at constant excitation can be written as

$$i_L = A + B\omega \qquad . \quad . \quad . \quad . \quad (66)$$

where $A$ and $B$ are constants which can be determined by the Kapp test. The loss torque will therefore be

$$T_L = \frac{F(A + B\omega)}{9\cdot81} \text{ kg-m} \quad . \quad . \quad . \quad (67)$$

and damping torque due to loss,

$$T_{dL} = \frac{\partial T_L}{\partial \omega} = \frac{FB}{9\cdot81} \text{ kg-m per mechanical rad/s} \quad . \quad (68)$$

For measurement of negative damping, the stator of the a.c. machine having been connected to the busbars, the rotor was brought up to 2 000 r.p.m. by the d.c. motor and synchronized to the supply by means of the switch (D) in the rotor circuit (Fig. 7). With the field current of the d.c. motor held constant the resistance (E) in the armature circuit of this machine was adjusted until a small phase-swinging oscillation of the two machines was just maintained. It was assumed that under these conditions the positive damping of the d.c. machine was equal and opposite to the negative damping inherent in the induction motor. This test was repeated for a number of values of the variable reactance (B) in the rotor circuit. When performing the tests the input of the d.c. machine was so adjusted, by control of its field current, that the angle $\alpha$ was very small, thus justifying the omission of terms in $\sin \alpha$ when calculating the negative damping torque. The predicted curve and the experimental points are shown in Fig. 9.

It was found impossible to prevent an increase in oscillation when the added reactance (B) was reduced to below 1 ohm, as the maximum positive damping which the d.c. machine could supply was less than $40 \times 10^{-3}$ kg-m per rad/s.

In calculating the value for the a.c. machine it was assumed that the eddy-current loss was constant and independent of the swinging displacement. On this assumption the eddy-current loss cannot provide any damping. It may be justified in the following manner: the resistance voltages in the rotor and stator under conditions of test were small, being of the order of 1% of the terminal voltages, which were maintained constant; thus the rate of change of flux linkages in the stator and rotor must have
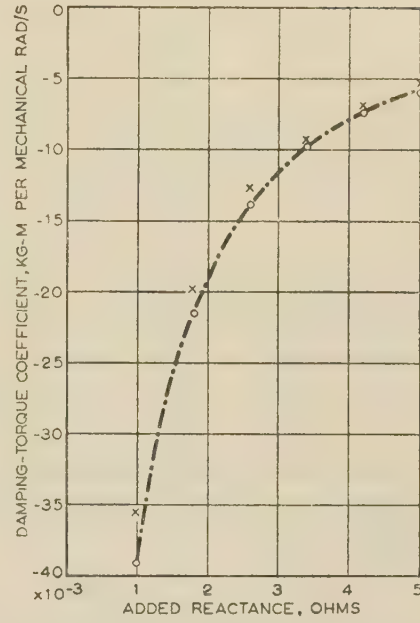


Fig. 9.—Variation of inherent damping-torque coefficient with added rotor reactance.

○ Theoretical.
× Experimental.

been very nearly constant. The frequency of the supply was practically constant, and since this was applied to both rotor and stator, the velocity of the rotating field must have been the same with respect to each of these members. If the velocity and magnitude of this field were constant, the eddy-current loss must have been nearly constant also.
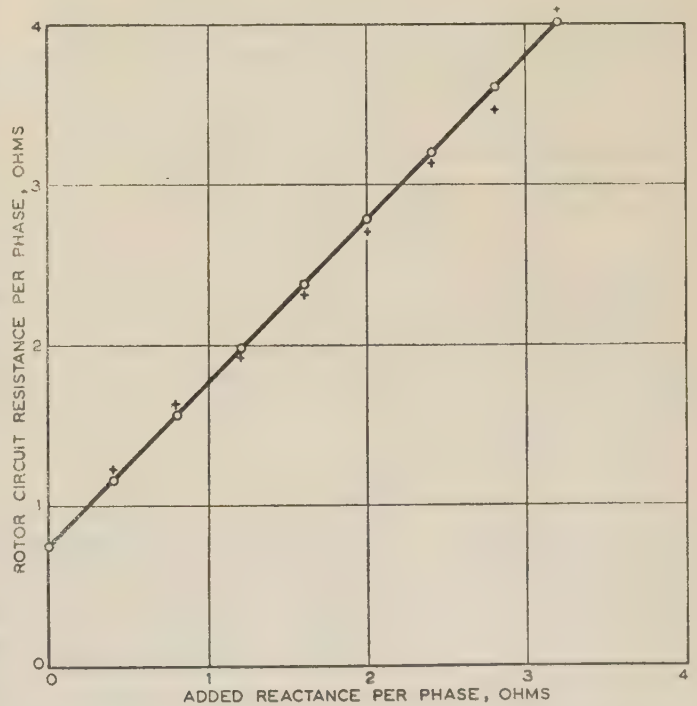


Fig. 10.—Stabilization with additional resistance in rotor circuit.

○ Theoretical.
× Experimental.

### (3.2) Stabilization with Added Resistance in Rotor

The possibility of stabilizing a double-synchronous-speed machine by the addition of resistance in the rotor circuit, as suggested by eqns. (61) and (62), has been verified experimentally. For this test three variable resistances, one in series with each rotor phase, were introduced.

The stator of the a.c. machine was fed from a 400-volt 3-phase 50 c/s supply, and the voltage applied to the rotor, kept in phase with the stator voltage with the help of the phase shifter, was maintained at such a value as to satisfy the condition $V_S^2/X_S = V_R^2/X_R$. The a.c. machine was excited on the stator side, run up to speed with the help of the d.c. motor and then synchronized on the rotor side to the proper voltage. The supply to the d.c. machine was then switched off to ensure that no positive damping was contributed from that side. Finally, the series resistance on the rotor side was varied until the machine was just on the point of executing sustained oscillations. Repetition of this procedure with different total rotor reactances gave the resistance necessary in the rotor circuit for any given rotor-circuit reactance to ensure stable running. Fig. 10 shows the rotor-circuit resistances per phase necessary to provide stability for different reactances added in each rotor phase.

### (3.3) Comments on the Results

Fig. 9 shows that the total negative-damping-torque coefficient for an added reactance of 1 ohm, is of the order of $40 \times 10^{-3}$ kg-m per mechanical rad/s, while for the same added reactance it can be seen from Fig. 10 that increasing the rotor resistance to about 1·8 ohms per phase completely eliminates the inherent negative damping and stabilizes the machine. Fig. 10 also shows that a lower resistance can achieve a stabilizing result with a lower added series reactance. There is an increased rotor copper loss, but it should be borne in mind that there is also a doubled output in this type of machine for a given frame size. There is also the possibility of stabilizing with the help of series capacitors, a study of which may yield fruitful results, although it is perhaps doubtful if the extra cost is economically justifiable.

### (4) ACKNOWLEDGMENTS

### (5) REFERENCES

(1) KASSJANOW, W. T.: 'Die Theorie der doppeltgespeisten Induktionsmaschine', *Elektrotechnik und Maschinenbau*, 1932, **51**, p. 453.
(2) MESSING, E.: 'Theory of Double Field Induction Motor', *Archiv für Elektrotechnik*, 1933, **27**, p. 279.
(3) ARNOLD, E.: 'Weschelstromtechnik' (Springer).
(4) HERSCHDORFER, J.: 'Theory of the Double Field Induction Motor', *Archiv für Elektrotechnik*, 1932, **26**, p. 620.
(5) TSCHERDANZEV, J.: 'Theory of Doubly Fed Induction Machine', *ibid.*, 1926, **15**, p. 257.
(6) LEONHARD, A.: 'Asynchronous and Synchronous Running of the General Doubly Fed Three Phase Machine', *ibid.*, 1936, **30**, p. 483.
(7) KLOSS, M.: 'The Three-Phase Doubly Fed Motor for Double Synchronous Speed', *Elektrotechnische Zeitschrift*, 1935, **56**, p. 885.
(8) STEUDEL, H.: 'Der Betriebsverhalten der Doppelfeldmaschine', Dissertation, Technische Hochschule, Berlin, 1933.
(9) HANNAKAM, L.: 'Stabilisierung des Betriebs der doppeltgespeisten Asynchronmaschine durch die Anwurfmaschine', *Elektrotechnische Zeitschrift*, 1954, **75**, p. 654.
(10) CONCORDIA, C., CRARY, S. B., and KRON, G.: 'The Doubly Fed Machine', *Transactions of the American I.E.E.*, 1942, **61**, p. 286.
(11) LYON, W. V., and EDGERTON, H. E.: 'Transient Angular Oscillations of Synchronous Machinery', *ibid.*, 1930, **49**, p. 686.
(12) PRESCOTT, J. C., and RICHARDSON, J. E.: 'The Inherent Instability of Synchronous Machinery', *Journal I.E.E.*, 1934, **75**, p. 497.

### (6) APPENDIX: DERIVATION OF TORQUE EXPRESSIONS

$$V_S = (R_S + j\omega_S L_S)I_{S1} + jM\omega_S I_{R1}\varepsilon^{-j\alpha} \qquad (17)$$

$$0 = jM(\omega_S - \omega)\varepsilon^{j\alpha}I_{S1} + [R_R + j(\omega_S - \omega)L_R]I_{R1} \qquad (18)$$

$$I_{S1} = \frac{[R_R + j(\omega_S - \omega)L_R]V_S}{[R_S R_R - L_S\omega_S L_R(\omega_S - \omega) + M^2\omega_S(\omega_S - \omega)] + j[R_R L_S\omega_S + R_S L_R(\omega_S - \omega)]} \qquad (19)$$

Putting

$$A = R_S R_R - L_S\omega_S L_R(\omega_S - \omega) + M^2\omega_S(\omega_S - \omega)$$
$$B = R_R L_S\omega_S + R_S L_R(\omega_S - \omega)$$

and rationalizing,

$$I_{S1} = \frac{V_S[R_R + j(\omega_S - \omega)L_R](A - jB)}{A^2 + B^2} \qquad (69)$$

$$I_{R1} = -jM(\omega_S - \omega)V_S\varepsilon^{j\alpha}\frac{A - jB}{A^2 + B^2} \qquad (70)$$

$E'_{R1}$ = e.m.f. induced in the rotor phase due to currents in the stator

$$= -jM(\omega_S - \omega)\varepsilon^{j\alpha}I_{S1}$$

Therefore

$$E'_{R1} = -jM(\omega_S - \omega)\varepsilon^{j\alpha}V_S[R_R + j(\omega_S - \omega)L_R]\frac{A - jB}{A^2 + B^2}$$
$$\qquad (71)$$

whence

$$E'^*_{R1} = \frac{M(\omega_S - \omega)}{A^2 + B^2}V_S[L_R(\omega_S - \omega) + jR_R](A + jB)\varepsilon^{-j\alpha} \qquad (72)$$

where * indicates the conjugate.

Similarly

$$0 = jM(\omega_R + \omega)\varepsilon^{-j\alpha}I_{R2} + [R_S + j(\omega_R + \omega)L_S]I_{S2} \qquad (21)$$

$$V_R = (R_R + j\omega_R L_R)I_{R2} + jM\omega_R I_{S2}\varepsilon^{j\alpha} \qquad (22)$$

$$I_{R2} = \frac{[R_S + j(\omega_R + \omega)L_S]V_R}{[R_S R_R - L_S(\omega_R + \omega)L_R\omega_R + M^2(\omega_R + \omega)\omega_R] + j[R_R L_S(\omega_R + \omega) + (R_S L_R\omega_R)]} \qquad (24)$$

Putting

$$C = R_S R_R - L_S(\omega_R + \omega)L_R\omega_R + M^2(\omega_R + \omega)\omega_R$$

$$D = R_R L_S(\omega_R + \omega) + R_S L_R \omega_R$$

and rationalizing,

$$I_{R2} = [R_S + j(\omega_R + \omega)L_S]V_R\frac{C - jD}{C^2 + D^2} \qquad . \quad (73)$$

$$I_{S2} = [-jM(\omega_R + \omega)\varepsilon^{-j\alpha}V_R]\frac{C - jD}{C^2 + D^2} \quad . \quad . \quad (74)$$

$E'_{R2}$ = e.m.f. induced in the rotor phase due to currents in the stator.

$$= -jM\omega_R\varepsilon^{j\alpha}I_{S2}$$

Therefore

$$E'_{R2} = -jM\omega_R\varepsilon^{j\alpha}[-jM(\omega_R + \omega)\varepsilon^{-j\alpha}V_R]\frac{C - jD}{C^2 + D^2} \qquad (75)$$

whence

$$E'^{*}_{R2} = -M^2\omega_R(\omega_R + \omega)V_R\frac{C + jD}{C^2 + D^2} \qquad . \quad . \quad . \quad (76)$$

where * indicates the conjugate.

From the above values of $E'^{*}_{R1}$, $I_{R1}$, $E'^{*}_{R2}$ and $I_{R2}$, the four hypothetical torques, in kilogramme-metres, can be derived thus:

where

$$a_1 = -(R_S X_R + R_R X_S)R_S^2 R_R^2$$

$$a_2 = -(R_S X_R + R_R X_S)X_m^2 R_S R_R$$

$$a_3 = -(R_S X_R + R_R X_S)(R_S^2 X_R^2 + R_R^2 X_S^2)$$

$$a_4 = -(R_S X_R + R_R X_S)X_m^2 R_S R_R$$

$$a_5 = -(R_S X_R + R_R X_S)(X_m^2 - X_S X_R)^2$$

$$b_1 = R_S^2 R_R^2(R_S R_R - X_S X_R)$$

$$b_2 = 2R_S^2 R_R^2 X_m^2$$

$$b_3 = \{R_S R_R[(X_m^2 - X_S X_R)^2 - R_S R_R X_S X_R]$$
$$+ R_S R_R(X_m^2 - X_S X_R)(R_S R_R - X_S X_R)$$
$$+ (R_S X_R + R_R X_S)^2(R_S R_R + X_m^2 - X_S X_R)\}$$

$$b_4 = (X_m^2 - X_S X_R)2R_S R_R X_m^2$$

$$b_5 = [(X_m^2 - X_S X_R)^3 - (X_m^2 - X_S X_R)R_S R_R X_S X_R]$$

$$d_1 = (R_S^2 R_R^2 + R_R^2 X_S^2)(R_S^2 R_R^2 + R_S^2 X_R^2)$$

$$d_2 = 2R_S R_R X_m^2(2R_S^2 R_R^2 + R_S^2 X_R^2 + R_R^2 X_S^2)$$

$$d_3 = [4R_S^2 R_R^2 X_m^4 + (X_m^2 - X_S X_R)^2(2R_S^2 R_R^2 + R_2 X_R^2 + R_R^2 X_S^2)$$
$$+ R_S^2 X_R^2(R_S^2 R_R^2 + R_S^2 X_R^2) + R_R^2 X_S^2(R_S^2 R_R^2 + R_R^2 X_S^2)]$$

$$d_4 = 2R_S R_R X_m^2[2(X_m^2 - X_S X_R)^2 + (R_S^2 X_R^2 + R_R^2 X_S^2)]$$

$$d_5 = [(X_m^2 - X_S X_R)^4 + R_S^2 R_R^2 X_S^2 X_R^2$$
$$+ (X_m^2 - X_S X_R)^2(R_S^2 X_R^2 + R_R^2 X_S^2)]$$

$$T_1 = -\frac{3p}{9\cdot81(\omega_S - \omega)}\mathscr{R}E'^{*}_{R1}I_{R1} = -\frac{3pV_S^2 R_R M^2(\omega_S - \omega)}{9\cdot81(A^2 + B^2)} \qquad . \quad . \quad . \quad . \quad . \quad . \quad . \quad . \quad (77)$$

$$T_2 = -\frac{3p}{9\cdot81\omega_R}\mathscr{R}E'^{*}_{R2}I_{R2} = -\frac{3pV_R^2 R_S M^2(\omega_R + \omega)}{9\cdot81(C^2 + D^2)} \qquad . \quad . \quad . \quad . \quad . \quad . \quad . \quad . \quad (78)$$

$$T_3 = -\frac{3p}{9\cdot81(\omega_S - \omega)}\mathscr{R}E'^{*}_{R1}I_{R2}$$

$$= -\frac{3pMV_S V_R}{9\cdot81(A^2 + B^2)(C^2 + D^2)}\{[R_S L_R(\omega_S - \omega) - R_R L_S(\omega_R + \omega)][(AC + BD)\cos\alpha - (AD - BC)\sin\alpha]$$
$$+ [R_S R_R + L_S L_R(\omega_S - \omega)(\omega_R + \omega)][(AD - BC)\cos\alpha + (AC + BD)\sin\alpha]\} \qquad (79)$$

$$T_4 = -\frac{3p}{9\cdot81\omega_R}\mathscr{R}E'^{*}_{R2}I_{R1} = \frac{3pMV_S V_R}{9\cdot81(A^2 + B^2)(C^2 + D^2)}[M^2(\omega_S - \omega)(\omega_R + \omega)][(AD - BC)\cos\alpha + (AC + BD)\sin\alpha] . \quad . \quad (80)$$

and

$$T_G = T_1 + T_2 + T_3 + T_4$$

For the double synchronous speed case, expressing these formulae in terms of slip $s$, and reactances, where

$$s = \frac{\omega_S - \omega}{\omega_S} = \frac{\omega_R + \omega}{\omega_R}$$

and noting that $\omega_R = -\omega_S$; $X_S = L_S\omega_S$; $X_R = L_R\omega_S$; $X_m = M\omega_S$:

$$A = R_S R_R + s(X_m^2 - X_S X_R) = C$$

$$B = R_R X_S + sR_S X_R \quad \text{and} \quad D = -R_S X_R - sR_R X_S$$

and the formulae become

$$T_1 = -\frac{3pV_S^2}{9\cdot81\omega_S}\frac{sR_R X_m^2}{\{(R_S^2 R_R^2 + R_R^2 X_S^2) + s(2X_m^2 R_S R_R) + s^2[(X_m^2 - X_S X_R)^2 + R_S^2 X_R^2)]\}} \qquad . \quad . \quad . \quad . \quad (81)$$

$$T_2 = -\frac{3pV_R^2}{9\cdot81\omega_S}\frac{sR_S X_m^2}{\{(R_S^2 R_R^2 + R_S^2 X_R^2) + s(2X_m^2 R_S R_R) + s^2[(X_m^2 - X_S X_R)^2 + R_R^2 X_S^2)]\}} \qquad . \quad . \quad . \quad . \quad (82)$$

and

$$T_3 + T_4 = -\left[\frac{(a_1 + a_2 s + a_3 s^2 + a_4 s^3 + a_5 s^4)\cos\alpha + (b_1 + b_2 s + b_3 s^2 + b_4 s^3 + b_5 s^4)\sin\alpha}{(d_1 + d_2 s + d_3 s^2 + d_4 s^3 + d_5 s^4)}\right]\frac{3pMV_S V_R}{9\cdot81} \qquad . \quad . \quad (83)$$

# DISCUSSION ON
## 'THE MEASUREMENT AND PREDICTION OF INDUCTION MOTOR STRAY LOSS AT LARGE SLIPS'*

**Mr. A. H. Maggs** (*communicated*): The authors state that to minimize stray loss in induction motors the number of slots per pole should be as small as possible, and in support of this thesis refer to page 174 of P. L. Alger's book, 'The Nature of Polyphase Induction Machines'. It should be noted, however, that Alger is discussing the effect of varying the number of rotor slots in relation to a given number of stator slots, and he does not mention the question of varying the stator slots also and what effect this would have.

In the writer's experience, which includes a variety of types of induction machine, single- and 3-phase, with and without commutators, those with relatively large numbers of slots per pole are generally better from an all-round point of view than those with relatively small numbers. Since in a given size of machine the ampere-turns per pole are about the same whatever the number of slots per pole may be, it follows that for a small number the ampere-turns per slot must be large. Thus for a given length of air-gap the zigzag leakage flux density is also large, the tooth-tip saturation more pronounced and the magnitude of the flux pulsations correspondingly large. One has only to visualize a machine, having a given air-gap, in which the numbers of slots, stator and rotor, are made increasingly large towards infinity to realize that, not only is the zigzag leakage flux density reduced inversely at some power greater than unity, but despite the increase in the frequency of flux pulsation the losses arising therefrom are progressively reduced.

A relatively large number of slots per pole is particularly advantageous in single-phase machines of both commutator and non-commutator types, where a low leakage reactance is desirable in order to secure a high specific torque output. Also in these machines a large number of slots greatly reduces the risk of incurring that part of the double-frequency hum and vibration which is excited by the forces associated with the zigzag leakage flux and is most pronounced at high current loadings. The prominence of this noise or vibration also depends on the

* BARTON, T. H., and AHMAD, V.: Monograph No. 219 U, January, 1957 (104 C, p. 299).

uniformity of the air-gap, the bearing fit and the general mechanical design. It is most important to ensure that the critical speed of the rotor is not at or too close to twice line frequency; preferably it should be higher.

Three-phase a.c. commutator motors, more particularly the shunt type with separate induction regulator, also yield appreciably better speed/torque characteristics when designed with relatively large numbers of slots per pole. In the shunt machine the leakage reactance, which includes the through reactance of the regulator, materially affects the characteristics.

The arguments often advanced in favour of a small number of slots are better space factor and lower winding costs. The writer is of the opinion that other considerations, some of which have been enumerated above, outweigh these arguments. A less massive coil in a narrower slot ensures better transfer of heat from the coil to the core, from which heat is mainly dispersed. Concurrently a slightly smaller total amount of copper is required for a designed output. The difference in cost between the larger and smaller numbers of slots which are usual and practicable can only be of second-order importance in the production of laminations, and, in addition, the difference in winding costs, especially when the coils are wound in jointless groups, can only be very small, bearing in mind that the total numbers of turns are almost if not exactly equal for both numbers of coils. The reduction in copper weight may even reverse the difference, since copper is a relatively expensive material.

**Dr. T. H. Barton** and **Mr. V. Ahmad** (*in reply*): We are grateful for Mr. Magg's remarks and agree with him that, contrary to our statement in the conclusion to our paper, the stray loss associated with the zigzag leakage flux will decrease as the number of slots is increased whilst keeping the ratio of rotor to stator slots constant. When writing the paper we were concerned principally with the resultant increase in frequency, and, not being machine designers, omitted to consider the compensating effect of the reduced flux density. We would like to apologize to Mr. Alger for any inconvenience which our incorrect reference to his book may have caused him.

# PROCEEDINGS OF THE INSTITUTION OF ELECTRICAL ENGINEERS

## CONTENTS